MASARYK UNIVERSITY

FACULTY OF SCIENCE

DEPARTMENT OF EXPERIMENTAL BIOLOGY

Mobile Genetic Elements: Friends or Foes of Staphylococci?

HABILITATION THESIS

Tibor Botka

BRNO 2026

ABSTRACT

This habilitation thesis addresses the dual role of mobile genetic elements in staphylococci: their role in the development of pathogenicity and their application in the treatment of difficult-to-treat infections. The first part presents the author's contribution to research on resistance- and virulence-associated plasmids, prophage-mediated lysogenic conversion, and interactions between bacteriophages and chromosomal islands. The author was involved in the discovery and characterization of new genetic elements, the mechanisms of their transfer via generalized and lateral transduction, and the development of novel methodologies for their study. The second part focuses on the author's research on the therapeutic potential of lytic bacteriophages. It covers publications on the genomics, lytic activity, and structure of bacteriophages of the genus *Kayvirus*, demonstrating their suitability for phage therapy. An important part of the author's work is the application of phage-antibiotic synergy, which demonstrates that this approach can enhance antibacterial efficacy, suppress the emergence of resistance, and broaden the spectrum of treatable staphylococcal strains. Attention is also paid to the safety aspects of phage therapy, in which knowledge from both fields—lytic phages and the transfer of the staphylococcal mobilome encoding pathogenic determinants—is integrated. Overall, the presented results advanced our understanding of phage-host interactions and the dynamics of mobile genetic elements, while contributing to the development of safe and effective phage-based antimicrobial strategies.

ACKNOWLEDGEMENTS

I would like to express my sincere gratitude to everyone who has, directly or indirectly, contributed to joint publications, applied research results, grants awarded, or conference presentations, as well as to my professional development over the past few years.

Many thanks to all current and former colleagues from the Laboratory of Molecular Diagnostics of Microorganisms, whose expertise and teamwork have been indispensable to both my research and my daily academic life. First and foremost, I would like to thank my supervisor throughout my studies, Doc. Vladislava Růžičková, for her long-standing guidance, support, and trust in my work. I would especially like to express my gratitude to the former and current heads of the laboratory, Prof. Jiří Doškař and Prof. Roman Pantůček, respectively, whose scientific vision, deep knowledge, and constant support have been invaluable. I would also like to thank all the students whose work I have supervised or consulted on for their contributions to my research, including publications and successful grant proposals.

I extend my sincere thanks to my colleagues from other departments at Masaryk University for their interdisciplinary collaboration and knowledge sharing, which has significantly enhanced the quality and scope of my research. I would like to thank the Department of Microbiology, the Department of Biochemistry, CEITEC MU, and St. Anne's University Hospital in Brno for essential cooperation on applied research projects. I also want to thank the Core Facilities at Masaryk University for providing access to cutting-edge infrastructure. As close collaboration between academia and industry drives progress in applied biomedical sciences, I would like to acknowledge my colleagues from the biotechnology industry. I am deeply grateful to my colleagues at foreign institutions, whose collaboration has broadened my academic horizons and enriched my research experience.

Above all, I would like to express my deep and heartfelt gratitude to my wife and children. Thanks to their understanding and unwavering support, I have been able to carry out this demanding work as a researcher and academic. Their encouragement and patience during long work hours, weekends spent writing, and periods of my absence were indispensable for the completion of this work and for my academic career as a whole.

CONTENT

ABBREVIATIONS 6

1 STRUCTURE OF THE THESIS AND THE AUTHOR'S CONTRIBUTION 8

2 INTRODUCTION 13

3 MGE CONTRIBUTING TO STAPHYLOCOCCAL PATHOGENICITY 16

3.1 PLASMIDS 17

3.1.1 ANTIMICROBIAL RESISTANCE-ENCODING PLASMIDS 17

3.1.2 VIRULENCE FACTOR-ENCODING PLASMIDS 20

3.2 TEMPERATE PHAGES 23

3.2.1 LYSOGENIC CONVERSION 25

3.3 PHAGE-INDUCIBLE CHROMOSOMAL ISLANDS 28

3.4 TRANSDUCTION 32

3.4.1 GENERALIZED TRANSDUCTION 34

3.4.2 LATERAL TRANSDUCTION 35

4 PHAGE-BASED APPROACHES TO FIGHT STAPHYLOCOCCAL INFECTIONS 37

4.1 *KAYVIRUS* PHAGES 39

4.2 PHAGE-ANTIBIOTICS SYNERGY (PAS) 43

4.3 SAFETY ASPECTS OF PHAGE AND PAS-BASED THERAPY 47

5 CONCLUSIONS AND OUTLOOK 50

6 REFERENCES 53

7 APPENDICES 64

APPENDIX 1 64

APPENDIX 2 95

APPENDIX 3 119

APPENDIX 4 136

APPENDIX 5 152

APPENDIX 6 169

APPENDIX 7 178

APPENDIX 8 187

APPENDIX 9 212

APPENDIX 10 226

APPENDIX 11 238

APPENDIX 12 254

APPENDIX 13 277

APPENDIX 14 297

APPENDIX 15.....310
APPENDIX 16.....318
APPENDIX 17.....325
APPENDIX 18.....336

ABBREVIATIONS

AI	Artificial Intelligence
AMO	Amoxicillin
attB	Bacterial Attachment Site
CA-MRSA	Community-Acquired Methicillin-Resistant *Staphylococcus aureus*
CC	Clonal Complex
CEITEC	Central European Institute of Technology
CF	Cystic Fibrosis
CIP	Ciprofloxacin
CoNS	Coagulase-Negative Staphylococci
CRISPR	Clustered Regularly Interspaced Short Palindromic Repeats
DNA	Deoxyribonucleic Acid
DR	Direct Repeat
EDIN	Epidermal Cell Differentiation Inhibitor
ET	Exfoliative Toxin
ETA	Exfoliative Toxin A
ETA-B	Exfoliative Toxin A Phage Group B
ETB	Exfoliative Toxin B
HGT	Horizontal Gene Transfer
IleRS	Isoleucyl-tRNA Synthetase (wild type)
$IleRS^R$	Mutated IleRS (induces low-level mupirocin resistance)
IleRS2	Alternative IleRS (induces high-level mupirocin resistance)
IS	Insertion Sequence
ITR	Inverted Terminal Repeat
LTR	Long Terminal Repeat
MGE	Mobile Genetic Element
MLS(B)	Macrolide-Lincosamide-Streptogramin B
MOI	Multiplicity of Infection

MRSA	Methicillin-Resistant *Staphylococcus aureus*
ONT	Oxford Nanopore Technology
ORF	Open Reading Frame
oriT	Origin of Transfer
PAS	Phage-Antibiotic Synergy
PFU	Plaque-Forming Unit
PICI	Phage-Inducible Chromosomal Island
PVL	Panton-Valentine Leukocidin
QCM-D	Quartz Crystal Microbalance with Dissipation Monitoring
RBP	Receptor-Binding Protein
RM	Restriction-Modification
SaPI	*Staphylococcus aureus* Pathogenicity Island
SCC	Staphylococcal Cassette Chromosome
SeCI	*Staphylococcus epidermidis* Chromosomal Island
SePI	*Staphylococcus epidermidis* Pathogenicity Island
SeRI	*Staphylococcus epidermidis* Resistance Island
SE	Staphylococcal Enterotoxin
SEA	Staphylococcal Enterotoxin A
SSSS	Staphylococcal Scalded Skin Syndrome
SSTI	Skin and Soft Tissue Infection
ST	Sequence Type
T4SS	Type IV Secretion System
TerL	Terminase Large Subunit
TerS	Terminase Small Subunit
TSST-1	Toxic Shock Syndrome Toxin 1
tRNA	Transfer RNA
WTA	Wall Teichoic Acid

1 STRUCTURE OF THE THESIS AND THE AUTHOR'S CONTRIBUTION

This habilitation thesis presents a compilation of selected scientific papers focusing on the impact of mobile genetic elements (MGEs) on staphylococci and their pathogenicity. The first part deals with the role of MGEs as sources of factors that determine virulence and antimicrobial resistance, which bacteria exploit to enhance their fitness. On the other hand, the second part presents how to utilize phages to combat pathogenic bacterial strains, thereby improving or supplementing traditional therapeutic approaches. As this work presents my research results and recently published relevant knowledge, it does not constitute an exhaustive review of the staphylococcal mobilome. Therefore, not all types of MGEs are mentioned, and individual areas are not necessarily covered equally.

My contributions include the characterization of antimicrobial resistance- and virulence-associated plasmids, the role of prophages in bacterial virulence and anti-phage defense, and the investigation of horizontal gene transfer among staphylococcal species. Our findings revealed a new, distinct lineage of large exfoliative toxin B-encoding plasmids, a previously unknown abortive system of prophage origin, and provided new insights into the variability of temperate phages and plasmids of *Staphylococcus aureus*. With my colleagues, including students I supervised, we investigated the mobilization of plasmids and chromosomal islands of *Staphylococcus epidermidis* by temperate bacteriophages. We were the first to compare their genomics and provide evidence of a phage-inducible chromosomal island transfer in this species. Thus, we have substantially contributed to knowledge of interactions between phages and phage-inducible chromosomal islands that shape the dynamics of the staphylococcal mobilome. One of my major contributions is the innovative application of long-read sequencing to characterize complete encapsidated genophores, providing new insight into generalized and lateral transduction and the effects of environmental stress on mobilome transmission.

Furthermore, I focused on the phenotypic and genomic characterization of lytic phages, including their therapeutic potential and safety. We demonstrated that phages of the genus *Kayvirus* are highly suitable for therapeutic use due to their broad host range, safety, and ability to suppress the spread of bacterial MGEs. An important part of my research in the field of phage therapy is the exploitation of synergistic effects when combining phages and antibiotics, as well

as other translational approaches to improve strategies against difficult-to-treat staphylococcal infections. In addition to the enhanced lytic efficacy of phage-antibiotic combinations, we have also described their effects on changes in the susceptibility of staphylococcal strains, the suppression of biofilm growth, and the inhibition of antimicrobial resistance emergence. Through our collaboration with structural virologists, we have uncovered the relationships between genomics and the mechanisms of phage infection. Together, these studies connect fundamental research of bacterial evolution with the development of novel antimicrobial strategies and the assessment of their safety.

The publications listed below comprise 17 selected peer-reviewed original research articles and one review that highlight my contributions to the field. I am the first, co-first, or corresponding author of six of the presented articles, making the core of this thesis. My contribution to each work is detailed in the tables below. The manuscripts are arranged chronologically from the most recent, and the Journal Impact Factor (JIF) and JIF quartile or decile ranking are provided based on data from Web of Science (Journal Citation Reports, Clarivate). Full papers are attached as the Appendix.

[1] Pantůček R, Doškař J, Boštík J, Kocourková D, Petrzik K, Koptíková J, Benešík M, Plevka P, Füzik T, Mašlaňová I, Botka T, Nepeřený J, Zeller D, Kuntová L, Snopková K, Hrala M, Chumchalová J, Holý D, Moša M (2026) Past and present phage therapy research and practice in the Czech Republic – contribution to phage therapy in Europe. *Virology Journal*. https://doi.org/10.1186/s12985-026-03296-x (JCR 2025: IF = 4.0; Q1 – Virology)

Experimental work (%)	Supervision (%)	Manuscript (%)	Research direction (%)
N/A	10	10	10

[2] Bíňovský J, Šiborová M, Zlatohurska M, Nováček J, Bárdy P, Baška R, Škubník K, Botka T, Benešík M, Pantůček R, Tripsianes K, Plevka P (2026) Conformational changes of the baseplate regulating tail contraction of *Staphylococcus* phage 812. *EMBO Journal* 45:5514–5536. https://doi.org/10.1038/s44318-026-00834-9 (JCR 2025: IF = 8.4; Q1 – Biochemistry & Molecular Biology)

Experimental work (%)	Supervision (%)	Manuscript (%)	Research direction (%)
5	-	10	10

[3] Siváková A, Figallová E, Botka T (corresp. author), Vacek L, Tkadlec J, Vrbský J, Osowski M, Petráš P, Polaštík Kleknerová D, Dvořáčková M, Urbanová P, Pantůček R, Růžička F (2026) The combination of mupirocin and *Kayvirus* broadens the decolonization effect against *Staphylococcus aureus*. *Applied Microbiology and Biotechnology* 110:157. https://doi.org/10.1007/s00253-026-13814-0 (JCR 2025: IF = 4.7; Q2 – Biotechnology & Applied Microbiology)

Experimental work (%)	Supervision (%)	Manuscript (%)	Research direction (%)
20	80	60	70

[4] Cieniková Z, Nováček J, Šiborová M, Popelářová B, Füzik T, Botka T, Benešík M, Bárdy P, Pantůček R, Plevka P (2026) Genome anchoring, retention, and release by neck proteins of *Staphylococcus* phage 812. *Communications Biology* 9:199. https://doi.org/10.1038/s42003-025-09477-8 (JCR 2025: IF = 5.8; D1 – Biology)

Experimental work (%)	Supervision (%)	Manuscript (%)	Research direction (%)
10	-	10	15

[5] Botka T, Smetanová S, Vinco A, Kučerová E, Rovňáková K, Siváková A, Mašlaňová I, Pantůček R (2025) Virion content unpacked by long-read sequencing: stress-induced changes in transmitted staphylococcal mobilome due to phage-satellite interactions. *Nucleic Acids Research* 53:gkaf1165. https://doi.org/10.1093/nar/gkaf1165 (JCR 2025: IF = 15; D1 – Biochemistry & Molecular Biology)

Experimental work (%)	Supervision (%)	Manuscript (%)	Research direction (%)
60	90	80	90

[6] Komárková M, Benešík M, Procházková T, Vinco A, Laichmanová M, Smetanová S, Jelínek P, Moša M, Botka T, Šoóš M, Pantůček R (2025) Compatibility of antimicrobial preservatives with therapeutic bacteriophages of the genera *Pbunavirus* and *Kayvirus*. *European Journal of Pharmaceutics and Biopharmaceutics* 214:114781. https://doi.org/10.1016/j.ejpb.2025.114781 (JCR 2025: IF = 5.0; Q1 – Pharmacology & Pharmacy)

Experimental work (%)	Supervision (%)	Manuscript (%)	Research direction (%)
-	20	10	15

[7] Šimečková H, Bárdy P, Kuntová L, Macháčová E, Botka T, Bíňovský J, Houser J, Farka Z, Plevka P, Pantůček R, Mašlaňová I (2025) CRISPR-Cas10-assisted structural modification of staphylococcal *Kayvirus* for imaging and biosensing applications. *ACS Synthetic Biology* 14:2979–2986. https://doi.org/10.1021/acssynbio.5c00387 (JCR 2025: IF = 4.5; Q1 – Biochemical research methods)

Experimental work (%)	Supervision (%)	Manuscript (%)	Research direction (%)
15	-	10	10

[8] Mašlaňová I, Kovařovic V, Botka T, Švec P, Sedláček I, Šedo O, Finstrlová A, Neumann-Schaal M, Kirstein S, Schwendener S, Staňková E, Rovňáková K, Petráš P, Doškař J, Perreten V, Pantůček R (2025) Evidence of *in vitro mecB*-mediated β-lactam antibiotic resistance transfer to *Staphylococcus aureus* from *Macrococcus psychrotolerans* sp. nov., a psychrophilic bacterium from food-producing animals and human clinical specimens. *Applied and Environmental Microbiology* 91:e0165224. https://doi.org/10.1128/aem.01652-24 (JCR 2025: IF = 4.2; Q2 – Biotechnology & Applied Microbiology)

Experimental work (%)	Supervision (%)	Manuscript (%)	Research direction (%)
20	-	15	20

[9] Obořilová R, Kučerová E, Botka T, Vaisocherová-Lísalová H, Skládal P, Farka Z (2025) Piezoelectric biosensor with dissipation monitoring enables the analysis of bacterial lytic agent activity. *Scientific Reports* 15:3419. https://doi.org/10.1038/s41598-024-85064-x (JCR 2025: IF = 4.9; Q1 – Multidisciplinary Sciences)

Experimental work (%)	Supervision (%)	Manuscript (%)	Research direction (%)
5	50	20	50

[10] Vacek L, Polaštík Kleknerová D, Lipový B, Holoubek J, Matysková D, Černá E, Brtníková J, Jeklová E, Kobzová Š, Janda L, Lišková L, Diabelko D, Botka T, Pantůček R, Růžička F, Vojtová L (2024) Phage therapy combined with Gum Karaya injectable hydrogels for treatment of methicillin-resistant *Staphylococcus aureus* deep wound infection in a porcine model. *International Journal of Pharmaceutics* 660:124348. https://doi.org/10.1016/j.ijpharm.2024.124348 (JCR 2024: IF = 5.2; Q1 – Pharmacology & Pharmacy)

Experimental work (%)	Supervision (%)	Manuscript (%)	Research direction (%)
5	10	10	15

[11] Kuntová L, Mašlaňová I, Obořilová R, Šimečková H, Finstrlová A, Bárdy P, Šiborová M, Troianovska L, Botka T, Gintar P, Šedo O, Farka Z, Doškař J, Pantůček R (2023) *Staphylococcus aureus* prophage-encoded protein causes abortive infection and provides population immunity against kayviruses. *mBio* 14:e0249022. https://doi.org/10.1128/mbio.02490-22 (JCR 2023: IF = 5.1; Q1 – Microbiology)

Experimental work (%)	Supervision (%)	Manuscript (%)	Research direction (%)
10	20	10	15

[12] Kovařovic V, Finstrlová A, Sedláček I, Petráš P, Švec P, Mašlaňová I, Neumann-Schaal M, Šedo O, Botka T, Staňková E, Doškař J, Pantůček R (2023) *Staphylococcus brunensis* sp. nov. isolated from human clinical specimens with a staphylococcal cassette chromosome-related genomic island outside of the *rlmH* gene bearing the *ccrDE* recombinase gene complex. *Microbiology Spectrum* 11:e0134223. https://doi.org/10.1128/spectrum.01342-23 (JCR 2023: IF = 3.7; Q2 – Microbiology)

Experimental work (%)	Supervision (%)	Manuscript (%)	Research direction (%)
15	15	10	15

[13] Fišarová L*, Botka T*, Du X*, Mašlaňová I, Bárdy P, Pantůček R, Benešík M, Roudnický P, Winstel V, Larsen J, Rosenstein R, Peschel A, Doškař J (2021) *Staphylococcus epidermidis* phages transduce antimicrobial resistance plasmids and mobilize chromosomal islands. *mSphere* 6:e00223-21. https://doi.org/10.1128/mSphere.00223-21 *co-first authors (JCR 2021: IF = 5.029; Q2 – Microbiology)

Experimental work (%)	Supervision (%)	Manuscript (%)	Research direction (%)
30	30	50	50

[14] Botka T, Pantůček R, Mašlaňová I, Benešík M, Petráš P, Růžičková V, Havlíčková P, Varga M, Žemličková H, Koláčková I, Florianová M, Jakubů V, Karpíšková R, Doškař J (2019) Lytic and genomic properties of spontaneous host-range *Kayvirus* mutants prove their suitability for upgrading phage therapeutics against staphylococci. *Scientific Reports* 9:5475. https://doi.org/10.1038/s41598-019-41868-w (JCR 2019: IF = 3.998; Q1 – Multidisciplinary Sciences)

Experimental work (%)	Supervision (%)	Manuscript (%)	Research direction (%)
70	40	80	70

[15] Fišarová L, Pantůček R, Botka T, Doškař J (2019) Variability of resistance plasmids in coagulase-negative staphylococci and their importance as a reservoir of antimicrobial resistance. *Research in Microbiology* 170:105–111. https://doi.org/10.1016/j.resmic.2018.11.004 (JCR 2019: IF = 3.217; Q2 – Microbiology)

Experimental work (%)	Supervision (%)	Manuscript (%)	Research direction (%)
30	20	40	20

[16] Botka T, Růžičková V, Svobodová K, Pantůček R, Petráš P, Čejková D, Doškař J (2017) Two highly divergent lineages of exfoliative toxin B-encoding plasmids revealed in impetigo strains of *Staphylococcus aureus*. *International Journal of Medical Microbiology* 307:291–296. https://doi.org/10.1016/j.ijmm.2017.05.005 (JCR 2017: IF = 3.298; Q2 – Microbiology)

Experimental work (%)	Supervision (%)	Manuscript (%)	Research direction (%)
90	50	90	80

[17] Botka T, Růžičková V, Konečná H, Pantůček R, Rychlík I, Zdráhal Z, Petráš P, Doškař J (2015) Complete genome analysis of two new bacteriophages isolated from impetigo strains of *Staphylococcus aureus*. *Virus Genes* 51:122–131. https://doi.org/10.1007/s11262-015-1223-8 (JCR 2015: IF = 1.285; Q4 – Genetics & Heredity)

Experimental work (%)	Supervision (%)	Manuscript (%)	Research direction (%)
90	20	90	60

[18] Tkadlec J, Vařeková E, Pantůček R, Doškař J, Růžičková V, Botka T, Fila L, Melter O (2015) Characterization of *Staphylococcus aureus* strains isolated from Czech cystic fibrosis patients: High rate of ribosomal mutation conferring resistance to MLS(B) antibiotics as a result of long-term and low-dose azithromycin treatment. *Microbial Drug Resistance* 21:416–423. https://doi.org/10.1089/mdr.2014.0276 (JCR 2015: IF = 2.529; Q2 – Infectious Diseases)

Experimental work (%)	Supervision (%)	Manuscript (%)	Research direction (%)
20	-	5	-

Please note that, in this work, AI was used to check grammar, list abbreviations used in the text, and refine certain sentences; however, these changes were always thoroughly reviewed.

2 INTRODUCTION

The genus *Staphylococcus* comprises Gram-positive, facultatively anaerobic cocci that colonize the skin and mucous membranes of humans and animals. While many species are commensal, *S. aureus* stands out as a major opportunistic pathogen responsible for a wide range of infections—from superficial skin lesions to life-threatening conditions such as sepsis, endocarditis, and pneumonia. Its pathogenicity is driven by an arsenal of virulence factors, including toxins, enzymes, and adhesion molecules [1]. In addition to *Staphylococcus aureus*, coagulase-negative staphylococci (CoNS), such as *Staphylococcus epidermidis*, *Staphylococcus haemolyticus*, and newly described species like *Staphylococcus ratti* and *Staphylococcus brunensis*, have gained attention for their clinical relevance. These species, often isolated from laboratory animals and human clinical samples, may act as reservoirs of antimicrobial resistance and virulence genes, contributing to zoonotic transmission and nosocomial infections (Appendix 12, 15) [2–4].

Staphylococcal genomes are highly dynamic (**Fig. 1**), shaped by MGEs, including prophages, chromosomal islands, plasmids, transposons, insertion sequences (ISs), and staphylococcal cassette chromosomes (SCCs). These elements facilitate horizontal gene transfer, enabling rapid adaptation to environmental pressure, including acquisition of antibiotic resistance [5]. Pangenomic analyses revealed that the accessory genome of staphylococci is enriched for genes associated with virulence, antimicrobial resistance, and metabolic versatility. These genes are frequently located on MGEs, underscoring their central role in shaping pathogenic potential and ecological fitness.

Fascinated by the crucial role of MGEs in the evolution of staphylococci, I have been studying their role in the emergence of pathogenic strains since my studies. My early work, therefore, focused on plasmids and temperate bacteriophages (briefly phages).

Plasmids play a pivotal role in the dissemination of antimicrobial resistance and virulence traits. In already known as well as newly described staphylococcal species, plasmids have been identified that carry genes conferring resistance to heavy metals and antibiotics (e.g., *blaZ*, *ermC*) and stress-response mechanisms (Appendix 12, 15, 16) [3, 4, 6]. The mosaic structure and mobilization systems of staphylococcal plasmids suggest their frequent horizontal transfer

across species boundaries. Related genera, such as *Macrococcus*, are also reservoirs of plasmids that can modify the pathogenic phenotype of staphylococci (Appendix 8) [7].

Prophages, integrated genomes of temperate phages, are integral components of staphylococcal genomes. Most strains harbor multiple prophages that influence virulence, immune evasion, and resistance to lytic phages. For example, temperate siphoviruses encoding Panton-Valentine leukocidin (PVL) are able to convert a non-toxigenic strain of *S. aureus* into a highly effective toxin producer (Appendix 3) [8, 9]. Some prophages encode proteins involved in anti-phage mechanisms protecting the lysogenized host, including the harbored prophage. They can also trigger abortive infection upon exposure to a lytic phage, which kills the lysogen but protects the rest of the population by arresting lytic phage propagation (Appendix 11) [10].

Temperate phages are the main mediators of horizontal transfer of the staphylococcal mobilome. They can transfer plasmids and large regions of the bacterial genome (Appendix 5, 13) [11, 12]. Currently, the importance of interactions between temperate phages and phage-inducible chromosomal islands (PICIs) is increasingly recognized, as they significantly contribute to mobilome transduction and mitigate the negative impact of phage infection on bacterial populations (Appendix 5) [12–14].

S. aureus is a prominent member of the ESKAPE group (*Enterococcus faecium*, *S. aureus*, *Klebsiella pneumoniae*, *Acinetobacter baumannii*, *Pseudomonas aeruginosa*, *Enterobacter* spp.) of highly virulent, antibiotic-resistant species often found in hospital settings. That is why my work on characterizing and identifying the mechanisms behind the emergence of pathogenic strains has evolved into an interest in how to combat them. The difficult-to-treat infections caused by staphylococci require new therapeutic approaches, including the reintroduction of phage therapy. However, the efficacy of phage therapy is challenged by the presence of specific and non-specific anti-phage mechanisms. This necessitates the use of phages with a broad host range or their combination with other antimicrobial agents. To conduct this research, I secured funding through a junior grant from the Czech Health Research Council, and later received a grant from the Technology Agency of the Czech Republic, under which I collaborated with biotechnology companies to translate our findings into practical applications. We combined phages with antibiotics to produce synergistic effects, reduce antibiotic dosages, and limit the emergence of resistant mutants (Appendix 3, 5, 9) [9, 12, 15]. Nevertheless, ensuring the safety of phage therapy requires knowledge from both of my areas of interest to carefully select a suitable lytic phage and to monitor host-phage genomic

interactions to prevent unintended consequences, such as horizontal gene transfer of virulence or resistance determinants (Appendix 14) [16]. While working on grant-funded projects, we also developed new methodologies for studying phages, mobilome-phage and mobilome-host interactions, with significant contributions from students whose work I supervised or consulted on. This primarily involves monitoring bacterial lysis using piezoelectric biosensors (Appendix 9) [15] and identifying and characterizing transduced genophores at the level of individual virions using long-read sequencing (Appendix 5) [12].

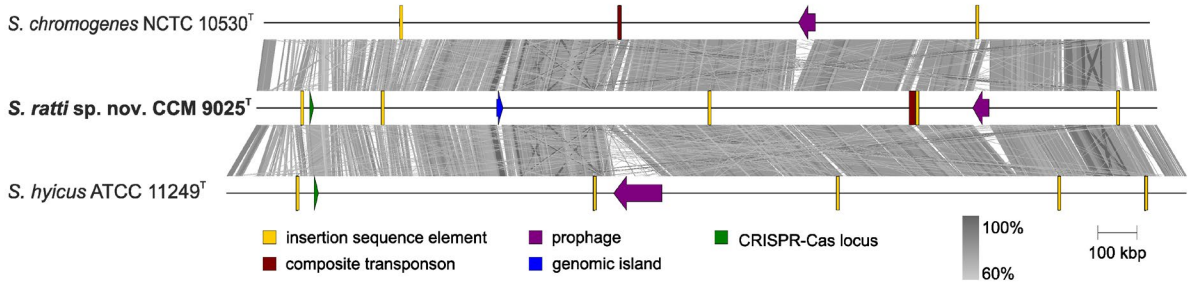

Figure 1: An example of the distribution of the accessory genome comprising MGE in CoNS. While accessory elements represent regions with the lowest homology, the core genome shows high homology across species. The map shows nucleotide sequence identity above 60%. The locations of variable genetic elements are color-coded as shown in the legend. Reproduced from Kovařovic *et al.* (2022) [2].

3 MGE CONTRIBUTING TO STAPHYLOCOCCAL PATHOGENICITY

Staphylococci primarily include pathogenic and opportunistic species that pose a particular threat to immunocompromised individuals in hospital environments [1, 17]. Staphylococcal infections, especially the nosocomial ones, can be significantly complicated by antibiotic resistance. Therefore, the emergence of multidrug-resistant strains of bacterial species of the genus *Staphylococcus* is a serious health problem. According to the World Health Organization, *S. aureus* is one of the six most common bacterial species in Europe that exhibit antibiotic resistance, making it a priority for the development of novel antimicrobial agents [18]. Another staphylococcal species, *S. epidermidis*, typically colonizes the skin as a natural commensal but is also an opportunistic pathogen, and the most common cause of infections by coagulase-negative staphylococci (CoNS) [19]. Like *S. aureus*, it is a significant agent of nosocomial disease worldwide, causing infections in immunocompromised patients, in patients with implants, and through invasive medical devices [20]. CoNS do not typically produce invasive toxins like *S. aureus* [21, 22], but carry genes conferring resistance to all classes of antibiotics and thus serve as reservoirs of antimicrobial resistance factors for pathogens from the genus *Staphylococcus* via horizontal gene transfer (HGT) (Appendix 12) [2, 3, 23]. Similarly, related genera, such as macrococci, may harbor a variety of MGEs, including newly described plasmids, prophages, and genomic islands, which may confer selective advantages to other bacteria and enhance their survival.

MGEs, often associated with antimicrobial resistance and virulence factors, represent up to 25% of the staphylococcal genomes, while core genes linked mostly to central metabolism and the basic functions of the cell make up about 56-75% of the total genome across the evolutionary lineages of staphylococcal strains of a given species [24–26]. Our previous studies focused on MGEs, including temperate phages that can convert a non-toxigenic strain into a producer of exfoliative toxin A by lysogenization (Appendix 17) [27], large plasmids encoding exfoliative toxin B and antimicrobial resistance (Appendix 16) [6], resistance plasmids in CoNS (Appendix 15) [4], novel staphylococcal genomic island (Appendix 12) [3], or prophage-encoded resistance to lytic phages (Appendix 11) [10].

MGEs can be spread via various mechanisms, including transduction, conjugation, and transformation. While transformation is not very efficient in staphylococci, phage-mediated transduction is considered the most important way of MGE spread [28]. We, together with other authors, showed that temperate phages are effective mediators of HGT of plasmids, phage-inducible chromosomal islands (PICIs), and other widespread staphylococcal MGEs (Appendix 13) [11, 29]. PICIs typically carry genes for virulence factors such as superantigens (toxic shock syndrome toxin or enterotoxin genes), resistance factors (the *fusB* gene conferring resistance to fusidic acid), adhesins, anticoagulants, or immunomodulation factors [30, 31]. Together with prophages, PICIs can mediate the lateral transduction of large chromosomal regions through packaging during delayed excision (Appendix 5) [12, 32].

In summary, staphylococci have long been important pathogens due to their variable mobilome, which enables the acquisition of virulence and resistance genes, including through interspecies transfer. This allows rapid emergence of new strains adapted to the environment, especially the hospital environment, further accelerating the emergence of dangerous strains under selection pressure.

3.1 Plasmids

3.1.1 Antimicrobial resistance-encoding plasmids

The genes responsible for antibiotic resistance, including to tetracyclines, amphenicols, macrolides, lincosamides, streptogramins, and aminoglycosides, are found in staphylococcal plasmids (Appendix 15) [4]. Both coagulase-positive and coagulase-negative staphylococci carrying resistance-encoding plasmids have been isolated from hospitals, veterinary facilities, and polluted waters. A global *S. aureus* plasmidome analysis, covering 1395 human and animal isolates from six continents, found plasmids in 66.8% of strains and identified 35 distinct plasmid-borne antimicrobial resistance genes [33]. Although staphylococcal plasmids vary greatly, very similar ones have been detected across multiple staphylococcal species over large geographic areas. Their high similarity in DNA sequences and structure, as we have explored, suggests that horizontal gene transfer may have occurred among strains across different environments (Appendix 12, 15) [2–4].

Many species of coagulase-negative staphylococci are potential pathogens and serve as reservoirs of antimicrobial resistance genes [34]. In our work on plasmid variability, 48 of

62 CoNS strains analyzed carried one or more plasmids harboring various resistance determinants, suggesting an essential role of these MGEs in antimicrobial resistance and its spread (Appendix 15) [4]. Similar antimicrobial resistance patterns were observed in human and veterinary strains, which can be explained by the use of the same antibiotic class in both environments and by the horizontal transfer of resistance-encoding plasmids. Their stable carriage in *S. aureus* was confirmed in electroporation experiments.

An interesting plasmid-IS interplay was described in the IS257 element and pT181-like plasmids in *S. aureus* and CoNS [35, 36]. The IS element plays an important role in the integration of plasmids into the chromosome or into larger plasmids and affects the expression of resistance genes. Such interactions between MGEs may contribute to observed inter- and intra-plasmid rearrangements (Appendix 15) [4].

Most of our understanding of plasmid transfer comes from studies on *S. aureus*, where phage-mediated transduction involving small to medium-sized plasmids is common, often mediated by temperate siphoviruses of the subfamily *Azeredovirinae* [37, 38]. Therefore, our studies on transduction in *S. epidermidis* bring important insight. As shown in **Table 1**, using five *S. epidermidis* phages of the *Rockefellervirus* genus, all the tested phages were capable of transducing plasmids ranging in size from 4 kbp to 19 kbp with high frequencies up to 10^{-4} among *S. epidermidis* strains from different clonal complexes (Appendix 13) [11]. We successfully transduced plasmids encoding resistance to streptomycin, tetracycline, and chloramphenicol.

Larger resistance plasmids can be transferred by conjugation, in which DNA is delivered through a mating pore complex involving a coupling protein and a relaxase, which binds, cleaves, and attaches to *oriT* to form a relaxosome [39]. Moreover, approximately 85% of non-conjugative *S. aureus* plasmids can be mobilized using their own *oriT* and relaxase or the sequence mimicking the *oriT* of a conjugative plasmid carried by the same cell [33, 40]. Also, large resistance plasmids can undergo inter-species transfer, as was demonstrated with the methicillin-resistance-encoding large *Macrococcus psychrotolerans* plasmid (Appendix 8) [7]. This 66.4 kb-long *mecB*-harboring plasmid p19Msa1099_1 was transferred *in vitro* to *S. aureus* strain RN4220 via conjugation. Moreover, a small cryptic plasmid p19Msa1099_8 was mobilized and co-transferred.

Table 1: Transductions of *S. epidermidis* mobile genetic elements.

Donor strain	Mobile genetic element			Transduction system			
	Name	Size (bp)	Resistance gene(s)	Recipient strain	Phage	Selection antibiotic	Frequency
SE27	pSE27_S	4,397	*aad(6)*	SE459	27	Streptomycin	NA[a]
SE27	pSE27_T	4,439	*tetK*	1457	48	Tetracycline	5.0×10^{-4}
SE48	$SeCI_{SE48}$	14,835		1457	48	-	NA[b]
SE459	pSE459_T	18,761	*tetK*	1457	459	Tetracycline	1.6×10^{-7}
1457 (pBTn)	pBTn	11,256	*bla, erm, cat*	A6C	48	Chloramphenicol	5.4×10^{-5}
					456	Chloramphenicol	3.7×10^{-5}
					459	Chloramphenicol	6.9×10^{-5}
					E72	Chloramphenicol	6.1×10^{-5}
1457 (pBTn)	pBTn	11,256	*bla, erm, cat*	1457	48	Chloramphenicol	6.1×10^{-6}
					456	Chloramphenicol	3.9×10^{-7}
					459	Chloramphenicol	2.0×10^{-7}
					E72	Chloramphenicol	9.3×10^{-7}

[a]Not applicable due to the emergence of spontaneous streptomycin-resistant mutants.
[b]Not applicable due to no antibiotic selection.
Adapted from Fišarová *et al.* (2021) [11] (Appendix 13).

In addition to the circular plasmids, we identified a 150-kb megaplasmid with covalently closed linear topology in *M. psychrotolerans* (Appendix 8) [7]. These plasmids have 14.1-kb inverted terminal repeats (ITRs) terminated by a covalent closure site (**Fig. 2**). They encode proteins responsible for mobilization (MobA/MobL) and protein domains found in type IV secretion systems (T4SS), which indicates their ability to transfer via conjugation, and the multidrug efflux pump NorA, which can confer resistance to fluoroquinolones and other structurally unrelated drugs. Whether they can be transferred to staphylococci remains unclear and presents a future experimental challenge.

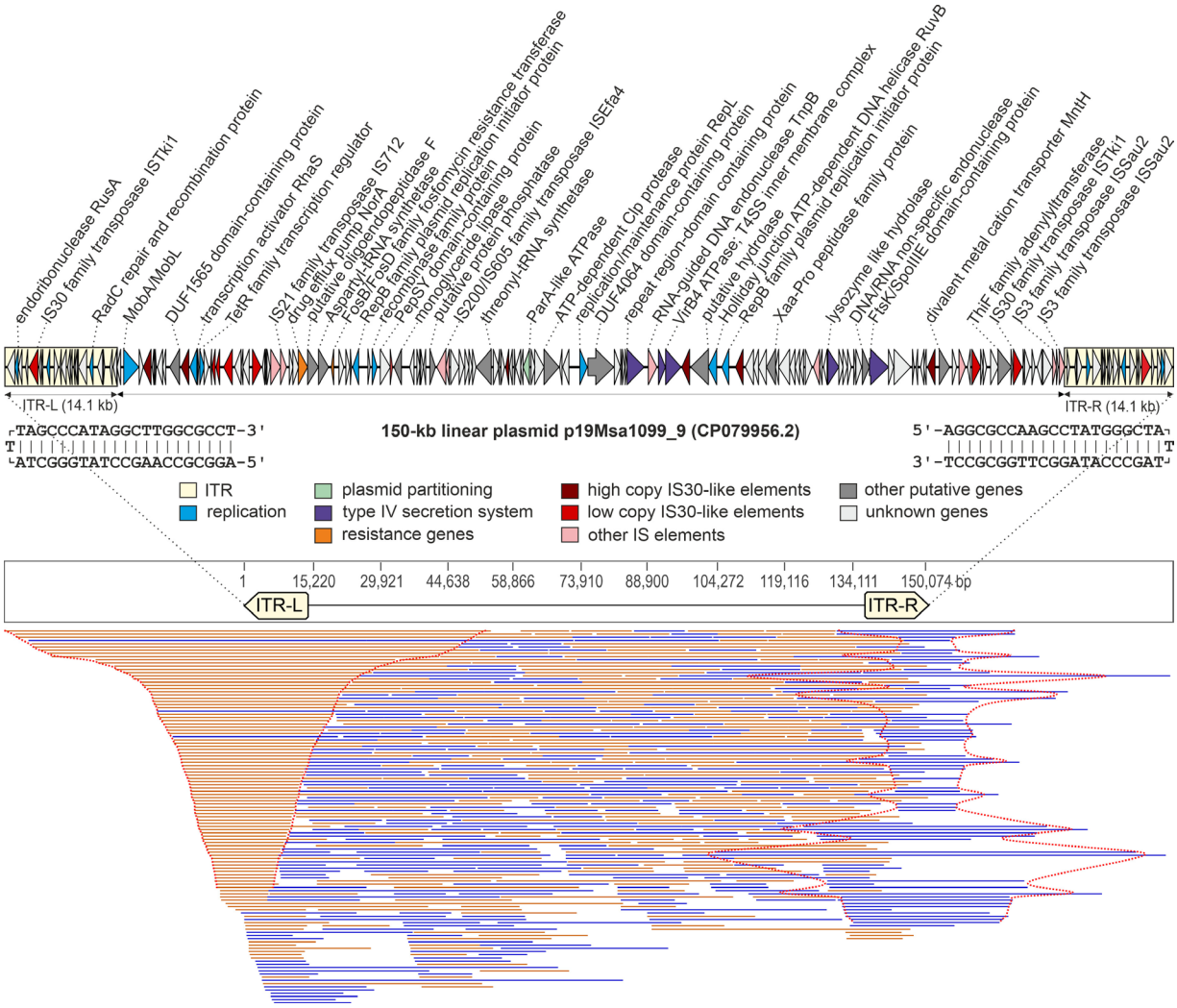

Figure 2: Genetic map of *Macrococcus psychrotolerans* linear plasmid p19Msa1099_9. Arrows show the position and orientation of predicted coding regions. The predicted genes are color-coded according to the legend. The sequences of the physical ends of the hairpin plasmid are shown below the gene map. The mapping of sequencing reads longer than 10 kb to the assembled plasmid sequence revealed a centrally symmetric alignment of reads to the covalently closed ends of the hairpin plasmid. These reads resulted from the unfolding of the terminal hairpin structure during Oxford Nanopore sequencing technology (ONT) as it passed through the nanopore, and therefore, the unmapped parts correspond to the complementary strand (highlighted by a red dotted line). Reproduced from Mašlaňová *et al.* (2025) [7] (Appendix 8).

3.1.2 VIRULENCE FACTOR-ENCODING PLASMIDS

In addition to well-known antimicrobial resistance plasmids, these elements can encode toxins and other factors that increase staphylococcal invasiveness (Appendix 16) [6, 41, 42]. Plasmid-encoded enterotoxins in *S. aureus* cause food poisoning, with the responsible genes, *sed* and *sej*, often located in close proximity on small plasmids [41]. Interestingly, we found plasmid-born enterotoxin genes in a large portion of *S. aureus* strains isolated from cystic

fibrosis patients in the Czech Republic (Appendix 18) [43]. A later study confirmed that the high prevalence of enterotoxin genes in cystic fibrosis *S. aureus* strains is also in the USA [44]. Although the role of enterotoxins in respiratory infections remains unclear, their greater prevalence in airway specimens than in skin isolates suggests that these toxins confer a selective advantage.

Exfoliative toxin B (ETB), an active serine protease produced by some *S. aureus* strains, is closely associated with toxin-mediated epidermolytic skin disorders in humans [45]. ETB is usually encoded by a large 38–41-kb penicillinase-type plasmid [42] and cleaves the cadherin-like transmembrane glycoprotein desmoglein 1 [46], which manifests clinically as blistering skin disease *pemphigus neonatorum* in neonates and *bullous impetigo* and generalized staphylococcal scalded skin syndrome (SSSS) in young children and adults [45]. It was shown that ETB is produced by approximately 21% of *S. aureus* isolates from impetigo cases in the Czech Republic [47]. The early studies on ETB-producing strains described a large *etb* gene-positive plasmid pRW001 [48], and the complete sequences of $pETB_{TY4}$ [42] and $pETB_{TY825}$ [49] have been determined.

To date, our study on ETB plasmids is the most recent and presents a molecular characterization of 13 *etb* gene-positive clinical strains of *S. aureus*, along with a comparative analysis of their ETB plasmids (Appendix 16) [6]. In this study, conservative ($pETB_{TY4}$-based) ETB plasmids resided in strains of clonal complex CC121 and shared a common 33-kb core sequence. All $pETB_{TY4}$-based plasmids also carried genetic determinants for the epidermal cell differentiation inhibitor (EDIN) C, bacteriocin, and cadmium resistance (*cadD* and *cadX*). They differed from each other in the content of two variable DNA regions, so we distinguished four types of $pETB_{TY4}$-based plasmids (**Fig. 3**). For example, the type III plasmids contain an insertion of the beta-lactamase-encoding transposon Tn552 described by Rowland and Dyke [50], and plasmid type IV has an additional large multi-resistance segment including cadmium resistance genes [49] in the locus occupied by the *cad* operon in other $pETB_{TY4}$-based plasmids. Nevertheless, the cadmium resistance genes in type IV and other $pETB_{TY4}$-based plasmids do not share a common origin and differ in structure (Appendix 16) [6]. The existence of only a few variants of $pETB_{TY4}$-based plasmids and their exclusive association with CC121 suggests a very low probability of horizontal transfer. These plasmids have no *tra* or *mob* operon genes. The mobilization via a relaxase-*in trans* mechanism [40] using *oriT* mimic sequences, which were found in all $pETB_{TY4}$-based plasmids, seems improbable, as none of the investigated

S. aureus strains carried an additional conjugative plasmid. The rare bacteriophage-mediated horizontal transfer via transduction remains the most probable way of dissemination of these plasmids among staphylococci (Appendix 16) [6].

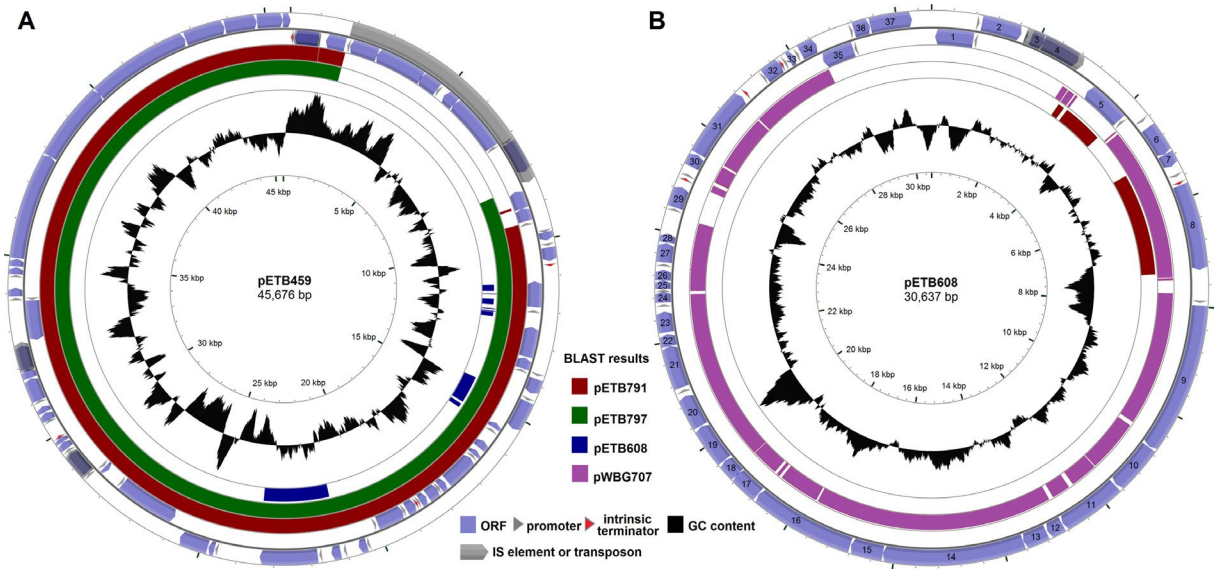

Figure 3: Circular maps of ETB-plasmid nucleotide sequences: (A) pETB459 (type III) and (B) pETB608 (type V). Nucleotide sequence similarities to $pETB_{TY4}$-based plasmids of pETB type I (pETB791), II (pETB797), and to conjugative plasmid pWBG707 are shown with a 70% (A) and 85% (B) identity cut-offs. Reproduced from Botka *et al.* (2017) [6] (Appendix 16).

A distinct plasmid pETB608 (**Fig. 3**), encoding ETB-like toxin and two other serine proteases, together with two EDIN A-like proteins, was described in only one *S. aureus* strain of ST130 and hence seems to be an evolutionarily recent (Appendix 16) [6]. All encoded serine proteases contained conserved regions that harbored the same catalytic triad. While the ETB-like protein showed 84% similarity to ETB, the rest of the serine proteases showed only about 50% similarity to already known proteins. Plasmid pETB608 encodes two EDIN A-like proteins; one showed 93% similarity to the same-sized precursor of EDIN A [51] and could be considered a new variant. The second showed 65% similarity to EDIN A, probably due to genomic rearrangements leading to its truncation (Appendix 16) [6].

The negative effect of EDINs A and C on wound repair and epidermal differentiation has been demonstrated previously [42, 52]. EDIN is a risk factor for deep-seated staphylococcal tissue infections following bacteremia [53]. Therefore, ETB-producing strains are assumed to be more virulent than those producing other types of exfoliative toxins [54]. Hence, the predicted EDIN A-like proteins and trypsin-like serine proteases encoded by pETB608 could be of high clinical relevance (Appendix 16) [6].

The presence of the plasmid conjugation transfer (*tra*)A–M genes is not associated with *S. aureus* lineage [55]. Thus, the *tra* operon in pETB608 implies its ability to self-transmit by conjugation, which is not limited to ST130 strains (Appendix 16) [6]. However, the mechanism of horizontal transfer of this unique virulence-encoding plasmid has not yet been elucidated.

3.2 TEMPERATE PHAGES

During productive phage infection, called the lytic cycle, viable virions containing a genophore comprising one or slightly more than one copy of the phage genome are synthesized using the host apparatus, phage-encoded proteins, and the phage genome template. After cell lysis, a newly released progeny binds to the surface of other bacterial cells and injects its DNA into their cytoplasm. Strictly lytic (or virulent) phages can undergo only productive infection in permissive cells, sometimes with an intermediate stage called the carrier state [56], but never integrate their genome into the host chromosome and transfer it vertically to subsequent generations. Temperate phages can alternatively integrate their genome into the host chromosome at a specific attachment (*attB*) site, forming a so-called prophage that replicates with the host chromosome and is vertically transferred from the initial infected cell to its progeny through cell division. Some stress factors can lead to DNA damage and the emergence of single-stranded DNA bound by polymerizing RecA proteins [57]. In addition to SOS response induction via the autocatalytic cleavage of the LexA repressor, this nucleoprotein complex also leads to the cleavage of the prophage CI-like repressor, thereby activating promoters of the lytic cycle, which enable prophage excision, virion formation, and release from the cell.

All known and described temperate phages infecting staphylococci belong to the class *Caudoviricetes* and have a siphoviral morphology (**Fig. 4**), which means icosahedral heads and long, flexible, non-contractile tails [58]. Their genomes typically span 40–50 kb and are organized into functional modules (groups of genes) for lysogeny, DNA replication, packaging, morphogenesis of head (capsid) and tail, and lysis (**Fig. 5**). The modules of a given function are interchangeable during co-infections or recombination with prophages, leading to genomic mosaicism (Appendix 17) [27].

Temperate bacteriophages are a major driver of genomic plasticity in staphylococci, with a significant impact on their fitness, including virulence. Therefore, we investigated how they can change the host phenotype through lysogenic conversion (Appendix 17) [27]. Many

S. aureus prophages encode important virulence factors, e.g. Panton-Valentine leukocidin, enterotoxin A, exfoliative toxin A, and immune-evasion proteins, and can rapidly shift harmless commensal to pathogen [59].

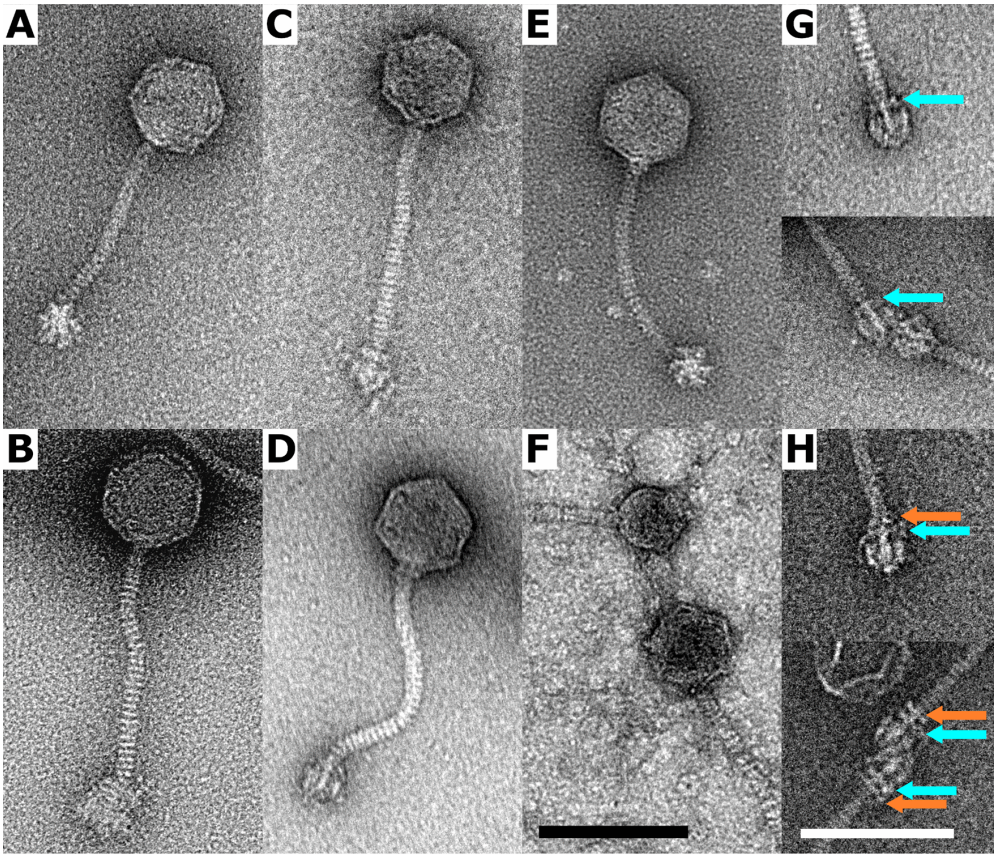

Figure 4: Transmission electron microscope images of negatively stained virions of *S. epidermidis* siphoviruses. (A) Phage 27; (B) phage 459; (C) phage 456; (D) phage E72; (E) phage 48; and (F) phage 48 and phage 48-derived particle with altered capsid architecture due to interaction with PICI-encoded proteins. (G) Detail of the baseplate of phage E72. In a specific baseplate conformation, a ring of density is present at the end of the tail (cyan arrow). (H) Detail of the baseplate of phage 456. An extra ring of density is located above the one present in phage E72 (orange arrow). Bars, 100 nm; black for images A to F (all at the same scale) and white for images G and H. Reproduced from Fišarová *et al.* (2021) [11] (Appendix 13).

Moreover, during the assembly of phage particles, mistakenly recognized bacterial DNA can be packaged into procapsids instead of the phage genome, and thus spread into other bacteria permissive to phage adsorption [60]. The ability to transduce host DNA depends on the phage lifecycle and mechanism of DNA packaging. Only temperate phages have been described as effectively mediating horizontal gene transfer via transduction in staphylococci, employing different mechanisms (Appendix 5, 13, 14, 17) [11, 12, 16, 27, 61].

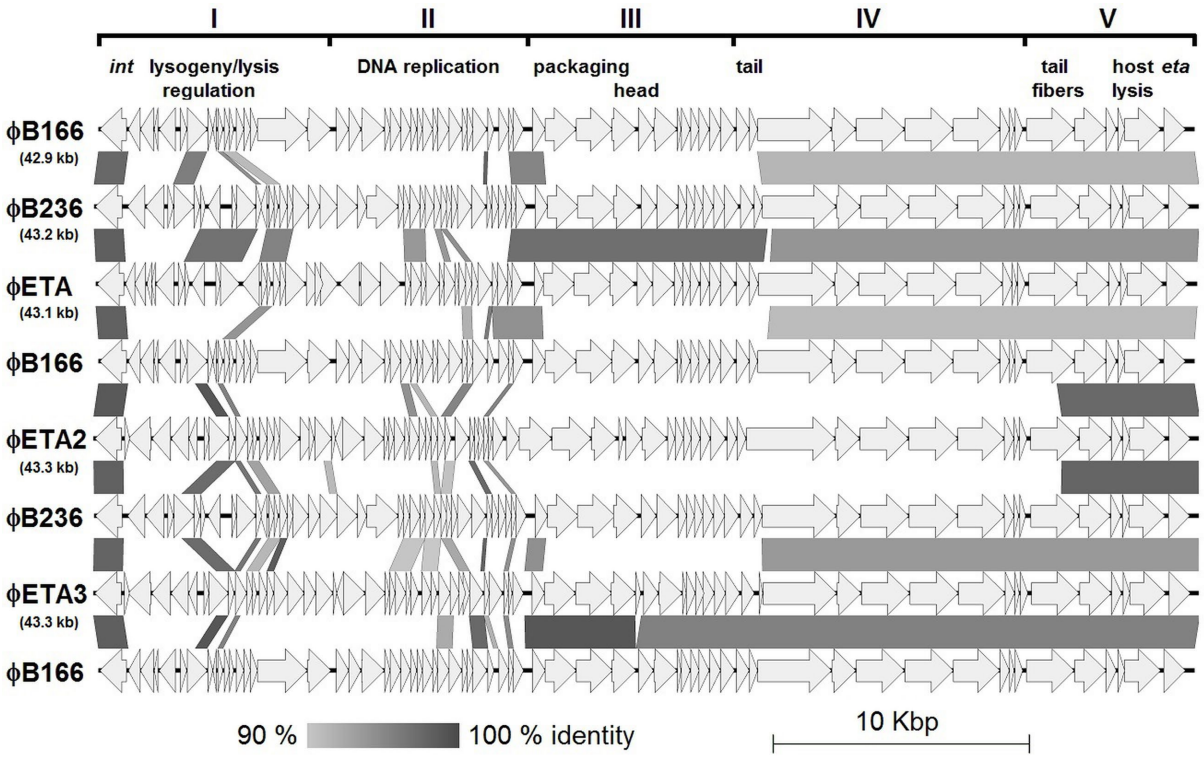

Figure 5: Alignment of the genome maps of phages B166, B236, ETA, ETA2, and ETA3. Regions I–V and modules are depicted on the top line. ORFs are represented by full arrows and intergenic sequences by abscissa. Shaded boxes express the sequence identity levels between genomes. The phage genome sizes are noted in brackets. Reproduced from Botka *et al.* (2015) [27] (Appendix 17).

3.2.1 LYSOGENIC CONVERSION

Lysogenic conversion represents a key evolutionary mechanism through which staphylococci acquire new virulence traits and adapt to diverse environments. This is caused by the integration of a temperate phage genome that carries a gene unrelated to its own life cycle, which changes the phenotype of the lysogenized bacterium. While the presence of a prophage confers immunity to superinfection [62], the extra genetic content may encode defense systems against lytic phages (Appendix 11) [10] or virulence factors (Appendix 17) [27, 61]. Contrary to the gain of new properties through positive lysogenic conversion, negative lysogenic conversion may lead to loss of function when the prophage integrates into the coding region of a gene [63].

Among the most important prophage-encoded factors are secreted toxins, many of which modulate host immunity or cause tissue damage. Staphylococcal exfoliative toxins (ETs), enterotoxins (SEs), and Panton–Valentine leukocidin (PVL) illustrate the impact of phage-borne genes on the clinical significance of *S. aureus* strains.

Prominent examples of lysogenic conversion mediators are some members of the *Phietavirus* genus that harbor the *eta* gene encoding exfoliative toxin A (ETA) (Appendix 17) [27, 47]. ETA-converting phages are of the B1 morphotype (Appendix 17) [27] and can be classified into six ETA-B groups [64]. We demonstrated that phietaviruses B166 and B236 integrate into a defined chromosomal locus and induce ETA production in the recipient strain, proving positive lysogenic conversion (Appendix 17) [27]. Prophage-borne ETA and plasmid-borne ETB have been identified as the major causative agents of the blistering skin diseases associated with *S. aureus* infection [65]. Some ET-producing *S. aureus* strains carry both the ETA prophage and the ETB plasmid. According to our results, ETA prophages in these cases belong exclusively to the ETA-B1 or ETA-B5 groups and contain DNA replication and packaging genes that differ from those of other ETA phages (Appendix 17) [27]. This suggests the presence of undescribed interactions between these MGEs.

Several enterotoxins responsible for staphylococcal food poisoning and implicated in various inflammatory diseases, especially enterotoxin A (SEA), are encoded by siphoviral prophages, which facilitates their rapid horizontal transfer [66]. As superantigens, SEs bypass conventional antigen presentation by cross-linking MHC class II molecules with T-cell receptors, triggering massive, polyclonal T-cell activation [67]. This leads to a cytokine storm characterized by fever, emesis, and systemic inflammation. The phage-encoded nature of many SEs contributes to the episodic emergence of highly toxigenic strains (Appendix 18) [43, 68].

Panton–Valentine leukocidin is a bicomponent pore-forming toxin composed of LukS-PV and LukF-PV subunits, which are encoded by phiSa2-like temperate siphoviruses of *Triavirus* (former *3alikevirus*) and *Biseptimavirus* (former *77likevirus*) genus [69]. PVL targets human neutrophils and forms lytic pores, leading to rapid cell death. Neutrophil destruction releases inflammatory mediators that amplify tissue damage. Clinically, PVL-positive *S. aureus* strains are strongly associated with severe skin and soft-tissue infections (SSTIs), recurrent abscesses, and necrotizing pneumonia (Appendix 3) [9, 70]. PVL production is often associated with the worldwide-disseminated *S. aureus* clonal complex (CC) 8, especially the community-acquired methicillin-resistant (CA-MRSA) USA300 clone, which predominates in North America [71].

We found out that the prophage-carried PVL genes can be replaced by the *pdps*$_{Sau}$ abortive system gene, which targets kayviruses (**Fig. 6**), lytic phages used in phage therapy (Appendix 11, 14) [10, 16]. The mechanism of Pdps$_{Sau}$ action does not alter the adsorption of infecting phages or the phage genome delivery, but it halts phage DNA replication (Appendix 11) [10].

The predicted Pdp_{Sau} protein structure shows a membrane-binding α-helix at its N terminus, which is likely associated with changes in cell membrane polarity and permeability observed after infection, leading to prophage-activated cell death.

Besides this, *S. aureus* prophages provide various other anti-phage systems, like a widespread tail-activated system targeting different incoming phages as well as induced phage progeny [72]. Because it must be turned off during prophage induction, this system allows regulation of lysogeny, phage immunity, and autoimmunity. The next example is the restriction-modification (RM) system *Sau*42I, encoded by the *S. aureus* quadruple-converting phage 42, which also encodes staphylokinase and enterotoxin A, and whose integration results in the loss of beta-hemolysin gene expression [73]. Another example is the phage-encoded invasion factor TarP, which glycosylates wall teichoic acid (WTA) polymers, thereby impairing WTA immunogenicity and host defense, and also converts the podoviral receptor, making podoviruses unable to infect these lysogens [74]. However, *tarP* dissemination is restricted to a few clonal complexes (CC) for unclear reasons; type I restriction-modification (RM) systems may play a role.

Overall, through the continual acquisition, loss, and recombination of prophages, staphylococci maintain a dynamic accessory genome that enables rapid adaptation to host, antimicrobial pressure, and ecological competition. Notably, horizontal transfer of anti-phage mechanisms may significantly impact the efficacy of phage therapy of antibiotic-resistant staphylococcal infections.

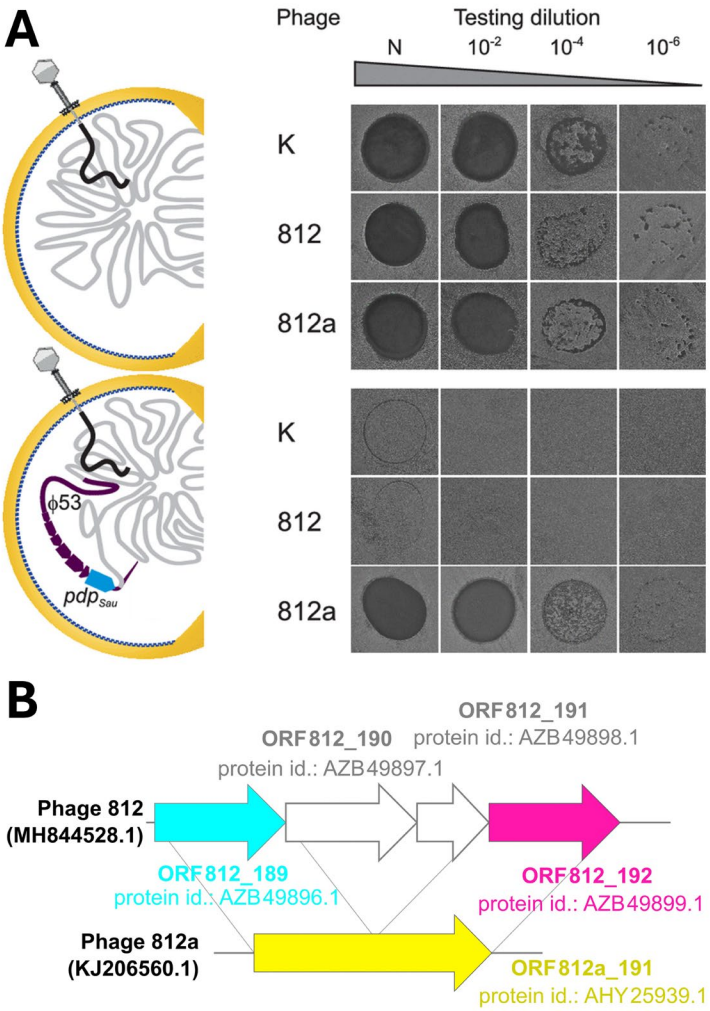

Figure 6: (A) Impact of *pdp*$_{Sau}$ gene expression on *Kayvirus* lytic action demonstrated by drop assay performed with lytic phages K, 812, and 812a on phage-sensitive strain RN4220 compared to Pdp$_{Sau}$-encoding lysogen RN4220 (53+). If single plaques appeared at any dilution, the strain was considered susceptible. (B) Phage 812a can replicate on strains with the *pdp*$_{Sau}$ gene due to a deletion that fused ORF189 and ORF192 of the parental phage 812. Adapted from Kuntová *et al.* (2023) [10] (Appendix 11).

3.3 PHAGE-INDUCIBLE CHROMOSOMAL ISLANDS

Phage-inducible chromosomal islands (PICIs) act as highly mobile phage satellites. In *S. aureus*, they are called pathogenicity islands (SaPIs) because they carry several superantigen genes, especially those for toxic shock syndrome toxin-1 (TSST-1). In *S. epidermidis*, pathogenicity (SePI) and resistance (SeRI) islands are known to carry genes for enterotoxins and fusidic acid resistance [30, 75]. The PICI of our interest contains accessory genes of unknown function, probably the anti-phage system (unpublished), and is simply referred to as chromosomal island (SeCI) (Appendix 13) [11]. In *S. aureus*, PICIs are usually

of simple genomic architecture [76], whereas those of *S. epidermidis* can be similar (Appendix 13) [11], but are mostly composite [77] (**Fig. 7**).

PICIs are integrated into the bacterial chromosome but can be induced by helper phage or by induced prophage to excise, replicate, and package their DNA into phage-like particles, facilitating the horizontal transfer and interfering with phage propagation [78]. The phage-encoded PICI derepressors, such as dUTPase, Sri, and ORF15 in phage 80α, play a key role in PICI mobilization [79]. In *S. epidermidis* phages, we proposed an involvement of capsid proteins in PICI mobilization (Appendix 13) [11].

PICIs mostly act as parasites of helper phages and alter phage propagation in various ways. Proteins PtiA, PtiM, and PtiB, or their homologs, are involved in the inhibition of phage late transcription through the interaction with phage transcriptional regulator RinA [80]. Next, PICI-encoded capsid-remodeling proteins can redirect phage capsid architecture, leading to the formation of small-headed virions (**Fig. 4F**) that are unable to carry the entire phage genome, but can accommodate more than one copy of PICI (Appendix 5) [12]. The bacterial uptake of incomplete phage DNAs that cannot promote phage infection might play a role in prophage evolution through recombination.

We also showed that PICI trimers can be packaged into normal phage particles instead of phage genophores (Appendix 5) [12], which is facilitated by inhibition of the phage terminase small subunit, as described for *S. aureus* SaPIs [81]. The distribution of phage and island genophores in released virions varied depending on the helper phage, its life cycle, the host strain used, and the action of other inducing agents, such as antibiotics (Appendix 5) [12] (**Fig. 8**). Induction agents usually cause DNA damage resulting in an SOS response [82] and an excision of the helper prophage followed by the mobilization of PICI [83].

In addition to their importance as anti-phage systems and sources of virulence factors and antimicrobial resistance, these MGEs play a significant role in the spread of bacterial genes.

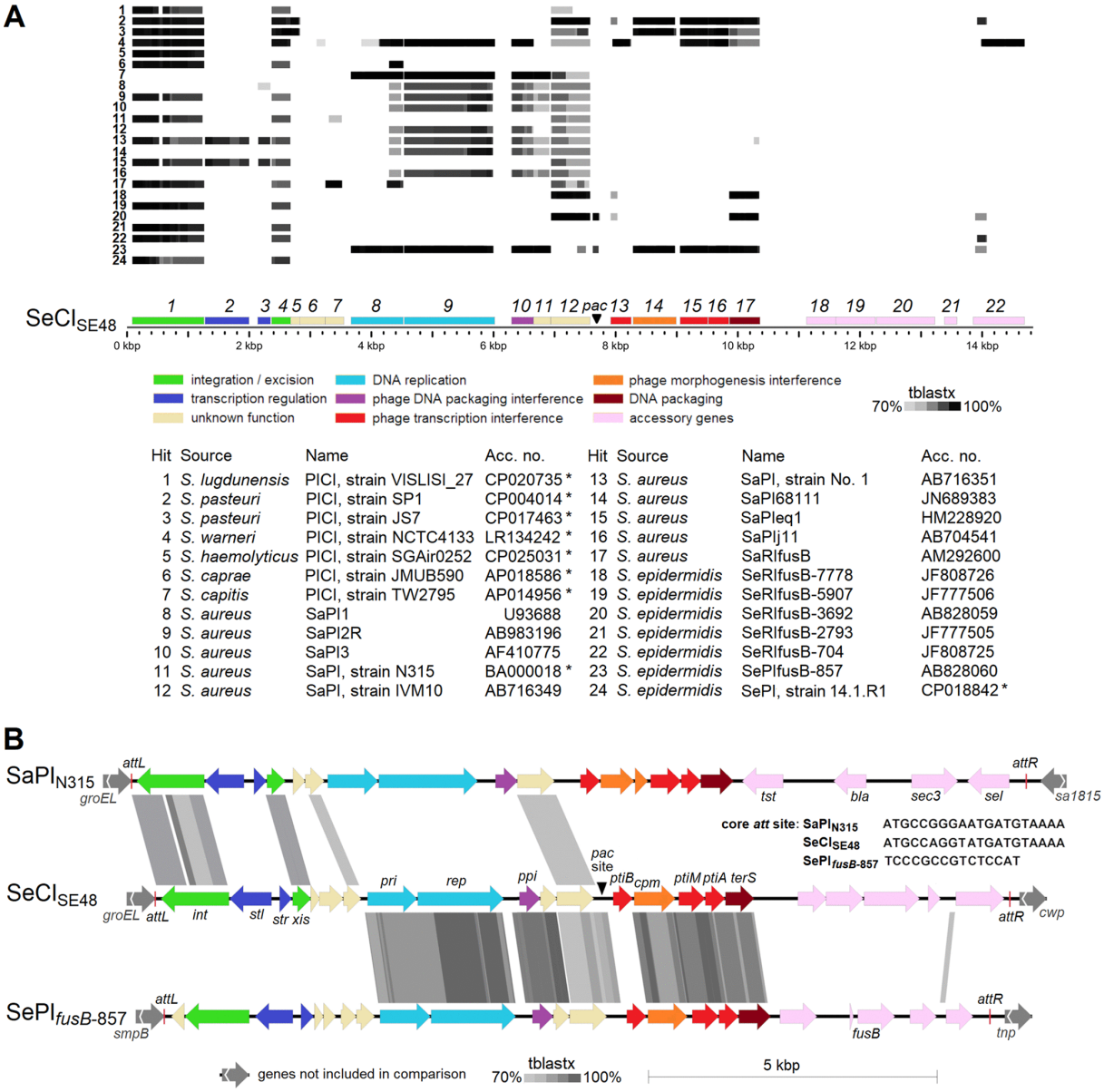

Hit	Source	Name	Acc. no.	Hit	Source	Name	Acc. no.
1	*S. lugdunensis*	PICI, strain VISLISI_27	CP020735 *	13	*S. aureus*	SaPI, strain No. 1	AB716351
2	*S. pasteuri*	PICI, strain SP1	CP004014 *	14	*S. aureus*	SaPI68111	JN689383
3	*S. pasteuri*	PICI, strain JS7	CP017463 *	15	*S. aureus*	SaPIeq1	HM228920
4	*S. warneri*	PICI, strain NCTC4133	LR134242 *	16	*S. aureus*	SaPIj11	AB704541
5	*S. haemolyticus*	PICI, strain SGAir0252	CP025031 *	17	*S. aureus*	SaRIfusB	AM292600
6	*S. caprae*	PICI, strain JMUB590	AP018586 *	18	*S. epidermidis*	SeRIfusB-7778	JF808726
7	*S. capitis*	PICI, strain TW2795	AP014956 *	19	*S. epidermidis*	SeRIfusB-5907	JF777506
8	*S. aureus*	SaPI1	U93688	20	*S. epidermidis*	SeRIfusB-3692	AB828059
9	*S. aureus*	SaPI2R	AB983196	21	*S. epidermidis*	SeRIfusB-2793	JF777505
10	*S. aureus*	SaPI3	AF410775	22	*S. epidermidis*	SeRIfusB-704	JF808725
11	*S. aureus*	SaPI, strain N315	BA000018 *	23	*S. epidermidis*	SePIfusB-857	AB828060
12	*S. aureus*	SaPI, strain IVM10	AB716349	24	*S. epidermidis*	SePI, strain 14.1.R1	CP018842 *

Figure 7: Comparison of staphylococcal phage-inducible chromosomal islands. (A) *S. epidermidis* SeCI$_{SE48}$ compared to islands identified in staphylococcal genomes available in GenBank. SeCI$_{SE48}$ genes are color-coded according to their product function, and the corresponding gene product number is given above them. Chromosomal islands obtained from complete genomes of staphylococcal strains as 20-kb sequences starting with the integrase gene are indicated with asterisks. (B) Detailed comparison of SeCI$_{SE48}$ with SePI$_{fusB-857}$ and SaPI$_{N315}$. Genes are color-coded according to their product function. Identity based on tblastx comparison is represented by shaded boxes with a 70% cutoff. Reproduced from Fišarová *et al.* (2021) [11] (Appendix 13).

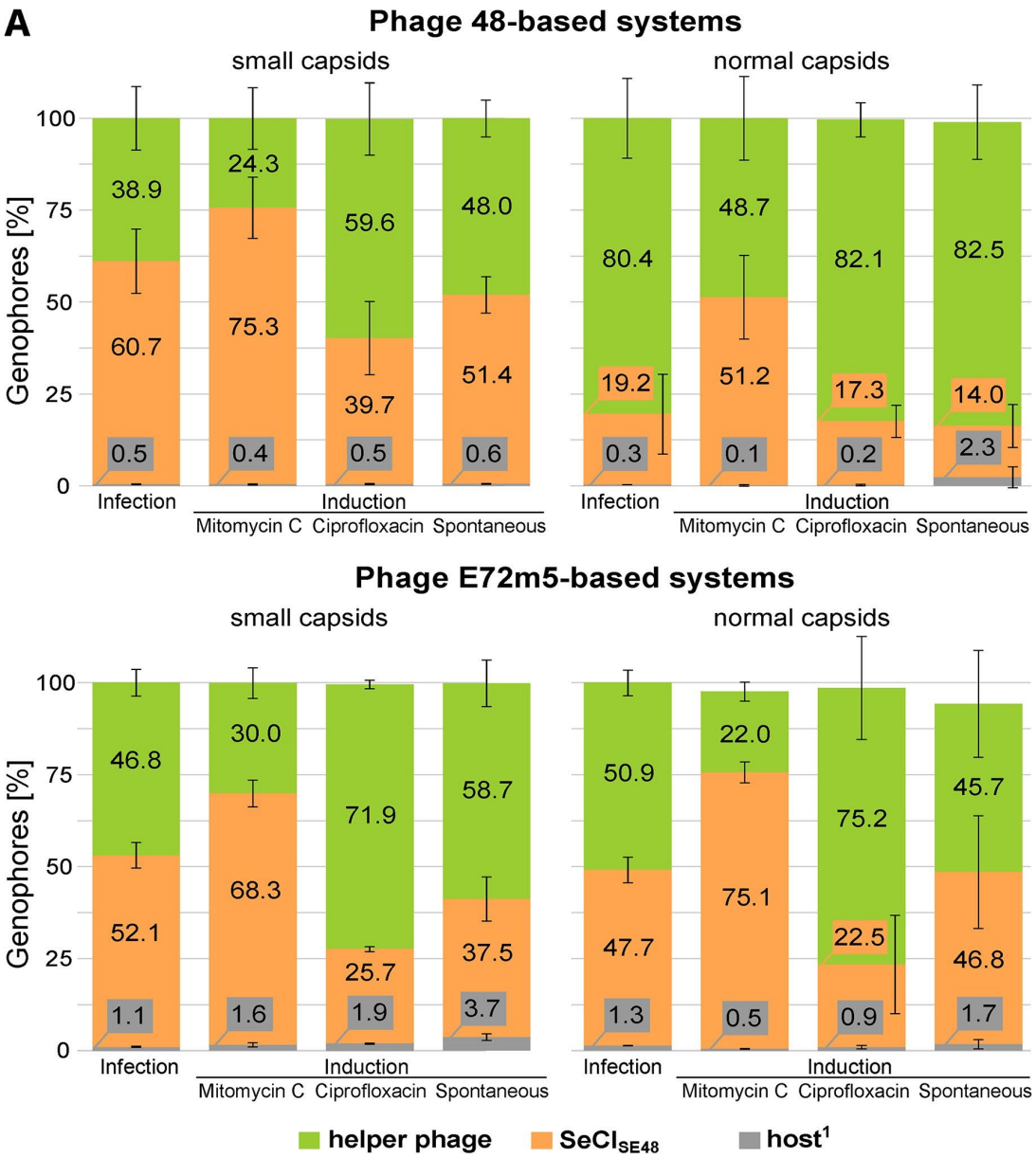

Figure 8: Relative abundance of full-length genophores with different origins in released normal and small-headed particles after helper phage 48 and E72m5 infection and induction. The results are presented as means of three biological replicates with standard deviations shown as whiskers. In phage 48-based systems, there was a statistically significant difference in the abundance of phage-inducible chromosomal island $SeCI_{SE48}$ and phage genophores from small particles upon mitomycin C induction, and in genophores from normal particles except for mitomycin C induction. In phage E72m5-based systems, this difference was observed in genophores from small particles except for infection, and from normal particles after mitomycin C and ciprofloxacin induction. [1]Genophores mapped to chromosomal or plasmid reference. Adapted from Botka *et al.* (2025) [12] (Appendix 5).

3.4 TRANSDUCTION

Transduction is the most important way of horizontal gene transfer in staphylococci [84]. Currently, three types of transduction, i.e., the transfer of non-phage DNA by phage particles, can be distinguished: specialized, generalized, and lateral. The ability to promote transduction is tightly associated with the DNA packaging mechanism of phages, most often *pac*- or *cos*-type. In *cos*-phages, the terminase complex recognizes the *cos* site for the initial and final cuts, making cohesive ends and packaging genophores with a precise one-unit genome length [85]. As a consequence, the transducing ability of these phages is restricted to cases of aberrant prophage excision, when the *cos*-site is preserved and enables the packaging of the phage genome with the adjacent segment of bacterial DNA. In rare cases, pseudo-*cos* sites can be distinguished by phage terminase in bacterial or plasmid DNA. However, these two pseudo-*cos* sites must occur within a distance equal to up to the capsid capacity to be successfully packaged [86].

Pac-type packaging of phage genophores is based on an initial imprecise cut of the phage DNA concatemer at the *pac* site by the terminase complex, followed by DNA packaging until the head capacity is full (Appendix 5) [12, 86] (**Fig. 9A**). Subsequently, the DNA is cut a second time in a *pac*-site-independent manner, and the resulting end serves as the initiation site for packaging into a new empty prohead. As a result, the phage genophore inside the capsid is terminally redundant and circularly permuted. The redundancy of phage genophores ranges from 2% to 10% of the genome length [87], a range we also confirmed for staphylococcal *pac*-phages (Appendix 5) [12]. We have shown that in case the PICI is packaged, the redundancy in small-headed particles is greater, 7%–16% of the genome length, which probably enables the packaging of various PICIs using the same capsid morphogenesis mechanism. Interestingly, the DNA-terminase complex can package genophores from the same concatemer intermittently into both types of procapsids (**Fig. 9B**).

Known strictly lytic staphylococcal phages are incapable of efficient transduction because they destroy the host genome and use it to synthesize copies of their own genome (Appendix 14) [16, 88]. In general, no naturally occurring strictly lytic phage capable of efficiently transducing chromosomal bacterial DNA has been described to date. Only a few lactococcal phages have been shown to transduce plasmids under certain conditions; transduction has also been reported using mutants of the *E. coli* T4 phage [89, 90].

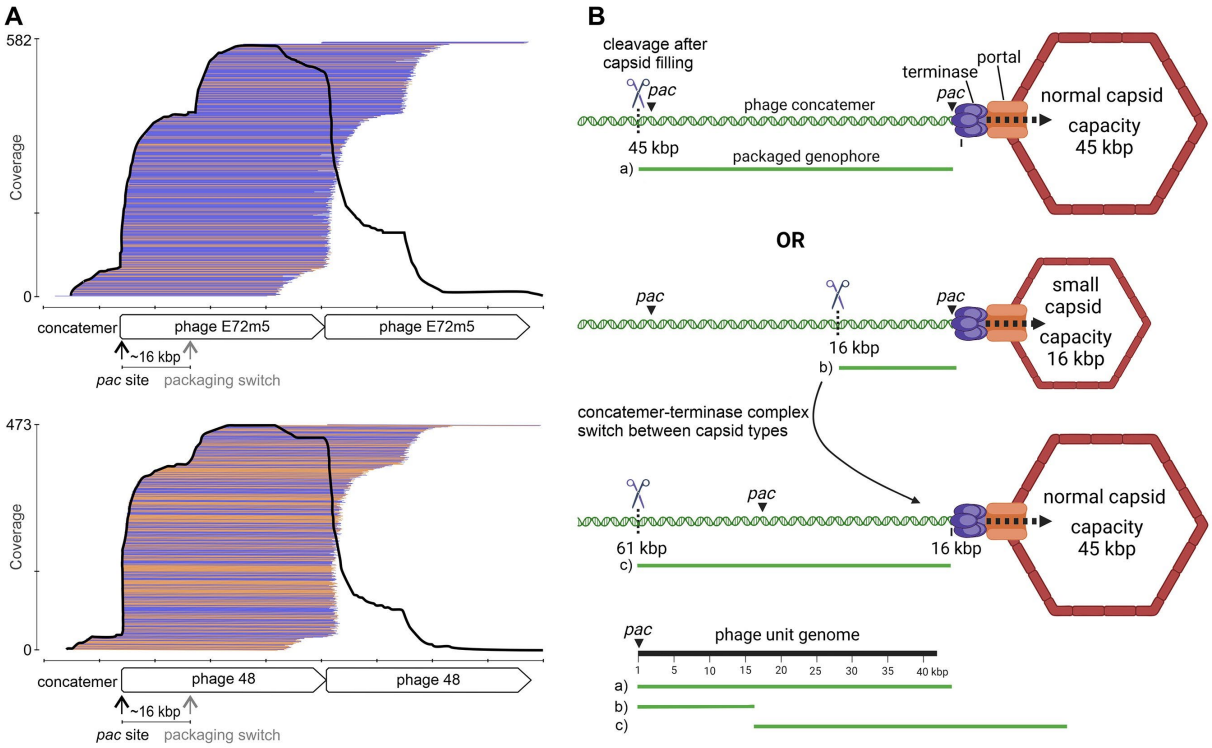

Figure 9: Mapping of phage genophore sequences to the phage concatemer (A), and mechanism of the concatemer–terminase complex switching between the two types of capsids (B). The obvious bounce in coverage (A) indicates a switch during the packaging of the concatemer, as depicted in part B. Packaging of phage DNA concatemers starts imprecisely from the *pac* site (A and Ba). This results in genophores of ~45 kbp in length with the same or similar start, which manifests in increased coverage at the *pac* site (A). However, the concatemers may first be packaged into small capsids, resulting in 16-kbp genophores with a start at the *pac* site (Bb). Subsequently, genophores packaged into normal particles have a similar start at around 16 kbp from the *pac* site (Bc), as reflected by a typical change in phage genome coverage (A; schematically in part B, below). Analogously, the same mechanism applies to the SeCI concatemers. The color of the mapped genophores indicates their orientation to the reference (blue for forward; orange for reverse). Reproduced from Botka *et al.* (2025) [12] (Appendix 5).

Studies, including ours, usually assess transduction by quantifying the frequency of successfully transduced elements carrying selection markers, particularly antibiotic resistance genes, using phage titers measured by plaque-forming units (Appendix 13) [11, 29, 60]. However, such an approach does not account for particles carrying non-phage DNA and is inherently limited, as it overlooks the broad spectrum of transducible MGEs and focuses only on the transduction outcome. Therefore, it biases estimates of transduction dynamics and fails to provide a comprehensive knowledge of the true extent of horizontal gene transfer. Our novel long-read sequencing-based approach has been developed to characterize full-length encapsidated genophores, thereby enabling us to assess transduction dynamics and quantify virion content without bias from antibiotic selection (Appendix 5) [12]. A similar approach was used in recent work on the mobilization of bacterial genomic DNA in the gut microbiome [91].

3.4.1 GENERALIZED TRANSDUCTION

In staphylococci, the specialized transduction via aberrant prophage excision is poorly described [29], while the generalized and lateral transduction promoted by *pac*-phages and *pac*-PICIs appear to be the main HGT mechanisms (Appendix 5, 13) [11, 12]. As the phage terminase small subunit (TerS) and the PICI TerS recognize different *pac* sequences, PICIs expand the transduction repertoire of phages. The generalized transduction occurs when the phage or PICI TerS recognizes the pseudo-*pac* site. As only the initial recognition and cut (via phage large terminase subunit TerL) are required, relatively large segments of the bacterial chromosome or several plasmid copies can be gradually packaged (Appendix 5) [12, 92]. Despite earlier hypotheses, pseudo-*pac* sites are not simple sequence homologs of phage and PICI *pac* sites. They have some consensus region, but rather with a specific sequence structure than with sequence identity [93]. Generalized transduction is a packaging error in which the terminase complex packages bacterial DNA instead of the phage DNA. Therefore, its efficacy is relatively low, which is reflected in the frequency of transduction typically of 10^{-7}, and up to 10^{-4} in staphylococcal phages with the highest transducing potential (Appendix 13) [11].

Generalized transduction is most often assessed via resistance plasmid transfer. We have shown that staphylococcal temperate phages transduce plasmids conferring resistance to streptomycin, tetracycline, or chloramphenicol across staphylococcal strains of the same or different species (Appendix 13) [11, 61]. We also demonstrated that DNA-damaging agents, such as ciprofloxacin, increase the abundance of plasmid sequences in released virions (Appendix 5) [12]. The possible cause is the linearization of plasmids due to DNA damage, which facilitates the packaging. Plasmids can be packaged into virions in the form of capsid-fulfilling multimers, or as monomers and plasmid fragments that are too small to allow correct virion assembly (Appendix 5) [12, 94]. Therefore, a mechanism similar to that observed in phage T4 is proposed, in which additional DNA is transferred into already filled capsids regardless of the presence of concatemers [94, 95]. Plasmids or chromosomal fragments might be co-transduced together with phage or PICI genomes, or their copies might fill the capsids on their own [96, 97].

3.4.2 LATERAL TRANSDUCTION

Lateral transduction is the most effective way of horizontal gene transfer in staphylococci [98]. It enables the transfer of chromosomal DNA at a frequency more than 1000 times higher than that observed in generalized or specialized transduction [99]. It occurs when a terminase complex starts phage or PICI DNA packaging while the prophage or PICI is still integrated in the host chromosome. As a result of a *pac*-type packaging, multiple virions contain chromosomal DNA downstream of the *pac* site (**Fig. 10**). The lateral transduction was discovered in staphylococci through comparison of horizontal transfer rates and short-read sequencing of virion content [98, 99] and was confirmed in our work by whole-genophore sequencing using long reads (Appendix 5) [12]. Moreover, it was proposed that in PICI, concatemeric islands can form within the host chromosome when packaging is initiated at the *pac* site prior to excision [32]. We confirmed this by observing multi-copy PICI genophores, including adjacent host sequences, in normal-sized capsids (Appendix 5) [12] (**Fig. 10**).

The frequency of bacterial DNA packaging decreases with distance from the phage or PICI *pac* site (Appendix 5) [12, 32] (**Fig. 10A)**. According to studies on *pac*-phage P22, a series of 2–12 packaging events occurs after initial cleavage, and the DNA packaging series length increases with time after infection [100, 101]. It is not known whether multiple series can be initiated on a single concatemer molecule.

It was shown that phage- or PICI-mediated lateral transduction can be exploited by defense islands to spread [102]. Defense islands, clusters of antiphage system genes (e.g. RM systems or CRISPR-Cas), are often localized near prophage or PICI. Therefore, they can be mobilized at higher frequencies than more distant regions. This way, naïve strains can be converted even if the systems are not encoded directly by the phage or PICI. Interestingly, although it reduces its burst size, the spread of antiphage systems may also benefit the phage that mediates lateral transduction, because these systems target competing phages rather than the mediating phage itself.

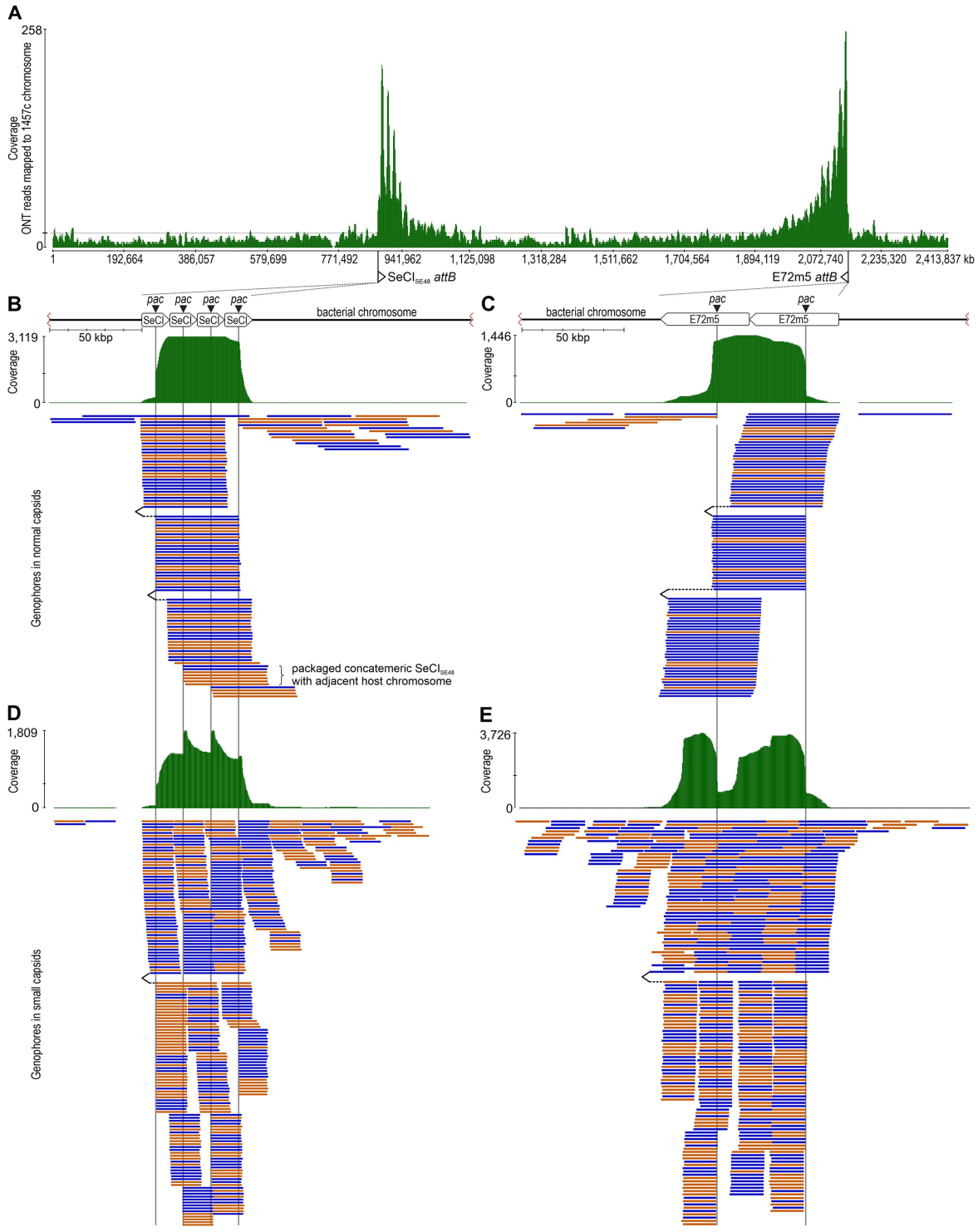

Figure 10: Mapping of sequencing reads to the host, phage E72m5, and PICI (SeCI$_{SE48}$) genomes. Reads were mapped to the MGE-less host genome to improve visualization of highly covered MGE regions (A). Coverage decreased with distance from the integration site (*attB*) in the packaging direction, reflecting lateral transduction of host DNA. To show the structure of packaged genophores, reads were mapped to multimeric PICI (B, D) or phage (C, E) genomes. Coverage patterns were consistent with cyclic genome permutation and imprecise packaging initiation at *pac* sites. Genophores containing both the MGE (or multiple copies of the MGE) and host sequence were detected (B–E), indicating that concatemer formation can occur before MGE excision. Genophore orientation relative to the reference genome is shown in blue (forward) and orange (reverse). Reproduced from Botka *et al.* (2025) [12] (Appendix 5).

4 PHAGE-BASED APPROACHES TO FIGHT STAPHYLOCOCCAL INFECTIONS

A deeper insight into the phage biology is essential not only for understanding bacterial evolution, but also for designing safe therapeutic applications of bacteriophages. Therefore, the following chapter focuses on the exploitation of lytic phages as antimicrobial agents.

Phages were discovered in the early 20th century, and phage therapy subsequently became widely used to treat bacterial infections (Appendix 1) [103]. However, with the discovery and introduction of antibiotics into clinical practice during World War II, it was quickly replaced by more broadly applicable antibiotic therapy, which was better suited to acute conditions. The spread of antibiotic resistance and the emergence of difficult-to-treat multidrug-resistant strains, combined with stagnation in antibiotic research, have driven demand for new treatment approaches. This has brought phage therapy back into the spotlight, a field that had persisted mainly in post-communist countries in Europe and Asia.

Phage therapy is based on lytic bacteriophages, exploiting their life cycle, during which phages use the bacterial metabolic machinery for replication [104]. Following phage multiplication, the host bacterium is lysed, and newly formed viral particles are released, infecting the next bacterial cells. This process continues until the bacterial population is substantially reduced or eradicated. The suppression of bacterial infection is not solely the result of phage-mediated lysis but also involves the host immune response, which is stimulated by bacterial lysis products and by phages themselves. For example, phage particles can opsonize bacteria, making them more recognizable to the immune system [105].

Phage therapy offers several important advantages over conventional antibiotic treatment. The main advantage (which, paradoxically, led to antibiotics prevailing over phages in the first half of the 20th century) is its high specificity toward the target pathogen, which minimizes disruption of the commensal and symbiotic microbiota that contribute to human immune homeostasis [106]. Another important advantage is the ability of some phages to degrade bacterial biofilms, which represent a significant barrier to antibiotic penetration and are a common cause of antimicrobial resistance in bacteria colonizing medical devices and hospital surfaces [107].

To ensure the safety of the therapy, only lytic phages that are incapable of the lysogenic cycle and of efficient transduction are used. In human medicine, phage therapy is routinely used at specialized clinics in Georgia and Russia (Appendix 1) [103]. In the European Union, phages are most often used under compassionate programs; however, phage therapy is easily accessible especially in Poland (Hirszfeld Institute of Immunology and Experimental Therapy) and Belgium (BT Consortium). The phage-based preparation Stafal®, registered for the topical treatment of staphylococcal infections since the late 1980s, has been produced in Czechoslovakia and later in the Czech Republic, but is currently discontinued despite its proven effectiveness and lower treatment costs compared to antibiotics (Appendix 1, 14) [16, 103, 108]. Several phage therapy trials and studies have been carried out in the United Kingdom, Belgium, France, Germany, and the USA. In the Czech Republic, DUOFAG® by MB PHARMA, a bacteriophage cocktail for topical administration targeting *S. aureus* and *P. aeruginosa*, is currently undergoing clinical trials (EUCT ID: 2024-518307-22-01).

Despite these advantages, phage therapy also has limitations, particularly regarding the universality of its application. In our research, we focus on overcoming these limitations. Phage-resistant bacterial strains occur naturally, and resistant mutants may emerge through ongoing coevolution between bacteria and phages. Nevertheless, this evolutionary process also leads to the emergence of phage mutants capable of overcoming bacterial resistance. These mutants can be rapidly isolated and propagated to generate therapeutic preparations effective against newly resistant bacterial strains (Appendix 14) [16, 109]. This represents a major advantage of phage therapy, allowing therapeutic preparations to be updated quickly and at substantially lower cost than developing new antibiotics.

However, since the discovery of bacteriophages, new insights have been gained regarding the types of phage life cycles or their ability to transfer genes encoding virulence or antimicrobial resistance factors. Current safety requirements, therefore, call for a much more detailed characterization of phages and a more precise preparation of phage products compared to the past. For this reason, the introduction of phage therapy into current clinical practice has been time-consuming, and only recently have quality criteria for phage therapy medicinal products been established in the EU (Appendix 1) [103, 110].

As an alternative to whole phages, their derivatives, such as endolysins, can be used; these are known as enzybiotics. Such lytic enzymes can be modified using genetic engineering techniques and produced via heterologous expression, which offers several advantages,

including eliminating the need for toxinogenic production strains [111]. Enzybiotics are being introduced into clinical practice; however, effective drug-delivery methods need to be explored [112, 113]. Currently, gel-based cosmetics, such as FAGOCARE PLUS® by FAGOFARMA, that combine phages and phage enzymes are available on the Czech market (Appendix 1) [103]. When using phage derivatives, we can also benefit from the arsenal of temperate phages, which significantly expands our options. This applies not only to individual lytic enzymes but also to so-called tailocins.

Tailocins are products of prophage remnants that no longer carry genetic information for the capsid, replication, or other regulatory functions, and thus form a tail-like structure capable of binding to and disrupting the cell wall of a permissive bacterium [114, 115]. Many bacterial species, particularly Gram-negative ones, actively utilize these phage remnants in competition within polymicrobial communities. Tailocins represent a promising therapeutic approach because their specificity can be modified, and since they do not transfer genetic material, there is no risk of complications associated with the transfer of unwanted virulence or resistance genes.

4.1 *KAYVIRUS* PHAGES

For the treatment of staphylococcal infections, well-characterized, strictly lytic phages belonging to the genus *Kayvirus* with myoviral morphology and broad host ranges (**Fig. 11**) are considered particularly promising (Appendix 14) [16, 116–118], as are *Rosenblumvirus* P68 and related podoviruses (Appendix 9) [15, 119, 120]. As we focus on characterizing the lytic abilities, genome (**Fig. 12**), and virion structure (**Fig. 13**) of *Kayvirus* 812 and its spontaneous mutants (Appendix 2, 4, 14) [16, 121, 122], the following chapter is devoted to this genus.

Kayviruses (named after type phage K or *Kayvirus kay*) are often used in antistaphylococcal preparations, such as Stafal® of DUOFAG®, and phage therapy-related studies due to their broad host range (Appendix 1, 3, 14) [9, 16, 103, 108, 118, 123]. Because their spontaneous mutants emerge relatively frequently, they are well-suited for isolating phage strains capable of overcoming bacterial resistance to the parental phage. In our previous paper, five spontaneous phage mutants were isolated as rare plaques on phage-resistant *S. aureus* strains, showing a 42% broader host range than the wild type, determined on a set of 186 MRSA strains representing globally circulating human and livestock-associated clones (Appendix 14) [16]

(**Fig. 11**). We have demonstrated that some kayviruses can kill *S. epidermidis* strains (Appendix 5) [12], an opportunistic pathogen of growing significance (Appendix 13) [11].

Kayviral genomes are linear, double-stranded DNA molecules composed of unique and repetitive terminal regions (**Fig. 12**). The unit genomes (the non-redundant part of the genome comprising a unique region and a single long terminal repeat) are about 140 kb in size and contain more than 200 genes [124]. Genomes lack a clear modular architecture, unlike that of staphylococcal siphoviruses. Early-expressed host-takeover genes are carried by identical long terminal repeats (LTRs) of approx. 8 kbp. The majority of *Kayvirus* genomes encode tRNAs and contain group I introns, often encoding a homing endonuclease, which are located in genes involved in DNA metabolism, morphogenesis, and lysis (Appendix 14) [16, 109, 125]. The function of introns is not fully understood, but they may play a role in competition between co-infecting phages [126]. Next, identified non-coding RNAs likely contribute to the regulation of gene expression [127].

During phage propagation, random mutations occur (**Fig. 12**), and some may affect phage infectivity (**Fig. 11**). Phages carrying beneficial mutations can be isolated on bacteria resistant to the parental phage. Such selection leads to observation of genomic changes in genes related to host range or phage fitness (Appendix 14) [16]. In kayviruses, we observed changes like endolysin gene truncation or point mutations in receptor-binding protein-encoding genes.

Two different receptor-binding proteins (RBPs) determine the host range of *Kayvirus* phages. One of the RBPs is necessary for binding onto the backbone of wall teichoic acids (WTA), while the second one binds to N-acetyl-α-D-glucosamine (α-GlcNAc) [128]. We have shown that in kayviruses, the homologs of the α-GlcNAc-binding RBP exhibit higher variability, suggesting that the corresponding gene is a mutation hotspot important for host specificity (Appendix 14) [16]. Other significant mutations that overcome anti-phage mechanisms include a truncation of the endolysin gene [109] and a deletion that fuses *orf189* (encoding a regulatory protein) and *orf192* (encoding a putative membrane protein) in phage 812 (Appendix 14) [16]. According to our results, phage 812-derived mutants carrying the fusion gene can successfully eradicate hosts expressing the $Pdps_{au}$ abortive infection prophage-encoded system (**Fig. 6**), which effectively inhibits infection by parental phage 812 or phage K (Appendix 11) [10].

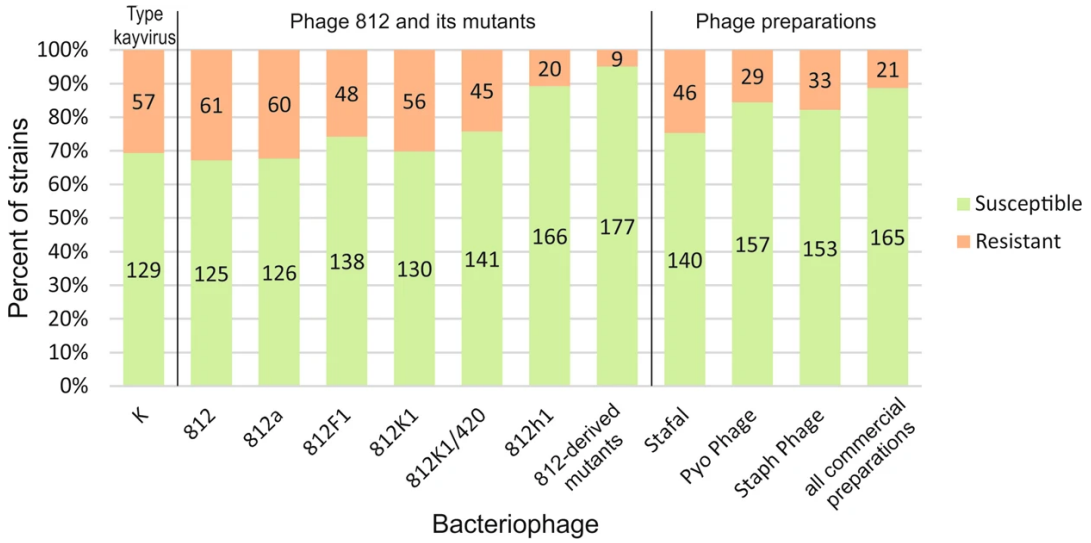

Figure 11: Lytic activity of phages K, 812 and its mutants, and kayviruses from commercial preparations Stafal (Bohemia Pharmaceuticals, Czech Republic), PyoPhage (Eliava Biopreparations, Georgia), and StaphPhage (Microgen, Russia), determined on a set of MRSA strains. Susceptibility of strains to at least one of the 812-derived mutants and at least one of the commercial preparations is shown. Reproduced from Botka *et al.* (2019) [16] (Appendix 14).

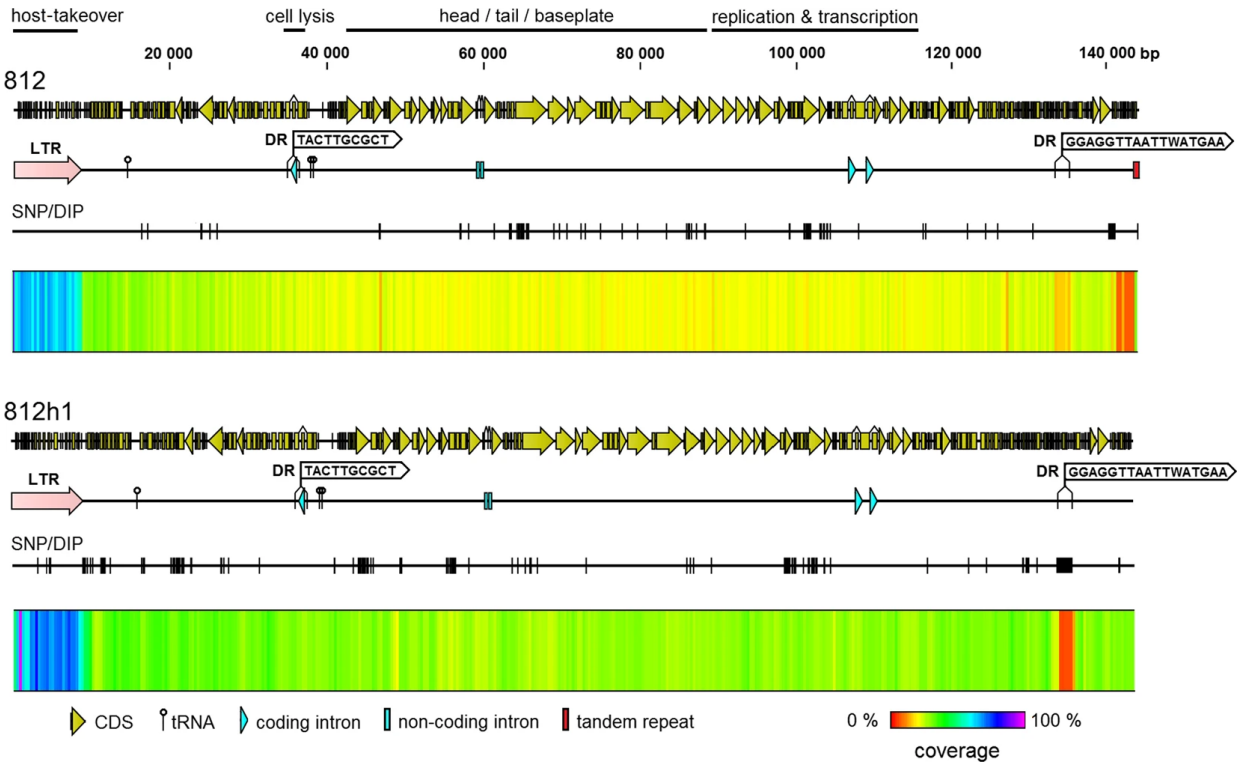

Figure 12: Coverage differences of genomic regions achieved by mapping of sequencing reads to unit genomes of phages 812 and 812h1. Long terminal repeats (LTRs) were delimited by excessively high coverage at the left ends of the genomes due to the alignment of reads from both LTRs. The genome annotations are illustrated on three feature lines: the top line shows coding sequences; the middle line indicates the location of LTR, tRNA genes, introns, and the direct repeats (DR) serving as recombination sites in the endolysin gene, and a 2-kb deletion/insertion polymorphism in phage 812h1; and the bottom lines show the positions of single-nucleotide (SNP) and deletion/insertion (DIP) polymorphisms. Reproduced from Botka *et al.* (2019) [16] (Appendix 14).

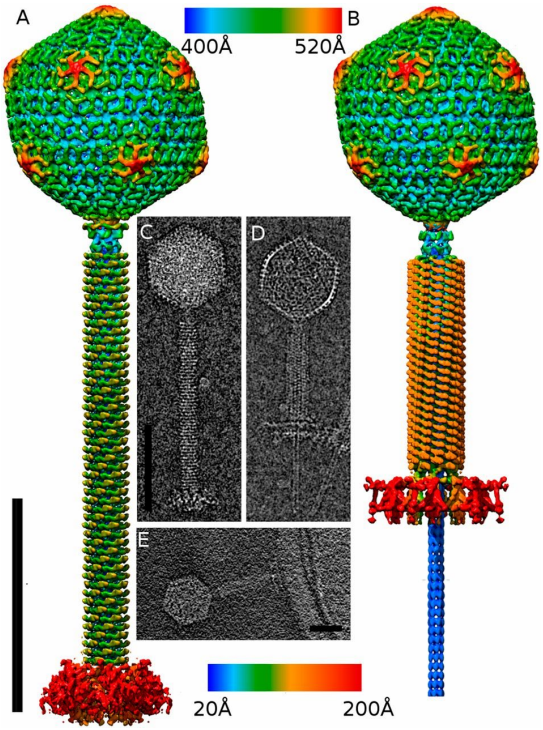

Figure 13: Virions of bacteriophage 812 in native conformation (A) and after tail contraction (B). The heads are rainbow-colored according to the distance from the head center. The tails and baseplates are rainbow-colored according to the distance from the tail sixfold axis. (C and D) Cryo-EM images of native and contracted phage 812 virions. (E) Cryo-tomogram of phage 812 virions attached to an *S. aureus* cell. (Scale bars, 1,000 Å.). Reproduced from Nováček *et al.* (2016) [129].

We have been collaborating extensively with CEITEC MU to uncover the mechanisms of *Kayvirus* phage infection. The genus exhibits typical myoviral morphology, characterized by an icosahedral capsid and a long, double-layered contractile tail (**Fig. 13**). Phage 812 capsid has a diameter of 90 nm and is linked to the 240-nm tail by neck proteins [129]. Contraction of the tail sheath facilitates penetration of the tail tube through the bacterial cell, forming a channel for the phage genome to enter the cytoplasm. The binding of the virion to the staphylococcal cell is a very complex process that requires rotation of the receptor-binding and tripod protein complexes that form the baseplate arms. This reorients the receptor-binding proteins away from the capsid and disrupts the interaction between the tripod proteins and the tail sheath. The changes to the tripod complexes lead to the release of the central spike and weld proteins, thereby exposing peptidoglycan-degrading domains of the hub proteins (Appendix 2) [122]. Baseplate arms change is transmitted through wedge modules to the tail sheath initiator proteins, followed by tail sheath contraction, during which it shortens to 50% and pushes the tail tube 10–30 nm into the bacterial cytoplasm.

The genome release is regulated by neck proteins (portal, adaptor, stopper, tail terminator, and two types of decoration proteins), which are also important during the virion assembly and DNA packaging (Appendix 4) [121]. The portal complex interacts with the genomic left LTR and thus anchors the phage genome within the capsid, where the adaptor complex induces a local B-to-A form transition of the DNA. The tail sheath contraction disrupts DNA-protein binding, allowing the genome to enter the neck, where it is stacked, possibly due to the local A form, until a subsequent tail tube structural change, induced by its interaction with the *S. aureus* cell, releases it. Genome ejection proceeds from the right genophore end toward the left end, while the left redundant part remains anchored to the portal as residual DNA.

We modified the structure of phage 812h1 by inserting a polyhistidine tag into an unstructured exposed loop on the surface of the tail sheath protein (Appendix 7) [130]. A two-strain editing strategy was applied, utilizing homologous recombination followed by CRISPR-Cas10-assisted counter-selection of the recombinant phages. The His-tagged phage particles can be recognized by specific antibodies, enabling their use in imaging and biosensing applications.

Structural stability is necessary to maintain the lytic activity of therapeutic phages in medicinal preparations, an important aspect of the practical application of phage therapy. On the other hand, in dosage forms, antimicrobial preservatives are often used to ensure microbial quality, but they may adversely affect the stability of phage particles. We tested kayviruses with twelve commonly used preservatives for thirteen weeks (Appendix 6) [131]. A complete loss of lytic potential was observed with diazolidinyl urea and benzalkonium chloride. Acceptable level of phage titer decrease was observed with m-cresol, sodium propionate, sodium benzoate, and phenylethyl alcohol; while thimerosal, parabens, and monopropylene glycol had minimal or no impact. Considering the properties of preservatives that interact least with phages, a compromise between stability and preservative safety will be required in pharmaceutical practice.

4.2 PHAGE-ANTIBIOTICS SYNERGY (PAS)

An increasingly important strategy for combating bacterial infections involves combining phages with antibiotics. Numerous studies have demonstrated enhanced antimicrobial efficacy resulting from phage-antibiotic synergy (PAS) against *Escherichia coli*, *P. aeruginosa*, *K. pneumoniae*, *A. baumannii* [132–134], *S. aureus* (Appendix 3, 9) [9, 15], and *S. epidermidis* (Appendix 5) [12]. The efficacy of such combinations is influenced by the effect of antibiotics on the phage replication cycle, including enhanced production of phage progeny within infected bacterial hosts, as evidenced by phage plaque size enhancement [135, 136]. Nevertheless, some combinations may be antagonistic yet still usable in therapy, as we showed in our study of the *Kayvirus*-mupirocin combination for *S. aureus* decolonization (Appendix 3) [9].

Due to emerging mupirocin resistance, we investigated the mupirocin-*Kayvirus* coadministration as a potential strategy to broaden the range of treatable *S. aureus* strains and to prevent the development of new resistance (Appendix 3) [9]. We assessed interactions between mupirocin and the lytic phage in PVL-positive strains with varying levels of mupirocin

resistance. In mupirocin-susceptible strains, due to altered protein synthesis caused by inhibition of isoleucyl-tRNA synthetase by mupirocin, phage efficacy was decreased, whereas mupirocin efficacy was unaffected (**Fig. 14**). However, in mupirocin-resistant strains susceptible to phages, phage proliferation and bacterial lysis were observed even in the presence of mupirocin, thanks to an altered or alternative synthetase that allowed protein synthesis to continue. In low-level mupirocin-resistant strains, the phage remained active at low to moderate mupirocin concentrations, preventing the emergence of new resistant strains due to mutations in the isoleucyl-tRNA synthetase gene.

Another interesting phenomenon that we have previously shown is a change in the sensitivity of the staphylococcal host to phage. Using a piezoelectric biosensor with dissipation technique (QCM-D), we observed a synergistic effect between subinhibitory concentrations of amoxicillin and the *Rosenblumvirus* P68, which together lysed the P68-resistant *S. aureus* strain RN4220 (Appendix 9) [15] (**Fig. 15A, 15B)**. Our results indicate that this synergy also hinders the development of bacterial aggregates, which are the initial stages of biofilm formation (**Fig. 15C**).

PAS-related results indicate that the combined treatment may enable reductions in antibiotic dosage while maintaining therapeutic efficacy. Combined therapy may also prevent the development of resistance because cross-resistance between phages and antibiotics is expected to be limited (Appendix 3) [9, 137]. Moreover, in chronic polymicrobial infections, shifts in dominant pathogens during treatment are common; therefore, it may be beneficial when some pathogens are susceptible to phages and others to antibiotics. Furthermore, the inclusion of established antibiotics in combined formulations could facilitate regulatory approval by pharmaceutical authorities, particularly with regard to patient safety considerations. Unlike therapeutics based solely on phages, the presence of conventional antibiotics may also reduce ethical concerns associated with the design of future clinical trials [138].

We also investigated the combination of phage 812K1/420 with a slightly antibacterial gum Karaya-based hydrogel in a porcine model of deep staphylococcal SSTIs (Appendix 10) [139]. The gum Karaya injectable hydrogels and hydrogel films represent an effective, non-toxic, and easy-to-apply delivery system that supports wound healing and re-epithelialization. In the model, this combination showed a synergistic effect when significantly reducing the bacterial load (2.5log CFU/g of tissue) within one week. Local signs of inflammation were

significantly reduced, with clear evidence of re-epithelialization and no adverse effects observed.

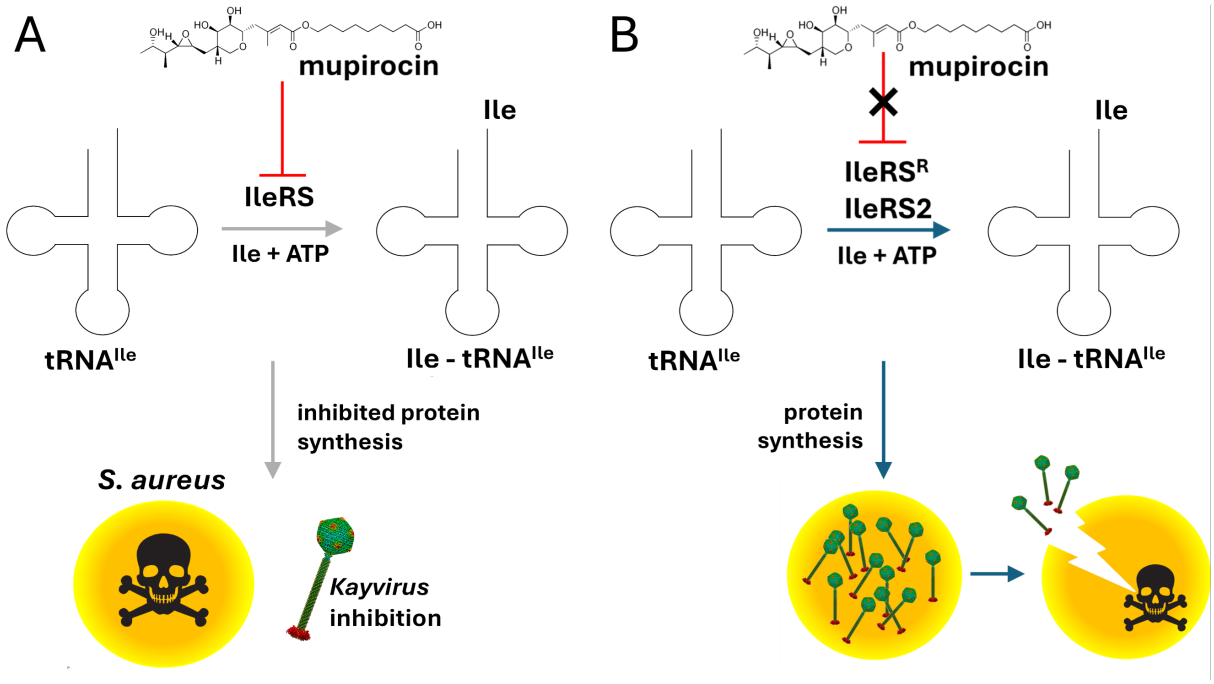

Figure 14: Phage-mupirocin interplay. (A) Mupirocin inhibits Ile-tRNA synthetase (IleRS), thereby blocking protein synthesis in bacteria. This also inhibits the propagation of the infecting phage. (A) Alternative or mutated IleRS enables bacteria to survive exposure to mupirocin. At the same time, in the case of phage infection, it allows the phage to propagate and kill the bacterial host.

To develop effective preparations combining phages and antimicrobial agents, it is essential to evaluate not only their antimicrobial activity but also the biological properties of the selected phages and the impact of antibiotics on phage stability. Combined preparations are also subject to regulatory requirements regarding the microbiological quality and functional compatibility of both components (Appendix 6) [131]. Since preservatives can interfere with both phages and antibiotics, primary packaging that prevents contamination and facilitates dosing seems most suitable for topical application. However, interactions between phages and such packaging, including adhesion to the inner surface and mechanical damage from the application mechanism, should be assessed. We prepared a functional sample that enables topical spray application and dosing of stable mixtures of *Kayvirus* phages 812 or 812h1 (titer $\geq 10^8$ PFU/ml) with ciprofloxacin (c = 0.125 mg/l) or amoxicillin (c = 8 mg/l) that exhibit an additive to synergistic effect [140]. The resulting formulation can be easily prepared and has a shelf life of up to 2 months.

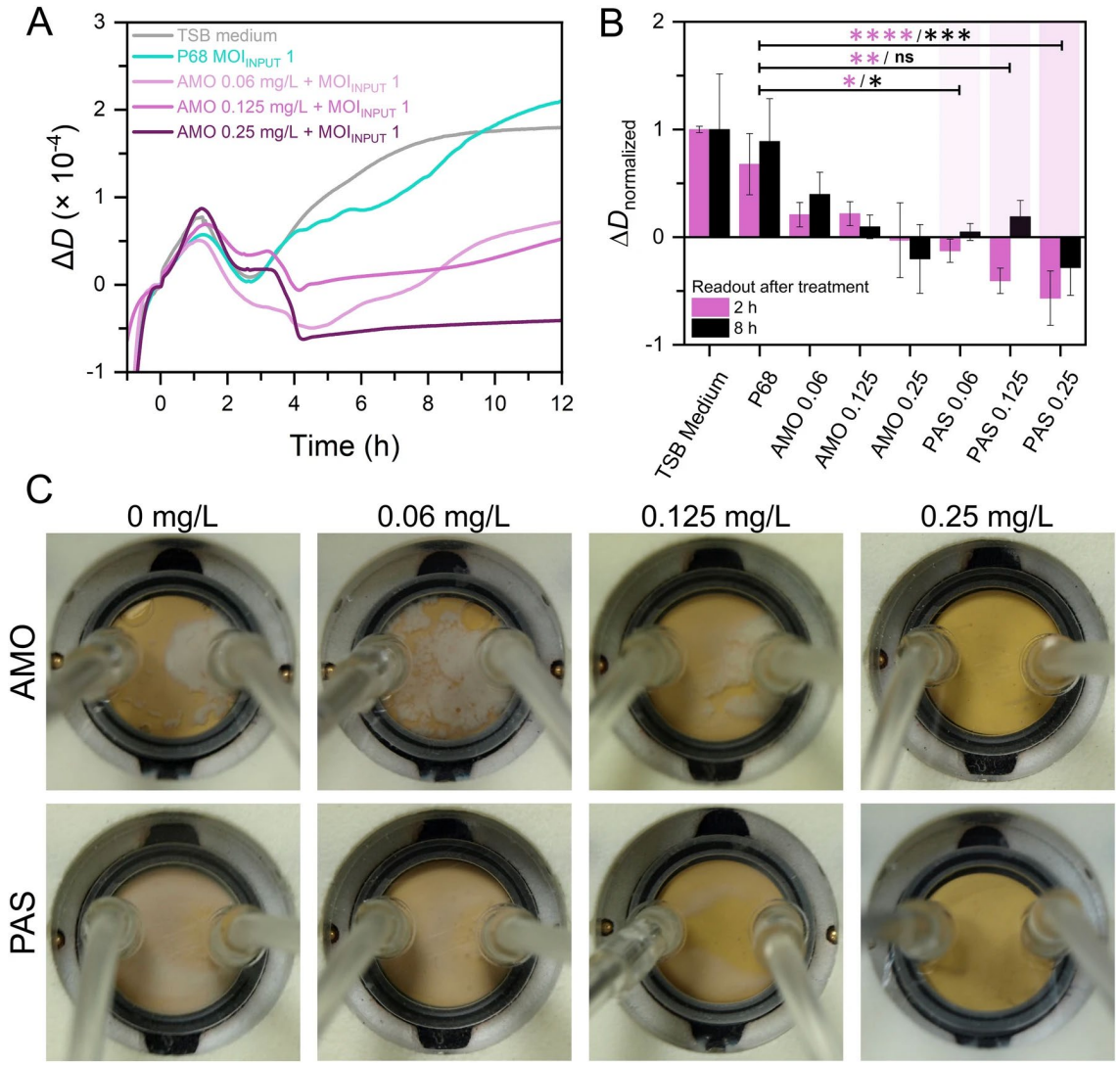

Figure 15: (A) Changes in QCM-D dissipation signal over time for the lysis of *S. aureus* RN4220 by phage P68 (MOI_{INPUT} = 1) alone and in combination with amoxicillin (AMO; 0.06 mg/L, 0.125 mg/mL, and 0.25 mg/L). (B) Normalized dissipation changes read out at 2 h and 8 h after the addition of various lytic agent combinations. Error bars represent standard deviations, and the statistical significances are marked with asterisks (**** for $p < 0.0001$, *** for $p < 0.001$, ** for $p < 0.01$, * for $p < 0.05$, and ns for $p > 0.05$). (C) The appearance of the QCM-D measuring cell after 24 h of measurement for AMO alone (concentrations provided above the corresponding panels) and PAS (utilizing 10^7 PFU/mL of phage P68), showing the differences in the constitution of the formed bacterial biofilm (white layer). In the case of PAS, a compact biofilm was not formed. Reproduced from Obořilová *et al.* (2025) [15] (Appendix 9).

4.3 SAFETY ASPECTS OF PHAGE AND PAS-BASED THERAPY

Phages are natural components of all human body niches and generally do not elicit adverse immune responses [105]. Moreover, they likely play an important role in shaping mammalian-bacterial interactions and may exert anti-inflammatory effects. There are concerns about endotoxin release during phage therapy [141]. Nevertheless, endotoxin concentration can increase up to 20-fold even during antibiotic treatment [142], and endotoxin production is typical for Gram-negative bacteria.

Only limited information is available on the impact of phage infection on bacterial exotoxin production, which may represent a potential safety concern. Generally, as the bacterial population is rapidly reduced by lytic phages, which is associated with bacterial genome destruction and inhibition of transcription [143] and translation [144] of host genes, exotoxin production is expected to be reduced. To date, no complications associated with excessive exotoxin production have been reported during therapy with strictly lytic phages. Toxins may pose a serious health risk when present in phage preparation due to the phage propagation on toxinogenic host strains. Therefore, the use of non-toxinogenic strains or proper purification of phage lysates is necessary [145]. In the case of kayviruses, we usually perform bacterial DNA removal followed by tangential flow filtration with a 300-kDa pore size to ensure their purity (Appendix 6) [131].

Since clinical strains of staphylococci carry a wide range of MGEs, it is essential to examine the impact of phage therapy and combination therapy on the release and spread of these elements, which often confer bacterial virulence or antimicrobial resistance. Therefore, we have explored MGE mobilization in the *S. epidermidis* model under different conditions: phage (*Kayvirus* 812h1), antibiotic (ciprofloxacin), and combined treatment compared to spontaneous induction (Appendix 5) [12] (**Fig. 16**). As expected, treatment with ciprofloxacin increased the prophage induction [146], but treatment with the *Kayvirus* 812h1 strongly reduced the titer of the induced temperate phage (Appendix 5) [12] (**Fig. 17**). At the cellular level, upregulated prophage gene expression was reported during infection with the related *Kayvirus* type phage K in *S. aureus* [127], likely due to host DNA damage from kayviral infection. However, lytic phage host takeover mechanisms probably disrupt the maturation of induced phage particles, reducing the number of infectious virions released at the population level.

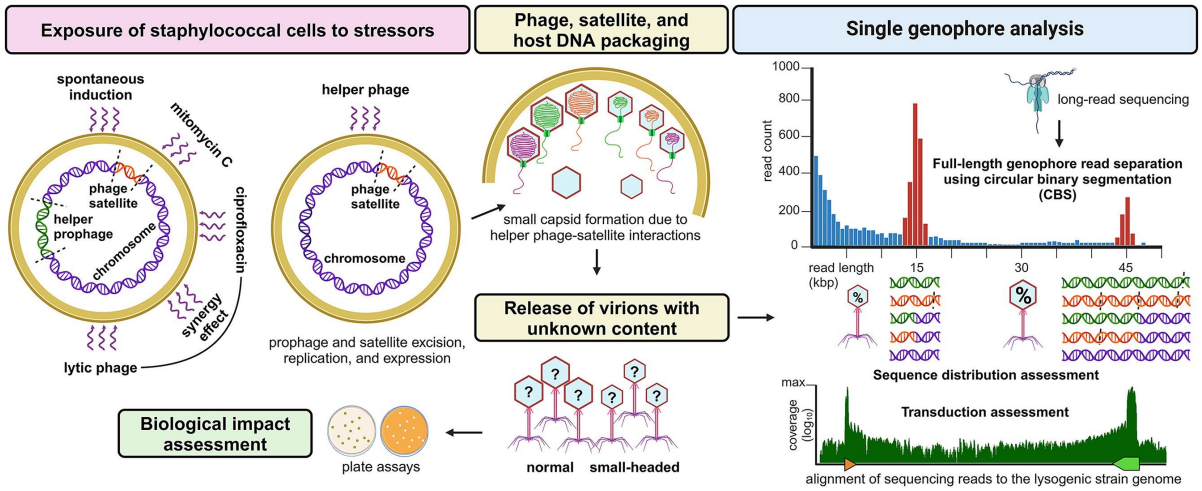

Figure 16: Diagram of the single-virion approach to evaluating the packaging of various types of MGEs and the transduction of bacterial DNA under different conditions: *Kayvirus* infection, ciprofloxacin treatment, combined phage-antibiotic treatment, and spontaneous induction. Reproduced from Botka *et al.* (2025) [12] (Appendix 5).

When the treatment was combined with the antibiotic ciprofloxacin, we observed an increase in both the titer of induced phage and the relative amount of packaged MGEs compared to treatment with phage alone (**Fig. 17**), but the increase was not statistically significant compared to ciprofloxacin alone (Appendix 5) [12]. This increase may result from a lower input ratio of therapeutic phage and, therefore, a lower number of cells infected at the beginning of treatment, thereby allowing ciprofloxacin to induce prophage and MGEs in uninfected bacteria. In addition to the fact that the number of released transducing particles did not pose a greater risk than in the case of antibiotic treatment, the phage-antibiotic combination resulted in a six-order-of-magnitude decrease in the number of viable staphylococcal cells, more than with either the antibiotic or the therapeutic phage alone (**Fig. 17**). Furthermore, the advantage of administering the phage alone in inhibiting transducing particles was equalized when a higher phage input ratio was used in combination with ciprofloxacin.

The phage-ciprofloxacin synergistic combinations have already been used to treat infections caused by *S. aureus* or *P. aeruginosa* [147, 148]. As this combined approach appears to be the best in terms of treatment efficacy while not increasing the risk of spreading resistance and virulence genes, we prepared a utility model representing a mixture of phages and ciprofloxacin acting synergistically against *S. aureus* and *P. aeruginosa*, intended for the treatment of respiratory diseases and other bacterial infections [149]. This utility model protects a formulation combining bacteriophages and ciprofloxacin in a buffering system that simultaneously enhances the ciprofloxacin solubility and preserves the biological activity of bacteriophages of the genera *Kayvirus* and *Pbunavirus*. This preparation is designed for

administration via nebulization. To date, successful tests have been conducted on a cascade impactor and a lung model; however, the advantages of combining lytic phage and ciprofloxacin therapy need to be confirmed *in vivo*.

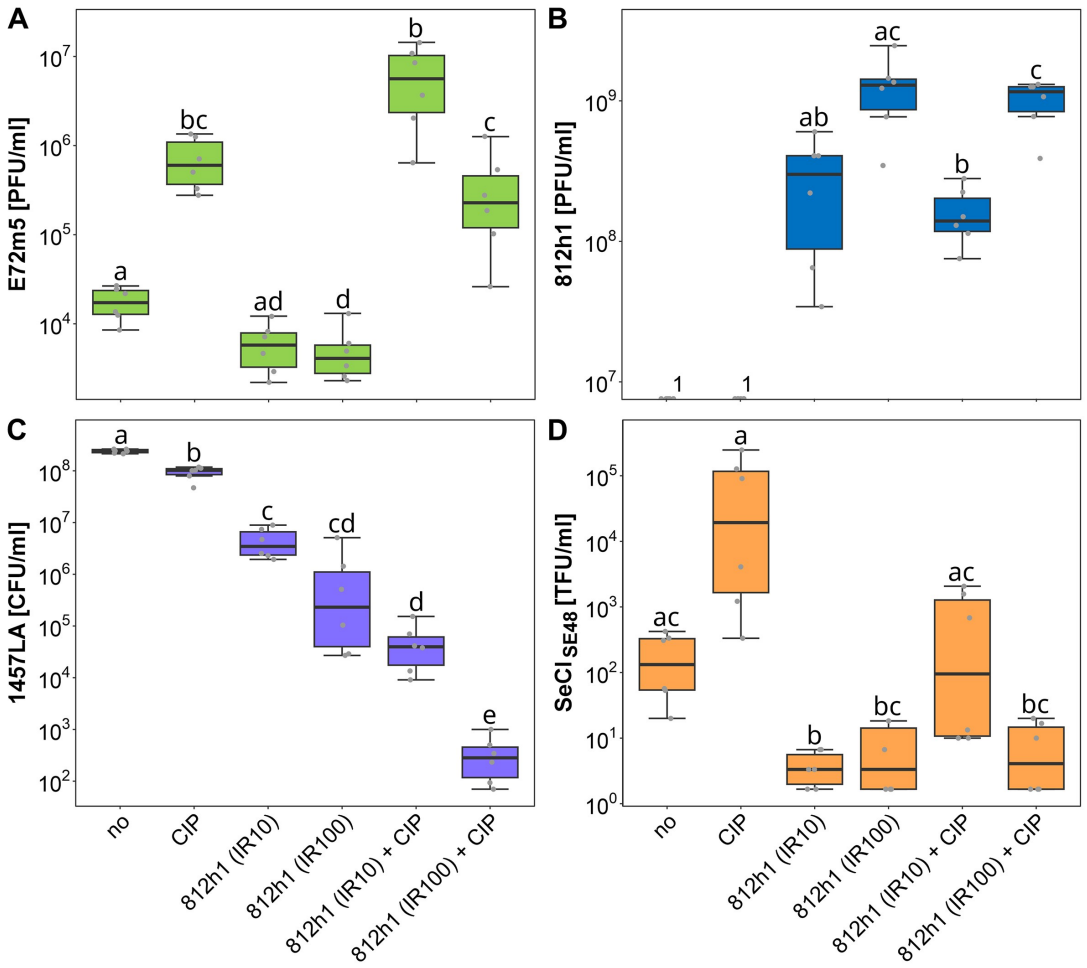

Figure 17: Effect of stress factors on prophage induction, therapeutic phage propagation, bacterial cell count reduction, and $SeCI_{SE48}$ transduction. Counts of released induced phage E72m5 virions (A), infecting phage 812h1 virions (B), viable cell counts of 1457LA culture (C), and $SeCI_{SE48}$-carrying transductant-forming units (D) after spontaneous induction (no treatment) and treatment with ciprofloxacin (CIP), phage 812h1 at input ratios (IR) 10 and 100, and their combination. The difference between values was assessed statistically for each system: Different small letters above boxplots indicate statistically significant differences between groups ($P < .05$). Groups sharing at least one letter are not significantly different from each other. [1]No 812h1 virions were released after spontaneous and ciprofloxacin-mediated induction, as the phage 812h1 was not used. Reproduced from Botka *et al.* (2025) [12] (Appendix 5).

5 Conclusions and Outlook

This thesis demonstrates that mobile genetic elements (MGEs) are the principal drivers of staphylococcal evolution and adaptation. Through horizontal gene transfer, MGEs enable the rapid dissemination of antimicrobial resistance genes, virulence determinants, and anti-phage defense systems across staphylococcal strains, thereby shaping their pathogenicity. At the same time, bacteriophages, a major component of the staphylococcal mobilome, represent promising therapeutic tools capable of addressing the growing challenge of antimicrobial resistance. My work presented in this thesis, therefore, highlights the dual role of MGEs as both contributors to bacterial pathogenicity and valuable instruments for its control. Although the text is divided thematically into separate sections, reading them makes it clear to the reader that the various aspects of the mobilome are interconnected, reflecting complex relationships not only between the MGE and the host but also among the MGEs themselves.

A substantial part of this work concerns plasmids as important vehicles for genetic exchange. Comparative analyses of resistance and virulence plasmids revealed extensive diversity among staphylococcal species, pointing to CoNS as important reservoirs due to interspecies dissemination of clinically relevant determinants. Moreover, the demonstration of conjugative transfer of resistance plasmids from *Macrococcus* sp. to *S. aureus* highlighted the importance of non-staphylococcal reservoirs in the emergence of novel pathogenic lineages. The characterization of ETB-encoding plasmids provided new insights into their evolution, genetic organization, and epidemiology of staphylococcal epidermolytic diseases. The identification of previously undescribed plasmid variants carrying virulence-associated genes further expanded current knowledge of the staphylococcal plasmidome. Our findings support the view that plasmids are key factors in bacterial adaptation and, therefore, need to be continuously analyzed in both clinical and environmental settings.

Another important part of this work targets temperate bacteriophages. The genomic characterization of ETA-converting phages, together with experimental demonstrations of their role in lysogenic conversion, provided direct evidence of the importance of prophages in shaping staphylococcal genomes and pathogenicity. Our results show that prophages are not passive genetic cargo but actively modify host phenotypes, including susceptibility to other phages, which influences microbial competition. The identification and characterization of

prophage-associated anti-phage systems emphasize the complexity of phage-host interactions and have important implications for the efficacy of phage therapy.

An important outcome of this thesis is the detailed investigation of phage-mediated transduction as the dominant mechanism of horizontal gene transfer in staphylococci. Using long-read sequencing, complete encapsidated genophores were characterized for the first time, allowing direct observation of the genetic cargo transmitted by phage particles. This approach provided exceptional insight into the dynamics of generalized and lateral transduction and revealed how environmental stressors, antibiotics, and lytic phage infection influence the composition of DNA packaged into virions. The results showed the phage-inducible chromosomal islands as substantial contributors to genetic mobility, which can alter phage propagation to facilitate their own dissemination. Our findings advance the understanding of bacterial gene flow and establish a framework for future studies investigating mobilome dynamics in polymicrobial communities.

The second major topic of this thesis is the therapeutic exploitation of bacteriophages. Extensive characterization of lytic *Kayvirus* phages demonstrated their suitability for phage therapy of staphylococcal infections due to their broad host range, safety, and ability to generate mutants able to overcome bacterial anti-phage mechanisms. Structural and genomic analyses contributed to a deeper understanding of host recognition, infection mechanisms, and genome delivery processes. These findings not only support the clinical application of kayviruses but also provide knowledge relevant to the design and improvement of future phage preparations.

One of the most promising strategies for the therapy of difficult-to-treat bacterial infections is based on phage-antibiotic synergy. Our studies demonstrated that combining phages with conventional antibiotics may substantially broaden the range of treatable strains, suppress the emergence of resistance, and enhance antibacterial efficacy. Importantly, analyses of phage-antibiotic interactions highlighted the need for careful optimization of combination regimens. The preparation of prototype formulations containing therapeutic phages and antibiotics illustrates the translational potential of our research and provides a foundation for future clinical development. Besides efficacy, the safety of phage-based therapy is equally important. Our results indicate that treatment with lytic phages does not increase the risk of mobilome dissemination beyond that associated with antibiotic treatment and, under certain conditions, can even significantly reduce the release of transducing particles from the bacterial population.

My work helps to resolve key concerns surrounding phage therapy and supports its integration into modern antimicrobial strategies.

In future work, we need to address several limitations of standard research approaches, as most studies were conducted under laboratory conditions with a limited number of bacterial strains and bacteriophages. Consequently, the observed mechanisms of horizontal gene transfer and phage-host interactions may not fully reflect the complexity of natural microbial communities. Next, the molecular mechanisms governing intra-mobilome interactions among plasmids, temperate and lytic phages, PICI, and staphylococcal defense systems remain poorly characterized and warrant further investigation. Understanding intra-mobilome and host-mobilome networks is essential for insight into the evolutionary trajectories of staphylococci and for developing methods to limit the spread of virulence and resistance determinants. Moreover, uncovering these interactions may help specifically target the application of phage therapy or elucidate still-unclear phenomena, such as pseudolysogeny. Long-read sequencing-based methods, together with epigenomic analysis and single-cell approaches, will be among the most useful tools that I want to focus on in my future research.

Concerning my applied research, I will focus on evaluating synergies and their molecular mechanisms in phage cocktails and combinations of phages with antibiotics or phage-derived enzymes, and validating these approaches on animal models. Since most *in vitro* testing is conducted on monocultures, which can lead to different results when translated into practice, it will be useful to test the efficacy of phages on polymicrobial communities, including biofilms, which better reflect *in vivo* conditions. Similarly, more effort is needed to understand the pharmacokinetics and pharmacodynamics of phage and combined preparations. With advances in artificial intelligence (AI), it may be possible, for example, to quickly and efficiently identify suitable phage enzymes with anti-biofilm activity not only in lytic phage sequences but also in databases of bacterial genomes, which contain a vast number of prophages, including incomplete rudiments. Modifications of these proteins can also be designed to broaden or enhance their antibacterial effect. Phage proteins, such as receptor-binding proteins, can also be used to detect bacteria. The development of advanced AI-based methods may significantly accelerate scientific progress.

6 REFERENCES

1. Otto M (2014) *Staphylococcus aureus* toxins. *Curr Opin Microbiol* 17:32–37. https://doi.org/10.1016/j.mib.2013.11.004

2. Kovařovic V, Sedláček I, Petráš P, Králová S, Mašlaňová I, Švec P, Neumann-Schaal M, Botka T, Gelbíčová T, Staňková E, Doškař J, Pantůček R (2022) *Staphylococcus ratti* sp. nov. isolated from a lab rat. *Pathogens* 11:51. https://doi.org/10.3390/pathogens11010051

3. Kovařovic V, Finstrlová A, Sedláček I, Petráš P, Švec P, Mašlaňová I, Neumann-Schaal M, Šedo O, Botka T, Staňková E, Doškař J, Pantůček R (2023) *Staphylococcus brunensis* sp. nov. isolated from human clinical specimens with a staphylococcal cassette chromosome-related genomic island outside of the *rlmH* gene bearing the *ccrDE* recombinase gene complex. *Microbiol Spectr* 11:e0134223. https://doi.org/10.1128/spectrum.01342-23

4. Fišarová L, Pantůček R, Botka T, Doškař J (2019) Variability of resistance plasmids in coagulase-negative staphylococci and their importance as a reservoir of antimicrobial resistance. *Res Microbiol* 170:105–111. https://doi.org/10.1016/j.resmic.2018.11.004

5. Malachowa N, DeLeo FR (2010) Mobile genetic elements of *Staphylococcus aureus*. *Cell Mol Life Sci* 67:3057–3071. https://doi.org/10.1007/s00018-010-0389-4

6. Botka T, Růžičková V, Svobodová K, Pantůček R, Petráš P, Čejková D, Doškař J (2017) Two highly divergent lineages of exfoliative toxin B-encoding plasmids revealed in impetigo strains of *Staphylococcus aureus*. *Int J Med Microbiol* 307:291–296. https://doi.org/10.1016/j.ijmm.2017.05.005

7. Mašlaňová I, Kovařovic V, Botka T, Švec P, Sedláček I, Šedo O, Finstrlová A, Neumann-Schaal M, Kirstein S, Schwendener S, Staňková E, Rovňáková K, Petráš P, Doškař J, Perreten V, Pantůček R (2025) Evidence of *in vitro mecB*-mediated β-lactam antibiotic resistance transfer to *Staphylococcus aureus* from *Macrococcus psychrotolerans* sp. nov., a psychrophilic bacterium from food-producing animals and human clinical specimens. *Appl Environ Microbiol* 91:e0165224. https://doi.org/10.1128/aem.01652-24

8. Boakes E, Kearns AM, Ganner M, Perry C, Hill RL, Ellington MJ (2011) Distinct bacteriophages encoding Panton-Valentine leukocidin (PVL) among international methicillin-resistant *Staphylococcus aureus* clones harboring PVL. *J Clin Microbiol* 49:684–692. https://doi.org/10.1128/JCM.01917-10

9. Siváková A, Figallová E, Botka T, Vacek L, Tkadlec J, Vrbský J, Osowski M, Petráš P, Polaštík Kleknerová D, Dvořáčková M, Urbanová P, Pantůček R, Růžička F (2026) The combination of mupirocin and *Kayvirus* broadens the decolonization effect against *Staphylococcus aureus*. *Appl Microbiol Biotechnol* 110:157. https://doi.org/10.1007/s00253-026-13814-0

10. Kuntová L, Mašlaňová I, Obořilová R, Šimečková H, Finstrlová A, Bárdy P, Šiborová M, Troianovska L, Botka T, Gintar P, Šedo O, Farka Z, Doškař J, Pantůček R (2023) *Staphylococcus aureus* prophage-encoded protein causes abortive infection and provides population immunity against kayviruses. *mBio* 14:e0249022. https://doi.org/10.1128/mbio.02490-22

11. Fišarová L, Botka T, Du X, Mašlaňová I, Bárdy P, Pantůček R, Benešík M, Roudnický P, Winstel V, Larsen J, Rosenstein R, Peschel A, Doškař J (2021) *Staphylococcus epidermidis* phages transduce antimicrobial resistance plasmids and mobilize chromosomal islands. *mSphere* 6:e00223-21. https://doi.org/10.1128/mSphere.00223-21

12. Botka T, Smetanová S, Vinco A, Kučerová E, Rovňáková K, Siváková A, Mašlaňová I, Pantůček R (2025) Virion content unpacked by long-read sequencing: stress-induced changes in

transmitted staphylococcal mobilome due to phage-satellite interactions. *Nucleic Acids Res* 53:gkaf1165. https://doi.org/10.1093/nar/gkaf1165

13. Penadés JR, Christie GE (2015) The phage-inducible chromosomal islands: A family of highly evolved molecular parasites. *Annu Rev Virol* 2:181–201. https://doi.org/10.1146/annurev-virology-031413-085446

14. Novick RP (2019) Pathogenicity islands and their role in staphylococcal biology. *Microbiol Spectr* 7:. https://doi.org/10.1128/microbiolspec.GPP3-0062-2019

15. Obořilová R, Kučerová E, Botka T, Vaisocherová-Lísalová H, Skládal P, Farka Z (2025) Piezoelectric biosensor with dissipation monitoring enables the analysis of bacterial lytic agent activity. *Sci Rep* 15:3419. https://doi.org/10.1038/s41598-024-85064-x

16. Botka T, Pantůček R, Mašlaňová I, Benešík M, Petráš P, Růžičková V, Havlíčková P, Varga M, Žemličková H, Koláčková I, Florianová M, Jakubů V, Karpíšková R, Doškař J (2019) Lytic and genomic properties of spontaneous host-range *Kayvirus* mutants prove their suitability for upgrading phage therapeutics against staphylococci. *Sci Rep* 9:5475. https://doi.org/10.1038/s41598-019-41868-w

17. Heilmann C, Ziebuhr W, Becker K (2019) Are coagulase-negative staphylococci virulent? *Clin Microbiol Infect* 25:1071–1080. https://doi.org/10.1016/j.cmi.2018.11.012

18. Shrivastava SR, Shrivastava PS, Ramasamy J (2018) Responding to the challenge of antibiotic resistance: World Health Organization. *J Res Med Sci* 23:21. https://doi.org/10.4103/1735-1995.228593

19. Schoenfelder SMK, Lange C, Eckart M, Hennig S, Kozytska S, Ziebuhr W (2010) Success through diversity - how *Staphylococcus epidermidis* establishes as a nosocomial pathogen. *Int J Med Microbiol* 300:380–386. https://doi.org/10.1016/j.ijmm.2010.04.011

20. Piette A, Verschraegen G (2009) Role of coagulase-negative staphylococci in human disease. *Vet Microbiol* 134:45–54. https://doi.org/10.1016/j.vetmic.2008.09.009

21. Otto M (2012) Molecular basis of *Staphylococcus epidermidis* infections. *Semin Immunopathol* 34:201–214. https://doi.org/10.1007/s00281-011-0296-2

22. von Eiff C, Peters G, Heilmann C (2002) Pathogenesis of infections due to coagulase-negative staphylococci. *Lancet Infect Dis* 2:677–685. https://doi.org/10.1016/s1473-3099(02)00438-3

23. Schwarz S, Feßler AT, Loncaric I, Wu C, Kadlec K, Wang Y, Shen J (2018) Antimicrobial resistance among staphylococci of animal origin. *Microbiol Spectr* 6:. https://doi.org/10.1128/microbiolspec.ARBA-0010-2017

24. Lindsay JA, Holden MTG (2004) *Staphylococcus aureus*: superbug, super genome? *Trends Microbiol* 12:378–385. https://doi.org/10.1016/j.tim.2004.06.004

25. Bosi E, Monk JM, Aziz RK, Fondi M, Nizet V, Palsson BØ (2016) Comparative genome-scale modelling of *Staphylococcus aureus* strains identifies strain-specific metabolic capabilities linked to pathogenicity. *Proc Natl Acad Sci U S A* 113:E3801-3809. https://doi.org/10.1073/pnas.1523199113

26. Chaudhry V, Patil PB (2016) Genomic investigation reveals evolution and lifestyle adaptation of endophytic *Staphylococcus epidermidis*. *Sci Rep* 6:19263. https://doi.org/10.1038/srep19263

27. Botka T, Růžičková V, Konečná H, Pantůček R, Rychlík I, Zdráhal Z, Petráš P, Doškař J (2015) Complete genome analysis of two new bacteriophages isolated from impetigo strains of *Staphylococcus aureus*. *Virus Genes* 51:122–131. https://doi.org/10.1007/s11262-015-1223-8

28. Lindsay JA (2014) *Staphylococcus aureus* genomics and the impact of horizontal gene transfer. *Int J Med Microbiol* 304:103–109. https://doi.org/10.1016/j.ijmm.2013.11.010

29. Bowring JZ, Su Y, Alsaadi A, Svenningsen SL, Parkhill J, Ingmer H (2022) Screening for highly transduced genes in *Staphylococcus aureus* revealed both lateral and specialized transduction. *Microbiol Spectr* 10:e0242321. https://doi.org/10.1128/spectrum.02423-21

30. Madhusoodanan J, Seo KS, Remortel B, Park JY, Hwang SY, Fox LK, Park YH, Deobald CF, Wang D, Liu S, Daugherty SC, Gill AL, Bohach GA, Gill SR (2011) An enterotoxin-bearing pathogenicity island in *Staphylococcus epidermidis*. *J Bacteriol* 193:1854–1862. https://doi.org/10.1128/JB.00162-10

31. Fillol-Salom A, Martínez-Rubio R, Abdulrahman RF, Chen J, Davies R, Penadés JR (2018) Phage-inducible chromosomal islands are ubiquitous within the bacterial universe. *ISME J* 12:2114–2128. https://doi.org/10.1038/s41396-018-0156-3

32. Chee MSJ, Serrano E, Chiang YN, Harling-Lee J, Man R, Bacigalupe R, Fitzgerald JR, Penadés JR, Chen J (2023) Dual pathogenicity island transfer by piggybacking lateral transduction. *Cell* 186:3414-3426.e16. https://doi.org/10.1016/j.cell.2023.07.001

33. Tian X, Zhang Z, Hou W, Li J, Kang S, Mai Z, Zhong N, Lu L, Shi C (2026) Plasmidomic landscape of *Staphylococcus aureus* and the emergence of a CC5 subclade harboring the conjugative plasmid pSK41: implications for food safety and antimicrobial resistance. *NPJ Sci Food* 10:78. https://doi.org/10.1038/s41538-026-00733-7

34. John J, George S, Nori SRC, Nelson-Sathi S (2019) Phylogenomic analysis reveals the evolutionary route of resistant genes in *Staphylococcus aureus*. *Genome Biol Evol* 11:2917–2926. https://doi.org/10.1093/gbe/evz213

35. Werckenthin C, Schwarz S, Roberts MC (1996) Integration of pT181-like tetracycline resistance plasmids into large staphylococcal plasmids involves IS257. *Antimicrob Agents Chemother* 40:2542–2544. https://doi.org/10.1128/AAC.40.11.2542

36. Yui Eto K, Firth N, Davis AM, Kwong SM, Krysiak M, Lee YT, O'Brien FG, Grubb WB, Coombs GW, Bond CS, Ramsay JP (2019) Evolution of a 72-kilobase cointegrant, conjugative multiresistance plasmid in community-associated methicillin-resistant *Staphylococcus aureus* isolates from the early 1990s. *Antimicrob Agents Chemother* 63:e01560-19. https://doi.org/10.1128/AAC.01560-19

37. Dyer DW, Rock MI, Lee CY, Iandolo JJ (1985) Generation of transducing particles in *Staphylococcus aureus*. *J Bacteriol* 161:91–95. https://doi.org/10.1128/jb.161.1.91-95.1985

38. Mašlaňová I, Doškař J, Varga M, Kuntová L, Mužík J, Malúšková D, Růžičková V, Pantůček R (2013) Bacteriophages of *Staphylococcus aureus* efficiently package various bacterial genes and mobile genetic elements including SCC*mec* with different frequencies. *Environ Microbiol Rep* 5:66–73. https://doi.org/10.1111/j.1758-2229.2012.00378.x

39. Wong JJW, Lu J, Glover JNM (2012) Relaxosome function and conjugation regulation in F-like plasmids - a structural biology perspective. *Mol Microbiol* 85:602–617. https://doi.org/10.1111/j.1365-2958.2012.08131.x

40. Ramsay JP, Kwong SM, Murphy RJT, Yui Eto K, Price KJ, Nguyen QT, O'Brien FG, Grubb WB, Coombs GW, Firth N (2016) An updated view of plasmid conjugation and mobilization in *Staphylococcus*. *Mob Genet Elem* 6:e1208317. https://doi.org/10.1080/2159256X.2016.1208317

41. Zhang S, Iandolo JJ, Stewart GC (1998) The enterotoxin D plasmid of *Staphylococcus aureus* encodes a second enterotoxin determinant (sej). *FEMS Microbiol Lett* 168:227–233. https://doi.org/10.1111/j.1574-6968.1998.tb13278.x

42. Yamaguchi T, Hayashi T, Takami H, Ohnishi M, Murata T, Nakayama K, Asakawa K, Ohara M, Komatsuzawa H, Sugai M (2001) Complete nucleotide sequence of a *Staphylococcus aureus*

exfoliative toxin B plasmid and identification of a novel ADP-ribosyltransferase, EDIN-C. *Infect Immun* 69:7760–7771. https://doi.org/10.1128/IAI.69.12.7760-7771.2001

43. Tkadlec J, Vařeková E, Pantůček R, Doškař J, Růžičková V, Botka T, Fila L, Melter O (2015) Characterization of *Staphylococcus aureus* strains isolated from Czech cystic fibrosis patients: High rate of ribosomal mutation conferring resistance to MLS(B) antibiotics as a result of long-term and low-dose azithromycin treatment. *Microb Drug Resist* 21:416–423. https://doi.org/10.1089/mdr.2014.0276

44. Fischer AJ, Kilgore SH, Singh SB, Allen PD, Hansen AR, Limoli DH, Schlievert PM (2019) High prevalence of *Staphylococcus aureus* enterotoxin gene cluster superantigens in cystic fibrosis clinical isolates. *Genes* 10:1036. https://doi.org/10.3390/genes10121036

45. Plano LRW (2004) *Staphylococcus aureus* exfoliative toxins: how they cause disease. *J Invest Dermatol* 122:1070–1077. https://doi.org/10.1111/j.1523-1747.2004.22144.x

46. Rouva G, Vergadi E, Krasagakis K, Galanakis E (2025) Understanding host's response to staphylococcal scalded skin syndrome. *Acta Paediatr* 114:241–247. https://doi.org/10.1111/apa.17462

47. Růžičková V, Pantůček R, Petráš P, Machová I, Kostýlková K, Doškař J (2012) Major clonal lineages in impetigo *Staphylococcus aureus* strains isolated in Czech and Slovak maternity hospitals. *Int J Med Microbiol* 302:237–241. https://doi.org/10.1016/j.ijmm.2012.04.001

48. Jackson MP, Iandolo JJ (1986) Sequence of the exfoliative toxin B gene of *Staphylococcus aureus*. *J Bacteriol* 167:726–728. https://doi.org/10.1128/jb.167.2.726-728.1986

49. Hisatsune J, Hirakawa H, Yamaguchi T, Fudaba Y, Oshima K, Hattori M, Kato F, Kayama S, Sugai M (2013) Emergence of *Staphylococcus aureus* carrying multiple drug resistance genes on a plasmid encoding exfoliative toxin B. *Antimicrob Agents Chemother* 57:6131–6140. https://doi.org/10.1128/AAC.01062-13

50. Rowland SJ, Dyke KG (1990) Tn552, a novel transposable element from *Staphylococcus aureus*. *Mol Microbiol* 4:961–975. https://doi.org/10.1111/j.1365-2958.1990.tb00669.x

51. Inoue S, Sugai M, Murooka Y, Paik SY, Hong YM, Ohgai H, Suginaka H (1991) Molecular cloning and sequencing of the epidermal cell differentiation inhibitor gene from *Staphylococcus aureus*. *Biochem Biophys Res Commun* 174:459–464. https://doi.org/10.1016/0006-291x(91)91438-i

52. Aepfelbacher M, Essler M, Huber E, Sugai M, Weber PC (1997) Bacterial toxins block endothelial wound repair. Evidence that Rho GTPases control cytoskeletal rearrangements in migrating endothelial cells. *Arterioscler Thromb Vasc Biol* 17:1623–1629. https://doi.org/10.1161/01.atv.17.9.1623

53. Munro P, Benchetrit M, Nahori M-A, Stefani C, Clément R, Michiels J-F, Landraud L, Dussurget O, Lemichez E (2010) The *Staphylococcus aureus* epidermal cell differentiation inhibitor toxin promotes formation of infection foci in a mouse model of bacteremia. *Infect Immun* 78:3404–3411. https://doi.org/10.1128/IAI.00319-10

54. Mulligan ME, Murray-Leisure KA, Ribner BS, Standiford HC, John JF, Korvick JA, Kauffman CA, Yu VL (1993) Methicillin-resistant *Staphylococcus aureus*: a consensus review of the microbiology, pathogenesis, and epidemiology with implications for prevention and management. *Am J Med* 94:313–328. https://doi.org/10.1016/0002-9343(93)90063-u

55. McCarthy AJ, Lindsay JA (2012) The distribution of plasmids that carry virulence and resistance genes in *Staphylococcus aureus* is lineage associated. *BMC Microbiol* 12:104. https://doi.org/10.1186/1471-2180-12-104

56. Mäntynen S, Laanto E, Oksanen HM, Poranen MM, Díaz-Muñoz SL (2021) Black box of phage-bacterium interactions: exploring alternative phage infection strategies. *Open Biol* 11:210188. https://doi.org/10.1098/rsob.210188

57. Nanda AM, Thormann K, Frunzke J (2015) Impact of spontaneous prophage induction on the fitness of bacterial populations and host-microbe interactions. *J Bacteriol* 197:410–419. https://doi.org/10.1128/JB.02230-14

58. Ingmer H, Gerlach D, Wolz C (2019) Temperate phages of *Staphylococcus aureus*. *Microbiol Spectr* 7:. https://doi.org/10.1128/microbiolspec.GPP3-0058-2018

59. Lindsay JA (2019) Staphylococci: Evolving genomes. *Microbiol Spectr* 7:. https://doi.org/10.1128/microbiolspec.GPP3-0071-2019

60. Mašlaňová I, Stříbná S, Doškař J, Pantůček R (2016) Efficient plasmid transduction to *Staphylococcus aureus* strains insensitive to the lytic action of transducing phage. *FEMS Microbiol Lett* 363:fnw211. https://doi.org/10.1093/femsle/fnw211

61. Zeman M, Mašlaňová I, Indráková A, Šiborová M, Mikulášek K, Bendíčková K, Plevka P, Vrbovská V, Zdráhal Z, Doškař J, Pantůček R (2017) *Staphylococcus sciuri* bacteriophages double-convert for staphylokinase and phospholipase, mediate interspecies plasmid transduction, and package *mecA* gene. *Sci Rep* 7:46319. https://doi.org/10.1038/srep46319

62. Moller AG, Lindsay JA, Read TD (2019) Determinants of phage host range in *Staphylococcus* species. *Appl Environ Microbiol* 85:e00209-19. https://doi.org/10.1128/AEM.00209-19

63. Carroll JD, Cafferkey MT, Coleman DC (1993) Serotype F double- and triple-converting phage insertionally inactivate the *Staphylococcus aureus* beta-toxin determinant by a common molecular mechanism. *FEMS Microbiol Lett* 106:147–155. https://doi.org/10.1111/j.1574-6968.1993.tb05951.x

64. Holochová P, Růžičková V, Dostálová L, Pantůček R, Petrás P, Doškař J (2010) Rapid detection and differentiation of the exfoliative toxin A-producing *Staphylococcus aureus* strains based on phiETA prophage polymorphisms. *Diagn Microbiol Infect Dis* 66:248–252. https://doi.org/10.1016/j.diagmicrobio.2009.10.008

65. Ladhani S (2001) Recent developments in staphylococcal scalded skin syndrome. *Clin Microbiol Infect* 7:301–307. https://doi.org/10.1046/j.1198-743x.2001.00258.x

66. Zeaki N, Susilo YB, Pregiel A, Rådström P, Schelin J (2015) Prophage-encoded staphylococcal enterotoxin A: Regulation of production in *Staphylococcus aureus* strains representing different *sea* regions. *Toxins* 7:5359–5376. https://doi.org/10.3390/toxins7124889

67. Deacy AM, Gan SK-E, Derrick JP (2021) Superantigen recognition and interactions: Functions, mechanisms and applications. *Front Immunol* 12:731845. https://doi.org/10.3389/fimmu.2021.731845

68. Fisher EL, Otto M, Cheung GYC (2018) Basis of virulence in enterotoxin-mediated staphylococcal food poisoning. *Front Microbiol* 9:436. https://doi.org/10.3389/fmicb.2018.00436

69. Coombs GW, Baines SL, Howden BP, Swenson KM, O'Brien FG (2020) Diversity of bacteriophages encoding Panton-Valentine leukocidin in temporally and geographically related *Staphylococcus aureus*. *PloS One* 15:e0228676. https://doi.org/10.1371/journal.pone.0228676

70. Lina G, Piémont Y, Godail-Gamot F, Bes M, Peter MO, Gauduchon V, Vandenesch F, Etienne J (1999) Involvement of Panton-Valentine leukocidin-producing *Staphylococcus aureus* in primary skin infections and pneumonia. *Clin Infect Dis* 29:1128–1132. https://doi.org/10.1086/313461

71. Planet PJ (2017) Life after USA300: The rise and fall of a superbug. *J Infect Dis* 215:S71–S77. https://doi.org/10.1093/infdis/jiw444

72. Rostøl JT, Quiles-Puchalt N, Iturbe-Sanz P, Lasa Í, Penadés JR (2024) Bacteriophages avoid autoimmunity from cognate immune systems as an intrinsic part of their life cycles. *Nat Microbiol* 9:1312–1324. https://doi.org/10.1038/s41564-024-01661-6

73. Dempsey RM, Carroll D, Kong H, Higgins L, Keane CT, Coleman DC (2005) *Sau*42I, a *Bcg*I-like restriction-modification system encoded by the *Staphylococcus aureus* quadruple-converting phage Phi42. *Microbiology* 151:1301–1311. https://doi.org/10.1099/mic.0.27646-0

74. Gerlach D, Sieber RN, Larsen J, Krusche J, De Castro C, Baumann J, Molinaro A, Peschel A (2022) Horizontal transfer and phylogenetic distribution of the immune evasion factor *tarP*. *Front Microbiol* 13:951333. https://doi.org/10.3389/fmicb.2022.951333

75. Chen H-J, Chang Y-C, Tsai J-C, Hung W-C, Lin Y-T, You S-J, Tseng S-P, Teng L-J (2013) New structure of phage-related islands carrying *fusB* and a virulence gene in fusidic acid-resistant *Staphylococcus epidermidis*. *Antimicrob Agents Chemother* 57:5737–5739. https://doi.org/10.1128/AAC.01433-13

76. Novick RP, Ram G (2017) Staphylococcal pathogenicity islands-movers and shakers in the genomic firmament. *Curr Opin Microbiol* 38:197–204. https://doi.org/10.1016/j.mib.2017.08.001

77. Banaszkiewicz S, Calland JK, Mourkas E, Sheppard SK, Pascoe B, Bania J (2019) Genetic diversity of composite enterotoxigenic *Staphylococcus epidermidis* pathogenicity islands. *Genome Biol Evol* 11:3498–3509. https://doi.org/10.1093/gbe/evz259

78. Ibarra-Chávez R, Brady A, Chen J, Penadés JR, Haag AF (2022) Phage-inducible chromosomal islands promote genetic variability by blocking phage reproduction and protecting transductants from phage lysis. *PLoS Genet* 18:e1010146. https://doi.org/10.1371/journal.pgen.1010146

79. Tormo-Más MA, Mir I, Shrestha A, Tallent SM, Campoy S, Lasa I, Barbé J, Novick RP, Christie GE, Penadés JR (2010) Moonlighting bacteriophage proteins derepress staphylococcal pathogenicity islands. *Nature* 465:779–782. https://doi.org/10.1038/nature09065

80. Ram G, Chen J, Ross HF, Novick RP (2014) Precisely modulated pathogenicity island interference with late phage gene transcription. *Proc Natl Acad Sci U S A* 111:14536–14541. https://doi.org/10.1073/pnas.1406749111

81. Ram G, Chen J, Kumar K, Ross HF, Ubeda C, Damle PK, Lane KD, Penadés JR, Christie GE, Novick RP (2012) Staphylococcal pathogenicity island interference with helper phage reproduction is a paradigm of molecular parasitism. *Proc Natl Acad Sci U S A* 109:16300–16305. https://doi.org/10.1073/pnas.1204615109

82. Anderson DG, Kowalczykowski SC (1998) Reconstitution of an SOS response pathway: derepression of transcription in response to DNA breaks. *Cell* 95:975–979. https://doi.org/10.1016/s0092-8674(00)81721-3

83. Ubeda C, Maiques E, Knecht E, Lasa I, Novick RP, Penadés JR (2005) Antibiotic-induced SOS response promotes horizontal dissemination of pathogenicity island-encoded virulence factors in staphylococci. *Mol Microbiol* 56:836–844. https://doi.org/10.1111/j.1365-2958.2005.04584.x

84. McCarthy AJ, Witney AA, Lindsay JA (2012) *Staphylococcus aureus* temperate bacteriophage: carriage and horizontal gene transfer is lineage associated. *Front Cell Infect Microbiol* 2:6. https://doi.org/10.3389/fcimb.2012.00006

85. Feiss M, Siegele DA (1979) Packaging of the bacteriophage lambda chromosome: dependence of cos cleavage on chromosome length. *Virology* 92:190–200. https://doi.org/10.1016/0042-6822(79)90224-1

86. Chiang YN, Penadés JR, Chen J (2019) Genetic transduction by phages and chromosomal islands: The new and noncanonical. *PLoS Pathog* 15:e1007878. https://doi.org/10.1371/journal.ppat.1007878

87. Casjens SR, Gilcrease EB (2009) Determining DNA packaging strategy by analysis of the termini of the chromosomes in tailed-bacteriophage virions. *Methods Mol Biol* 502:91–111. https://doi.org/10.1007/978-1-60327-565-1_7

88. Carlton RM, Noordman WH, Biswas B, de Meester ED, Loessner MJ (2005) Bacteriophage P100 for control of *Listeria monocytogenes* in foods: genome sequence, bioinformatic analyses, oral toxicity study, and application. *Regul Toxicol Pharmacol* RTP 43:301–312. https://doi.org/10.1016/j.yrtph.2005.08.005

89. Marcelli B, Karsens H, Nijland M, Oudshoorn R, Kuipers OP, Kok J (2020) Employing lytic phage-mediated horizontal gene transfer in *Lactococcus lactis*. *PLoS ONE* 15:e0238988. https://doi.org/10.1371/journal.pone.0238988

90. Young KK, Edlin GJ, Wilson GG (1982) Genetic analysis of bacteriophage T4 transducing bacteriophages. *J Virol* 41:345–347. https://doi.org/10.1128/JVI.41.1.345-347.1982

91. Borodovich T, Buttimer C, Wilson JS, Bardy P, Smith M, Hill C, Khokhlova EV, Harte M, Govi B, Fogg PCM, Hill C, Shkoporov AN (2026) Large-scale capsid-mediated mobilisation of bacterial genomic DNA in the gut microbiome. *Nat Commun* 17:2046. https://doi.org/10.1038/s41467-026-68726-4

92. Wolput S, Lood C, Fillol-Salom A, Casters Y, Albasiony A, Cenens W, Vanoirbeek K, Kerremans A, Lavigne R, Penadés JR, Aertsen A (2024) Phage-host co-evolution has led to distinct generalized transduction strategies. *Nucleic Acids Res* 52:7780–7791. https://doi.org/10.1093/nar/gkae489

93. Maier JL, Gin C, Callahan B, Sheriff EK, Duerkop BA, Kleiner M (2024) Pseudo-*pac* site sequences used by phage P22 in generalized transduction of *Salmonella*. *PLoS Pathog* 20:e1012301. https://doi.org/10.1371/journal.ppat.1012301

94. Zhang Z, Kottadiel VI, Vafabakhsh R, Dai L, Chemla YR, Ha T, Rao VB (2011) A promiscuous DNA packaging machine from bacteriophage T4. *PLoS Biol* 9:e1000592. https://doi.org/10.1371/journal.pbio.1000592

95. Vafabakhsh R, Kondabagil K, Earnest EE, Lee KS, Zhang Z, Dai L, Dahmen KA, Rao VB, Ha T (2014) Single-molecule packaging initiation in real time by a viral DNA packaging machine from bacteriophage T4. *Proc Natl Acad Sci U S A* 111:15096–15101. https://doi.org/10.1073/pnas.1407235111

96. Coren JS, Pierce JC, Sternberg N (1995) Headful packaging revisited: the packaging of more than one DNA molecule into a bacteriophage P1 head. *J Mol Biol* 249:176–184. https://doi.org/10.1006/jmbi.1995.0287

97. Leffers G, Rao VB (1996) A discontinuous headful packaging model for packaging less than headful length DNA molecules by bacteriophage T4. *J Mol Biol* 258:839–850. https://doi.org/10.1006/jmbi.1996.0291

98. Chen J, Quiles-Puchalt N, Chiang YN, Bacigalupe R, Fillol-Salom A, Chee MSJ, Fitzgerald JR, Penadés JR (2018) Genome hypermobility by lateral transduction. *Science* 362:207–212. https://doi.org/10.1126/science.aat5867

99. Humphrey S, Fillol-Salom A, Quiles-Puchalt N, Ibarra-Chávez R, Haag AF, Chen J, Penadés JR (2021) Bacterial chromosomal mobility via lateral transduction exceeds that of classical mobile genetic elements. *Nat Commun* 12:6509. https://doi.org/10.1038/s41467-021-26004-5

100. Jackson EN, Jackson DA, Deans RJ (1978) *Eco*RI analysis of bacteriophage P22 DNA packaging. *J Mol Biol* 118:365–388. https://doi.org/10.1016/0022-2836(78)90234-6

101. Adams MB, Hayden M, Casjens S (1983) On the sequential packaging of bacteriophage P22 DNA. *J Virol* 46:673–677. https://doi.org/10.1128/JVI.46.2.673-677.1983

102. Kuang X, Gorzynski J, Touchon M, Shkoporov A, Rocha EPC, Fitzgerald JR, Chen J, Rostøl JT, Penadés JR (2026) Bacteriophages mobilize bacterial defense systems via lateral transduction. *Sci Adv* 12:eadx5749. https://doi.org/10.1126/sciadv.adx5749

103. Pantůček R, Doškař J, Boštík J, Kocourková D, Petrzik K, Koptíková J, Benešík M, Plevka P, Füzik T, Mašlaňová I, Botka T, Nepeřený J, Zeller D, Kuntová L, Snopková K, Hrala M, Moša M (2026) Past and present phage therapy research and practice in the Czech Republic – contribution to phage therapy in Europe. *Virol J*. https://doi.org/10.1186/s12985-026-03296-x

104. Lin DM, Koskella B, Lin HC (2017) Phage therapy: An alternative to antibiotics in the age of multi-drug resistance. *World J Gastrointest Pharmacol Ther* 8:162–173. https://doi.org/10.4292/wjgpt.v8.i3.162

105. Van Belleghem JD, Dąbrowska K, Vaneechoutte M, Barr JJ, Bollyky PL (2018) Interactions between bacteriophage, bacteria, and the mammalian immune system. *Viruses* 11:10. https://doi.org/10.3390/v11010010

106. Belkaid Y, Hand TW (2014) Role of the microbiota in immunity and inflammation. *Cell* 157:121–141. https://doi.org/10.1016/j.cell.2014.03.011

107. Pawłuszkiewicz K, Busłowicz T, Korgiel M, Faltus A, Kucharczyk E, Porębska B, Pochciał P, Kucharczyk N, Paluch E (2025) Bacteriophage-based approach against biofilm infections associated with medical devices: A narrative review of ESKAPE pathogens. *Int J Mol Sci* 26:8699. https://doi.org/10.3390/ijms26178699

108. Straka M, Hubenáková Z, Janošíková L, Bugalová A, Minich A, Wawruch M, Liptáková A, Drahovská H, Slobodníková L (2024) *In vitro* susceptibility of clinical and carrier strains of *Staphylococcus aureus* to STAFAL® phage preparation. *Int J Mol Sci* 25:12885. https://doi.org/10.3390/ijms252312885

109. Benešík M, Nováček J, Janda L, Dopitová R, Pernisová M, Melková K, Tišáková L, Doškař J, Žídek L, Hejátko J, Pantůček R (2018) Role of SH3b binding domain in a natural deletion mutant of *Kayvirus* endolysin LysF1 with a broad range of lytic activity. *Virus Genes* 54:130–139. https://doi.org/10.1007/s11262-017-1507-2

110. Fuerst-Wilmes M, Respondek V, Schramm M, Lilienthal N, Buss K, Duechting A (2025) Regulation of phage therapy medicinal products: developments, challenges, and opportunities. *Front Cell Infect Microbiol* 15:1631359. https://doi.org/10.3389/fcimb.2025.1631359

111. Zeng T, Liu S, Zou P, Yao X, Chen Q, Wei L, Wang Q, Zhang C, Zheng Y, Yu R (2024) Create artilysins from a recombinant library to serve as bactericidal and antibiofilm agents targeting *Pseudomonas aeruginosa*. *Int J Biol Macromol* 273:132990. https://doi.org/10.1016/j.ijbiomac.2024.132990

112. Fowler VG, Das AF, Lipka-Diamond J, Ambler JE, Schuch R, Pomerantz R, Cassino C, Jáuregui-Peredo L, Moran GJ, Rupp ME, Lachiewicz AM, Kuti JL, Wise RA, Kaye KS, Zervos MJ, Nichols WG (2024) Exebacase in addition to standard-of-care antibiotics for *Staphylococcus aureus* bloodstream infections and right-sided infective endocarditis: A phase 3, superiority-design, placebo-controlled, randomized clinical trial (DISRUPT). *Clin Infect Dis* 78:1473–1481. https://doi.org/10.1093/cid/ciae043

113. Jun SY, Jang IJ, Yoon S, Jang K, Yu K-S, Cho JY, Seong M-W, Jung GM, Yoon SJ, Kang SH (2017) Pharmacokinetics and tolerance of the phage endolysin-based candidate drug SAL200 after a single intravenous administration among healthy volunteers. *Antimicrob Agents Chemother* 61:e02629-16. https://doi.org/10.1128/AAC.02629-16

114. Backman T, Burbano HA, Karasov TL (2024) Tradeoffs and constraints on the evolution of tailocins. *Trends Microbiol* 32:1084–1095. https://doi.org/10.1016/j.tim.2024.04.001

115. Acedo JZ, Chiorean S, Vederas JC, van Belkum MJ (2018) The expanding structural variety among bacteriocins from Gram-positive bacteria. *FEMS Microbiol Rev* 42:805–828. https://doi.org/10.1093/femsre/fuy033

116. Dvořáčková M, Růžička F, Benešík M, Pantůček R, Dvořáková-Heroldová M (2019) Antimicrobial effect of commercial phage preparation Stafal® on biofilm and planktonic forms of methicillin-resistant *Staphylococcus aureus*. *Folia Microbiol* 64:121–126. https://doi.org/10.1007/s12223-018-0622-3

117. Suchithra KV, Hameed A, Rekha PD, Stothard P, Arun AB (2025) A novel *Kayvirus* species phage RuSa1 removes biofilm and lyses multiple clinical strains of methicillin resistant *Staphylococcus aureus*. *Sci Rep* 15:7358. https://doi.org/10.1038/s41598-025-92032-6

118. Jurado A, Gómez-Cambronero CC, Rodríguez A, Lopez D, García P, Fernández L (2026) Broad-host-range *Kayvirus* phages preferentially infect *Staphylococcoccus aureus* cells with β-glycosylated WTA, the most common bacterial form in the human host. *Int J Antimicrob Agents* 67:107755. https://doi.org/10.1016/j.ijantimicag.2026.107755

119. Hrebík D, Štveráková D, Škubník K, Füzik T, Pantůček R, Plevka P (2019) Structure and genome ejection mechanism of *Staphylococcus aureus* phage P68. *Sci Adv* 5:eaaw7414. https://doi.org/10.1126/sciadv.aaw7414

120. Głowacka-Rutkowska A, Gozdek A, Empel J, Gawor J, Żuchniewicz K, Kozińska A, Dębski J, Gromadka R, Łobocka M (2018) The ability of lytic staphylococcal podovirus vB_SauP_phiAGO1.3 to coexist in equilibrium with its host facilitates the selection of host mutants of attenuated virulence but does not preclude the phage antistaphylococcal activity in a nematode infection model. *Front Microbiol* 9:3227. https://doi.org/10.3389/fmicb.2018.03227

121. Cieniková Z, Nováček J, Šiborová M, Popelářová B, Füzik T, Botka T, Benešík M, Bárdy P, Pantůček R, Plevka P (2026) Genome anchoring, retention, and release by neck proteins of *Staphylococcus* phage 812. *Commun Biol* 9:199. https://doi.org/10.1038/s42003-025-09477-8

122. Bíňovský J, Šiborová M, Zlatohurska M, Nováček J, Bárdy P, Baška R, Škubník K, Botka T, Benešík M, Pantůček R, Tripsianes K, Plevka P (2026) Conformational changes of the baseplate regulating tail contraction of *Staphylococcus* phage 812. *EMBO J* 45:5514–5536. https://doi.org/10.1038/s44318-026-00834-9

123. Apiratwarrasakul S, Sresuwadjarey P, Phumthanakorn N, Withatanung P, Thongdee M, Lerdsittikul V (2025) The broad-spectrum *Kayvirus* phage disrupts biofilms formed by methicillin-resistant *Staphylococcus aureus* and methicillin-resistant *Staphylococcus pseudintermedius*. *Virology* 611:110657. https://doi.org/10.1016/j.virol.2025.110657

124. Łobocka M, Hejnowicz MS, Dąbrowski K, Gozdek A, Kosakowski J, Witkowska M, Ulatowska MI, Weber-Dąbrowska B, Kwiatek M, Parasion S, Gawor J, Kosowska H, Głowacka A (2012) Genomics of staphylococcal Twort-like phages--potential therapeutics of the post-antibiotic era. *Adv Virus Res* 83:143–216. https://doi.org/10.1016/B978-0-12-394438-2.00005-0

125. Gu J, Liu X, Yang M, Li Y, Sun C, Lu R, Song J, Zhang Q, Lei L, Feng X, Du C, Yu H, Yang Y, Han W (2013) Genomic characterization of lytic *Staphylococcus aureus* phage GH15: providing new clues to intron shift in phages. *J Gen Virol* 94:906–915. https://doi.org/10.1099/vir.0.049197-0

126. Birkholz EA, Morgan CJ, Laughlin TG, Lau RK, Prichard A, Rangarajan S, Meza GN, Lee J, Armbruster E, Suslov S, Pogliano K, Meyer JR, Villa E, Corbett KD, Pogliano J (2024) An intron endonuclease facilitates interference competition between coinfecting viruses. *Science* 385:105–112. https://doi.org/10.1126/science.adl1356

127. Finstrlová A, Mašlaňová I, Blasdel Reuter BG, Doškař J, Götz F, Pantůček R (2022) Global transcriptomic analysis of bacteriophage-host interactions between a *Kayvirus* therapeutic phage and *Staphylococcus aureus*. *Microbiol Spectr* 10:e0012322. https://doi.org/10.1128/spectrum.00123-22

128. Azam AH, Hoshiga F, Takeuchi I, Miyanaga K, Tanji Y (2018) Analysis of phage resistance in *Staphylococcus aureus* SA003 reveals different binding mechanisms for the closely related Twort-like phages ϕSA012 and ϕSA039. *Appl Microbiol Biotechnol* 102:8963–8977. https://doi.org/10.1007/s00253-018-9269-x

129. Nováček J, Šiborová M, Benešík M, Pantůček R, Doškař J, Plevka P (2016) Structure and genome release of Twort-like *Myoviridae* phage with a double-layered baseplate. *Proc Natl Acad Sci U S A* 113:9351–9356. https://doi.org/10.1073/pnas.1605883113

130. Šimečková H, Bárdy P, Kuntová L, Macháčová E, Botka T, Bíňovský J, Houser J, Farka Z, Plevka P, Pantůček R, Mašlaňová I (2025) CRISPR-Cas10-assisted structural modification of staphylococcal *Kayvirus* for imaging and biosensing applications. *ACS Synth Biol* 14:2979–2986. https://doi.org/10.1021/acssynbio.5c00387

131. Komárková M, Benešík M, Procházková T, Vinco A, Laichmanová M, Smetanová S, Jelínek P, Moša M, Botka T, Šoóš M, Pantůček R (2025) Compatibility of antimicrobial preservatives with therapeutic bacteriophages of the genera *Pbunavirus* and *Kayvirus*. *Eur J Pharm Biopharm* 214:114781. https://doi.org/10.1016/j.ejpb.2025.114781

132. Ryan EM, Alkawareek MY, Donnelly RF, Gilmore BF (2012) Synergistic phage-antibiotic combinations for the control of *Escherichia coli* biofilms *in vitro*. *FEMS Immunol Med Microbiol* 65:395–398. https://doi.org/10.1111/j.1574-695X.2012.00977.x

133. Oechslin F, Piccardi P, Mancini S, Gabard J, Moreillon P, Entenza JM, Resch G, Que Y-A (2017) Synergistic interaction between phage therapy and antibiotics clears *Pseudomonas aeruginosa* infection in endocarditis and reduces virulence. *J Infect Dis* 215:703–712. https://doi.org/10.1093/infdis/jiw632

134. Morris TC, Reyneke B, Khan S, Khan W (2025) Phage-antibiotic synergy to combat multidrug resistant strains of Gram-negative ESKAPE pathogens. *Sci Rep* 15:17235. https://doi.org/10.1038/s41598-025-01489-y

135. Kaur S, Harjai K, Chhibber S (2012) Methicillin-resistant *Staphylococcus aureus* phage plaque size enhancement using sublethal concentrations of antibiotics. *Appl Environ Microbiol* 78:8227–8233. https://doi.org/10.1128/AEM.02371-12

136. Kim M, Jo Y, Hwang YJ, Hong HW, Hong SS, Park K, Myung H (2018) Phage-antibiotic synergy via delayed lysis. *Appl Environ Microbiol* 84:e02085-18. https://doi.org/10.1128/AEM.02085-18

137. Zhang Q-G, Buckling A (2012) Phages limit the evolution of bacterial antibiotic resistance in experimental microcosms. *Evol Appl* 5:575–582. https://doi.org/10.1111/j.1752-4571.2011.00236.x

138. Dickey J, Perrot V (2019) Adjunct phage treatment enhances the effectiveness of low antibiotic concentration against *Staphylococcus aureus* biofilms *in vitro*. *PloS One* 14:e0209390. https://doi.org/10.1371/journal.pone.0209390

139. Vacek L, Polaštík Kleknerová D, Lipový B, Holoubek J, Matysková D, Černá E, Brtníková J, Jeklová E, Kobzová Š, Janda L, Lišková L, Diabelko D, Botka T, Pantůček R, Růžička F, Vojtová L (2024) Phage therapy combined with Gum Karaya injectable hydrogels for treatment of methicillin-resistant *Staphylococcus aureus* deep wound infection in a porcine model. *Int J Pharm* 660:124348. https://doi.org/10.1016/j.ijpharm.2024.124348

140. Komárková M, Kučerová E, Siváková A, Botka T (2025) Stabilní směs terapeutických bakteriofágů rodu *Kayvirus* a antibiotik účinných proti *Staphylococcus aureus* ve sprejových aplikátorech [Stable mixture of therapeutic bacteriophages of the *Kayvirus* genus and antibiotics effective against *Staphylococcus aureus* in spray applicators]. Functional sample NU21J-05-00035_Gfunk01, assignees: *Masaryk University*. https://is.muni.cz/publication/2537302/Gfunk_NU21J_05_00035.pdf

141. Chung KM, Nang SC, Tang SS (2023) The safety of bacteriophages in treatment of diseases caused by multidrug-resistant bacteria. *Pharmaceuticals* 16:1347. https://doi.org/10.3390/ph16101347

142. Hurley JC (1992) Antibiotic-induced release of endotoxin: a reappraisal. *Clin Infect Dis* 15:840–854. https://doi.org/10.1093/clind/15.5.840

143. Xu L, Liang L, Yuan L, Yao Y, Hua X, Feng Y (2025) A phage transcription factor displaces the host σ factor and stabilizes its own σ factor. *Nucleic Acids Res* 53:gkaf683. https://doi.org/10.1093/nar/gkaf683

144. Gerovac M, Chihara K, Wicke L, Böttcher B, Lavigne R, Vogel J (2024) Phage proteins target and co-opt host ribosomes immediately upon infection. *Nat Microbiol* 9:787–800. https://doi.org/10.1038/s41564-024-01616-x

145. Hietala V, Horsma-Heikkinen J, Carron A, Skurnik M, Kiljunen S (2019) The removal of endo- and enterotoxins from bacteriophage preparations. *Front Microbiol* 10:1674. https://doi.org/10.3389/fmicb.2019.01674

146. Goerke C, Köller J, Wolz C (2006) Ciprofloxacin and trimethoprim cause phage induction and virulence modulation in *Staphylococcus aureus*. *Antimicrob Agents Chemother* 50:171–177. https://doi.org/10.1128/AAC.50.1.171-177.2006

147. Roszak M, Dołęgowska B, Cecerska-Heryć E, Serwin N, Jabłońska J, Grygorcewicz B (2022) Bacteriophage-ciprofloxacin combination effectiveness depends on *Staphylococcus aureus-Candida albicans* dual-species communities' growth model. *Microb Drug Resist* 28:613–622. https://doi.org/10.1089/mdr.2021.0324

148. Hong Q, Chang RYK, Assafiri O, Morales S, Chan H-K (2024) Optimizing *in vitro* phage-ciprofloxacin combination formulation for respiratory therapy of multi-drug resistant *Pseudomonas aeruginosa* infections. *Int J Pharm* 652:123853. https://doi.org/10.1016/j.ijpharm.2024.123853

149. Moša M, Benešík M, Botka T, Figallová E (2026) Směs fágů a ciprofloxacinu působící synergicky proti bakteriím *S. aureus* a *P. aeruginosa* zaměřená na léčbu respiračních onemocnění a jiné bakteriální infekce [A synergistic combination of phages and ciprofloxacin against *S. aureus* and *P. aeruginosa*, designed for the treatment of respiratory diseases and other bacterial infections]. CZ Utility Model 39377, assignees: *MB PHARMA s.r.o. and Masaryk University*. https://isdv.upv.gov.cz/webapp/resdb.print_detail.det?pspis=PUV/43931

7 APPENDICES

This section comprises the author's publications that constitute this habilitation thesis. All publications are used under the Open Access policy terms or with the publisher's permission.

APPENDIX 1

Pantůček R, Doškař J, Boštík J, Kocourková D, Petrzik K, Koptíková J, Benešík M, Plevka P, Füzik T, Mašlaňová I, Botka T, Nepeřený J, Zeller D, Kuntová L, Snopková K, Hrala M, Chumchalová J, Holý D, Moša M (2026) Past and present phage therapy research and practice in the Czech Republic – contribution to phage therapy in Europe. *Virology Journal*. https://doi.org/10.1186/s12985-026-03296-x

(JCR 2025: IF = 4.0; Q1 – Virology)

CC BY 4.0

Virology Journal

REVIEW | Article in Press

Past and present phage therapy research and practice in the Czech Republic – contribution to phage therapy in Europe

Roman Pantůček · Jiří Doškař · Josef Boštík · Dana Kocourková · Karel Petrzik · Jana Koptíková · Martin Benešík · Pavel Plevka · Tibor Füzik · Ivana Mašlaňová · Tibor Botka · Jiří Nepeřený · Daniel Zeller · Lucie Kuntová · Kateřina Snopková · Matěj Hrala · Marek Moša

Received: 20 April 2026 / Accepted: 29 August 2026
© The Author(s) 2026

Abstract

Renewed interest in bacteriophage therapy, driven by the global rise of antimicrobial resistance, is accelerating efforts to establish its rational, evidence-based use in clinical practice. This review provides a comprehensive overview of the historical milestones, current status, and potential of phage applications in the Czech Republic. We show that the country has built on a long tradition of phage therapy, integrating academic research, industrial capabilities, and clinical practice. Since 2000, more than 30 competitively funded projects have addressed key challenges in phage safety, genomic characterization, formulation, delivery, phage-antibiotic synergy, and GMP-compliant manufacturing. Clinical translation is advancing through named-patient basis treatments and the ongoing trials. Beyond human medicine, phage applications have also been explored in veterinary medicine, food safety, and agriculture. Overall, the evidence reviewed indicates that the country has established substantial expertise and infrastructure for phage research and implementation, positioning it as an important European contributor to the development of phage therapy. In a concluding discussion, this review identifies key priorities for sustainable access to phage preparations and the broader integration of phage-based interventions into healthcare systems within the rapidly evolving European regulatory framework.

This Article in Press is shared early to give you faster access to new research. It is citable and carries a permanent DOI. The final edited version will replace it automatically.

Roman Pantůček and Jiří Doškař contributed equally to this work as co-first authors.

Graphical abstract

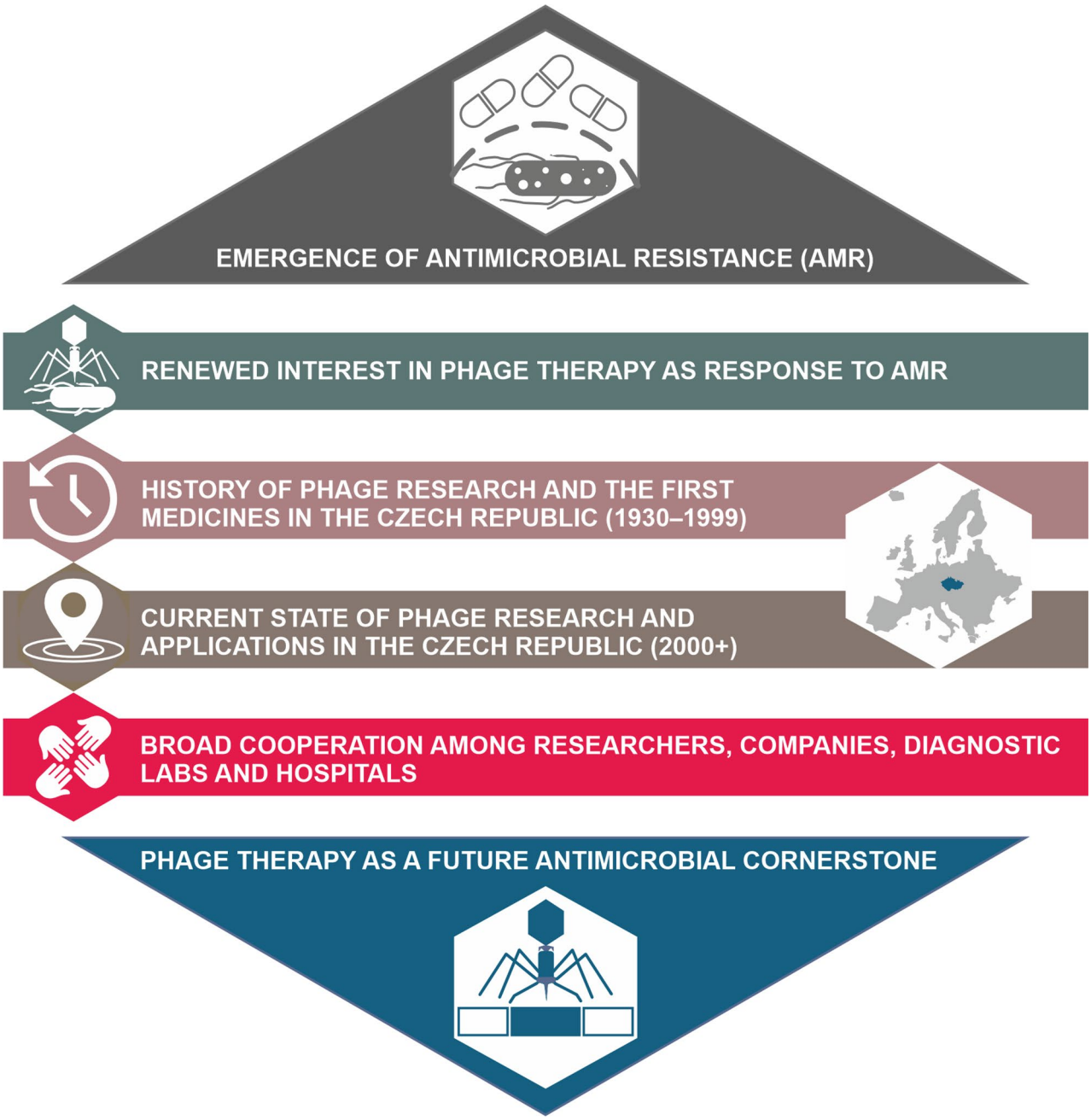

Keywords Phage therapy · Bacteriophage · Non-traditional antibacterial therapies · Stafal · Biocontrol · Enzybiotics · Staphylococcal infections · Osteomyelitis · Kayvirus · Plant pathogenic bacteria

Introduction

The growing antimicrobial resistance of most bacterial pathogens to currently available antibiotics is one of the most critical global health challenges [1]. The development of new antibiotic classes is both time-intensive and economically demanding, and no novel classes have been introduced in recent years. Consequently, alternative

therapeutic strategies are urgently needed to either replace or complement conventional antibiotics. Among these non-traditional approaches, phage therapy stands out as a promising option [2].

In the early 20th century, the concept of phage therapy was widely regarded as hopeful; however, after the discovery and widespread introduction of antibiotics, phage production and clinical use declined in most Western countries, while they continued to develop in the former Soviet Union and post-Soviet countries [3]. Modern clinical phage applications in Western Europe reemerged in the early 2000s primarily through personalized compassionate-use treatments [4], in collaboration with established phage therapy centers in Georgia [5] and Poland [6]. A multidisciplinary network of European experts has since been actively shaping scientific discourse and infrastructure development, formulating recommendations to overcome regulatory and formulation challenges and facilitate clinical implementation [7–10]. The first randomized controlled trials were launched, marking a transition from case reports to structured evaluation [4, 11]. This was followed by regulatory progress, most notably in Belgium, where the implementation of a magistral preparation framework enabled patient-specific phage formulations with pharmaceutical oversight [12]. Partial failures of large randomized trials, such as PhagoBurn and studies targeting urinary tract infections, highlighted the need for optimized trial design, appropriate phage selection, dosing strategies, and quality control [13–15]. In contrast, personalized bacteriophage therapy has demonstrated promising clinical outcomes in retrospective analyses of difficult-to-treat infections, with clinical improvement and bacterial eradication in nearly two-thirds of cases, and enhanced bacteriophage efficacy when combined with antibiotics [16].

Importantly, the European Society of Clinical Microbiology and Infectious Diseases (ESCMID) Study Group for Non-Traditional Antibacterial Therapy (ESGNTA) has emerged, bringing together clinicians, microbiologists, and phage researchers across Europe. The group develops microbiological guidelines, supports clinical trials, promotes research on phage-derived enzymes, and encourages the establishment of academic phage therapy centers [17, 18]. National phage therapy programs are being introduced into academic medical centers, thereby accelerating case-based treatment under compassionate-use or personalized protocols. Recent major initiatives include the Phage Therapy Unit (PTU) at the Hirszfeld Institute of Immunology and Experimental Therapy in Poland - the first dedicated center in the EU [19], the Belgian BT Consortium [16], Phage4Cure in Germany [20], the PHAGEinLYON clinical program [21], the Lausanne University Hospital through the PhageEU Coalition [22], the Becky Mayer Centre for Phage Research at the University of Leicester [23], and Portugal also adheres to the highest clinical and quality standards and has implemented a framework for the hospital use of bacteriophages [24]. These centers are intensively developing clinical infrastructure and research hubs, often using standardized personalized phage cocktails, optimizing formulations, and establishing phage biobanks [25]. In parallel, commercial engagement has expanded rapidly, with dozens of biotechnology companies developing phage-based therapeutics, diagnostics, and production technologies, including advanced Good Manufacturing Practice (GMP)-compliant phage production. The European Pharmacopoeia Commission has approved a general chapter of the European Pharmacopoeia (Ph. Eur.) on bacteriophages, effective from 2025, establishing an official regulatory framework that enables controlled clinical application and facilitates future marketing authorization in accordance with national regulations [26]. Rapid progress in molecular technologies, including omics-based phage characterization [27] and the integration of artificial intelligence (AI) into phage selection or design [28], is increasingly helping to overcome long-standing technical challenges and bringing phage therapy closer to routine clinical implementation.

In response to the global challenge of antimicrobial resistance, interest in bacteriophage therapy has resurged, driving a wide range of research initiatives in the Czech Republic as well. This review traces the historical development of phage therapy in the Czech Republic (part of former Czechoslovakia) and addresses current challenges related to safety, efficacy, and practical implementation. It summarizes data on past and present research projects spanning clinical, veterinary, and technological domains, conducted across academic institutions and commercial initiatives recorded to 2025 (Fig. 1). The literature and historical record search was performed by a multidisciplinary team of authors with complementary expertise in phage research, medical and biotechnological applications, providing a rigorous and balanced assessment of the available sources.

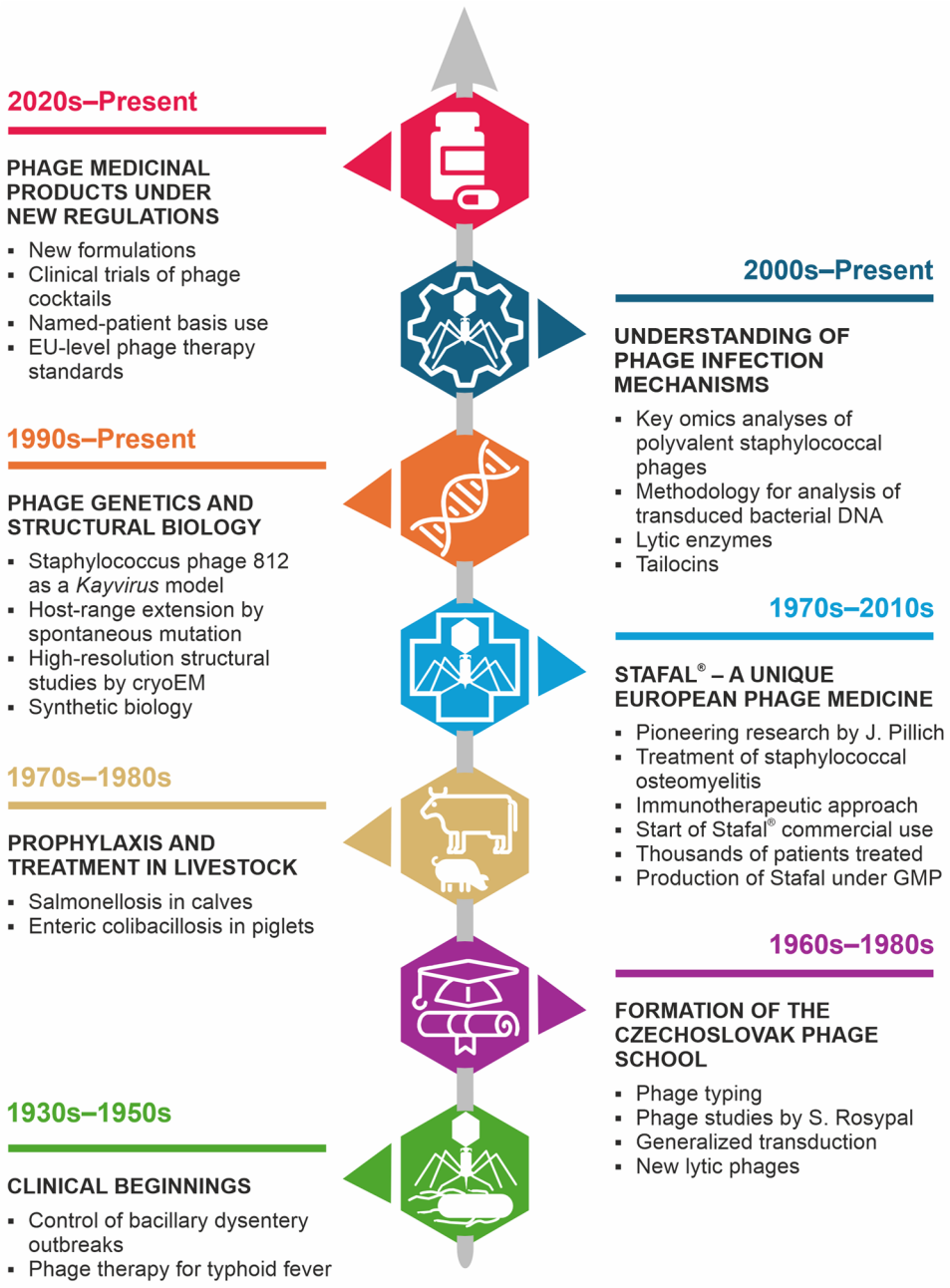

Fig. 1 Timeline of key milestones in therapeutic bacteriophage research in Czechoslovakia and the Czech Republic

Early research in Czechoslovakia (1930 –1950 s)

In Czechoslovakia, the first attempts at phage therapy began before World War II. The early experiments closely reflected contemporary Soviet research that explored the therapeutic potential of bacteriophages. At the National Institute of Public Health in Prague, František Vaníček, Ludmila Mlčochová and Karel Raška were among the pioneers who, in the 1930s, developed a bacteriophage preparation intended for the treatment of bacillary dysentery. Raška [29] documented the effective therapeutic and, in particular, prophylactic use of a strain-specific bacteriophage to control a large outbreak of bacillary dysentery in an industrial workforce that affected several thousand employees over several weeks, where conventional hygienic measures and available chemotherapeutics had failed. At the end of the war, during a severe dysentery outbreak in Terezín Concentration Camp, which

affected both the ghetto and the Small Fortress, and was associated with a mortality rate of 20–40%, a total of 916 L of bacteriophage lysate were dispatched to control the epidemic [30]. Between 1943 and 1946, in collaboration with Ludvík Hloucal, the team also produced a phage preparation directed against typhoid fever [31].

These fundamentals of phage therapy proved critical during the postwar period, most notably in a prolonged dysentery outbreak in a children's home in 1958 in the former Czechoslovakia. Procházka [32] reported the successful application of a specific *Shigella sonnei* phage for prophylaxis and therapy, which terminated an epidemic that had persisted for more than 12 weeks and was resistant to sulfonamides and multiple antibiotics, achieving full control within five days. Their study provides early clinical evidence that well-prepared, strain-specific monovalent bacteriophages, formulated as coated tablets and administered after gastric neutralization with sodium bicarbonate 30 min prior to dosing, can achieve high therapeutic efficacy. Phage preparations were produced in cooperation with the Institute of Epidemiology and Microbiology of the National Institute of Public Health in Prague and were used mainly as part of anti-epidemic measures [30], unlike in Poland and Georgia, where the phage treatment became a standalone clinical program.

Since the 1960s, knowledge of bacteriophage biology has expanded primarily through their wide use in phage typing, particularly in staphylococci. New staphylococcal lytic bacteriophages belonging to the current subfamily *Twortvirinae* were isolated, and their activity was studied not only against *S. aureus*, but also other staphylococcal species [33–36].

Formation of the Czechoslovak Phage School during the 1960–1990 s

Jiří Pillich

At the end of the 1960s, the Institute of Biophysics of the Czechoslovak Academy of Sciences in Brno initiated the development of bacteriophage-based therapeutic preparations under the leadership of Dr. Jiří Pillich [37]. His work was primarily focused on the treatment of staphylococcal infections with lytic bacteriophage preparations based on bacteriophage 131 [38], currently classified to the *Kayvirus* genus (family *Herelleviridae*), which includes phage strains referred to as polyvalent, exhibiting lytic activity against a wide range of *S. aureus* strains and even other *Staphylococcus* spp [39, 40]. Pillich collaborated closely with clinicians across Czechoslovakia and regularly disseminated findings on these preparations at conferences. Several case reports have shown favorable outcomes with these treatment procedures for managing chronic infections, particularly osteomyelitis, when staphylococcal phage lysate was administered locally to accessible wound sites and simultaneously to potential reservoirs of infectious agents, such as the nasopharynx [41–44]. The authors reported good experience with the sequential administration of phage after antibiotic treatment (oxacillin, gentamicin, lincomycin) and consider prolonged antibiotic treatment to be contraindicated [45].

During the 1980s, Pillich expanded his research toward immunological applications of phage-derived preparations and developed the anti-staphylococcal vaccine Stava for parenteral administration, prepared with bacteriophages [46]. Their approach was inspired by the clinically validated Staphage Lysate (SPL), used to treat staphylococcal infections [47], although research at the time focused primarily on therapeutic outcomes rather than on elucidating the underlying mechanisms of action. Pillich also worked on preparing phage lysates from clinical strains *of Pseudomonas aeruginosa* for use as immunological agents [48].

In the 1990s, Pillich initiated an international collaboration with John C. Balcarek and Immunology Laboratories Inc. (USA) and developed innovative methods for preparing protein-based vaccines using bacteriophages [49]. A branch of the Immunology Laboratories was subsequently established in Brno; however, after both Pillich and Balcarek passed away, the research was never commercialized. Their idea of integrating phage technology with basic immunological mechanisms, in which bacterial components generated by phage lytic activity play a significant role, remains relevant although largely unexplored [50].

Stafal® – the only registered phage product in the era preceding EU-wide pharmaceutical regulations

Stafal® is the best-known Czech phage-based product for the treatment of *S. aureus* infections, and the most prominent outcome of Pillich's work [51]. Initially produced at laboratory scale in the Institute of Biophysics in Brno, manufacturing was transferred in 1983 to pharmaceutical conditions at the Institute of Serums and Vaccines (ÚSOL) in Prague. The product was formulated as an unpurified phage lysate produced on synthetic medium. The same year, the Czech "Commission for New Drugs" approved its clinical testing. In an initial trial of chronic and post-traumatic osteomyelitis, Stafal® treatment was well tolerated and resulted in complete recovery in 50% of patients and clinical improvement in the remaining ones [52].

Following these early studies Stafal® was used for a broad spectrum of staphylococcal infections, including chronic and/or recurrent infections in otorhinolaryngology (rhinitis chronica, pharyngitic chronica, recurrent furunculosis of the nose, and otitis media) [53–55], skin and soft-tissue infections [56] and infection complications of underlying diseases such as chronic venous insufficiency and diabetes mellitus, demonstrating high healing rates and rapid improvement in diabetic patients suffering from foot ulcers, as well as effective eradication of methicillin-resistant *S. aureus* (MRSA) carriage [57]. The economic benefits of Stafal® in the treatment of skin and soft tissue infections were analyzed by Jarčuška [58], who concluded that Stafal® treatment is more cost-effective than treatment with commonly used antibiotics and reduces the duration of antibiotic treatment.

Stafal® was officially registered by the Czech State Institute for Drug Control (SÚKL) in 1989 for topical application in laboratory-confirmed staphylococcal infections. In 1994, joint-stock company SEVAC was established as the successor to ÚSOL and continued production for both therapeutic and prophylactic indications. During this period, Stafal® was frequently administered together with the antistaphylococcal immunomodulator Stava as part of a combined therapeutic strategy [59–61]. By 1996, a total of 1,189 patients had been treated with this combination therapy, including 632 patients with chronic osteomyelitis (unpublished data from Sevapharma).

Through subsequent privatization, production passed to companies Sevapharma in 1997, then to IMMUNA, and subsequently to IMMUNA CZ and Bohemia Pharmaceuticals. Although manufacturing continued, Czech registration expired in 2008 due to non-renewal by the manufacturer, but the product remains registered in Slovakia (Table 1). EU-wide registration was not achieved due to unmet requirements set by the European Medicines Agency (EMA). Upon expiration, the rights and associated phage and bacterial strains were transferred to the AUMED company.

The in vitro activity of Stafal® was investigated, focusing on currently circulating *S. aureus* strains, demonstrating high effectiveness and a broad host range, with efficacy exceeding 90% depending on the set of strains tested [39, 62–64]. A study on biofilm-forming MRSA strains shows that the preparation can also eradicate biofilms, although achieving a reduction requires phage concentrations roughly ten times higher than those needed for planktonic bacteria [65].

Stafal® represents a significant milestone in the history of phage therapy in Central Europe, demonstrating both the therapeutic potential of bacteriophages and the complex interplay of regulatory hurdles and commercial sustainability under modern pharmaceutical standards, factors that ultimately led to the discontinuation of the

Table 1 Number of Stafal® packages (unit corresponds to 10 ml per package, where specified) produced after its registration as a medicinal product for topical use

Period	Producer	Approx. output	Note
1990–1994	ÚSOL	2,000 units/year	Routine production
1995–1997	SEVAC	3,000 units/year	Czech market
1998–2011	Sevapharma	3,000 units/year	Czech registration expired in 2008, then available for the Slovak market
2011–2013	IMMUNA, then IMMUNA CZ	6,000 units/year	Slovak market, in Czechia available for import under a specific treatment program
2012	IMMUNA CZ	1,500 vials, lyophilized batch	For a clinical trial as part of the registration process
2014–2018	Bohemia Pharmaceuticals	total 13,400 units	Slovak market, GMP production

product. Its discontinuation also reflected reluctance among some physicians to accept clinical indications at a time when antibiotic treatment remained effective, a lack of strong promotion, and insufficient coverage of phage biology and therapeutic applications in recent medical education.

AUMED has recently focused on developing a phage-based topical preparation to reduce *S. aureus* skin colonization associated with atopic dermatitis, in line with current trends in new treatment modalities, to restore skin barrier function and alleviate disease exacerbations [66].

Czech contributions to phage genetics and structural biology

Kayvirus Research: From phage 812 broad host-range mutants to molecular biology supporting the efficacy and safety of phage therapy

Kayviruses are among the most important therapeutic bacteriophages because of their strictly lytic lifestyle, broad activity, high antibacterial efficacy, and long history of clinical and experimental use in antistaphylococcal phage therapy. During the 1980s and 1990s, progress in molecular biology allowed detailed study of interactions between phages, bacterial cells, and the treated host organism. In the Czech Republic, this line of research was led by Prof. Stanislav Rosypal and his team at the Faculty of Science of Masaryk University in Brno. They had conducted systematic studies on polyvalent staphylococcal phages since the 1970s. The subject of interest was phage 812 (genus *Kayvirus*), obtained from the Institute for Experimental Epidemiology in Wernigerode, Germany, a close relative of the reference *Staphylococcus* phage K [67, 68]. Early investigations characterized its genetic features and led to the isolation of numerous spontaneous mutants selected as rare plaques on resistant strains, which expanded its host range [69–71]. Later, they demonstrated that together these mutants can lyse more than 95% of *S. aureus* strains across a broad spectrum of isolates, as well as strains of several additional staphylococcal species [39]. The isolation of spontaneous mutants with an expanded host range represents a distinctive approach in the Czech Republic. It provides a practical alternative to continuous environmental phage isolation, significantly facilitating the updating of therapeutic preparations in which the host spectrum is a key determinant of efficacy [63].

In subsequent years, they aimed to clarify the factors influencing the phage lytic properties, host range, and the nature of host-cell resistance, which resulted in the first description of the molecular-genetic structure of the *Kayvirus* genome [39]. Genome sequencing has clarified the molecular basis of host-range expansion in kayviruses, identifying specific genomic changes (Fig. 2) linked to distinct host-range phenotypes [63] and extending earlier comparative genomic analyses of polyvalent staphylococcal phages of this genus [72]. Among the characterized phage 812 variants, the highly virulent phage 812K1/420 carries a deletion in the endolysin gene, specifically affecting the Ami2 domain [73], and a mutation that leads to a fusion gene, allowing the phage to overcome the Pdp_{Sau} (Abi) defense system [74]. Global transcriptomics of *Kayvirus* infections further clarified phage-host interactions: infection triggers general stress responses in *S. aureus*, does not activate major virulence determinants, and exhibits minimal interaction with resident prophages, all of which support the genetic safety of *Kayvirus* phages for therapeutic purposes [75]. Proteomic studies, conducted using 2-DE SDS-PAGE and MALDI-MS, characterized key structural virion proteins, highlighted the abundance of bacterial Ig-like domain proteins that may influence adhesion to the host, penetration and immunogenicity, and identified possible post-translational modifications of some structural proteins, as documented by spot train patterns [76].

From phage structure to therapy: Mechanistic insights enabling clinical translation

Tailed bacteriophages in the order *Caudovirales* provide a convenient platform for linking molecular architecture to therapeutic function, and advances in structural biology enable rational phage design. Structural analyses have shown that tailed phages share a conserved virion organization: an icosahedral capsid built from HK97-like major

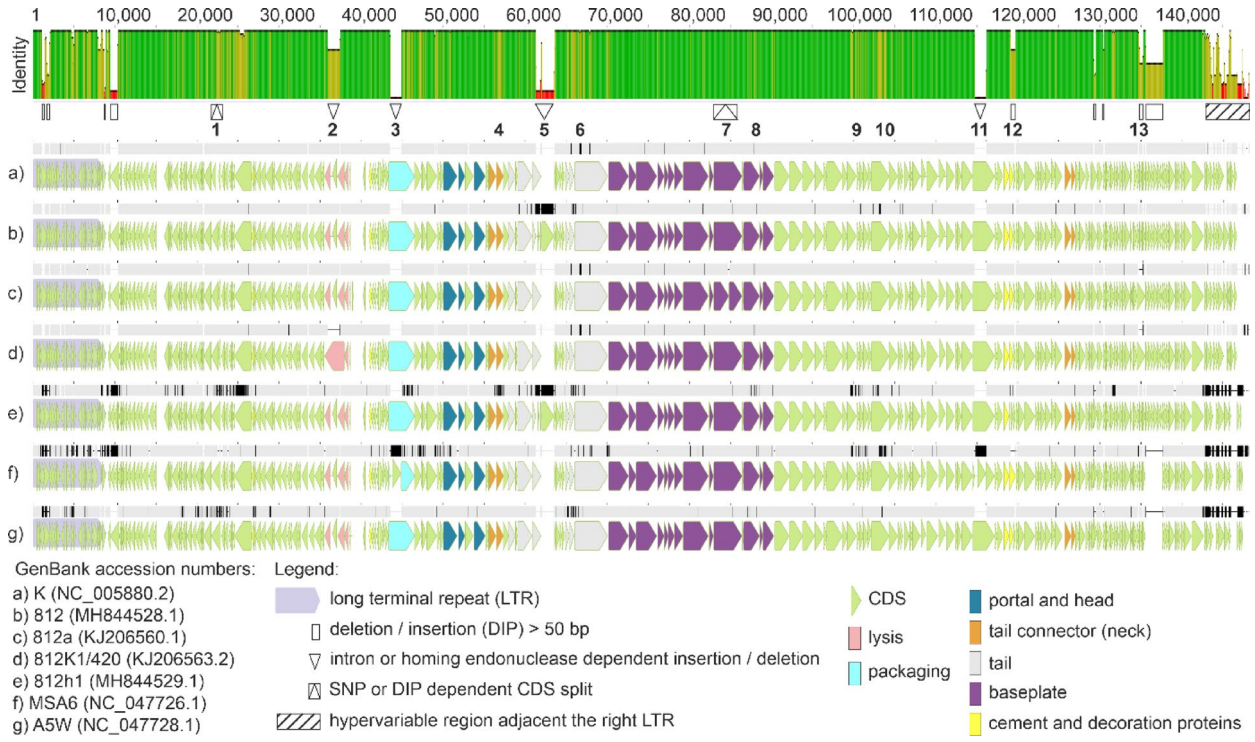

Fig. 2 Multiple alignment of genomic sequences of kayviruses K, 812, 812a, 812K1/420, 812h1, MSA6, and A5W. The graph shows 100% identity in green, identity between 100% and 30% in greenish-brown, and identity below 30% in red. Regions identical to the consensus are shown in light grey, while regions of disagreement are shown in black. The Mauve plug-in in Geneious Prime 2026.0.2 (https://www.geneious.com) was used for the alignment and visualization. The major variations are found in genes encoding the following proteins: (1) ATPase, (2) endolysin, (3) large terminase, (4) stopper protein, (5) tail tube protein, (6) tape measure protein, (7) tripod protein, (8) receptor binding protein, (9) DNA primase, (10) ribonucleotide reductase, 11) RecA recombinase, 12) Ig-like domain protein, and 13) gene fusion, which enables overcoming the Pdp_{Sau} anti-phage system

capsid proteins that package the dsDNA genome, a dodecameric portal complex, and a neck that mechanically couples the head to the tail [77]. The tail forms a specialized genome-delivery apparatus whose morphology underlies the classical division into contractile myophages, long-tailed siphophages, and short-tailed podophages (Fig. 3). Across these phage groups, due to horizontal gene transfer, modular genome sequences encoding baseplate-mediated receptor-binding, cell wall penetration, and lytic proteins are exchanged and reused, resulting in diversified infection strategies. Recent works advance the field of phage biology by resolving high-resolution structures using cryo-electron microscopy (cryoEM) and other progressive techniques [78], showing that structural variations translate into distinct receptor specificities, adsorption dynamics, and genome-delivery mechanisms [79–82].

CryoEM of a *Kayvirus* phage strain enabled the first high-resolution reconstruction of the virion and the elucidation of its genome delivery mechanism [79]. The structural data revealed how neck proteins anchor, retain, and release the viral genome [83]. Recent high-resolution studies of the phage 812 virion structure, including baseplate remodeling during adsorption and tail contraction, have produced a detailed atlas of virion proteins and a roadmap for understanding how *Herelleviridae* phages effectively overcome barriers of the Gram-positive cell wall [84]. The growing mechanistic insight into phage architecture and mechanisms of infection thus provides a means for the structure-guided engineering of phage host range, binding avidity, and environmental stability, directly supporting the development of optimized, clinically applicable phage therapeutics. We showed that knowledge of virion component structure enables the rational engineering of *Kayvirus* particles, as demonstrated by CRISPR-Cas10-assisted insertion of a polyhistidine tag into the tail sheath protein of phage 812h1 [85].

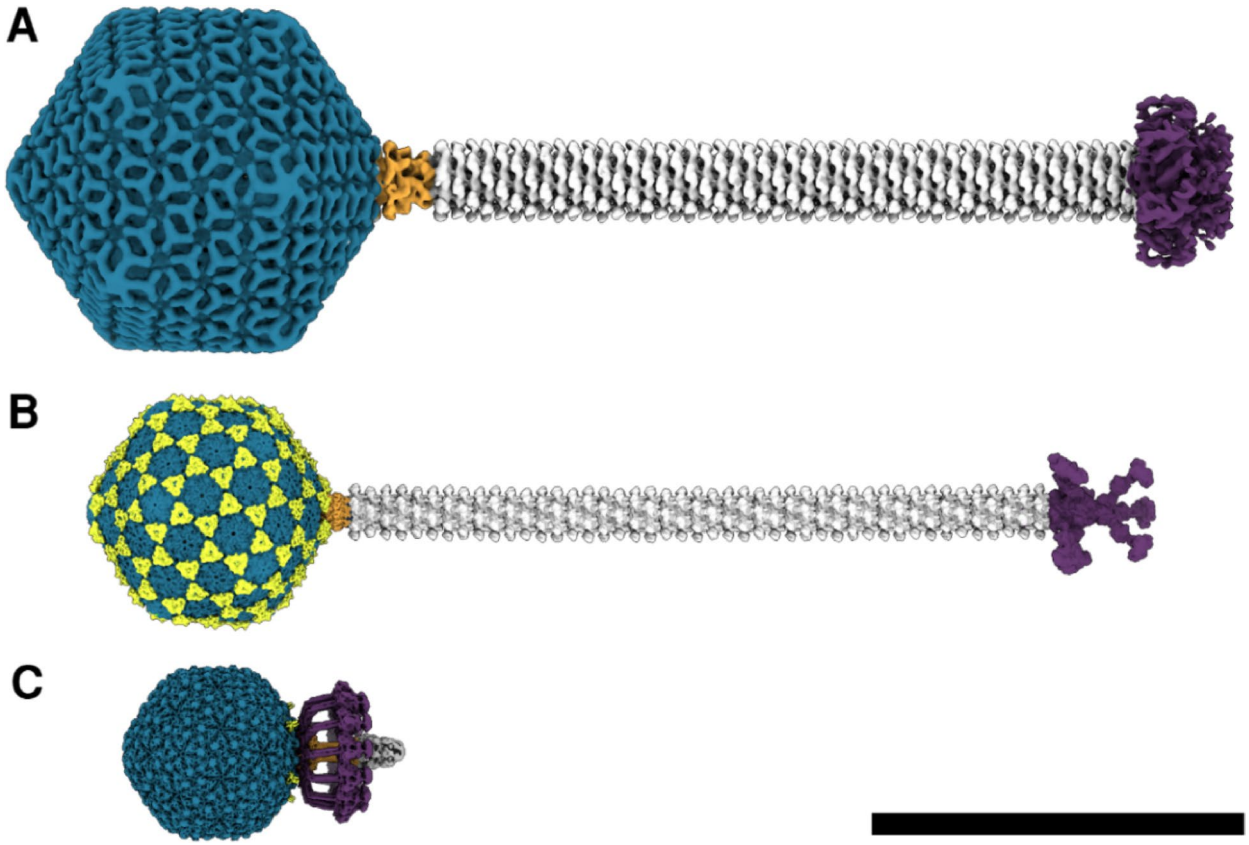

Fig. 3 Isosurface representations of composite cryo-electron microscopy maps of three distinct virion myo-, sipho- and podo-morphotypes, respectively: (**A**) *Staphylococcus* phage 812 (*Kayvirus*); (**B**) *Pseudomonas aeruginosa* phage JBD30 (*Casadabanvirus*); (**C**) *Staphylococcus aureus* phage p68 (*Rosenblumvirus*). The maps are color-coded by the structural features: turquoise - capsid/major capsid proteins; lime - capsid decoration proteins/minor capsid proteins; orange - portal/tail connector proteins; white - tail; grey - tail knob; plum - baseplate/receptor binding proteins. The scale bar represents 100 nm. Following EMDB datasets were used - phi812: EMD-8210, EMD-4051, EMD-8203, and EMD-8218; phiJBD30: EMD-19,439, EMD-19,256, EMD-19,265, EMD-19,264, and EMD-19,267; phi68: EMD-4459

This approach enables site-specific functionalization for imaging, biosensing, and diagnostic applications without impairing phage infectivity, underscoring the potential of structure-guided modifications for versatile phage therapeutics.

Research on horizontal gene transfer in therapeutic staphylococcal phages

Horizontal gene transfer (HGT) mediated by bacteriophages represents a key safety consideration in the production and clinical application of phage preparations [9]. Research on temperate staphylococcal bacteriophages at Masaryk University in Brno began with a strong focus on the mechanisms of plasmid-mediated antibiotic resistance transduction [86]. Subsequent research has focused on the relationships of temperate phages [87] and pointed out the potential for multiple lysogeny [88], which poses an inherent risk of stable integration of prophages into the bacterial chromosome, where they can alter bacterial gene expression and induce lysogenic conversion. At the same time, the classification system and PCR diagnostics for these phages were established [89–91].

In particular, phages and prophages of serological group B (*pac*-type phages) [92] very frequently mediate the generalized transduction of antibiotic-resistance determinants, including plasmid-borne genes such as *blaZ* and *tetK* [93, 94], specialized [95, 96] and lateral transduction [97, 98], and even transduction of large chromosomal

resistance elements of the staphylococcal cassette chromosome *mec* (SCC*mec*) that can be encapsidated, including the methicillin resistance *mecA* gene [99]. Transduction enables the efficient transfer of plasmids within and between *S. aureus* lineages, even between strains insensitive to phage lytic action, as adsorption and genophore delivery are efficient, thereby greatly facilitating the horizontal spread of resistance in natural populations [100].

The development of a qPCR-based approach enabled the reliable detection and quantification of specific resistance and virulence genes encapsidated by staphylococcal siphoviruses, confirming that diverse chromosomal loci, plasmids, staphylococcal pathogenicity islands (SaPIs), SCC*mec*, and other mobile genetic elements can be inadvertently packaged at variable frequencies, especially by serogroup B *pac*-type phages [94]. Recently, long-read nanopore sequencing has enabled single-virion resolution of full-length packaged genophores, thereby enabling the characterization of encapsidated DNA. This sequencing-based approach provided high-resolution insights into the dynamics of a lytic phage and a temperate transducing phage, overcoming the limitations of traditional transduction assays by directly identifying the complete repertoire of mobilizable DNA in *vivo*. In an *S. epidermidis* model carrying a phage-inducible chromosomal island, the *Kayvirus* phage 812h1 strain did not enhance the mobilization of staphylococcal mobile genetic elements relative to antibiotic treatment, providing robust evidence for the genetic safety of phage-based therapeutics [101].

More recently, long-read metagenomics methods have significantly expanded the analytical resolution of the capsid-mediated mobilization of bacterial genomic DNA in complex biological samples [102, 103]. Direct, molecularly resolved sequence data demonstrate that the phage-mediated HGT is an active, frequent, and widespread process, indicating ongoing generalized transduction, specialized transduction, lateral transduction, and gene transfer agent-mediated DNA packaging, as well as prophage induction, recombination and integration into phylogenetically distant hosts. Until recently, interactions between bacteriophage strains and their hosts could only be assessed by plaque assays, which detect phages capable of forming visible plaques on a reference host. The Phage Recovery and Investigation in Single-droplet Microenvironments platform, described by Zhang et al. [104], uses droplet microfluidics to encapsulate host bacteria and phages in water-in-oil microdroplets, enabling direct isolation, quantification, and characterization of phages from complex samples. When combined with sequencing, PRISM greatly expands the ability to recover and analyze diverse bacteriophages from environmental sources.

In line with these findings, it is strongly recommended that any use of therapeutic phage preparations should consistently exclude transducing particles, both induced temperate prophages from production strains and lytic phages prone to mispackaging, since even low levels of transduction-competent virions pose a significant biological risk by potentially spreading virulence or antibiotic resistance genes or serve as platforms for further recombination events, potentially leading to the emergence of new mosaic phages with altered genetic content. PCR techniques, sequencing and droplet microfluidics methodological advances, provide an essential toolkit for the pre-clinical screening of therapeutic phage preparations (Fig. 4), enabling rigorous detection and exclusion of transducing phages.

Applied research and development driving phage therapy implementation in the Czech Republic

Recent phage therapy research in the Czech Republic reflects a multidisciplinary approach that integrates clinical, veterinary, and technological perspectives, building on a long-standing historical tradition of bacteriophage research and therapeutic applications. Comprehensive research conducted over the past 20 years has enabled the development and implementation of phage-based products across multiple fields (Fig. 5). Since 2000, more than 30 projects across academic, clinical, and industrial institutions have been implemented in the Czech Republic with a total funding of approximately €19 million (https://starfos.tacr.cz) from several national grant agencies, primarily the Technology Agency of the Czech Republic, the Ministry of Industry, the Ministry of Health, and the National Agency for Agricultural Research. These initiatives encompass a wide range of applications, from preclinical models to infection control and livestock health, leveraging the adaptability of phage-based technologies (Table 2). Importantly, these sustained efforts strengthen the national readiness for emerging European regulatory

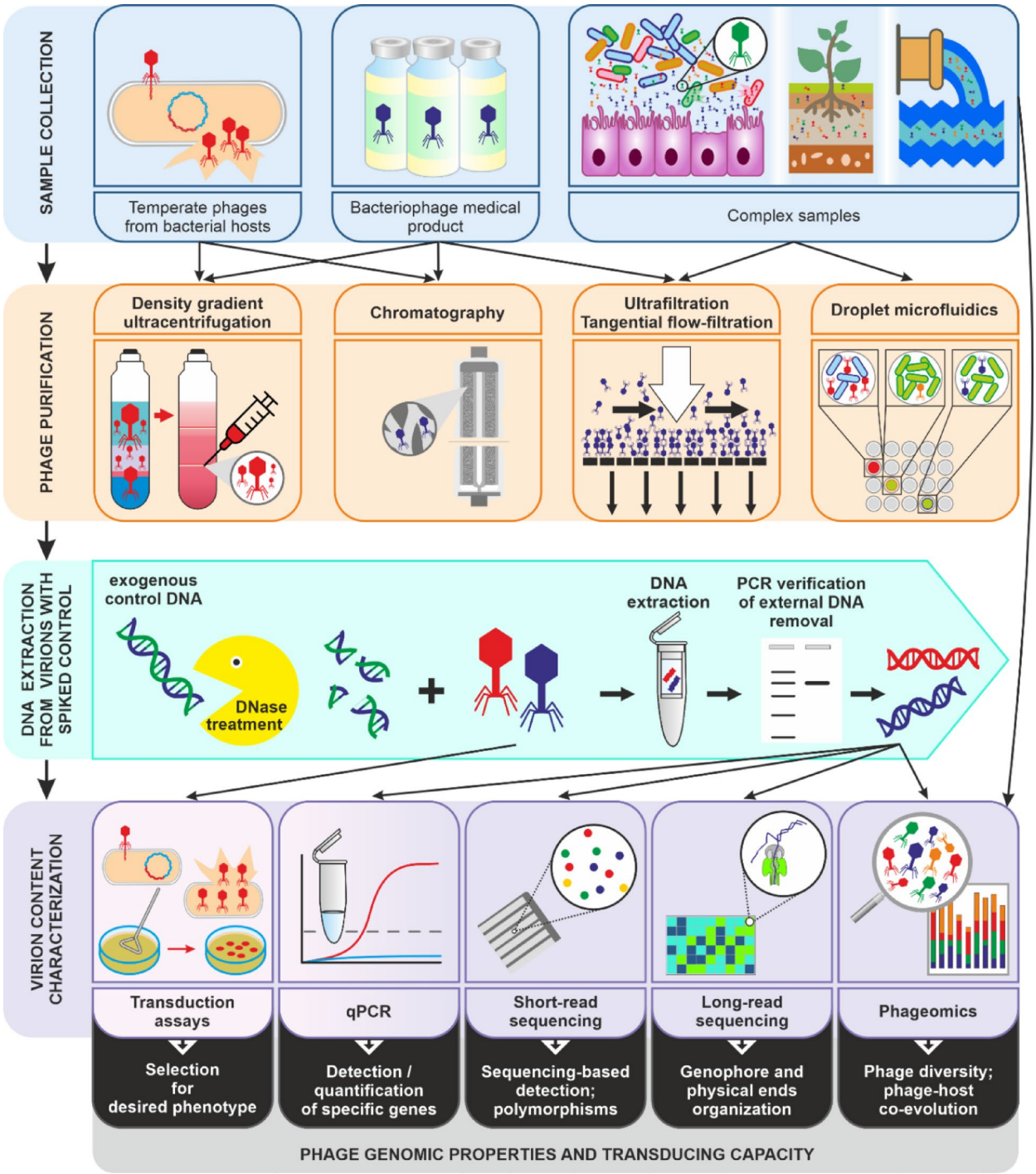

Fig. 4 Standardized workflow for evaluating the genetic safety of phage therapeutics, integrating phage sample collection and purification, enzymatic bacterial host DNA depletion from phage samples, and a wide range of analytical methods for assessing the genetic cargo of bacteriophage capsids

frameworks governing bacteriophage-derived medicinal products, ensuring that established infrastructure, expertise, and validated technologies can be rapidly aligned with upcoming legal requirements.

A central component of this progress has been the refinement of modern phage manufacturing pipelines within the general EU regulatory framework for biological medicinal products. Clinical-grade production of

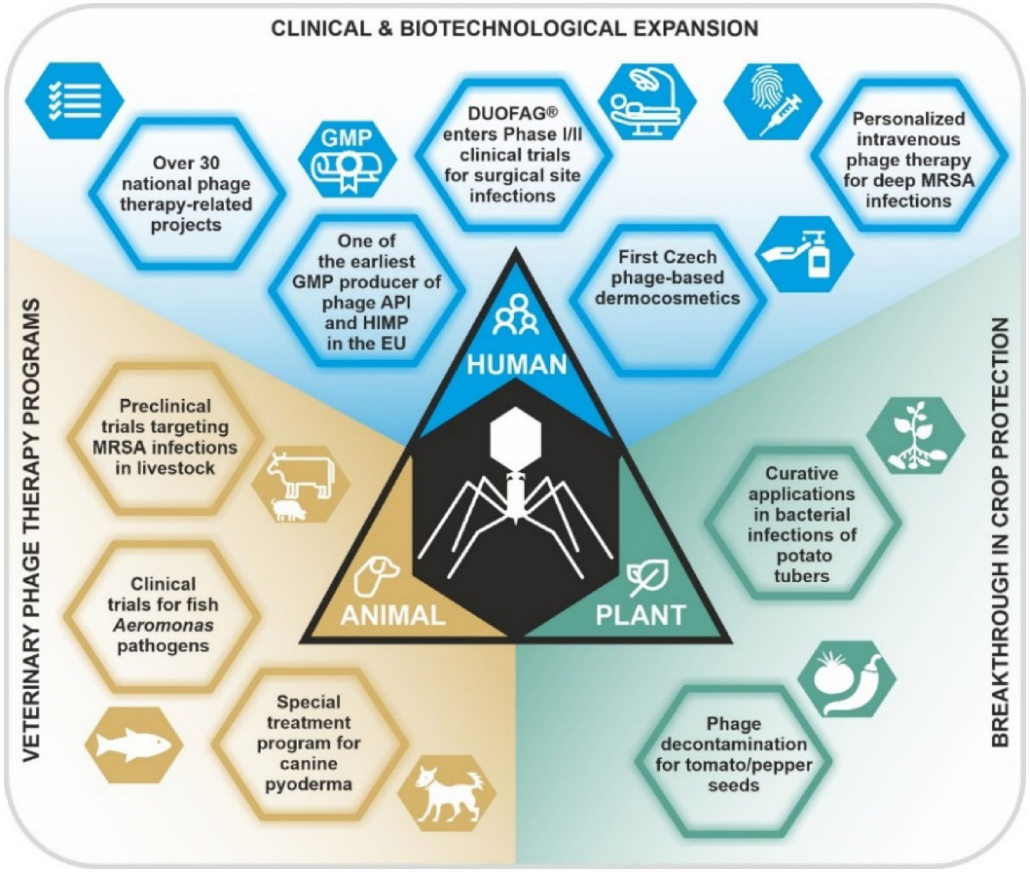

Fig. 5 Main areas of research on bacteriophages and their use in human and veterinary medicine and agriculture in the Czech Republic since the 2000s

phage-based Active Pharmaceutical Ingredients (APIs) and Human Investigational Medicinal products (HIMPs) requires manufacturing in GMP-compliant facilities under appropriate regulatory authorization, accompanied by technical documentation demonstrating their identity, purity, safety, and compliance with Ph. Eur. quality standards. Consistent with these standards, the clinical-grade production of phage APIs is currently supported by facilities like MB PHARMA, which holds the necessary regulatory authorization. Alongside manufacturing activities, Czech companies collaborate with academic research facilities focused on the practical introduction of phage therapy. They are working to isolate new phage variants to reflect the sensitivity of current pathogen samples obtained in cooperation with hospital clinical microbiology departments in the Czech Republic. Their research focuses on the rapid isolation of new phage strains from wastewater, the environment, or the laboratory evolution of their mutants, enabling them to respond flexibly to resistant bacteria. The phage bank of MB PHARMA and FAGOFARMA companies currently includes more than 100 characterized phages targeting *S. aureus*, *P. aeruginosa*, *Klebsiella pneumoniae*, *Acinetobacter baumannii*, *Cutibacterium acnes*, and *Aeromonas salmonicida* bacteria (Fig. 6). To routinely identify clinically relevant phages directly from minimally processed samples, a method based on virion protein fingerprints was developed [105].

The primary goal is to translate phage therapies into clinically viable products, which requires collaboration between pharmacists, and highlights the importance of formulation science. A recent study by Komárková et al. [106] systematically evaluated the compatibility of antimicrobial preservatives to ensure the microbiological quality and stability of phages during long-term storage. The freeze-dried tablets they designed containing therapeutic bacteriophages of the genera *Kayvirus* and *Pbunavirus* met Ph. Eur. standards and maintained high phage titers, with superior stability compared to liquid formulations [107]. Growing interest in advanced delivery

Table 2 Overview of selected phage therapy projects and applications in the Czech Republic that have been implemented in the last five years

Area / Topic	Investigators	Target Pathogens	Formulation / Delivery	Status / Outcome
Human medical applications				
Bacteriophage therapy for surgical site infections	MB PHARMA, FNUSA	*S. aureus*, *P. aeruginosa*	Liquid formulation, phage cocktail DUOFAG®	Human / Clinical trial
Recurrent bacterial vaginosis	AUMED	*Gardnerella vaginalis*, *S. aureus*, *Streptococcus* spp.	Local phage preparation	In vitro / Ongoing
Inhaled phage therapy	MB PHARMA, MU	*S. aureus*, *P. aeruginosa*	Phage – antibiotic synergy	In vitro, nematode / Utility model
MRSA prevention	FAGOFARMA	*S. aureus*	Phage cocktail, nasal spray	In vitro / Ongoing
Superficial wound infections	MU	*S. aureus*	Antibiotics enhancing phage efficacy	Ex vivo / Utility model
Nosocomial infections	MU, CAS, FNUSA	*S. aureus*, *P. aeruginosa*	Phages + antimicrobial synergy, semisolid hydrogel	In vitro / Utility model
Nosocomial infections	FAGOFARMA, FNO	*S. aureus*, *K. pneumoniae*, *A. baumannii*, *P. aeruginosa*	Phage cocktail against nosocomial infections	In vitro, animal / Prototype, validated technology
Phage sensitivity testing	MB PHARMA, FAGOFARMA	*S. aureus*	Test kit for evaluating phage antimicrobial activity	In vitro / Patent, validated technology
Cosmetics				
Dermocosmetics	MB PHARMA	*S. aureus*, *C. acnes*	Semisolid hydrogel, FAGOCARE®	In vitro, dermatological testing / Commercial product
Skin Spray and Bioactive gel	AUMED Pharma	*S. aureus*, *C. acnes*	Semisolid hydrogel or spray, Phage Glow	In vitro, dermatological testing / Commercial product
Technologies & Carriers and Formulations				
Encapsulation in nanostructures	MB PHARMA, TU Liberec	ESKAPE pathogens	Nanofiber air filter material with phages	In vitro / Prototype, utility model
Nanofiber wound dressings	CTU, UCT, FAGOFARMA	*S. aureus*, *P. aeruginosa*	Soluble nanomaterials	In vitro / Terminated prematurely
Wound dressings	Biolytics	*S. aureus*	Hydrogel wound dressings	In vitro / Prototype
Nanobiotechnologies for diagnostics, biosensors	MU	*S. aureus*	Monoclonal antibodies for detection	In vitro, animal / Utility model
In vivo imaging of phage infection	FAGOFARMA	*S. aureus*	Labeling of bacteria with radiopharmaceuticals	In vitro, animal / Validated technology
Enzybiotics				
Phage endolysins, antistaphylococcal	VRI, FNUSA	*S. aureus*	Recombinant endolysins	In vitro / Validated technology
Phage endolysins for biofilm-associated infections	DYNTEC, CAS, FAGOFARMA	ESKAPE pathogens	Phage + endolysin synergy	In vitro, animal / Patent
Dermocosmetics	FAGOFARMA	*S. aureus*, *C. acnes*	Phage + endolysin synergy, semisolid hydrogel FAGOCARE PLUS®	In vitro / Commercial product
Veterinary applications				
Infections in livestock	Bentley Czech, VRI	*S. aureus*	Topical gel, topical spray	In vitro, animal / Utility model
Infections in fish farming, cattle and bees	MB PHARMA, DYNTEC, FAGOFARMA	*S. aureus*; *A. salmonicida*; *Paenibacillus larvae*	Liquid formulation, phage cocktail FISHPHAG AS, One Health applications	In vitro, animal / Clinical trial
Salmonellosis in livestock	SEVARON	*Salmonella* Typhimurium	Phage-based medicinal product	In vitro, animal / Certified methodology
Canine pyoderma	Bioveta	*S. pseudintermedius*	Phage lysate, liquid	In vitro, animal / Special treatment program
Pyoderma in cats and dogs	BC CAS, CEITEC, LabMediaServis	*S. pseudintermedius*	Phage cocktail, semisolid hydrogel	In vitro, animal / Clinical trial
Poultry diseases	BC CAS, PTACY, LabMediaServis	*E. coli*	Liquid phage cocktail, One Health application	In vitro, animal / Ongoing project

Table 2 (continued)

Area / Topic	Investigators	Target Pathogens	Formulation / Delivery	Status / Outcome
Poultry diseases	VRI	Various bacterial pathogens	Phage cocktail	In vitro, animal / Ongoing project
Agriculture				
Biological protection of potatoes	BC CAS, Potato Res. Inst., VESA, UCT	*Dickeya solani*	Liquid tuber treatment	Field trial / Certified methodology
Biological protection of greenhouse tomatoes	BC CAS	*Pseudomonas syringae*, *Xanthomonas* spp.	Preventive phage cocktails	Field trial / Prototype, patent

BC CAS, Biology Centre of the CAS in České Budějovice; CAS, Czech Academy of Sciences; CEITEC, Central European Institute of Technology; CTU, Czech Technical University in Prague; FNO, University Hospital Ostrava; FNUSA, St. Anne's University Hospital, Brno; MU, Masaryk University; TU Liberec, Technical University Liberec; VRI, Veterinary Research Institute, Brno; UCT, University of Chemistry and Technology, Prague; VESA, Velhartice Potato Breeding; VUTBR, Brno University of Technology

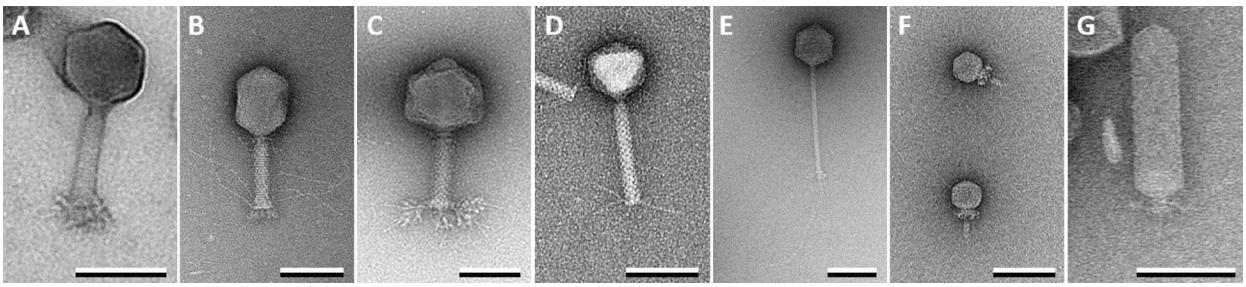

Fig. 6 Micrographs showing extensive structural diversity of lytic bacteriophages with particular emphasis on variation in their tail appendices. Selected phages from the MB PHARMA and FAGOFARMA collections, visualized using transmission electron microscopy. The scale bar represents 100 nm. **A**) Unclassified *Acinetobacter* phage, **B**) *Aeromonas* phage from genus *Tulanevirus*, **C**) *Klebsiella* phage from genus *Alcyoneusvirus*, **D**) *Pseudomonas* phage from genus *Pbunavirus*, **E**) *Klebsiella* phage from genus *Sugarlandvirus*, **F**) *Staphylococcus* phage from genus *Andhravirus*, and **G**) *Aeromonas* phage from genus *Lahexavirus*

approaches to stabilize and protect bacteriophages has accelerated the exploration of nanocarrier-based encapsulation strategies. Recent work has demonstrated that optimally formulated stearylamine-modified niosomes effectively encapsulate bacteriophages, enhancing their stability under harsh pH conditions and improving their antibacterial efficacy [108].

There has been an increase in parallel efforts in collaboration with academic institutions to develop alternative or complementary therapeutic strategies for treating skin and soft tissue infections, particularly through preclinical testing. Multidisciplinary teams have validated an in vivo porcine infection model for testing non-traditional therapeutics [109] and have utilized it to investigate topical bacteriophage delivery systems targeting pathogens such as *S. aureus* and *P. aeruginosa* based on bioactive polysaccharide injectable hydrogels [110]. These studies have been instrumental in establishing clinical evidence supporting phage therapy, determining optimal dosing strategies and assessing the safety profile of staphylococcal and pseudomonal phages, which are central to Czech therapeutic programs [111]. Efforts are focused on characterization and design of active phage proteins, such as endolysins [112]. An integral part of this research is the development of interesting application formulations that combine phages and enzybiotics [113].

The synergistic potential of combining phages and antibiotics has also been investigated, demonstrating a significantly enhanced antimicrobial efficacy [101, 114]. In addition, the possibility of staphylococcal decolonization has been expanded to include a combined use of *Kayvirus* phage 812K1/420 and mupirocin [115]. Although interactions between these agents are predominantly antagonistic, their combination can suppress the emergence

of strains with low-level mupirocin resistance and broaden the spectrum of antimicrobial activity to include strains with high-level mupirocin resistance [115].

Advanced nanobiotechnological methods, such as atomic force microscopy complemented by surface plasmon resonance and a piezoelectric biosensor with dissipation monitoring, have been developed to observe phage lytic activity on planktonic cultures or biofilms in real time [114, 116]. These novel tools, often at single-cell resolution, offer new approaches to characterizing phage potency and assessing phage-antibiotic interactions during their antimicrobial action.

Tailocins as precision phage-related antimicrobials

Tailocins (phage tail-like bacteriocins) are evolutionarily derived remnants of temperate phages that retain the receptor-binding and membrane-penetrating machinery of contractile (R-type) or non-contractile flexible (F-type) phage tails but lack capsids and nucleic acids metabolism genomes [117]. They bind to specific surface receptors on susceptible bacteria and induce rapid cell death through membrane depolarization [118]. Their targeted antibacterial activity has been previously demonstrated across multiple applications, from human-related anti-infective and prophylactic applications to the eradication of a wide range of phytopathogenic bacteria [119]. Tailocins represent a promising class of next-generation antimicrobials with the potential to precisely target specific pathogens by modifying receptor-binding proteins through synthetic biology, utilizing the vast diversity of bacteriophages [120].

Tailocin research in the Czech Republic was pioneered by Jan Šmarda, Sr. at the Faculty of Medicine, Masaryk University, whose work focused on bacteriocins produced by enterobacteria. Investigations of environmental isolates led to the identification of both R-type and F-type particles in *Pragia fontium* and *Budvicia aquatica* [121, 122] with inhibitory effects against selected Enterobacterales, such as *Yersinia enterocolitica* [123]. More recent research has expanded to *Pseudomonas* spp. from Antarctic sampling, enabling the first identification of tailocins from extreme polar environments and revealing their widespread genomic distribution and ecological role in mediating antagonistic interactions between closely related strains [124, 125]. Their antibacterial activity against human multidrug-resistant clinical isolates and phytopathogenic pseudomonads has been systematically evaluated, underscoring their relevance in medical microbiology, agriculture, and environmental contexts [126–128].

Human health-related phage applications

Bacteriophages as next-generation cosmetic actives

Due to the regulatory complexity associated with registering bacteriophage-based medicinal products and concurrent commercial interest in alternative business models, the development of phage-based products in the Czech Republic has shifted partially toward cosmetic applications. At present, two hydrogel-based preparations incorporating bacteriophage components are available on the Czech market. The first comprises bacteriophage-containing dermocosmetic products under the Phage Glow brand (Aumed Pharma), designed specifically for acne-prone and eczematous skin, available as either a polyethylene glycol (PEG)-based bioactive hydrogel or a hydroxyethylcellulose (HEC)-based skin spray. The second product, FAGOCARE® gel (FAGOFARMA), utilizes purified bacteriophages that specifically target *S. aureus* and *C. acnes* and represents a microbiome-oriented cosmetic approach. These cosmetic products exemplify a pragmatic approach to utilizing phage-derived technologies outside the pharmaceutical regulatory framework, while exploiting their antibacterial specificity and microbiome-modulating potential to support healthy skin features.

Regulatory framework and clinical access to bacteriophage therapy in the Czech Republic

Historically approved phage preparations persisted in Czechia and Slovakia as remnants of the pre-EU regulatory era, governed by local legislation. With the harmonization of European rules for medicinal product manufacturing, these older formulations no longer meet current standards. In the Czech Republic, the access of patients to bacteriophage therapy is at present limited to either clinical trials, or a variant of the named-patient scheme (compassionate-use), utilizing an exemption granted by the Ministry of Health of the Czech Republic, in which a pharmacy is permitted to use an active substance without a monograph in the Czech or Ph. Eur. for the magistral preparation of a medicinal product for a specific patient. To ensure the safe and controlled use of non-monograph active substances, an application for the exemption pathway should be supported by a comprehensive risk-assessment dossier.

To facilitate this process, a Ministry of Health working group on bacteriophage therapy – comprising clinicians, pharmacists, manufacturers, the State Institute for Drug Control (SÚKL), patient representatives, and healthcare payers – was established in 2025. This group has drafted and published guidance documents and application templates aiming to streamline the regulatory pathway for clinicians and manufacturers intending to pursue this exemption mechanism. Consequently, development efforts are focusing on optimizing production processes, media formulation, phage purification, and the implementation of robust quality-control methodologies. In the absence of a dedicated regulatory pathway, development follows the standard requirements for quality, safety and efficacy, supported by the European Pharmacopoeia Chaps. 5.31 *Phage Therapy Medicinal Products* and 2.7.38 *Bacteriophage Potency Determination*.

Phage therapy clinical trials under contemporary regulatory standards

Initiatives over the last two years have emphasized the importance of transitioning from experimental phage use to structured preclinical and clinical evaluation, supported by collaborations among academic institutions, hospitals, and biotechnology companies. One illustrative example of this shift is the investigational medicinal product DUOFAG®, a topically administered, defined bacteriophage cocktail developed by MB PHARMA, currently undergoing clinical trials (EUCT ID: 2024-518307-22-01). DUOFAG® comprises *Kayvirus* phages targeting *Staphylococcus* spp. and a *Pbunavirus* phage active against *P. aeruginosa*. DUOFAG® is being evaluated in a Phase IIa trial for safety, tolerability, and preliminary efficacy in the treatment of surgical site infections. An interim safety analysis, following the completion of Cohort I (Phase I), showed a favorable safety profile [129]. As of April 2026, 14 patients have been enrolled in the second cohort (http://www.duofag.cz/). In February 2026, the Czech State Institute for Drug Control authorized a follow-up phase IIb clinical trial of this HIMP (EUCT ID: 2025-522752-45-00).

Another clinically relevant phage therapy initiative involved the participation of the Cystic Fibrosis Center at the Motol University Hospital (Prague) in a multicenter study evaluating the safety and tolerability of BX004-A (developed by BiomX), a three-phage nebulized cocktail (phage genera *Bruynoghevirus*, *Pbunavirus*, and *Pakpunavirus*) targeting *P. aeruginosa* for the treatment of chronic pulmonary infections in patients with cystic fibrosis. The program initially comprised a Phase Ib/IIa trial (ClinicalTrials.gov ID: NCT05010577; Registration Date: 2021-08-11), which showed that inhaled BX004-A was generally safe and well tolerated in adult cystic fibrosis patients, with efficient pulmonary delivery and exploratory evidence of reduced bacterial sputum burden, although definitive efficacy conclusions were limited by small sample size [130]. These encouraging early-phase results supported progression to a Phase IIb multicenter study of HIMP comprising five phage strains (ClinicalTrials.gov ID: NCT06998043; Registration Date: 2025-05-28) designed to evaluate efficacy and safety over an extended dosing period, which was subsequently terminated prematurely due to an unexpectedly high incidence of adverse events. These studies exemplify the application of contemporary clinical research standards to bacteriophage-based therapeutics, reflecting an increasing convergence with conventional drug development pathways, and underscore the safety challenges associated with advanced-stage inhaled phage therapy.

A further example of clinically oriented bacteriophage development in the Czech Republic is TRIOFAG®, a bacteriophage preparation formulated to target bacterial isolates collected from Czech hospitals, particularly from multiple departments of University Hospital Ostrava. TRIOFAG® comprises phages active against *S. aureus* (phage genus *Kayvirus*), *Acinetobacter baumannii* (phage genus *Saclayvirus*, and an unclassified phage), and *Klebsiella pneumoniae* (phage genera *Sugarlandvirus*, *Jiaodavirus*, and an unclassified phage), in a dosage form suitable for respiratory tract bacterial infections. Two *Acinetobacter* bacteriophages together lysed 57% of 71 uncharacterized clinical isolates from two Czech hospitals and 23% of 30 previously described genetically diverse strains [131]. On the other hand, *Klebsiella* phages showed a narrow spectrum, significantly influenced by genetic and capsular heterogeneity, which requires complex phage cocktails tested on well-defined, clinically relevant contemporary strains described in recent epidemiological research [132]. Preclinical safety evaluation of TRIOFAG® in a rat model (late 2024 to early 2025) showed no observable toxicity after repeated daily oral administration (http://www.triofag.cz/).

The first reported case of intravenous phage therapy within a hospital special treatment program

The first published case report describes modern systemic human phage therapy of MRSA spondylodiscitis and demonstrates that individualized intravenous bacteriophage treatment can be safe, feasible, and clinically effective. The case involved a patient with a deep-seated, spinal stabilization implant-associated infection refractory to prolonged antibiotic therapy. A personalized bacteriophage preparation targeting the causative pathogen *S. aureus* (produced by FAGOFARMA) was administered intravenously as part of a hospital-based special treatment program approved in 2024. Administration of a *Kayvirus* bacteriophage (strain DSM 33476) preparation led to sustained remission after the discontinuation of both the phage and antibiotics [133]. Importantly, this first case generated critical safety and feasibility data for future clinical development and provided a practical regulatory and clinical framework for compassionate-use phage therapy, demonstrating successful coordination between clinicians, a GMP-capable manufacturer, and national regulatory authorities.

Veterinary applications

Phage therapy in Czech veterinary medicine has evolved substantially over time, reflecting changing epidemiological and economic priorities. In contrast, current veterinary phage research is increasingly driven by antimicrobial resistance, regulatory constraints on antibiotic use, and One Health considerations. Contemporary priorities include multidrug-resistant pathogens of clinical, economic, and zoonotic significance. A common therapeutic target is *Staphylococcus* spp. in livestock, and the prevention of zoonotic transmission of a specific *S. aureus* ST398 genetic lineage. Emerging research focuses on pathogenic *E. coli* strains affecting poultry, livestock, and pets. In veterinary medicine, phage therapy in the Czech Republic follows the EU regulatory framework for veterinary medicinal products. Routine use requires marketing authorization based on evidence of quality, safety and efficacy. When no suitable authorized veterinary medicinal product is available, Czech legislation also permits the use of unregistered phage preparations through an approved veterinary special treatment programme authorized by the Institute for State Control of Veterinary Biologicals and Medicines (ÚSKVBL).

Early veterinary applications of phage therapy

In the 1960–1980 s, bacteriophages were primarily explored as cost-effective tools for farm-level prophylaxis and the treatment of infections that caused significant economic losses in intensive livestock production, emphasizing practical feasibility, reduced mortality, and improved production performance. One of the first systematic field evaluations of bacteriophage therapy in veterinary medicine was conducted in a discontinued *Salmonella* bacteriophage preparation, historically referred to as Bacteriophage STM (Bioveta), designed for the prevention and control of salmonellosis in calves. The research demonstrated that the oral administration of a bacteriophage

preparation targeting *Salmonella enteritidis* and *Salmonella* Typhimurium was both therapeutically effective and prophylactically protective against salmonellosis in calves [134].

An early Czech study systematically evaluated the susceptibility of *Escherichia coli* strains isolated from piglets to T-even bacteriophages and demonstrated that a high proportion of clinical isolates were sensitive, predominantly to phage T2. The authors developed a scalable method for high-titer phage production and showed, in field applications, that oral phage administration was safe and associated with a reduced incidence and severity of colibacillosis and edema disease in piglets [135].

Both bacteriophages and phage-derived endolysins have been investigated as potential tools to control *Paenibacillus larvae*, the etiological agent of American foulbrood (AFB), one of the most destructive and persistent diseases affecting honeybee colonies. Early experimental work conducted at the Apiculture Research Institute in Dol in the late 1970s and early 1980s led to the isolation and characterization of a *P. larvae* bacteriophage (designated BLA), exhibiting siphoviral morphology and predominantly temperate behavior, yet capable of effective lytic activity against multiple *P. larvae* strains under laboratory conditions [136]. A recent project (Table 2) shifted attention to phage-derived endolysins, specifically a conserved N-acetylmuramoyl-L-alanine amidase that mediates efficient cell wall degradation and can be applied independently as a specific antimicrobial agent. Nevertheless, due to the exceptional resilience of *P. larvae* spores, their long-term environmental persistence, and the intracellular localization of infection in honeybee larvae, classical phage therapy faces substantial practical limitations in AFB control.

Currently available phage products for veterinary use

There is great interest in using phages to treat canine pyoderma, one of the most prevalent dermatological conditions in dogs, typically caused by *Staphylococcus pseudintermedius* including multidrug-resistant and methicillin-resistant strains, which significantly limit treatment options. This renewed interest led to the redevelopment of a phage-based preparation designated Bacteriophage SI (Bioveta), originally discontinued in 1994, to comply with current regulatory standards. Between 2021 and 2024, the product underwent clinical trials in veterinary practice (experimental project no. 14/2020), resulting in approval under the Czech veterinary special therapeutic program. Subcutaneous administration of a phage lysate containing a phage from the subfamily *Twortvirinae* produced positive outcomes in 50 of the 66 treated dogs (excellent in 29, very good in 16, good in 5) (unpublished data from Bioveta). Notably, clinical improvement was also observed in dogs without detectable *S. pseudintermedius* or with isolates resistant to phage lysis, suggesting potential immunomodulatory effects beyond direct bacteriolysis [137]. The effect of the topical application of three wide-host-range phages in a patented hydrogel was recently tested in a controlled infection model in guinea pigs infected with *S. pseudintermedius* in a BC CAS, CEITEC, and LabMediaServis research project (Table 2).

The veterinary clinical trial of another phage-based product, FISHPHAG AS (authorization No. 001/2025/CT), was approved by the Czech regulatory authority in January 2025. FISHPHAG AS is a bacteriophage-based preparation containing phages belonging to the *Biquartavirus* genus developed to target *Aeromonas salmonicida* and intended for use in the prevention and management of furunculosis in salmonid aquaculture. These phages lysed up to 88% of 32 field *A. salmonicida* isolates characterized previously [138, 139]. The trial was conducted by DYNTEC at two aquaculture facilities in the Vysočina and Moravian Karst regions during the summer of 2025. In total, approximately 70,000 fish of the family *Salmonidae* (*Salvelinus alpinus* × *Salvelinus fontinalis* and *Oncorhynchus mykiss*) were included in flow-through tank systems. FISHPHAG AS demonstrated a favourable safety profile, with minimal mortality observed across the treated groups (unpublished data from DYNTEC). The assessment of efficacy was limited by low bacterial prevalence, relatively low phage concentrations, and continuous water flow; nevertheless, the treated tanks consistently exhibited a reduction in bacterial load compared to untreated controls. The detectable persistence of phages in treated tanks suggested short-term environmental stability and likely in situ replication. Overall, the results indicated a positive trend toward efficacy under real-world aquaculture conditions, despite substantial methodological constraints.

Food industry, agriculture and environmental applications

Phages used in the food industry or agriculture can prevent or eliminate contamination of farm raw materials and products by pathogenic bacteria. The study by Hlucháňová et al. [140] demonstrated that, although bacteriophage P100 (LISTEX™ P100) is a biologically innovative and targeted approach to controlling *Listeria monocytogenes* in ready-to-eat foods, its efficacy is limited in complex matrices, such as steak tartare. They thus highlighted the crucial importance of the food matrix type and the specific susceptibility of the strain for effective elimination. LISTEX was also used by the cheese producer A.W. Loštice.

Bacteriophages have substantial potential as environmentally friendly biocontrol agents against bacterial plant diseases, however, their practical application in agriculture remains challenging [141]. In Czech agronomy, phage research is targeting the most abundant and devastating plant pathogens, particularly those that cause post-harvest yield losses in potatoes, tomatoes, cabbages, carrots, beets, and other crops such as *Dickeya* sp., *Pectobacterium* sp., and *Kosakonia* sp. Another target is biotrophic pathogens that infect leaves or fruits, such as *Pseudomonas syringae*. In this respect, Czech research parallels research conducted in Poland and Denmark [142]; however, it utilizes its own sources of lytic phages. An exception is the identification of a biotic agent in the semi-industrial production of biomass from *Arthronema africanum*, a filamentous cyanobacterium known for its antitumor properties. The study revealed a novel temperate bacteriophage in the *A. africanum* production strain that was absent in related strains and species [143].

The pectinolytic bacteria *Dickeya solani* and *Pectobacterium* sp. infect potato tubers through lenticels or surface wounds under moist conditions, causing bacterial soft rot. A mixture of *Limestonevirus* bacteriophages, the novel *Certrevirus*, and *Berlinvirus* [144, 145], forms the basis for laboratory experiments using tuber disks, as well as for preventive and curative applications in controlled glasshouse experiments. The application of the phage solution to tuber disks and wounded tubers did not completely eliminate the infection. However, it reduced the development of soft rot symptoms by 59.5–91.4% [146, 147]. In glasshouse experiments, phage application reduced blackleg symptoms by approximately 87% when applied preventatively, and by 50% when applied curatively [148]. The effectiveness of phages depends on their concentration in the environment, the rate of tuber injury, and the order of their application. In the field, weather conditions, especially soil moisture content, primarily influence the protective effect of phages. To increase phage accessibility, the field applicator was modified to spray phages directly onto tubers during planting. Plants protected from both mild and severe bacterial infections had greater leaf cover (Fig. 7).

Eliminating the pathogen in the early stages of infection is generally more economical and effective than curing diseased plants later on. This is particularly true for seed-transmitted bacterial pathogens, such as *Xanthomonas* sp., which affects pepper and tomato plants. A novel *Foxunavirus* has been isolated that was specific for five of the twenty-one tested strains of *X. campestris* pv. *campestris* [149] and two *Schitoviridae* viruses have been isolated that are specific to a wide range of *Xanthomonas* hosts. The use of specific phage composition for decontaminating pepper and tomato seeds, as well as gardening tools, has been recently patented [150, 151]. Other phages with podovirus morphology belonging to the genera *Pollyceevirus* and *Ghunavirus* have also been reported to infect plant *Pseudomonas* spp. and *Xanthomonas* spp [152].

Discussion on key prerequisites for further progress in integrating phage therapy into clinical practice

Phage therapy research and clinical application have a long tradition in the Czech Republic, further strengthened in recent decades through structured education and the systematic training of a new generation of researchers. Over the past 25 years, several dozen undergraduate and doctoral students, especially those primarily trained at Masaryk University in Brno, have contributed to this field through diploma and PhD theses addressing key aspects of phage biology directly relevant to therapeutic development. Notably, many of these graduates have transitioned into the biotechnology sector and are now employed by companies such as MB PHARMA and

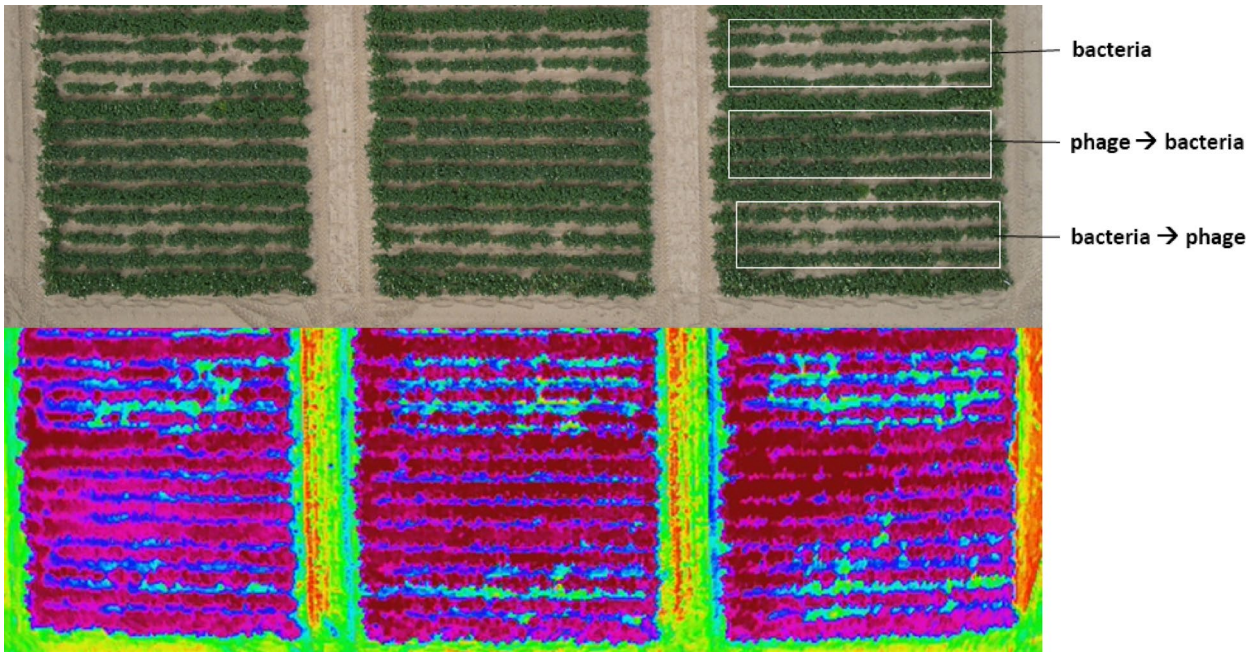

Fig. 7 Visible light and infrared view of three repetitions of a potato planting field test. Sixty potato plants in three rows and three replicates were infected with *Dickeya* alone, treated with a phage cocktail before infection, or treated with a phage cocktail after the bacterial infection. The tuber yield of phage-treated plants was then 4–16% higher after a severe *Dickeya* infection and 25–34% higher after a mild infection simulation [147]

FAGOFARMA, strengthening the national infrastructure and ensuring continuity between academic research, industrial development, and clinical implementation.

Beyond their immediate therapeutic relevance, bacteriophages represent a powerful platform for fundamental research in molecular biology, microbial ecology, and evolutionary genetics. Phage genomes remain vast and only partially characterized reservoirs of genetic diversity, with a substantial proportion of their genes encoding proteins of unknown function. Systematic functional exploration of this genetic "dark matter" is likely to uncover novel regulatory elements, structural insights, antimicrobial strategies, enzymes, and biomolecular tools, thereby expanding both our understanding of virus–host interactions and the translational potential of phages in biotechnology and next-generation therapeutics.

Despite substantial research activity, significant public investment, strong technical capabilities of phage developers, and early steps toward clinical translation, several challenges remain before phage therapy can become a reliable component of modern medicine. Addressing these gaps will require strategic investment in collaborative phage banks, regulatory alignment, and systems-level research to unlock the full clinical potential of bacteriophages as a response to antimicrobial resistance. Ultimately, sustained collaboration among academia, healthcare providers, biotechnology companies, and regulators will determine whether phage therapy can transition from a promising alternative into an integrated, patient-centered pillar of antimicrobial treatment. Based on this review and recent advances, we have identified several priority gaps that largely mirror challenges observed internationally [153].

Hybrid therapeutic models. The Czech experience illustrates the complementary roles of standardized and personalized phage therapy. The ongoing DUOFAG® study may provide important evidence regarding the feasibility and clinical value of standardized phage preparations, which offer commercial and regulatory advantages under contemporary regulatory conditions. At the same time, broader implementation of named-patient-basis use in the Czech Republic highlights the importance of individualized phage selection for difficult-to-treat infections

and benefits from regulatory mechanisms that enable rapid clinical use of well-characterized phages outside traditional marketing authorization pathways and well-established GMP-compliant production.

Phage sourcing and infrastructure. Specialized therapeutic phage banks are increasingly recognized as critical infrastructure. However, development of phage collections remains fragmented, and there is currently no nationally coordinated, interoperable phage repository with harmonized release criteria. Nevertheless, sustainable access to therapeutic phages will require continued support for phage repositories, standardized quality-control procedures, and coordinated mechanisms for sharing phages and reference bacterial strains among clinical, academic, and industrial partners, which applies internationally.

Governance, **coordination**, **financing and sustainable clinical implementation.** Beyond product-oriented development, further progress in phage therapy in the Czech Republic requires structured regulatory dialogue, stakeholder coordination, and the establishment of a sustainable clinical infrastructure within major hospitals accessible nationwide to enable systematic, case-by-case clinical use. However, long-term sustainability is still compromised by fragmented, predominantly project-based funding that fails to provide a stable foundation for unified clinical pathways and hospital-based therapeutic programs. The absence of clearly defined reimbursement mechanisms for both personalized phage preparations and standardized products further limits implementation, imposing financial burdens on healthcare providers and generating uncertainty for biotechnology companies and investors. Slow regulatory harmonization and uncertain payer pathways continue to limit scalable implementation; however, a stakeholder working group established in 2025 aims to address these gaps.

Target pathogens and systems biology. Czech phage research has traditionally focused on clinically important multidrug-resistant pathogens, particularly *Staphylococcus* spp., supported by extensive expertise in the biology, genomics, and epidemiology of these bacteria, and, more recently, on *P. aeruginosa*, *K. pneumoniae*, and *A. baumannii*. However, many clinically relevant pathogens still lack suitable therapeutic phages in local collections. Future developments are likely to extend toward preventive applications, such as targeted decolonization of MRSA carriers before high-risk surgical procedures. Such approaches could reduce antibiotic use while preserving the commensal microbiota. Their successful implementation, however, will require a deeper understanding of phage-host-microbiome interactions, including the long-term consequences of pathogen elimination and the microbiome restoration.

Synergy or antagonism between phages and antibiotics. Phage-antibiotic synergy (PAS) is highly context dependent, with synergy or antagonism varying according to the specific bacterial strain, phage, antibiotic, and treatment conditions. It therefore cannot be reliably predicted from genomic data alone. Promising in vitro findings frequently fail to translate into in vivo efficacy, where factors such as the site of infection, biofilm formation, pharmacokinetics, host immune responses, and microbiome interactions critically shape therapeutic outcomes. There are additional uncertainties regarding the optimal sequencing, dosing, and timing of combined phage-antibiotic administration. Addressing these gaps will require validated protocols for assessing PAS and the integration of harmonized in vitro and in vivo testing frameworks into routine microbiology laboratories that already collect isolates and support clinical trials and personalized therapeutic decision-making.

Host range prediction and innovation. Bacteria and their bacteriophages undergo continuous coevolution, generating resistance patterns that cannot be reliably derived from genomic data alone. Phage host range cannot be predicted solely from individual bacterial markers such as receptor genes, CRISPR arrays, and restriction-modification systems, because infection outcomes depend on complex interactions between phage and bacterial genes, many of which remain functionally uncharacterized. The growing diversity of identified bacterial defense systems, which has historically been underestimated, is now recognized as a major determinant of host range, but they are not the sole source of the resistance either. These limitations underscore the need for large, systematically curated datasets that capture diverse phage-host combinations. Although contemporary research programs increasingly mandate the use of AI, robust training datasets remain scarce. Progress will require unified, AI-ready databases integrating well-characterized phage genomes, bacterial host genomes that include receptor patterns and defense profiles, and quantitative phenotypic measures (e.g., adsorption kinetics, efficiency of plating, and

antibiotic synergy), including clinical metadata, coordinated across manufacturers, hospitals, and laboratories, with prospective wet-lab validation.

Immunopharmacology and formulation. Specialized preclinical immunogenicity studies in pig and rodent models are ongoing in the Czech programs, and indicate substantial interindividual variability in immune responses to bacteriophage preparations. These findings underscore the need for coordinated studies on immunogenicity, phage titer at a given dose, repeated dosing, and formulation-specific immune responses in early human cohorts to formulate rational strategies and administration in future clinical trials. Further research should build on Pillich's early concepts to clarify the immunological mechanisms underlying phage therapy, including the beneficial role of bacterial components in phage preparations for immune modulation versus the direct bactericidal activity of lytic phages themselves.

Adaptive phage innovation and regulatory flexibility. The long-term clinical sustainability of phage therapy depends on the capacity to continuously expand and update the therapeutic phage repertoire in response to bacterial evolution. Bacterial resistance to phages is frequently driven by the horizontal dissemination of defense systems within specific clonal complexes, rather than solely by *de novo* receptor mutations. Effective countermeasures require both the systematic isolation of new strictly lytic phages from environmental sources and the adaptive evolution ("training") or rational engineering of existing phages to overcome emerging resistance. However, current regulatory pathways are not optimally configured to accommodate this dynamic biological reality. Newly isolated phages appropriately require comprehensive genomic and safety evaluation prior to clinical use, yet phage mutants that differ only by limited genomic modifications (Fig. 2) and restore activity against resistant strains are often subjected to the same extensive validation framework as entirely new entities. This lack of proportionate regulatory differentiation slows down timely therapeutic updates and limits the practical exploitation of phage adaptability. To preserve clinical efficacy and ensure long-term viability, regulatory models need to evolve toward agile, risk-based frameworks that enable rapid substitution or updating of phage strains within defined phage species – analogous to the periodic reformulation of influenza vaccines – while maintaining rigorous standards of safety, quality, and traceability.

Production host strain optimization and regulatory gaps in manufacturing. Safe and scalable phage manufacturing depends critically on the selection and optimization of bacterial propagation strains; however, scientific and regulatory gaps remain. Production hosts should ideally be free of antibiotic-resistance determinants, virulence factors, and inducible prophages, yet suitable naturally occurring strains of bacterial pathogens are not always available. Advances in synthetic biology provide opportunities to engineer improved propagation hosts by removing undesirable genetic elements and enhancing stability and phage yield, but regulatory guidance for such engineered production strains remains insufficiently defined. In individualized settings, the patient's own bacterial isolate can be considered as a temporary production host, particularly when rapid adaptation is required or the patient's condition is time-sensitive. However, this approach raises additional biosafety and quality-control challenges that need to be addressed through validated downstream purification and sensitive analytical platforms, including qPCR, ELISA, HPLC, and mass spectrometry, to detect residual contaminants, prophage particles, or other bacterial by-products. Compounding these challenges, phage genomes themselves still contain a high proportion of genes with unknown or poorly characterized functions, limiting comprehensive risk assessment and complicating the regulatory evaluation of both phages and their production systems. These uncertainties highlight the need for clearer, risk-based regulatory frameworks and targeted research to standardize production-host qualification, analytical control strategies, and genomic safety assessment in phage manufacturing.

Education, perception, and clinical acceptance. Awareness and understanding of phage therapy remain limited, and a degree of skepticism persists within part of the Czech medical and scientific community. It is based on the assumption that phages are similar to other antimicrobial agents, but their biological nature and mechanisms of action are fundamentally different, requiring a different approach that accounts for their viral nature. Despite growing international evidence of the safety and efficacy of phage therapy, outdated perceptions, insufficient knowledge of modern phage biology among physicians, and the absence of standardized clinical frameworks continue to hinder its wider adoption. Promotion within scientific societies, the targeted professional education of

physicians, robust communication of clinical data, and structured implementation procedures will be essential to build trust and facilitate the responsible integration of phage therapy into routine healthcare.

Acknowledgements The authors wish to thank Marta Šiborová (CEITEC, Masaryk University, Brno; currently University of Copenhagen), Pavol Bárdy (Faculty of Science, Masaryk University, Brno; currently University of York), Pavel Dřevínek (Department of Medical Microbiology, Second Faculty of Medicine, Charles University, Prague), Martin Faldyna (Veterinary Research Institute, Brno), Antonín Přidal (Mendel University in Brno), and David Šmajs and Renáta Karpíšková (Faculty of Medicine, Masaryk University, Brno) for their valuable help and Michaela Navrátilová and Kristína Létalová (Masaryk University) for technical assistance. Schematic diagrams were created using icons from the Power-user add-in icon library (Power-user SAS, France; https://www.powerusersoftwares.com) for Microsoft PowerPoint.

Author contributions R.P. and J.D. designed the review concept and wrote the original draft. R.P., J.K., K.P., M.B., T.F., I.M., and T.B. designed display items. J.K. drew all the drawings in the manuscript. J.D., T.B., and T.F. analyzed data. All authors contributed to drafting and reviewed the manuscript.

Funding The authors gratefully acknowledge supported by the National Institute of Virology and Bacteriology project (Programme EXCELES, ID Project No. LX22NPO5103, funded by the European Union - Next GenerationEU and Programme NW26A-NIVB, funded by the Ministry of Health of the Czech Republic).

Data availability Accession numbers of reused datasets are indicated in the legends of Figs. 2 and 3. Information on projects focused on phage therapy was extracted from the STARFOS database (https://starfos.tacr.cz), a public database on research, development, and innovation operated by the Research, Development and Innovation Council of the Czech Republic in cooperation with the Office of the Government of the Czech Republic.

Declarations

Ethics approval and consent to participate No ethical approval was required, as the study did not involve human or animal subjects or specimens.

Consent for publication Not applicable.

Competing interests Josef Boštík, Dana Kocourková, Jiří Nepeřený, Martin Benešík, Daniel Zeller, and Marek Moša are employees of companies that manufacture bacteriophage products. The authors declare that their institutional affiliation did not influence the product development, commercial involvement, scientific processing, interpretation, or conclusions presented in this article.

Open Access This article is licensed under a Creative Commons Attribution 4.0 International License, which permits use, sharing, adaptation, distribution and reproduction in any medium or format, as long as you give appropriate credit to the original author(s) and the source, provide a link to the Creative Commons licence, and indicate if changes were made. The images or other third party material in this article are included in the article's Creative Commons licence, unless indicated otherwise in a credit line to the material. If material is not included in the article's Creative Commons licence and your intended use is not permitted by statutory regulation or exceeds the permitted use, you will need to obtain permission directly from the copyright holder. To view a copy of this licence, visit http://creativecommons.org/licenses/by/4.0/.

References

1. Ho CS, Wong CTH, Aung TT, Lakshminarayanan R, Mehta JS, Rauz S, McNally A, Kintses B, Peacock SJ, de la Fuente-Nunez C, et al. Antimicrobial resistance: a concise update. Lancet Microbe. 2025;6(1):100947.
2. Theuretzbacher U, Piddock LJV. Non-traditional antibacterial therapeutic options and challenges. Cell Host Microbe. 2019;26(1):61–72.
3. Chanishvili N. Bacteriophages as therapeutic and prophylactic means: Summary of the Soviet and post Soviet experiences. Curr Drug Deliv. 2016;13(3):309–23.
4. McCallin S, Sacher JC, Zheng J, Chan BK. Current state of compassionate phage therapy. Viruses. 2019;11(4):343.
5. Chanishvili N, Myelnikov D, Blauvelt TK. Professor Giorgi Eliava and the Eliava Institute of Bacteriophage. Phage-Therapy Appl Res. 2022;3(2):71–80.

6. Żaczek M, Weber-Dąbrowska B, Międzybrodzki R, Łusiak-Szelachowska M, Górski A. Phage therapy in Poland - a centennial journey to the first ethically approved treatment facility in Europe. Front Microbiol. 2020;11:1056.
7. Alavidze Z, Aminov R, Betts A, Bardiau M, Taudeau L, Caplin J, Chanishvili N, Coffey A, Cooper I, De Vos D, et al. Silk route to the acceptance and re-implementation of bacteriophage therapy: Expert round table on acceptance and re-implementation of bacteriophage therapy. Biotechnol J. 2016;11(5):595–600.
8. Sybesma W, Rohde C, Bardy P, Pirnay JP, Cooper I, Caplin J, Chanishvili N, Coffey A, De Vos D, Scholz AH, et al. Silk Route to the Acceptance and Re-Implementation of Bacteriophage Therapy-Part II. Antibiotics. 2018;7(2):35.
9. Rohde C, Resch G, Pirnay JP, Blasdel BG, Debarbieux L, Gelman D, Gorski A, Hazan R, Huys I, Kakabadze E, et al. Expert opinion on three phage therapy related topics: Bacterial phage resistance, phage training and prophages in bacterial production strains. Viruses. 2018;10(4):178.
10. Nale JY, Clokie MR. Preclinical data and safety assessment of phage therapy in humans. Curr Opin Biotechnol. 2021;68:310–7.
11. Pires DP, Costa AR, Pinto G, Meneses L, Azeredo J. Current challenges and future opportunities of phage therapy. FEMS Microbiol Rev. 2020;44(6):684–700.
12. Pirnay JP, Verbeken G. Magistral phage preparations: Is this the model for everyone? Clin Infect Dis. 2023;77(Suppl 5):S360–9.
13. Jault P, Leclerc T, Jennes S, Pirnay JP, Que YA, Resch G, Rousseau AF, Ravat F, Carsin H, Le Floch R, et al. Efficacy and tolerability of a cocktail of bacteriophages to treat burn wounds infected by *Pseudomonas aeruginosa* (PhagoBurn): a randomised, controlled, double-blind phase 1/2 trial. Lancet Infect Dis. 2019;19(1):35–45.
14. Pirnay JP, Kutter E. Bacteriophages: it's a medicine, Jim, but not as we know it. Lancet Infect Dis. 2021;21(3):309–11.
15. Górski A, Borysowski J, Międzybrodzki R. Phage therapy: Towards a successful clinical trial. Antibiotics. 2020;9(11):827.
16. Pirnay JP, Djebara S, Steurs G, Griselain J, Cochez C, De Soir S, Glonti T, Spiessens A, Vanden Berghe E, Green S, et al. Personalized bacteriophage therapy outcomes for 100 consecutive cases: a multicentre, multinational, retrospective observational study. Nat Microbiol. 2024;9(6):1434–53.
17. Suh GA, Scobie ESGNTA, Esgnta A, Piuzzi NS, Bartak V, Anyaehie UE, Arciola CR, Batailler C, Benes M, et al. 2025 ICM: Role of unconventional medications. J Arthroplasty. 2025;41(1):S151–6.
18. McCallin S, Drulis-Kawa Z, Ferry T, Pirnay JP, Nir-Paz R. ESGNTA ESCMID study group for non-traditional antibacterials. Phages and phage-borne enzymes as new antibacterial agents. Clin Microbiol Infect. 2025;31(6):910–21.
19. Żaczek M, Górski A, Weber-Dąbrowska B, Letkiewicz S, Fortuna W, Rogoz P, Pasternak E, Międzybrodzki R. A thorough synthesis of phage therapy unit activity in Poland-Its history, milestones and international recognition. Viruses. 2022;14(6):1170.
20. Willy C, Bugert JJ, Classen AY, Deng L, Duchting A, Gross J, Hammerl JA, Korf IHE, Kuhn C, Lieberknecht-Jouy S, et al. Phage therapy in Germany-Update 2023. Viruses. 2023;15(2):588.
21. Ferry T, Bouar ML, Briot T, Roussel-Gaillard T, Perpoint T, Roux S, Ader F, Valour F, Kassai B, Boussaha I, et al. Access to phage therapy at Hospices Civils de Lyon in 2022: Implementation of the PHAGEinLYON Clinic programme. Int J Antimicrob Agents. 2024;64(6):107372.
22. de Villiers H, Golliard G, Vuattoux X, Resch G. Rational design of a potent two-phage cocktail against a contemporary *Acinetobacter baumannii* strain recovered from a burned patient at the Lausanne University Hospital. Viruses. 2025;17(11):1441.
23. Jones JD, Trippett C, Suleman M, Clokie MRJ, Clark JR. The future of clinical phage therapy in the United Kingdom. Viruses. 2023;15(3):721.
24. Alves J, Carvalho AC, Capela C, Faria B, Leite R, Meneses L, Pires DP, Azeredo J. Bacteriophage therapy: a review and the Portuguese landscape. Revista Portuguesa de Doenças Infecciosas. 2026;20(1):140.
25. Pirnay JP, Ferry T, Resch G. Recent progress toward the implementation of phage therapy in Western medicine. FEMS Microbiol Rev. 2022;46(1):fuab040.
26. Fuerst-Wilmes M, Respondek V, Schramm M, Lilienthal N, Buss K, Duechting A. Regulation of phage therapy medicinal products: developments, challenges, and opportunities. Front Cell Infect Microbiol. 2025;15:1631359.
27. Skurnik M, Alkalay-Oren S, Boon M, Clokie M, Sicheritz-Pontén T, Dąbrowska K, Hatfull GF, Hazan R, Jalasvuori M, Kiljunen S, et al. Phage therapy. Nat Rev Method Prim. 2025;5(1):9.
28. Doud MB, Robertson JM, Strathdee SA. Optimizing phage therapy with artificial intelligence: a perspective. Front Cell Infect Microbiol. 2025;15:1611857.
29. Raška K. Bacteriophagy and its significance in the treatment and prevention of bacillary dysentery [in Czech]. Časopis Lékařů Českých. 1944;83(2):55.
30. Kříž J, Beranová R. History of the National Institute of Public Health in Prague [in Czech]. Acta Hyg Epidermiol Microbiol. 2005;SI:1–185.
31. Hloucal L, Cvrček Z, Vaníček F, Mlčochová L. Treatment of typhoid fever with bacteriophage [in Czech]. Časopis Lékařů Českých. 1947;86:774–89.

32. Procházka D. Successful use of a bacteriophage in a dysentery epidemic in a children's home [Article in German]. Zentralbl Bakteriol I Orig. 1967;202(3):369–73.
33. Pulverer G, Pillich J, Kocur M. Zwei neue gegen pathogene Staphylokokken wirksame Bakteriophagen. Zentralbl Bakteriol I Orig. 1966;201(3):321–5.
34. Pulverer G, Pillich J, Klein A. New bacteriophages of *Staphylococcus epidermidis*. J Infect Dis. 1975;132(5):524–31.
35. Hájek V, Horák V. Typing coagulase-positive staphylococci of different origin with Blouse and Meekins' phages. J Hyg Epidemiol Microbiol Immunol. 1984;29(3):317–22.
36. Hájek V, Horák V. A comparison of the lytic activity of poultry, human, and bovine phages with staphylococci of different origin. Zentralbl Bakteriol Orig A. 1978;242(4):446–55.
37. Pillich J, Výmola F, Buda J. Assumptions for successful therapy using staphylococcal phage lysates. Zentralbl Bakteriol Orig. 1969;210(3):377–81.
38. Pillich J, Pulverer G, Vojtíšková M. Activity of polyvalent staphylococcal bacteriophages. Zentralbl Bakteriol Parasit Infekt Hyg Ser A. 1976;5(I Abt Suppl):81–6.
39. Pantůček R, Rosypalová A, Doškař J, Kailerová J, Ružičková V, Borecká P, Snopková S, Horváth R, Götz F, Rosypal S. The polyvalent staphylococcal phage 812: Its host-range mutants and related phages. Virology. 1998;246(2):241–52.
40. O'Flaherty S, Ross RP, Meaney W, Fitzgerald GF, Elbreki MF, Coffey A. Potential of the polyvalent anti-*Staphylococcus* bacteriophage K for control of antibiotic-resistant staphylococci from hospitals. Appl Environ Microbiol. 2005;71(4):1836–42.
41. Výmola F, Buda J, Pillich J. Staphylococcal necrosis cured with a staphylococcal phage lysate [in German]. Zentralbl Bakteriol Orig. 1968;206(3):377–83.
42. Buda J, Výmola F, Pillich J. Skin necrosis of the lower extremity healed with staphylococcal phagolysates [in Czech]. Rozhl Chir. 1966;45(2):132–9.
43. Závadský Z, Pillich J. Imunizace a bakteriofágový lyzát v terapii chronických osteomyelitid. Acta Chir Orthop Traumatol Čechoslov. 1974;41:61–4.
44. Pillich J, Továrek J, Fait M. A contribution to the treatment of acute hematogenous and chronic osteomyelitis in children [in German]. Z Orthop. 1978;116:40–6.
45. Výmola F, Lochman O, Buda J, Pillich J. Staphylococcal osteomyelitis. Ann N Y Acad Sci. 1974;236(0):508–14.
46. Pillich J, Haklová J, Toufarová D, Kubíčková D, Jandová D. The use of STAVA - a phage lysate of *Staphylococcus aureus*, as a vaccine with immunomodulating properties. In Bacteria and The Host. Edited by Rýc M, Franček J. Prague: Avicenum; 1986: 369 – 71.
47. Dean JH, Silva JS, McCoy JL, Chan SP, Baker JJ, Leonard C, Herberman RB. *In vitro* human reactivity to staphylococcal phage lysate. J Immunol. 1975;115(4):1060–4.
48. Sekaninová G, Kolárová M, Pillich J, Seménka J, Slavíková H, Kubícková D, Zajícová V. *Pseudomonas aeruginosa* phage lysate as an immunobiological agent – 1. Selection of clinical strains for phage lysate preparation. Folia Microbiol. 1999;44(1):93–7.
49. Pillich J, Balcarek JC. Compositions and methods for treatment of microbial infections. US 8920815 B2, Issued December 30, 2014. United States Patent; 2013.
50. Gorski A, Miedzybrodzki R, Borysowski J, Dabrowska K, Wierzbicki P, Ohams M, Korczak-Kowalska G, Olszowska-Zaremba N, Lusiak-Szelachowska M, Klak M, et al. Phage as a modulator of immune responses: practical implications for phage therapy. Adv Virus Res. 2012;83:41–71.
51. Pillich J, Výmola F. Antistaphylococcal phage lysate for topical use. CS 203719 B1, Issued May 15, 1983. Prague: Office for Inventions and Discoveries of Czechoslovakia; 1979.
52. Domorázkova E, Stránský V. Stafal SEVAC for local use - Results of the clinical trials at three clinical sites [in Czech]. Zpravy SEVAC (Institute Serums Vaccines Prague). 1985;4:130–9.
53. Bláha K, Výmola F, Jedličková Z. Experience with phage therapy in otorhinolaryngology [in Czech]. Československá Otolaryngologie. 1985;14(2):66–9.
54. Ryšánková J. The use of phage therapy in chronic staphylococcal diseases in otorhinolaryngology [in Czech]. Československá Otolaryngologie. 1980;29:56–8.
55. Kynčlová S. Therapeutic use of staphylococcal phage lysate in chronic and recurrent respiratory diseases [in Czech]. Česko-Slovenská Pediatr. 1984;39:646–51.
56. Jarčuška P, Rošák M, Novotný M. Clinically effective treatment with anti-staphylococcal phage lysate in a patient with complicated skin and soft tissue infection caused by a methicillin-resistant strain of *Staphylococcus epidermidis* [in Slovak]. Derma. 2014;14(1–3):1–8.
57. Zelenková H. Anti-*Staphylococcus* phage lysate in the treatment of chronic crural wounds caused by chronic venous insufficiency and *diabetes mellitus* [in Slovak]. Kazuistiky v Diabetologii. 2014;12:15–9.
58. Jarčuška P. Economic aspects of the treatment of skin and soft tissue infections with anti-staphylococcal phage lysate [in Slovak]. Slov Chir. 2015;12(1):15–8.
59. Výmola F, Vrbová E, Pillich J. Successful treatment of staphylococcal infections. Combined chemo- and immunotherapy [in Czech]. Czech Med. 1988;4:206–9.

60. Vondrák J, Katzer Z. STAVA and STAFAL preparations in the complex treatment of surgical infections [in Czech]. Plzeňský Lékařský Sborník. 1989:243–5.
61. Březina Z. A few notes on the immunomodulators STAVA and STAFAL [in Czech]. Prakt Lek. 1986;11:430–731.
62. Straka M, Hubenaková Z, Janošíková L, Bugalová A, Minich A, Wawruch M, Liptáková A, Drahovská H, Slobodníková L. *In vitro* susceptibility of clinical and carrier strains of *Staphylococcus aureus* to STAFAL® phage preparation. Int J Mol Sci. 2024;25(23):12885.
63. Botka T, Pantůček R, Mašlaňová I, Benešík M, Petráš P, Růžičková V, Havlíčková P, Varga M, Žemlíčková H, Koláčková I, et al. Lytic and genomic properties of spontaneous host-range *Kayvirus* mutants prove their suitability for upgrading phage therapeutics against staphylococci. Sci Rep. 2019;9(1):5475.
64. Dvořáčková M, Růžicka F, Heroldová MD, Vacek L, Bezděková D, Benešík M, Petráš P, Pantůček R. Therapeutic potential of bacteriophages for staphylococcal infections and selected methods for susceptibility testing of staphylococci. Epidemiol Mikrobiologie Imunol. 2020;69(1):10–8.
65. Dvořáčková M, Růžička F, Benešík M, Pantůček R, Dvořáková-Heroldová M. Antimicrobial effect of commercial phage preparation Stafal® on biofilm and planktonic forms of methicillin-resistant *Staphylococcus aureus*. Folia Microbiol. 2019;64(1):121–6.
66. Subramanian G, Lam WJ, Tham EH, Chandran NS, Sampath P. Decoding atopic dermatitis: pathophysiology, clinical diagnosis, and treatments. Trends Mol Med. 2026;32(4):416–7.
67. Gill JJ. Revised genome sequence of *Staphylococcus aureus* bacteriophage K. Genome Announc. 2014;2(1):e01173–13.
68. O'Flaherty S, Coffey A, Edwards R, Meaney W, Fitzgerald GF, Ross RP. Genome of staphylococcal phage K: a new lineage of Myoviridae infecting gram-positive bacteria with a low G+C content. J Bacteriol. 2004;186(9):2862–71.
69. Rosypal S, Rosypalová A. A spontaneous mutant of polyvalent phage 812 capable of growth in *Staphylococcus aureus* NCTC 8511 carrying prophage 53. Folia Fac Sci Univ Purk Brun. 1970;11:37–47.
70. Doškař J, Rosypal S. Restriction-deficient mutants of *Staphylococcus aureus* strains resistant to polyvalent phage 812. Scripta Fac Sci Natur Univ Masaryk Brun. 1986;16:337–46.
71. Rosypal S, Rosypalová A, Doškař J, Pakrová E. The use of the polyvalent phage 812 and its host-range mutants to the differentiation of *Staphylococcus aureus*. Scripta Fac Sci Natur Univ Purk Brun. 1986;16:317–36.
72. Łobocka M, Hejnowicz MS, Dabrowski K, Gozdek A, Kosakowski J, Witkowska M, Ulatowska MI, Weber-Dabrowska B, Kwiatek M, Parasion S, et al. Genomics of staphylococcal Twort-like phages-potential therapeutics of the post-antibiotic era. Adv Virus Res. 2012;83:143–216.
73. Benešík M, Nováček J, Janda L, Dopitová R, Pernisová M, Melková K, Tišáková L, Doškař J, Žídek L, Hejátko J, Pantůček R. Role of SH3b binding domain in a natural deletion mutant of *Kayvirus* endolysin LysF1 with a broad range of lytic activity. Virus Genes. 2018;54(1):130–9.
74. Kuntová L, Mašlaňová I, Obořilová R, Šimečková H, Finstrlová A, Bardy P, Šiborová M, Troianovska L, Botka T, Gintar P, et al. *Staphylococcus aureus* prophage-encoded protein causes abortive infection and provides population immunity against *Kayviruses*. mBio. 2023;14(2):e02490–22.
75. Finstrlová A, Mašlaňová I, Blasdel Reuter BG, Doškař J, Götz F, Pantůček R. Global transcriptomic analysis of bacteriophage-host interactions between a *Kayvirus* therapeutic phage and *Staphylococcus aureus*. Microbiol Spectr. 2022;10(3):e00123–22.
76. Eyer L, Pantůček R, Zdráhal Z, Konečná H, Kašpárek P, Ružičková V, Hernychová L, Preisler J, Doškař J. Structural protein analysis of the polyvalent staphylococcal bacteriophage 812. Proteomics. 2007;7(1):64–72.
77. Rossmann MG, Rao VB. Viral Molecular Machines. New York: Springer; 2012.
78. Bárdy P, Hrebík D, Pantůček R, Plevka P. Future prospects of structural studies to advance our understanding of phage biology. Microbiol Aust. 2019;40(1):42–6.
79. Nováček J, Šiborová M, Benešík M, Pantůček R, Doškař J, Plevka P. Structure and genome release of Twort-like *Myoviridae* phage with a double-layered baseplate. Proc Natl Acad Sci USA. 2016;113(33):9351–6.
80. Hrebík D, Štveráková D, Škubník K, Füzik T, Pantůček R, Plevka P. Structure and genome ejection mechanism of *Staphylococcus aureus* phage P68. Sci Adv. 2019;5(10):eaaw7414.
81. Šiborová M, Füzik T, Procházková M, Nováček J, Benešík M, Nilsson AS, Plevka P. Tail proteins of phage SU10 reorganize into the nozzle for genome delivery. Nat Commun. 2022;13(1):5622.
82. Valentová L, Füzik T, Nováček J, Hlavenková Z, Pospíšil J, Plevka P. Structure and replication of *Pseudomonas aeruginosa* phage JBD30. EMBO J. 2024;43(19):4384–405.
83. Cieniková Z, Nováček J, Šiborová M, Popelářová B, Füzik T, Botka T, Benešík M, Bárdy P, Pantůček R, Plevka P. Genome anchoring, retention, and release by neck of *Staphylococcus* phage 812 proteins. Commun Biol. 2026;9:199.
84. Bíňovský J, Šiborová M, Zlatohurska M, Nováček J, Bárdy P, Baška R, Škubník K, Botka T, Benešík M, Pantůček R, et al. Conformational changes of the baseplate regulating tail contraction of Staphylococcus phage 812. EMBO J. 2026;45:5514–36.

85. Šimečková H, Bárdy P, Kuntová L, Macháčová E, Botka T, Bíňovský J, Houser J, Farka Z, Plevka P, Pantůček R, Mašlaňová I. CRISPR-Cas10-assisted structural modification of staphylococcal *Kayvirus* for imaging and biosensing applications. ACS Synth Biol. 2025;14(8):2979–86.
86. Rosypal S. Transduction of plasmids in *Staphylococcus aureus*. Folia Fac Sci Univ Purk Brun. 1981;22:5–22.
87. Doškař J, Pallová P, Pantůček R, Rosypal S, Růžičková V, Pantůčková P, Kailerová J, Klepárník K, Malá Z, Boček P. Genomic relatedness of *Staphylococcus aureus* phages of the International Typing Set and detection of serogroup A, B, and F prophages in lysogenic strains. Can J Microbiol. 2000;46(11):1066–76.
88. Borecká P, Rosypal S, Pantůček R, Doškař J. Localization of prophages of serological group B and F on restriction fragments defined in the restriction map of *Staphylococcus aureus* NCTC 8325. FEMS Microbiol Lett. 1996;143(2–3):203–10.
89. Goerke C, Pantucek R, Holtfreter S, Schulte B, Zink M, Grumann D, Broker BM, Doskar J, Wolz C. Diversity of prophages in dominant *Staphylococcus aureus* clonal lineages. J Bacteriol. 2009;191(11):3462–8.
90. Kahánková J, Pantůček R, Goerke C, Růžičkova V, Holochová P, Doškař J. Multilocus PCR typing strategy for differentiation of *Staphylococcus aureus* siphoviruses reflecting their modular genome structure. Environ Microbiol. 2010;12(9):2527–38.
91. Pantůček R, Doškař J, Růžičková V, Kašpárek P, Oráčova E, Kvardová V, Rosypal S. Identification of bacteriophage types and their carriage in *Staphylococcus aureus*. Arch Virol. 2004;149(9):1689–703.
92. Ingmer H, Gerlach D, Wolz C. Temperate phages of Staphylococcus aureus. Microbiol Spectr. 2019;7(5):GPP3–0058.
93. Varga M, Kuntová L, Pantůček R, Mašlaňová I, Růžičková V, Doškař J. Efficient transfer of antibiotic resistance plasmids by transduction within methicillin-resistant *Staphylococcus aureus* USA300 clone. FEMS Microbiol Lett. 2012;332(2):146–52.
94. Mašlaňová I, Doškař J, Varga M, Kuntová L, Mužík J, Malúšková D, Růžičková V, Pantůček R. Bacteriophages of *Staphylococcus aureus* efficiently package various bacterial genes and mobile genetic elements including SCC*mec* with different frequencies. Environ Microbiol Rep. 2013;5(1):66–73.
95. Quiles-Puchalt N, Martinez-Rubio R, Ram G, Lasa I, Penadés JR. Unravelling bacteriophage phi11 requirements for packaging and transfer of mobile genetic elements in *Staphylococcus aureus*. Mol Microbiol. 2014;91(3):423–37.
96. Fišarová L, Botka T, Du X, Mašlaňová I, Bárdy P, Pantůček R, Benešík M, Roudnický P, Winstel V, Larsen J, et al. *Staphylococcus epidermidis* phages transduce antimicrobial resistance plasmids and mobilize chromosomal islands. mSphere. 2021;6(3):00223–21.
97. Chen J, Quiles-Puchalt N, Chiang YN, Bacigalupe R, Fillol-Salom A, Chee MSJ, Fitzgerald JR, Penadés JR. Genome hypermobility by lateral transduction. Science. 2018;362(6411):207–12.
98. Chee MSJ, Serrano E, Chiang YN, Harling-Lee J, Man R, Bacigalupe R, Fitzgerald JR, Penadés JR, Chen J. Dual pathogenicity island transfer by piggybacking lateral transduction. Cell. 2023;186(16):3414–e2616.
99. Chlebowicz MA, Mašlaňová I, Kuntova L, Grundmann H, Pantůček R, Doškař J, van Dijl JM, Buist G. The Staphylococcal Cassette Chromosome mec type V from *Staphylococcus aureus* ST398 is packaged into bacteriophage capsids. Int J Med Microbiol. 2014;304(5–6):764–74.
100. Mašlaňová I, Stříbná S, Doškař J, Pantůček R. Efficient plasmid transduction to *Staphylococcus aureus* strains insensitive to the lytic action of transducing phage. FEMS Microbiol Lett. 2016;363:19.
101. Botka T, Smetanová S, Vinco A, Kučerová E, Rovňáková K, Siváková A, Mašlaňová I, Pantůček R. Virion content unpacked by long-read sequencing: stress-induced changes in transmitted staphylococcal mobilome due to phage-satellite interactions. Nucleic Acids Res. 2025;53(20):gkaf1165.
102. Wirbel J, Hickey AS, Chang D, Enright NJ, Dvorak M, Chanin RB, Schmidtke DT, Bhatt AS. Long-read metagenomics reveals phage dynamics in the human gut microbiome. Nature. 2026;649(8098):982–90.
103. Borodovich T, Buttimer C, Wilson JS, Bardy P, Smith M, Hill C, Khokhlova EV, Harte M, Govi B, Fogg PCM, et al. Large-scale capsid-mediated mobilisation of bacterial genomic DNA in the gut microbiome. Nat Commun. 2026;17(1):2046.
104. Zhang H, Boeckman J, Gupte R, Prejean A, Miller J, Rodier A, de Figueiredo P, Liu M, Gill J, Han A. PRISM: A unified platform for phage isolation and characterization from single-droplet microenvironments. Sci Adv. 2026;12(13):eaeb2362.
105. Štveráková D, Šedo O, Benešík M, Zdráhal Z, Doškař J, Pantůček R. Rapid identification of intact staphylococcal bacteriophages using matrix-assisted laser desorption Ionization-time-of-flight mass spectrometry. Viruses. 2018;10(4):176.
106. Komárková M, Benešík M, Procházková T, Vinco A, Laichmanová M, Smetanová S, Jelínek P, Moša M, Botka T, Šoóš M, Pantůček R. Compatibility of antimicrobial preservatives with therapeutic bacteriophages of the genera *Pbunavirus* and *Kayvirus*. Eur J Pharm Biopharm. 2025;214:114781.
107. Komárková M, Benešík M, Černá E, Sedláčková L, Mosa M, Vojtová L, Franc A, Pantůček R. The pharmaceutical quality of freeze-dried tablets containing therapeutic bacteriophages against *Pseudomonas aeruginosa* and *Staphylococcus aureus*. Int J Pharm. 2025;671:125199.
108. George AH, Jelínek P, Benešík M, Košiarčiková S, Mikšátko J, Pečurlić I, Moša M, Šoóš M. Preparation and characterization of niosomes for bacteriophage delivery. Small Sci. 2026;6(1):e202500530.

109. Raška F, Lipový B, Kobzová S, Vacek L, Jarošová R, Kleknerová D, Matiašková K, Makovický P, Vícenová M, Jeklová E, et al. Development of a porcine model of skin and soft-tissue infection caused by *Staphylococcus aureus*, including methicillin-resistant strains suitable for testing topical antimicrobial agents. Anim Model Exp Med. 2025;8(3):544–57.
110. Vacek L, Polaštík Kleknerová D, Lipový B, Holoubek J, Matysková D, Černá E, Brtníková J, Jeklová E, Kobzová S, Janda L, et al. Phage therapy combined with Gum Karaya injectable hydrogels for treatment of methicillin-resistant *Staphylococcus aureus* deep wound infection in a porcine model. Int J Pharm. 2024;660:124348.
111. Matysková D, Vacek L, Růžička F, Lipový B. The potential of phage therapy in the treatment of skin and soft tissue infections. Dermatol Prax. 2023;17(3):146–8.
112. Vacek L, Kobzová S, Čmelík R, Pantůček R, Janda L. Enzybiotics LYSSTAPH-S and LYSDERM-S as potential therapeutic agents for chronic MRSA wound infections. Antibiotics. 2020;9(8):519.
113. Moša M, Benešík M. A mixture to prepare lyophilised tablets with antimicrobial effect on bacteria *Staphylococcus aureus* and *Pseudomonas aeruginosa* containing bacteriophages and lytic enzymes with an optimum stability and efficiency of active constituents. CZ 310423 B6, Issued April 24, 2025. Prague: Industrial Property Office of the Czech Republic; 2025.
114. Obořilová R, Kučerová E, Botka T, Vaisocherová-Lísalová H, Skládal P, Farka Z. Piezoelectric biosensor with dissipation monitoring enables the analysis of bacterial lytic agent activity. Sci Rep. 2025;15(1):3419.
115. Siváková A, Figallová E, Botka T, Vacek L, Tkadlec J, Vrbský J, Osowski M, Petráš P, Polaštík Kleknerová D, Dvořáčková M, et al. The combination of mupirocin and *Kayvirus* broadens the decolonization effect against *Staphylococcus aureus*. Appl Microbiol Biotechnol. 2026;110(1):157.
116. Obořilová R, Šimecková H, Pastucha M, Klimovic S, Víšová I, Přibyl J, Vaisocherová-Lísalová H, Pantůček R, Skládal P, Mašlaňová I, Farka Z. Atomic force microscopy and surface plasmon resonance for real-time single-cell monitoring of bacteriophage-mediated lysis of bacteria. Nanoscale. 2021;13(31):13538–49.
117. Scholl D. Phage tail-like bacteriocins. Annu Rev Virol. 2017;4(1):453–67.
118. Latrová K, Dolejšová T, Motlová L, Mikusová G, Bosák J, Snopková K, Šmajs D, Konopásek I, Fišer R. R-Type fonticins produced by *Pragia fontium* form large pores with high conductance. J Bacteriol. 2023;205(1):e00315–22.
119. Ibarguren C, Bleriot I, Blasco L, Fernandez-Garcia L, Ortiz-Cartagena C, Arman L, Barrio-Pujante A, Rodriguez OM, Garcia-Contreras R, Wood TK, Tomas M. The world of phage tail-like bacteriocins: State of the art and biotechnological perspectives. Microbiol Res. 2025;295:128121.
120. Woudstra C, Sorensen AN, Sorensen MCH, Brondsted L. Strategies for developing phages into novel antimicrobial tailocins. Trends Microbiol. 2024;32(10):996–1006.
121. Šmarda J. Production of bacteriocin-like agents of *Budvicia aquatica* and *Pragia fontium*. Zentralbl Bakteriol Mikrob Hyg Ser A. 1987;265(1–2):74–81.
122. Šmarda J, Benada O. Phage tail-like (high-molecular-weight) bacteriocins of *Budvicia aquatica* and *Pragia fontium* (*Enterobacteriaceae*). Appl Environ Microbiol. 2005;71(12):8970–3.
123. Snopková K, Chaloupková E, Hrala M, Šmajs D. Characterization of tailocins of *Pragia fontium* 24613 and the tailocin loci within the family *Budviciaceae*. Res Microbiol. 2025;176(1–2):104261.
124. Snopková K, Sedláček I, Šmajs D. First evidence of high-molecular-weight bacteriocin (tailocin) produced by Antarctic *Pseudomonas* spp. Czech Polar Rep. 2018;8(2):178–85.
125. Snopková K, Dufková K, Chamrad I, Lenobel R, Čejková D, Kosina M, Hrala M, Hola V, Sedláček I, Šmajs D. Pyocin-mediated antagonistic interactions in *Pseudomonas* spp. isolated in James Ross Island, Antarctica. Environ Microbiol. 2022;24(3):1294–307.
126. Snopková K, Sedlář K, Nováková D, Staňková E, Sedláček I, Šedo O, Holá V. *Pseudomonas rossensis* sp. nov., a novel psychrotolerant species produces antimicrobial agents targeting resistant clinical isolates of *Pseudomonas aeruginosa*. Curr Res Microb Sci. 2025;8:100353.
127. Snopková K, Dufková K, Šmajs D. *Pseudomonas prosekii* isolated in Antarctica inhibits plantpathogenic strains of *Pseudomonas viridiflava* and *Pseudomonas fluorescens*. Czech Polar Rep. 2022;11(2):270–8.
128. Snopková K, Dufková K, Klimešová P, Vanerková M, Růžicka F, Holá V. Prevalence of bacteriocins and their co-association with virulence factors within *Pseudomonas aeruginosa* catheter isolates. Int J Med Microbiol. 2020;310(8):151454.
129. Štveráková D, Benešík M, Peichlová M, Kubíček L, Maduda D, Staffa R, Procházková T, Dostál D, Buňata M, Moša M. DUOFAG® - Bacteriophages for the treatment of surgical wound infections [in Czech]. In Congress of Clinical Microbiology, Infectious Diseases and Epidemiology, 11th Edition. September 18–20, 2025, Hradec Králové, Czech Republic; 2025.
130. Weiner I, Kahan-Hanum M, Buchstab N, Zelcbuch L, Navok S, Sherman I, Nicenboim J, Axelrod T, Berko-Ashur D, Olshina M, et al. Phage therapy with nebulized cocktail BX004-A for chronic *Pseudomonas aeruginosa* infections in cystic fibrosis: a randomized first-in-human trial. Nat Commun. 2025;16(1):5579.
131. Nemec A, Krizova L, Maixnerova M, van der Reijden TJ, Deschaght P, Passet V, Vaneechoutte M, Brisse S, Dijkshoorn L. Genotypic and phenotypic characterization of the *Acinetobacter calcoaceticus-Acinetobacter baumannii*

complex with the proposal of *Acinetobacter pittii* sp. nov. (formerly *Acinetobacter* genomic species 3) and *Acinetobacter nosocomialis* sp. nov. (formerly *Acinetobacter* genomic species 13TU). Res Microbiol. 2011;162(4):393–404.
132. Davidova-Gerzova L, Lausova J, Sukkar I, Nechutna L, Kubackova P, Krutova M, Bezdicek M, Dolejska M. Multidrug-resistant ESBL-producing *Klebsiella pneumoniae* complex in Czech hospitals, wastewaters and surface waters. Antimicrob Resist Infect Control. 2024;13(1):141.
133. Arientová S, Beran O, Belšan T, Holub M. Successful systemic phage therapy for implant-associated MRSA spondylodiscitis. Int J Infect Dis. 2026;164:108357.
134. Procházka R, Boleslav E. Clinical verification of bacteriophages against *Salmonella* infections in calves [in Czech]. Veterinářství. 1979;29(9):396–7.
135. Staroštík L, Kaláb D. Use of bacteriophage for prophylaxis and treatment of *E. coli* infections in piglets [in Czech]. Veterinářství. 1965;15:495–7.
136. Drobníková V, Ludvík J. Bacteriophage of *Bacillus larvae*. J Apic Res. 2015;21(1):53–6.
137. Nepeřený J, Vrzal V. Use of phagolysate in the treatment of staphylococcal pyodermia in dogs [in Czech]. Veterinářství. 2022;72(9):496–501.
138. Palíková M, Navrátil S, Čížek A, Soukupová Z, Lang Š, Kopp R, Mareš J. Seasonal occurrence of diseases in a recirculation system for salmonid fish in the Czech Republic. Acta Vet Brno. 2014;83(3):201–7.
139. Dvořáková Prokešová M, Gebauer T, Korytář T, Bušová M, Pojezdal Ľ, Lieke T, Tran HQ, Ferrocino I, Franciosa I, Zare M, et al. Performance, immune response, disease resistance, and gut microbiota of rainbow trout, *Oncorhynchus mykiss* (Walbaum, 1792) juveniles fed ground leonardite with a high humic substance content. Aquaculture. 2024;580:740308.
140. Hlucháňová L, Kořená K, Juřicová H. Vacuum-packed steak tartare: Prevalence of *Listeria monocytogenes* and evaluation of efficacy of Listex™ P100. Foods. 2022;11(4):533.
141. Korniienko N, Kharina A, Budzanivska I, Burketová L, Kalachova T. Phages of phytopathogenic bacteria: High potential, but challenging application. Plant Prot Sci. 2022;58(2):81–91.
142. Carstens AB, Djurhuus AM, Kot W, Hansen LH. A novel six-phage cocktail reduces *Pectobacterium atrosepticum* soft rot infection in potato tubers under simulated storage conditions. FEMS Microbiol Lett. 2019;366(9):fnz101.
143. Petrzik K, Lukavský J, Koloniuk I. Novel virus on filamentous *Arthronema africanum* cyanobacterium. Microb Ecol. 2021;81(2):454–9.
144. Petrzik K, Kmoch M, Brazdová S, Ševčík R. Complete genome sequences of novel *Berlinvirus* and novel *Certrevirus* lytic for *Pectobacterium* sp. causing soft rot and black leg disease of potato. Virus Genes. 2021;57(3):302–5.
145. Petrzik K, Vacek J, Brazdová S, Ševčík R, Koloniuk I. Diversity of limestone bacteriophages infecting *Dickeya solani* isolated in the Czech Republic. Arch Virol. 2021;166(4):1171–5.
146. Beňo F, Horsáková I, Kmoch M, Petrzik K, Krátká G, Ševčík R. Bacteriophages as a strategy to protect potato tubers against *Dickeya dianthicola* and *Pectobacterium carotovorum* soft rot. Microorganisms. 2022;10(12):2369.
147. Petrzik K, Vacek J, Kmoch M, Binderová D, Brázdová S, Lenz O, Ševčík R. Field use of protective bacteriophages against pectinolytic bacteria of potato. Microorganisms. 2023;11(3):620.
148. Kmoch M, Vacek J, Loubová V, Petrzik K, Brázdová S, Ševčík R. Potential of *Limestonevirus* bacteriophages for ecological control of *Dickeya solani* causing bacterial potato blackleg. Agriculture. 2024;14(3):497.
149. Neoralová M, Brázdová S, Eichmeier A, Petrzik K. Complete genome sequence of *Xanthomonas phage* M29, a new member of *Foxunavirus* isolated in the Czech Republic. Virus Genes. 2023;59(6):874–7.
150. Petrzik K, Brázdová S. The Xe_PB119 bacteriophage strain, a preparation based on this bacteriophage strain and their use against bacterial spot on tomatoes and peppers. CZ 309961 B6, Issued January 25, 2024. Prague: Industrial Property Office of the Czech Republic; 2024.
151. Petrzik K, Brázdová S. The Xe_NED111 bacteriophage strain, a preparation based on this bacteriophage strain and their use against bacterial spot on tomatoes and peppers. CZ 309960 B6, Issued January 25, 2024. Prague: Industrial Property Office of the Czech Republic; 2024.
152. Korniienko N, Kharina A, Zrelovs N, Jindřichová B, Moravec T, Budzanivska I, Burketová L, Kalachova T. Isolation and characterization of two lytic phages efficient against phytopathogenic bacteria from *Pseudomonas* and *Xanthomonas* genera. Front Microbiol. 2022;13:853593.
153. Turner PE, Azeredo J, Buurman ET, Green S, Haaber JK, Haggstrom D, Kameda de Figueiredo Carvalho K, Kirchhelle C, Gonzalez Moreno M, Pirnay JP, Portillo MA. Addressing the research and development gaps in modern phage therapy. Phage-Therapy Appl Res. 2024;5(1):30–9.

Publisher's note Springer Nature remains neutral with regard to jurisdictional claims in published maps and institutional affiliations.

Authors and Affiliations

Roman Pantůček[1] · Jiří Doškař[1] · Josef Boštík[2] · Dana Kocourková[3,4] · Karel Petrzik[5] · Jana Koptíková[6] · Martin Benešík[1,3,4] · Pavel Plevka[7] · Tibor Füzik[7] · Ivana Mašlaňová[1] · Tibor Botka[1] · Jiří Nepeřený[8] · Daniel Zeller[9] · Lucie Kuntová[1] · Kateřina Snopková[1,10] · Matěj Hrala[11] · Marek Moša[3,4,12]

✉ Roman Pantůček
pantucek@sci.muni.cz

[1] Department of Experimental Biology, Faculty of Science, Masaryk University, Kamenice 5, Brno 625 00, Czech Republic

[2] AUMED a.s, Prague, Czech Republic

[3] MB PHARMA GROUP s.r.o, Prague, Czech Republic

[4] FAGOFARMA s.r.o, Prague, Czech Republic

[5] Biology Centre, Institute of Plant Molecular Biology, Department of Plant Virology, Czech Academy of Sciences, České Budějovice, Czech Republic

[6] Institute of Biostatistics and Analyses, Faculty of Medicine, Masaryk University, Brno, Czech Republic

[7] Central European Institute of Technology (CEITEC), Masaryk University, Brno, Czech Republic

[8] Bioveta, a.s., Ivanovice na Hané, Czech Republic

[9] DYNTEC spol. s r. o., Terezín, Czech Republic

[10] Faculty of Science, RECETOX, Masaryk University, Brno, Czech Republic

[11] Department of Biology, Faculty of Medicine, Masaryk University, Brno, Czech Republic

[12] Faculty of Science, Charles University, Prague, Czech Republic

APPENDIX 2

Bíňovský J, Šiborová M, Zlatohurska M, Nováček J, Bárdy P, Baška R, Škubník K, Botka T, Benešík M, Pantůček R, Tripsianes K, Plevka P (2026) Conformational changes of the baseplate regulating tail contraction of *Staphylococcus* phage 812. *EMBO Journal* 45:5514–5536. https://doi.org/10.1038/s44318-026-00834-9

(JCR 2025: IF = 8.4; Q1 – Biochemistry & Molecular Biology)

CC BY 4.0

Article

TRANSPARENT PROCESS OPEN ACCESS CHECK FOR UPDATES

THE EMBO JOURNAL

Conformational changes of the baseplate regulating tail contraction of *Staphylococcus* phage 812

Ján Bíňovský[1,2,4], Marta Šiborová[1,4], Maryna Zlatohurska[1], Jiří Nováček[1], Pavol Bárdy[3], Roman Baška[1], Karel Škubník[1], Tibor Botka[3], Martin Benešík[3], Roman Pantůček[3], Konstantinos Tripsianes[1] & Pavel Plevka[1]✉

Abstract

Phages with contractile tails employ elaborate mechanisms to penetrate bacterial cell walls and deliver their genomes into the host cytoplasm. Here, we used cryo-EM to show that the baseplate of phage 812, a member of the *Kayvirus* genus, which infects Gram-positive *Staphylococcus* strains, is formed of a core, wedge modules, and baseplate arms carrying receptor-binding proteins 1 and 2 and tripod complexes. Upon binding to a host cell, the receptor-binding proteins of phage 812 baseplate reorient and undergo conformational changes. The changes to the tripod complexes trigger the release of the central spike and weld proteins, which expose peptidoglycan-degrading domains of the hub proteins. Changes in the positions of baseplate arms are transmitted through wedge modules to tail sheath initiator proteins. The ring of the tail sheath initiator proteins expands and triggers the contraction of the tail sheath, which shortens to 50% and pushes the tail tube 10–30 nm into the bacterial cytoplasm. Homologous molecular mechanisms are probably shared by phages of the *Herelleviridae* family with contractile tails to infect Gram-positive bacteria.

Subject Categories Microbiology, Virology & Host Pathogen Interaction; Structural Biology
https://doi.org/10.1038/s44318-026-00834-9
Received 4 February 2025; Revised 25 May 2026;
Accepted 29 May 2026
Published online: 26 June 2026

Introduction

Tailed phages use baseplates at the end of their tails to attach to the host cell surface to initiate infection (Nobrega et al, 2018). The cell binding of phages with contractile tails is coupled with a conformational change to the baseplate that triggers tail sheath contraction (Leiman and Shneider, 2012). The tail tube penetrates the cell wall and enables the ejection of the phage genome into the bacterial cytoplasm. Most of the phages with contractile tails and contractile injection systems (CISs) structurally characterized to date attack Gram-negative bacteria (Taylor et al, 2016; Li et al, 2023; Wang et al, 2023; Yang et al, 2023a, 2023b; Yu et al, 2024; Sonani et al, 2024; Marín-Arraiza et al, 2025). Current knowledge regarding the mechanisms employed to breach the cell walls of Gram-positive bacteria is limited.

Phages of the genus *Kayvirus* of the family *Herelleviridae* (Barylski et al, 2020) exhibit high lytic activity against the Gram-positive bacterium *Staphylococcus aureus* (Botka et al, 2019; Łobocka et al, 2012; Vandersteegen et al, 2011). This human pathogen can cause skin and epithelial infections, as well as bacteremia that can develop into life-threatening sepsis (Kwiecinski and Horswill, 2020; Grunenwald et al, 2018). *S. aureus* is frequently resistant to antibiotics, which has renewed interest in phage therapy (Venturini et al, 2022; Petrovic Fabijan et al, 2020; Uyttebroek et al, 2022). The best studied *Kayvirus*, phage K, shares 98.5% of the genome identity with a polyvalent phage 812. Host range mutants of phage 812 were shown to infect more than 90% of *S. aureus* isolates (Pantůček et al, 1998; Botka et al, 2019). Major components of the *S. aureus* cell wall are peptidoglycan and teichoic acids (van Dalen et al, 2020). Phage 812 and related *Kayvirus* phages recognize the backbone and side-chain moieties of the wall teichoic acid (Xia et al, 2011; Takeuchi et al, 2016; Krusche et al, 2025).

It has been shown that a virion of 812 is formed by an icosahedral head with a diameter of 90 nm and a 240-nm-long tail that ends with a lentil-shaped baseplate (Nováček et al, 2016). Upon binding to the *S. aureus* cell wall, the baseplate transforms into a double-layered disc-shaped conformation. Furthermore, the structure of phage A511 of the *Herelleviridae* family, which infects Gram-positive *Listeria* and is morphologically similar to 812, has also been determined (Guerrero-Ferreira et al, 2019). However, the resolutions of the previous studies of 812 and A511 were limited to 13 and 14 Å, respectively, which prevented the identification of some of the baseplate components and characterization of their conformational changes that enable cell wall binding, tail contraction, and genome delivery.

The naming convention for baseplate components was established in the pioneering studies of phage T4. The core of the baseplate is formed by the central hub (Taylor et al, 2016, 2018), which serves as a centerpiece for the baseplate assembly and a

[1]Central European Institute of Technology, Brno, Czech Republic. [2]National Centre for Biomolecular Research, Faculty of Science, Masaryk University, Brno, Czech Republic. [3]Department of Experimental Biology, Faculty of Science, Masaryk University, Brno, Czech Republic. [4]These authors contributed equally: Ján Bíňovský, Marta Šiborová.
✉E-mail: pavel.plevka@ceitec.muni.cz

 © The Author(s)

platform for the tail tube polymerization. Six wedge complexes encircle the core and provide the foundation for tail sheath assembly (Taylor et al, 2016, 2018). Baseplate core proteins of contractile-tailed phages exhibit high structural conservation (Taylor et al, 2016, 2018; Veesler and Cambillau, 2011). In addition, the structures of the baseplate core proteins are shared by CISs (Park et al, 2018; Ge et al, 2020; Weiss et al, 2022; Xu et al, 2022; Desfosses et al, 2019; Jiang et al, 2019; Cai et al, 2024). The outer baseplate of contractile-tailed phages can be either simple, containing one or two tail fibers to bind to host cellular receptors (Li et al, 2023; Wang et al, 2023; Yang et al, 2023a, 2023b; Yu et al, 2024; Sonani et al, 2024), or more intricate, such as that of T4 (Taylor et al, 2016).

Here, we used a combination of cryogenic electron microscopy (cryo-EM), X-ray crystallography, nuclear magnetic resonance spectroscopy (NMR), and AlphaFold2 predictions to build the molecular structure of the tail and baseplate in extended and contracted conformations of a *Kayvirus* representative, phage 812. Based on a comparison of the pre- and post-contraction structures, we propose a sequence of conformational changes that propagate from the baseplate periphery to the core and trigger the tail sheath contraction.

Results and discussion

The structure of the baseplate of 812 with extended tail

The structure of the pre-contraction 812 baseplate with imposed sixfold symmetry was previously determined to a resolution of 13 Å using cryo-EM (Nováček et al, 2016). Here, we show that the 812 baseplate, similar to that of A511 (Guerrero-Ferreira et al, 2019), is only approximately sixfold symmetric. An initial asymmetric reconstruction with distinct threefold symmetric features enabled the determination of the overall baseplate structure to a resolution of 5.9 Å after imposing the C3 symmetry (Fig. 1A–E; Appendix Fig. S1A,B and Appendix Table S1). The baseplate of 812 is lentil-shaped with a diameter of 655 Å and height of 310 Å, and its constituent proteins can be assigned to a core, six wedge modules, and six arms decorated with three types of putative receptor-binding proteins (Fig. 1A–E; Appendix Fig. S1C–O and Appendix Tables S1 and S2).

Each of the baseplate arms is formed by the arm scaffold protein (gp117) and the arm segment proteins (gp118) (Fig. 1A–E). The baseplate arm provides attachment sites for proteins with putative receptor-binding functions: two trimers of the tripod proteins (gp119), a trimer of receptor-binding protein 1 (RBP1, gp121), and a trimer of receptor-binding protein 2 (RBP2, gp123) (Fig. 1A–D). The trimer of tripod proteins located closer to the tail axis (inner tripod) is oriented with its receptor-binding domains pointing away from the phage head (Fig. 1A–D). In contrast, the receptor-binding domains of tripod proteins attached to the baseplate arm further away from the tail axis (outer tripod) point toward the phage head (Fig. 1B–D). Trimers of RBP1 and RBP2 are attached to the end of the baseplate arm (Fig. 1A–D). The RBP1 reaches from one baseplate arm to the neighboring one, where it interacts with RBP2 (Fig. 1A,B). RBP2 points toward the tail sheath (Fig. 1C,D). In every alternating baseplate arm, the RBP1-RBP2 interaction is mediated by a coupler protein (gp122) (Fig. 1A,D).

The threefold symmetry of the 812 baseplate is most apparent in the distinct conformations of the alternating baseplate arms and the positions of the putative receptor-binding proteins attached to them (Fig. 1A–D). The alternating arrangement of baseplate arms is caused by different angles at which the arms point away from the tail axis (Fig. 1C,D). The upper baseplate arms radiate from the tail axis at an angle of 72°, while the lower baseplate arms radiate at an angle of 62°. The differences in the baseplate arm angles position the six inner tripods to form a shape of an equilateral triangle when viewed along the tail axis towards the phage head (Fig. 1A). The distinct angles of baseplate arms also influence the interactions of tripod proteins with the tail sheath. The outer tripod attached to the upper baseplate arm interacts with the first tail sheath disc (Fig. 1C,D; Appendix Fig. S2A). In contrast, the outer tripod bound to the lower baseplate arm does not interact with the tail sheath (Fig. 1C,D; Appendix Fig. S2B).

Each baseplate arm protrudes radially from a wedge module. A localized reconstruction of the wedge modules and baseplate core reached a resolution of 3.0 Å (Fig. 2A–F; Appendix Figs. S1C,D, S3, and S4 and Appendix Table S1). Each wedge module is a heterotrimer formed by two copies of wedge protein (gp116) and an N-terminal part of the arm scaffold protein (gp117) (Fig. 2A–F; Appendix Fig. S4). Two neighboring wedge modules that connect to the upper and lower baseplate arms assume distinct conformations (Appendix Fig. S5A–C).

Six wedge modules encircle the baseplate core, composed of tail tube initiator, tail sheath initiator, hub, assembly, central spike, and weld proteins (Fig. 2A–F; Appendix Fig. S5A–F). The hexamer of tail tube initiator proteins (gp113) and trimer of hub proteins (gp110) form a channel, which extends the tail tube channel into the baseplate. The trimer of central spike proteins (gp112), bound to the three copies of weld protein (gp111), plugs the baseplate channel at the level of the hub proteins (Fig. 2A,B). The hexamer of tail tube initiator proteins is surrounded by six copies of each of the tail sheath initiator (gp115) and assembly proteins (gp114), which are placed above each other (Fig. 2A,B; Appendix Fig. S5).

It is likely that the overall threefold symmetry of the 812 baseplate is determined during assembly by the asymmetric addition of baseplate proteins to the trimer of hub proteins. The structural differences propagate into the baseplate periphery, resulting in the alternating angles of the baseplate arms relative to the tail axis (Fig. 1B–D). The same mechanism is probably employed to establish the threefold symmetry of the A511 baseplate (Guerrero-Ferreira et al, 2019). In contrast, baseplate core proteins of structurally characterized phages were shown to be arranged with quasi-sixfold symmetry (Taylor et al, 2016; Li et al, 2023; Wang et al, 2023; Yang et al, 2023a, 2023b; Yu et al, 2024; Sonani et al, 2024).

Central spike protein blocks the baseplate channel and protrudes from the baseplate

The trimer of central spike proteins of 812 blocks the baseplate channel and protrudes more than 30 nm from the baseplate (Fig. 3A,B). The central spike protein can be divided into oligosaccharide-binding (OB), β-prism, coiled-coil, knob, and petal domains (Fig. 3B; Appendix Fig. S6A and Appendix Table S3). The OB and β-prism domains were resolved in the reconstruction of the pre-contraction 812 baseplate (Fig. 2A). The structure of the coiled-

© The Author(s)

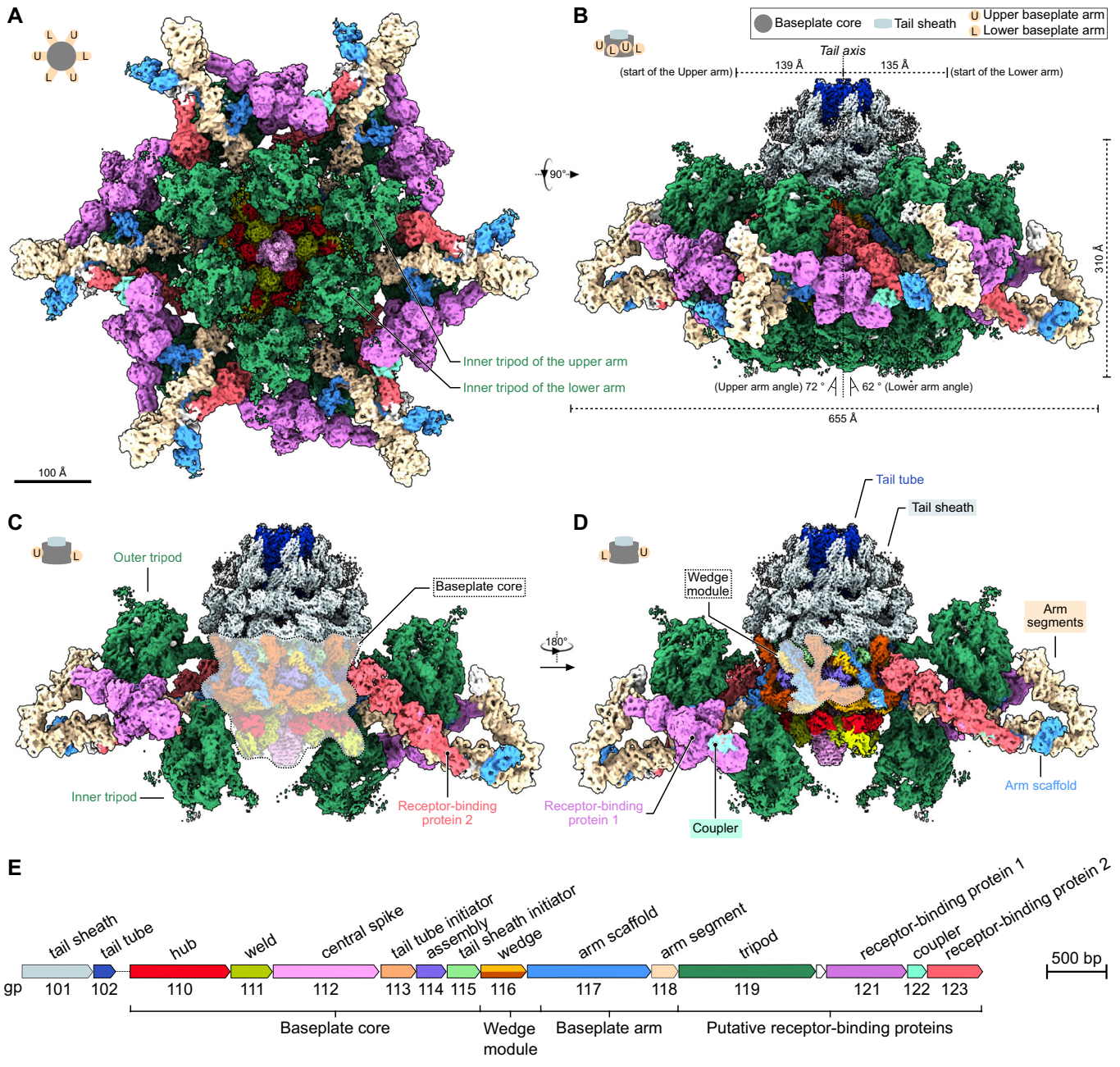

Figure 1. Structure of phage 812 baseplate.

(A–D) The composite cryo-EM map of the 812 baseplate is viewed along **(A)** and perpendicular **(B–D)** to the tail axis. Protein components of the baseplate and tail are colored according to the scheme depicted in **(E)**. Pictograms indicate the upper and lower baseplate arms. The height and width of the baseplate, tail axis, angles of baseplate arms relative to the tail axis, and distances of baseplate arms from the tail axis are indicated. **(C, D)** Side views of the 812 baseplate, with two front and two rear baseplate arms removed to display the wedge modules and baseplate core. **(E)** Scheme of part of the 812 genome encoding tail and baseplate genes.

coil domain was predicted using AlphaFold2 (Jumper et al, 2021) (Fig. 3B; Appendix Fig. S6A), and structures of the knob and petal domains were determined by cryo-EM and single-particle reconstruction of a recombinantly produced central spike protein (Fig. 3B; Appendix Fig. S7A–J and Appendix Table S1). The OB and β-prism domains have conserved structures shared by central spike proteins of other phages and CISs (Ge et al, 2020; Jiang et al, 2019; Xu et al, 2022; Li et al, 2023; Yang et al, 2023a, 2023b; Yu et al, 2024; Sonani et al, 2024; Desfosses et al, 2019; Weiss et al, 2022). The two domains bind to the inside of the channel formed by the hub proteins (Fig. 2A,B; Appendix Fig. S4). The coiled-coil, knob, and petal domains protrude from the 812 baseplate and are not resolved in the cryo-EM reconstruction of the baseplate, due to the coiled-coil domain's flexibility (Fig. 3A). Structural prediction indicates that the coiled-coil domains from the three central spike proteins form a 22-nm-long fiber, reminiscent of the tail needle from phage P22 (Bhardwaj et al, 2009) (Fig. 3B; Appendix Fig. S6A). The knob domain has a tumor necrosis factor-like fold

 © The Author(s)

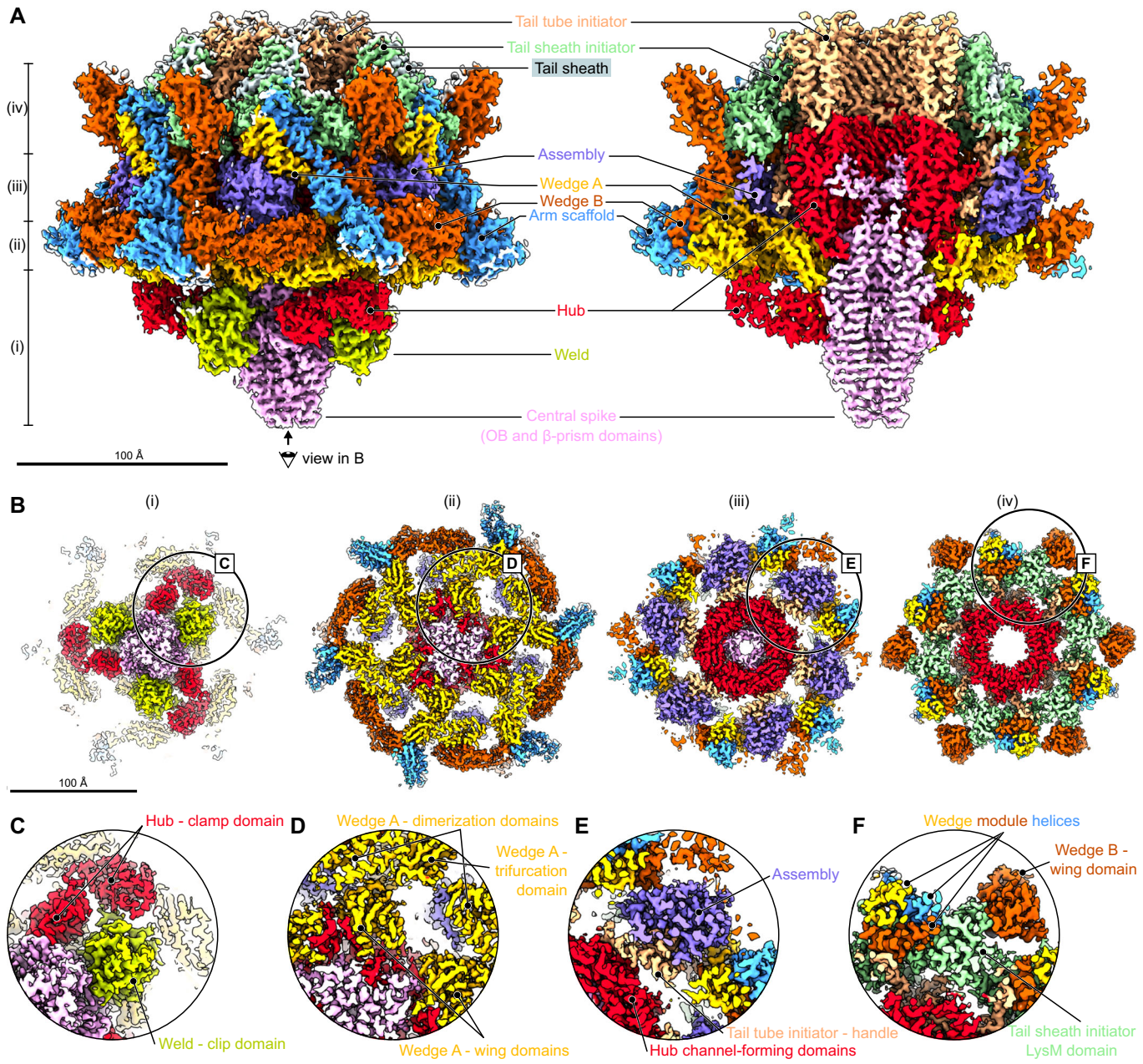

Figure 2. Structure of 812 wedge modules and baseplate core.

(A–F) The cryo-EM map of wedge modules and baseplate core. Individual proteins are colored according to the scheme depicted in Fig. 1E. Names of selected proteins and protein domains are indicated. **(A)** Side view of wedge modules and baseplate core shown as a whole (left) and with front half removed (right). The positions of sections shown in panel B are indicated on the left. **(B)** Sections through the wedge modules and baseplate core viewed towards the phage head. Positions of close-up views of selected regions displayed in **(C–F)** are indicated as black circles. **(C–F)** Close-up views of selected regions from sections in **(B)**.

(Eck and Sprang, 1989), similar to that of the head domains of receptor-binding proteins from lactococcal phages Tuc2009 and 1358 (Legrand et al, 2016; Farenc et al, 2014; McCabe et al, 2015) and a lectin from *Burkholderia cenocepacia* (Šulák et al, 2010) which indicates that the knob domain may bind to saccharides from the bacterial cell wall. The petal domain of the central spike protein has an α/β-barrel fold structurally similar to phosphodiesterases, such as the GlpQ protein from *B. subtilis* that cleaves teichoic acid during phosphate starvation (Myers et al, 2016; Shi et al, 2008). In addition, the petal domain includes two conserved histidines commonly found in active sites of phosphodiesterases, suggesting the domain's putative cleavage activity (Fig. 3C).

Phages with contractile tails and CISs attacking Gram-negative bacteria pierce the outer bacterial membranes using puncturing tips formed of proteins with β-prism or β-helix domains (Browning et al, 2012; Kanamaru et al, 2002; Shneider et al, 2013). In contrast, to infect Gram-positive *S. aureus*, phage 812 has to penetrate a 50–70-nm-thick layer of teichoic acids and peptidoglycan. Therefore, we propose that the knob and petal domains of the central spike of 812 bind to and degrade the host teichoic acids to expose

© The Author(s)

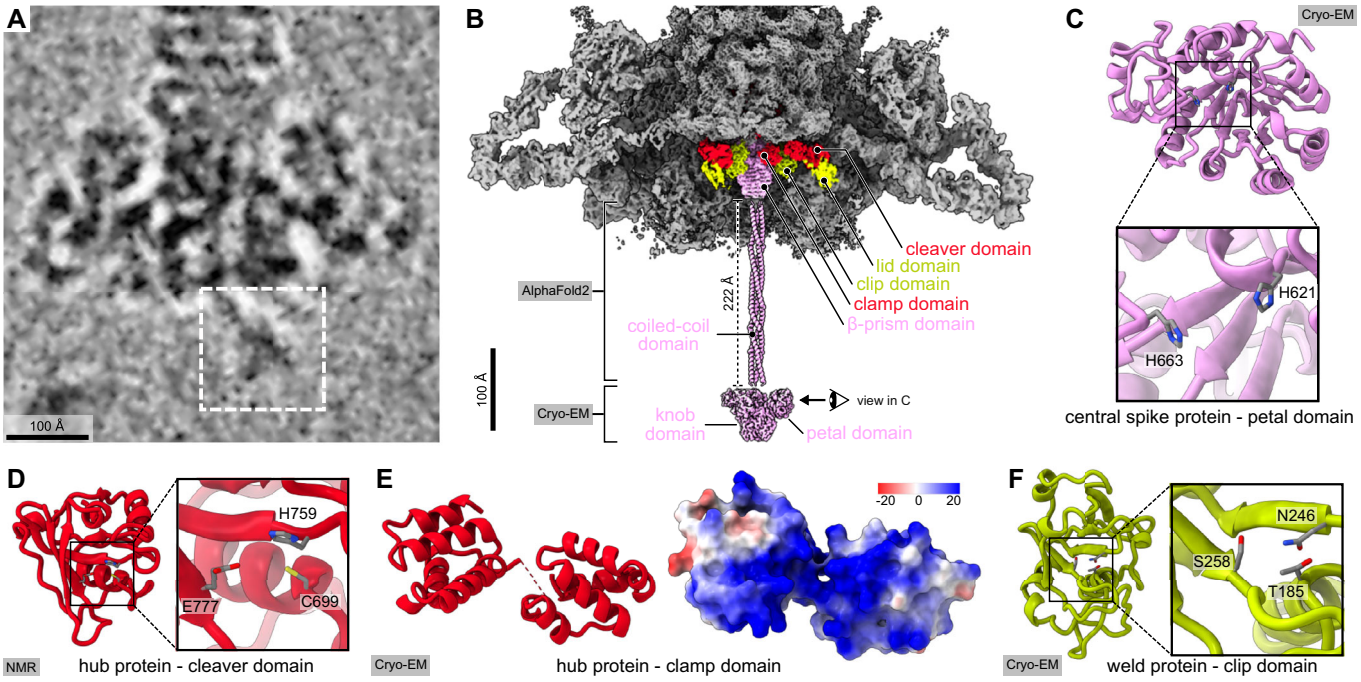

Figure 3. Central spike, hub, and weld proteins.

(A) Cryo-electron micrograph of the 812 baseplate. The white dashed rectangle indicates the putative position of the coiled-coil, knob, and petal domains of the trimer of central spike proteins. **(B)** Composite cryo-EM map of 812 baseplate and cryo-EM map of the knob and petal domains of the central spike protein trimer. The baseplate is shown in gray except for the central spike (pink), hub (red), and weld (green) proteins. The front part of the baseplate has been removed. The coiled-coil domains of the central spike proteins predicted using AlphaFold2 are shown in cartoon representation. **(C, D)** Cartoon representations of the petal domain of the central spike protein **(C)** and the cleaver domain of the hub protein **(D)**. Side chains of residues forming putative hydrolytic sites are shown in stick representation. Insets show details of the putative hydrolytic sites. **(E)** Cartoon (left) and surface (right) representations of the clamp domain of the hub protein. The molecular surface is colored according to Coulombic electrostatic potential in the range from −20 to 20 kcal/(mol·e) at 298 K. **(F)** Cartoon representation of the clip domain of the weld protein. Side chains of residues forming a putative receptor-binding site are shown as sticks. The structures shown in **(C–F)** were determined using cryo-EM or NMR, as indicated.

the peptidoglycan layer for degradation by the cleaver domain of the hub protein (see below).

Hub proteins facilitate penetration of the tail tube through the cell wall and cell membrane

The three hub proteins form a ring, extending the tail channel into the 812 baseplate (Fig. 2A–C). The hub protein can be divided into channel-forming domains I to IV and clamp and cleaver domains (Appendix Fig. S6B and Appendix Table S3). The channel-forming domains I and III have beta-barrel folds and are positioned next to each other so that the head-proximal interface formed by the trimer of hub proteins has pseudo-sixfold symmetry for binding the hexamer of tube initiator proteins (Appendix Figs. S4 and S6B). In contrast, the channel-forming domains II and IV of the hub protein, positioned below domains I and III, respectively, are structurally distinct and form interfaces for binding the trimer of central spike proteins to the inside of the hub channel (Appendix Figs. S4 and S6B). The channel-forming domains I-IV are structurally similar to those of the gp27 of phage T4, for which the domain naming convention was established (Kanamaru et al, 2002). Homologs of the channel-forming domains can also be identified among phages with long non-contractile tails (Tal proteins) (Veesler and Cambillau, 2011; Kizziah et al, 2020) and CISs (Vgrg-like proteins) (Taylor et al, 2018; Büttner et al, 2016; Leiman et al, 2009) (Appendix Table S3).

The cleaver domain of the hub protein, the structure of which was determined using NMR (Fig. 3D; Appendix Fig. S6B and Appendix Table S4), has the characteristic fold of the cysteine- and histidine-dependent amido-hydrolase/peptidase (CHAP) (Bateman and Rawlings, 2003), and contains the conserved catalytic triad Cys699-His759-Glu777 (Sanz-Gaitero et al, 2014) (Fig. 3D). Accordingly, zymogram analysis demonstrated that a recombinant cleaver domain degrades *S. aureus* cell walls (hence the name cleaver) (Appendix Fig. S8A,B), which agrees with previous functional studies of hub protein homologs from the related phage K (Becker et al, 2008; Paul et al, 2011). The clamp domain of the hub protein is formed by ten short α-helices that connect the central spike protein to weld proteins (Figs. 2B,C and 3E). The clamp domain is structurally similar to pore-forming saposin-like proteins, which employ positively charged residues to interact with the negatively charged surfaces of lipid membranes (Appendix Table S3) (Willis et al, 2011; Lee et al, 2006). Since the clamp domain of the 812 hub protein contains a long positively charged patch of residues, as the saposin-like proteins do (Fig. 3E), we speculate that it may bind the *S. aureus* membrane to facilitate its penetration by a tail tube. In addition to gp27 of T4 featuring a lysozyme domain, more hub proteins equipped with enzymatic domains have been reported recently (Yu et al, 2024; Cai et al, 2024). Therefore, we propose that the hub proteins of 812 and related phages enable genome delivery by degrading peptidoglycan to facilitate penetration of the tail tube through the cell wall.

 © The Author(s)

Tail tube initiator, weld, assembly, and tail sheath initiator proteins complete the baseplate core

Three weld proteins bind to the central spike, hub, and three inner tripod proteins, connecting them together (Figs. 1C,D and 2A–C; Appendix Figs. S4, S6C–E, and S9A–D). Six assembly and six tail sheath initiator proteins surround the hub and tail tube initiator proteins to complete the structure of the baseplate core (Fig. 2A,B,E,F; Appendix Figs. S4 and S10A–C). The tube initiator and sheath initiator proteins are organized with sixfold symmetry. In contrast, the central spike, weld, hub, and assembly proteins are organized with threefold symmetry that determines the overall organization of the baseplate when the 812 tail is in extended conformation.

The weld protein of 812 can be divided into the N-terminal lid and C-terminal clip domains, which are connected by a 14-residue-long linker (Appendix Fig. S6D). The lid domain interacts with an inner tripod and serves as a lid covering the peptidase site of the cleaver domain of the hub protein (Appendix Fig. S9A–D). Therefore, releasing the weld protein from the baseplate upon host cell binding exposes the active site of the cleaver domain of the hub protein to hydrolyze the cell wall peptidoglycan. The clip domain of the weld protein, located closer to the tail axis, binds the weld protein to the central spike protein (Fig. 2C; Appendix Fig. S9A–D). The clip domain has the CHAP protein fold similar to that of the cleaver domain of the hub protein (Gillespie et al, 2015; Wu et al, 2019) (Fig. 3F). However, the clip domain lacks the conserved catalytic residues Cys-His-Glu required for the peptidoglycan cleavage (Fig. 3F) (Sanz-Gaitero et al, 2014). Thus, the clip domain is likely enzymatically inactive, but may have retained peptidoglycan-binding ability, similar to the RipD protein from *M. tuberculosis* (Böth et al, 2014). There is no homolog of the weld protein in the baseplate of the related phage A511 (Guerrero-Ferreira et al, 2019; Habann et al, 2014). The weld protein may be unnecessary for A511 because of the differences in the cell wall composition between *Staphylococcus* and *Listeria*.

The assembly protein of 812 is formed by a compact bundle of nine α-helices. The assembly protein interacts with the wedge protein and the C-terminal handle of the tail tube initiator protein (Fig. 2E; Appendix Fig. S4). There are proteins with a compact globular structure and in the equivalent position in the baseplates of pyocin R2 and phages Pam3, E217, A-1, and Milano (Appendix Table S3), indicating the structural role of these proteins in baseplate cores (Ge et al, 2020; Li et al, 2023; Yang et al, 2023a; Yu et al, 2024; Sonani et al, 2024).

The hexamer of tail tube initiator proteins binds to the trimer of hub proteins and, on the other side, to a hexamer of tail tube proteins (Fig. 2A). The tail tube initiator protein can be divided into the N-terminal β-barrel domain and the C-terminal α-helical handle, which stretches along the hub protein and reaches the assembly protein in the baseplate core (Appendix Figs. S4 and S6C). The tail tube initiator proteins from pyocin R2 and phages E217 and Pam3 contain extensions similar to the C-terminal handle of the 812 tail tube initiator protein, suggesting an evolutionary link between phage and pyocin baseplates (Leiman and Shneider, 2012; Veesler and Cambillau, 2011).

The tail sheath initiator protein of 812 is composed of the LysM and handshake domains (Appendix Fig. S6E). The handshake domain, containing two β-strands, interacts with the N- and C-termini of tail sheath proteins from the first tail sheath disc and the C-terminus of tail sheath protein from the second tail sheath disc to form a five-stranded β-sheet (Appendix Fig. S10B,C). Therefore, the interactions of the tail sheath and tail sheath initiator proteins can initiate assembly of the 812 tail sheath. Proteins containing domains with structures similar to the handshake domain are integral to the baseplates of most CISs and phages with contractile tails (Taylor et al, 2018; Büttner et al, 2016; Maxwell et al, 2013) (Appendix Table S3).

Wedge modules attach baseplate arms to the baseplate core

Wedge modules are structural components of phage baseplates, which enable the attachment of peripheral baseplate proteins to the baseplate core (Taylor et al, 2016; Watts and Coombs, 1990). Here, we show that the wedge module of 812 is formed by two wedge proteins with different conformations, A and B, and the N-terminal 176 residues of the arm scaffold protein (Fig. 2A; Appendix Figs. S4, S5B,C, and S6F,G). Wedge protein can be divided into N-terminal α-helices, wing, trifurcation, and dimerization domains (Appendix Fig. S6F,G), and the part of the arm scaffold protein belonging to the wedge module can be divided into N-terminal α-helices and a trifurcation domain (Fig. 4A–D). Individual parts of the 812 wedge module are structurally conserved and can also be found in the baseplate of phage T4 (Taylor et al, 2016). The N-terminal helices and trifurcation domains mediate contacts between the proteins forming the wedge module (Fig. 2F; Appendix Fig. S5A–C). The wing domain of wedge protein A binds to the hub and central spike proteins (Fig. 2D). In contrast, the wing domain of wedge protein B binds to the tail sheath initiator protein (Fig. 2F). The six wedge modules form an iris around the baseplate core (Appendix Fig. S5A), as described in phage T4 (Taylor et al, 2016). Dimerization domains of wedge proteins mediate interactions between neighboring wedge modules (Appendix Fig. S5A). Even though the neighboring wedge modules differ in their conformations due to the overall threefold symmetry of the baseplate, the contacts between the dimerization domains are similar (Appendix Fig. S5A–F).

Baseplate arms provide attachment sites for putative receptor-binding proteins

To address the flexibility of the lower and upper baseplate arms from a phage with the extended tail, a series of sub-particle reconstructions were performed, resulting in resolutions ranging from 3.8 to 6.3 Å (Appendix Figs. S1E–O and S3 and Appendix Table 1). Baseplate arms of 812 are formed by docking loop 1, linker 1, bulge domain including docking loop 2, linker 2, elbow domain, linker 3, and C-terminal domain of the arm scaffold protein that are reinforced by six dimers of the arm segment proteins named A–F (Fig. 4A,B,D; Appendix Fig. S11A–E). We employed X-ray crystallography to determine the structure of the arm segment protein (Fig. 4C; Appendix Table S5) and AlphaFold2 (Jumper et al, 2021) to predict the structures of the arm scaffold protein domains (Appendix Fig. S11A). The structures were fitted and refined into the sub-particle reconstruction cryo-EM maps of the upper and lower arms. The arm segment protein is composed of an N-terminal α-helix followed by a three-stranded β-sheet and a

© The Author(s)

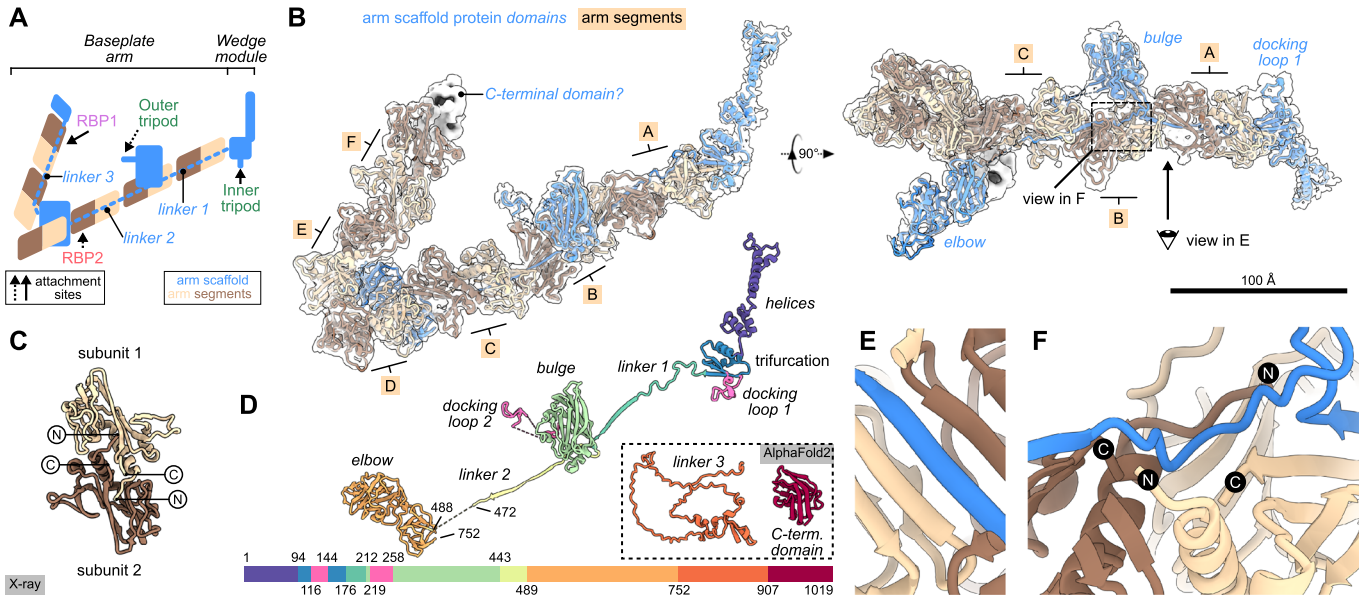

Figure 4. Structure of baseplate arm.

(A) Schematic representation of the baseplate arm and part of the wedge module. Attachment sites of tripods, RBP1, and RBP2 are indicated. **(B)** Composite cryo-EM map of the lower baseplate arm with structures of arm scaffold and arm segment proteins shown in cartoon. The distal end of the baseplate arm, probably corresponding to the C-terminal domain of the arm scaffold protein, is shown as a white surface. Parts of the baseplate arm with fitted structures are shown as white semi-transparent surfaces. Arm segment dimers A to F are indicated. **(C)** The structure of the dimer of arm segment proteins, determined using X-ray crystallography, is shown in a cartoon. **(D)** Cartoon representation of the domains of the arm scaffold protein. Domain names and selected chain termini are indicated. Domain structures predicted using AlphaFold2 and not fitted into the cryo-EM maps are shown in a dotted rectangle. The linear diagram (bottom) representing arm scaffold protein domains is colored according to the structures. **(E, F)** Cartoon representation of the interaction of the C-terminal β-strands of arm segment proteins with the arm scaffold protein. Views are indicated in **(B)**.

bundle of loops and short β-strands (Fig. 4C). The overall structure of the arm segment protein is similar to that of gp8 from phage T4 and gp105 from phage A511 (Guerrero-Ferreira et al, 2019; Leiman et al, 2003). The interactions between the C-terminal β-strands of arm segment proteins from neighboring dimers are mediated by linkers of the arm scaffold protein (Fig. 4E,F). The linkers of the arm scaffold protein fill the gaps between the dimers of arm segment proteins, creating continuous, seven-stranded β-sheets, as has been speculated previously (Guerrero-Ferreira et al, 2019). The cryo-EM map contains resolved density only for the linker 1 and a part of the linker 2 (Fig. 4D). The density likely belonging to the remainder of linker 2, linker 3, and the C-terminal domain could be observed in a difference map after the subtraction of the densities belonging to the arm segment proteins (Appendix Fig. S11B–E).

The arm scaffold protein provides attachment sites for two trimers of tripod proteins, one trimer of RBP1, and one trimer of RBP2. The 28-residue-long docking loop 1 of the arm scaffold protein forms the binding site for the inner tripod complex, while the 40-residue-long docking loop 2 enables attachment of the outer tripod complex (Fig. 4A,B,D). The docking loops have triangular structures that fit into crevices formed by the trimers of tripod proteins (Appendix Fig. S12A–D). Despite the different length, the docking loops have hydrophobic residues arranged in equivalent positions in the inner and outer tripod crevices (Appendix Fig. S12E).

Predicted structure of the elbow domain of the arm scaffold protein with a double β-sandwich fold could be placed at the periphery of baseplate arms, where it forms a protuberance pointing towards the neighboring baseplate arm (Fig. 4B). Close to the elbow domain, a low-resolution density emerging from below the arm segment C likely belongs to a part of the arm scaffold protein that attaches RBP2 (Appendix Fig. S11D). Arm segment dimers D, E, and F create an arch at the baseplate periphery, with the linker 3 likely running along the segments (Fig. 4A; Appendix Fig. S11B,C). RBP1 is attached to the baseplate arm where a low-resolution density emerges from the arm segment F (Appendix Fig. S11E). At the end of the baseplate arm, a density was identified that could accommodate the C-terminal domain of the arm scaffold protein with a predicted β-sandwich fold, although it could not be positioned in the reconstruction with confidence (Appendix Fig. S11E).

Baseplate of 812 contains 12 tripod protein complexes

The most prominent components of the 812 baseplate are the twelve trimers of tripod proteins (Fig. 1A–D). We predicted structures of the tripod proteins in 812 with an extended tail using AlphaFold2 (Jumper et al, 2021) and refined their structure in the corresponding parts of the reconstructions of the baseplate arms (Fig. 5A–E; Appendix Fig. S13A,B). The tripod protein can be divided into spine, flap, fiber, base, fin, leg, anchor, and hook domains (Fig. 5E). The flap domain contains an insertion loop, three of which play a role in the attachment of the tripod complex to the arm scaffold protein (Fig. 5C–E). The base and fin domains of tripod proteins have ten-stranded β-sandwich folds of carbohydrate-binding module families 16 and 61 (Cid et al, 2010; Bae et al, 2008) (Fig. 5E; Appendix Table S3), indicating that they may bind glycans from the *S. aureus* cell wall. The leg domain includes fifteen β-strands, eight forming a β-sandwich that is structurally similar to lectin-like protein Cwp84 from *C. difficile* (Bradshaw et al, 2014) (Fig. 5E; Appendix Table S3), suggesting

 © The Author(s)

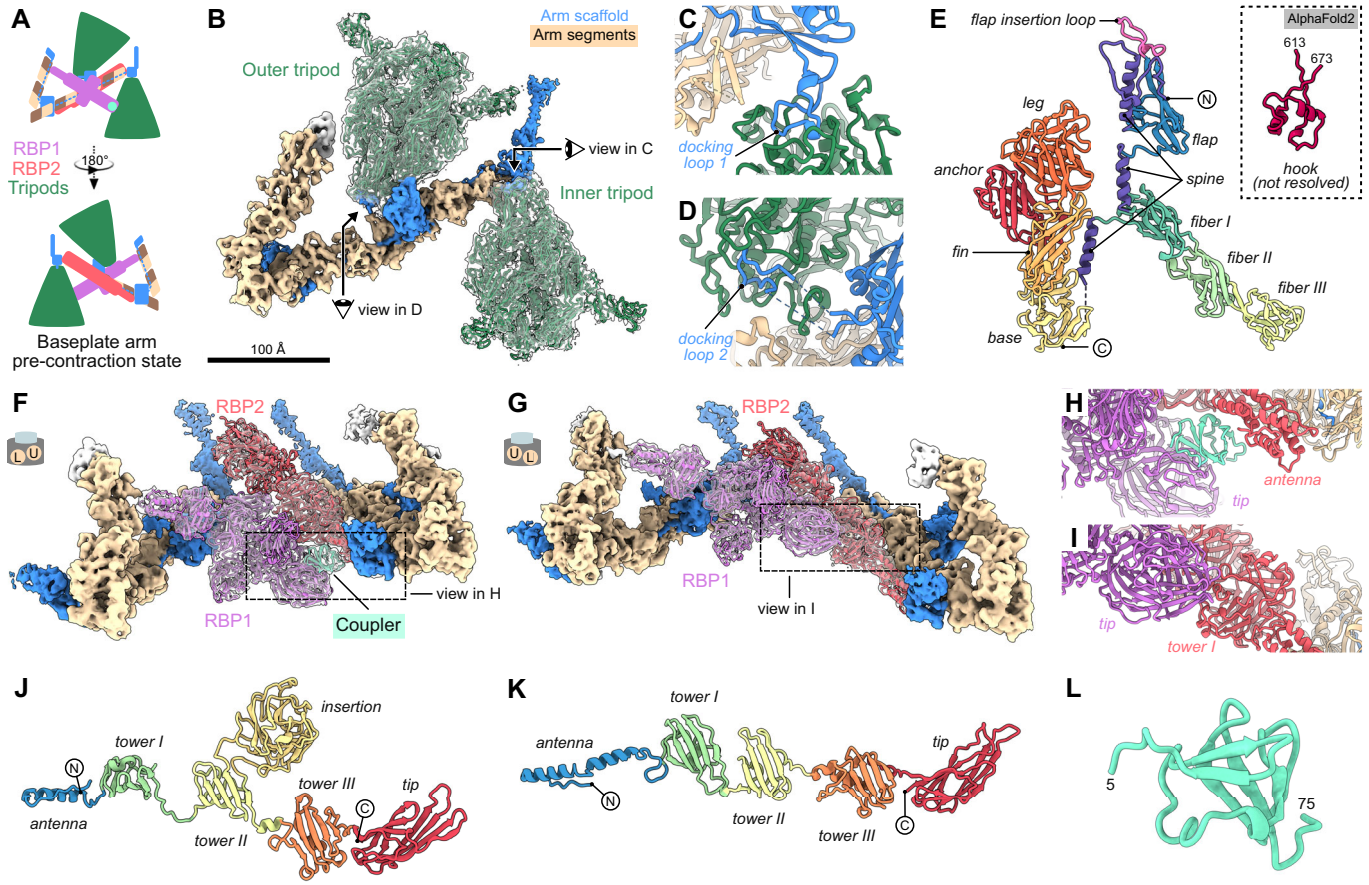

Figure 5. Tripod and receptor-binding proteins of the 812 baseplate.

(A) Schematic representation of the baseplate arm and part of the wedge module of 812 with the extended tail. **(B)** Composite cryo-EM map of the lower baseplate arm. Part of the map corresponding to the inner and outer tripod protein trimers is shown as a white semi-transparent surface. Part of the map corresponding to the arm scaffold and arm segment proteins is shown as an opaque surface colored according to the protein type. Structures of the tripod proteins are shown in cartoon representation. Views of **(C, D)** are indicated. **(C, D)** Detailed views of attachment sites of inner **(C)** and outer **(D)** tripod protein trimers to the docking loops 1 and 2, respectively, of the arm scaffold protein. **(E)** The structure of the tripod protein is shown in cartoon representation and colored by domains. Domain names and chain termini are indicated. **(F, G)** Composite cryo-EM maps of the two neighboring baseplate arms. Parts of maps corresponding to RBP1, RBP2 **(F, G)**, and coupler **(F)** proteins are shown as a white semi-transparent surface. Parts of maps corresponding to the arm scaffold and arm segment proteins are shown as opaque surfaces colored according to the protein type. Structures of RBP1, RBP2, and coupler proteins are shown in cartoon representation. Views of **(H, I)** are indicated. **(H, I)** Detailed views of RBP1, RBP2, and coupler protein interactions are indicated in **(H)** and **(I)**. **(J, K)** Structures of RBP1 **(J)** and RBP2 **(K)** monomers are shown in cartoon representation and colored by domains. **(L)** The structure of the coupler protein is shown in a cartoon.

another possible receptor-binding site. The anchor domain with a β-sandwich fold is followed by the hook domain with sequence similarity to LysM proteins, indicating it may bind peptidoglycan (Buist et al, 2008) (Fig. 5E; Appendix Fig. S14 and Appendix Table S3).

Receptor-binding and coupler proteins

The baseplate of 812 contains six trimers of each of RBP1 and RBP2 with putative receptor-binding activities (Fig. 1A–D). We employed AlphaFold2 (Jumper et al, 2021) to predict the structures of RBP1 and RBP2 and refine them in the corresponding parts of the cryo-EM map of the pre-contraction baseplate (Fig. 5F–L). RBP1 consists of an antenna domain, three tower domains, and a tip domain, all positioned along the symmetry axis of the trimer, and a wing domain protruding laterally from the second tower domain (Fig. 5J). The tower domains are structurally similar to each other and contain characteristic six-stranded β-sheets. The antenna domain mediates the binding of RBP1 to the end of the baseplate arm near the arm segment F, and the tip domain of RBP1 points towards the neighboring baseplate arm (Fig. 5F,G). RBP2 has the same domain composition as RBP1, except for the wing domain, which is missing (Fig. 5K). In the baseplate, the antenna domain of RBP2 binds near arm segment C, and the tip domain is in contact with a wedge module (Fig. 5F,G; Appendix Fig. S2). Baseplate of 812 before tail contraction contains three copies of coupler proteins. One coupler protein connects the tip domain of RBP1 from a lower baseplate arm to the antenna domain of RBP2 from the neighboring upper baseplate arm (Fig. 5F). In contrast, RBP1 from the upper baseplate arm interacts directly with RBP2 from the lower baseplate arm (Fig. 5G). Resolved structure of the coupler protein (residues 5–75 out of 124) contains two β-sheets (Fig. 5L) and the closest structural homolog is the tail fiber assembly protein from phage Mu, where it serves as a chaperone for correct folding of the tail fiber (North et al, 2019).

© The Author(s)

Rearrangement of RBPs and tripod complexes during tail contraction

Tailed phages use receptor-binding proteins from their baseplates to attach to host cells. For phages with contractile tails, the receptor binding is accompanied by reorganization of the baseplates, which may include conformational changes to individual proteins (Nobrega et al, 2018; Taylor et al, 2016; Nováček et al, 2016). It has been proposed that the reorganization starts at the baseplate periphery, propagates to the inner baseplate, and triggers the contraction of the tail sheath (Leiman and Shneider, 2012; Taylor et al, 2016). The overall asymmetric reconstruction of the baseplate of 812 with the contracted tail reached the resolution of 6.6 Å (Appendix Fig. S7A and Appendix Table S1). The post-contraction baseplate has the shape of a six-pointed star with a diameter of 713 Å and a thickness of 344 Å (Fig. 6A–C). The conformational change transforms the baseplate to sixfold symmetry, with all six baseplate arms protruding at 83° and positioned at the same distance from the tail axis (Fig. 6A–C; Appendix Fig. S7B). Focused reconstructions including tail sheath initiator, wedge module, inner tripod and tail sheath proteins show that the central part of the baseplate is stable, reaching local resolutions up to 3.1 Å (Appendix Figs. S7C,D and S15). The sub-particle reconstruction of the post-contraction baseplate arm contains resolved density of arm segment protein dimers A-C as well as of the docking loop 1, linker 1, bulge domain with the docking loop 2, and part of the linker 2 of the arm scaffold protein, inner and outer tripods, and RBP2 (Fig. 6D; Appendix Figs. S7E,F and S15). RBP1, arm segments D-F, and the remainder of the arm scaffold protein are not resolved in the reconstruction of the post-contraction baseplate, likely due to the flexibility of the structure (Fig. 6A–D). Comparing the structures of the baseplates of 812 particles with extended and contracted tails enabled us to describe conformational changes controlling the baseplate rearrangement and tail sheath contraction. The reorganization of the 812 baseplate is probably initiated by the interaction of the RBP1 with teichoic acid as its putative receptor. In the post-contraction baseplate, RBP2 trimers are oriented parallel with the tail axis, and their tip domains face away from the phage head (Fig. 6A–D). The movement of RBP1 and RBP2 provides space for the outer tripod complexes to rotate ~170° to point their receptor-binding domains away from the phage head (Fig. 6A±D). The inner tripod complexes assume positions with their axes parallel to the tail axis (Fig. 6A–D).

The interactions between the tripod complexes and the docking loops 1 and 2 of the arm scaffold protein are preserved after the baseplate reorganization (Fig. 6E,F). As described above, the docking loop 2 of the arm scaffold protein, which binds the outer tripod complex, is twelve residues longer than the docking loop 1 that binds the inner tripod complex (Appendix Fig. 12E). The extra residues of the docking loop 2 enable the ~170° rotation of the outer tripod complexes during the baseplate transformation.

The tripod complexes not only rotate, but also undergo complex conformational changes (Figs. 5E and 6G): (i) The second and third spine helices move towards the first spine helix by 10 and 16 Å, respectively. (ii) The fiber domain moves 13 Å towards the flap domain and rotates 20° counterclockwise around the tripod threefold symmetry axis when looking from the bottom of the tripod. (iii) The base domain shifts 24 Å along the third spine helix while rotating 174° around an axis perpendicular to the tripod symmetry axis. (iv) The fin domain moves 56 Å to protrude laterally from the tripod. (v) The three leg domains detach from the flap domains and move 88 Å to interact with each other under the base domains. (vi) The anchor and hook domains were not resolved in the cryo-EM reconstruction of the baseplate from a phage with a contracted tail (Fig. 6G); however, phage particles attached to the cell wall contain density at the bottom of the tripod complexes, suggesting that the anchor and hook domains stretch along the tripod threefold axis toward the cell wall (Appendix Fig. S16A,B). Similar density under the tripod complexes was observed in micrographs of contracted phage A511 attached to *Listeria* cells, and in the baseplate reconstructions of the spontaneously contracted 812 (Nováček et al, 2016) and A511 (Guerrero-Ferreira et al, 2019). Because of their positioning after the tripod conformational change and their sequence similarity to peptidoglycan-binding proteins of the LysM family (Appendix Fig. S14), we speculate that the hook domains of 812 and related phages bind the host cell wall.

The conformational change of tripod proteins is required to form tripod-tripod interactions in phages with contracted tails. In particular, the rotation and translation of the base domain are essential to expose an interface to which a fiber domain of the neighboring tripod complex binds through an interface with a buried surface area of 1900 Å^2 (Appendix Fig. S17A,B). Each inner tripod complex connects two inner tripods from neighboring baseplate arms and an outer tripod complex attached to the same baseplate arm. In addition, one fiber domain of each outer tripod complex interacts with tower domains 1 and 2 of RBP2 (Fig. 6B). The contacts mediated by the fiber domains probably stabilize the baseplate structure in phages with contracted tails.

Overall, the recognition and adhesion of 812 to the host cell requires re-orientation of the RBP1, RBP2, and conformational changes of tripod complexes, affecting the positions of the six arms of the post-contraction baseplate. Less extensive conformational changes were described for the receptor-binding proteins of other phages (Li et al, 2023; Šiborová et al, 2022; Sciara et al, 2010).

Conformational changes to the baseplate core prompt tail sheath contraction

The structure of wedge modules and baseplate core is affected by the rearrangement of receptor-binding proteins and baseplate arms, which in turn trigger the contraction of the tail sheath. The polypeptide chains of arm scaffold proteins link baseplate arms of 812 to the wedge modules (Fig. 4A,B). Therefore, the changes in the position and orientation of baseplate arms cause the iris-like structure formed by the wedge modules to expand in diameter from 104 to 122 Å (Appendix Fig. S5A,D). The expansion of the iris is enabled by the movement of the dimerization and trifurcation domains relative to each other, which brings the six wedge modules to an identical conformation (Appendix Fig. S5D,E). In contrast, the interactions between the dimerization domains of wedge proteins remain the same as in the baseplate of the extended tail (Appendix Fig. S5F). A similar expansion was described for gp6 and gp7 during the transition of the T4 baseplate from its extended to contracted state (Taylor et al, 2016). In phage 812, the expansion of the diameter of the tail sheath initiator hexamer, which probably occurs together with that of the wedge iris, is enabled by the partial unfolding of the linker helices between LysM and handshake domains (Appendix Fig. S10A–F). The unfolding of the linker enables the tail sheath initiator proteins to maintain the same contacts within the hexamer and with wedge modules as in the baseplate of the extended tail (Appendix Fig. S10C,F,G,H). The handshake domain of the tail sheath initiator protein inclines 17° (Appendix Fig. S10B,E)

 © The Author(s)

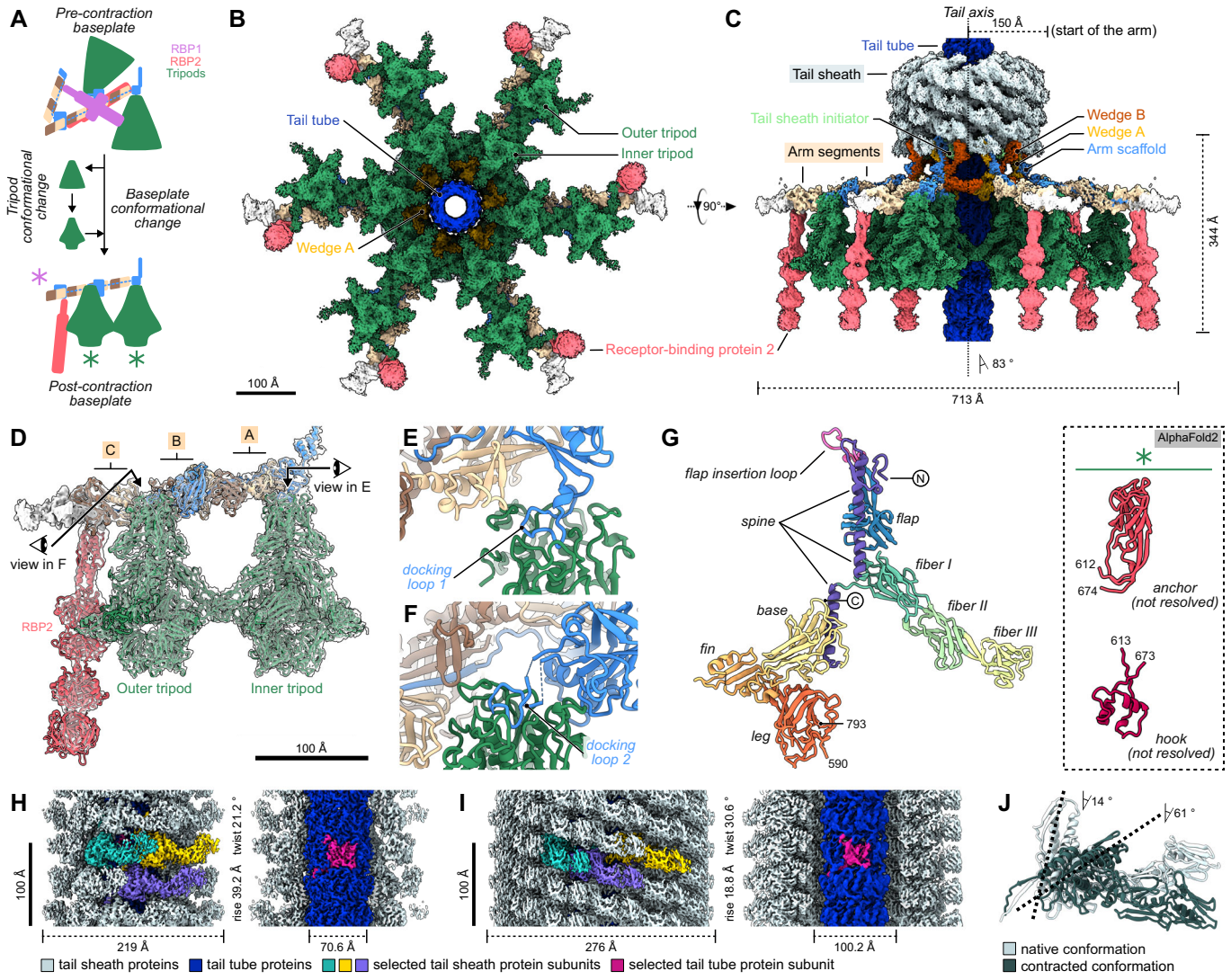

Figure 6. Structures of the 812 baseplate, tripods, and tail sheath after the tail sheath contraction.

(A) Schematic representation of conformational changes of the baseplate arm and tripod complexes. The pink asterisk indicates the putative attachment site of RBP1, which was not resolved in the reconstruction of the contracted baseplate. Green asterisks indicate the putative position of the anchor and hook domains of tripod proteins, which were not resolved in the reconstruction. **(B, C)** Composite cryo-EM maps of the contracted baseplate are viewed along **(B)** and perpendicular to **(C)** the tail axis. Proteins are colored according to Fig. 1D, and the names of selected components are indicated. **(C)** The height and width of the baseplate, position of the tail axis, angle of baseplate arms relative to the tail axis, and distance of baseplate arms from the tail axis are indicated. **(D)** Composite cryo-EM map of the baseplate arm from the contracted baseplate. The distal end of the baseplate arm that could not be interpreted is shown as a white surface. Part of the baseplate arm with fitted structures is shown as a white semi-transparent surface. Structures are shown in cartoon representation. Views of **(E, F)** are indicated. **(E, F)** Detailed views of attachment sites of inner **(E)** and outer **(F)** tripod protein trimers to the docking loops 1 and 2, respectively, of the arm scaffold protein. **(G)** Cartoon representation of the tripod protein is colored by domains. The structures of the anchor and hook domains of the tripod protein, which were not resolved in the cryo-EM reconstruction of the contracted baseplate, were predicted using AlphaFold2, and their putative positions are indicated in panel A by green asterisks. Domain names and chain termini are indicated. **(H, I)** Cryo-EM map of the extended tail **(H)** and composite cryo-EM map of the contracted tail **(I)**. For each panel, complete maps are shown on the left, and maps with the front half of the tail sheath removed shown on the right. Protein components are colored according to the legend below the panel. **(J)** Comparison of the structures of tail sheath proteins in extended and contracted conformations. The structures are shown in cartoon representation, and their domains II were superimposed. Angles of the long axes of domain I relative to the tail axis are indicated for each conformation.

and, together with the wedge iris expansion, triggers the contraction of the tail sheath, as discussed below.

The tail of 812 in extended conformation can bend

Contractile tails of phages differ in their length and mechanical properties. Tail bending up to 90° has been observed for *Herelleviridae* phages infecting *Staphylococcus* (Nováček et al, 2016; Klumpp et al, 2010), *Listeria* phage A511 (Guerrero-Ferreira et al, 2019), and phage Milano (Sonani et al, 2024) from the genus *Schmittlotzvirus* of an unclassified family. In contrast, the ~100-nm-long tails of *Straboviridae* phages, represented by T4, are rigid (Kostyuchenko et al, 2005). The flexibility of the longer tails was speculated to be an adaptation to withstand mechanical forces without breaking (Nováček et al, 2016; Zinke et al, 2022). To explain the ability of the 812 tail to bend without breaking, we determined the structure of the extended 812 tail to a

© The Author(s)

resolution of 4.2 Å (Fig. 6H; Appendix Fig. S7G and Appendix Table S1). Both tail tube and tail sheath proteins are arranged as six-start helices with a rise of 39.2 Å and twist of 21.2°.

The tail tube protein of 812 has an eight-stranded β-barrel fold with a protruding stacking loop, characteristic of tail tube proteins of long-tailed phages and CISs (Zinke et al, 2022) (Appendix Fig. S18A–D). Whereas the outer surface of the 812 tail tube features roughly equal distribution of positively and negatively charged residues, the inner surface of the tail tube is negatively charged, probably to facilitate the passage of the phage DNA during ejection (Appendix Fig. S18B,C). The ability of phage Milano to bend was attributed to the missing loop in the β-barrel domain of the tail tube protein (Sonani et al, 2024). The phage Milano tail tube straightening, after contraction, was speculated to be caused by the negative electrostatic potential of its outer surface (Sonani et al, 2024). However, since the tail tube of 812 contains the loop between the β-strands 6 and 7 (Appendix Fig. S18D) and its outer surface charges are balanced (Appendix Fig. S18B), its bending and straightening are likely enabled by different mechanisms.

The sheath protein of 812 can be divided into domains I-IV, according to the convention established for the tail sheath protein (gp18) of phage T4 (Leiman and Shneider, 2012) (Appendix Fig. S19A). In an extended tail, the domains I and II of the 812 tail sheath proteins interact with tail tube proteins and mediate contacts between tail sheath proteins (Appendix Fig. S19B,C). Domains III and IV are positioned successively next to domain II at the tail surface (Appendix Fig. S19B). The two-stranded β-sheet of domain I is augmented by accepting the N- and C-termini of tail sheath proteins from a disc positioned closer to the phage head (Appendix Fig. S19C). By mediating the handshake interactions, the domain I interconnects tail sheath proteins from successive discs. These interactions are conserved in the tail sheath structures of numerous phages and CISs (Taylor et al, 2016; Ge et al, 2020; Jiang et al, 2019; Xu et al, 2022; Li et al, 2023; Yang et al, 2023a, 2023b; Yu et al, 2024; Sonani et al, 2024; Desfosses et al, 2019; Weiss et al, 2022; Wang et al, 2023; Kudryashev et al, 2015; Ouyang et al, 2022). The domain II of the tail sheath protein is formed by six β-strands surrounded by eight α-helices, whereas domains III and IV each contain a beta-sandwich flanked by an α-helix (Appendix Fig. S19A). Domain III contacts domain IV of the tail sheath protein from the disc located closer to the baseplate (Appendix Fig. S19D). Additionally, domain IV interacts with domain II of the neighboring tail sheath protein from the same disc (Appendix Fig. S19D). The domain IV of the T4 gp18 is not involved in intersubunit contacts (Aksyuk et al, 2009); however, the bulkier domain III of the T4 tail sheath protein (168 residues) interacts with another tail sheath protein from the disc closer to the phage head (Aksyuk et al, 2009). We speculate that interactions of domains III and IV of the 812 tail sheath proteins allow a spring-like movement of the subunits relative to each other, which enables 812 tail bending (Appendix Fig. S19E).

Contraction of the tail sheath

In phages with contractile tails and CISs, the rearrangement of the baseplate induced by binding to a target cell wall triggers the contraction of the tail sheath, which transforms from the extended state to a lower energy contracted state (Maghsoodi et al, 2019). The released energy of the tail sheath contraction is used to drive the tail tube through the host cell wall (Ge et al, 2020; Li et al, 2023; Yu et al, 2024; Nováček et al, 2016; Guerrero-Ferreira et al, 2019). The contracted tail sheath of 812, which was reconstructed to a resolution of 3.2 Å, broadens to 276 Å in diameter (Fig. 6I; Appendix Fig. S7J and Appendix Table S1). The sheath broadening is coupled to a change in the rise and twist of the six-start helix formed by the tail sheath proteins to 18.8 Å and 30.6°, respectively. The successive discs of the contracted tail sheath are brought closer to each other due to the tilting of domain I by 47° compared to its extended conformation (Fig. 6J) while maintaining the intersubunit handshake interactions among domains I from successive discs (Appendix Fig. S19F,G). During contraction, the individual domains of the tail sheath protein of phage 812, unlike those of T4 and some CISs (Jiang et al, 2019; Aksyuk et al, 2009; Ge et al, 2015), move relative to each other, which enables the formation of the more extensive contacts between the subunits (Appendix Fig. S19H). The buried surface area of intersubunit contacts per tail sheath monomer increases from ~5500 Å in the extended tail sheath to ~9500 Å in the contracted tail sheath. We speculate that the enlarged contacts stabilize the straight structure of the contracted tail sheath, which is less flexible than the extended one.

It has been shown for phages T4 and A511 and R-type diffocin that the contraction of the tail sheath is gradual and occurs as a wave along the tail axis (Guerrero-Ferreira et al, 2019; Cai et al, 2024; Maghsoodi et al, 2019; Moody, 1973). In agreement with the previous in vitro observations, we captured particles of 812 with a partially contracted tail sheath attached to the *S. aureus* cell wall (Appendix Fig. S16). Furthermore, the cryo-EM reconstructions of baseplate-proximal parts of the tail sheath in the extended and contracted state provide structures of discrete intermediates of contraction (Appendix Figs. S1D and S7C). The first three baseplate-proximal tail sheath discs of the extended 812 tail sheath differ in conformation from those in the central part of the extended tail sheath (Appendix Fig. S20A,B). The deviation occurs gradually, with the first tail sheath disc being the most affected (Appendix Fig. S20B). Similar deviations of baseplate-proximal tail sheath proteins were observed in the R2 pyocin and T6SS (Ge et al, 2020; Nazarov et al, 2018). The first three sheath discs of 812 have their organization shifted toward that of the contracted tail sheath, which may reduce the activation energy required to initiate the tail sheath contraction (Fraser et al, 2021).

In the contracted tail sheath of 812, the structures of the first six baseplate-proximal tail sheath discs deviate from those of the central part of the contracted tail sheath (Appendix Fig. S20C,D). Similar to the extended tail sheath, the first contracted sheath disc is the most affected, and the sixth one the least affected (Appendix Fig. S20D). The first two baseplate-proximal sheath discs have the rise increased by 5.5 Å relative to the tail sheath disc from the center of the contracted tail sheath (Appendix Fig. S20D). The absence of a twist difference may be due to the more extensive contacts between consecutive tail sheath discs than in the extended tail, which is probably incompatible with deviations in the angle of the helical twist. Interactions with the sheath initiator and wedge module proteins likely cause the altered structure of the baseplate-proximal tail sheath discs and directly couple the conformational changes of baseplate proteins with the sheath contraction.

Changes in the baseplate structure required for cell wall penetration

Phages with contractile tails infecting Gram-positive bacteria employ enzymes that degrade teichoic acid and peptidoglycan to

 © The Author(s)

facilitate tail tube penetration through the cell wall (van Dalen et al, 2020; Fernandes and São-José, 2018). Phage 812 may use the petal domain of the central spike protein to cleave teichoic acid (Fig. 3B,C); however, the central spike protein needs to be released from the tail channel to enable the genome ejection. We speculate that the conformational change to inner tripods, which disrupts their interaction with weld proteins, triggers the release of the weld and central spike proteins from the baseplate. Dissociation of the weld protein is required to enable the cleaver domains of the hub protein to interact with and degrade the cell wall peptidoglycan (Appendix Fig. S9). This indicates that the weld and central spike proteins of 812 are released before the cell wall penetration by the tail tube. In contrast, the central spike proteins of phages T4 and E217, which infect Gram-negative bacteria, are released from baseplates after puncturing the host outer membrane (Li et al, 2023; Nishima et al, 2011; Wenzel et al, 2020).

Relative rotation of consecutive tail sheath discs in the extended 812 tail is 21.2°, whereas that of the contracted tail sheath is 30.6°. Since the tail contains 51 tail sheath discs, as the 812 tail sheath contracts, the tip of the tail tube is pushed through the teichoic acid and peptidoglycan layers while rotating about its axis by 475° (see "Methods"). The rotation of the hub proteins at the tip of the tail tube can enhance their peptidoglycan degradation activity by bringing them into contact with more substrate. Once the peptidoglycan layer is breached, the clamp domains of the hub proteins can interact with the *S. aureus* cytoplasmic membrane. It was shown that after the penetration of the outer membrane and peptidoglycan layer, gp27 from T4 (a homolog of the hub protein from 812) remains associated with the tip of the tail tube and probably interacts with the ejected tape measure protein to form a pore through the inner membrane of *E. coli* (Hu et al, 2015). The tail tube of 812 penetrates 10–30 nm into the *S. aureus* cytoplasm, depending on the thickness of the cell wall, which varies between 50 and 70 nm (Nováček et al, 2016). Therefore, unlike in T4, the hub proteins of 812 are probably not required to form a pore in the *S. aureus* membrane, and their role in genome delivery may be limited to facilitation of the penetration of the cell wall and cytoplasmic membrane by the tail tube tip. Whether the hub and other baseplate core proteins remain associated with the tip of the tail tube after the membrane penetration remains unknown.

Conclusions

In this study, we employed a combination of cryo-EM, X-ray crystallography, NMR, and structure prediction methods to elucidate the intricate mechanisms employed by phage 812 to penetrate the *S. aureus* cell wall in preparation for transferring its genetic material into the host cytoplasm. While most of the previously structurally characterized phages with contractile tails target Gram-negative bacteria, our focus has been on 812 attacking *S. aureus*, a representative of Gram-positive bacteria, which are comparatively less explored. We show that the baseplate of the phage 812 comprises a core, wedge modules, and baseplate arms that carry RBP1, RBP2, and tripod complexes (Fig. 1A–D). Upon binding to the *S. aureus* cell wall, the baseplate symmetry transitions from threefold to sixfold, which is enabled by a series of conformational changes that propagate from the baseplate periphery to the core (Fig. 6A–C). Based on our results, we propose a model of 812 cell adhesion and penetration (Fig. 7A–E). During the attachment, the putative receptor-binding proteins reorient, and tripod complexes undergo conformational changes to enable host cell surface binding (Fig. 7A,B). Subsequently, the central spike proteins degrade cell wall teichoic acids (Fig. 7A,B). In contrast, phages employ central spike proteins with rigid β-prism or β-helix domains to penetrate the outer membrane of Gram-negative bacteria (Browning et al, 2012; Kanamaru et al, 2002; Shneider et al,

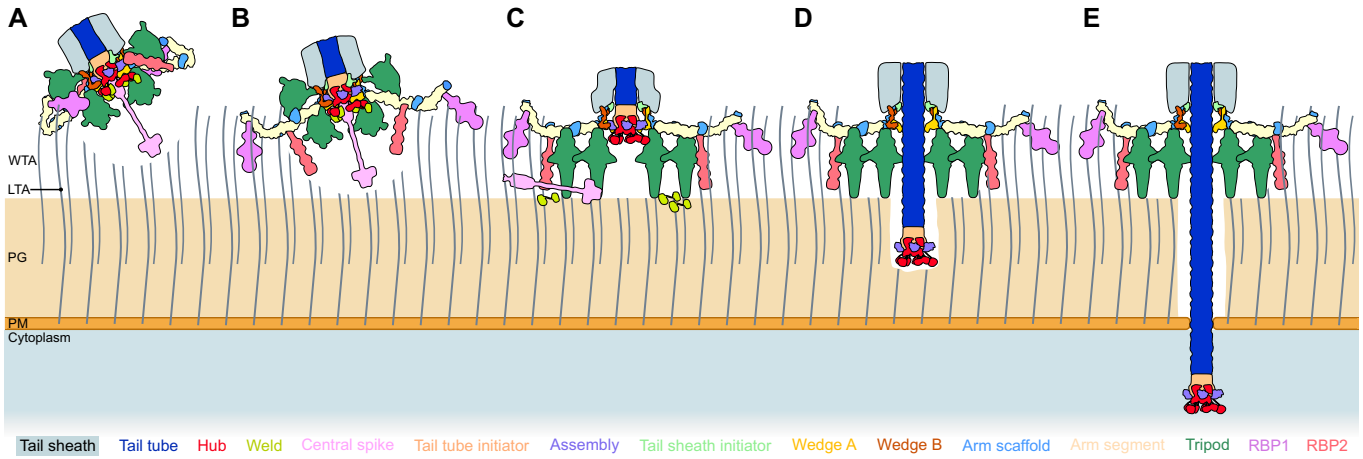

Figure 7. Scheme of 812 cell adhesion and penetration mechanism.

(A) The baseplate of phage 812 meets the cell wall of *S. aureus*, trimers of RBP1 bind to teichoic acid, and the petal domains of the central spike proteins cleave teichoic acid below the baseplate. **(B)** Trimers of RBP2 rotate and bind to teichoic acid. **(C)** Tripod complexes undergo a conformational change and anchor the baseplate to the cell wall. Central spike and weld proteins detach from the baseplate. The diameter of the iris formed by wedge modules increases, leading to a conformational change to tail sheath initiator proteins and baseplate-proximal sheath discs. The remaining baseplate core proteins detach from the sheath initiator and wedge module proteins. **(D)** As the contraction of the sheath discs propagates towards the phage head, the tail tube with tail tube initiator, hub, and assembly proteins at its tip is driven through the cell wall. The cleaver domain of the hub protein degrades the peptidoglycan. **(E)** The tail tube penetrates the cytoplasmic membrane, and its tip reaches the cytoplasm. However, it is not known whether the baseplate core proteins remain associated with the tip of the tail tube during the membrane penetration. WTA wall teichoic acid, LTA lipoteichoic acid, PG peptidoglycan, PM plasma membrane. The scheme is colored according to the list of proteins at the bottom.

© The Author(s)

2013). The conformational changes to the tripod complexes of 812 trigger the release of the central spike and weld proteins from the baseplate, which enables the hub proteins to cleave peptidoglycan (Fig. 7C,D) and facilitate penetration of the tail tube through the cell membrane (Fig. 7D,E). Changes in the baseplate arms' positions relayed through wedge modules to the hexamer of tail sheath initiator proteins cause an expansion of its diameter, triggering a tail sheath contraction (Fig. 7C–E). The structures of the baseplate core, tail sheath, and tail tube proteins of 812 are similar to those of phages and CISs targeting Gram-negative bacteria CISs (Park et al, 2018; Ge et al, 2020; Weiss et al, 2022; Xu et al, 2022; Desfosses et al, 2019; Jiang et al, 2019; Sonani et al, 2024; Yang et al, 2023a; Li et al, 2023; Yu et al, 2024; Taylor et al, 2016; Wang et al, 2023), indicating that the mechanism triggering the tail sheath contraction is conserved among the phages infecting hosts with distinct cell wall properties. The baseplate-proximal tail sheath discs of the extended 812 particle have an altered structure, which may lower the energy barrier required to initiate the tail sheath contraction. The tail sheath shortens from 200 to 96 nm upon contraction (Nováček et al, 2016), pushing the tail tube's tip through the peptidoglycan layer and plasma membrane 10–30 nm into the cytoplasm, depending on the local thickness of the *S. aureus* cell wall. The hub proteins with putative peptidoglycan-degrading activity are positioned at the tip of the 812 tail tube and may facilitate its penetration through the cell wall. In contrast, T4 baseplate lysozymes are released from the baseplate into the periplasmic peptidoglycan layer of Gram-negative *E. coli* (Kanamaru et al, 2002; Arisaka et al, 2003). The molecular characterization of the 812 baseplate structure and the mechanism of cell wall binding open up the possibility of a rational design of engineered bacteriophages to target specific bacterial strains.

Methods

Reagents and Tools Table

Reagent/resource	Reference or source	Identifier or catalog number
Experimental models		
Phage phi812K1/420	Novacek et al, 2016	KJ206563.2
S. aureus	Czech Collection of Microorganisms	CCM 885
S. aureus	Czech Collection of Microorganisms	SA 812 (CCM 4028)
E. coli BL21(DE3)	SIGMA	CMC0014
Recombinant DNA		
pET28a(+)	Merck	69864
pET28b(+)	Merck	69864
Custom pET22b	Plevka Lab	
Antibodies		
Oligonucleotides and other sequence-based reagents		
PCR primers	This study	Methods
Chemicals, enzymes, and other reagents		
Lipoteichoic acid from *S. aureus*	Sigma	L2515
Turbonuclease	Abnova	P5381
Peptone	OXOID	LP0037
LB broth	Sigma	L7275
IPTG	Sigma	I6758
$^{15}NH_4Cl$	Cambridge Isotope Laboratories	NLM-467-PK
Software		
Localized reconstruction tool	Ilca, et al, 2015, Plevka Lab	github.com/fuzikt/localrec
Relion 3.1	Zivanov, et al, 2020	
Relion 4.0	Kimanius, et al, 2021	
Relion 5.0	Kimanius, et al, 2021	
EMAN2	Tang, et al, 2007	https://github.com/cryoem/eman2
CrYOLO	Wagner, 2019	https://cryolo.readthedocs.io/en/stable/
Topaz	Bepler, et al, 2019	http://topaz.csail.mit.edu
Isolde	Croll, 2018	https://tristanic.github.io/isolde/
ChimeraX	Pettersen, 2021	https://www.cgl.ucsf.edu/chimerax/
Other		
Holey-carbon-coated Cu grid R2/1, mesh 200	Quantifoil	
Cu grid R1.2/1.3, mesh 200	Quantifoil	
Morpheus I & II crystallization screen	Molecular Dimensions	https://moleculardimensions.com
Midas	Molecular Dimensions	https://moleculardimensions.com
JCSG-plus	Molecular Dimensions	https://moleculardimensions.com

Bacteriophage 812 propagation and purification

For the 812 virion preparation, 150 mL of meat peptone broth (13 g/l nutrient broth, 3 g/l yeast extract, 5 g/l tryptone, pH 7.2) was inoculated with 2.5 ml of the overnight planktonic culture of *S. aureus* SA 812 (CCM 4028) and incubated at 37 °C with aeration until the culture reached an optical density (OD_{600}) of 0.5–0.6. Next, the culture was supplemented with 2 mM $CaCl_2$ and infected with 15 ml of phage lysate (~ 108 PFU/ml). The mixture was incubated at 37 °C with shaking at 340 RPM. After 2–3 h, the first signs of bacterial lysis appeared, and the mixture was placed in the fridge at 4 °C overnight. The next day, the lysate was centrifuged for 30 min at 5000 × *g* and 4 °C to remove cell debris. The supernatant was collected, filtered through a 0.45-µm filter, and stored at 4 °C. Phage particles were pelleted by centrifugation at 54,000 × *g* for 2.5 h at 4 °C using a Beckman 50.2 Ti rotor. The supernatant was

 © The Author(s)

discarded, and 100 µl of phage buffer (10 mM NaCl, 10 mM $CaCl_2$, 50 mM Tris-HCl, pH 8) was added to each centrifuge tube. The pellets were left to dissolve overnight at 4 °C with shaking. The next day, the resuspended phage sample was loaded onto a cesium chloride step gradient (1.4, 1.45, 1.5, and 1.7 g/ml), prepared in the phage buffer, and centrifuged at 40,000 RPM for 4 h at 4 °C using a Beckman SW41Ti rotor. After centrifugation, the visible bands were collected and dialyzed against phage buffer overnight at 4 °C.

Induction of 812 tail contraction and genome release in vitro

To induce contraction of the 812 tail, a previously reported protocol was modified (Fokine et al, 2004). The purified phage sample (10^{12} PFU/ml) in phage buffer was supplemented with teichoic acid from *Staphylococcus aureus* (SIGMA) at a concentration of 100 µg/ml, then diluted 10x using a solution of 3 M urea in the phage buffer and incubated at 42 °C for 45 min. After incubation, the sample was diluted 3x in the phage buffer and treated with Turbonuclease (Abnova) at a final concentration of 3.5 U/ml for 15 min at room temperature. Phage particles were pelleted by centrifugation at 75,000 × *g* at 4 °C for 1 h using a 50.2 Ti rotor (Beckman Coulter) and resuspended in the phage buffer.

Identification of structural proteins of the phage baseplate

The purified 812 phage was resuspended in Laemmli buffer and boiled for 3 min. Subsequently, the sample was treated with Turbonuclease (Abnova) at a final concentration of 2 U/µl for 15 min at room temperature. Proteins from the phage particles were separated using tricine gradient gel electrophoresis. Major protein bands were cut from the gel and used for mass spectrometry analysis. Mass spectrometry data processing and analyses were performed using FlexAnalysis 3.4 and MS BioTools (Bruker Daltonics). Mascot software (Matrix Science, London, UK) was used for sequence searches in exported MS/MS spectra against the National Center for Biotechnology Information database and a local database supplied with the expected protein sequences. The mass tolerance of peptides and MS/MS fragments for MS/MS ion searches was 50 parts per million and 0.5 Da, respectively. The oxidation of methionine and propionyl-amidation of cysteine as optional modifications, and one enzyme mis-cleavage were set for all searches. Peptides with a statistically significant peptide score ($P < 0.05$) were considered.

Cryo-EM phage sample preparation, data collection, motion correction, and CTF estimation

Purified 812 (10^{11} PFU/ml) in phage buffer (4 µl), either in the extended or contracted state, was pipetted onto a holey carbon-coated copper grid (R2/1, mesh 200; Quantifoil), blotted, and vitrified by plunging into liquid ethane using a Vitrobot Mark IV (FEI). The vitrified sample was transferred to a Titan Krios electron microscope (Thermo Fisher) operated under cryogenic conditions and at an acceleration voltage of 300 kV. The beam was aligned for parallel illumination in NanoProbe mode, and coma-free alignments were performed to remove the residual beam tilt. Micrographs of 812 with an extended tail were collected at a magnification of ×105,000 using a K3 direct electron detector (Gatan) operating in counting mode, resulting in a calibrated pixel size of 0.8336 Å/pix. Imaging was done under low-dose conditions (total dose 40.8 e-/Å^2) and with defocus values ranging from −0.5 to −2.0 µm. A two-second exposure was fractioned into 40 frames and saved as a movie. Micrographs of 812 in a contracted state were collected at a magnification of × 130,000 using a K2 Summit direct electron detector (Gatan) operating in counting mode, resulting in a calibrated pixel size of 1.057 Å/pix. Imaging was done under low-dose conditions (total dose 42 e-/Å^2) and with defocus values ranging from −1.0 to −2.4 µm. A seven-second exposure was fractioned into 40 frames and saved as a movie. Automated data acquisitions were performed using the software Serial EM. The movies were corrected for global and local motion during acquisition using MotionCor2 (Zheng et al, 2017), and saved as dose-weighted micrographs. Defocus values were estimated from aligned non-dose-weighted micrographs using the program Gctf (Zhang, 2016).

Reconstruction of the baseplate of phage 812 with an extended tail

A total of 444 particles were manually picked from a random 1000 micrographs using Relion (Scheres, 2015) and used to train Topaz (Bepler et al, 2019). Automated picking with Topaz on 26,731 micrographs yielded 64,874 particle coordinates. Particles were initially extracted into a 1280 px box and binned 4× (320 px box size, 3.3344 Å/px). Two rounds of 3D multireference classification followed by two rounds of reference-free 2D classification resulted in a selection of 17,393 particles. Particles were 3D refined with no symmetry imposed, and the previously reconstructed native baseplate (EMD-8210), low-pass-filtered to 60 Å, was used as an initial model. Two rounds of subsequent 3D classifications yielded 4195 particles, which were re-extracted with 2× binning into a 640 px box (1.6672 Å/px). A further round of 3D classification yielded a final set of 3586 particles. After correction of anisotropic magnification and beam tilt, an asymmetric reconstruction reached a resolution of 8.4 Å after post-processing; imposing C3 symmetry improved the resolution to 5.9 Å after post-processing.

To improve the reconstruction of the core and wedge proteins, 8470 particles of a 3D refined baseplate were re-extracted with 2× binning into a 640 px box (1.6672 Å/px). After one round of 3D refinement and 3D classification with a mask including the core and wedge modules and no symmetry imposed, particles were assigned to optics groups, and CTF refinements were carried out. A subsequent re-extraction of 8368 particles to a 640 px box rescaled to a 512 px box (1.042 Å/px) was followed by 3D refinement with C3 symmetry imposed. After one round of CTF refinements and Bayesian polishing, the final map reached the resolution of 3.0 Å after post-processing using a structure-derived mask.

To improve the reconstruction of the baseplate-proximal tail, the 3D refined baseplate map was segmented, and the segment containing the tail sheath initiator protein and the first three disks of tail sheath and tail tube protein was used to calculate the center-of-mass coordinates for targeted re-extraction. Using this offset, 8919 particles of 3D refined baseplate were re-extracted into a 640 px box and binned 2× to a 320 px box (1.6672 Å/px). Four rounds of asymmetric 3D refinements and classifications reduced the dataset to 4071 particles. These particles were re-extracted into

© The Author(s)

a 640 px box and rescaled to a 512 px box (1.042 Å/px), then 3D refined with C3 symmetry imposed. After three rounds of CTF refinements and Bayesian polishing, the final map reached the resolution of 3.4 Å after post-processing using a structure-derived mask.

To improve the reconstruction of the lower and upper baseplate arms, the 3D refined baseplate map was segmented, and the segments corresponding to the lower and upper arms were used to calculate the center-of-mass coordinates for a modified localized reconstruction protocol (Ilca et al, 2015) (github.com/fuzikt/localrec). Using these offsets, 26,748 particles for each arm were re-extracted into a 720 px box and binned 2× to a 360 px box (1.6672 Å/px). One round of 3D refinement and classification produced 22,031 particles for the lower arm, and 19,727 particles for the upper arm; further 3D classifications revealed classes with variable conformations. To address the heterogeneity for each arm, maps of the lower and upper arms were segmented into several subparts, and center-of-mass coordinates were calculated for every subpart. For each arm subpart, one or two rounds of 3D refinement with Blush regularization and 3D classification were performed; when a subpart reconstruction reached ~4.5 Å resolution, particles were assigned to optics groups and subjected to CTF refinements. Structure-derived masks were used for post-processing to generate the final subpart maps.

In all the above cases, the resolution after post-processing was calculated according to the gold standard FSC = 0.143 criterion. The local resolution for each map was computed using Relion (Kimanius et al, 2021).

Reconstruction of the baseplate of phage 812 with a contracted tail

Out of 15,371 micrographs of phages in the post-contraction state, the first 1000 micrographs were used to manually pick 7539 particles using crYOLO (Wagner et al, 2019). Particles were then extracted and binned 4× to a 208 px box size (4.228 Å/px) using Relion (Zivanov et al, 2020). After a single round of reference-free 2D classification, all aligned particles were re-extracted unbinned to an 832 px box size (1.057 Å/px) with re-centering of the offsets to x,y,z coordinates equal to 0,0,0. Then, particles were imported into Topaz (Bepler et al, 2019) with a down-sampling factor of 8. After training the neural network, the positions of particles were predicted using a radius of $r = 36$ and a picking threshold of $t = 0$. After the picking coordinates were corrected for the sampling factor, 54,841 particles were extracted using a 960 px box size and binned 4× to a 240 px box size (4.228 Å/px) using Relion (Kimanius et al, 2021). After several rounds of reference-free 2D classification, 31,308 particles were subject to asymmetric 3D reconstruction and classification, using the previously reconstructed post-contraction baseplate (EMD-8212) low-pass-filtered to 60 Å as an initial model. The resulting 25,487 particles were re-extracted to a 1280 px box and binned 2× to obtain a 640 px box size (2.114 Å/px). After 3D classification, 21,264 particles were 3D refined, and the final asymmetric map reached the resolution of 6.6 Å after post-processing. Another 3D refinement with C6 symmetry imposed yielded a final map with a resolution of 4.4 Å after post-processing.

To improve the reconstruction of the core, wedge module, and inner tripod proteins, 3D refined post-contraction baseplate particles were re-extracted to a 720 px box (1.057 Å/px), and a 3D refinement was performed using a focused mask encompassing selected regions. The particles were assigned to their respective optics groups, and several rounds of CTF refinements (anisotropic magnification estimation, beam tilt, trefoil, and tetrafoil aberrations estimation, and fitting of the defocus and astigmatism parameters per particle) were performed. Then, two rounds of Bayesian polishing and subsequent 3D refinements and CTF refinements were performed. The final map reached the resolution of 3.1 Å after post-processing. The final post-processing step was also performed using a mask encompassing the first six tail sheath discs, core, wedge module, and inner tripod proteins, and a subunit of the arm segment protein, resulting in a map with a resolution of 4.1 Å after post-processing.

To improve the reconstruction of the post-contraction baseplate arm, the 3D refined post-contraction baseplate map was segmented, and the segment corresponding to the arm was used to calculate the center-of-mass coordinates for a modified localized reconstruction protocol (Ilca et al, 2015) (github.com/fuzikt/localrec). Using these offsets, 152,894 particles were re-extracted into a 480 px box and binned 2× to a 240 px box (2.114 Å/px). After subtraction of the surrounding signal, three rounds of asymmetric 3D refinements and classifications were performed to select particles with the most pronounced density belonging to the RBP2 protein. A total of 15,390 particles were re-extracted into a 480 px box unbinned (1.057 Å/px), assigned to optics groups, and subjected to two rounds of 3D and CTF refinements, yielding a final map with a resolution of 4.1 Å after post-processing.

To improve the reconstruction of the arm segment B, bulge domain of the arm scaffold protein, and the top part of the outer tripod proteins, 93,601 particles from early 3D classification of the post-contraction baseplate arm were subjected to two rounds of 3D refinement with Blush regularization and 3D classification using a focused mask encompassing the selected region. The baseplate arm map was segmented, and center-of-mass coordinates were calculated for a subpart including the selected region. Using the coordinate offsets, 56,778 particles were re-extracted into a 256 px box unbinned (1.057 Å/px), and the surrounding signal was subtracted. One round of 3D and CTF refinements yielded a final map with a resolution of 4.4 Å after post-processing.

In all the above cases, the resolution after post-processing was calculated according to the gold standard FSC = 0.143 criterion. The local resolution for each map was computed using Relion (Kimanius et al, 2021).

Reconstruction of the extended tail

The 812 tails were manually boxed using the program e2helixboxer.py from the EMAN2 suite (Tang et al, 2007), and the helical segments were extracted in a 360 px box using Relion (Zivanov et al, 2020). Tail edges and bent and damaged particles were removed from the dataset by multiple rounds of reference-free 2D classification. A map of the 812 tail in its extended conformation (EMD-4051), low-pass-filtered to 50 Å, was used as an initial model for the 3D refinement of 18,188 particles using a helical refinement protocol with C6 symmetry imposed. The helical refinement and the per particle CTF refinement were iterated until convergence. The final map reached a resolution of 4.2 Å after post-processing. The resolution after post-processing was calculated according to

 © The Author(s)

the gold standard FSC = 0.143 criterion. Local resolution maps were computed using Relion (Zivanov et al, 2020).

Reconstruction of the contracted tail

A total of 106,091 particles were manually picked from 4833 micrographs using the program e2helixboxer.py from the EMAN2 suite (Tang et al, 2007), and the helical segments were extracted using a 400 px box size (1.061 Å/px) in Relion (Zivanov et al, 2020). Tail edges and bent and damaged particles were removed from the dataset by multiple rounds of reference-free 2D classification. Then, 85,549 particles were subjected to several rounds of 3D refinement and classification with C6 symmetry imposed. A map of the contracted tail determined previously (EMD-4052) filtered to 50 Å was used as an initial model for the 3D refinement of 69,969 particles using a helical refinement protocol with C6 symmetry imposed. The final map reached an average resolution of 3.0 Å after post-processing. The resolution after post-processing was calculated according to the gold standard FSC = 0.143 criterion. The local resolution map was computed using Relion (Zivanov et al, 2020).

Localized reconstruction of the tail tube from the phage with a contracted tail

Information about particle positions and orientations from the final reconstruction of the post-contraction baseplate was used to extract sub-particle images of the tail tube with a modified localized reconstruction protocol (Ilca et al, 2015) (github.com/fuzikt/localrec). The initial set of 25,203 sub-particles centered on the contact region between the tail tube and wedge A proteins was extracted to a 256 px box size (1.057 Å/px) and subjected to several rounds of reference-free 2D classifications in Relion (Zivanov et al, 2020). After the initial 3D refinement with imposed C6 symmetry, a single 3D classification was performed. The selected 12,906 particles belonging to the best class were further refined with imposed C6 symmetry and maximum allowed deviations from previous orientations of 10°. The final map reached an average resolution of 3.6 Å after post-processing. The resolution after post-processing was calculated according to the gold standard FSC = 0.143 criterion. The local resolution map was computed using Relion (Zivanov et al, 2020).

Calculation of tail tube rotation during tail sheath contraction

Electron micrographs of the phages with extended tails were used to determine that the tail contains 51 tail sheath discs. The rotation between consecutive discs of tail sheath proteins is 21.1° in the extended tail sheath and 30.6° in the contracted tail. The rotation of the tail tip upon tail contraction was calculated as follows. Taking the first tail sheath disc as a reference point, the rotation of 50 tail sheath discs with a 21.1° twist equals the overall rotation of 1055°. For the contracted tail sheath, the rotation of 50 tail sheath discs with the 30.6° twist equals the overall rotation of 1530°. The overall rotation of the extended tail sheath was subtracted from the overall rotation of the contracted tail sheath, resulting in a difference of 475°.

Cryo-EM of 812 attached to *S. aureus* cell wall fragments

S. aureus SA 812 was cultured in 100 ml of meat peptone broth (1 g of Lab-Lemco (Difco), 5 g of yeast extract powder L21 (Oxoid), 10 g of peptone L37 (Oxoid), and 5 g of NaCl were dissolved in distilled water to a final volume of 1000 ml, and the pH was adjusted to 7.4 using 10 M NaOH) at 37 °C until OD_{600} = 0.3. Cells were harvested by centrifugation at 3000 × *g* for 15 min. The resulting pellet was resuspended in 80% isopropanol to a final volume of 10 ml and incubated for 1 h at room temperature. The suspension was centrifuged at 1000 × *g* at room temperature for 15 min. The resulting supernatant was transferred to another tube, and cell wall fragments were harvested by centrifugation at 20,000 × *g* for 30 min. The resulting pellet was resuspended in 100 µl of the phage buffer and mixed with 812 at MOI 10, relative to the starting bacterial culture. After 5 min of incubation at room temperature, the sample was applied to a holey carbon-coated copper grid for electron microscopy (R2/1, mesh 200; Quantifoil), blotted, and vitrified by plunging into liquid ethane using a Vitrobot Mark IV (FEI), blot force 2, blotting time 2 s. Grids were imaged at a magnification of ×17,000, using a Tecnai TF20 operated (FEI) under cryogenic conditions and at an acceleration voltage of 200 kV.

Production of the recombinant cleaver domain of the hub protein

The DNA segment encoding the cleaver domain of the hub protein (residues 650-808) was amplified from the genomic DNA of phage 812 by PCR using forward and reverse primers (5'GTAGCCATG-GAACAAAGTAGTGGA3' and 5'TAGGATCCTTTATTTCTTAT CGTAAA3'). Using restriction cloning, the amplicon was cloned into the vector pET28a(+) (Novagen/Merck), providing a T7 tag and a His6 tag at the C-terminus of the protein. An *E. coli* expression strain BL21(DE3) was transformed with the construct using a standard heat shock procedure (45 s at 42 °C). An overnight culture was used to inoculate 1 l of 2% Luria-Bertani broth (Oxoid) supplemented with kanamycin (50 µg/mL) and cultivated at 37 °C until OD_{600} = 0.5. The protein expression was induced with 0.4 mM IPTG, and was allowed to progress for 4–6 h at 30 °C.

For nuclear magnetic resonance spectroscopy (NMR), the cleaver domain was produced in M9 minimal medium supplemented with traces of metals, vitamins, and 2 g/L [^{13}C]glucose or 0.5 g/L $^{15}NH_4Cl$ (Cambridge Isotope Laboratories). *E. coli* BL21 (DE3) was grown to OD_{600} = 0.5, and the gene expression was induced with 0.4 mM IPTG and continued at 30 °C for 12 h. The cultures were harvested, resuspended in the sonication buffer (100 mM Tris-Cl, pH 8, 500 mM NaCl, 4 mM DTT, 10 mM imidazole, 0.1% TritonX-100), and subjected to sonication (Sartorius Labsonic® M), followed by centrifugation at 14,000×*g* and 4 °C for 45 min. The supernatant was filtered (0.45 µm cut-off, Corning Inc.), loaded into a 5 ml Histrap column (GE Healthcare), pre-equilibrated with the loading buffer, and connected to an AKTA FPLC system (GE Healthcare). After the column was washed with 15 column volumes of the loading buffer (50 mM Tris-Cl, 300 mM NaCl, 20 mM imidazole), gradient elution was performed using the elution buffer (50 mM Tris-Cl, 300 mM NaCl, 500 mM imidazole). Fractions with protein were pooled, concentrated, and loaded onto a HiLoad 16/600 Superdex 75 pg size-exclusion chromatography column (GE Healthcare Life Sciences), followed by an isocratic elution with 100 mM Na-phosphate, pH

© The Author(s)

6.8, 150 mM NaCl. Purified protein was pooled, and the buffer was exchanged by performing two washes with 20 mM Na-phosphate buffer, pH 6.8, using an Amicon Ultra 15 filter (10 kDa cut-off, Millipore). While exchanging the buffer, the sample was concentrated to 20 mg/ml. For the NMR studies, the protein was concentrated at 35 mg/ml while buffer-exchanged to 25 mM Na-phosphate, pH 6.6, and 100 mM NaCl.

Zymogram analysis

The cleaver domain of the hub protein after Histrap purification was separated on a conventional 12.5% polyacrylamide gel using SDS-PAGE. Polyacrylamide gels (12.5%) for zymograms contained 0.5% bacterial cell walls, prepared from *S. aureus* CCM 885 cells, autoclaved at 121 °C for 5 min. Samples of the cleaver domain were mixed with loading buffer (1% SDS, 6% sucrose, 100 mM dithiothreitol, 10 mM Tris, pH 6.8, 0.0625% bromophenol blue) and boiled for 5 min before loading onto SDS-PAGE gels and zymograms. The SDS-gel and zymogram were separated using gel electrophoresis. After the gel electrophoresis, the zymogram was washed for 30 min with distilled water to remove SDS. To renature the cleaver domain, the zymogram was soaked at room temperature in distilled water for 2–4 h, and then for 1 h in the buffer containing 150 mM Na-phosphate, pH 7.0, 0.1% TritonX-100, and 10 mM $MgCl_2$. The zymogram was stained for 3 h with 0.1% methylene blue in 0.001% KOH and washed with water. The peptidoglycan-hydrolytic activity of the cleaver domain of the hub protein was detected as a clear zone on a dark blue background.

NMR structure determination of the cleaver domain of the hub protein

NMR spectra were recorded at 298 K in an 850 MHz Bruker Avance III spectrometer equipped with a $^{1}H/^{13}C/^{15}N$ TCI cryogenic probe head with z-axis gradients. The composition of the NMR sample was 1.8 mM uniformly ^{13}C-, ^{15}N-labeled cleaver domain in a buffer containing 25 mM sodium phosphate, pH 6.6, 100 mM NaCl, 1.5 mM DTT, and 10% D_2O for the lock. Three sparsely sampled 4D NMR experiments were acquired: 4D HC(CC-TOCSY(CO)) NH, 4D $^{13}C,^{15}N$ edited HMQC-NOESY-HSQC (HCNH), and 4D $^{13}C,^{13}C$ edited HMQC-NOESY-HSQC (HCCH). Sequential and aliphatic side-chain assignments were obtained automatically using the 4D-CHAINS algorithm (Evangelidis et al, 2018) and checked manually. Backbone dihedral angle restraints were derived from TALOS (Shen et al, 2009) using a combination of five kinds (H^N, H^α, C^α, C^β, N) of chemical shift assignments for each residue in the sequence. NOE cross-peaks from the two 4D NOESY spectra (HCNH and HCCH) were assigned automatically by CYANA 3.0 (Güntert, 2009) in structure calculations with torsion angle dynamics. Unambiguous distance and torsion angle restraints (Appendix Table S3) were used in a water refinement calculation (Linge et al, 2003), applying the RECOORD protocol (Nederveen et al, 2005). The quality of the NMR-derived structure ensembles was validated using PSVS (Bhattacharya et al, 2007).

Production of recombinant central spike protein

The gene for the central spike protein was amplified from the genomic DNA of phage 812 using forward and reverse primers (5'AGATTGGTGGCTCGGATGATTTAAATGTAAAAGGATTA GTTTTA3' and 5'GAGGAGAGTTAAGACTTATTAAATCTTTT-TATATTCATCTAGGTAGTTTGTAAA3'). Compared to the full-length gene, the first 17 nucleotide triplets from the 5' end of the amplified gene were omitted, as they code for the first 17 residues of the central spike protein, which were predicted to be disordered by the secondary structure prediction using the program Phyre (Kelley et al, 2015). The truncated gene was cloned into a vector derived from pET22b, which was modified to provide a His6-SUMO-tag fusion followed by the Ulp1 cleavage site at the N-terminus of the protein. The *E. coli* expression strain BL21(DE3) was transformed with the construct using a standard heat shock procedure (45 s at 42 °C). An overnight culture was used to inoculate 2% Luria-Bertani broth (Sigma) supplemented with ampicillin (50 µg/ml). Cells were cultivated at 37 °C and 250 rpm until $OD_{600} = 0.5$, followed by cultivation at 16 °C and 250 rpm for 24 h without the induction of expression, as soluble central spike protein was only produced after non-induced leaky expression. Cells were harvested in a typical yield of 8 g per liter of cell culture, resuspended in 2.5 ml of the loading buffer (50 mM Na/K phosphate, pH 7, 200 mM NaCl) per gram of cell pellet, and subjected to chemical disintegration (0.5% octylthioglucoside, 1 mg/ml lysozyme, 2 U/ml Turbonuclease, 1 mM PMSF, 5 mM TCEP) at 6 °C overnight. The lysate was centrifuged at 20,000 × *g* and 8 °C for 30 min. The resulting supernatant was filtered (0.45 µm cut-off, Corning Inc.) and loaded into a 5 ml Histrap column (GE Healthcare) pre-equilibrated with the loading buffer and connected to an AKTA FPLC system (GE Healthcare). After the column was washed with 15 column volumes of the loading buffer, gradient elution was performed using the elution buffer (50 mM Na/K phosphate, pH 7.0, 200 mM NaCl, 500 mM imidazole). Eluted fractions containing the central spike protein, as determined by SDS-PAGE analysis using 12.5% polyacrylamide gels, were pooled and supplemented with 5 mM TCEP before the cleavage of the purification tag overnight at 6 °C using the in-house prepared Ulp1 protease. The cleavage solution was desalted using a HiPrep™ 26/10 Desalting column (Cytiva) before reverse affinity chromatography using the 5 ml Histrap column (GE Healthcare). Cleaved protein collected in the flow-through fraction was concentrated (30 kDa cut-off; Amicon® Ultra; Merc Millipore) and loaded into a Superdex 16/600 200 pg column (GE Healthcare) pre-equilibrated with the loading buffer (50 mM Na/K phosphate, pH 7.0, 200 mM NaCl), followed by an isocratic elution. Monodisperse fractions were analyzed by SDS-PAGE and concentrated to a final concentration of 5 mg/ml.

Cryo-EM reconstruction of recombinant central spike protein

The purified central spike protein sample was diluted in buffer (50 mM Na/K phosphate, pH 7.0, 200 mM NaCl) to a concentration of 0.8 mg/ml and then diluted 10x in water. Four µl of the central spike protein at a concentration of 0.08 mg/ml were applied onto a holey carbon-coated copper grid (R1.2/1.3, mesh 200; Quantifoil) glow-discharged for 60 s from both sides. The excess of the sample was blotted for 1 s with filter paper (Whatman No. 1) using blot force -2 and immediately plunge-frozen in liquid ethane using a Vitrobot Mark IV (FEI). The instrument chamber was maintained at 100% humidity and at 4 °C. Cryo-EM data were

 © The Author(s)

collected using a Titan Krios TEM (Thermo Fisher Scientific) operated at 300 kV and equipped with a K2 Summit direct electron detector (Gatan). The beam was aligned for parallel illumination in NanoProbe mode, and the residual beam tilt was removed by coma-free alignments. The software SerialEM was used to acquire the data in the electron counting mode at ×130,000 magnification, corresponding to a calibrated pixel size of 1.04 Å/px over a defocus range of −0.3 to −3.0 µm. The exposure of 8 s with a dose rate of 6.6 e^-/px/s was fractionated into 40 frames (total dose 57 e^-/Å^2, 1.425 e^-/Å^2 per frame). A total of 3120 micrographs were collected. For each movie, the drift and gain correction was performed with MotionCor2 (Zheng et al, 2017), while the contrast-transfer function was estimated using the program Gctf (Zhang, 2016). crYOLO (Wagner et al, 2019) was used to pick particles from micrographs denoised using the program janni (Wagner, 2019). Particles were manually picked from 10 micrographs and used to train the neural network. The resulting 487,160 coordinates were used to extract particles to a 256 px box size and binned 2× to a 128 px box size (2.08 Å/px) using Relion (Zivanov et al, 2020). Several rounds of 2D classification sorted out classes of the central spike protein's C-terminal domains, containing 226,791 particles. These particles were re-extracted and binned to a 128 px box size (2.08 Å/px) using Relion 5.0 beta (github.com/3dem/relion/tree/ver5.0). Three additional rounds of reference-free 2D classification resulted in 135,736 particles, which were used for 3D reconstruction using the initial model generated by the stochastic gradient descent algorithm within Relion. Subsequent 3D classifications did not improve the quality or resolution of the reconstruction. Therefore, all 135,736 particles were re-extracted unbinned to a 256 px box (1.04 Å/px) and assigned to their respective optics groups. Several rounds of CTF refinements, including anisotropic magnification estimation, beam tilt and trefoil aberrations estimation, and fitting of the defocus and astigmatism parameters per micrograph, improved the resolution of the post-processed map to 3.6 Å. Then, two rounds of Bayesian polishing and subsequent 3D refinement with Blush regularization and CTF refinements were performed. The final map reached a resolution of 3.2 Å. The resolution after post-processing was calculated according to the gold standard FSC = 0.143 criterion. Local resolution maps were computed using Relion (Kimanius et al, 2021).

Production of recombinant Arm segment protein

The gene encoding the arm segment protein was cloned into the pET-28b(+) vector (Novagen/Merck), providing a His6 tag at the C-terminus of the protein. An *E. coli* expression strain BL21(DE3) was transformed with the construct using a standard heat shock procedure (45 s at 42 °C). An overnight culture was used to inoculate 2% Luria-Bertani broth (Sigma) supplemented with 1 mM $MgCl_2$, 1% glucose, and ampicillin (50 µg/ml), followed by cultivation at 37 °C and 250 rpm until OD_{600} = 0.5. The expression was induced with 0.4 mM IPTG at 18 °C and was allowed to progress for 17 h. Cells were harvested and lysed using the lysis buffer (0.5% octyl-thioglucoside, 1 mg/ml lysozyme, 2 U/ml Turbonuclease, 1 mM PMSF, 5 mM TCEP) at room temperature for 30 min, and subsequently disintegrated with an Emulsiflex C3 (Avestin). After centrifugation at 20,000×*g* and 8 °C for 30 min, the supernatant was filtered (0.45 µm cut-off, Corning Inc.) and loaded into a 5 ml Histrap column (GE Healthcare) pre-equilibrated with the loading buffer (50 mM HEPES, pH 8, 200 mM NaCl, 40 mM imidazole) connected to an AKTA Pure FPLC system (GE Healthcare). The protein was eluted in one step using the elution buffer (50 mM HEPES, pH 8, 200 mM NaCl, 500 mM imidazole). Eluted fractions containing the arm segment protein, detected by SDS-PAGE analysis on 12% polyacrylamide gels, were loaded into a Superdex 16/600 75 pg column (GE Healthcare) pre-equilibrated with the loading buffer (50 mM HEPES, pH 8, 200 mM NaCl), followed by an isocratic elution. Monodisperse fractions were analyzed by SDS-PAGE and concentrated to a final concentration of 14 mg/ml.

Crystallization and X-ray structure determination of recombinant arm segment protein

The arm segment protein was crystallized by vapor diffusion using the sitting-drop method at 21 °C. The protein sample at a concentration of 14 mg/ml was used to prepare drops with protein to precipitant ratios of 200 nl:100 nl, 100 nl:100 nl, and 100 nl:200 nl in MRC 3-drop 96-well plates using a Dragonfly robot (SPT Labtech) with a range of commercially available screens (Molecular Dimensions, Hampton Research, Qiagen-Nextal). Thick needle-like crystals were observed in the drops containing the solution of 1.6 M LiCl, 0.1 M Tris, pH 7.5, 25% w/v PEG 4000. The same crystallization solution was used to prepare hanging drops for vapor diffusion. Crystals were harvested from the hanging drops and flash-vitrified in liquid nitrogen.

Diffraction data were recorded at 100 K on the Proxima-2A beamline at the Soleil synchrotron (Paris, France). Native crystals were soaked in I3C using the I3C phasing kit (Hampton Research), and the dataset was phased using the multiple wavelength anomalous dispersion method. The diffraction data from the crystals soaked with I3C were collected at 12.67 ke$^-$V and 5.00 ke$^-$V. The structure of the arm segment protein was determined using the program SHELXD (Schneider and Sheldrick, 2002). The native diffraction data recorded from the crystals of the arm segment protein were phased using the program Phaser (McCoy et al, 2007), and the structure was determined using the anomalous data as a molecular replacement model. Refinement was performed manually using the program *Coot* (Emsley et al, 2010) and automatically in *REFMAC5* (Vagin et al, 2004). The structures were validated using *MolProbity* (Williams et al, 2018).

Structure prediction, determination, and refinement using cryo-EM maps

The structures of phage proteins were predicted using the program Alphafold2 (Jumper et al, 2021) and fitted into their densities as rigid bodies or by individual domains using the programs Chimera (Pettersen et al, 2004) or ChimeraX (Meng et al, 2023), and then adjusted interactively using ISOLDE (Croll, 2018). The structures were iteratively improved using the real-space refinement implemented in the *Phenix* package (Liebschner et al, 2019), and corrected manually using programs *Coot* (Emsley et al, 2010) and ISOLDE (Croll, 2018). The geometry evaluation of models was performed using *MolProbity* (Williams et al, 2018).

© The Author(s)

Visualization and structure analysis

Chimera (Pettersen et al, 2004) and ChimeraX (Meng et al, 2023) were used to visualize maps and structures. PISA web server (Krissinel and Henrick, 2007) was used to calculate interface areas. Sequences were analyzed using Clustal Omega (Sievers and Higgins, 2018) available via the EMBL-EBI server (Madeira et al, 2022) and visualized with Jalview (Waterhouse et al, 2009).

Construction of the composite maps

Composite maps of pre- and post-contraction baseplates were constructed in ChimeraX using the *volume maximum* command. Given variable resolution and quality of consensus, focused and sub-particle maps, the numeric threshold levels were adjusted individually, and the command option *scaleFactors fromLevels* was used. In case of the pre-contraction baseplate, sub-particle reconstructions of lower (Appendix Fig. S1F–K) and upper (Appendix Fig. S1M–O) baseplate arms were combined with the overall reconstruction of the lower (Appendix Fig. S1E) and upper (Appendix Fig. S1L) baseplate arm, respectively. Then, newly constructed maps of the lower and upper arms were combined with reconstructions of the core and wedge module proteins (Appendix Fig. S1C) and baseplate-proximal tail (Appendix Fig. S1D) to create the final composite map of the pre-contraction baseplate.

In the case of the post-contraction baseplate, sub-particle reconstruction of the arm segment B (Appendix Fig. S7F) was combined with the post-processed reconstruction of the baseplate arm (Appendix Fig. S7E). To better visualize the density of the RBP2, a refined map (without post-processing) of the baseplate arm was segmented, and the density corresponding to the RBP2 and an unassigned density at the baseplate periphery were extracted. This map was then combined with the baseplate arm map created in the previous step. Finally, the newly constructed map of the baseplate arm was combined with the reconstruction of the core, wedge module, inner tripod, and baseplate-proximal tail sheath proteins (Appendix Fig. S7C) and reconstructions of the tail tube (Appendix Fig. S7I) stacked onto each other to create the final composite map of the post-contraction baseplate.

Data availability

Links to the deposited structural data: https://www.ebi.ac.uk/pdbe/entry/pdb/9TIC, https://www.ebi.ac.uk/pdbe/entry/pdb/9TID, https://www.ebi.ac.uk/pdbe/entry/pdb/9TIE, https://www.ebi.ac.uk/pdbe/entry/pdb/9TIF, https://www.ebi.ac.uk/pdbe/entry/pdb/9TIG, https://www.ebi.ac.uk/pdbe/entry/pdb/9TIH, https://www.ebi.ac.uk/pdbe/entry/pdb/9TII, https://www.ebi.ac.uk/pdbe/entry/pdb/9TIJ, https://www.ebi.ac.uk/pdbe/entry/pdb/9TIK, https://www.ebi.ac.uk/pdbe/entry/pdb/9TIL, https://www.ebi.ac.uk/pdbe/entry/pdb/9TIM, https://www.ebi.ac.uk/pdbe/entry/pdb/9TIN, https://www.ebi.ac.uk/pdbe/entry/pdb/9TIO, https://www.ebi.ac.uk/pdbe/entry/pdb/9TIP, https://www.ebi.ac.uk/pdbe/entry/pdb/9TIR, https://www.ebi.ac.uk/pdbe/entry/pdb/9TIS, https://www.ebi.ac.uk/pdbe/entry/pdb/9TIT, https://www.ebi.ac.uk/pdbe/entry/pdb/9TIW, https://www.ebi.ac.uk/pdbe/entry/pdb/9EUJ, https://www.ebi.ac.uk/pdbe/entry/pdb/9EUK, https://www.ebi.ac.uk/pdbe/entry/pdb/9F04, https://www.ebi.ac.uk/pdbe/entry/pdb/9F05, https://www.ebi.ac.uk/pdbe/entry/pdb/9F06, https://www.ebi.ac.uk/pdbe/entry/pdb/9EUL, https://www.ebi.ac.uk/pdbe/entry/pdb/9EUM, https://www.ebi.ac.uk/pdbe/entry/pdb/9FKO, https://www.ebi.ac.uk/emdb/EMD-55950, https://www.ebi.ac.uk/emdb/EMD-55951, https://www.ebi.ac.uk/emdb/EMD-55952, https://www.ebi.ac.uk/emdb/EMD-55953, https://www.ebi.ac.uk/emdb/EMD-55954, https://www.ebi.ac.uk/emdb/EMD-55955, https://www.ebi.ac.uk/emdb/EMD-55956, https://www.ebi.ac.uk/emdb/EMD-55957, https://www.ebi.ac.uk/emdb/EMD-55958, https://www.ebi.ac.uk/emdb/EMD-55959, https://www.ebi.ac.uk/emdb/EMD-55960, https://www.ebi.ac.uk/emdb/EMD-55961, https://www.ebi.ac.uk/emdb/EMD-55962, https://www.ebi.ac.uk/emdb/EMD-55963, https://www.ebi.ac.uk/emdb/EMD-55964, https://www.ebi.ac.uk/emdb/EMD-55966, https://www.ebi.ac.uk/emdb/EMD-55967, https://www.ebi.ac.uk/emdb/EMD-55968, https://www.ebi.ac.uk/emdb/EMD-55969, https://www.ebi.ac.uk/emdb/EMD-55977, https://www.ebi.ac.uk/emdb/EMD-19972, https://www.ebi.ac.uk/emdb/EMD-19973, https://www.ebi.ac.uk/emdb/EMD-55978, https://www.ebi.ac.uk/emdb/EMD-50093, https://www.ebi.ac.uk/emdb/EMD-50094, https://www.ebi.ac.uk/emdb/EMD-50095, https://www.ebi.ac.uk/emdb/EMD-19974. Cryo-EM maps and structure coordinates were deposited into the Electron Microscopy Data Bank (EMDB) and Protein Data Bank (PDB), respectively, with the following accession numbers: Structure of whole baseplate and baseplate-proximal tail of phage with extended tail computed with no symmetry imposed: EMD-55950. Structure of whole baseplate and baseplate-proximal tail of phage with extended tail computed with imposed threefold symmetry: EMD-55951 and PDB-9TIC. Structure of core and wedge module proteins of phage with extended tail computed with imposed threefold symmetry: EMD-55952 and PDB-9TID. Structure of baseplate-proximal tail of phage with extended tail computed with imposed threefold symmetry: EMD-55953 and PDB-9TIE. Structure of the lower baseplate arm of phage with extended tail computed with no symmetry imposed: EMD-55954 and PDB-9TIF. Structure of lower baseplate arm (segment A) of phage with extended tail computed with no symmetry imposed: EMD-55955 and PDB-9TIG. Structure of lower baseplate arm (segment B) of phage with extended tail computed with no symmetry imposed: EMD-55956 and PDB-9TIH. Structure of lower baseplate arm (segments C, D) of phage with extended tail computed with no symmetry imposed: EMD-55957 and PDB-9TII. Structure of lower baseplate arm (segments D, E, F) of phage with extended tail computed with no symmetry imposed: EMD-55958 and PDB-9TIJ. Structure of lower baseplate arm (uRBP1-lRBP2) of phage with extended tail computed with no symmetry imposed: EMD-55959 and PDB-9TIK. Structure of lower baseplate arm (lRBP1-uRBP2) of phage with extended tail computed with no symmetry imposed: EMD-55960 and PDB-9TIL. Structure of upper baseplate arm of phage with extended tail computed with no symmetry imposed: EMD-55961 and PDB-9TIM. Structure of upper baseplate arm (segment A) of phage with extended tail computed with no symmetry imposed: EMD-55962 and PDB-9TIN. Structure of upper baseplate arm (segment B) of phage with extended tail computed with no symmetry imposed: EMD-55963 and PDB-9TIO. Structure of upper baseplate arm (segments C, D, E, F) of phage with extended tail computed with no symmetry imposed: EMD-55964 and PDB-9TIP. Composite structure of whole baseplate and baseplate-proximal tail of phage with extended tail: EMD-55977. Structure of whole baseplate and

 © The Author(s)

baseplate-proximal tail of phage with contracted tail computed with no symmetry imposed: EMD-55966. Structure of whole baseplate and baseplate-proximal tail of phage with contracted tail computed with imposed sixfold symmetry: EMD-55967 and PDB-9TIR. Structure of core, wedge module, arm segment, inner tripod, and baseplate-proximal tail sheath proteins of phage with contracted tail computed with imposed sixfold symmetry: EMD-19972 and PDB-9EUJ. Structure of core, wedge module, and inner tripod proteins of phage with contracted tail computed with imposed sixfold symmetry: EMD-19973 and PDB-9EUK. Structure of baseplate arm of phage with contracted tail computed with no symmetry imposed: EMD-55968 and PDB-9TIS. Structure of baseplate arm (segment B) of phage with contracted tail computed with no symmetry imposed: EMD-55969 and PDB-9TIT. Composite structure of whole baseplate, baseplate-proximal tail sheath, and tail tube of phage with contracted tail: EMD-55978 and PDB-9TIW. Structure of extended tail computed with imposed sixfold symmetry: EMD-50093 and PDB-9F04. Structure of tail tube of phage with contracted tail computed with imposed sixfold symmetry: EMD-50094 and PDB-9F05. Structure of contracted tail sheath computed with imposed sixfold symmetry: EMD-50095 and PDB-9F06. Structure of central spike protein (knob and petal domains) computed with imposed threefold symmetry: EMD-19974 and PDB-9EUL. The NMR structure of the cleaver domain of the hub protein was deposited to PDB under the accession number 9EUM. The X-ray structure of the arm segment protein was deposited to PDB under the accession number 9FKO. All custom scripts used during the single-particle data reconstruction are available at https://github.com/fuzikt/starpy.

The source data of this paper are collected in the following database record: biostudies:S-SCDT-10_1038-S44318-026-00834-9.

Expanded view data, supplementary information, appendices are available for this paper at https://doi.org/10.1038/s44318-026-00834-9.

Peer review information

A peer review file is available at https://doi.org/10.1038/s44318-026-00834-9

References

Aksyuk AA, Leiman PG, Kurochkina LP, Shneider MM, Kostyuchenko VA, Mesyanzhinov VV, Rossmann MG (2009) The tail sheath structure of bacteriophage T4: a molecular machine for infecting bacteria. EMBO J 28:821–829

Arisaka F, Kanamaru S, Leiman P, Rossmann MG (2003) The tail lysozyme complex of bacteriophage T4. Int J Biochem Cell Biol 35:16–21

Bae B, Ohene-Adjei S, Kocherginskaya S, Mackie RI, Spies MA, Cann IKO, Nair SK (2008) Molecular basis for the selectivity and specificity of ligand recognition by the family 16 carbohydrate-binding modules from *Thermoanaerobacterium polysaccharolyticum* ManA. J Biol Chem 283:12415–12425

Barylski J, Enault F, Dutilh BE, Schuller MB, Edwards RA, Gillis A, Klumpp J, Knezevic P, Krupovic M, Kuhn JH et al (2020) Analysis of spounaviruses as a case study for the overdue reclassification of tailed phages. Syst Biol 69:110–123

Bateman A, Rawlings ND (2003) The CHAP domain: a large family of amidases including GSP amidase and peptidoglycan hydrolases. Trends Biochem Sci 28:234–237

Becker SC, Foster-Frey J, Donovan DM (2008) The phage K lytic enzyme LysK and lysostaphin act synergistically to kill MRSA. FEMS Microbiol Lett 287:185–191

Bepler T, Morin A, Rapp M, Brasch J, Shapiro L, Noble AJ, Berger B (2019) Positive-unlabeled convolutional neural networks for particle picking in cryo-electron micrographs. Nat Methods 16:1153–1160

Bhardwaj A, Walker-Kopp N, Casjens SR, Cingolani G (2009) An evolutionarily conserved family of virion tail needles related to bacteriophage P22 gp26: correlation between structural stability and length of the α-helical trimeric coiled Coil. J Mol Biol 391:227–245

Bhattacharya A, Tejero R, Montelione GT (2007) Evaluating protein structures determined by structural genomics consortia. Proteins 66:778–795

Böth D, Steiner EM, Izumi A, Schneider G, Schnell R (2014) RipD (Rv1566c) from *Mycobacterium tuberculosis*: adaptation of an NlpC/p60 domain to a non-catalytic peptidoglycan-binding function. Biochem J 457:33–41

Botka T, Pantůček R, Mašlaňová I, Benešík M, Petráš P, Růžičková V, Havlíčková P, Varga M, Žemličková H, Koláčková I et al (2019) Lytic and genomic properties of spontaneous host-range Kayvirus mutants prove their suitability for upgrading phage therapeutics against staphylococci. Sci Rep 9:5475

Bradshaw WJ, Kirby JM, Thiyagarajan N, Chambers CJ, Davies AH, Roberts AK, Shone CC, Acharya KR (2014) The structure of the cysteine protease and lectin-like domains of Cwp84, a surface layer-associated protein from *Clostridium difficile*. Acta Crystallogr D Biol Crystallogr 70:1983–1993

Browning C, Shneider MM, Bowman VD, Schwarzer D, Leiman PG (2012) Phage pierces the host cell membrane with the iron-loaded spike. Structure 20:326–339

Buist G, Steen A, Kok J, Kuipers OP (2008) LysM, a widely distributed protein motif for binding to (peptido)glycans. Mol Microbiol 68:838–847

Büttner CR, Wu Y, Maxwell KL, Davidson AR (2016) Baseplate assembly of phage Mu: defining the conserved core components of contractile-tailed phages and related bacterial systems. Proc Natl Acad Sci USA 113:10174–10179

Cai X, He Y, Yu I, Imani A, Scholl D, Miller JF, Zhou ZH (2024) Atomic structures of a bacteriocin targeting Gram-positive bacteria. Nat Commun 15:7057

Cid M, Pedersen HL, Kaneko S, Coutinho PM, Henrissat B, Willats WGT, Boraston AB (2010) Recognition of the helical structure of β-1,4-galactan by a new family of carbohydrate-binding modules. J Biol Chem 285:35999–36009

Croll TI (2018) *ISOLDE*: a physically realistic environment for model building into low-resolution electron-density maps. Acta Crystallogr D Struct Biol 74:519–530

Desfosses A, Venugopal H, Joshi T, Felix J, Jessop M, Jeong H, Hyun J, Heymann JB, Hurst MRH, Gutsche I et al (2019) Atomic structures of an entire contractile injection system in both the extended and contracted states. Nat Microbiol 4:1885–1894

Eck MJ, Sprang SR (1989) The structure of tumor necrosis factor-α at 2.6 Å resolution. J Biol Chem 264:17595–17605

Emsley P, Lohkamp B, Scott WG, Cowtan K (2010) Features and development of *Coot*. Acta Crystallogr D Biol Crystallogr 66:486–501

Evangelidis T, Nerli S, Nováček J, Brereton AE, Karplus PA, Dotas RR, Venditti V, Sgourakis NG, Tripsianes K (2018) Automated NMR resonance assignments and structure determination using a minimal set of 4D spectra. Nat Commun 9:384

Farenc C, Spinelli S, Vinogradov E, Tremblay D, Blangy S, Sadovskaya I, Moineau S, Cambillau C (2014) Molecular insights on the recognition of a *Lactococcus lactis* cell wall pellicle by the phage 1358 receptor binding protein. J Virol 88:7005–7015

Fernandes S, São-José C (2018) Enzymes and mechanisms employed by tailed bacteriophages to breach the bacterial cell barriers. Viruses 10:396

Fokine A, Chipman PR, Leiman PG, Mesyanzhinov VV, Rao VB, Rossmann MG (2004) Molecular architecture of the prolate head of bacteriophage T4. Proc Natl Acad Sci USA 101:6003–6008

© The Author(s)

Fraser A, Prokhorov NS, Jiao F, Pettitt BM, Scheuring S, Leiman PG (2021) Quantitative description of a contractile macromolecular machine. Sci Adv 7:eabf9601

Ge P, Scholl D, Leiman PG, Yu X, Miller JF, Zhou ZH (2015) Atomic structures of a bactericidal contractile nanotube in its pre- and postcontraction states. Nat Struct Mol Biol 22:377–382

Ge P, Scholl D, Prokhorov NS, Avaylon J, Shneider MM, Browning C, Buth SA, Plattner M, Chakraborty U, Ding K et al (2020) Action of a minimal contractile bactericidal nanomachine. Nature 580:658–662

Gillespie JJ, Phan IQH, Scheib H, Subramanian S, Edwards TE, Lehman SS, Piitulainen H, Sayeedur Rahman M, Rennoll-Bankert KE, Staker BL et al (2015) Structural insight into how bacteria prevent interference between multiple divergent type IV secretion systems. mBio 6:e01867–15

Grunenwald CM, Bennett MR, Skaar EP (2018) Nonconventional therapeutics against *Staphylococcus aureus*. Microbiol Spectr. https://doi.org/10.1128/microbiolspec.gpp3-0047-2018

Guerrero-Ferreira RC, Hupfeld M, Nazarov S, Taylor NM, Shneider MM, Obbineni JM, Loessner MJ, Ishikawa T, Klumpp J, Leiman PG (2019) Structure and transformation of bacteriophage A511 baseplate and tail upon infection of *Listeria* cells. EMBO J 38:e99455

Güntert P (2009) Automated structure determination from NMR spectra. Eur Biophys J 38:129–143

Habann M, Leiman PG, Vandersteegen K, Van den Bossche A, Lavigne R, Shneider MM, Bielmann R, Eugster MR, Loessner MJ, Klumpp J (2014) Listeria phage A511, a model for the contractile tail machineries of SPO1-related bacteriophages. Mol Microbiol 92:84–99

Hu B, Margolin W, Molineux IJ, Liu J (2015) Structural remodeling of bacteriophage T4 and host membranes during infection initiation. Proc Natl Acad Sci USA 112:E4919–E4928

Ilca SL, Kotecha A, Sun X, Poranen MM, Stuart DI, Huiskonen JT (2015) Localized reconstruction of subunits from electron cryomicroscopy images of macromolecular complexes. Nat Commun 6:8843

Jiang F, Li N, Wang X, Cheng J, Huang Y, Yang Y, Yang J, Cai B, Wang Y-P, Jin Q et al (2019) Cryo-EM Structure and assembly of an extracellular contractile injection system. Cell 177:370–383.e15

Jumper J, Evans R, Pritzel A, Green T, Figurnov M, Ronneberger O, Tunyasuvunakool K, Bates R, Žídek A, Potapenko A et al (2021) Highly accurate protein structure prediction with AlphaFold. Nature 596:583–589

Kanamaru S, Leiman PG, Kostyuchenko VA, Chipman PR, Mesyanzhinov VV, Arisaka F, Rossmann MG (2002) Structure of the cell-puncturing device of bacteriophage T4. Nature 415:553–557

Kelley LA, Mezulis S, Yates CM, Wass MN, Sternberg MJE (2015) The Phyre2 web portal for protein modeling, prediction and analysis. Nat Protoc 10:845–858

Kimanius D, Dong L, Sharov G, Nakane T, Scheres SHW (2021) New tools for automated cryo-EM single-particle analysis in RELION-4.0. Biochem J 478:4169–4185

Kizziah JL, Manning KA, Dearborn AD, Dokland T (2020) Structure of the host cell recognition and penetration machinery of a *Staphylococcus aureus* bacteriophage. PLoS Pathog 16:e1008314

Klumpp J, Lavigne R, Loessner MJ, Ackermann H-W (2010) The SPO1-related bacteriophages. Arch Virol 155:1547–1561

Kostyuchenko VA, Chipman PR, Leiman PG, Arisaka F, Mesyanzhinov VV, Rossmann MG (2005) The tail structure of bacteriophage T4 and its mechanism of contraction. Nat Struct Mol Biol 12:810–813

Krissinel E, Henrick K (2007) Inference of macromolecular assemblies from crystalline state. J Mol Biol 372:774–797

Krusche J, Beck C, Lehmann E, Gerlach D, Daiber E, Mayer C, Müller J, Onallah H, Würstle S, Wolz C et al (2025) Characterization and host range prediction of *Staphylococcus aureus* phages through receptor-binding protein analysis. Cell Rep 44:115369

Kudryashev M, Wang RY-R, Brackmann M, Scherer S, Maier T, Baker D, DiMaio F, Stahlberg H, Egelman EH, Basler M (2015) Structure of the type VI secretion system contractile sheath. Cell 160:952–962

Kwiecinski JM, Horswill AR (2020) *Staphylococcus aureus* bloodstream infections: pathogenesis and regulatory mechanisms. Curr Opin Microbiol 53:51–60

Lee JH, Yang S-T, Rho S-H, Im YJ, Kim SY, Kim YR, Kim M-K, Kang GB, Kim JI, Rhee JH et al (2006) Crystal structure and functional studies reveal that PAS factor from *Vibrio vulnificus* is a novel member of the saposin-fold family. J Mol Biol 355:491–500

Legrand P, Collins B, Blangy S, Murphy J, Spinelli S, Gutierrez C, Richet N, Kellenberger C, Desmyter A, Mahony J et al (2016) The atomic structure of the phage Tuc2009 baseplate tripod suggests that host recognition involves two different carbohydrate binding modules. mBio 7:e01781–15

Leiman PG, Basler M, Ramagopal UA, Bonanno JB, Sauder JM, Pukatzki S, Burley SK, Almo SC, Mekalanos JJ (2009) Type VI secretion apparatus and phage tail-associated protein complexes share a common evolutionary origin. Proc Natl Acad Sci USA 106:4154–4159

Leiman PG, Shneider MM (2012) Contractile tail machines of bacteriophages. In: Rossmann MG, Rao VB (eds) Viral molecular machines. Springer US, Boston, MA, pp 93–114

Leiman PG, Shneider MM, Kostyuchenko VA, Chipman PR, Mesyanzhinov VV, Rossmann MG (2003) Structure and location of gene product 8 in the bacteriophage T4 baseplate. J Mol Biol 328:821–833

Li F, Hou C-FD, Lokareddy RK, Yang R, Forti F, Briani F, Cingolani G (2023) High-resolution cryo-EM structure of the *Pseudomonas* bacteriophage E217. Nat Commun 14:4052

Liebschner D, Afonine PV, Baker ML, Bunkóczi G, Chen VB, Croll TI, Hintze B, Hung L-W, Jain S, McCoy AJ et al (2019) Macromolecular structure determination using X-rays, neutrons and electrons: recent developments in *Phenix*. Acta Crystallogr D Struct Biol 75:861–877

Linge JP, Williams MA, Spronk CAEM, Bonvin AMJJ, Nilges M (2003) Refinement of protein structures in explicit solvent. Proteins 50:496–506

Łobocka M, Hejnowicz MS, Dąbrowski K, Gozdek A, Kosakowski J, Witkowska M, Ulatowska MI, Weber-Dąbrowska B, Kwiatek M, Parasion S et al (2012) Genomics of Staphylococcal twort-like phages - potential therapeutics of the post-antibiotic era. In: Małgorzata Łobocka, Wacław Szybalski (eds) Advances in virus research. Elsevier, pp 143–216

Madeira F, Pearce M, Tivey ARN, Basutkar P, Lee J, Edbali O, Madhusoodanan N, Kolesnikov A, Lopez R (2022) Search and sequence analysis tools services from EMBL-EBI in 2022. Nucleic Acids Res 50:W276–W279

Maghsoodi A, Chatterjee A, Andricioaei I, Perkins NC (2019) How the phage T4 injection machinery works including energetics, forces, and dynamic pathway. Proc Natl Acad Sci USA 116:25097–25105

Marín-Arraiza L, Roa-Eguiara A, Pape T, Sofos N, Hendriks IA, Lund Nielsen M, Steiner-Rebrova EM, Taylor NMI (2025) Structural characterization of an extracellular contractile injection system from *Photorhabdus luminescens* in extended and contracted states. Nat Commun 16:9327

Maxwell KL, Fatehi Hassanabad M, Chang T, Pirani N, Bona D, Edwards AM, Davidson AR (2013) Structural and functional studies of gpX of *Escherichia coli* phage P2 reveal a widespread role for LysM domains in the baseplates of contractile-tailed phages. J Bacteriol 195:5461–5468

McCabe O, Spinelli S, Farenc C, Labbé M, Tremblay D, Blangy S, Oscarson S, Moineau S, Cambillau C (2015) The targeted recognition of *Lactococcus lactis* phages to their polysaccharide receptors: Receptor binding to lactococcal phage 1358. Mol Microbiol 96:875–886

McCoy AJ, Grosse-Kunstleve RW, Adams PD, Winn MD, Storoni LC, Read RJ (2007) *Phaser* crystallographic software. J Appl Crystallogr 40:658–674

 © The Author(s)

Meng EC, Goddard TD, Pettersen EF, Couch GS, Pearson ZJ, Morris JH, Ferrin TE (2023) UCSF CHIMERAX: tools for structure building and analysis. Protein Sci 32:e4792

Moody MF (1973) Sheath of bacteriophage T4. J Mol Biol 80:613–635

Myers CL, Li FKK, Koo B-M, El-Halfawy OM, French S, Gross CA, Strynadka NCJ, Brown ED (2016) Identification of two phosphate starvation-induced wall teichoic acid hydrolases provides first insights into the degradative pathway of a key bacterial cell wall component. J Biol Chem 291:26066–26082

Nazarov S, Schneider JP, Brackmann M, Goldie KN, Stahlberg H, Basler M (2018) Cryo- EM reconstruction of Type VI secretion system baseplate and sheath distal end. EMBO J 37:e97103

Nederveen AJ, Doreleijers JF, Vranken W, Miller Z, Spronk CAEM, Nabuurs SB, Güntert P, Livny M, Markley JL, Nilges M et al (2005) RECOORD: a recalculated coordinate database of 500+ proteins from the PDB using restraints from the BioMagResBank. Proteins 59:662–672

Nishima W, Kanamaru S, Arisaka F, Kitao A (2011) Screw motion regulates multiple functions of T4 phage protein gene product 5 during cell puncturing. J Am Chem Soc 133:13571–13576

Nobrega FL, Vlot M, De Jonge PA, Dreesens LL, Beaumont HJE, Lavigne R, Dutilh BE, Brouns SJJ (2018) Targeting mechanisms of tailed bacteriophages. Nat Rev Microbiol 16:760–773

North OI, Sakai K, Yamashita E, Nakagawa A, Iwazaki T, Büttner CR, Takeda S, Davidson AR (2019) Phage tail fibre assembly proteins employ a modular structure to drive the correct folding of diverse fibres. Nat Microbiol 4:1645–1653

Nováček J, Šiborová M, Benešík M, Pantůček R, Doškař J, Plevka P (2016) Structure and genome release of Twort-like Myoviridae phage with a double-layered baseplate. Proc Natl Acad Sci USA 113:9351–9356

Ouyang R, Costa AR, Cassidy CK, Otwinowska A, Williams VCJ, Latka A, Stansfeld PJ, Drulis-Kawa Z, Briers Y, Pelt DM et al (2022) High-resolution reconstruction of a Jumbo-bacteriophage infecting capsulated bacteria using hyperbranched tail fibers. Nat Commun 13: 7241

Pantůček R, Rosypalová A, Doškař J, Kailerová J, Růžičková V, Borecká P, Snopková Š, Horváth R, Götz F, Rosypal S (1998) The polyvalent Staphylococcal phage φ812:its host-range mutants and related phages. Virology 246:241–252

Park Y-J, Lacourse KD, Cambillau C, DiMaio F, Mougous JD, Veesler D (2018) Structure of the type VI secretion system TssK–TssF–TssG baseplate subcomplex revealed by cryo-electron microscopy. Nat Commun 9:5385

Paul VD, Rajagopalan SS, Sundarrajan S, George SE, Asrani JY, Pillai R, Chikkamadaiah R, Durgaiah M, Sriram B, Padmanabhan S (2011) A novel bacteriophage tail-associated muralytic enzyme (TAME) from Phage K and its development into a potent antistaphylococcal protein. BMC Microbiol 11:226

Petrovic Fabijan A, Lin RCY, Ho J, Maddocks S, Ben Zakour NL, Iredell JR, Westmead Bacteriophage Therapy Team, Khalid A, Venturini C, Chard R et al (2020) Safety of bacteriophage therapy in severe *Staphylococcus aureus* infection. Nat Microbiol 5:465–472

Pettersen EF, Goddard TD, Huang CC, Couch GS, Greenblatt DM, Meng EC, Ferrin TE (2004) UCSF Chimera—a visualization system for exploratory research and analysis. J Comput Chem 25:1605–1612

Pettersen EF, Goddard TD, Huang CC, Meng EC, Couch GS, Croll TI, Morris JH, Ferrin TE (2021) UCSF ChimeraX: Structure visualization for researchers, educators, and developers. Protein Sci 30:70–82

Sanz-Gaitero M, Keary R, Garcia-Doval C, Coffey A, van Raaij MJ (2014) Crystal structure of the lytic CHAPK domain of the endolysin LysK from *Staphylococcus aureus* bacteriophage K. Virol J 11:133

Scheres SHW (2015) Semi-automated selection of cryo-EM particles in RELION-1.3. J Struct Biol 189:114–122

Schneider TR, Sheldrick GM (2002) Substructure solution with *SHELXD*. Acta Crystallogr D Biol Crystallogr 58:1772–1779

Sciara G, Bebeacua C, Bron P, Tremblay D, Ortiz-Lombardia M, Lichière J, van Heel M, Campanacci V, Moineau S, Cambillau C (2010) Structure of lactococcal phage p2 baseplate and its mechanism of activation. Proc Natl Acad Sci USA 107:6852–6857

Shen Y, Delaglio F, Cornilescu G, Bax A (2009) TALOS+: a hybrid method for predicting protein backbone torsion angles from NMR chemical shifts. J Biomol NMR 44:213–223

Shi L, Liu J-F, An X-M, Liang D-C (2008) Crystal structure of glycerophosphodiester phosphodiesterase (GDPD) from *Thermoanaerobacter tengcongensis*, a metal ion-dependent enzyme: Insight into the catalytic mechanism: crystal structure of GDPD. Proteins 72:280–288

Shneider MM, Buth SA, Ho BT, Basler M, Mekalanos JJ, Leiman PG (2013) PAAR-repeat proteins sharpen and diversify the type VI secretion system spike. Nature 500:350–353

Šiborová M, Füzik T, Procházková M, Nováček J, Benešík M, Nilsson AS, Plevka P (2022) Tail proteins of phage SU10 reorganize into the nozzle for genome delivery. Nat Commun 13:5622

Sievers F, Higgins DG (2018) Clustal Omega for making accurate alignments of many protein sequences. Protein Sci 27:135–145

Sonani RR, Palmer LK, Esteves NC, Horton AA, Sebastian AL, Kelly RJ, Wang F, Kreutzberger MAB, Russell WK, Leiman PG et al (2024) An extensive disulfide bond network prevents tail contraction in *Agrobacterium tumefaciens* phage Milano. Nat Commun 15:756

Šulák O, Cioci G, Delia M, Lahmann M, Varrot A, Imberty A, Wimmerová M (2010) A TNF-like trimeric lectin domain from *Burkholderia cenocepacia* with specificity for fucosylated human histo-blood group antigens. Structure 18:59–72

Takeuchi I, Osada K, Azam AH, Asakawa H, Miyanaga K, Tanji Y (2016) The presence of two receptor-binding proteins contributes to the wide host range of Staphylococcal twort-like phages. Appl Environ Microbiol 82:5763–5774

Tang G, Peng L, Baldwin PR, Mann DS, Jiang W, Rees I, Ludtke SJ (2007) EMAN2: an extensible image processing suite for electron microscopy. J Struct Biol 157:38–46

Taylor NMI, Prokhorov NS, Guerrero-Ferreira RC, Shneider MM, Browning C, Goldie KN, Stahlberg H, Leiman PG (2016) Structure of the T4 baseplate and its function in triggering sheath contraction. Nature 533:346–352

Taylor NMI, van Raaij MJ, Leiman PG (2018) Contractile injection systems of bacteriophages and related systems. Mol Microbiol 108:6–15

Uyttebroek S, Chen B, Onsea J, Ruythooren F, Debaveye Y, Devolder D, Spriet I, Depypere M, Wagemans J, Lavigne R et al (2022) Safety and efficacy of phage therapy in difficult-to-treat infections: a systematic review. Lancet Infect Dis 22:e208–e220

Vagin AA, Steiner RA, Lebedev AA, Potterton L, McNicholas S, Long F, Murshudov GN (2004) *REFMAC*5 dictionary: organization of prior chemical knowledge and guidelines for its use. Acta Crystallogr D Biol Crystallogr 60:2184–2195

van Dalen R, Peschel A, van Sorge NM (2020) Wall teichoic acid in *Staphylococcus aureus* host interaction. Trends Microbiol 28:985–998

Vandersteegen K, Mattheus W, Ceyssens P-J, Bilocq F, De Vos D, Pirnay J-P, Noben J-P, Merabishvili M, Lipinska U, Hermans K et al (2011) Microbiological and molecular assessment of bacteriophage ISP for the control of *Staphylococcus aureus*. PLoS ONE 6:e24418

Veesler D, Cambillau C (2011) A common evolutionary origin for tailed-bacteriophage functional modules and bacterial machineries. Microbiol Mol Biol Rev 75:423–433

Venturini C, Petrovic Fabijan A, Fajardo Lubian A, Barbirz S, Iredell J (2022) Biological foundations of successful bacteriophage therapy. EMBO Mol Med 14:e12435

© The Author(s)

Wagner T (2019) MPI-Dortmund/sphire-janni: JANNI 0.0.5.
Wagner T, Merino F, Stabrin M, Moriya T, Antoni C, Apelbaum A, Hagel P, Sitsel O, Raisch T, Prumbaum D et al (2019) SPHIRE-crYOLO is a fast and accurate fully automated particle picker for cryo-EM. Commun Biol 2:1–13
Wang Z, Fokine A, Guo X, Jiang W, Rossmann MG, Kuhn RJ, Luo Z-H, Klose T (2023) Structure of Vibrio phage XM1, a simple contractile DNA injection machine. Viruses 15:1673
Waterhouse AM, Procter JB, Martin DMA, Clamp M, Barton GJ (2009) Jalview version 2—a multiple sequence alignment editor and analysis workbench. Bioinformatics 25:1189–1191
Watts NR, Coombs DH (1990) Structure of the bacteriophage T4 baseplate as determined by chemical cross-linking. J Virol 64:143–154
Weiss GL, Eisenstein F, Kieninger A-K, Xu J, Minas HA, Gerber M, Feldmüller M, Maldener I, Forchhammer K, Pilhofer M (2022) Structure of a thylakoid-anchored contractile injection system in multicellular cyanobacteria. Nat Microbiol 7:386–396
Wenzel S, Shneider MM, Leiman PG, Kuhn A, Kiefer D (2020) The central spike complex of bacteriophage T4 contacts PpiD in the periplasm of *Escherichia coli*. Viruses 12:1135
Williams CJ, Headd JJ, Moriarty NW, Prisant MG, Videau LL, Deis LN, Verma V, Keedy DA, Hintze BJ, Chen VB et al (2018) MolProbity: more and better reference data for improved all-atom structure validation. Protein Sci 27:293–315
Willis C, Wang CK, Osman A, Simon A, Pickering D, Mulvenna J, Riboldi-Tunicliffe A, Jones MK, Loukas A, Hofmann A (2011) Insights into the membrane interactions of the saposin-like proteins Na-SLP-1 and Ac-SLP-1 from human and dog hookworm. PLoS ONE 6:e25369
Wu X, Zhao Y, Sun L, Jiang M, Wang Q, Wang Q, Yang W, Wu Y (2019) Crystal structure of CagV, the *Helicobacter pylori* homologue of the T4 ss protein VirB8. FEBS J 286:4294–4309
Xia G, Corrigan RM, Winstel V, Goerke C, Gründling A, Peschel A (2011) Wall teichoic acid-dependent adsorption of staphylococcal siphovirus and myovirus. J Bacteriol 193:4006–4009
Xu J, Ericson CF, Lien Y-W, Rutaganira FUN, Eisenstein F, Feldmüller M, King N, Pilhofer M (2022) Identification and structure of an extracellular contractile injection system from the marine bacterium *Algoriphagus machipongonensis*. Nat Microbiol 7:397–410
Yang F, Jiang Y-L, Zhang J-T, Zhu J, Du K, Yu R-C, Wei Z-L, Kong W-W, Cui N, Li W-F et al (2023a) Fine structure and assembly pattern of a minimal myophage Pam3. Proc Natl Acad Sci USA 120:e2213727120
Yang F, Wang L, Zhou J, Xiao H, Liu H (2023b) In situ structures of the ultra-long extended and contracted tail of myoviridae phage P1. Viruses 15:1267
Yu R-C, Yang F, Zhang H-Y, Hou P, Du K, Zhu J, Cui N, Xu X, Chen Y, Li Q et al (2024) Structure of the intact tail machine of *Anabaena* myophage A-1(L). Nat Commun 15:2654
Zhang K (2016) Gctf: real-time CTF determination and correction. J Struct Biol 193:1–12
Zheng SQ, Palovcak E, Armache J-P, Verba KA, Cheng Y, Agard DA (2017) MotionCor2: anisotropic correction of beam-induced motion for improved cryo-electron microscopy. Nat Methods 14:331–332
Zinke M, Schröder GF, Lange A (2022) Major tail proteins of bacteriophages of the order Caudovirales. J Biol Chem 298:101472
Zivanov J, Nakane T, Scheres SHW (2020) Estimation of high-order aberrations and anisotropic magnification from cryo-EM data sets in RELION-3.1. IUCrJ 7:253–267

Acknowledgements

We gratefully acknowledge the core facilities Cryo-electron microscopy and tomography, Biomolecular Interactions and Crystallography, Proteomics, and Josef Dadok National NMR Centre of CIISB, Instruct-CZ Centre, supported by MEYS CR (LM2023042) and European Regional Development Fund-Project "UP CIISB" (No. CZ.02.1.01/0.0/0.0/18_046/0015974). We gratefully acknowledge support from the National Institute of Virology and Bacteriology (Program EXCELES, Project ID No. LX22NPO5103) - Funded by the European Union - Next Generation EU and the project New Technologies for Translational Research in Pharmaceutical Sciences /NETPHARM, project ID OP JAC CZ.02.01.01/00/22_008/0004607, which is co-funded by the European Union. This work received funding from the ERC Consolidator Grant No. 101043452 to PP. Computational resources were provided by the e-INFRA CZ project (ID:90254), supported by the Ministry of Education, Youth and Sports of the Czech Republic.

Author contributions

Ján Bíňovský: Data curation; Formal analysis; Validation; Investigation; Visualization; Methodology; Writing—original draft; Writing—review and editing. **Marta Šiborová**: Validation; Investigation; Visualization; Methodology; Writing—original draft. **Maryna Zlatohurska**: Investigation. **Jiří Nováček**: Supervision; Investigation; Methodology. **Pavol Bárdy**: Investigation. **Roman Baška**: Investigation. **Karel Škubník**: Investigation. **Tibor Botka**: Investigation. **Martin Benešík**: Investigation. **Roman Pantůček**: Supervision; Methodology. **Konstantinos Tripsianes**: Formal analysis. **Pavel Plevka**: Conceptualization; Resources; Supervision; Funding acquisition; Validation; Methodology; Writing—original draft; Project administration; Writing—review and editing.

Source data underlying figure panels in this paper may have individual authorship assigned. Where available, figure panel/source data authorship is listed in the following database record: biostudies:S-SCDT-10_1038-S44318-026-00834-9.

Disclosure and competing interests statement

The authors declare no competing interests.

Open Access This article is licensed under a Creative Commons Attribution 4.0 International License, which permits use, sharing, adaptation, distribution and reproduction in any medium or format, as long as you give appropriate credit to the original author(s) and the source, provide a link to the Creative Commons licence, and indicate if changes were made. The images or other third party material in this article are included in the article's Creative Commons licence, unless indicated otherwise in a credit line to the material. If material is not included in the article's Creative Commons licence and your intended use is not permitted by statutory regulation or exceeds the permitted use, you will need to obtain permission directly from the copyright holder. To view a copy of this licence, visit http://creativecommons.org/licenses/by/4.0/. Creative Commons Public Domain Dedication waiver http://creativecommons.org/publicdomain/zero/1.0/ applies to the data associated with this article, unless otherwise stated in a credit line to the data, but does not extend to the graphical or creative elements of illustrations, charts, or figures. This waiver removes legal barriers to the re-use and mining of research data. According to standard scholarly practice, it is recommended to provide appropriate citation and attribution whenever technically possible.

© The Author(s) 2026

APPENDIX 3

Siváková A, Figallová E, Botka T (corresp. author), Vacek L, Tkadlec J, Vrbský J, Osowski M, Petráš P, Polaštík Kleknerová D, Dvořáčková M, Urbanová P, Pantůček R, Růžička F (2026) The combination of mupirocin and *Kayvirus* broadens the decolonization effect against *Staphylococcus aureus*. *Applied Microbiology and Biotechnology* 110:157. https://doi.org/10.1007/s00253-026-13814-0

(JCR 2025: IF = 4.7; Q2 – Biotechnology & Applied Microbiology)

CC BY 4.0

Applied Microbiology and Biotechnology (2026) 110:157
https://doi.org/10.1007/s00253-026-13814-0

RESEARCH

The combination of mupirocin and *Kayvirus* broadens the decolonization effect against *Staphylococcus aureus*

Alena Siváková[1] · Eliška Figallová[2] · Tibor Botka[2] · Lukáš Vacek[1] · Jan Tkadlec[3] · Jan Vrbský[1] · Martin Osowski[1] · Petr Petráš[4] · Dominika Polaštík Kleknerová[1] · Milada Dvořáčková[1] · Pavlína Urbanová[1] · Roman Pantůček[2] · Filip Růžička[1]

Received: 27 January 2026 / Revised: 20 March 2026 / Accepted: 31 March 2026
© The Author(s) 2026, modified publication 2026

Abstract

Staphylococcus aureus strains cause a wide range of infections in humans, often with the potential for complications such as surgical site infections. The production of Panton-Valentin leukocidin (PVL) by certain strains of *S. aureus* is clinically associated with chronic or recurrent infections, which typically require decolonization, most often with mupirocin. As increased mupirocin use promotes the emergence of resistance, this study investigated the coadministration of mupirocin and therapeutic *Kayvirus* bacteriophage as a potential strategy to enhance treatment efficacy and prevent the development of new resistance. We collected and evaluated 37 PVL-encoding *S. aureus* strains from wound samples. Among these, 22% were methicillin-resistant, and 11% were resistant to the tested phage, but all were susceptible to mupirocin. To assess interactions between mupirocin and the phage in PVL-positive strains with varying levels of mupirocin resistance, we used lysogenization by PVL-encoding phage and adaptive laboratory evolution of clinical strains. In mupirocin-susceptible strains, lytic phage efficacy decreased due to altered protein synthesis caused by the interaction of mupirocin with isoleucyl-tRNA synthetase, whereas mupirocin efficacy was unaffected. In contrast, the advantage of combined administration was observed in mupirocin-resistant strains susceptible to phages, as their altered or alternative synthetase allowed protein synthesis to continue, enabling phage proliferation and bacterial lysis, even in the presence of mupirocin. This in vitro study demonstrates that mupirocin in combination with *Kayvirus* broadens the spectrum of strains susceptible to treatment and that the phage used prevents the development of mupirocin resistance.

Key points

- *Mupirocin-phage combination broadens the anti-staphylococcal effect in vitro.*
- *Combination treatment reduces the emergence of mupirocin resistance.*
- *Mupirocin action is not inhibited by phage therapy.*

Keywords *Staphylococcus aureus* · Panton-Valentine leukocidin · Decolonization · Mupirocin · Phage therapy · *Kayvirus*

Alena Siváková and Eliška Figallová contributed equally to this work.

✉ Tibor Botka
tibor.botka@mail.muni.cz

[1] Department of Microbiology, Faculty of Medicine, Masaryk University and St. Anne's University Hospital, Brno, Czech Republic

[2] Department of Experimental Biology, Faculty of Science, Masaryk University, Brno, Czech Republic

[3] Department of Medical Microbiology, Second Faculty of Medicine, Charles University and University Hospital Motol and Homolka, Prague, Czech Republic

[4] National Reference Laboratory for Staphylococci, National Institute of Public Health, Prague, Czech Republic

Introduction

Infections remain a leading cause of death worldwide, and reducing their impact is an urgent global public health priority (Murray et al. 2022). *Staphylococcus aureus* is the predominant human pathogen, with an all-cause, age-standardized mortality rate of 14.6 per 100,000 population (Ikuta et al. 2022). It causes a wide range of infections, including bloodstream infections (BSIs) and skin and soft tissue infections (SSTIs), of which it is the leading cause (Tong et al. 2015). Approximately 30% of the human population carries this bacterium asymptomatically (Wertheim et al. 2005). However, *S. aureus* carriage can pose a significant risk in certain clinical contexts such as cardiac surgery (Langenberg et al. 2018), acute leukemia (Ghaffary et al. 2024), and hemodialysis (Hassoun-Kheir et al. 2023), requiring eradication. Due to the rise of antimicrobial resistance (AMR), methicillin-resistant *S. aureus* (MRSA) has been a major focus of recent research (Murray et al. 2022). Although MRSA decolonization has been achieved using antibiotic-based regimens, such approaches carry the risk of selecting for resistant *S. aureus* strains (Eed et al. 2019).

The clinical significance of *S. aureus* is amplified by its wide array of virulence factors, including toxins with superantigen activity and cytotoxins. Among the toxins, Panton-Valentine leukocidin (PVL), encoded by prophage-borne *lukS-PV* and *lukF-PV* genes, is a well-known toxin that causes leukocyte destruction and tissue necrosis. PVL is commonly associated with chronic necrotic skin lesions and severe necrotizing pneumonia (Genestier et al. 2005; Löffler et al. 2010). Patients colonized with PVL-producing *S. aureus* strains commonly suffer from recurring skin lesions and have an elevated risk of surgical site infections (Hoppe et al. 2019; Leistner et al. 2022); therefore, they may benefit from prophylactic decolonization.

Traditional *S. aureus* decolonization regimens utilize nasally administered mupirocin combined with chlorhexidine soap for body washing. However, this treatment fails in upwards of 30% of patients and must be repeated (Cool-Foley et al. 1991; Rossi et al. 1996; Wagenlehner et al. 2007; Ammerlaan et al. 2011). Colonization of non-nasal sites, such as the throat or wounds, is associated with higher rates of eradication failure (Mollema et al. 2010; Lindgren et al. 2018). Resistance to both chlorhexidine (CHX-R) and mupirocin (Mu-R) has been reported, with variable prevalence across regions: for example, Mu-R 9.1% and CHX-R 5.8% in Saudi Arabia, and Mu-R 19.3% in the USA (Antonov et al. 2015; Yankey and Isaacson 2018). Mupirocin acts by inhibiting bacterial isoleucyl-tRNA synthetase, thereby blocking protein synthesis. Two types of mupirocin resistance have been previously described: high-level resistance (Mu-HR), mediated by an alternative isoleucyl-tRNA synthetase encoded by the *mupA* or *mupB* genes, which are typically carried on plasmids (Hodgson et al. 1994; Seah et al. 2012), and low-level resistance (Mu-LR), resulting from *mupA* carried on the chromosome or from point mutations in the wild-type *ileS* gene encoding isoleucyl-tRNA synthetase. Although Mu-LR strains respond to mupirocin treatment, this type of resistance has been described as the cause of decolonization therapy failure (Hetem and Bonten 2013).

Novel approaches are urgently needed to enhance the efficacy of decolonization and combat the emergence of resistance. Bacteriophages offer promising therapeutic potential because of their pathogen specificity and synergy with antibiotics (Comeau et al. 2007; Obořilová et al. 2025). In this study, we investigated the combination of mupirocin with the therapeutic phage 812K1/420 of the *Kayvirus* genus (Pantůček et al. 1998; Botka et al. 2019). We evaluated, in vitro, the efficacy of this combined therapy against clinical PVL+ *S. aureus* isolates and assessed its potential in preventing de novo emergence of mupirocin resistance. We focused on PVL+ strains as a typical target of decolonization; however, our conclusions apply to *S. aureus* in general.

Materials and methods

Staphylococcus aureus isolates

Between January 2021 and December 2022, 17 *S. aureus* isolates positive for PVL-encoding genes (PVL+ strains) and two non-PVL strains were collected from adult patients treated for SSTIs in various hospital departments (surgery, internal medicine, psychiatry, oncology, and others) (Table S1). Samples were collected from four hospitals that provide care to patients from the Moravian region (labeled AS): St. Anne's University Hospital, the Center for Cardiovascular Surgery and Transplantation in Brno, Masaryk Memorial Cancer Institute, and the Hospital of the Merciful Brothers in Brno, Czech Republic. Samples from suspected SSTIs (e.g., pus and wound swab) were cultured on blood agar (Oxoid, UK) and blood agar with 10% NaCl (Oxoid, UK). *S. aureus* strains were deposited in the Collection of Microorganisms of the Department of Microbiology, St. Anne's University Hospital and Faculty of Medicine, Masaryk University, Czech Republic. The National Reference Laboratory (NRL) for Staphylococci of the National Institute of Public Health (NIPH) provided 20 PVL+ *S. aureus* isolates (labeled NRL/St) from SSTIs in hospitals across the Bohemian region (Table S1). Bacterial identification was carried out using MALDI-TOF MS (Bruker Daltonics, USA) according to the manufacturer's instructions. All bacterial isolates were obtained from routine diagnostic

samples, with only anonymized data regarding their origin included in this study.

Detection of the Panton-Valentine leukocidin genes

The PVL *lukS-PV* and *lukF-PV* genes (GenBank accession: X72700.1) and the *S. aureus* species-confirming *nuc* gene were detected using real-time PCR and primers, as described previously (Galia et al. 2019). PVL+ *S. aureus* strain NRL/St 22/167 (isolated from a blood culture, NIPH NRL collection) and NRL/St 22/195 (Table S1) served as positive controls after the PCR amplicons were confirmed using Sanger sequencing. DNA isolation was performed using the 3DMed isolation kit (3D Biomedicine Science and Technology Co., China) and the KingFisher Flex device (Thermo Scientific, USA), according to the manufacturer's instructions. The 10 µL reaction mixture consisted of 0.5 µL of DNA template, 0.5 µL of primers (10 µM) each, 5 µL of LightCycler 480 SYBR Green I Master (Roche, Switzerland), and 3.5 µL of nuclease-free water. End-point real-time PCR was performed using a CFX96 Real-time PCR system (Bio-Rad, USA).

Antimicrobial susceptibility testing

Using the standardized disc (Oxoid, UK) diffusion method on Mueller-Hinton agar (MHA, Oxoid, UK), all isolates were tested against cefoxitin, erythromycin, clindamycin, trimethoprim/sulfamethoxazole, tetracycline, mupirocin, gentamicin, rifampicin, linezolid, ciprofloxacin, tigecycline, and ceftaroline. *S. aureus* ATCC 25923 was used as a control strain. The minimum inhibitory concentrations (MICs) of vancomycin (Erba Lachema, Czechia) and mupirocin (Fagron a.s., Czechia) were determined in accordance with the ISO standard 20776-1:2019 using the broth microdilution method in cation-adjusted MHB (Oxoid, UK). Methicillin resistance was assayed by PCR detection of the *mecA* gene, as described by Belguesmia et al. (2021). Methicillin-resistant *S. aureus* ATCC 43300 was used as a control. For mupirocin-resistant *S. aureus* strains, resistance was verified using the microdilution method, which determined the exact MIC. All results were interpreted according to EUCAST guidelines (version 16.0, 2026). Methicillin-resistant *S. aureus* ATCC 43300 was used as a control. The mechanism of resistance to mupirocin was determined by PCR detection of *mupA,* as described by Eed et al. (2019).

Phage 812K1/420 susceptibility testing

Phage strains 812 (wild type) and 812K1/420 have been described previously (Pantůček et al. 1998; Botka et al. 2019). The ability of the phage to propagate on the analyzed strains was confirmed by the appearance of single plaques after a drop test using serial dilution of the phage lysate as previously described by Pantůček et al. (1998). Next, to demonstrate the ability of phage 812K1/420 to overcome the abortive system determined by Pdp_{Sau} protein, we tested the phage susceptibility of the *S. aureus* strains RN4220, RN4220 (53^{+}), NCTC 8325, and NRL 02/947 (Kuntová et al. 2023).

Determination of clonal relatedness of Panton-Valentine leukocidin-producing *S. aureus* strains

PVL+ *S. aureus* isolates were characterized by *spa* typing as described by Harmsen et al. (2003). Individual *spa* types were assigned using the Ridom StaphType software package, version 2.2.1 (Ridom, Germany). Based on a previously described high concordance (0.954–0.979) between *spa*-typing and MLST in determining the clonal complex (CC) (O'Hara et al. 2016), the CCs were inferred from *spa* types using information available in the SpaServer database (http://spaserver.ridom.de), from previously published studies (Blanco et al. 2011; Egyir et al. 2014; Kinross et al. 2017; Durand et al. 2018; Klein et al. 2020; Monecke et al. 2021; Tabaja et al. 2021; Rakonjac et al. 2022; Quero et al. 2023; Yin et al. 2024), or from whole-genome sequences using MLST 2.0 tool (Larsen et al. 2012).

Pulsed-field gel electrophoresis (PFGE) was conducted as described by Pantůček et al. (1996). *Sma*I (New England Biolabs, USA) macrorestriction fragments were separated with a CHEF Mapper XA System (Bio-Rad Laboratories, CA) using 1.2% agarose in 1 × Tris-acetate-EDTA (TAE) buffer at 14 °C, 5.5 V/cm, pulse times of 1–55 s for 24 h. *Sma*I-cleaved DNA from *S. aureus* strain NCTC 8325 served as the ladder. The gel was stained with ethidium bromide for 30 min, destained in water, and visualized under UV light at a wavelength of 302 nm. PFGE analysis was performed using the BIONUMERICS software version 8.1 (bioMérieux, Applied Maths, Belgium).

Preparation of PVL+ strain with high-level resistance to mupirocin

To prepare the PVL+ Mu-HR strain, a non-PVL Mu-HR SSTI isolate AS 21/64 (Table S1) was lysogenized (Holochová et al. 2010) using the PVL-converting temperate phage phiSa2 07/415, which originated from the MRSA strain NRL/St 07/415. Next, single colonies were cultivated three times in medium containing 1 mM sodium citrate to obtain a pure lysogen culture. PCR detection of the prophage and PVL genes, as well as PFGE of *Sma*I macrorestriction fragments, confirmed the presence of an integrated prophage (Fig. S1). One culture was randomly selected, and the strain was designated AS 21/64L.

Preparation of PVL+ strains with low-level resistance to mupirocin

Two PVL+ Mu-LR strains were prepared using adaptive laboratory evolution (ALE). PVL+ strains NRL/St 21/350 and AS 22/149 were repeatedly exposed to mupirocin to evolve low-level resistance, which is described as an MIC range of 8–64 mg/L (Patel et al. 2009). ALE was performed in a 96-well plate using a liquid culture of approximately 1×10^6 CFU/mL in Mueller-Hinton broth (MHB; Oxoid, UK) in three biological replicates. The concentration of mupirocin was initially set at the MIC for each strain. Every 24 h, it was doubled, and 100 µL of the culture was transferred into a new well with fresh medium. The remaining 100 µL of the culture was plated on Mueller-Hinton agar (MHA) at the respective mupirocin concentrations and incubated overnight at 37 °C. Individual colonies were then picked and streaked onto MHA with or without mupirocin as a growth control. Strains designated NRL/St 21/350R and AS 22/149R were cultivated from randomly selected resistant colonies on plates with 8 mg/L mupirocin.

Measurement of the combined effect of mupirocin with phage on distantly related strains

To determine the combined effect of administration, PVL+ isolates representing distinct PFGE profile groups: NRL/St 21/219, AS 22/130, NRL/St 20/786, NRL/St 21/377, NRL/St 21/350, AS 22/149 (selected randomly), and AS 21/64L were used. The strains were grown overnight on separate plates with 1.5% Tryptone Soya Agar (TSA; Oxoid, UK), and individual colonies were inoculated into 10 mL of MHB with adjusted Ca^{2+} and Mg^{2+} ions according to CLSI standards. Fresh cultures were grown at 37 °C with orbital shaking (120 rpm) until the late exponential phase and then diluted to 2×10^8 CFU/mL. In addition to the growth and negative controls, seven conditions of phage and/or mupirocin (0.03 mg/L) treatment were tested in a 96-well plate (JetBiofil, China): (1) phage immediate addition, (2) phage addition after 8 h, (3) immediate addition of mupirocin, (4) mupirocin addition after 8 h, (5) addition of mupirocin immediately and phage after 8 h, (6) addition of phage immediately and mupirocin after 8 h, and (7) simultaneous immediate addition of phage with mupirocin. The input ratio (IR or MOI_{INPUT}) of phages to bacteria (PFU/CFU) was 0.1. Measurements were performed over 48 h at 37 °C with mild shaking in 10-min intervals, using a spectrophotometer (Tecan Infinite M200 PRO, Tecan Trading AG, Switzerland). Optical density (OD) was measured at 850 nm, the optimal wavelength for evaluating interactions between bacterial cultures and antibiotics (Truong et al. 2021). A viable cell count of the remaining bacteria was performed after 48 h of incubation by plating the cells, resuspended in an equal volume of fresh medium adjusted with citrate, on 1.5% TSA. All experiments were performed in biological triplicates and technical duplicates.

Spectrophotometric measurement of the effect of mupirocin and phage on Mu-HR PVL+ strain

Strain AS 21/64L was grown overnight on 1.5% TSA, and individual colonies were inoculated into 10 mL of MHB with adjusted Ca^{2+} and Mg^{2+} ions according to CLSI standards. Fresh cultures were grown at 37 °C with orbital shaking (120 rpm) until the late exponential phase and then diluted to 2×10^8 CFU/mL. In addition to growth and negative control, the following treatments were tested in a 96-well plate: mupirocin at 0.03, 4, and 128 mg/L; phage (IR 0.1); and phage with mupirocin at all three concentrations. Agents were immediately added to the bacterial culture in plates. Measurements (OD_{850}) were performed over 24 h at 37 °C with mild shaking in 10-min intervals, using an Infinite M200 PRO microplate reader. The experiment was performed in nine biological replicates.

Measurement of the combined effect of mupirocin with phage on strains with various susceptibility profiles

Representative *S. aureus* PVL+ strains with different susceptibility to mupirocin and the phage were selected to determine the efficacy of the combined administration of mupirocin and the phage, that is, a phage-susceptible and mupirocin-susceptible strain NRL/St 21/350, a phage-resistant and mupirocin-susceptible strain NRL/St 20/303, a phage-susceptible and mupirocin-resistant strain with a low level of resistance (Mu-LR) NRL/St 21/350R, and a phage-susceptible and mupirocin-resistant strain with a high level of resistance (Mu-HR) AS 21/64L. A non-PVL strain AS 22/143 served as a double-resistant control. 96-well cell culture plates were inoculated with representative *S. aureus* strains (2×10^8 CFU/mL) in MHB with adjusted Ca^{2+} and Mg^{2+} according to CLSI standards, phage 812K1/420 (IR = 0.1), and mupirocin at final concentrations of 4 mg/L and 128 mg/L. Microtiter plates were incubated at 37 °C for 24 h with a 10-s shaking interval for each 10-min measurement period in a Tecan Infinite M200 PRO microplate reader, with OD measured at 850 nm. After incubation, the plate was centrifuged at 500 × g for 10 min to pellet bacterial debris and cells. The growth medium containing the phage/antibiotic was removed, and the cells were resuspended in an equal volume of fresh medium with citrate adjustment. Viable cell counts were determined using the plating method. Measurements were performed for growth control, growth with the addition of mupirocin alone, growth with the addition of phage alone, and growth with a combination

of phage and mupirocin in biological triplicates and technical duplicates.

Whole-genome sequencing, assembly, and bioinformatics

The DNA of wild-type strains and their Mu-LR derivatives was isolated as previously described (Fišarová et al. 2021), with a modification in the final step: DNA was extracted from the supernatant using a Genomic DNA Clean & Concentrator-25 kit (ZymoResearch, USA) according to the manufacturer's instructions.

For sequencing on the Oxford Nanopore Technology platform, libraries were prepared using a Ligation Sequencing Kit V14 (SQK-LSK114) according to the manufacturer's instructions and sequenced using FLO-FLG114 flow cells (R10.4.1) in a MinION device (Oxford Nanopore Technologies, UK). The device was controlled using MinKNOW version 24.02.16 (Oxford Nanopore Technologies, UK), which was also used for base-calling (super accuracy mode) and trimming.

Complete genomes were assembled using Flye version 2.9.5 (Lin et al. 2016) and annotated using the NCBI Prokaryotic Genome Annotation Pipeline (Li et al. 2021). Resistance genes were identified using AMRFinderPlus version 3.12.8 (Feldgarden et al. 2021) with the V3.12–2024-05-02.2.2 database using a species-specific point mutation search set for *S. aureus*. Whole-genome sequences were aligned using the Mauve Plugin (Darling et al. 2004), and multiple sequence alignment was performed using Clustal Omega version 1.2.3, both in Geneious Prime version 2025.2.2 (https://www.geneious.com). Changes in isoleucyl-tRNA synthetase (IleS) amino acid sequences were compared to the NCBI reference sequence WP_000384706.

Phage-mupirocin interaction assessment

Viable cell count (CFU/ml) data were converted to percentages, with 100% assigned to the highest observed value. These data were arranged according to the SynergyFinder v3.18.0 manual (Ianevski et al. 2022) and processed in R v4.5.2 with the additional synergyfinder v3.18.0 package (Zheng et al. 2022), which was also used for descriptive statistics. For data processing, the input data were transformed and processed using a built-in "viability" option. The phage-mupirocin interaction was calculated using Bliss and Loewe additivity models.

Statistical analysis

For each *S. aureus* strain, differences in bacterial viable cell counts (CFU/mL) among treatment groups were assessed using Kruskal-Wallis followed by Dunn's multiple comparison post hoc test with Benjamini-Hochberg false discovery rate correction in R (version 4.5.2). Differences in final blank-corrected OD_{850} values among treatment groups were determined using one-way ANOVA followed by Tukey's honest significant difference (HSD) test in R. Statistical significance was set at $p < 0.05$. Results of the post hoc tests are presented using letter-based groupings, i.e., treatment groups sharing a common letter do not differ significantly. The efficacy of phage/mupirocin, based on spectrophotometric measurements, was analyzed using the Centroid Index with the software Centroid_Index_Calculator designed by Hosseini et al. (2024) and originally intended for quantifying phage efficacy.

Results

Characterization and clinical background of *Staphylococcus aureus* isolates

Characterization of individual PVL+ *S. aureus* isolates, including antibiotic and phage susceptibility and relatedness, is shown in Table 1. All PVL+ *S. aureus* strains were susceptible to mupirocin (MIC = 0.125 mg/L), and four (10.8%) were resistant to phage 812K1/420. Clinical isolates in this study comprised 21.6% MRSA and 10.8% MLSB-resistant strains. A total of 16 *spa* types and 8 CCs were identified (Table 1; Table S1). PFGE fingerprint patterns after *Sma*I cleavage clustered according to assigned CCs and revealed seven restriction profiles (Fig. S2), while CC398 samples were not cleavable as was previously described (Bens et al. 2006).

Antimicrobial effect of mupirocin and phage on distinct PVL+ strains

To evaluate the potential of mupirocin therapy broadened by a therapeutic phage, seven strains, representing each PFGE group, were treated with both agents alone and in combination, administered sequentially and simultaneously (Fig. 1a). For sequential administration, we chose an interval of 8 h as the time during which subpopulations resistant to the initial agent may arise, as this is often a complication of clinical treatment (Patel et al. 2009). In clinical use, mupirocin is also administered at intervals of 8 to 12 h (Poovelikunnel et al. 2015). Since phage-antibiotic synergy is usually reported for sub-inhibitory antibiotic concentrations, a ¼ MIC of mupirocin was used (0.03 mg/L).

The antibacterial effects of different treatment approaches were quantified using a Centroid Index (CI) calculated from 48-h growth measurements obtained by spectrophotometry. Changes in the position of the centroid indicate shifts in the distribution of cell population densities over time. This facilitates the comparison of bacterial growth curves, which

Table 1 Characterization of Panton-Valentine leukocidin-producing (PVL+) *S. aureus* strains under study

Strain	Resistance profile	MIC MUP (mg/L)	Phage susceptibility	PFGE pattern	*spa* type	CC
AS 21/97	-	0.125	S	IV	t355	CC152
AS 21/99	-	0.06	S	III	t021	CC30
AS 21/143	-	0.125	S	IV	t355	CC152
AS 21/152	-	0.125	S	IV	t355	CC152
AS 21/157	-	0.125	S	IV	t355	CC152
AS 22/3	-	0.125	S	IV	t355	CC152
AS 22/71	-	0.125	S	IV	t355	CC152
AS 22/96	-	0.125	S	V	t6465	CC121
AS 22/101	-	0.125	S	IV	t1172	CC152
AS 22/103	-	0.125	S	IV	t355	CC152
AS 22/105	-	0.125	S	III	t433	CC30
AS 22/107	-	0.125	S	III	t433	CC30
AS 22/112	-	0.125	S	IV	t355	CC152
AS 22/130	-	0.125	S	IV	t355	CC152
AS 22/149	-	0.125	S	VII	t3207	CC45
AS 22/150	$iMLS_B$	0.125	S	III	t342	CC30
AS 22/155	-	0.125	S	IV	t355	CC152
NRL/St 20/085	-	0.125	R	III	t1848	CC30
NRL/St 20/095	-	0.125	S	III	t021	CC30
NRL/St 20/168	MRSA, MLS_B, TE	0.125	S	NT	t021	CC30
NRL/St 20/183	-	0.125	S	III	t433	CC30
NRL/St 20/197	MRSA, ERY, CIP	0.125	S	II	t008	CC8
NRL/St 20/212	-	0.125	S	III	t021	CC30
NRL/St 20/269	MRSA, ERY, TE, CIP	0.125	R	III	t276	CC30
NRL/St 20/303	MRSA, TE, CN	0.125	R	I	t903	CC1153
NRL/St 20/382	-	0.125	S	III	t433	CC30
NRL/St 20/621	MRSA, MLS_B, TE	0.125	S	NT	t034	CC398
NRL/St 20/632	-	0.125	S	III	t021	CC30
NRL/St 20/715	SXT	0.125	S	V	t21515	UNK
NRL/St 20/786	-	0.125	S	V	t435	CC121
NRL/St 20/905	MLS_B	0.125	S	NT	t034	CC398
NRL/St 21/049	SXT	0.125	S	V	t7002	CC121
NRL/St 21/219	MRSA, ERY, CIP	0.125	S	II	t008	CC8
NRL/St 21/350	-	0.125	S	III	t433	CC30
NRL/St 21/377	MRSA, TE	0.125	R	VI	t044	CC80
NRL/St 22/195	MRSA, ERY, CIP	0.125	S	II	t008	CC8
NRL/St 22/197	-	0.125	S	IV	t355	CC152

MIC MUP, minimum inhibitory concentration of mupirocin; *MRSA*, methicillin-resistant *S. aureus*; *$iMLS_B$*, inducible type of resistance to macrolides, lincosamides, and streptogramin B; *MLS_B*, constitutive resistance to macrolides, lincosamides, and streptogramin B; *ERY*, erythromycin; *CIP*, ciprofloxacin; *TE*, tetracycline; *CN*, gentamicin; *SXT*, trimethoprim/sulfamethoxazole; *S*, phage-susceptible; *R*, phage-resistant; *NT*, non-typeable due to *Sma*I resistance; *CC*, clonal complex; *UNK*, unknown CC

may exhibit different trends due to various factors. The CI value ranges from 0 to 1, with 1 indicating a phage that completely eradicates the bacterial strain and 0 indicating a completely ineffective phage.

The application of phage 812K1/420 at the beginning of the measurement was highly effective in phage-susceptible strains, whereas application after 8 h had no significant eradication effect (Fig. 1a). The efficacy of mupirocin alone was generally low due to the use of a sub-inhibitory concentration, but it was noticeably higher in susceptible isolates than in the resistant strain AS 21/64L. In this strain, the addition of phage 8 h after treatment with mupirocin resulted in improved efficacy compared to mupirocin alone. Moreover, simultaneous administration led

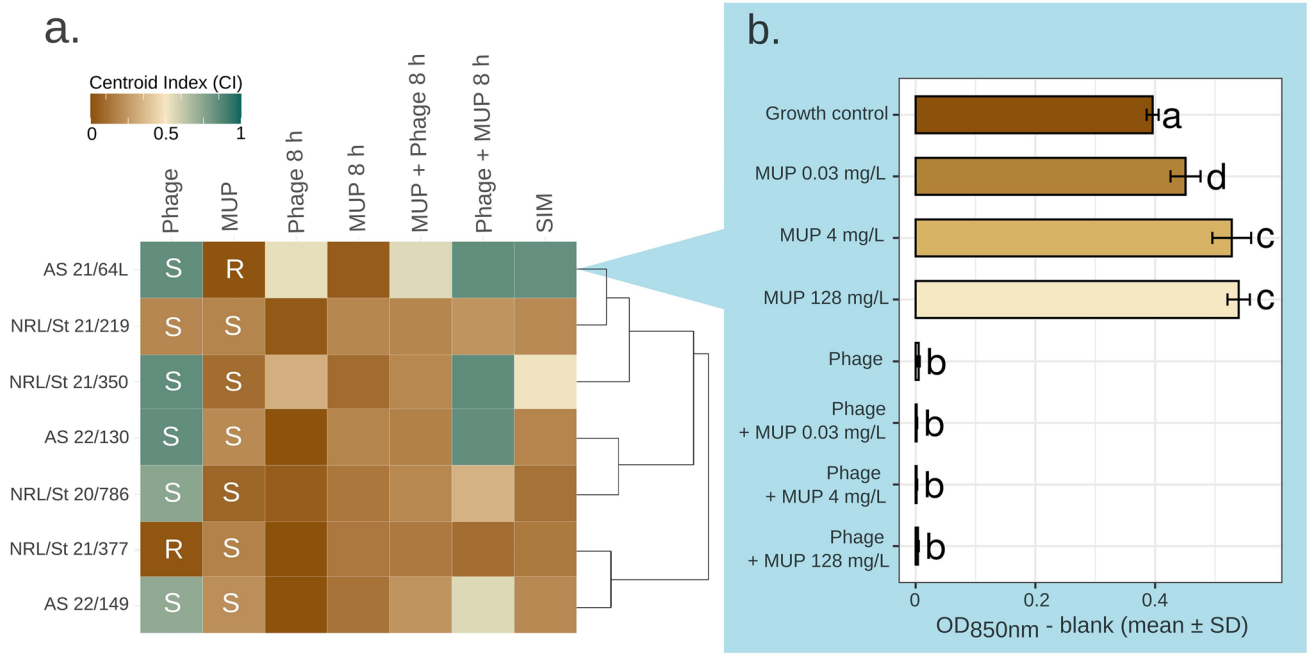

Fig. 1 Effect of phage 812K1/420 and mupirocin (MUP) sequential and simultaneous treatment on selected PVL+ *S. aureus* isolates representing different clusters according to PFGE and *spa*-typing. **a** Heatmap showing mean Centroid Index (CI) values calculated based on 48-h spectrophotometric measurement in three biological replicates of bacterial cultures treated with phage 812K1/420 alone ("phage"), mupirocin (0.03 mg/L) alone ("MUP"), their delayed administration ("phage 8 h" and "MUP 8 h", respectively), phage-mupirocin combination administered simultaneously ("SIM") or sequentially ("MUP + phage 8 h"—mupirocin followed by phage after 8 h; "phage + MUP 8 h"—phage followed by MUP after 8 h). Higher CI values indicate better treatment outcomes. Strains are clustered according to PFGE analysis, without expressing their similarity as branch lengths. Each isolate is shown as either susceptible (S) or resistant (R) to both the phage and mupirocin. **b** Strain AS 21/64L growth reduction via optical density after 24 h of treatment using different mupirocin concentrations. Bars represent the mean ± SD of nine biological replicates. Bars not sharing a common letter (a–d) indicate significant differences ($p < 0.05$; ANOVA with Tukey's HSD post hoc test). Exact *p*-values are listed in Table S3

to significantly better outcomes, which was also observed in strain NRL/St 21/350.

In most cases, the efficacy of simultaneous coadministration did not differ considerably from that of mupirocin alone (Fig. 1a). In the case of mupirocin administration 8 h after phage treatment, its effect was primarily determined by whether the culture had already been eradicated due to prior phage infection. If so, the result was identical to that of treatment with phage alone; otherwise, the efficiency was reduced compared to phage administration alone. The addition of mupirocin reduced phage 812K1/420 efficacy to varying degrees in all mupirocin-susceptible strains. In contrast, the mupirocin-resistant strain AS 21/64L did not inhibit phage 812K1/420 propagation during combined treatment, even at higher mupirocin concentrations (Fig. 1b; Table S3).

Interestingly, strain NRL/St 21/350 exhibited partial phage inhibition, despite its susceptibility to mupirocin (Fig. 1a). The strain does not carry any plasmids and harbors genes and point mutations involved in fosfomycin and trimethoprim resistance (Table S2). Next, it encodes a major facilitator superfamily (MFS) efflux membrane protein, Tet38, responsible for the extrusion of organic compounds and antibiotics (Truong-Bolduc et al. 2018). We hypothesize that this may be responsible for partial mupirocin removal, allowing at least minimal phage propagation.

To evaluate the effect of the PVL-encoding prophage on susceptibility to mupirocin, strain AS 21/64L was compared with the parental strain AS 21/64 (Fig. S1). Their growth during the different treatments was very similar, except at the highest mupirocin concentration tested, where the lysogen showed better growth than the wild type, consistent with previously published results (Rendueles et al. 2023).

Antimicrobial effect of simultaneous treatment with mupirocin and phage on PVL+ strains with different susceptibility profiles

To assess the efficacy of the simultaneous combined treatment on strains with different phage/mupirocin susceptibility profiles, viable cell counts (CFU/mL) were determined after 24 h of treatment in five representative isolates (Fig. 2; Table S3). A sub-inhibitory concentration for Mu-LR strains of 4 mg/L (32 × MIC for susceptible strains) and a high concentration of 128 mg/L were used to assess interactions

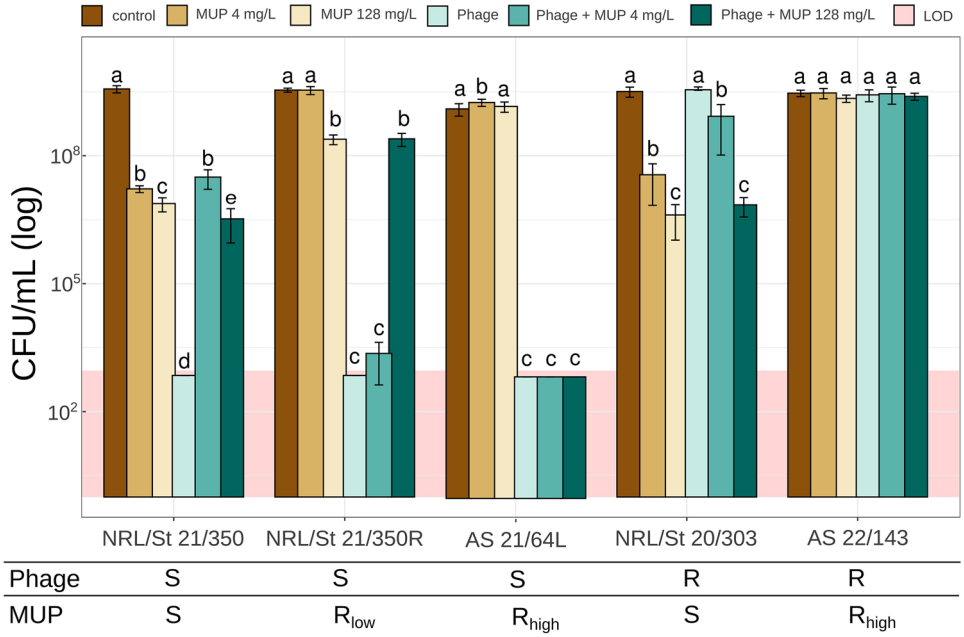

Fig. 2 Effect of phage 812K1/420 and mupirocin (MUP) simultaneous treatment on selected PVL+ *S. aureus* isolates with different susceptibility profiles. Viable cell count after 24 h of mono- or combination treatments was assessed. Treatments included mupirocin (4 mg/L, 128 mg/L), phage alone, and phage-MUP combination. Each isolate is shown as either susceptible (S) or resistant (R) to both the phage and mupirocin. Data are shown as means ± SD of three biological replicates. Statistically distinct groups are denoted by different letters (a-e) above bars ($p < 0.05$, Kruskal-Wallis with Dunn's post hoc test); CFU/mL values below the limit of detection (LOD) are shown in pale pink. Exact *p*-values are listed in Table S3

of the phage and mupirocin under different treatment conditions.

In mupirocin-susceptible isolates, the combination treatment exhibited the same efficacy as mupirocin, regardless of their susceptibility to phage (Fig. 2; Table S3). The exception was strain NRL/St 21/350, where the combination of the highest concentration of mupirocin (128 mg/L) with phage had a slightly, but statistically significantly, higher antibacterial effect than mupirocin alone. As a result, the interactions between the phage and mupirocin in this strain showed Bliss and Loewe synergy scores close to zero (additivity), while in other strains, they were strongly negative, indicating an inhibitory effect (Table S4). In the Mu-LR strain, the combination treatment with a sub-inhibitory mupirocin concentration, as well as phage alone, significantly reduced viable cell counts by at least five orders of magnitude compared to the untreated control or mupirocin-only treatment ($p < 0.05$). However, the highest concentration of mupirocin led to phage inactivation, and the outcome of combined treatment was the same as using mupirocin alone.

In the case of Mu-HR strains, the combined treatment showed the same outcome as phage treatment alone. In the phage-susceptible Mu-HR strain, treatment with both phage alone and phage-mupirocin combination resulted in significantly more effective eradication than mupirocin alone ($p < 0.05$). These results demonstrate that the addition of mupirocin does not compromise the high antibacterial effect of the therapeutic phage on Mu-HR strains. Moreover, eradication was highly effective, with no regrowth of culture after 24 h (Fig. 2), or even after 48 h (Fig. S1), as confirmed by both OD measurements and CFU/mL determination for strain AS 21/64L. Only the control non-PVL strain AS 22/143 remained unaffected due to its resistance to both agents.

The effect of the phage-mupirocin combination on the emergence of low-level mupirocin-resistant strains

Phage reproduction relies on the bacterial protein synthesis machinery; therefore, we propose that inhibition of phage activity by mupirocin in susceptible strains is due to its interference with protein synthesis by binding to bacterial isoleucyl-tRNA synthetase (Sutherland et al. 1985). Therefore, phage propagation was maintained in strains encoding an alternative isoleucyl-tRNA synthetase (Fig. S3).

To simulate the emergence of strains with low-level resistance to mupirocin, which occurs as a result of mupirocin treatment in a clinical setting (Miller et al. 1996), strains NRL/St 21/350 (GenBank accession: JBRKZN010000001) and AS 22/149 (JBRKZM010000001) were subjected to ALE to obtain their Mu-LR derivatives.

The genomes of both derived strains, designated NRL/St 21/350R (JBRKZP010000001) and AS 22/149R (JBRKZO010000001), respectively, contained de novo mutations in the *ileS* gene, which encodes isoleucyl-tRNA synthetase (Fig. S4). Because it was the only affected gene product, it can be concluded that this was the cause of the low-level mupirocin resistance.

While the amino acid sequence of NRL/St 21/350 IleS (MGS5385280) was identical to that of the reference IleS (NCBI RefSeq: WP_000384706), the homologue of AS 22/149 (MGS5377755) showed many single-nucleotide changes (Table 2; Fig. S4) and a 98.1% pairwise identity without impact on the mupirocin susceptibility of the strain. In Mu-LR strains NRL/St 21/350R (MGS5346550) and AS 22/149R (MGS5401978), three and two de novo mutations, respectively, appeared in IleS compared to the wild types. Four of them, Gly593Asp and Arg632Ile in NRL/St 21/350R and His585Tyr and Ser634Phe in AS 22/149R, were localized near the previously described Val-to-Phe mutations (V588F and V631F), which are assumed to disrupt the hydrophobic pocket in the Rossman fold responsible for mupirocin binding (Antonio et al. 2002).

To simulate changes in mupirocin concentration during treatment, three concentrations were tested (0.03 mg/L, 4 mg/L, and 128 mg/L). When low concentrations of mupirocin (0.03 mg/L and 4 mg/L) were used in combination with the phage, the inhibitory effect on Mu-LR derivatives compared to wild types was evident (Fig. 3). In contrast, when a high concentration of mupirocin (128 mg/L) was used, an almost identical inhibitory effect of the antibiotic was observed, either administered alone or in combination, and the use of phage did not provide any additional effect. Thus, when a high concentration of mupirocin was used, the growth of both the susceptible and Mu-LR strains was inhibited. However, at the lowest mupirocin concentration (0.03 mg/L), the growth of the Mu-LR strains was inhibited only in the presence of phage 812K1/420, which also contributed to the growth reduction at a concentration of 4 mg/L. Therefore, the presence of the phage could serve as protection against Mu-LR subpopulations emerging due to decreasing concentrations of mupirocin during treatment.

Table 2 Amino acid substitutions in the IleS encoded by wild-type strains NRL/St 21/350 and AS 22/149 and their low-level mupirocin-resistant (Mu-LR) derivatives, compared to reference isoleucyl-tRNA synthetase (WP_000384706)

Strain	NRL/St 21/350	NRL/St 21/350R	AS 22/149	AS 22/149R
Phenotype	MUP-susceptible	MUP-resistant	MUP-susceptible	MUP-resistant
[a]Amino acid change in IleS relative to the reference	no	Ser191Ala*	Asn213Asp	Asn213Asp
		Gly593Asp*	Ala223Ser	Ala223Ser
		Arg632Ile*	Asn257Asp	Asn257Asp
			Glu259Gln	Glu259Gln
			Ile263Val	Ile263Val
			Asp276Gly	Asp276Gly
			Ala280Asp	Ala280Asp
			Tyr288Phe	Tyr288Phe
			Thr289Ser	Thr289Ser
			Glu306Lys	Glu306Lys
			Asp313Glu	Asp313Glu
			Gln421Lys	Gln421Lys
			Glu472Asp	Glu472Asp
			Ser570Ala	Ser570Ala
			Thr814Ser	His585Tyr*
			Asp866Glu	Ser634Phe*
			Val877Ala	Thr814Ser
				Asp866Glu
				Val877Ala

De novo mutations in Mu-LR derivatives are marked with an asterisk

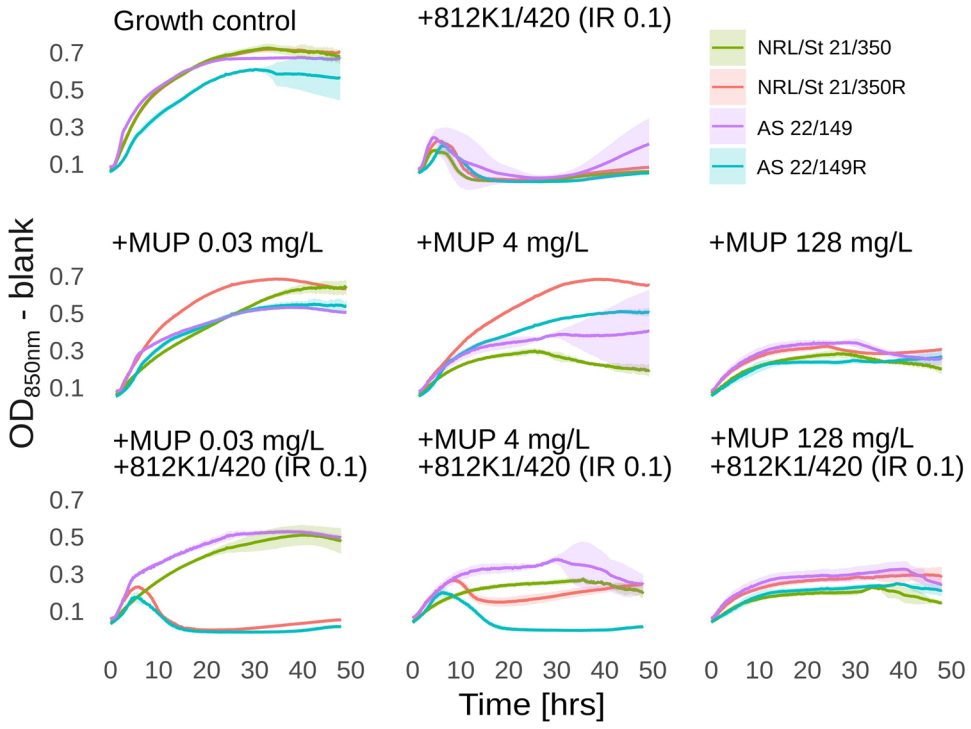

Fig. 3 Growth properties of mupirocin-susceptible *S. aureus* strains AS 22/149, NRL/St 21/350, and their Mu-LR derivatives AS 22/149R and NRL/St 21/350R, respectively, in the presence of phage 812K1/420 (IR = 0.1), mupirocin (MUP; $c = 0.03$, 4, and 128 mg/L), and their combination. Data are shown as means ± SD of three biological replicates

Ability of phage 812K1/420 to infect Pdp_{Sau}-positive strains

In some strains, the prophage-carried PVL genes can be replaced by the pdp_{Sau} abortive system gene, which targets kayviruses (Kuntová et al. 2023). Thus, selecting PVL+ isolates might overestimate the evaluation of phage lytic effect on *S. aureus*. Phage 812K1/420 was proven to propagate on Pdp_{Sau}-negative prophage-less strain RN4220 as well as Pdp_{Sau}-positive strains RN4220 (53^+) and NCTC 8325, while the parental phage 812 propagated only on RN4220, demonstrating its inhibition by Pdp_{Sau} (Fig. S5). These *S. aureus* strains were chosen to observe only the prophage effect, given their shared genetic background (Herbert et al. 2010), and the results were confirmed on clinical isolate NRL 02/947 (Fig. S5).

Discussion

Decolonization is crucial for treating and preventing *S. aureus* infections; however, conventional decolonization regimens may lead to the development of resistance to the substances used (Patel et al. 2009). Therefore, antimicrobials not applied for general treatment are typically used. Conventional decolonization regimens primarily use mupirocin, a topical antibiotic with a short biological half-life, making it unsuitable for systemic treatment (Eed et al. 2019). Despite its widespread use, clinical outcomes remain suboptimal in the long term, as strict disinfection regimens using topical antibiotics are unsuccessful in a substantial proportion of cases (Cool-Foley et al. 1991; Rossi et al. 1996; Wagenlehner et al. 2007; Ammerlaan et al. 2011). Although this study focused on PVL-positive strains, its conclusions are applicable to *S. aureus* in general.

To enhance decolonization, we evaluated the therapeutic *Kayvirus* 812K1/420, a part of the clinical phage preparation Stafal, currently registered in Slovakia but discontinued (Straka et al. 2024). Phage 812K1/420 is a derivative of phage 812a (Botka et al. 2019), which is a spontaneous mutant of phage 812 isolated on the *S. aureus* strain NCTC 8511 (53^+) (Pantůček et al. 1998). Phage 812a can propagate on strains producing the Pdp_{Sau} protein, which induces abortive infection targeting kayviruses (Kuntová et al. 2023). This is enabled by a deletion that fuses *orf189* and *orf192* of the parental phage 812 (Botka et al. 2019). The same deletion is preserved in phage 812K1/420, and its phenotypic expression was confirmed in this study, demonstrating that targeting PVL+ *S. aureus* did not result in selection bias. Phage 812K1/420 has a broader host range also due to the deletion of the middle amidase domain of the encoded endolysin (Benešík et al. 2018; Botka et al. 2019). It previously exhibited lytic activity in 82.7% of *S. aureus* strains (Pantůček et al. 1998) and 75% of clinical MRSA isolates (Botka et al. 2019). In our study, 89.2% ($n = 33$) of 37 PVL+ isolates were phage-susceptible. Furthermore, kayviruses can be prepared in stable formulations (Komárková et al. 2025), facilitating production and distribution of the

combined therapy. Combining a general-acting antibiotic with the polyvalent *Kayvirus* may provide broader efficacy than personalized single phages or phage cocktails, which are often limited by their host range (Hatfull et al. 2022). The range of strains susceptible to the phage-mupirocin combination could be further expanded by substituting with a more virulent *Kayvirus* strain or by using their cocktails (Botka et al. 2019).

Although we observed mostly an inhibitory effect of mupirocin on phage 812K1/420 in mupirocin-susceptible strains, the effect of the antibiotic itself remained unchanged. Similarly, previous studies have found that concurrent mupirocin-phage therapy accelerates MRSA eradication and decreases phage titers (Chhibber et al. 2014). Phage propagation depends on the host ability to synthesize proteins; therefore, the suppression of the phage effect results from the bacterial isoleucyl-tRNA synthetase inhibition by mupirocin. Mu-HR strains that utilize alternative tRNA ligases thus remained susceptible to phage. Next, we observed changes in the isoleucyl-tRNA synthetase gene that appeared de novo in strains that acquired a low level of resistance to mupirocin while remaining susceptible to phage.

In North America, the CC8 USA300 clone predominates in SSTIs (Talan et al. 2011). This study includes three PVL+ strains of the globally disseminated CC8, all of which were t008, MRSA, and susceptible to both phage and mupirocin. While in the USA, in 2020, 58% of invasive MRSA strains were CC8 and 2.6% were Mu-HR (Centers for Disease Control and Prevention 2025); in the Czech Republic, fewer than 5% of MRSA isolates have been assigned to CC8 (Tkadlec et al. 2021). No clinical PVL+ Mu-HR isolate was represented among the strains in this study, which could be considered a limitation. Instead, we used the non-PVL Mu-HR SSTI isolate AS 21/64 (CC1), which was lysogenized by a PVL-encoding phage. Lysogenization is a natural process, and we demonstrated that the prophage had no effect on mupirocin and phage resistance of the strain, allowing us to consider the results equivalent to those of a native PVL+ Mu-HR isolate. Although in some locations Mu-HR strains occur primarily in the most widespread CCs (Virgillio et al. 2025), plasmids encoding high-level mupirocin resistance are generally not strictly associated with any CC (Pérez-Roth et al. 2006), nor is resistance to phage 812K1/420 (Botka et al. 2019). Therefore, we assume that the effectiveness of the combined decolonization approach is not influenced by the clonal complex, but rather by strain-specific resistance mechanisms. However, the strain must be resistant to both agents to prevent the antimicrobial effect of the mupirocin-phage combination.

As mupirocin concentration decreases post-application due to its instability and metabolization (Conly and Johnston 2002; Poovelikunnel et al. 2015), sub-inhibitory concentrations may lead to selection of Mu-LR subpopulations, which were effectively suppressed by phage 812K1/420 in vitro. Thus, combination therapy may prevent the emergence of new Mu-LR subpopulations during the declining phase of antibiotic efficacy, enabling prolonged treatment, which is otherwise limited to a few days due to concerns regarding resistance development (Poovelikunnel et al. 2015). Simultaneous therapy may also prevent the emergence of resistance to either agent, as observed in clinical practice (Schooley et al. 2017). Due to the rising antibiotic resistance and limited new agents, novel applications of existing agents, including nanomupirocin and PEGylated chitosan, have been investigated (Azeez et al. 2024; Cern et al. 2024). Their use in combination with phages in semi-solid formulations, such as gels and creams, represents a promising treatment strategy.

In summary, combined treatment did not demonstrate synergistic effects, as the combination was not more effective in eradicating a given bacterial population than the individual components alone. However, coadministration of mupirocin with the 812K1/420 therapeutic phage broadens the spectrum of susceptible *S. aureus* strains, which is particularly important from the perspective of decolonization therapy in countries with high mupirocin resistance. Furthermore, the addition of bacteriophage inhibits the spread of mupirocin resistance by targeting strains that are both mupirocin-resistant and phage-susceptible, including those with de novo mutations conferring resistance to mupirocin. Importantly, phage addition does not compromise the overall antibacterial effect of mupirocin, supporting their potential use as a complementary therapeutic strategy.

Supplementary Information The online version contains supplementary material available at https://doi.org/10.1007/s00253-026-13814-0.

Acknowledgements The authors would like to extend their gratitude to Zuzana Švagerová, Laura Claudie Hermanová, and Kristína Létalová for their time and practical contributions and to Tereza Kočí for her valuable comments on the revisions. We would like to thank Prof. Freiberger from the Genetic Laboratory of the Center of Cardiovascular and Transplant Surgery in Brno for the Sanger sequencing of PCR amplicons.

Author contribution TB, AS, EF, LV, RP, and FR conceived and designed the research. EF, AS, TB, LV, JT, JV, MO, PP, DKP, MD, and PU performed research. EF, TB, AS, and JT analyzed the data. TB, AS, and EF wrote the manuscript. All authors read and approved the manuscript. AS and EF contributed equally to this work.

Funding Open access publishing supported by the institutions participating in the CzechELib Transformative Agreement. This work was supported by the Ministry of Health of the Czech Republic, in cooperation with the Czech Health Research Council, under project No. NU21J-05-00035, and by a Grant from Masaryk University MUNI/A/1759/2025.

Data availability The data underlying this article are available in the article, its online supplementary materials, and in subject-specific public repositories. Sequencing data of strains NRL/St 21/350 (Biosample

SAMN52216007, genome sequence accession JBRKZN010000001), NRL/St 21/350R (Biosample SAMN52216392, genome sequence accession JBRKZP010000001), AS 22/149 (Biosample SAMN52215998, genome sequence accession JBRKZM010000001), and AS 22/149R (Biosample SAMN52216391, genome sequence accession JBRKZO010000001) are deposited within NCBI BioProject PRJNA1337322. Source data of the measurements presented in Fig.1, Fig. 2, Fig. 3, and Fig. S1 are available in the Zenodo repository (https://doi.org/10.5281/zenodo.17530980).

Declarations

Ethical approval This article does not contain any studies with human or animal participants.

Competing interests The authors declare no competing interests.

Open Access This article is licensed under a Creative Commons Attribution 4.0 International License, which permits use, sharing, adaptation, distribution and reproduction in any medium or format, as long as you give appropriate credit to the original author(s) and the source, provide a link to the Creative Commons licence, and indicate if changes were made. The images or other third party material in this article are included in the article's Creative Commons licence, unless indicated otherwise in a credit line to the material. If material is not included in the article's Creative Commons licence and your intended use is not permitted by statutory regulation or exceeds the permitted use, you will need to obtain permission directly from the copyright holder. To view a copy of this licence, visit http://creativecommons.org/licenses/by/4.0/.

References

Ammerlaan HSM, Kluytmans JAJW, Berkhout H, Buiting A, De Brauwer EIGB, Van Den Broek PJ, Van Gelderen P, Leenders S, Ott A, Richter C, Spanjaard L, Spijkerman IJB, Van Tiel FH, Voorn GP, Wulf MWH, Van Zeijl J, Troelstra A, Bonten MJM, Van De Berg CMF, Bosman J, Bremer A, Bril W, Commeren D, Van Essen G, Gigengack-Baars A, Van Kasteren MME, Lommerse EJM, Mascini E, Renders NHM, Van Rijen M, Schellekens J, Smeets E, Sprangers T, Vandenbroucke-Grauls CMJE, Verbon A, Verduin K, Wagenvoort JHT, Van Wijngaarden P (2011) Eradication of carriage with methicillin-resistant *Staphylococcus aureus*: effectiveness of a national guideline. J Antimicrob Chemother 66:2409–2417. https://doi.org/10.1093/jac/dkr243

Antonio M, McFerran N, Pallen MJ (2002) Mutations affecting the Rossman fold of isoleucyl-tRNA synthetase are correlated with low-level mupirocin resistance in *Staphylococcus aureus*. Antimicrob Agents Chemother 46:438–442. https://doi.org/10.1128/AAC.46.2.438-442.2002

Antonov NK, Garzon MC, Morel KD, Whittier S, Planet PJ, Lauren CT (2015) High prevalence of mupirocin resistance in *Staphylococcus aureus* isolates from a pediatric population. Antimicrob Agents Chemother 59:3350–3356. https://doi.org/10.1128/AAC.00079-15

Azeez S, Sathiyaseelan A, Venkatesan K, Wang M-H (2024) Fabrication of mupirocin-loaded PEGylated chitosan nanoparticulate films for enhanced wound healing. Int J Mol Sci 25:9188. https://doi.org/10.3390/ijms25179188

Belguesmia Y, Spano G, Drider D (2021) Potentiating effects of leaderless enterocin DD14 in combination with methicillin on clinical methicillin-resistant *Staphylococcus aureus* S1 strain. Microbiol Res 252:126864. https://doi.org/10.1016/j.micres.2021.126864

Benešík M, Nováček J, Janda L, Dopitová R, Pernisová M, Melková K, Tišáková L, Doškař J, Žídek L, Hejátko J, Pantůček R (2018) Role of SH3b binding domain in a natural deletion mutant of *Kayvirus* endolysin LysF1 with a broad range of lytic activity. Virus Genes 54:130–139. https://doi.org/10.1007/s11262-017-1507-2

Bens CCPM, Voss A, Klaassen CHW (2006) Presence of a novel DNA methylation enzyme in methicillin-resistant *Staphylococcus aureus* isolates associated with pig farming leads to uninterpretable results in standard pulsed-field gel electrophoresis analysis. J Clin Microbiol 44:1875–1876. https://doi.org/10.1128/JCM.44.5.1875-1876.2006

Blanco R, Tristan A, Ezpeleta G, Larsen AR, Bes M, Etienne J, Cisterna R, Laurent F (2011) Molecular epidemiology of Panton-Valentine leukocidin-positive *Staphylococcus aureus* in Spain: emergence of the USA300 clone in an autochthonous population. J Clin Microbiol 49:433–436. https://doi.org/10.1128/JCM.02201-10

Botka T, Pantůček R, Mašlaňová I, Benešík M, Petráš P, Růžičková V, Havlíčková P, Varga M, Žemličková H, Koláčková I, Florianová M, Jakubů V, Karpíšková R, Doškař J (2019) Lytic and genomic properties of spontaneous host-range *Kayvirus* mutants prove their suitability for upgrading phage therapeutics against staphylococci. Sci Rep 9:5475. https://doi.org/10.1038/s41598-019-41868-w

Centers for Disease Control and Prevention (2025) Emerging infections program, healthcare-associated infections – community interface surveillance report: invasive Staphylococcus aureus, 2020. Available at: https://www.cdc.gov/healthcare-associated-infections/media/pdfs/2020-MRSA-Report-508.pdf. Accessed 10 Mar 2026

Cern A, Skoczen SL, Snapp KS, Hod A, Zilbersheid D, Bavli Y, Alon-Maimon T, Bachrach G, Wei X, Berman B, Yassour M, Cedrone E, Neun BW, Dobrovolskaia MA, Clogston JD, Stern ST, Barenholz Y (2024) Nano-mupirocin as tumor-targeted antibiotic: physicochemical, immunotoxicological and pharmacokinetic characterization, and effect on gut microbiome. J Control Release 373:713–726. https://doi.org/10.1016/j.jconrel.2024.07.045

Chhibber S, Gupta P, Kaur S (2014) Bacteriophage as effective decolonising agent for elimination of MRSA from anterior nares of BALB/c mice. BMC Microbiol 14:212. https://doi.org/10.1186/s12866-014-0212-8

Comeau AM, Tétart F, Trojet SN, Prère M-F, Krisch HM (2007) Phage-antibiotic synergy (PAS): β-lactam and quinolone antibiotics stimulate virulent phage growth. PLoS One 2:e799. https://doi.org/10.1371/journal.pone.0000799

Conly JM, Johnston BL (2002) Mupirocin – are we in danger of losing it? Can J Infect Dis Med Microbiol 13:157–159. https://doi.org/10.1155/2002/692581

Cool-Foley AA, Nathan C, O'Donovan C, Simon D (1991) Eradication of methicillin-resistant *Staphylococcus aureus* vaginitis with mupirocin. Ann Pharmacother 25:1331–1333. https://doi.org/10.1177/106002809102501209

Darling ACE, Mau B, Blattner FR, Perna NT (2004) Mauve: multiple alignment of conserved genomic sequence with rearrangements. Genome Res 14:1394–1403. https://doi.org/10.1101/gr.2289704

Durand G, Javerliat F, Bes M, Veyrieras J-B, Guigon G, Mugnier N, Schicklin S, Kaneko G, Santiago-Allexant E, Bouchiat C, Martins-Simões P, Laurent F, Van Belkum A, Vandenesch F, Tristan A (2018) Routine whole-genome sequencing for outbreak investigations of *Staphylococcus aureus* in a national reference center. Front Microbiol 9:511. https://doi.org/10.3389/fmicb.2018.00511

Eed EM, Ghonaim MM, Khalifa AS, Alzahrani KJ, Alsharif KF, Taha AA (2019) Prevalence of mupirocin and chlorhexidine resistance among methicillin-resistant coagulase-negative staphylococci isolated during methicillin-resistant *Staphylococcus aureus* decolonization strategies. Am J Infect Control 47:1319–1323. https://doi.org/10.1016/j.ajic.2019.05.004

Egyir B, Guardabassi L, Sørum M, Nielsen SS, Kolekang A, Frimpong E, Addo KK, Newman MJ, Larsen AR (2014) Molecular epidemiology and antimicrobial susceptibility of clinical *Staphylococcus aureus* from healthcare institutions in Ghana. PLoS One 9:e89716. https://doi.org/10.1371/journal.pone.0089716

Feldgarden M, Brover V, Gonzalez-Escalona N, Frye JG, Haendiges J, Haft DH, Hoffmann M, Pettengill JB, Prasad AB, Tillman GE, Tyson GH, Klimke W (2021) AMRFinderPlus and the reference gene catalog facilitate examination of the genomic links among antimicrobial resistance, stress response, and virulence. Sci Rep 11:12728. https://doi.org/10.1038/s41598-021-91456-0

Fišarová L, Botka T, Du X, Mašlaňová I, Bárdy P, Pantůček R, Benešík M, Roudnický P, Winstel V, Larsen J, Rosenstein R, Peschel A, Doškař J (2021) *Staphylococcus epidermidis* phages transduce antimicrobial resistance plasmids and mobilize chromosomal islands. mSphere 6:e00223–21. https://doi.org/10.1128/mSphere.00223-21.

Galia L, Ligozzi M, Bertoncelli A, Mazzariol A (2019) Real-time PCR assay for detection of *Staphylococcus aureus*, Panton-Valentine leucocidin and methicillin resistance directly from clinical samples. AIMS Microbiol 5:138–146. https://doi.org/10.3934/microbiol.2019.2.138

Genestier A-L, Michallet M-C, Prévost G, Bellot G, Chalabreysse L, Peyrol S, Thivolet F, Etienne J, Lina G, Vallette FM, Vandenesch F, Genestier L (2005) *Staphylococcus aureus* Panton-Valentine leukocidin directly targets mitochondria and induces Bax-independent apoptosis of human neutrophils. J Clin Invest 115:3117–3127. https://doi.org/10.1172/JCI22684

Ghaffary S, Javidnia A, Beheshtirouy S, Sadeghi J, Akbari AM, Hamishehkar H, Sarbakhsh P, Sanaat Z, Nikanfar A, Esfahani A, Chavoshi SH, Nejati B, Raeisi M, Gholami N (2024) Comparison of global decolonization efficacy with mupirocin nasal drop and chlorhexidine mouthwash in acute leukemia patients: randomized clinical trial. Support Care Cancer 32:42. https://doi.org/10.1007/s00520-023-08232-1

Harmsen D, Claus H, Witte W, Rothgänger J, Claus H, Turnwald D, Vogel U (2003) Typing of methicillin-resistant *Staphylococcus aureus* in a university hospital setting by using novel software for *spa* repeat determination and database management. J Clin Microbiol 41:5442–5448. https://doi.org/10.1128/JCM.41.12.5442-5448.2003

Hassoun-Kheir N, Buetti N, Olivier V, Perez M, Frossard J, Renzi G, Schrenzel J, Saudan P, Harbarth S (2023) Targeted mupirocin-based decolonization for *Staphylococcus aureus* carriers and the subsequent risk of mupirocin resistance in haemodialysis patients – a longitudinal study over 20 years. J Hosp Infect 135:55–58. https://doi.org/10.1016/j.jhin.2023.01.019

Hatfull GF, Dedrick RM, Schooley RT (2022) Phage therapy for antibiotic-resistant bacterial infections. Annu Rev Med 73:197–211. https://doi.org/10.1146/annurev-med-080219-122208

Herbert S, Ziebandt A-K, Ohlsen K, Schäfer T, Hecker M, Albrecht D, Novick R, Götz F (2010) Repair of global regulators in *Staphylococcus aureus* 8325 and comparative analysis with other clinical isolates. Infect Immun 78:2877–2889. https://doi.org/10.1128/IAI.00088-10

Hetem DJ, Bonten MJM (2013) Clinical relevance of mupirocin resistance in *Staphylococcus aureus*. J Hosp Infect 85:249–256. https://doi.org/10.1016/j.jhin.2013.09.006

Hodgson JE, Curnock SP, Dyke KG, Morris R, Sylvester DR, Gross MS (1994) Molecular characterization of the gene encoding high-level mupirocin resistance in *Staphylococcus aureus* J2870. Antimicrob Agents Chemother 38:1205–1208. https://doi.org/10.1128/AAC.38.5.1205

Holochová P, Růžičková V, Pantůček R, Petráš P, Janisch R, Doškař J (2010) Genomic diversity of two lineages of exfoliative toxin A-converting phages predominating in *Staphylococcus aureus* strains in the Czech Republic. Res Microbiol 161:260–267. https://doi.org/10.1016/j.resmic.2010.03.008

Hoppe P-A, Holzhauer S, Lala B, Bührer C, Gratopp A, Hanitsch LG, Humme D, Kieslich M, Kallinich T, Lau S, Leistner R, Niebank M, Pokrywka A, Ringe H, Schaper A-S, Schröder J-T, Schwarz C, Staab D, Stegemann MS, Thee S, Varnholt V, Von Bernuth H, Weber-Carstens S, Wendt A, Krüger R (2019) Severe infections of Panton-Valentine leukocidin positive *Staphylococcus aureus* in children. Medicine 98:e17185. https://doi.org/10.1097/MD.0000000000017185

Hosseini N, Chehreghani M, Moineau S, Charette SJ (2024) Centroid of the bacterial growth curves: a metric to assess phage efficiency. Commun Biol 7:673. https://doi.org/10.1038/s42003-024-06379-z

Ianevski A, Giri AK, Aittokallio T (2022) SynergyFinder 3.0: an interactive analysis and consensus interpretation of multi-drug synergies across multiple samples. Nucleic Acids Res 50:W739–W743. https://doi.org/10.1093/nar/gkac382

Ikuta KS, Swetschinski LR, Robles Aguilar G, Sharara F, Mestrovic T, Gray AP, Davis Weaver N, Wool EE, Han C, Gershberg Hayoon A, Aali A, Abate SM, Abbasi-Kangevari M, Abbasi-Kangevari Z, Abd-Elsalam S, Abebe G, Abedi A, Abhari AP, Abidi H, Aboagye RG, Absalan A, Abubaker Ali H, Acuna JM, Adane TD, Addo IY, Adegboye OA, Adnan M, Adnani QES, Afzal MS, Afzal S, Aghdam ZB, Ahinkorah BO, Ahmad A, Ahmad AR, Ahmad R, Ahmad Sajjad, Ahmad Sohail, Ahmadi S, Ahmed A, Ahmed H, Ahmed JQ, Ahmed Rashid T, Ajami M, Aji B, Akbarzadeh-Khiavi M, Akunna CJ, Al Hamad H, Alahdab F, Al-Aly Z, Aldeyab MA, Aleman AV, Alhalaiqa FAN, Alhassan RK, Ali BA, Ali L, Ali SS, Alimohamadi Y, Alipour V, Alizadeh A, Aljunid SM, Allel K, Almustanyir S, Ameyaw EK, Amit AML, Anandavelane N, Ancuceanu R, Andrei CL, Andrei T, Anggraini D, Ansar A, Anyasodor AE, Arabloo J, Aravkin AY, Areda D, Aripov T, Artamonov AA, Arulappan J, Aruleba RT, Asaduzzaman M, Ashraf T, Athari SS, Atlaw D, Attia S, Ausloos M, Awoke T, Ayala Quintanilla BP, Ayana TM, Azadnajafabad S, Azari Jafari A, B DB, Badar M, Badiye AD, Baghcheghi N, Bagherieh S, Baig AA, Banerjee I, Barac A, Bardhan M, Barone-Adesi F, Barqawi HJ, Barrow A, Baskaran P, Basu S, Batiha A-MM, Bedi N, Belete MA, Belgaumi UI, Bender RG, Bhandari B, Bhandari D, Bhardwaj P, Bhaskar S, Bhattacharyya K, Bhattarai S, Bitaraf S, Buonsenso D, Butt ZA, Caetano Dos Santos FL, Cai J, Calina D, Camargos P, Cámera LA, Cárdenas R, Cevik M, Chadwick J, Charan J, Chaurasia A, Ching PR, Choudhari SG, Chowdhury EK, Chowdhury FR, Chu D-T, Chukwu IS, Dadras O, Dagnaw FT, Dai X, Das S, Dastiridou A, Debela SA, Demisse FW, Demissie S, Dereje D, Derese M, Desai HD, Dessalegn FN, Dessalegni SAA, Desye B, Dhaduk K, Dhimal M, Dhingra S, Diao N, Diaz D, Djalalinia S, Dodangeh M, Dongarwar D, Dora BT, Dorostkar F, Dsouza HL, Dubljanin E, Dunachie SJ, Durojaiye OC, Edinur HA, Ejigu HB, Ekholuenetale M, Ekundayo TC, El-Abid H, Elhadi M, Elmonem MA, Emami A, Engelbert Bain L, Enyew DB, Erkhembayar R, Eshrati B, Etaee F, Fagbamigbe AF, Falahi S, Fallahzadeh A, Faraon EJA, Fatehizadeh A, Fekadu G, Fernandes JC, Ferrari A, Fetensa G, Filip I, Fischer F, Foroutan M, Gaal PA, Gadanya MA, Gaidhane AM, Ganesan B, Gebrehiwot M, Ghanbari R, Ghasemi Nour M, Ghashghaee A, Gholamrezanezhad A, Gholizadeh A, Golechha M, Goleij P, Golinelli D, Goodridge A, Gunawardane DA, Guo Y, Gupta RD, Gupta S, Gupta VB, Gupta VK, Guta A, Habibzadeh P, Haddadi Avval A, Halwani R, Hanif A, Hannan MdA, Harapan H, Hassan S, Hassankhani H, Hayat K, Heibati B, Heidari G, Heidari M, Heidari-Soureshjani R, Herteliu C, Heyi DZ, Hezam K, Hoogar P, Horita N, Hossain MM, Hosseinzadeh M, Hostiuc M, Hostiuc S, Hoveidamanesh S, Huang J, Hussain S, Hussein NR, Ibitoye SE, Ilesanmi OS, Ilic IM, Ilic MD, Imam MT, Immurana M, Inbaraj LR, Iradukunda A, Ismail NE, Iwu CCD, Iwu CJ, J LM, Jakovljevic M, Jamshidi E, Javaheri T, Javanmardi F, Javidnia J, Jayapal SK, Jayarajah U, Jebai R, Jha RP, Joo T, Joseph N, Joukar F, Jozwiak JJ, Kacimi SEO, Kadashetti V, Kalankesh LR, Kalhor R, Kamal VK, Kandel H, Kapoor N, Karkhah S, Kassa BG, Kassebaum NJ, Katoto PD, Keykhaei M, Khajuria H, Khan

A, Khan IA, Khan M, Khan MN, Khan MA, Khatatbeh MM, Khater MM, Khayat Kashani HR, Khubchandani J, Kim H, Kim MS, Kimokoti RW, Kissoon N, Kochhar S, Kompani F, Kosen S, Koul PA, Koulmane Laxminarayana SL, Krapp Lopez F, Krishan K, Krishnamoorthy V, Kulkarni V, Kumar N, Kurmi OP, Kuttikkattu A, Kyu HH, Lal DK, Lám J, Landires I, Lasrado S, Lee S, Lenzi J, Lewycka S, Li S, Lim SS, Liu W, Lodha R, Loftus MJ, Lohiya A, Lorenzovici L, Lotfi M, Mahmoodpoor A, Mahmoud MA, Mahmoudi R, Majeed A, Majidpoor J, Makki A, Mamo GA, Manla Y, Martorell M, Matei CN, McManigal B, Mehrabi Nasab E, Mehrotra R, Melese A, Mendoza-Cano O, Menezes RG, Mentis A-FA, Micha G, Michalek IM, Micheletti Gomide Nogueira De Sá AC, Milevska Kostova N, Mir SA, Mirghafourvand M, Mirmoeeni S, Mirrakhimov EM, Mirza-Aghazadeh-Attari M, Misganaw AS, Misganaw A, Misra S, Mohammadi E, Mohammadi M, Mohammadian-Hafshejani A, Mohammed S, Mohan S, Mohseni M, Mokdad AH, Momtazmanesh S, Monasta L, Moore CE, Moradi M, Moradi Sarabi M, Morrison SD, Motaghinejad M, Mousavi Isfahani H, Mousavi Khaneghah A, Mousavi-Aghdas SA, Mubarik S, Mulita F, Mulu GBB, Munro SB, Muthupandian S, Nair TS, Naqvi AA, Narang H, Natto ZS, Naveed M, Nayak BP, Naz S, Negoi I, Nejadghaderi SA, Neupane Kandel S, Ngwa CH, Niazi RK, Nogueira De Sá AT, Noroozi N, Nouraei H, Nowroozi A, Nuñez-Samudio V, Nutor JJ, Nzoputam CI, Nzoputam OJ, Oancea B, Obaidur RM, Ojha VA, Okekunle AP, Okonji OC, Olagunju AT, Olusanya BO, Omar Bali A, Omer E, Otstavnov N, Oumer B, P A M, Padubidri JR, Pakshir K, Palicz T, Pana A, Pardhan S, Paredes JL, Parekh U, Park E-C, Park S, Pathak A, Paudel R, Paudel U, Pawar S, Pazoki Toroudi H, Peng M, Pensato U, Pepito VCF, Pereira M, Peres MFP, Perico N, Petcu I-R, Piracha ZZ, Podder I, Pokhrel N, Poluru R, Postma MJ, Pourtaheri N, Prashant A, Qattea I, Rabiee M, Rabiee N, Radfar A, Raeghi S, Rafiei S, Raghav PR, Rahbarnia L, Rahimi-Movaghar V, Rahman M, Rahman MA, Rahmani AM, Rahmanian V, Ram P, Ranjha MMAN, Rao SJ, Rashidi M-M, Rasul A, Ratan ZA, Rawaf S, Rawassizadeh R, Razeghinia MS, Redwan EMM, Regasa MT, Remuzzi G, Reta MA, Rezaei N, Rezapour A, Riad A, Ripon RK, Rudd KE, Saddik B, Sadeghian S, Saeed U, Safaei M, Safary A, Safi SZ, Sahebazzamani M, Sahebkar A, Sahoo H, Salahi Saina, Salahi Sarvenaz, Salari H, Salehi S, Samadi Kafil H, Samy AM, Sanadgol N, Sankararaman S, Sanmarchi F, Sathian B, Sawhney M, Saya GK, Senthilkumaran S, Seylani A, Shah PA, Shaikh MA, Shaker E, Shakhmardanov MZ, Sharew MM, Sharifi-Razavi A, Sharma P, Sheikhi RA, Sheikhy A, Shetty PH, Shigematsu M, Shin JI, Shirzad-Aski H, Shivakumar KM, Shobeiri P, Shorofi SA, Shrestha S, Sibhat MM, Sidemo NB, Sikder MK, Silva LMLR, Singh JA, Singh P, Singh S, Siraj MS, Siwal SS, Skryabin VY, Skryabina AA, Socea B, Solomon DD, Song Y, Sreeramareddy CT, Suleman M, Suliankatchi Abdulkader R, Sultana S, Szócska M, Tabatabaeizadeh S-A, Tabish M, Taheri M, Taki E, Tan K-K, Tandukar S, Tat NY, Tat VY, Tefera BN, Tefera YM, Temesgen G, Temsah M-H, Tharwat S, Thiyagarajan A, Tleyjeh II, Troeger CE, Umapathi KK, Upadhyay E, Valadan Tahbaz S, Valdez PR, Van Den Eynde J, Van Doorn HR, Vaziri S, Verras G-I, Viswanathan H, Vo B, Waris A, Wassie GT, Wickramasinghe ND, Yaghoubi S, Yahya GATY, Yahyazadeh Jabbari SH, Yigit A, Yiğit V, Yon DK, Yonemoto N, Zahir M, Zaman BA, Zaman SB, Zangiabadian M, Zare I, Zastrozhin MS, Zhang Z-J, Zheng P, Zhong C, Zoladl M, Zumla A, Hay SI, Dolecek C, Sartorius B, Murray CJL, Naghavi M (2022) Global mortality associated with 33 bacterial pathogens in 2019: a systematic analysis for the Global Burden of Disease Study 2019. Lancet 400:2221–2248. https://doi.org/10.1016/S0140-6736(22)02185-7.

Kinross P, Petersen A, Skov R, Van Hauwermeiren E, Pantosti A, Laurent F, Voss A, Kluytmans J, Struelens MJ, Heuer O, Monnet DL, the European human LA-MRSA study group (2017) Livestock-associated meticillin-resistant *Staphylococcus aureus* (MRSA) among human MRSA isolates, European Union/European Economic Area countries, 2013. Eurosurveillance 22:16–00696. https://doi.org/10.2807/1560-7917.ES.2017.22.44.16-00696.

Klein S, Hannesen J, Zanger P, Heeg K, Boutin S, Nurjadi D (2020) Entry of Panton–Valentine leukocidin-positive methicillin-resistant *Staphylococcus aureus* into the hospital: prevalence and population structure in Heidelberg, Germany 2015–2018. Sci Rep 10:13243. https://doi.org/10.1038/s41598-020-70112-z

Komárková M, Benešík M, Procházková T, Vinco A, Laichmanová M, Smetanová S, Jelínek P, Moša M, Botka T, Šoóš M, Pantůček R (2025) Compatibility of antimicrobial preservatives with therapeutic bacteriophages of the genera *Pbunavirus* and *Kayvirus*. Eur J Pharm Biopharm 214:114781. https://doi.org/10.1016/j.ejpb.2025.114781

Kuntová L, Mašlaňová I, Obořilová R, Šimečková H, Finstrlová A, Bárdy P, Šiborová M, Troianovska L, Botka T, Gintar P, Šedo O, Farka Z, Doškař J, Pantůček R (2023) *Staphylococcus aureus* prophage-encoded protein causes abortive infection and provides population immunity against Kayviruses. mBio 14:e02490–22. https://doi.org/10.1128/mbio.02490-22.

Langenberg JCM, Kluytmans JAJW, Mulder PGH, Romme J, Ho GH, Van Der Laan L (2018) Peri-operative nasal eradication therapy prevents *Staphylococcus aureus* surgical site infections in aortoiliac surgery. Surg Infect 19:510–515. https://doi.org/10.1089/sur.2018.029

Larsen MV, Cosentino S, Rasmussen S, Friis C, Hasman H, Marvig RL, Jelsbak L, Sicheritz-Pontén T, Ussery DW, Aarestrup FM, Lund O (2012) Multilocus sequence typing of total-genome-sequenced bacteria. J Clin Microbiol 50:1355–1361. https://doi.org/10.1128/JCM.06094-11

Leistner R, Hanitsch LG, Krüger R, Lindner AK, Stegemann MS, Nurjadi D (2022) Skin infections due to Panton-Valentine leucocidin–producing *S. aureus*. Dtsch Arztebl Int 119:775–784. https://doi.org/10.3238/arztebl.m2022.0308

Li W, O'Neill KR, Haft DH, DiCuccio M, Chetvernin V, Badretdin A, Coulouris G, Chitsaz F, Derbyshire MK, Durkin AS, Gonzales NR, Gwadz M, Lanczycki CJ, Song JS, Thanki N, Wang J, Yamashita RA, Yang M, Zheng C, Marchler-Bauer A, Thibaud-Nissen F (2021) RefSeq: expanding the prokaryotic genome annotation pipeline reach with protein family model curation. Nucleic Acids Res 49:D1020–D1028. https://doi.org/10.1093/nar/gkaa1105

Lin Y, Yuan J, Kolmogorov M, Shen MW, Chaisson M, Pevzner PA (2016) Assembly of long error-prone reads using de Bruijn graphs. Proc Natl Acad Sci USA 113:E8396–E8405. https://doi.org/10.1073/pnas.1604560113

Lindgren A-K, Nilsson AC, Åkesson P, Gustafsson E, Melander E (2018) Eradication of methicillin-resistant *Staphylococcus aureus* (MRSA) throat carriage: a randomised trial comparing topical treatment with rifampicin-based systemic therapy. Int J Antimicrob Agents 51:642–645. https://doi.org/10.1016/j.ijantimicag.2017.08.021

Löffler B, Hussain M, Grundmeier M, Brück M, Holzinger D, Varga G, Roth J, Kahl BC, Proctor RA, Peters G (2010) *Staphylococcus aureus* panton-valentine leukocidin is a very potent cytotoxic factor for human neutrophils. PLoS Pathog 6:e1000715. https://doi.org/10.1371/journal.ppat.1000715

Miller MA, Dascal A, Portnoy J, Mendelson J (1996) Development of mupirocin resistance among methicillin-resistant *Staphylococcus aureus* after widespread use of nasal mupirocin ointment. Infect Control Hosp Epidemiol 17:811–813. https://doi.org/10.1086/647242

Mollema FPN, Severin JA, Nouwen JL, Ott A, Verbrugh HA, Vos MC (2010) Successful treatment for carriage of methicillin-resistant

Staphylococcus aureus and importance of follow-up. Antimicrob Agents Chemother 54:4020–4025. https://doi.org/10.1128/AAC.01240-09

Monecke S, Müller E, Braun SD, Armengol-Porta M, Bes M, Boswihi S, El-Ashker M, Engelmann I, Gawlik D, Gwida M, Hotzel H, Nassar R, Reissig A, Ruppelt-Lorz A, Senok A, Somily AM, Udo EE, Ehricht R (2021) Characterisation of *S. aureus*/MRSA CC1153 and review of mobile genetic elements carrying the fusidic acid resistance gene *fusC*. Sci Rep 11:8128. https://doi.org/10.1038/s41598-021-86273-4.

Murray CJL, Ikuta KS, Sharara F, Swetschinski L, Aguilar GR, Gray A, Han C, Bisignano C, Rao P, Wool E, Johnson SC, Browne AJ, Chipeta MG, Fell F, Hackett S, Haines-Woodhouse G, Hamadani BHK, Kumaran EAP, McManigal B, Achalapong S, Agarwal R, Akech S, Albertson S, Amuasi J, Andrews J, Aravkin A, Ashley E, Babin F-X, Bailey F, Baker S, Basnyat B, Bekker A, Bender R, Berkley JA, Bethou A, Bielicki J, Boonkasidecha S, Bukosia J, Carvalheiro C, Castañeda-Orjuela C, Chansamouth V, Chaurasia S, Chiurchiù S, Chowdhury F, Donatien RC, Cook AJ, Cooper B, Cressey TR, Criollo-Mora E, Cunningham M, Darboe S, Day NPJ, Luca MD, Dokova K, Dramowski A, Dunachie SJ, Bich TD, Eckmanns T, Eibach D, Emami A, Feasey N, Fisher-Pearson N, Forrest K, Garcia C, Garrett D, Gastmeier P, Giref AZ, Greer RC, Gupta V, Haller S, Haselbeck A, Hay SI, Holm M, Hopkins S, Hsia Y, Iregbu KC, Jacobs J, Jarovsky D, Javanmardi F, Jenney AWJ, Khorana M, Khusuwan S, Kissoon N, Kobeissi E, Kostyanev T, Krapp F, Krumkamp R, Kumar A, Kyu HH, Lim C, Lim K, Limmathurotsakul D, Loftus MJ, Lunn M, Ma J, Manoharan A, Marks F, May J, Mayxay M, Mturi N, Munera-Huertas T, Musicha P, Musila LA, Mussi-Pinhata MM, Naidu RN, Nakamura T, Nanavati R, Nangia S, Newton P, Ngoun C, Novotney A, Nwakanma D, Obiero CW, Ochoa TJ, Olivas-Martinez A, Olliaro P, Ooko E, Ortiz-Brizuela E, Ounchanum P, Pak GD, Paredes JL, Peleg AY, Perrone C, Phe T, Phommasone K, Plakkal N, Ponce-de-Leon A, Raad M, Ramdin T, Rattanavong S, Riddell A, Roberts T, Robotham JV, Roca A, Rosenthal VD, Rudd KE, Russell N, Sader HS, Saengchan W, Schnall J, Scott JAG, Seekaew S, Sharland M, Shivamallappa M, Sifuentes-Osornio J, Simpson AJ, Steenkeste N, Stewardson AJ, Stoeva T, Tasak N, Thaiprakong A, Thwaites G, Tigoi C, Turner C, Turner P, Doorn H, Velaphi S, Vongpradith A, Vongsouvath M, Vu H, Walsh T, Walson JL, Waner S, Wangrangsimakul T, Wannapinij P, Wozniak T, Sharma TEMWY, Yu KC, Zheng P, Sartorius B, Lopez AD, Stergachis A, Moore C, Dolecek C, Naghavi M (2022) Global burden of bacterial antimicrobial resistance in 2019: a systematic analysis. Lancet 399:629–655. https://doi.org/10.1016/S0140-6736(21)02724-0

O'Hara FP, Suaya JA, Ray GT, Baxter R, Brown ML, Mera RM, Close NM, Thomas E, Amrine-Madsen H (2016) Spa typing and multilocus sequence typing show comparable performance in a macroepidemiologic study of *Staphylococcus aureus* in the United States. Microb Drug Resist 22:88–96. https://doi.org/10.1089/mdr.2014.0238

Obořilová R, Kučerová E, Botka T, Vaisocherová-Lísalová H, Skládal P, Farka Z (2025) Piezoelectric biosensor with dissipation monitoring enables the analysis of bacterial lytic agent activity. Sci Rep 15:3419. https://doi.org/10.1038/s41598-024-85064-x

Pantůček R, Götz F, Doškař J, Rosypal S (1996) Genomic variability of *Staphylococcus aureus* and the other coagulase-positive *Staphylococcus* species estimated by macrorestriction analysis using pulsed-field gel electrophoresis. Int J Syst Evol Microbiol 46:216–222. https://doi.org/10.1099/00207713-46-1-216

Pantůček R, Rosypalová A, Doškař J, Kailerová J, Růžičková V, Borecká P, Snopková Š, Horváth R, Götz F, Rosypal S (1998) The polyvalent staphylococcal phage φ812: its host-range mutants and related phages. Virology 246:241–252. https://doi.org/10.1006/viro.1998.9203

Patel JB, Gorwitz RJ, Jernigan JA (2009) Mupirocin resistance. Clin Infect Dis 49:935–941. https://doi.org/10.1086/605495

Pérez-Roth E, López-Aguilar C, Alcoba-Florez J, Méndez-Álvarez S (2006) High-level mupirocin resistance within methicillin-resistant *Staphylococcus aureus* pandemic lineages. Antimicrob Agents Chemother 50:3207–3211. https://doi.org/10.1128/AAC.00059-06

Poovelikunnel T, Gethin G, Humphreys H (2015) Mupirocin resistance: clinical implications and potential alternatives for the eradication of MRSA. J Antimicrob Chemother 70:2681–2692. https://doi.org/10.1093/jac/dkv169

Quero S, Serras-Pujol M, Párraga-Niño N, Torres C, Navarro M, Vilamala A, Puigoriol E, De Los Ríos JD, Arqué E, Serra-Pladevall J, Romero A, Molina D, Paredes R, Pedro-Botet ML, Reynaga E (2023) Methicillin-resistant and methicillin-sensitive *Staphylococcus aureus* in pork industry workers, Catalonia, Spain. One Health 16:100538. https://doi.org/10.1016/j.onehlt.2023.100538

Rakonjac B, Lepšanović Z, Šuljagić V, Jovčić B, Kojić M, Larsen AR, Đurić M, Ćirković I (2022) Predominance of t355/ST152/SCC*mec* V clonal type among PVL-positive MRSA isolates in a tertiary care hospital in Belgrade, Serbia. PLoS One 17:e0273474. https://doi.org/10.1371/journal.pone.0273474

Rendueles O, De Sousa JA, Rocha EP (2023) Competition between lysogenic and sensitive bacteria is determined by the fitness costs of the different emerging phage-resistance strategies. eLife 12:e83479. https://doi.org/10.7554/eLife.83479.

Rossi T, Peltonen R, Laine J, Eerola E, Vuopio-Varkila J, Kotilainen P (1996) Eradication of the long-term carriage of methicillin-resistant *Staphylococcus aureus* in patients wearing dentures: a follow-up of 10 patients. J Hosp Infect 34:311–320. https://doi.org/10.1016/S0195-6701(96)90111-5

Schooley RT, Biswas B, Gill JJ, Hernandez-Morales A, Lancaster J, Lessor L, Barr JJ, Reed SL, Rohwer F, Benler S, Segall AM, Taplitz R, Smith DM, Kerr K, Kumaraswamy M, Nizet V, Lin L, McCauley MD, Strathdee SA, Benson CA, Pope RK, Leroux BM, Picel AC, Mateczun AJ, Cilwa KE, Regeimbal JM, Estrella LA, Wolfe DM, Henry MS, Quinones J, Salka S, Bishop-Lilly KA, Young R, Hamilton T (2017) Development and use of personalized bacteriophage-based therapeutic cocktails to treat a patient with a disseminated resistant *Acinetobacter baumannii* infection. Antimicrob Agents Chemother 61:e00954-17. https://doi.org/10.1128/AAC.00954-17

Seah C, Alexander DC, Louie L, Simor A, Low DE, Longtin J, Melano RG (2012) *Mup*B, a new high-level mupirocin resistance mechanism in *Staphylococcus aureus*. Antimicrob Agents Chemother 56:1916–1920. https://doi.org/10.1128/AAC.05325-11

Straka M, Hubenáková Z, Janošíková L, Bugalová A, Minich A, Wawruch M, Liptáková A, Drahovská H, Slobodníková L (2024) In vitro susceptibility of clinical and carrier strains of *Staphylococcus aureus* to STAFAL® phage preparation. Int J Mol Sci 25:12885. https://doi.org/10.3390/ijms252312885

Sutherland R, Boon RJ, Griffin KE, Masters PJ, Slocombe B, White AR (1985) Antibacterial activity of mupirocin (pseudomonic acid), a new antibiotic for topical use. Antimicrob Agents Chemother 27:495–498. https://doi.org/10.1128/AAC.27.4.495

Tabaja H, Hindy J-R, Kan SS (2021) Epidemiology of methicillin-resistant *Staphylococcus aureus* in Arab countries of the Middle East and North African region. Mediterr J Hematol Infect Dis 13:e2021050. https://doi.org/10.4084/MJHID.2021.050

Talan DA, Krishnadasan A, Gorwitz RJ, Fosheim GE, Limbago B, Albrecht V, Moran GJ, The EMERGEncy ID Net Study Group (2011) Comparison of *Staphylococcus aureus* from skin and soft-tissue infections in US emergency department patients, 2004 and 2008. Clin Infect Dis 53:144–149. https://doi.org/10.1093/cid/cir308

Tkadlec J, Capek V, Brajerova M, Smelikova E, Melter O, Bergerova T, Polivkova S, Balejova M, Hanslianova M, Fackova D, Neradova K,

Tejkalova R, Vagnerova I, Bartonikova N, Chmelarova E, Drevinek P, Krutova M (2021) The molecular epidemiology of methicillin-resistant *Staphylococcus aureus* (MRSA) in the Czech Republic. J Antimicrob Chemother 76:55–64. https://doi.org/10.1093/jac/dkaa404

Tong SYC, Davis JS, Eichenberger E, Holland TL, Fowler VG (2015) *Staphylococcus aureus* infections: epidemiology, pathophysiology, clinical manifestations, and management. Clin Microbiol Rev 28:603–661. https://doi.org/10.1128/CMR.00134-14

Truong VK, Chapman J, Cozzolino D (2021) Monitoring the bacterial response to antibiotic and time growth using near-infrared spectroscopy combined with machine learning. Food Anal Methods 14:1394–1401. https://doi.org/10.1007/s12161-021-01994-6

Truong-Bolduc QC, Wang Y, Hooper DC (2018) Tet38 efflux pump contributes to fosfomycin resistance in *Staphylococcus aureus*. Antimicrob Agents Chemother 62:e00927-18. https://doi.org/10.1128/AAC.00927-18

Virgillio AM, Felton EA, Jackson JK, Kennedy SJ, Becker DN, Lima A, Atrubin K, Cella E, Azarian T, Silbert S, Shaw LN, Kim K (2025) Genomic and phenotypic characterization of mupirocin-resistant *Staphylococcus aureus* clinical isolates. Open Forum Infect Di 12:ofaf374. https://doi.org/10.1093/ofid/ofaf374.

Wagenlehner FME, Naber KG, Bambl E, Raab U, Wagenlehner C, Kahlau D, Höller C, Witte W, Weidner W, Lehn N, Harbarth S, Linde H-J (2007) Management of a large healthcare-associated outbreak of Panton-Valentine leucocidin-positive meticillin-resistant *Staphylococcus aureus* in Germany. J Hosp Infect 67:114–120. https://doi.org/10.1016/j.jhin.2007.07.006

Wertheim HF, Melles DC, Vos MC, Van Leeuwen W, Van Belkum A, Verbrugh HA, Nouwen JL (2005) The role of nasal carriage in *Staphylococcus aureus* infections. Lancet Infect Dis 5:751–762. https://doi.org/10.1016/S1473-3099(05)70295-4

Yankey H, Isaacson G (2018) Efficacy of topical 2% mupirocin ointment for treatment of tympanostomy tube otorrhea caused by community-acquired methicillin resistant *Staphylococcus aureus*. Int J Pediatr Otorhinolaryngol 109:36–39. https://doi.org/10.1016/j.ijporl.2018.03.024

Yin N, Michel C, Makki N, Deplano A, Milis A, Prevost B, Miendje-Deyi VY, Hallin M, Martiny D (2024) Emergence and spread of a mupirocin-resistant variant of the European epidemic fusidic acid-resistant impetigo clone of *Staphylococcus aureus*, Belgium, 2013 to 2023. Euro Surveill 29:2300668. https://doi.org/10.2807/1560-7917.ES.2024.29.19.2300668

Zheng S, Wang W, Aldahdooh J, Malyutina A, Shadbahr T, Tanoli Z, Pessia A, Tang J (2022) Synergyfinder plus: toward better interpretation and annotation of drug combination screening datasets. Genom Proteom Bioinf 20:587–596. https://doi.org/10.1016/j.gpb.2022.01.004

APPENDIX 4

Cieniková Z, Nováček J, Šiborová M, Popelářová B, Füzik T, Botka T, Benešík M, Bárdy P, Pantůček R, Plevka P (2026) Genome anchoring, retention, and release by neck proteins of *Staphylococcus* phage 812. *Communications Biology* 9:199. https://doi.org/10.1038/s42003-025-09477-8

(JCR 2025: IF = 5.8; D1 – Biology)

CC BY 4.0

communications biology

A Nature Portfolio journal

Article

https://doi.org/10.1038/s42003-025-09477-8

Genome anchoring, retention, and release by neck proteins of *Staphylococcus* phage 812

Check for updates

Zuzana Cieniková [1], Jiří Nováček [1], Marta Šiborová [1,3], Barbora Popelářová [1,2], Tibor Füzik [1], Tibor Botka [2], Martin Benešík[2], Pavol Bárdy [2,4], Roman Pantůček [2] & Pavel Plevka [1] ✉

The virion of *Staphylococcus* phage 812 is formed by a capsid and a contractile tail joined together by neck proteins. The neck proteins are crucial for virion assembly, DNA packaging, and the regulation of genome release, but their functions are not completely understood. Here, we show that the neck of phage 812 consists of portal, adaptor, stopper, tail terminator, and two types of decoration proteins. A dodecameric DNA-binding site at the surface of the portal complex anchors the phage genome inside the capsid. The adaptor complex induces a local B-to-A form transition of the DNA in the neck channel that could slow or pause genome translocation during ejection. The central channel of a stopper complex that is not attached to the tail terminator complex is closed by gating loops. In contrast, in the phage 812 virion, the gating loops are in an open conformation, and the DNA extends into the tail. The structure of neck proteins is not affected by tail sheath contraction. Therefore, the expulsion of tail tape measure proteins triggers the genome release.

Lytic phage 812, strain K1/420, and closely related kayviruses from the family *Herelleviridae* infect a wide range of *Staphylococcus aureus* strains. Kayviruses are promising candidates for phage therapy against human infections caused by *S. aureus*, a Gram-positive pathogen[1–3]. The virion of phage 812 is formed by an icosahedral capsid enclosing a 150 kbp-long, AT-rich dsDNA genome, and a double-layered contractile tail terminated by a baseplate[2,4]. The tail, possessing helical symmetry, is attached to the capsid by the neck. The neck of long-tailed phages is formed by a dodecamer of portal proteins, a dodecamer of adaptor proteins, a hexamer of stopper proteins, and a hexamer of tail terminator proteins[5–10]. Adaptor and stopper proteins are collectively called head completion or head-to-tail joining proteins. Tail terminator is also called tail completion or tail-to-head joining protein.

The neck is involved in numerous functions during the phage infection cycle. The portal complex nucleates capsid assembly[11,12]. In the completed prohead, the portal dodecamer occupies the position of a pentamer of capsid proteins at one of the icosahedral vertices. During genome filling, the packaging terminase complex docks onto the portal complex and threads genomic DNA through its central channel into the capsid[13–15]. In phage T4, the packaging starts with the insertion of about 500 bp of the genomic leading end into the capsid and its anchoring to the portal complex[16]. The crown domain of the portal complex located inside the capsid was proposed to function as a sensor for the completion of genome packaging in phages SPP1 and P22[17,18]. After the termination of the packaging and detachment of the terminase, head completion proteins assemble at the portal complex and ensure genome retention in tailless proheads[19,20]. Multiple mechanisms of genome retention in virions of long-tailed phages have been described: in the *Bacillus* phage SPP1, the genome is held inside the neck channel by the stopper proteins[6], whereas in the *Staphylococcus* phage 80α it is stopped by the tail completion protein located inside the neck channel[21], and in the phages Pam3 and λ by the tail tape measure proteins at the neck-to-tail junction[9,22]. The DNA double-strand is inherently asymmetric and flexible, and thus can only be characterized using localized structural studies bypassing symmetry averaging, which are challenging even with state-of-the-art equipment and methodologies[21,22].

Here, we present cryo-electron microscopy (cryo-EM) structures of the neck of the phage 812 virion and genome release intermediate, as well as the crystal structure of a hexamer of stopper proteins. We show that a positively charged belt at the surface of the portal complex binds the DNA inside the capsid. In the absence of attachment to the tail terminator complex, the central channel of the stopper protein hexamer is closed by gating loops. In the phage 812 virion, where the stopper complex is attached to the tail

[1]CEITEC Masaryk University, Kamenice 753/5, 625 00, Brno, Czech Republic. [2]Department of Experimental Biology, Faculty of Science, Masaryk University, Kamenice 753/5, 625 00, Brno, Czech Republic. [3]Present address: Novo Nordisk Foundation Centre for Protein Research, Faculty of Health and Medical Sciences, University of Copenhagen, 2200 Copenhagen, Denmark. [4]Present address: York Structural Biology Laboratory, Department of Chemistry, University of York, York, YO10 5DD, UK. ✉e-mail: pavel.plevka@ceitec.muni.cz

terminator complex, the central channel is open and DNA protrudes into the tail. The portal and adaptor complexes bend the DNA inside the neck channel and induce its local transition to an A-form. These observations led us to propose a mechanism for how the neck proteins of *Herelleviridae* phages anchor, retain, and modulate the release of the phage genome.

Results and Discussion

Neck structure of phage 812 virion

The cryo-EM structures of the phage 812 neck solved with imposed sixfold and twelvefold symmetries both achieved a resolution of 4.2 Å (Fig. 1, S1–S5 and Table S1). The neck of phage 812 consists of four types of proteins forming the channel: a dodecamer of gp91 portal proteins, a dodecamer of gp96 adaptor proteins, a hexamer of gp97 stopper proteins, and a hexamer of gp99 tail terminator proteins (Fig. 1A and Tables S2–S4). The outer surface of the neck is decorated with gp164 stopper decoration proteins and gp56 terminator decoration proteins, which are organized as hexamers of homodimers (Fig. 1A). The density of putative neck whisker proteins surrounding the adaptor complex was not sufficiently resolved to enable structure determination and gene product identification (Fig. 1B).

Portal complex

The portal complex of phage 812 has the shape of a spool, with an inner 30 Å-wide channel. The portal protein can be divided into wing, crown, stem, and clip domains (Fig. S6A and Table S3)[5]. The wing and crown domains are inside the capsid, the stem domains traverse the capsid, and the clip domains are inserted into the adaptor complex outside the capsid (Fig. 1A–C). The crown domains form a conical funnel that opens towards the center of the head. In the phage 812 virion, three sections of the dsDNA genome encircle the crown and the wing domains (Fig. 1B). The outer surface of the wing domain has an overall positive charge (Fig. S7 and Table S5). This feature is conserved in phages from the *Herelleviridae* family (Fig. S8), and was also found in herpesviruses (Fig. S9)[23]. In contrast, the surfaces of the wing domains of phages from other families are mostly negatively charged (Fig. S9). Portal complexes were shown to interact with the packaged DNA and thus influence genome topology and retention[16,18]. The role of the positive charges of wing domains of phage 812 portal proteins in DNA binding is discussed below.

Adaptor proteins

The dodecamer of adaptor proteins has the overall shape of a funnel (Fig. S6B). The adaptor protein of phage 812 is composed of an α-helical core, a β-hairpin, and a β-sandwich domain. The channel inside the adaptor complex broadens to 80 Å in diameter. The channel chamber is walled by the α-helical cores (Fig. 1B, C). β-hairpins of the twelve adaptor proteins assemble into a cylindrical tube with a diameter of <30 Å, inserted into the stopper complex (Fig. 1B, C). The diameter of the adaptor β-hairpin tube channel is remarkably conserved among both sipho- and myophages with known structures[8–10,21,22,24–26], and is probably optimized for the translocation of straight B-form dsDNA. The β-sandwich subdomains of phage 812 adaptor proteins are positioned on the outer surface of the neck and are in contact with the capsid (Fig. 1B, C). The adaptor protein of phage 812 is structurally

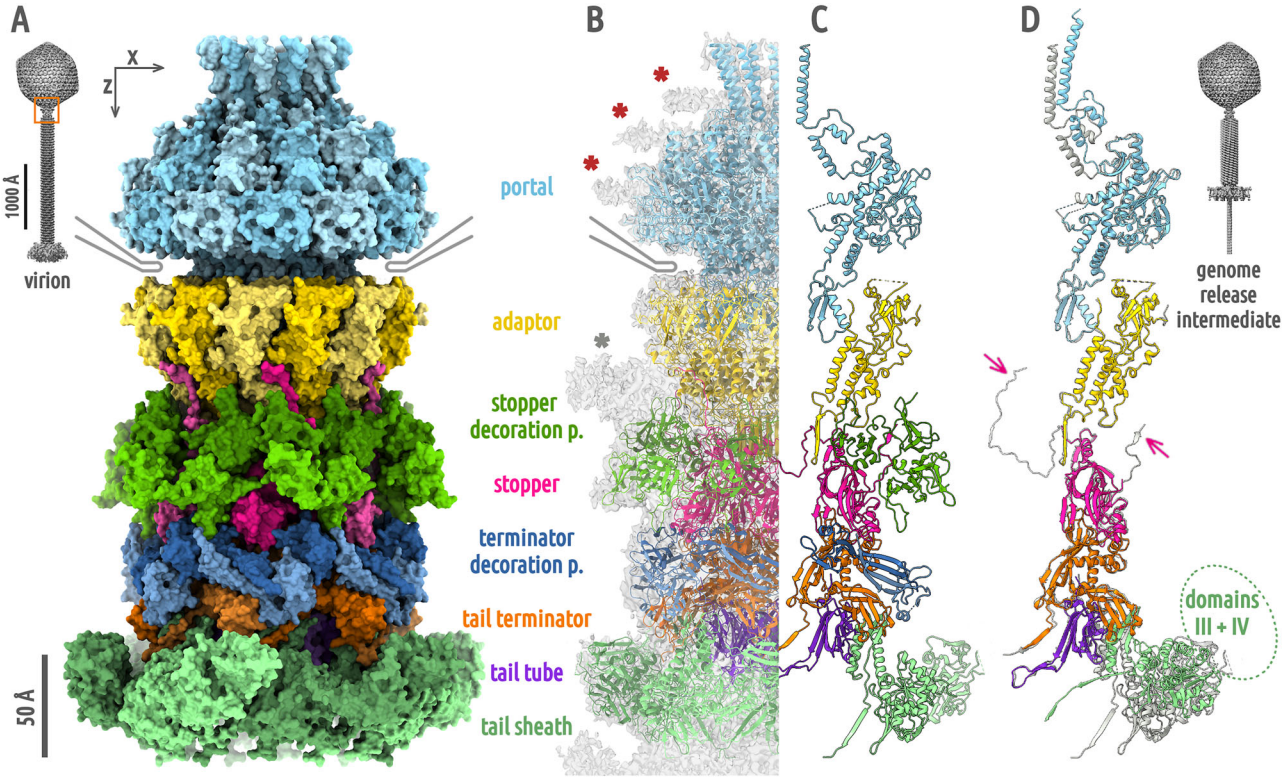

Fig. 1 | Structure of phage 812 neck. A Neck proteins of phage 812 virion are shown in surface representation: portal in light blue, adaptor in gold, stopper in magenta, tail terminator in orange, stopper decoration in forest green, terminator decoration in steel blue, tail tube in violet, and tail sheath in light green. The capsid is indicated schematically in gray. The neck region is outlined with an orange box in the overview of the virion. **B** Neck proteins of the virion are shown in cartoon representation, with the cryo-EM map reconstructed with imposed C6-symmetry (EMD-18462) shown as semi-transparent light gray surface. The densities of three DNA rings encircling the portal complex are marked with red asterisks, and the density of putative neck whisker proteins with a gray asterisk. **C** Cartoon representation of monomers of neck proteins of the phage 812 virion. Domains III and IV of the tail sheath protein are shown as semi-transparent. **D** Comparison of the structure of neck proteins in virion (light gray) and in genome release intermediate (in color). Decoration proteins were not present in the genome release intermediate and are not shown for the virion. Magenta arrows indicate the N- and C-termini of the stopper protein resolved only in the virion. Domains III and IV of the tail sheath protein from the neck-proximal disc are not resolved to a high resolution in the structure of the phage 812 genome release intermediate. Their approximate position is indicated by a light green dotted oval. The inset shows the overall structure of the genome release intermediate.

similar to its homolog in the *Mycolicibacterium* phage Mycofy1, where an α-helical core, a β-hairpin, and a β-sandwich domain were also described[26].

Stopper proteins

The hexamer of stopper proteins of phage 812 is shaped as a ring, with extensions stretching towards the adaptor complex (Fig. 1A). The stopper protein is composed of a β-barrel core, a tetra-cysteine loop, a β-hairpin gating loop, and an external β-sandwich domain (Fig. S6C). Six β-barrel cores delimit the neck channel to 40 Å in diameter. The β-hairpin gating loops in the phage 812 virion line the channel and are sandwiched between hairpin loops of tail terminator proteins. The twelvefold symmetry of the adaptor complex is preserved at the interface with the hexamer of stopper proteins, as the stopper protein forms similar intermolecular contacts with a pair of neighboring adaptor proteins (Fig. S10). The phage 812 stopper protein has a close structural resemblance to its homologs from *Pseudomonas* phages E217 and Pa193, which however lack the external β-sandwich domain[10,25].

Tail terminator proteins

The tail terminator complex of phage 812 has the shape of a six-armed clamp with an inner 40 Å-wide channel (Fig. 1B, C). The tail terminator protein is formed by a core domain composed of a β-sheet flanked by α-helices and a β-sandwich domain (Fig. S6D). The core β-sheets line the central channel and are surrounded by α-helices on the outside (Fig. 1C). The β-sandwich domain binds to tail sheath proteins (Fig. 1A, B). The tail terminator protein of phage 812 bears a structural similarity to its homologs in phages E217 and Pa193, apart from the β-sandwich domain present solely in phage 812[10,25].

Tail tube and tail sheath proteins

The structures of the phage 812 tail tube and tail sheath were determined previously to resolutions of 9 and 6 Å, respectively[4]. Here, we present the structures of neck-adjacent tail tube and tail sheath proteins determined to a resolution of 4.3 Å (Fig. S3C). The tail tube protein consists of a β-sheet domain, six of which build a β-barrel that forms the tail channel (Fig. 1A–C, S6H). A hexamer of tail sheath proteins surrounds each ring of tail tube proteins (Fig. 1A, B). The tail sheath protein can be divided into domains I–IV[27]. Domains I and II are adjacent to the tail tube. Domains III and IV are located at the outer face of the tail sheath (Fig. S6G). Domains III and IV are less resolved in the cryo-EM reconstruction due to their flexibility, and were interpreted using predicted structures.

Stopper and terminator decoration proteins

The decoration proteins of phage 812 neck form elongated dimers spanning, in a zigzag pattern, the adaptor-stopper junction (stopper decoration protein) and stopper-terminator junction (terminator decoration protein) (Fig. 1A). The stopper decoration protein is composed of an N-terminal globular domain containing a β-sheet flanked by two α-helices, and a C-terminal β-barrel domain (Fig. S6E). The terminator decoration protein contains 15-residue-long N- and C-terminal antiparallel β-strands and a small globular central domain (Fig. S6F). In the phage 812 virion, the stopper decoration proteins interact with a density of putative neck whiskers and probably enable their attachment (Fig. 1B). We hypothesize that the decoration proteins reinforce the interfaces between adaptor and stopper, and stopper and terminator complexes, since phage 812 particles that had lost the neck decoration proteins often have deformed or broken necks (Fig. S11A). It is also possible that the neck whisker and decoration proteins play a role of chaperones that are important for a successful self-assembly of phage 812 virions.

Stopper complex ensures genome retention in the capsid before tail attachment

After the completion of phage genome packaging and dissociation of the packaging terminase, adaptor and stopper proteins attach to the portal complex[19]. The resulting genome-filled assembly intermediate retains the packaged genome until tail attachment[20]. We solved a 2.2 Å resolution structure of the stopper protein of phage 812 using X-ray crystallography (Fig. S2C and Table S6). The protein forms hexamers in solution and in the crystal (Fig. 2 and S12), which differ in structure from those in the phage 812 particle (Fig. 2A–C and S13). In the crystal structure, the six gating loops of the stopper protein form α-helices and restrict the central channel to 4.5 Å (Fig. 2A). Similarly, the central channel of the stopper complex in the tailless DNA-filled particle of phage SPP1 is blocked by gating loops in α-helical conformations (Fig. S13A–B)[8]. Therefore, we speculate that phage 812 stopper proteins use the gating loops to ensure the retention of the phage genome before the tail attachment.

Tail attachment induces opening of the phage 812 stopper channel

The gating loops of the stopper proteins in the phage 812 virion are in β-hairpin conformations that leave the central channel open (Fig. 2B and S13C). To transform from the closed conformation observed in the crystal structure into the open form in the phage 812 virion, stopper proteins rotate 15° and pull the gating loops away from the adaptor complex (Fig. S13D). This rotation is induced by the attachment of the tail terminator complex, which pushes tetra-cysteine loops of stopper proteins outwards (Fig. S13CF). The Cys-Pro-Cys-$(X)_n$-Cys-X-X-Cys pattern of the tetra-cysteine loop is conserved in stopper proteins of phages from the family *Herelleviridae* (Fig. S13E), but not among any other phage groups. Thanks to proline and cross-strand zinc coordination (Fig. 2D), the loop is stable and moves as a rigid body together with the core β-barrel domain of the stopper protein (Table S7). The gating loop changes conformation to a β-hairpin and lines the inner surface of the neck channel, which delimits the local channel diameter to 40 Å (Fig. S13CF). The α-helix-to-β-strand transformation of the gating loop is enabled by the residues Gly106, Gly113, and Gly118, which serve as hinges and provide conformational freedom to the polypeptide chain. These glycine residues are conserved within the *Herelleviridae* family (Fig. S13E). The coupled conservation of the tetra-cysteine motif and the glycine hinges of the gating loop in stopper proteins indicates that the mechanism of genome gating is shared among *Herelleviridae* phages.

Genome release is not dependent on changes in neck structure

We induced genome release in purified phage 812 virions by in vitro treatment with urea. The capsids showed a continuum of residual genome density, as the mechanisms that ensure completion of DNA ejection in vivo cannot occur. We selected capsids with the lowest average inner density, and we termed this dataset 'genome release intermediates' (Fig. S14). We solved the structure of the neck of the genome release intermediates using twelvefold and sixfold symmetries to resolutions of 3.1 and 3.6 Å, respectively (Fig. S14–17 and Table S1). The neck of the genome release intermediate lacks decoration proteins, which have been stripped during the tail contraction treatment, and there is no resolved density for the N- and C-termini of stopper proteins that interact with the stopper decoration proteins in the virion (Fig. 1D and S18A–B). The crown domains of portal proteins are shifted 8.9 Å away from the core of the portal complex and rotated 28° counterclockwise around the portal central axis, when looking from the head center, relative to their position in the virion (Fig. 1D, RMSD of 6.1 Å over 5,256 portal protein Cα atom pairs). This structural change is likely due to the absence of most of the packaged DNA in the genome release intermediate. Aside from the change in position, enabled by flexible linkers connecting crown and wing domains of portal proteins, minimal difference was observed when crown domain models of virion and genome release intermediate were compared. The other domains of portal proteins were not affected by tail contraction and genome release (RMSD of 1.1 Å over 4,368 Cα atom pairs). Adaptor, stopper, tail terminator, and neck-adjacent tail tube complexes of the genome release intermediate are in the same conformations as in the virion (RMSD of 0.78 Å over 6942 Cα atom pairs available for comparison, Fig. 1D). The absence of structural differences between the neck proteins of the phage 812 genome-containing particles

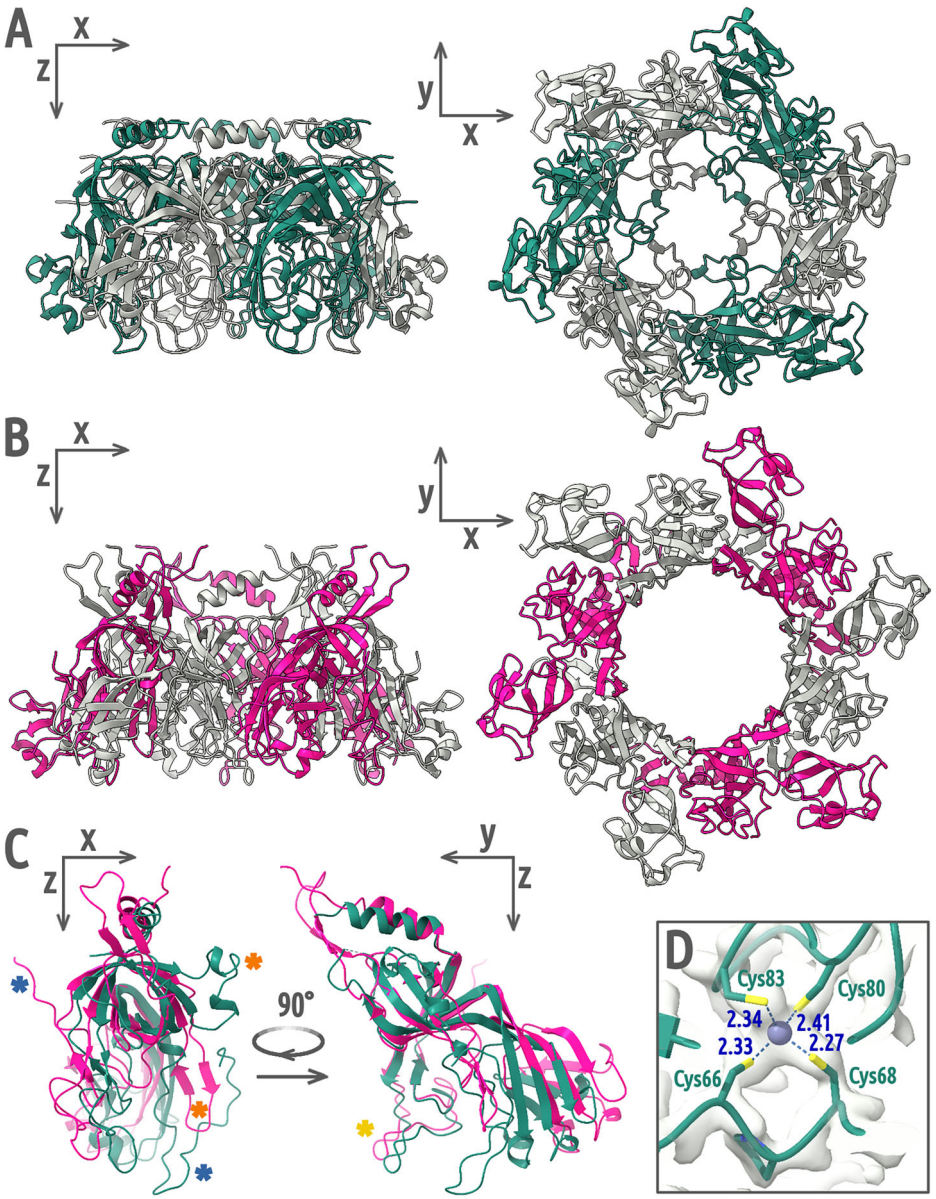

Fig. 2 | Structure of stopper protein in crystal and phage 812 particle. A–B A hexamer of stopper proteins in the crystal (**A**) and in the virion (**B**), shown in cartoon representation. Alternating subunits are shown in color and in gray. **C** Structural alignment of stopper protein monomers from the crystal (teal) and the virion (magenta). The two positions of the gating loop are indicated with orange asterisks, those of the C-terminus with blue asterisks, and those of the tetra-cysteine loop with a golden asterisk. **D** A zinc atom (blue sphere) is coordinated between four cysteine side chains in the crystal structure of the tetra-cysteine loop. Distances are reported in angstroms.

and genome release intermediates indicates that no conformational change to the neck is involved in the regulation of phage 812 genome release. Therefore, it is likely that the genome release is enabled by the release of the tail tape measure proteins, as discussed below.

Changes in the neck-to-tail contacts caused by tail contraction

The tail terminator complex caps the tail and interacts with the terminal hexamers of tail tube and tail sheath proteins. The core β-sheets of six tail terminator proteins build a β-barrel of the same size and shape as the tail tube β-barrel, extending the tail channel seamlessly into the neck (Fig. S6DH). The interaction is strengthened by N-termini of tail tube proteins which insert into gaps between cores and β-sandwich domains of tail terminator proteins. Tail sheath contraction and genome ejection have no effect on the conformation of the terminal tail tube complex nor on its interface with the tail terminator complex (Fig. 1D).

The interfaces between tail sheath and tail terminator proteins, and between tail sheath proteins from two consecutive discs in the tail of the phage 812 virion, are similar (Fig. 3A). Tail terminator or tail sheath proteins from a hexamer located closer to the phage head provide C-terminal β-strands to complement β-turns of domains I of tail sheath proteins from a disc located further away from the head (Fig. 3A). Inter-disc β-sheet complementation was observed also in phages E217, Pam3, and Pa193 and appears to be a conserved feature of phages with contractile tails[9,10,25]. The tail terminator protein of phage 812 is unique in having an outer β-sandwich domain that clamps tail sheath domain I against the tail tube (Fig. 1). After tail sheath contraction of phage 812, the inter-disc contacts between tail sheath proteins are preserved, and domains I and C-terminal β-strands of tail sheath proteins move as rigid bodies to their positions in the contracted tail sheath[4]. In contrast, the tail terminator protein does not change conformation upon tail contraction, and the domain I of the interacting tail sheath protein remains locked in the native position while the other tail sheath protein domains move (Fig. 3B and S6I). Domain II moves to the canonical contracted position, while outer domains III and IV are not well resolved in the reconstruction, indicating that they become mobile (Fig. 3C). The helix connecting domain I to domain II is partially unraveled to accommodate the increased distance between the locked domain I and the shifted domain II (Fig. 3B). In comparison, following the tail contraction of phage E217, domains I of neck-adjacent tail sheath proteins move away from the gateway protein gp29, a homolog of phage 812 tail terminator protein, as gp29 lacks a β-sandwich domain locking the tail sheath domain I.

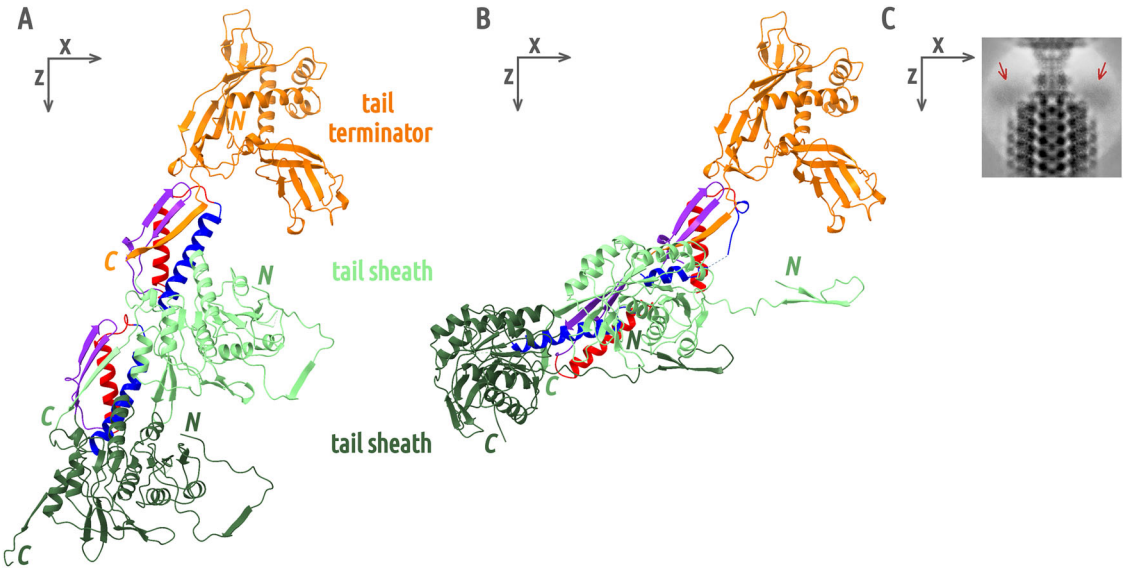

Fig. 3 | Tail terminator and tail sheath proteins in native and contracted tail. **A** Comparison of intermolecular contacts between tail terminator and tail sheath proteins in the phage 812 virion. A tail terminator protein is shown as an orange cartoon, an adjacent tail sheath protein in light green (domains III and IV were omitted) and a tail sheath protein from the second disc in dark green. Domain I segments of the tail sheath proteins highlighted in blue (α-helix residues 490–513), red (α-helix residues 522–538), and violet (β-turn residues 551–563) interact with the C-terminus of the adjacent tail sheath or tail terminator protein. **B** Comparison of contacts between tail terminator and tail sheath proteins after tail contraction. Domains III and IV of tail sheath proteins were omitted for clarity. The coloring of the proteins is identical to (**A**). The C-terminal β-strand of the tail terminator protein, and violet and red segments of domain I of the adjacent tail sheath protein, retain the same position as in the native structure. However, residues 490–513 (in blue), which in the native tail form an α-helix, reorganize. In contrast, the homologous interface between two adjacent tail sheath proteins retains the same structure as in the native tail, but its position is shifted. **C** Cryo-EM image of the neck/tail junction of the phage after tail contraction, showing the disordered state of domains III and IV of tail sheath proteins from the neck-adjacent disc (red arrows).

The C-terminal β-strand of gp29 of phage E217 swings outwards to accommodate the conformational change[10].

Binding of the DNA to the outer surface of the portal complex

A section of dsDNA, which we named 'anchor DNA', encircles the portal complex at the level of wing domains in the cryo-EM reconstruction of the phage 812 genome release intermediate (Fig. 4A, B and S18). In an asymmetric reconstruction, this DNA is resolved as a split ring with a right-handed twist and a radius of 65 Å (Fig. 4A, B). The DNA is in the B-form. The diameter of the portal complex at the level of the DNA binding site is such that the DNA makes one helical turn per portal monomer, permitting an analysis of DNA-portal interactions in twelve and sixfold symmetrized maps (Fig. 4C–E and S18A, B). Side chains of Arg137, Arg145, and Lys425 of the portal protein form salt bridges with DNA backbone phosphates (Fig. 4C–E). These DNA-binding side chains are stabilized by contacts with negatively charged side chains of Glu139 and Glu142 (Fig. S19). Positively charged DNA-binding sites of neighboring portal proteins are separated by negatively charged valleys formed by Asp130, Asp132, Glu134, and Glu424 (Fig. S7B, C). The DNA minor groove facing the portal protein is narrowed to 3 Å, from *ca* 6 Å in straight B-form DNA (Fig. 4F)[28]. The side chain of Lys138 extends into the minor groove and interacts with two consecutive base pairs (labeled as F5:R6 and F6:R5 on strands F and R, Fig. 4EH). The nucleotide identity of these two base pairs cannot be determined based on the cryo-EM map due to rotational and inter-particle averaging. However, molecular simulations with all nucleotide combinations of these two base pairs (Table S8) show that a strong base pair (containing G and C) is disfavored in both positions due to the presence of the guanine N2 hydrogen donor clashing with the Lys138 NZ hydrogen donor (Table S9). This belt of charged side chains on the wing domains of phage 812 portal complex therefore provides a high-avidity, shape-specific, and sequence-sensitive binding site for B-form DNA.

To determine the sequence of the genome interacting with the portal complex, we sequenced the DNA in phage 812 virions and genome release intermediates. A long terminal repeat (LTR) of 8.5 kbp flanks both chromosomal ends of the phage 812 genome packaged in virions[2]. The repeats are conventionally named as left, the repeat at the 5' end of the genomic sequence, and right, the 3' end repeat downstream of the genomic sequence[29]. The vast majority of sequence reads from the genome release intermediate start at position 1 of the LTR (Fig. 4G and S18C), indicating that the DNA retained in the capsid corresponds to the left end of the phage 812 genome. This sequence is likely to be the sequence bound to the portal complex (Fig. 4A–B). Our results also demonstrate that phage 812 genome ejection proceeds from the right chromosome end toward the left end, which corresponds to a first in, last out direction.

In the asymmetric cryo-EM reconstruction of the phage 812 genome release intermediate, the ends of the anchor DNA split ring are positioned next to each other (Fig. 4A–B). One end of the DNA points toward the portal-capsid junction, and the other end points to the top of the portal crown. The crown funnel, connected to the core of the portal complex by flexible loops, is tilted 3.5° off the neck axis towards the opening in the anchor DNA ring (Fig. S20), indicating that the tilting is caused by the interactions of the DNA loop with the portal crown. Furthermore, the twelve crown termini of portal proteins fold into six structures reminiscent of molten globules (Fig. S18D–F) and contain 41% of residues with charged side chains, making their interaction with DNA plausible.

The interaction of the genome with the portal complex is described here for the phage 812 genome release intermediate. We speculate, however, that the primary purpose of the molten-globule portal crown structures and of the B-DNA-binding circular belt formed by wing domains is to anchor the leading end of the genome inserted into the capsid during the initial stage of genome packaging. Based on the evidence that the genome ejection proceeds in the first in, last out direction, the interaction of the end of the DNA with the portal would be established at the beginning of genome packaging and retained until its ejection. DNA anchoring may prevent its accidental escape from the capsid caused by slippage of the packaging terminase[16]. Furthermore, the DNA anchoring also constrains the movement of the genome inside the capsid, which may prevent its knotting[30], and initiate coaxial genome spooling (Fig. S11B).

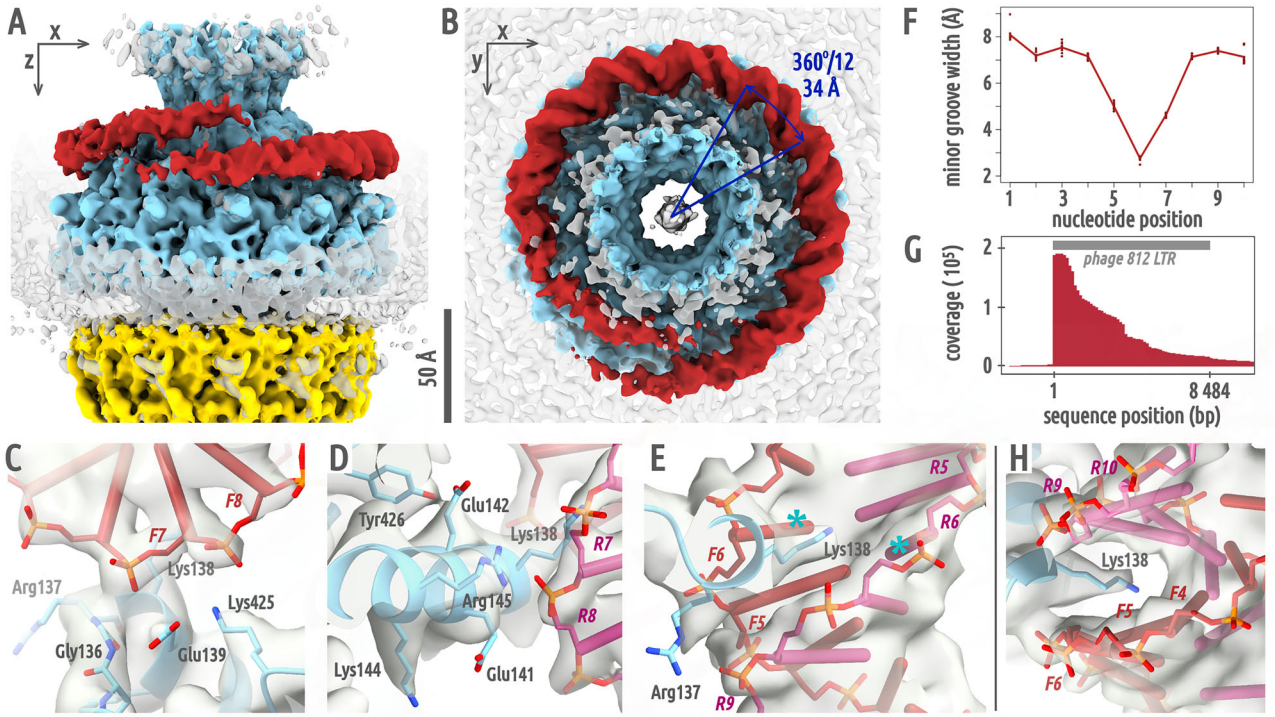

Fig. 4 | DNA forms split ring encircling portal complex of phage 812 genome release intermediate. A, **B** Surface representation of an asymmetric cryo-EM reconstruction of the neck of phage 812 genome release intermediate (EMD-18395), low-pass filtered to 6 Å and zone-colored based on its structural components: dsDNA in red, portal proteins in light blue, adaptor proteins in gold; remaining density in semi-transparent gray. The arc distance between neighboring portal wing domains described by the anchor DNA is 34 Å (indicated in navy blue), which corresponds to one B-DNA helix turn. **C**–**E** Interactions between side chains of portal proteins and DNA in C12-symmetrized reconstruction of the neck of the genome release intermediate (EMD-18213). The two DNA strands are colored in primary red (strand F) and rose red (strand R). Turquoise asterisks denote the bases forming putative hydrogen bonds with the Lys138 side chain. **F** Plot of the average van der Waals width of the minor groove over one helical turn of the DNA anchored to the portal complex (n = 12 helical turns). **G** Mapping of sequence reads of DNA remaining in phage 812 capsids after genome release onto phage 812 long terminal repeat (LTR). **H** Shape of the DNA minor groove facing the portal protein binding site.

Interaction of the portal complex with DNA inside the neck channel

In the phage 812 virion, DNA fills the neck channel and is in contact with tunnel loops of the portal proteins (Fig. 5A). Each tunnel loop interacts with the crown base of the same portal protein subunit, which pushes the loop against channel DNA (Fig. 5A). The neck channel of the genome release intermediate contains residual DNA (Fig. 5B). The crown domains of portal proteins of the genome release intermediate are raised relative to their positions in the virion, which releases the pressure on the tunnel loops that ease away from DNA (Fig. 5B). Nevertheless, an asymmetric reconstruction of the portal channel of the genome release intermediate shows that the tunnel loops remain in contact with DNA (Fig. 5C). Tunnel loops (residues 376–381) are stabilized by interactions with the backbone of the DNA (Fig. 5C–D). The side chain of Lys381 extends towards DNA phosphates (Fig. 5E). We speculate that the lowering of the crown caused by the pressure exerted by the encapsidated DNA leads to a compression of the portal tunnel loops and tighter contact with the channel DNA (Fig. 5A–B). It was hypothesized that this conformational switch sends the headful packaging termination signal through DNA to the terminase of phage SPP1[17], and a similar mechanism could also trigger packaging termination in phage 812.

B-to-A DNA transition inside the neck channel could regulate genome translocation

In the asymmetric reconstruction of the neck of the genome release intermediate, the DNA leans away from the central axis at the portal/adaptor junction (Fig. 6A, B). The bent DNA forms asymmetric contacts with side chains of Lys334 from portal clip domains (Fig. 6A, B). Rings of lysines lining the inside of the portal channel at the clip domain level were previously identified in many tailed phages and were speculated to interact with the channel DNA[6,31,32]. Inside the adaptor chamber, the DNA switches from the B to the A-form over one helical turn before resuming the B-form upon entering the β-hairpin tube of the adaptor complex (Fig. 6A). A-form DNA is characterized by a wider diameter compared to the B-form, an off-center displacement of nucleic base pairs, and an exposed minor groove (Fig. S21)[28]. The A-form region of the DNA interacts asymmetrically *via* its minor groove with short loops (residues 265–272) of adaptor proteins at the exit from the adaptor chamber, where side chains of Met269 and Tyr270 are positioned to form hydrophobic interactions with DNA ribose sugars (Fig. 6AC). In the narrow β-hairpin tube of the adaptor complex, with a van der Waals diameter of <24 Å, the B-DNA is recentered on the channel axis by contacts between DNA backbone phosphates and Glu254 side chains (Fig. 6AD). The transition from an off- to on-axis position is enabled by a bend in the DNA double-strand due to a sharp narrowing of its minor groove (Fig. 6E, F and S22).

There is a similar widening and off-centricity of the channel DNA in the adaptor chamber of the phage 812 virion as in the genome release intermediate (Fig. S23). The B-to-A conversion must be therefore reversible and could occur when genome progression through the neck is slowed or paused. B-to-A transitions are typically induced by dehydration or by DNA-remodeling proteins and are sequence-dependent[33]. We hypothesize that in phage 812, the double strand bends inside the adaptor β-hairpin tube (Fig. 6E, F and S22A), is pressed against hydrophobic loops of the adaptor proteins (Fig. 6C), undergoes a flipping of ribose sugars to the exposed 3'-endo conformation, and so triggers DNA conversion to the A-form[34]. AT-rich dsDNA is prone to bending under the influence of positive ions[35–37], and GC-rich dsDNA enables B-to-A form conversion[33,38]. Therefore, an AT-rich DNA tract located in the adaptor β-hairpin tube followed by a GC-rich tract located in the adaptor chamber is susceptible to forming the structure

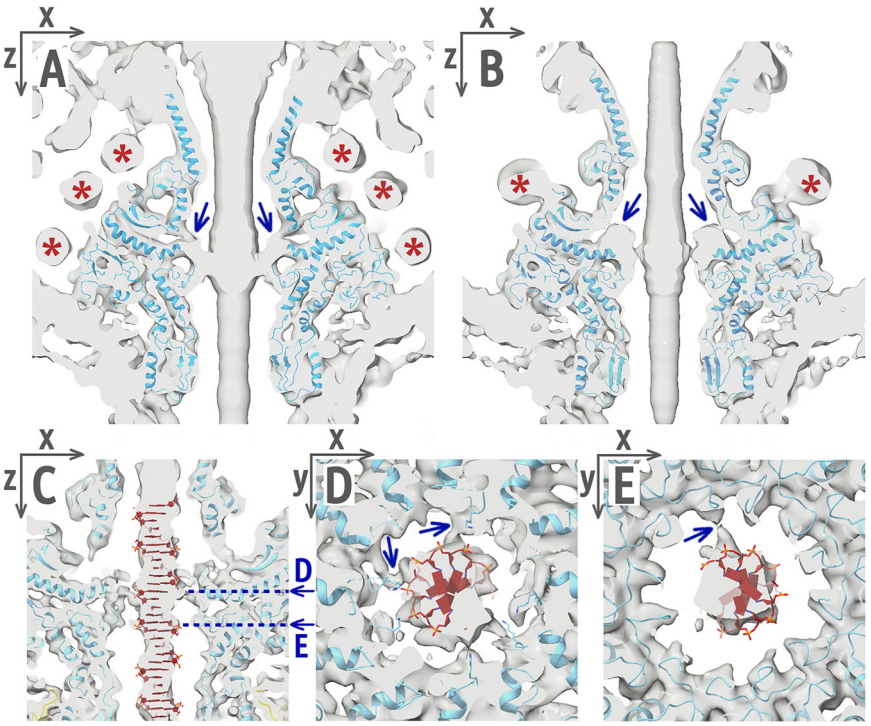

Fig. 5 | Cross-sections through cryo-EM maps of phage 812 portal channel. A, **B** Twelvefold-symmetrized reconstructions of the portal in the virion (A, EMD-18445) and genome release intermediate (B, EMD-18213) are shown as gray semi-transparent surface. Portal proteins are shown in light blue in cartoon representation. Blue arrows indicate the position of tunnel loops, and red asterisks denote DNA rings around the portal complex. **C**–**E** Asymmetric reconstruction of the portal channel of the phage 812 genome release intermediate (EMD-18372) viewed perpendicular to (**C**) and along (**D**, **E**) the tail axis. The portal complex is in light-blue cartoon representation, the adaptor complex in gold, and the DNA in red. The tunnel loops of portal proteins (residues 375–392) extend towards the DNA. The contacts with the DNA phosphate backbone are mediated by side chains of Lys381 (**D**) and the flexible loop Gly376–Gly379 (**E**), which are indicated by blue arrows.

observed in phage 812 adaptor channel. This DNA remodeling could ease the pressure of the DNA packaged inside the virion capsid on tail tape measure proteins in the tail tube, as the off-axis A-DNA region likely transfers part of this pressure to the adaptor complex. A similar arrangement of dsDNA inside the neck was observed in phage φ29 virion, in which the genomic DNA appears to adopt a toroidal shape inside the chamber of the lower collar complex, while the DNA terminus occupies the lower collar tube and is in contact with the tail tape measure protein-analog gp3[39,40]. During genome delivery, the A-form conversion in the adaptor chamber of phage 812 could provide a means to strategically pause DNA ejection that can be encoded into the genomic sequence through modulating the AT/GC composition of the translocating DNA. Indeed, the sequencing of the residual capsid DNA of phage 812 after the induction of genome ejection shows an accumulation of reads of certain lengths (Fig. S24), consistent with genome ejection pausing. The pausing may contribute to the regulation of phage gene expression in the initial stages of infection, help to avoid targeting by bacterial immune systems before phage counter-proteins are synthesized, and prevent phage DNA degradation during phage-induced cleavage of the host genome, as observed in phage T5[41,42]. Pull on the stalled DNA caused by its diffusion in the bacterial cytoplasm or by the activity of RNA polymerase could resume the genome ejection[43,44].

Genomic end and the tail tape measure protein

The van der Waals diameter of the channel formed by the stopper, tail terminator, and tail tube proteins is >30 Å, and the walls are negatively charged, allowing an unhindered passage of DNA (Fig. 7 and S25). In the asymmetric reconstruction of the neck/tail junction of the phage 812 virion, the four neck-proximal rings of the tail tube are occupied by dsDNA (Fig. 7A). In the fifth ring of the tail tube, the end of the DNA double-strand is in head-to-head contact with a trimeric density that we attribute to the N-termini of the tail tape measure proteins (TMP) (Fig. 7A). Thus, the packaged genome is poised for ejection upon the release of the TMP complex from the tail tube. Unlike phage 80α[21], phage 812 does not contain a tail completion protein blocking DNA inside the neck channel, pointing at different genome gating mechanisms used by these two phages.

The length of the channel from the adaptor complex to the fourth tail tube ring in the phage 812 virion is 269 Å, which corresponds to a DNA length of *ca* 85 bp (Fig. 7)[28]. The DNA has a pitch of *ca* 35 Å/turn, typical for B-form DNA[28], but a shallow minor groove caused by an off-axis displacement of the bases (Fig. 7B), which is a mark of A-form DNA[28]. The 85 terminal base pairs of the right end of phage 812 long terminal repeat contain four poly(G):poly(C) tracts, which could facilitate the formation of the hybrid B/A-form (Fig. 7C)[38]. Phages from the *Twortvirinae* subfamily of *Herelleviridae* have genomes with an AT content above 70%, therefore the presence of clustered G-tracts at the end of phage 812 genome is particularly notable. We hypothesize that the hybrid DNA form is caused by the pressure exerted by the packaged genome since the A-form of DNA accommodates 30% more base pairs per axial length than the B-form[28]. A complete conversion of the DNA end to the wider A-form is prevented by the limited 31 Å van der Waals diameter and the negative surface charge of the tail tube channel (Fig. S25). In the structure of the phage λ virion, the genomic end is likewise located inside the tail channel and has a hybrid B/A conformation with a shallow minor groove[22]. This DNA remodeling could serve to dissipate the energy of impact exerted by the DNA end on the tail tape measure protein when the DNA descends into the tail tube after head-to-tail joining, analogous to suspension coils in a car.

DNA compresses the tail tape measure proteins

The TMP complex acts as a scaffold for tail tube assembly and determines its length[45–48]. However, in the phage 812 virion, the tail tube exceeds the length of the TMP trimer by four rings of tail tube proteins (Fig. 7). This length difference corresponds to 166 Å, which is 8% of the total tail tube length, or *ca* 110 amino acid residues arranged in an α-helix. Mass spectrometry data indicate that both N- and C-termini of TMP are present in phage 812 virions (Fig. S26). Therefore, we hypothesize that the TMP trimer inside the tail tube of the phage 812 virion is longitudinally compressed by the DNA released from the neck after head-to-tail joining. Based on the secondary structure prediction of phage 812 TMP (Fig. S26A) and known structures of its homologs[24,49], we speculate that the TMPs form a trimer with parallel α-helical coiled-coil segments interspersed with segments without a specific secondary structure. The segments without predicted secondary structure account for 42% of the total sequence, and, unlike coiled coils, can be compressed. TMP compression could disrupt its interactions with tail tube proteins and facilitate TMP release prior to genome ejection.

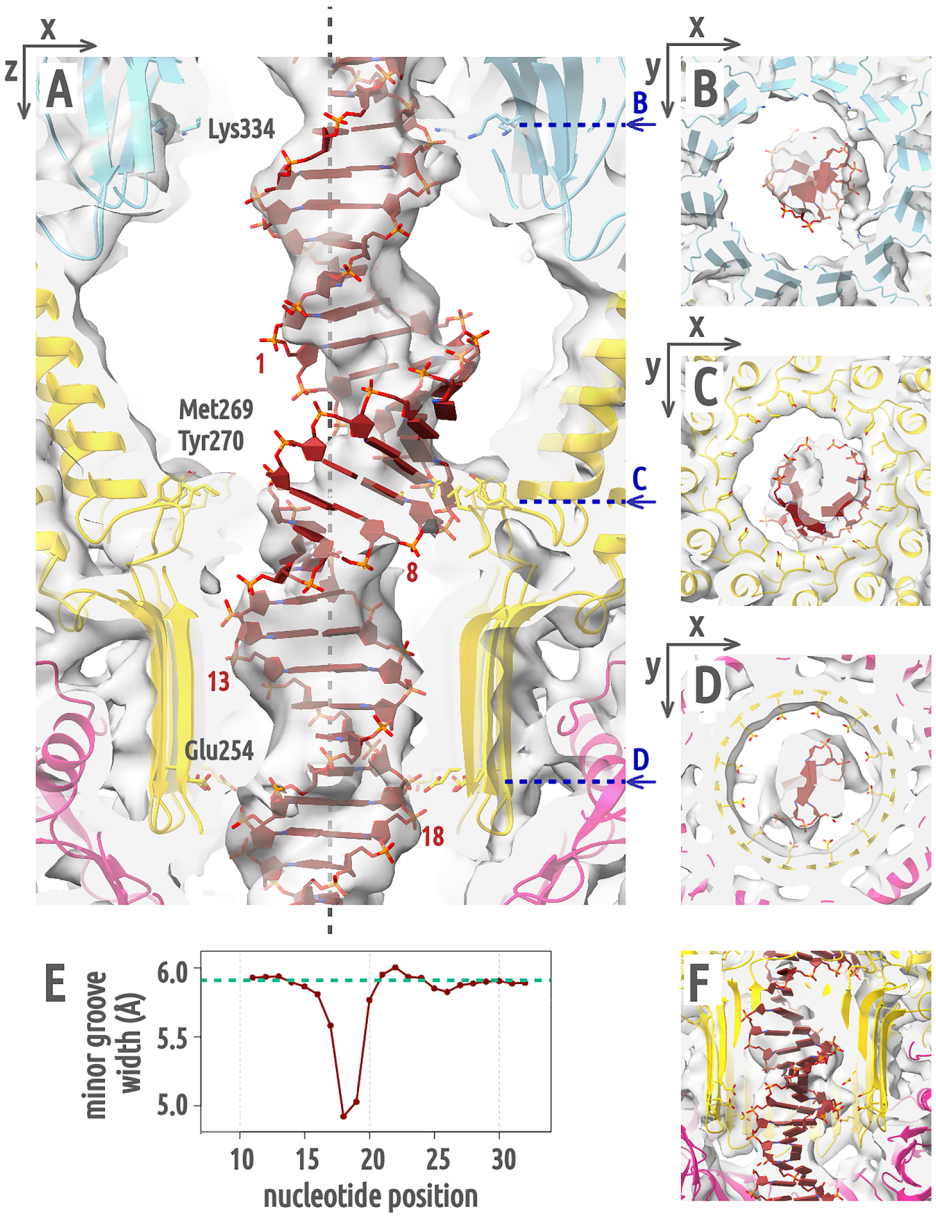

Fig. 6 | DNA converts to A-form in adaptor channel. A–D An asymmetric reconstruction of the adaptor channel of the genome release intermediate (EMD-18372) is shown as gray semi-transparent surface. Portal proteins are shown in cartoon representation in light blue, adaptor proteins in gold, stopper proteins in magenta, and DNA in red. The position of the central channel *z*-axis is indicated by a dashed gray line. Side chains of Lys334 of portal proteins and Glu254, Met269, and Tyr270 of adaptor proteins are shown in stick representation. The numbering of nucleotides for the measurement of the minor groove width in panel (**E**) is indicated in panel (**A**) on the strand oriented in the head-to-tail direction. Nucleotides 1–10 are in the A-form. **E** Plot of the Van der Waals width of the DNA minor groove. The dashed turquoise line represents the minor groove width of an ideal B-form DNA. **F** Cross-section through the channel density tilted -24° along *x*, showing the narrow minor groove of DNA near the Glu254 ring.

Conclusions

The comparison of the structures of phage 812 virion and contracted particle highlights the mechanistic roles that the neck proteins and the DNA play in the phage life cycle, from genome packaging through virion assembly to genome ejection (Fig. 8). The portal provides a circular, high-avidity binding site that anchors the leading end of the phage genome and thus influences its spooling inside the head. Pressure exerted by the packaged genome induces a lowering of the crown of the portal complex. The B-to-A-form DNA remodeling by side chains of the portal and adaptor complexes stabilize the genome in the virion and could strategically pause its translocation during ejection. The stopper proteins in the closed conformation block the central channel with their gating loops, suggesting a mechanism for securing the genome inside tailless heads. Conformational changes to the gating loops, induced by the attachment of the tail terminator complex during virion assembly, open the stopper channel and permit the progression of the genomic end into the tail tube. The hybrid B/A-form adopted by terminal G-tracts of the phage DNA and the compression of the tail tape measure protein trimer likely serve to disperse the force exerted by the fully packaged genome. Contrary to expectations, the neck proteins of phage 812 do not play a direct role in regulating the genome ejection from the capsid, as the tail sheath contraction does not affect their structure. Instead, disruption of the interactions of TMPs with the baseplate, induced by baseplate binding to a host cell[4], likely enables expulsion of the TMPs and genome ejection by unblocking the tail tube channel.

Methods

Preparation of phage samples

Staphylococcus phage 812, strain K1/420, was propagated in *S. aureus* (strain CCM 4028, Czech Collection of Microorganisms) planktonic cultures grown at 37 °C in meat peptone broth supplemented with $CaCl_2$ to 2 mM final concentration[4]. The phage lysate was centrifuged at 5000 × g and 4 °C for 30 min then filtered through 0.45 µm membrane to remove cell debris. Phages were pelleted by centrifugation at 54,000 × g for 2.5 h, then gently dissolved in 500 µL of phage buffer (50 mM Tris pH 8, 10 mM NaCl, 10 mM $CaCl_2$). The sample was purified on a CsCl step density gradient (1.45, 1.5 and 1.7 g/mL of CsCl in phage buffer) by centrifugation at 194,000 × g for 4 h. Collected fractions containing phage particles were dialyzed against the phage buffer over-night. For the preparation of genome release intermediates with contracted tails used for cryo-EM data collection, the phage sample was supplemented with lipoteichoic acid (LTA) from *S. aureus*

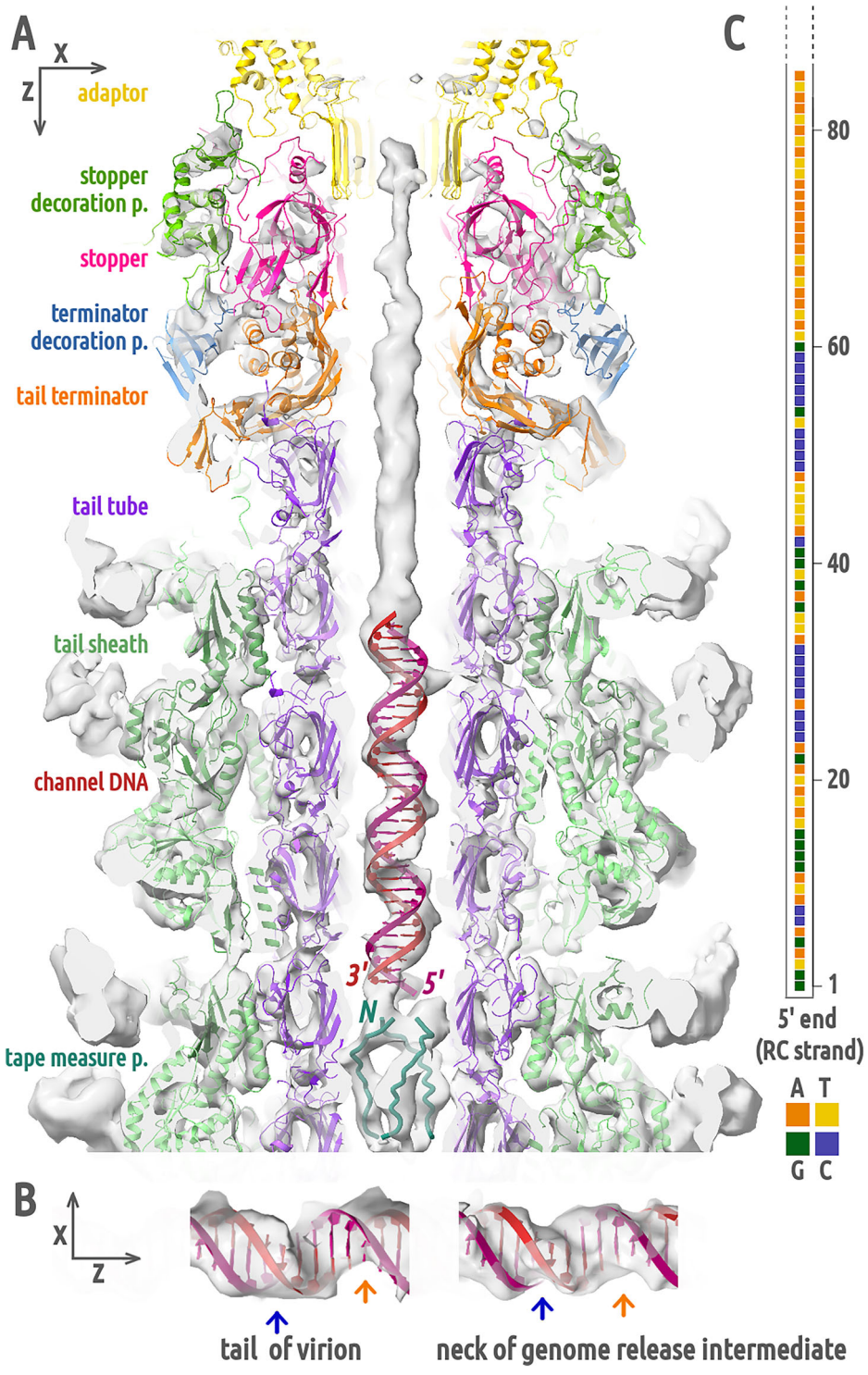

Fig. 7 | Structure of terminus of phage DNA and tail tape measure protein in virion tail. A An asymmetric reconstruction of the neck-to-tail junction (EMD-18516) is shown as gray semi-transparent surface. Adaptor proteins are shown in cartoon representation in gold, stopper proteins in magenta, tail terminator proteins in orange, stopper decoration proteins in forest green, terminator decoration proteins in steel blue, tail tube proteins in violet, and tail sheath proteins in light green. An ideal B-form dsDNA (in red) was placed into the helical density inside the tail tube channel. The first 14 residues of three TMPs (in turquoise) were fitted into the channel density starting at the fifth ring of the tail tube. **B** Comparison of reconstructed DNA densities in phage 812 tail channel of the virion and neck channel of the genome release intermediate with a B-form DNA model. The neck channel DNA has clear major (orange arrow) and minor (blue arrow) groove valleys typical for B-form DNA. The tail channel DNA has a deep major groove and a shallow minor groove caused by an off-center displacement of the base-pair densities, indicating a hybrid B/A form. **C** The reverse complement (RC) sequence (85 right-end base pairs) of the phage 812 long terminal repeat is aligned with the DNA density in panel A from the adaptor β-hairpin tube to the end of the genome.

(SIGMA) to a final concentration of 100 µg/mL, then diluted 1:10 using the phage buffer with the addition of urea at a final concentration of 3 M, and incubated for 2 h at 42 °C. The sample was then diluted 1:3 with the phage buffer, incubated for 15 min at room temperature with Turbonuclease (Abnova) at a final concentration of 30 µg/mL, and pelleted for 1 h at 75,000 × g. The pellet was resuspended in 100 µL of the phage buffer. For the preparation of particles with contracted tails used for residual genome sequencing, a second phage sample was treated with a tail contraction protocol modified as follows: the dilution ratio to urea-supplemented phage buffer was 1:20, the incubation was carried out for 2 h at 42 °C then 1 h at 4 °C, and LTA was omitted.

Mass spectrometry analysis of phage samples

To establish the identity of protein components, a virion sample treated with Turbonuclease was analyzed by 1D tricine 15% SDS-PAGE. Selected gel bands were excised and after destaining and washing, each gel area was incubated with trypsin. Liquid chromatography–tandem mass spectrometry (LC–MS/MS) analysis was performed using UltiMate 3000 RSLC system (Thermo Fisher Scientific) on-line coupled with Impact II Ultra-High Resolution Qq-Time-Of-Flight mass spectrometer (Bruker). Exported MS/MS spectra were analyzed in Proteome Discoverer 1.4 (Thermo Fisher Scientific) using in-house Mascot 2.6.2 (Matrixscience) search engine. Mascot MS/MS ion searches were done against *Staphylococcus* phage 812

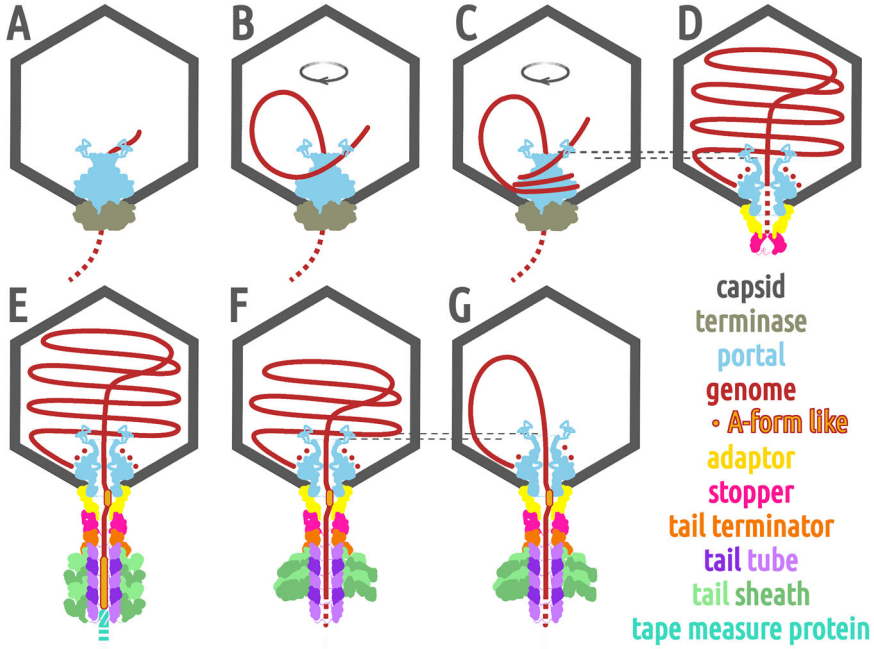

Fig. 8 | Functions of neck proteins in phage 812 genome packaging and ejection. Phage components are shown schematically, with capsid in dark gray, terminase in beige, portal in light blue, adaptor in gold, stopper in magenta, tail terminator in orange, tail tube in violet, tail sheath in light green, TMP in turquoise, and DNA in red. **A** Left DNA end inserted into the capsid interacts with the crown of the portal complex. **B**–**C** DNA binds to and loops around the wing domains of portal proteins, which directs coaxial spooling of the packaged genome. **D** The packaged genome compresses the portal crown, which could contribute to the termination of packaging and replacement of the terminase complex with adaptor and stopper complexes. Stopper gating loops in the closed conformation ensure genome retention. **E** When the tail binds to the neck, the stopper gating loops open and the genomic end descends into the tail tube. TMP and the A-form DNA inside the adaptor channel prevent the genome from further progress. **F** During genome ejection, a sequence-induced transition to A-form DNA inside the adaptor channel can pause the progress of the genome release. **G** In the last stage of genome ejection, the portal crown is lifted and the residual DNA from the left LTR remains anchored to the portal protein wing domains.

proteome (UniProt ID UP000203789) and GPM cRAP contaminant database (http://www.thegpm.org/crap/, version 2018-11-22).

Resequencing of phage 812 K1/420 genome

Considering the limitations of the 454-sequencing method used for the previous determination of the phage 812 K1/420 genome (GenBank acc. no. KJ206563.1), a hybrid approach with both short and long reads was used to determine the precise full-length genome sequence as packaged in the capsid.

The phage lysate was pelleted by high-speed centrifugation at 54,000 × g and resuspended in 400 µL of the phage buffer. One µL of DNase I (1U/µL; Thermo Scientific) and 1 µL of RNase A (10 mg/mL, New England BioLabs) were added, and the solution was incubated for 30 min at 37 °C. Next, 30 µL of 10% SDS and 10 µL of proteinase K (20 mg/mL; Sigma-Aldrich) were added, and the sample was incubated for 15 min at 55 °C. DNA was purified using Genomic DNA Clean & Concentrator-10 (ZymoResearch) according to the manufacturer's instructions for genomic DNA isolation (the addition of 2 volumes of ChIP DNA Binding Buffer to the DNA sample).

For Oxford Nanopore sequencing, the library was prepared using an SQK-LSK114 kit (Oxford Nanopore Technologies, UK) according to the manufacturer's instructions, using Long Fragment Buffer (LFB) in the washing step. The library was sequenced with a FLO-FLG114 flow cell in a MinION device (Oxford Nanopore Technologies). The device was controlled with the software MinKNOW v23.11.4 (Oxford Nanopore Technologies), which was also used for base-calling (Super-accurate model) and trimming.

For Illumina sequencing, a 500 bp sequencing library was prepared with an NEBNext Ultra II DNA library prep kit for Illumina (New England BioLabs). The samples were sequenced using a MID output cartridge in 150 bp paired-end mode on an Illumina NextSeq sequencing platform (Illumina, San Diego, CA, USA). The quality of sequencing reads was analyzed with FastQC v0.11.8[50]. Bases of lower quality (average quality below 20) and adaptors were trimmed using the sliding window model in Trimmomatic Galaxy v0.39[51].

The complete genome was obtained using hybrid assembly in Unicycler Galaxy v0.5.0[52]. Long terminal repeats were determined based on read coverage levels[2], and confirmed by long-read mapping in Geneious Prime v2025.0.3 using the Minimap2 v2.24 plugin (https://www.geneious.com). Genes were annotated using RAST[53], with manual inspection using NCBI BLAST[54], InterPro[55], and based on the results of this study (Table S2).

Independently, long-read sequencing was used to identify residual DNA in phage particles after genome ejection. The DNA isolation procedure was the same as above, using 400 µL of purified contracted viral particles in the phage buffer and the protocol of the Genomic DNA Clean & Concentrator-10 kit (ZymoResearch) for the isolation of PCR products/DNA fragments (addition of 5 volumes of ChIP DNA Binding Buffer to the DNA sample). The sequencing library was prepared as described above, using Short Fragment Buffer (SFB) in the washing step. The sequencing was performed on an Oxford Nanopore platform as described above. For subsequent analysis, remaining Oxford Nanopore adaptor sequences (Top strand: 5'-TTTTTTTTCCTGTACTTCGTTCAGTTACGTATTGCT-3'; Bottom strand: 5'-GCAATACGTAACTGAACGAAGTACAGG-3') were trimmed from sequencing reads using the BBDuk plug-in v38.84 (Geneious Prime v2025.0.3) with the following parameters: Kmer Length = 15, Maximum Substitutions = 1; Maximum Substitutions + INDELS = 1; Trim partial adaptors from ends with kmer length = 2. The trimmed reads with a maximum length corresponding to the LTR (8,484 bp, 93% of all reads) were mapped to the reference genome 812 K1/420 (KJ206563.2) using the Geneious mapper (Geneious Prime v2025.0.3) with the following parameters: Map multiple best matches: Randomly; Maximum Gaps Per Read: 15%; Maximum Gap Size: 50; Minimum Overlap Identity: 90%; Word Length: 12.

Cryo-electron microscopy

The phage sample (3.5–4.0 µL) was applied onto glow-discharged holey carbon-coated copper grids (Quantifoil R2/1, 200 or 300 mesh) and vitrified in liquid ethane using a Vitrobot Mark IV (Thermo Fisher Scientific). Cryo-EM data were collected on a Krios TEM (Thermo Fisher Scientific) operating at 300 kV. The beam was aligned for parallel illumination in NanoProbe mode, and coma-free alignments were performed to remove the residual beam tilt. The virion sample was acquired using a Falcon II detector (Thermo Fisher Scientific) in linear mode with 1 s exposure at a magnification of 75,000 ×, resulting in a pixel size of 1.061 Å. Genome release

intermediates with contracted tails were collected with SerialEM 3.7.14[56] using a K2 Summit detector (Gatan) equipped with an energy filter and the slit set to 20 eV. The data were collected with 7 s exposure at a magnification of 130,000 × in super-resolution counting mode, resulting in a non-super-resolution pixel size of 1.057 Å. Complete details of the acquisition process are listed in the Supplementary Information (Table S1).

Cryo-EM data processing

Dose-fractionated movies were aligned and dose-weighted using MotionCor2 1.4.0[57], and defocus estimation was performed using Gctf 1.0.6[58]. For phage virions, capsids were manually picked with EMAN2 *e2boxer*[59]. Capsids of genome release intermediates with contracted tails were automatically picked with Gautomatch 0.56[60] and virion-like capsids containing genome were removed by 2D classification in Relion 3.1[61]. Further removal of partially full capsids was performed by radially averaging capsid images using xmipp 3.0[62] and discarding images with the highest average inner capsid density calculated using R 4.1.2[63]. 3D refinement with imposed icosahedral symmetry was done with the Relion auto-refine procedure using phage 812 virion capsid (EMD-8304)[4] as an initial model. Neck vertices were identified by expanding the icosahedral symmetry of aligned capsids and subjecting them to 2D classifications in Relion with fixed orientations while applying a soft neck mask on the capsid vertex corresponding to the null in-plane angle. Neck sub-particles were extracted using a modified local extraction protocol[64] and refined applying C6 or C12 symmetries using a modified version of Relion that allows for a free rotational search while restricting the orientational search of tilt and psi angles. The post-processing of refined maps was performed in Relion. The pixel size of the dataset acquired on the Falcon II detector was adjusted to 1.080 Å during the post-processing step. Map resolution was estimated by Fourier shell correlation using the 0.143 threshold criterion. Local resolution estimation was performed by sampling the volume using a soft spherical mask 12.5 Å in diameter, then the map was low-pass filtered and B-factor sharpened during post-processing according to local resolution estimates. Asymmetric and symmetry-reducing reconstructions were achieved by symmetry-expanding the pre-aligned particle dataset and performing focused 3D classifications without orientational searches. For the reconstruction of the portal crown and the anchor DNA in genome release intermediates, the density of the capsid was subtracted from the particle images prior to sub-particle extraction. To compare reconstructions of portal tunnel loops in the virion and genome release intermediate, we performed automated B-factor sharpening[65] and detector MTF correction on each map in Relion, then applied a ΔB-factor of 179 Å2 and a low-pass filter with a 6 Å cut-off to the maps. Detailed workflow charts of the reconstruction steps are provided in the Supplementary Information (Fig. S1 and S14).

Model building and refinement in cryo-EM density

Protein main chains were traced in the reconstructed maps in Coot 0.9[66] and identified by comparison with structure predictions based on the primary sequence generated by RaptorX[67] or AlphaFold2[68]. The highest-ranking prediction models (for AlphaFold2 after force-field relaxation) were fitted into the maps and rebuilt in Coot. The models were refined iteratively using ISOLDE 1.4[69] and the Phenix 1.19[70] real space refinement protocol, and their quality was assessed by MolProbity 4.5.2[71] and the Phenix validation protocol (Tables S1 and S4). A circular pseudo-model of the anchor dsDNA was created in Coot, by generating a 10 bp random-sequence B-form DNA, performing restrained flexible fitting into the cryo-EM density, and extending the model 12-fold. The geometry of the DNA model was refined in the C12-symmetrized map in the presence of the portal complex using Phenix and validated using DNAtco 3.2[72]. The circular model was extended by 19 bp, then flexibly fitted to the asymmetric split-ring density in Coot. A random-sequence 63 bp-long pseudo-model of the neck channel dsDNA was generated using Web 3DNA 2.0[73] as an 11 bp-long A-form DNA flanked by B-form DNA regions, flexibly fitted to the asymmetric density in Coot, refined in Phenix in the presence of portal and adaptor dodecamers without applying symmetry operators, and validated by DNAtco. Simulated electron densities of ideal A- and B-form DNA were generated using xmipp from atomic models created in Coot.

Preparation of recombinant stopper protein gp97

The isolation of phage genomic DNA was performed by phenol/chloroform/isoamyl extraction[2,74]. The coding sequence for gp97 of phage 812 K1/420 was PCR-amplified from the phage DNA and inserted using ligation-independent cloning into a pET22T vector carrying N-terminal hexahistidine and SUMO Smt3 tags under the control of a T7 promoter, then introduced into an *E. coli* BL21(DE3) cell line (Novagen). The cells were grown in 1 L of autoinduction medium (ZYP-5052)[75] at 30 °C and 250 RPM until proliferation arrest, harvested by centrifugation (20 min at 3,000 × g), resuspended in 50 mM Tris pH 8.0, 150 mM NaCl, 1 mg/mL lysozyme, 0.5% n-octyl β-D-thioglucopyranoside, 125 U/mL Turbonuclease (Abnova), and lysed using EmulsiFlex-C3 (Avestin). The lysate was clarified by centrifugation (20 min at 21,000 × g, 10 °C) and filtration through a 0.45 µm membrane. The sample was then subjected to nickel affinity chromatography in a HisTrap HP column (GE Healthcare) equilibrated with 50 mM Tris pH 8.0, 150 mM NaCl, 20 mM imidazole buffer, and eluted with 350 mM imidazole buffer. The eluted fractions were buffer exchanged into 50 mM Tris pH 8.0, 100 mM NaCl in a HiPrep 26/10 Desalting column (GE Healthcare). After the cleavage of N-terminal tags by in-house produced Ulp1ac protease (at 4 °C overnight), the sample was loaded into a HisTrap column to remove the cleaved His_6-Smt3 tag. The untagged protein in the flowthrough was concentrated in Amicon® Ultra-15 centrifugal filter units (Merck) with a 10 kDa cut-off, and subjected to size exclusion chromatography (HiLoad 16/600 Superdex 200 pg column, GE Healthcare, calibrated using Cytiva LMW and HMW Gel Filtration Calibration kits). Fractions containing homogenous gp97 were pooled, concentrated to 3.3 mg/mL, and used for crystallization using the hanging drop vapor diffusion method by mixing the sample with 1.6 M NaCl, 8% PEG 6000, 20% glycerol, and 3% dextran sulfate sodium salt in a 1:2 ratio. The identity of the purified protein was verified by mass spectrometry prior to crystallization.

X-ray data collection, processing, and model building

The crystals were flash frozen in liquid nitrogen without additional cryoprotectant and used to collect X-ray diffraction data at 77 K at the PROXIMA-1 beamline at the Soleil synchrotron (France) using the Dectris Pilatus 6 M detector at 12.67 keV with an oscillation angle of 0.1°. The data were indexed and processed to a resolution of 2.2 Å in space group $P6_12_12_1$ using the XDS software package (version 2016-11-01)[76] and scaled and merged with CCP4 Suite 6.4 Aimless[77]. Further processing was carried out in CCP4 Suite 8.0[78]: phasing was performed in Phaser 2.8.3[79] using molecular replacement with segmented subdomains from an AlphaFold2 gp97 structural model, and the model was iteratively rebuilt in Coot 0.9[66] and refined in reciprocal space in RefMac5 5.8[80], and in real space in ISOLDE 1.4[69]. The data and model validation was carried out with Phenix 1.19 Xtriage[81] and MolProbity 4.5.2[71]. The hexameric state of gp97 was validated using PDBePISA 1.48[82], and the structural features of the metal-coordinating tetra-cysteine site were assessed using the CheckMyMetal tool[83]. Further details about data processing and validation are listed in the Supplementary Information (Table S6).

Bioinformatic analysis

A structural comparison of neck proteins against the full PDB database was carried out using the Dali server[84]. A structural homology query of the stopper gp97 tetra-cysteine motif was performed with HHpred[85] against the PDB70 database. A sequence similarity search with gp97 against non-redundant sequences of *Caudoviricetes* was done with NCBI PSI-BLAST[54] using the BLOSUM62 scoring matrix and default parameters. Representative species of *Herelleviridae* genera (Table S10) were selected according to the International Committee on Taxonomy of Viruses classification, a multiple sequence alignment of their stopper proteins was generated with Cobalt[86], and the consensus motifs were visualized as sequence logos[87].

Similarly, to analyze the conservation of positively charged residues on the portal wing surface, the protein sequence of portal gp91 was queried against *Herelleviridae* using PSI-BLAST, then a multiple sequence alignment of portals of *Herelleviridae* representative species was generated with MAFFT[88], and a guide tree using Phylo.io 1.0[89]. Secondary structure predictions of phage proteins were carried out with RaptorX-Property[90]. Structural predictions of portal monomers of five species spanning across *Herelleviridae* clusters were generated using AlphaFold2 and aligned to the structure of the phage 812 portal dodecamer. The electrostatic surface potential of atomic models was calculated with the UCSF ChimeraX 1.9[91] *coulombic* command, and the lipophilicity potential with the command *mlp*, using the default settings. Molecular interfaces were inspected with PDBePISA 1.48[82], and hydrogen bonds and salt bridges were annotated based on the intermolecular distance between donor and acceptor atom centers scoring below 4.0 Å[92]. DNA minor groove widths were measured as cross-strand P_i-to-P_{i+4} separations reduced by 2×2.9 Å, corresponding to two phosphate van der Waals radii[93]. A circular 120 bp-long dsDNA model refined in Phenix was used for the calculation of the minor groove width of the anchor DNA bound to the portal complex, and values were averaged over 10 bp repeats. To calculate the minor groove width of the neck channel DNA, an ideal B-form dsDNA spanning the channel from the adaptor β-hairpin tube to the stopper was fitted into the density and refined in real-space in Coot. Curvature and base pair inclination of the DNA were calculated using Curves + [94]. The estimation of hydrogen bond lengths between Lys138 NZ of the portal protein and minor groove base edges of the two closest base pairs of the anchor DNA was performed by placing the refined atomic model into the C12-symmetrized map, mutating the two base pairs to all 16 Watson-Crick nucleotide combinations, and running a short minimization for each in ISOLDE at 20 °C in an Amber14 force-field, repeating the process three times. Portal crown tilt in the genome release intermediate was measured by rigidly fitting two identical crown dodecamers (residues 437–507) into the C12-symmetrized and the asymmetric map using UCSF Chimera 1.15[95]. One dodecamer was then aligned on the second dodecamer by Matchmaker, and the reported transformation matrix was used to calculate pivot point, rotation axis and XZ plane rotation angle. Figures were generated in UCSF Chimera 1.15[95], UCSF ChimeraX 1.9[91], ACD/ChemSketch 2022.2.0[96], and R 4.1.2[63].

Statistics and reproducibility

Cryo-EM data were collected on two independent samples, with 30,553 resp. 15,371 acquired images. For resolution estimation of cryo-EM maps, particle datasets were randomly split into two subsets equal in size and reconstructed independently. DNA sequencing and subsequent analysis were performed using established workflows detailed in the Methods section. The DNA of the phage was sequenced using two independent samples and two different platforms. Using the built-in statistics in Geneious Prime v2025.0.3, the coverage of the consensus sequence of phage 812 strain K1/420 (KJ206563.2) was 607.0 × (SD 111.7) for Illumina sequencing reads (NCBI SRA ID SRR36294882), and 3,013.7 × (SD 2,318.2) for Oxford Nanopore sequencing reads (NCBI SRA ID SRR36291690). Residual DNA in empty capsids was analyzed using a set of 332,896 Oxford Nanopore sequencing reads (NCBI SRA ID SRR33751657).

Reporting summary

Further information on research design is available in the Nature Portfolio Reporting Summary linked to this article.

Data availability

The GenBank/ENA/DDBJ accession number of the phage 812 strain K1/420 genome is KJ206563.2. The whole-genome sequencing reads (NCBI BioSample ID SAMN53543416) and residual phage DNA sequencing reads (NCBI BioSample ID SAMN48784668) were deposited in the NCBI under the BioProject ID PRJNA1269267. Cryo-EM density maps are available in the Electron Microscopy Data Bank under accession IDs EMD-18048, EMD-18065, EMD-18213, EMD-18369, EMD-18372, EMD-18385, EMD-18395, EMD-18445, EMD-18462, EMD-18489, EMD-18516, EMD-18912, and EMD-18919. Atomic coordinates and X-ray structure factors are available in the Protein Data Bank under accession IDs 8Q01, 8Q1I, 8Q7D, 8QEM, 8QEK, 8QGR, 8QJE, 8QKH, 8R5G, and 8R69. Mass spectrometry data were deposited to the ProteomeXchange Consortium *via* PRIDE[97] partner repository under dataset identifier PXD071586. Unedited image of SDS-PAGE of phage 812 is included in Supplementary Information (Fig. S27). Numeric source data for plots are supplied as Supplementary Data 1, and processed mass spectrometry data of phage 812 as Supplementary Data 2. All other data are available from the corresponding author on reasonable request.

Received: 10 July 2025; Accepted: 22 December 2025;
Published online: 08 January 2026

References

1. McCallin, S., Sarker, S. A., Sultana, S., Oechslin, F. & Brüssow, H. Metagenome analysis of Russian and Georgian Pyophage cocktails and a placebo-controlled safety trial of single phage versus phage cocktail in healthy Staphylococcus aureus carriers. *Environ. Microbiol.* **20**, 3278–3293 (2018).
2. Botka, T. et al. Lytic and genomic properties of spontaneous host-range Kayvirus mutants prove their suitability for upgrading phage therapeutics against staphylococci. *Sci. Rep.* **9**, 5475 (2019).
3. Arroyo-Moreno, S. et al. Insights into gene transcriptional regulation of kayvirus bacteriophages obtained from therapeutic mixtures. *Viruses* **14**, 626 (2022).
4. Nováček, J. et al. Structure and genome release of Twort-like Myoviridae phage with a double-layered baseplate. *Proc. Natl. Acad. Sci. USA* **113**, 9351–9356 (2016).
5. Tavares, P., Zinn-Justin, S. & Orlova, E. V. Genome gating in tailed bacteriophage capsids. In *Viral Molecular Machines* (eds Rossmann, M. G. & Rao, V. B.) 585–600 (Springer US, 2012).
6. Chaban, Y. et al. Structural rearrangements in the phage head-to-tail interface during assembly and infection. *Proc. Natl. Acad. Sci. USA* **112**, 7009–7014 (2015).
7. Bárdy, P. et al. Structure and mechanism of DNA delivery of a gene transfer agent. *Nat. Commun.* **11**, 3034 (2020).
8. Orlov, I. et al. CryoEM structure and assembly mechanism of a bacterial virus genome gatekeeper. *Nat. Commun.* **13**, 7283 (2022).
9. Yang, F. et al. Fine structure and assembly pattern of a minimal myophage Pam3. *Proc. Natl. Acad. Sci. USA* **120**, e2213727120 (2023).
10. Li, F. et al. High-resolution cryo-EM structure of the Pseudomonas bacteriophage E217. *Nat. Commun.* **14**, 4052 (2023).
11. Hsiao, C. L. & Black, L. W. Head morphogenesis of bacteriophage T4 II. The role of gene 40 in initiating prehead assembly. *Virology* **91**, 15–25 (1978).
12. Prevelige, P. E. Jr, Thomas, D. & King, J. Nucleation and growth phases in the polymerization of coat and scaffolding subunits into icosahedral procapsid shells. *Biophys. J.* **64**, 824–835 (1993).
13. Sun, S. et al. The structure of the phage T4 DNA packaging motor suggests a mechanism dependent on electrostatic forces. *Cell* **135**, 1251–1262 (2008).
14. Daudén, M. I. et al. Large terminase conformational change induced by connector binding in bacteriophage T7. *J. Biol. Chem.* **288**, 16998–17007 (2013).
15. Woodson, M. et al. A viral genome packaging motor transitions between cyclic and helical symmetry to translocate dsDNA. *Sci. Adv.* **7**, eabc1955 (2021).
16. Ray, K., Ma, J., Oram, M., Lakowicz, J. R. & Black, L. W. Single-molecule and FRET fluorescence correlation spectroscopy analyses of phage DNA packaging: colocalization of packaged phage T4 DNA ends within the capsid. *J. Mol. Biol.* **395**, 1102–1113 (2010).

17. Orlova, E. V. et al. Structure of the 13-fold symmetric portal protein of bacteriophage SPP1. *Nat. Struct. Biol.* **6**, 842–846 (1999).
18. Lokareddy, R. K. et al. Portal protein functions akin to a DNA-sensor that couples genome-packaging to icosahedral capsid maturation. *Nat. Commun.* **8**, 14310 (2017).
19. Casjens, S. R. Bacteriophage lambda FII gene protein: Role in head assembly. *J. Mol. Biol.* **90**, 1–20 (1974).
20. Lhuillier, S. et al. Structure of bacteriophage SPP1 head-to-tail connection reveals mechanism for viral DNA gating. *Proc. Natl. Acad. Sci. UAE* **106**, 8507–8512 (2009).
21. Kizziah, J. L., Mukherjee, A., Parker, L. K. & Dokland, T. Structure of the Staphylococcus aureus bacteriophage 80α neck shows details of the DNA, tail completion protein, and tape measure protein. *Structure* **33**, 1063–1073.e2 (2025).
22. Gu, Z., Wu, K. & Wang, J. Structural morphing in the viral portal vertex of bacteriophage lambda. *J. Virol.* **98**, e00068–24 (2024).
23. Liu, Y.-T., Jih, J., Dai, X., Bi, G.-Q. & Zhou, Z. H. Cryo-EM structures of herpes simplex virus type 1 portal vertex and packaged genome. *Nature* **570**, 257–261 (2019).
24. Ayala, R. et al. Nearly complete structure of bacteriophage DT57C reveals architecture of head-to-tail interface and lateral tail fibers. *Nat. Commun.* **14**, 8205 (2023).
25. Iglesias, S. M. et al. Cryo-EM analysis of Pseudomonas phage Pa193 structural components. *Commun. Biol.* **7**, 1275 (2024).
26. Li, X. et al. Cryo-EM Reveals structural diversity in prolate-headed mycobacteriophage Mycofy1. *J. Mol. Biol.* **437**, 169126 (2025).
27. Leiman, P. G. & Shneider, M. M. Contractile tail machines of bacteriophages. In *Viral Molecular Machines* (eds Rossmann, M. G. & Rao, V. B.) 93–114 (Springer US, Boston, MA, 2012).
28. Sinden, R. R., Pearson, C. E., Potaman, V. N. & Ussery, D. W. DNA: structure and function. In *Advances in Genome Biology* (eds. Verma, R. S.) 1–141 (Elsevier, 1998).
29. Łobocka, M. et al. Chapter 5 - Genomics of staphylococcal twort-like phages - potential therapeutics of the post-antibiotic era. In *Advances in Virus Research* (eds Łobocka, M. & Szybalski, W.) 143–216 (Academic Press, 2012).
30. Arsuaga, J., Vázquez, M., Trigueros, S., Sumners, D. W. & Roca, J. Knotting probability of DNA molecules confined in restricted volumes: DNA knotting in phage capsids. *Proc. Natl. Acad. Sci. USA* **99**, 5373–5377 (2002).
31. Guasch, A. et al. Detailed architecture of a DNA translocating machine: the high-resolution structure of the bacteriophage φ29 connector particle. *J. Mol. Biol.* **315**, 663–676 (2002).
32. Sun, L. et al. Cryo-EM structure of the bacteriophage T4 portal protein assembly at near-atomic resolution. *Nat. Commun.* **6**, 7548 (2015).
33. Kulkarni, M. & Mukherjee, A. Sequence dependent free energy profiles of localized B-to A-form transition of DNA in water. *J. Chem. Phys.* **139**, 10B617_1 (2013).
34. Tolstorukov, M. Y., Jernigan, R. L. & Zhurkin, V. B. Protein–DNA Hydrophobic Recognition in the Minor Groove is Facilitated by Sugar Switching. *J. Mol. Biol.* **337**, 65–76 (2004).
35. Mirzabekov, A. D. & Rich, A. Asymmetric lateral distribution of unshielded phosphate groups in nucleosomal DNA and its role in DNA bending. *Proc. Natl. Acad. Sci. USA* **76**, 1118–1121 (1979).
36. Shui, X., McFail-Isom, L., Hu, G. G. & Williams, L. D. The B-DNA Dodecamer at high resolution reveals a spine of water on sodium. *Biochemistry* **37**, 8341–8355 (1998).
37. Hancock, S. P., Hiller, D. A., Perona, J. J. & Jen-Jacobson, L. The energetic contribution of induced electrostatic asymmetry to dna bending by a site-specific protein. *J. Mol. Biol.* **406**, 285–312 (2011).
38. Minchenkova, L. E., Schyolkina, A. K., Chernov, B. K. & Ivanov, V. I. CC/GG contacts facilitate the B to A transition of DMA in solution. *J. Biomol. Struct. Dyn.* **4**, 463–476 (1986).
39. Tang, J. et al. DNA poised for release in bacteriophage ø29. *Structure* **16**, 935–943 (2008).
40. Xu, J., Wang, D., Gui, M. & Xiang, Y. Structural assembly of the tailed bacteriophage ϕ29. *Nat. Commun.* **10**, 2366 (2019).
41. Lanni, Y. T. First-step-transfer deoxyribonucleic acid of bacteriophage T5. *Bacteriol. Rev.* **32**, 227–242 (1968).
42. de Frutos, M., Letellier, L. & Raspaud, E. DNA Ejection from bacteriophage T5: analysis of the kinetics and energetics. *Biophys. J.* **88**, 1364–1370 (2005).
43. Molineux, I. J. & Panja, D. Popping the cork: mechanisms of phage genome ejection. *Nat. Rev. Microbiol.* **11**, 194–204 (2013).
44. Chen, Y.-J. et al. Two-stage dynamics of in vivo bacteriophage genome ejection. *Phys. Rev. X* **8**, 021029 (2018).
45. Katsura, I. & Hendrix, R. W. Length determination in bacteriophage lambda tails. *Cell* **39**, 691–698 (1984).
46. Hendrix, R. W. & Casjens, S. R. Protein cleavage in bacteriophage λ tail assembly. *Virology* **61**, 156–159 (1974).
47. Xu, J., Hendrix, R. W. & Duda, R. L. Chaperone–protein interactions that mediate assembly of the bacteriophage lambda tail to the correct length. *J. Mol. Biol.* **426**, 1004–1018 (2014).
48. Seul, A. et al. Biogenesis of a bacteriophage long non-contractile tail. *J. Mol. Biol.* **433**, 167112 (2021).
49. Kizziah, J. L., Manning, K. A., Dearborn, A. D. & Dokland, T. Structure of the host cell recognition and penetration machinery of a Staphylococcus aureus bacteriophage. *PLoS Pathog.* **16**, e1008314 (2020).
50. Wingett, S. W. & Andrews, S. FastQ Screen: A tool for multi-genome mapping and quality control. *F1000Research* **7**, 1338 (2018).
51. Bolger, A. M., Lohse, M. & Usadel, B. Trimmomatic: a flexible trimmer for Illumina sequence data. *Bioinformatics* **30**, 2114–2120 (2014).
52. Wick, R. R., Judd, L. M., Gorrie, C. L. & Holt, K. E. Unicycler: Resolving bacterial genome assemblies from short and long sequencing reads. *PLoS Comput. Biol.* **13**, e1005595 (2017).
53. Brettin, T. et al. RASTtk: A modular and extensible implementation of the RAST algorithm for building custom annotation pipelines and annotating batches of genomes. *Sci. Rep.* **5**, 8365 (2015).
54. NCBI Resource Coordinators Database resources of the national center for biotechnology information. *Nucleic Acids Res.* **41**, D8–D20 (2013).
55. Mitchell, A. L. et al. InterPro in 2019: improving coverage, classification and access to protein sequence annotations. *Nucleic Acids Res.* **47**, D351–D360 (2019).
56. Mastronarde, D. N. Automated electron microscope tomography using robust prediction of specimen movements. *J. Struct. Biol.* **152**, 36–51 (2005).
57. Zheng, S. Q. et al. MotionCor2: anisotropic correction of beam-induced motion for improved cryo-electron microscopy. *Nat. Methods* **14**, 331–332 (2017).
58. Zhang, K. Gctf: Real-time CTF determination and correction. *J. Struct. Biol.* **193**, 1–12 (2016).
59. Tang, G. et al. EMAN2: An extensible image processing suite for electron microscopy. *J. Struct. Biol.* **157**, 38–46 (2007).
60. Zhang, K. Gautomatch. *MRC Laboratory of Molecular Biology*. https://www2.mrc-lmb.cam.ac.uk/ (2020).
61. Scheres, S. H. W. A bayesian view on cryo-EM structure determination. *J. Mol. Biol.* **415**, 406–418 (2012).
62. de la Rosa-Trevín, J. M. et al. Xmipp 3.0: An improved software suite for image processing in electron microscopy. *J. Struct. Biol.* **184**, 321–328 (2013).
63. R Core Team. *R: A Language and Environment for Statistical Computing*. (R Foundation for Statistical Computing, Vienna, Austria, 2022).
64. Ilca, S. L. et al. Localized reconstruction of subunits from electron cryomicroscopy images of macromolecular complexes. *Nat. Commun.* **6**, 8843 (2015).

65. Rosenthal, P. B. & Henderson, R. Optimal determination of particle orientation, absolute hand, and contrast loss in single-particle electron cryomicroscopy. *J. Mol. Biol.* **333**, 721–745 (2003).
66. Emsley, P., Lohkamp, B., Scott, W. G. & Cowtan, K. D. Features and development of Coot. *Acta Crystallogr. Sect. D* **66**, 486–501 (2010).
67. Wang, S., Sun, S., Li, Z., Zhang, R. & Xu, J. Accurate de novo prediction of protein contact map by ultra-deep learning model. *PLoS Comput. Biol.* **13**, e1005324 (2017).
68. Jumper, J. et al. Highly accurate protein structure prediction with AlphaFold. *Nature* **596**, 583–589 (2021).
69. Croll, T. I. ISOLDE: a physically realistic environment for model building into low-resolution electron-density maps. *Acta Crystallogr. Sect. D* **74**, 519–530 (2018).
70. Liebschner, D. et al. Macromolecular structure determination using X-rays, neutrons and electrons: recent developments in Phenix. *Acta Crystallogr. Sect. D* **75**, 861–877 (2019).
71. Williams, C. J. et al. MolProbity: More and better reference data for improved all-atom structure validation. *Protein Sci.* **27**, 293–315 (2018).
72. Černý, J. et al. Structural alphabets for conformational analysis of nucleic acids available at dnatco.datmos.org. *Acta Crystallogr. Sect. D* **76**, 805–813 (2020).
73. Li, S., Olson, W. K. & Lu, X.-J. Web 3DNA 2.0 for the analysis, visualization, and modeling of 3D nucleic acid structures. *Nucleic Acids Res.* **47**, W26–W34 (2019).
74. Sambrook, J. E., Fritsch, E. F. & Maniatis, T. *Molecular Cloning: A Laboratory Manual*. (Cold Spring Harbor Laboratory Press, Cold Spring Harbor, NY, 1989).
75. Studier, F. W. Protein production by auto-induction in high-density shaking cultures. *Protein Expr. Purif.* **41**, 207–234 (2005).
76. Kabsch, W. XDS. *Acta Crystallogr. D Biol. Crystallogr.* **66**, 125–132 (2010).
77. Evans, P. R. & Murshudov, G. N. How good are my data and what is the resolution? *Acta Crystallogr. Sect. D* **69**, 1204–1214 (2013).
78. Winn, M. D. et al. Overview of the CCP4 suite and current developments. *Acta Crystallogr. Sect. D* **67**, 235–242 (2011).
79. McCoy, A. J. et al. Phaser crystallographic software. *J. Appl. Crystallogr.* **40**, 658–674 (2007).
80. Murshudov, G. N. et al. REFMAC5 for the refinement of macromolecular crystal structures. *Acta Crystallogr. Sect. D* **67**, 355–367 (2011).
81. Zwart, P., Grosse-Kunstleve, R. W. & Adams, P. *Xtriage and Fest: Automatic Assessment Of X-ray Data And Substructure Structure Factor Estimation*. www:https://cci.lbl.gov (2005).
82. Krissinel, E. & Henrick, K. Inference of Macromolecular Assemblies from Crystalline State. *J. Mol. Biol.* **372**, 774–797 (2007).
83. Zheng, H. et al. CheckMyMetal: a macromolecular metal-binding validation tool. *Acta Crystallogr. Sect. D* **73**, 223–233 (2017).
84. Holm, L. Dali server: structural unification of protein families. *Nucleic Acids Res.* **50**, W210–W215 (2022).
85. Hildebrand, A., Remmert, M., Biegert, A. & Söding, J. Fast and accurate automatic structure prediction with HHpred. *Proteins Struct. Funct. Bioinforma.* **77**, 128–132 (2009).
86. Papadopoulos, J. S. & Agarwala, R. COBALT: constraint-based alignment tool for multiple protein sequences. *Bioinformatics* **23**, 1073–1079 (2007).
87. Crooks, G., Hon, G., Chandonia, J.-M. & Brenner, S. WebLogo: a sequence logo generator. *Genome Res.* **14**, 1188–1190 (2004).
88. Katoh, K., Rozewicki, J. & Yamada, K. D. MAFFT online service: multiple sequence alignment, interactive sequence choice and visualization. *Brief. Bioinform.* **20**, 1160–1166 (2019).
89. Robinson, O., Dylus, D. & Dessimoz, C. Phylo.io: Interactive viewing and comparison of large phylogenetic trees on the web. *Mol. Biol. Evol.* **33**, 2163–2166 (2016).
90. Wang, S., Li, W., Liu, S. & Xu, J. RaptorX-Property: a web server for protein structure property prediction. *Nucleic Acids Res.* **44**, W430–W435 (2016).
91. Pettersen, E. F. et al. UCSF ChimeraX: Structure visualization for researchers, educators, and developers. *Protein Sci.* **30**, 70–82 (2021).
92. Barlow, D. J. & Thornton, J. M. Ion-pairs in proteins. *J. Mol. Biol.* **168**, 867–885 (1983).
93. Laughton, C. & Luisi, B. The mechanics of minor groove width variation in DNA, and its implications for the accommodation of ligands. *J. Mol. Biol.* **288**, 953–963 (1999).
94. Blanchet, C., Pasi, M., Zakrzewska, K. & Lavery, R. CURVES+ web server for analyzing and visualizing the helical, backbone and groove parameters of nucleic acid structures. *Nucleic Acids Res.* **39**, W68–W73 (2011).
95. Pettersen, E. F. et al. UCSF Chimera—a visualization system for exploratory research and analysis. *J. Comput. Chem.* **25**, 1605–1612 (2004).
96. ACD/ChemSketch. *ACD/Labs*. https://www.acdlabs.com/resource/acd-labs-releases-v2022-software-update/ (2022).
97. Perez-Riverol, Y. et al. The PRIDE database at 20 years: 2025 update. *Nucleic Acids Res.* **53**, D543–D553 (2025).

Acknowledgements

We gratefully acknowledge the Cryo-electron Microscopy and Tomography Core Facility and Proteomics Core Facility of the CEITEC MU of CIISB, Instruct-CZ Centre, supported by the Ministry of Education, Youth and Sports of the Czech Republic (MEYS CR) infrastructure project LM2023042, and the European Regional Development Fund - Projects "UP CIISB" (No. CZ.02.1.01/0.0/0.0/18_046/0015974) and "Innovation of Czech Infrastructure for Integrative Structural Biology" (No. CZ.02.01.01/00/23_015/0008175). Computational resources were provided by the e-INFRA CZ project (ID: 90254), supported by MEYS CR. This work was supported by the project National Institute of Virology and Bacteriology (Programme EXCELES, ID Project No. LX22NPO5103) - Funded by the European Union - Next Generation EU, and the project New Technologies for Translational Research in Pharmaceutical Sciences / NETPHARM, project ID OP JAC CZ.02.01.01/00/22_008/0004607, which is co-funded by the European Union. This work also received funding from ERC Consolidator Grant No. 101043452 to P.P., and from the Ministry of Health of the Czech Republic in cooperation with the Czech Health Research Council under project No. NU21J-05–00035 to T.B.

Author contributions

M.B., M.S., Z.C. and P.B. purified the phage samples. Z.C., J.N. and M.S. performed cryo-EM data collection and processing, and Z.C. and T.F. performed cryo-EM data analysis. B.P. cloned, purified, and crystallized the stopper protein. B.P. and P.P. collected and processed crystallographic data. Z.C. carried out X-ray data analysis, X-ray and cryo-EM structural determination, deposition of atomic coordinates and maps, bioinformatic analysis and figure preparation. T.B. performed the sequencing and assembly of the phage 812 genome, and sequencing and analysis of residual capsid DNA after genome ejection. T.B. and R.P. performed the genome annotation. P.P. and R.P. designed and supervised the research. Z.C. and P.P. wrote the manuscript. All authors participated in critical reading of the manuscript and approved the final version.

Competing interests

The authors declare no competing interests.

Additional information

Supplementary information The online version contains supplementary material available at https://doi.org/10.1038/s42003-025-09477-8.

Correspondence and requests for materials should be addressed to Pavel Plevka.

Peer review information *Communications Biology* thanks the anonymous reviewers for their contribution to the peer review of this work. Primary Handling Editors: Robert Kingsley and Mengtan Xing. A peer review file is available.

Reprints and permissions information is available at http://www.nature.com/reprints

Publisher's note Springer Nature remains neutral with regard to jurisdictional claims in published maps and institutional affiliations.

Open Access This article is licensed under a Creative Commons Attribution 4.0 International License, which permits use, sharing, adaptation, distribution and reproduction in any medium or format, as long as you give appropriate credit to the original author(s) and the source, provide a link to the Creative Commons licence, and indicate if changes were made. The images or other third party material in this article are included in the article's Creative Commons licence, unless indicated otherwise in a credit line to the material. If material is not included in the article's Creative Commons licence and your intended use is not permitted by statutory regulation or exceeds the permitted use, you will need to obtain permission directly from the copyright holder. To view a copy of this licence, visit http://creativecommons.org/licenses/by/4.0/.

© The Author(s) 2026

APPENDIX 5

Botka T, Smetanová S, Vinco A, Kučerová E, Rovňáková K, Siváková A, Mašlaňová I, Pantůček R (2025) Virion content unpacked by long-read sequencing: stress-induced changes in transmitted staphylococcal mobilome due to phage-satellite interactions. *Nucleic Acids Research* 53:gkaf1165. https://doi.org/10.1093/nar/gkaf1165
(JCR 2025: IF = 15; D1 – Biochemistry & Molecular Biology)

CC BY 4.0

Nucleic Acids Research, 2025, **53**, gkaf1165
https://doi.org/10.1093/nar/gkaf1165
Molecular and Structural Biology

Virion content unpacked by long-read sequencing: stress-induced changes in transmitted staphylococcal mobilome due to phage-satellite interactions

Tibor Botka[1], Soňa Smetanová[1,2], Adam Vinco[1], Eliška Kučerová[1], Kristína Rovňáková[1], Alena Siváková[3], Ivana Mašlaňová[1], Roman Pantůček[1,*]

[1]Department of Experimental Biology, Faculty of Science, Masaryk University, Brno 625 00, Czech Republic
[2]RECETOX, Faculty of Science, Masaryk University, Brno 625 00, Czech Republic
[3]Department of Microbiology, St Anne's University Hospital and Faculty of Medicine, Masaryk University, Brno 625 00, Czech Republic
*To whom correspondence should be addressed. Email: pantucek@sci.muni.cz

Abstract

The evolution of the virulence and antibiotic resistance of staphylococci, important opportunistic pathogens, is strongly determined by their mobilome, which can spread by phage virions or small-headed particles resulting from the hijacking of helper phage machinery by phage satellites named phage-inducible chromosomal islands (PICIs). Despite known mechanisms of the formation of transducing particles, it has not yet been possible to analyze their DNA content at the single-virion level. Using the *Staphylococcus epidermidis* model and long-read nanopore sequencing, we determined the sequence structure and ratio of phage and PICI genophores, plasmid, and bacterial DNA packaged in normal and small-headed virions. It was shown that the ratios vary mainly depending on the helper phage and the antimicrobial used for induction. When the effect of a strictly lytic phage and its combination with ciprofloxacin on a packaged mobilome was analyzed, no significant increase in mobilome dissemination was observed compared to antibiotics alone. Here, we demonstrate a novel approach for the analysis of transduced bacterial mobilome and show *in vitro* that lytic phage-based therapeutic strategies do not increase the risk of mobile genetic element transfer.

Graphical abstract

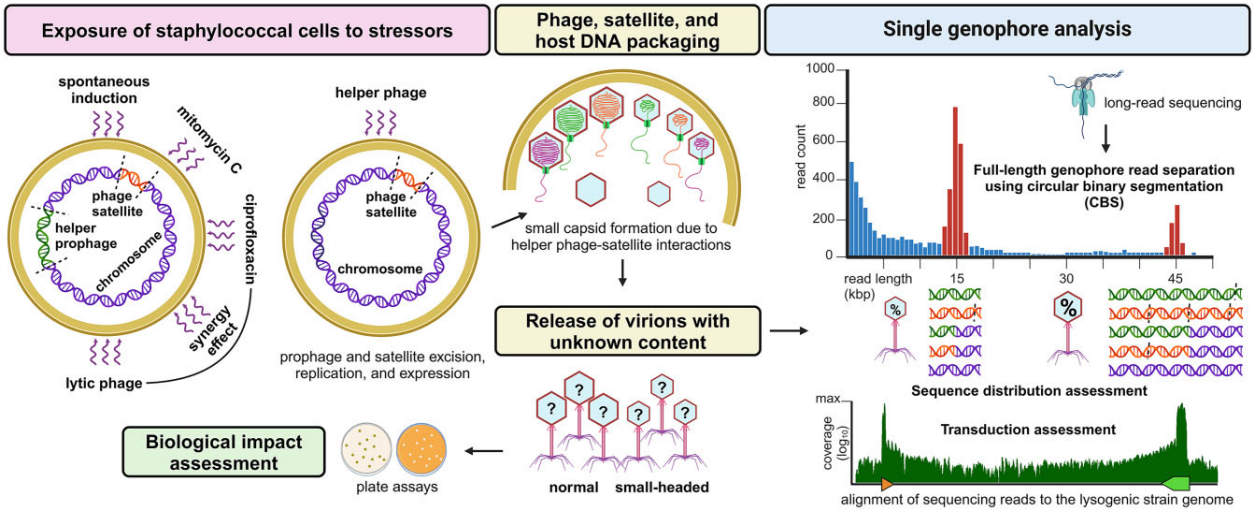

Introduction

Staphylococcal infections pose a serious problem in hospitalized patients, especially when complicated by antibiotic resistance [1, 2]. While *Staphylococcus aureus* is a known coagulase-positive opportunistic pathogen, coagulase-negative *Staphylococcus epidermidis* has been assumed to be a common human commensal, part of normal skin microbiota [3]. However, even *S. epidermidis* has recently become an increasing contributor to nosocomial infections [4] that can be complicated by increasing invasivity [5] and biofilm formation [2]. The evolution of staphylococci is significantly driven by the acquisition of mobile genetic elements (MGEs), a source of pathogenicity-associated genes that can spread by intra- and interspecies horizontal gene transfer, lead-

Received: February 21, 2025. **Revised:** September 26, 2025. **Accepted:** September 29, 2025
© The Author(s) 2025. Published by Oxford University Press.
This is an Open Access article distributed under the terms of the Creative Commons Attribution License (https://creativecommons.org/licenses/by/4.0/), which permits unrestricted reuse, distribution, and reproduction in any medium, provided the original work is properly cited.

Downloaded from https://academic.oup.com/nar/article/53/20/gkaf1165/8317317 by Masarykova Univerzita user on 04 February 2026

ing to the emergence and evolution of drug-resistant strains [6, 7].

Temperate phages often carry accessory genes that increase the virulence of lysogenic hosts [8–11] and can mediate generalized or specialized transduction [12–14]. In *S. aureus* prophages, lateral transduction was discovered [15] when the packaging was initiated from the prophage *pac* site before the prophage excision. The packaging via a headful mechanism then continues by encapsidating the adjacent bacterial DNA up to hundreds of kilobases downstream from the prophage sequence [16].

Prophage excision can be triggered by SOS response-inducing antimicrobials or phage infection [17, 18], causing the subsequent spread of phage genome and accessory genes in the environment by lysogenic conversion [19] or by the acquisition of transduced MGE [12, 20–24]. This process can lead to the emergence of bacterial strains that are resistant to the applied therapy. Therefore, in the context of mobilome induction, the safety of all therapeutic approaches, including phage therapy (which is experiencing increased interest), should be considered.

Besides common MGEs such as plasmids and prophages, a family of phage-inducible chromosomal islands (PICIs), which frequently harbor genes for virulence and resistance factors [25–27], can be mobilized by helper phages [28]. Their mobilization can be associated with helper phage capsid remodeling, which results in the formation of small-headed virions [13, 29, 30]. This causes a reduction in phage spread in the host population due to a decreased number of virions carrying the phage genome and the fact that small-headed particles are unable to carry the entire phage genome, so infection by such a virion does not lead to productive phage infection [31, 32].

Since PICIs employ the same mechanism of DNA packaging as helper phages, they can mediate generalized [33] and lateral transduction [34]. As the phage terminase small subunit (TerS) and the PICI TerS recognize different *pac* sequences, PICIs expand the transduction repertoire of phages.

Previous studies have assessed transduction by quantifying the frequency of successfully transduced elements carrying selection markers, particularly antibiotic resistance genes, using the plaque-forming units titer [13, 24, 35], which does not reflect particles carrying non-phage DNA and biases the estimation of the transduction dynamics. Moreover, such traditional approaches are inherently limited as they overlook the broader spectrum of MGEs that can be transduced and focus only on the final step of transduction, which may be influenced by host anti-MGE mechanisms, both inhibitory [36, 37] and promotive [38]. Consequently, these methods used alone fail to provide a comprehensive view of the mobilome dynamics and the true extent of horizontal gene transfer.

Here we introduce a novel, sequencing-based approach that overcomes these limitations by directly identifying and quantifying full-length genophores packaged in individual virions, including both normal and small-headed particles modified by PICIs. Using a single-genophore resolution, we analyze the packaging mechanisms and distribution of phage, PICI, plasmid, and chromosomal DNA under different stress factors. Notably, the study demonstrates that *in vitro* treatment combining lytic phage and antibiotics does not increase the risk of MGE spread compared to antibiotics alone, providing important insights into the safety of phage-based therapy.

Materials and methods

Biological resources

Two helper *S. epidermidis* siphophages were used: phage 48 [39] and phage E72m5 (in this study). Phage 48 was propagated on *S. epidermidis* strain SE48 [39], and phage E72m5 on *S. epidermidis* strain 1457 [40]. Phage 812h1 [41] of the *Kayvirus* genus was used to assess the effect of phage-based therapy on transduction compared to antibiotic treatment. All bacterial strains used in this study are listed in Table 1.

Lysogenization of *S. epidermidis* strains was performed as described previously [8]. Genome editing was performed using the plasmid pIMAY, as described previously [42]. The sequences for homologous recombination were amplified using the primers listed in Supplementary Table 1. For the deletion of prophage 1457 from strain 1457 (pos. 1 793 020–1 835 461 bp in GenBank reference genome CP020463.1), pIMAY and the insert were cleaved using *SalI*-HF and *XmaI* (New England Biolabs, USA) and ligated using the Quick Ligation Kit (New England Biolabs), obtaining strain 1457c.

Strain 1457LA_ermC was prepared by replacement of a part of the $SeCI_{SE48}$ sequence in position 889 868–891 129 bp of the strain 1457LA genome (CP180177.1) by an *ermC* cassette from pCN51 vector (KR781468, pos. 2101–3361 bp) [43] of the same size. The *ermC* gene and the homologous arms were assembled with the linearized vector using NEBuilder HiFi DNA Assembly Master Mix (New England Biolabs). In both cases, the obtained constructs were transformed into *Escherichia coli* DC10B and verified using the Sanger sequencing service (Eurofins Genomics, Germany). The corresponding construct was then electroporated into strain 1457 for deletion of prophage 1457 and 1457LA for size-conserved insertion of the *ermC* gene.

Preparation of phage lysates, phage enumeration, and efficiency of plating determination

The high-titer phage lysates were prepared using phages and their propagation strains in meat-peptone broth (MPB) prepared from 13 g of nutrient broth (Oxoid, UK), 3 g yeast extract (Oxoid), 5 g peptone (Oxoid), and distilled water to a final volume of 1 l (pH 7.4), and supplemented with $CaCl_2$ to a final concentration of 2 mM. The input ratio (IR or MOI_{INPUT}) of phages was 0.1. Bacterial debris was removed by centrifugation at 3100 × *g* for 30 min, and supernatants were filtered using a polyethersulfone membrane filter with a pore size of 0.45 μm (TPP, Switzerland).

For phage titer determination by the double-layer agar (DLA) method, respective dilutions of phage lysates were mixed with overnight bacterial cultures and soft 0.7% meat-pepton agar (MPA) with the addition of $CaCl_2$ to a final concentration of 2 mM. MPA (1.5%) plates were overlayed with this suspension and incubated at 37°C overnight. The number of plaque-forming units per milliliter (PFU/ml) was assessed as the mean of three technical replicates for each dilution. The efficiency of plating was calculated as the ratio of titers obtained on the strains of interest.

Transmission electron microscopy

For electron microscopy, virions were purified in a CsCl density gradient [44] and then diluted to an A_{280} of 0.5–1.0. Negatively stained samples were prepared by applying 4 μl of the diluted sample onto copper grids coated with a 12-nm carbon

Downloaded from https://academic.oup.com/nar/article/53/20/gkaf1165/8317317 by Masarykova Univerzita user on 04 February 2026

Table 1. Properties and use of *S. epidermidis* and other staphylococcal strains in this study.

Strain	MGE content			Properties and use	Reference
	$SeCI_{SE48}$	Prophage	Plasmid		
SE48	YES	NO	pSE48_1, pSE48_2	Propagation strain for phage 48; infection system with phage 48	Dean *et al.* [39]
SE48L	YES	48	pSE48_1, pSE48_2	Lysogen of strain SE48; used in induction systems	This study
1457	NO	1457	p1457	Propagation strain for phage E72m5; sensitive to phage 812h1	Galac *et al.* [40]
1457($SeCI_{SE48}$+)	YES	1457	p1457	Infection system with phage E72m5	Fišarová *et al.* [13]
1457LA	YES	E72m5	p1457	Used in induction systems	This study
1457LA_ermC	YES[a]	E72m5	p1457	Used for transduction experiments with erythromycin selection	This study
1457c	NO	NO	p1457	Cured for prophage 1457; control infection system with phage E72m5	This study
S. aureus 1137	NO	NO	NO	Propagation strain for phage 812h1; resistant to phage E72m5	AUMED s.r.o., Czechia
S. cohnii A6C	NO	NO	2.7-kb	Sensitive to phage E72m5; resistant to phage 812h1	Dean *et al.* [39]

[a]$SeCI_{SE48}$ with the incorporated *ermC* gene. GenBank acc. nos. of listed strains: SE48 (CP066303), SE48L (CP180175), 1457 (CP020463), 1457($SeCI_{SE48}$+) (CP180176), 1457LA (CP180177), 1457LA_ermC (CP194848), and 1457c (CP180178). GenBank acc. nos. of listed MGEs: $SeCI_{SE48}$ (MW368309); prophages 48 (MW364972), 1457 (CP020463), and E72m5 (PV036961); plasmids pSE48_1 (CP066304), pSE48_2 (CP066305), and p1457 (CP020462).

layer and stained with 2% uranyl acetate. Samples were observed using a Tecnai F20 electron microscope (Thermo Fisher Scientific, USA) operated at 200 kV with ×50 000 magnification.

Minimum inhibitory concentration of antimicrobials and induction efficiency determination

Antimicrobial susceptibility testing was performed using the broth microdilution method (Trios, Czechia) in accordance with ISO standard 20776–1:2019. The minimum inhibitory concentration (MIC) of gentamicin, oxacillin, and ciprofloxacin was interpreted in accordance with EUCAST guidelines (version 14.0, 2024) [45]. Methicillin-resistant *S. aureus* ATCC 43300 was used as a control strain. MIC of mitomycin C (SERVA Electrophoresis GmbH, Germany) was assessed as a concentration that fully inhibited bacterial growth after 18 h of incubation at 37°C. The induction of prophages by these antimicrobials was evaluated using a drop plaque assay with overnight incubation at 37°C of the lysates obtained using 1.0×, 0.75×, and 0.5× MIC of the respective antibiotics and 2 mg/l of the final concentration of mitomycin C (4× MIC for strain SE48L and 8× MIC for 1457LA). The number of PFU/ml was assessed by the DLA method as the mean of three technical replicates.

Adsorption assay

An overnight culture of the strain 1457LA was inoculated into fresh MPB and cultivated with aeration at 37°C to an OD_{600} = 0.6 (≈ 10^8 CFU/ml). The culture was mixed with 812h1 phage lysate (IR = 10) and $CaCl_2$ to a final concentration of 2 mM and cultivated at 37°C with aeration. Samples were taken at 0, 2, 5, 10, 15, and 20 min after inoculation. For adsorption assay of phage E72m5 on strains 1457 and A6C (IR = 0.5), brain heart infusion (BHI) broth (Oxoid), OD_{600} = 1.9–2.0 (≈ 1 × 10^9 CFU/ml), $CaCl_2$ final concentration of 4 mM, and sampling at 0, 2, 5, 10, 20, and 30 min were used to follow the same conditions as used in the transduction assays. The percentage of free virions in the supernatant after cell pelleting at 9700 × *g* for 2 min was determined using the DLA method in three technical replicates.

Preparation of induced phage lysates

Induced lysates were prepared using 500 ml of fresh bacterial cultures in MPB grown to OD_{600} = 0.25 and 2 mg/l of the final concentration of mitomycin C or 1× MIC of ciprofloxacin. After incubation at 37°C for 2 h with gentle aeration (80 rpm), the cultures were stored in the dark, statically, at room temperature overnight. Spontaneously induced lysates were prepared from 1 l of bacterial culture without the addition of an inducing agent. Bacterial debris was removed by centrifugation at 3100 × *g* for 30 min, and supernatants were filtered using a polyethersulfone membrane filter with a pore size of 0.22 μm (TPP, Switzerland).

Treatment of strain 1457LA with a lytic *Kayvirus* phage

A shaken overnight culture of strain 1457LA was inoculated into 100 ml of fresh MPB and cultured to OD_{600} ≈ 0.25. Phage 812h1 (IR = 10 or 100) or phage 812h1 and 1× MIC of ciprofloxacin were added. This was followed by incubation with gentle shaking (80 rpm) at 37°C for 2 h. Lysis was finalized in the dark, statically, at room temperature overnight. Bacterial debris was filtered out, and titers of induced phage E72m5 and lytic phage 812h1 and viable cell counts were determined for six biological replicates, which were measured in technical triplicates for each dilution. To distinguish the growth characteristics of the therapeutic phage 812h1 and induced phage E72m5, *S. aureus* strain 1137 (sensitive to phage 812h1 and resistant to phage E72m5), *Staphylococcus cohnii* strain A6C (sensitive to phage E72m5 and resistant to phage 812h1), and *S. epidermidis* strain 1457 (sensitive to both phages) were used. To determine viable cell counts, tryptone soya agar (TSA; Oxoid) was used.

Transductions

Transducing lysates from spontaneous and ciprofloxacin (1× MIC) induction, phage 812h1 infection (IR = 10 or 100), and the combined treatment with phage 812h1 and ciprofloxacin were prepared as described earlier using *S. epidermidis* strain 1457LA_ermC. An overnight culture of recipient strain *S. cohnii* A6C grown in BHI broth was diluted to OD_{600} = 1.9–2.0 (≈ 1 × 10^9 CFU/ml) and enriched with $CaCl_2$ to a fi-

Downloaded from https://academic.oup.com/nar/article/53/20/gkaf1165/8317317 by Masarykova Univerzita user on 04 February 2026

nal concentration of 4 mM. Tenfold dilutions of transducing lysates were mixed with an equal volume of recipient and incubated at 37°C for 30 min. Aliquots of each transduction assay were plated in technical triplicate on BHI agar plates supplemented with sodium citrate at a final concentration of 20 mM and erythromycin at a final concentration of 5 μg/ml and incubated at 37°C for 36 h. For each treatment, the titer of phage E72m5, the number of transductant-forming units per milliliter of transducing lysate (TFU/ml), and the transduction frequency (TFU/PFU) were calculated for each of the six biological replicates, along with the descriptive statistics.

Extraction of DNA from virions

Lysates were concentrated using Amicon 30 kDa MWCO (Sartorius) to a final volume of 40 ml and centrifuged at 64 000 × *g* for 2.5 h at 6°C using a Beckman Avanti J-30I high-speed centrifuge. Each pellet was spontaneously resuspended in 400 μl of DNase buffer (2.5 mM $MgCl_2$, 0.1 mM $CaCl_2$, 10 mM Tris–HCl, pH 7.5) overnight at 4°C. The samples were treated with 2 μl DNase I (2500 U/ml; Thermo Scientific, cat. no.: 90083) and 5 μl RNase A (10 mg/ml; Thermo Scientific) for 90 min at 37°C. Next, 10 μl Proteinase K (20 mg/ml; Sigma–Aldrich) and 30 μl of 10% sodium dodecyl sulfate (SDS) were added, followed by incubation on a shaking thermoblock at 55°C, 250 rpm for 15 min. The DNA was extracted using a Genomic DNA Clean & Concentrator-10 kit (Zymo Research) according to the manufacturer's instructions. The absence of external DNA was confirmed by the polymerase chain reaction (PCR) detection (Supplementary Fig. 1) of control DNA of *Pseudomonas* phage LUZ19 [46], added in a total amount of 30 ng to the samples before treatment. Primers LUZ19-mcp_F (CTTCGACATGCGCAAGGAAG) and LUZ19-mcp_R (CGGTCAGGTCCAGTTTCTCC), targeting the gene encoding the major capsid protein of phage LUZ19, were used for external DNA detection. Primers endlys_F (CCATAGAACGGTGAGGACAGG) and endlys_R (TGGAGTGGGTGAGAATCCCTT), targeting endolysin gene of phage 812h1 [41]; and primers SeCI_F (CGTTGAGGGCTTGAAATGGG) and SeCI_R (GCACCTAACACTTGGCGTTT), targeting *gp12* and *gp13* of $SeCI_{SE48}$ [13], were used for internal control (Supplementary Fig. 1). The sequencing data obtained were also mapped on the phage LUZ19 genome sequence (NC_010326) using Minimap2 v2.24 plug-in in Geneious Prime v2025.2.2 (https://www.geneious.com/) with the following setup: Data Type: Oxford Nanopore (more sensitive), K-Mer Length: 28.

Bacterial DNA extraction

The bacterial DNA was isolated as previously described [13] with some modifications. First, 10 ml of stationary overnight bacterial culture cultivated in TSB at 37°C was centrifuged at 3000 × *g* and 10°C for 10 min, washed with 5 ml of wash solution [10 mM Tris–HCl, 10 mM ethylenediaminetetraacetic acid (EDTA), 10 mM EGTA, 1 M NaCl, pH 7.5], and resuspended in Tris-EDTA buffer with lysostaphin (50 μg/ml; Sigma–Aldrich), achromopeptidase (1000 U/ml; Sigma–Aldrich), mutanolysin (40 U/ml; Sigma–Aldrich), and RNase A (200 μg/ml; Thermo Scientific) in a total volume of 500 μl, followed by incubation for 1–2 h at 37°C until lysis appeared. Then, 100 μl of 10% SDS and 20 μl of proteinase K (20 mg/ml; Sigma–Aldrich) were added, and the sample was incubated for 30 min at 55°C, followed by cooling to 4°C and centrifugation at 9700 × *g* for 10 min. The DNA was extracted from the supernatant using a Genomic DNA Clean & Concentrator-25 kit (ZymoResearch) according to the manufacturer's instructions.

Whole-genome sequencing, annotation, and mapping

Libraries of DNA from phage particles were prepared using a Ligation Sequencing Kit V14 (SQK-LSK114; Oxford Nanopore Technologies, UK) according to the manufacturer's instructions. Libraries were sequenced with FLO-FLG114 flow cells (R10.4.1) in a MinION device (Oxford Nanopore Technologies, UK). The device was controlled with the software MinKNOW v23.11.7 (Oxford Nanopore Technologies, UK), which was also used for base-calling (super accuracy mode) and trimming. Biological triplicates were prepared for all evaluated systems. The obtained sequences of packaged DNA were mapped to reference sequences of the source MGEs and bacterial chromosomes. Sequencing read mapping and statistics were computed using Geneious Prime v2025.2.2 (https://www.geneious.com/) and the Geneious mapper plug-in (Minimum quality mapping: 10). The specific mapping parameters and reference genomes used are listed in the corresponding supplementary tables.

To obtain whole bacterial and phage genomes, the Oxford Nanopore Technologies (ONT) platform, using a Rapid Barcoding Kit V14 (SQK-RAD114) or a Ligation Sequencing Kit V14 (SQK-LSK114), and the Illumina platform (Illumina, USA) were used. Illumina sequencing was performed with a NextSeq sequencer using a NextSeq 500/550 Hi Output Kit v2.5 (75 cycles) and a 150-bp paired-end mode. Reads were trimmed using the sliding window model in Trimmomatic Galaxy v0.38.1 [47]. Complete genomes were obtained via hybrid assembly using Unicycler Galaxy v0.5.0 [48] or Flye v2.9.5 [49] for ONT-only sequenced genomes. Phage E72m5 genome was annotated using Pharokka v1.3.2 [50] with manual inspection using BLAST (http://blast.ncbi.nlm.nih.gov/). Bacterial genomes were annotated using the NCBI Prokaryotic Genome Annotation Pipeline [51].

Determination of normal and small-sized genophore ratio

DNA samples were analyzed using an Advanced Analytical Fragment Analyzer (Agilent) 12-capillary instrument using an Agilent DNF-468 HS Genomic DNA 50 kb Kit (DNF-468-0500). Samples were first diluted to a concentration of 1–10 ng/μl and then mixed with the diluent marker according to the user manual. Peak delineation was evaluated using the instrument's proprietary software PROsize with manual correction.

Identification of full-length genophores and determination of the sequencing read fraction with an ambiguous origin, and other statistical analyses

Circular binary segmentation (CBS) [52, 53] was used to distinguish reads representing full-length genophores in normal and small-headed virions from a background consisting of fragmented DNA (Fig. 1). The robustness of the CBS method setting was tested under different parameters. The results are accessible on Zenodo (zenodo.org). Based on the literature search [52, 53] and our robustness testing results, the significance level for the test to accept change points (*alpha*) was

Downloaded from https://academic.oup.com/nar/article/53/20/gkaf1165/8317317 by Masarykova Univerzita user on 04 February 2026

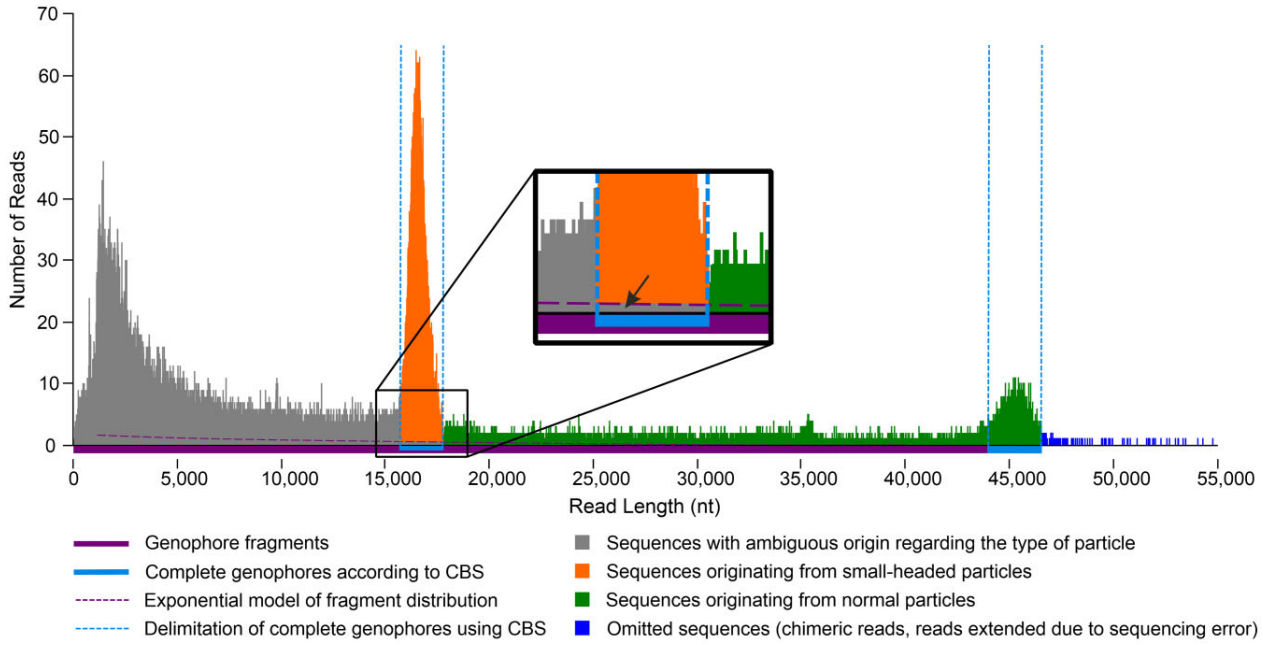

Figure 1. Distribution of sequenced reads and determination of complete genophores from small and normal capsids using CBS. The fraction of sequences with ambiguous origin in the peak of the genophores carried in small capsids (indicated by a black arrow) was estimated using an exponential function. Most sequencing lengths have very low abundance (0 or 1); they are densely clustered on the *x*-axis, which causes the exponential model to appear low and makes the abundant sequencing lengths seem visually overrepresented. The figure displays data from the phage E72m5 infection system (NCBI SRA acc. no. SRR32323969).

finally set to 0.01, the minimum number of markers for a changed segment (*min_width*) was 2, and the number of permutations (*nperm*) was 10 000. Using CBS, sequencing data were divided into homogeneous segments with significantly different average read counts to define genophores from normal and small capsids statistically. The range of genophore sequence lengths was determined so that the segment with the minimum (or maximum) sequence length in the peak formed by the genophores of a given capsid type had an average read count ≥2. If no segment in the peak was ≥2 (which was often the case for genophore sequences in normal capsids), the span of the segment with the highest average read count value was used. Length ranges were described for each biological replicate separately and for the combined data from infection systems. An exponential regression model was used to calculate the relative number of sequences with ambiguous origin in terms of particle type in a set of complete genophores from small-headed particles determined by CBS (Fig. 1). Sequencing data of each biological replicate with lengths ≥1 000 and ≤40 000 nt (excluding those within the range of genophores from small-headed particles) was used to build the model, from which the number of these sequences was predicted.

Differences in median values and Cliff's Delta [54] were used to characterize differences between genophore length ranges from different biological replicates (statistical testing was not performed because large sample sizes make even negligible differences statistically significant). A *t*-test was used for statistical testing of differences between the relative abundances of genophores of different origins in released normal and small-headed particles, as well as between the relative content of phage and $SeCI_{SE48}$ genome copies in the sequencing data. Differences between counts of released virions of infecting phage 812h1, induced phage E72m5, and viable cell counts of 1457LA culture after treatments were tested using Analysis of variance with the Games–Howell *post-hoc* test [55] due to unequal variances. Values were logarithmically transformed, and outlying values were excluded prior to testing to obtain normally distributed data. Differences in the number of TFUs between various treatments were analyzed using the nonparametric Kruskal–Wallis test followed by Dunn's post-hoc test, due to the high frequency of zero and low values. For the purposes of statistical testing, values below 10 TFU/ml (≈ LOD; limit of detection) were replaced by the constant $10/\sqrt{2}$ [56].

Statistical analyses were performed in R v4.3.2 [57] using additional R packages PSCBS [52, 53] (CBS algorithm), ggplot2 [58] (various graphs), and rstatix [59] (statistical testing).

Phage-antibiotic interaction assessment

Experimental data on viable cell count (CFU/ml) and prophage induction (PFU/ml) of six biological replicates were converted to percentages, with 100% assigned to the highest observed value in both cases. These data were arranged according to the SynergyFinder v3.12.0 manual [60] and processed in R v4.3.3 [57] with the additional package synergyfinder v3.12.0 [61], also used for descriptive statistics calculation. For data processing, the input data were transformed and processed using a built-in "viability" option. The phage-antibiotic interaction was calculated using Bliss, zero interaction potency (ZIP), highest single agent (HSA), and Loewe additivity models and visualized.

Results

Model systems for staphylococcal mobilome analysis

To analyze the distribution and structure of the packaged mobilome after phage infection, we chose two source *S. epider-*

Downloaded from https://academic.oup.com/nar/article/53/20/gkaf1165/8317317 by Masarykova Univerzita user on 04 February 2026

midis strains (Table 1) carrying previously characterized PICI $SeCI_{SE48}$ [13], which is a suitable model MGE due to its high transducibility and similarity with various PICIs in genes affecting integration, transcription, or packaging. The first included strain, SE48, is a natural carrier of $SeCI_{SE48}$ and a propagation strain for helper phage 48. The second strain used was 1457 with integrated $SeCI_{SE48}$, designated 1457($SeCI_{SE48}$+). This strain served as a host for phage E72m5, a spontaneous mutant of phage E72 that is unable to propagate on 1457($SeCI_{SE48}$+) [13]. To analyze the distribution of the mobilome after prophage induction, we prepared a lysogen of strain SE48, designated SE48L, containing prophage 48; and a lysogen of strain 1457($SeCI_{SE48}$+) with phage E72m5, designated 1457LA. This lysogenization resulted in the curing of natural prophage 1457 in 1457LA; thus, there was no interference between prophages 1457 and E72m5 during induction. Strains SE48 and 1457($SeCI_{SE48}$+) were exposed to infection by transducing helper phages 48 and E72m5, respectively, while the corresponding lysogens were exposed to antimicrobial agents mitomycin C and ciprofloxacin, which were selected based on their highest induction potential (Supplementary Table 2). Strain 1457LA was also treated with the lytic therapeutic phage 812h1 of the *Kayvirus* genus [41] alone or in combination with ciprofloxacin. During the lytic cycle of helper phage E72m5, both normal phage virions and small-headed virions resulting from the interaction with $SeCI_{SE48}$-encoded capsid morphogenesis protein were produced (Supplementary Fig. 2), as occurred with phage 48 [13]. To study the effectiveness of $SeCI_{SE48}$ transduction after each treatment, strain 1457LA_ermC containing $SeCI_{SE48}$ with an inserted erythromycin resistance gene was used as a donor, and *S. cohnii* A6C, which is susceptible to the transducing phage E72m5 and resistant to the lytic phage 812h1, as a recipient.

For each host-phage/prophage system, independent biological triplicates were prepared and analyzed. Phage E72m5 infection of strain 1457c, which does not carry prophages or $SeCI_{SE48}$, served as a control for phage genophore length and distribution determination (Supplementary Tables S3 and S4).

ONT sequencing-based approach for size and origin determination of packaged genophores

After the external genetic material was eliminated using DNase I, the DNA inside the released virions was extracted and sequenced. The successful external DNA elimination was proved by PCR (Supplementary Fig. 1) and mapping of sequencing reads to the genome sequence of phage LUZ19, whose DNA was added as a control prior to sample treatment, with a negative result. We prepared an ONT sequencing library without the DNA fragmentation step to preserve as many of the full-length DNA molecules packaged in the phage particles as possible. We distinguished full-length genophore sequences originating from normal and small-headed particles from fragmented DNA based on their abundance using the CBS algorithm (Fig. 1 and Supplementary Table 3). This approach enabled us to eliminate the bias caused by DNA fragments of unclear origin in terms of particle type, which may also be parts of the same genophore. The origin of genophores from both particle types was subsequently identified by mapping to reference sequences (Supplementary Table 4). For all replicates, we were able to analyze sequences of complete genophores from small capsids determined using CBS. However, due to fragmentation, it was not possible to use CBS to detect complete genophores from normal capsids in some replicates from induction systems (Supplementary Table 3). Still, analysis of reads ranging from 25 to 46 kb ensured that they originated exclusively from normal capsids, while no two or more reads belonged to the same genophore, and excessively long reads (chimeric or caused by sequencing error) were eliminated.

Due to DNA fragmentation, the portion of reads determined as complete genophores from small-headed particles included a small fraction of fragmented DNA from normal particles. Their abundance was estimated using an exponential function (Fig. 1). Because they could not be individually identified, they could not be accurately quantified or removed. As expected, their proportion was generally higher in induced samples due to a higher level of DNA fragmentation (Supplementary Table 3A), but in all assessed cases, this was below 4.7%. This clearly shows that the analysis of the genophores from small-headed particles was not considerably biased.

We compared the median lengths of genophore reads determined by CBS from biological replicates of all systems. Data obtained from the infection systems of both phages had the highest consistency, as the replicates differed negligibly and exhibited the lowest fragmentation (Supplementary Table 3A). Therefore, the length of the genophores was determined based on these data (Supplementary Table 3B).

The approach used enables the accurate separate quantification of genophores of different origins for each capsid type by size, but not a relative quantification of genophores of both capsid types. The reason for this is that the probability of DNA being sequenced on the ONT platform decreases with increasing length, and also due to the higher probability of fragmentation of larger DNA molecules during library preparation. This led, in most cases, to a multiple overrepresentation of sequenced genophores from small-headed virions (Supplementary Table 4). To determine the proportion of normal and small-headed particles, we used an analysis of isolated DNA with an Agilent Fragment Analyzer. As the quantitative accuracy of the kit used is ±30%, it was a rough estimation (Supplementary Table 5).

Genophore size determination

Phage and $SeCI_{SE48}$ genophores are terminally redundant and circularly permuted, which results from a headful packaging mechanism. Sequence alignment showed slightly imprecise packaging initiation from the phage and $SeCI_{SE48}$ *pac* sites (Figs 2 and 3). For phage 48, the median size of full-length genophores of normal virions was 43.8 kbp (±2% using 5th–95th percentile range) (Supplementary Table 3B). Relative to the 42.5-kbp unit genome of phage 48, this represents 103.1% (max. 105% using 95th percentile) of its genome. The median size of full-length genophores in phage 48-derived small-headed virions was 15.9 kbp (± 4%), representing 37.4% of the phage unit genome and 107% (max. 111.7%) of the 14.8-kbp $SeCI_{SE48}$ genome (Supplementary Table 3B).

For phage E72m5, the median size of full-length genophores of normal virions was 45.3 kbp (±1%) (Supplementary Table 3B). This corresponds to 102.5% (max. 103.5%) of the 44.2-kbp phage unit genome. The median size of full-length genophores in phage E72m5-derived small-headed virions was 16.5 kbp (± 4%), representing

Downloaded from https://academic.oup.com/nar/article/53/20/gkaf1165/8317317 by Masarykova Univerzita user on 04 February 2026

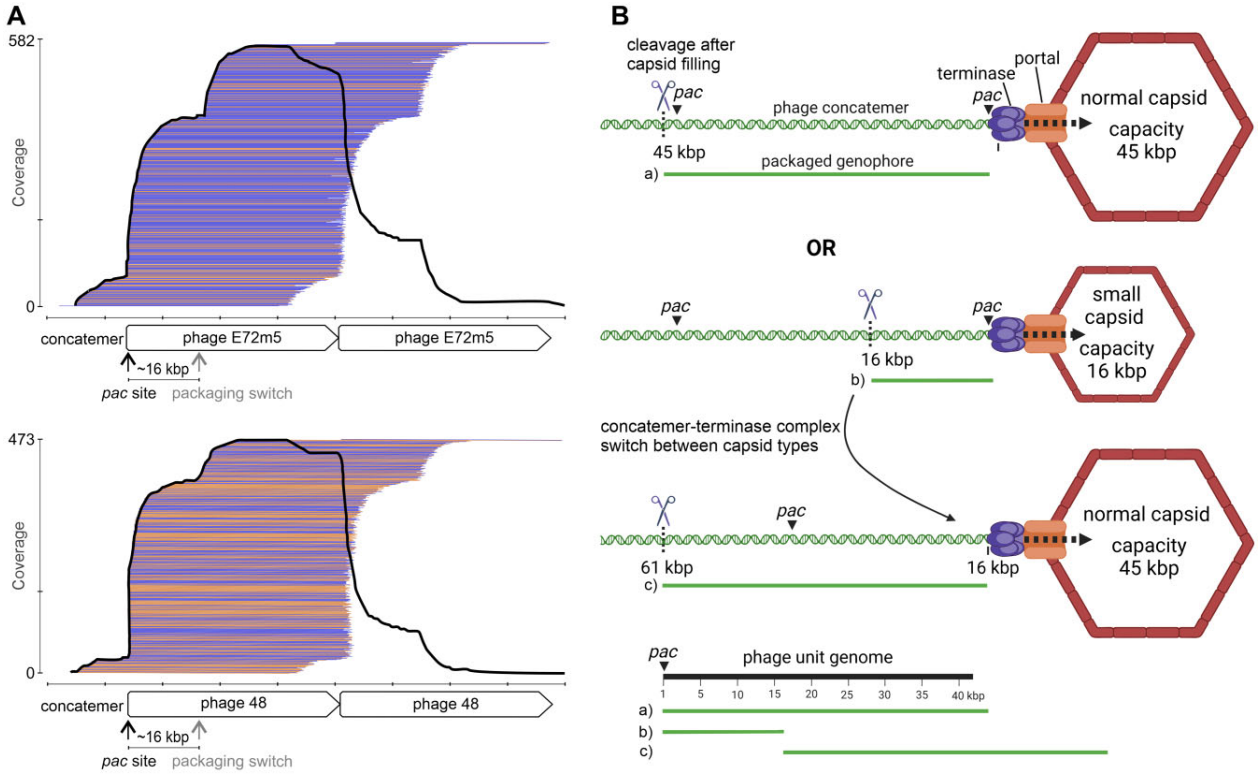

Figure 2. Mapping of phage genophore sequences to the phage concatemer (**A**), and mechanism of the concatemer–terminase complex switching between the two types of capsids (**B**). The obvious bounce in coverage (A) indicates a switch during the packaging of the concatemer, as depicted in part B. Packaging of phage DNA concatemers starts imprecisely from the *pac* site (A and Ba). This results in genophores of ∼45 kbp in length with the same or similar start, which can be observed as an increased coverage at the *pac* site (A). However, the concatemers may first be packaged into small capsids. This results in genophores of 16 kbp with a start at the *pac* site (Bb). Subsequently, genophores packaged into normal particles have a similar start at around 16 kbp from the *pac* site (Bc), which is reflected by a typical change in phage genome coverage (A; schematically in part B, below). Analogously, the same mechanism applies to the SeCI concatemers. Data obtained after treatment of strains 1457LA and SE48L with ciprofloxacin were used for mapping (**A**). The color of the mapped genophores indicates their orientation to the reference (blue for forward; orange for reverse). The figure was partly created in BioRender. Botka (2025) https://BioRender.com/l80g597.

37.4% of the phage unit genome and 111.5% (max. 115.6%) of the $SeCI_{SE48}$ genome (Supplementary Table 3B). The normal capsid capacity of phages 48 and E72m5 enabled the packaging of a three-copy multimer of the $SeCI_{SE48}$ (Fig. 3).

Distribution of MGE and host DNA in normal and small-headed particles

We observed packaging of the same concatemers into normal and small proheads for both phages E72m5 and 48 (Fig. 2). This could be explained by the fact that the phage-encoded large terminase subunit is involved in the packaging of both phage and $SeCI_{SE48}$ concatemers. It recognizes and binds to a prohead portal, which is also of phage origin in both cases. Hence the DNA-terminase complex has no specificity to a particular capsid type and can switch between normal and small proheads. Switching between both types of particles during packaging of the same concatemer was observed as an apparent increase in the coverage of sequencing reads from ∼16 kbp downstream of the *pac* site (Fig. 2A), corresponding to the capacity of the small-headed particle (Fig. 2B). The level of observed increase was proportional to the abundance of small particles (Supplementary Table 5).

The relative amount of phage, $SeCI_{SE48}$, and host DNA-derived genophores in each capsid type is given in Supplementary Table S4 for all the analyzed systems. Despite the variability among biological replicates, evident trends can be observed in the distribution of genophores of different origins depending on the helper phage and the agent used for induction (Fig. 4A). After infection or the spontaneous and ciprofloxacin-mediated induction of phage 48, the ratio of phage to $SeCI_{SE48}$ genophores in the released small-headed particles was approximately equimolar (there was no statistically significant difference). In normal-sized particles, phage genophores clearly prevailed. Mitomycin C-mediated induction resulted in a predominance of $SeCI_{SE48}$ genophores in small capsids and equimolar distribution in normal capsids.

After infection, the ratio of phage E72m5 and $SeCI_{SE48}$ genophores was approximately equimolar in both normal and small-headed particles (Fig. 4A). The results were similar for spontaneous induction, where a small but statistically significant difference ($P < .05$) in distribution was observed in the case of small capsids. Ciprofloxacin-mediated induction resulted in an abundance of phage E72m5 genophores in all released virions. In both strains, 1457LA and SE48L, induction with mitomycin C led to a considerable increase in the relative amount of $SeCI_{SE48}$ genophores in small and normal capsids when compared to all other systems.

In both lysogenic strains, the direction of packaging of the helper prophage and $SeCI_{SE48}$ is toward each other, which is reflected in the increased frequency of packaging of chromoso-

Downloaded from https://academic.oup.com/nar/article/53/20/gkaf1165/8317317 by Masarykova Univerzita user on 04 February 2026

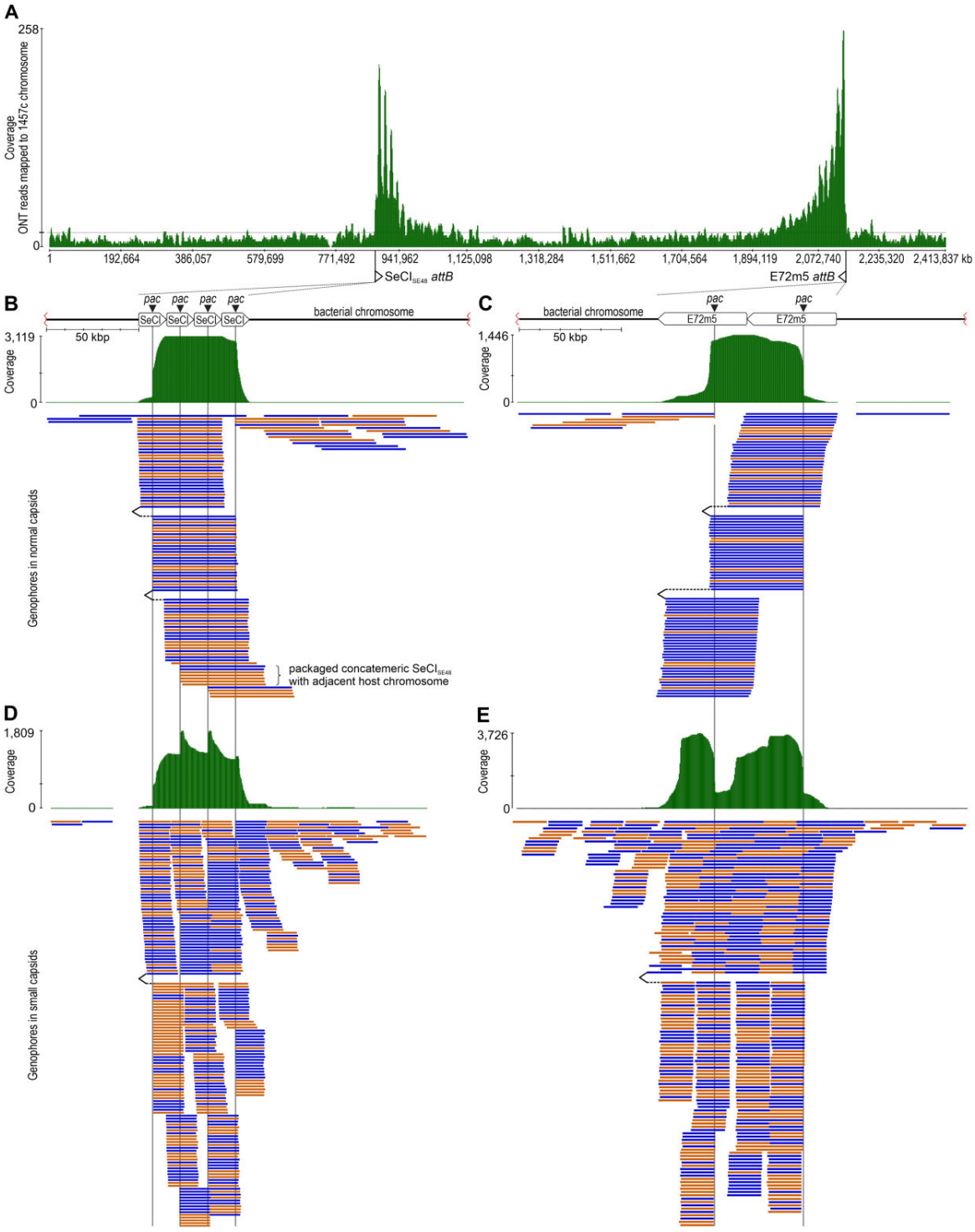

Figure 3. Mapping of sequencing reads to the host, phage, and SeCI$_{SE48}$ genomes. All ONT reads from two biological replicates (NCBI SRA acc. nos. SRR32323971 and SRR32323983) of spontaneous induction in strain 1457LA were mapped to the 1457c genome sequence to eliminate highly covered SeCI$_{SE48}$ and E72m5 regions for clarity (**A**). For both MGEs, the integration site (*attB*) is depicted with an arrow indicating the direction of packaging. The coverage decreases in the direction of the packaging with distance from the MGE position. This corresponds to the frequency of packaging of host sequences into virions due to lateral transduction. To show the sequence organization of SeCI$_{SE48}$ and phage E72m5 complete packaged genophores, these were mapped to multimeric SeCI$_{SE48}$ (**B**, **D**) or E72m5 (**C**, **E**) genomes, respectively. A coverage corresponding to the cyclic permutation of the genomes with an inaccurate start of packaging at the *pac* sites can be observed. An integrated multimeric form was used to demonstrate genophores resulting from lateral transduction. Genophores containing both the MGE and host sequence or multiple copies of the MGE and host sequence were present (B–E). This indicates that concatemer formation may also occur prior to MGE excision. This was proved by the occurrence of genophores in normal capsids containing SeCI$_{SE48}$ multimers with an adjacent host chromosome (B). Data obtained after treatment of strain 1457(SeCI$_{SE48}$+) with phage E72m5 (B, C) and ciprofloxacin (D, E) were used for mapping. Only part of the total read count is depicted; the color of the mapped genophores indicates their orientation to the reference (blue for forward; orange for reverse).

Downloaded from https://academic.oup.com/nar/article/53/20/gkaf1165/8317317 by Masarykova Univerzita user on 04 February 2026

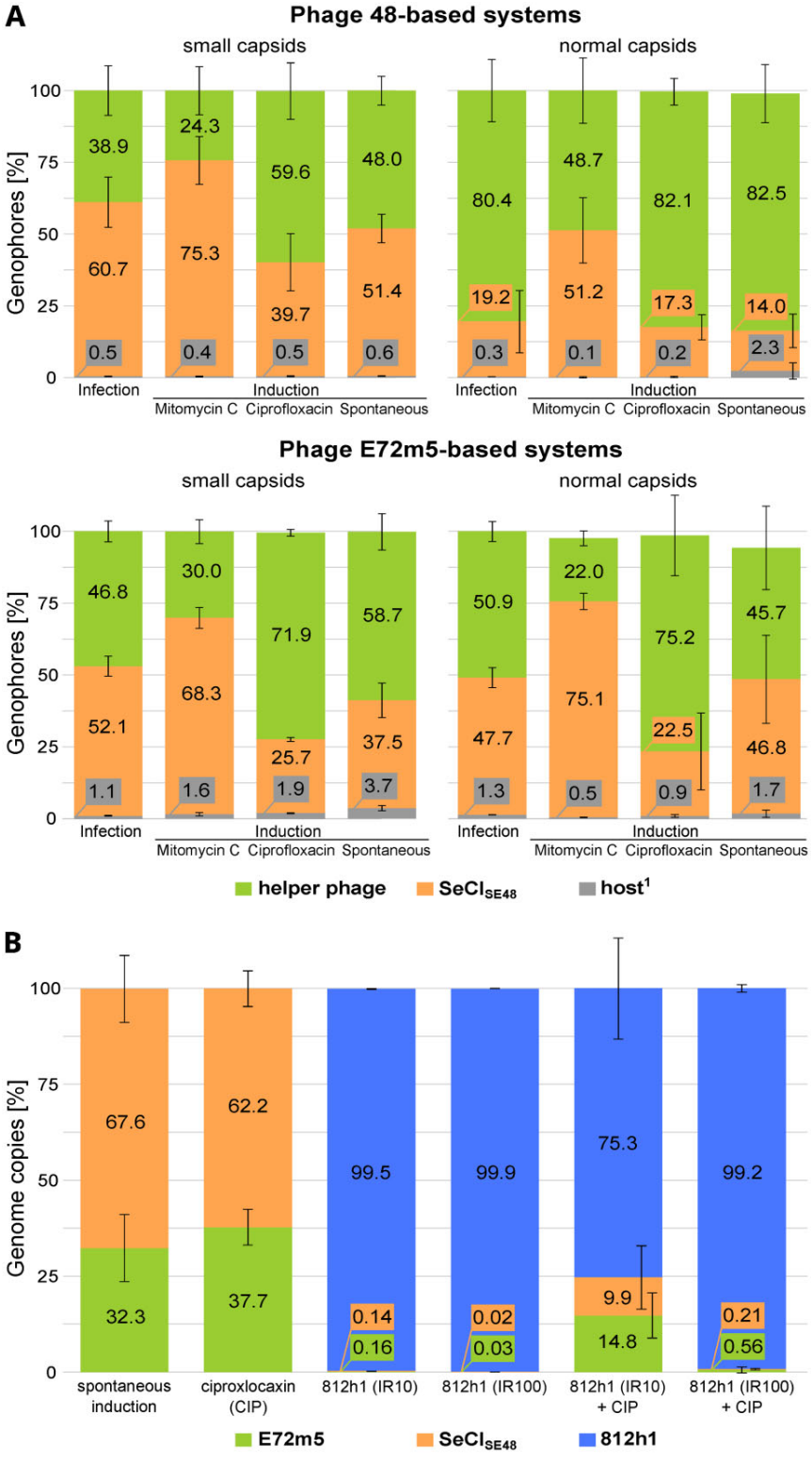

Figure 4. Relative abundance of full-length genophores with different origins in released normal and small-headed particles after helper phage 48 and E72m5 infection and induction (**A**). Relative content of phage and SeCI$_{SE48}$ genome copies in sequencing data obtained from particles released spontaneously and after treatment of strain 1457LA with ciprofloxacin, lytic phage 812h1, and their combination (**B**). The results are presented as means of three biological replicates with standard deviations shown as whiskers. In phage 48-based systems (part A), there was a statistically significant difference in the abundance of SeCI$_{SE48}$ and phage genophores from small particles upon mitomycin C induction, and in genophores from normal particles except for mitomycin C induction. In phage E72m5-based systems, this difference was observed in genophores from small particles except for infection, and from normal particles after mitomycin C and ciprofloxacin induction. Furthermore, a statistically significant difference was observed in the abundance of SeCI$_{SE48}$ and phage genome copies (part B) after spontaneous induction and ciprofloxacin induction. Source data and more detailed results for each replicate are given in Supplementary Tables S4 and S7. [1]Genophores mapped to chromosomal or plasmid reference.

Downloaded from https://academic.oup.com/nar/article/53/20/gkaf1165/8317317 by Masarykova Univerzita user on 04 February 2026

mal sequences between these elements due to lateral transduction (Fig. 3A). Rare full-length reads from small-headed particles containing slightly more than one copy of the 15-kb plasmid p1457 (CP020462) of the strains 1457 and 1457LA were detected (Supplementary Table S4). From all systems, only one multimeric read of p1457, with a size of 43.7 kb (slightly below the capacity of the normal particle determined using CBS), was detected in sequencing reads obtained after E72m5 infection (biological replicate SRR32323981). Both cases suggest packaging from a concatemer during plasmid replication. No plasmid sequences from strains SE48 and SE48L were detected as multimers among the full-length reads from small-headed and normal particles. Despite this, using all sequencing reads from each system, the coverage (Minimap2 v2.24 plug-in, Data Type: Oxford Nanopore, K-Mer Length: 28) of an 8-kb pSE48_1 ranged from 1× in infection to 266× in ciprofloxacin induction, which was 7.1×10^4 times and 1.4×10^2 times lower compared to $SeCI_{SE48}$, respectively. The coverage of 1-kb pSE48_2 ranged from 15× in infection to 2206× in ciprofloxacin induction, which was 4.7×10^3 times and 17.3 times lower compared to $SeCI_{SE48}$, respectively.

The relative abundance of normal particles and small-headed particles differed according to the helper phage and its life cycle (Supplementary Table S5). For phage 48, normal particles were slightly overrepresented after infection. For infection with phage E72m5, small-headed particles were almost twice as abundant as normal ones. For both lysogens SE48L and 1457LA, antimicrobial-mediated prophage induction led to a substantial increase in the number of small-headed particles.

Impact of antimicrobial agents on the induction of MGEs

We further investigated the impact of the *in vitro* treatment of strain 1457LA culture with ciprofloxacin (1× MIC), therapeutic lytic phage 812h1, and their combination on the mobilization of genetic elements. Considering the moderately efficient adsorption (Supplementary Table S6) of phage 812h1 on strain 1457LA cells (60% of virions adsorbed in 20 min), we chose two different input ratios ($IR = MOI_{INPUT}$) of the phage, 10 and 100. In addition to the analysis of sequencing reads ≥500 nt from all released virions (Supplementary Table 7), viable cell count and phage titer were determined on selectively permissive strains *S. aureus* 1137 and *S. cohnii* A6C (Supplementary Table 8). The occurrence of MGE in a total number of virions was expressed as the mean percentage of genome copies calculated as the coverage of a given MGE relative to the sum of the coverage of all reference sequences (Fig. 4B). An increase in the induction of prophage E72m5 was observed whenever ciprofloxacin was used (Fig. 5A). After treatment with ciprofloxacin, the released particles of both types together contained almost 40% of phage E72m5 genome copies and ∼60% of $SeCI_{SE48}$ copies (not genophores, as $SeCI_{SE48}$ is packaged into phage particles as a trimer, and the phage genome is incomplete in small-headed particles) (Fig. 4B). This ratio was similar to spontaneous induction, but the use of ciprofloxacin resulted in a significantly higher release of E72m5 virions (Fig. 5A). After treatment with phage 812h1 alone, its genome significantly predominated, making up to 99.9% of genome copies (Fig. 4B). Phage 812h1 infection led to a 100-fold lower titer of the induced phage E72m5 compared to ciprofloxacin treatment (Fig. 5A) and the reduction in induced phage titer was also statistically significant for a higher IR of phage 812h1 compared even to untreated spontaneous induction.

The combination with ciprofloxacin had no effect on the resulting titer of phage 812h1 (Fig. 5B). Compared to the phage 812h1-only treatment, an increased titer of induced phage E72m5 (Fig. 5A) and an increased relative amount of packaged MGEs was detected in the combined treatment using phage 812h1 and ciprofloxacin (Fig. 4), especially at the lower input ratio of phage 812h1. Nevertheless, the number of released phage E72m5 virions in the combined treatment was not statistically significantly different from the ciprofloxacin-only treatment (Fig. 5A). Importantly, the combined treatment led to the highest decrease in the number of viable bacterial cells (Fig. 5C). The application of phage 812h1 at an input ratio of 100 together with ciprofloxacin was statistically significantly the most effective treatment, and resulted in a 6 order of magnitude decrease in viable cell count compared to ciprofloxacin-only or no treatment.

Furthermore, the type of interaction between phage 812h1 and ciprofloxacin was evaluated as synergistic in the inhibition of strain 1457LA (Supplementary Fig. 3A) using SynergyFinder 3.0 [60]. We calculated the overall synergy score as the mean of score values for both the phage IRs used: Bliss and ZIP models 0.35 (*P*-value 4.56×10^{-9}), HSA model 1.05 (*P*-value 6.68×10^{-19}), and Loewe additivity model 0.64 (*P*-value 2.76×10^{-5}). Calculated positive values indicate synergy, while negative values indicate antagonism. The effect of ciprofloxacin on the stability of prophage E72m5 when the culture was co-treated with phage 812h1 was found to be antagonistic (Supplementary Fig. 3B). The scores for each of the models applied were: Bliss -26.67 (*P*-value 1.00×10^{-5}), ZIP -5.33 (*P*-value 2.54×10^{-1}), HSA -26.63 (*P*-value 1.03×10^{-5}), and Loewe -26.63 (*P*-value 1.03×10^{-5}).

Using strain 1457LA_ermC containing $SeCI_{SE48}$ with an inserted erythromycin resistance gene, we experimentally determined the number of transducing particles released after each treatment (Fig. 5D). We used the *S. cohnii* strain A6C, which is susceptible to the transducing phage E72m5 and resistant to the lytic phage 812h1, as a recipient. About 75% of E72m5 virions adsorbed onto the strain A6C cells, while over 99% adsorbed onto *S. epidermidis* strain 1457 (Supplementary Table S6) within 30 minutes of cocultivation. The relatively low efficiency of adsorption and potential anti-MGE mechanisms may account for the lower number of transductants obtained compared to what was expected based on the abundance of $SeCI_{SE48}$-carrying small-headed and normal particles (Supplementary Tables S4 and S5). The results (Fig. 5D; Supplementary Table S9) showed that the lowest absolute and relative amounts of transducing particles were produced when the lytic phage was used alone or at a higher input ratio in combination with ciprofloxacin. When the antibiotic was combined with a lower input ratio of phage 812h1, the values were comparable to those obtained from spontaneous induction. The highest absolute and relative amounts of transducing particles were detected when ciprofloxacin was used alone.

Discussion

Despite the fact that several recent sequencing-based studies have focused on transductomics [34, 62, 63], the approaches

Downloaded from https://academic.oup.com/nar/article/53/20/gkaf1165/8317317 by Masarykova Univerzita user on 04 February 2026

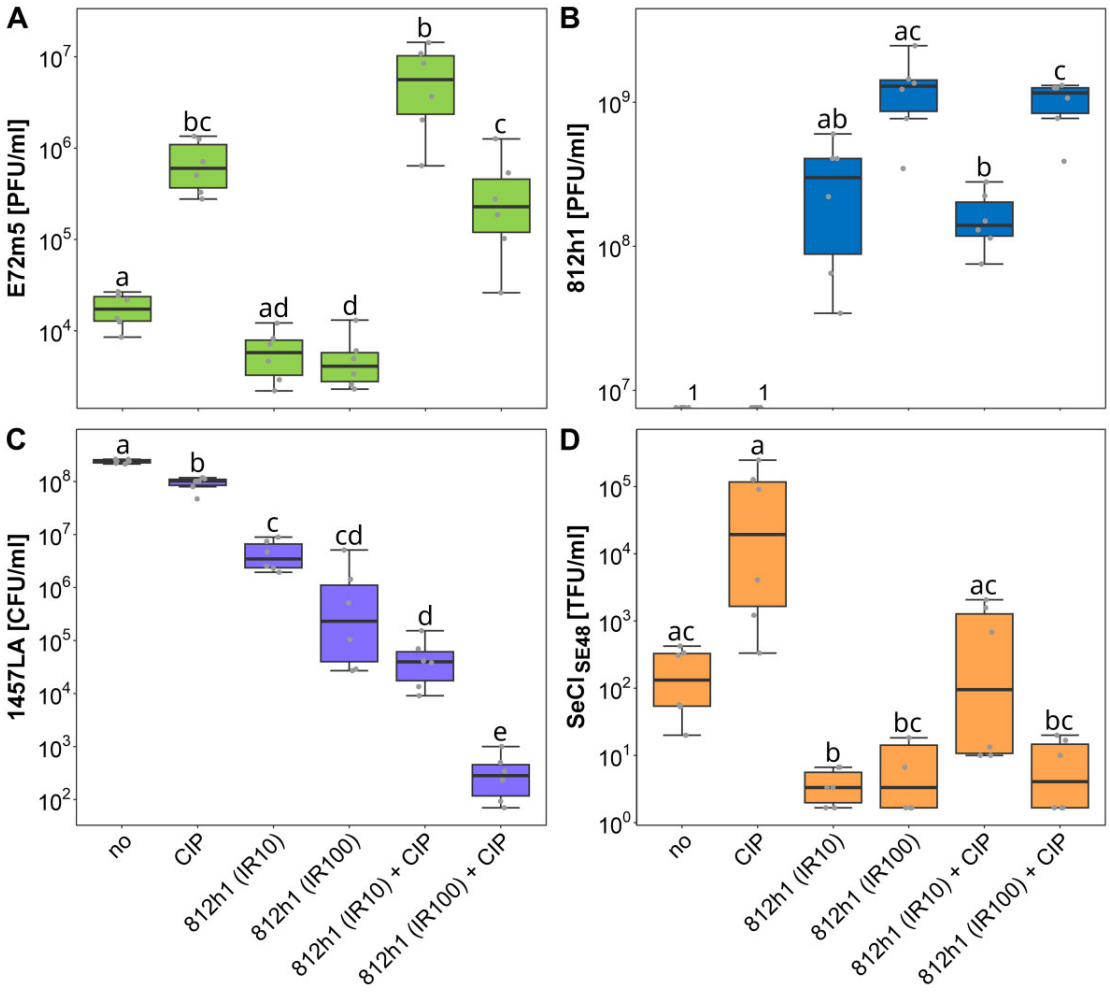

Figure 5. Effect of stress factors on prophage induction, therapeutic phage propagation, bacterial cell count reduction, and $SeCI_{SE48}$ transduction. Counts of released induced phage E72m5 virions (**A**), infecting phage 812h1 virions (**B**), viable cell counts of 1457LA culture (**C**), and $SeCI_{SE48}$-carrying transductant-forming units (**D**) after spontaneous induction (no treatment) and treatment with ciprofloxacin (CIP), phage 812h1 at input ratios (IR) 10 and 100, and their combination. The difference between values was assessed statistically for each system: Different small letters above boxplots indicate statistically significant differences between groups ($P < .05$). Groups sharing at least one letter are not significantly different from each other. Source data and more detailed results are given in Supplementary Tables S8 and S9. [1]No 812h1 virions were released after spontaneous and ciprofloxacin-mediated induction, as the phage 812h1 was not used.

used have not been able to effectively compare and quantify individual genophores in phage and phage-derived small-headed particles. Previous approaches in staphylococci based on indirect evidence using Southern blot analysis only confirmed the presence of phage and PICI DNA in normal as well as small-headed capsids [32]. Here we present an ONT-based approach for transduced mobilome analysis suitable for the identification of phage, PICI, chromosome, and plasmid genophores in individual particle types after infection with helper phage, induction by SOS-response inducing agents, and/or infection with a lytic phage.

Sequence analysis clearly shows that both phage and $SeCI_{SE48}$ genophores are terminally redundant and circularly permuted, and are therefore packaged via a headful mechanism starting with an imprecise cleavage at the *pac* site. The redundancy of phage genophores in normal particles was consistent with the previously published value of 2%–10% of genome length [64]. The redundancy of $SeCI_{SE48}$ genophores in small-headed particles was greater, 7%–16% of the genome length. Since the capacity of the small heads was 36%–37% of the normal ones for both helper phages, the size plasticity of $SeCI_{SE48}$ genophores enables the packaging of complete PICI into small-headed particles derived from phages with different capsid sizes. At the same time, it probably enables the packaging of various PICIs using the same capsid morphogenesis mechanism.

We confirmed that, besides normal virions, the phage genome is also packaged into small-headed particles, where it is incomplete [32]. The uptake of these incomplete phage DNAs might be an important mechanism of prophage evolution through recombination, as the recipient cell does not undergo phage-mediated lysis. Next, we confirmed the assumption that, besides the small-headed particles, PICIs are packaged into normal virions as trimers [65], and are thus transferred completely by both capsid types.

In normal capsids, multi-copy $SeCI_{SE48}$ genophores including adjacent host sequences formed during lateral transduction were detected (Fig. 3B). This confirms the previously

Downloaded from https://academic.oup.com/nar/article/53/20/gkaf1165/8317317 by Masarykova Univerzita user on 04 February 2026

proposed formation of concatemeric islands within the host chromosome when PICI does not undergo the typical chronological order of excision, replication, and packaging of DNA, but the packaging is initiated from the *pac* site before the excision [34]. Detected reads consisting of phage and extensive adjacent chromosomal sequences indicate lateral transduction mediated by delayed prophage excision (Fig. 3C and E). Lateral transduction enables the transfer of chromosomal DNA with a more than 1000 times higher frequency than can be observed in generalized or specialized transduction [15]. Accordingly, the distribution of sequencing reads mapped to the host chromosome (Fig. 3A), and at the same time, the very low number of detected plasmids transmitted by generalized transduction showed that lateral transduction occurred much more frequently than other transduction types.

As shown in lateral transduction, the frequency of packaging decreases with distance from the *pac* site (Fig. 3A). Given the same (headful) mechanism of encapsidation, this probably also applies to phage and PICI concatemers. However, in terms of the frequency of individual gene transfer, the distance of a given gene from the *pac* site is limiting for lateral transduction of the host chromosome, but not for the packaging of concatemers, because the complete set of genes of a given unit genome is packaged in every single packaging event. According to a study on *pac*-phage P22 with a headful packaging mechanism [66, 67], a series of 2–12 packaging events occurs after cleavage at the *pac* site, while the DNA packaging series length increases with time after infection. It is not known whether the number of packaging events in a single series is limited by concatemer length, or whether multiple series can be initiated on a single concatemer molecule [68].

The model system described is generalizable to staphylococcal PICIs mobilized by the *pac*-type helper phages, which contribute most to the formation of transducing particles [69], though some PICIs can utilize *cos*-type helper phages. In this case, PICI carries a *cos* site recognized by the phage TerS, leading to competition between PICI and phage concatemers for the packaging complexes [70]. However, *cos*-type packaging is assumed to mediate specialized transduction only [69]. Recently, capsid-forming PICIs (cf-PICIs) have been reported to be possibly present in staphylococci [71]. Unlike other PICIs, cf-PICIs are completely independent of the phage packaging complex and do not interfere with phage reproduction. Disregarding transduction events, only phage DNA is packaged into phage capsids, while only cf-PICI DNA is packaged into cf-PICI capsids.

The low packaging frequency of the plasmids of strains SE48 and 1457 is consistent with our previous unsuccessful attempts to transduce them [13]. Considering the increased abundance of SE48 plasmid sequences in released virions after ciprofloxacin induction and the fact that no multimeric SE48 plasmids were detected in free virions as a capsid-fulfilling genophore, it should be considered that they could be carried as observed monomers and plasmid fragments with an unknown preference for particle type. The size of small plasmid sequences is insufficient for the headful mechanism of packaging required for the virion assembly [72]. Therefore, we hypothesize that the promiscuity of the packaging machinery may play a role, similarly as in the phage T4, in which DNA is transferred into the finished phage heads in the same way as into the proheads [72], while the presence of a concatemer may not be necessary [73]. Packaging could be facilitated by the linearization of plasmids due to DNA damage by induction agents, which would correspond to the observed notably higher abundance of strain SE48 plasmid sequences in the data from inductions than from infections. Thus, these small DNAs could be co-transduced together with phage or PICI genomes, or fill the capsids in multiple separate copies, as described for phages P1 [74] and T4 [75].

The distribution of phage and island genophores varied depending on the helper phage, its life cycle, and the host strain used. For helper phage 48 and $SeCI_{SE48}$, similar ratios were observed in a given particle type across systems, except for induction by mitomycin C. The fact that phage 48 genophores clearly predominated in normal particles while island abundance increased in small-headed particles indicates a co-evolutionary trade-off that allows the efficient propagation of both elements. This is consistent with the fact that phage 48 has been repeatedly propagated on strain SE48, naturally containing the island $SeCI_{SE48}$, since the 70's [39]. In contrast, the ratios of phage E72m5 and $SeCI_{SE48}$ genophores in normal and small particles within each system were similar. The difference in genophore distribution after infection and induction may be caused by an observed deletion in prophage E72m5 at position 42 828–43 309 bp of the reference (GenBank acc. no. PV036961). This resulted in the fusion gene consisting of parts of *orf70* and *orf72*. The function of the corresponding genes is not known, but they are located in the region between *rinB* and *rinA* genes, which affect DNA packaging into procapsids [76].

During DNA packaging, two types of terminase complexes are formed, consisting of phage-encoded large subunit (TerL) and small subunit (TerS) encoded either by the phage or by $SeCI_{SE48}$. Since the specificity of the terminase complex is determined by the TerS, and phage and $SeCI_{SE48}$ encode distinct TerS proteins that recognize their own *pac* sites, there is probably no competition between these two types of terminase complexes for DNA concatemers. However, $SeCI_{SE48}$ encodes the Ppi (phage auxiliary encapsidation inhibitor) protein [13], which can reduce the efficiency of phage DNA packaging by binding to phage TerS [31]. It remains unclear how this affects the phages used. Both phages encode identical small terminase subunits, however, the sequences starting with a putative *pac* site upstream of the corresponding gene differ (71.8% identity). The different efficiency of phage and $SeCI_{SE48}$ genome recognition by the terminase complexes can explain the differences in the genophore distribution in both helper phages. Small-headed particles formed a much larger proportion of the virions released after any E72m5 induction or infection than in phage 48. Short co-evolution may have played a role in easier $SeCI_{SE48}$ induction in strain 1457LA, leading to a higher expression of island-encoded genes compared to SE48L.

Mitomycin C and ciprofloxacin efficiently increased titers of induced phages when compared to spontaneous induction, but had different impacts on the ratio of packaged genophores. Mitomycin C-mediated induction significantly increased the portion of $SeCI_{SE48}$ genophores, forming a majority in both types of particles for both helper prophages. While mitomycin C acts via cross-linking strands of the DNA double helix [77], ciprofloxacin inhibits DNA replication by blocking DNA gyrase and topoisomerase IV [78]. The resulting double-stranded DNA breaks cause an SOS response [79] and thus an excision of the helper prophage. Triggering its lytic cycle then leads to the mobilization of PICI [80]. The *S. aureus* pathogenicity island (SaPI) operon I containing the *terS* gene encoding a small terminase subunit can be induced

Downloaded from https://academic.oup.com/nar/article/53/20/gkaf1165/8317317 by Masarykova Univerzita user on 04 February 2026

by the SOS response of the host cell, and thus, the packaging of bacterial DNA from pseudo-*pac* sites can appear even if the phage is not the helper phage of the SaPI and the SaPI is not mobilized [65]. Based on this, we suppose that the reason for the effect of mitomycin C could be the additional expression of the $SeCI_{SE48}$ operon, which encodes TerS and capsid modulation proteins, which could be expressed directly via the SOS response even before PICI derepression and excision. The different induction outcomes may be related to the higher MIC multiple used for mitomycin C compared to ciprofloxacin or to a different mechanism of action. The effect of mitomycin C and ciprofloxacin on PICI mobilization has already been studied in *S. aureus*, with the conclusion that both agents enhance island transfer [80]. However, these conclusions were based on the presence of genophores of small-headed particles without further differentiation of their origin. Therefore, they rather support our conclusion that both agents can increase the relative abundance of small-headed particles.

The treatment of the staphylococcal culture with ciprofloxacin led to increased production of infectious particles of induced prophage, as described previously [17]. Despite the reported upregulation of prophage gene expression upon the phage K infection of *S. aureus* [81], treatment with the closely related therapeutic phage 812h1 led to a drastic reduction in the titer of the released temperate phage compared to ciprofloxacin use. The upregulation of prophage gene expression can be explained by the SOS response caused by the host DNA damage by phage 812h1 nucleases, which causes prophage excision. However, intracellular temperate phage DNA awaiting packaging may subsequently be damaged by phage 812h1 host-takeover mechanisms, resulting in low numbers of released mature and infectious temperate phage virions (Fig. 5A). Therefore, purely complete genophore reads could not be used for analysis due to a shortage of them caused by the fragmentation and high abundance of phage 812h1 sequencing data (Fig. 4B).

Although the combined treatment led to an increase in both the titer of induced phage and the relative amount of packaged mobilome compared to treatment with phage alone, the values observed were not statistically significantly higher than those observed for the treatment with ciprofloxacin alone. Most probably, this is because with a lower input ratio of therapeutic phage, a lower number of cells are infected in the initial phase, allowing the induction of prophage and subsequently PICI in the remaining uninfected bacterial population due to the SOS response triggered by ciprofloxacin.

Importantly, the combined treatment led to a six-order-of-magnitude decrease in the number of viable bacterial cells, and it was more effective than the antibiotic or therapeutic phage alone. Based on the results obtained using various interaction models, we proved that this interaction was synergistic. Similarly, ciprofloxacin with phages has already been used to eradicate *S. aureus* or *Pseudomonas aeruginosa* based on phage-antibiotic synergy [82, 83]. Therefore, this combined approach appears to be the best in terms of treatment efficacy while not increasing the risk of spreading resistance and virulence genes compared to standard antibiotic treatment. The application of lytic phage has been shown to reduce the risk of MGE transduction to levels comparable to spontaneous induction, or even significantly lower, depending on the quantity of phage used and its combination with antibiotics. Nevertheless, the advantages of therapy combining lytic phage and ciprofloxacin need to be confirmed *in vivo*.

This work contributes to the elucidation of the interactions between phages, PICIs, and host DNA packaging; it significantly advances our understanding of the biology of transduction and provides a robust framework for assessing the risks associated with horizontal gene transfer in therapeutic contexts.

Acknowledgements

We gratefully acknowledge the CF Genomics and CF Bioinformatics supported by the NCMG research infrastructure (LM2023067), the CF Cryo-electron Microscopy and Tomography of CEITEC MU of the CIISB (LM2023042), and the RECETOX research infrastructure (LM2023069), all funded by the Ministry of Education, Youth and Sports of the Czech Republic, for their support in obtaining the scientific data presented in this paper. The authors thank Prof. Rob Lavigne (Faculty of BioScience Engineering, KU Leuven, Belgium) for supplying the phage LUZ19. The graphical abstract was created in BioRender.com (Botka, 2025) and can be accessed at https://BioRender.com/h74x186.

Author contributions: Tibor Botka (Conceptualization [lead], Data curation [lead], Formal analysis [supporting], Funding acquisition [equal], Investigation [equal], Methodology [equal], Project administration [equal], Resources [equal], Supervision [lead], Validation [equal], Visualization [lead], Writing—original draft [lead], Writing—review & editing [lead]), Soňa Smetanová (Data curation [equal], Formal analysis [lead], Validation [equal], Visualization [supporting], Writing—review & editing [supporting]), Adam Vinco (Investigation [equal], Writing—review & editing [supporting]), Eliška Kučerová (Formal analysis [supporting], Investigation [supporting], Visualization [supporting], Writing—review & editing [supporting]), Kristína Rovňáková (Investigation [equal], Writing—review & editing [supporting]), Alena Siváková (Investigation [supporting], Writing—review & editing [supporting]), Ivana Mašlaňová (Resources [supporting], Writing—review & editing [supporting]), and Roman Pantucek (Conceptualization [supporting], Funding acquisition [equal], Methodology [supporting], Project administration [equal], Resources [equal], Supervision [equal], Visualization [equal], Writing—original draft [equal], Writing—review & editing [equal])

Supplementary data

Supplementary data is available at NAR online.

Conflict of interest

None declared.

Funding

This work was supported by the Ministry of Health of the Czech Republic in cooperation with the Czech Health Research Council under project No. NU21J-05–00035 and a National Institute of Virology and Bacteriology project (Program EXCELES, ID project no. LX22NPO5103) funded by the European Union–Next Generation EU. Funding to pay the Open Access publication charges for this article was provided by Czech Republic Institutions (CzechElib affiliated) through the Fully OA Open Access Agreement (82929901).

Downloaded from https://academic.oup.com/nar/article/53/20/gkaf1165/8317317 by Masarykova Univerzita user on 04 February 2026

Data availability

The data underlying this article are available in the article, its online supplementary materials, and in subject-specific public repositories. Sequencing data are deposited within BioProject PRJNA1198866 (https://www.ncbi.nlm.nih.gov/bioproject/PRJNA1198866), except for the genome of phage E72m5 deposited under GenBank acc. no. PV036961. Whole-genome sequences of *S. epidermidis* strains obtained in this work are deposited under the following GenBank acc. nos.: SE48L (CP180175), 1457(SeCI$_{SE48}$+) (CP180176), 1457LA (CP180177), 1457LA_ermC (CP194848), and 1457c (CP180178). BioSample accession numbers and Sequence Read Archive (SRA) data for biological replicates are listed in Supplementary Tables S3 and S7. The following sequences taken from the GenBank database were also used in this paper: *S. epidermidis* strains SE48 (CP066303) and 1457 (CP020463); SeCI$_{SE48}$ (MW368309); phage 48 (MW364972) and prophage 1457 (CP020463); plasmids pSE48_1 (CP066304), pSE48_2 (CP066305), and p1457 (CP020462). The results of testing the robustness of the CBS method under different parameters are accessible on Zenodo (https://doi.org/10.5281/zenodo.17054370).

References

1. Samia NI, Robicsek A, Heesterbeek H *et al.* Methicillin-resistant *Staphylococcus aureus* nosocomial infection has a distinct epidemiological position and acts as a marker for overall hospital-acquired infection trends. *Sci Rep* 2022;12:17007. https://doi.org/10.1038/s41598-022-21300-6
2. Schoenfelder SM, Lange C, Eckart M *et al.* Success through diversity - how *Staphylococcus epidermidis* establishes as a nosocomial pathogen. *Int J Med Microbiol* 2010;300:380–6. https://doi.org/10.1016/j.ijmm.2010.04.011
3. Otto M. *Staphylococcus epidermidis*—the 'accidental' pathogen. *Nat Rev Micro* 2009;7:555–67. https://doi.org/10.1038/nrmicro2182
4. McCann MT, Gilmore BF, Gorman SP. *Staphylococcus epidermidis* device-related infections: pathogenesis and clinical management. *J Pharm Pharmacol* 2008;60:1551–71. https://doi.org/10.1211/jpp.60.12.0001
5. Guo Y, Du X, Krusche J *et al.* Invasive *Staphylococcus epidermidis* uses a unique processive wall teichoic acid glycosyltransferase to evade immune recognition. *Sci Adv* 2023;9:eadj2641. https://doi.org/10.1126/sciadv.adj2641
6. Otto M. Coagulase-negative staphylococci as reservoirs of genes facilitating MRSA infection: staphylococcal commensal species such as *Staphylococcus epidermidis* are being recognized as important sources of genes promoting MRSA colonization and virulence. *Bioessays* 2013;35:4–11. https://doi.org/10.1002/bies.201200112
7. Ingmer H, Gerlach D, Wolz C. Temperate phages of *Staphylococcus aureus*. *Microbiol Spectr* 2019;7:0058–2018. https://doi.org/10.1128/microbiolspec.GPP3-0058-2018
8. Botka T, Růžičková V, Konečná H *et al.* Complete genome analysis of two new bacteriophages isolated from impetigo strains of *Staphylococcus aureus*. *Virus Genes* 2015;51:122–31. https://doi.org/10.1007/s11262-015-1223-8
9. Otter JA, Kearns AM, French GL *et al.* Panton-Valentine leukocidin-encoding bacteriophage and gene sequence variation in community-associated methicillin-resistant *Staphylococcus aureus*. *Clin Microbiol Infect* 2010;16:68–73. https://doi.org/10.1111/j.1469-0691.2009.02925.x
10. van Wamel WJ, Rooijakkers SH, Ruyken M *et al.* The innate immune modulators staphylococcal complement inhibitor and chemotaxis inhibitory protein of *Staphylococcus aureus* are located on beta-hemolysin-converting bacteriophages. *J Bacteriol* 2006;188:1310–5. https://doi.org/10.1128/JB.188.4.1310-1315.2006
11. Holden MT, Lindsay JA, Corton C *et al.* Genome sequence of a recently emerged, highly transmissible, multi-antibiotic- and antiseptic-resistant variant of methicillin-resistant *Staphylococcus aureus*, sequence type 239 (TW). *J Bacteriol* 2010;192:888–92. https://doi.org/10.1128/JB.01255-09
12. Penadés JR, Chen J, Quiles-Puchalt N *et al.* Bacteriophage-mediated spread of bacterial virulence genes. *Curr Opin Microbiol* 2015;23:171–8. https://doi.org/10.1016/j.mib.2014.11.019
13. Fišarová L, Botka T, Du X *et al. Staphylococcus epidermidis* phages transduce antimicrobial resistance plasmids and mobilize chromosomal islands. *mSphere* 2021;6:e00223–21. https://doi.org/10.1128/mSphere.00223-21
14. Xia G, Wolz C. Phages of *Staphylococcus aureus* and their impact on host evolution. *Infect Genet Evol* 2014;21:593–601. https://doi.org/10.1016/j.meegid.2013.04.022
15. Chen J, Quiles-Puchalt N, Chiang YN *et al.* Genome hypermobility by lateral transduction. *Science* 2018;362:207–12. https://doi.org/10.1126/science.aat5867
16. Davidson AR. A common trick for transferring bacterial DNA. *Science* 2018;362:152–3. https://doi.org/10.1126/science.aav1723
17. Goerke C, Koller J, Wolz C. Ciprofloxacin and trimethoprim cause phage induction and virulence modulation in *Staphylococcus aureus*. *Antimicrob Agents Chemother* 2006;50:171–7. https://doi.org/10.1128/AAC.50.1.171-177.2006
18. Rohde C, Resch G, Pirnay JP *et al.* Expert opinion on three phage therapy related topics: bacterial phage resistance, phage training and prophages in bacterial production strains. *Viruses* 2018;10:178. https://doi.org/10.3390/v10040178
19. Brüssow H, Canchaya C, Hardt WD. Phages and the evolution of bacterial pathogens: from genomic rearrangements to lysogenic conversion. *Microbiol Mol Biol Rev* 2004;68:560–602. https://doi.org/10.1128/MMBR.68.3.560-602.2004
20. Haaber J, Leisner JJ, Cohn MT *et al.* Bacterial viruses enable their host to acquire antibiotic resistance genes from neighbouring cells. *Nat Commun* 2016;7:13333. https://doi.org/10.1038/ncomms13333
21. Hossain M, Aslan B, Hatoum-Aslan A. Tandem mobilization of anti-phage defenses alongside SCC*mec* elements in staphylococci. *Nat Commun* 2024;15:8820. https://doi.org/10.1038/s41467-024-53146-z
22. Winstel V, Kuhner P, Krismer B *et al.* Transfer of plasmid DNA to clinical coagulase-negative staphylococcal pathogens by using a unique bacteriophage. *Appl Environ Microbiol* 2015;81:2481–8. https://doi.org/10.1128/AEM.04190-14
23. Scharn CR, Tenover FC, Goering RV. Transduction of staphylococcal cassette chromosome *mec* elements between strains of *Staphylococcus aureus*. *Antimicrob Agents Chemother* 2013;57:5233–8. https://doi.org/10.1128/AAC.01058-13
24. Mašlaňová I, Stříbna S, Doškař J *et al.* Efficient plasmid transduction to *Staphylococcus aureus* strains insensitive to the lytic action of transducing phage. *FEMS Microbiol Lett* 2016;363:fnw211. https://doi.org/10.1093/femsle/fnw211
25. Madhusoodanan J, Seo KS, Remortel B *et al.* An enterotoxin-bearing pathogenicity island in *Staphylococcus epidermidis*. *J Bacteriol* 2011;193:1854–62. https://doi.org/10.1128/JB.00162-10
26. Chen HJ, Tsai JC, Hung WC *et al.* Identification of *fusB*-mediated fusidic acid resistance islands in *Staphylococcus epidermidis* isolates. *Antimicrob Agents Chemother* 2011;55:5842–9. https://doi.org/10.1128/AAC.00592-11
27. Novick RP, Schlievert P, Ruzin A. Pathogenicity and resistance islands of staphylococci. *Microbes Infect* 2001;3:585–94. https://doi.org/10.1016/S1286-4579(01)01414-9
28. Fillol-Salom A, Martinez-Rubio R, Abdulrahman RF *et al.* Phage-inducible chromosomal islands are ubiquitous within the

Downloaded from https://academic.oup.com/nar/article/53/20/gkaf1165/8317317 by Masarykova Univerzita user on 04 February 2026

bacterial universe. *ISME J* 2018;12:2114–28. https://doi.org/10.1038/s41396-018-0156-3
29. Damle PK, Wall EA, Spilman MS *et al.* The roles of SaPI1 proteins gp7 (CpmA) and gp6 (CpmB) in capsid size determination and helper phage interference. *Virology* 2012;432:277–82. https://doi.org/10.1016/j.virol.2012.05.026
30. Hawkins NC, Kizziah JL, Penadés JR *et al.* Shape shifter: redirection of prolate phage capsid assembly by staphylococcal pathogenicity islands. *Nat Commun* 2021;12:6408. https://doi.org/10.1038/s41467-021-26759-x
31. Ram G, Chen J, Kumar K *et al.* Staphylococcal pathogenicity island interference with helper phage reproduction is a paradigm of molecular parasitism. *Proc Natl Acad Sci USA* 2012;109:16300–5. https://doi.org/10.1073/pnas.1204615109
32. Ubeda C, Olivarez NP, Barry P *et al.* Specificity of staphylococcal phage and SaPI DNA packaging as revealed by integrase and terminase mutations. *Mol Microbiol* 2009;72:98–108. https://doi.org/10.1111/j.1365-2958.2009.06634.x
33. Chen J, Ram G, Penadés JR *et al.* Pathogenicity island-directed transfer of unlinked chromosomal virulence genes. *Molecular Cell* 2015;57:138–49. https://doi.org/10.1016/j.molcel.2014.11.011
34. Chee MSJ, Serrano E, Chiang YN *et al.* Dual pathogenicity island transfer by piggybacking lateral transduction. *Cell* 2023;186:3414–26. https://doi.org/10.1016/j.cell.2023.07.001
35. Bowring JZ, Su Y, Alsaadi A *et al.* Screening for highly transduced genes in *Staphylococcus aureus* revealed both lateral and specialized transduction. *Microbiol Spectr* 2022;10:e02423–21. https://doi.org/10.1128/spectrum.02423-21
36. Kogay Wolf R, YI and Koonin EV. Defence systems and horizontal gene transfer in bacteria. *Environ Microbiol* 2024;26:e16630. https://doi.org/10.1111/1462-2920.16630
37. Vasu K, Nagaraja V. Diverse functions of restriction-modification systems in addition to cellular defense. *Microbiol Mol Biol Rev* 2013;77:53–72. https://doi.org/10.1128/MMBR.00044-12
38. Watson BNJ, Staals RHJ, Fineran PC. CRISPR-Cas-mediated phage resistance enhances horizontal gene transfer by transduction. *mBio* 2018;9:e02406–17. https://doi.org/10.1128/mBio.02406-17
39. Dean BA, Williams RE, Hall F *et al.* Phage typing of coagulase-negative staphylococci and micrococci. *J Hyg* 1973;71:261–70. https://doi.org/10.1017/S0022172400022737
40. Galac MR, Stam J, Maybank R *et al.* Complete genome sequence of *Staphylococcus epidermidis* 1457. *Genome Announc* 2017;5:e00450–17. https://doi.org/10.1128/genomeA.00450-17
41. Botka T, Pantůček R, Mašlaňová I *et al.* Lytic and genomic properties of spontaneous host-range *Kayvirus* mutants prove their suitability for upgrading phage therapeutics against staphylococci. *Sci Rep* 2019;9:5475. https://doi.org/10.1038/s41598-019-41868-w
42. Monk IR, Shah IM, Xu M *et al.* Transforming the untransformable: application of direct transformation to manipulate genetically *Staphylococcus aureus* and *Staphylococcus epidermidis*. *mBio* 2012;3:e00277–11. https://doi.org/10.1128/mBio.00277-11
43. Charpentier E, Anton AI, Barry P *et al.* Novel cassette-based shuttle vector system for Gram-positive bacteria. *Appl Environ Microbiol* 2004;70:6076–85. https://doi.org/10.1128/AEM.70.10.6076-6085.2004
44. Mašlaňová I, Doškař J, Varga M *et al.* Bacteriophages of *Staphylococcus aureus* efficiently package various bacterial genes and mobile genetic elements including SCC*mec* with different frequencies. *Environ Microbiol Rep* 2013;5:66–73. https://doi.org/10.1111/j.1758-2229.2012.00378.x
45. EUCAST. *The European Committee on Antimicrobial Susceptibility Testing. Breakpoint tables for interpretation of MICs and zone diameters. Version 14.0. EUCAST Development Laboratory for Antimicrobial Susceptibility Testing of bacteria*, Växjö, Sweden, 2024. https://www.eucast.org/fileadmin/src/media/PDFs/EUCAST_files/Breakpoint_tables/v_14.0_Breakpoint_Tables.xlsx
46. Lammens E, Ceyssens PJ, Voet M *et al.* Representational difference analysis (RDA) of bacteriophage genomes. *J Microbiol Methods* 2009;77:207–13. https://doi.org/10.1016/j.mimet.2009.02.006
47. Bolger AM, Lohse M, Usadel B. Trimmomatic: a flexible trimmer for Illumina sequence data. *Bioinformatics* 2014;30:2114–20. https://doi.org/10.1093/bioinformatics/btu170
48. Wick RR, Judd LM, Gorrie CL *et al.* Unicycler: resolving bacterial genome assemblies from short and long sequencing reads. *PLoS Comput Biol* 2017;13:e1005595. https://doi.org/10.1371/journal.pcbi.1005595
49. Lin Y, Yuan J, Kolmogorov M *et al.* Assembly of long error-prone reads using de Bruijn graphs. *Proc Natl Acad Sci USA* 2016;113:E8396–405. https://doi.org/10.1073/pnas.1604560113
50. Bouras G, Nepal R, Houtak G *et al.* Pharokka: a fast scalable bacteriophage annotation tool. *Bioinformatics* 2023;39:btac776. https://doi.org/10.1093/bioinformatics/btac776
51. Li W, O'Neill KR, Haft DH *et al.* RefSeq: expanding the Prokaryotic Genome Annotation Pipeline reach with protein family model curation. *Nucleic Acids Res* 2021;49:D1020–8. https://doi.org/10.1093/nar/gkaa1105
52. Olshen AB, Venkatraman ES, Lucito R *et al.* Circular binary segmentation for the analysis of array-based DNA copy number data. *Biostatistics* 2004;5:557–72. https://doi.org/10.1093/biostatistics/kxh008
53. Venkatraman ES, Olshen AB. A faster circular binary segmentation algorithm for the analysis of array CGH data. *Bioinformatics* 2007;23:657–63. https://doi.org/10.1093/bioinformatics/btl646
54. Meissel K, Yao ES. Using Cliff's Delta as a Non-Parametric Effect Size Measure: an Accessible Web App and R Tutorial. *Pract Assess Res Eval* 2024;29:2. https://doi.org/10.7275/pare.1977
55. Lee S, Lee DK. What is the proper way to apply the multiple comparison test? *Korean J Anesthesiol* 2018;71:353–60. https://doi.org/10.4097/kja.d.18.00242
56. Antweiler RC. Evaluation of statistical treatments of left-censored environmental data using coincident uncensored data sets. II. Group comparisons. *Environ Sci Technol* 2015;49:13439–46. https://doi.org/10.1021/acs.est.5b02385
57. R Core Team. *A Language and Environment for Statistical Computing*. R Foundation for Statistical Computing, Vienna, Austria, 2023. https://cran.r-project.org/
58. Wickham H. ggplot2, Elegant Graphics for Data Analysis. Springer-Verlag, New York, NY, 2009. https://doi.org/10.1007/978-0-387-98141-3.
59. Kassambara A. rstatix: pipe-Friendly Framework for Basic Statistical Tests. R package version 0.7.2, 2023. https://rpkgs.datanovia.com/rstatix/
60. Ianevski A, Giri AK, Aittokallio T. SynergyFinder 3.0: an interactive analysis and consensus interpretation of multi-drug synergies across multiple samples. *Nucleic Acids Res* 2022;50:W739–43. https://doi.org/10.1093/nar/gkac382
61. Zheng S, Wang W, Aldahdooh J *et al.* SynergyFinder Plus: toward better interpretation and annotation of drug combination screening datasets. *Genomics Proteomics Bioinformatics* 2022;20:587–96. https://doi.org/10.1016/j.gpb.2022.01.004
62. Kleiner M, Bushnell B, Sanderson KE *et al.* Transductomics: sequencing-based detection and analysis of transduced DNA in pure cultures and microbial communities. *Microbiome* 2020;8:158. https://doi.org/10.1186/s40168-020-00935-5
63. Wolput S, Lood C, Fillol-Salom A *et al.* Phage-host co-evolution has led to distinct generalized transduction strategies. *Nucleic Acids Res* 2024;52:7780–91. https://doi.org/10.1093/nar/gkae489
64. Casjens SR, Gilcrease EB. Determining DNA packaging strategy by analysis of the termini of the chromosomes in tailed-bacteriophage virions. *Methods Mol Biol* 2009;502:91–111. https://doi.org/10.1007/978-1-60327-565-1_7
65. Ubeda C, Maiques E, Tormo MA *et al.* SaPI operon I is required for SaPI packaging and is controlled by LexA. *Mol Microbiol*

Downloaded from https://academic.oup.com/nar/article/53/20/gkaf1165/8317317 by Masarykova Univerzita user on 04 February 2026

2007;65:41–50.
https://doi.org/10.1111/j.1365-2958.2007.05758.x
66. Jackson EN, Jackson DA, Deans RJ. *Eco*RI analysis of bacteriophage P22 DNA packaging. *J Mol Biol* 1978;118:365–88. https://doi.org/10.1016/0022-2836(78)90234-6
67. Adams MB, Hayden M, Casjens S. On the sequential packaging of bacteriophage P22 DNA. *J Virol* 1983;46:673–7. https://doi.org/10.1128/jvi.46.2.673-677.1983
68. Casjens S, Weigele P. DNA Packaging by Bacteriophage P22. *Viral Genome Packaging Machines: Genetics, Structure, and Mechanism*. Springer, Boston, MA, 2005; pp.80–8. https://doi.org/10.1007/0-387-28521-0.
69. Chiang YN, Penadés JR, Chen J. Genetic transduction by phages and chromosomal islands: the new and noncanonical. *PLoS Pathog* 2019;15:e1007878. https://doi.org/10.1371/journal.ppat.1007878
70. Quiles-Puchalt N, Carpena N, Alonso JC *et al.* Staphylococcal pathogenicity island DNA packaging system involving cos-site packaging and phage-encoded HNH endonucleases. *Proc Natl Acad Sci USA* 2014;111:6016–21. https://doi.org/10.1073/pnas.1320538111
71. Alqurainy N, Miguel-Romero L, Sousa Md *et al.* A widespread family of phage-inducible chromosomal islands only steals bacteriophage tails to spread in nature. *Cell Host & Microbe* 2023;31:69–82. https://doi.org/10.1016/j.chom.2022.12.001
72. Zhang Z, Kottadiel VI, Vafabakhsh R *et al.* A promiscuous DNA packaging machine from bacteriophage T4. *PLoS Biol* 2011;9:e1000592. https://doi.org/10.1371/journal.pbio.1000592
73. Vafabakhsh R, Kondabagil K, Earnest T *et al.* Single-molecule packaging initiation in real time by a viral DNA packaging machine from bacteriophage T4. *Proc Natl Acad Sci USA* 2014;111:15096–101. https://doi.org/10.1073/pnas.1407235111
74. Coren JS, Pierce JC, Sternberg N. Headful packaging revisited: the packaging of more than one DNA molecule into a bacteriophage P1 head. *J Mol Biol* 1995;249:176–84. https://doi.org/10.1006/jmbi.1995.0287
75. Leffers G, Rao VB. A discontinuous headful packaging model for packaging less than headful length DNA molecules by bacteriophage T4. *J Mol Biol* 1996;258:839–50. https://doi.org/10.1006/jmbi.1996.0291
76. Ferrer MD, Quiles-Puchalt N, Harwich MD *et al.* RinA controls phage-mediated packaging and transfer of virulence genes in Gram-positive bacteria. *Nucleic Acids Res* 2011;39:5866–78. https://doi.org/10.1093/nar/gkr158
77. Kwan BW, Chowdhury N, Wood TK. Combatting bacterial infections by killing persister cells with mitomycin C. *Environ Microbiol* 2015;17:4406–14. https://doi.org/10.1111/1462-2920.12873
78. Rehman A, Patrick WM, Lamont IL. Mechanisms of ciprofloxacin resistance in *Pseudomonas aeruginosa*: new approaches to an old problem. *J Med Microbiol* 2019;68:1–10. https://doi.org/10.1099/jmm.0.000873
79. Anderson DG, Kowalczykowski SC. Reconstitution of an SOS response pathway: derepression of transcription in response to DNA breaks. *Cell* 1998;95:975–9. https://doi.org/10.1016/S0092-8674(00)81721-3
80. Ubeda C, Maiques E, Knecht E *et al.* Antibiotic-induced SOS response promotes horizontal dissemination of pathogenicity island-encoded virulence factors in staphylococci. *Mol Microbiol* 2005;56:836–44. https://doi.org/10.1111/j.1365-2958.2005.04584.x
81. Finstrlová A, Mašlaňová I, Blasdel Reuter BG *et al.* Global transcriptomic analysis of bacteriophage-host interactions between a *Kayvirus* therapeutic phage and *Staphylococcus aureus*. *Microbiol Spectr* 2022;10:e00123–22. https://doi.org/10.1128/spectrum.00123-22
82. Roszak M, Dolegowska B, Cecerska-Heryc E *et al.* Bacteriophage-ciprofloxacin combination effectiveness depends on *Staphylococcus aureus-Candida albicans* dual-species communities' growth model. *Microb Drug Resist* 2022;28:613–22. https://doi.org/10.1089/mdr.2021.0324
83. Hong Q, Chang RYK, Assafiri O *et al.* Optimizing *in vitro* phage-ciprofloxacin combination formulation for respiratory therapy of multi-drug resistant *Pseudomonas aeruginosa* infections. *Int J Pharm* 2024;652:123853. https://doi.org/10.1016/j.ijpharm.2024.123853

Received: February 21, 2025. **Revised:** September 26, 2025. **Accepted:** September 29, 2025
© The Author(s) 2025. Published by Oxford University Press.
This is an Open Access article distributed under the terms of the Creative Commons Attribution License (https://creativecommons.org/licenses/by/4.0/), which permits unrestricted reuse, distribution, and reproduction in any medium, provided the original work is properly cited.

Downloaded from https://academic.oup.com/nar/article/53/20/gkaf1165/8317317 by Masarykova Univerzita user on 04 February 2026

APPENDIX 6

Komárková M, Benešík M, Procházková T, Vinco A, Laichmanová M, Smetanová S, Jelínek P, Moša M, Botka T, Šoóš M, Pantůček R (2025) Compatibility of antimicrobial preservatives with therapeutic bacteriophages of the genera *Pbunavirus* and *Kayvirus*. *European Journal of Pharmaceutics and Biopharmaceutics* 214:114781. https://doi.org/10.1016/j.ejpb.2025.114781 (JCR 2025: IF = 5.0; Q1 – Pharmacology & Pharmacy)

CC BY 4.0

European Journal of Pharmaceutics and Biopharmaceutics 214 (2025) 114781

Contents lists available at ScienceDirect

European Journal of Pharmaceutics and Biopharmaceutics

journal homepage: www.elsevier.com/locate/ejpb

Research paper

Compatibility of antimicrobial preservatives with therapeutic bacteriophages of the genera *Pbunavirus* and *Kayvirus*☆

Marie Komárková [a], Martin Benešík [b], Tereza Procházková [b], Adam Vinco [a], Monika Laichmanová [c], Soňa Smetanová [a,d], Petr Jelínek [e], Marek Mošа [b,f], Tibor Botka [a], Miroslav Šoóš [e], Roman Pantůček [a,*]

[a] Department of Experimental Biology, Division of Genetics and Molecular Biology, Faculty of Science, Masaryk University, 611 37 Brno, Czech Republic
[b] MB Pharma s.r.o., 120 00 Prague, Czech Republic
[c] Department of Experimental Biology, Czech Collection of Microorganisms, Faculty of Science, Masaryk University, 625 00 Brno, Czech Republic
[d] RECETOX, Faculty of Science, Masaryk University, 625 00 Brno, Czech Republic
[e] Department of Chemical Engineering, University of Chemistry and Technology, 166 28 Prague, Czech Republic
[f] Faculty of Science, Charles University, 128 00 Prague, Czech Republic

ARTICLE INFO

Keywords:
Phage therapy
Dosage forms formulations
Excipients
Antimicrobial preservative
Bacteriophages
Kayvirus
Pbunavirus
Pseudomonas aeruginosa
Staphylococcus aureus

ABSTRACT

Implementing bacteriophages into dosage forms is a significant step for the practical application of phage therapy. While designing a dosage form, bacteriophages as active ingredients may be exposed to excipients, guaranteeing microbial quality. However, only a few antimicrobial preservatives have been studied regarding their interaction with bacteriophages during long-term storage. Here, the stability of the staphylococcal *Kayvirus* and pseudomonal *Pbunavirus* with twelve commonly used preservatives was monitored for thirteen weeks to assess the risk of destabilisation of phage suspensions by excipients. The effectiveness of preservatives on the test bacteria, yeast and mould was determined using a microdilution method and the phage lytic activity by plaque enumeration. The antimicrobial activity of preservatives with bacteriophages was confirmed, except benzalkonium chloride and chlorhexidine digluconate, which showed precipitation and were classified as incompatible. A complete loss of phage potency in both tested phages occurred with diazolidinyl urea and in *Kayvirus* with benzalkonium chloride. For both phages, a slight decrease in titer, by one order of magnitude, was observed with m-cresol, sodium propionate, sodium benzoate, and phenylethyl alcohol. For *Kayvirus*, thimerosal, parabens, and mono propylene glycol and for *Pbunavirus*, phenoxyethanol also met the criteria. The decrease by two or more orders was determined for the remaining cases. This study helps select antimicrobial preservatives for optimizing dosage formulations with the therapeutically applicable bacteriophages.

1. Introduction

Phage therapy involves the use of bacterial viruses in the treatment of bacterial infections and represents a promising alternative to antibiotic therapy against multidrug-resistant bacteria [1,2]. The most common target pathogens considered for phage therapy are *Pseudomonas aeruginosa* and *Staphylococcus aureus* [3]. An important step when implementing phage therapy in practice is the development of a dosage form that meets the requirements for the microbiological quality defined by the European Pharmacopoeia [4]. Microbiological quality is based on aseptic and sterile preparation and the application of pharmaceutical preservatives. Due to the narrow antimicrobial spectrum, phages do not guarantee this quality themselves, so preservatives ensure long-term protection of the dosage form against contamination, for example, when repeated patient self-applications. During phage product preparation and storage, the bacteriophages are exposed to physicochemical

Abbreviations: CCM, Czech Collection of Microorganisms; CFU, Colony Forming Units; CLSI, Clinical and Laboratory Standards Institute; DLS, Dynamic Light Scattering; DSM, German Collection of Microorganisms (Deutche Sammlung von Mikroorganismen); IT, Initial Titer; LB, Luria-Bertani; PES, Polyethersulfone; PFU, Plaque Forming Units; PSS, Physiological Saline Solution; TFF, Tangential Flow Filtration; TSB, Tryptone Soya Broth; TY, Tryptone-Yeast.

☆ This article is part of a special issue entitled: 'Excipients' published in European Journal of Pharmaceutics and Biopharmaceutics.

* Corresponding author.
E-mail address: pantucek@sci.muni.cz (R. Pantůček).

https://doi.org/10.1016/j.ejpb.2025.114781
Received 12 December 2024; Received in revised form 9 May 2025; Accepted 9 June 2025
Available online 10 June 2025
0939-6411/© 2025 The Author(s). Published by Elsevier B.V. This is an open access article under the CC BY license (http://creativecommons.org/licenses/by/4.0/).

parameters like pH and temperature fluctuation, mechanical stress, UV light, or interactions with excipients that influence phage integrity and infectivity, and thus antibacterial effectivity in phage dosage form. The excipients required in multi-dose products for phage application [5–8] are antimicrobial preservatives, classified according to chemical structure into groups with specific mechanisms of action, as shown in Table 1 [9–15].

However, the interactions between bacteriophages and pharmaceutical preservatives have been the subject of a limited number of studies. The stability of phages against *Cutibacterium acnes* and *Klebsiella oxytoca* in a hydrogel containing a range of preservatives was tested [16]. Merabishvili *et al.* [17] monitored the effect of antimicrobial preservatives, but also of disinfectants and antibiotics in commercial preparations used in the treatment of burns, on the titer stability in a cocktail containing bacteriophages against *P. aeruginosa*, *Acinetobacter baumanii*, and *S. aureus*. In Russian and Georgian liquid phage preparations, quinazoline or 8-hydroxyquinoline sulfate monohydrate are used as antimicrobial preservatives [18]. Moreover, the combination of bacteriophages and preservatives can be applied in several other fields, such as food preservation against *Listeria monocytogenes* [19] or removal of viable bacteria from surfaces and skin [20,21]. The studies above indicated that preservatives can reduce the phage titer during long-term storage. Therefore, possible incompatibility should be clarified when developing a dosage form containing bacteriophages. These incompatibilities are potentially based on physicochemical properties of phage particles, such as size and morphology, charge, or protein parameters [6,22] and are often linked to the mechanism of action of the antimicrobial preservatives (Table 1).

Here, we investigate the long-term effect of pharmaceutical preservatives belonging to various chemical classes on the stability of the staphylococcal *Kayvirus* and the pseudomonal *Pbunavirus*. The members of these phage genera have been frequently and successfully applied for personalized bacteriophage therapy in various administration routes, including topical or intravenous administration, nebulization or nasal spray [7]. Both myovirus-like morphotype phages are frequently used in phage therapeutic cocktails, which target *P. aeruginosa* and *S. aureus* [23,24]. In this regard, knowledge of the interaction between excipients and bacteriophages may be a significant step toward improving the quality of dosage forms for bacteriophage administration and implementing phage therapy in clinical practice [6]. We aimed to determine if the presence of selected antimicrobial preservatives at the maximum recommended concentration influences the efficacy and stability of the bacteriophages. On the other hand, we tested whether bacteriophage suspension affects the preservative activity, especially during more extended storage periods. In addition, we have included the method of dynamic light scattering to assess the physicochemical aspect of the state of phage particles suspended in a preservative solution.

2. Materials and Methods

2.1. Bacteriophages and phage propagation

Staphylococcus bacteriophage DSM 33473 (genus *Kayvirus*), *Pseudomonas* bacteriophage DSM 33593 (genus *Pbunavirus*), and bacterial strains for phage propagation *S. aureus* DSM 33466 and *P. aeruginosa* DSM 33599 were deposited in the German Collection of Microorganisms and Cell Cultures (Leibniz Institute, Braunschweig, Germany). The

Table 1
Commonly used antimicrobial preservatives, their basic chemical properties, mode of action, and use in different applications. Assessed antimicrobial preservatives are marked in bold and were chosen as frequently applied representatives of individual chemical classes [8–15].

Chemical structure	Examples	Mechanism of action	Potential phage incompatibility	Effectiveness	Application
Organic acids and their salts	**Sodium propionate** Benzoic acid **Sodium benzoate** Dehydroacetic acid	Dissipation of the proton motive force, acidification of the cell cytoplasm	Interactions influenced by pH changes	Antifungal and antibacterial	Foodstuffs, peroral, parenteral, and dermal preparations, cosmetics
Phenols	**M-cresol** Triclosan Chlorocresol	Protein denaturation, membrane disruption	Mild protein denaturation	Lower Gram-negative bacteria effect and mould	Injection and disinfection
Alcohols	Benzylalcohol **Phenoxyethanol** **Phenylethyl alcohol** Chlorbutanol	Protein denaturation, membrane disruption, and protein synthesis inhibition	Mild protein denaturation	Antibacterial and lower antifungal effect	Dermal, ocular, nasal, and otic preparations, injection, disinfection
Quaternary ammonium compounds	**Benzalkonium chloride** Benzethonium chloride Cetrimide Carbethopendecinium bromide	Disruption of the cytoplasmic membrane based on the positive charge of compounds	Destabilization of phage particles via charge interactions or interference with adsorption	The broad spectrum of Gram-positive and Gram-negative bacteria, mould, yeast, and some viruses	Peroral, dermal, ocular, nasal, and otic preparations, injections, disinfection, cosmetics, antiseptics
Biguanides	**Chlorhexidine digluconate** Chlorhexidine diacetate Chlorhexidine dihydrochloride	Disruption of the cytoplasmic membrane based on the positive charge of compounds	Destabilization of phage particles via charge interactions or interference with adsorption	Antibacterial, antifungal, and antiviral (lipophilic viruses)	Dermal and ocular preparations, antiseptic
Heavy metal derivatives (organomercury compounds)	Phenylmercuric nitrate Phenylmercuric acetate **Thimerosal**	Enzyme inhibition due to binding to protein −SH group	Cysteine-containing proteins can be inactivated by metal-thiol binding	Antifungal and antibacterial	Parenteral, dermal, ocular, and otic preparations, antiseptic
Urea compounds	**Diazolidinyl urea** Imidazolidinyl urea	Formaldehyde release, protein and nucleotide synthesis disruption	Crosslink or denature phage proteins	Antibacterial and lower antifungal effect	Disinfection and dermal preparations
Diols	**Mono propylene glycol**	Disruption of the cytoplasmic membrane	Not expected at low concentration	Antifungal and lower effect on Gram-negative bacteria	A variety of parenteral and nonparenteral products, disinfection
Esters of 4-hydroxy-benzoic acid	**Methylparaben** Ethylparaben **Propylparaben** Butylparaben	Dissipation of the proton motive force, membrane disruption, and protein synthesis inhibition	Possible effect on phage infectivity depending on protein conformation	Antifungal and antibacterial	Foodstuffs, parenteral, dermal, and ocular preparations, cosmetics

bacteriophages are included in the liquid purified preservative-free phage cocktail Duofag® (MB PHARMA, Czech Republic), currently in clinical trial (Clinical Trial to Demonstrate the Safety and Efficacy of DUOFAG®, ClinicalTrials.gov ID NCT06319235).

DSM 33473 lysate was prepared in 1 L of tryptone-yeast (TY) broth composed of 7 g Tryptone (Oxoid, Basingstoke Hampshire, UK), 10 g Yeast Extract Powder (Oxoid), and 3 g NaCl to 1000 mL of water (pH 7.4). The culture of strain DSM 33466 was grown to $OD_{600} = 0.3$, then $CaCl_2$ to 7 mM final concentration and 1/10 vol of phage stock (10^9 PFU/mL) were added and incubated for three hours at 37 °C and 130 rpm. Phage DSM 33593 was propagated in 500 mL of Luria-Bertani (LB) broth with exponentially grown culture of strain DSM 33599 to $OD_{600} = 0.3$, then $MgCl_2$ to 7 mM concentration and 1/10 vol of the phage stock (10^9 PFU/mL) were added and incubated for 1 h at 37 °C and 130 rpm, then for 1 h at 30 °C and 60 rpm and then for 1 h at room temperature in the dark without shaking. Final lysates were filtered using a 0.22 µm polyethersulfone (PES) membrane in a vacuum Nalgene Rapid-Flow filtration unit (Thermo Fisher Scientific, USA).

2.2. Purification of phage lysates

Phage purification was performed as previously optimized [25] to meet available guidelines [26–29]. Briefly, the lysate with pH adjusted to 8 and $MgCl_2$ added to 2 mM was mixed with benzonase endonuclease EMPROVE EXPERT (Merck, Germany) to a final concentration of 3000 U/L, and incubated for 120 min at 37 °C and 80 rpm to remove bacterial DNA. Tangential flow filtration (TFF) with a Pellicon 2 Mini Ultrafiltration Cassette Biomax Module with a 300 kDa membrane (Merck, Germany) in a Pall Centramate 500 S Benchtop TFF System (Pall, USA) was used for sequential volume-reduction of phage lysates to 1/10 of the volume. The lysates were mixed in the TFF system with trisodium citrate at 1 % (w/v) and sodium deoxycholate at 2 % (w/v), and gradually washed with buffers with a decreasing concentration of these components to transfer the phage suspension to a Physiological Saline Solution (PSS) containing 0.85 % (w/v) NaCl. The final suspension reduced to 150 mL was filter-sterilized using a 0.22 µm PES membrane syringe filter (filtraTECH, France).

2.3. Antimicrobial preservatives

Twelve antimicrobial preservatives were assessed: sodium propionate (≥99.0 %), m-cresol (99 %), benzalkonium chloride (≥95.0 %), chlorhexidine digluconate (20 % w/v solution), diazolidinyl urea (≥95.0 %), and methylparaben (≥100.0 %, analytical standard) purchased from Sigma-Aldrich Chemical (St. Louis, MO, USA); phenoxyethanol (≥99.0 %, for synthesis), phenylethyl alcohol (≥99.0 %, for synthesis), and propylparaben (≥98.0 %, Ph.Eur.) from Carl Roth (Karlsruhe, Germany); sodium benzoate (≥99.8 %) from PENTA (Prague, Czech Republic); thimerosal (100 %, for antimicrobial preservation) from Gihon (Mar del Plata, Argentina); and mono propylene glycol (≥99.5 %) from Badische Anilin & Soda-Fabrik (Ludwigshafen, Germany). Stock solutions were prepared double-concentrated in PSS and filter-sterilized, except the benzalkonium chloride and phenoxyethanol, which were sterilized by autoclaving for 15 min at 121 °C and the parabens, which were dissolved in mono propylene glycol under aseptic conditions. The concentrations for the stability study shown in Table 2 were based on the maximum of the ordinarily applied dosages according to available literature [15].

2.4. Preparation of suspensions and stability study

The purified phage suspensions (10^9 PFU/mL) mixed with preservative solution in a 1:1 ratio to a 4 mL volume were prepared and stored at 6 ± 2 °C in the 5 mL brown glass vials (Thermo Fisher Scientific, USA). These vials of hydrolytic class I were treated with 1 % HCl overnight and rinsed with distilled water before sterilization to prevent alkali metals interactions. The control suspension contained PSS. The stability of the phage titer was determined by a standard spot-test plaque assay using the double-layer agar method to obtain a homogeneous lawn of the indicator strain [30], when only a countable number of plaques (1 to 50) was evaluated. The tested intervals were 24 h, fourteen days, five, nine, and thirteen weeks of storage. The results are presented as mean

Table 2
Assessment of the compatibility of antimicrobial preservatives with the tested bacteriophages based on the effect of antimicrobial preservatives on the phage titer of the suspension in a physiological saline solution. The phage potency change was assessed according to the one-sided Mann-Whitney *U* test (data in Table S8), which compared the initial titer and the titer after 24 h of preservative exposure. The Kruskal-Wallis test (data in Table S9) with Dunn's post-hoc test (data in Table S10) described the phage potency change from 24 h to 13 weeks. For both tests, the phage potency was interpreted as stable (p-value > 0.05) or decreasing when there were statistically significant differences (p-value ≤ 0.05). When the titer decrease after 13 weeks was three or more log PFU/mL, the preservative was considered unsuitable for phage products. The preservative was considered moderately suitable when the decrease was two log PFU/mL.

Preservative	Final concentration	*Kayvirus* DSM 33473				*Pbunavirus* DSM 33593			
		Trend of phage potency value [a]	Change in initial titer after 24 h of exposure (log PFU/mL)	Decrease in titer after 13 weeks (log PFU/mL)	Suitability for phage dosage forms	Trend of phage potency value [a]	Change in initial titer after 24 h of exposure (log PFU/mL)	Decrease in titer after 13 weeks (log PFU/mL)	Suitability for phage dosage forms
Sodium benzoate	2 % (w/w)	st/st	0	0	yes	dcr [b]/dcr	0	1	yes
Sodium propionate	10 % (w/w)	st/st	0	0	yes	st/st	0	0	yes
Phenoxyethanol	2 % (v/v)	st/dcr	0	2	moderate	st/st	0	0	moderate [d]
Phenylethyl alcohol	1 % (v/v)	st/dcr	0	1	yes	st/st	0	0	yes
Mono propylene glycol	50 % (v/v)	st/st	0	0	yes	st/dcr	0	2	moderate
M-cresol	0.3 % (v/v)	st/st	0	1	yes	st/dcr	0	1	yes
Methylparaben	0.06 % (w/w)	st/st	0	0	yes	st/dcr	0	2	moderate
Propylparaben	0.12 % (w/w)	st/st	0	0	yes	dcr/dcr	0	2	moderate
Thimerosal	0.1 % (w/w)	st/dcr	0	1	yes	dcr [b]/dcr	1	7	no
Benzalkonium chloride	0.02 % (w/w)	dcr [b]/dcr	5	9	no	st/dcr	0	3	no
Chlorhexidine digluconate	0.01 % (v/v)	st/dcr	0	2	no [c]	st/dcr	0	2	no [c]
Diazolidinyl urea	0.5 % (w/w)	dcr [b]/dcr	5	9	no	dcr [b]/dcr	5	9	no

Legend: [a], Mann-Whitney *U* test / Kruskal-Wallis test; st, stable; dcr, statistically significant decrease (p-value < 0.05); [b], marginally statistically significant decrease (p-value = 0.05); [c], precipitation in storage suspension (Tables S1–S3); [d], incompatibility based on the results of DLS.

values of biological triplicates and technological duplicates as recommended previously [31].

2.5. Effectivity of antimicrobial preservatives

The antimicrobial effect of preservatives was tested using the test microorganisms specified in the European Pharmacopoeia (Ph. Eur. 11th edition, chapter 5.1.3. Efficacy of antimicrobial preservation), namely *P. aeruginosa* CCM 1961, *S. aureus* CCM 4516, *Escherichia coli* CCM 4517, *Candida albicans* CCM 8215, and *Aspergillus brasiliensis* CCM 8222 obtained from the Czech Collection of Microorganisms (Masaryk University, Brno, Czech Republic, https://ccm.sci.muni.cz/en). The modified broth microdilution method was used for susceptibility testing [32] in biological and technological duplicates at five tested time intervals. Briefly, the sample was mixed with 10 × concentrated broth in a ratio of 1:9 into 500 μL. The LB broth was used for *P. aeruginosa*, TY broth for *S. aureus*, and Tryptone Soya Broth (TSB) (Oxoid) for other test microorganisms. 200 μl of the mixture was pipetted into 96-well microtiter plates with flat bottoms (Anicrin, Italy) and inoculated with a suspension to a final concentration of 5×10^3–5×10^4 colony forming units (CFU)/mL using an inoculator device with a pin 1 mm in diameter. Every plate contained PSS with inoculated broth and PSS with non-inoculated broth as positive and negative controls, respectively. The plates were incubated at 37 °C for 18 h, and for *C. albicans* and *A. brasiliensis* for 48 h. The turbidity was determined by visual comparison with the controls.

2.6. Dynamic light scattering

Dynamic light scattering (DLS) with 3D LS spectrometer (LS Instruments, Switzerland) was used for the measurements performed at the angle of 90° and temperature of 25 °C after 24 h and fourteen days of sample storage. Due to the low variability of biological samples, the final size of particles was determined as an average of three DLS measurements (20 s) of two biological replicates, which was sufficient to obtain statistically relevant data. The PSS with antimicrobial preservative solutions and purified phage suspension without a preservative were applied like blank. As the DLS-calculated size is viscosity-dependent, the viscosity of samples was measured in the double gap geometry using Rheometer MCR 702e (Anton Paar, Austria).

2.7. Assessment of compatibility between phages and preservatives

No specific pharmacopeial guidance exists yet for preservatives in phage products; therefore, the assessment criteria were selected to meet established regulatory considerations. Compatibility between phages and preservatives during long-term exposure was evaluated using four tests: I) Antimicrobial Efficacy – the growth of test microorganisms has been inhibited in the presence of bacteriophage, indicating the stability of the preservative effect; II) Formulation Stability – the preservative or used solvent did not cause sample precipitation or other signs of instability; III) Impact on Bacteriophage Stability – the preservative did not cause chemical degradation or disruption of bacteriophage virions and/or did not induce phage aggregation; IV) Impact on Bacteriophage Viability – the phage titer has not decreased below the previously recommended value 10^7 PFU/mL [17].

2.8. Statistical analysis

Non-parametric tests relevant to the number of replicates were applied. The Mann-Whitney *U* test was applied to assess the decrease in the initial titer after 24 h and the change in the DLS signal after 24 h and 14 days. The Kruskal-Wallis test with Dunn's post-hoc was used to test phage titer during time intervals. The Statistica version 14.0.0.15 (TIBCO Software, CA, USA) with R version 4.3.2 (rOpenSci initiative, https://ropensci.org/, Vienna, Austria) was applied for statistical analysis and OriginPro 2023 (OriginLab Corporation, MA, USA) for the visualization of data.

3. Results

3.1. Study of bacteriophage-preservative incompatibility

When designing bacteriophage dosage forms, it is essential to test the compatibility of phages with all excipients, including preservatives. The antimicrobial effect of the tested preservatives without bacteriophages was proven on all the used test microorganisms except for chlorhexidine digluconate, which precipitated after five weeks of storage (Table S1) and caused the detection of antimicrobial interactions to be impossible. The phage presence did not disrupt the effect of the antimicrobial preservatives except for benzalkonium chloride, which precipitated with both phages used (Tables S2 and S3). These precipitation events made it impossible to detect the effectivity of the preservative by the microdilution method since it created turbidity without inoculation. We did not notice any influence of the assessed bacteriophages without antimicrobial preservatives on the growth of the test microorganisms, except for strain *S. aureus* CCM 4516, which is sensitive to staphylococcal phage DSM 33473 (Table S2).

3.2. Physicochemical interaction between bacteriophages and antimicrobial preservatives

The physical state of bacteriophage particles after exposure to antimicrobial preservatives was analyzed by the DLS measurement technique. According to the results, the average value of virion size in standardly applied physiological saline solution without antimicrobial preservatives and with phage suspension of 10^9 PFU/mL was 117.26 ± 3.79 nm in the case of *Kayvirus* and 92.87 ± 4.16 nm for *Pbunavirus* (Fig. 1, Table S4). No significant difference ($p > 0.05$) compared to these values in the blank purified phage suspension was observed for most tested preservatives and for both tested phages (Fig. 1, Tables S4 and S5).

The particle size exceeded the instrument measurement range in the case of benzalkonium chloride, chlorhexidine digluconate, and in the case of phenoxyethanol after 14 days with *Pbunavirus* DSM 33593 (Table S4). These results confirmed the benzalkonium chloride and chlorhexidine digluconate incompatibilities demonstrated in the microdilution method and pointed out further possible incompatibility with phenoxyethanol (Fig. 1).

3.3. Stability of phage titer with antimicrobial preservatives

Due to their antimicrobial nature, the inhibition effect of antimicrobial preservatives is critical for interpreting the lytic activity of a bacteriophage. To bypass any inhibition of the bacterial lawn by an antimicrobial preservative itself during phage titration, only dilutions with countable plaques were considered. The results on phage titer stability during storage are shown in Tables S6 and S7. In the purified phage suspension without preservative, there was a minimal titer decrease of no more than a tenth of one order of magnitude, i.e., 0.08 ± 0.01 log PFU/mL for *Kayvirus* and 0.16 ± 0.18 log PFU/mL for *Pbunavirus*. With sodium benzoate, phenoxyethanol, phenylethyl alcohol, m-cresol, mono propylene glycol, parabens, and chlorhexidine digluconate, the titers decreased by approximately at most two orders of magnitude (Fig. 2, Table 2). Both phages were most stable without a titer decrease during storage with sodium propionate (Fig. 2). On the other hand, a complete loss of titer was observed for staphylococcal *Kayvirus* DSM 33473 with benzalkonium chloride, while pseudomonal *Pbunavirus* DSM 33593 exhibited a decrease of approximately three orders of magnitude (Fig. 2, Table 2). A significant decrease in potency was induced by thimerosal in *Pbunavirus* DSM 33593, while for the *Kayvirus* DSM 33473, the titer decreased by approximately one order of

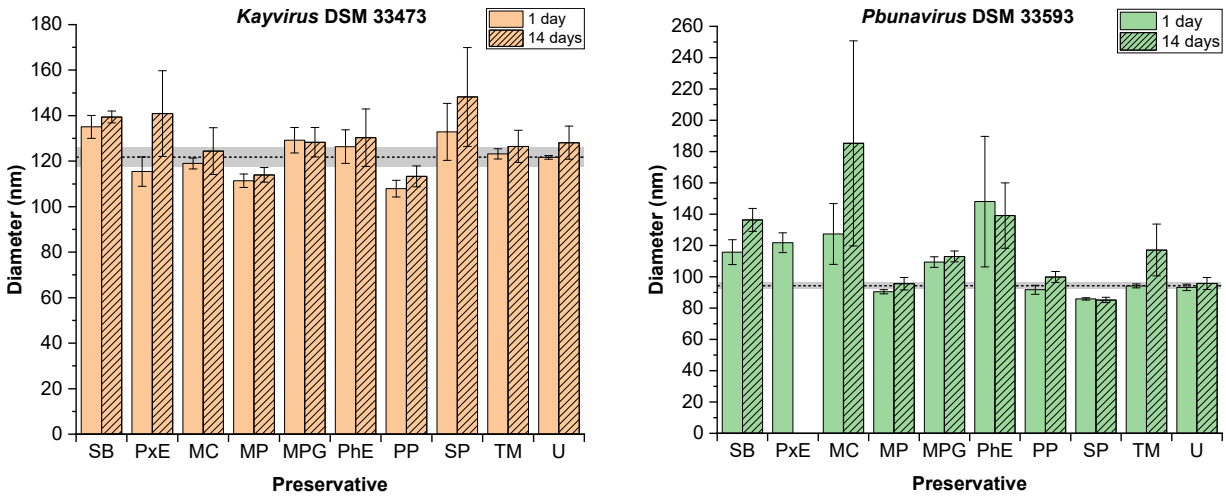

Fig. 1. The size range of particles in phage suspension with variant antimicrobial preservatives measured by dynamic light scattering. The size of phage particles (nm) in suspensions with preservatives is shown as mean value ± SD (n = 2), *Kayvirus* DSM 33473 on the left (orange), and *Pbunavirus* DSM 33593 on the right (green). The dashed lines with grey shadow represent the mean value of the phage particle size in suspension without the preservatives. In the case of chlorhexidine digluconate, and benzalkonium chloride, the size of signal exceeded the instrument measuring range, so these preservatives are excluded from the figure, as in the case of phenoxyethanol with DSM 33593 after 14 days. Abbreviations: SB, sodium benzoate; PxE, Phenoxyethanol; MC, M-cresol; MP, Methylparaben; MPG, Mono propylene glycol; PhE, Phenylethyl alcohol; PP, Propylparaben; SP, Sodium propionate; TM, Thimerosal; U, Diazolidinyl urea.

magnitude (Fig. 2). Both phages lost potency after two weeks of storage with diazolidinyl urea.

According to phage stability and preservative compatibility results, we classified preservatives into suitable and unsuitable groups for dosage forms with evaluated phage (Table 2).

4. Discussion

Bacteriophage virions are nucleoprotein particles with lipid-free capsids, and excipients can influence their chemical nature and stability, leading to potential incompatibilities [22], which introduces unique formulation challenges. This study aims to recommend antimicrobial preservatives applied to a broad spectrum of dosage forms against microbial contaminants [15] that cause a minimal decrease in phage potency and retain antimicrobial activity when developing new dosage forms. According to our classification, phage-compatible preservatives were organic acid salts, phenols, alcohols, and parabens. Of these suitable candidates, interaction with parabens was previously investigated in the case of *Pbunavirus* and *Kayvirus* phages. Merabishvili *et al.* [17] demonstrated that Sulfamylon containing paraben excipients caused a decrease in initial titer 10^9 PFU/mL of at most two orders of magnitude in *Kayvirus* ISP and *Pbunavirus* 14–1, which is partly consistent with our results. Nevertheless, the storage conditions at 37 °C for 24 h they applied correspond rather to conditions on human skin, but not to long-term storage of the dosage form. In addition, their exploration concerned the interaction between bacteriophages and burn wound care products containing multiple components [17], including antibiotics and other excipients, which may have affected phage titer. When examining the interaction between multiple excipients and phages, it is necessary to point out that the phage titer stability in mono propylene glycol, both with and without parabens, was comparable. This suggests that the presence of parabens does not significantly affect the stability of *Kayvirus* titers relative to mono propylene glycol alone (Fig. 2). Furthermore, the slight decrease in titer observed indicates that mono propylene glycol may serve as a suitable solvent for compounds that are poorly soluble or insoluble in water, supporting its potential application in phage therapy formulations containing *Kayvirus*.

Chemical and physical interactions between various excipients and bacteriophages are essential for phage compatibility and should not be neglected. In previous studies, the authors demonstrated phage aggregation and fragmentation after exposure to physicochemical factors using DLS analysis [33,34]. Here, DLS analysis showed colloidal instability of chlorhexidine digluconate, leading to the formation of large clusters despite the still weak effect of the antimicrobial preservative on phage potency. The formation of clusters is connected with the production of chlorhexidine salts in the presence of some substances, including chlorides, which is typical for chlorhexidine in concentrations greater than 0.05 % w/v, but it is also possible in concentrations below 0.01 % w/v [15]. Also, previous studies have focused on the interaction between chlorhexidine digluconate and *Pbunavirus* or *Kayvirus* genera members, but did not notice the precipitation of chlorhexidine digluconate. When stored at 37 °C for 24 h, the authors proved the negative influence on *Kayvirus* with initial titers of 10^5 and 10^9 PFU/mL and chlorhexidine in concentrations of 0.02–0.2 % [17,35]. Chlorhexidine digluconate in concentration 0.05 % caused a decrease in the initial titer 10^9 log PFU/mL by at most two orders of magnitude for *Pbunavirus* 14–1 [17], corresponding to DSM 33593. However, the antimicrobial preservative was an active ingredient of the anti-infective solution Hibidil with other excipients, which makes the comparison problematic. The different compound concentrations, storage time, and temperature in previous studies can explain the observed differences in the compatibility of chlorhexidine digluconate and assessed phages, especially the absence of precipitation in contrast with our study. It points out that these factors must be considered during the development of phage therapy products.

The significant physicochemical interactions with bacteriophage were confirmed in the case of benzalkonium chloride. Using benzalkonium chloride resulted in a highly turbid appearance of both phage samples, indicating aggregation. However, it reduced the phage titer differently, depending on the phage used. We hypothesize that the cause is charge-based interactions between a negatively charged phage particle [36,37] and the cationic compound, as described previously [15,36]. We presume that these charge-based interactions have a dissimilar influence on the titers of assessed bacteriophages, because their particles have different protein composition and structure. The negative influence of benzalkonium chloride in concentration 0.002–5 % on *Kayvirus* has been previously noticed but the high storage temperature and lower used phage initial titer 10^5 PFU/mL probably caused a more rapid titer decrease after 24 h with no sign of precipitation [35] in contrast with our study, as in the case of chlorhexidine. The charge-based interaction of phages is another factor that restricts the application of some cationic substances.

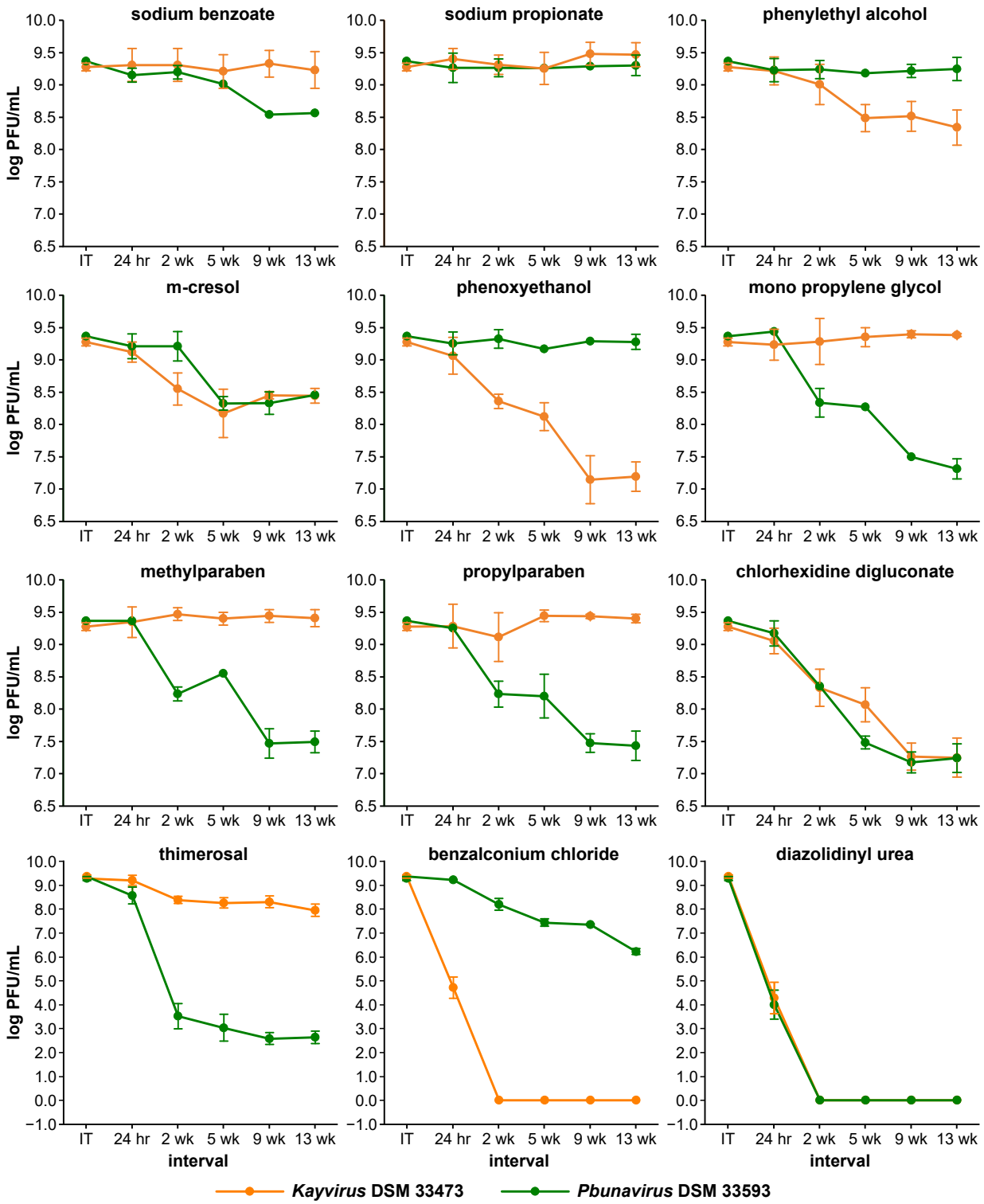

Fig. 2. Stability of *Kayvirus* and *Pbunavirus* phage titer with antimicrobial preservatives. The values of phage titer in physiological saline solution at five assessed time points are expressed as log PFU/mL. The initial titer (IT) is shown. Values on axis y are adjusted according to the decrease rate in the titer. Data are shown as mean values ± SD (n = 3). The axis x does not represent a continuous timescale; discrete time categories are connected by lines for visual clarity.

Another important feature of applied excipients is their safety. Our study confirms that the organic mercury compound thimerosal is a suitable preservative for preparations containing *Kayvirus*, and probably other *Twortvirinae* members regarding titer stability. This is supported by the fact that thimerosal has been used to preserve bacteriophage products, for example, Stafal®, containing *Kayvirus* [38]. Still, the application of thimerosal is being phased out due to toxicity and adverse reactions. Although phenoxyethanol caused a decrease in titer of around two orders of magnitude (Table 2), it represents a safer variant [39]. The difference between assessed phage genera in tolerance to thimerosal is another undesirable factor that restricts the application of this excipient in phage cocktails. We presume that this difference in titer loss is connected with the structural changes of distinct phage proteins during exposure to thimerosal, caused by mercury binding through thiol groups

of the proteins [40]. In sum, the protein incompatibility and toxicity of this compound [15] rather exclude its application for phage therapy products.

Diazolidinyl urea caused a loss of potency in both phages, probably due to the inactivation effect of the released formaldehyde, whose antiviral effect is generally described. For this reason, it could be more applicable as an antiviral agent for preventing contamination by phages [21,41]. Moreover, this preservative is often applied for cosmetics preservation, similar to benzalkonium chloride (Table 1). These possible negative interactions based on the virucidal effect of applied excipients in phage therapy products, for example, for skin application, should be controlled, especially in the design of clinical trials, as was pointed out, e.g., during the PhagoBurn study [42].

To summarize, the presented assessment of antimicrobial preservative-phage compatibility is helpful for future studies that will be of interest in optimizing pharmaceutical phage therapy products and the interaction between bacteriophages, excipients, and microbiological contaminants. The assessed brands of preservatives in this study have a high degree of quality and purity, but not all were suitable for pharmaceutical application. Still, it is possible to implement the results of this study during future optimisation with preservatives in pharmaceutical grade. The non-invasive and facile DLS method may play a significant role in describing possible incompatibilities of individual phage strains and excipients. The phage strain with target bacteria and many other features of the dosage form should be considered, including antimicrobial preservative concentration, combination with antibiotics, storage temperature and time, and the interactions with other excipients, packaging material, or simultaneously administered products.

CRediT authorship contribution statement

Marie Komárková: Writing – review & editing, Writing – original draft, Visualization, Validation, Methodology, Investigation, Formal analysis, Data curation, Conceptualization. **Martin Benešík:** Writing – review & editing, Supervision, Methodology, Conceptualization. **Tereza Procházková:** Writing – review & editing, Methodology, Investigation. **Adam Vinco:** Writing – review & editing, Investigation, Formal analysis. **Monika Laichmanová:** Writing – review & editing, Methodology, Investigation. **Soňa Smetanová:** Writing – review & editing, Validation, Formal analysis, Data curation. **Petr Jelínek:** Writing – review & editing, Visualization, Methodology, Investigation, Formal analysis. **Marek Moša:** Writing – review & editing, Resources, Funding acquisition. **Tibor Botka:** Writing – review & editing, Funding acquisition. **Miroslav Šoóš:** Writing – review & editing, Supervision, Conceptualization. **Roman Pantůček:** Writing – review & editing, Writing – original draft, Visualization, Supervision, Project administration, Funding acquisition, Conceptualization.

Declaration of Competing Interest

The authors declare the following financial interests/personal relationships which may be considered as potential competing interests: Martin Benešík, Tereza Procházková and Marek Moša are employees of a company that manufactures bacteriophage products.

Acknowledgments

This work was supported by the project National Institute of Virology and Bacteriology (Programme EXCELES, Project ID LX22NPO5103) - Funded by the European Union - Next Generation EU to R.P. The authors gratefully acknowledge funding from the Ministry of Health of the Czech Republic (NU21J-05-00035) to T.B. and the project co-funded with public support from the Technology Agency of the Czech Republic under the TREND Programme and funded under the National Recovery Plan from the European Recovery and Resilience Facility (FW10010112) to M.M. Authors also thank RECETOX Research Infrastructure (LM2023069) funded by the Ministry of Education, Youth and Sports of the Czech Republic for its supportive background.

The authors wish to thank Dana Kadaňková (Masaryk University, Brno), Kateřina Plachá, Rostislav Halouzka, and Dominik Chmelík (MB Pharma s.r.o., Prague), and Aleš Franc (Masaryk University, Faculty of Pharmacy, Brno), for their valuable help. The graphical abstract was created with BioRender.com.

Appendix A. Supplementary data

Supplementary data to this article can be found online at https://doi.org/10.1016/j.ejpb.2025.114781.

Data availability

All data are available in the Supplementary material online.

References

[1] D.P. Pires, A.R. Costa, G. Pinto, L. Meneses, J. Azeredo, Current challenges and future opportunities of phage therapy, FEMS Microbiol. Rev. 44 (2020) 684–700, https://doi.org/10.1093/femsre/fuaa017.
[2] S. Uyttebroek, B. Chen, J. Onsea, F. Ruythooren, Y. Debaveye, D. Devolder, et al., Safety and efficacy of phage therapy in difficult-to-treat infections: a systematic review, Lancet Infect. Dis. 22 (2022) e208–e220, https://doi.org/10.1016/S1473-3099(21)00612-5.
[3] S.A. Gómez-Ochoa, M. Pitton, L.G. Valente, C.D. Sosa Vesga, J. Largo, A. C. Quiroga-Centeno, et al., Efficacy of phage therapy in preclinical models of bacterial infection: a systematic review and meta-analysis, Lancet Microbe 3 (2022) e956–e968, https://doi.org/10.1016/S2666-5247(22)00288-9.
[4] J.P. Pirnay, T. Ferry, G. Resch, Recent progress toward the implementation of phage therapy in Western medicine, FEMS Microbiol. Rev. 46 (2022), https://doi.org/10.1093/femsre/fuab040 fuab040.
[5] H. Duyvejonck, M. Merabishvili, M. Vaneechoutte, S. de Soir, R. Wright, V. P. Friman, et al., Evaluation of the stability of bacteriophages in different solutions suitable for the production of magistral preparations in Belgium, Viruses 13 (2021) 865, https://doi.org/10.3390/v13050865.
[6] D.J. Malik, I.J. Sokolov, G.K. Vinner, F. Mancuso, S. Cinquerrui, G. T. Vladisavljevic, et al., Formulation, stabilisation and encapsulation of bacteriophage for phage therapy, Adv. Colloid Interface Sci. 249 (2017) 100–133, https://doi.org/10.1016/j.cis.2017.05.014.
[7] J.P. Pirnay, S. Djebara, G. Steurs, J. Griselain, C. Cochez, S. De Soir, et al., Personalized bacteriophage therapy outcomes for 100 consecutive cases: a multicentre, multinational, retrospective observational study, Nat. Microbiol. 9 (2024) 1434–1453, https://doi.org/10.1038/s41564-024-01705-x.
[8] R.Y.K. Chang, S. Morales, Y. Okamoto, H.K. Chan, Topical application of bacteriophages for treatment of wound infections, Transl. Res. 220 (2020) 153–166, https://doi.org/10.1016/j.trsl.2020.03.010.
[9] M.J. Akers, Sterile Drug Products: Formulation, Packaging, Manufacturing and Quality, Informa Healthcare, London, UK, 2010.
[10] K.A. Fitzgerald, A. Davies, A.D. Russell, Sensitivity and resistance of *Escherichia coli* and *Staphylococcus aureus* to chlorhexidine, Lett. Appl. Microbiol. 14 (1992) 33–36, https://doi.org/10.1111/j.1472-765X.1992.tb00641.x.
[11] P. Gilbert, D. Pemberton, D.E. Wilkinson, Barrier properties of the gram-negative cell envelope towards high molecular weight polyhexamethylene biguanides, J. Appl. Bacteriol. 69 (1990) 585–592, https://doi.org/10.1111/j.1365-2672.1990.tb01552.x.
[12] R.I. Mahato, A.S. Narang. Pharmaceutical Dosage Forms and Drug Delivery, 3rd ed., CRC Press, Boca Raton, 2018 https://doi.org/10.1201/9781315156941.
[13] E. Ortega Morente, M.A. Fernandez-Fuentes, M.J. Grande Burgos, H. Abriouel, R. Perez Pulido, A. Galvez, Biocide tolerance in bacteria, Int. J. Food Microbiol. 162 (2013) 13–25, https://doi.org/10.1016/j.ijfoodmicro.2012.12.028.
[14] A.D. Russell, I. Chopra, Understanding Antibacterial Action and Resistance, 2nd ed., Ellis Horwood, Hertfordshire, UK, 1996.
[15] R.C. Rowe, P.J. Sheskey, M.E. Quinn, Handbook of Pharmaceutical Excipients, Sixth ed., Pharmaceutical Press and American Pharmacist Association, London, UK, 2009.
[16] T.L. Brown, H. Ku, G. Mnatzaganian, M. Angove, S. Petrovski, M. Kabwe, et al., The varying effects of a range of preservatives on *Myoviridae* and *Siphoviridae* bacteriophages formulated in a semi-solid cream preparation, Lett. Appl. Microbiol. 71 (2020) 203–209, https://doi.org/10.1111/lam.13299.
[17] M. Merabishvili, R. Monserez, J. van Belleghem, T. Rose, S. Jennes, D. De Vos, et al., Stability of bacteriophages in burn wound care products, PLoS One 12 (2017) e0182121, https://doi.org/10.1371/journal.pone.0182121.
[18] A.M. Pinto, M.A. Cerqueira, M. Banobre-Lopes, L.M. Pastrana, S. Sillankorva, Bacteriophages for chronic wound treatment: From traditional to novel delivery systems, Viruses 12 (2020) 235, https://doi.org/10.3390/v12020235.
[19] A. Chibeu, L. Agius, A. Gao, P.M. Sabour, A.M. Kropinski, S. Balamurugan, Efficacy of bacteriophage LISTEXP100 combined with chemical antimicrobials in reducing

Listeria monocytogenes in cooked turkey and roast beef, Int. J. Food Microbiol. 167 (2013) 208–214, https://doi.org/10.1016/j.ijfoodmicro.2013.08.018.
[20] E. Stachler, A. Kull, T.R. Julian, Bacteriophage treatment before chemical disinfection can enhance removal of plastic-surface-associated *Pseudomonas aeruginosa*, Appl. Environ. Microbiol. 87 (2021) e00980–21, https://doi.org/10.1128/AEM.00980-21.
[21] L. Chen, W.J. Lee, Y. Ma, S.S. Jang, K. Fong, S. Wang, The efficacy of different sanitizers against MS2 bacteriophage introduced onto plastic or stainless steel surfaces, Curr. Res. Food Sci. 5 (2022) 175–181, https://doi.org/10.1016/j.crfs.2022.01.004.
[22] E. Jończyk-Matysiak, N. Łodej, D. Kula, B. Owczarek, F. Orwat, R. Międzybrodzki, et al., Factors determining phage stability/activity: challenges in practical phage application, Expert Rev. Anti Infect. Ther. 17 (2019) 583–606, https://doi.org/10.1080/14787210.2019.1646126.
[23] K. Leskinen, H. Tuomala, A. Wicklund, J. Horsma-Heikkinen, P. Kuusela, M. Skurnik, et al., Characterization of vB_SauM-fRuSau02, a Twort-like bacteriophage isolated from a therapeutic phage cocktail, Viruses 9 (2017) 258, https://doi.org/10.3390/v9090258.
[24] M. Merabishvili, J.P. Pirnay, G. Verbeken, N. Chanishvili, M. Tediashvili, N. Lashkhi, et al., Quality-controlled small-scale production of a well-defined bacteriophage cocktail for use in human clinical trials, PLoS One 4 (2009) e4944, doi:10.1371/journal.pone.0004944.
[25] M. Komárková, M. Benešík, E. Černá, L. Sedláčková, M. Moša, L. Vojtová, et al., The pharmaceutical quality of freeze-dried tablets containing therapeutic bacteriophages against *Pseudomonas aeruginosa* and *Staphylococcus aureus*, Int. J. Pharm. 671 (2025) 125199, https://doi.org/10.1016/j.ijpharm.2025.125199.
[26] T. Luong, A.C. Salabarria, R.A. Edwards, D.R. Roach, Standardized bacteriophage purification for personalized phage therapy, Nat. Protoc. 15 (2020) 2867–2890, https://doi.org/10.1038/s41596-020-0346-0.
[27] B. Lapras, C. Marchand, C. Merienne, M. Medina, C. Kolenda, F. Laurent, et al., Rationalisation of the purification process for a phage active pharmaceutical ingredient, Eur. J. Pharm. Biopharm. 203 (2024) 114438, https://doi.org/10.1016/j.ejpb.2024.114438.
[28] V. Hietala, J. Horsma-Heikkinen, A. Carron, M. Skurnik, S. Kiljunen, The removal of endo- and enterotoxins from bacteriophage preparations, Front. Microbiol. 10 (2019) 1674, https://doi.org/10.3389/fmicb.2019.01674.
[29] C.E. Frasch, L. van Alphen, J. Holst, J.T. Poolman, E. Rosenqvist, Outer membrane protein vesicle vaccines for meningococcal disease, in: A.J. Pollard, M.C. Maiden, (Eds.), Meningococcal Vaccines, Humana Press, New York, NY, 2001, pp. 81-107, doi:10.1385/1-59259-148-5:81.
[30] M.R.J. Clokie, A.M. Kropinski, Bacteriophages Methods and Protocols, in: Isolation, Characterization, and Interactions 1, Humana Press, New York, NY, 2009, https://doi.org/10.1007/978-1-60327-164-6.
[31] S.T. Abedon, T.I. Katsaounis, Detection of bacteriophages: Statistical aspects of plaque assay, in: D.R. Harper, S.T. Abedon, B.H. Burrowes, M.L. McConville, (Eds.), Bacteriophages Biology, Technology, Therapy, Springer, Cham, 2021, pp. 539-560, doi:10.1007/978-3-319-41986-2_17.
[32] CLSI, M07-A10 - Methods for Dilution Antimicrobial Susceptibility Tests for Bacteria that Grow Aerobically. Approved Standard, 10th ed., Clinical and Laboratory Standards Institute, Wayne, PA, 2015.
[33] T. Dharmaraj, M.J. Kratochvil, J.D. Pourtois, Q. Chen, M. Hajfathalian, A. Hargil, et al., Rapid assessment of changes in phage bioactivity using dynamic light scattering, PNAS Nexus 2 (2023) gad406, https://doi.org/10.1093/pnasnexus/pgad406.
[34] B. Szermer-Olearnik, M. Drab, M. Makosa, M. Zembala, J. Barbasz, K. Dabrowska, et al., Aggregation/dispersion transitions of T4 phage triggered by environmental ion availability, J. Nanobiotechnol. 15 (2017) 32, https://doi.org/10.1186/s12951-017-0266-5.
[35] S. Agún, L. Fernández, E. González-Menéndez, B. Martínez, A. Rodríguez, P. García, Study of the interactions between bacteriophage phiIPLA-RODI and four chemical disinfectants for the elimination of *Staphylococcus aureus* contamination, Viruses 10 (2018) 103, https://doi.org/10.3390/v10030103.
[36] M.H. Ly-Chatain, S. Moussaoui, A. Vera, V. Rigobello, Y. Demarigny, Antiviral effect of cationic compounds on bacteriophages, Front. Microbiol. 4 (2013) 46, https://doi.org/10.3389/fmicb.2013.00046.
[37] M. Horká, D. Štveráková, J. Šalplachta, K. Šlais, M. Šiborová, F. Růžička, et al., Electrophoretic techniques for purification, separation and detection of *Kayvirus* with subsequent control by matrix-assisted laser desorption/ionization time-of-flight mass spectrometry and microbiological methods, J. Chromatogr. A 1570 (2018) 155–163, https://doi.org/10.1016/j.chroma.2018.07.078.
[38] M. Dvorackova, F. Ruzicka, M. Benesik, R. Pantucek, M. Dvorakova-Heroldova, Antimicrobial effect of commercial phage preparation Stafal® on biofilm and planktonic forms of methicillin-resistant *Staphylococcus aureus*, Folia Microbiol. 64 (2019) 121–126, https://doi.org/10.1007/s12223-018-0622-3.
[39] I. Lowe, J. Southern, The antimicrobial activity of phenoxyethanol in vaccines, Lett. Appl. Microbiol. 18 (1994) 115–116, https://doi.org/10.1111/j.1472-765x.1994.tb00820.x.
[40] J.G. Elferink, Thimerosal: a versatile sulfhydryl reagent, calcium mobilizer, and cell function-modulating agent, Gen. Pharmacol. 33 (1999) 1–6, https://doi.org/10.1016/s0306-3623(98)00258-4.
[41] C. Campagna, M. Villion, S.J. Labrie, C. Duchaine, S. Moineau, Inactivation of dairy bacteriophages by commercial sanitizers and disinfectants, Int. J. Food Microbiol. 171 (2014) 41–47, https://doi.org/10.1016/j.ijfoodmicro.2013.11.012.
[42] P. Jault, T. Leclerc, S. Jennes, J.P. Pirnay, Y.A. Que, G. Resch, et al., Efficacy and tolerability of a cocktail of bacteriophages to treat burn wounds infected by *Pseudomonas aeruginosa* (PhagoBurn): A randomised, controlled, double-blind phase 1/2 trial, Lancet Infect. Dis. 19 (2019) 35–45, https://doi.org/10.1016/S1473-3099(18)30482-1.

APPENDIX 7

Šimečková H, Bárdy P, Kuntová L, Macháčová E, Botka T, Bíňovský J, Houser J, Farka Z, Plevka P, Pantůček R, Mašlaňová I (2025) CRISPR-Cas10-assisted structural modification of staphylococcal *Kayvirus* for imaging and biosensing applications. *ACS Synthetic Biology* 14:2979–2986. https://doi.org/10.1021/acssynbio.5c00387

(JCR 2025: IF = 4.5; Q1 – Biochemical research methods)

CC BY 4.0

ACS SyntheticBiology

Open Access
This article is licensed under CC-BY 4.0

pubs.acs.org/synthbio
Letter

CRISPR-Cas10-Assisted Structural Modification of Staphylococcal *Kayvirus* for Imaging and Biosensing Applications

Hana Šimečková, Pavol Bárdy, Lucie Kuntová, Eliška Macháčová, Tibor Botka, Ján Bíňovský, Josef Houser, Zdeněk Farka, Pavel Plevka, Roman Pantůček, and Ivana Mašlaňová*

Cite This: *ACS Synth. Biol.* 2025, 14, 2979−2986

Read Online

ACCESS | Metrics & More | Article Recommendations | Supporting Information

ABSTRACT: Recent advances in genome editing techniques based on CRISPR-Cas have opened up new possibilities in bacteriophage engineering and, thus, enabled key developments in medicine, nanotechnology, and synthetic biology. Although staphylococcal phage genomes have already been edited, the modification of their structural proteins has not yet been reported. Here, the structure of *Staphylococcus* phage 812h1 of the *Kayvirus* genus was modified by inserting a poly histidine tag into an exposed loop of the tail sheath protein. A two-strain editing strategy was applied, utilizing homologous recombination followed by CRISPR-Cas10-assisted counter-selection of the recombinant phages. The His-tagged phage particles can be recognized by specific antibodies, enabling the modified bacteriophages to be employed in numerous techniques. The attachment of the engineered phage to bacteria was visualized by fluorescence microscopy, and its functionality was confirmed using biolayer interferometry biosensing, enzyme-linked immunosorbent assay, and flow cytometry, demonstrating that the genetic modification did not impair its biological activity.

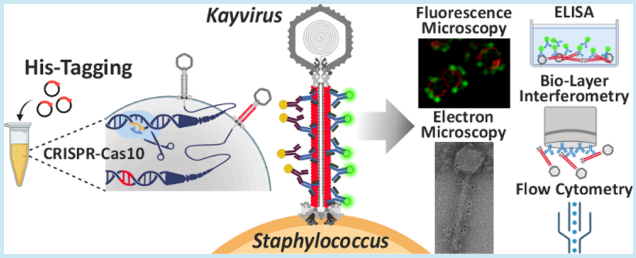

KEYWORDS: *Bacteriophage, CRISPR-Cas10, Staphylococcus aureus, Biosensing Techniques, Poly histidine Tag, Herelleviridae*

Downloaded via MASARYK UNIV on February 4, 2026 at 10:05:59 (UTC).
See https://pubs.acs.org/sharingguidelines for options on how to legitimately share published articles.

INTRODUCTION

Bacteriophages, natural predators of bacteria, are integral components of a wide range of ecosystems and profoundly influence bacterial evolution.[1] Fundamental phage research and studies of its applications in medicine, the food industry, and biotechnology are being intensively conducted worldwide. Technological advances in genetic engineering open up new possibilities for improving phage properties, and modified bacteriophages are powerful tools in current science.[2−4]

Phage particles are complex viral DNA−protein assemblies with diverse biological functions and effects on target cells. Genetic modifications of phages focus on extending their host range,[5,6] increasing their antibacterial efficacy,[7,8] and the development of reporter phages for pharmaceutical research and biotechnology applications.[9] Modified phage particles can also act as selective bioreceptors in various detection tools,[10] deliver a programmed CRISPR-Cas system,[11−13] or serve as antibacterial drones.[14,15] However, the efficient genome editing of lytic bacteriophages, which do not integrate DNA into the bacterial chromosome, poses several challenges due to their rapid replication cycle,[16] degradation of the host chromosome early in infection,[17] or compartmentalization of their genome from the rest of the cell.[18]

An effective genome-editing strategy that has been successfully implemented in recent years is CRISPR-assisted genome editing. This approach is based on homologous recombination followed by the counter-selection of rare recombinants using the CRISPR-Cas machinery. It has enabled the successful modification of various phages targeting *Escherichia coli*,[19−21] *Streptococcus thermophilus*,[22] *Vibrio cholerae*,[23] *Lactococcus lactis*,[24] *Klebsiella pneumoniae*,[25] *Pseudomonas aeruginosa*,[26] and *Listeria monocytogenes*.[27]

The CRISPR-Cas10 (Type III-A) system to counter-selection of recombinant staphylococcal phages was also applied to the genome editing of *Staphylococcus aureus* kayviruses from the family *Herelleviridae*.[28,29] However, this was performed as a proof-of-concept study, introducing simple nucleotide substitutions into the gene for the phage DNA polymerase, resulting in silent mutations. Structural studies of kayviruses,[30] the availability of genomes in public databases, the integration of proteomic data into this framework,[31] and new insights into phage-host interactions obtained from transcriptomic studies[32] bring possibilities for more challenging genome editing of this phage group.

Received: May 28, 2025
Revised: July 22, 2025
Accepted: July 23, 2025
Published: July 28, 2025



ACS Publications
© 2025 The Authors. Published by American Chemical Society

https://doi.org/10.1021/acssynbio.5c00387
ACS Synth. Biol. 2025, 14, 2979−2986

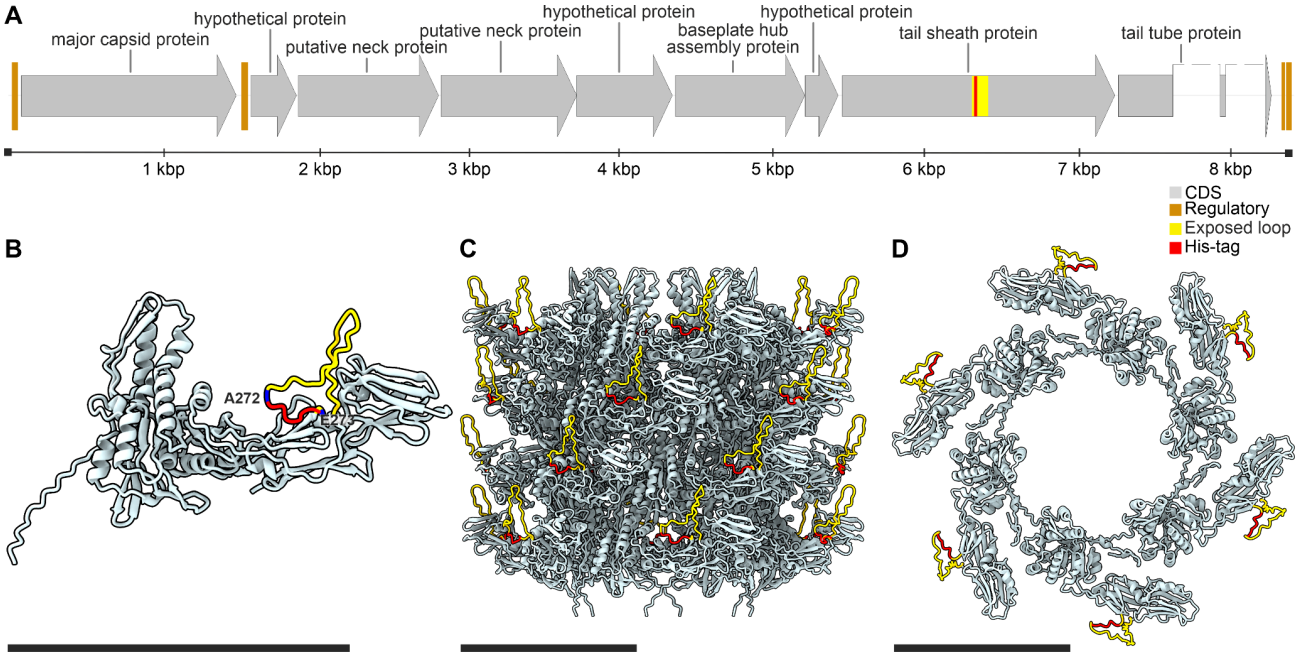

Figure 1. Scheme depicting the introduction of a poly histidine tag into the phage 812h1 tail sheath protein. (A) Part of the 812h1 phage head−tail structural genome module (GenBank: MH844529.1, sequence region: 51781 − 60096) showing the proposed insertion of a His-tag-encoding sequence (red) into the sequence encoding the exposed loop (yellow) within the TSP (GenBank: AZB50028.1, region 271 − 297). (B) Predicted structure of the modified TSP with an exposed loop (yellow) and inserted His-tag (red). The delimiting residues of the insertion Ala272 and Glu273 are highlighted in blue. (C) Modified TSPs with exposed loops (yellow) and inserted His-tags (red), modeled based on the structure of the four tail sheath protein hexamer discs (PDB: 9F04).[36] Side view of the tail sheath is shown. (D) Top view of a modeled single tail sheath protein hexamer disc shown in panel C. Scale bars are 10 nm (black).

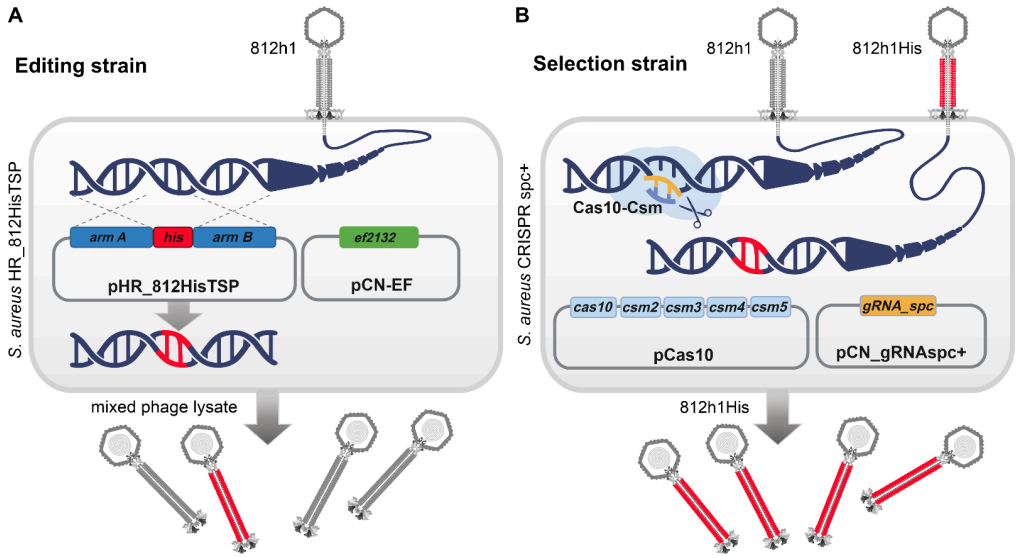

Figure 2. Two-strain CRISPR-Cas10-based editing strategy. (A) Genome editing of phage 812h1. The *S. aureus* HR_812HisTSP editing strain carrying the pHR_812HisTSP and pCN-EF vectors mediates the insertion of a *his*-tag sequence into the gene for the tail sheath protein. After homologous recombination facilitated by recombinase EF2132 between arms A and B, a mixed phage progeny is produced, containing a majority of the wild-type phages (gray) and recombinant phages (red) bearing a His-tag within the tail sheath. (B) Selection of recombinant phages. The *S. aureus* CRISPR spc+ selection strain carrying pCas10 and pCN_gRNAspc+ mediates the recognition and degradation of unedited DNA of phage 812h1 (gray). The Cas10-Csm effector complex is composed of five *cas-csm* genes and is guided to its target by a gRNA with a specific spacer (orange). Recombinant phage 812h1His with an insertion in the genome escapes CRISPR recognition and produces uniform recombinant phage progeny (red).

Here, we present structural modification of the highly virulent and polyvalent *Staphylococcus* phage 812h1[33] of the *Kayvirus* genus using a modified CRISPR-Cas10-assisted editing and selection strategy. Kayviruses are widely employed in phage therapeutic preparations and are generally considered safe for clinical application.[34,35] We incorporated a multifunctional poly histidine tag, broadly employed in biological applications, into the tail sheath protein (TSP). The introduced His-tag enabled biosensing detection, ultraresolution visualization using fluorescence and electron microscopy, and the study of phage-host

https://doi.org/10.1021/acssynbio.5c00387
ACS Synth. Biol. 2025, 14, 2979−2986

Table 1. Plasmid Vectors Used in This Study

Vector	Length (bp)	Selection marker[a]	Purpose	Reference
pCas10 = p*crispr-cas*/Δ*cas1*Δ*cas2*	10,910	cmp^R	A component of CRISPR-Cas10 counter-selection that carries genes for the Cas10-Csm effector complex, ensuring the degradation of the targeted DNA.	29
pCN_gRNAspc-	6,526	ery^R	A component of CRISPR-Cas10 counter-selection that carries a gRNA scaffold without any spacer that targets phage 812h1.	This work
pCN_gRNAspc+	6,561	ery^R	A component of CRISPR-Cas10 counter-selection that carries a gRNA with the spacer that targets the *tsp* gene of phage 812h1.	This work
pCN-EF= pCN-EF2132tet	7,266	cmp^R	This vector carries the gene for an enterococcal recombinase EF2132.	37
pHR_812HisTSP	6,267	ery^R	A vector complementary to pCN-EF that carries the editing segment HR_812HisTSP for homologous recombination.	This work
pCas9counter	9,533	ery^R	This vector backbone was used to construct pHR_812HisTSP, compatible with pCN-EF.	37
pCN51	6,430	ery^R	This vector was used to construct the vectors pCN_gRNAspc+ and pCN_gRNAspc-.	45

[a]Legend: cmp^R, resistance to chloramphenicol (25 μg/mL); ery^R, resistance to erythromycin (10 μg/mL).

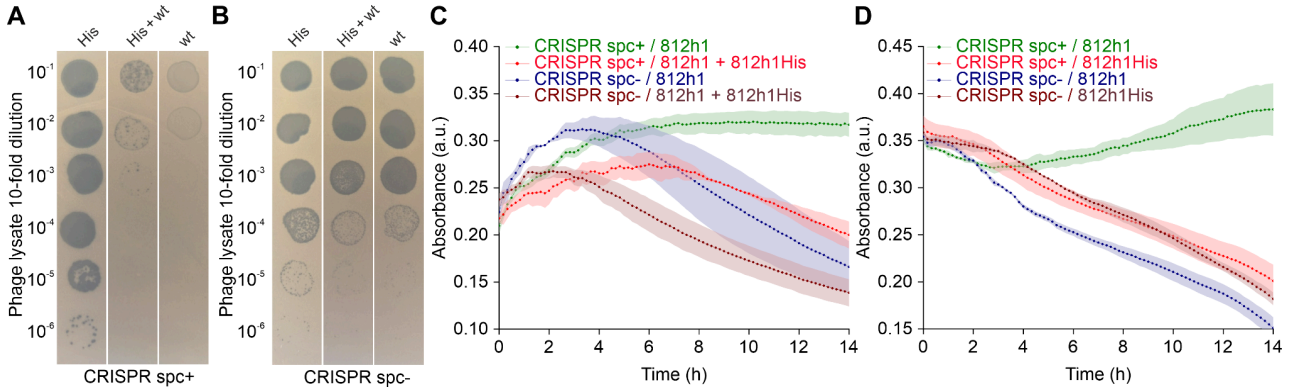

Figure 3. Efficiency of *S. aureus* CRISPR-Cas10 selection system. (A) Double-layer agar overlay plaque spot assay showing the sensitivity of the *S. aureus* CRISPR spc+ strain to the 812h1His (His) phage, mixed phage lysate (His + wt), and phage 812h1 (wt). Wild-type phage 812h1 does not propagate efficiently on the *S. aureus* CRISPR spc+ strain. (B) A plaque spot assay showing the sensitivity of the *S. aureus* CRISPR spc- strain to the 812h1His phage, mixed phage lysate, and phage 812h1. (C) Turbidity assay showing the sensitivity of the *S. aureus* CRISPR spc+ selection strain to mixed phage progeny comprising 812h1 and 812h1His phages. Wild-type phages 812h1 are recognized by the Cas10 effector complex and do not lyse the *S. aureus* CRISPR spc+ selection strain (green). The control *S. aureus* CRISPR spc- strain without a specific spacer is sensitive to 812h1 phages (blue). The mixed phage lysate, which contains a population of 812h1His phages, can lyse both the selection strain (red) and the strain without the specific spacer (brown). (D) Turbidity assay showing the sensitivity of the *S. aureus* CRISPR spc+ selection strain to wild-type phages 812h1 and phage 812h1His. The modified 812h1His phages overcame the CRISPR-Cas10 immune system and efficiently lysed the *S. aureus* strain CRISPR spc+ strain (red). The control *S. aureus* CRISPR spc- strain is sensitive to both wild-type phage 812h1 (blue) and phage 812h1His (brown). The *S. aureus* CRISPR spc+ strain is not sensitive to phage 812h1 (green).

interactions. This demonstrates that the modified phage can be broadly utilized as a model viral particle for monitoring and diagnostic applications in various sample matrices.

RESULTS AND DISCUSSION

The lytic staphylococcal bacteriophage 812h1 with a broad host range, previously derived from phage 812,[33] was chosen for structural modifications. The virion of phage 812 consists of an isometric head, a long tail with a contractile sheath, and a double-layered baseplate.[30] The tail consists of tail sheath proteins (TSPs) arranged in hexamer discs surrounding the central tail tube channel (Figure 1CD). Based on the TSP structure (PDB: 5LI2),[30] an unstructured exposed loop on the surface of TSP (Figure 1BCD, Figure S1) was selected as a target site for introducing modifications. A DNA sequence encoding a string of six histidine residues (6× His) was designed for insertion into the TSP gene (Figure 1A) between the codons for alanine (Ala272) and glutamic acid (Glu273) of the TSP (Figure 1B) using CRISPR-Cas10-assisted phage genome editing derived from the system developed by Bari et al.[28,29]

The wild-type phage genome was genetically modified by homologous recombination using editing strain *S. aureus* HR_HisTSP (Figure 2A) derived from laboratory strain *S. aureus* RN4220. The strain contained plasmid pCN-EF2132tet (pCN-EF), which encodes enterococcal recombinase EF2132 for increasing recombination efficiency[37] and the compatible vector pHR_812HisTSP carrying the template for the homologous recombination (Table 1). The editing template contained an 18-nucleotide *his*-tag (6× CAT) flanked by two 520-bp homologous arms that target the editing site within the exposed loop of the *tsp* gene, between the triplets GCA and GAA (GenBank: MH844529.1, positions 57988 and 57991, respectively; Figure 1A). The phage progeny resulting from propagation of the high-titer phage lysate (10^9 PFU/mL) on the editing strain was counter-selected using the *S. aureus* CRISPR spc+ selection strain, which harbors the effector vector p*crispr-cas*/Δ*cas1*Δ*cas2*[29] (abbreviated pCas10) encoding the endonuclease complex Cas10-Csm[28] and the vector pCN_gRNAspc+ carrying the CRISPR-Cas10 gRNA scaffold with a spacer that targets only the unmodified *tsp* gene (Figure

https://doi.org/10.1021/acssynbio.5c00387
ACS Synth. Biol. 2025, 14, 2979−2986

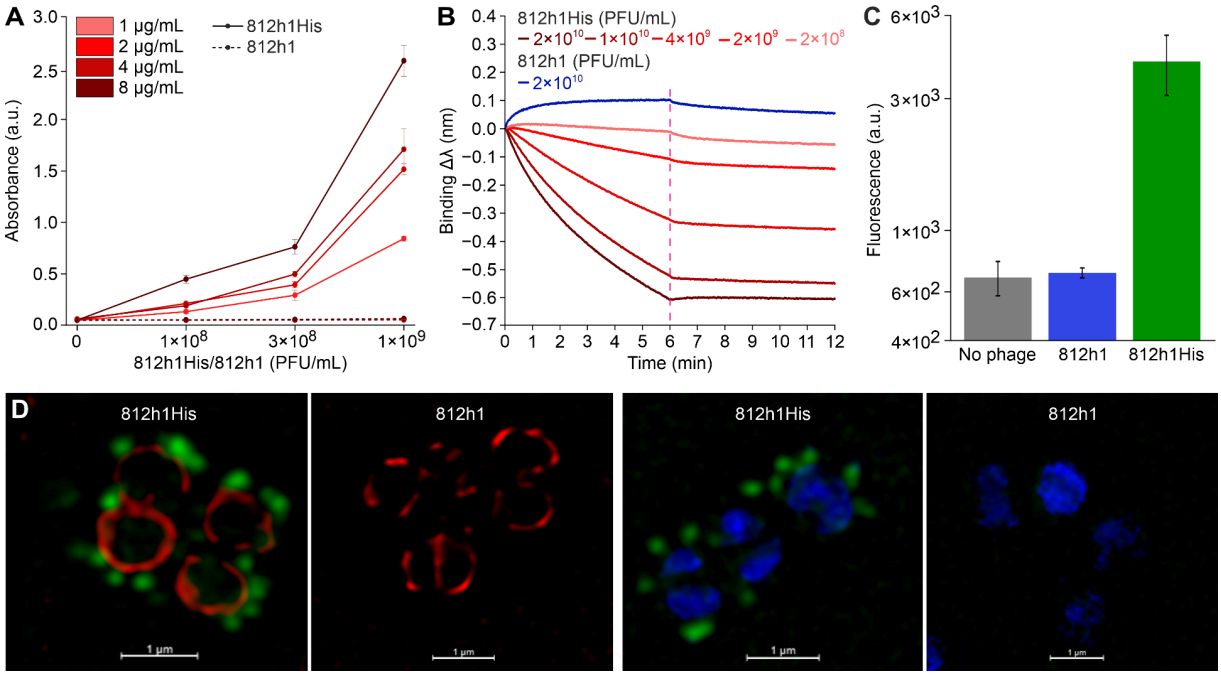

Figure 4. Binding of anti-His antibodies to modified phage 812h1His. (A) ELISA confirmation of the accessibility of the poly histidine tag on phage 812h1His virion surface. A pronounced concentration-dependent binding of the anti-HisAF488 antibody to immobilized 812h1His phage was demonstrated utilizing HRP-anti-mouse antibody as a label. In contrast, binding of the anti-HisAF488 antibody to immobilized 812h1 was not observed. Three immobilization concentrations of phages and four antibody concentrations were tested. (B) Real-time detection of 812h1His phage by Bio-Layer Interferometry. A concentration-dependent binding of the phage 812h1His to the immunosensor was monitored (red color gradient), displaying an inverse binding profile. The dissociation starts in 6 min (red dash line). The control sample of unmodified phage 812h1 displayed low-level nonspecific positive binding (blue). (C) Detection of recombinant phage using flow cytometry determination of the median fluorescence intensity (MFI) exhibited by *S. carnosus* TM300 cells after binding of fluorescently labeled phage 812h1His (green), wild-type phage 812h1 (blue), or no phage (gray). The MFI (812h1His) was significantly elevated ($p < 0.001$) compared to MFI (812h1) as determined by one-way ANOVA and Tukey's HSD posthoc test. (D) Ultrahigh-resolution fluorescence microscopy of 812h1His−anti-HisAF488 phage-antibody complex (green) adsorbed on the *S. carnosus* TM300 strain, stained by cell membrane-binding SynaptoRed (red) or DNA-binding DAPI (blue) fluorescent dyes. The control samples of wild-type phage 812h1 gave no phage-specific green fluorescence signal. Scale bar, 1 μm.

2B, Table 1). The *S. aureus* CRISPR spc- strain lacking the specific spacer in the gRNA was used as a control (Table 1).

The ability of modified phages to escape CRISPR-Cas-mediated selection was tested in the *S. aureus* CRISPR spc+ selection strain by using a spot plaque assay (Figure 3A). At a concentration of 1×10^9 PFU/mL, phage 812h1 did not form any plaques on *S. aureus* CRISPR spc+, whereas it propagated unimpeded on *S. aureus* CRISPR spc- (Figure 3B). After the editing step, the titer was 1×10^9 PFU/mL on the *S. aureus* CRISPR spc- strain, while the titer on the *S. aureus* CRISPR spc+ strain was $(0.9–1.7) \times 10^6$ PFU/mL, indicating the emergence of recombinant 812h1His phages with 0.1% recombination efficiency (Figure 3AB). After four passages on the *S. aureus* CRISPR spc+ strain, a homogeneous 812h1His phage progeny was obtained with an almost identical titer on both CRISPR spc+ and CRISPR spc- strains (Figure 3AB). The stability of the 812h1His phage was confirmed by repeated propagation on *S. aureus* RN4220 spc-, with no change in efficiency of plating on *S. aureus* RN4220 spc- and *S. aureus* RN4220 spc+ strains. The modified 812h1His phages retained their infectivity and demonstrated the ability to eradicate *S. aureus* culture in a turbidity assay (Figure 3CD).

The long-read sequencing confirmed the insertion of the *his*-tag sequence into the *tsp* gene, resulting in the rescue of recombinant 812h1His phages from the immune system of the *S. aureus* CRISPR spc+ strain (Figure S2). Sequence analysis showed an 85.7% occurrence of complete (6× CAT) *his*-tag insertion at 1061 × coverage (SD = 0.9). The remaining 14.3% of recombinant phages contained shortened variants of the *his*-tag sequence; however, no uniform sequence subpopulation was identified (Figure S2).

The spatial accessibility of the poly histidine tag on the virion surface was confirmed using an enzyme-linked immunosorbent assay (ELISA) with peroxidase-modified anti-mouse antibody (HRP-anti-mouse), indicating a specific binding of a monoclonal mouse anti-His IgG antibody conjugated with Alexa Fluor 488 (anti-HisAF488) to the phage 812h1His, while absent from the phage 812h1 (Figure 4A). In addition, we tested if the interaction between the poly histidine tag and the His-tag specific antibody can occur in the complex sample of 50% human serum (Figure S3). The signals of phage 812h1His were in all cases higher than the signals of 812h1, which successfully confirmed the specificity of the interaction, even in serum.

Next, a biolayer interferometry (BLI) biosensor with an anti-HIS-(HIS2)-functionalized surface was employed for monitoring the binding capabilities of 812h1His to an immunosensor in real-time (Figure 4B). We observed a pronounced concentration-dependent association of 812h1His with the biosensor surface. Due to the relatively large size of the phage particle, which is approximately 330 nm long,[30] its specific binding to the surface exhibited an inverse (negative) response (Figure 4B), consistent with previous observations for other large complexes and viruses.[38−40] In contrast, phage 812h1 exhibited a low positive signal response, likely from residual nonspecific binding

https://doi.org/10.1021/acssynbio.5c00387
ACS Synth. Biol. 2025, 14, 2979−2986

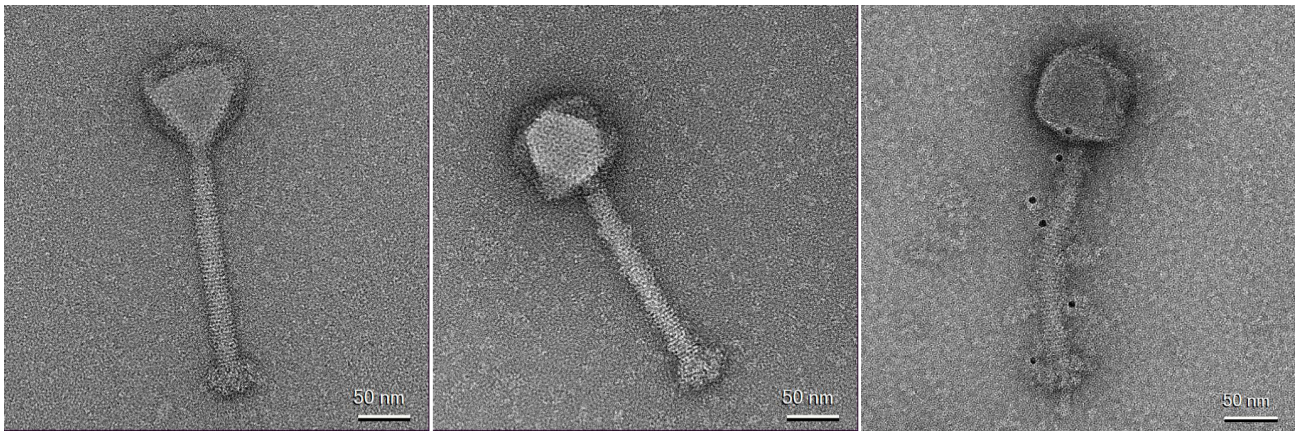

Figure 5. Transmission electron microscopy of phage particles with a monoclonal mouse anti-HisAF488 antibody (from left): wild-type phage 812h1; 812h1His−anti-HisAF488 phage-antibody complex; anti-mouse IgG-6 nm gold secondary antibody binding to 812h1His−anti-HisAF488 phage-antibody complex. Scale bar: 50 nm.

of small molecules present in the phage sample. Our BLI detection assay thus demonstrates the ability of the immunosensor to distinguish the specific binding of large phage particles from residuals that adsorb nonspecifically. Each modified phage particle contained 312 His-tagged TSP copies,[30] which are expected to form multivalent interactions with antibodies at the sensor surface. The enhanced overall avidity of the interaction is probably responsible for the observed high binding stability and very low dissociation rate (Figure 4B).

Staphylococcus carnosus was used as an organism for immunological detection assays, owing to the absence of protein A in its cell wall, to which the Fc fragments of commonly used commercial anti-His antibodies have high affinity.[41] Fluorescently labeled 812h1His−anti-HisAF488 phage-antibody complex bound to *S. carnosus* TM300 exhibited a 6-fold increase in median fluorescence intensity measured by flow cytometry compared to the control (Figure 4C). This strong signal enabled the visualization of phage binding using ultrahigh-resolution fluorescence microscopy (Figure 4D). Moreover, the modified bacteriophage tail sheaths were visualized by immunodetection and transmission electron microscopy using 6 nm Colloidal Gold AffiniPure Goat Anti-Mouse IgG secondary antibody (anti-mouse IgG-6 nm gold), which specifically bound to anti-HisAF488 in the phage TSP (Figure 5).

CONCLUSIONS

Labeling phage virion proteins is challenging due to their compact and highly organized structure. Success depends on the structure−function relationship of virion components, making structural data essential for rational engineering. High-resolution structures or reliable models thus help identify suitable insertion sites while minimizing the disruption of essential functions or assembly pathways. Surface-exposed, flexible loops are preferred insertion sites for reporter tags, as they are less likely to affect structural integrity or critical interactions.

This study demonstrates the potential of CRISPR-Cas10-based phage engineering to create customizable structure-guided virion modifications for *Kayvirus* strains. An accessible poly histidine tag incorporated into the phage tail sheath enabled site-specific functionalization of the phage surface, which provides a range of applications, including the immunodetection of viral particles using advanced microscopic techniques, the immobilization of phages on biosensor platforms, and the phage-based flow cytometric detection of bacterial strains.

MATERIAL AND METHODS

Bacteria, Bacteriophage, Culture Conditions. *Escherichia coli* TOP10F' (Invitrogen) was used for cloning. The transformants were cultivated at 37 °C with shaking at 120 rpm in Luria−Bertani (LB) medium (Oxoid) supplemented, if required, with ampicillin (100 μg/mL). Strains for phage editing and modified phage selection were derived from *S. aureus* RN4220.[42,43] *Staphylococcus carnosus* TM300[44] was used for phage-antibody immunological assays. Staphylococcal strains were cultured at 37 or 30 °C with shaking at 120 rpm in Meat-Peptone Broth (MPB) medium[33] supplemented, if required, with chloramphenicol (25 μg/mL) and/or erythromycin (10 μg/mL). Bacteriophage 812h1 and its propagation have been described previously.[33]

DNA and Plasmid Vectors. The plasmid vectors used are given in Table 1. Custom-designed DNA primers and oligonucleotides (Table S1) were purchased from Sigma-Aldrich (Merck). The homology arms segment HR_812HisTSP was synthesized (Twist Bioscience). The cloning and plasmid vector construction workflow using restriction enzymes is described in the Supporting Information.

Indirect Enzyme-Linked Immunosorbent Assay (ELISA) for His-Phage Testing. Unless stated otherwise, incubations were performed at room temperature for one h with gentle shaking, followed by four washes in washing buffer (50 mM Tris, 0.05% Tween 20, 1 mM KF, pH 7.4). Microlon high-binding 96-well microtiter plate (Greiner Bio-One) was coated with phage 812h1 or 812h1His in coating buffer (100 μL in each well; 50 mM Na_2CO_3/$NaHCO_3$, 0,05% NaN_3, pH 9.6) and incubated overnight at 4 °C. Each sample well was treated as follows: blocked with 20% SuperBlock TBS (Thermo Fisher Scientific) in washing buffer, incubated with 6×-His Tag Monoclonal Antibody (HIS.H8) Alexa Fluor 488 (anti-HisAF488) (Invitrogen) at various dilutions (1, 2, 4, and 8 μg/mL in assay buffer consisting of 10% SuperBlock TBS, 0.05% Tween 20, 50 mM Tris, 150 mM NaCl, 1 mM KF, 0.5% PEG, pH 7.5), and incubated with the Peroxidase AffiniPure Goat Anti-Mouse IgG (H+L) (Jackson ImmunoResearch) in assay buffer (0.22 μg/mL). After the final washing, a TMB-Complete2 substrate solution (TestLine Clinical Diagnostics) was added for

https://doi.org/10.1021/acssynbio.5c00387
ACS Synth. Biol. 2025, 14, 2979−2986

color development, followed by stopping the reaction with 1 M H_2SO_4 and reading absorbance at 450 nm using a Synergy HT microplate reader (Bio-Tek Instruments).

Bio-Layer Interferometry (BLI) Biosensing. An Octet RED96e system (ForteBio) was employed for a BLI detection binding assay of recombinant phages. All BLI steps were performed in phage buffer at 25 °C. The association and dissociation were monitored for 360 s while being shaken at 1000 rpm in 200 μL of the samples. The phages 812h1 (2×10^{10} PFU/mL) or 812h1His (ranging from 2×10^{8} to 2×10^{10} PFU/mL) diluted in phage buffer and the Octet Anti-HIS (HIS2) precoated biosensors (Sartorius) pre-equilibrated for 120 s in phage buffer were used. The experiment was performed in biological duplicates. Data were collected using Data Analysis v.11.1 software (ForteBio).

Flow-Cytometry and Fluorescence Microscopy. Bacteriophage 812h1His (at 1×10^{10} PFU/mL) was incubated with a 6×-His Tag Monoclonal Antibody (HIS.H8) Alexa Fluor 488 (anti-HisAF488) at a final concentration of 1 μg/mL for 2 h at 4 °C; then, the *S. carnosus* TM300 cell suspension in phage buffer ($OD_{600\ nm} = 0.6$) was added to achieve an input ratio of 10:1 and the mixture was incubated for 10 min. The samples were washed with phage buffer and analyzed with a CytoFLEX S flow cytometer (Beckman Coulter). Three independent biological experiments were performed in a technical triplicate. Data was acquired from 50,000 events per sample and analyzed using the software CytExpert v.2.5 (Beckman Coulter).

For fluorescence microscopy, the staphylococcal cells were stained with DAPI (Thermo Fisher Scientific) or SynaptoRed (Biotium) and washed with phage buffer according to the manufacturer's recommendations. The stained cells were mixed with fluorescently labeled 812h1His−anti-HisAF488 phage-antibody complex and imaged using high-resolution microscopy (ZEISS Elyra 7 with Lattice SIM).

Transmission Electron Microscopy and Immunoelectron Microscopy. For the immunoelectron microscopy, the purified bacteriophage 812h1His (at 1×10^{10} PFU/mL) was incubated with 6×-His Tag Monoclonal Antibody (HIS.H8) Alexa Fluor 488 (anti-HisAF488) (final concentration 1 μg/mL; Invitrogen) for 2 h at 4 °C, and then 6 nm Colloidal Gold AffiniPureTM Goat Anti-Mouse IgG (Jackson ImmunoResearch) was added according to the manufacturer's recommendations. All negatively stained samples were prepared by double staining in 2% uranyl acetate. All samples were observed with a Tecnai F20 Transmission Electron Microscope (FEI Company) operated at 200 kV at a magnification of 150,000×.

Data Visualization and Statistical Analyses. The statistical evaluation, data visualization, and graphing were done using OriginPro 2023 v.10.0 (OriginLab Corporation). Fluorescence microscopy image processing was done using ZEN Lite v.3.11 (Carl Zeiss Microscopy). The structure of the modified tail sheath protein was predicted by AlphaFold2.[46] Structures were visualized using ChimeraX.[47]

■ ASSOCIATED CONTENT

Data Availability Statement

The sequences of new plasmid constructs and data associated with this work are provided in the Zenodo depository https://doi.org/10.5281/zenodo.15463060. Sequencing data of modified 812h1His phage were deposited in GenBank under the BioProject number PRJNA1268361.

Supporting Information

The Supporting Information is available free of charge at https://pubs.acs.org/doi/10.1021/acssynbio.5c00387.

Additional experimental details: the structure of the 812h1His tail sheath (Figure S1), sequence analysis of the *tsp* gene region in modified phages 812h1His (Figure S2), detection of modified phages 812h1His in 50% human blood serum by ELISA (Figure S3), primers and oligonucleotides used in this study (Table S1) and Supplementary Methods (PDF)

■ AUTHOR INFORMATION

Corresponding Author

Ivana Mašlaňová − *Department of Experimental Biology, Faculty of Science, Masaryk University, Brno 611 37, Czech Republic;* orcid.org/0000-0002-2597-2848; Email: maslanova@mail.muni.cz

Authors

Hana Šimečková − *Department of Experimental Biology, Faculty of Science, Masaryk University, Brno 611 37, Czech Republic*

Pavol Bárdy − *Department of Experimental Biology, Faculty of Science, Masaryk University, Brno 611 37, Czech Republic; Department of Chemistry, York Structural Biology Laboratory, University of York, Heslington, York YO10 5DD, United Kingdom*

Lucie Kuntová − *Department of Experimental Biology, Faculty of Science, Masaryk University, Brno 611 37, Czech Republic*

Eliška Macháčová − *Department of Biochemistry, Faculty of Science, Masaryk University, Brno 625 00, Czech Republic*

Tibor Botka − *Department of Experimental Biology, Faculty of Science, Masaryk University, Brno 611 37, Czech Republic*

Ján Bíňovský − *Central European Institute of Technology, Masaryk University, Brno 625 00, Czech Republic; National Centre for Biomolecular Research, Faculty of Science, Masaryk University, Brno 625 00, Czech Republic;* orcid.org/0000-0001-7647-5211

Josef Houser − *Central European Institute of Technology, Masaryk University, Brno 625 00, Czech Republic; National Centre for Biomolecular Research, Faculty of Science, Masaryk University, Brno 625 00, Czech Republic*

Zdeněk Farka − *Department of Biochemistry, Faculty of Science, Masaryk University, Brno 625 00, Czech Republic;* orcid.org/0000-0002-6842-7081

Pavel Plevka − *Central European Institute of Technology, Masaryk University, Brno 625 00, Czech Republic*

Roman Pantůček − *Department of Experimental Biology, Faculty of Science, Masaryk University, Brno 611 37, Czech Republic;* orcid.org/0000-0002-3950-675X

Complete contact information is available at: https://pubs.acs.org/10.1021/acssynbio.5c00387

Author Contributions

The manuscript was written through the contributions of all authors. H.Š., P.B., and I.M. designed research; H.Š., P.B., L.K., E.M., T.B., and I.M. performed experiments; H.Š., P.B., E.M., T.B., J.B., J.H., and Z.F. analyzed, validated, and interpreted data; H.Š., R.P., and I.M. wrote the original manuscript; all authors revised and edited the manuscript; H.Š., T.B., J.B., R.P., and I.M. prepared visualizations; Z.F., P.P., R.P., and I.M. supervised students; Z.F., P.P., R.P., and I.M. obtained funding.

Funding

This research was conducted within the framework of the Ministry of Health of the Czech Republic Research Programme (NU22-05-00042). The study was partly supported by the project National Institute of Virology and Bacteriology (Programme EXCELES, ID Project No. LX22NPO5103) - Funded by the European Union - Next Generation EU. We gratefully acknowledge the Cellular imaging (CELLIM) core facility, supported by the Czech-BioImaging large RI project (LM2023050) and funded by the Ministry of Education, Youth and Sports of the Czech Republic (MEYS CR). We also gratefully acknowledge the Cryo-electron Microscopy and Tomography and Biomolecular Interactions and Crystallography core facilities of CEITEC MU of the CIISB, Instruct-CZ Centre, supported by MEYS CR (LM2023042) and the European Regional Development Fund Project "Innovation of Czech Infrastructure for Integrative Structural Biology" (CZ.02.01.01/00/23_015/0008175) for their support with obtaining scientific data presented in this paper. The students wish to thank the Grant Agency of Masaryk University for its support (MUNI/A/1603/2024).

Notes

The authors declare no competing financial interest.

■ ACKNOWLEDGMENTS

We acknowledge Prof. Asma Hatoum-Aslan (University of Illinois) for providing us with the p*crispr-cas*/Δ*cas*1Δ*cas*2 plasmid. Plasmids pCN-EF2132tet and pCas9counter (Addgene plasmids #107191 and #107192, respectively) were a gift from Steve Salipante (University of Washington). We wish to thank Pavel Payne (CEITEC, Masaryk University) for his valuable help and helpful discussions. Jiří Nováček and Zuzana Hlavenková (Cryo-electron Microscopy and Tomography Core Facility, CEITEC, Masaryk University) are gratefully acknowledged for transmission electron microscopy and immunoelectron microscopy, as is Jakub Pospíšil (CELLIM Core Facility, CEITEC, Masaryk University) for ultrahigh-resolution fluorescence microscopy. The graphical abstract was partly created in BioRender.

■ REFERENCES

(1) Clokie, M. R. J.; Millard, A. D.; Letarov, A. V.; Heaphy, S. Phages in Nature. *Bacteriophage* **2011**, *1*, 31−45.
(2) Bárdy, P.; Pantůček, R.; Benešík, M.; Doškař, J. Genetically Modified Bacteriophages in Applied Microbiology. *J. Appl. Microbiol.* **2016**, *121*, 618−633.
(3) Chen, Y.; Batra, H.; Dong, J.; Chen, C.; Rao, V. B.; Tao, P. Genetic Engineering of Bacteriophages against Infectious Diseases. *Front. Microbiol.* **2019**, *10*, (954). DOI: 10.3389/fmicb.2019.00954.
(4) Pires, D. P.; Cleto, S.; Sillankorva, S.; Azeredo, J.; Lu, T. K. Genetically Engineered Phages: A Review of Advances over the Last Decade. *Microbiol. Mol. Biol. Rev.* **2016**, *80*, 523−543.
(5) Yosef, I.; Goren, M. G.; Globus, R.; Molshanski-Mor, S.; Qimron, U. Extending the Host Range of Bacteriophage Particles for DNA Transduction. *Mol. Cell* **2017**, *66*, 721−728.
(6) Jia, H.-J.; Jia, P.-P.; Yin, S.; Bu, L.-K.; Yang, G.; Pei, D.-S. Engineering Bacteriophages for Enhanced Host Range and Efficacy: Insights from Bacteriophage-Bacteria Interactions. *Front. Microbiol.* **2023**, *14*, 1172635.
(7) Edgar, R.; Friedman, N.; Molshanski-Mor, S.; Qimron, U. Reversing Bacterial Resistance to Antibiotics by Phage-Mediated Delivery of Dominant Sensitive Genes. *Appl. Environ. Microbiol.* **2012**, *78*, 744−751.
(8) Łobocka, M.; Dąbrowska, K.; Górski, A. Engineered Bacteriophage Therapeutics: Rationale, Challenges and Future. *BioDrugs* **2021**, *35*, 255−280.
(9) Meile, S.; Du, J.; Staubli, S.; Grossmann, S.; Koliwer-Brandl, H.; Piffaretti, P.; Leitner, L.; Matter, C. I.; Baggenstos, J.; Hunold, L.; et al. Engineered Reporter Phages for Detection of *Escherichia coli*, *Enterococcus*, and *Klebsiella* in Urine. *Nat. Commun.* **2023**, *14*, (4336). DOI: 10.1038/s41467-023-39863-x.
(10) Farooq, U.; Yang, Q.; Ullah, M. W.; Wang, S. Bacterial Biosensing: Recent Advances in Phage-Based Bioassays and Biosensors. *Biosens. Bioelectron.* **2018**, *118*, 204−216.
(11) Bikard, D.; Euler, C. W.; Jiang, W.; Nussenzweig, P. M.; Goldberg, G. W.; Duportet, X.; Fischetti, V. A.; Marraffini, L. A. Exploiting CRISPR-Cas Nucleases to Produce Sequence-Specific Antimicrobials. *Nat. Biotechnol.* **2014**, *32*, 1146−1150.
(12) Cobb, L. H.; Park, J.; Swanson, E. A.; Beard, M. C.; McCabe, E. M.; Rourke, A. S.; Seo, K. S.; Olivier, A. K.; Priddy, L. B. Crispr-Cas9Modified Bacteriophage for Treatment of *Staphylococcus aureus* Induced Osteomyelitis and Soft Tissue Infection. *PloS One* **2019**, *14*, No. e0220421.
(13) Gencay, Y. E.; Jasinskytė, D.; Robert, C.; Semsey, S.; Martínez, V.; Petersen, A. Ø.; Brunner, K.; de Santiago Torio, A.; Salazar, A.; Turcu, I. C.; et al. Engineered Phage with Antibacterial CRISPR-Cas Selectively Reduce *E. coli* Burden in Mice. *Nat. Biotechnol.* **2024**, *42*, 265−274.
(14) Ram, G.; Ross, H. F.; Novick, R. P.; Rodriguez-Pagan, I.; Jiang, D. Conversion of Staphylococcal Pathogenicity Islands to CRISPR-Carrying Antibacterial Agents That Cure Infections in Mice. *Nat. Biotechnol.* **2018**, *36*, 971−976.
(15) Novick, R. P. Antibacterial Particles and Predatory Bacteria as Alternatives to Antibacterial Chemicals in the Era of Antibiotic Resistance. *Curr. Opin. Microbiol.* **2021**, *64*, 109−116.
(16) Shabbir, M. A. B.; Hao, H.; Shabbir, M. Z.; Wu, Q.; Sattar, A.; Yuan, Z. Bacteria vs. Bacteriophages: Parallel Evolution of Immune Arsenals. *Front. Microbiol.* **2016**, *7*, (1292). DOI: 10.3389/fmicb.2016.01292.
(17) Rees, P. J.; Fry, B. A. The Morphology of Staphylococcal Bacteriophage K and DNA Metabolism in Infected *Staphylococcus aureus*. *J. Gen. Virol.* **1981**, *53*, 293−307.
(18) Chaikeeratisak, V.; Nguyen, K.; Khanna, K.; Brilot, A. F.; Erb, M. L.; Coker, J. K.; Vavilina, A.; Newton, G. L.; Buschauer, R.; Pogliano, K.; et al. Assembly of a Nucleus-Like Structure During Viral Replication in Bacteria. *Science* **2017**, *355*, 194−197.
(19) Kiro, R.; Shitrit, D.; Qimron, U. Efficient Engineering of a Bacteriophage Genome Using the Type I-E CRISPR-Cas System. *RNA Biol.* **2014**, *11*, 42−44.
(20) Tao, P.; Wu, X.; Tang, W.-C.; Zhu, J.; Rao, V. Engineering of Bacteriophage T4 Genome Using CRISPR-Cas9. *ACS Synth. Biol.* **2017**, *6*, 1952−1961.
(21) Adler, B. A.; Hessler, T.; Cress, B. F.; Lahiri, A.; Mutalik, V. K.; Barrangou, R.; Banfield, J.; Doudna, J. A. Broad-Spectrum CRISPR-Cas13a Enables Efficient Phage Genome Editing. *Nat. Microbiol.* **2022**, *7*, 1967−1979.
(22) Martel, B.; Moineau, S. CRISPR-Cas: An Efficient Tool for Genome Engineering of Virulent Bacteriophages. *Nucleic Acids Res.* **2014**, *42*, 9504−9513.
(23) Box, A. M.; McGuffie, M. J.; O'Hara, B. J.; Seed, K. D. Functional Analysis of Bacteriophage Immunity through a Type I-E CRISPR-Cas System in *Vibrio cholerae* and Its Application in Bacteriophage Genome Engineering. *J. Bacteriol.* **2016**, *198*, 578−590.
(24) Lemay, M.-L.; Renaud, A. C.; Rousseau, G. M.; Moineau, S. Targeted Genome Editing of Virulent Phages Using CRISPR-Cas9. *Bio-Protoc.* **2018**, *8*, (e2674). DOI: 10.21769/BioProtoc.2674.
(25) Shen, J.; Zhou, J.; Chen, G.-Q.; Xiu, Z.-L. Efficient Genome Engineering of a Virulent *Klebsiella* Bacteriophage Using CRISPR-Cas9. *J. Virol.* **2018**, *92*, No. e00534-18.
(26) Chen, Y.; Yan, B.; Chen, W.; Zhang, X.; Liu, Z.; Zhang, Q.; Li, L.; Hu, M.; Zhao, X.; Xu, X. Development of the CRISPR-Cas12a System

for Editing of *Pseudomonas aeruginosa* Phages. *iScience* **2024**, *27*, 110210.
(27) Hupfeld, M.; Trasanidou, D.; Ramazzini, L.; Klumpp, J.; Loessner, M. J.; Kilcher, S. A Functional Type II-a CRISPR-Cas System from *Listeria* Enables Efficient Genome Editing of Large Non-Integrating Bacteriophage. *Nucleic Acids Res.* **2018**, *46*, 6920−6933.
(28) Bari, S. M. N.; Walker, F. C.; Cater, K.; Aslan, B.; Hatoum-Aslan, A. Strategies for Editing Virulent Staphylococcal Phages Using CRISPR-Cas10. *ACS Synth. Biol.* **2017**, *6*, 2316−2325.
(29) Nayeemul Bari, S.M.; Hatoum-Aslan, A. CRISPR-Cas10 Assisted Editing of Virulent Staphylococcal Phages. *Methods Enzymol.* **2019**, *616*, 385−409.
(30) Nováček, J.; Šiborová, M.; Benešík, M.; Pantůček, R.; Doškař, J.; Plevka, P. Structure and Genome Release of Twort-Like *Myoviridae* Phage with a Double-Layered Baseplate. *Proc. Natl. Acad. Sci. U.S.A.* **2016**, *113*, 9351−9356.
(31) Eyer, L.; Pantůček, R.; Zdráhal, Z.; Konečná, H.; Kašpárek, P.; Růžičková, V.; Hernychová, L.; Preisler, J.; Doškař, J. Structural Protein Analysis of the Polyvalent Staphylococcal Bacteriophage 812. *Proteomics* **2007**, *7*, 64−72.
(32) Finstrlová, A.; Mašlaňová, I.; Blasdel Reuter, B. G.; Doškař, J.; Götz, F.; Pantůček, R. Global Transcriptomic Analysis of Bacteriophage-Host Interactions between a *Kayvirus* Therapeutic Phage and *Staphylococcus aureus*. *Microbiol. Spectr.* **2022**, *10*, No. e00123-22.
(33) Botka, T.; Pantůček, R.; Mašlaňová, I.; Benešík, M.; Petráš, P.; Růžičková, V.; Havlíčková, P.; Varga, M.; Zemličková, H.; Koláčková, I.; et al. Lytic and Genomic Properties of Spontaneous Host-Range *Kayvirus* Mutants Prove Their Suitability for Upgrading Phage Therapeutics against Staphylococci. *Sci. Rep.* **2019**, *9*, (5475). DOI: 10.1038/s41598-019-41868-w.
(34) Ajuebor, J.; Buttimer, C.; Arroyo-Moreno, S.; Chanishvili, N.; Gabriel, E. M.; O'Mahony, J.; McAuliffe, O.; Neve, H.; Franz, C.; Coffey, A. Comparison of *Staphylococcus* Phage K with Close Phage Relatives Commonly Employed in Phage Therapeutics. *Antibiotics (Basel)* **2018**, *7* (37), 37.
(35) Petrovic Fabijan, A.; Lin, R. C. Y.; Ho, J.; Maddocks, S.; Ben Zakour, N. L.; Iredell, J. R.; et al. Safety of Bacteriophage Therapy in Severe *Staphylococcus aureus* Infection. *Nat. Microbiol.* **2020**, *5*, 465−472.
(36) Bíňovský, J.; Šiborová, M.; Nováček, J.; Bárdy, P.; Baška, R.; Škubník, K.; Botka, T.; Benešík, M.; Pantůček, R.; Tripsianes, K.; et al. Cell Attachment and Tail Contraction of *Staphylococcus aureus* Phage phi812. *bioRxiv* **2024**, DOI: 10.1101/2024.09.19.613683, preprint.
(37) Penewit, K.; Holmes, E. A.; McLean, K.; Ren, M.; Waalkes, A.; Salipante, S. J. Efficient and Scalable Precision Genome Editing in *Staphylococcus aureus* through Conditional Recombineering and CRISPR/Cas9-Mediated Counterselection. *mBio* **2018**, *9*, No. e00067-18.
(38) Needham, P.; Page, R. C.; Yehl, K. Phage-Layer Interferometry: A Companion Diagnostic for Phage Therapy and a Bacterial Testing Platform. *Sci. Rep.* **2024**, *14*, (6026). DOI: 10.1038/s41598-024-55776-1.
(39) Åman, T.; Auer, S.; Hytönen, V. P.; Määttä, J. A. Performance of Label-Free Biosensors as a Function of Layer Thickness. *Biosens. Bioelectron. X* **2024**, *21*, 100556.
(40) De Keyser, P.; Kalichuk, V.; Zögg, T.; Wohlkönig, A.; Schenck, S.; Brunner, J.; Pardon, E.; Steyaert, J. A Biosensor-Based Phage Display Selection Method for Automated, High-Throughput Nanobody Discovery. *Biosens. Bioelectron.* **2025**, *271*, 116951.
(41) Deisenhofer, J. Crystallographic Refinement and Atomic Models of a Human Fc Fragment and Its Complex with Fragment B of Protein a from *Staphylococcus aureus* at 2.9- and 2.8-.ANG. Resolution. *Biochemistry* **1981**, *20*, 2361−2370.
(42) Kreiswirth, B. N.; Löfdahl, S.; Betley, M. J.; O'Reilly, M.; Schlievert, P. M.; Bergdoll, M. S.; Novick, R. P. The Toxic Shock Syndrome Exotoxin Structural Gene Is Not Detectably Transmitted by a Prophage. *Nature* **1983**, *305*, 709−712.
(43) Nair, D.; Memmi, G.; Hernandez, D.; Bard, J.; Beaume, M.; Gill, S.; Francois, P.; Cheung, A. L. Whole-Genome Sequencing of *Staphylococcus aureus* Strain RN4220, a Key Laboratory Strain Used in Virulence Research, Identifies Mutations That Affect Not Only Virulence Factors but Also the Fitness of the Strain. *J. Bacteriol.* **2011**, *193*, 2332−2335.
(44) Wagner, E.; Doskar, J.; Götz, F. Physical and Genetic Map of the Genome of *Staphylococcus carnosus* TM300. *Microbiology* **1998**, *144*, 509−517.
(45) Charpentier, E.; Anton, A. I.; Barry, P.; Alfonso, B.; Fang, Y.; Novick, R. P. Novel Cassette-Based Shuttle Vector System for Gram-Positive Bacteria. *Appl. Environ. Microbiol.* **2004**, *70*, 6076−6085.
(46) Jumper, J.; Evans, R.; Pritzel, A.; Green, T.; Figurnov, M.; Ronneberger, O.; Tunyasuvunakool, K.; Bates, R.; Zidek, A.; Potapenko, A.; et al. Highly Accurate Protein Structure Prediction with AlphaFold. *Nature* **2021**, *596*, 583−589.
(47) Pettersen, E. F.; Goddard, T. D.; Huang, C. C.; Meng, E. C.; Couch, G. S.; Croll, T. I.; Morris, J. H.; Ferrin, T. E. UCSF ChimeraX: Structure Visualization for Researchers, Educators, and Developers. *Protein Sci.* **2021**, *30*, 70−82.

https://doi.org/10.1021/acssynbio.5c00387
ACS Synth. Biol. 2025, 14, 2979−2986

APPENDIX 8

Mašlaňová I, Kovařovic V, Botka T, Švec P, Sedláček I, Šedo O, Finstrlová A, Neumann-Schaal M, Kirstein S, Schwendener S, Staňková E, Rovňáková K, Petráš P, Doškař J, Perreten V, Pantůček R (2025) Evidence of *in vitro mecB*-mediated β-lactam antibiotic resistance transfer to *Staphylococcus aureus* from *Macrococcus psychrotolerans* sp. nov., a psychrophilic bacterium from food-producing animals and human clinical specimens. *Applied and Environmental Microbiology* 91:e0165224. https://doi.org/10.1128/aem.01652-24
(JCR 2025: IF = 4.2; Q2 – Biotechnology & Applied Microbiology)

CC BY 4.0

AMERICAN SOCIETY FOR MICROBIOLOGY | Applied and Environmental Microbiology

Check for updates

| Microbial Genetics | Full-Length Text

Evidence of *in vitro mecB*-mediated β-lactam antibiotic resistance transfer to *Staphylococcus aureus* from *Macrococcus psychrotolerans* sp. nov., a psychrophilic bacterium from food-producing animals and human clinical specimens

Ivana Mašlaňová,[1] Vojtěch Kovařovic,[1,2] Tibor Botka,[1] Pavel Švec,[3] Ivo Sedláček,[3] Ondrej Šedo,[4] Adéla Finstrlová,[1] Meina Neumann-Schaal,[5] Sarah Kirstein,[5] Sybille Schwendener,[6,7] Eva Staňková,[3] Kristína Rovňáková,[1] Petr Petráš,[8] Jiří Doškař,[1] Vincent Perreten,[6] Roman Pantůček[1]

AUTHOR AFFILIATIONS See affiliation list on p. 20.

ABSTRACT Macrococci are usually found as commensals on the skin and mucosa of animals and have been isolated from mammal-derived fermented foods; however, they can also act as opportunistic pathogens. Here, we used whole-genome sequencing, comparative genomics, extensive biotyping, MALDI-TOF mass spectrometry, and chemotaxonomy to characterize *Macrococcus* sp. strains isolated from livestock and human-related specimens. Based on the results of polyphasic taxonomy, we propose the species *Macrococcus psychrotolerans* sp. nov. (type strain NRL/St 95/376^T = CCM 8659^T = DSM 111350^T) belonging to the *Macrococcus caseolyticus* phylogenetic clade. It grows at 4°C, and the core genome of the isolates contains suspected genes contributing to low-temperature tolerance. Variable genetic elements include prophages, chromosomal islands, a composite staphylococcal cassette chromosome island, and many plasmids that affect the overall genome expansion and adaptation to specific ecological settings of the studied isolates. Large plasmids carrying the methicillin resistance gene *mecB* were identified in *M. psychrotolerans* sp. nov. strains and confirmed as self-transmissible to *Staphylococcus aureus in vitro*. In addition to plasmids with circular topology, a 150-kb-long linear plasmid with 14.1-kb-long inverted terminal repeats, harboring many IS elements and putative genes for a type IV secretion system was revealed. The described strains were isolated from human clinical material, food-producing animals, meat, and a wooden cheese board and have the potential to proliferate at refrigerator temperatures. Their presence in the food chain and human infections indicates that attention needs to be paid to this potential novel opportunistic pathogen.

IMPORTANCE The study offers insights into the phenotypic and genomic features of a novel species of the genus *Macrococcus* that occurs in livestock, food, and humans. The large number of diverse mobile genetic elements contributes to the adaptation of macrococci to various environments. The ability of the described microorganisms to grow at refrigerator temperatures, enabled by genes that are predicted to contribute to low-temperature tolerance, raises food safety concerns. Confirmed *in vitro* conjugative transfer of plasmid-borne *mecB* gene to *S. aureus* poses a significant risk of spread of broad β-lactam resistance. In addition, the intergeneric plasmid transfer to *S. aureus* is indicative of horizontal gene transfer events that may be more frequent than generally accepted. Determining a complete sequence and gene content of linear megaplasmid with exceptional topology for the *Staphylococcaceae* family suggests its possible role in shuttling adaptive traits through an exchange of genetic information.

Editor Sophie Roussel, Anses, Maisons-Alfort Laboratory for Food Safety, Maisons-Alfort, France

Address correspondence to Roman Pantůček, pantucek@sci.muni.cz.

The authors declare no conflict of interest.

See the funding table on p. 20.

Received 23 August 2024
Accepted 18 February 2025
Published 11 March 2025

Copyright © 2025 Mašlaňová et al. This is an open-access article distributed under the terms of the Creative Commons Attribution 4.0 International license.

Downloaded from https://journals.asm.org/journal/aem on 04 February 2026 by 147.251.86.90.

KEYWORDS Gram-positive cocci, methicillin resistance, cephalosporin resistance, conjugation, food safety, cold temperature tolerance, linear plasmid

Macrococci are Gram-positive, coagulase-negative, and catalase-positive cocci and are phylogenetically closely related to the *Mammaliicoccus* genus. Currently, the *Macrococcus* genus comprises 12 species according to the List of Prokaryotic Names with Standing in Nomenclature (LPSN) (1). They are usually found as commensals on the skin and mucosa of mammals, from where they may also contaminate milk and meat. Case reports on infections by *Macrococcus canis* and *Macrococcus caseolyticus* have been noted in lambs (2), bovine mastitis (3), diseased broiler chicken (4), dogs (5, 6), and skin wound infections, or vulvitis and vaginitis in humans (7, 8). A recent study reported high animal mortality rates associated with infections caused by these bacteria (4). *Macrococcus* species possess various putative enzymatic virulence factors, including lipases, nucleases, and proteases (9). These enzymes are responsible for the ability of the bacteria to cause infection and survive in the host. The genus has gained attention in recent years due to acquiring multiple antibiotic resistance mechanisms through mobile genetic elements (MGEs), including the methicillin resistance genes *mecB* and/or *mecD* (3, 10–13). These genes can be located on a staphylococcal cassette chromosome (SCC*mec*) (14); however, the *mecD* gene was mainly detected on resistance islands McRI$_{mecD}$ (15) and *mecB* was in addition found on plasmids (16–18). The presence of an almost identical *mecB*-containing plasmid in *Macrococcus canis* and *Staphylococcus aureus* indicates that an exchange of genes between both genera may occur (16, 19).

Comparative genomics studies (7, 9, 15) revealed high plasticity of macrococcal genomes, their pathogenic potential, and the importance of MGEs in horizontal gene transfer (HGT) and pathogenesis. In addition to the acquisition of β-lactam resistance genes, macrococci can acquire other resistance genes by HGT, which leads to multidrug-resistant strains (10, 15, 20, 21). The importance of HGT in the evolutionary processes occurring in macrococci was also supported by the description of *Macrococcus armenti* (22), which acquired antimicrobial genetic elements recently (23).

In this study, a polyphasic taxonomic approach using phenotypic and genotypic methods revealed the taxonomic position of six *Macrococcus* sp. isolates originating from livestock, meat, wooden cheese board, and human clinical samples. The objective is also to characterize MGEs involved in HGT that contribute to genomic plasticity in macrococci and can be transferred to other opportunistic bacterial pathogens of the *Staphylococcaceae* family. The results of genome annotation underscore their significance in medicine and food microbiology.

RESULTS

Phylogenetic relationship of novel *Macrococcus* sp. isolates

Six *Macrococcus* sp. isolates were collected from specimens of different origins between 1995 and 2021 (Table 1). Methicillin-resistant *Macrococcus* sp. strains 19Msa1099, 19Msa1047, and 19Msa0499 were collected during a previous study focused on the characterization of macrococci from the nasal cavities of calves and pigs in Switzerland (21).

The phylogenetic analysis of the investigated strains based on complete 16S rRNA gene sequences demonstrated that they belong to the *M. caseolyticus* phylogenetic clade (Fig. 1A). The pairwise nucleotide sequence alignment of the 16S rRNA gene of the most genomically distant isolates NRL/St 95/376^T and 19Msa1099 exhibited 99.8% similarity. The NRL/St 95/376^T strain, representing the investigated group, exhibited 99.6% pairwise nucleotide similarity with the *M. caseolyticus* subsp. *caseolyticus* DSM 20597^T type strain. More precise taxonomic classification of the analyzed strains was determined based on their phylogenetic divergence at the whole-genome level. The calculated average nucleotide identity (ANI) values < 95.5% and digital DNA-DNA hybridization (dDDH) values < 63.5% distinguished all six strains from their closest relatives *M. caseolyticus*, *M. canis*, and *M. armenti* (Table S1), as also shown by

Downloaded from https://journals.asm.org/journal/aem on 04 February 2026 by 147.251.86.90.

TABLE 1 Source of strains of *Macrococcus psychrotolerans* sp. nov.

Strain[a]	Collection numbers[a]	Source	Year of isolation	Locality
NRL/St 95/376^T	CCM 8659^T, DSM 111350^T	Wooden cheese board	1995	České Budějovice, Czech Republic
NRL/St 13/116	ND	Human, swab from nose	2013	Příbram, Czech Republic
NRL/St 21/332	ND	Human, pus from wound on leg	2021	Prague, Czech Republic
19Msa1099	CCM 9224	Pork meat	2019	Bern, Switzerland
19Msa0499[b]	ND	Calf, nasal swab sample	2019	Bern, Switzerland
19Msa1047[b]	ND	Calf, nasal swab sample	2019	Bern, Switzerland

[a]NRL/St, National Reference Laboratory for Staphylococci, National Institute of Public Health (Prague); CCM, Czech Collection of Microorganisms; DSM, German Collection of Microorganisms and Cell Cultures; ND, not deposited.
[b]Strains 19Msa1047 and 19Msa0499 were originally published as *M. caseolyticus* (21).

protein-coding core genome analysis at the nucleotide and protein level (Fig. 1B and C). The ANI and dDDH values of all six strains were below the threshold values for species delimitation, which are 95%–96% and 70%, respectively (24).

Discrimination of *Macrococcus* spp. by MALDI-TOF MS and DNA fingerprinting techniques

Using cluster analysis of matrix-assisted laser desorption/ionization-time-of-flight mass spectrometry (MALDI-TOF MS) data, five of the six novel isolates were separated into a contiguous cluster distinct from phylogenetically related *Macrococcus* spp. (Fig. 2A). The exception to this pattern was strain NRL/St 13/116, grouped more distantly from other isolates. This distinction can be attributed to the close similarity of mass spectra to those of the related *M. caseolyticus* species (Fig. 2A). Therefore, under routine MALDI-TOF MS analysis conditions, strains of *M. psychrotolerans* sp. nov. may not be assigned to the correct *Macrococcus* species. However, when an alternative MALDI matrix (25) that enables the ionization of proteins over a broader range of molecular weights was employed, the novel isolates were grouped into a coherent dendrogram subbranch due to the detection of more species-specific signals (Fig. 2B), which is more accurate for identifying macrococci.

Numerical analysis of the repetitive sequence-based PCR (rep-PCR) fingerprints obtained with the $(GTG)_5$ primer (Fig. 3A) and the ribotype profiles obtained by automated ribotyping with the restriction enzyme *Eco*RI (Fig. 3B) grouped all six strains analyzed into a single cluster that was clearly distinct from the fingerprints of the type strains of the validly named *Macrococcus* species. Minor differences due to the presence or absence of some DNA bands allowed the differentiation of certain strains at the strain level; nevertheless, their fingerprints shown by both techniques were visually very similar or identical for strains 19Msa1099, 19Msa1047, and 19Msa0499. These results suggest that both methods are more suitable for the identification of *M. psychrotolerans* sp. nov. than for strain typing.

Phenotype and physiology

All six investigated strains exhibited typical phenotypic traits corresponding to the basic characteristics of the genus *Macrococcus*. They grew well on standard media used for the routine cultivation of macrococci, e.g., plate count agar (PCA), tryptone soya agar (TSA), nutrient agar (NA), mannitol salt agar (MSA), brain heart infusion agar (BHI), and P agar. All six isolates formed Gram-stain-positive spherical and non-motile cocci. Cells of 890 ± 75 × 610 ± 95 nm occur in pairs or clusters with adjacent sides flattened (Fig. 4). Abundant growth was obtained at a wide range of temperatures (1–45°C) in tryptone soy broth (TSB) and salinities (0%–10% NaCl). All six isolates grew between pH 6.0 and 9.0.

The strains were catalase and oxidase-positive, resistant to bacitracin and susceptible to furazolidone. Complete results of extensive biochemical and physiological testing of the six investigated strains using the conventional tests and the commercial kits API ZYM, API 50CH, and Biolog GEN III MicroPlate test panels are given in the Protologue below. The strain-dependent test results found in the analyzed group are shown in Table S2.

Downloaded from https://journals.asm.org/journal/aem on 04 February 2026 by 147.251.86.90.

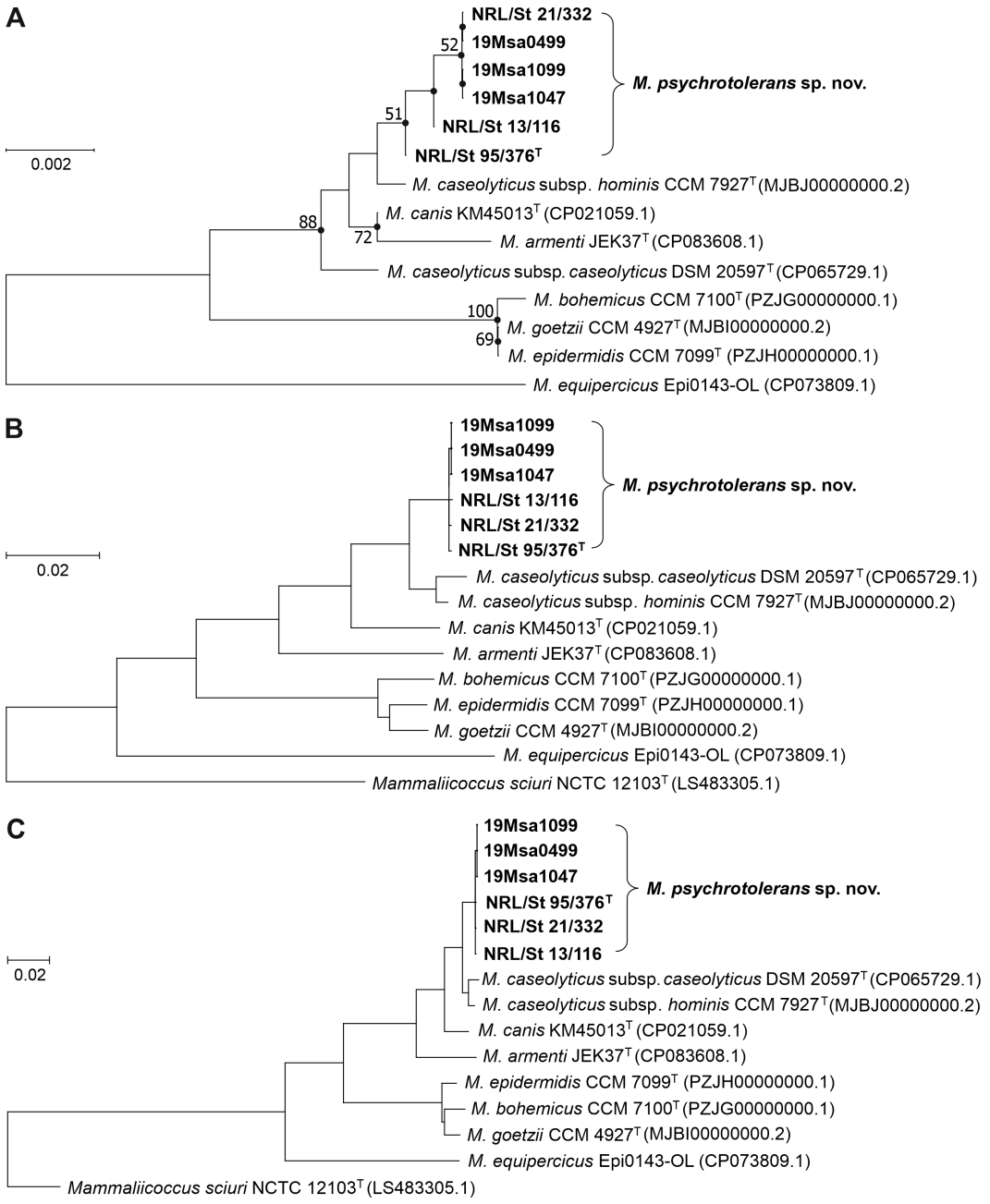

FIG 1 Evolutionary analyses of *Macrococcus caseolyticus* phylogenetic clade, including *M. psychrotolerans* sp. nov. (A) Unrooted phylogenetic tree based on complete 16S rRNA gene sequences extracted from whole-genomic sequencing data (GenBank accession numbers of the reference genomes are in parentheses and those of the studied strains in Table S5). The evolutionary history was inferred using the maximum likelihood method and Tamura–Nei model. Filled circles indicate that the corresponding nodes were also obtained in the tree constructed by the neighbor-joining method. The percentage of 500 tree replications above 50% in which the associated taxa clustered together is shown next to the branches. The tree is drawn to scale, with branch lengths measured in the number of substitutions per site. (B) Nucleotide sequence-based phylogenetic tree of concatenated alignment of 92 core genes constructed using up-to-date bacterial core gene (UBCG) set. (C) Protein sequence-based phylogenetic tree of concatenated alignment of 92 core genes constructed using UBCG. The maximum likelihood tree was inferred using RAxML software and set to 100 replicates.

Antimicrobial susceptibility testing using the disc diffusion method showed that all six strains are susceptible to erythromycin, fusidic acid, gentamicin, chloramphenicol, rifampicin, trimethoprim, trimethoprim/sulfamethoxazole, tetracycline, tigecycline, and

Downloaded from https://journals.asm.org/journal/aem on 04 February 2026 by 147.251.86.90.

tobramycin and resistant to penicillin G. Antibiotic susceptibility was strain dependent when tested with ampicillin, oxacillin, cefoxitin, ceftobiprole, ceftaroline, ciprofloxacin, norfloxacin, levofloxacin, clindamycin, linezolid, and novobiocin (Table S3).

Extensive biotyping showed, in agreement with the results of whole-genome phylogeny, DNA fingerprinting techniques, and MALDI-TOF MS data, that the investigated group of six isolates represents a new species of the genus *Macrococcus*. Notably, the ability of the analyzed strains to grow at 1°C in broth seems to be a unique phenotypic feature among the members of *Macrococcus*, which gave the name to the proposed species *Macrococcus psychrotolerans* sp. nov. Physiological and biochemical tests enabling the differentiation of *M. psychrotolerans* sp. nov. from the phylogenetically closely related *Macrococcus* spp. are shown in Table 2.

Cellular fatty acids were analyzed at two temperatures (37°C and 15°C) to understand the role of fatty acids in adaptation to lower temperatures. All six strains resemble a typical fatty acid profile of *Macrococcus* spp. at 37°C (Table 3, complete data in Table S4). Unsaturated fatty acids were enriched at low temperatures on average almost 2× in all strains. There was no statistically significant difference between the isolates of the Czech

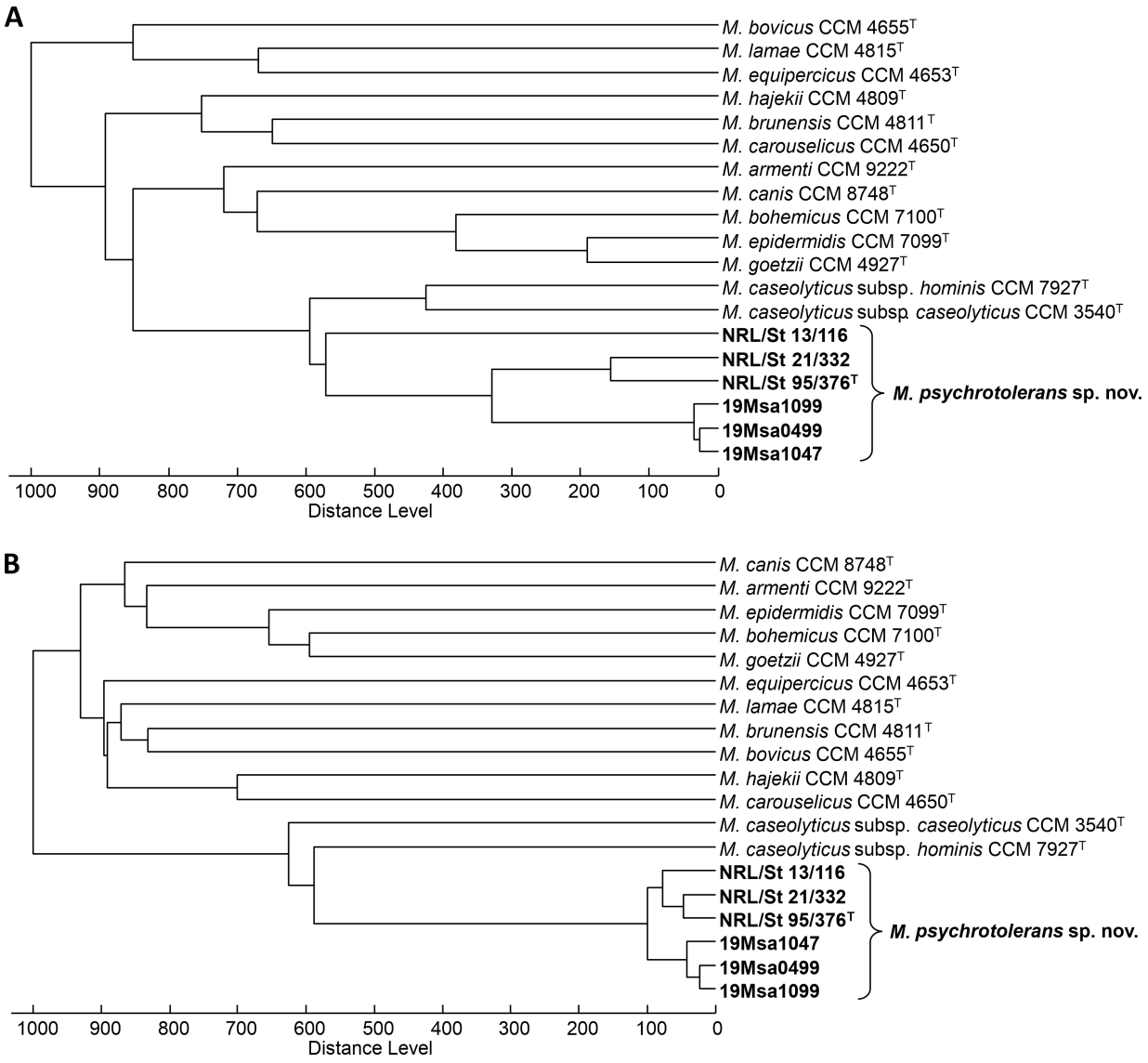

FIG 2 Dendrograms based on MALDI-TOF MS profiles of *Macrococcus psychrotolerans* sp. nov. strains and other members of the genus *Macrococcus* (A) using α-Cyano-4-hydroxycinnamic acid (CHCA) as a standard MALDI matrix; (B) using alternative MALDI matrix—strongly acidified ferulic acid. The dendrograms were generated using the correlation distance measure with the average linkage algorithm (UPGMA).

Downloaded from https://journals.asm.org/journal/aem on 04 February 2026 by 147.251.86.90.

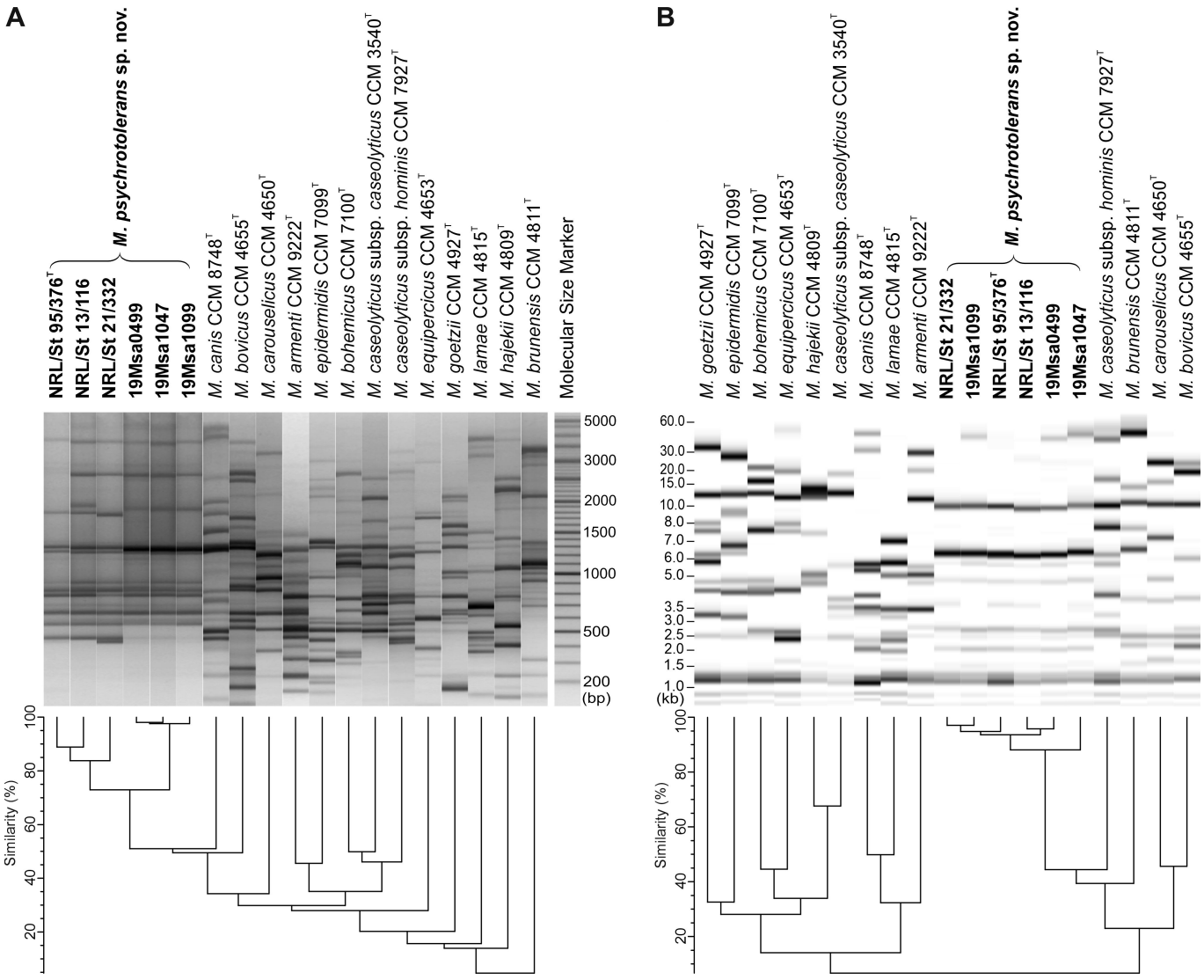

FIG 3 Cluster analysis of DNA fingerprinting data from *Macrococcus psychrotolerans* sp. nov. strains and the type strains of validly named *Macrococcus* spp. (A) Dendrogram based on cluster analysis of rep-PCR fingerprints obtained with the $(GTG)_5$ primer. (B) Dendrogram based on cluster analysis of *Eco*RI ribotype patterns obtained with automated ribotyping using the RiboPrinter system. Both dendrograms were calculated with Pearson's correlation coefficients with the UPGMA clustering method.

Republic and Switzerland, but in tendency (at 37°C), Swiss isolates showed a higher abundance of saturated fatty acids compared to the Czech isolates.

Genomic characterization of *M. psychrotolerans* sp. nov.

The *M. psychrotolerans* sp. nov. genomes have a chromosome size of 2.04–2.10 Mb with G+C content of 37.0%–37.2% and contain 2102–2432 predicted protein-coding genes and 79 RNAs (Table S5). They exhibited high similarity, differing primarily in the content of variable genomic elements (Fig. 5). The chromosomes of strains 19Msa1047, 19Msa1099, and 19Msa0499 were almost identical, as also indicated by dDDH and ANI values (Table S1).

The pan-genome of all six *M. psychrotolerans* sp. nov. representatives and the phylogenetically closest *M. caseolyticus* subsp. *caseolyticus* CCM 3540^T, *M. caseolyticus* subsp. *hominis* CCM 7927^T, and *M. canis* KM45013^T strains share 1659 orthologous clusters of encoded proteins. Thirty-seven distinctive orthologous protein clusters were identified as typical for six *M. psychrotolerans* sp. nov. genomes (Table S6). When we

Downloaded from https://journals.asm.org/journal/aem on 04 February 2026 by 147.251.86.90.

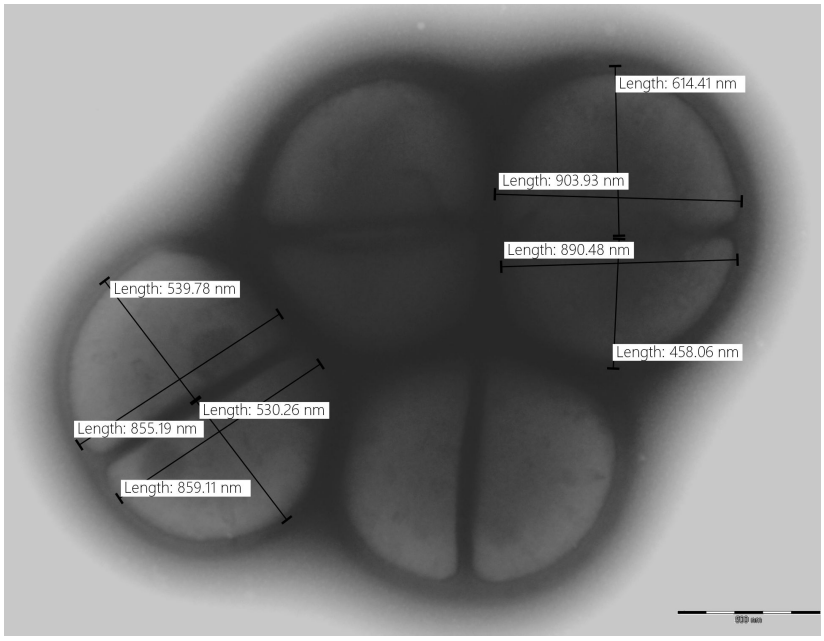

FIG 4 Transmission electron microscopy image of type strain *Micrococcus psychrotolerans* sp. nov. NRL/St 95/376^T, performed with Morgagni 268D Philips electron microscope. Negative staining was performed using 2% ammonium molybdate. Bar represents 500 nm.

focused on protein coding sequences that were previously not identified in any of the micrococcal genomes available in GenBank from known micrococcal species, 23 unique chromosomal core genes and 14 plasmid-borne genes shared by all isolates were identified for the *M. psychrotolerans* sp. nov. genomes (Table S6). The unique chromosomal genes are often hypothetical or encode integral membrane proteins responsible for the ATP-powered translocation of many substrates across membranes. Distinctive plasmid genes are related to the toxin-antitoxin system essential for maintaining plasmids in a population of cells.

A detailed comparison of representative core genome sequences of *M. psychrotolerans* sp. nov. with closely related micrococci revealed several unique genes with suspected roles in psychrotolerance. One of the distinct operons, consisting of seven genes, encodes proteins involved in acetoin catabolism (dihydrolipoyl dehydrogenase, thiamine pyrophosphate-dependent dehydrogenase, alpha-ketoacid dehydrogenase, dihydrolipoamide acetyltransferase, and dihydrolipoamide acetyltransferase) (Table S6). According to the Gene Ontology (GO) enrichment analysis (26) among strains belonging to *M. psychrotolerans* sp. nov., these genes belong to an enrichment pathway related to glycolytic processes and/or to the acetoin metabolism process, which involves the breakdown of carbohydrates into pyruvate, accompanied by the production of metabolites with a possible role in the psychrotolerance of these microorganisms (27).

In addition, all the *M. psychrotolerans* sp. nov. strains encode three different putative cold shock proteins, also identified sporadically in genomes classified in GenBank as *M. canis*, *M. caseolyticus,* or *M. armenti*, where the reciprocal amino acid identity ranges from 96.9% to 93.9% (query coverage 98%). The cold shock protein annotated as CspA (GenBank: WZE69993) shares 62.5% amino acid identity (94% query coverage) with the cold shock protein CspA (GenBank:VWQ03685) of *Escherichia coli*. Two other cold shock proteins (GenBank: WZE71216 and WZE71217) belonging to the CspC protein superfamily (UniProt: P0A9Y6) are genes located upstream that belong to the putative acetoin catabolism operon and separated by three genes from this operon.

Downloaded from https://journals.asm.org/journal/aem on 04 February 2026 by 147.251.86.90.

TABLE 2 Differentiation of *Macrococcus psychrotolerans* sp. nov. from closely related macrococci

Test[a]	*M. psychrotolerans* sp. nov.[b]	*M. canis*[b]	*M. caseolyticus* subsp. *caseolyticus*[b]	*M. caseolyticus* subsp. *hominis*[b]	*M. armenti*[b]
Growth at 1°C[c]	+/+	–/n.a.	–/n.a.	–/–	–/n.a.
Growth on mannitol salt agar	+/+	+/+	+/+	+/+	–/–
Voges-Proskauer test	–/d	+/+	+/+	+/+	–/–
Nitrate reduction	+/d	+/+	+/+	+/+	+/+
Pyrrolidonyl arylamidase	+/+	+/+	–/d	+/+	+/+
Acid from[d]:					
Glycerol	+/w	w/w	+/+	+/+	–/–
Ribose	+/+	–/–	+/+	+/+	+/+
Galactose	–/–	–/–	+/+	–/–	+/d
Mannitol	–/–	+/+	–/–	+/+	–/d
N-acetyl glucosamine	–/–	–/–	–/–	–/–	w/w
Lactose	–/–	–/–	+/+	–/–	+/d
Yellowish pigment	–/d	–/–	–/–	+/+	–/–

[a]+, positive; –, negative; w, weak reaction; d, 11%–89% strains positive; n.a., not assessed.
[b]Result of type strain/result from species description (5, 7, 22). Data for *M. psychrotolerans* sp. nov. and the type strains of closely related *Macrococcus* spp. were taken from this study in two replications.
[c]Growth in TSB after 7 days.
[d]API 50CH test (bioMérieux).

Chromosomal MGEs

The *M. psychrotolerans* sp. nov. strains have up to two complete prophages in their genomes integrated into three different *att* sites (Fig. 5). The prophage genomes exhibit low similarities to any known viruses from the order *Caudovirales* according to NCBI entries. They are likely yet undescribed phage genera. Prophages have a modular structure typical for staphylococcal siphoviruses (28) but a distinct gene composition. Comparative analysis showed that the prophages designated phiMP$_{NRL/St\ 13/116}$ (47.2 kb), phiMP$_{NRL/St\ 21/332}$ (49.3 kb), and phiMP$_{19Msa1099a}$ (52.3 kb) are highly similar in their major genomic modules to the previously described phage ϕMC1 (7) from *M. caseolyticus* subsp. *hominis* strain CCM 7927^T (coverage 57% and nucleotide identity 96.5%) and with the prophage identified in *M. caseolyticus* strain IMD0819 (3) (coverage 62% and identity 91.5%) but differ in their integrase genes (Fig. 6).

The prophages phiMP$_{NRL/St13/116}$ and phiMP$_{NRL/St21/332}$ share 95.7% mutual identity and are integrated into bacterial genomes downstream of the *glnA* gene encoding type I glutamate-ammonia ligase (GenBank: QYA77299.1). Two prophages were identified in strains 19Msa1099, 19Msa0499, and 19Msa1047. The first, designated phiMP$_{19Msa1099a}$,

TABLE 3 Abundance (% of total fatty acids) of pairs of major saturated and unsaturated fatty acids of *Macrococcus psychrotolerans* sp. nov. isolates cultivated at two different temperatures

Fatty acid	Results obtained for tested strains and temperatures											
	NRL/St 95/376^T		NRL/St 13/116		NRL/St 21/332		19Msa1099		19Msa0499		19Msa1047	
	15°C	37°C	15°C	37°C	15°C	37°C	15°C	37°C	15°C	37°C	15°C	37°C
$C_{14:1}$ ω9c	8.9	1.7	8.6	2.0	7.7	3.1	9.3	1.2	8.9	0.8	8.1	0.7
$C_{14:0}$	19.6	30.5	18.3	31.8	19.7	30.2	20.9	34.0	21.3	39.0	23.8	38.3
$C_{16:1}$ ω11c	26.0	14.4	26.5	16.9	28.37	17.6	29.8	16.2	30.2	14.4	30.0	13.1
$C_{16:0}$	2.4	13.0	2.4	11.8	2.6	11.1	2.3	14.0	2.5	19.7	3.3	20.7
$C_{18:1}$ ω13c	31.6	22.8	30.1	17.7	30.9	21.7	28.7	18.5	27.5	10.9	26.2	10.7
$C_{18:0}$	1.0	6.7	1.0	4.2	1.0	4.5	0.7	6.3	0.8	7.7	1.1	8.8
$C_{20:1}$ ω15c	3.0	1.0	2.5	0.6	2.3	1.3	1.8	0.5	1.7	0.2	1.4	nd[a]
$C_{20:0}$	0.9	1.1	0.6	0.6	0.7	0.7	0.3	0.7	0.4	0.4	0.6	0.4
Saturated	26.3	54.5	25.9	56.2	26.3	50.9	26.3	58.8	27.1	69.8	30.5	71.7
Unsaturated	70.7	40.9	68.8	39.0	70.7	45.3	70.6	37.0	70.1	26.7	66.7	24.8

[a]nd, not detected.

Downloaded from https://journals.asm.org/journal/aem on 04 February 2026 by 147.251.86.90.

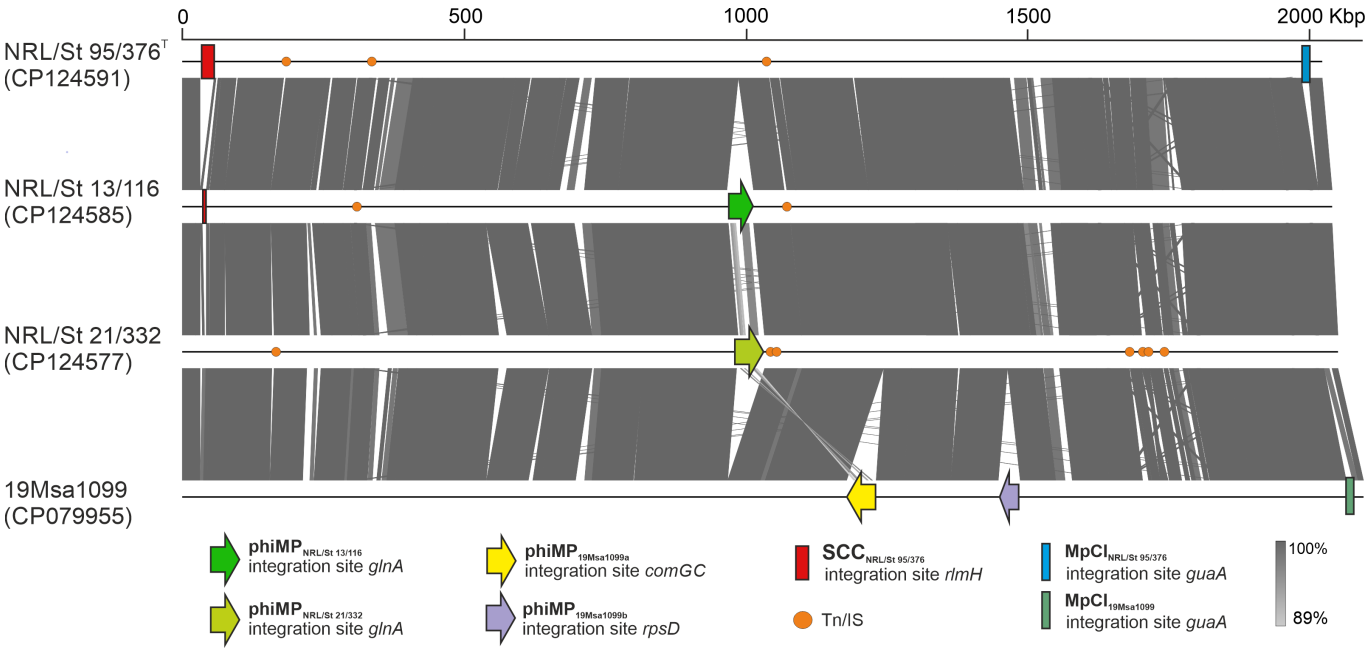

FIG 5 Genome comparison of selected *Macrococcus psychrotolerans* sp. nov. isolates. MGEs, i.e., prophages (phi), SCC, *M. psychrotolerans* chromosomal islands (MpCI), and transposons or insertion sequences are shown and color-coded as in the legend. Chromosomes of strains 19Msa1099, 19Msa0499, and 19Msa1047 share >99% identity and 19Msa1099 is shown as representative.

is integrated into the *comGC* gene, a part of the *comG* operon involved in binding of transforming DNA, which is, thus, disrupted by a negative lysogenic conversion process. The same integration site has been described previously in phage ϕMC1 (7). The second 38.6 kb-long prophage designated phiMP$_{19Msa1099b}$ is integrated into the *rpsD* gene encoding 30S ribosomal protein S4 (WP_219492567.1).

Comparative genomic analyses revealed the presence of 12.7 kb chromosomal island (CI) in strain NRL/St 95/376^T (designated MpCI$_{NRL/St\ 95/376}$) and 11.2 kb CI in strains 19Msa1099, 19Msa1047, and 19Msa0499 (designated MpCI$_{19Msa1099}$) at the same integration site between the tRNA$_{Ser}$ gene and the guanosine monophosphate (GMP) synthetase gene *guaA* (GenBank: WZE70899.1) (Fig. 7). These CI belong based on conserved modular structure, with genes clustered according to function, into phage inducible chromosomal islands group (29). A putative site-specific integrase of MpCI$_{NRL/St\ 95/376}$ exhibits 76.5% amino acid identity the MpCI$_{19Msa1099}$ integrase. In other *Macrococcus* spp. genomes except for *M. armenti* (23), this CI is absent or is replaced by a gene for putative SdrD B-like domain-containing protein (GenBank: WP_219503173.1), which is similar to the SpaA isopeptide-forming pilin-related protein (GenBank: WP_146606923.1). A structurally similar genomic island integrated into the *guaA* gene has been reported in *Mammaliicoccus fleurettii* along with the gene *erm*(45) for macrolides-lincosamides-streptogramin B (MLS$_B$) resistance (23, 30) (Fig. 7). MpCI$_{NRL/St\ 95/376}$ encodes a putative SAM-dependent type IIS restriction-modification enzyme (GenBank: WP_101142918), suggesting a possible protective function of this element from the host immune system. MpCI$_{19Msa1099}$ carries a gene for an Abi-like family protein (GenBank: WP_219493404) similar to the *Lactococcus* sp. abortive infection protein, which is involved in bacteriophage resistance (31).

Macrococcus psychrotolerans sp. nov. strain NRL/St 95/376^T carries a 24.86-kb-long composite island designated SCC$_{NRL/St\ 95/376}$ that belongs to SCC elements with *ccrB$_{m2}$A$_{m2}$* recombinase gene complex. The SCC$_{NRL/St\ 95/376}$ element is bordered by an almost identical 28 bp direct repeat (TGAATCGTATCAYAAGTAATGAGGTTTA) and inserted into the *rlmH* gene. It has 23 putative CDS. The *ccr* gene complex shares homology with *ccr* genes of *M. canis* KM45013 SCC*mec* (32) and *M. caseolyticus* JCSC7096 (18). Apart from

Downloaded from https://journals.asm.org/journal/aem on 04 February 2026 by 147.251.86.90.

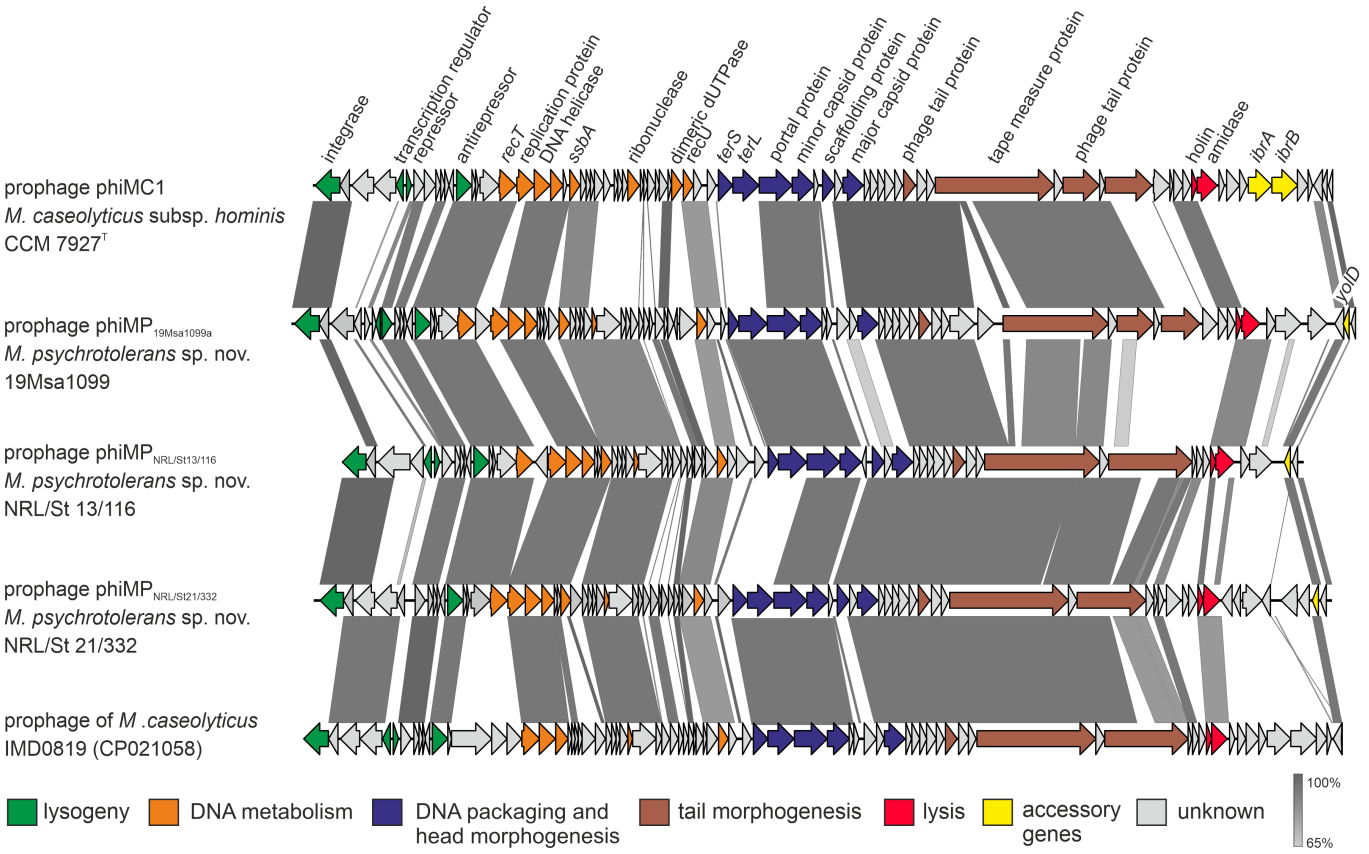

FIG 6 Genome comparison of bacteriophages identified in *Macrococcus psychrotolerans* sp. nov. with closely related bacteriophages from *Macrococcus caseolyticus*. Genomes were aligned using the blastn algorithm, and similar regions with more than 65% identity are indicated. Arrows represent the positions and orientations of the coding regions. Predicted genome modules are color-coded according to the legend.

the conserved *ccr* gene complex, the cassette harbors a DNA methyltransferase gene and a cluster of genes with unknown functions.

Multiple plasmid carriage, including a linear megaplasmid in *M. psychrotolerans* sp. nov.

Multiple plasmids are present in all six investigated *M. psychrotolerans* sp. nov. strains, ranging from 5 to 11 plasmid replicons. Plasmids smaller than 10 kb contained predominantly *repUS56* and *rep7a* genes (Table S7), which are the dominant replication genes in plasmids belonging to the *M. caseolyticus* phylogenetic group, with a prevalence of 35% and 34%, respectively, and are frequently associated with antimicrobial resistance (20). The identified plasmid replicons also frequently contain genes for both mobilization and toxin-antitoxin systems (Table S7).

Large 66.4-kb to 68.6-kb *mecB* gene-carrying plasmids were identified in three methicillin-resistant *M. psychrotolerans* sp. nov. strains 19Msa1099, 19Msa0499, and 19Msa1047 (Table S7) (21). The presence of the *mecB*-encoding plasmid is consistent with the phenotypic resistance of these three strains to oxacillin and cefoxitin (Table S3). These plasmids also harbor genes with homology to the type IV conjugative DNA transfer secretion system (GenBank: QYA38970.1), which seems to be widely used as a means for transferring plasmids in Gram-positive bacteria (33, 34).

In addition to the circular plasmids, almost identical 150 kb-long megaplasmids p19Msa1099_9, p19Msa0499_10, and p19Msa1047_11 with a covalently closed linear topology have been identified in the three strains 19Msa1099, 19Msa0499, and 19Msa1047. The plasmids have 14.1-kb-long inverted terminal repeats (ITRs) terminated by a covalent closure site apparent from centrally symmetric long sequencing reads

Downloaded from https://journals.asm.org/journal/aem on 04 February 2026 by 147.251.86.90.

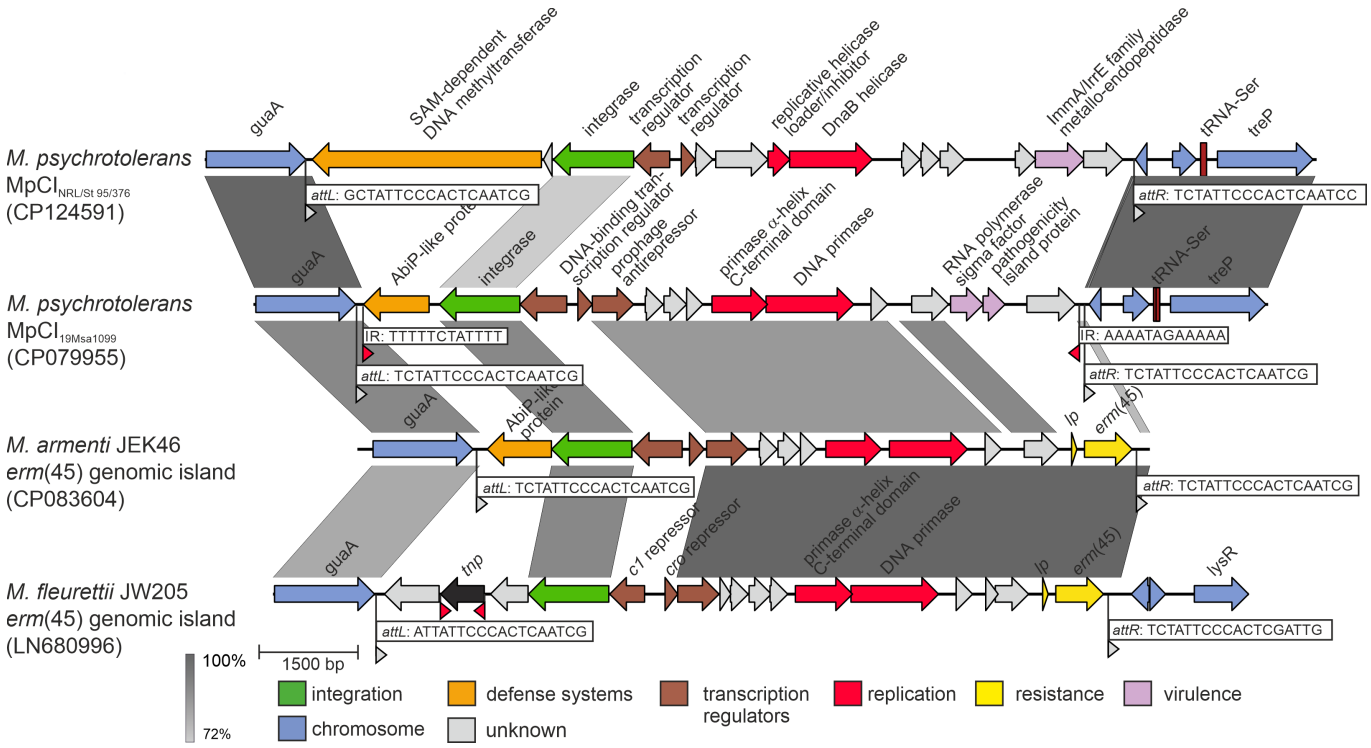

FIG 7 Global alignment of phage-inducible chromosomal islands identified in *Macrococcus psychrotolerans* sp. nov. strains NRL/St 95/376^T and 19Msa1099. $MpCI_{19Msa1099}$ is identical to islands in 19Msa1047 and 19Msa0499. The GenBank accession numbers of whole genomic sequences are provided.

originating from double-stranded plasmid ends (Fig. 8). The first and last T bases have no complementary counterparts and link both DNA chains (Fig. 8). The gene homologs for the RadC protein and the endoribonuclease RusA, which are involved in DNA repair and homologous recombination, were annotated inside ITRs. The linear plasmid also encodes two distinct RepB family plasmid replication initiator proteins, proteins responsible for mobilization (MobA/MobL), cell division (FtsK/SpoIIIE domain-containing protein), and plasmid segregation (ParA-like ATPase). There are several predicted genes in the plasmid sequence that encode protein domains found in type IV secretion systems (T4SS) (Fig. 8). The gene homolog for the multidrug efflux pump NorA (Fig. 8), which can confer resistance to fluoroquinolones and other structurally unrelated drugs, was identified in the plasmid (35). In addition to these genes, there are a number of IS elements and genes with unknown functions (Fig. 8).

In vitro mecB-mediated β-lactam antibiotic resistance transfer to *Staphylococcus aureus* by conjugation

The ability of 66.4 kb-long *mecB*-harboring plasmid p19Msa1099_1 (GenBank: CP079957) to transfer from *M. psychrotolerans* sp. nov. 19Msa1099 into the laboratory strain *S. aureus* RN4220 (pT181) was demonstrated. Together with p19Msa1099_1, the transferred 1.9 kb cryptic plasmid p19Msa1099_8 was detected in the *S. aureus* transconjugants. Analysis of sequence reads of the obtained transconjugants showed a mean coverage of 574.1 for the RN4220 genome, 1,244.2 for plasmid pT181, 23.1 for plasmid p19Msa1099_1, and 238.8 for plasmid 19Msa1099_8. There was no evidence of sequence reads mapping to the chromosome of the donor strain 19Msa1099. The stability of the *mecB* gene-carrying plasmid in the *S. aureus* RN4220 (pT181, p19Msa1099_1, p19Msa1099_8) cells during replication is 80% when the cultures were grown for 24 hours on plates without antibiotic selection. The resistance phenotype of tested penicillins and cephalosporins of the transconjugant *S. aureus* after acquiring the *mecB* gene-carrying plasmid was almost the same as the donor *M. psychrotolerans* sp. nov. 19Msa1099. Ceftobiprole resistance

Downloaded from https://journals.asm.org/journal/aem on 04 February 2026 by 147.251.86.90.

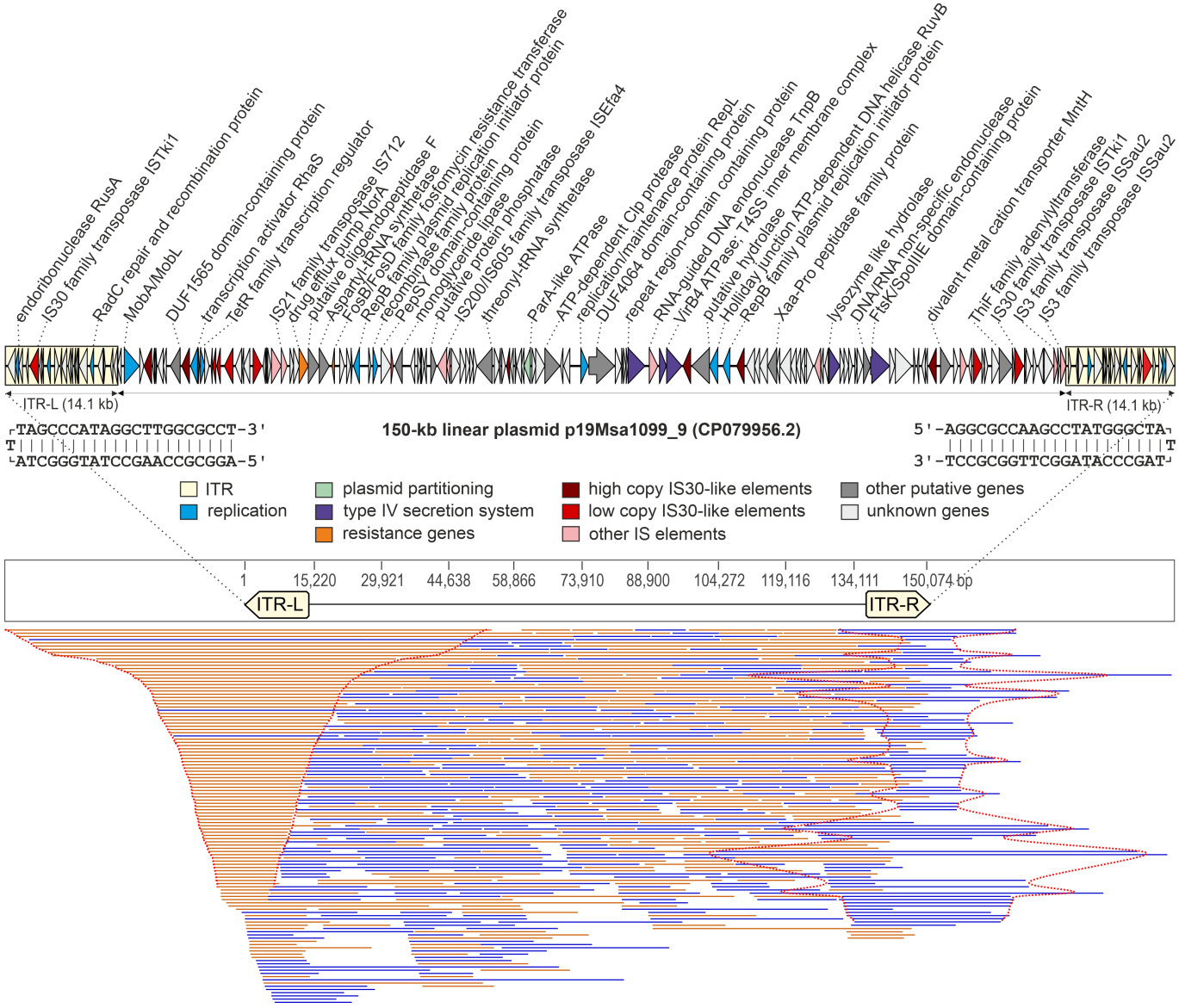

FIG 8 Genetic map of linear plasmid p19Msa1099_9 (GenBank accession number CP079956.2). Arrows show the position and orientation of predicted coding regions. The predicted genes are color-coded according to the legend. The sequences of physical ends of the hairpin plasmid are shown below the gene map. The mapping of sequencing reads longer than 10 kb to the assembled plasmid sequence revealed a centrally symmetric alignment of reads to the covalently closed ends of the hairpin plasmid. These reads resulted from the unfolding of the terminal hairpin structure during Oxford Nanopore sequencing technology (ONT) as it passed through the nanopore, and therefore, the unmapped parts correspond to the complementary strand (highlighted by a red dotted line). The mean coverage calculated from all ONT reads by Geneious mapper was 881× with a standard deviation of 215.

and decreased ceftaroline susceptibility resulted from acquiring the *mecB* gene in the *S. aureus* transconjugant (Table S3).

Taxonomic description of *M. psychrotolerans* sp. nov.

Macrococcus psychrotolerans sp. nov. (psy.chro.to´ler.ans. Gr. masc. adj. *psychros* cold; L. pres. part. *tolerans* tolerating; N.L. part. adj. *psychrotolerans* cold-tolerating).

Cells are Gram-stain positive spherical cocci with variable size of 890 ± 75 × 610 ± 95 nm, occurring predominantly in pairs, or tetrads and clusters, aerobic, non-spore-forming and non-motile. Colonies on TSA agar are circular, whole margin, flat, smooth, matt to glossy, 2 mm in diameter after 48 h of growth, and predominantly beige. Negative hemolytic activity on Columbia sheep-blood agar. Positive growth on PCA,

Downloaded from https://journals.asm.org/journal/aem on 04 February 2026 by 147.251.86.90.

TSA, NA, MSA, BHI, and P agar. Strains grow in the presence of up to 10% NaCl, at 1°C and 45°C, but not at 50°C, and in the range of pH 6 to pH 9. Catalase, oxidase, and pyrrolidonyl arylamidase positive. Coagulase, arginine dihydrolase, urease, and ornithine decarboxylase negative. Susceptible to furazolidone (100 µg) and resistant to bacitracin (10 IU). Hydrolysis of esculin and Tween 80 negative. Variable reactions were obtained for the hydrolysis of DNA, gelatine and glycerol, nitrate reduction, Voges-Proskauer test, clumping factor, and novobiocin resistance.

Enzymatic reactions tested with the API ZYM kit were positive for alkaline phosphatase, esterase (C4), and esterase lipase (C8), negative for lipase (C14), valine arylamidase, cystine arylamidase, trypsin, α-galactosidase, β-galactosidase, β-glucuronidase, β-glucosidase, N-acetyl-β-glucosaminidase, α-mannosidase, and α-fucosidase and variable for α-glucosidase, α-chymotrypsin, acid phosphatase, leucine arylamidase, and naphthol-AS-Bi-phosphohydrolase.

Acid production from substrates tested with the API 50CH kit was positive for ribose, D-glucose, D-fructose, maltose, and trehalose; negative for erythritol, D-arabinose, L-arabinose, D-xylose, L-xylose, adonitol, β-methyl-D-xyloside, galactose, mannose, sorbose, rhamnose, dulcitol, inositol, mannitol, sorbitol, α-methyl-D-mannoside, α-methyl-D-glucoside, N-acetyl glucosamine, amygdaline, arbutin, salicin, cellobiose, lactose, melibiose, inulin, melezitose, D-raffinose, starch, glycogen, xylitol, β-gentiobiose, D-turanose, D-lyxose, D-tagatose, D-fucose, L-fucose, D-arabitol, L-arabitol, 2 keto-gluconate, and 5 keto-gluconate and variable for glycerol, sucrose, and gluconate.

Phenotype characterization using Biolog GEN III MicroPlate test panels exhibited positive reactions for the utilization of dextrin, D-maltose, D-fructose, glycerol, D-glucose-6-PO_4, D-fructose-6-PO_4, L-alanine, L-histidine, L-serine, D-gluconic acid, L-lactic acid, α-keto glutaric acid, acetoacetic acid, α-hydroxy-butyric acid, formic acid, and acetic acid; borderline utilization of inosine; negative reactions for the utilization of D-cellobiose, gentiobiose, sucrose, stachyose, D-raffinose, α-D-lactose, D-melibiose, β-methyl-D-glucoside, D-salicin, N-acetyl-D-glucosamine, N-acetyl-β-D-mannosamine, N-acetyl-D-galactosamine, N-acetyl neuraminic acid, D-mannose, D-galactose, 3-methyl glucose, L-rhamnose, D-sorbitol, D-mannitol, D-arabitol, myo-inositol, D-aspartic acid, D-serine, L-arginine, L-aspartic acid, pectin, D-galacturonic acid, L-galactonic acid lactone, D-glucuronic acid, mucic acid, quinic acid, D-saccharic acid, p-hydroxy phenylacetic acid, D-lactic acid methyl ester, citric acid, D-malic acid, bromo-succinic acid, Tween 40, γ-amino-butyric acid, β-hydroxy-D,L-butyric acid, and propionic acid; and variable reactions for the utilization of D-trehalose, α-D-glucose, D-turanose, D-fucose, L-fucose, gelatine, glycyl-L-proline, L-glutamic acid, L-pyroglutamic acid, glucuronamide, methyl pyruvate, L-malic acid, and α-keto butyric acid. The strains grow in the presence of 1% sodium lactate, nalidixic acid, lithium chloride, potassium tellurite, aztreonam, and sodium butyrate; do not grow in the presence of fusidic acid, troleandomycin, rifamycin SV, minocycline, lincomycin, guanidine HCl, niaproof 4, vancomycin, tetrazolium violet, tetrazolium blue, and sodium bromate, and the growth was variable for D-serine when tested using Biolog GEN III MicroPlate test panels.

The type strain NRL/St 95/376^T contains menaquinones MK-6 (99.3%) and MK-7 (0.7%), and the peptidoglycan type is L-Lys-Gly_{3-4} (A11.2, A3α). The predominant fatty acids are $C_{14:0}$ (30.5%), $C_{18:1}$ ω13c (22.8%, identified as $C_{18:1}$ ω9c by the MIDI system), $C_{16:1}$ ω11c (14.4%), $C_{16:0}$ (13.0%), $C_{18:0}$ (6.7%), and $C_{14:1}$ ω9c (1.7%, not identified by the MIDI system). Furthermore, $C_{16:0}$ alcohol (2.3%) and $C_{18:0}$ alcohol [1.9%, identified as $C_{18:3}$ ω6c (6, 9, 12) by the MIDI system] are detectable. The genomic DNA G+C content of the type strain NRL/St 95/376^T is 37.2%. Type strain NRL/St 95/376^T (= CCM 8659^T = DSM 111350^T) was isolated from a wooden cheese board.

DISCUSSION

Macrococcus species belong to the normal flora of several mammals, and some species may be occasionally associated with animal infections, particularly livestock and pets. Certain species of the genus *Macrococcus* have been found in food products, mainly

Downloaded from https://journals.asm.org/journal/aem on 04 February 2026 by 147.251.86.90.

raw milk and dairy products. Bello et al. (36) suggested the reclassification of certain *Macrococcus* spp. into the novel genus *Macrococcoides* based on conserved signature indels as the main taxonomic criterium without studying other traits. According to LPSN (1), we consider the *Macrococcoides* genus to be a synonym due to nomenclature inaccuracies. Here, we described *M. psychrotolerans* sp. nov., which is closely related to the *M. caseolyticus* phylogenetic group and, like *M. caseolyticus,* includes isolates from animal husbandry and meat and dairy processing environments. *M. caseolyticus* is the most studied species of the *Macrococcus* genus and is used as a starter culture, contributing to the aroma and flavor of fermented foods. However, concerns are arising regarding food safety due to recent findings of methicillin and other antibiotic resistance genes in *M. caseolyticus*. These genes pose a risk to human health, as they can be transferred to other bacteria, particularly staphylococcal species present in food (11). The emergence of human-related isolates suggests that these organisms may sporadically enter the human clinical field.

The genome of *M. psychrotolerans* sp. nov. only differs marginally from related *M. caseolyticus* in G+C genome content, genome size, and median number of proteins encoded by the core genome. In contrast to other macrococci, strains of *M. psychrotolerans* sp. nov. can grow at refrigerator temperatures. The ability of a microorganism to survive and grow at low temperatures can allow the contamination of food such as meat or dairy products, which was noted in a recent metagenomic study in which *Macrococcus* sp. represented the predominant genus next to *Lactococcus* sp. during refrigerated meat storage (37). Comparative analysis of *M. psychrotolerans* sp. nov. genomes revealed the presence of a combination of genes for acetoin metabolism, butanediol dehydrogenase (BDH), ABC transporter genes, and three genes encoding cold shock proteins, which may support the ability of this bacteria to grow at low temperatures. Beckering et al. (27) found that the *Bacillus subtilis* gene cluster encoding the ABC transporter for acetoin was upregulated by a rapid decrease in temperature from 37°C to 15°C. It suggests that metabolic derivatives of acetoin could function as cryoprotectants under cold shock conditions (27). One probable metabolite with a possible cryoprotective function is 2,3-butanediol (38), which is metabolized from acetoin by 2,3-butanediol dehydrogenase (39). It has a low freezing point of −60°C and, in combination with specific proteins, can act as an antifreeze compound (40).

Members of small cold shock proteins are the most common bacterial proteins that react to temperature decreases and have canonical nucleic acid-binding sequence motifs (41). The homolog of CspA identified in *M. psychrotolerans* sp. nov. strains is related to extensively studied CspA (GenBank: WP_000014594) of *E. coli* (62.5% amino acid identity). It protects mRNA secondary structures and, thus, has a fundamental effect on cellular transcription during a rapid decrease in temperature (42). In the other two products of *csp* genes classified into the CspC protein superfamily, canonical nucleic acid-binding sequence motifs RNP1 and RNP2 have been predicted to bind to single-stranded RNA and DNA (41). Both the *csp* genes are localized in tandem, have distinct promoters and terminators, and have a lower G+C content (31.21% on average) than the genome average, indicating their horizontal transfer. Nevertheless, both *csp* gene products exhibit high mutual amino acid identity, differing in only two amino acids. A BLAST search only sporadically found the presence of these genes in sequence records of *M. caseolyticus* and *M. canis* and of the genus *Lysinibacillus* belonging to *Bacillales* (*Caryophanales*). However, the genes had a distinct regulatory sequence for transcription, and no information about the phenotype related to growth at low temperatures is known.

The cellular fatty acid profiles of *M. psychrotolerans* sp. nov. showed a clear overlap with *M. canis* and *M. caseolyticus* but combine features of both related species. The abundance of *iso*-fatty acids is lower than in *M. caseolyticus*, while the fatty alcohol abundance is far lower than in *M. canis* (5). In contrast, the type strain of *M. psychrotolerans* sp. nov. contained higher amounts of the unsaturated $C_{18:1}$ ω13c (identified as $C_{18:1}$ ω9c in the MIDI system) and $C_{16:0}$. The ratio of saturated and unsaturated

Downloaded from https://journals.asm.org/journal/aem on 04 February 2026 by 147.251.86.90.

fatty acids is a potential key feature for temperature adaptation and the regulation of membrane fluidity and might be one of the features relevant for the psychrotolerance of *M. psychrotolerans* sp. nov. Thus, we studied the fatty acid profile at two different temperatures (37°C as for published reference strains and 15°C). In all isolates, we observed the shift from saturated to non-saturated fatty acids by a factor of almost 2, which is a common principle in many species to modify the fluidity of the membrane (43, 44).

All *M. psychrotolerans* sp. nov. genomes contain one or more prophages integrated into different *att* sites. Prophage phiMP$_{19Msa1099a}$, identified in three *M. psychrotolerans* sp. nov. strains 19Msa1099, 19Msa0499, and 19Msa1047, is integrated into the *comGC* gene. The *comG* operon-encoded proteins exhibit similarity to genes for type IV pillar assembly (45) and for the secretion of some proteins in Gram-negative bacteria (46). Its insertional inactivation in *comGC* leads to a loss of transformability and the failure to bind DNA by cells growing in competency state (46, 47). We described this phenomenon previously in *M. caseolyticus* subsp. *hominis*, in which this negative lysogenic conversion led to nearly identical genomes of unrelated strains (7). Therefore, we hypothesize that the insertional inactivation of the *comGC* gene by prophage contributed to the loss of the ability of natural transformation in the three *M. psychrotolerans* sp. nov. strains. This may be the reason for their almost complete identity, despite the fact they originate from different sources, but we cannot exclude the possibility of a clonal relationship.

The variable part of the genomes of strains NRL/St 95/376^T, 19Msa1099, 19Msa1047, and 19Msa0499 includes CIs integrated into the 3′ end of the GMP synthetase gene (*guaA*), a known integration site for genomic islands, transposons, and bacteriophages in various bacterial species (48, 49). Also, a number of staphylococcal pathogenicity islands (SaPIs) integrate into this site (50). The MpCI$_{19Msa1099}$ identified in 19Msa1099, 19Msa1047, and 19Msa0499 strains exhibits 86.7% nucleotide similarity (57% query coverage) with an island identified in *M. armenti* (23) and 87.4% nucleotide similarity (53% query coverage) with an 11.5 kb genomic island of *M. fleurettii* encoding an MLS$_B$ resistance methylase Erm(45) (30), which suggests that there is an intra- and interspecies and intergeneric transmission of whole islands or their parts.

Most *M. psychrotolerans* sp. nov. strains contain a high number of plasmids, including conjugative plasmids larger than 66 kb encoding the *mecB* gene and also linear megaplasmids (Table S7). *M. psychrotolerans* sp. nov. strains were isolated in different regions and may inhabit various habitats. The *mecB* gene-carrying plasmids and linear megaplasmids were only carried by strains 19Msa1099, 19Msa0499, and 19Msa1047 isolated in Switzerland. This indicates variability in antibiotic resistance and may also suggest recent plasmid acquisition from other bacteria.

The *mecB*-encoded penicillin-binding protein 2a (PBP2a)-related transpeptidase was found on large plasmids and SCC*mec* elements in *Macrococcus* spp. (7, 17, 18, 21, 32). The *mecB* gene-encoding plasmids identified in strains 19Msa0499, 19Msa1099, and 19Msa1047 are similar to plasmid pSAWWU4229 (GenBank: LT799381) from *S. aureus* strain UKM4229 obtained from a 67-year-old cardiology patient with no signs of infection (19), to plasmid pKM0218 from *M. canis* (16) and to plasmid pMCCL2 (GenBank: AP009486) from *M. caseolyticus* (17). This pMCCL2 carries the *mec* gene complex (*mecB-mecR1*$_m$-*mecI*$_m$-*blaZ*$_m$) as part of a transposon Tn*6045* (18), which is also carried on plasmids of strains 19Msa0499, 19Msa1099, and 19Msa1047. Similarly, plasmids with high nucleotide similarity were identified in methicillin-resistant *M. caseolyticus* isolated from cattle in Switzerland (21) and England and Wales (10, 15). Evidence of the occurrence of similar plasmids in different locations and isolates suggests that they are transferable *in vivo* or in the environment. *M. psychrotolerans* sp. nov. strains harbor several plasmids that carry genes for mobilization (*mobA*, *mobC*, and *mobL*), suggesting their possible role in horizontal transfer.

Here, we proved *in vitro* conjugative transfer of *mecB* encoding plasmid p19Msa1099_1 from *M. psychrotolerans* sp. nov. to *S. aureus*. This intergeneric transfer poses a risk of spreading resistance to beta-lactams to other human opportunistic

Downloaded from https://journals.asm.org/journal/aem on 04 February 2026 by 147.251.86.90.

pathogens. As observations of *mecB* in *S. aureus* are rare, the role of *mecB*-encoded PBP2a in conferring resistance to anti-MRSA cephalosporin antibiotics is underexplored. Here, we showed that acquiring the *mecB* gene leads to resistance to ceftobiprole and ceftaroline (Table S3), similar to introducing mutated *mecA* into the susceptible *S. aureus* background (51). However, the sequence coverage of the transferred plasmid p19Msa1099_1 was 24 times lower than the coverage of the entire *S. aureus* RN4220 chromosome. Also, the phenotypic test showed frequent plasmid losses at cell division. We hypothesize that the plasmid is not uniformly maintained in the bacterial cell population, and its segregation stability is low for unknown reasons (52). In addition to the *mecB* encoding plasmid, a 1.9 kb cryptic plasmid was transmitted to the analyzed transconjugants. Whether plasmid 19Msa1099_8 encodes for a function that is beneficial for the acquisition or maintenance of p19Msa1099_1 remains unknown.

Linear megaplasmids have been found in a limited number of bacterial species. These plasmids are extrachromosomal DNA elements that are divided into hairpin elements or elements with 5′-end attached proteins (53). Both types are characterized by an invertron-like structure with ITRs. The assembly of a complete plasmid p19Msa1099_9 was achieved by obtaining high-quality nanopore sequencing reads with lengths exceeding the ITRs. The ONT platform further enabled the sequencing of unwound plasmid strands that contained the DNA hairpin closure, allowing the identification of the junction site of both strands. As there were no obvious nicks in the sequence, a linear hairpin structure could be confirmed. Comparative analysis of the nucleotide sequences with other linear plasmids in the GenBank found no sequence similarity. However, at the protein level, a low similarity and similar gene structure with the linear plasmid of *Mammaliicoccus sciuri* strain B9-58B isolated from retail pork has been identified (54). The linear plasmid contains a large number of IS30-like elements (Fig. 8) that are widely distributed in bacteria and are involved in the transfer of genetic information and shuttling of adaptive traits and, thus, influences the genomic content (55). Predicted genes of possible replication relevance are scattered throughout the plasmid. We identified the two putative genes encoding the RepB family initiation protein (Fig. 8). RepB is a hexameric replication initiator typical for the rolling-circle replicons evolutionarily related to viral initiators, whereas other plasmid initiators are purified as monomers or dimers (56). The plasmid encodes the VirB4 ATPase, several putative hydrolases, and the protein containing the FtsK domain, which are part of the multiprotein secretion apparatus, the type IV secretion system (T4SS), that is necessary for the conjugative transfer of DNA to a recipient cell. VirB4 exhibits similarity to the TraE protein involved in the process of DNA translocation, FtsK-homologous protein transfers double-stranded DNA to the recipient cell, and hydrolases play a key role in the assembly of T4SS (34).

MATERIALS AND METHODS

Bacterial strains

Strains NRL/St 95/376^T, NRL/St 13/116, and NRL/St 21/332 were isolated in various routine clinical laboratories in the Czech Republic and identified in the Reference Laboratory for Staphylococci (National Institute of Public Health, Prague, Czech Republic). Strains 19Msa1099, 19Msa1047, and 19Msa0499 were isolated previously (21). Representative strains have been deposited in the Czech Collection of Microorganisms (Masaryk University, Brno, Czech Republic, http://www.sci.muni.cz/ccm) and the Leibniz Institute DSMZ-German Collection of Microorganisms and Cell Cultures (Braunschweig, Germany, https://www.dsmz.de) (Table 1). Reference type strains of validly named *Macrococcus* spp. were obtained from the Czech Collection of Microorganisms.

Phenotypic characterization

The morphological, biochemical, and physiological characterization of analyzed macrococci was performed as previously described (7, 57, 58). The growth of strains

Downloaded from https://journals.asm.org/journal/aem on 04 February 2026 by 147.251.86.90.

was tested in a basic set of staphylococcal media: Columbia sheep-blood Agar (Oxoid), Plate Count Agar (Oxoid), Tryptone Soya Agar (Oxoid), CM3 Nutrient Agar (Oxoid), Brain Heart Infusion Agar (Oxoid), Mannitol Salt Agar (HiMedia), and P agar at mesophile temperature conditions. The tested temperatures were 1°C, 3°C, 7°C, 10°C, 15°C, 25°C, 37°C, 42°C, 45°C, 48°C, and 50°C. The tested salinity was 0%, 2%, 7%, 8%, 9%, 10%, and 11% NaCl in Tryptone Soy Broth (TSB) (Oxoid). The tested pH levels (in TSB) were 5, 6, 7, 8, 9, 10, and 11. The commercial kits API ZYM, API 50 CH (bioMérieux), and Biolog GEN III MicroPlate (Biolog) were used as specified by the manufacturers. Antimicrobial susceptibility was tested by the disc diffusion method using Oxoid disks except for ceftobiprole and ceftaroline, which were from Bio-Rad, on Mueller-Hinton agar and interpreted according to the EUCAST guidelines for coagulase-negative staphylococci (59) as described previously (60).

Transmission electron microscopy

A 200-mesh carbon/formvar-coated grid was placed on a drop of suspension of bacteria in water for 20 min. Bacterial cells on the grid were negatively stained with 2% ammonium molybdate and treated with UV light. A Morgagni 268D Philips (ThermoFisher Scientific, The Netherlands) transmission electron microscope was used to visualize bacterial cells.

Matrix-assisted laser desorption/ionization-time-of-flight mass spectrometry analysis

The samples were prepared by the standard extraction protocol described by Freiwald and Sauer (61). In addition to the standard saturated solution of alpha-cyano-4-hydroxycinnamic acid (CHCA) in water:acetonitrile:TFA (47.5:50:2.5, vol/vol), an alternative matrix solution was utilized, composed of 12.5 mg mL^{-1} ferulic acid in water:acetonitrile:formic acid (50:33:17, vol/vol), as proposed by Madonna et al. (25). MALDI-TOF mass spectra were obtained using an Ultraflextreme instrument (Bruker Daltonics) operated in linear positive mode using the software FlexControl v3.4. Mass spectra were processed using FlexAnalysis v3.4 (Bruker Daltonics) and BioTyper software v3.1 (Bruker Daltonics). A MALDI-TOF mass spectra-based dendrogram was constructed using the Pearson's product moment coefficient as a measure of similarity, and the unweighted pair group average linked method (UPGMA) as a grouping method.

Genotypic analysis by fingerprinting techniques

Repetitive sequence-based PCR (rep-PCR) fingerprinting with the $(GTG)_5$ primer was used to genotypically screen the investigated macrococci. DNA extraction from the bacterial cells, PCR conditions, and fingerprint analysis were performed as previously described (62). Further characterization included automated ribotyping with the restriction enzyme *Eco*RI, performed with the RiboPrinter Microbial Characterisation System (DuPont Qualicon) according to the manufacturer's instructions. Numerical analysis of rep-PCR fingerprints and ribotype patterns was performed using BioNumerics v7.6 (Applied Maths, Belgium). The dendrograms were calculated with Pearson's correlation coefficients with the UPGMA clustering method. The ribotype patterns were imported into the software BioNumerics using the load samples import script provided by the manufacturer.

Chemotaxonomic analyses

Analyses were performed in the proposed type strain NRL/St 95/376^T at the Leibniz Institute DSMZ-German Collection of Microorganisms and Cell Cultures (https://www.dsmz.de). Fatty acid methyl ester (FAME) profiles were analyzed after saponification, methylation, and extraction following the protocol of Sasser (63). The FAME mixtures were separated by gas chromatography and detected by a flame ionization

Downloaded from https://journals.asm.org/journal/aem on 04 February 2026 by 147.251.86.90.

detector. In subsequent analysis, fatty acids were identified by gas chromatography-mass spectrometry (GC-MS) run on an Agilent GC-MS 7000D system (64). The position of single double bonds was confirmed by derivatization to the corresponding dimethyl disulfide adduct (65). Peaks were identified based on retention time and mass spectra. If the MIDI database TSBA6 resulted in a different identification, it is mentioned in the Protologue to allow comparison to the literature.

Isolation and structure analyses of the peptidoglycan were performed according to published protocols with some modifications. In brief, the amino acid composition of the total hydrolysate (4 N HCl, 100°C, 16 h) of the peptidoglycan was analyzed by GC-MS using Protocol 10 by Schumann (66). The partial hydrolysate (4 N HCl, 100°C, 45 min) of the peptidoglycan was analyzed by high-resolution liquid chromatography-mass spectrometry as described previously (66, 67). Enantiomeric analysis was performed by liquid chromatography as described previously (68). Respiratory quinones were extracted and analyzed as described previously (64). Identity was confirmed by mass spectrometry as described previously (67).

Conjugative transfer of methicillin resistance

The protocol for conjugation between donor *M. psychrotolerans* sp. nov. strain 19Msa1099 and recipient *S. aureus* RN4220 (pT181) (69) was based on the original method by Forbes and Schaberg (70) with the following modifications: The cultures were grown overnight at 37°C in TSB, diluted 1:50 in TSB, and grown with aeration at 37°C to OD_{600} = 0.4 (approximately 10^8 CFU mL^{-1}). The cultures were mixed 1:1 and filtered through a sterile 0.45 µm cellulose acetate filter (Ahlstrom-Munksjö, Finland). The filter was placed on a TSA plate without antibiotics, with the side with the bacterial lawn touching the agar surface, and incubated overnight at 37°C. The cells were washed from the filter into 1 mL of TSB, plated at various dilutions on TSA plates with 2.5 µg mL^{-1} tetracycline (Sigma-Aldrich) and 1.25 µg mL^{-1} oxacillin sodium salt (Sigma-Aldrich), and incubated overnight at 37°C. Individual tiny colonies were passaged on TSA plates with 2.5 µg mL^{-1} tetracycline and 0.25 µg mL^{-1} oxacillin.

For simple calculation of plasmid stability during cell replication, the culture grown on TSA with oxacillin 0.25 µg mL^{-1} was resuspended in TSB and diluted and plated on TSA without oxacillin to obtain individual colonies. The colonies were replicated on plates with oxacillin 0.25 µg mL^{-1}, and plasmid stability was calculated as the ratio of the number of oxacillin-resistant colonies over the number of input colonies.

Genome sequencing and assembly

The sequencing of strains 19Msa1099, 19Msa1047, and 19Msa0499 was performed in a previous study as described by Keller et al. (21). For strains NRL 95/St 376^T, NRL/St 13/116, and NRL/St 21/332, the genomic DNA was extracted from pure cultures cultivated in Meat Peptone Broth as described previously (71). The 500 bp sequencing library for the Illumina platform was prepared with a NEBNext Ultra II DNA library prep kit for Illumina (New England BioLabs). The samples were sequenced using a MID output cartridge in 150 bp paired-end mode in an Illumina NextSeq sequencing platform (Illumina, San Diego, CA, USA). The quality of reads was assessed with FastQC v0.11.9 (72).

For sequencing using the Oxford Nanopore technology (ONT), the library was prepared using the SQK-RAD004 Rapid sequencing kit (Oxford Nanopore Technologies, Oxford, UK) according to the manufacturer's instructions, and sequenced with a FLO-FLG001 flow cell (R9.4.1) in a MinION device (Oxford Nanopore Technologies, Oxford, UK). The device was controlled with the software MinKNOW v22.12.7 (Oxford Nanopore Technologies, UK) also used for base calling and trimming. To verify the genetic background of the transconjugants and for the linear megaplasmid assembly, the SQK-LSK114 Ligation sequencing kit and SQK-RBK114-24 Rapid barcoding kit (Oxford Nanopore Technologies) and FLO-FLG114 flow cells (R10.4.1) were used. The software MinKNOW v24.02.16 (Oxford Nanopore Technologies) was used for base calling and trimming. In all cases, only reads with a *q*-score ≥10 were used for assembly. Long

Downloaded from https://journals.asm.org/journal/aem on 04 February 2026 by 147.251.86.90.

sequencing reads were mapped to the reference chromosomal and plasmid sequences using the built-in Geneious Mapper (Minimum mapping quality: 10) in Geneious Prime v2024.0.5 (GraphPad Software, New Zealand).

Complete bacterial genome sequences were assembled using Trycycler v0.5.0 (73). The resulting assemblies were first polished with Medaka using long reads (https://github.com/nanoporetech/medaka) and then Polypolish using short reads (74). The coverage of the final assembly was inspected by mapping sequencing reads using the plugin module Minimap2 (75) for ONT reads and Bowtie 2 (76) for Illumina reads in Geneious Prime.

Phylogenic and pangenome analyses

An almost complete 16S rRNA gene was sequenced by Sanger sequencing (Eurofins Genomics, Ebersberg, Germany) as described previously (77). The whole 16S rRNA gene sequences for phylogenetic analyses were extracted from WGS data obtained in this study and the NCBI Genome database and compared by EzBioCloud (78). The phylogenetic analyses were performed with the software MEGA v11 (79). Genetic distances were corrected using the Tamura-Nei model, and the evolutionary history was inferred using the maximum-likelihood and neighbor-joining methods, using a bootstrap test based on 500 replications (80). The up-to-date bacterial core gene (UBCG) pipeline v3.0 with default settings was used for whole-genome phylogenetic analysis based on 92 core gene sequences (81).

Average nucleotide identity (ANI) and digital DNA-DNA hybridization (dDDH) values were determined to evaluate the genomic similarity between strains. The dDDH values were calculated according to the d4 formula using a web-based genome-to-genome distance calculator (GGDC) v3.0 (82). Cluster analysis based on ANI values and a heat map of ANI identity were obtained using fastANI v1.33 (83).

Bioinformatics analyses

Complete genomes were annotated using the NCBI Prokaryotic Genome Annotation Pipeline (84) and further examined manually with the NCBI BLAST tool (https://blast.ncbi.nlm.nih.gov). MGEs were identified with PHASTER (85), PhiSpy v4.2.21 (86), IslandViewer 4 (87), VRprofile2 (88), and ISFinder (89). Virulence and resistance genes were predicted using ABRicate (https://github.com/tseemann/abricate) with the CARD (90), Resfinder v4.5.0 (91), and VFDB (92) databases. Predicted protein sequences were clustered using web-based OrthoVenn3 with a default cutoff *e*-value of 1*e*−5 and inflation value of 1.5 (93). The pairwise sequence alignments of multiple loci and whole genomes were visualized using EasyFig v2.2.5 (94).

ACKNOWLEDGMENTS

Daniel Krsek (National Reference Laboratory for Diagnostic Electron Microscopy of Infectious Agents, National Institute of Public Health, Prague, Czech Republic) is gratefully acknowledged for transmission electron microscopy, as are Anika Wasner and Gesa Martens (DSMZ-German Collection of Microorganisms and Cell Cultures) for technical assistance.

This work was supported by a National Institute of Virology and Bacteriology project (Programme EXCELES, Project ID No. LX22NPO5103)—Funded by the European Union-Next Generation EU to R.P. The CIISB, Instruct-CZ Centre of the Instruct-ERIC EU consortium, funded by the Ministry of Education, Youth and Sports of the Czech Republic (MEYS CR) infrastructure project (LM2023042), is gratefully acknowledged for the financial support of the measurements at the CEITEC Proteomics Core Facility (CF). We acknowledge the CF Genomics and the CF Bioinformatics supported by the NCMG research infrastructure (LM2023067) funded by the MEYS CR for their support in obtaining scientific data presented in this paper. P.P. was supported by the Ministry of Health, Czech Republic—conceptual development of research organization (The National Institute of

Downloaded from https://journals.asm.org/journal/aem on 04 February 2026 by 147.251.86.90.

Public Health—NIPH, 75010330). Computational resources were supplied by the e-INFRA CZ project (ID: 90254), supported by the MEYS CR. The Czech Collection of Microorganisms (Masaryk University) partly funded this study. The Grant Agency of Masaryk University (MUNI/A/1603/2024) supported the research activities of students.

AUTHOR AFFILIATIONS

[1]Department of Experimental Biology, Section of Genetics and Molecular Biology, Faculty of Science, Masaryk University, Brno, Czech Republic
[2]Institute of Microbiology, Czech Academy of Sciences, BIOCEV, Vestec, Czech Republic
[3]Department of Experimental Biology, Czech Collection of Microorganisms, Faculty of Science, Masaryk University, Brno, Czech Republic
[4]Central European Institute of Technology, Masaryk University, Brno, Czech Republic
[5]Leibniz Institute DSMZ-German Collection of Microorganisms and Cell Cultures, Braunschweig, Germany
[6]Division of Bacterial Molecular Epidemiology and Infectious Diseases, Institute of Veterinary Bacteriology, Vetsuisse Faculty, University of Bern, Bern, Switzerland
[7]Clinic of Conservative and Preventive Dentistry, Center for Dental Medicine, University of Zurich, Zurich, Switzerland
[8]Centre for Epidemiology and Microbiology, National Institute of Public Health, Prague, Czech Republic

AUTHOR ORCIDs

Ivana Mašlaňová http://orcid.org/0000-0002-2597-2848
Vojtěch Kovařovic http://orcid.org/0009-0004-0971-9764
Tibor Botka http://orcid.org/0000-0003-2708-3718
Pavel Švec http://orcid.org/0000-0002-1051-5177
Ivo Sedláček http://orcid.org/0000-0003-1717-187X
Meina Neumann-Schaal http://orcid.org/0000-0002-1641-019X
Sarah Kirstein http://orcid.org/0009-0006-0692-9410
Sybille Schwendener http://orcid.org/0009-0008-5661-8260
Vincent Perreten http://orcid.org/0000-0001-5722-9445
Roman Pantůček http://orcid.org/0000-0002-3950-675X

FUNDING

Funder	Grant(s)	Author(s)
Ministerstvo Školství, Mládeže a Tělovýchovy	LX22NPO5103, LM2023042, LM2023067, 90254	Roman Pantůček Ondrej Šedo
Ministerstvo Zdravotnictví Ceské Republiky	NIPH 75010330	Petr Petráš
Masarykova Univerzita	MUNI/A/1603/2024	Jiří Doškař

AUTHOR CONTRIBUTIONS

Ivana Mašlaňová, Conceptualization, Data curation, Investigation, Methodology, Validation, Visualization, Writing – original draft, Writing – review and editing | Vojtěch Kovařovic, Data curation, Formal analysis, Investigation, Writing – review and editing | Tibor Botka, Formal analysis, Investigation, Software, Validation, Visualization, Writing – review and editing | Pavel Švec, Investigation, Validation, Visualization, Writing – review and editing | Ivo Sedláček, Conceptualization, Data curation, Formal analysis, Investigation, Methodology, Resources, Validation, Writing – original draft, Writing – review and editing | Ondrej Šedo, Data curation, Formal analysis, Investigation, Visualization, Writing – review and editing | Adéla Finstrlová, Data curation, Investigation, Writing – original draft | Meina Neumann-Schaal, Data curation, Investigation, Resources, Validation,

Downloaded from https://journals.asm.org/journal/aem on 04 February 2026 by 147.251.86.90.

Writing – review and editing | Sarah Kirstein, Data curation, Investigation, Visualization, Writing – review and editing | Sybille Schwendener, Data curation, Investigation, Validation, Writing – review and editing | Eva Staňková, Investigation, Validation | Kristína Rovňáková, Investigation, Methodology | Petr Petráš, Formal analysis, Funding acquisition, Investigation, Resources, Writing – review and editing | Jiří Doškař, Conceptualization, Funding acquisition, Resources, Supervision, Writing – review and editing | Vincent Perreten, Conceptualization, Project administration, Resources, Writing – review and editing | Roman Pantůček, Conceptualization, Formal analysis, Funding acquisition, Methodology, Project administration, Resources, Supervision, Visualization, Writing – original draft, Writing – review and editing

DATA AVAILABILITY

All sequence data associated with the analyzed strains have been deposited in GenBank under BioProject accession numbers PRJNA952914 and PRJNA744395. The GenBank accession numbers of complete genomes of strains NRL/St 95/376^T, NRL/St 13/116, and NRL/St 21/332 are CP124591-CP124597, CP124585-CP124590, and CP124577-CP124584, respectively. Whole genomic sequences of strains 19Msa1099 (CP079955-CP079964), 19Msa0499 (CP079969-CP079980), and 19Msa1047 (CP080013-CP080023) have been published previously (21). The ONT sequencing data from an *S. aureus* transconjugant have been deposited under BioSample accession number SAMN41884817. The partial 16S rRNA gene sequence of type strain NRL/St 95/376^T obtained by Sanger sequencing was deposited under GenBank accession number PP341307.

ADDITIONAL FILES

The following material is available online.

Supplemental Material

Supplemental material (AEM01652-24-s0001.xlsx). Tables S1 to S7.

REFERENCES

1. Parte AC, Sardà Carbasse J, Meier-Kolthoff JP, Reimer LC, Göker M. 2020. List of prokaryotic names with standing in nomenclature (LPSN) moves to the DSMZ. Int J Syst Evol Microbiol 70:5607–5612. https://doi.org/10.1099/ijsem.0.004332
2. de la Fuente R, Suarez G, Ruiz Santa Quiteria JA, Meugnier H, Bes M, Freney J, Fleurette J. 1992. Identification of coagulase negative staphylococci isolated from lambs as *Staphylococcus caseolyticus*. Comp Immunol Microbiol Infect Dis 15:47–52. https://doi.org/10.1016/0147-9571(92)90101-v
3. Schwendener S, Cotting K, Perreten V. 2017. Novel methicillin resistance gene *mecD* in clinical *Macrococcus caseolyticus* strains from bovine and canine sources. Sci Rep 7:43797. https://doi.org/10.1038/srep43797
4. Li G, Du X, Zhou D, Li C, Huang L, Zheng Q, Cheng Z. 2018. Emergence of pathogenic and multiple-antibiotic-resistant *Macrococcus caseolyticus* in commercial broiler chickens. Transbound Emerg Dis 65:1605–1614. https://doi.org/10.1111/tbed.12912
5. Gobeli Brawand S, Cotting K, Gómez-Sanz E, Collaud A, Thomann A, Brodard I, Rodriguez-Campos S, Strauss C, Perreten V. 2017. *Macrococcus canis* sp. nov., a skin bacterium associated with infections in dogs. Int J Syst Evol Microbiol 67:621–626. https://doi.org/10.1099/ijsem.0.001673
6. Cotting K, Strauss C, Rodriguez-Campos S, Rostaher A, Fischer NM, Roosje PJ, Favrot C, Perreten V. 2017. *Macrococcus canis* and *M. caseolyticus* in dogs: occurrence, genetic diversity and antibiotic resistance. Vet Dermatol 28:559–e133. https://doi.org/10.1111/vde.12474
7. Mašlaňová I, Wertheimer Z, Sedláček I, Švec P, Indráková A, Kovařovic V, Schumann P, Spröer C, Králová S, Šedo O, Krištofová L, Vrbovská V, Füzik T, Petráš P, Zdráhal Z, Ružičková V, Doškař J, Pantůček R. 2018. Description and comparative genomics of *Macrococcus caseolyticus* subsp. *hominis* subsp. nov., *Macrococcus goetzii* sp. nov., *Macrococcus epidermidis* sp. nov., and *Macrococcus bohemicus* sp. nov., novel macrococci from human clinical material with virulence potential and suspected uptake of foreign DNA by natural transformation. Front Microbiol 9:1178. https://doi.org/10.3389/fmicb.2018.01178
8. Jost G, Schwendener S, Liassine N, Perreten V. 2021. Methicillin-resistant *Macrococcus canis* in a human wound. Infect Genet Evol 96:105125. https://doi.org/10.1016/j.meegid.2021.105125
9. Carroll LM, Pierneef R, Mafuna T, Magwedere K, Matle I. 2023. Genus-wide genomic characterization of *Macrococcus*: insights into evolution, population structure, and functional potential. Front Microbiol 14:1181376. https://doi.org/10.3389/fmicb.2023.1181376
10. MacFadyen AC, Fisher EA, Costa B, Cullen C, Paterson GK. 2018. Genome analysis of methicillin resistance in *Macrococcus caseolyticus* from dairy cattle in England and Wales. Microb Genom 4:000191. https://doi.org/10.1099/mgen.0.000191
11. Ramos GLPA, Vigoder HC, Nascimento JS. 2021. Technological applications of *Macrococcus caseolyticus* and its impact on food safety. Curr Microbiol 78:11–16. https://doi.org/10.1007/s00284-020-02281-z
12. Mazhar S, Hill C, McAuliffe O. 2018. The genus *Macrococcus*: an insight into its biology, evolution, and relationship with *Staphylococcus*. Adv Appl Microbiol 105:1–50. https://doi.org/10.1016/bs.aambs.2018.05.002
13. Schwendener S, Perreten V. 2021. Complete circular genome sequence of a *mecB*- and *mecD*-containing strain of *Macrococcus canis*. Microbiol Resour Announc 10:e00408-21. https://doi.org/10.1128/MRA.00408-21
14. Schwendener S, Keller JE, Overesch G, Perreten V. 2021. Novel SCCmec element containing the methicillin resistance gene *mecD* in *Macrococcus bohemicus*. J Glob Antimicrob Resist 24:360–362. https://doi.org/10.1016/j.jgar.2021.02.001
15. Schwendener S, Perreten V. 2022. The *bla* and *mec* families of β-lactam resistance genes in the genera *Macrococcus*, *Mammaliicoccus* and *Staphylococcus*: an in-depth analysis with emphasis on *Macrococcus*. J

Downloaded from https://journals.asm.org/journal/aem on 04 February 2026 by 147.251.86.90.

Antimicrob Chemother 77:1796–1827. https://doi.org/10.1093/jac/dkac107
16. Chanchaithong P, Perreten V, Schwendener S. 2019. *Macrococcus canis* contains recombinogenic methicillin resistance elements and the *mecB* plasmid found in *Staphylococcus aureus*. J Antimicrob Chemother 74:2531–2536. https://doi.org/10.1093/jac/dkz260
17. Baba T, Kuwahara-Arai K, Uchiyama I, Takeuchi F, Ito T, Hiramatsu K. 2009. Complete genome sequence of *Macrococcus caseolyticus* strain JCSCS5402, reflecting the ancestral genome of the human-pathogenic staphylococci. J Bacteriol 191:1180–1190. https://doi.org/10.1128/JB.01058-08
18. Tsubakishita S, Kuwahara-Arai K, Baba T, Hiramatsu K. 2010. Staphylococcal cassette chromosome mec-like element in *Macrococcus caseolyticus*. Antimicrob Agents Chemother 54:1469–1475. https://doi.org/10.1128/AAC.00575-09
19. Becker K, van Alen S, Idelevich EA, Schleimer N, Seggewiß J, Mellmann A, Kaspar U, Peters G. 2018. Plasmid-encoded transferable *mecB*-mediated methicillin resistance in *Staphylococcus aureus*. Emerg Infect Dis 24:242–248. https://doi.org/10.3201/eid2402.171074
20. Zhang Y, Min S, Sun Y, Ye J, Zhou Z, Li H. 2022. Characteristics of population structure, antimicrobial resistance, virulence factors, and morphology of methicillin-resistant *Macrococcus caseolyticus* in global clades. BMC Microbiol 22:266. https://doi.org/10.1186/s12866-022-02679-8
21. Keller JE, Schwendener S, Neuenschwander J, Overesch G, Perreten V. 2022. Prevalence and characterization of methicillin-resistant *Macrococcus* spp. in food producing animals and meat in Switzerland in 2019. Schweiz Arch Tierheilkd 164:153–164. https://doi.org/10.17236/sat00343
22. Keller JE, Schwendener S, Overesch G, Perreten V. 2022. *Macrococcus armenti* sp. nov., a novel bacterium isolated from the skin and nasal cavities of healthy pigs and calves. Int J Syst Evol Microbiol 72:005245. https://doi.org/10.1099/ijsem.0.005245
23. Keller JE, Schwendener S, Nováková D, Pantůček R, Perreten V. 2023. Letter to the editor: novel antimicrobial genetic elements in methicillin-resistant *Macrococcus armenti*. Microb Drug Resist 29:65–68. https://doi.org/10.1089/mdr.2022.0162
24. Kim M, Oh HS, Park SC, Chun J. 2014. Towards a taxonomic coherence between average nucleotide identity and 16S rRNA gene sequence similarity for species demarcation of prokaryotes. Int J Syst Evol Microbiol 64:346–351. https://doi.org/10.1099/ijs.0.059774-0
25. Madonna AJ, Basile F, Ferrer I, Meetani MA, Rees JC, Voorhees KJ. 2000. On-probe sample pretreatment for the detection of proteins above 15 KDa from whole cell bacteria by matrix-assisted laser desorption/ionization time-of-flight mass spectrometry. Rapid Commun Mass Spectrom 14:2220–2229. https://doi.org/10.1002/1097-0231(20001215)14:23<2220::AID-RCM155>3.0.CO;2-4
26. Thomas PD, Ebert D, Muruganujan A, Mushayahama T, Albou LP, Mi H. 2022. PANTHER: making genome-scale phylogenetics accessible to all. Protein Sci 31:8–22. https://doi.org/10.1002/pro.4218
27. Beckering CL, Steil L, Weber MHW, Völker U, Marahiel MA. 2002. Genomewide transcriptional analysis of the cold shock response in *Bacillus subtilis*. J Bacteriol 184:6395–6402. https://doi.org/10.1128/JB.184.22.6395-6402.2002
28. Kahánková J, Pantůček R, Goerke C, Růžičková V, Holochová P, Doškař J. 2010. Multilocus PCR typing strategy for differentiation of *Staphylococcus aureus* siphoviruses reflecting their modular genome structure. Environ Microbiol 12:2527–2538. https://doi.org/10.1111/j.1462-2920.2010.02226.x
29. Penadés JR, Christie GE. 2015. The phage-inducible chromosomal islands: a family of highly evolved molecular parasites. Annu Rev Virol 2:181–201. https://doi.org/10.1146/annurev-virology-031413-085446
30. Wipf JRK, Schwendener S, Nielsen JB, Westh H, Perreten V. 2015. The new macrolide-lincosamide-streptogramin B resistance gene *erm*(45) is located within a genomic island in *Staphylococcus fleurettii*. Antimicrob Agents Chemother 59:3578–3581. https://doi.org/10.1128/AAC.00369-15
31. Tangney M, Fitzgerald GF. 2002. Effectiveness of the lactococcal abortive infection systems AbiA, AbiE, AbiF and AbiG against P335 type phages. FEMS Microbiol Lett 210:67–72. https://doi.org/10.1111/j.1574-6968.2002.tb11161.x
32. Gómez-Sanz E, Schwendener S, Thomann A, Gobeli Brawand S, Perreten V. 2015. First staphylococcal cassette chromosome mec containing a *mecB*-carrying gene complex independent of transposon Tn6045 in a *Macrococcus canis* isolate from a canine infection. Antimicrob Agents Chemother 59:4577–4583. https://doi.org/10.1128/AAC.05064-14
33. Shintani M, Sanchez ZK, Kimbara K. 2015. Genomics of microbial plasmids: classification and identification based on replication and transfer systems and host taxonomy. Front Microbiol 6:242. https://doi.org/10.3389/fmicb.2015.00242
34. Goessweiner-Mohr N, Arends K, Keller W, Grohmann E. 2013. Conjugative type IV secretion systems in Gram-positive bacteria. Plasmid 70:289–302. https://doi.org/10.1016/j.plasmid.2013.09.005
35. Neyfakh AA, Borsch CM, Kaatz GW. 1993. Fluoroquinolone resistance protein NorA of *Staphylococcus aureus* is a multidrug efflux transporter. Antimicrob Agents Chemother 37:128–129. https://doi.org/10.1128/AAC.37.1.128
36. Bello S, Mudassir SH, Rudra B, Gupta RS. 2023. Phylogenomic and molecular markers based studies on *Staphylococcaceae* and *Gemella* species. Proposals for an emended family *Staphylococcaceae* and three new families (*Abyssicoccaceae* fam. nov., *Salinicoccaceae* fam. nov. and *Gemellaceae* fam. nov.) harboring four new genera, *Lacicoccus* gen. nov., *Macrococcoides* gen. nov., *Gemelliphila* gen. nov., and *Phocicoccus* gen. nov. Antonie Van Leeuwenhoek 116:937–973. https://doi.org/10.1007/s10482-023-01857-6
37. Li X, Wang H, Guo C, Wang L. 2024. Profiling of microbial populations present in ground beef and plant-based meat analogues. LWT 196:115845. https://doi.org/10.1016/j.lwt.2024.115845
38. Almada L, Guibert EE, Rodriguez JV. 2002. A simple GC method for determination of cryoprotector diols 1,4-butanediol or 2,3-butanediol in isolated rat hepatocytes. Cryo Letters 23:113–120. https://www.ingentaconnect.com/content/cryo/cryo/2002/00000023/00000002/art00006.
39. Xiao Z, Xu P. 2007. Acetoin metabolism in bacteria. Crit Rev Microbiol 33:127–140. https://doi.org/10.1080/10408410701364604
40. Lu P, Bai R, Gao T, Chen J, Jiang K, Zhu Y, Lu Y, Zhang S, Xu F, Zhao H. 2024. Systemic metabolic engineering of *Enterobacter aerogenes* for efficient 2,3-butanediol production. Appl Microbiol Biotechnol 108:146. https://doi.org/10.1007/s00253-023-12911-8
41. Ermolenko DN, Makhatadze GI. 2002. Bacterial cold-shock proteins. Cell Mol Life Sci 59:1902–1913. https://doi.org/10.1007/pl00012513
42. Zhou Z, Tang H, Wang W, Zhang L, Su F, Wu Y, Bai L, Li S, Sun Y, Tao F, Xu P. 2021. A cold shock protein promotes high-temperature microbial growth through binding to diverse RNA species. Cell Discov 7:15. https://doi.org/10.1038/s41421-021-00246-5
43. Freese E, Sass H, Rütters H, Schledjewski R, Rullkötter J. 2008. Variable temperature-related changes in fatty acid composition of bacterial isolates from German Wadden sea sediments representing different bacterial phyla. Org Geochem 39:1427–1438. https://doi.org/10.1016/j.orggeochem.2008.06.005
44. Suutari M, Laakso S. 1994. Microbial fatty acids and thermal adaptation. Crit Rev Microbiol 20:285–328. https://doi.org/10.3109/10408419409113560
45. Pelicic V. 2023. Mechanism of assembly of type 4 filaments: everything you always wanted to know (but were afraid to ask). Microbiology (Reading) 169:001311. https://doi.org/10.1099/mic.0.001311
46. Chung YS, Dubnau D. 1998. All seven *comG* open reading frames are required for DNA binding during transformation of competent *Bacillus subtilis*. J Bacteriol 180:41–45. https://doi.org/10.1128/JB.180.1.41-45.1998
47. Brooks MR, Padilla-Vélez L, Khan TA, Qureshi AA, Pieper JB, Maddox CW, Alam MT. 2020. Prophage-mediated disruption of genetic competence in *Staphylococcus pseudintermedius*. mSystems 5:e00684-19. https://doi.org/10.1128/mSystems.00684-19
48. Mingoia M, Morici E, Tili E, Giovanetti E, Montanari MP, Varaldo PE. 2013. Characterization of Tn5801.Sag, a variant of *Staphylococcus aureus* Tn916 family transposon Tn5801 that is widespread in clinical isolates of *Streptococcus agalactiae*. Antimicrob Agents Chemother 57:4570–4574. https://doi.org/10.1128/AAC.00521-13
49. Song L, Pan Y, Chen S, Zhang X. 2012. Structural characteristics of genomic islands associated with GMP synthases as integration hotspot among sequenced microbial genomes. Comput Biol Chem 36:62–70. https://doi.org/10.1016/j.compbiolchem.2012.01.001
50. Novick RP, Christie GE, Penadés JR. 2010. The phage-related chromosomal islands of Gram-positive bacteria. Nat Rev Microbiol 8:541–551. https://doi.org/10.1038/nrmicro2393
51. Chan LC, Basuino L, Diep B, Hamilton S, Chatterjee SS, Chambers HF. 2015. Ceftobiprole- and ceftaroline-resistant methicillin-resistant

Downloaded from https://journals.asm.org/journal/aem on 04 February 2026 by 147.251.86.90.

Staphylococcus aureus. Antimicrob Agents Chemother 59:2960–2963. https://doi.org/10.1128/AAC.05004-14
52. Sengupta M, Austin S. 2011. Prevalence and significance of plasmid maintenance functions in the virulence plasmids of pathogenic bacteria. Infect Immun 79:2502–2509. https://doi.org/10.1128/IAI.00127-11
53. Dib JR, Wagenknecht M, FarÃas ME, Meinhardt F. 2015. Strategies and approaches in plasmidome studies-uncovering plasmid diversity disregarding of linear elements? Front Microbiol 6:463. https://doi.org/10.3389/fmicb.2015.00463
54. Neyaz L, Karki AB, Fakhr MK. 2020. Draft genome sequence of megaplasmid-bearing *Staphylococcus sciuri* strain B9-58B, isolated from retail pork. Microbiol Resour Announc 9:e01474-19. https://doi.org/10.1128/MRA.01474-19
55. Lysnyansky I, Calcutt MJ, Ben-Barak I, Ron Y, Levisohn S, Methé BA, Yogev D. 2009. Molecular characterization of newly identified IS3, IS4 and IS30 insertion sequence-like elements in *Mycoplasma bovis* and their possible roles in genome plasticity. FEMS Microbiol Lett 294:172–182. https://doi.org/10.1111/j.1574-6968.2009.01562.x
56. Boer DR, Ruiz-Masó JA, Rueda M, Petoukhov MV, Machón C, Svergun DI, Orozco M, del Solar G, Coll M. 2016. Conformational plasticity of RepB, the replication initiator protein of promiscuous streptococcal plasmid pMV158. Sci Rep 6:20915. https://doi.org/10.1038/srep20915
57. Pantůček R, Švec P, Dajcs JJ, Machová I, Černohlávková J, Šedo O, Gelbíčová T, Mašlaňová I, Doškař J, Zdráhal Z, Růžičková V, Sedláček I. 2013. *Staphylococcus petrasii* sp. nov. including *S. petrasii* subsp. *petrasii* subsp. nov. and *S. petrasii* subsp. *croceilyticus* subsp. nov., isolated from human clinical specimens and human ear infections. Syst Appl Microbiol 36:90–95. https://doi.org/10.1016/j.syapm.2012.11.004
58. Kovařovic V, Sedláček I, Petráš P, Králová S, Mašlaňová I, Švec P, Neumann-Schaal M, Botka T, Gelbíčová T, Staňková E, Doškař J, Pantůček R. 2022. *Staphylococcus ratti* sp. nov. isolated from a lab rat. Pathogens 11:51. https://doi.org/10.3390/pathogens11010051
59. EUCAST. 2024. Breakpoint tables for interpretation of MICs and zone diameters, version 14.0. The European Committee on Antimicrobial Susceptibility Testing. Available from: http://www.eucast.org
60. Kovařovic V, Finstrlová A, Sedláček I, Petráš P, Švec P, Mašlaňová I, Neumann-Schaal M, Šedo O, Botka T, Staňková E, Doškař J, Pantůček R. 2023. *Staphylococcus brunensis* sp. nov. isolated from human clinical specimens with a staphylococcal cassette chromosome-related genomic island outside of the *rlmH* gene bearing the *ccrDE* recombinase gene complex. Microbiol Spectr 11:e0134223. https://doi.org/10.1128/spectrum.01342-23
61. Freiwald A, Sauer S. 2009. Phylogenetic classification and identification of bacteria by mass spectrometry. Nat Protoc 4:732–742. https://doi.org/10.1038/nprot.2009.37
62. Švec P, Pantůček R, Petráš P, Sedláček I, Nováková D. 2010. Identification of *Staphylococcus* spp. using $(GTG)_5$-PCR fingerprinting. Syst Appl Microbiol 33:451–456. https://doi.org/10.1016/j.syapm.2010.09.004
63. Sasser M. 1990. Identification of bacteria by gas chromatography of cellular fatty acids, MIDI technical note 101, Revision July 2006 ed. MIDI Inc., Newark, DE. Available from: http://midi-inc.com/pdf/MIS_Technote_101.pdf
64. Vieira S, Huber KJ, Neumann-Schaal M, Geppert A, Luckner M, Wanner G, Overmann J. 2021. *Usitatibacter rugosus* gen. nov., sp. nov. and *Usitatibacter palustris* sp. nov., novel members of *Usitatibacteraceae* fam. nov. within the order *Nitrosomonadales* isolated from soil. Int J Syst Evol Microbiol 71:004631. https://doi.org/10.1099/ijsem.0.004631
65. Moss CW, Lambert-Fair MA. 1989. Location of double bonds in monounsaturated fatty acids of *Campylobacter cryaerophila* with dimethyl disulfide derivatives and combined gas chromatography-mass spectrometry. J Clin Microbiol 27:1467–1470. https://doi.org/10.1128/jcm.27.7.1467-1470.1989
66. Schumann P. 2011. Peptidoglycan structure. Methods Microbiol 38:101–129. https://doi.org/10.1016/B978-0-12-387730-7.00005-X
67. Schumann P, Kalensee F, Cao J, Criscuolo A, Clermont D, Köhler JM, Meier-Kolthoff JP, Neumann-Schaal M, Tindall BJ, Pukall R. 2021. Reclassification of Haloactinobacterium glacieicola as Occultella glacieicola gen. nov., comb. nov., of Haloactinobacterium album as Ruania alba comb. nov, with an emended description of the genus Ruania, recognition that the genus names Haloactinobacterium and Ruania are heterotypic synonyms and description of Occultella aeris sp. nov., a halotolerant isolate from surface soil sampled at an ancient copper smelter. Int J Syst Evol Microbiol 71:004769. https://doi.org/10.1099/ijsem.0.004769
68. Kämpfer P, McInroy JA, Clermont D, Neumann-Schaal M, Criscuolo A, Busse H-J, Glaeser SP. 2021. *Leucobacter soli* sp. nov., from soil amended with humic acid. Int J Syst Evol Microbiol 71:005156. https://doi.org/10.1099/ijsem.0.005156
69. Chlebowicz MA, Mašlaňová I, Kuntová L, Grundmann H, Pantůček R, Doškař J, van Dijl JM, Buist G. 2014. The staphylococcal cassette chromosome mec type V from *Staphylococcus aureus* ST398 is packaged into bacteriophage capsids. Int J Med Microbiol 304:764–774. https://doi.org/10.1016/j.ijmm.2014.05.010
70. Forbes BA, Schaberg DR. 1983. Transfer of resistance plasmids from *Staphylococcus epidermidis* to *Staphylococcus aureus*: evidence for conjugative exchange of resistance. J Bacteriol 153:627–634. https://doi.org/10.1128/jb.153.2.627-634.1983
71. Fišarová L, Botka T, Du X, Mašlaňová I, Bárdy P, Pantůček R, Benešík M, Roudnický P, Winstel V, Larsen J, Rosenstein R, Peschel A, Doškař J. 2021. *Staphylococcus epidermidis* phages transduce antimicrobial resistance plasmids and mobilize chromosomal islands. mSphere 6:e00223-21. https://doi.org/10.1128/mSphere.00223-21
72. Wingett SW, Andrews S. 2018. FastQ Screen: a tool for multi-genome mapping and quality control. F1000Res 7:1338. https://doi.org/10.12688/f1000research.15931.2
73. Wick RR, Judd LM, Cerdeira LT, Hawkey J, Méric G, Vezina B, Wyres KL, Holt KE. 2021. Trycycler: consensus long-read assemblies for bacterial genomes. Genome Biol 22:266. https://doi.org/10.1186/s13059-021-02483-z
74. Wick R.R, Holt KE. 2022. Polypolish: short-read polishing of long-read bacterial genome assemblies. PLoS Comput Biol 18:e1009802. https://doi.org/10.1371/journal.pcbi.1009802
75. Li H. 2018. Minimap2: pairwise alignment for nucleotide sequences. Bioinformatics 34:3094–3100. https://doi.org/10.1093/bioinformatics/bty191
76. Langmead B, Salzberg SL. 2012. Fast gapped-read alignment with Bowtie 2. Nat Methods 9:357–359. https://doi.org/10.1038/nmeth.1923
77. Pantůček R, Sedláček I, Petráš P, Koukalová D, Švec P, Štětina V, Vancanneyt M, Chrastinová L, Vokurková J, Růžičková V, Doškař J, Swings J, Hájek V. 2005. *Staphylococcus simiae* sp. nov., isolated from South American squirrel monkeys. Int J Syst Evol Microbiol 55:1953–1958. https://doi.org/10.1099/ijs.0.63590-0
78. Yoon SH, Ha SM, Kwon S, Lim J, Kim Y, Seo H, Chun J. 2017. Introducing EzBioCloud: a taxonomically united database of 16S rRNA gene sequences and whole-genome assemblies. Int J Syst Evol Microbiol 67:1613–1617. https://doi.org/10.1099/ijsem.0.001755
79. Tamura K, Stecher G, Kumar S. 2021. MEGA11: molecular evolutionary genetics analysis version 11. Mol Biol Evol 38:3022–3027. https://doi.org/10.1093/molbev/msab120
80. Felsenstein J. 1985. Confidence limits on phylogenies: an approach using the bootstrap. Evolution 39:783–791. https://doi.org/10.1111/j.1558-5646.1985.tb00420.x
81. Na SI, Kim YO, Yoon SH, Ha SM, Baek I, Chun J. 2018. UBCG: up-to-date bacterial core gene set and pipeline for phylogenomic tree reconstruction. J Microbiol 56:280–285. https://doi.org/10.1007/s12275-018-8014-6
82. Meier-Kolthoff JP, Carbasse JS, Peinado-Olarte RL, Göker M. 2022. TYGS and LPSN: a database tandem for fast and reliable genome-based classification and nomenclature of prokaryotes. Nucleic Acids Res 50:D801–D807. https://doi.org/10.1093/nar/gkab902
83. Jain C, Rodriguez-R LM, Phillippy AM, Konstantinidis KT, Aluru S. 2018. High throughput ANI analysis of 90K prokaryotic genomes reveals clear species boundaries. Nat Commun 9:5114. https://doi.org/10.1038/s41467-018-07641-9
84. Li W, O'Neill KR, Haft DH, DiCuccio M, Chetvernin V, Badretdin A, Coulouris G, Chitsaz F, Derbyshire MK, Durkin AS, Gonzales NR, Gwadz M, Lanczycki CJ, Song JS, Thanki N, Wang J, Yamashita RA, Yang M, Zheng C, Marchler-Bauer A, Thibaud-Nissen F. 2021. RefSeq: expanding the prokaryotic genome annotation pipeline reach with protein family model curation. Nucleic Acids Res 49:D1020–D1028. https://doi.org/10.1093/nar/gkaa1105
85. Arndt D, Grant JR, Marcu A, Sajed T, Pon A, Liang Y, Wishart DS. 2016. PHASTER: a better, faster version of the PHAST phage search tool. Nucleic Acids Res 44:W16–W21. https://doi.org/10.1093/nar/gkw387
86. Edwards R, Decewicz P, Katelyn D, Laurasisk S. 2022. linsalrob/PhiSpy: dropped prophages (v.4.2.21). Zenodo 2022:5945762. Available from: https://doi.org/10.5281/zenodo.3475716
87. Bertelli C, Laird MR, Williams KP, Lau BY, Hoad G, Winsor GL, Brinkman FS, Simon Fraser University Research Computing Group. 2017.

Downloaded from https://journals.asm.org/journal/aem on 04 February 2026 by 147.251.86.90.

IslandViewer 4: expanded prediction of genomic islands for larger-scale datasets. Nucleic Acids Res 45:W30–W35. https://doi.org/10.1093/nar/gkx343
88. Wang M, Goh YX, Tai C, Wang H, Deng Z, Ou HY. 2022. VRprofile2: detection of antibiotic resistance-associated mobilome in bacterial pathogens. Nucleic Acids Res 50:W768–W773. https://doi.org/10.1093/nar/gkac321
89. Siguier P, Perochon J, Lestrade L, Mahillon J, Chandler M. 2006. ISfinder: the reference centre for bacterial insertion sequences. Nucleic Acids Res 34:D32–D36. https://doi.org/10.1093/nar/gkj014
90. Jia B, Raphenya AR, Alcock B, Waglechner N, Guo P, Tsang KK, Lago BA, Dave BM, Pereira S, Sharma AN, Doshi S, Courtot M, Lo R, Williams LE, Frye JG, Elsayegh T, Sardar D, Westman EL, Pawlowski AC, Johnson TA, Brinkman FSL, Wright GD, McArthur AG. 2017. CARD 2017: expansion and model-centric curation of the comprehensive antibiotic resistance database. Nucleic Acids Res 45:D566–D573. https://doi.org/10.1093/nar/gkw1004
91. Bortolaia V, Kaas RS, Ruppe E, Roberts MC, Schwarz S, Cattoir V, Philippon A, Allesoe RL, Rebelo AR, Florensa AF, et al. 2020. ResFinder 4.0 for predictions of phenotypes from genotypes. J Antimicrob Chemother 75:3491–3500. https://doi.org/10.1093/jac/dkaa345
92. Liu B, Zheng D, Zhou S, Chen L, Yang J. 2022. VFDB 2022: a general classification scheme for bacterial virulence factors. Nucleic Acids Res 50:D912–D917. https://doi.org/10.1093/nar/gkab1107
93. Sun J, Lu F, Luo Y, Bie L, Xu L, Wang Y. 2023. OrthoVenn3: an integrated platform for exploring and visualizing orthologous data across genomes. Nucleic Acids Res 51:W397–W403. https://doi.org/10.1093/nar/gkad313
94. Sullivan MJ, Petty NK, Beatson SA. 2011. Easyfig: a genome comparison visualizer. Bioinformatics 27:1009–1010. https://doi.org/10.1093/bioinformatics/btr039

Downloaded from https://journals.asm.org/journal/aem on 04 February 2026 by 147.251.86.90.

APPENDIX 9

Obořilová R, Kučerová E, Botka T, Vaisocherová-Lísalová H, Skládal P, Farka Z (2025) Piezoelectric biosensor with dissipation monitoring enables the analysis of bacterial lytic agent activity. *Scientific Reports* 15:3419. https://doi.org/10.1038/s41598-024-85064-x
(JCR 2025: IF = 4.9; Q1 – Multidisciplinary Sciences)

CC BY 4.0

scientific reports

Check for updates

OPEN

Piezoelectric biosensor with dissipation monitoring enables the analysis of bacterial lytic agent activity

Radka Obořilová[1,2]✉, Eliška Kučerová[3], Tibor Botka[3], Hana Vaisocherová-Lísalová[4], Petr Skládal[1] & Zdeněk Farka[1,2]✉

Antibiotic-resistant strains of *Staphylococcus aureus* pose a significant threat in healthcare, demanding urgent therapeutic solutions. Combining bacteriophages with conventional antibiotics, an innovative approach termed phage-antibiotic synergy, presents a promising treatment avenue. However, to enable new treatment strategies, there is a pressing need for methods to assess their efficacy reliably and rapidly. Here, we introduce a novel approach for real-time monitoring of pathogen lysis dynamics employing the piezoelectric quartz crystal microbalance (QCM) with dissipation (QCM-D) technique. The sensor, a QCM chip modified with the bacterium *S. aureus* RN4220 Δ*tarM*, was utilized to monitor the activity of the enzyme lysostaphin and the phage P68 as model lytic agents. Unlike conventional QCM solely measuring resonance frequency changes, our study demonstrates that dissipation monitoring enables differentiation of bacterial growth and lysis caused by cell-attached lytic agents. Compared to reference turbidimetry measurements, our results reveal distinct alterations in the growth curve of the bacteria adhered to the sensor, characterized by a delayed lag phase. Furthermore, the dissipation signal analysis facilitated the precise real-time monitoring of phage-mediated lysis. Finally, the QCM-D biosensor was employed to evaluate the synergistic effect of subinhibitory concentrations of the antibiotic amoxicillin with the bacteriophage P68, enabling monitoring of the lysis of P68-resistant wild-type strain *S. aureus* RN4220. Our findings suggest that this synergy also impedes the formation of bacterial aggregates, the precursors of biofilm formation. Overall, this method brings new insights into phage-antibiotic synergy, underpinning it as a promising strategy against antibiotic-resistant bacterial strains with broad implications for treatment and prevention.

Keywords Piezoelectric biosensor, Antimicrobial treatment, Phage therapy, Phage-antibiotic synergy, Multidrug-resistant bacteria, *Staphylococcus aureus*

Staphylococcus aureus stands out as a leading cause of life-threatening complications, particularly within healthcare facilities, often culminating in severe, and sometimes even fatal, outcomes[1]. The escalating threat posed by antibiotic-resistant bacteria highlights the importance of exploring new treatment strategies and diagnostic methods. Bacteriophages, commonly referred to as phages, represent a promising alternative to antibiotics in the global fight against antibiotic resistance[2]. Clinical applications of tailored phage therapies have demonstrated efficacy in infection treatment, reducing severe complications, such as amputations or even mortality[3].

Recent studies have demonstrated that combining phages with subinhibitory antibiotic concentrations can yield superior outcomes compared to individual therapies, a phenomenon termed phage-antibiotic synergy (PAS)[4,5]. This synergy may result from bacterial defense mechanism inefficacy against two different agents or accelerated bacterial population eradication due to the increased phage progeny[6–8].

[1]Department of Biochemistry, Faculty of Science, Masaryk University, Kamenice 5, 625 00 Brno, Czech Republic. [2]Central European Institute of Technology, Masaryk University, Kamenice 5, 625 00 Brno, Czech Republic. [3]Department of Experimental Biology, Section of Genetics and Molecular Biology, Faculty of Science, Masaryk University, Kamenice 5, 625 00 Brno, Czech Republic. [4]FZU – Institute of Physics of the Czech Academy of Sciences, Na Slovance 1999/2, 182 00 Prague, Czech Republic. ✉email: radka.oborilova@ceitec.muni.cz; farka@mail.muni.cz

Phages, ubiquitously present in various environments, including the human body, interact with and regulate bacterial populations[9]. Particularly, lytic phages are preferred for therapy due to their rapid adaptability, which is crucial for personalized treatments in antibiotic-resistant cases[10]. However, some phages can facilitate horizontal gene transfer through transduction or lysogeny, potentially fostering the emergence of pathogenic strains[11,12]. In addition, the historical oversight of phage therapy caused by the widespread success of antibiotics has led to a lack of relevant studies and regulatory frameworks regarding its clinical applications[13]. Initial research indicated the relative safety of phage therapy; however, further studies are needed[14,15], making a demand for the development of safe, rapid, and reliable methods of phage testing to underpin their biomedical applications.

Conventional methods of bacterial lysis monitoring rely on microbiological cultivation or techniques assessing changes in cell integrity, such as microscopy and flow cytometry[16]. However, these methods have numerous limitations, including only indirect lysis evidence (e.g., culture turbidity), lack of the ability to determine lytic agent concentration over time, low throughput and sensitivity, and laborious sample preparation via staining that can compromise cell viability[17]. Moreover, some methods, like turbidimetry, are only effective for continuous measurement in planktonic cultures and not in biofilms, commonly encountered in healthcare settings[18]. Thus, advanced instrumental methods are required for accurate elucidation of phage interactions with bacterial populations on biologically relevant surfaces or tissues.

Staphylococcal biofilms are complex microbial communities embedded in a self-produced extracellular matrix[19]. Their occurrence is usually associated with enhanced pathogenicity and resistance to various antimicrobials. The extracellular matrix comprises extracellular DNA (eDNA), polysaccharides, and proteins originating from dead cells. The ratio of these components and the conditions for the biofilm formation are strain-dependent. Biofilm formation is usually triggered in stressful environments, e.g., cold temperatures, high salt concentrations, or the presence of antibiotics[20]. Several phases of biofilm development can be distinguished: initial attachment, multiplication of the bacterial cells, clearance of eDNA, maturation of the biofilm, and finally, its dispersal with the colonization of new niches[21]. Common culture-based methods for biofilm characterization include crystal violet staining of the biofilm biomass and streaking of culture on the specialized agar plates with Congo red dye. Both methods are laborious, and their results are only semiquantitative[22].

Biosensors, especially those from a label-free family, offer a solution to overcome the drawbacks of the conventional methods. They allow direct monitoring of bacterial behavior on the sensor surface over time with high sensitivity, facilitate controlled addition of lytic agents or removal of metabolites for further assessment, and enable straightforward quantitative evaluation and automation of bacterial lysis monitoring. Sensitive label-free techniques based on optical surface plasmon resonance (SPR)[23] and piezoelectric quartz crystal microbalance (QCM)[24] designed for monitoring biochemical events at the sensor surface show great promise. However, these approaches are commonly used for bacteria detection[25,26] or to study bacterial interactions[27,28] and only rarely focus on real-time monitoring of bacterial growth[29,30]. In our previous work, we demonstrated the potential of SPR for real-time monitoring of phage-mediated lysis of bacteria on a chip[23]. However, as far as we know, there are no reports on real-time monitoring of bacterial lysis using QCM.

The QCM method, first described in air by Sauerbrey[31], determines the mass changes on the surface of the quartz crystal by monitoring its resonance frequency shift. Recently adapted for liquid environments, QCM holds significant potential in life sciences, particularly with quartz crystal microbalance with dissipation monitoring (QCM-D), which also assesses surface viscoelastic changes[32]. These effects can relate to bacterial cell adhesion[33], growth, and biofilm formation, as well as to bacterial lysis. QCM was also demonstrated to enable monitoring of the biofilm formation[34,35] and studying lytic agent effects on artificially constructed biological membranes, simulating cell surfaces[36].

The aim of the present study was to advance QCM-D to enable real-time and precise monitoring of bacterial lysis in the presence of a complex lytic system, mimicking PAS therapy mechanisms on a chip. To achieve this, we have developed a novel QCM-D methodology using two complex biological systems involving the lysis of *S. aureus* by the enzyme lysostaphin and the phage P68[37]. The approach was based on monitoring changes in resonance frequency and dissipation upon the addition or removal of even a minimal mass caused by the disruption of bacterial integrity and subsequent lysis. Figure 1 illustrates the course of the experiments on the QCM sensor surface, where bacteria were immobilized on a poly-L-lysine (PLL) layer, and the lysis was induced by the enzyme lysostaphin or phage P68. Lysostaphin is an endopeptidase isolated from *Staphylococcus simulans*. In most staphylococcal species, it causes lysis by cleaving the pentaglycine bridges of peptidoglycan[38–40]. Due to its highly specific interaction and precise mechanism of action[41], lysostaphin can induce rapid lysis of both bacterial cells and biofilms[42]. Phage P68 is a well-characterized podovirus of the *Rountreeviridae* family, known for its short tail and high lytic activity[43,44]. The achieved results demonstrated that studying bacterial lysis on a sensor surface using dissipation monitoring may unveil differences in the formation and eradication of resistant biofilms. Furthermore, the implemented flow system allowed monitoring of metabolites released during the complex bacterium-phage interaction, along with the supply of fresh culture medium. Finally, we employed the developed approach to evaluate the synergistic effect of subinhibitory concentrations of the antibiotic amoxicillin (AMO) and phage P68, enabling the monitoring of lysis in the P68-insensitive *S. aureus* strain.

Materials and methods

Chemicals, buffers, and cultivation media

Acetone and isopropanol were purchased from Penta (Czech Republic). Poly-L-lysine (PLL), cysteamine hydrochloride, glutaraldehyde, antibiotic amoxicillin (AMO), and lysostaphin (specific activity ≥ 3990 U/mg) were obtained from Sigma-Aldrich (USA). Growth media were obtained from Oxoid (UK). All other common chemicals were obtained from Sigma-Aldrich (USA), Carl Roth (Germany), or Penta (Czech Republic). Unpolished and polished quartz crystals (resonance frequency of 10 MHz) were purchased from Krystaly,

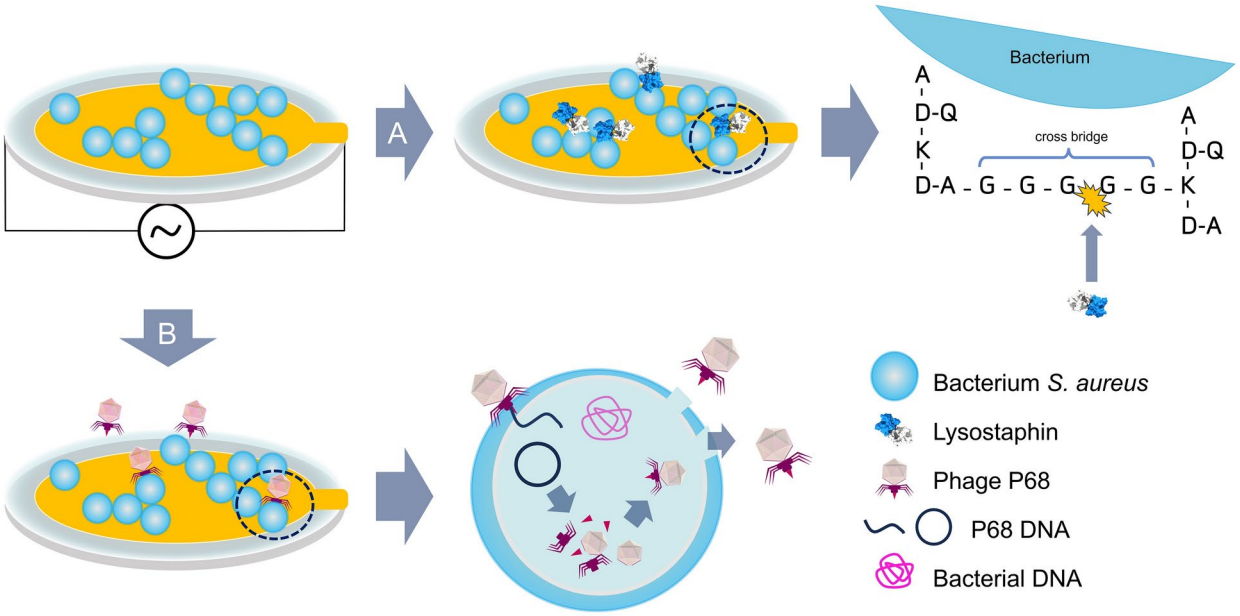

Fig. 1. Schematic representation of the course of the experiment on the surface of the QCM-D sensor. (**A**) Monitoring of bacterial lysis by lysostaphin with the detail of the cleavage of the pentaglycine bridge of bacterial peptidoglycan (A – L-alanine, D-Q – D-glutamine, K – L-lysine, D-A – D-alanine, G – L-glycine). (**B**) Phage-mediated lysis on the sensor with the detail of the lytic cycle of the phage in the bacterium.

Hradec Králové (Czech Republic). LIVE/DEAD *Bac*Light Bacterial Viability Kit was purchased from Invitrogen (USA).

The used buffers and cultivation media included Tris-buffered saline (TBS; 50 mM Tris, 150 mM NaCl, pH 7.5), phosphate-buffered saline (PBS; 50 mM NaH_2PO_4/Na_2HPO_4, 150 mM NaCl, pH 7.4), phage buffer (50 mM Tris, 10 mM NaCl, 10 mM $CaCl_2$, pH 8.0), and tryptone soya broth (TSB; CM0129, 0.9 g of TSB dissolved in distilled water to 30 mL, pH 7.4).

Cultivation of *S. aureus*

Four *S. aureus* strains were employed in this study, including two laboratory strains (RN4220 and RN4220 Δ*tarM*) and two clinical strains (13/791 and 10/234). Laboratory bacterial strains *S. aureus* RN4220[45] and *S. aureus* RN4220 Δ*tarM*[46] were obtained from Prof. A. Peschel (University of Tübingen, Germany). The deletion of the gene encoding glycosyltransferase TarM, which ensures a precise glycosylation profile of teichoic acid in the bacterial cell wall, makes the RN4220 Δ*tarM* strain highly sensitive to phages from the former *Podoviridae* family, specifically the phage P68 used in this work[46,47]. This phage-bacterium combination results in a very efficient lysis, thus serving as a suitable model. Clinical exfoliative toxin-producing strains *S. aureus* 13/791[48] and *S. aureus* 10/234[49] isolated from child blisters were obtained from Dr. P. Petráš (National Institute of Public Health, Czech Republic).

The RN4220 Δ*tarM* strain was selected for the optimization of QCM measurements due to its sensitivity to phage P68, whereas the RN4220 strain served as a control. The following strains were chosen for PAS turbidimetry measurement: RN4220 Δ*tarM* – sensitive to the phage and AMO, RN4220 – insensitive to the phage, sensitive to AMO, 13/791 – sensitive to the phage, resistant to AMO, and 10/234 – resistant to the phage and AMO. Subsequently, the combination of strain RN4220 and phage P68 with AMO was selected for QCM measurement of PAS because of the most pronounced synergistic effect. AMO was selected based on disc diffusion assays with different antibiotics on *S. aureus* strain RN4220 Δ*tarM*, where phage P68 showed enlarged plaques in the presence of AMO (Figure S1A). In addition, phage P68 gained the ability to propagate on strain RN4220 in the presence of AMO (Figure S1B,C). Thus, the chosen phage-antibiotic combination served as a suitable model with unambiguous data interpretation.

The bacteria were grown overnight in TSB medium at 37 °C without agitation to an optical density at 600 nm (OD_{600}) of ~ 1.8. The cells were centrifuged at 4,600 g for 10 min and resuspended in TBS buffer for efficient immobilization on the sensor surface. The viability of bacteria on the sensor surface after the immobilization was evaluated using fluorescence microscopy. The number of bacteria on the sensor was estimated to be ~ 2.5×10^7 cells, corresponding to approximately 10^8 colony-forming units (CFU) per mL in a measuring cell with a total volume of ~ 100 µL.

Preparation of phage P68

The phage P68[37] (GenBank acc. no. NC_004679.1) was purchased from Félix d'Hérelle Reference Center for Bacterial Viruses (Université Laval, Canada). The propagating strain *S. aureus* RN4220 Δ*tarM* was freshly grown in TSB to OD_{600} of 0.4. Afterward, the lysate containing phage P68 was added to achieve the input ratio (phage-

to-bacteria ratio; IR or MOI_{INPUT}) of ~ 10 and allowed to propagate at 37 °C with mild shaking until the bacterial lysis occurred. The resulting bacterial lysate was filtered through a 0.45-µm polyethersulfone syringe filter (TPP, Switzerland), and the sterile lysate was stored at 4 °C for further processing.

The phage was purified by centrifugation at 64,000 g for 2.5 h at 4 °C (Avanti J-30I with JA-30.50 Ti rotor, Beckman Coulter, USA). The pellet was resuspended in 300 µL of phage buffer overnight at 4 °C. The residual dissolved proteins were removed by extraction with chloroform (1:1 of total sample volume). The viral particles were purified by ultracentrifugation in the CsCl gradient, as described previously[43]. The viable virus particles were quantified by double agar layer plaque assay as plaque-forming units (PFU) per mL.

Bacterial lysis monitored by turbidimetry

The lysis experiments in solution were performed in non-binding 96-well polystyrene microtiter plates (Greiner, Austria), utilizing the UPCON S-Pro reader (Labrox, Finland). The lysis was evaluated turbidimetrically as the decrease of OD_{600} using strains *S. aureus* RN4220 and *S. aureus* RN4220 Δ*tarM*. The bacterial culture was diluted in a TSB medium, and varying amounts of lysis agents (either lysostaphin or phage P68 in TSB) were added, always in a volume ratio of 1:4. The lysis was monitored for 10 h at 37 °C. The lysostaphin-mediated lysis was tested using the resulting concentrations of 0, 1, 10, and 100 µg/mL, with *S. aureus* diluted to OD_{600} of ~ 0.9 (2×10^8 CFU/mL) using a TSB medium. In the case of phage-mediated lysis, the MOI_{INPUT} levels of 0, 0.01, 0.1, and 1 were tested.

In the study of PAS, two laboratory *S. aureus* strains (RN4220 and RN4220 Δ*tarM*) and two clinical strains (13/791 and 10/234) were tested to evaluate the susceptibility and resistance of each phage-antibiotic combination. Bacterial cultures (75 µL) were inoculated in the TSB medium, and 75 µL of phage P68 in the TSB medium with a resulting MOI_{INPUT} of 1 or 10 was added. Then, 50 µL of AMO, diluted in distilled water to a final concentration of 0.25 mg/L for laboratory strains and 32 mg/L for clinical strains, was added. The lysis in the case of PAS was monitored for 15 h at 37 °C.

The subinhibitory concentration of AMO was determined for all bacterial strains tested as follows: Bacterial inoculum was prepared by diluting the overnight culture with TSB to a final OD_{600} of ~ 0.25. In each well, 150 µL of this inoculum was mixed with 50 µL of AMO solutions, prepared by two-fold serial dilution, with the highest concentration of 32 mg/L, and the lowest one of 0.01 mg/L. Bacterial growth control and medium sterility control were included. The plate was incubated at 37 °C for 20 h with a 10-min measurement interval at 600 nm in an Infinite M200 microplate reader (Tecan, Switzerland). The minimum inhibitory concentration (MIC) was evaluated as the concentration with no signs of bacterial growth. Similar to what has been described previously[50], we defined MIC_{50} of the 18-h OD_{600} values as the lowest AMO concentration that inhibited equal or more than 50% of the bacterial growth determined by bacterial control.

Optimization of immobilization and monitoring of bacterial lysis using QCM

All QCM measurements were performed using the OpenQCM device (Novaetech, Italy). First, bacteria immobilization on the gold surface of 10 MHz QCM sensors was optimized. The polished and unpolished surfaces, each activated or non-activated, were compared. Each sensor was first cleaned in acetone (2×10 min) and isopropanol (1×15 min) in the ultrasonic bath. Then, the sensor was washed with distilled water and dried with compressed air. The activation of gold was performed by 500 µL of cysteamine hydrochloride (20 µg/mL) in distilled water for 2 h, followed by 500 µL of 5% glutaraldehyde in PBS for 1 h at room temperature. The sensor was then washed, inserted into the measuring cell, and the binding of PLL (10 µg/mL) was carried out at the flow rate of 20 µL/min for 20 min. Alternatively, direct binding of PLL was performed in 500 µL droplets for 1 h utilizing the same concentration. Finally, the bacterial culture of *S. aureus* in the TBS buffer was injected (~ 10^9 CFU/mL) with a flow rate of 25 µL/min for 25 min.

The experiments with lysostaphin as a lytic agent took place at room temperature, with TBS as a running buffer. Lysostaphin concentrations of 0, 1, 3, 10, 30, and 100 µg/mL were injected for 35 min, followed by 1 h for monitoring the changes on the sensor surface. In the case of phages, the concentrations of 0, 10^7, 10^8, 10^9, and 10^{10} PFU/mL were applied in the flow system for 10 min, with a monitoring time of 6 h from the phage addition. The TSB growth medium was used as a running buffer, and the measurement took place at 37 °C inside a heated box.

The PAS experiments were started by immobilizing the bacteria on the sensor surface, as described above. This was followed by replacing the running buffer with the TSB medium, and after 1 h, AMO in a resulting concentration of 0, 0.06, 0.125, or 0.25 mg/L was injected into the running medium. Subsequently, phage P68 with a resulting MOI_{INPUT} of 1 was also added to the running medium for ~ 2.5 h. The measurement took place at 37 °C for 15 h. The flow rate in all lysis experiments was 25 µL/min. The subinhibitory concentration of AMO for QCM measurements with the bacterial strain *S. aureus* RN4220 was determined in the same way as described for turbidimetry, but utilizing the dissipation signal.

Verification of bacteria viability by fluorescence microscopy

After the immobilization of bacteria on the sensor surface, the cell culture was stained using the LIVE/DEAD *Bac*Light Bacterial Viability Kit according to the manufacturer's instructions. The primary objective was to assess the relative viability of bacteria on the sensor after the immobilization without emphasizing their absolute numbers. The kit includes SYTO 9 (3.34 mM) and propidium iodide (PI; 20 mM) dyes, which intercalate into the DNA of the cell and enable evaluating viability based on their different permeability through the bacterial membrane. Both dyes were mixed in a 1:1 ratio (v/v) and diluted (3 µL of the mixture in 1 mL of TBS buffer). The solution was then injected into the measuring system, staining bacteria on the sensor surface.

The stained samples were observed using the BX41 fluorescence microscope (Olympus, Japan) with the veTEC monochromatic camera (Omegon, Germany) and a mercury-vapor lamp as an excitation source. SYTO

9 emission was observed using a fluorescein isothiocyanate filter cube (U-MWB2; excitation 475 ± 30 nm, emission > 520 nm, dichroic mirror 500 nm), and the PI was visualized using a tetramethyl rhodamine isocyanate filter cube (U-MWG2; excitation 530 ± 40 nm, emission > 590 nm, dichroic mirror 570 nm). The images were processed using the ImageJ software (National Institutes of Health, USA) and are presented with artificial colors.

AFM visualization of the sensor surface

The evaluation of the roughness of polished and unpolished QCM sensors and the visualization of bacteria on the sensor surfaces were carried out using AFM in air. Before AFM scanning, each QCM sensor was washed with distilled water and dried with compressed air. The scanning was done using Dimension FastScan Bio (Bruker, USA) in PeakForce Tapping mode. A ScanAsyst-Air probe (Bruker, USA) with a spring constant of 0.4 N/m was used. The 10 µm × 10 µm images were recorded at the resolution of 1024 px × 1024 px. The images were processed in the Gwyddion software (Czech Metrology Institute, Czech Republic)[51].

Statistical data evaluation

The statistical evaluation was performed in OriginPro 2022 (OriginLab, USA). All turbidimetric measurements were performed in three technical replicates. Assessment of the bacteria immobilization on the sensor activated by PLL was performed five times for both the polished and the unpolished sensors. QCM measurements were repeated in two (phage- and lysostaphin-mediated lysis) or three (PAS) biological replicates, depending on the complexity and length of the measurement. Bar graphs were plotted as mean values, with error bars representing the standard deviations. In dot charts, each point corresponds to one measurement. The data was normalized according to the formula:

$$\Delta D_{\mathrm{normalized}} = \frac{\Delta L \cdot \Delta I_{\mathrm{m}}}{\Delta I \cdot \Delta L_{\mathrm{m}}}$$

where ΔL is the difference in the signal before and after the lysis, ΔI is the difference in the signal before and after the immobilization, and ΔL_{m} and ΔI_{m} are the signal differences in the TSB medium. It must be noted that in the case of the temperature of 37 °C, ΔL is affected by both the lysis and the potential bacteria growth. The standard deviations were calculated considering the error propagation. The statistical evaluation of the data was carried out by a one-way ANOVA, and the statistical significances were marked with asterisks (**** for $p < 0.0001$, *** for $p < 0.001$, ** for $p < 0.01$, * for $p < 0.05$, and ns for $p > 0.05$).

In addition to the normalization method employed here, simpler processes, such as studying the lysis in buffer at room temperature, can be explained in more details as proposed by Olsson et al.[52], quantifying the sensor coverage and layer thickness.

Results and discussion

Evaluation of bacterial strain and lytic agent models

The enzyme lysostaphin and phage P68 were used as model lytic agents. With lysostaphin, the complete eradication of the bacterial cultures of *S. aureus* RN4220 and *S. aureus* RN4220 Δ*tarM* was observed by turbidimetry for all the studied concentrations (1, 10, and 100 µg/mL) within 1.5 h (Figure S2A,B).

Turbidimetry was also used to select the most effective model bacteria-phage combination (MOI_{INPUT} of 0, 0.01, 0.1, and 1) for lysis monitoring. Figure S2C shows the incomplete eradication of *S. aureus* RN4220 Δ*tarM*; the lysis was observed approximately 1 h after the phage injection, corresponding with the literature[23]. On the other hand, *S. aureus* RN4220 was not eradicated by the P68 phage, even at the highest tested MOI_{INPUT} (Figure S2D). Hence, *S. aureus* RN4220 Δ*tarM* was selected as a suitable model for optimizing QCM-D experiments with the lysis induced by phage P68.

Optimization of *S. aureus* immobilization for real-time QCM and QCM-D measurements

The preparation of the QCM-D measurement started with modifying the gold-coated QCM sensors. Two types of sensors, polished and unpolished, were compared, and their roughness was characterized by AFM (Figure S3A,B). The unpolished sensor had a more fragmented surface, with a ~ 1 µm height range, unlike the polished with a height range of ~ 10 nm. Gentle electrostatic binding of bacteria to the sensor surface via PLL was performed[23]. The adhesion of PLL to gold (adsorption) and cysteamine-glutaraldehyde-activated sensor surfaces (covalent binding) was verified, resulting in a resonance frequency decrease of 20 to 25 Hz within 10 min for both crystal types (Figure S3C). Thus, as the results of both modification approaches were similar, further experiments were carried out with the simpler adsorption-based method.

Both crystal types were compared by monitoring the *S. aureus* immobilization on QCM sensors in the TBS buffer. Figure S4A shows the frequency and dissipation changes in time for both crystal types. The introduction of running TBS buffer after the immobilization did not result in a significant decrease in the dissipation signal that would indicate the detachment of the bacteria from the surface. This is further supported by the statistical data evaluation (Figure S4B), demonstrating that the bacteria bind efficiently without detachment and the resulting signal changes have an acceptable error. The binding of bacteria to the surface of the polished sensor resulted in a resonance frequency change of − 163 ± 62 Hz, while the changes in the case of the unpolished sensor reached − 533 ± 63 Hz. The higher surface roughness of the unpolished crystal, connected with a larger surface area, increased the number of bacteria immobilized on the sensor up to threefold. Thus, for further optimizations, the unpolished crystal was chosen for its higher yield.

Maintaining the viability and metabolic activity of bacteria is necessary for the implementation of the lytic cycle of the phage, phage reproduction, and subsequent lysis of the bacterium. The effect of immobilization on viability was verified using the LIVE/DEAD *Bac*Light Bacterial Viability Kit utilizing fluorescence microscopy. Figure S5 compares bacterial viability on polystyrene Petri dishes and polished and unpolished QCM sensors functionalized with PLL. It was shown that the immobilization did not affect the viability of the bacteria; almost all bacteria on the sensor surface were observed to be alive.

Lysostaphin as a model for QCM and QCM-D monitoring of bacterial lysis

Lysostaphin is a very effective lytic agent suitable for optimizing the QCM setup in the study of bacterial lysis. A typical lysis curve demonstrating the changes in resonance frequency and dissipation in time is shown in Figure S6A. The buffer flowed over *S. aureus*-functionalized sensors for 20 min, followed by the injection of lysostaphin (10 µg/mL), first causing a frequency decrease by 117 ± 2 Hz due to the binding of the enzyme to the surface, followed by the frequency increase by 210 ± 120 Hz, associated with the cleavage of bacterial peptidoglycan and subsequent lysis of bacteria and release of cell fragments. The dissipation curve showed exactly the opposite trend, agreeing with the expectation. The enzyme binding caused only a slight increase in dissipation of $(0.05 \pm 0.02) \times 10^{-4}$, followed by a significant decrease by $(1.17 \pm 0.13) \times 10^{-4}$ during the subsequent lysis. The signal changes during the lysis strongly depended on the number of immobilized bacteria. As shown in Figure S6B, when normalized by the number of immobilized cells, the frequency and dissipation changes during the lysis on polished and unpolished sensors were not significantly different ($p > 0.05$). For studying lysis with simpler enzyme-based lytic agents, such as lysostaphin, the difference between QCM and QCM-D is insignificant; lysostaphin binding and bacterial lysis were successfully detected in both cases, concluding that both the QCM and the QCM-D are suitable for measurements in a buffer environment at room temperature.

The AFM visualization of the sensor surfaces with attached bacteria without and with lysostaphin lysis (Fig. 2A) revealed changes in the roughness of the polished sensor after the lysis. On the other hand, with an unpolished sensor, only the absence of bacteria could be identified due to its higher roughness. Nevertheless, unpolished sensors were chosen for further experiments for their higher responses and easier handling; as the unpolished crystals are slightly thicker, better sealing of the measuring cell can be achieved, reducing the number of bubbles present throughout the experiments.

After the general optimizations, lysostaphin concentrations of 0, 1, 3, 10, 30, and 100 µg/mL were examined utilizing the unpolished crystals (Fig. 2B,C). For the low concentrations (≤ 10 µg/mL), the course of the curves was consistent with the one described above. However, at higher concentrations of 30 and 100 µg/mL, the lysis was followed by a further decrease in frequency and an increase in dissipation that lasted until the end of the lysostaphin injection. In a reference experiment with lysostaphin adsorbing to the sensor surface, the frequency and dissipation changes were significantly lower (Figure S7). Thus, the binding of bacterial residues to the sensor surface is the probable explanation for the signal changes in the later phases of the bacterium-lysostaphin interactions. It should be noted that sensor surface blocking was not carried out in these experiments. However,

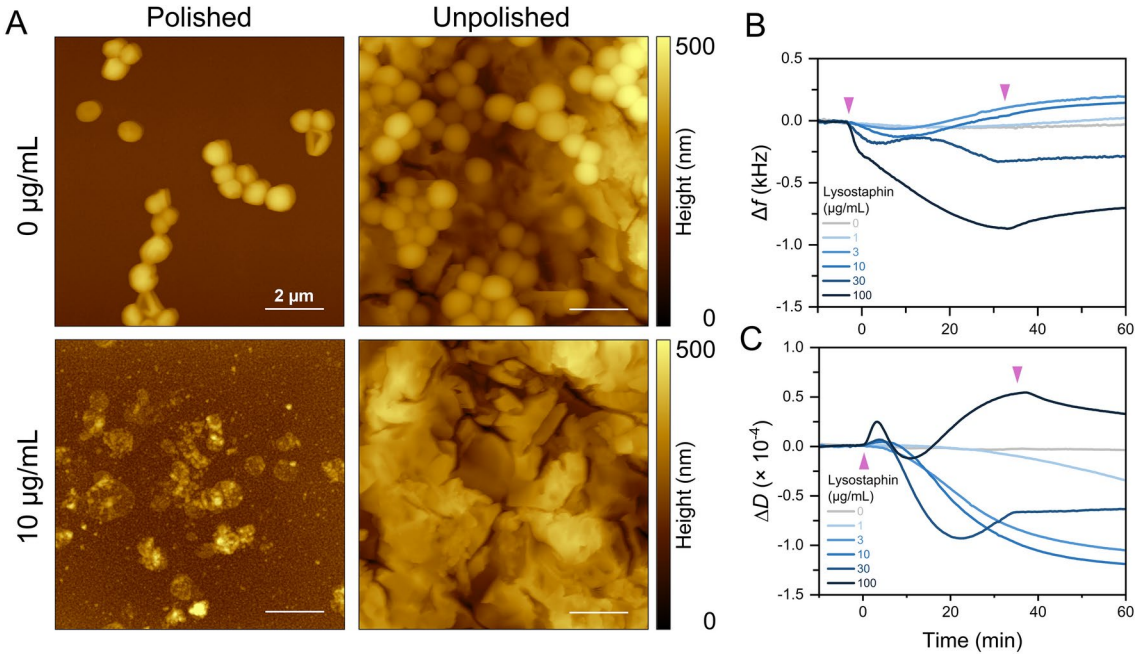

Fig. 2. Lysostaphin-induced lysis of *S. aureus* RN4220 Δ*tarM* on polished and unpolished QCM sensors modified with PLL. (**A**) AFM visualization of QCM sensors with attached *S. aureus* without and with lysostaphin (10 µg/mL). Monitoring the changes of (**B**) resonance frequency and (**C**) dissipation of unpolished sensors during the lysis by various lysostaphin concentrations. The purple arrows indicate the start and end of the lysostaphin injection.

similar behavior for higher enzyme concentrations was previously observed also using SPR with the surface blocked using 1% bovine serum albumin[23]. The choice of a particular blocking agent can be a complex problem and should be addressed in further studies. For example, antifouling surfaces with specifically attached cells can be considered[53].

QCM and QCM-D monitoring of phage-mediated lysis

To carry out phage-mediated lysis, it is necessary to ensure optimal conditions for virus multiplication and the completion of the lytic cycle. Thus, the experiments were conducted at an elevated temperature of 37 °C, with the TSB growth medium as a running buffer. A typical *S. aureus* growth curve without lysis is shown in Fig. 3A. First, the immobilization of bacteria took place in the TBS buffer for greater yield and better adhesion of the cells to the surface (phase I). Next, an injection of TSB growth medium was carried out. When TSB is injected into the measuring cell, binding of proteins from the medium on the sensor surface can occur. During the

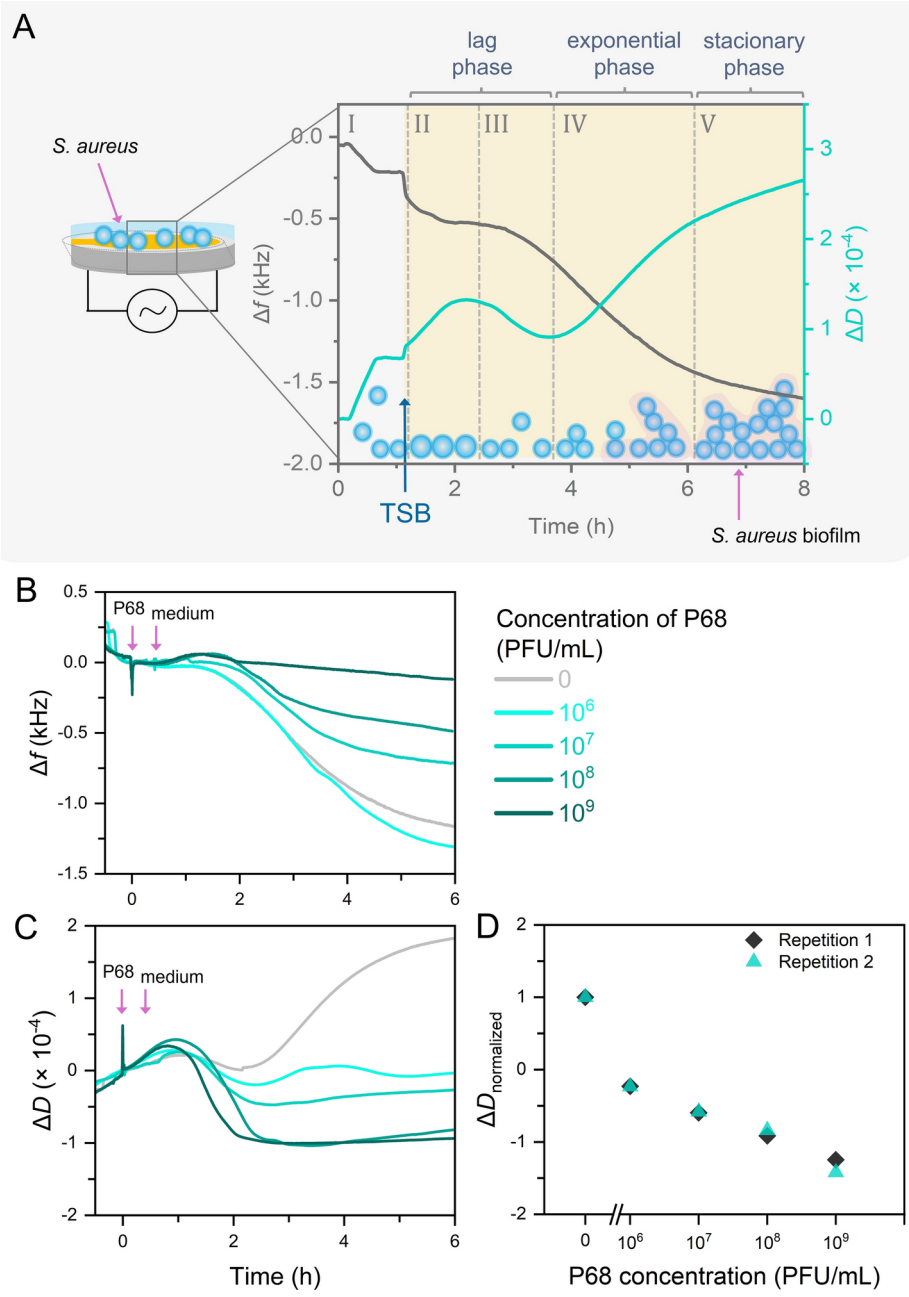

Fig. 3. QCM-D monitoring of *S. aureus* RN4220 Δ*tarM* on the surface of the piezoelectric sensor modified with PLL. (**A**) Growth of *S. aureus* without the presence of lytic agent. Changes in (**B**) frequency and (**C**) dissipation in real-time monitoring of lysis by various concentrations of phage P68. (**D**) Dissipation data (differences between the maximum dissipation value reached after the phage addition and the minimum value) for individual phage concentrations normalized to the number of immobilized bacteria.

medium injection, the dissipation increased by $(0.135 \pm 0.019) \times 10^{-4}$, and the resonance frequency decreased by 215 ± 27 Hz within 5 min. This effect was utilized to block the sensor surface, limiting non-specific interactions of lysis agents with PLL.

The dissipation continued to increase and reached a maximum of 1 h after the TSB addition (phase II). According to Liyun Wang et al., who investigated the behavior of a bacterial culture on the polyethylene terephthalate surface using fluorescence microscopy, bacteria on a solid surface can increase their volume through metabolic processes and nutrient uptake[54]. In our study, the increase in dissipation was likely caused by such processes along with cell growth. After that, a decrease in dissipation signal was observed, which could be associated with the release of reversibly attached cells from the surface of the sensor or a reduction in the number of bacteria due to their spontaneous death (phase III). This was followed by bacterial growth, primarily in the form of biofilm, which involves bacterial division and extracellular matrix production (phase IV). As demonstrated by the increasing dissipation, the viscosity of the biofilm kept increasing until the stationary phase was finally reached (phase V). In comparison, monitoring the frequency provides less information because the difference between the binding and the lysis cannot be distinguished. This highlights the importance of monitoring dissipation in QCM-D for the study of phage-mediated lysis. The information on the changes in the character of the bacterial culture and the development of the biofilm on the sensor surface during phases II and III would be unclear by only monitoring the frequency signal. After the characterization of the growth curve, the bacterial culture was lysed using different bacteriophage concentrations (10^6 to 10^9 PFU/mL; Fig. 3B,C). The lysis was observed as a frequency decrease after a defined time shift, agreeing with the turbidimetric measurements (Figure S2). The decreasing trend in frequency during the lysis was similar to that of bacteria binding to the surface, suggesting that binding occurs in both cases; during the immobilization or growth, new bacteria attach, whereas during the lysis, remnants of lysed bacteria adhere. Conversely, the dissipation signal of the lysis showed an opposite trend compared to the binding of the bacteria, highlighting the importance of dissipation in assessing phage-mediated lysis. This effect is most pronounced when comparing the control without the phage with the lowest phage concentration of 10^6 PFU/mL; the dissipation clearly shows the lysis progress, whereas the frequency signal combines the growth, lysis, and the possible deposition of lysed bacterial residues.

Figure 3D shows dissipation changes normalized to the number of immobilized bacteria for individual phage concentrations, revealing a decreasing trend in the dissipation with the increasing phage concentration for both replicates. Furthermore, a reference experiment (Figure S8) demonstrated that phage binding to the sensor surface does not result in a change in frequency or dissipation to the same extent as lysostaphin, regardless of the concentration.

Thus, we have demonstrated that the combination of frequency and dissipation monitoring provides complex information on the phage lysis, distinguishing the lysis of bacteria from the adherence of their lysed remnants to the sensor surface. This represents a significant advantage compared to the observation of phage-mediated lysis by SPR[23], which combines the effect of lysis and adherence into a single measured signal (change of refractive index).

QCM-D monitoring of PAS

The PAS effect was observed in the phage P68 combined with AMO as a plaque enlargement on strain RN4220 Δ*tarM* and phage propagation on strain RN4220 (Figure S1). We hypothesize that the effect of AMO, which inhibits bacterial cell wall biosynthesis and repair, resulted in either more efficient phage adsorption or a delayed lysis effect[55], leading to increased phage burst size and, thus, larger plaques. As strains expressing the accessory cell wall teichoic acid glycosyltransferase TarM are resistant to podoviruses, such as P68[47], the effect of AMO on cell wall structure probably plays a role in the observed gain of the ability of phage P68 to infect the strain RN4220 efficiently.

To maintain the advantages of synergistic effect (selectivity and suppression of the formation of resistant mutants), the phage must be able to propagate on a given strain. This occurs either by the treatment with an antibiotic that modifies the susceptibility of the strain or by using its subinhibitory concentration, which partially inhibits the host population but does not kill, allowing the phage to propagate[56], in some cases even more effectively than without the antibiotic[55]. Moreover, the PAS-based approach can minimize the harmful effect of antibiotics on the natural microbiota[57]. Another important aspect of the PAS effect is the ability of phages to penetrate and disrupt the biofilm to make it accessible to antibiotics[58].

Four *S. aureus* strains (RN4220, RN4220 Δ*tarM*, 10/234, and 13/791) were subjected to individual and combination in vitro treatment to assess the synergistic effect. First, the subinhibitory concentration of AMO for *S. aureus* strain RN4220 was determined using turbidimetry (Figure S9A) and QCM (Figure S9B). The methods provided different results, showing a subinhibitory cut-off at 4 mg/L using turbidimetry and 0.06 mg/L using QCM. This can be explained by the different numbers of target bacteria and the fact that turbidimetry evaluates planktonic culture, whereas QCM studies bacteria immobilized directly on the sensor surface. A reference experiment (Figure S10) confirmed that binding of AMO to the sensor surface without bacteria does not cause a significant change in the signal, consistent with the previous experiments with lysostaphin.

Furthermore, the effect of the synergy of phage P68 with AMO on the individual *S. aureus* strains was evaluated. Turbidimetry showed complete eradication of the P68-susceptible strain RN4220 Δ*tarM* (Figure S11A) and P68-resistant strain RN4220 (Figure S11B) in the combined treatment, in contrast to individual phage P68 treatment, which failed to eradicate even the susceptible strain. In the case of the clinical strain 13/791, the PAS accelerated the lysis process, although complete lysis was not achieved within the observed timeframe of 15 h (Figure S11C). Finally, no effect was observed in the highly resistant strain 10/234 (Figure S11D). Thus, due to the most pronounced synergistic effect, *S. aureus* RN4220 was used for further lysis monitoring experiments.

Figure 4A shows changes in dissipation over time for the lysis of P68-resistant *S. aureus* RN4220 using the phage P68 ($MOI_{INPUT} = 1$) alone and in combination with AMO (concentrations 0.06, 0.125, and 0.25 mg/L).

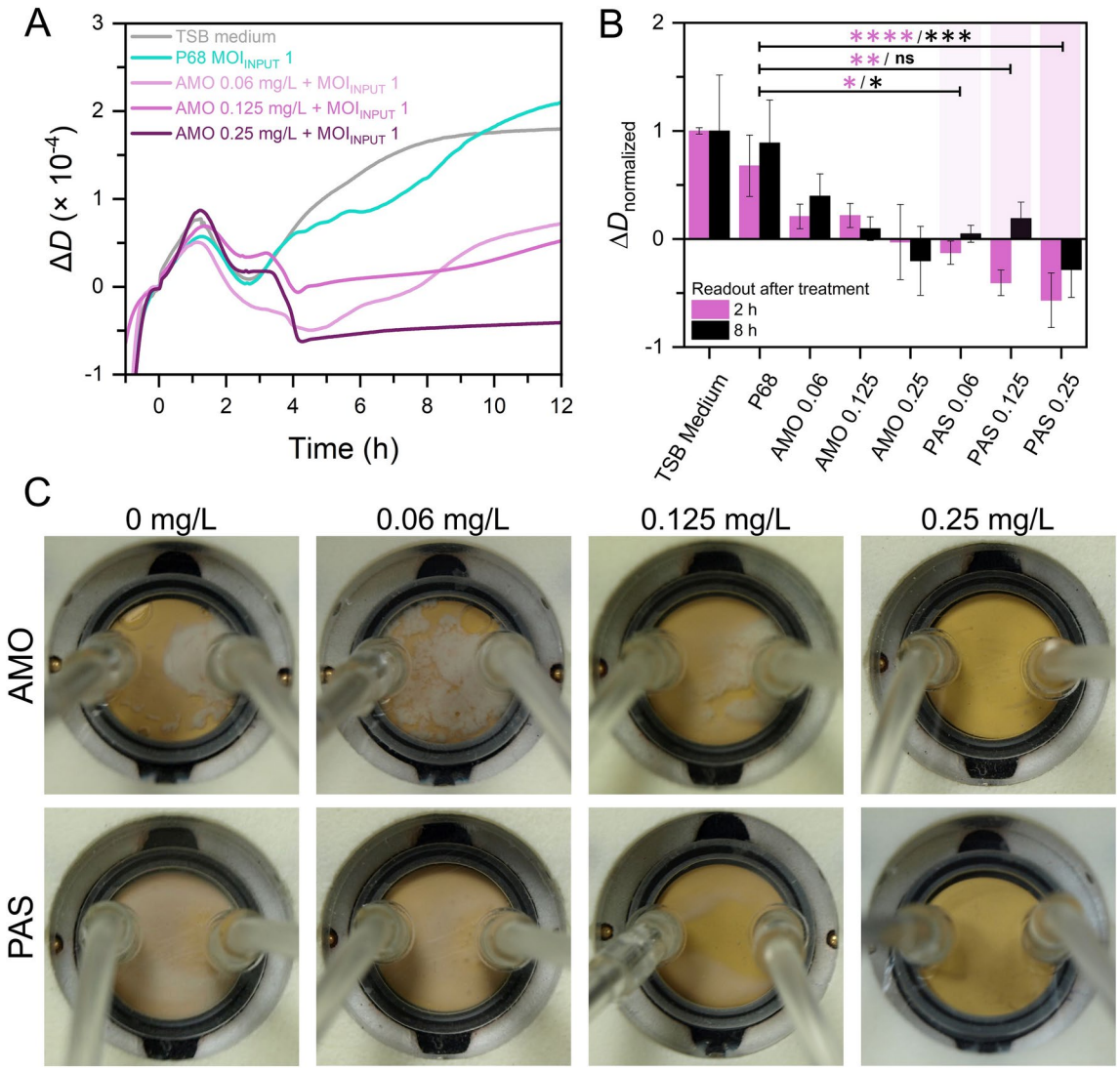

Fig. 4. (**A**) Changes in QCM-D dissipation signal over time for the lysis of *S. aureus* RN4220 by phage P68 ($MOI_{INPUT} = 1$) alone and in combination with AMO (0.06 mg/L, 0.125 mg/mL, and 0.25 mg/L). (**B**) Normalized dissipation changes read out at 2 h and 8 h after the addition of various lytic agent combinations. Error bars represent standard deviations, and the statistical significances are marked with asterisks (**** for $p < 0.0001$, *** for $p < 0.001$, ** for $p < 0.01$, * for $p < 0.05$, and ns for $p > 0.05$). (**C**) The appearance of the QCM-D measuring cell after 24 h of measurement for AMO alone (concentrations provided above the corresponding panels) and PAS (utilizing 10^7 PFU/mL of phage P68), showing the differences in the constitution of the formed bacterial biofilm (white layer). In the case of PAS, a compact biofilm was not formed.

When using the phage P68 alone, the trend of the dissipation curve remained comparable to the case of negative control in the TSB medium. In the combined treatment experiment, no significant difference was observed compared to the control in the dissipation trend during the antibiotic injection step (time between 1–2 h) with all the studied AMO concentrations. However, upon the subsequent addition of phage P68 (in the time of 2.5 h), the bacterial growth ceased, followed by the sharp decrease in dissipation due to the lysis after another ~ 45 min of PAS with AMO concentrations of 0.125 mg/L and 0.25 mg/L. There was no further increase in the dissipation signal, indicating no bacterial multiplication on the sensor surface. In contrast, the lowest studied AMO concentration of 0.06 mg/L did not show a significant decrease in dissipation upon phage addition, and bacterial growth persisted.

Considering the dynamics of bacterial culture growth and lysis, dissipation changes were read at two distinct time points: 2 h after the addition of phage P68, corresponding to the maximum signal decrease, and 8 h after the addition of phage P68, at the beginning of the stationary phase observed in the control sample without treatment. The two readouts are compared in Fig. 4B as normalized values. The readout after 2 h gives a significantly more pronounced decrease in the signal for the PAS treatment. On the other hand, the readout at 8 h shows a further increase in the signal, likely due to the insufficient eradication of all bacteria. It is, therefore, useful for monitoring further culture development and biofilm growth. The phage alone did not cause a significant change in the

dissipation signal for neither of the readout times ($p > 0.05$). However, statistically significant differences were observed between the use of phage P68 alone and its synergistic mixture with AMO, demonstrating a significant effect of PAS on the initially P68-resistant *S. aureus* RN4220 bacterial culture. The comparison of readout at 2 h and 8 h after the phage injection showed that the readout at 2 h provided statistically more significant results for monitoring bacterial culture lysis by the synergistic effect of phage and antibiotic, making this time more suitable for data evaluation. It must be noted that assessing frequency and dissipation changes is not the only way of data evaluation. Kinetic parameters of the interactions can also be evaluated, as proposed by Rajaram et al.[59].

In addition, photos of the sensors were taken 24 h after the measurement (Fig. 4C). Using an ineffective AMO concentration of 0.06 mg/L resulted in a biofilm with a similar appearance to the control with no lytic agent. Despite increasing the flow rate to 44 mL/min, the biofilm remained intact and could not be detached from the sensor surface. Conversely, in all synergistic combinations, the remnants of the bacterial culture were washed away by the high flow, and no compact biofilm was formed, even at the lowest AMO concentration. Finally, QCM was used to compare the lysis of the P68-resistant strain RN4220 with the susceptible strain RN4220 Δ*tarM* (Figure S12). Unlike the injection of phage P68 alone, the combination of phage and subinhibitory AMO concentrations resulted in significant bacterial lysis and a substantial dissipation decrease within ~ 45 min for both strains.

Overall, these results agree with observations by turbidimetry (Figure S11) and provide insights into bacterial behavior during lysis on the surface, where bacteria commonly proliferate and pose significant clinical challenges. Furthermore, the ability to monitor bacterial growth and lysis in a moderate flow can facilitate the addition of lytic agents and fresh nutrients and the collection of metabolites or cells at various growth and lysis phases for further complementary studies, such as investigating the presence of signaling molecules and genetic changes.

It should be noted that the current literature lacks comprehensive studies on bacterial behavior and lysis on surfaces toward creating robust *pathogen-on-a-chip* models. When developing such models, emphasis should be placed on scenarios resembling real-life situations where bacteria colonize mucous membranes and tissues and grow resistant biofilms. Appropriate consideration of surrounding conditions, such as body temperature, nutrient presence, and the inherent interactions between bacteria and phages, is essential. This proof-of-concept study showed that label-free QCM-D biosensors can address these gaps and provide critical insights into bacterial lysis mechanisms.

QCM-D is an affordable device with the possibility of multi-channel measurement and automation of the entire process. As the price of sensors is low (QCM sensors with Au electrodes can be obtained for €5 per piece), they can be disposed of after the measurement, not risking potential contamination due to their cleaning and reuse. In addition, both sides of the resonator can be used for experiments, further reducing the price per experiment. After optimization and appropriate technical implementation, the method can be used in clinical practice to rapidly determine the effect of lytic agents (phages, antibiotics, or other antimicrobials) or to determine whether the phage-antibiotic combination exhibits the desired efficiency, minimizing the requirement for time-consuming culture experiments.

Conclusions

In this study, we report on a new label-free biosensor concept for sensitive real-time monitoring of bacterial lysis in a microfluidic chip. We demonstrate that by monitoring dissipation changes during lysis reactions by means of quartz crystal microbalance technique, it is possible to distinguish between lysis by cell-attached agent and other processes, such as bacteria culture growth. *S. aureus* lysis mechanisms, induced by both enzyme lysostaphin and phage P68, were investigated as model complex biological systems. Our investigations uncovered distinct mechanisms of bacterial lysis, both enzyme- and phage-mediated, shedding light on previously unexplored dynamics under viable culture conditions. Notably, we observed a unique pattern of phage-mediated lysis on a solid surface, involving bacterial growth and detachment from surfaces, a phenomenon with important implications for understanding biofilm dynamics and antibiotic resistance. Furthermore, our study revealed the potential of phage-antibiotic synergy in lysing even non-susceptible *S. aureus* strains. This finding underscores the promise of our approach in tackling infections caused by multidrug-resistant bacterial strains and biofilms, offering a significant contribution to the field of antimicrobial therapy.

Data availability

The datasets generated during the study are available from the corresponding author on reasonable request.

Received: 11 September 2024; Accepted: 30 December 2024
Published online: 27 January 2025

References

1. Kouijzer, I. J. E., Fowler, V. G. & Ten Oever, J. Redefining *Staphylococcus aureus* bacteremia: A structured approach guiding diagnostic and therapeutic management. *J Infect* **86**, 9–13. https://doi.org/10.1016/j.jinf.2022.10.042 (2023).
2. Hatfull, G. F., Dedrick, R. M. & Schooley, R. T. Phage therapy for antibiotic-resistant bacterial infections. *Annu. Rev. Med.* **73**, 197–211. https://doi.org/10.1146/annurev-med-080219-122208 (2022).
3. Uyttebroek, S. et al. Safety and efficacy of phage therapy in difficult-to-treat infections: A systematic review. *Lancet Infect. Dis.* **22**, e208–e220. https://doi.org/10.1016/S1473-3099(21)00612-5 (2022).
4. Akturk, E. et al. Synergistic action of phage and antibiotics: Parameters to enhance the killing efficacy against mono and dual-species biofilms. *Antibiotics* **8**, 103. https://doi.org/10.3390/antibiotics8030103 (2019).
5. Dickey, J. & Perrot, V. Adjunct phage treatment enhances the effectiveness of low antibiotic concentration against *Staphylococcus aureus* biofilms *in vitro*. *PLoS ONE* **14**, e0209390. https://doi.org/10.1371/journal.pone.0209390 (2019).
6. Li, X. et al. Characterization of a novel bacteriophage Henu2 and evaluation of the synergistic antibacterial activity of phage-antibiotics. *Antibiotics* **10**, 174. https://doi.org/10.3390/antibiotics10020174 (2021).

7. Nazarov, P. A. MDR pumps as crossroads of resistance: Antibiotics and bacteriophages. *Antibiotics* **11**, 734. https://doi.org/10.3390/antibiotics11060734 (2022).
8. Leclerc, Q. J., Lindsay, J. A. & Knight, G. M. Modelling the synergistic effect of bacteriophage and antibiotics on bacteria: Killers and drivers of resistance evolution. *PLoS Comput. Biol.* **18**, e1010746. https://doi.org/10.1371/journal.pcbi.1010746 (2022).
9. Jędrusiak, A., Fortuna, W., Majewska, J., Górski, A. & Jończyk-Matysiak, E. Phage interactions with the nervous system in health and disease. *Cells* **12**, 1720. https://doi.org/10.3390/cells12131720 (2023).
10. Botka, T. et al. Lytic and genomic properties of spontaneous host-range *Kayvirus* mutants prove their suitability for upgrading phage therapeutics against staphylococci. *Sci. Rep.* **9**, 5475. https://doi.org/10.1038/s41598-019-41868-w (2019).
11. Fišarová, L. et al. *Staphylococcus epidermidis* phages transduce antimicrobial resistance plasmids and mobilize chromosomal islands. *mSphere* **6**, e00223-e321. https://doi.org/10.1128/mSphere.00223-21 (2021).
12. Botka, T. et al. Complete genome analysis of two new bacteriophages isolated from impetigo strains of *Staphylococcus aureus*. *Virus Genes* **51**, 122–131. https://doi.org/10.1007/s11262-015-1223-8 (2015).
13. Naureen, Z. et al. Comparison between American and European legislation in the therapeutical and alimentary bacteriophage usage. *Acta Biomed. Ateneo Parm* **91**, e2020023. https://doi.org/10.23750/abm.v91i13-S.10815 (2020).
14. Liu, D. et al. The safety and toxicity of phage therapy: A review of animal and clinical studies. *Viruses* **13**, 1268. https://doi.org/10.3390/v13071268 (2021).
15. Podlacha, M. et al. Interactions of bacteriophages with animal and human organisms safety issues in the light of phage therapy. *Int. J. Mol. Sci.* **22**, 8937. https://doi.org/10.3390/ijms22168937 (2021).
16. Melo, L. D. R., Monteiro, R., Pires, D. P. & Azeredo, J. Phage-host interaction analysis by flow cytometry allows for rapid and efficient screening of phages. *Antibiotics* **11**, 164. https://doi.org/10.3390/antibiotics11020164 (2022).
17. Gan, B.-H., Cai, X., Javor, S., Köhler, T. & Reymond, J.-L. Synergistic effect of propidium iodide and small molecule antibiotics with the antimicrobial peptide dendrimer G3KL against gram-negative bacteria. *Molecules* **25**, 5643. https://doi.org/10.3390/molecules25235643 (2020).
18. Zheng, Y., He, L., Asiamah, T. K. & Otto, M. Colonization of medical devices by staphylococci. *Environ. Microbiol.* **20**, 3141–3153. https://doi.org/10.1111/1462-2920.14129 (2018).
19. Foulston, L., Elsholz, A. K. W., DeFrancesco, A. S. & Losick, R. The extracellular matrix of *Staphylococcus aureus* biofilms comprises cytoplasmic proteins that associate with the cell surface in response to decreasing pH. *mBio* **5**, e01667-e1714. https://doi.org/10.1128/mBio.01667-14 (2014).
20. Schilcher, K. & Horswill, A. R. Staphylococcal biofilm development: Structure, regulation, and treatment strategies. *Microbiol. Mol. Biol. Rev.* **84**, e00026-e119. https://doi.org/10.1128/MMBR.00026-19 (2020).
21. Moormeier, D. E. & Bayles, K. W. *Staphylococcus aureus* biofilm: A complex developmental organism. *Mol. Microbiol.* **104**, 365–376. https://doi.org/10.1111/mmi.13634 (2017).
22. Shrestha, L., Bhattarai, N. R. & Khanal, B. Comparative evaluation of methods for the detection of biofilm formation in coagulase-negative staphylococci and correlation with antibiogram. *Infect. Drug Resist.* **11**, 607–613. https://doi.org/10.2147/IDR.S159764 (2018).
23. Obořilová, R. et al. Atomic force microscopy and surface plasmon resonance for real-time single-cell monitoring of bacteriophage-mediated lysis of bacteria. *Nanoscale* **13**, 13538–13549. https://doi.org/10.1039/d1nr02921e (2021).
24. Forinová, M. et al. A comparative assessment of a piezoelectric biosensor based on a new antifouling nanolayer and cultivation methods: Enhancing *S. aureus* detection in fresh dairy products. *Curr. Res. Biotechnol.* **6**, 100166. https://doi.org/10.1016/j.crbiot.2023.100166 (2023).
25. Lim, H. J., Saha, T., Tey, B. T., Tan, W. S. & Ooi, C. W. Quartz crystal microbalance-based biosensors as rapid diagnostic devices for infectious diseases. *Biosens. Bioelectron.* **168**, 112513. https://doi.org/10.1016/j.bios.2020.112513 (2020).
26. Park, J.-H., Cho, Y.-W. & Kim, T.-H. Recent advances in surface Plasmon resonance sensors for sensitive optical detection of pathogens. *Biosensors* **12**, 180. https://doi.org/10.3390/bios12030180 (2022).
27. Shrivastav, A. M. et al. Engineering the penetration depth of nearly guided wave surface plasmon resonance towards application in bacterial cells monitoring. *Sens. Actuators B Chem.* **345**, 130338. https://doi.org/10.1016/j.snb.2021.130338 (2021).
28. Latag, G. V., Nakamura, T., Palai, D., Mondarte, E. A. Q. & Hayashi, T. Investigation of three-dimensional bacterial adhesion manner on model organic surfaces using quartz crystal microbalance with energy dissipation monitoring. *ACS Appl. Bio Mater.* **6**, 1185–1194. https://doi.org/10.1021/acsabm.2c01012 (2023).
29. Salazar, J. et al. Real-time detection of the bacterial biofilm formation stages using QCM-based sensors. *Chemosensors* **11**, 68. https://doi.org/10.3390/chemosensors11010068 (2023).
30. Amer, M.-A. et al. Multichannel QCM-based system for continuous monitoring of bacterial biofilm growth. *IEEE Trans. Instrum. Meas.* **69**, 2982–2995. https://doi.org/10.1109/TIM.2019.2929280 (2020).
31. Sauerbrey, G. Verwendung von Schwingquarzen zur Wägung dünner Schichten und zur Mikrowägung. *Z Physik* **155**, 206–222. https://doi.org/10.1007/BF01337937 (1959).
32. Skládal, P. Piezoelectric biosensors: Shedding light on principles and applications. *Microchim. Acta* **191**, 184. https://doi.org/10.1007/s00604-024-06257-9 (2024).
33. Alexander, T. E., Lozeau, L. D. & Camesano, T. A. QCM-D characterization of time-dependence of bacterial adhesion. *Cell Surf.* **5**, 100024. https://doi.org/10.1016/j.tcsw.2019.100024 (2019).
34. Olsson, A. L. J. QCM-D for non-destructive real-time assessment of *Pseudomonas aeruginosa* biofilm attachment to the substratum during biofilm growth. *Colloids Surf. B Biointerfaces* **136**, 928–934. https://doi.org/10.1016/j.colsurfb.2015.10.032 (2015).
35. Ripa, R., Shen, A. Q. & Funari, R. Detecting *Escherichia coli* biofilm development stages on gold and titanium by quartz crystal microbalance. *ACS Omega* **5**, 2295–2302. https://doi.org/10.1021/acsomega.9b03540 (2020).
36. Swana, K. W., Camesano, T. A. & Nagarajan, R. Formation of a fully anionic supported lipid bilayer to model bacterial inner membrane for QCM-D studies. *Membranes* **12**, 558. https://doi.org/10.3390/membranes12060558 (2022).
37. Vybiral, D. et al. Complete nucleotide sequence and molecular characterization of two lytic *Staphylococcus aureus* phages: 44AHJD and P68. *FEMS Microbiol. Lett.* **219**, 275–283. https://doi.org/10.1016/S0378-1097(03)00028-4 (2003).
38. Jayakumar, J., Kumar, V. A., Biswas, L. & Biswas, R. Therapeutic applications of lysostaphin against *Staphylococcus aureus*. *J. Appl. Microbiol.* **131**, 1072–1082. https://doi.org/10.1111/jam.14985 (2021).
39. Bastos, M. D. C. D. F., Coutinho, B. G. & Coelho, M. L. V. Lysostaphin: A staphylococcal bacteriolysin with potential clinical applications. *Pharmaceuticals* **3**, 1139–1161. https://doi.org/10.3390/ph3041139 (2010).
40. Schindler, C. A. & Schuhardt, V. T. Lysostaphin: A new bacteriolytic agent for the *Staphylococcus*. *Proc. Natl. Acad. Sci. U.S.A.* **51**, 414–421. https://doi.org/10.1073/pnas.51.3.414 (1964).
41. Gonzalez-Delgado, L. S. et al. Two-site recognition of *Staphylococcus aureus* peptidoglycan by lysostaphin SH3b. *Nat. Chem. Biol.* **16**, 24–30. https://doi.org/10.1038/s41589-019-0393-4 (2020).
42. Wu, J. A., Kusuma, C., Mond, J. J. & Kokai-Kun, J. F. Lysostaphin disrupts *Staphylococcus aureus* and *Staphylococcus epidermidis* biofilms on artificial surfaces. *Antimicrob. Agents Chemother.* **47**, 3407–3414. https://doi.org/10.1128/AAC.47.11.3407-3414.2003 (2003).
43. Hrebík, D. et al. Structure and genome ejection mechanism of *Staphylococcus aureus* phage P68. *Sci Adv* **5**, eaaw7414. https://doi.org/10.1126/sciadv.aaw7414 (2019).
44. Aleshkin, A. V. et al. Phagebiotics in treatment and prophylaxis of healthcare-associated infections. *Bacteriophage* **6**, e1251379. https://doi.org/10.1080/21597081.2016.1251379 (2016).

45. Kreiswirth, B. N. et al. The toxic shock syndrome exotoxin structural gene is not detectably transmitted by a prophage. *Nature* **305**, 709–712. https://doi.org/10.1038/305709a0 (1983).
46. Brown, S. et al. Methicillin resistance in *Staphylococcus aureus* requires glycosylated wall teichoic acids. *Proc. Natl. Acad. Sci. U.S.A.* **109**, 18909–18914. https://doi.org/10.1073/pnas.1209126109 (2012).
47. Li, X. An accessory wall teichoic acid glycosyltransferase protects *Staphylococcus aureus* from the lytic activity of *Podoviridae*. *Sci. Rep.* **5**, 17219. https://doi.org/10.1038/srep17219 (2015).
48. Botka, T. et al. Two highly divergent lineages of exfoliative toxin B-encoding plasmids revealed in impetigo strains of *Staphylococcus aureus*. *Int. J. Med. Microbiol.* **307**, 291–296. https://doi.org/10.1016/j.ijmm.2017.05.005 (2017).
49. Růžičková, V. et al. Major clonal lineages in impetigo *Staphylococcus aureus* strains isolated in Czech and Slovak maternity hospitals. *Int. J. Med. Microbiol.* **302**, 237–241. https://doi.org/10.1016/j.ijmm.2012.04.001 (2012).
50. Tiwari, S., Nizet, O. & Dillon, N. Development of a high-throughput minimum inhibitory concentration (HT-MIC) testing workflow. *Front. Microbiol.* **14**, 1079033. https://doi.org/10.3389/fmicb.2023.1079033 (2023).
51. Nečas, D. & Klapetek, P. Gwyddion: An open-source software for SPM data analysis. *Open Phys* **10**, 181–188. https://doi.org/10.2478/s11534-011-0096-2 (2012).
52. Olsson, A. L. J., Wargenau, A. & Tufenkji, N. Optimizing bacteriophage surface densities for bacterial capture and sensing in quartz crystal microbalance with dissipation monitoring. *ACS Appl. Mater. Interfaces* **8**, 13698–13706. https://doi.org/10.1021/acsami.6b02227 (2016).
53. Víšová, I., Houska, M. & Vaisocherová-Lísalová, H. Biorecognition antifouling coatings in complex biological fluids: A review of functionalization aspects. *Analyst* **147**, 2597–2614. https://doi.org/10.1039/d2an00436d (2022).
54. Wang, L., Fan, D., Chen, W. & Terentjev, E. M. Bacterial growth, detachment and cell size control on polyethylene terephthalate surfaces. *Sci. Rep.* **5**, 15159. https://doi.org/10.1038/srep15159 (2015).
55. Kim, M. et al. Phage-antibiotic synergy via delayed lysis. *Appl. Environ. Microbiol.* **84**, e02085-e2118. https://doi.org/10.1128/AEM.02085-18 (2018).
56. Chhibber, S., Kaur, T. & Sandeep Kaur. Co-therapy using lytic bacteriophage and linezolid: Effective treatment in eliminating methicillin resistant *Staphylococcus aureus* (MRSA) from diabetic foot infections. *PLoS ONE* **8**, e56022. https://doi.org/10.1371/journal.pone.0056022 (2013).
57. Bhargava, K., Nath, G., Bhargava, A., Aseri, G. K. & Jain, N. Phage therapeutics: From promises to practices and prospectives. *Appl. Microbiol. Biotechnol.* **105**, 9047–9067. https://doi.org/10.1007/s00253-021-11695-z (2021).
58. Łusiak-Szelachowska, M., Weber-Dąbrowska, B. & Górski, A. Bacteriophages and lysins in biofilm control. *Virol. Sin.* **35**, 125–133. https://doi.org/10.1007/s12250-019-00192-3 (2020).
59. Rajaram, K. et al. Real-time analysis of dual-display phage immobilization and autoantibody screening using quartz crystal microbalance with dissipation monitoring. *Int. J. Nanomed.* **10**, 5237. https://doi.org/10.2147/IJN.S84800 (2015).

Acknowledgements

This work was supported by grant NU21J-05-00035 from the Ministry of Health of the Czech Republic, by a National Institute of Virology and Bacteriology project (Program EXCELES, ID project no. LX22NPO5103) funded by the European Union – Next Generation EU, by Ministry of Education of the Czech Republic within the OP-JAK project SENDISO no. CZ.02.01.01/00/22_008/0004596, and by the project MUNI/G/1125/2022 funded by Masaryk University. T.B. gratefully acknowledges the financial support of the research project No. FW10010112 co-financed with state support from the Technology Agency of the Czech Republic under the TREND Programme and funded within the National Recovery Plan from the European Recovery and Resilience Facility. H.V.-L. was supported by the Czech Science Foundation (No. 24-10671S). CIISB, Instruct-CZ Centre, funded by MEYS CR (LM2023042) and European Regional Development Fund-Project "UP CIISB" (No. CZ.02.1.01/0.0/0.0/18_046/0015974) is gratefully acknowledged for the financial support of the measurements at the CF Nanobiotechnology.

Author contributions

Radka Obořilová: Conceptualization, Methodology, Formal analysis, Investigation, Data Curation, Writing – Original Draft, Writing – Review & Editing, Visualization; Eliška Kučerová: Investigation, Writing – Review & Editing; Tibor Botka: Methodology, Validation, Resources, Writing – Review & Editing, Funding acquisition; Hana Vaisocherová-Lísalová: Resources, Writing – Review & Editing, Funding acquisition; Petr Skládal: Methodology, Resources, Writing – Review & Editing, Funding acquisition; Zdeněk Farka: Conceptualization, Methodology, Resources, Writing – Original Draft, Writing – Review & Editing, Visualization, Supervision, Funding acquisition.

Declarations

Competing interests

The authors declare no competing interests.

Additional information

Supplementary Information The online version contains supplementary material available at https://doi.org/10.1038/s41598-024-85064-x.

Correspondence and requests for materials should be addressed to R.O. or Z.F.

Reprints and permissions information is available at www.nature.com/reprints.

Publisher's note Springer Nature remains neutral with regard to jurisdictional claims in published maps and institutional affiliations.

Open Access This article is licensed under a Creative Commons Attribution 4.0 International License, which permits use, sharing, adaptation, distribution and reproduction in any medium or format, as long as you give appropriate credit to the original author(s) and the source, provide a link to the Creative Commons licence, and indicate if changes were made. The images or other third party material in this article are included in the article's Creative Commons licence, unless indicated otherwise in a credit line to the material. If material is not included in the article's Creative Commons licence and your intended use is not permitted by statutory regulation or exceeds the permitted use, you will need to obtain permission directly from the copyright holder. To view a copy of this licence, visit http://creativecommons.org/licenses/by/4.0/.

© The Author(s) 2025

APPENDIX 10

Vacek L, Polaštík Kleknerová D, Lipový B, Holoubek J, Matysková D, Černá E, Brtníková J, Jeklová E, Kobzová Š, Janda L, Lišková L, Diabelko D, Botka T, Pantůček R, Růžička F, Vojtová L (2024) Phage therapy combined with Gum Karaya injectable hydrogels for treatment of methicillin-resistant *Staphylococcus aureus* deep wound infection in a porcine model. *International Journal of Pharmaceutics* 660:124348.

https://doi.org/10.1016/j.ijpharm.2024.124348

(JCR 2024: IF = 5.2; Q1 – Pharmacology & Pharmacy)

Reprinted based on the author's right to include this Elsevier article in his own thesis. (https://www.elsevier.com/about/policies-and-standards/copyright)

International Journal of Pharmaceutics 660 (2024) 124348

Contents lists available at ScienceDirect

International Journal of Pharmaceutics

journal homepage: www.elsevier.com/locate/ijpharm

Phage therapy combined with Gum Karaya injectable hydrogels for treatment of methicillin-resistant *Staphylococcus aureus* deep wound infection in a porcine model

L. Vacek [a], D. Polaštík Kleknerová [a], B. Lipový [b,c], J. Holoubek [b], D. Matysková [b], E. Černá [c], J. Brtníková [c], E. Jeklová [d], Š. Kobzová [d], L. Janda [d], L. Lišková [e], D. Diabelko [a], T. Botka [f], R. Pantůček [f], F. Růžička [a,*], L. Vojtová [c]

[a] Department of Microbiology, St. Anne's University Hospital and Faculty of Medicine, Masaryk University, Pekařská 53, 602 00 Brno, Czech Republic
[b] Department of Burns and Plastic Surgery, Faculty of Medicine, Masaryk University, Kamenice 5, 625 00 Brno, Czech Republic
[c] Advanced Biomaterials Group, Central European Institute of Technology, Brno University of Technology, Purkyňova 656/123, 612 00 Brno, Czech Republic
[d] Clinical Immunology and Immunology of Infectious Diseases, Veterinary Research Institute, Hudcova 296/70, 621 00 Brno, Czech Republic
[e] Department of Histology and Embryology, Faculty of Medicine, Masaryk University, Kamenice 5, 625 00 Brno, Czech Republic
[f] Department of Experimental Biology, Faculty of Science, Masaryk University, Kamenice 753/5, 625 00 Brno, Czech Republic

ARTICLE INFO

Keywords:
Bacteriophage
Phage therapy
Gum Karaya
Hydrogel film
Injectable hydrogel
Staphylococcus aureus
MRSA

ABSTRACT

Skin and soft tissue infections (SSTIs) represent a significant healthcare challenge, particularly in the context of increasing antibiotic resistance. This study investigates the efficacy of a novel therapeutic approach combining bacteriophage (phage) therapy with a gum Karaya (GK)-based hydrogel delivery system in a porcine model of deep staphylococcal SSTIs. The study exploits the lytic activity and safety of the Staphylococcus phage 812K1/420 of the *Kayvirus* genus, which is active against methicillin-resistant *Staphylococcus aureus* (MRSA). The GK injectable hydrogels and hydrogel films, developed by our research group, serve as effective, non-toxic, and easy-to-apply delivery systems, supporting moist wound healing and re-epithelialization. In the porcine model, the combined treatment showed a synergistic effect, leading to a significant reduction in bacterial load (2.5 log CFU/gram of tissue) within one week. Local signs of inflammation were significantly reduced by day 8, with clear evidence of re-epithelialization and wound contraction. Importantly, no adverse effects of the GK-based delivery system were observed throughout the study. The results highlight the potential of this innovative therapeutic approach to effectively treat deep staphylococcal SSTIs, providing a promising avenue for further research and clinical application in the field of infections caused by antibiotic-resistant bacteria.

1. Introduction

Skin and soft tissue infections (SSTIs) encompass a wide range of pathological conditions, from mild superficial infections to severe necrotizing infections requiring intensive care unit (ICU) admission and pose a significant risk of subsequent complications and mortality. The primary line of treatment relies on targeted antibiotic therapy, which is based on the results of microbiological testing (Esposito et al., 2016; Ki and Rotstein, 2008).

Despite the availability of a wide range of antibiotics, infections caused by highly resistant bacterial strains are rapidly emerging. In the ongoing battle against antibiotic resistance, the need to explore alternative therapies becomes increasingly urgent (Chen et al., 2023; World Health Organization, 2023). Our research aims to contribute to the potential use of phage therapy in the treatment of infections caused by methicillin-resistant *Staphylococcus aureus* (MRSA), represented here by a porcine model of deep SSTI.

The main advantages of phage therapy include the bactericidal effect (strict use of lytic phages is a prerequisite), multiplication of phage particles in the presence of the target (bacterial cells), minimal disruption of the normal microbiome due to specific recognition of the host bacterial cell, and no measurable toxicity to eukaryotic cells. Other advantages include the low risk of resistance, the versatility of use, relatively low production costs, and, when using certain phages

* Corresponding author.
E-mail address: filip.ruzicka@fnusa.cz (F. Růžička).

https://doi.org/10.1016/j.ijpharm.2024.124348
Received 20 February 2024; Received in revised form 24 May 2024; Accepted 14 June 2024
Available online 15 June 2024
0378-5173/© 2024 Elsevier B.V. All rights are reserved, including those for text and data mining, AI training, and similar technologies.

containing polysaccharide depolymerases, the possibility to degrade biofilms (Loc-Carrillo and Abedon, 2011).

Although phages are generally considered to be non-toxic, they can interact with the immune system and, therefore, potentially lead to inappropriate immune responses (Kaźmierczak et al., 2021). However, there is little evidence of such reactions, and they do not pose a significant problem in the use of phage therapy. Recent evidence from clinical trials suggests that phage therapy, as currently practised, has few, if any, side effects (Górski et al., 2016; Loc-Carrillo and Abedon, 2011; Petrovic Fabijan et al., 2020).

Phage preparations also benefit from an appropriate delivery system. Our group has already developed such systems based on gum Karaya (GK) polysaccharide – injectable hydrogels and hydrogel films (Drápalová et al., 2023; Lipový et al., 2018; Postulkova et al., 2018). The physical, chemical, antimicrobial, and cytotoxic evaluation showed that the properties of prepared biopolymer-based injectable hydrogels and hydrogel films meet all the necessary requirements for wound treatment. In the present study, we aimed to demonstrate in a porcine model that phage treatment using a suitable GK-based delivery system can constitute an effective topical therapy for deep SSTIs caused by methicillin-resistant *S. aureus*.

2. Materials and methods

2.1. Preparation of GK based injectable hydrogels and hydrogel films for wound dressings

GK injectable hydrogels and hydrogel films were fabricated using either freeze-thawing (injectable hydrogels) or freeze-drying method (hydrogel films).

Injectable hydrogels and hydrogel films were prepared from deacetylated GK, which was prepared from original GK (commercial-grade, M_w of approx. 9500 kg/mol, Sigma-Aldrich, Darmstadt, Germany). Deacetylation was performed to increase polysaccharide solubility as described in Postulkova et al. (2017). First, GK was dispersed in ultrapure water (2 wt%) and deacetylated using a 1 M solution of NaOH (Lach-Ner, Neratovice, Czech Republic), which was followed by HCl neutralization (Lach-Ner, Neratovice, Czech Republic). Deacetylated GK was then purified by filtration to remove the rest of the impurities, precipitated in ethanol, and freeze-dried to obtain a dried powder.

Other components of the deacetylated hydrogel/hydrogel films included polyvinyl alcohol (PVA; M_n = 130 kg/mol, 99 % hydrolyzed; Sigma-Aldrich, Darmstadt, Germany), and anhydrous glycerol purchased from Penta s.r.o. (Czech Republic). The stock solutions of deacetylated GK and PVA were dissolved separately; GK was dissolved in water at 90 °C and PVA at 100 °C according to Drápalová et al. (2023). Then, liquid components were all mixed together in a ratio of 1:1 (GK: PVA) with the addition of anhydrous glycerol; the mixture was then homogenized using a magnetic stir bar overnight, forming a GK-based polymer blend. The same blend was used for both types of hydrogels, with the final form of injectable hydrogels with a high water content and dry hydrogel film with no water present in the polymer matrix. Injectable hydrogels were fabricated using the freeze–thaw method, where samples were frozen in liquid nitrogen and stored in the freezer. Frozen injectable hydrogels were left at room temperature (23 °C) until fully thawed before use in *in vitro* and *in vivo* experiments. Hydrogel films were fabricated using freeze-drying in a 5 × 5 cm plastic mold with hydrogel dry mass accounting for 0.025 g/cm^2 in a lyophilizer (Epsilon 2–10, Martin Christ, Germany) at –35 °C at a low pressure of 1 mBar for 15 h, followed by the secondary drying step at 25 °C under a pressure of 0.01 mBar.

2.2. Phage strain selection and host range

The polyvalent Staphylococcus phage 812, strain 812K1/420 of the genus *Kayvirus* (GenBank/ENA/DDBJ accession number KJ206563.2), was isolated previously (Botka et al., 2019), characterized by cryo-electron microscopy (Nováček et al., 2016), and deposited in the collection of the Department of Experimental Biology, Masaryk University (Brno, Czech Republic). A high proportion of MRSA strains are susceptible to this phage (Botka et al., 2019; Dvořáčková et al., 2020). High-titer phage lysate was prepared in 1 L of minimal broth composed of 5 g Tryptone (Oxoid), 2 g Yeast Extract Powder (Oxoid), and 5 g NaCl, dissolved in distilled water to a volume of 1 L (pH 7.4). 40 mL of an 18-hour culture of prophage-free strain *S. aureus* RN4220 was added and incubated at 37 °C with continuous shaking to OD_{600} = 0.25. Then 100 mL of phage lysate of titer 10^9 PFU/mL and $CaCl_2$ (to the final concentration of 2 mM) were added, followed by incubation for 3–4 h at 37 °C with continuous shaking until complete lysis. The obtained lysate was filtered through the Rapid-Flow sterile bottle-top filter (Nalgene) with a polyethersulfone (PES) membrane and a pore size of 0.2 μm. Subsequently, tangential flow filtration was performed under sterile conditions using a Vivaflow 200 Cassette (Item no. VF20P4) with a 100 kDa PES membrane (Sartorius), during which the medium was replaced with a sterile buffer (10 mM Tris-HCl – pH 7.5; 2.5 mM $MgCl_2$; 0.1 mM $CaCl_2$). After reducing the purified phage suspension to one–tenth volume, the 0.22 μm PES membrane syringe filter (TPP, Switzerland) was used for the final sterilization. The *S. aureus* strain FS159 (provided by the Czech Collection of Microorganisms, entry CCM 4890) exhibiting an almost 100 % efficiency of plating for the used phage, was used for phage titration.

2.3. Phage strain stability and activity in GK based injectable hydrogels

To assess the phage strain stability in injectable hydrogels, 10 μL of the purified phage suspension (10^{11} PFU/mL) was diluted in 990 μL of GK hydrogel, thoroughly mixed and incubated at 37 °C for 24 h. 10 μL of phage stock suspension diluted in 990 μL of Phosphate Buffered Saline (PBS) (pH 7.4) was used as a control sample.

The number of active phage particles after 24-hour incubation was determined by the Double Layer Agar technique (DLA) (Sambrook and Russell, 2001). Briefly, the *S. aureus* FS159 host strain was cultured overnight at 37 °C in nutrient broth (Sigma-Aldrich, USA) and prepared according to the manufacturer's instructions. For use in the DLA method, the same culture medium was supplemented with agar (Sigma-Aldrich, USA) at final concentrations of 1.5 % and 0.7 % for the bottom and top agar layers, respectively.

Phage samples in GK or normal saline were serially diluted ten-fold with PBS (pH 7.4), and 100 μL of each dilution was spread evenly on the bottom agar. Bacterial host cells were washed three times with normal saline, added to 2.5 ml of top agar layer supplemented with 0.002 M $CaCl_2$, gently homogenized, and poured onto a bottom agar layer. The plates were gently swirled, dried at room temperature for 10 min and then inverted and incubated at 37 °C overnight. The number of plaque–forming units was counted and compared to the control sample.

2.4. Phage elution assay

A release profile of phage particles from the GK hydrogel films was assessed in PBS (pH 7.4). Briefly, hydrogel films (1 cm in diameter) were saturated with 100 μL of the stock phage preparation (10^{11} PFU/mL) and incubated at 37 °C for 1 h. Then, the hydrogel film samples were transferred to fresh 1 mL of PBS at specific time intervals (0.25, 0.5, 1, 2, 4 and 8 h) and incubated while shaking at 150 rpm. The number of active phage particles in the eluate samples was determined by the DLA technique described in section 2.3 and expressed as the percentage of active phage particles of the stock phage preparation.

2.5. In vitro evaluation of the antibacterial effect of GK hydrogel film/injectable hydrogel containing phage preparation on staphylococcal infection

An antimicrobial effect of individual components has been determined previously (Botka et al., 2019; Drápalová et al., 2023; Dvořáčková et al., 2020; Lipový et al., 2018). An antimicrobial effect of GK hydrogel film/injectable hydrogel containing phage preparation on staphylococcal infection was evaluated by growth curve measurement as previously described by Vacek et al. (2020). Briefly, the *S. aureus* FS159 strain was cultured in 20 mL of nutrient broth at 37 °C overnight. The bacterial cells were then washed three times with PBS and resuspended in a nutrient broth supplemented with 0.002 M $CaCl_2$ and adjusted to the density of 0.5 McFarland standard (approx. 1.5×10^8 CFU/mL).

The bacterial suspension (1000 μL) and tested antimicrobial preparations were mixed in a 24-well microplate (Sigma-Aldrich, USA). The following antimicrobial preparations were tested: hydrogel film (1 cm in diameter) alone; hydrogel film (1 cm in diameter) saturated with 100 μL of the stock phage preparation (10^{11} PFU/mL); injectable hydrogel alone (100 μL); injectable hydrogel (100 μL) saturated with 100 μL of the stock phage preparation (10^{11} PFU/mL); 100 μL of the stock phage preparation (10^{11} PFU/mL) alone; 100 μL of PBS (serving as growth control).

Microplates were incubated at 37 °C with shaking in Tecan Infinite M200 PRO microplate reader (Tecan Trading, Trasadingen, Switzerland), and optical density (A = 600 nm) was measured every 30 min for 20 h. The average growth curve and standard deviations were calculated for each variant after background subtraction.

2.6. In vivo experiments (porcine model)

The animal care protocol for this experiment followed the Czech Guidelines for Animal Experimentation and was approved by the Central Commission for Animal Welfare of the Ministry of Agriculture of the Czech Republic (serial No. MZe 2181). A total of six pigs were used throughout the experiment. Two pigs (40 wounds) were used for the development and progress assessment of deep skin and soft tissue infection in the animal model. The remaining four (80 wounds) were used to assess the antimicrobial potential of GK-based phage preparations.

2.6.1. Development of deep skin and soft tissue infection

Two pigs were used to develop and evaluate the progression of deep skin and soft tissue infection in the animal model. Female 15-week-old pigs of the hybrid Large White (50 %) × Landrace (50 %) (Bioprodukt Knapovec a.s., Ústí nad Orlicí, Czech Republic) with an average body weight of 75 ± 5 kg were used for the study. The pigs were housed individually in enriched environment pens in the accredited barrier-type Animal facilities of the Veterinary Research Institute, Brno. The pigs were fed a standard commercial diet (De Heus, Marefy, Czech Republic) twice a day ad libitum and had unlimited access to drinking water.

All surgical procedures were performed under general anaesthesia. Premedication and analgesia during the surgery were provided by subcutaneous administration of butorphanol (0.1 mg/kg of body weight; BW), a synthetic opioid agonist–antagonist analgesic. Anaesthesia was induced with a combination of tiletamine/zolazepam (2 mg/kg BW), ketamine (2 mg/kg of BW) and xylazine (2 mg/kg of BW) administered intramuscularly. General anaesthesia was then maintained by intravenous propofol administration (8–15 mg/kg BW).

Full-thickness skin defects were surgically performed on the backs of pigs after antisepsis (povidone-iodine alcoholic solution, followed by 2 % peracetic acid). Skin excisions were performed in strictly defined areas of 5 × 5 cm. Twenty skin defects were performed in each pig, ten on each side of the spine (Fig. 1). Fascial incisions were performed inside the defects to support infection development.

The methicillin-resistant *S. aureus* strain NRL/Atb 5921 (sequence type ST22, spa type t020, SCC*mec* type IV) was used for wound infection. This strain is multiresistant, including resistance to oxacillin, amoxicillin/clavulanic acid, or 3rd generation cephalosporins. 5 mL of bacterial inoculum (concentration approx. 10^9 CFU/mL) were diffusely applied into the sterile gauzes that individually covered surgically induced skin defects. Once the wounds were infected, occlusive dressing was fixed on the pigs' back. Animals were dressed in an elastic dress to minimize the dislocation of the bandages. Immediately after surgery, a second analgesic drug, meloxicam (0.1 mg/kg BW), was administered subcutaneously and then continued at a dose of 0.1 mg/kg BW once a day for the next 3 days.

2.6.2. Microbiological assessment of infection development

To assess the level of bacterial load in the wounds during the study, microbiological and histopathological samples were taken on days 4, 7, 11, and 14 post-infection (later referred to as treatment days 1, 4, 8, and 11, respectively). Pre-operative antibiotic prophylaxis was used to reduce the risk of contaminating agents interfering with the induced infection. More specifically, ceftazidime pentahydrate (2 g) and Shotapen (combination of Benzathine benzylpenicillin 10 mg/kg, Procaine benzylpenicillin 10 mg/kg and Dihydrostreptomycin sulphate 20.5 mg/

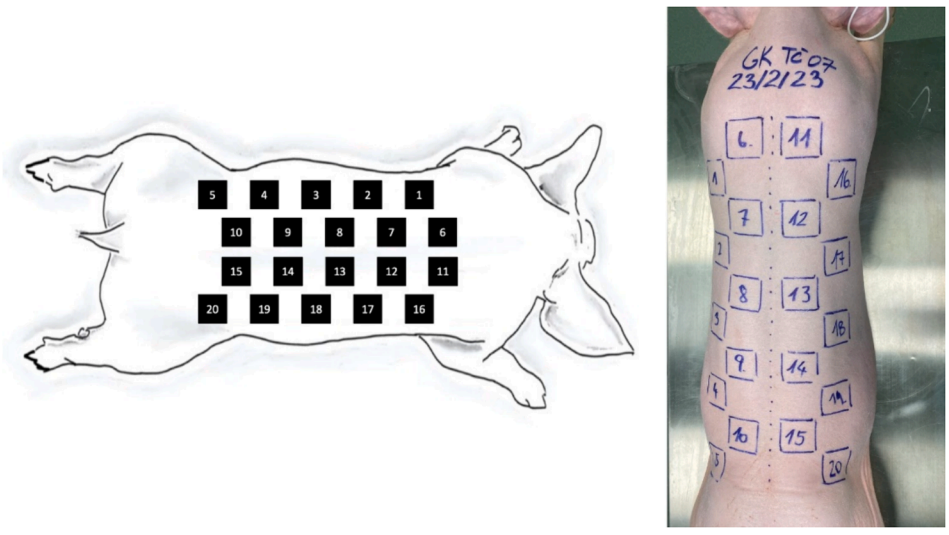

Fig. 1. Position of skin defects on the back of a pig in the animal model. A total of 20 skin defects were performed in each pig, ten on each side of the spine.

kg) were administered prior to sampling. The staphylococcal strain used in this study is resistant to these antibiotics by using EUCAST methods and interpretive criteria (The European Committee on Antimicrobial Susceptibility Testing, 2023).

The bacterial load within the tissue was assessed by processing the tissue biopsy samples. Tissue samples were taken using an 8 mm biopsy punch (Medplus, Czech Republic), placed in 2 mL of sterile PBS, and homogenized (Stomacher® 80 Biomaster, Seward, UK). Serial ten-fold dilutions of the homogenate were plated onto blood agar and blood agar supplemented with 10 % NaCl. Plates were incubated at 37 °C for 24 h, after which the colony-forming units (CFU) counts were enumerated and the CFU per gram of the tissue was calculated according to the following formula:

$$\text{CFU per gram of tissue} = \text{number of colonies (CFU)} \times \text{plated volume} \times \text{dilution} / \text{weight}$$

Bacterial colonies were subsequently analyzed by Matrix-Assisted Laser Desorption/Ionization Time-of-Flight Mass Spectrometry (MALDI-TOF MS; Bruker, Switzerland) to verify the presence of the expected bacterial species in infected wounds and to detect any contamination of the samples. In addition, pulsed-field gel electrophoresis (PFGE) was used as a molecular typing tool to confirm *S. aureus* strain identity in wounds.

2.6.3. Histopathological assessment of infection development

Tissue samples for histopathological examination were fixated in a 10 % formaldehyde solution for 24 h. The material was processed according to standardized protocols using a tissue samples processor ETP PLUS (Intelsint Srl, Italy). All samples were embedded into paraffin blocks using a TES 99 Paraffin Embedding Center (Medite Medical, Germany). Samples were cut using a Thermo Scientific Microm HM 325 Rotary Microtome (Thermo Fisher Scientific, Austria). Serial slices were mounted on standard slides (Knittel Glass Gmbh, Germany) and stained by Haematoxylin-eosin and Gram staining (Bamed, Czech Republic). The prepared slides were examined for signs of inflammation, fibrosis, vascular dilatation, and the number and localization of staphylococcal cells.

2.6.4. Visual assessment of the antibacterial effect of combined GK injectable hydrogel/hydrogel film with phage preparation on staphylococcal infection

In addition to the microbiological and histopathological assessment, the visual appearance and the local signs of wound infection, such as purulent discharge, redness, or induration, were assessed.

2.6.5. Assessment of GK injectable hydrogel and hydrogel film antibacterial effect on staphylococcal infection

Four wounds on both animals (8 wounds) mentioned in section 2.6.2 were dedicated to assessing the bacterial load in wounds during the experiment when only GK injectable hydrogels and hydrogel films without phage preparation were used. Microbiological and histopathological samples were taken on days 4, 7, 11, and 14 post-infection and processed identically to the process mentioned in previous sections 2.6.2, 2.6.3, and 2.6.4.

2.6.6. Assessment of the antibacterial effect of combined GK injectable hydrogel/hydrogel film with phage preparation on staphylococcal infection

Four pigs (80 wounds) were used to assess the effects of combination therapy with either hydrogel films-phage preparation or injectable hydrogel-phage preparation combination. Infection was introduced as described above (section 2.6.2). On days 4, 7, 11 and 14, with day 4 being the first day of infection treatment, GK hydrogel films/injectable hydrogels supplemented with staphylococcal phage preparation at concentrations of 10^8 or 10^9 PFU/wound were applied to the wound surface after microbiological and histological sampling. Hereinafter, days 4, 7, 11, and 14 of the experiment will be referred to as treatment days 1, 4, 8, and 11, respectively.

The following combinations were applied to the wounds: GK hydrogel film + phage preparation (10^9 PFU/wound), GK hydrogel film + phage preparation (10^8 PFU/wound), GK injectable hydrogel + phage preparation (10^9 PFU/wound), GK injectable hydrogel + phage preparation (10^8 PFU/wound) (i.e. 4 different combinations each applied to 4 wounds per pig, i.e., 16 wounds per four pigs for each treatment option). The remaining four wounds served as treatment controls (1x hydrogel film only without phage preparation, 1x injectable hydrogel only without phage preparation, and 2x untreated wound per pig). The locations of individual treatment options varied among experimental animals to ensure randomization of treatment options among wound sites. An example of the application scheme for each treatment is shown in Fig. 2. Microbiological and histopathological samples were collected on treatment days 1, 4, 8, and 11 and processed identically to the process described in sections 2.6.2, 2.6.3, and 2.6.4.

2.7. Statistical analysis

To statistically evaluate the efficacy of each treatment option, bacterial loads (expressed as log CFU/gram tissue) in samples from control animals and wound samples from treated animals were compared. A two-sample *t*-test (for each sampling time, i.e., treatment days 1, 4, 8, and 11) was used to compare the efficacy of each treatment option compared with samples from control animals. An ANOVA test was used to compare the efficacy of each treatment option among themselves. Paired t-tests comparing the results on treatment days 1 vs 4, 1 vs 8, and 1 vs 11 were used to determine the time point at which the bacterial load in the wound was significantly reduced. Therefore, the effect of the treatment was statistically significant. The level of significance considered for all tests was $\alpha = 0.05$. Statistica v.14 software (TIBCO Software, USA) was used for statistical analysis.

3. Results

3.1. Stability and activity of the phage in GK-based hydrogels

The phage preparation stability was assessed in GK injectable hydrogel and compared to the stability of this preparation in PBS (pH 7.4), which served as a control. The number of active phage particles after 24-hour incubation was determined using the Double-Layer Agar

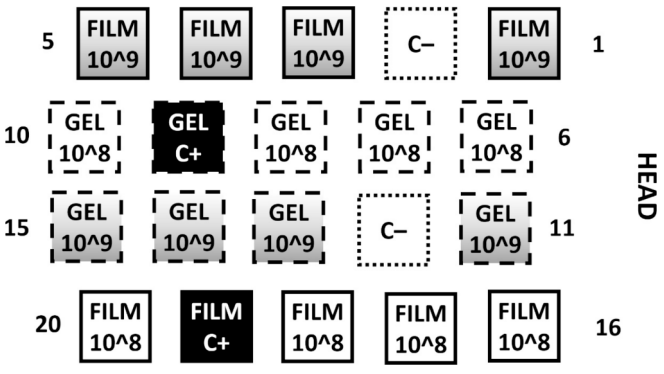

Fig. 2. An example of the location of treatment options among skin defects on the back of the porcine model. A total of 20 skin defects were created, and the following treatment options were used: **FILM 10^9** = gum Karaya (GK) hydrogel film + phage preparation (10^9 PFU/wound), **FILM 10^8** = GK hydrogel film + phage preparation (10^8 PFU/wound), **GEL 10^9** = GK injectable hydrogel + phage preparation (10^9 PFU/wound), **GEL 10^8** = GK injectable hydrogel + phage preparation (10^8 PFU/wound), **FILM C+** = GK hydrogel film without phage preparation, **GEL C+** = GK injectable hydrogel without phage preparation, **C–** = untreated wound.

technique (DLA). The results showed that there was no statistical difference ($p = 0.405$) between the stability of phage preparation in GK injectable hydrogel and PBS (pH 7.4); the numbers of active phage particles after 24 h were 9.1 ± 0.11 and 8.8 ± 0.41 log PFU/mL, respectively.

3.2. Phage elution assay

A release profile of phage particles from GK hydrogel films was assessed in PBS (pH 7.4) at specific time intervals (0.25, 0.5, 1, 2, 4 and 8 h). The number of active phage particles in the eluate samples was determined by the DLA technique and expressed as the percentage of active phage particles of the stock phage preparation. The maximum number of 95.7 ± 0.3 % of released active phage particles was achieved after 1 h of elution time. Longer elution time (up to 8 h) did not increase the number of released particles further (Fig. 3).

3.3. In vitro evaluation of the antibacterial effect of GK hydrogel film/injectable hydrogel containing phage preparation on staphylococcal infection

An antimicrobial effect of either GK hydrogel film or injectable hydrogel containing phage preparation on staphylococcal infection was evaluated by growth curve measurement. The antimicrobial preparations tested were: hydrogel film (1 cm in diameter) alone; hydrogel film (1 cm in diameter) saturated with 100 μL of the stock phage preparation (10^{11} PFU/mL); injectable hydrogel alone (100 μL); injectable hydrogel (100 μL) saturated with 100 μL of the stock phage preparation (10^{11} PFU/mL); 100 μL of the stock phage preparation (10^{11} PFU/mL) alone; 100 μL of PBS (serving as growth control). All tested variants containing the phage preparation successfully reduced bacterial numbers within 4 h and did not allow bacterial regrowth throughout the experiment. The hydrogel film (alone) and injectable hydrogel (alone) samples had only a limited effect on bacterial growth and lowered the optical density of samples at the 20-hour time point from 0.674 ± 0.008 to 0.604 ± 0.005 or 0.541 ± 0.001, respectively (Fig. 4).

3.4. Microbiological and histopathological assessment of infection progression

To assess the bacterial load in the wounds during the experiment without treatment, microbiological and histopathological samples were taken on days 4, 7, 11, and 14 post-infection (also referred to as treatment days 1, 4, 8, and 11, respectively). Tissue bacterial load was assessed by microbiological evaluation of tissue biopsy samples and histopathological evaluation.

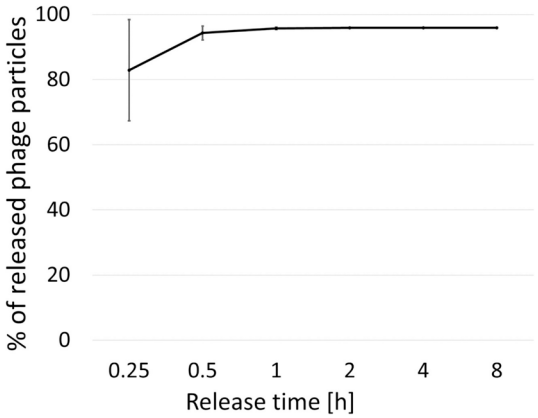

Fig. 3. A release profile of phage particles from GK hydrogel films. The maximum number of 95.7 ± 0.3 % of released active phage particles was achieved after 1 h of elution time.

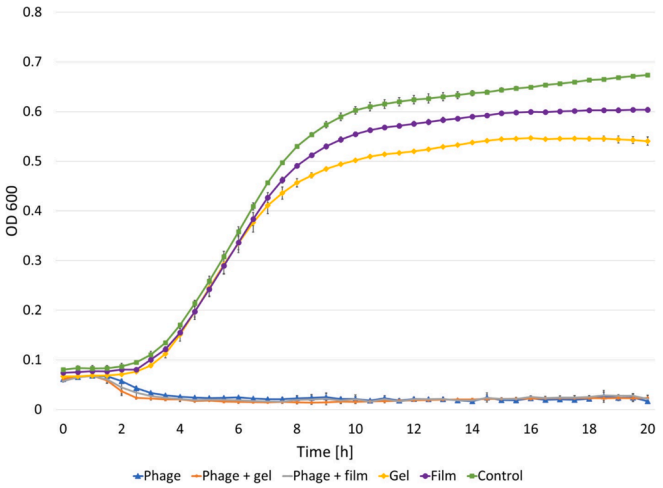

Fig. 4. The antimicrobial effect of gum Karaya hydrogel film/injectable hydrogel containing phage preparation on staphylococcal infection was evaluated by growth curve measurement. The antimicrobial preparations tested were as follows: **Film** – hydrogel film (1 cm in diameter) alone; **Phage + film** – hydrogel film (1 cm in diameter) saturated with 100 μL of the stock phage preparation (10^{11} PFU/mL); **Gel** – injectable hydrogel alone (100 μL); **Phage + gel** – injectable hydrogel (100 μL) saturated with 100 μL of the stock phage preparation (10^{11} PFU/mL); **Phage** – 100 μL of the stock phage preparation (10^{11} PFU/mL) alone; **Control** – 100 μL of PBS (serving as growth control). All tested variants containing phage preparation effectively reduced bacterial numbers within 4 h and did not allow bacterial regrowth throughout the experiment. Hydrogel film (alone) and injectable hydrogel (alone) samples had a limited effect on bacterial growth.

The deep skin and soft tissue infection fully developed within three days, reaching an average number of 6.1 ± 0.4 log CFU/gram of tissue. Throughout the experiment, the average number of bacterial cells in the tissue (biopsy samples) increased significantly ($p = 0.003$) to the final amounts of 7.2 ± 0.4 log CFU/gram of tissue (Fig. 6, Control animals; Fig. 9, top line). The expected bacterial species in infected wounds was confirmed by MALDI-TOF MS and strain similarity to the original *S. aureus* strain NRL/Atb 5921 used for wound infection was verified by PFGE (data not shown).

The full development of deep skin and soft tissue infection was further confirmed by histopathological evaluation. The specimens were characterized by significant tissue infiltration by inflammatory cells with a predominance of polymorphonuclear cells and macrophages accompanied by apparent vasodilatation. Gram staining revealed extensive areas of staphylococcal cells within the wound tissue and on its surface (Fig. 5).

3.5. Evaluation of the antibacterial effect of GK injectable hydrogel and hydrogel film on staphylococcal infection

Four wounds on both animals mentioned in the previous section (3.4) were used to assess the bacterial load in the wounds during the test when only GK injectable hydrogels and hydrogel films without the phage preparation were used. Microbiological and histopathological samples were taken on days 4, 7, 11, and 14 post-infection. The numbers of bacteria present in the samples were not significantly different from untreated wound samples ($p > 0.05$).

3.6. Assessment of the antibacterial effect of combined GK injectable hydrogel/hydrogel film with phage preparation on staphylococcal infection

The study demonstrated a statistically significant therapeutic effect of antimicrobial dressings containing a phage preparation on infection caused by the multidrug-resistant *S. aureus* strain NRL/Atb 5921. The

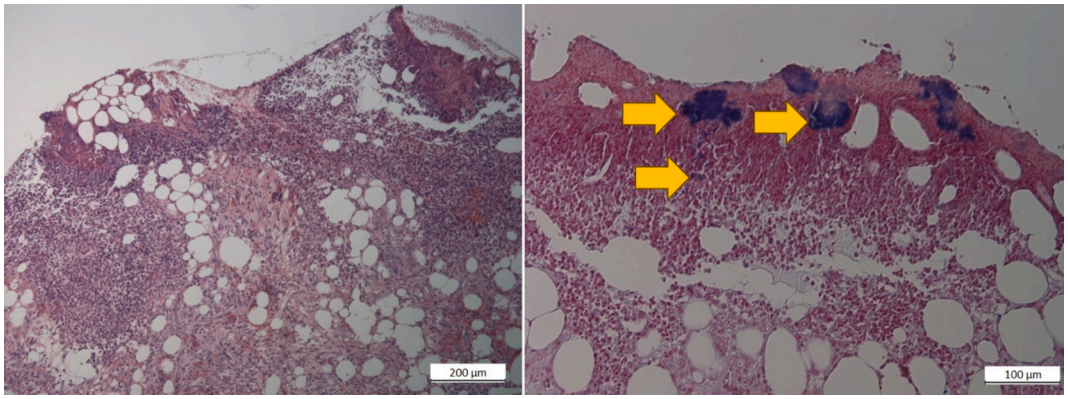

Fig. 5. A histopathological evaluation of deep skin and soft tissue infection development three days after the infection. Samples were stained with **Haematoxylin-eosin staining (left)** and **Gram staining (right)**. Samples were characterized by significant tissue infiltration by inflammatory cells with a predominance of polymorphonuclear cells and macrophages accompanied by apparent vasodilatation (200× magnification). Gram staining showed extensive areas of staphylococcal cells (yellow darts) within the wound tissue and on its surface (400× magnification). (For interpretation of the references to colour in this figure legend, the reader is referred to the web version of this article.)

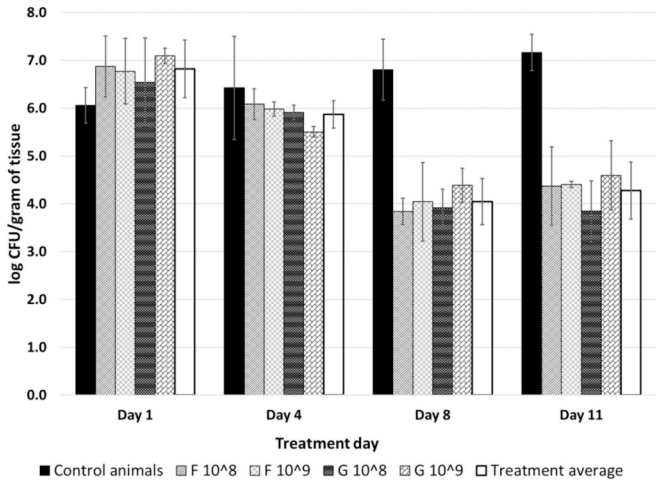

Fig. 6. Evaluation of the antibacterial effect of combined gum Karaya injectable hydrogel/hydrogel film with phage preparation on staphylococcal infection, hydrogel films only, injectable hydrogel only or untreated wounds during the treatment of methicillin-resistant *S. aureus* infection. The **graph shows the amount of the pathogen in the tissue** on each treatment day. **Control animals** = amount of pathogen in wounds of control animals (no treatment) over time. **F 10^8** = treatment using GK hydrogel film containing phage preparation at a concentration of 10^8 PFU/wound. **F 10^9** = treatment using GK hydrogel film containing phage preparation at a concentration of 10^9 PFU/wound. **G 10^8** = treatment using GK injectable hydrogel containing phage preparation concentration at a of 10^8 PFU/wound. **G 10^9** = treatment using GK injectable hydrogel containing phage preparation at a concentration of 10^9 PFU/wound. **Treatment average** = average amount of pathogen in the tissue calculated as an average of all tested treatment options. A significant reduction in bacterial load was achieved within one week of treatment (Day 8 and Day 11; $p < 0.001$). Treatment options were not significantly different from each other at any timepoint ($p > 0.05$).

data obtained from the microbiological evaluation of biopsy tissue samples showed average initial levels of 6.8 ± 0.52 log CFU/gram of tissue. The bacterial load in the wounds decreased to 4.3 ± 0.59 log CFU/gram of tissue ($p < 0.001$), with a mean reduction of 2.5 log CFU/gram of tissue between day 1 (samples were collected prior to the first treatment administration) and day 11 of the treatment of infection.

Specifically, 11-day treatment using GK hydrogel film containing 10^8 PFU/wound of phage resulted in a reduction to 4.4 ± 0.82 log CFU/gram tissue ($p < 0.001$). Treatment using GK hydrogel film containing 10^9 PFU/wound of phage preparation resulted in a reduction to 4.4 ± 0.06 log CFU/gram tissue ($p < 0,001$). Treatment using GK injectable hydrogel containing phage preparation at a concentration of 10^8 PFU/wound resulted in a reduction to values of 3.8 ± 0.64 log CFU/gram tissue ($p < 0.001$), and treatment using GK injectable hydrogel containing 1 mL of phage preparation at a concentration of 10^9 PFU/wound led to a reduction to values of 4.6 ± 0.72 log CFU/gram tissue ($p < 0.001$). It was statistically confirmed that the treatments were not significantly different from each other at any timepoint ($p > 0.05$). A significant reduction in bacterial load was achieved within one week of treatment, $p < 0.001$ (see Fig. 6, Control animals vs. other results, and Supplementary Fig. 1).

Wounds left untreated or treated only with GK hydrogel film or injectable hydrogel without phage preparation were gradually contaminated by phage preparation during the study. Therefore, these results were not considered statistically relevant.

3.7. Histopathological evaluation of the antibacterial effect of combined GK injectable hydrogel/hydrogel film with phage preparation on staphylococcal infection

Haematoxylin-eosin-stained samples from the treatment day 1 (samples were collected prior to the first treatment administration), were characterized by significant tissue infiltration by inflammatory cells with a predominance of polymorphonuclear cells and macrophages accompanied by apparent vasodilatation. Treatment day 4 showed tissue hyperemia, vasodilation, neoangiogenesis, infiltration by inflammatory cells (polymorphonuclear cells, macrophages), and increased fibroblast activity. On treatment day 8, inflammatory cells were distributed in the wound periphery. On treatment day 11, neoangiogenesis, reduction of inflammatory infiltrate, increased fibroblast activity (collagen production), and gradual organization of the granulation tissue margins were observed (Fig. 7).

Gram stainingof the samples collected on treatment day 1 (samples were collected prior to the first administration of treatment) showed extensive areas of staphylococcal cells within the wound tissue and on its surface. On treatment day 4, only a few localized areas of staphylococcal cells were visible within the wound tissue. On treatment days 8 and 11, no areas of staphylococcal cells were visible within the wound tissue (Fig. 8).

3.8. Visual assessment of the antibacterial effect of combined GK injectable hydrogel/hydrogel film with phage preparation on staphylococcal infection

In addition to the assessment of the antibacterial effect of the

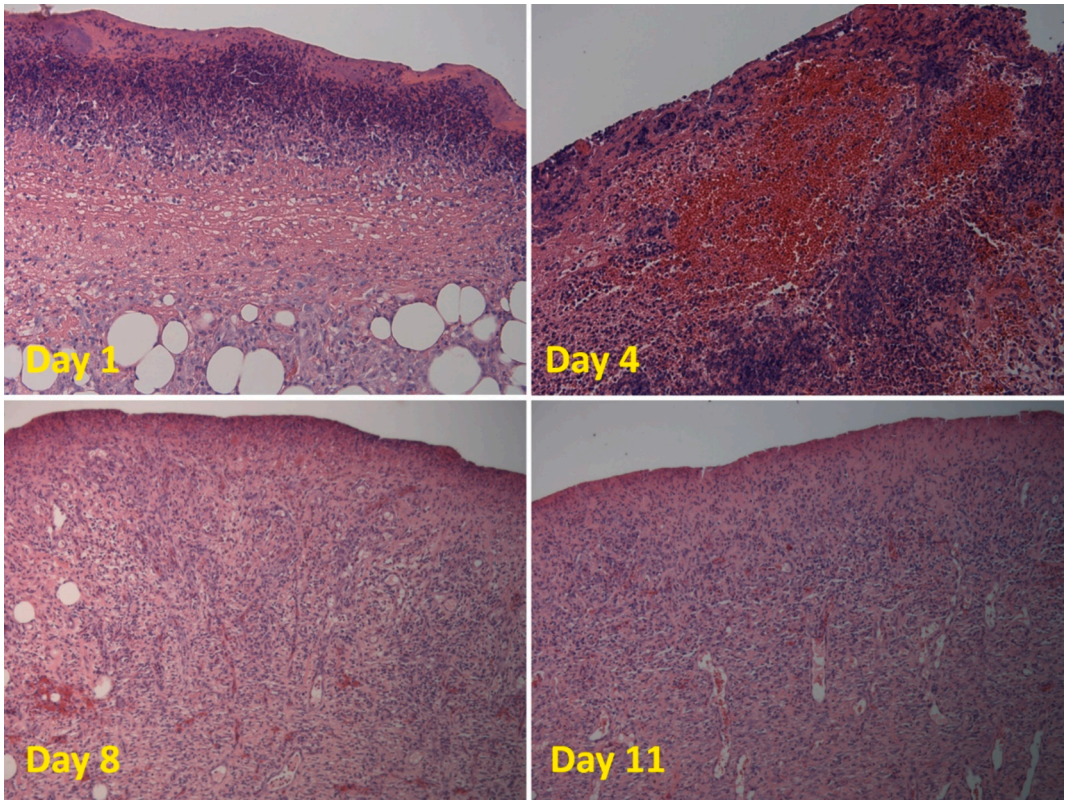

Fig. 7. Histopathological evaluation of the antibacterial effect of the combined gum Karaya hydrogel film/injectable hydrogel with phage preparation on staphylococcal infection. On the treatment day 1 (samples were obtained prior to the first treatment administration), **Haematoxylin-eosin-stained samples** were characterized by a significant tissue infiltration by inflammatory cells with a predominance of polymorphonuclear cells and macrophages accompanied by apparent vasodilatation. Day 4 of treatment showed tissue hyperemia, vasodilation, neoangiogenesis, infiltration by inflammatory cells (polymorphonuclear cells, macrophages), and increased fibroblast activity. On treatment day 8, inflammatory cells were distributed in the wound periphery. On treatment day 11, neoangiogenesis, reduction of inflammatory infiltrate, increased fibroblast activity (collagen production), and gradual organization of granulation tissue margins were observed.

combination of the GK injectable hydrogel/hydrogel film with phage preparation on staphylococcal infection, the visual appearance of the wounds was compared to the wounds of untreated control animals. The wounds of untreated animals showed local signs of inflammation with purulent discharge, which persisted till the end of the experiment. In contrast, the wounds of treated animals showed local signs of inflammation up to day 4 only. Since treatment day 8, local signs of inflammation have receded, with clear evidence of re-epithelization and wound contraction (Fig. 9).

4. Discussion

Skin and soft tissue infections (SSTIs) cover a wide range of pathological conditions, from mild superficial infections to severe necrotizing infections requiring hospitalization in an intensive care unit (ICU). Hospital-acquired infections have a significant impact on the morbidity and mortality of hospitalized patients. In surgical departments, particularly in burn units, wound infections are the most common local complication (Posluszny et al., 2011). Treatment of such infections is often complicated by the ever-increasing antibiotic resistance. These infections prolong hospital stays and increase treatment costs, thus having a significant negative economic impact (Dadgostar, 2019).

SSTIs are often caused by Gram-positive pathogens, with *S. aureus* being the most common causative agent. In practice, highly resistant bacterial strains are rapidly emerging, most commonly methicillin-resistant *S. aureus* (MRSA) strains. Despite the emergence of highly resistant microorganisms and the urgent medical need for new antimicrobials, their development has slowed down and is not fast enough to prevent the emergence of new highly resistant bacterial strains. In the last 20 years, only two new classes of antibiotics (lipopeptides and oxazolidinones) have been developed and approved by international drug agencies – the US Food and Drug Administration and the European Medicines Agency (Tacconelli et al., 2018). The main reasons for this slowdown include the high cost of developing new antibiotics and the limited choice of suitable candidates. The limited development of new antibiotics highlights the need for alternative therapies against bacterial infections. One promising alternative is bacteriophage (phage) therapy (Abedon et al., 2011; Górski et al., 2016; Lawrence et al., 2019; Loc-Carrillo and Abedon, 2011; Ofir and Sorek, 2018).

A recent systematic review (Uyttebroek et al., 2022) addressing the safety and efficacy of phage therapy, which includes 52 safety studies and 59 efficacy studies, concluded that only 7 % of patients developed mild side effects that persisted for the duration of phage therapy, while no side effects were observed in the remaining patients. At the same time, clinical improvement was observed in 79 % of patients, and bacterial eradication was observed in 87 % of patients treated with phage therapy.

More specifically, two observational studies focusing on chronic wounds involving 20 (Gupta et al., 2019) and 48 patients (Patel et al., 2021), respectively, showed mild side effects in only one patient. Nevertheless, a significant therapeutic effect was observed in all of them. As another example, a randomized clinical trial (phase I) on the safety of phage therapy in patients with chronic tibial ulcers found no difference between the treated ($n = 20$) and untreated ($n = 22$) groups, with no side effects observed in any of the groups.

The main advantages of phage therapy comprise the bactericidal effect (strict use of lytic phages is necessary), multiplication of phage particles in the presence of the target (bacterial cells), minimal

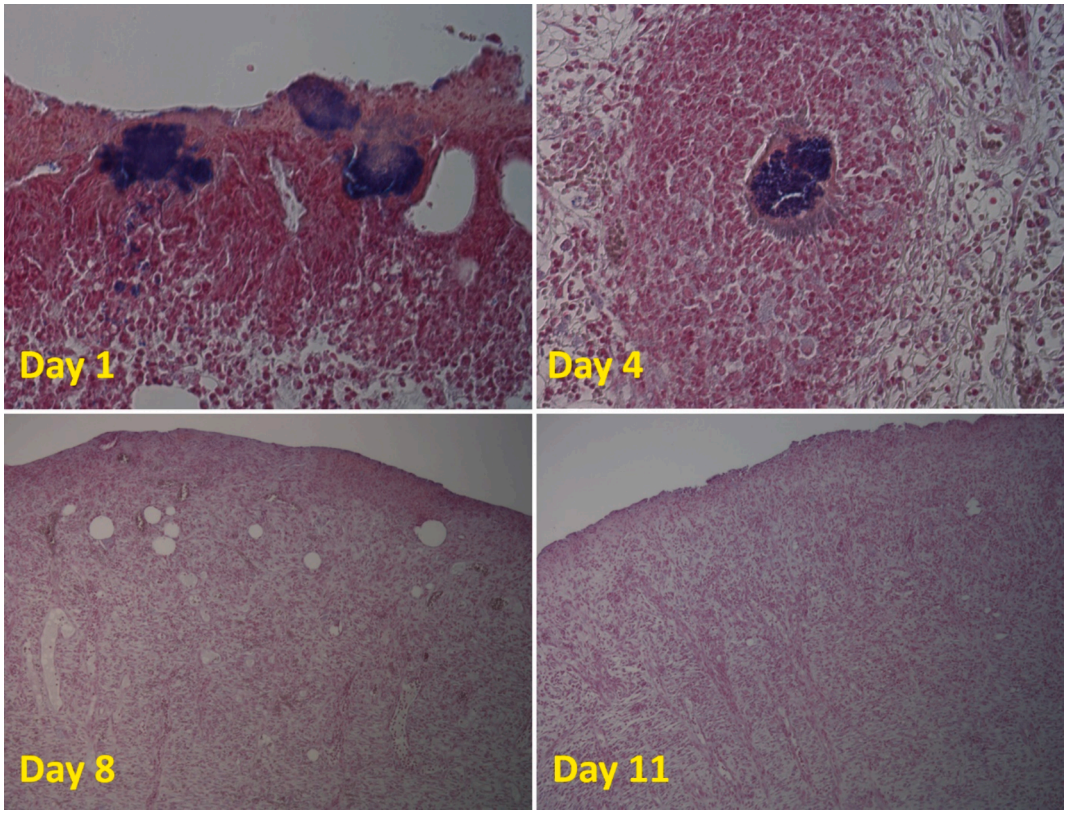

Fig. 8. Histopathological evaluation of the antibacterial effect of the combined gum Karaya hydrogel film/injectable hydrogel with phage preparation on staphylococcal infection. On treatment day 1 (samples were collected prior to the first treatment administration), **Gram staining** showed extensive areas of staphylococcal cells within the wound tissue and on its surface. On treatment day 4, only a few localized areas of staphylococcal cells were visible within the wound tissue. On treatment days 8 and 11, no areas of staphylococcal cells were visible within the wound tissue. Day 1 – 200× magnification, Day 4 – 400× magnification, Day 8 – 100× magnification, Day 11 – 100× magnification.

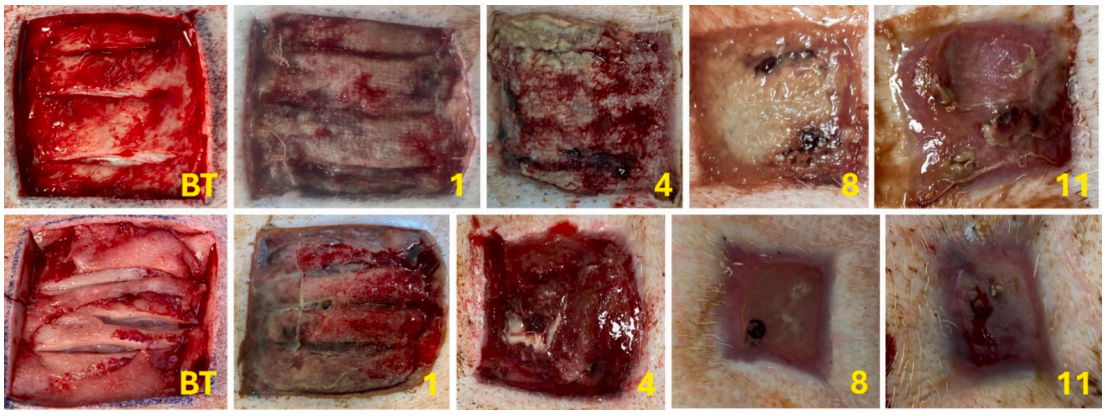

Fig. 9. Visual evaluation of the antibacterial effect of the combined gum Karaya hydrogel with phage preparation on staphylococcal infection. **Top row: untreated wounds; bottom row: treated wounds**. Deep skin and soft tissue defects were surgically performed three days before the treatment (top and bottom left photographs, **"BT"**). Other photographs were taken on **days 1, 4, 8, and 11** of the study. The wounds of untreated animals showed local signs of inflammation, with purulent discharge remaining till the end of the experiment. In contrast, the wounds of treated animals (both GK injectable hydrogel or hydrogel film with phage preparation) showed local signs of inflammation up to day 4 only. Since treatment day 8, local signs of inflammation have receded, with clear evidence of re-epithelization and wound contraction.

disruption of the normal microbiome due to specific recognition of the host bacterial cell and low to unmeasurable toxicity to eukaryotic cells. Other advantages can be found, such as low induction of resistance (especially when using phage cocktails or personalized phage therapy), versatility of use or relatively low production costs (Loc-Carrillo and Abedon, 2011; Principi et al., 2019). Bacteriophages of the genus *Kayvirus* (family *Herelleviridae*) are very promising agents due to their high lytic activity and polyvalence (a wide range of *S. aureus* and even non-*S. aureus* staphylococcal species can be targeted). The genomic (Cui et al., 2017; Łobocka et al., 2012; Vandersteegen et al., 2011), transcriptomic (Finstrlová et al., 2022), proteomic (Eyer et al., 2007), immunological (Kaźmierczak et al., 2021), and structural (Nováček et al., 2016) characterization of phages from the genus *Kayvirus* suggests that the phages are safe for medical use.

The phage 812K1/420 used in this study (GenBank/ENA/DDBJ accession number KJ206563.2) does not carry genes for antibiotic resistance, bacterial virulence factors or sequences derived from mobile elements. Similarly, no acquisition of the genes for lysogeny was found in the analyzed phage genomes (Botka et al., 2019). A host range of the phage 812K1/420 was previously investigated and described, e.g. in Botka et al. (2019), where 75.8 % of methicillin-resistant *S. aureus* (MRSA) strains were susceptible (n = 186), or in Dvořáčková et al. (2020), where 90.4 % of *S. aureus* strains tested (n = 867) were susceptible to the Stafal® preparation (containing a cocktail of Kayviruses including 812 K1/420). In the study, an even higher proportion of MRSA strains were susceptible to this preparation (99.0 %, n = 196).

Phage preparations also benefit from an appropriate delivery system. A growing body of evidence suggests that hydrogel films effectively absorb phage into the dry hydrogel matrix due to its high absorption capacity (Postulkova et al., 2018), cover the wound, deliver phages to the wound site, and release them into the moist wound site due to their hydrophilic characteristics (Kaur et al., 2019). Injectable hydrogels possess similar properties, such as hydrogel films, and they effectively deliver and release phages into the wound site (Chang et al., 2021). Compared to hydrogel films, injectable hydrogel possesses moldability, filling and covering the whole wound site (Yang et al., 2022) while providing a hydrated environment suitable for phage migration within the hydrogel and into the wound (Yan et al., 2021).

Moreover, the hydrophilic character of both used materials, injectable hydrogels and hydrogel films, allows moist wound healing, provide optimal conditions for re-epithelization, improves the fluid balance in the wound bed (exudate or transudate management), and supports complete wound closure (Chang et al., 2020; Kim et al., 2021; Pinto et al., 2020; Shen et al., 2021).

In this study, we have successfully induced deep staphylococcal SSTI in a porcine model. Most studies classify a bacterial load of 10^5 CFU/gram of tissue or higher as critical for acute or chronic wound infection (Robson and Heggers, 1969). In addition, Breidenbach and Trager (1995) demonstrated that a critical bacteria load of $\geq 10^4$ CFU/gram of tissue is required to cause infection in complex extremity wounds. Both criteria were met within three days when the deep SSTI fully developed and achieved an average number of 6.1 ± 0.4 log CFU/gram of tissue. During the study, the average number of bacterial cells within the tissue (biopsy samples) of control animals continued to increase ($p = 0.003$) to the final amount of 7.2 ± 0.4 log CFU/gram of tissue.

Further, we have demonstrated that both the GK hydrogel films and injectable hydrogels can be successfully used as an effective phage delivery system that simultaneously supports moist wound healing and provides optimal conditions for re-epithelialization. To our knowledge, this is the first study to evaluate the combined effects of GK and phage therapy. Although GK hydrogel films or injectable hydrogels alone could not suppress the staphylococcal infection, the synergistic activity resulted in an average reduction of 2.5 log CFU/gram of tissue of staphylococcal pathogen within one week of treatment. Local signs of inflammation were observed in the wounds of treated animals up to treatment day 4. By treatment day 8, local signs of inflammation had receded, with clear evidence of re-epithelization and wound contraction. No side effects of the GK polysaccharide hydrogel film or injectable hydrogel treatment were observed during the study.

No statistically significant differences between the four treatment modalities were found at any time point. Nevertheless, it can be assumed that injectable gels may be more suitable for, e.g., deep, irregular wounds that produce less exudate, while films could be suited for superficial, regular wounds that produce more exudate as they have the potential to absorb more exudate.

The results of the presented study highlight the potential of the GK-based delivery systems for phage therapy as a viable and safe option for the treatment of SSTIs. Further, this approach enables the treatment strategy to be adjusted for specific situations or individuals and offers a promising avenue for future research and clinical applications in the treatment of infections caused by antibiotic-resistant bacteria.

4.1. Limitations of the study

A certain limitation of the presented study lies in the gradual spread of the phage particles to wounds that were not primarily treated using either the GK hydrogel film or injectable hydrogel supplemented by phage preparation in animals subjected to such treatment. However, this might be rather due to the haematogenic spread of phage particles than cross-contamination of the wounds. This phenomenon limits the testing of preparations with and without phages on a single individual and, therefore, does not allow a direct comparison of the antimicrobial effect of these preparations on a given individual.

5. Conclusions

Skin and soft tissue infections (SSTIs) pose a significant challenge in medical practice, particularly in surgical departments and burn units, where complications like wound infections are prevalent. The increasing antibiotic resistance complicates the treatment of these infections, leading to prolonged hospitalization and increased economic burden.

Given the limited development of new antibiotics in recent decades, alternative therapies are urgently needed. Bacteriophage (phage) therapy is emerging as a promising option, offering advantages such as bactericidal activity, minimal disruption of the normal microbiome, and minimal toxicity to eukaryotic cells. Phages of the genus *Kayvirus*, particularly the assessed strain 812K1/420, exhibit high lytic activity and safety for medical use.

This study explores using a *Herelleviridae* phage in a novel delivery system based on GK hydrogel films and injectable hydrogels. The results demonstrate the efficacy of this combined approach in the treatment of deep staphylococcal SSTIs in a porcine model. The GK hydrogels and hydrogel films, when used as a delivery system for phage therapy, contribute to moist wound healing, optimal conditions for re-epithelialization, and wound closure.

Notably, the study shows a synergistic effect of GK and phage therapy, resulting in a significant reduction in bacterial load within one week of treatment. Local signs of inflammation were reduced and there was evidence of re-epithelialization and wound contraction. Importantly, no adverse effects of the GK polysaccharide hydrogel film or injectable hydrogel were observed during the study.

These results highlight the potential of the GK-based delivery system for phage therapy as a viable and safe option for the treatment of deep wound SSTIs. This offers a promising avenue for future research and clinical applications in the treatment of infections caused by antibiotic-resistant bacteria.

CRediT authorship contribution statement

L. Vacek: Writing – review & editing, Writing – original draft, Visualization, Validation, Project administration, Methodology, Investigation, Formal analysis, Data curation, Conceptualization. **D. Polaštík Kleknerová:** Investigation, Formal analysis, Data curation. **B. Lipový:** Writing – review & editing, Writing – original draft, Visualization, Validation, Supervision, Resources, Project administration, Methodology, Investigation, Funding acquisition, Formal analysis, Data curation, Conceptualization. **J. Holoubek:** Writing – review & editing, Writing – original draft, Investigation, Data curation. **D. Matysková:** Writing – review & editing, Writing – original draft, Investigation, Data curation. **E. Černá:** Writing – review & editing, Writing – original draft, Visualization, Validation, Methodology, Investigation, Formal analysis, Data curation. **J. Brtníková:** Writing – review & editing, Writing – original draft, Visualization, Validation, Methodology, Investigation, Formal analysis, Data curation. **E. Jeklová:** Writing – review & editing, Writing – original draft, Validation, Methodology, Investigation, Data curation. **Š. Kobzová:** Writing – review & editing, Methodology, Investigation,

Formal analysis, Data curation. **L. Janda:** Writing – review & editing, Validation, Methodology, Investigation, Funding acquisition, Formal analysis, Data curation, Conceptualization. **L. Lišková:** Writing – review & editing, Visualization, Methodology, Investigation, Formal analysis, Data curation. **D. Diabelko:** Writing – review & editing, Investigation, Formal analysis, Data curation. **T. Botka:** Writing – review & editing, Methodology, Investigation, Conceptualization. **R. Pantůček:** Writing – review & editing, Writing – original draft, Visualization, Validation, Methodology, Investigation, Formal analysis, Data curation, Conceptualization. **F. Růžička:** Writing – review & editing, Writing – original draft, Visualization, Validation, Supervision, Resources, Project administration, Methodology, Investigation, Funding acquisition, Formal analysis, Data curation, Conceptualization. **L. Vojtová:** Writing – review & editing, Writing – original draft, Visualization, Validation, Supervision, Resources, Project administration, Methodology, Investigation, Funding acquisition, Formal analysis, Data curation, Conceptualization.

Declaration of competing interest

The authors declare that they have no known competing financial interests or personal relationships that could have appeared to influence the work reported in this paper.

Data availability

We hasuppl_fig_1_BW.xlsx“ data file anve attached supplementary Fig. 1 as a ”Staphylococcus_d uploaded data to the Mendeley data repository (Reserved DOI: 10.17632/hbx9bfnp3m.1).

Acknowledgements

The *Staphylococcus aureus* strain NRL/Atb 5921 was kindly provided by Prof. Helena Žemličková (National Reference Laboratory for Antibiotics, National Institute of Public Health – Prague, Czech Republic). This work was supported by the Ministry of Heath of the Czech Republic, grant number NU20-05-00166.

Appendix A. Supplementary data

Supplementary data to this article can be found online at https://doi.org/10.1016/j.ijpharm.2024.124348.

References

Abedon, S.T., Kuhl, S.J., Blasdel, B.G., Kutter, E.M., 2011. Phage treatment of human infections. Bacteriophage 1, 66–85. https://doi.org/10.4161/bact.1.2.15845.

Botka, T., Pantůček, R., Mašlaňová, I., Benešík, M., Petráš, P., Růžičková, V., Havlíčková, P., Varga, M., Žemličková, H., Koláčková, I., Florianová, M., Jakubů, V., Karpíšková, R., Doškař, J., 2019. Lytic and genomic properties of spontaneous host-range Kayvirus mutants prove their suitability for upgrading phage therapeutics against staphylococci. Sci. Rep. 9, 5475. https://doi.org/10.1038/s41598-019-41868-w.

Breidenbach, W.C., Trager, S., 1995. Quantitative culture technique and infection in complex wounds of the extremities closed with free flaps. Plast. Reconstr. Surg. 95, 860–865.

Chang, R.Y.K., Morales, S., Okamoto, Y., Chan, H.-K., 2020. Topical application of bacteriophages for treatment of wound infections. Transl. Res. 220, 153–166. https://doi.org/10.1016/j.trsl.2020.03.010.

Chang, R.Y.K., Okamoto, Y., Morales, S., Kutter, E., Chan, H.-K., 2021. Hydrogel formulations containing non-ionic polymers for topical delivery of bacteriophages. Int. J. Pharm. 605, 120850 https://doi.org/10.1016/j.ijpharm.2021.120850.

Chen, L., Kumar, S., Wu, H., 2023. A review of current antibiotic resistance and promising antibiotics with novel modes of action to combat antibiotic resistance. Arch. Microbiol. 205, 356. https://doi.org/10.1007/s00203-023-03699-2.

Cui, Z., Guo, X., Dong, K., Zhang, Y., Li, Q., Zhu, Y., Zeng, L., Tang, R., Li, L., 2017. Safety assessment of Staphylococcus phages of the family Myoviridae based on complete genome sequences. Sci. Rep. 7, 41259. https://doi.org/10.1038/srep41259.

Dadgostar, P., 2019. Antimicrobial resistance: implications and costs. Infect. Drug Resist. 12, 3903–3910. https://doi.org/10.2147/IDR.S234610.

Drápalová, E., Michlovská, L., Poštulková, H., Chamradová, I., Lipový, B., Holoubek, J., Vacek, L., Růžička, F., Hanslianová, M., Svobodová, T., Černá, E., Hrdličková, B., Vojtová, L., 2023. Antimicrobial cost-effective transparent hydrogel films from renewable gum karaya/chitosan polysaccharides for modern wound dressings. ACS Appl. Polym. Mater. 5, 2774–2786. https://doi.org/10.1021/acsapm.3c00025.

Dvořáčková, M., Růžička, F., Dvořáková Heroldová, M., Vacek, L., Bezděková, D., Benešík, M., Petráš, P., Pantůček, R., 2020. Možnosti terapeutického ovlivnění stafylokokových infekcí prostřednictvím bakteriofágů a vybrané metody testování citlivosti stafylokoků in vitro. Epidemiol. Mikrobiol. Imunol. 69, 10–18. ISSN 1210-7913.

Esposito, S., Bassetti, M., Bonnet, E., Bouza, E., Chan, M., De Simone, G., Dryden, M., Gould, I., Lye, D.C., Saeed, K., Segreti, J., Unal, S., Yalcin, A.N., 2016. Hot topics in the diagnosis and management of skin and soft-tissue infections. Int. J. Antimicrob. Agents 48, 19–26. https://doi.org/10.1016/j.ijantimicag.2016.04.011.

Eyer, L., Pantůček, R., Zdráhal, Z., Konečná, H., Kašpárek, P., Růžičková, V., Hernychová, L., Preisler, J., Doškař, J., 2007. Structural protein analysis of the polyvalent staphylococcal bacteriophage 812. Proteomics 7, 64–72. https://doi.org/10.1002/pmic.200600280.

Finstrlová, A., Mašlaňová, I., Blasdel Reuter, B.G., Doškař, J., Götz, F., Pantůček, R., 2022. Global Transcriptomic analysis of bacteriophage-host interactions between a Kayvirus Therapeutic Phage and Staphylococcus aureus. Microbiol. Spectr. 10, e0012322.

Górski, A., Międzybrodzki, R., Weber-Dąbrowska, B., Fortuna, W., Letkiewicz, S., Rogóż, P., Jończyk-Matysiak, E., Dąbrowska, K., Majewska, J., Borysowski, J., 2016. Phage therapy: combating infections with potential for evolving from merely a treatment for complications to targeting diseases. Front. Microbiol. 7, 1515. https://doi.org/10.3389/fmicb.2016.01515.

Gupta, P., Singh, H.S., Shukla, V.K., Nath, G., Bhartiya, S.K., 2019. Bacteriophage therapy of chronic nonhealing wound: clinical study. Int. J. Low. Extrem. Wounds 18, 171–175. https://doi.org/10.1177/1534734619835115.

Kaur, P., Gondil, V.S., Chhibber, S., 2019. A novel wound dressing consisting of PVA-SA hybrid hydrogel membrane for topical delivery of bacteriophages and antibiotics. Int. J. Pharm. 572, 118779 https://doi.org/10.1016/j.ijpharm.2019.118779.

Kaźmierczak, Z., Majewska, J., Miernikiewicz, P., Międzybrodzki, R., Nowak, S., Harhala, M., Lecion, D., Kęska, W., Owczarek, B., Ciekot, J., Drab, M., Kędzierski, P., Mazurkiewicz-Kania, M., Górski, A., Dąbrowska, K., 2021. Immune response to therapeutic staphylococcal bacteriophages in mammals: kinetics of induction, immunogenic structural proteins, natural and induced antibodies. Front. Immunol. 12, 639570 https://doi.org/10.3389/fimmu.2021.639570.

Ki, V., Rotstein, C., 2008. Bacterial skin and soft tissue infections in adults: a review of their epidemiology, pathogenesis, diagnosis, treatment and site of care. Can. J. Infect. Dis. Med. Microbiol. 19, 173–184. https://doi.org/10.1155/2008/846453.

Kim, H.Y., Chang, R.Y.K., Morales, S., Chan, H.-K., 2021. Bacteriophage-delivering hydrogels: current progress in combating antibiotic resistant bacterial infection. Antibiotics 10, 130. https://doi.org/10.3390/antibiotics10020130.

Lawrence, Baldridge, Handley, 2019. Phages and human health: more than idle hitchhikers. Viruses 11, 587. https://doi.org/10.3390/v11070587.

Lipový, B., Holoubek, J., Vacek, L., Růžička, F., Nedomová, E., Poštulková, H., Vojtová, L., 2018. Antimicrobial effect of novel hydrogel matrix based on natural polysaccharide Sterculia urens. Epidemiol. Mikrobiol. Imunol. 67, 166–174.

Łobocka, M., Hejnowicz, M.S., Dąbrowski, K., Gozdek, A., Kosakowski, J., Witkowska, M., Ulatowska, M.I., Weber-Dąbrowska, B., Kwiatek, M., Parasion, S., Gawor, J., Kosowska, H., Głowacka, A., 2012. Genomics of Staphylococcal Twort-like Phages -. In: Potential Therapeutics of the Post-Antibiotic Era, in: Advances in Virus Research. Academic Press, pp. 143–216. https://doi.org/10.1016/B978-0-12-394438-2.00005-0.

Loc-Carrillo, C., Abedon, S.T., 2011. Pros and cons of phage therapy. Bacteriophage 1, 111–114. https://doi.org/10.4161/bact.1.2.14590.

Nováček, J., Šiborová, M., Benešík, M., Pantůček, R., Doškař, J., Plevka, P., 2016. Structure and genome release of Twort-like Myoviridae phage with a double-layered baseplate. Proc. Natl. Acad. Sci. 113, 9351–9356. https://doi.org/10.1073/pnas.1605883113.

Ofir, G., Sorek, R., 2018. Contemporary phage biology: from classic models to new insights. Cell 172, 1260–1270. https://doi.org/10.1016/j.cell.2017.10.045.

Patel, D.R., Bhartiya, S.K., Kumar, R., Shukla, V.K., Nath, G., 2021. Use of customized bacteriophages in the treatment of chronic nonhealing wounds: a prospective study. Int. J. Low. Extrem. Wounds 20, 37–46. https://doi.org/10.1177/1534734619881076.

Petrovic Fabijan, A., Lin, R.C.Y., Ho, J., Maddocks, S., Ben Zakour, N.L., Iredell, J.R., Khalid, A., Venturini, C., Chard, R., Morales, S., Sandaradura, I., Gilbey, T., 2020. Safety of bacteriophage therapy in severe Staphylococcus aureus infection. Nat. Microbiol. 5, 465–472. https://doi.org/10.1038/s41564-019-0634-z.

Pinto, A.M., Cerqueira, M.A., Bañobre-Lópes, M., Pastrana, L.M., Sillankorva, S., 2020. Bacteriophages for chronic wound treatment: from traditional to novel delivery systems. Viruses 12, 235. https://doi.org/10.3390/v12020235.

Posluszny, J.A., Conrad, P., Halerz, M., Shankar, R., Gamelli, R.L., 2011. Surgical burn wound infections and their clinical implications. J. Burn Care Res. 32, 324–333. https://doi.org/10.1097/BCR.0b013e31820aaffe.

Postulkova, H., Chamradova, I., Pavlinak, D., Humpa, O., Jancar, J., Vojtova, L., 2017. Study of effects and conditions on the solubility of natural polysaccharide gum karaya. Food Hydrocoll. 67, 148–156. https://doi.org/10.1016/j.foodhyd.2017.01.011.

Postulkova, H., Nedomova, E., Hearnden, V., Holland, C., Vojtova, L., 2018. Hybrid hydrogels based on polysaccharide gum karaya, poly(vinyl alcohol) and silk fibroin. Mater. Res. Express 6, 035304. https://doi.org/10.1088/2053-1591/aaf45d.

Principi, N., Silvestri, E., Esposito, S., 2019. Advantages and limitations of bacteriophages for the treatment of bacterial infections. Front. Pharmacol. 10, 513. https://doi.org/10.3389/fphar.2019.00513.

Robson, M.C., Heggers, J.P., 1969. Bacterial quantification of open wounds. Mil. Med. 134, 19–24.

Sambrook, J., Russell, D.W., 2001. Molecular cloning: a laboratory manual. Cold Spring Harbor Laboratory Press, New York, N.Y., United States.

Shen, H.-Y., Liu, Z.-H., Hong, J.-S., Wu, M.-S., Shiue, S.-J., Lin, H.-Y., 2021. Controlled-release of free bacteriophage nanoparticles from 3D-plotted hydrogel fibrous structure as potential antibacterial wound dressing. J. Control. Release 331, 154–163. https://doi.org/10.1016/j.jconrel.2021.01.024.

Tacconelli, E., Carrara, E., Savoldi, A., Harbarth, S., Mendelson, M., Monnet, D.L., Pulcini, C., Kahlmeter, G., Kluytmans, J., Carmeli, Y., Ouellette, M., Outterson, K., Patel, J., Cavaleri, M., Cox, E.M., Houchens, C.R., Grayson, M.L., Hansen, P., Singh, N., Theuretzbacher, U., Magrini, N., Aboderin, A.O., Al-Abri, S.S., Awang Jalil, N., Benzonana, N., Bhattacharya, S., Brink, A.J., Burkert, F.R., Cars, O., Cornaglia, G., Dyar, O.J., Friedrich, A.W., Gales, A.C., Gandra, S., Giske, C.G., Goff, D.A., Goossens, H., Gottlieb, T., Guzman Blanco, M., Hryniewicz, W., Kattula, D., Jinks, T., Kanj, S.S., Kerr, L., Kieny, M.-P., Kim, Y.S., Kozlov, R.S., Labarca, J., Laxminarayan, R., Leder, K., Leibovici, L., Levy-Hara, G., Littman, J., Malhotra-Kumar, S., Manchanda, V., Moja, L., Ndoye, B., Pan, A., Paterson, D.L., Paul, M., Qiu, H., Ramon-Pardo, P., Rodríguez-Baño, J., Sanguinetti, M., Sengupta, S., Sharland, M., Si-Mehand, M., Silver, L.L., Song, W., Steinbakk, M., Thomsen, J., Thwaites, G.E., van der Meer, J.W., Van Kinh, N., Vega, S., Villegas, M. V., Wechsler-Fördös, A., Wertheim, H.F.L., Wesangula, E., Woodford, N., Yilmaz, F. O., Zorzet, A., 2018. Discovery, research, and development of new antibiotics: the WHO priority list of antibiotic-resistant bacteria and tuberculosis. Lancet Infect. Dis. 18, 318–327. https://doi.org/10.1016/S1473-3099(17)30753-3.

The European Committee on Antimicrobial Susceptibility Testing, 2023. Breakpoint tables for interpretation of MICs and zone diameters. Version 14.0 [WWW Document]. URL https://www.eucast.org/clinical_breakpoints (accessed 3.1.23).

Uyttebroek, S., Chen, B., Onsea, J., Ruythooren, F., Debaveye, Y., Devolder, D., Spriet, I., Depypere, M., Wagemans, J., Lavigne, R., Pirnay, J.-P., Merabishvili, M., De Munter, P., Peetermans, W.E., Dupont, L., Van Gerven, L., Metsemakers, W.-J., 2022. Safety and efficacy of phage therapy in difficult-to-treat infections: a systematic review. Lancet. Infect. Dis. 22, e208–e220. https://doi.org/10.1016/S1473-3099(21)00612-5.

Vacek, L., Kobzová, Š., Čmelík, R., Pantůček, R., Janda, L., 2020. Enzybiotics LYSSTAPH-S and LYSDERM-S as potential therapeutic agents for chronic MRSA wound infections. Antibiotics 9, 519. https://doi.org/10.3390/antibiotics9080519.

Vandersteegen, K., Mattheus, W., Ceyssens, P.-J., Bilocq, F., De Vos, D., Pirnay, J.-P., Noben, J.-P., Merabishvili, M., Lipinska, U., Hermans, K., Lavigne, R., 2011. Microbiological and molecular assessment of bacteriophage ISP for the control of Staphylococcus aureus. PLoS One 6, e24418.

World Health Organization, 2023. Antimicrobial resistance [WWW Document]. URL https://www.who.int/news-room/fact-sheets/detail/antimicrobial-resistance (accessed 1.8.24).

Yan, W., Banerjee, P., Liu, Y., Mi, Z., Bai, C., Hu, H., To, K.K.W., Duong, H.T.T., Leung, S. S.Y., 2021. Development of thermosensitive hydrogel wound dressing containing Acinetobacter baumannii phage against wound infections. Int. J. Pharm. 602, 120508 https://doi.org/10.1016/j.ijpharm.2021.120508.

Yang, X., Wang, B., Peng, D., Nie, X., Wang, J., Yu, C.-Y., Wei, H., 2022. Hyaluronic acid-based injectable hydrogels for wound dressing and localized tumor therapy: a review. Adv. Nanobiomed Res. 2, 2200124. https://doi.org/10.1002/anbr.202200124.

APPENDIX 11

Kuntová L, Mašlaňová I, Obořilová R, Šimečková H, Finstrlová A, Bárdy P, Šiborová M, Troianovska L, Botka T, Gintar P, Šedo O, Farka Z, Doškař J, Pantůček R (2023) *Staphylococcus aureus* prophage-encoded protein causes abortive infection and provides population immunity against kayviruses. *mBio* 14:e0249022.

https://doi.org/10.1128/mbio.02490-22

(JCR 2023: IF = 5.1; Q1 – Microbiology)

CC BY 4.0

AMERICAN SOCIETY FOR MICROBIOLOGY | mBio®

RESEARCH ARTICLE

Staphylococcus aureus Prophage-Encoded Protein Causes Abortive Infection and Provides Population Immunity against Kayviruses

Lucie Kuntová,[a] Ivana Mašlaňová,[a] Radka Obořilová,[a,b,c] Hana Šimečková,[a] Adéla Finstrlová,[a] Pavol Bárdy,[d] Marta Šiborová,[b] Liudmyla Troianovska,[a] Tibor Botka,[a] Petr Gintar,[b,e] Ondrej Šedo,[b] Zdeněk Farka,[a,b,c] Jiří Doškař,[a] Roman Pantůček[a]

[a]Department of Experimental Biology, Faculty of Science, Masaryk University, Brno, Czech Republic
[b]Central European Institute of Technology, Masaryk University, Brno, Czech Republic
[c]Department of Biochemistry, Faculty of Science, Masaryk University, Brno, Czech Republic
[d]Department of Chemistry, York Structural Biology Laboratory, University of York, York, United Kingdom
[e]National Centre for Biomolecular Research, Faculty of Science, Masaryk University, Brno, Czech Republic

Lucie Kuntová and Ivana Mašlaňová contributed equally to this work. Author order was determined alphabetically.

ABSTRACT Both temperate and obligately lytic phages have crucial roles in the biology of staphylococci. While superinfection exclusion among closely related temperate phages is a well-characterized phenomenon, the interactions between temperate and lytic phages in staphylococci are not understood. Here, we present a resistance mechanism toward lytic phages of the genus *Kayvirus*, mediated by the membrane-anchored protein designated Pdp_{Sau} encoded by *Staphylococcus aureus* prophages, mostly of the Sa2 integrase type. The prophage accessory gene pdp_{Sau} is strongly linked to the lytic genes for holin and ami2-type amidase and typically replaces genes for the toxin Panton-Valentine leukocidin (PVL). The predicted Pdp_{Sau} protein structure shows the presence of a membrane-binding α-helix in its N-terminal part and a cytoplasmic positively charged C terminus. We demonstrated that the mechanism of action of Pdp_{Sau} does not prevent the infecting kayvirus from adsorbing onto the host cell and delivering its genome into the cell, but phage DNA replication is halted. Changes in the cell membrane polarity and permeability were observed from 10 min after the infection, which led to prophage-activated cell death. Furthermore, we describe a mechanism of overcoming this resistance in a host-range *Kayvirus* mutant, which was selected on an *S. aureus* strain harboring prophage 53 encoding Pdp_{Sau}, and in which a chimeric gene product emerged via adaptive laboratory evolution. This first case of staphylococcal interfamily phage-phage competition is analogous to some other abortive infection defense systems and to systems based on membrane-destructive proteins.

IMPORTANCE Prophages play an important role in virulence, pathogenesis, and host preference, as well as in horizontal gene transfer in staphylococci. In contrast, broad-host-range lytic staphylococcal kayviruses lyse most *S. aureus* strains, and scientists worldwide have come to believe that the use of such phages will be successful for treating and preventing bacterial diseases. The effectiveness of phage therapy is complicated by bacterial resistance, whose mechanisms related to therapeutic staphylococcal phages are not understood in detail. In this work, we describe a resistance mechanism targeting kayviruses that is encoded by a prophage. We conclude that the defense mechanism belongs to a broader group of abortive infections, which is characterized by suicidal behavior of infected cells that are unable to produce phage progeny, thus ensuring the survival of the host population. Since the majority of staphylococcal strains are lysogenic, our findings are relevant for the advancement of phage therapy.

Editor Alison Buchan, University of Tennessee at Knoxville

Copyright © 2023 Kuntová et al. This is an open-access article distributed under the terms of the Creative Commons Attribution 4.0 International license.

Address correspondence to Roman Pantůček, pantucek@sci.muni.cz.

The authors declare no conflict of interest.

Received 19 September 2022
Accepted 19 January 2023
Published 13 February 2023

Downloaded from https://journals.asm.org/journal/mbio on 04 February 2026 by 147.251.86.90.

KEYWORDS *Staphylococcus aureus*, lysogeny, phage resistance, abortive infection, *Kayvirus*, cell death, phage therapy, bacteriophage evolution, bacteriophage therapy, bacteriophages

Bacteriophages are widespread across ecosystems and are among the most numerous entities on earth. Bacteria are constantly threatened by phage infection, and 20 to 40% of daily bacterial death is caused by bacteriophages (1). Conversely, the integrated genomes of prophages often promote beneficial phenotypic changes in their hosts (2) and play a major role in horizontal gene transfer, thus contributing to the evolution of bacterial pathogens (3).

Most *Staphylococcus aureus* isolates carry multiple siphoviral prophages in their genome (4) with an impact on virulence, toxin production, immune evasion, and host preference (5) as well as the mobilization of variable genetic elements (6) and dissemination of antibiotic resistance by transduction (7–9). Besides temperate staphylococcal siphoviruses, there are the strictly lytic myoviruses (10) and podoviruses (11) that are believed to be suitable for use as antimicrobial agents.

Over the last 2 decades, interest in using phages for the treatment of bacterial infections has increased enormously. Based on current clinical trials, phage therapy is efficient, safe, and acceptable for treatment in human medicine (12). The therapeutic potential of kayviruses with the type phage K (13) led to the characterization of many phage strains of this genus with an extremely broad host range (14) as was demonstrated for phage 812 (15). Kayviruses were studied to clarify their polyvalence (15, 16), lytic activity (17–19), synergistic effect with antibiotics (20), and interaction with the immune system (21); to describe their structure and genome delivery (22); and for safety assessments for therapy (23, 24). This progress in the implementation of kayviruses into safe phage therapy has been achieved by the characterization of staphylococcal phage-host interactions at the omics level, such as comparative genomics (10, 14, 15, 25), transcriptomics (26, 27), and proteomics studies (28).

One of the limitations of using kayviruses in medical practice is the possible resistance of staphylococcal species to these phages. During the constant competition between phages and their hosts, multiple bacterial phage resistance systems targeting various stages of the phage life cycle have evolved (29, 30). In staphylococci, these include various mechanisms, such as targeting foreign DNA by restriction modification (31), CRISPR-Cas immunity (32), protection against entry into the host cell through the modification of wall teichoic acids (33), overproduction of staphylococcal protein A (34), prophage-induced immunity (35), interference with phage reproduction mediated by pathogenicity islands (36), and the different host factors required for phage reproduction (37).

Some antiphage systems in staphylococci are yet to be discovered, namely, the large group of mechanisms categorized as abortive infections. Here, we report that temperate siphoviruses can protect the staphylococcal population from destruction by virulent *Kayvirus* phages by an abortive infection mechanism.

RESULTS AND DISCUSSION

Prophages induce insensitivity of *S. aureus* to kayviruses. Prophageless *S. aureus* strains ISP8 and 1039 were lysogenized by prophages 11, 29, 42E, 47, 53, 71, 77, 80α, 83A, 84, 85, or 96 and tested for susceptibility to lytic kayviruses 812, 812a, and K. The integration of prophages 47, 53, and 80α resulted in a resistant phenotype to the lytic phages 812 and K. Phage 53 was used for the lysogenization of multiple strains, including methicillin-resistant *S. aureus* (MRSA) USA300 (Table 1), which led to the establishment of a resistant phenotype to phages 812 and K independently of the genetic background of the lysogens. In models of cured strains NCTC 8511 (53^+)c and ISP8 (53^+)c, it was shown that sensitivity to both phages 812 and K is renewed after the prophage is lost. Similarly, *S. aureus* NCTC 8325, which is naturally resistant to phage 812, regained its sensitivity after all of its prophages were removed (Table 1). In contrast to phages 812 and K, prophages 47, 53, and 80α do not affect sensitivity to phage 812a, the phage 812 host-range mutant that originated during passaging phage 812 on *S. aureus* strain NCTC 8511 with prophage 53 (38) (Table 1).

Downloaded from https://journals.asm.org/journal/mbio on 04 February 2026 by 147.251.86.90.

TABLE 1 Staphylococcal strains used in this study and their sensitivity to lytic phages[a]

Bacteria and strain	Presence of pdp_{Sau}	Prophage content; strain characteristics	Reference or source	Sensitivity to kayvirus		
				K	812	812a
S. aureus						
RN4220	−	No prophage; propagation strain for phage K	95	+	+	+
CCM 4028 (= SA812)	−	Sa2int, Sa3int; propagation strain for phage 812	38	+	+	+
RN4220 (pCN51)	−	No prophage	This study	+	+	+
RN4220 (pCN51-pdp_{Sau})	+	No prophage	This study	−	−	+
RN4220 (pCN51-pdp_{Sau}-orf812a_191)	+	No prophage	This study	+	+	+
RN4220 (53^+)	+	Sa7int	This study	−	−	+
RN4220 (53^+) (pCN51-orf812a_191)	+	Sa7int	This study	+	+	+
NCTC 8325	+	Sa2int, Sa3int, Sa5int	Culture collection	−	−	+
ISP8 (= 8325-4)	−	No prophage; cured for phi11, phi12, phi13	96	+	+	+
ISP8 (47^+)	+	Sa2int	This study	−	−	+
ISP8 (53^+)	+	Sa7int	64	−	−	+
ISP8 (53^+)c	−	No prophage; cured for phi53	64	+	+	+
1039 (= CCM 4890)	−	No prophage	97	+	+	+
NCTC 8511	−	Sa2int, Sa3int, Sa6int	Culture collection	+	+	+
NCTC 8511 (53^+) (= S26)	+	Sa2int, Sa3int, Sa6int, Sa7int	38	−	−	+
NCTC 8511 (53^+)c	−	Sa2int, Sa3int, Sa6int, cured for phi53	This study	+	+	+
USA300	−	Sa2int, Sa3int	98	+	+	+
USA300c	−	No prophage; cured for $phiSa2_{USA}$ and $Sa3_{USA}$	99	+	+	+
USA300c (53^+)	+	Sa7int	This study	−	−	+
E48 (= NRL 02/947)	+	Sa2int, Sa3int, clinical MRSA isolate	100	−	−	+
S. epidermidis						
Tü 3298	−	ND	101	+	+	−
Tü 3298 (pCN51-pdp_{Sau})	+	ND	This study	−	−	−

[a]+, sensitive; −, resistant; ND, not determined.

The studied prophages 47, 53, and 80α that induced immunity to kayviruses 812 and K are unrelated or only distantly related to each other based on their whole-genome sequence. Phage 47 belongs to group A by the original serological classification and to integrase type Sa2. Phages 53 and 80α belong to group B and integrase types Sa7 and Sa5, respectively. Each integrase type possesses a different *att* site; thus, the insertion inactivation of a bacterial gene is not the cause of the induced nonsensitivity. Comparative genomic analyses of phages 47, 53, and 80α revealed only one common gene corresponding to ORF016 coding for an unknown protein (UniProtKB accession no. Q4ZDJ8) in the previously published bacteriophage 53 genome (39). This gene was designated pdp_{Sau} (phage defense protein of *S. aureus*).

A set of MRSA strains was subsequently screened for the pdp_{Sau} gene using PCR. All pdp_{Sau}-positive strains exhibited resistance to wild-type phage 812. Strain E48 (ST8/t024/staphylococcal cassette chromosome *mec* element IV [SCC*mec* IV]) related to USA300 (40) as a representative of the most frequent genotype that naturally carried the pdp_{Sau} gene (Table 1) was genome sequenced and used for further analyses.

Phage sensitivity assay in an artificial expression system. To verify the direct association between the pdp_{Sau} gene and a phage-resistant phenotype, the pdp_{Sau} gene was cloned in the expression vector pCN51 under a cadmium-inducible promoter (41) and electroporated into *S. aureus* RN4220, which is naturally sensitive to phages 812 and K. The Pdp_{Sau} protein was detected by mass spectrometry after SDS-PAGE of the proteins from lysed cells both in the naturally occurring lysogen and the artificial system, where 28% of the protein sequence (amino acid range 39 to 178) was covered by nine tryptic peptides. A strain harboring the construct pCN51-pdp_{Sau} exhibited a resistant phenotype to both phages after the overexpression, the same as the lysogenic strain *S. aureus* RN4220 (53^+) (Fig. 1A). This proved that the protein Pdp_{Sau} alone is sufficient to induce resistance to phages 812 and K. Next, the construct pCN51-pdp_{Sau} was transformed into the coagulase-negative *Staphylococcus epidermidis* Tü 3298 strain (Table 1), where the expression of the pdp_{Sau} gene also led to the induction of a resistant phenotype.

Downloaded from https://journals.asm.org/journal/mbio on 04 February 2026 by 147.251.86.90.

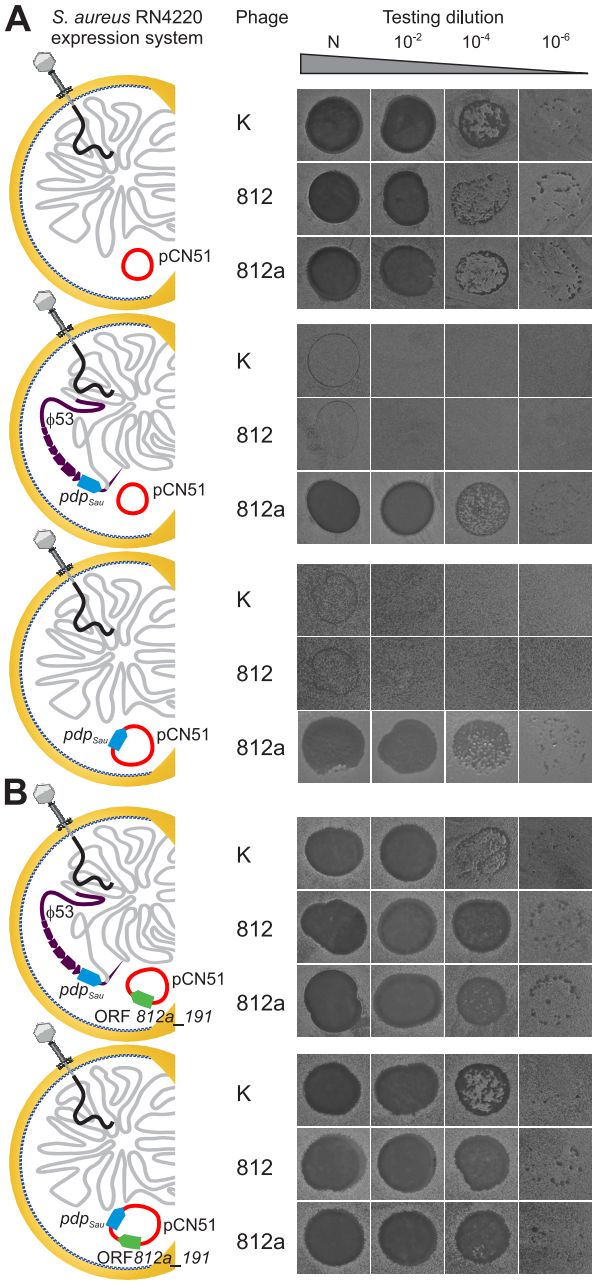

FIG 1 Impact of pdp_{Sau} gene expression on *Kayvirus* lytic action demonstrated by drop assay performed with phages K, 812, and 812a on *S. aureus* RN4220 derivatives. Testing was performed at four phage concentrations, nondiluted phage with a titer of 10^9 PFU/mL (N) and dilutions of 10^{-2}, 10^{-4}, and 10^{-6}. Four types of resulting lytic zones were distinguished—confluent lysis, semiconfluent lysis, single plaques, growth inhibition, or no lysis. If single plaques appeared at any dilution, the strain was considered susceptible. (A) Phage-sensitive control strain RN4220 (pCN51) compared to wild-type phage resistant RN4220 (53^+) (pCN51) and RN4220 (pCN51-pdp_{Sau}) harboring pdp_{Sau} gene on prophage 53 or plasmid pCN51, respectively. Phage 812a replicates effectively on strains with the pdp_{Sau} gene. (B) *S. aureus* strains RN4220 (53^+) (pCN51-ORF812a_191) and RN4220 (pCN51-pdp_{Sau}-ORF812a_191) coexpressing pdp_{Sau} and ORF 812a_191, which restores the sensitive phenotype. The restoration of the phage-sensitive phenotype occurs both in the lysogenic strain with prophage-encoded pdp_{Sau} and the strain with coexpressed pdp_{Sau} and ORF 812a_191 from a common promoter.

The pdp_{Sau} gene prevalence in *S. aureus* whole-genome sequences. Analyses of the prevalence of pdp_{Sau}-encoding prophages in more than 60 thousand *Staphylococcaceae* genomes available in the NCBI database matched a set of 41 bacterial genomes with this gene. The pdp_{Sau} gene was found solely on *S. aureus* prophage regions. A gene with lower similarity was found in the prophage genomes of coagulase-negative staphylococci and the genus *Aerococcus* (Fig. 2A). The extracted prophage sequences were classified by BLAST

Downloaded from https://journals.asm.org/journal/mbio on 04 February 2026 by 147.251.86.90.

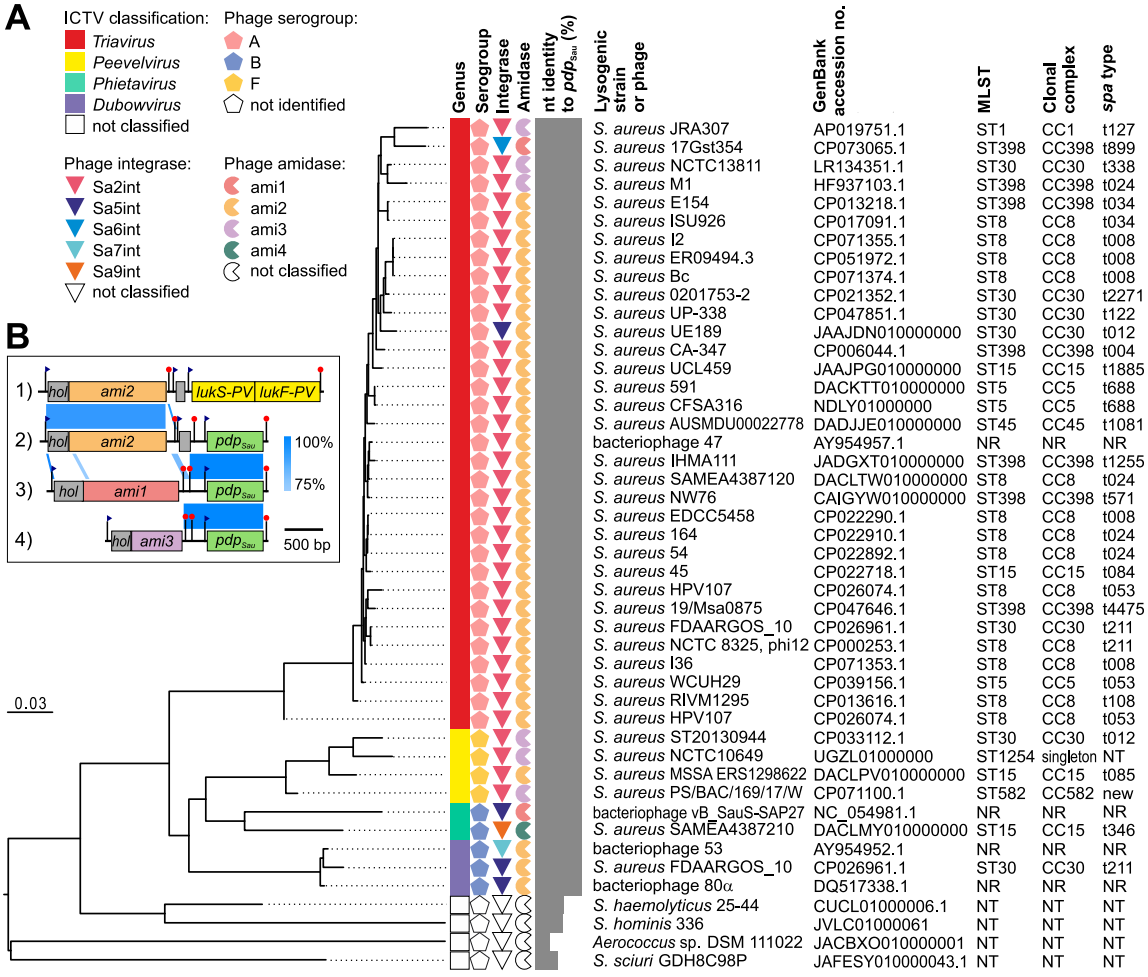

FIG 2 Phylogenetic insights into prophages harboring pdp_{Sau} gene identified in whole-genome sequences of *Staphylococcaceae* family and their characteristics. (A) Bacteriophage and prophage genomes extracted from whole-genome sequences that matched pdp_{Sau} were compared using the Genome-BLAST Distance Phylogeny method with the settings recommended for prokaryotic viruses (90). The resulting intergenomic distances were used to infer a balanced minimum evolution tree with branch support via FASTME including Subtree Pruning and Regrafting (SPR) postprocessing (91). The branch lengths of the resulting tree are scaled in terms of the respective distance formula used. Phage genomes were characterized by phage type corresponding to serological group (65), integrase gene type (44), and amidase gene type (42). The nucleotide identity of pdp_{Sau} homologs to ORF016 of phage 53 is shown. Multilocus sequence type and staphylococcal protein A (*spa*) type were derived from the genome assemblies. NR, not relevant; NT, not typeable. (B) Nucleotide sequence alignment showing the gene structure of lytic modules and accessory genes in the genomes of four *S. aureus* prophages as follows: (i) phi PVL (92), (ii) phi 53 (39), (iii) prophage vB_StaphS-IVBph354 (93), and (iv) prophage from strain PS/BAC/169/17/W (94). ORFs with proven or predicted functions are depicted as colored boxes. Nucleotide identity between genomic regions is indicated by blue-shaded regions. Putative promoters and terminators are depicted as blue flags and red pins, respectively.

search and *in silico* PCR into the genera *Triavirus*, *Phietavirus*, *Peevelvirus*, and/or *Dubowvirus* (Fig. 2A). The most frequent ones (85%) were prophages harboring Sa2 integrase, and the rest comprised integrase types Sa5, Sa6, Sa7, and Sa9. The gene organization of the lytic module shows that pdp_{Sau} is always localized downstream of the gene for amidase in the lysis module (Fig. 2B) and is typically linked to amidase ami2 according to the previous classification system (42). The presence of the pdp_{Sau} gene adjacent to ami2 was also confirmed by PCR in multiple lysogenic MRSA strain E48. The ami2 lytic module of pdp_{Sau}-positive phages was homologous with Panton-Valentine leukocidin (PVL)-converting phages (100% nucleotide [nt] identity) (Fig. 2B), which leads to the hypothesis that it has the same origin as in PVL-encoding phages (43). As determined previously (44), the crossover point for the integration of the PVL toxin-encoding complex is situated at the end of the phage amidase open reading frame (ORF), and the pdp_{Sau} locus possibly recombines at this crossover point.

Next, we tested whether there was a relationship between the presence of the pdp_{Sau} gene and clonal complexes of whole-genome sequenced lysogenic strains. Predominant genotypes from clonal complexes CC5, CC8, CC15, CC30, and ST398 (Fig. 2A) are typical

Downloaded from https://journals.asm.org/journal/mbio on 04 February 2026 by 147.251.86.90.

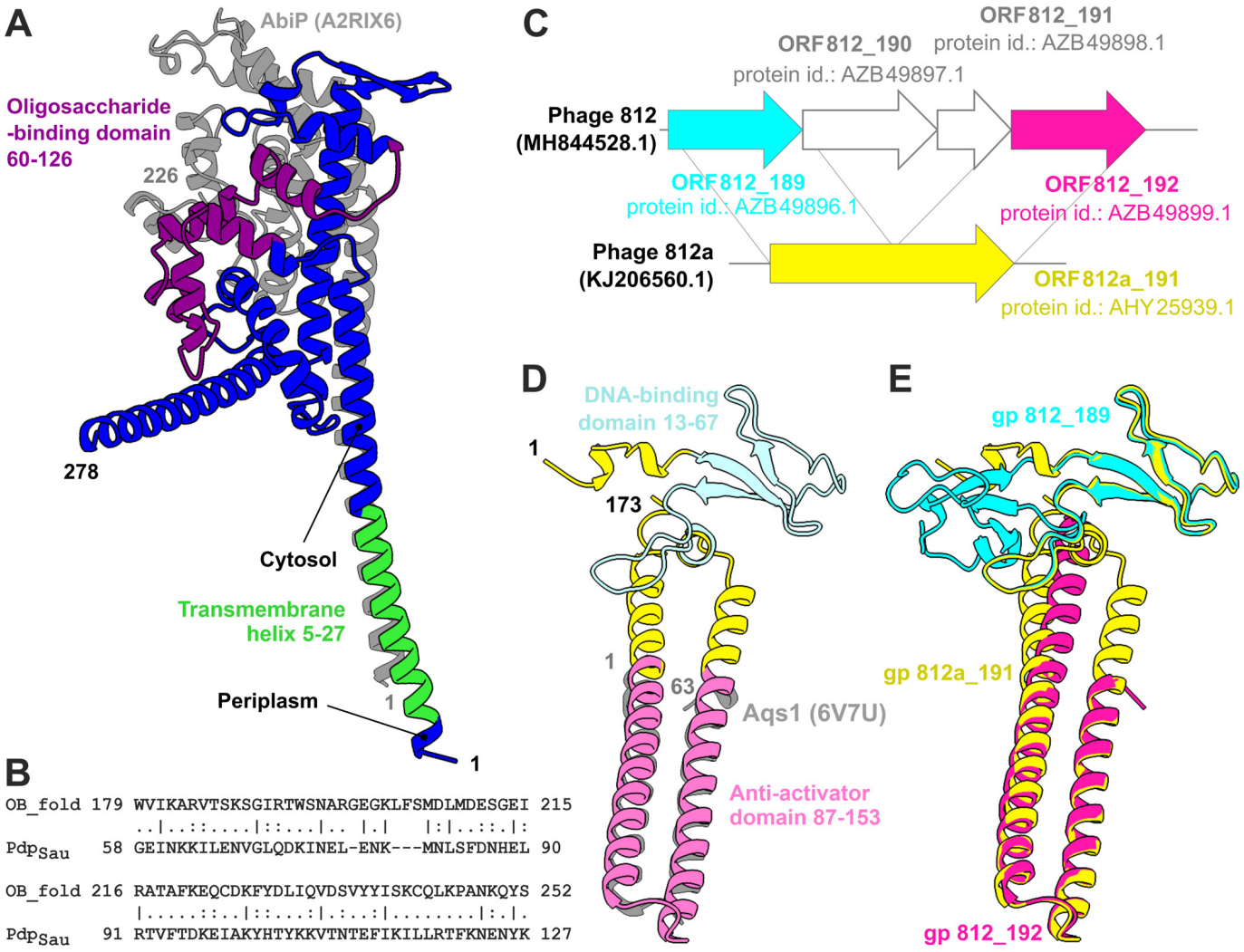

FIG 3 Structure prediction of immunity protein Pdp$_{Sau}$ and new fusion protein restoring phage sensitivity encoded by phage mutant 812a. (A) 3D structure prediction of Pdp$_{Sau}$ (blue) with N-terminal transmembrane helix (lime green) and oligosaccharide-binding fold-like region (purple) highlighted. The structure is superimposed with the predicted structure of characterized immunity protein AbiP (A2RIX6) from *Lactococcus* (gray). (B) EMBOSS Needle pairwise alignment (BLOSUM62) of oligosaccharide-binding (OB) domains of RPA replication protein (UniProtKB accession no. Q24492) with OB_fold hit in Pdp$_{Sau}$ protein (score, 25; similarity, 40.5%). (C) Sequence alignment of genomic loci encoding ORF 812_189 and ORF 812_192 in phage 812 and fusion ORF 812a_191 in the genome of host-range mutant phage 812a, depicting the emerging deletion. (D) 3D structure prediction of fusion protein ORF812a_191, superimposed with the solved structure of the antiactivator Aqs1 (PDB accession no. 6V7U; gray). (E) Structural alignment of gene products encoded by ORF 812_189 (cyan), ORF 812_192 (magenta), and fusion ORF 812a_191 (yellow).

for community isolates where prophage-induced immunity to kayviruses may represent an evolutionary advantage, e.g., for survival and dissemination in a wastewater environment as an important reservoir for lytic phages (45).

Transmembrane protein Pdp$_{Sau}$ is structurally similar to apoptotic protein. Region 5 to 27 of the 278-amino acid (aa) protein Pdp$_{Sau}$ contains many hydrophobic residues and protein topology prediction classified it as a transmembrane domain (TMHMM, probability of N-in, 0.985) (Fig. 3A). Furthermore, structure comparison of the Pdp$_{Sau}$ protein region 3 to 28 suggests a weak similarity of the region to *Enterococcus faecalis* RNAI protein (2KV5) and *S. aureus* PepA1 protein (4B19) (see Table S1 in the supplemental material). RNAI forms part of the *par* locus and has the function of an Fst toxin for the stable maintenance of plasmids in cells (46). Fst translocated across a membrane induces changes in membrane integrity, leading to the disruption of cell division (47). PepA1 protein, similarly to Fst, forms a membrane-binding α-helix in a 22-residue part of its N terminus (48). The liquid chromatography-tandem mass spectrometry (LC-MS/MS) analysis (see Table S2 in the supplemental material) revealed a predominant allocation of Pdp$_{Sau}$ protein in the membrane fraction compared to the cytoplasmic one; therefore, we assume Pdp$_{Sau}$ is embedded in the

Downloaded from https://journals.asm.org/journal/mbio on 04 February 2026 by 147.251.86.90.

membrane. The cytoplasmic C-terminal domain of Pdp_{Sau} is positively charged. Pairwise sequence alignment (Fig. 3B) confirmed the presence of an oligosaccharide-binding fold (UniProtKB accession no. Q24492), which often facilitates DNA-binding function (49). Both transmembrane and DNA-binding domains were described in the lactococcal phage-defense abortive system protein AbiP (UniProtKB accession no. A2RIX6) (50). We thus compared protein models generated by Alphafold2 of Pdp_{Sau} to AbiP, which despite the low amino acid identity exhibited a significant structural similarity demonstrated by their pairwise superimposing (Fig. 3A; see also Table S1).

Based on protein structure predictions, we hypothesize that Pdp_{Sau} is one of the apoptotic-like membrane proteins associated with abortive systems (Abi), whose modes of action involve degradation or depolarization of the cell membrane (50). In Gram-positive bacteria, Abi systems provide resistance against phage infection that can lead to cell death and target various stages of the cell life cycle (50–52). Other classes of Abi systems target tRNAs or mRNAs and cleave essential proteins in the host translation apparatus, resulting in growth arrest and nonproductive infection (53), or compete with native replicase proteins (54).

The *pdp*$_{Sau}$ gene does not affect *Kayvirus* adsorption and genome release but blocks its DNA replication. To study the mechanism of action of Pdp_{Sau}, the strains RN4220, RN4220 (53^{+}), and RN4220 (pCN51-*pdp*$_{Sau}$) were infected with the wild-type phage 812. The reaction of strains to infection with phage was monitored by turbidity assay. Strains expressing *pdp*$_{Sau}$ exhibited growth of the bacterial culture upon infection with phage 812, which was slowed down for the first 4 h compared to uninfected culture, whereas the absence of the *pdp*$_{Sau}$ gene led to lysis of the culture (see Fig. S1 in the supplemental material). The expression level of the *pdp*$_{Sau}$ gene during phage 812 infection was determined using quantitative reverse transcription-PCR (RT-qPCR). Neither overexpression nor downregulation of the *pdp*$_{Sau}$ gene was detected at 0, 5, 10, and 20 min of infection with phage 812 compared to the sample without the addition of phage (see Table S3 in the supplemental material). The change in the expression of the *pdp*$_{Sau}$ gene is therefore not essential for the activation of the phage defense mechanism.

Next, we examined specific steps of the phage life cycle—adsorption, genome delivery, transcription, and replication—to determine at which point the cycle is arrested. The comparison of adsorption rate (see Fig. S2 in the supplemental material) showed that phage 812 virions adsorb efficiently onto both *pdp*$_{Sau}$-positive and -negative cells; thus, Pdp_{Sau} does not affect adsorption.

We recently showed that *Kayvirus* transcription starts immediately after the entry of phage DNA into the host cells (26). To verify that *Kayvirus* phage 812 genome delivery and the transcription of its DNA occurs in *pdp*$_{Sau}$-positive *S. aureus* strains, the transcripts of the early (anti-sigma factor, orf 812_132; GenBank accession no. AZB49840.1), middle (putative DNA-binding protein, 812_143; GenBank accession no. AZB49851.1), and late (baseplate wedge protein, 812_118; GenBank accession no. AZB49826.1) phase of infection (26) were quantified by RT-qPCR (see Fig. S3 in the supplemental material). The presence of transcripts of all of the tested loci confirmed that the DNA of phage 812 is inside cells and accessible to the host transcription apparatus. Based on the facts that phage DNA is present inside the cell and Pdp_{Sau} is structurally similar to lactococcal AbiP, we hypothesize that similarly to AbiP, the binding of a nucleic acid to Pdp_{Sau} activates the phage resistance mechanism.

The replication of phage 812 was examined using the absolute quantification of the *mcp* gene for major capsid protein during infection (see Fig. S4 in the supplemental material). Rees and Fry in their original study of the phage K replisome (55) described that during the first half of the latent period, the number of phage DNA molecules increased from 1 copy to 27 phage equivalents. This observation is consistent with quantitative PCR (qPCR) results, where we detected about a 30-fold increase in the amount of phage 812 DNA in the sensitive control strain RN4220 20 min postinfection (Fig. S4). After 30 min, the copy number of the *mcp* gene increased about 40-fold in control RN4220 compared to those of *pdp*$_{Sau}$-positive strains, where the *mcp* copy number only increased 2-fold. The very low increase in the genome copy number leads to the presumption that the phage replication in *pdp*$_{Sau}$-positive strains is either not activated or is stalled at the very beginning.

Downloaded from https://journals.asm.org/journal/mbio on 04 February 2026 by 147.251.86.90.

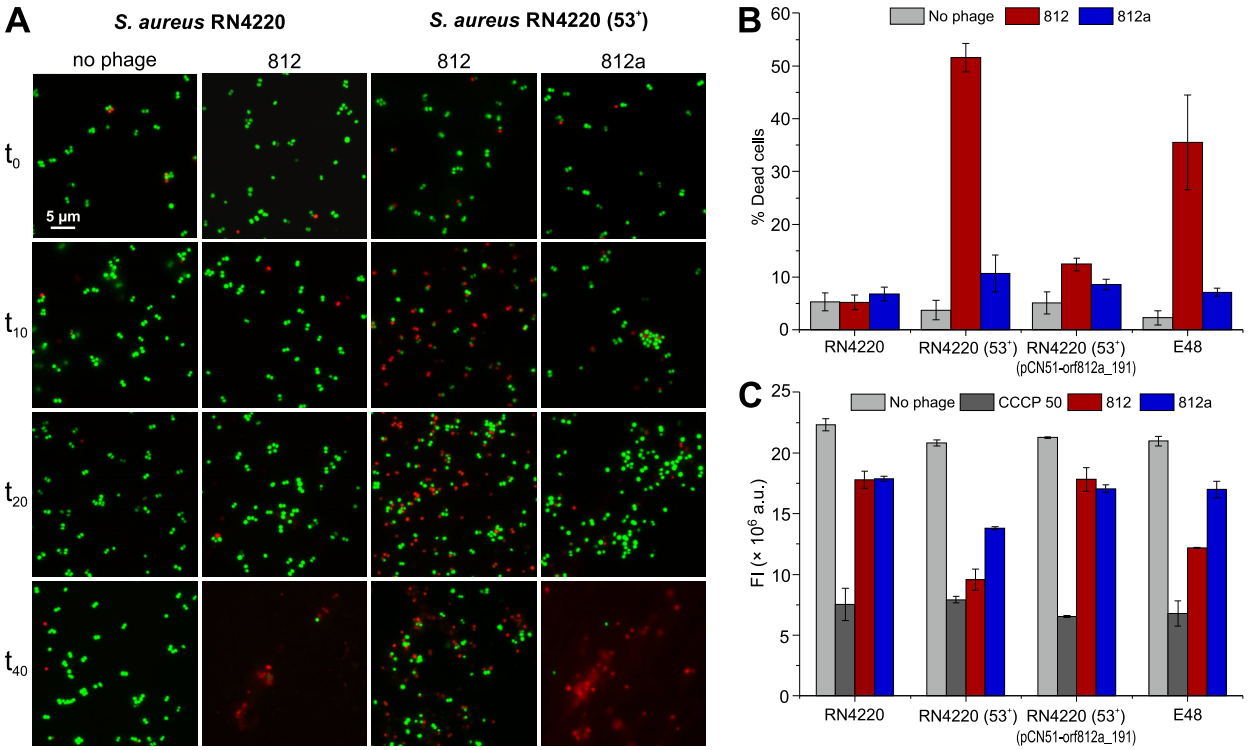

FIG 4 Changes in *S. aureus* membrane permeability through Pdp_{Sau}-based phage defense mechanism illustrated by LIVE/DEAD staining. (A) Fluorescence microscopy of *S. aureus* infected with phages 812 or 812a and no phage control sample, visualized by fluorescence microscopy at time points 0, 10, 20, and 40 min after the onset of infection. Propidium iodide, a red-fluorescent nucleic acid-binding dye, which cannot enter cells with intact membranes, was used as a marker for the loss of membrane integrity and cell death. Dead cells are represented by red dots and live cells by green dots. (B) Percentage of dead bacterial cells 10 min after the onset of infection. *S. aureus* cultures were infected with phages 812 or 812a and compared with noninfected strains. (C) Changes in membrane polarity examined by BacLight bacterial membrane potential kit assay on *S. aureus* RN4220, RN4220 (53^+), RN4220 (53^+) (pCN51-orf812a_191), and clinical MRSA strain E48 treated with phages 812 or 812a at an MOI_{input} of 10. Treatment with the ionophore carbonyl cyanide 3-chlorophenylhydrazone, component B (CCCP) at a final concentration of 50 mM was used as a positive control of depolarization. The decrease in membrane potential was measured as a loss of red fluorescence emitted by carbocyanine dye $DiOC_2(3)$ (3,3′-diethyloxa-carbocyanine iodide).

***pdp_{Sau}* impacts cell membrane potential and permeability in *Kayvirus*-infected cells.** Due to the assumed transmembrane localization of Pdp_{Sau} protein, the changes in the cell membrane integrity 10 to 40 min postinfection in strains RN4220 and RN4220 (53^+) were assessed using LIVE/DEAD cell staining. In the RN4220 strain, we observed live cells until the release of new phage progeny after 40 min (Fig. 4A). Compared to the pdp_{Sau} gene-negative strain RN4220, we observed a presence of dead cells 10 min postinfection and subsequent increase in cell counts with no cell lysis after 40 min postinfection in pdp_{Sau} gene-positive strain RN4220 (53^+) (Fig. 4A and B). This indicates halted phage propagation followed by a rapid growth of live cells starting from 20 min after infection (Fig. 4A). In this way, the bacterial population survives due to an abortive defense mechanism.

Changes in membrane permeability are connected with membrane potential. The carbocyanine dye staining showed a statistically significant reduction in red fluorescence (P value < 0.01) in the pdp_{Sau}-negative nonlysogenic strain RN4220 compared to that in the pdp_{Sau}-positive lysogenic strain RN4220 (53^+), indicating a change in membrane potential (Fig. 4C). This was also observed in the control MRSA strain E48 (Fig. 4B and C). Similarly, the abortive Rex system of bacteriophage lambda characterized by termination of macromolecular synthesis, loss of active transport, ATP hydrolysis, and altruistic cell death is explained by depolarization of the cytoplasmic membrane due to activation of the membrane component of the system (56).

Kayviruses can escape prophage-induced bacterial resistance mechanism. Bacteriophage 812 host-range mutants are capable of growing on pdp_{Sau}-positive strains. This capability was first observed in a mutant designated 812a, which was obtained as rare plaques after plating phage 812 (mutation frequency, 9.9×10^{-9}; efficiency of plating, 0.43)

Downloaded from https://journals.asm.org/journal/mbio on 04 February 2026 by 147.251.86.90.

on the lysogenic strain *S. aureus* NCTC 8511 (53^+) (38). Phage 812a propagated efficiently on all of the analyzed lysogenic pdp_{Sau}-positive strains, as determined by phage drop plaque assays (Table 1; Fig. 1A), turbidity assay (Fig. S1), and microscopic observation of the infected cells (Fig. 4A).

Whole-genome sequencing of phage 812a (15) revealed a deletion leading to a new fusion gene with a possible role in overcoming the action of Pdp_{Sau}. The deletion in phage 812 genome includes a locus encoding four hypothetical genes (ORF 812_189 to ORF 812_192; GenBank accession no. MH844528.1). After the deletion, ORF 812_189 and ORF 812_192 form a fusion gene in phage 812a annotated as ORF 812a_191 (GenBank accession no. KJ206560.1) (Fig. 3C and E). The new 173-aa fusion protein has a conserved DNA-binding domain on its N terminus (residues 13 to 67) with a zinc finger motif similar to Miz-1 protein (HHpred, 2N26; probability, 98.81%; e value, 6.4e−9) (57) and to the transcription repressor CTCF from eukaryotes (HHpred, 6QNX, probability: 98.4%, e-value 1.4e−7) (58). The tertiary structure of the protein in the C-terminal region 87 to 153 is similar to the antiactivator Aqs1 of *Pseudomonas* phage DSM3 (DALI search, PDB accession no. 6V7U; Z-score = 6.5) (Fig. 3D), which is involved in blocking a host phage-resistance mechanism by inhibiting the DNA-binding domain of a host cell regulator (59).

To verify the direct association of the new fusion gene with overcoming the resistance mechanism, ORF 812a_191 was coexpressed with pdp_{Sau} under one promoter in *S. aureus* RN4220 (pCN51-pdp_{Sau}-orf812a_191), which led to restored sensitivity to phages 812 and K. The same phenomenon was confirmed in the *S. aureus* RN4220 (53^+) (pCN51-orf812a_191) system, which naturally carries pdp_{Sau} in the genome (Fig. 1B; see also Fig. S1). No change in membrane potential or permeability was observed when *S. aureus* strain RN4220 (53^+) (pCN51-orf812a_191) was infected with phage 812 (Fig. 4B and C).

Conclusions. The described defense mechanism encoded by a prophage accessory gene protects the staphylococcal bacterial population against virulent lytic phages via abortive infection. Because it is encoded by prophages in various clonal lineages, we assume it was spread by horizontal gene transfer. An analogy can be found in the abortive mechanisms of lactococci (53) but even in a group of Gram-negative bacteria (60), where the responsible genes are also carried by mobile genetic elements. The interaction of the prophage gene product with the infecting phage halts the replication of its DNA and leads to changes in the permeability of the cell membrane. Based on these findings, we conclude that the infected part of the bacterial host population is sacrificed to stop the lytic infection by the *Kayvirus* and prevent the release of its new progeny. The bacteria benefit from a lysogenic conversion that allows them to escape the lytic action of *Kayvirus* at the population level. Therefore, we believe that this novel mechanism of phage competition in staphylococci leads to the stable maintenance of prophages protecting their hosts. Kayviruses can evolve through mutations and regain the ability to lyse lysogenic strains, thus maintaining their wide range of hosts, which is important for their use in phage therapy.

MATERIALS AND METHODS

Bacterial and bacteriophage strains and culture conditions. The strains used in this study are listed in Table 1. Staphylococcal strains were routinely grown in meat peptone broth (MPB) and/or meat peptone agar (MPA) according to Botka et al. (15). *Escherichia coli* strains were grown at 37°C with shaking at 160 rpm in LB medium. Phage 812, deposited in the Czech Collection of Microorganisms under number CCM 7911, and phage 812a were described previously (38). Bacteriophage K was kindly provided by G. Xia (University of Manchester, UK) (61). *S. aureus* phages from the International Typing Set (62) and phage 80α (63) were described previously. Lysogenized strains were prepared as previously described (64), and the presence of prophages was verified by PCR (65). The phage-cured *S. aureus* strain USA300 (designated USA300c) was generated by deleting native prophages $Sa2int_{USA300}$ and $Sa3int_{USA300}$ using the plasmid pKOR1 as described for *S. aureus* Newman (66). Phage-cured strains ISP8 (53^+)c and NCTC 8511 (53^+)c were prepared by using UV light and recognized by replica plating on MPA medium inoculated with an indicator strain (64).

Construction of plasmid vectors and protein preparation. The expression vectors constructed in this study are derived from high-copy-number shuttle vector plasmid pCN51 with cadmium-inducible promoter (41) and are listed in Table 1. The protein-coding regions were amplified by PCR with primers designed for restriction enzyme cloning (see Table S4 in the supplemental material). Restriction endonucleases BamHI and EcoRI (New England Biolabs) were used for cloning by ligation with T4 DNA ligase (New England Biolabs). Plasmid constructs were transformed into competent *E. coli* Top10F′ (Invitrogen) and then into *E. coli* BL21(DE3) (Invitrogen) for protein expression or transferred into electrocompetent *S. aureus* cells (67). All constructs were verified by

Downloaded from https://journals.asm.org/journal/mbio on 04 February 2026 by 147.251.86.90.

Sanger sequencing in the Eurofins MWG Operon sequencing facility (Ebersberg, Germany). The expression and coexpression of cloned genes from plasmid constructs were verified by mass spectrometry.

Phage susceptibility testing. The double agar overlay technique (MPA with 2 mM $CaCl_2$) was used for phage susceptibility testing and the isolation of phage mutants. The phage lysates of a titer of 10^9 PFU/mL were diluted up to 10^{-6} and applied in triplicates by spotting 10-μL aliquots onto soft agar lawns inoculated with the tested *S. aureus* strain. Plates were incubated overnight at 37°C. The strain was only evaluated as sensitive if the phage formed plaques.

Adsorption assays. The adsorption efficiency of phages 812 and 812a onto *S. aureus* strains RN4220 and RN4220 (53^+) was determined as described previously (33). Briefly, the adsorption was analyzed using a multiplicity of infection (MOI_{input}) of 0.1, and the adsorption rate (%) was calculated by determining the number of unbound phage particles in the supernatant and subtracting it from the total number of input PFU as a ratio of the total number of input PFU. The adsorption rate was estimated 5 min after phage infection.

Bacterial cell growth assays during phage infection. Bacterial strains were cultivated aerobically in 20 mL of MPB to the logarithmic phase (optical density at 600 nm [OD_{600}] = 0.4 to 0.45) at 37°C. A transparent 96-well cell culture plate (SPL Life Sciences) with a transparent cover and an Infinite 200 PRO (Tecan) microplate reader were used for the turbidimetric assay. The experiments were carried out in triplicates in a total volume of 200 μL per well at 37°C with continuous orbital shaking (amplitude, 4 mm) for 24 h using the recommended protocol and instrument settings (absorbance, 600 nm; 20 flashes; 0 ms settle time). Phage infection assay was done at an MOI_{input} of 5 or 10 with the addition of $CaCl_2$ to a final concentration of 2 mM.

DNA extraction for phage gene quantification in infected cells. Bacterial culture grown to an OD_{600} of 0.4 to 0.45 in 50 mL MPB at 37°C was mixed with phages 812 or 812a at an MOI_{input} of 0.1 and incubated with shaking. The 1.5-mL aliquots were taken at sampling time points 0, 2, 5, 10, 15, 20, and 30 min and centrifuged at 10,000 $\times$ *g* for 2 min. Pellets were frozen using liquid nitrogen and kept at −80°C. DNA was extracted from each aliquot sample using a High Pure PCR template preparation kit (Roche) with prolonged lysis with lysostaphin (Sigma-Aldrich) added to a final concentration of 10 μg/mL.

cDNA preparation. Total RNA was extracted using the TRI reagent (Sigma-Aldrich) from *S. aureus* cells infected with phages at sampling time points 0, 2, 5, 10, 15, 20, and 30 min, harvested as described above. The procedure was done in RNase-free tubes according to the manufacturer's instructions with the following modifications for the lysis of Gram-positive bacteria: 10^8 cells were lysed in 1 mL of TRI reagent and transferred to lysing matrix B with 0.1 mm silica spheres (MP Biomedicals) and homogenized for 2 min. The silica spheres were collected by centrifugation for 3 min at 10,000 $\times$ *g* at 4°C. Purified RNA was used for cDNA synthesis in a reverse transcription assay using a high-capacity cDNA reverse transcription kit (Applied Biosystems).

qPCR and RT-qPCR of phage genes at different times of infection. Each reaction mixture (20 μL) contained 10 μL of 2$\times$ LightCycler 480 SYBR green I master (Roche), forward and reverse primers (each 10 μM) listed in Table S4, and template DNA or cDNA diluted into a volume of 5 μL. Reactions were carried out in triplicates using a LightCycler 480 Instrument II (Roche) according to Mašlaňová et al. (68). An initial denaturation of DNA at 95°C for 10 min was followed by 30 cycles of amplification (95°C for 15 s, 55°C for 20 s, 72°C for 15 s) and a dissociation phase at 95°C for 15 s, 60°C for 60 s, 95°C for 5 s, and 60°C for 15 s. The amplification efficiency of qPCR was calculated from threshold cycle (C_T) values of standard curves prepared from the plasmid or genomic DNA for each reaction, and a linear regression curve through the data points was generated. The measurements were done in biological and technical triplicates. The expression level was analyzed from crossing point (Cp) values using a one-way analysis of variance (ANOVA) test. All statistical analyses were performed in R v4.2.1. (https://cran.r-project.org/).

Protein identification by mass spectrometry. Vertical one-dimensional SDS-PAGE was performed as described previously (69). Separation zones corresponding to the molecular weight of the expected protein (33 $\pm$ 5 kDa) were excised from the gel, and after destaining and washing procedures, they were digested with trypsin (Promega) for 2 h at 40°C. Tryptic peptides extracted from gels were subjected to LC-MS/MS analysis using an UltiMate 3000 RSLCnano liquid chromatography system (Thermo Fisher Scientific) connected on-line to an Impact II ultra-high resolution Qq-time-of-flight mass spectrometer (Bruker, Germany). MS/MS data were searched against a custom database of expected amino acid sequences and in parallel against the NCBIprot database (https://ftp.ncbi.nih.gov/blast/db/FASTA/) using an in-house Mascot search engine version 2.4.1 (Matrix Science, UK).

To obtain cytoplasmic (C) and membrane (M) protein fractions, the isolation method described previously (70) was used with changes for the final processing of the membrane fraction. The pelleted membrane fraction was washed twice with 50 mM ammonium bicarbonate (AB), centrifuged at 20,000 $\times$ *g* for 10 min, and solubilized in SDT lysis buffer (4% SDS, 0.1 M dithiothreitol, 0.1 M Tris-HCl, pH 7.6). Solubilized proteins were processed using filter-aided sample preparation (FASP) and digested with SOLu-trypsin dimethylated (Merck) in 50 mM AB. Recovered peptides were cleaned using ethyl acetate extraction. LC-MS/MS analyses of both fractions were performed in an RSLCnano liquid chromatography system on-line connected to an Orbitrap Exploris 480 mass spectrometer (Thermo Fisher Scientific). Peptides were separated using an analytical EASY-Spray column (Acclaim PepMap C_{18} column; 2-μm particles, 75 μm $\times$ 500 mm; Thermo Fisher Scientifics; part number ES903) during a 138-min gradient elution (mobile phase A, 0.1% formic acid in water; mobile phase B, 0.1% formic acid in 80% acetonitrile). MS data were acquired in a data-dependent strategy with a defined number of scans based on precursor abundance with survey scan (*m/z* 350 to 2,000). The resolution of the survey scan was 120,000 (at *m/z* 200) with a target value of 1 $\times$ 10^6 ions and maximum injection time of 500 ms. High-energy collisional dissociation-tandem mass spectrometry (HCD-MS/MS) data (30% relative fragmentation energy) were recorded at 15,000 resolution (maximum injection time, 50 ms). MaxQuant software version 2.0.3.0 with inbuild search engine Andromeda (Max-Planck-Institute of Biochemistry) was used for data evaluation. Searches were done against the *S. aureus* NCTC 8325 reference proteome (UP000008816) and cRAP contaminants database version 2012.01.01. Carbamidomethylation of cysteine was set as a fixed modification while oxidation (M), deamidation

Downloaded from https://journals.asm.org/journal/mbio on 04 February 2026 by 147.251.86.90.

(N, Q), and acetylation (protein N-term) were set as variable modifications. Trypsin was used as the protein-cleaving enzyme with two allowed missed cleavages. Peptides and proteins with a false discovery rate of <1% were considered for final data evaluation. All identified proteins including the protein of interest (UniProtKB accession no. Q2FYE0) are listed in Table S2 in the supplemental material. Mass spectrometry data were deposited in the ProteomeXchange Consortium via the PRIDE partner repository under database identifier PXD036676.

Bacterial membrane permeability and membrane polarity assays. *S. aureus* strains RN4220, RN4220 (53^+), RN4220 (53^+) (pCN51-orf812a_191), and E48 were routinely grown in MPB. The bacterial culture was 100-fold diluted in MPB supplemented with 0.5 μM $Cd(NO_3)_2$ to induce expression where needed and incubated at 37°C with shaking to an OD_{600} of 0.35 to 0.40. The phage 812 or 812a was added at an MOI_{input} of 5. The bacterial cells without phages were used as a negative control. The 1.5-mL aliquots were taken at sampling times 0, 10, 20, and 40 min, centrifuged at 10,000 $\times$ *g* for 2 min, and the pellets were washed once and resuspended in 150 μL of 50 mM Tris-HCl (pH 7.5) for membrane permeability assay and in 150 μL of phosphate-buffered saline (PBS) buffer for membrane polarity assay. The cell suspension was stained using a LIVE/DEAD BacLight bacterial viability kit (Invitrogen) as recommended by the manufacturer. The kit contains SYTO 9 and propidium iodide (PI), which have different permeabilities through the bacterial membrane. The stained bacterial samples were observed with an Olympus BX41 fluorescence microscope (Olympus, Japan). The SYTO 9 emission was observed using a fluorescein isothiocyanate (FITC) filter cube (U-MWB2; excitation 475 $\pm$ 30 nm; emission >520 nm; dichroic mirror (DM) 500 nm) and the PI using a tetramethyl rhodamine isocyanate (TRITC) filter cube (U-MWG2; excitation 530 $\pm$ 40 nm; emission >590 nm; DM 570 nm). The measurements were done in biological and technical triplicates.

Changes in membrane polarity were detected with a BacLight bacterial membrane potential kit (Invitrogen) containing carbocyanine dye $DiOC_2(3)$ (3,3′-diethyloxa-carbocyanine iodide) and compared with the control ionophore carbonyl cyanide 3-chlorophenylhydrazone, component B (CCCP) at a final concentration of 50 μM, both diluted in dimethyl sulfoxide (DMSO). The precipitation of $DiOC_2(3)$ indicates changes in potential at the bacterial membrane, and its natural green emission shifts to red (71). The decrease in membrane potential was observed as a loss of red fluorescence using an Upcon S-Pro reader (Labrox, Finland) in a black nonbinding 96-well microplate (Greiner, Austria). Kinetic measurements were performed from the addition of ionophores for 1 h, and the intensity value was evaluated at 20 min. The filters used in this case were 485 $\pm$ 10 nm for excitation and 616 $\pm$ 8.5 nm for emission (DM excitation, 450 to 492 nm; emission, 520 to 550 nm). The measurements were done in biological and technical triplicates. The effect of phage addition on membrane depolarization in the tested strains was analyzed using analysis of variance (ANOVA) followed by *post hoc* Tukey tests performed in R v4.2.1.

Protein structure prediction. The transmembrane domain of Pdp_{Sau} was predicted using TMHMM version 2.0 (72). The DNA-binding domain in Pdp_{Sau} was predicted using DRNApred (73). HHpred (74), Phyre2 (75), and DALI search (76) were used for Pdp_{Sau}, estimating the similarity to distantly related proteins based on the secondary and tertiary structure prediction. The three-dimensional (3D) models of Pdp_{Sau} and orf812a_191 protein structures were predicted by AlphaFold, developed by DeepMind (77). Chimera version 1.15.rc (78) and ChimeraX version 1.2.5 (79) were used for the visualization of 3D protein structures.

Whole-genome sequencing. The bacterial culture was prepared and enzymatically treated as previously described (80). The genomic DNA was extracted using a Genomic DNA Clean & Concentrator-25 kit (Zymo Research) according to the manufacturer's instructions. For sequencing on the Oxford Nanopore platform, the library was prepared using an SQK-RAD004 rapid sequencing kit (Oxford Nanopore Technologies) according to the manufacturer's instructions. The library was sequenced with a FLO-FLG001 flow cell (R9.4.1) in a MinION device (Oxford Nanopore Technologie). The device was controlled with MinION software release 22.05.5 (Oxford Nanopore Technologies). Basecalling, demultiplexing, and barcode trimming were performed using standalone ONT Guppy software version 6.1.7 using the config file dna_r9.4.1_450bps_sup.cfg with a default minimum q-score threshold of 10. For Illumina-based sequencing, the 500-bp sequencing library was prepared with an xGen DNA Lib Prep EZ (Integrated DNA Technologies, Belgium). The samples were sequenced using a 600v3 Miseq sequencing cartridge in a 2 $\times$ 300 paired end mode using an Illumina MiSeq sequencing platform (Illumina). Illumina reads were trimmed and filtered using Trimmomatic version 0.38.1 with the sliding window model using average quality required 20 (81). The complete bacterial genome sequence was obtained using a hybrid assembly with Unicycler version 0.4.8 (82) using a minimal k-mer size of 0.2 and highest k-mer size of 0.95 with 10 k-mer steps used in a SPAdes assembly. The resulting assembly was polished with Pilon version 1.24 (83). The genome was annotated using the NCBI Prokaryotic Genome Annotation Pipeline (84).

Genomic sequences used in this study and bioinformatic analyses. Whole genomic sequences with the pdp_{Sau} gene were identified by BLAST search (https://blast.ncbi.nlm.nih.gov/). Prophage sequences from this data set were extracted manually based on their integration sites (42). The PubMLST website was used for multilocus sequence type (MLST) determination (85). Spa-types were derived with RIDOM Spa server (86). Phage and prophage genomes were characterized based on *in silico* PCR (87) using primers targeting structural genes corresponding to the serological group (65), integrase gene type (44), and amidase genes (42). Promoter sequences were predicted using the BPROM webserver (88), and terminator sites were predicted using ARNold (89).

Data availability. The complete genome sequence of *S. aureus* strain E48 (=NRL 02/947) has been deposited in GenBank/ENA/DDBJ under accession numbers CP103850 (chromosome) and CP103849 (plasmid). The associated BioProject and BioSample accession numbers are PRJNA873286 and SAMN30496472, respectively.

SUPPLEMENTAL MATERIAL

Supplemental material is available online only.

FIG S1, PDF file, 1.3 MB.

Downloaded from https://journals.asm.org/journal/mbio on 04 February 2026 by 147.251.86.90.

FIG S2, PDF file, 1.3 MB.
FIG S3, PDF file, 1.3 MB.
FIG S4, PDF file, 1.3 MB.
TABLE S1, XLSX file, 0.01 MB.
TABLE S2, XLSX file, 2.6 MB.
TABLE S3, XLSX file, 0.02 MB.
TABLE S4, XLSX file, 0.01 MB.

ACKNOWLEDGMENTS

This work was supported by a National Institute of Virology and Bacteriology project (Program EXCELES, ID project no. LX22NPO5103) funded by the European Union - Next Generation EU, a grant (18-13064S) from the Czech Science Foundation to R.P., grants (NU22-05-00042 and NU21J-05-00035) from the Ministry of Health of the Czech Republic to I.M. and T.B., respectively, a project from the Grant Agency of Masaryk University (MUNI/A/1325/2021) to J.D., and Wellcome Trust grant 224067/Z/21/Z to P.B.

We gratefully acknowledge the CIISB, Instruct-CZ Centre of Instruct-ERIC EU consortium, and the NCMG research infrastructure funded by the Ministry of Education, Youth and Sports of the Czech Republic (LM2018127) and European Regional Development Fund-Project "UP CIISB" (no. CZ.02.1.01/0.0/0.0/18_046/0015974) for their financial support of the measurements at the Proteomics, Nanobiotechnology, and Cryo-electron Microscopy and Tomography Core Facilities of CEITEC MU. The computational resources were supplied by the project e-INFRA CZ funded by the Ministry of Education, Youth and Sports of the Czech Republic (LM2018140).

We thank P. Formanová (Faculty of Science, Masaryk University) for valuable help with the pilot experiments. We thank C. Wolz (Interfaculty Institute of Microbiology and Infection Medicine, University of Tübingen) for providing the delysogenized *S. aureus* USA300c strain.

REFERENCES

1. Suttle CA. 2007. Marine viruses-major players in the global ecosystem. Nat Rev Microbiol 5:801–812. https://doi.org/10.1038/nrmicro1750.
2. Feiner R, Argov T, Rabinovich L, Sigal N, Borovok I, Herskovits AA. 2015. A new perspective on lysogeny: prophages as active regulatory switches of bacteria. Nat Rev Microbiol 13:641–650. https://doi.org/10.1038/nrmicro3527.
3. Humphrey S, Fillol-Salom A, Quiles-Puchalt N, Ibarra-Chavez R, Haag AF, Chen J, Penadés JR. 2021. Bacterial chromosomal mobility via lateral transduction exceeds that of classical mobile genetic elements. Nat Commun 12:6509. https://doi.org/10.1038/s41467-021-26004-5.
4. Naorem RS, Goswami G, Gyorgy S, Fekete C. 2021. Comparative analysis of prophages carried by human and animal-associated *Staphylococcus aureus* strains spreading across the European regions. Sci Rep 11:18994. https://doi.org/10.1038/s41598-021-98432-8.
5. Ingmer H, Gerlach D, Wolz C. 2019. Temperate phages of *Staphylococcus aureus*. Microbiol Spectr 7:7.5.1. https://doi.org/10.1128/microbiolspec.GPP3-0058-2018.
6. Novick RP. 2003. Mobile genetic elements and bacterial toxinoses: the superantigen-encoding pathogenicity islands of *Staphylococcus aureus*. Plasmid 49:93–105. https://doi.org/10.1016/S0147-619X(02)00157-9.
7. Fillol-Salom A, Alsaadi A, Sousa JAM, Zhong L, Foster KR, Rocha EPC, Penades JR, Ingmer H, Haaber J. 2019. Bacteriophages benefit from generalized transduction. PLoS Pathog 15:e1007888. https://doi.org/10.1371/journal.ppat.1007888.
8. Haaber J, Leisner JJ, Cohn MT, Catalan-Moreno A, Nielsen JB, Westh H, Penadés JR, Ingmer H. 2016. Bacterial viruses enable their host to acquire antibiotic resistance genes from neighbouring cells. Nat Commun 7:13333. https://doi.org/10.1038/ncomms13333.
9. Mašlaňová I, Stříbná S, Doškař J, Pantůček R. 2016. Efficient plasmid transduction to *Staphylococcus aureus* strains insensitive to the lytic action of transducing phage. FEMS Microbiol Lett 363:fnw211. https://doi.org/10.1093/femsle/fnw211.
10. Łobocka M, Hejnowicz MS, Dąbrowski K, Gozdek A, Kosakowski J, Witkowska M, Ulatowska MI, Weber-Dąbrowska B, Kwiatek M, Parasion S, Gawor J, Kosowska H, Głowacka A. 2012. Genomics of staphylococcal Twort-like phages-potential therapeutics of the post-antibiotic era. Adv Virus Res 83:143–216. https://doi.org/10.1016/B978-0-12-394438-2.00005-0.
11. Hrebík D, Štveraková D, Škubník K, Füzik T, Pantůček R, Plevka P. 2019. Structure and genome ejection mechanism of *Staphylococcus aureus* phage P68. Sci Adv 5:eaaw7414. https://doi.org/10.1126/sciadv.aaw7414.
12. Petrovic Fabijan A, Lin RCY, Ho J, Maddocks S, Ben Zakour NL, Iredell JR, Westmead Bacteriophage Therapy Team. 2020. Safety of bacteriophage therapy in severe *Staphylococcus aureus* infection. Nat Microbiol 5:465–472. https://doi.org/10.1038/s41564-019-0634-z.
13. O'Flaherty S, Coffey A, Edwards R, Meaney W, Fitzgerald GF, Ross RP. 2004. Genome of staphylococcal phage K: a new lineage of Myoviridae infecting gram-positive bacteria with a low G+C content. J Bacteriol 186:2862–2871. https://doi.org/10.1128/JB.186.9.2862-2871.2004.
14. Ajuebor J, Buttimer C, Arroyo-Moreno S, Chanishvili N, Gabriel E, O'Mahony J, McAuliffe O, Neve H, Franz C, Coffey A. 2018. Comparison of Staphylococcus phage K with close phage relatives commonly employed in phage therapeutics. Antibiotics 7:37. https://doi.org/10.3390/antibiotics7020037.
15. Botka T, Pantůček R, Mašlaňová I, Benešík M, Petráš P, Růžičková V, Havlíčková P, Varga M, Žemličková H, Koláčková I, Florianová M, Jakubů V, Karpíšková R, Doškař J. 2019. Lytic and genomic properties of spontaneous host-range Kayvirus mutants prove their suitability for upgrading phage therapeutics against staphylococci. Sci Rep 9:5475. https://doi.org/10.1038/s41598-019-41868-w.
16. Sáez Moreno D, Visram Z, Mutti M, Restrepo-Cordoba M, Hartmann S, Kremers AI, Tišáková L, Schertler S, Wittmann J, Kalali B, Monecke S, Ehricht R, Resch G, Corsini L. 2021. ε^2-Phages are naturally bred and have a vastly improved host range in *Staphylococcus aureus* over wild type phages. Pharmaceuticals (Basel) 14:325. https://doi.org/10.3390/ph14040325.
17. Sanz-Gaitero M, Keary R, Garcia-Doval C, Coffey A, van Raaij MJ. 2013. Crystallization of the CHAP domain of the endolysin from *Staphylococcus aureus* bacteriophage K. Acta Crystallogr Sect F Struct Biol Cryst Commun 69:1393–1396. https://doi.org/10.1107/S1744309113030133.
18. Benešík M, Novaček J, Janda L, Dopitová R, Pernisová M, Melková K, Tišáková L, Doškař J, Žídek L, Hejátko J, Pantůček R. 2018. Role of SH3b binding domain in a natural deletion mutant of Kayvirus endolysin LysF1 with a broad range of lytic activity. Virus Genes 54:130–139. https://doi.org/10.1007/s11262-017-1507-2.
19. Horgan M, O'Flynn G, Garry J, Cooney J, Coffey A, Fitzgerald GF, Ross RP, McAuliffe O. 2009. Phage lysin LysK can be truncated to its CHAP domain

Downloaded from https://journals.asm.org/journal/mbio on 04 February 2026 by 147.251.86.90.

and retain lytic activity against live antibiotic-resistant staphylococci. Appl Environ Microbiol 75:872–874. https://doi.org/10.1128/AEM.01831-08.
20. Simon K, Pier W, Kruttgen A, Horz HP. 2021. Synergy between phage Sb-1 and oxacillin against methicillin-resistant *Staphylococcus aureus*. Antibiotics 10:849. https://doi.org/10.3390/antibiotics10070849.
21. Kaźmierczak Z, Majewska J, Miernikiewicz P, Międzybrodzki R, Nowak S, Harhala M, Lecion D, Kęska W, Owczarek B, Ciekot J, Drab M, Kędzierski P, Mazurkiewicz-Kania M, Górski A, Dąbrowska K. 2021. Immune response to therapeutic staphylococcal bacteriophages in mammals: kinetics of induction, immunogenic structural proteins, natural and induced antibodies. Front Immunol 12:639570. https://doi.org/10.3389/fimmu.2021.639570.
22. Nováček J, Šiborová M, Benešík M, Pantůček R, Doškař J, Plevka P. 2016. Structure and genome release of Twort-like Myoviridae phage with a double-layered baseplate. Proc Natl Acad Sci U S A 113:9351–9356. https://doi.org/10.1073/pnas.1605883113.
23. Zelasko S, Górski A, Dabrowska K. 2017. Delivering phage therapy *per os*: benefits and barriers. Expert Rev Anti Infect Ther 15:167–179. https://doi.org/10.1080/14787210.2017.1265447.
24. Kifelew LG, Warner MS, Morales S, Vaughan L, Woodman R, Fitridge R, Mitchell JG, Speck P. 2020. Efficacy of phage cocktail AB-SA01 therapy in diabetic mouse wound infections caused by multidrug-resistant *Staphylococcus aureus*. BMC Microbiol 20:204. https://doi.org/10.1186/s12866-020-01891-8.
25. Leskinen K, Tuomala H, Wicklund A, Horsma-Heikkinen J, Kuusela P, Skurnik M, Kiljunen S. 2017. Characterization of vB_SauM-fRuSau02, a Twort-like bacteriophage isolated from a therapeutic phage cocktail. Viruses 9:258. https://doi.org/10.3390/v9090258.
26. Finstrlová A, Mašlaňová I, Blasdel Reuter BG, Doškař J, Götz F, Pantůček R. 2022. Global transcriptomic analysis of bacteriophage-host interactions between a Kayvirus therapeutic phage and *Staphylococcus aureus*. Microbiol Spectr 10:e00123-22. https://doi.org/10.1128/spectrum.00123-22.
27. Arroyo-Moreno S, Buttimer C, Bottacini F, Chanishvili N, Ross P, Hill C, Coffey A. 2022. Insights into gene transcriptional regulation of *Kayvirus* bacteriophages obtained from therapeutic mixtures. Viruses 14:626. https://doi.org/10.3390/v14030626.
28. Eyer L, Pantůcek R, Zdráhal Z, Konecná H, Kaspárek P, Růzicková V, Hernychová L, Preisler J, Doskar J. 2007. Structural protein analysis of the polyvalent staphylococcal bacteriophage 812. Proteomics 7:64–72. https://doi.org/10.1002/pmic.200600280.
29. Dy RL, Richter C, Salmond GP, Fineran PC. 2014. Remarkable mechanisms in microbes to resist phage infections. Annu Rev Virol 1:307–331. https://doi.org/10.1146/annurev-virology-031413-085500.
30. van Houte S, Buckling A, Westra ER. 2016. Evolutionary ecology of prokaryotic immune mechanisms. Microbiol Mol Biol Rev 80:745–763. https://doi.org/10.1128/MMBR.00011-16.
31. Moller AG, Lindsay JA, Read TD. 2019. Determinants of phage host range in *Staphylococcus* species. Appl Environ Microbiol 85:e00209-19. https://doi.org/10.1128/AEM.00209-19.
32. Mo CY, Mathai J, Rostol JT, Varble A, Banh DV, Marraffini LA. 2021. Type III-A CRISPR immunity promotes mutagenesis of staphylococci. Nature 592:611–615. https://doi.org/10.1038/s41586-021-03440-3.
33. Winstel V, Liang C, Sanchez-Carballo P, Steglich M, Munar M, Broker BM, Penadés JR, Nubel U, Holst O, Dandekar T, Peschel A, Xia G. 2013. Wall teichoic acid structure governs horizontal gene transfer between major bacterial pathogens. Nat Commun 4:2345. https://doi.org/10.1038/ncomms3345.
34. Nordström K, Forsgren A. 1974. Effect of protein A on adsorption of bacteriophages to *Staphylococcus aureus*. J Virol 14:198–202. https://doi.org/10.1128/JVI.14.2.198-202.1974.
35. Moller AG, Winston K, Ji S, Wang J, Hargita Davis MN, Solis-Lemus CR, Read TD. 2021. Genes influencing phage host range in *Staphylococcus aureus* on a species-wide scale. mSphere 6:e01263-20. https://doi.org/10.1128/mSphere.01263-20.
36. Ibarra-Chávez R, Brady A, Chen J, Penadés JR, Haag AF. 2022. Phage-inducible chromosomal islands promote genetic variability by blocking phage reproduction and protecting transductants from phage lysis. PLoS Genet 18:e1010146. https://doi.org/10.1371/journal.pgen.1010146.
37. Stone E, Campbell K, Grant I, McAuliffe O. 2019. Understanding and exploiting phage-host interactions. Viruses 11:567. https://doi.org/10.3390/v11060567.
38. Pantůcek R, Rosypalová A, Doskar J, Kailerová J, Růzicková V, Borecká P, Snopková S, Horváth R, Götz F, Rosypal S. 1998. The polyvalent staphylococcal phage φ812: its host-range mutants and related phages. Virology 246:241–252. https://doi.org/10.1006/viro.1998.9203.
39. Kwan T, Liu J, DuBow M, Gros P, Pelletier J. 2005. The complete genomes and proteomes of 27 *Staphylococcus aureus* bacteriophages. Proc Natl Acad Sci U S A 102:5174–5179. https://doi.org/10.1073/pnas.0501140102.
40. Lepuschitz S, Huhulescu S, Hyden P, Springer B, Rattei T, Allerberger F, Mach RL, Ruppitsch W. 2018. Characterization of a community-acquired-MRSA USA300 isolate from a river sample in Austria and whole genome sequence based comparison to a diverse collection of USA300 isolates. Sci Rep 8:9467. https://doi.org/10.1038/s41598-018-27781-8.
41. Charpentier E, Anton AI, Barry P, Alfonso B, Fang Y, Novick RP. 2004. Novel cassette-based shuttle vector system for Gram-positive bacteria. Appl Environ Microbiol 70:6076–6085. https://doi.org/10.1128/AEM.70.10.6076-6085.2004.
42. Kahánková J, Pantůcek R, Goerke C, Růžičková V, Holochová P, Doškař J. 2010. Multilocus PCR typing strategy for differentiation of *Staphylococcus aureus* siphoviruses reflecting their modular genome structure. Environ Microbiol 12:2527–2538. https://doi.org/10.1111/j.1462-2920.2010.02226.x.
43. Coombs GW, Baines SL, Howden BP, Swenson KM, O'Brien FG. 2020. Diversity of bacteriophages encoding Panton-Valentine leukocidin in temporally and geographically related *Staphylococcus aureus*. PLoS One 15:e0228676. https://doi.org/10.1371/journal.pone.0228676.
44. Goerke C, Pantucek R, Holtfreter S, Schulte B, Zink M, Grumann D, Bröker BM, Doskar J, Wolz C. 2009. Diversity of prophages in dominant *Staphylococcus aureus* clonal lineages. J Bacteriol 191:3462–3468. https://doi.org/10.1128/JB.01804-08.
45. Göller PC, Elsener T, Lorgé D, Radulovic N, Bernardi V, Naumann A, Amri N, Khatchatourova E, Coutinho FH, Loessner MJ, Gómez-Sanz E. 2021. Multi-species host range of staphylococcal phages isolated from wastewater. Nat Commun 12:6965. https://doi.org/10.1038/s41467-021-27037-6.
46. Gobl C, Kosol S, Stockner T, Ruckert HM, Zangger K. 2010. Solution structure and membrane binding of the toxin *fst* of the par addiction module. Biochemistry 49:6567–6575. https://doi.org/10.1021/bi1005128.
47. Weaver KE, Weaver DM, Wells CL, Waters CM, Gardner ME, Ehli EA. 2003. *Enterococcus faecalis* plasmid pAD1-encoded Fst toxin affects membrane permeability and alters cellular responses to lantibiotics. J Bacteriol 185:2169–2177. https://doi.org/10.1128/JB.185.7.2169-2177.2003.
48. Sayed N, Nonin-Lecomte S, Rety S, Felden B. 2012. Functional and structural insights of a *Staphylococcus aureus* apoptotic-like membrane peptide from a toxin-antitoxin module. J Biol Chem 287:43454–43463. https://doi.org/10.1074/jbc.M112.402693.
49. Arcus V. 2002. OB-fold domains: a snapshot of the evolution of sequence, structure and function. Curr Opin Struct Biol 12:794–801. https://doi.org/10.1016/S0959-440X(02)00392-5.
50. Domingues S, McGovern S, Plochocka D, Santos MA, Ehrlich SD, Polard P, Chopin MC. 2008. The lactococcal abortive infection protein AbiP is membrane-anchored and binds nucleic acids. Virology 373:14–24. https://doi.org/10.1016/j.virol.2007.11.004.
51. Guo L, Sattler L, Shafqat S, Graumann PL, Bramkamp M. 2022. A bacterial dynamin-like protein confers a novel phage resistance strategy on the population level in *Bacillus subtilis*. mBio 13:e03753-21. https://doi.org/10.1128/mbio.03753-21.
52. Lau RK, Ye Q, Birkholz EA, Berg KR, Patel L, Mathews IT, Watrous JD, Ego K, Whiteley AT, Lowey B, Mekalanos JJ, Kranzusch PJ, Jain M, Pogliano J, Corbett KD. 2020. Structure and mechanism of a cyclic trinucleotide-activated bacterial endonuclease mediating bacteriophage immunity. Mol Cell 77:723–733. https://doi.org/10.1016/j.molcel.2019.12.010.
53. Lopatina A, Tal N, Sorek R. 2020. Abortive infection: bacterial suicide as an antiviral immune strategy. Annu Rev Virol 7:371–384. https://doi.org/10.1146/annurev-virology-011620-040628.
54. Belley A, Callejo M, Arhin F, Dehbi M, Fadhil I, Liu J, McKay G, Srikumar R, Bauda P, Bergeron D, Ha N, Dubow M, Gros P, Pelletier J, Moeck G. 2006. Competition of bacteriophage polypeptides with native replicase proteins for binding to the DNA sliding clamp reveals a novel mechanism for DNA replication arrest in *Staphylococcus aureus*. Mol Microbiol 62:1132–1143. https://doi.org/10.1111/j.1365-2958.2006.05427.x.
55. Rees PJ, Fry BA. 1981. The replication of bacteriophage K DNA in *Staphylococcus aureus*. J Gen Virol 55:41–51. https://doi.org/10.1099/0022-1317-55-1-41.
56. Parma DH, Snyder M, Sobolevski S, Nawroz M, Brody E, Gold L. 1992. The Rex system of bacteriophage lambda: tolerance and altruistic cell death. Genes Dev 6:497–510. https://doi.org/10.1101/gad.6.3.497.
57. Tremblay C, Bédard M, Bonin MA, Lavigne P. 2016. Solution structure of the 13th C2H2 zinc finger of Miz-1. Biochem Biophys Res Commun 473:471–475. https://doi.org/10.1016/j.bbrc.2016.03.034.
58. Li Y, Haarhuis JHI, Sedeno Cacciatore A, Oldenkamp R, van Ruiten MS, Willems L, Teunissen H, Muir KW, de Wit E, Rowland BD, Panne D. 2020.

Downloaded from https://journals.asm.org/journal/mbio on 04 February 2026 by 147.251.86.90.

The structural basis for cohesin-CTCF-anchored loops. Nature 578:472–476. https://doi.org/10.1038/s41586-019-1910-z.
59. Shah M, Taylor VL, Bona D, Tsao Y, Stanley SY, Pimentel-Elardo SM, McCallum M, Bondy-Denomy J, Howell PL, Nodwell JR, Davidson AR, Moraes TF, Maxwell KL. 2021. A phage-encoded anti-activator inhibits quorum sensing in *Pseudomonas aeruginosa*. Mol Cell 81:571–583. https://doi.org/10.1016/j.molcel.2020.12.011.
60. Owen SV, Wenner N, Dulberger CL, Rodwell EV, Bowers-Barnard A, Quinones-Olvera N, Rigden DJ, Rubin EJ, Garner EC, Baym M, Hinton JCD. 2021. Prophages encode phage-defense systems with cognate self-immunity. Cell Host Microbe 29:1620–1633. https://doi.org/10.1016/j.chom.2021.09.002.
61. Xia G, Corrigan RM, Winstel V, Goerke C, Grundling A, Peschel A. 2011. Wall teichoic acid-dependent adsorption of staphylococcal siphovirus and myovirus. J Bacteriol 193:4006–4009. https://doi.org/10.1128/JB.01412-10.
62. Doškar J, Pallová P, Pantucek R, Rosypal S, Ruzicková V, Pantucková P, Kailerová J, Klepárník K, Malá Z, Bocek P. 2000. Genomic relatedness of *Staphylococcus aureus* phages of the International Typing Set and detection of serogroup A, B, and F prophages in lysogenic strains. Can J Microbiol 46:1066–1076. https://doi.org/10.1139/cjm-46-11-1066.
63. Novick RP. 1963. Analysis by transduction of mutations affecting penicillinase formation in *Staphylococcus aureus*. J Gen Microbiol 33:121–136. https://doi.org/10.1099/00221287-33-1-121.
64. Borecká P, Rosypal S, Pantůcek R, Doskar J. 1996. Localization of prophages of serological group B and F on restriction fragments defined in the restriction map of *Staphylococcus aureus* NCTC 8325. FEMS Microbiol Lett 143:203–210. https://doi.org/10.1111/j.1574-6968.1996.tb08481.x.
65. Pantůcek R, Doskar J, Růzicková V, Kaspárek P, Orácová E, Kvardová V, Rosypal S. 2004. Identification of bacteriophage types and their carriage in *Staphylococcus aureus*. Arch Virol 149:1689–1703. https://doi.org/10.1007/s00705-004-0335-6.
66. Bae T, Baba T, Hiramatsu K, Schneewind O. 2006. Prophages of *Staphylococcus aureus* Newman and their contribution to virulence. Mol Microbiol 62:1035–1047. https://doi.org/10.1111/j.1365-2958.2006.05441.x.
67. Augustin J, Götz F. 1990. Transformation of *Staphylococcus epidermidis* and other staphylococcal species with plasmid DNA by electroporation. FEMS Microbiol Lett 66:203–207. https://doi.org/10.1111/j.1574-6968.1990.tb03997.x.
68. Mašlaňová I, Doškař J, Varga M, Kuntová L, Mužík J, Malúšková D, Růžičková V, Pantůček R. 2013. Bacteriophages of *Staphylococcus aureus* efficiently package various bacterial genes and mobile genetic elements including SCC*mec* with different frequencies. Environ Microbiol Rep 5:66–73. https://doi.org/10.1111/j.1758-2229.2012.00378.x.
69. Zeman M, Mašlaňová I, Indráková A, Šiborová M, Mikulášek K, Bendíčková K, Plevka P, Vrbovská V, Zdráhal Z, Doškař J, Pantůček R. 2017. *Staphylococcus sciuri* bacteriophages double-convert for staphylokinase and phospholipase, mediate interspecies plasmid transduction, and package mecA gene. Sci Rep 7:46319. https://doi.org/10.1038/srep46319.
70. Zheng X, Marsman G, Lacey KA, Chapman JR, Goosmann C, Ueberheide BM, Torres VJ. 2021. The cell envelope of *Staphylococcus aureus* selectively controls the sorting of virulence factors. Nat Commun 12:6193. https://doi.org/10.1038/s41467-021-26517-z.
71. Novo DJ, Perlmutter NG, Hunt RH, Shapiro HM. 2000. Multiparameter flow cytometric analysis of antibiotic effects on membrane potential, membrane permeability, and bacterial counts of *Staphylococcus aureus* and *Micrococcus luteus*. Antimicrob Agents Chemother 44:827–834. https://doi.org/10.1128/AAC.44.4.827-834.2000.
72. Krogh A, Larsson B, von Heijne G, Sonnhammer EL. 2001. Predicting transmembrane protein topology with a hidden Markov model: application to complete genomes. J Mol Biol 305:567–580. https://doi.org/10.1006/jmbi.2000.4315.
73. Yan J, Kurgan L. 2017. DRNApred, fast sequence-based method that accurately predicts and discriminates DNA- and RNA-binding residues. Nucleic Acids Res 45:e84. https://doi.org/10.1093/nar/gkx059.
74. Soding J, Biegert A, Lupas AN. 2005. The HHpred interactive server for protein homology detection and structure prediction. Nucleic Acids Res 33:W244–W248. https://doi.org/10.1093/nar/gki408.
75. Kelley LA, Mezulis S, Yates CM, Wass MN, Sternberg MJ. 2015. The Phyre2 web portal for protein modeling, prediction and analysis. Nat Protoc 10:845–858. https://doi.org/10.1038/nprot.2015.053.
76. Holm L, Rosenstrom P. 2010. Dali server: conservation mapping in 3D. Nucleic Acids Res 38:W545–W549. https://doi.org/10.1093/nar/gkq366.
77. Jumper J, Evans R, Pritzel A, Green T, Figurnov M, Ronneberger O, Tunyasuvunakool K, Bates R, Zidek A, Potapenko A, Bridgland A, Meyer C, Kohl SAA, Ballard AJ, Cowie A, Romera-Paredes B, Nikolov S, Jain R, Adler J, Back T, Petersen S, Reiman D, Clancy E, Zielinski M, Steinegger M, Pacholska M, Berghammer T, Bodenstein S, Silver D, Vinyals O, Senior AW, Kavukcuoglu K, Kohli P, Hassabis D. 2021. Highly accurate protein structure prediction with AlphaFold. Nature 596:583–589. https://doi.org/10.1038/s41586-021-03819-2.
78. Pettersen EF, Goddard TD, Huang CC, Couch GS, Greenblatt DM, Meng EC, Ferrin TE. 2004. UCSF Chimera - a visualization system for exploratory research and analysis. J Comput Chem 25:1605–1612. https://doi.org/10.1002/jcc.20084.
79. Pettersen EF, Goddard TD, Huang CC, Meng EC, Couch GS, Croll TI, Morris JH, Ferrin TE. 2021. UCSF ChimeraX: structure visualization for researchers, educators, and developers. Protein Sci 30:70–82. https://doi.org/10.1002/pro.3943.
80. Fišarová L, Botka T, Du X, Mašlaňová I, Bárdy P, Pantůček R, Benešík M, Roudnický P, Winstel V, Larsen J, Rosenstein R, Peschel A, Doškař J. 2021. *Staphylococcus epidermidis* phages transduce antimicrobial resistance plasmids and mobilize chromosomal islands. mSphere 6:e00223-21. https://doi.org/10.1128/mSphere.00223-21.
81. Bolger AM, Lohse M, Usadel B. 2014. Trimmomatic: a flexible trimmer for Illumina sequence data. Bioinformatics 30:2114–2120. https://doi.org/10.1093/bioinformatics/btu170.
82. Wick RR, Judd LM, Gorrie CL, Holt KE. 2017. Unicycler: resolving bacterial genome assemblies from short and long sequencing reads. PLoS Comput Biol 13:e1005595. https://doi.org/10.1371/journal.pcbi.1005595.
83. Walker BJ, Abeel T, Shea T, Priest M, Abouelliel A, Sakthikumar S, Cuomo CA, Zeng Q, Wortman J, Young SK, Earl AM. 2014. Pilon: an integrated tool for comprehensive microbial variant detection and genome assembly improvement. PLoS One 9:e112963. https://doi.org/10.1371/journal.pone.0112963.
84. Li W, O'Neill KR, Haft DH, DiCuccio M, Chetvernin V, Badretdin A, Coulouris G, Chitsaz F, Derbyshire MK, Durkin AS, Gonzales NR, Gwadz M, Lanczycki CJ, Song JS, Thanki N, Wang J, Yamashita RA, Yang M, Zheng C, Marchler-Bauer A, Thibaud-Nissen F. 2021. RefSeq: expanding the Prokaryotic Genome Annotation Pipeline reach with protein family model curation. Nucleic Acids Res 49:D1020–D1028. https://doi.org/10.1093/nar/gkaa1105.
85. Jolley KA, Bray JE, Maiden MCJ. 2018. Open-access bacterial population genomics: BIGSdb software, the PubMLST.org website and their applications. Wellcome Open Res 3:124. https://doi.org/10.12688/wellcomeopenres.14826.1.
86. Harmsen D, Claus H, Witte W, Rothganger J, Claus H, Turnwald D, Vogel U. 2003. Typing of methicillin-resistant *Staphylococcus aureus* in a university hospital setting by using novel software for spa repeat determination and database management. J Clin Microbiol 41:5442–5448. https://doi.org/10.1128/JCM.41.12.5442-5448.2003.
87. Bikandi J, San Millan R, Rementeria A, Garaizar J. 2004. *In silico* analysis of complete bacterial genomes: PCR, AFLP-PCR and endonuclease restriction. Bioinformatics 20:798–799. https://doi.org/10.1093/bioinformatics/btg491.
88. Solovyev V, Salamov A. 2011. Automatic annotation of microbial genomes and metagenomic sequences, p 61–78. *In* Li RW (ed), Metagenomics and its applications in agriculture, biomedicine and environmental studies, vol 1. Nova Science Publishers, Hauppauge, NY.
89. Macke TJ, Ecker DJ, Gutell RR, Gautheret D, Case DA, Sampath R. 2001. RNAMotif, an RNA secondary structure definition and search algorithm. Nucleic Acids Res 29:4724–4735. https://doi.org/10.1093/nar/29.22.4724.
90. Meier-Kolthoff JP, Goker M. 2017. VICTOR: genome-based phylogeny and classification of prokaryotic viruses. Bioinformatics 33:3396–3404. https://doi.org/10.1093/bioinformatics/btx440.
91. Lefort V, Desper R, Gascuel O. 2015. FastME 2.0: a comprehensive, accurate, and fast distance-based phylogeny inference program. Mol Biol Evol 32:2798–2800. https://doi.org/10.1093/molbev/msv150.
92. Kaneko J, Kimura T, Narita S, Tomita T, Kamio Y. 1998. Complete nucleotide sequence and molecular characterization of the temperate staphylococcal bacteriophage φPVL carrying Panton–Valentine leukocidin genes. Gene 215:57–67. https://doi.org/10.1016/S0378-1119(98)00278-9.
93. Kittl S, Brodard I, Overesch G, Kuhnert P, Jores J, Labroussaa F. 2021. Complete genome sequences of the methicillin-resistant strain *Staphylococcus aureus* 17Gst354 and its prophage *Staphylococcus* phage vB_StaphS-IVBph354. Microbiol Resour Announc 10:e0058621. https://doi.org/10.1128/MRA.00586-21.
94. Paredes C, Chi SI, Flint A, Weedmark K, McDonald C, Bearne J, Ramirez-Arcos S, Pagotto F. 2021. Complete genome sequence of *Staphylococcus aureus* PS/BAC/169/17/W, isolated from a contaminated platelet concentrate in England. Microbiol Resour Announc 10:e00841-21. https://doi.org/10.1128/MRA.00841-21.

Downloaded from https://journals.asm.org/journal/mbio on 04 February 2026 by 147.251.86.90.

95. Kreiswirth BN, Lofdahl S, Betley MJ, O'Reilly M, Schlievert PM, Bergdoll MS, Novick RP. 1983. The toxic shock syndrome exotoxin structural gene is not detectably transmitted by a prophage. Nature 305:709–712. https://doi.org/10.1038/305709a0.
96. Novick RP. 1967. Properties of a cryptic high-frequency transducing phage in *Staphylococcus aureus*. Virology 33:155–166. https://doi.org/10.1016/0042-6822(67)90105-5.
97. Yoshizawa Y. 1985. Isolation and characterization of restriction negative mutants of *Staphylococcus aureus*. Jikeikai Med J 32:415–421.
98. Diep BA, Gill SR, Chang RF, Phan TH, Chen JH, Davidson MG, Lin F, Lin J, Carleton HA, Mongodin EF, Sensabaugh GF, Perdreau-Remington F. 2006. Complete genome sequence of USA300, an epidemic clone of community-acquired meticillin-resistant *Staphylococcus aureus*. Lancet 367:731–739. https://doi.org/10.1016/S0140-6736(06)68231-7.
99. Rohmer C, Dobritz R, Tuncbilek-Dere D, Lehmann E, Gerlach D, George SE, Bae T, Nieselt K, Wolz C. 2022. Influence of *Staphylococcus aureus* strain background on Sa3int phage life cycle switches. Viruses 14:2471. https://doi.org/10.3390/v14112471.
100. Kuntová L, Pantůček R, Rájová J, Růžičková V, Petráš P, Mašlaňová I, Doškař J. 2012. Characteristics and distribution of plasmids in a clonally diverse set of methicillin-resistant *Staphylococcus aureus* strains. Arch Microbiol 194:607–614. https://doi.org/10.1007/s00203-012-0797-y.
101. Augustin J, Rosenstein R, Wieland B, Schneider U, Schnell N, Engelke G, Entian KD, Gotz F. 1992. Genetic analysis of epidermin biosynthetic genes and epidermin-negative mutants of *Staphylococcus epidermidis*. Eur J Biochem 204:1149–1154. https://doi.org/10.1111/j.1432-1033.1992.tb16740.x.

Downloaded from https://journals.asm.org/journal/mbio on 04 February 2026 by 147.251.86.90.

APPENDIX 12

Kovařovic V, Finstrlová A, Sedláček I, Petráš P, Švec P, Mašlaňová I, Neumann-Schaal M, Šedo O, Botka T, Staňková E, Doškař J, Pantůček R (2023) *Staphylococcus brunensis* sp. nov. isolated from human clinical specimens with a staphylococcal cassette chromosome-related genomic island outside of the *rlmH* gene bearing the *ccrDE* recombinase gene complex. *Microbiology Spectrum* 11:e0134223. https://doi.org/10.1128/spectrum.01342-23
(JCR 2023: IF = 3.7; Q2 – Microbiology)

CC BY 4.0

AMERICAN SOCIETY FOR MICROBIOLOGY | Microbiology Spectrum

| Evolution | Research Article

Staphylococcus brunensis sp. nov. isolated from human clinical specimens with a staphylococcal cassette chromosome-related genomic island outside of the *rlmH* gene bearing the *ccrDE* recombinase gene complex

Vojtěch Kovařovic,[1] Adéla Finstrlová,[1] Ivo Sedláček,[2] Petr Petráš,[3] Pavel Švec,[2] Ivana Mašlaňová,[1] Meina Neumann-Schaal,[4] Ondrej Šedo,[5] Tibor Botka,[1] Eva Staňková,[2] Jiří Doškař,[1] Roman Pantůček[1]

AUTHOR AFFILIATIONS See affiliation list on p. 17.

ABSTRACT Novel species of coagulase-negative staphylococci, which could serve as reservoirs of virulence and antimicrobial resistance factors for opportunistic pathogens from the genus *Staphylococcus*, are recognized in human and animal specimens due to advances in diagnostic techniques. Here, we used whole-genome sequencing, extensive biotyping, MALDI-TOF mass spectrometry, and chemotaxonomy to characterize five coagulase-negative strains from the *Staphylococcus haemolyticus* phylogenetic clade obtained from human ear swabs, wounds, and bile. Based on the results of polyphasic taxonomy, we propose the species *Staphylococcus brunensis* sp. nov. (type strain NRL/St 16/872^T = CCM 9024^T = LMG 31872^T = DSM 111349^T). The genomic analysis revealed numerous variable genomic elements, including staphylococcal cassette chromosome (SCC), prophages, plasmids, and a unique 18.8 kb-long genomic island SbCI$_{ccrDE}$ integrated into the ribosomal protein L7 serine acetyltransferase gene *rimL*. SbCI$_{ccrDE}$ has a cassette chromosome recombinase (*ccr*) gene complex with a typical structure found in SCCs. Based on nucleotide and amino acid identity to other known *ccr* genes and the distinct integration site that differs from the canonical methyltransferase gene *rlmH* exploited by SCCs, we classified the *ccr* genes as novel variants, *ccrDE*. The comparative genomic analysis of SbCI$_{ccrDE}$ with related islands shows that they can accumulate virulence and antimicrobial resistance factors creating novel resistance elements, which reflects the evolution of SCC. The spread of these resistance islands into established pathogens such as *Staphylococcus aureus* would pose a great threat to the healthcare system.

IMPORTANCE The coagulase-negative staphylococci are important opportunistic human pathogens, which cause bloodstream and foreign body infections, mainly in immunocompromised patients. The mobile elements, primarily the staphylococcal cassette chromosome *mec*, which confers resistance to methicillin, are the key to the successful dissemination of staphylococci into healthcare and community settings. Here, we present a novel species of the *Staphylococcus* genus isolated from human clinical material. The detailed analysis of its genome revealed a previously undescribed genomic island, which is closely related to the staphylococcal cassette chromosome and has the potential to accumulate and spread virulence and resistance determinants. The island harbors a set of conserved genes required for its mobilization, which we recognized as novel cassette chromosome recombinase genes *ccrDE*. Similar islands were revealed not only in the genomes of coagulase-negative staphylococci but also in *S. aureus*. The comparative genomic study contributes substantially to the understanding of the evolution and pathogenesis of staphylococci.

Editor Shannon D. Manning, Michigan State University, East Lansing, Michigan, USA

Address correspondence to Roman Pantůček, pantucek@sci.muni.cz.

Vojtěch Kovařovic and Adéla Finstrlová contributed equally to this article. To determine the order of the authors we flipped the coin.

The authors declare no conflict of interest.

See the funding table on p. 18.

Received 29 March 2023
Accepted 3 July 2023
Published 15 September 2023

Copyright © 2023 Kovařovic et al. This is an open-access article distributed under the terms of the Creative Commons Attribution 4.0 International license.

Downloaded from https://journals.asm.org/journal/spectrum on 04 February 2026 by 147.251.86.90.

KEYWORDS coagulase-negative staphylococci, phylogenetic analysis, comparative genomics, mobile genetic elements, genomic islands, cassette chromosome recombinase, polyphasic taxonomy, gram-positive pathogens

Staphylococci, mainly coagulase-positive *Staphylococcus aureus*, are the leading cause of a broad spectrum of diseases in humans and animals. Over the last three decades, coagulase-negative staphylococcal species (CoNS), with the most significant being *Staphylococcus epidermidis*, *Staphylococcus haemolyticus,* and *Staphylococcus hominis*, have been recognized as opportunistic pathogens, especially in immunocompromised patients. CoNS are a frequent cause of nosocomial infections related to catheters or medical devices aided by their ability to form a biofilm (1). Additionally, the gene pool of substrate utilization pathways and resistance determinants enables CoNS to occupy various niches, providing favorable conditions for the emergence of multidrug-resistant CoNS and their subsequent spread in healthcare environments (2).

The adaptation of *S. haemolyticus* strains to diverse environments is facilitated by frequent recombination among numerous insertion sequences (ISSha*1*) (3). Therefore, the standard microbial and molecular diagnostic tools have limited discriminatory power to reliably distinguish species closely related to *S. haemolyticus* (4). Only recently, molecular diagnostics approaches, mainly in-depth whole-genome characterization, have assigned atypical *S. haemolyticus* strains isolated from clinical specimens into the new species *Staphylococcus borealis* (5) and *Staphylococcus taiwanensis* (6). The core genome phylogeny also led to the reclassification of the *S. petrasii* phylogenetic complex (7, 8), which now consists of three species—*S. petrasii*, *S. croceilyticus*, and *S. pragensis* (9). All these species were isolated from various human biological samples, mainly from wounds, eye and ear infections, urinary infections, and blood samples (10).

The versatility of CoNS is associated with a significant reservoir of mobile genetic elements (MGEs). Notably, the methicillin resistance encoded by the staphylococcal chromosomal cassette (SCC) *mec* (SCC*mec*) significantly complicates healthcare and increases the need to use second-line antimicrobial drugs to treat staphylococcal infections (11). Apart from *mec* genes responsible for methicillin resistance, SCC*mec* carries numerous genes for virulence, such as phenol-soluble modulins (PSM-*mec*), plasmin, or heavy-metal and other resistance genes contributing to the survival of these strains in an environment (12–14). It is suspected that the SCC*mec* originates from CoNS species (15), but the natural mechanism of SCC transmission is still unknown. It can be transferred intra- and even interspecies by transduction (16), conjugation (17), or natural competence (18). The transfer of SCC*mec* is mediated by *ccr* chromosome cassette genes of the serine recombinase family. Three phylogenetically distinct *ccr* genes, namely *ccrA*, *ccrB*, and *ccrC,* have been delineated with nucleotide identities below 50%. These recombinases recognize a specific *att* site in the bacterial *rlmH* gene for ribosomal RNA large-subunit methyltransferase H (19). The recombinases CcrA and CcrB function together as a heterotetramer in the specific excision of the SCC (20), whereas the CcrC recombinase enables mobilization of the element without another recombinase (21).

The recent increase in the association of CoNS with nosocomial infections and improvements in diagnostic approaches make it possible to recognize other often overlooked species of this group related to human diseases. Investigation of these CoNS as a pool of genes for antimicrobial resistance and virulence can reveal the molecular mechanisms that lead to these opportunistic pathogens' evolution, adaptation, and success. This article reports the polyphasic characterization of five *Staphylococcus* sp. isolates from human clinical material to delineate a novel species. Whole-genome sequence analyses of the strains revealed a remarkable non-SCC genomic island harboring *ccrDE* cassette chromosome recombinase types.

Downloaded from https://journals.asm.org/journal/spectrum on 04 February 2026 by 147.251.86.90.

RESULTS

Phylogenetic relationship of the strains

Five unidentified *Staphylococcus* sp. strains were collected from various human clinical specimens from both mixed culture and monoculture between 2016 and 2022 (Table 1) and transferred to the National Reference Laboratory for Staphylococci (National Institute of Public Health, Prague) for long-term storage and further study. The phylogenetic analysis of complete 16S rRNA gene sequences consistently placed the five isolates in *S. haemolyticus* cluster group defined previously (22). The closest relatives were *Staphylococcus petrasii*, *Staphylococcus croceilyticus*, and *Staphylococcus pragensis,* with 16S rRNA gene sequence similarities ranging from 99.80 to 99.59%, while other species were below 99.4% similarity. The topology of the neighbor-joining (NJ) phylogenetic tree constructed with 16S rRNA gene sequences was similar to that of the maximum likelihood (ML) tree (Fig. 1A). Because the 16S rRNA analysis has limited discriminatory power in the genus *Staphylococcus* (5, 6, 23), the phylogenetic position of the new isolates was also assessed using the concatenated multilocus sequence data of six routinely used conserved housekeeping genes: *rpoB*, *hsp60*, *dnaJ*, *tufA*, *gap*, and *sodA* for discrimination of staphylococcal species (Fig. 1B). The ML phylogenetic tree for the housekeeping genes had a very similar topology to that of the 16S rRNA gene tree and to the additional phylogenetic trees constructed using the up-to-date bacterial core gene (UBCG) at the nucleotide and protein level (Fig. 1C and D).

The whole-genome phylogenetic distance from the related staphylococcal taxa with an ANI value of <92.3% (Table S3) and digital DNA-DNA hybridization (dDDH) of <45.6% determined the closest species *S. petrasii*; however, the values were below the species delineation thresholds, which are 95–96% and 70%, respectively (24). The whole-genome phylogeny thus confirmed that the five isolates represent a distinct *Staphylococcus* species designated *Staphylococcus brunensis* sp. nov.

Growth, morphological, biochemical, and chemotaxonomical characterization of analyzed isolates

All five isolates exhibited Gram-positive stain, irregular cells ranging in diameter from 433 nm to 1,210 nm (Fig. S1) arranged in pairs, tetrads, and clusters. They grew very well on

TABLE 1 Origin of the strains of *Staphylococcus brunensis* sp. nov. characterized in this study

Strain	Date of isolation	Locality	Specimen	Sex	Age	Diagnosis	Other microflora
NRL/St[a] 16/872[T] = CCM[b] 9024[T] = LMG[c] 31,872[T] = DSM[d] 111349[T]	Oct 2016	Karlovy Vary	Swab of ear	M	3 y	Acute otitis externa	Monoculture
NRL/St[a] 19/737 = CCM[b] 9023	Jul 2019	Prague	Wound pus	M	32 y	Surgical wound infection	*S. aureus*
NRL/St[a] 18/288 = P12563	Mar 2018	Lyon	Wound pus	M	51 y	Leg wound infection	NA[e]
NRL/St[a] 21/187 = P13332	Jul 2021	Karlovy Vary	Bile	M	83 y	Cholelithiasis and cholecystitis	*E. coli, Klebsiella pneumoniae, Citrobacter freundii,* and *Enterococcus faecalis*
NRL/St[a] 22/194 = P13326	Apr 2022	Prague	Swab of ear	M	6 m	Acute otitis media	Monoculture

[a]NRL/St, National Reference Laboratory for Staphylococci, National Institute for Public Health, Prague.
[b]CCM, Czech Collection of Microorganisms.
[c]LMG, Bacteria Collection at the Laboratorium voor Microbiologie Universiteit Gent.
[d]DSM, German Collection of Microorganisms and Cell Cultures.
[e]NA, not analyzed.

Downloaded from https://journals.asm.org/journal/spectrum on 04 February 2026 by 147.251.86.90.

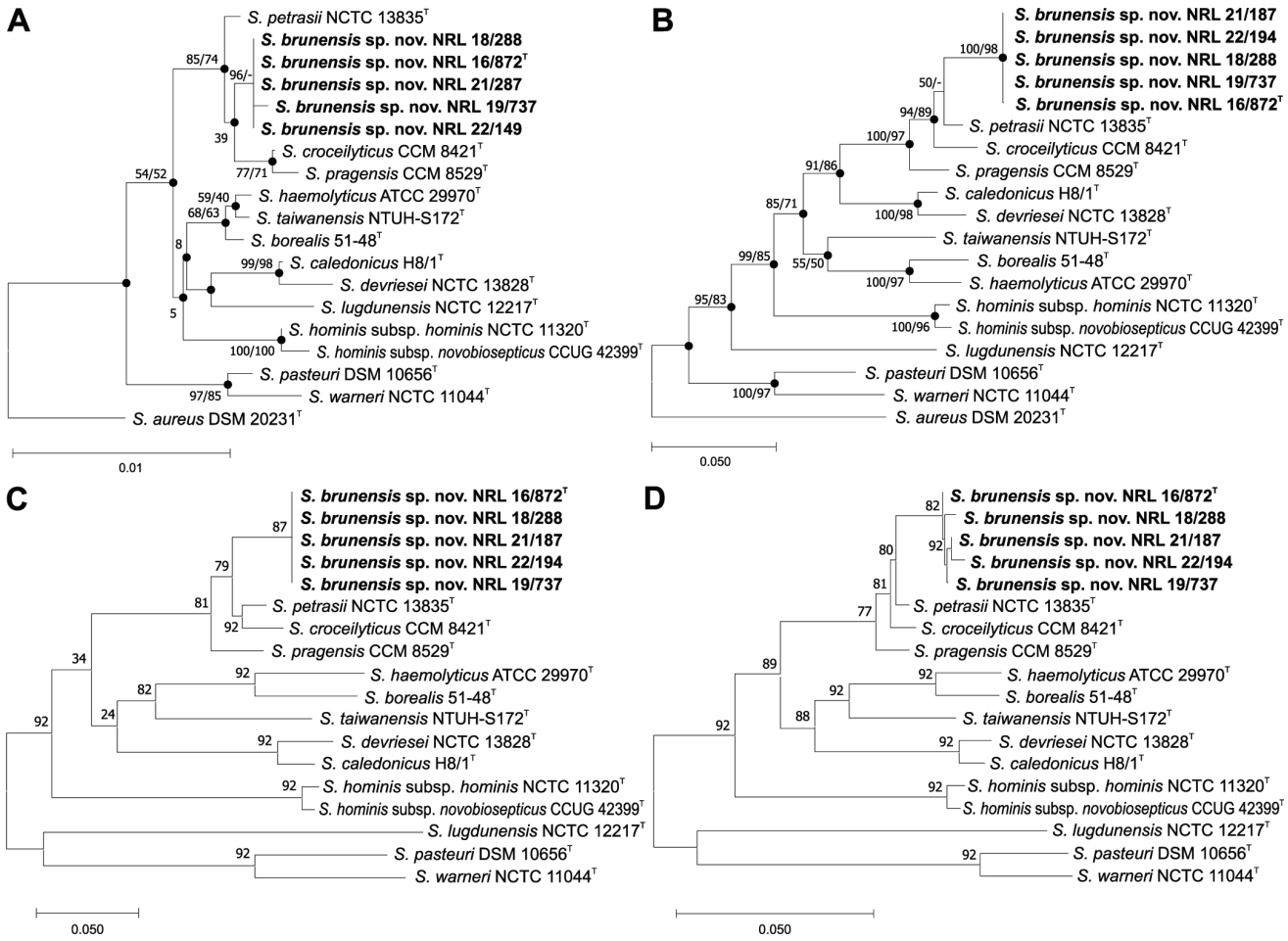

FIG 1 Evolutionary analyses of *Staphylococcus brunensis* sp. nov. and its closest relatives. GenBank accession numbers of used sequences are listed in Table S1. (A) Evolutionary history inferred using neighbor-joining (NJ) method based on complete 16S rRNA gene sequences extracted from whole-genome assemblies. Filled circles indicate that the corresponding nodes were also identified from analysis by the maximum likelihood (ML) method. The percentage of replicate trees above 50% in which the associated taxa clustered together in the bootstrap test (500 replicates) are shown next to the branches for the NJ and ML methods. *S. aureus* DSM 20231^T was used as an outgroup. The evolutionary distances are in the units of the number of base substitutions per site. All ambiguous positions were removed for each sequence pair. There were a total of 1,552 positions in the final data set. (B) Unrooted ML tree based on multilocus sequence analysis of concatenated nucleotide sequences from six loci—*rpoB*, *hsp60*, *dnaJ*, *tufA*, *gap,* and *sodA*—were extracted from whole-genome assemblies. Filled circles indicate that the corresponding nodes were also identified from analysis by the NJ method. There were a total of 3,952 positions in the final data set. Bootstrap probability values (percentages of 500 tree replications) greater than 50% are shown at branch points. The evolutionary distances are given as the number of substitutions per site. (C) Nucleotide sequence-based and (D) protein sequence-based phylogenetic tree of the concatenated alignment of 92 core genes constructed using up-to-date bacterial core gene (UBCG) set. The ML tree was inferred using RAxML software and 100 replicates. The threshold for the gene support index was set to 94% for the nucleotide and 80% for the protein-based tree. Gene support indices are given at branching points (the maximal possible value is 92). The bar indicates the number of substitutions per position.

tryptone soy agar (TSA), Columbia agar with blood, plate count agar, P agar, and nutrient agar, and did not grow in a thioglycollate medium. The Congo red agar method showed negativity in the production of polysaccharide intercellular adhesin (PIA) associated with biofilm formation. Phenotypic identification based on bacitracin resistance and sensitivity to furazolidone, positive catalase test, growth in the presence of NaCl above 10%, and microscopic morphology assigned five isolates as *Staphylococcus* sp. In contrast to the main characteristics of staphylococci, isolate NRL/St 19/737 exhibited atypical negative catalase activity. Test-dependent results were also observed for the Voges-Proskauer (VP) test (acetoin) and for β-glucuronidase. With detection of acetoin production, we only obtained positive results in all five strains when pyruvic acid served as substrate using the commercial VP test (Erba Lachema) instead of glucose as substrate for the

Downloaded from https://journals.asm.org/journal/spectrum on 04 February 2026 by 147.251.86.90.

TABLE 2 Differentiation of *Staphylococcus brunensis* sp. nov. from closely related staphylococci occurring in human clinical material

Test[d]	Result obtained for indicated type strain[a]/result from species description						
	S. brunensis sp. nov.[b]	*S. petrasii* CCM 8418^T	*S. croceilyticus* CCM 8421^T	*S. pragensis* CCM 8529^T	*S. haemolyticus* CCM 2737^T	*S. borealis* CCM 9145^T	*S. taiwanensis* CCM 9267^T
Arginine dihydrolase	+	+/+	+/+	−/−	+/+	+/+	+/+
Voges-Proskauer test	+	+/+	+/+	+/+	w/+	−/−	+/+
Urease	−	+/d	+/+	−/−	−/−	+/+	+/+
β-Glucuronidase[c]	+	−/−	+/+	−/−	+/d	+/d	−/−
DNA hydrolysis	−	w/d	−/−	+/+	+/d	w/−	−/−
Acid from: lactose	+	−/d	−/−	−/−	−/d	−/−	−/−
Galactose	+	−/d	−/−	−/−	+/d	−/nt	−/−
Mannose	−	+/+	−/−	−/−	−/−	−/d	−/−
Ribose	−	−/w	w/w	−/−	−/d	+/+	+/+
D-arabinose	−	−/−	+/+	−/−	−/−	−/−	−/−
N-Acetylglucosamine	−	−/−	−/−	−/−	+/+	+/d	−/−
Pale yellow pigment	−	−/−	+/+	−/−	-/-	+/+	−/−

[a]All data were taken from this study (in two replications).
[b]Presented data are uniform for all isolates of *S. brunensis* sp. nov.
[c]STAPHYtest 24 kit.
[d]+, positive; -, negative; w, weak reaction; d, 11–89% strains positive; nt, not tested.

conventional VP test. Similar results were obtained with the β-glucuronidase test, where all isolates were positive in the STAPHYtest 24 kit, but negative in the API ZYM kit due to a different substrate for enzyme detection. The differentiation of novel staphylococcal isolates from similar and/or closely related staphylococci occurring in human clinical material is shown in Table 2. The species *S. petrasii*, *S. pragensis,* and *S. haemolyticus* were phenotypically the most similar taxa to the aforementioned isolates. Strain-dependent utilization results are specified in Table S4. Complete characteristics of *S. brunensis* sp. nov. are stated in the protologue given subsequently.

Antibiotic susceptibility testing showed that all five strains are susceptible to cefoxitin, clindamycin, gentamicin, chloramphenicol, linezolid, oxacillin, rifampicin, tobramycin, trimethoprim, sulphamethox/trimethoprim (cotrimoxazole), tetracycline, and fusidic acid. Susceptibility to ciprofloxacin and levofloxacin was intermediate. Susceptibility to ampicillin, penicillin G, tigecycline, and erythromycin was strain-dependent (Table S4).

By using cluster analysis of matrix-assisted laser-desorption/ionization-time-of-flight mass spectrometry (MALDI-TOF MS) protein profiles, all five *S. brunensis* sp. nov. strains were separated into a coherent cluster distinguished from phylogenetically related

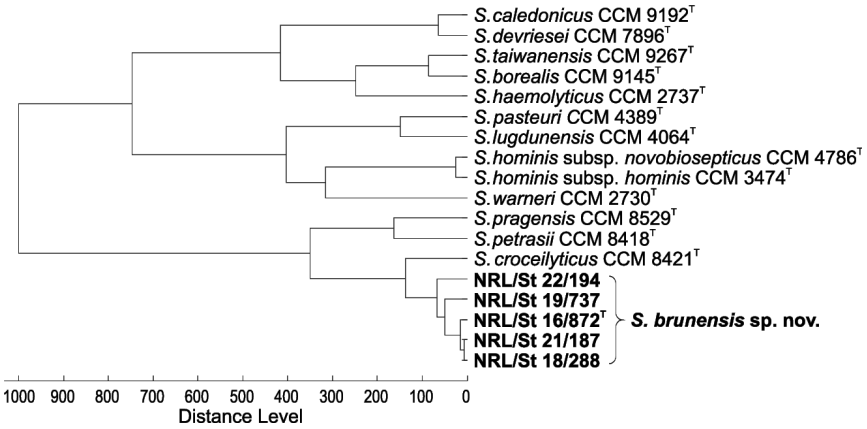

FIG 2 Dendrogram based on MALDI-TOF MS profiles of *Staphylococcus brunensis* sp. nov. and other phylogenetically related species. The dendrogram was generated using the correlation distance measure with the average linkage algorithm (UPGMA) settings of the software BioTyper version 3.1 (Bruker Daltonics).

Downloaded from https://journals.asm.org/journal/spectrum on 04 February 2026 by 147.251.86.90.

Staphylococcus spp., as shown in Fig. 2. All five strains share 35 signals within the *m/z* range 2–11 kDa, while five of these signals (*m/z* = 4130, 6660, 7614, 8258, and 10625) were found to be specific for *S. brunensis* sp. nov., being absent in the MALDI-TOF MS protein profiles of a comprehensive set of 65 *S. petrasii*, *S. croceilyticus*, and *S. pragensis* strains analyzed previously (10).

The chemotaxonomic analyses of type strain *S. brunensis* NRL/St 16/872^T showed predominantly menaquinone-7 (MK-7, 95%) and a small amount of MK-6 (4%) and MK-8 (1%). The major fatty acids were C $_{15:0\ anteiso}$ (38.6%) and C $_{17:0\ anteiso}$ (19.6%), followed by C $_{19:0\ anteiso}$ (8.3%), C $_{15:0\ iso}$ (6.3%), C $_{17:0\ iso}$ (6.9%), C $_{18:0}$ (6.8%), C $_{19:0\ iso}$ (4.4%), and C $_{20:0}$ (3.0%). A small amount of C $_{16:0\ iso}$ (1.8%), C $_{16:0}$ (1.2%), and C $_{18:0\ iso}$ (1.6%) fatty acids were also present. The detected peptidoglycan type is A3α (L-Lys-Gly$_{3-4}$, A11.2). All chemotaxonomic data are in-line with previous reported patterns (7).

DNA fingerprinting of *S. brunensis* sp. nov.

Screening of the investigated bacterial group by rep-PCR fingerprinting with primer (GTG)$_5$ showed their genotypic coherence. All five isolates had visually similar fingerprints, which were grouped into a single cluster and separated from the other entries in the in-house fingerprint database, which includes members of all recognized species of the genus *Staphylococcus*, including type strains of phylogenetically closely related

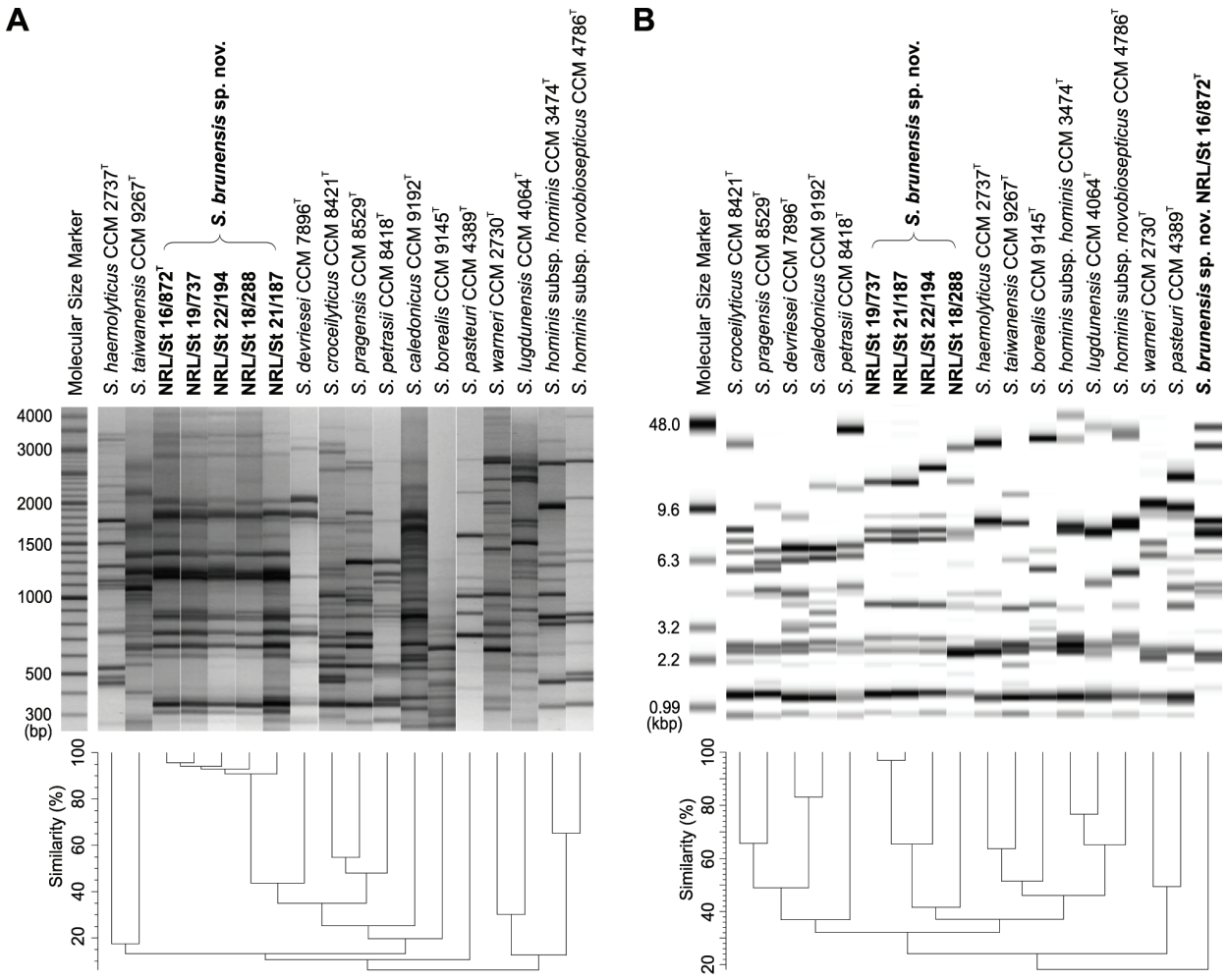

FIG 3 Cluster analysis of rep-PCR fingerprints and ribotype patterns obtained from *Staphylococcus brunensis* sp. nov. strains and the type strains of phylogenetically closely related *Staphylococcus* species. (A) Dendrogram based on (GTG)$_5$-PCR fingerprints. (B) Dendrogram based on cluster analysis of *Eco*RI ribotype patterns obtained using a RiboPrinter system. The dendrograms were calculated with Pearson's correlation coefficients with the UPGMA clustering method (*r*, expressed as percentage similarity values).

Downloaded from https://journals.asm.org/journal/spectrum on 04 February 2026 by 147.251.86.90.

species (Fig. 3A). The obtained results also suggest that this rapid and easy-to-perform method can be used for the identification of *S. brunensis* sp. nov., similarly to how we demonstrated for the identification of *Staphylococcus* spp. in our previous studies (8, 23, 25).

In contrast to the rep-PCR method, automated ribotyping with the restriction enzyme *Eco*RI revealed heterogeneity among the five examined strains (Fig. 3B). Three isolates, NRL/St 16/872^T, NRL/St 22/194, and NRL/St 18/288, exhibited unique fingerprint patterns that allowed differentiation at the strain level and indicated that they were not clonally related. The remaining two strains, NRL/St 19/737 and NRL/St 21/187, had visually identical ribotypes, despite being isolated in 2019 and 2021, respectively, at different locations and were therefore not considered clonally related. These results suggest that automated ribotyping with *Eco*RI can separate isolates of *S. brunensis* sp. nov. at the strain level, although some strains may have similar ribotype patterns. However, a reliable assessment of the discriminatory power of this technique for typing *S. brunensis* sp. nov. requires the analysis of a more significant number of strains from different localities and sources.

Genome characterization of *S. brunensis* sp. nov.

The comparison of sequenced genomes (Table S5) revealed a high degree of similarity between the isolates (Fig. 4). The *S. brunensis* sp. nov. genomes were 2.5–2.6 Mb long with GC content 33.3–33.4% encoding 2,500–2,700 CDS, 61−62 tRNAs, and 19 rRNAs. The pangenome consists of 2,230 core and 416 accessory, and 569 unique genes in total. The sequenced genomes differ in variable genomic elements, which constitute 5–8% of the genome and are associated with virulence and antimicrobial resistance genes, predominantly located at plasmids. All *S. brunensis* sp. nov. genomes possess a type IIU CRISPR-Cas complex with 15–20 variable spacers, some of which target siphoviral prophages as determined by blastn search. The core gene *kat* encoding catalase in the strain NRL/St 19/737 (locus tag MT339_07575) has a 1 bp deletion in homopolymer polyA, which introduces a premature stop codon at the 3' end of the gene. It is possible that the catalase-negative phenotype of the strain is associated with the loss of function of this gene, although a truncated protein without the first 22 amino acids could be produced.

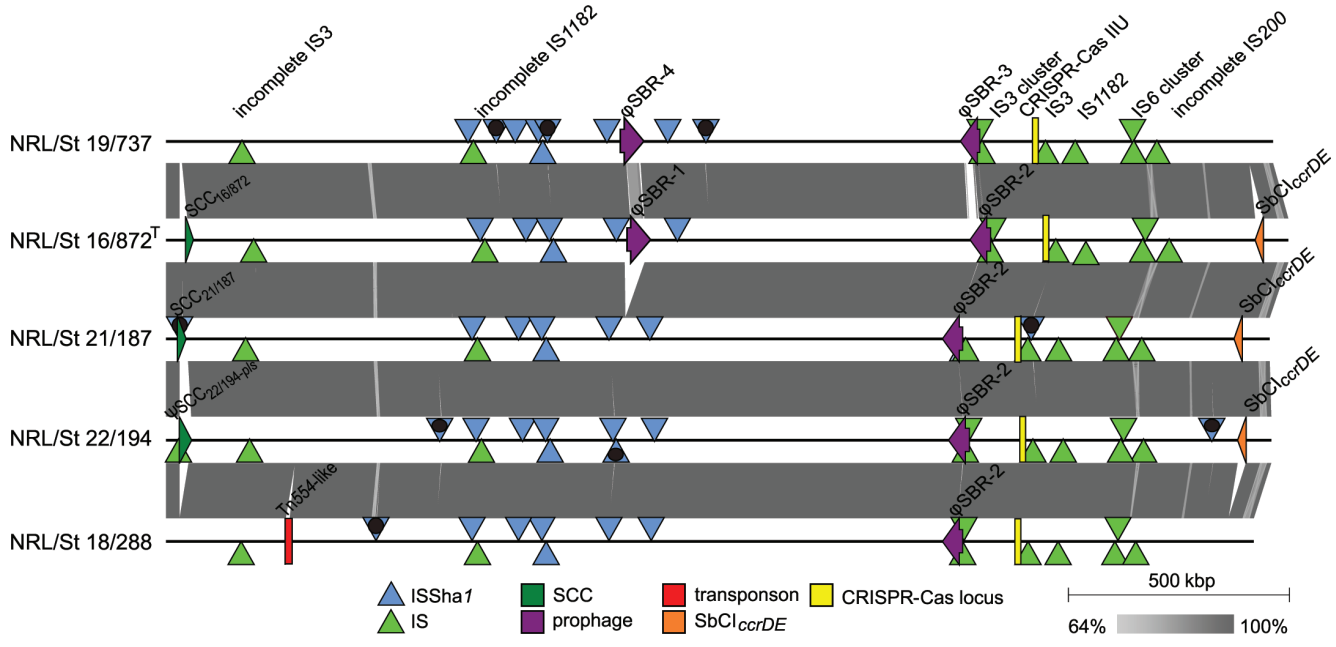

FIG 4 Genome comparison of *Staphylococcus brunensis* sp. nov. isolates. Mobile genetic elements are shown and color coded as in the legend. The ISSha*1* loci that are divergent for the respective strains are marked with black circles. Only nucleotide blast hits above 64% identity and longer than 2 kb are shown.

Downloaded from https://journals.asm.org/journal/spectrum on 04 February 2026 by 147.251.86.90.

TABLE 3 Plasmid contigs of *Staphylococcus brunensis* sp. nov. grouped by replication gene and gene content

Replication genes	Strain	Size (kb)	Antimicrobial resistance	Virulence factors	Saccharide utilization genes	Mobilization/toxin-antitoxin systems
rep39	NRL/St 16/872^T	31.2	*copZ*, *csoR*, *czrB*, *qacR*, *qacA*	*clp*	-	*mobA*
	NRL/St 18/288	21.9	*copZ*, *csoR*, *arsM*, *qacR*, *qacA*,	-	-	*fstP*
	NRL/St 21/187	22.9	*copZ*, *copA*, *csoR*, *arsR*, *arsM*	*clp*	-	*mobA*
rep20	NRL/St 16/872^T	27.2	*arsR*, *arsM*	*isaB*, *essG*	-	*mobC*, relaxaseP, *mobP*
	NRL/St 19/737 and NRL/St 18/288	33.9	*arsR*, *arsM*	*isaB*, *essG*	*mqo*, *hxlR*, *hxlA*, *hxlI*	*mobC*, relaxaseP, *mobP*
	NRL/St 21/187	22.9	*qacR*, *qacA*	*isaB*, *essG*	-	
rep39, *rep5b*, *rep21*, *rep10*, *rep20*	NRL/St 19/737	32.0	*blaZ*, *blaR*, *blaI*, *ermC*, *cadX*, *cadA*, *cadD*	-	-	*mobC*, relaxaseP, *mobP*
rep21	NRL/St 16/872^T, NRL/St 18/288, NRL/St 21/187, and NRL/St 22/194	2.8	*cadD*, *cadX*	-	-	-
rep13	NRL/St 16/872^T and NRL/St 21/187	2.6	-	-	-	-
rep5b	NRL/St 18/288	7.9	-	-	-	*mobC*, relaxase P
rep10	NRL/St 22/194	44.7	*ermC*			

The *S. brunensis* sp. nov. genomes harbor several large plasmids, which can be grouped by the presence of either *rep39* or *rep20* gene. Due to high sequence variability and mosaicism caused by interspersed IS*431*, it was not possible to determine a complete consensus sequence for all plasmids. The plasmid contigs comprise beta-lactam, heavy metal, and disinfectant resistance as well as virulence and saccharide utilization genes as shown in Table 3. All analyzed strains harbor a small *rep21* plasmid conferring cadmium resistance. The strain NRL/St 22/194 contains an additional *rep10* plasmid harboring the *ermC* gene similar to the pUSA05-1 plasmid from *S. aureus* (26). These two small plasmids are integrated into the *rep39*-type plasmid contig of strain NRL/St 19/737. Furthermore, two cryptic plasmids, one containing the *rep13* gene and the other containing *rep5b* gene were identified (Table 3).

The resistance to penicillin in *S. brunensis* sp. nov. NRL/St 18/288 is encoded by the *blaZ* gene located at a 9 kb Tn*554*-like transposon (Fig. 4) integrated into the chromosomal *isaB* gene. The chromosomes of *S. brunensis* sp. nov. harbor several copies of various full and partial IS elements from the IS*3*, IS*6*, IS*30*, IS*1182*, IS*200*/IS*605*, and ISha*1* families (Fig. 4). The IS*431* flanked composite transposon localized downstream of the *cspC* gene contains the gene for a short-chain dehydrogenase associated with survival in stress conditions (27). Each strain carries six to eight ISSha*1* copies integrated in six conserved and six variable loci, usually adjacent to rRNA genes. One copy of ISSha*1* is inserted in the SCC element of *S. brunensis* sp. nov. NRL/St 21/287 strain (Fig. 4).

The *S. brunensis* sp. nov. strains have one or two complete prophages in their genomes integrated into two different 18 bp *att* sites. The ΦSBR-1 prophage of NRL/St 16/872^T is integrated in the *att* site AATCCCTTACTTCCCGTT, located in the tRNA-Ser(gga) gene. The other strains encompass one or two CRISPR spacers homologous to the ΦSBR-1, and thus are immune to infection by this phage. The same *att* site is used by ΦSBR-4 in the genome of NRL/St 19/737. Both prophages are 45.4 kb long and share 79.3% nt identity. The next *att* site, AATCCCTCCGTTTCCGTT in tRNA-Ser(gct), is occupied by either ΦSBR-2 or ΦSBR-3. Prophage ΦSBR-2, which is 47 kb long, is integrated into the genomes of strains NRL/St 16/872^T, NRL/St 19/288, and NRL/St 21/287. The strain NRL/St 19/737 harbors a 43.5 kb ΦSBR-3 prophage, which shares 79% nt identity with ΦSBR-2 genome along 57% of its length; the difference is mainly in the morphogenesis module. Both ΦSBR-2 and ΦSBR-3 carry a putative accessory virulence factor sialic acid transporter (28) in the lysis gene module.

Two *S. brunensis* sp. nov. strains NRL/St 16/872^T and NRL/St 21/287 comprise an approximately 18.2 kb-long genomic island in the rRNA methyltransferase H gene *rlmH*

Downloaded from https://journals.asm.org/journal/spectrum on 04 February 2026 by 147.251.86.90.

(*orfX*). The genomic island was almost identical in both strains; the only difference is the presence of an insertion sequence ISSha*1* in strain NRL/St 21/287. The island is bordered by imperfect 18 bp-long direct repeats GAAGC(A/G)TATCATAA(G/A)TGA and harbor *ccrA1B2* genes; thus, according to the rules of the IWG-SCC (29) the element was designated $SCC_{NRL/St\ 16/872}$. The most similar element to $SCC_{NRL/St\ 16/872}$ is a composite island in genome of *S. hominis* C34847 (30), sharing 95.2% nt identity along 75% of their length. The $SCC_{CCM9024}$ carries genes for the type I restriction-modification (RM) system, sharing high homology with genes encoding a restriction (*hsdR*) and methylation (*hsdM*) subunit with the RM system of *S. hominis* C34847 and *S. aureus* NTUH-4729 (31). Interestingly, the *putP* gene, which encodes a sodium proline symporter, was wedged between the *ccrB2* gene and a set of three short hypothetical genes conserved in the *ccr* gene complex, thus disrupting the canonical organization of the complete *ccr* gene complex. Similarly, the *putP* gene and the flanking sequence from the *ccr* gene complex were found in SCC elements of various CoNS, *S. epidermidis* I1PPP121 (GenBank accession no. MH188479), *S. haemolyticus* BC05211 (KX181861), *S. hominis* J6 (LT963442), and *S. hominis* J11 (LT963438), and in plasmids of *S. warneri* 16A (CP031267) and *S. pasteuri* 3C (CP031281), pointing to a high degree of recombination occurring in staphylococci.

The strain NRL/St 22/194 also harbors an SCC element inserted into the *rlmH* gene bordered by the 21 bp imperfect repeat GG(C/A)GAAGC(A/G)TATCATAA(G/A)GTGA. The 26.6 kb pseudo-SCC element named $\psi SCC_{NRL/St\ 22/194\text{-}pls}$ has no recombinase genes, but carries several virulence genes, including the gene encoding plasmin sensitive protein (*pls*), poly(glycerol-phosphate) α-glycosyltransferase (*tagE*), and UDP-N-acetyl-muramate-L-alanine ligase (*murF*), which are also found in *S. aureus* composite island $SCCmec_{WAMRSA40}$ (32).

Novel genomic island harboring cassette chromosome recombinase genes *ccrDE*

The strains NRL/St 16/872^T, NRL/St 21/187 and NRL/St 22/194 harbor a mobile element of size 18.8 kb with cassette chromosome recombinase genes, integrated in the *rimJ/rimL* gene orthologous to the the ribosomal-protein-serine acetyltransferase gene *rimL* in *Escherichia coli* and *ydaF* in *Bacillus subtilis* (UniProt accession no. P13857 and P96579, respectively). The island designated *S. brunensis* chromosomal island *ccrDE* ($SbCI_{ccrDE}$) harbors another homologue of *rimL* with 70% nt identity to the original *rimL*; thus, it may complement the function of the truncated *rimL* gene. $SbCI_{ccrDE}$ is bordered by the tetranucleotide motif GAAA. Additionally, the 19 bp direct repeat ATTCCACAATGAAAT-CCAT was found on the integration site in *rimL* and inside the *rimL* homologue on the island, which suggests a complex recombination event.

$SbCI_{ccrDE}$ possesses a cluster of genes homologous to the *ccr* gene complex from SCC elements. The core of the *ccr* complex consists of two *ccr* genes, similar to SCC elements type IV or II. Additional genes in the *ccr* complex, that is the putative primase *polA*, cassette chromosome helicase *cch2*, three short proteins with the domains SAUGI, DUF960, and DUF1643, and a hypothetical protein (Fig. 5), were homologous to those in SCC*mec* type V, which has only one *ccrC* gene in the *ccr* complex. $SbCI_{ccrDE}$ *ccr* genes share more than 98% DNA sequence identity to *ccrA8B9* recombinases (Table S6) discovered recently in the *S. haemolyticus* genome (33). The values of nucleotide identity to currently known *ccrA1-7*, *ccrB1-8,* and *ccrC1-2* genes from SCCs range from 38.0 to 53.3% (Table S6). Although it is slightly above the threshold of 50.0% for the definition

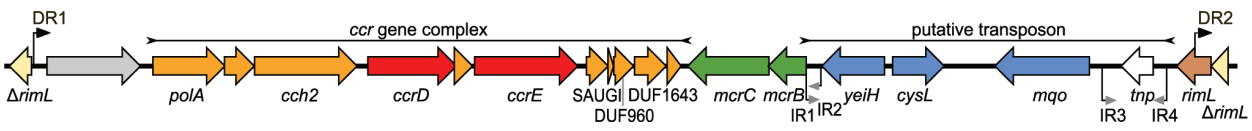

FIG 5 Annotated map of genes and possible functions in genomic island $SbCI_{ccrDE}$ harbored by *Staphylococcus brunensis* sp. nov. Genes are labeled according to known or putative function. Sequence of direct repeats DR1, DR2: 5′-ATTCCACAATGAAATCCAT-3′; sequence of inverted repeats IR1−IR4: 5′-TGGTTCTGTTGC-AAAGT-3′.

Downloaded from https://journals.asm.org/journal/spectrum on 04 February 2026 by 147.251.86.90.

of a gene variant according to the rules of IWG-SCC (29), the amino acid (aa) identity level of SbCI$_{ccrDE}$ recombinases to known CcrA, CcrB, and CcrC reaches a maximum of 39.9%, which is substantially lower than aa identity among Ccr allotypes, which range from 50.9 to 92.3%. Therefore, based on the borderline nucleotide identities and low protein identities to CcrA, CcrB, and CcrC allotypes, we propose designating the SbCI$_{ccr}$ recombinases as new allelic types *ccrD* and *ccrE* and reclassifying the described *ccrA8B9* recombinases accordingly (33). The CcrDE recombinases are able to excise the SbCI$_{ccrDE}$ element from its insertion sequence site, which has been detected by sequence read alignment and PCR analysis (Fig. S2).

Apart from the *ccr* gene complex, the island SbCI$_{ccrDE}$ carries the 5-methylcytosine-specific restriction enzyme *mcrB* and specificity subunit *mcrC* genes for the putative RM system (Fig. 5), commonly found on SCC elements, chromosomal islands, and prophages that help to maintain the mobile element in the genome (34). Approximately 5.8 kbp of the SbCI$_{ccrDE}$ is occupied by a putative transposon bordered by a perfect 17 bp inverted repeat of TGGTTCTGTTGCAAAGT. The transposon has one copy of the insertion sequence from the IS*6* family (sharing 95% nt identity to IS*431*$_{mec}$) and accessory genes encoding putative membrane protein (*yeiH*), putative transcriptional regulator (*cysL*), and malate chinonine oxidoreductase (*mqo*) (Fig. 5), which are frequently found on plasmids.

We surveyed the GenBank database for sequences resembling SbCI$_{ccrDE}$. In addition to *S. haemolyticus* BC5211 (33), we found related genomic islands with *ccrDE* in the genomes of *S. haemolyticus* (GenBank accession nos. CP033814 and CP102568), *S. hominis* subsp. *hominis* K1 (CP020618), and *S. borealis* GDY8P80P (35), and in *S. aureus* ER04332 and ER11327 (36), and related clones. The island is consistently inserted in the *rimL* gene, in a locus downstream of the conserved *metE* gene (Fig. 6A), which is 17–56 kb counterclockwise from the replication origin in CoNS species. However, in *S. aureus* strains, the *rimL* gene is located at the end of the *oriC* environ due to large-scale chromosomal inversion. The variable region of the islands comprises genes for an RM system (Fig. 6A). In *S. borealis* GDY8P80P, the island harbors many transposons with resistance genes to beta-lactam antibiotics, tetracycline, aminoglycosides, and other antimicrobials. The phylogenetic analysis of *ccrD* and *ccrE* genes from the related genomic islands (Fig. 6B) and the pairwise nucleotide identity comparison (Table S6) clearly distinguished two allotypes designated *ccrD1E1*, present in the genomes of *S. brunensis* sp. nov., *S. haemolyticus*, and *S. aureus*, and *ccrD2E2*, found in the genomes of *S. borealis* and *S. hominis* (Fig. 6B; Table S6).

Taxonomic description of *S. brunensis* sp. nov.

Staphylococcus brunensis (*bru.nen'sis* L. adj. brunensis from Bruna, the Roman name of the city of Brno, Czech Republic, where this and other staphylococcal species were first described).

Cells are Gram stain positive cocci, occurring predominantly in pairs and clusters, non-spore-forming, and nonmotile. Colonies on TSA agar are circular, whole margin, flat, smooth, shiny, 2 mm in diameter, aerobic, and white. Hemolytic activity on sheep blood agar, production of delta-hemolysin revealed in synergistic test with a beta-hemolytic producing strain (*S. pseudintermedius* CCM 4710). Growth in the presence of 12% NaCl, at 20°C and 45°C, but not at 15°C and 48°C. They are positive for pyrrolidonyl arylamidase, arginine dihydrolase, and nitrate reduction and negative for coagulase, clumping factor, oxidase, urease, VP test (acetoin, conventional tube test), hyaluronidase, thermostable nuclease, and ornithine decarboxylase; susceptible to furazolidon (100 µg) and novobiocin (5 µg), and resistant to bacitracin (10 IU); partially resistant to lysostaphin (200 mg L^{-1}) and resistant to lysozyme; negative for hydrolysis of esculin, gelatine, DNA, and Tween 80; positive on API ZYM for acid phosphatase, alkaline phosphatase (weak), esterase (C 4), and esterase lipase (C 8); negative on API ZYM for lipase (C14), valine arylamidase, cystine arylamidase, trypsin, α-chymotrypsin, naphthol-AS-BI-phosphohydrolase, α-galactosidase, β-galactosidase, β-glucuronidase, β-glucosidase, *N*-acetyl-β-glucosaminidase, α-mannosidase, and α-fucosidase. *S. brunensis* sp. nov.

Downloaded from https://journals.asm.org/journal/spectrum on 04 February 2026 by 147.251.86.90.

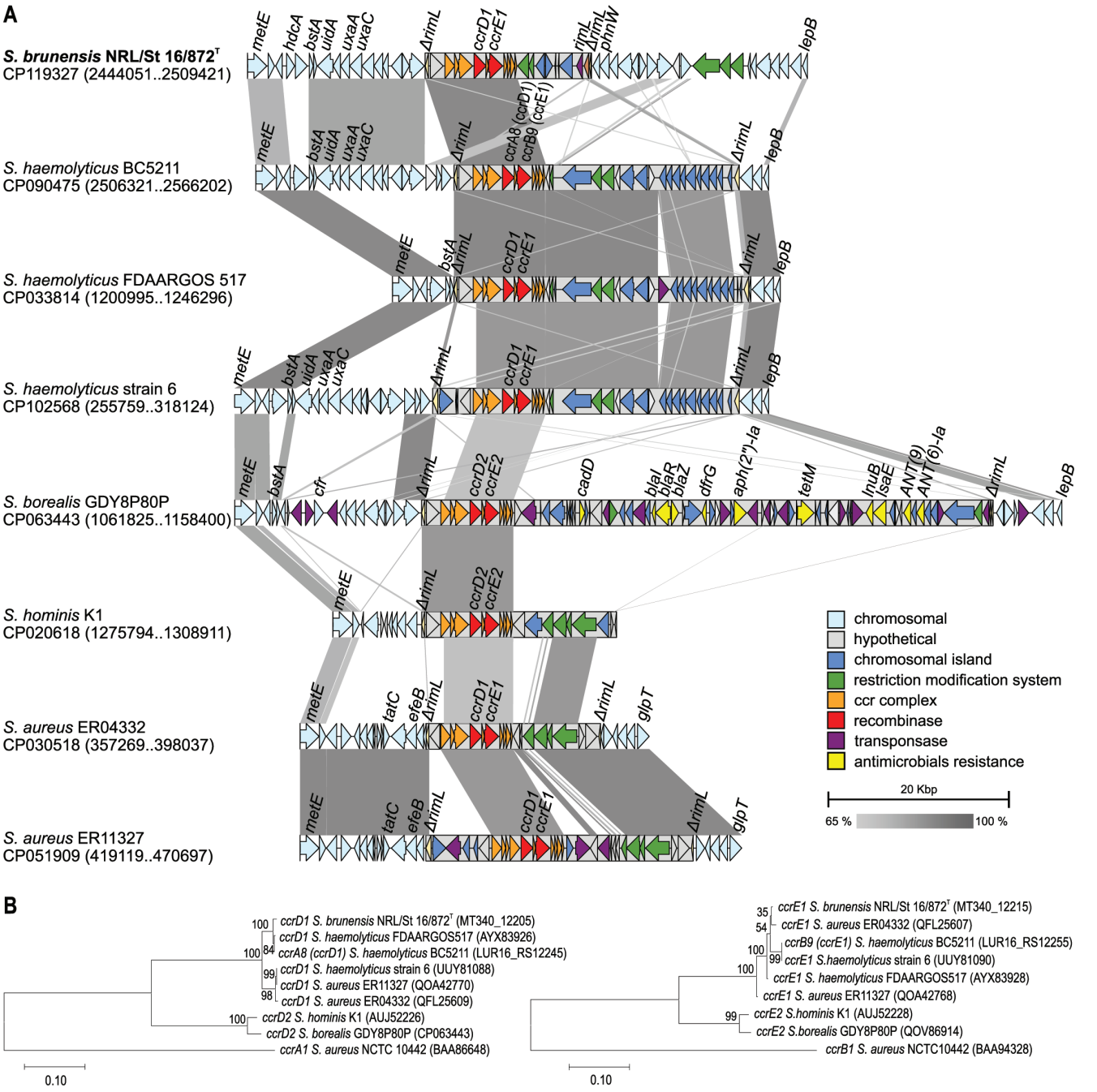

FIG 6 Comparative analysis of chromosomal islands harboring *ccrDE* cassette chromosome recombinases (CI_{ccrDE}). (A) Comparison of CI_{ccrDE} and flanking regions from different staphylococcal species. The genomic island CI_{ccrDE} is highlighted with a gray background. Genes are labeled according to known or putative functions, as shown in the legend. Only nucleotide blast hits above 65% identity and longer than 2 kb are shown. The position of the island is provided in parentheses next to the GenBank accession number. (B) Maximum likelihood trees of nucleotide sequences of *ccrD and ccrA8* recombinases with *ccrA1* as an outgroup, and *ccrE and ccrB9* recombinases with *ccrB1* as an outgroup, respectively. The trees were constructed using Tamura-Nei model with 500 bootstrap replicates. The evolutionary distances are in the number of base substitutions per site. The protein GenBank accession numbers or locus tags are shown in parentheses.

produce acid from glycerol (weak), galactose, D-glucose, D-fructose, maltose, lactose, sucrose, and trehalose. They do not produce acid from erythritol, D-arabinose, L-arabinose, ribose, D-xylose, L-xylose, adonitol, β-methyl-D-xyloside, mannose, sorbose, rhamnose, dulcitol, inositol, mannitol, sorbitol, α-methyl-D-mannoside, α-methyl-D-glucoside, *N*-acetyl glucosamine, amygdaline, arbutine, salicin, cellobiose, melibiose, inulin,

Downloaded from https://journals.asm.org/journal/spectrum on 04 February 2026 by 147.251.86.90.

melezitose, D-raffinose, starch, glycogen, xylitol, β-gentiobiose, D-turanose, D-lyxose, D-tagatose, D-fucose, L-fucose, D-arabitol, L-arabitol, gluconate, 2-keto-gluconate, and 5-keto-gluconate.

Variable biochemical reactions were obtained for catalase (4 of 5 positive), leucine arylamidase (2 of 5 positive), α-glucosidase (1 of 5 positive), and growth in 15% NaCl (4 of 5 positive) (Table S4).

Utilization (Biolog MicroPlate GEN III, protocol A) is positive for D-maltose, D-trehalose, D-turanose, α-D-glucose, D-fructose, D-galactose, glycerol, L-alanine, L-arginine, L-glutamic acid, L-serine, D-gluconic acid, acetic acid, and formic acid. Negative utilization for D-cellobiose, gentiobiose, stachyose, D-raffinose, D-melibiose, β-methyl-D-glucoside, D-salicin, *N*-acetyl-D-glucosamine, *N*-acetyl-D-galactosamine, *N*-acetyl neuraminic acid, 3-methyl glucose, D-fucose, L-fucose, L-rhamnose, inosine, D-sorbitol, D-mannitol, myo-inositol, D-glucose-6-PO4, D-aspartic acid, D-serine, gelatin, glycyl-L-proline, L-histidine, D-galacturonic acid, D-galactonic acid lactone, D-glucuronic acid, glucuronamide, mucic acid, quinic acid, D-saccharic acid, *p*-hydroxy phenylacetic acid, D-lactic acid methyl ester, citric acid, α-keto glutaric acid, D-malic acid, bromo-succinic acid, γ-amino-butyric acid, α-hydroxy-butyric acid, β-hydroxy-D,L-butyric acid, and propionic acid.

The type strain is NRL/St 16/872^T (= CCM 9024^T = DSM 111349^T = LMG 31872^T). The major respiratory quinone is menaquinone-7. The major fatty acids are $C_{15:0\ anteiso}$ and $C_{17:0\ anteiso}$. The peptidoglycan type is A3α (A11.2). The DNA G+C content of strain NRL/St 16/872^T is 33.40 mol%, calculated from the whole-genomic sequence. The species description is based on the characterization of five strains isolated from various human clinical materials. Most of the characteristics of the type strain NRL/St 16/872^T agree with the species description. The GenBank/ENA/DDBJ accession number for the 16S rRNA gene is OQ401401. The complete chromosome sequence of the type strain is available under GenBank accession number CP119327.

DISCUSSION

The recent molecular diagnostic methods and polyphasic taxonomic approach, including whole-genome sequencing, allow for more effective species differentiation of CoNS from various sources. Here, we described *S. brunensis* sp. nov., which occupies similar niches to the closely related species from the *S. petrasii* phylogenetic complex (10). The available isolates of *S. brunensis* sp. nov. were associated with the human ear and wound infections, whereas *S. petrasii* and *S. pragensis* predominated in wounds, blood, or urinary tract infections (Table S7). However, it is challenging for clinicians to determine whether these CoNS are causative agents of human diseases or suspected contaminants associated with the occurrence of these commensal bacteria on human skin.

The pathogenic potential of CoNS is related to immune evasion, invasion of host tissues, and biofilm formation, allowing them to persist on the surfaces of indwelling medical devices and thus cause chronic infections (1). The intercellular adhesion operon (*ica*), biofilm-associated protein (*bap*/*bhp*), and fibronectin-binding protein genes (*fnbA*/*fbe*) directly associated with biofilm production in *S. epidermidis* (37) have not been identified in either *S. brunensis* sp. nov. genomes or the other species from *S. petrasii* complex. Likewise, the *ica* operon homologue has not been detected in *S. haemolyticus* (3) and may be missing in this phylogenetic clade. Biofilm formation in the initial phase is influenced by molecules involved in surface adhesion. In staphylococci, these are microbial surface components recognizing adhesion matrix molecules (MSCRAMMs) (38). Homologs of cell wall-anchored serine-aspartate repeat-containing protein genes *sdrC, sdrG*, and *sdrH* have been identified in *S. petrasii* genomes (10) but not in *S. brunensis* sp. nov. However, gene homologues for elastin-binding protein (*ebp*), thermonuclease (*nuc*), autolysin E (*atlE*), and gene clusters (*cap5* or *cap8*) involved in the synthesis of capsular polysaccharides have been found in genomes of both *S. petrasii* (10) and *S. brunensis* sp. nov.

Downloaded from https://journals.asm.org/journal/spectrum on 04 February 2026 by 147.251.86.90.

A comparison of representative genome sequences revealed that the species *S. brunensis* sp. nov., *S. croceilyticus*, *S. petrasii*, and *S. pragensis* differ only marginally in genomic G+C content, genome size, and the median protein count encoded by the core genome. The major cause of interspecies differences in the *S. petrasii* complex is the accessory genome and variable genetic elements (Fig. S3). The role of these elements is best described in *S. aureus*, where HGT contributes to adaptation and evolution into successful lineages (39–41).

More than 90% of clinical staphylococcal isolates harbor plasmids of various size that can be classified to small multicopy plasmids or larger plasmids carrying several resistance determinants. However, only 5% (42) of staphylococcal plasmids are large multiresistance elements with the ability to mobilize or undergo conjugative transfer. Strains of *S. brunensis* sp. nov. harbor several large plasmids that encode genes for mobilization (*mobA*, *mobC*, *mobP*) and their spread by HGT is possible. The resistance genes are usually cointegrated between two copies of ISs that promote their spread (43). An example is IS*431* previously described in plasmids pSK41 and pGO1 (44), harboring linezolid and high-level resistance to vancomycin (45). It is probable that IS*431*, identified in *S. brunensis* plasmid sequences, is responsible for the mosaic structure of the elements and also promotes the spread of resistance genes across the genus *Staphylococcus*.

The plasmid-borne resistance to antibiotics and disinfectants suggests enhanced survival in healthcare environments. The resistance to beta-lactam (*blaZ*) and macrolide (*ermC*) antibiotics in *S. brunensis* sp. nov. strains correlates with resistance genes on plasmids and the Tn*554*-like transposon. Resistance to quaternary ammonium compounds (*qacA*), copper and heavy metals, and the hexulose utilization operon (*hxl*) in plasmids of *S. brunensis* sp. nov. suggests adaptation to various ecological niches similar to nosocomial and community-associated isolates of *S. haemolyticus* (46, 47).

The genomes of *S. brunensis* sp. nov. contain more insertion sequence elements than the closest relatives from *S. petrasii* complex (7, 8). The copy number variability of IS implies their recent capture and propagation and increases the genome plasticity among the strains. The most abundant ISSha*1* elements with 98% similarity to ISSha*1* from *S. haemolyticus* (3) are often located near rRNA genes and may contribute to variable ribotype patterns.

A significant MGE in the genome of *S. brunensis* sp. nov. is the genomic island $SbCI_{ccrDE}$ with unique recombinase genes *ccrD1E1*. Xiao et al. (33) reported the existence of these recombinases as *ccrA8B9* allotypes. Nevertheless, their amino acid sequences that were highly different from other known *ccrAB* variants place them among novel *ccrDE* alleles. This reclassification also made it possible to distinguish another apparent variant *ccrD2E2,* present in *S. hominis* and *S. borealis*. The *ccrDE* genes in all inspected staphylococcal genomes were present on a genomic island related to $SbCI_{ccrDE}$. Chromosomal islands with *ccrDE* (CI_{ccrDE}s) share gene structure similar to SCCs, such as conserved *ccr* complex, presence of variable regions, and flanking by direct repeats. However, unlike SCCs, which are canonicaly inserted in the *rlmH* (*orfX*) gene in the *oriC* environ (48), CI_{ccrDE}s are inserted in the *rimL* gene. The SCC-like islands with Ccr or closely related large serine recombinase were inserted in the *rlmH* in other genera of Gram-positive bacteria, that is the genera *Mammaliicoccus* and *Macrococcus*, *Enterococcus faecium*, *Bacillus cereus*, *Geobacillus vulcani*, and *Clostridioides difficile* (49–52). Hence, CI_{ccrDE}s might represent a new class of SCC elements integrated into the *rimL* gene due to the altered specificity of the *ccrDE* recombinases.

The molecular mechanism of the action of *ccrAB* recombinases requires specific sequences of around 60–70 bp and the presence of the central dinucleotide GA in the integration site, which are essential for the integration of the cassettes into the highly conserved *rlmH* gene (20). However, the *ccrAB* recombinases also act on non-canonical less conserved recombination sites (20). Xiao et al. (33) showed that the *ccrDE* recombinases are functional in excision and transfer of an SCC from *rlmH*, but they do not move together with the cassette. Here, we proved that the CI_{ccrDE} bearing the *ccrDE* genes is excised from the chromosome. Since CI_{ccrDE} has a similar size as pathogenicity islands

Downloaded from https://journals.asm.org/journal/spectrum on 04 February 2026 by 147.251.86.90.

and possesses a set of genes required for its replication (53), the element would perfectly fit into the phage capsid to be spread via transduction, which is a common transmission route of MGE in staphylococci (54, 55). The high sequence conservation of the *ccrDE* gene complex in various species corresponds with their spread through horizontal gene transfer.

The proportion and diversity of CI_{ccrDE} was low in the sequenced genomes deposited in the public databases, making it extremely difficult to identify the donor of *ccrDE* complex responsible for the formation of this element. Since we found *ccrD1E1* and *ccrD2E2* predominantly in CoNS genomes, it is possible that CoNS species are predisposed to forming this element and it can subsequently be transferred to *S. aureus*. The variable regions of CI_{ccrDE} are highly diverse in gene content, suggesting that the CI_{ccrDE} element evolved only recently in independent acquisition events, which are also common in the evolution of SCC*mec* (56) or staphylococcal pathogenicity islands (57). The benefit of CI_{ccrDE} for the bacterial host might be only marginal, so there is no selective pressure to maintain established element and disseminate it to more strains. The only widespread genes identified in all CI_{ccrDE}s that help to preserve the element are the RM system genes that differ in the CI_{ccrDE}s, suggesting that they come from various sources similar to canonical SCC elements (30, 31).

With the high selective pressure exerted on staphylococci by the use of antimicrobials, this element is a perfect candidate for the acquisition and spread of resistance and virulence genes. The SCC*mec* element underlying the successful spread of MRSA clones originated through joining of *ccr* gene complex with *mec* gene complex coming from multiple sources. The first signs of the accumulation of resistance genes in CI_{ccrDE} were observed in *S. borealis*, previously misidentified as *S. haemolyticus* (35), where the island comprised several transposons. A similar cluster of drug-resistance genes to that in CI_{ccrDE} of *S. borealis* was also reported in *S. aureus* on an SCC element (58) and a plasmid (59). We conclude that the gene structure of CI_{ccrDE} indicates its ability to act as a primordial element to accumulate virulence and antimicrobial resistance factors. The spread of the island to established pathogens such as *S. aureus* would thus represent a new threat to the healthcare system.

Conclusion

The identification of the new species *S. brunensis* within the *Staphylococcus* genus expands our understanding of the diversity of coagulase-negative staphylococci. The number of the strains available is still limited, but similar to its closest relative *S. petrasii*, it can be expected that more strains will be captured as better diagnostic methods are developed. Genome analysis of the new isolates has important implications for studying the role of coagulase-negative staphylococci as a reservoir of transmissible genes that can facilitate improved survival in the environment, resistance to antibiotic treatment, or increased virulence following horizontal transfer. Characterization of a previously unexplored genomic island closely related to the SCC indicates the potential for its interspecies transfer enabled by unique *ccrDE* recombinase genes in both coagulase-negative staphylococci and the more clinically significant *S. aureus*. Identifying the new type of MGE thus opens up new possibilities for future research of gene transfer mechanisms in the emergence of multidrug-resistant staphylococcal strains with implications for clinical practice. These findings deepen our understanding of the evolution and pathogenesis of staphylococci, shedding light on how these bacteria acquire and disseminate virulence traits and antibiotic resistance.

Downloaded from https://journals.asm.org/journal/spectrum on 04 February 2026 by 147.251.86.90.

MATERIALS AND METHODS

Bacterial strains, cultivation and phenotypic identification, and antimicrobial susceptibility testing

Simultaneously analyzed reference strains of *Staphylococcus* spp. were obtained from the Czech Collection of Microorganisms (CCM, Masaryk University, Brno). The strains grew well in a basic set of staphylococcal media at a temperature of 30–37°C. The morphological, biochemical, and physiological characterization was performed as previously mentioned (7, 60–62). Antimicrobial susceptibility testing by disc diffusion method on Mueller-Hinton agar with adherence to EUCAST guidelines (63) was performed as described previously (60).

Genome sequencing and bioinformatics analyses

The short-read sequencing was conducted for the type strain NRL/St 16/872^T (LGC Genomics, Berlin, Germany). The genomic DNA was isolated with a GenElute Bacterial Genomic DNA kit (Sigma-Aldrich, St. Louis, MO, USA) from pure culture colonies cultivated on Colombia sheep blood agar (Oxoid). The library was prepared using a Nextera XT DNA Library Preparation Kit (Illumina, San Diego, CA, USA) and sequenced externally by LGC Genomics (Berlin, Germany) on the NextSeq platform with 2 × 150 bp reads (Illumina). Genomes of all novel isolates were sequenced by Oxford Nanopore Technology (ONT). The genomic DNA was extracted as described previously (64). Sequencing libraries were prepared using an SQK-RAD004 rapid barcoding kit and sequenced with a FLO-FLG001 cell in a MinION device and MinKnow v21.10.4 software (Oxford Nanopore Technologies, Oxford, UK).

The software Guppy version 6.0.0 (Oxford Nanopore Technologies) with config dna_r9.4.1_450bps_sup.cfg and default settings was used for basecalling, demultiplexing, and barcode trimming. The ONT reads were filtered by quality mapping to Illumina reads using Filtlong version 0.2.1 (https://github.com/rrwick/Filtlong) with a minimum length of 1,500 bp and quality threshold set to 95% and mapping on Illumina reads where applicable. The quality of both long and short reads was assessed with FastQC version 0.11.9 (http://www.bioinformatics.babraham.ac.uk/projects/fastqc) and NanoStat (65). Complete chromosome and partial plasmid sequences were obtained using either a hybrid assembly with Unicycler version 0.4.9 (66) or a long-read-only assembly with Trycycler version 0.5.3 (67). The resulting contigs were further polished with Medaka version 1.6.1 (https://github.com/nanoporetech/medaka) and Polypolish version 0.5.0 (68). Sequences were manipulated and inspected in the cross-platform bioinformatics software Ugene version 38.1 (69). The genomes were annotated using the NCBI Prokaryotic Genome Annotation Pipeline (70). Nucleotide and protein multiple sequence aligment was performed with Clustal Omega (71). The multiple sequence alignment was visualized using EasyFig version 2.2.5 (72) and IslandCompare version 1.0 (73). Variable genetic content was identified with PhiSpy version 3.4 (74), MobilomeFinder (75), PlasmidFinder (76), IslandViewer 4 (77), ISFinder (78), and SCCmecFinder (79). The CRISPR/Cas system was characterized by CRISPRCasTyper (80). Virulence and resistance genes were predicted using Abricate (https://github.com/tseemann/abricate) with the CARD (81), Resfinder (82), and VFDB (83) databases.

Phylogenetic and pangenomic analyses

The partial 16S rRNA gene was sequenced by Sanger sequencing in the Eurofins MWG Operon sequencing facility (Ebersberg, Germany) with previously described primers (84). Whole-genome sequences of related staphylococcal species were obtained from the NCBI database (Table S1). The multilocus sequence data of six housekeeping genes (*rpoB*, *groEL*, *dnaJ*, *tufA*, *sodA*, and *gap*) that are commonly used in phylogenetic studies of the *Staphylococcaceae* were extracted from whole-genome sequence assemblies as follows (gene coordinates of *S. aureus*): 1420..1974 for *rpoB*, 270..826 for *hsp60*, 23..911 for *dnaJ*, 49..929 for *gap*, 383..1032 for *tufA*, and 50..480 for the *sodA* gene. The phylogenetic

Downloaded from https://journals.asm.org/journal/spectrum on 04 February 2026 by 147.251.86.90.

analyses were performed with the software MEGA version 11 (85). The UBCG collection of 92 conservative genes (86), the average nucleotide identity (ANI) (87), and digital DNA-DNA hybridization (dDDH) values by the d4 formula using the web-based genome-to-genome distance calculator (GGDC) version 3.0 (88) were used for calculations of overall genome relatedness indices. The pangenome was calculated with the OrthoVenn2 pipeline with proteins clustered at the default threshold (89).

DNA fingerprinting

For genotypic characterization of the investigated bacterial group, fingerprinting by repetitive sequence-based PCR (rep-PCR) with the primer $(GTG)_5$ (90) and automated ribotyping with the restriction enzyme *Eco*RI were performed. The isolation of DNA for rep-PCR fingerprinting, PCR conditions, and fingerprint analysis were performed as previously described (91). Automated ribotyping was performed using the RiboPrinter microbial characterization system (DuPont Qualicon) according to the manufacturer's instructions. Numerical analysis of rep-PCR fingerprints and *Eco*RI ribotype patterns was performed using BioNumerics version 7.6 (Applied Maths, Belgium). The ribotype patterns were imported into the BioNumerics software using the load samples import script provided by the manufacturer.

PCR analysis of mobilizable genomic island encoding Ccr recombinases

To determine whether a genomic island is mobilizable, we designed primers spanning the excision site and primers targeting the key genes present in the genomic island (Table S2). The PCR reaction was conducted using Quick-Load 2× master mix with standard buffer (New England Biolabs, Ipswich, MA, USA) and a 200 nM concentration of each primer. The genomic island product was further analyzed by Sanger sequencing (Eurofins Genomics, Germany).

Transmission electron microscopy

A 200-mesh carbon/formvar-coated grid was placed on a drop of suspension of bacteria in water for 20 min. Bacterial cells on the grid were negatively stained with 2% ammonium molybdate and treated with UV light. A Morgagni 268D Philips (ThermoFisher Scientific, The Netherlands) transmission electron microscope was used to visualize bacterial cells.

MALDI-TOF MS

Protein fingerprinting by means of MALDI-TOF MS using an Ultraflextreme instrument (Bruker Daltonics, Germany) was conducted after a standard extraction protocol (92). MALDI-TOF mass spectra were obtained using an UltrafleXtreme instrument (Bruker Daltonics) operated in linear positive mode using the software FlexControl version 3.4. Signals present in at least seven out of nine independent mass spectra acquired per sample were taken into account. Mass spectra were processed using FlexAnalysis version 3.4 (Bruker Daltonics) and BioTyper version 3.1 software (Bruker Daltonics) supplemented with database version 10.0.0.0 (9,607 entries).

Chemotaxonomic characterization

Respiratory quinones were extracted and analyzed as previously described (93). Identity was confirmed by mass spectrometry, as described by Schumann et al. (94). Analysis of the cellular fatty acid profile was performed using a Microbial Identification System (MIDI, Newark, DE) according to the Standard Protocol of the Sherlock Microbial Identification System software, version 6.1 (95). The fatty acids were identified using gas chromatography–mass spectrometry (GC-MS) according to the study of Vieira et al. (93).

Isolation and structural analysis of the peptidoglycan was performed according to published protocols with some modifications. Briefly, the amino acid composition of the

Downloaded from https://journals.asm.org/journal/spectrum on 04 February 2026 by 147.251.86.90.

total hydrolysate (4 N HCl, 100°C for 16 h) of the peptidoglycan was analyzed by GC/MS (protocol 10 by Schumann [96]). The partial hydrolysate (4 N HCl, 100°C, 0.75 h) of the peptidoglycan was analyzed by high-resolution liquid chromatography–mass spectrometry (LC-MS) as described previously (94, 96). Enantiomeric analysis was performed by liquid chromatography as described by reference 97.

ACKNOWLEDGMENTS

Daniel Krsek (National Reference Laboratory for Diagnostic Electron Microscopy of Infectious Agents, National Institute of Public Health, Prague, Czech Republic) is gratefully acknowledged for transmission electron microscopy, Anika Wasner, Anja Frühling, and Gesa Martens for technical assistance; Peter Schumann for helpful discussions (all Leibniz Institute DSMZ); and Tereza Gelbíčová (Department of Public Health, Faculty of Medicine, Masaryk University) for valuable help.

This work was supported by the project National Institute of Virology and Bacteriology (Programme EXCELES, ID Project No. LX22NPO5103)—Funded by the European Union-Next Generation EU to R. P. CIISB, Instruct-CZ Centre of Instruct-ERIC EU consortium, funded by MEYS CR infrastructure project LM2023042 and European Regional Development Fund-Project "UP CIISB" (No. CZ.02.1.01/0.0/0.0/18_046/0015974) is gratefully acknowledged for the financial support of the measurements at the CEITEC Proteomics Core Facility. Computational resources were supplied by the project e-INFRA CZ project (ID:90140), supported by the Ministry of Education, Youth and Sports of the Czech Republic. T. B. gratefully acknowledges funding from the Ministry of Health of the Czech Republic (NU21J-05–00035). P. P. was supported by a conceptual development of research organization funded by the Ministry of Health of the Czech Republic (NIPH, 75010330). The Grant Agency of Masaryk University (MUNI/A/1287/2022) to J. D. supported the research activities of students. This study was partly funded by the Czech Collection of Microorganisms.

AUTHOR AFFILIATIONS

[1]Department of Experimental Biology, Division of Genetics and Molecular Biology, Faculty of Science, Masaryk University, Brno, Czech Republic
[2]Department of Experimental Biology, Czech Collection of Microorganisms, Faculty of Science, Masaryk University, Brno, Czech Republic
[3]Reference Laboratory for Staphylococci, National Institute of Public Health, Praha, Czech Republic
[4]Leibniz Institute DSMZ-German Collection of Microorganisms and Cell Cultures, Braunschweig, Germany
[5]Central European Institute of Technology, Masaryk University, Brno, Czech Republic

AUTHOR ORCIDs

Adéla Finstrlová http://orcid.org/0000-0003-2343-4357
Ivo Sedláček http://orcid.org/0000-0003-1717-187X
Pavel Švec http://orcid.org/0000-0002-1051-5177
Ivana Mašlaňová http://orcid.org/0000-0002-2597-2848
Meina Neumann-Schaal http://orcid.org/0000-0002-1641-019X
Tibor Botka http://orcid.org/0000-0003-2708-3718
Jiří Doškař http://orcid.org/0000-0001-5216-9586
Roman Pantůček http://orcid.org/0000-0002-3950-675X

Downloaded from https://journals.asm.org/journal/spectrum on 04 February 2026 by 147.251.86.90.

FUNDING

Funder	Grant(s)	Author(s)
Ministerstvo Školství, Mládeže a Tělový-chovy (MŠMT)	LX22NPO5103, LM2023042, CZ.02.1.01/0.0/0.0/18_046/0015974, e-INFRA CZ ID:90140	Roman Pantůček Jiří Doškař Tibor Botka Ondrej Šedo Ivana Mašlaňová Adéla Finstrlová Vojtěch Kovařovic
Ministerstvo Zdravotnictví Ceské Republiky (MZCR)	NU21J-05-00035, NI 75010330	Petr Petráš Tibor Botka
Masarykova Univerzita (MU)	MUNI/A/1287/2022	Roman Pantůček Jiří Doškař Adéla Finstrlová Vojtěch Kovařovic

AUTHOR CONTRIBUTIONS

Vojtěch Kovařovic, Conceptualization, Data curation, Formal analysis, Investigation, Methodology, Software, Validation, Visualization, Writing – original draft, Writing – review and editing | Adéla Finstrlová, Conceptualization, Data curation, Formal analysis, Investigation, Methodology, Software, Supervision, Validation, Visualization, Writing – original draft, Writing – review and editing | Ivo Sedláček, Conceptualization, Data curation, Formal analysis, Investigation, Methodology, Resources, Supervision, Validation, Visualization, Writing – original draft, Writing – review and editing | Petr Petráš, Conceptualization, Data curation, Formal analysis, Funding acquisition, Investigation, Resources, Validation, Writing – original draft, Writing – review and editing | Pavel Švec, Conceptualization, Data curation, Formal analysis, Investigation, Methodology, Validation, Visualization, Writing – review and editing | Ivana Mašlaňová, Data curation, Formal analysis, Investigation, Software, Supervision, Validation, Writing – review and editing | Meina Neumann-Schaal, Conceptualization, Data curation, Investigation, Methodology, Resources, Validation, Visualization, Writing – review and editing | Ondrej Šedo, Conceptualization, Data curation, Funding acquisition, Investigation, Methodology, Validation, Visualization, Writing – review and editing | Tibor Botka, Funding acquisition, Investigation, Methodology, Software, Validation, Writing – review and editing | Eva Staňková, Data curation, Investigation, Validation, Writing – review and editing | Jiří Doškař, Conceptualization, Funding acquisition, Supervision, Writing – original draft, Writing – review and editing | Roman Pantůček, Conceptualization, Data curation, Formal analysis, Funding acquisition, Investigation, Project administration, Resources, Supervision, Visualization, Writing – original draft, Writing – review and editing

DATA AVAILABILITY

The complete genome sequences of new isolates NRL/St 16/872^T, NRL/St 19/737, NRL/St 18/288, NRL/St 21/187, and NRL/St 22/194 have been deposited in GenBank/ENA/DDBJ database under accession numbers CP119327–CP119331, JALGRI000000000, JALGRH000000000, JALGRG000000000, and CP116597–CP116599, respectively. The associated BioProject number is PRJNA779217. The accession number for the 16S rRNA gene of the type strain NRL/St 16/872^T is OQ401401.

ADDITIONAL FILES

The following material is available online.

Downloaded from https://journals.asm.org/journal/spectrum on 04 February 2026 by 147.251.86.90.

Supplemental Material

Supplemental tables and figures (Spectrum01342-23-S0001.pdf). Tables S1 to S5, Table S7, Figures S1 to S3.

Table S6 (Spectrum01342-23-S0002.xlsx). Pairwise identity matrices of nucleotide and amino acid sequences of cassette recombinases.

REFERENCES

1. Heilmann C, Ziebuhr W, Becker K. 2019. Are coagulase-negative staphylococci virulent? Clin Microbiol Infect 25:1071–1080. https://doi.org/10.1016/j.cmi.2018.11.012
2. Marincola G, Liong O, Schoen C, Abouelfetouh A, Hamdy A, Wencker FDR, Marciniak T, Becker K, Köck R, Ziebuhr W. 2021. Antimicrobial resistance profiles of coagulase-negative staphylococci in community-based healthy individuals in Germany. Front Public Health 9:684456. https://doi.org/10.3389/fpubh.2021.684456
3. Takeuchi F, Watanabe S, Baba T, Yuzawa H, Ito T, Morimoto Y, Kuroda M, Cui L, Takahashi M, Ankai A, Baba S, Fukui S, Lee JC, Hiramatsu K. 2005. Whole-genome sequencing of *Staphylococcus haemolyticus* uncovers the extreme plasticity of its genome and the evolution of human-colonizing staphylococcal species. J Bacteriol 187:7292–7308. https://doi.org/10.1128/JB.187.21.7292-7308.2005
4. Chaudhry V, Patil PB. 2020. Evolutionary insights into adaptation of *Staphylococcus haemolyticus* to human and non-human niches. Genomics 112:2052–2062. https://doi.org/10.1016/j.ygeno.2019.11.018
5. Pain M, Wolden R, Jaén-Luchoro D, Salvà-Serra F, Iglesias BP, Karlsson R, Klingenberg C, Cavanagh JP. 2020. *Staphylococcus borealis* sp. nov., isolated from human skin and blood. Int J Syst Evol Microbiol 70:6067–6078. https://doi.org/10.1099/ijsem.0.004499
6. Lin Y-T, Hung W-C, Wan T-W, Li H, Lee T-F, Hsueh P-R, Teng L-J. 2022. *Staphylococcus taiwanensis* sp. nov., isolated from human blood. Int J Syst Evol Microbiol 72. https://doi.org/10.1099/ijsem.0.005262
7. Pantůček R, Švec P, Dajcs JJ, Machová I, Černohlávková J, Šedo O, Gelbíčová T, Mašlaňová I, Doškař J, Zdráhal Z, Růžičková V, Sedláček I. 2013. *Staphylococcus petrasii* sp. nov. including *S. petrasii* subsp. petrasii subsp. nov. and *S. petrasii* subsp. *croceilyticus* subsp. nov., isolated from human clinical specimens and human ear infections. Syst Appl Microbiol 36:90–95. https://doi.org/10.1016/j.syapm.2012.11.004
8. Švec P, De Bel A, Sedláček I, Petráš P, Gelbíčová T, Černohlávková J, Mašlaňová I, Cnockaert M, Varbanovová I, Echahidi F, Vandamme P, Pantůček R. 2015. *Staphylococcus petrasii* subsp. *pragensis* subsp. nov., occurring in human clinical material. Int J Syst Evol Microbiol 65:2071–2077. https://doi.org/10.1099/ijs.0.000220
9. Madhaiyan M, Wirth JS, Saravanan VS. 2020. Phylogenomic analyses of the *Staphylococcaceae* family suggest the reclassification of five species within the genus *Staphylococcus* as heterotypic synonyms, the promotion of five subspecies to novel species, the taxonomic reassignment of five *Staphylococcus* species to *Mammaliicoccus* gen. nov., and the formal assignment of *Nosocomiicoccus* to the family *Staphylococcaceae*. Int J Syst Evol Microbiol 70:5926–5936. https://doi.org/10.1099/ijsem.0.004498
10. Vrbovská V, Kovařovic V, Mašlaňová I, Indráková A, Petráš P, Šedo O, Švec P, Fišarová L, Šiborová M, Mikulášek K, Sedláček I, Doškař J, Pantůček R. 2019. *Staphylococcus petrasii* diagnostics and its pathogenic potential enhanced by mobile genetic elements. Int J Med Microbiol 309:151355. https://doi.org/10.1016/j.ijmm.2019.151355
11. Uehara Y. 2022. current status of staphylococcal cassette chromosome *mec* (SCC*mec*). Antibiotics 11:86. https://doi.org/10.3390/antibiotics11010086
12. Qin L, McCausland JW, Cheung GYC, Otto M. 2016. PSM-Mec-A virulence determinant that connects transcriptional regulation, virulence, and antibiotic resistance in staphylococci. Front Microbiol 7:1293. https://doi.org/10.3389/fmicb.2016.01293
13. Bleiziffer I, Eikmeier J, Pohlentz G, McAulay K, Xia G, Hussain M, Peschel A, Foster S, Peters G, Heilmann C. 2017. The plasmin-sensitive protein pls in methicillin-resistant *Staphylococcus aureus* (MRSA) is a glycoprotein. PLoS Pathog 13:e1006110. https://doi.org/10.1371/journal.ppat.1006110
14. Chen H-J, Lin Y-T, Hung W-C, Tsai J-C, Hsueh P-R, Teng L-J. 2016. Distribution of staphylococcal cassette chromosome (SCC) mec element types in fusidic acid-resistant *Staphylococcus epidermidis* and identification of a novel SCC7684 element. Antimicrob Agents Chemother 60:5006–5009. https://doi.org/10.1128/AAC.00231-16
15. Tsubakishita S, Kuwahara-Arai K, Sasaki T, Hiramatsu K. 2010. Origin and molecular evolution of the determinant of methicillin resistance in staphylococci. Antimicrob Agents Chemother 54:4352–4359. https://doi.org/10.1128/AAC.00356-10
16. Scharn CR, Tenover FC, Goering RV. 2013. Transduction of staphylococcal cassette chromosome mec elements between strains of *Staphylococcus aureus*. Antimicrob Agents Chemother 57:5233–5238. https://doi.org/10.1128/AAC.01058-13
17. Ray MD, Boundy S, Archer GL. 2016. Transfer of the methicillin resistance genomic island among staphylococci by conjugation. Mol Microbiol 100:675–685. https://doi.org/10.1111/mmi.13340
18. Maree M, Thi Nguyen LT, Ohniwa RL, Higashide M, Msadek T, Morikawa K. 2022. Natural transformation allows transfer of SCC*mec*-mediated methicillin resistance in *Staphylococcus aureus* biofilms. Nat Commun 13:2477. https://doi.org/10.1038/s41467-022-29877-2
19. Boundy S, Safo MK, Wang L, Musayev FN, O'Farrell HC, Rife JP, Archer GL. 2013. Characterization of the *Staphylococcus aureus* rRNA methyltransferase encoded by *orfX*, the gene containing the staphylococcal chromosome cassette mec (SCC*mec*) insertion site. J Biol Chem 288:132–140. https://doi.org/10.1074/jbc.M112.385138
20. Misiura A, Pigli YZ, Boyle-Vavra S, Daum RS, Boocock MR, Rice PA. 2013. Roles of two large serine recombinases in mobilizing the methicillin-resistance cassette SCC*mec*. Mol Microbiol 88:1218–1229. https://doi.org/10.1111/mmi.12253
21. Ito T, Ma XX, Takeuchi F, Okuma K, Yuzawa H, Hiramatsu K. 2004. Novel type V staphylococcal cassette chromosome mec driven by a novel cassette chromosome recombinase, *ccrC*. Antimicrob Agents Chemother 48:2637–2651. https://doi.org/10.1128/AAC.48.7.2637-2651.2004
22. Takahashi T, Satoh I, Kikuchi N. 1999. Phylogenetic relationships of 38 taxa of the genus *Staphylococcus* based on 16S rRNA gene sequence analysis. Int J Syst Bacteriol 49:725–728. https://doi.org/10.1099/00207713-49-2-725
23. Pantůček R, Sedláček I, Indráková A, Vrbovská V, Mašlaňová I, Kovařovic V, Švec P, Králová S, Krištofová L, Kekláková J, Petráš P, Doškař J. 2018. *Staphylococcus edaphicus* sp. nov., isolated in Antarctica, harbors the *mecC* gene and genomic islands with a suspected role in adaptation to extreme environments. Appl Environ Microbiol 84:e01746-17. https://doi.org/10.1128/AEM.01746-17
24. Kim M, Oh HS, Park SC, Chun J. 2014. Towards a taxonomic coherence between average nucleotide identity and 16S rRNA gene sequence similarity for species demarcation of prokaryotes. Int J Syst Evol Microbiol 64:346–351. https://doi.org/10.1099/ijs.0.059774-0
25. Vrbovská V, Sedláček I, Zeman M, Švec P, Kovařovic V, Šedo O, Laichmanová M, Doškař J, Pantůček R. 2020. Characterization of *Staphylococcus intermedius* group isolates associated with animals from Antarctica and emended description of *Staphylococcus delphini*. Microorganisms 8:204. https://doi.org/10.3390/microorganisms8020204
26. Sabat AJ, Hermelijn SM, Akkerboom V, Juliana A, Degener JE, Grundmann H, Friedrich AW. 2017. Complete-genome sequencing elucidates outbreak dynamics of CA-MRSA USA300 (ST8-spa t008) in an academic hospital of Paramaribo, Republic of Suriname. Sci Rep 7:41050. https://doi.org/10.1038/srep41050
27. Pumirat P, Boonyuen U, Vanaporn M, Pinweha P, Tandhavanant S, Korbsrisate S, Chantratita N. 2014. The role of short-chain dehydrogenase/oxidoreductase, induced by salt stress, on host interaction of *B. pseudomallei*. BMC Microbiol 14:1. https://doi.org/10.1186/1471-2180-14-1

Downloaded from https://journals.asm.org/journal/spectrum on 04 February 2026 by 147.251.86.90.

28. North RA, Wahlgren WY, Remus DM, Scalise M, Kessans SA, Dunevall E, Claesson E, Soares da Costa TP, Perugini MA, Ramaswamy S, Allison JR, Indiveri C, Friemann R, Dobson RCJ. 2018. The sodium sialic acid symporter from *Staphylococcus aureus* has altered substrate specificity. Front Chem 6:233. https://doi.org/10.3389/fchem.2018.00233
29. International Working Group on the Classification of Staphylococcal Cassette Chromosome Elements (IWG-SCC). 2009. Classification of staphylococcal cassette chromosome mec (SCC*mec*): guidelines for reporting novel SCC*mec* elements. Antimicrob Agents Chemother 53:4961–4967. https://doi.org/10.1128/AAC.00579-09
30. McClure JA, Conly JM, Zhang K. 2021. Characterizing a novel staphylococcal cassette chromosome *mec* with a composite structure from a clinical strain of *Staphylococcus hominis*, C34847. Antimicrob Agents Chemother 65:e00777-21. https://doi.org/10.1128/AAC.00777-21
31. Lin Y-T, Tsai J-C, Chen H-J, Hung W-C, Hsueh P-R, Teng L-J. 2014. A novel staphylococcal cassette chromosomal element, SCC*fus*C, carrying *fus*C and *speG* in fusidic acid-resistant methicillin-resistant *Staphylococcus aureus*. Antimicrob Agents Chemother 58:1224–1227. https://doi.org/10.1128/AAC.01772-13
32. Wilson LK, Coombs GW, Christiansen K, Grubb WB, O'Brien FG. 2016. Characterization of a novel staphylococcal cassette chromosome composite island from community-associated MRSA isolated in aged care facilities in Western Australia. J Antimicrob Chemother 71:3372–3375. https://doi.org/10.1093/jac/dkw317
33. Xiao J, Huang J, Xue X, Wang C, Sun Y, Zheng L, Zhao X, Wang X, Zhao X, Xue H. 2023. Novel cassette chromosome recombinases CcrA8B9 catalyse the excision and integration of the staphylococcal cassette chromosome *mec* element. J Antimicrob Chemother 78:440–444. https://doi.org/10.1093/jac/dkac410
34. Vasu K, Nagaraja V. 2013. Diverse functions of restriction-modification systems in addition to cellular defense. Microbiol Mol Biol Rev 77:53–72. https://doi.org/10.1128/MMBR.00044-12
35. Chen L, Hu JX, Liu C, Liu J, Ma ZB, Tang ZY, Li YF, Zeng ZL. 2021. Identification of the multiresistance gene *poxtA* in oxazolidinone-susceptible *Staphylococcus haemolyticus* and *Staphylococcus saprophyticus* of pig and feed origins. Pathogens 10:601. https://doi.org/10.3390/pathogens10050601
36. Berbel Caban A, Pak TR, Obla A, Dupper AC, Chacko KI, Fox L, Mills A, Ciferri B, Oussenko I, Beckford C, Chung M, Sebra R, Smith M, Conolly S, Patel G, Kasarskis A, Sullivan MJ, Altman DR, van Bakel H. 2020. PathoSPOT genomic epidemiology reveals under-the-radar nosocomial outbreaks. Genome Med 12:96. https://doi.org/10.1186/s13073-020-00798-3
37. Ziebuhr W, Hennig S, Eckart M, Kränzler H, Batzilla C, Kozitskaya S. 2006. Nosocomial infections by *Staphylococcus epidermidis*: how a commensal bacterium turns into a pathogen. Int J Antimicrob Agents 28 Suppl 1:14–20. https://doi.org/10.1016/j.ijantimicag.2006.05.012
38. Foster TJ. 2019. The MSCRAMM family of cell-wall-anchored surface proteins of Gram-positive cocci. Trends Microbiol 27:927–941. https://doi.org/10.1016/j.tim.2019.06.007
39. Lindsay JA. 2019. Staphylococci: evolving genomes. Microbiol Spectr 7:GPP3-0071. https://doi.org/10.1128/microbiolspec.GPP3-0071-2019
40. Everitt RG, Didelot X, Batty EM, Miller RR, Knox K, Young BC, Bowden R, Auton A, Votintseva A, Larner-Svensson H, Charlesworth J, Golubchik T, Ip CLC, Godwin H, Fung R, Peto TEA, Walker AS, Crook DW, Wilson DJ. 2014. Mobile elements drive recombination hotspots in the core genome of *Staphylococcus aureus*. Nat Commun 5:3956. https://doi.org/10.1038/ncomms4956
41. Firth N, Jensen SO, Kwong SM, Skurray RA, Ramsay JP, Fischetti VA, Novick RP, Ferretti JJ, Portnoy DA, Braunstein M, Rood JI. 2018. Staphylococcal Plasmids, Transposable and integrative elements. Microbiol Spectr 6:GPP3-0030. https://doi.org/10.1128/microbiolspec.GPP3-0030-2018
42. Shearer JES, Wireman J, Hostetler J, Forberger H, Borman J, Gill J, Sanchez S, Mankin A, Lamarre J, Lindsay JA, Bayles K, Nicholson A, O'Brien F, Jensen SO, Firth N, Skurray RA, Summers AO. 2011. Major families of multiresistant plasmids from geographically and epidemiologically diverse staphylococci. G3 (Bethesda) 1:581–591. https://doi.org/10.1534/g3.111.000760
43. Caryl JA, Smith MCA, Thomas CD. 2004. Reconstitution of a staphylococcal plasmid-protein relaxation complex *in vitro*. J Bacteriol 186:3374–3383. https://doi.org/10.1128/JB.186.11.3374-3383.2004
44. Kwong SM, Ramsay JP, Jensen SO, Firth N. 2017. Replication of staphylococcal resistance plasmids. Front Microbiol 8:2279. https://doi.org/10.3389/fmicb.2017.02279
45. Bender J, Strommenger B, Steglich M, Zimmermann O, Fenner I, Lensing C, Dagwadordsch U, Kekulé AS, Werner G, Layer F. 2015. Linezolid resistance in clinical isolates of *Staphylococcus epidermidis* from German hospitals and characterization of two *cfr*-carrying plasmids. J Antimicrob Chemother 70:1630–1638. https://doi.org/10.1093/jac/dkv025
46. Pain M, Hjerde E, Klingenberg C, Cavanagh JP. 2019. Comparative genomic analysis of *Staphylococcus haemolyticus* reveals key to hospital adaptation and pathogenicity. Front Microbiol 10:2096. https://doi.org/10.3389/fmicb.2019.02096
47. Saroha T, Chaudhry V, Patil PB. 2022. Novel insights into the role of the mobilome in ecological diversification and success of *Staphylococcus haemolyticus* as an opportunistic pathogen. Microb Genom 8:000755. https://doi.org/10.1099/mgen.0.000755
48. Hiramatsu K, Ito T, Tsubakishita S, Sasaki T, Takeuchi F, Morimoto Y, Katayama Y, Matsuo M, Kuwahara-Arai K, Hishinuma T, Baba T. 2013. Genomic basis for methicillin resistance in *Staphylococcus aureus*. Infect Chemother 45:117–136. https://doi.org/10.3947/ic.2013.45.2.117
49. Mir-Sanchis I, Roman CA, Misiura A, Pigli YZ, Boyle-Vavra S, Rice PA. 2016. Staphylococcal SCC*mec* elements encode an active MCM-like helicase and thus may be replicative. Nat Struct Mol Biol 23:891–898. https://doi.org/10.1038/nsmb.3286
50. Sivertsen A, Janice J, Pedersen T, Wagner TM, Hegstad J, Hegstad K, Ellermeier CD. 2018. The *Enterococcus* cassette chromosome, a genomic variation enabler in enterococci. mSphere 3:e00402-18. https://doi.org/10.1128/mSphere.00402-18
51. Bjørkeng EK, Tessema GT, Lundblad EW, Butaye P, Willems R, Sollid JE, Sundsfjord A, Hegstad K. 2010. ccrABEnt serine recombinase genes are widely distributed in the *Enterococcus faecium* and *Enterococcus casseliflavus* species groups and are expressed in *E. faecium*. Microbiol 156:3624–3634. https://doi.org/10.1099/mic.0.041491-0
52. Schwendener S, Perreten V. 2022. The bla and mec families of beta-lactam resistance genes in the genera *Macrococcus*, *Mammaliicoccus* and *Staphylococcus*: an in-depth analysis with emphasis on *Macrococcus*. J Antimicrob Chemother 77:1796–1827. https://doi.org/10.1093/jac/dkac107
53. Bebel A, Walsh MA, Mir-Sanchis I, Rice PA. 2020. A novel DNA primase-helicase pair encoded by SCC*mec* elements. Elife 9:e55478. https://doi.org/10.7554/eLife.55478
54. Zeman M, Mašlaňová I, Indráková A, Šiborová M, Mikulášek K, Bendíčková K, Plevka P, Vrbovská V, Zdráhal Z, Doškař J, Pantůček R. 2017. *Staphylococcus sciuri* bacteriophages double-convert for staphylokinase and phospholipase, mediate interspecies plasmid transduction, and package *mecA* gene. Sci Rep 7:46319. https://doi.org/10.1038/srep46319
55. Chlebowicz MA, Mašlaňová I, Kuntová L, Grundmann H, Pantůček R, Doškař J, van Dijl JM, Buist G. 2014. The staphylococcal cassette chromosome *mec* type V from *Staphylococcus aureus* ST398 is packaged into bacteriophage capsids. Int J Med Microbiol 304:764–774. https://doi.org/10.1016/j.ijmm.2014.05.010
56. Rolo J, Worning P, Nielsen JB, Bowden R, Bouchami O, Damborg P, Guardabassi L, Perreten V, Tomasz A, Westh H, de Lencastre H, Miragaia M. 2017. Evolutionary origin of the Staphylococcal cassette Chromosome MEC (Sccmec). Antimicrob Agents Chemother 61:e02302–16. https://doi.org/10.1128/AAC.02302-16
57. Novick RP, Ram G. 2017. Staphylococcal pathogenicity islands-movers and shakers in the genomic firmament. Curr Opin Microbiol 38:197–204. https://doi.org/10.1016/j.mib.2017.08.001
58. Jiang N, Li J, Feßler AT, Wang Y, Schwarz S, Wu C. 2019. Novel pseudo-staphylococcal cassette chromosome mec element (phiSCCmecT55) in MRSA ST9. J Antimicrob Chemother 74:819–820. https://doi.org/10.1093/jac/dky457
59. Wendlandt S, Li B, Ma Z, Schwarz S. 2013. Complete sequence of the multi-resistance plasmid pV7037 from a porcine methicillin-resistant *Staphylococcus aureus*. Vet Microbiol 166:650–654. https://doi.org/10.1016/j.vetmic.2013.07.017

Downloaded from https://journals.asm.org/journal/spectrum on 04 February 2026 by 147.251.86.90.

60. Kovařovic V, Sedláček I, Petráš P, Králová S, Mašlaňová I, Švec P, Neumann-Schaal M, Botka T, Gelbíčová T, Staňková E, Doškař J, Pantůček R. 2022. *Staphylococcus ratti* sp. nov. isolated from a lab rat. Pathogens 11:51. https://doi.org/10.3390/pathogens11010051
61. Mašlaňová I, Wertheimer Z, Sedláček I, Švec P, Indráková A, Kovařovic V, Schumann P, Spröer C, Králová S, Šedo O, Krištofová L, Vrbovská V, Füzik T, Petráš P, Zdráhal Z, Ružičková V, Doškař J, Pantuček R. 2018. Description and comparative genomics of *Macrococcus caseolyticus* subsp. *hominis* subsp. nov., *Macrococcus goetzii* sp. nov., *Macrococcus epidermidis* sp. nov., and *Macrococcus bohemicus* sp. nov., novel macrococci from human clinical material with virulence potential and suspected uptake of foreign DNA by natural transformation. Front Microbiol 9:1178. https://doi.org/10.3389/fmicb.2018.01178
62. Freeman DJ, Falkiner FR, Keane CT. 1989. New method for detecting slime production by coagulase negative staphylococci. J Clin Pathol 42:872–874. https://doi.org/10.1136/jcp.42.8.872
63. EUCAST. 2022. Breakpoint tables for interpretation of MICs and zone diameters, *in press*. The European Committee on Antimicrobial Susceptibility Testing, Version 12. Available from: http://www.eucast.org
64. Fišarová L, Botka T, Du X, Mašlaňová I, Bárdy P, Pantůček R, Benešík M, Roudnický P, Winstel V, Larsen J, Rosenstein R, Peschel A, Doškař J. 2021. *Staphylococcus epidermidis* phages transduce antimicrobial resistance plasmids and mobilize chromosomal islands. mSphere 6:e00223-21. https://doi.org/10.1128/mSphere.00223-21
65. De Coster W, D'Hert S, Schultz DT, Cruts M, Van Broeckhoven C. 2018. NanoPack: visualizing and processing long-read sequencing data. Bioinformatics 34:2666–2669. https://doi.org/10.1093/bioinformatics/bty149
66. Wick RR, Judd LM, Gorrie CL, Holt KE. 2017. Unicycler: resolving bacterial genome assemblies from short and long sequencing reads. PLoS Comput Biol 13:e1005595. https://doi.org/10.1371/journal.pcbi.1005595
67. Wick RR, Judd LM, Cerdeira LT, Hawkey J, Méric G, Vezina B, Wyres KL, Holt KE. 2021. Trycycler: consensus long-read assemblies for bacterial genomes. Genome Biol 22:266. https://doi.org/10.1186/s13059-021-02483-z
68. Wick RR, Holt KE. 2022. Polypolish: short-read polishing of long-read bacterial genome assemblies. PLoS Comput Biol 18:e1009802. https://doi.org/10.1371/journal.pcbi.1009802
69. Okonechnikov K, Golosova O, Fursov M, UGENE team. 2012. Unipro UGENE: a unified bioinformatics toolkit. Bioinformatics 28:1166–1167. https://doi.org/10.1093/bioinformatics/bts091
70. Li W, O'Neill KR, Haft DH, DiCuccio M, Chetvernin V, Badretdin A, Coulouris G, Chitsaz F, Derbyshire MK, Durkin AS, Gonzales NR, Gwadz M, Lanczycki CJ, Song JS, Thanki N, Wang J, Yamashita RA, Yang M, Zheng C, Marchler-Bauer A, Thibaud-Nissen F. 2021. RefSeq: expanding the prokaryotic genome annotation pipeline reach with protein family model curation. Nucleic Acids Res 49:D1020–D1028. https://doi.org/10.1093/nar/gkaa1105
71. Madeira F, Pearce M, Tivey ARN, Basutkar P, Lee J, Edbali O, Madhusoodanan N, Kolesnikov A, Lopez R. 2022. Search and sequence analysis tools services from EMBL-EBI in 2022. Nucleic Acids Res 50:W276–W279. https://doi.org/10.1093/nar/gkac240
72. Sullivan MJ, Petty NK, Beatson SA. 2011. Easyfig: a genome comparison visualizer. Bioinformatics 27:1009–1010. https://doi.org/10.1093/bioinformatics/btr039
73. Bertelli C, Gray KL, Woods N, Lim AC, Tilley KE, Winsor GL, Hoad GR, Roudgar A, Spencer A, Peltier J, Warren D, Raphenya AR, McArthur AG, Brinkman FSL. 2022. Enabling genomic island prediction and comparison in multiple genomes to investigate bacterial evolution and outbreaks. Microb Genom 8:mgen000818. https://doi.org/10.1099/mgen.0.000818
74. Edwards R, Decewicz P, Katelyn D, Laurasisk S. 2021. Linsalrob/Phispy: Dropped Prophages (v.4.2.19). Zenodo. https://doi.org/10.5281/zenodo.5070204
75. Ou H-Y, He X, Harrison EM, Kulasekara BR, Thani AB, Kadioglu A, Lory S, Hinton JCD, Barer MR, Deng Z, Rajakumar K. 2007. MobilomeFINDER: web-based tools for in silico and experimental discovery of bacterial genomic islands. Nucleic Acids Res 35:W97–W104. https://doi.org/10.1093/nar/gkm380
76. Carattoli A, Zankari E, García-Fernández A, Voldby Larsen M, Lund O, Villa L, Møller Aarestrup F, Hasman H. 2014. *In silico* detection and typing of plasmids using plasmidfinder and plasmid multilocus sequence typing. Antimicrob Agents Chemother 58:3895–3903. https://doi.org/10.1128/AAC.02412-14
77. Bertelli C, Laird MR, Williams KP, Simon Fraser University Research Computing Group, Lau BY, Hoad G, Winsor GL, Brinkman FSL. 2017. IslandViewer 4: expanded prediction of genomic islands for larger-scale datasets. Nucleic Acids Res 45:W30–W35. https://doi.org/10.1093/nar/gkx343
78. Siguier P, Perochon J, Lestrade L, Mahillon J, Chandler M. 2006. Isfinder: the reference centre for bacterial insertion sequences. Nucleic Acids Res 34:D32–6. https://doi.org/10.1093/nar/gkj014
79. Kaya H, Hasman H, Larsen J, Stegger M, Johannesen TB, Allesøe RL, Lemvigh CK, Aarestrup FM, Lund O, Larsen AR, Limbago BM. 2018. Sccmecfinder, a web-based tool for typing of Staphylococcal cassette Chromosome MEC in Staphylococcus aureus using whole-genome sequence data. mSphere 3:e00612–17. https://doi.org/10.1128/mSphere.00612-17
80. Russel J, Pinilla-Redondo R, Mayo-Muñoz D, Shah SA, Sørensen SJ. 2020. CRISPRCasTyper: automated identification, annotation, and classification of CRISPR-Cas loci. CRISPR J 3:462–469. https://doi.org/10.1089/crispr.2020.0059
81. Jia B, Raphenya AR, Alcock B, Waglechner N, Guo P, Tsang KK, Lago BA, Dave BM, Pereira S, Sharma AN, Doshi S, Courtot M, Lo R, Williams LE, Frye JG, Elsayegh T, Sardar D, Westman EL, Pawlowski AC, Johnson TA, Brinkman FSL, Wright GD, McArthur AG. 2017. CARD 2017: expansion and model-centric curation of the comprehensive antibiotic resistance database. Nucleic Acids Res 45:D566–D573. https://doi.org/10.1093/nar/gkw1004
82. Zankari E, Hasman H, Cosentino S, Vestergaard M, Rasmussen S, Lund O, Aarestrup FM, Larsen MV. 2012. Identification of acquired antimicrobial resistance genes. J Antimicrob Chemother 67:2640–2644. https://doi.org/10.1093/jac/dks261
83. Chen L, Zheng D, Liu B, Yang J, Jin Q. 2016. VFDB 2016: hierarchical and refined dataset for big data analysis-10 years on. Nucleic Acids Res 44:D694–D697. https://doi.org/10.1093/nar/gkv1239
84. Pantůček R, Sedláček I, Petráš P, Koukalová D, Švec P, Štětina V, Vancanneyt M, Chrastinová L, Vokurková J, Růžičková V, Doškař J, Swings J, Hájek V. 2005. *Staphylococcus simiae* sp. nov., isolated from South American squirrel monkeys. Int J Syst Evol Microbiol 55:1953–1958. https://doi.org/10.1099/ijs.0.63590-0
85. Tamura K, Stecher G, Kumar S, Battistuzzi FU. 2021. Mega11: molecular evolutionary genetics analysis version 11. Mol Biol Evol 38:3022–3027. https://doi.org/10.1093/molbev/msab120
86. Na SI, Kim YO, Yoon SH, Ha SM, Baek I, Chun J. 2018. UBCG: up-to-date bacterial core gene set and pipeline for phylogenomic tree reconstruction. J Microbiol 56:280–285. https://doi.org/10.1007/s12275-018-8014-6
87. Jain C, Rodriguez-R LM, Phillippy AM, Konstantinidis KT, Aluru S. 2018. High throughput ANI analysis of 90K prokaryotic genomes reveals clear species boundaries. Nat Commun 9:5114. https://doi.org/10.1038/s41467-018-07641-9
88. Meier-Kolthoff JP, Klenk H-P, Göker M. 2014. Taxonomic use of DNA G+C content and DNA-DNA hybridization in the genomic age. Int J Syst Evol Microbiol 64:352–356. https://doi.org/10.1099/ijs.0.056994-0
89. Xu L, Dong Z, Fang L, Luo Y, Wei Z, Guo H, Zhang G, Gu YQ, Coleman-Derr D, Xia Q, Wang Y. 2019. OrthoVenn2: a web server for whole-genome comparison and annotation of orthologous clusters across multiple species. Nucleic Acids Res 47:W52–W58. https://doi.org/10.1093/nar/gkz333
90. Versalovic J, Schneider M, de Bruijn FJ, Lupski JR. 1994. Genomic fingerprinting of bacteria using repetitive sequence-based polymerase chain reaction. Methods Mol Cell Biol 5:25–40.
91. Švec P, Pantůček R, Petráš P, Sedláček I, Nováková D. 2010. Identification of *Staphylococcus* spp. using (GTG)5-PCR fingerprinting. Syst Appl Microbiol 33:451–456. https://doi.org/10.1016/j.syapm.2010.09.004
92. Freiwald A, Sauer S. 2009. Phylogenetic classification and identification of bacteria by mass spectrometry. Nat Protoc 4:732–742. https://doi.org/10.1038/nprot.2009.37
93. Vieira S, Huber KJ, Neumann-Schaal M, Geppert A, Luckner M, Wanner G, Overmann J. 2021. *Usitatibacter rugosus* gen. nov., sp. nov. and *Usitatibacter palustris* sp. nov., novel members of *Usitatibacteraceae* fam.

Downloaded from https://journals.asm.org/journal/spectrum on 04 February 2026 by 147.251.86.90.

nov. within the order *Nitrosomonadales* isolated from soil. Int J Syst Evol Microbiol 71:004631. https://doi.org/10.1099/ijsem.0.004631
94. Schumann P, Kalensee F, Cao J, Criscuolo A, Clermont D, Köhler JM, Meier-Kolthoff JP, Neumann-Schaal M, Tindall BJ, Pukall R. 2021. Reclassification of *Haloactinobacterium glacieicola* as *Occultella glacieicola* gen. nov., comb. nov., of *Haloactinobacterium album* as *Ruania alba* comb. nov, with an emended description of the genus *Ruania*, recognition that the genus names *Haloactinobacterium* and *Ruania* are heterotypic synonyms and description of *Occultella aeris* sp. nov., a halotolerant isolate from surface soil sampled at an ancient copper smelter. Int J Syst Evol Microbiol 71:004769. https://doi.org/10.1099/ijsem.0.004769
95. Sasser M. 1990. MIDI Technical Note 101, Revision July 2006 ed, *in press*. Identification of bacteria by gas chromatography of cellular fatty acids. MIDI Inc, Newark, DE. http://midi-inc.com/pdf/MIS_Technote_101.pdf.
96. Schumann P. 2011. Peptidoglycan structure. Methods Microbiol 38:101–129. https://doi.org/10.1016/b978-0-12-387730-7.00005-x
97. Kämpfer P, McInroy JA, Clermont D, Neumann-Schaal M, Criscuolo A, Busse H-J, Glaeser SP. 2021. *Leucobacter soli* sp. nov., from soil amended with humic acid. Int J Syst Evol Microbiol 71:005156. https://doi.org/10.1099/ijsem.0.005156

Downloaded from https://journals.asm.org/journal/spectrum on 04 February 2026 by 147.251.86.90.

APPENDIX 13

Fišarová L*, Botka T*, Du X*, Mašlaňová I, Bárdy P, Pantůček R, Benešík M, Roudnický P, Winstel V, Larsen J, Rosenstein R, Peschel A, Doškař J (2021) *Staphylococcus epidermidis* phages transduce antimicrobial resistance plasmids and mobilize chromosomal islands. *mSphere* 6:e00223-21. https://doi.org/10.1128/mSphere.00223-21 *co-first authors
(JCR 2021: IF = 5.029; Q2 – Microbiology)

CC BY 4.0

AMERICAN SOCIETY FOR MICROBIOLOGY | mSphere®

RESEARCH ARTICLE

Staphylococcus epidermidis Phages Transduce Antimicrobial Resistance Plasmids and Mobilize Chromosomal Islands

Lenka Fišarová,[a] Tibor Botka,[a] Xin Du,[b,c] Ivana Mašlaňová,[a] Pavol Bárdy,[a,d] Roman Pantůček,[a] Martin Benešík,[a] Pavel Roudnický,[d] Volker Winstel,[e,f] Jesper Larsen,[g] Ralf Rosenstein,[b,c] Andreas Peschel,[b,c] Jiří Doškař[a]

[a]Department of Experimental Biology, Faculty of Science, Masaryk University, Brno, Czech Republic
[b]Interfaculty Institute of Microbiology and Infection Medicine Tübingen, University of Tübingen, Tübingen, Germany
[c]Cluster of Excellence EXC2124 Controlling Microbes to Fight Infections, Tübingen, Germany
[d]Central European Institute of Technology, Masaryk University, Brno, Czech Republic
[e]Research Group Pathogenesis of Bacterial Infections, TWINCORE, Hannover, Germany
[f]Institute of Medical Microbiology and Hospital Epidemiology, Hannover Medical School, Hannover, Germany
[g]Department of Bacteria, Parasites, and Fungi, Statens Serum Institut, Copenhagen, Denmark

Lenka Fišarová, Tibor Botka, and Xin Du contributed equally to this work, and the order was determined based on participation in the study's conceptualization.

ABSTRACT *Staphylococcus epidermidis* is a leading opportunistic pathogen causing nosocomial infections that is notable for its ability to form a biofilm and for its high rates of antibiotic resistance. It serves as a reservoir of multiple antimicrobial resistance genes that spread among the staphylococcal population by horizontal gene transfer such as transduction. While phage-mediated transduction is well studied in *Staphylococcus aureus*, *S. epidermidis* transducing phages have not been described in detail yet. Here, we report the characteristics of four phages, 27, 48, 456, and 459, previously used for *S. epidermidis* phage typing, and the newly isolated phage E72, from a clinical *S. epidermidis* strain. The phages, classified in the family *Siphoviridae* and genus *Phietavirus*, exhibited an *S. epidermidis*-specific host range, and together they infected 49% of the 35 strains tested. A whole-genome comparison revealed evolutionary relatedness to transducing *S. aureus* phietaviruses. In accordance with this, all the tested phages were capable of transduction with high frequencies up to 10^{-4} among *S. epidermidis* strains from different clonal complexes. Plasmids with sizes from 4 to 19 kb encoding resistance to streptomycin, tetracycline, and chloramphenicol were transferred. We provide here the first evidence of a phage-inducible chromosomal island transfer in *S. epidermidis*. Similarly to *S. aureus* pathogenicity islands, the transfer was accompanied by phage capsid remodeling; however, the interfering protein encoded by the island was distinct. Our findings underline the role of *S. epidermidis* temperate phages in the evolution of *S. epidermidis* strains by horizontal gene transfer, which can also be utilized for *S. epidermidis* genetic studies.

IMPORTANCE Multidrug-resistant strains of *S. epidermidis* emerge in both nosocomial and livestock environments as the most important pathogens among coagulase-negative staphylococcal species. The study of transduction by phages is essential to understanding how virulence and antimicrobial resistance genes spread in originally commensal bacterial populations. In this work, we provide a detailed description of transducing *S. epidermidis* phages. The high transduction frequencies of antimicrobial resistance plasmids and the first evidence of chromosomal island transfer emphasize the decisive role of *S. epidermidis* phages in attaining a higher pathogenic potential of host strains. To date, such importance has been attributed only to *S. aureus* phages, not to those of coagulase-negative staphylococci. This study also proved that the described transducing bacteriophages represent valuable genetic modification tools in *S. epidermidis* strains where other methods for gene transfer fail.

Citation Fišarová L, Botka T, Du X, Mašlaňová I, Bárdy P, Pantůček R, Benešík M, Roudnický P, Winstel V, Larsen J, Rosenstein R, Peschel A, Doškař J. 2021. *Staphylococcus epidermidis* phages transduce antimicrobial resistance plasmids and mobilize chromosomal islands. mSphere 6:e00223-21. https://doi.org/10.1128/mSphere.00223-21.

Editor Patricia A. Bradford, Antimicrobial Development Specialists, LLC

Copyright © 2021 Fišarová et al. This is an open-access article distributed under the terms of the Creative Commons Attribution 4.0 International license.

Address correspondence to Andreas Peschel, andreas.peschel@uni-tuebingen.de, or Jiří Doškař, doskar@sci.muni.cz.

Received 8 March 2021
Accepted 21 April 2021
Published 12 May 2021

Downloaded from http://msphere.asm.org/ on May 14, 2021 by guest

KEYWORDS bacteriophages, *Staphylococcus epidermidis*, antibiotic resistance, horizontal gene transfer, pathogenicity islands, transduction

Staphylococcus epidermidis is a common commensal inhabitant of the skin and mucosal surfaces in healthy humans and the best characterized coagulase-negative staphylococcal (CoNS) species (1). In recent years, *S. epidermidis* has gained a lot of attention due to its increasing incidence in nosocomial infections (2). In addition to human diseases, it has also been reported to be the bacterium most frequently isolated from bovine mastitis (3, 4). Resistance to all classes of antibiotics in *S. epidermidis* has been reported (5), which together with its ability to form a biofilm on indwelling medical devices (6, 7) calls for new drugs or alternative methods for treatment. *S. epidermidis* is a highly diverse species that, in addition to mutation, also evolves by recombination and readily acquires mobile genetic elements (8). Although *S. epidermidis* contains few virulence genes in its genome, it acts as a reservoir of antimicrobial resistance genes, including methicillin resistance genes, and is involved in intra- and interspecies horizontal gene transfer associated with the emergence and evolution of drug-resistant strains (5, 9). This is evidenced by the presence of mobile genomic element sequences, including genes associated with pathogenicity islands, which are shared by *S. epidermidis* and *Staphylococcus aureus* (10). In *S. epidermidis*, pathogenicity and resistance islands (SePI and SeRI, respectively) are mostly composite (11) or resemble *S. aureus* phage-inducible chromosomal islands (PICIs) in their simpler genomic architecture (12–14).

Most of the horizontal gene transfer events in staphylococci are associated with bacteriophages belonging to the family *Siphoviridae* and occur by transduction, which is well studied in *S. aureus* (15–21). These phages induce lysogenic conversion (22–24), mobilize *S. aureus* pathogenicity islands (SaPIs) (25–27), and are essential for plasmid transduction (28, 29) and the lateral transfer of chromosomal genes (30, 31), highlighting the importance of siphoviruses for their evolution, which resulted in the highly adaptable pathogenesis strategies of *S. aureus*. There is a lack of such studies on *S. epidermidis*. Most knowledge on *S. epidermidis* siphoviruses is based on their use for phage typing (32, 33), morphological observations (34), lysogeny (35), and comparative genomics studies (36–38).

This work aimed to investigate the role of *S. epidermidis* phages in the spread of antimicrobial resistance genes. We characterized several new transducing bacteriophages and their capacity to transfer mobile genetic elements. Combined with comparative genomic analyses, these data suggest that *S. epidermidis* phages have a substantial impact on the fitness of host strains and their evolution.

RESULTS

Characterization of *S. epidermidis* transducing phages. Phages 27, 48, 456, and 459 were previously used for *S. epidermidis* phage typing (39, 40) but were not genomically and morphologically characterized, and their role in horizontal gene transfer was not estimated. Here, we compared the above-mentioned phages along with a new phage, E72, which was selected from a set of phages spontaneously induced from 37 clinical *S. epidermidis* strains based on its optimal growth properties and high-titer production.

Transmission electron microscopy showed that all the phages belonged to the family *Siphoviridae* and had similar morphologies (Fig. 1A to E). The diameters of the phage capsids were 65, 61, 68, 70, and 65 (±3) nm in phages 27, 48, 456, 459, and E72, respectively. Their tail lengths were in the range of 145 to 165 nm, and baseplate diameters were in the range of 25 to 30 nm. An exception was the phage 459 baseplate, with a diameter of 37 nm and a different, fuzzier shape than the rest of the studied phages (Fig. 1B).

In phage 48 propagated on strain SE48, small-headed phage-like particles with a capsid diameter of 48 nm were observed (Fig. 1F). Liquid chromatography-tandem

Downloaded from http://msphere.asm.org/ on May 14, 2021 by guest

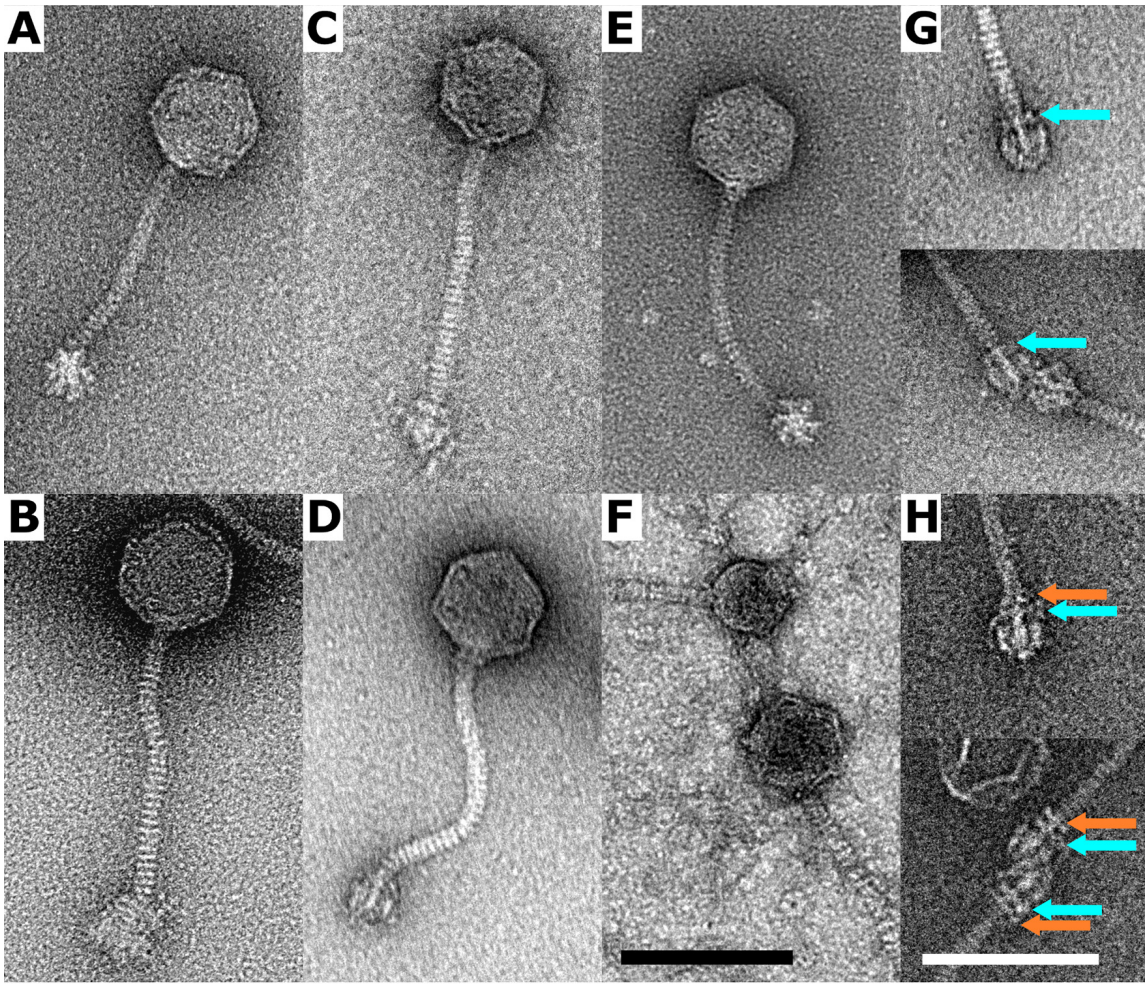

FIG 1 Transmission electron microscope images of negatively stained virions of *S. epidermidis* phietaviruses. (A) Phage 27; (B) phage 459; (C) phage 456; (D) phage E72; (E) phage 48; and (F) phage 48 and phage 48-derived particle with altered capsid architecture due to interaction with $SeCI_{SE48}$-encoded proteins. (G) Detail of the baseplate of phage E72. In a specific baseplate conformation, a ring of density is present at the end of the tail (cyan arrow). In total, 13 baseplates in this conformation were observed. (H) Detail of the baseplate of phage 456. An extra ring of density is located above the one present in phage E72 (orange arrow). In total, 15 baseplates in this conformation were observed. Bars, 100 nm; black for images A to F (all at the same scale) and white for images G and H.

mass spectrometry (LC-MS/MS) analysis of phage 48 virions identified 12 phage-encoded proteins (Table S1). In addition, a capsid morphogenesis protein encoded by the *cpm* gene (*gp14*; GenBank accession no. QRX38697) of the newly discovered chromosomal island of *S. epidermidis* strain SE48 was detected. This points to its effect on capsid remodeling associated with island mobilization, which was first observed and described in *S. epidermidis* here. The chromosomal island, designated $SeCI_{SE48}$, exhibited similarities in architecture and the integrase gene with *S. epidermidis* fusidic acid resistance islands (14) (Fig. 2).

The genomes of all the phages studied were assembled using short Illumina reads. They were arranged in functional modules, and their size was slightly above 40 kb (Fig. 3A). As no defined termini of genomic DNA were obvious from the Illumina read alignment, phages most likely use a headful packaging mechanism and have circularly permuted genomes with redundant ends (41). The analyzed *S. epidermidis* phages exhibited high average nucleotide identity (94 to 98%) to each other and 67 to 70% identity to *S. aureus* phietavirus 80α, suggesting that *Phietavirus* is a common phage genus in both staphylococcal species (Fig. 4). Comparison of the genomes of phages 27, 456, and 459 revealed high similarity in the virion structure module. Moreover,

Downloaded from http://msphere.asm.org/ on May 14, 2021 by guest

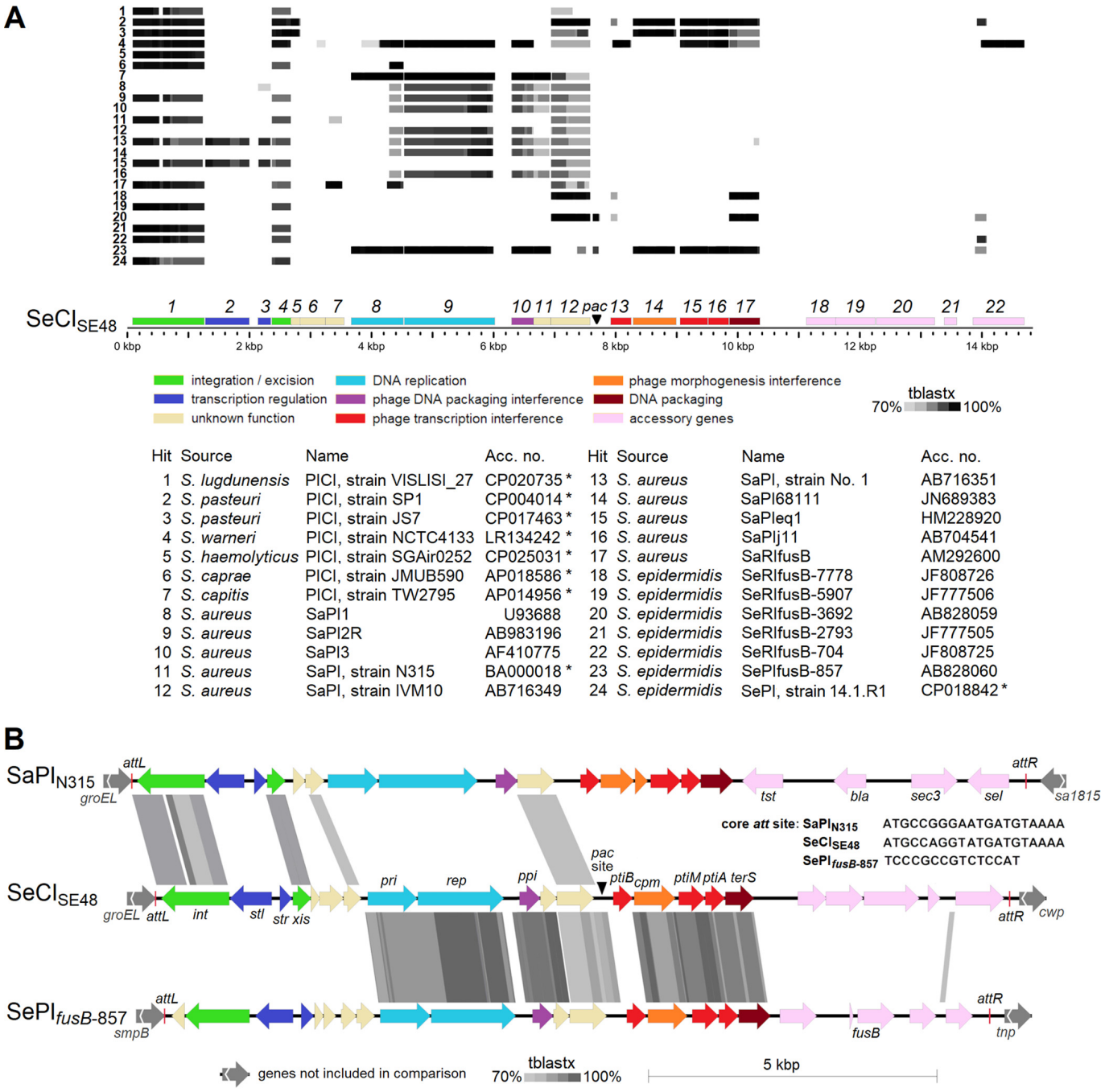

Hit	Source	Name	Acc. no.	Hit	Source	Name	Acc. no.
1	*S. lugdunensis*	PICI, strain VISLISI_27	CP020735 *	13	*S. aureus*	SaPI, strain No. 1	AB716351
2	*S. pasteuri*	PICI, strain SP1	CP004014 *	14	*S. aureus*	SaPI68111	JN689383
3	*S. pasteuri*	PICI, strain JS7	CP017463 *	15	*S. aureus*	SaPIeq1	HM228920
4	*S. warneri*	PICI, strain NCTC4133	LR134242 *	16	*S. aureus*	SaPIj11	AB704541
5	*S. haemolyticus*	PICI, strain SGAir0252	CP025031 *	17	*S. aureus*	SaRIfusB	AM292600
6	*S. caprae*	PICI, strain JMUB590	AP018586 *	18	*S. epidermidis*	SeRIfusB-7778	JF808726
7	*S. capitis*	PICI, strain TW2795	AP014956 *	19	*S. epidermidis*	SeRIfusB-5907	JF777506
8	*S. aureus*	SaPI1	U93688	20	*S. epidermidis*	SeRIfusB-3692	AB828059
9	*S. aureus*	SaPI2R	AB983196	21	*S. epidermidis*	SeRIfusB-2793	JF777505
10	*S. aureus*	SaPI3	AF410775	22	*S. epidermidis*	SeRIfusB-704	JF808725
11	*S. aureus*	SaPI, strain N315	BA000018 *	23	*S. epidermidis*	SePIfusB-857	AB828060
12	*S. aureus*	SaPI, strain IVM10	AB716349	24	*S. epidermidis*	SePI, strain 14.1.R1	CP018842 *

FIG 2 Comparison of phage-inducible chromosomal island SeCI$_{SE48}$ with selected chromosomal islands. (A) Islands identified in staphylococcal genomes available in GenBank. SeCI$_{SE48}$ genes are color coded according to their product function, and the corresponding gene product number is given above them. Chromosomal islands obtained from complete genomes of staphylococcal strains as 20-kb sequences starting with the integrase gene are indicated with asterisks. (B) Detailed comparison of SeCI$_{SE48}$ with SePI$_{fusB-857}$ and SaPI$_{N315}$. Genes are color coded according to their product function. Identity based on tblastx comparison is represented by shaded boxes with a cutoff of 70%.

phages 48 and 27 shared almost identical lysogeny and DNA metabolism modules, while the other modules differed (Fig. 3A; also, see Table S2 in the supplemental material).

When particular functional genome modules in their respective order were focused on, the following differences were observed. A comparison of the amino acid sequences of the terminase small subunit (TerS), which tends to be one of the least conserved phage proteins (42), divides known *S. epidermidis* phietaviruses into two subgroups, where phages 27, 48, and E72 represent one and phages 456 and 459 represent the

Downloaded from http://msphere.asm.org/ on May 14, 2021 by guest

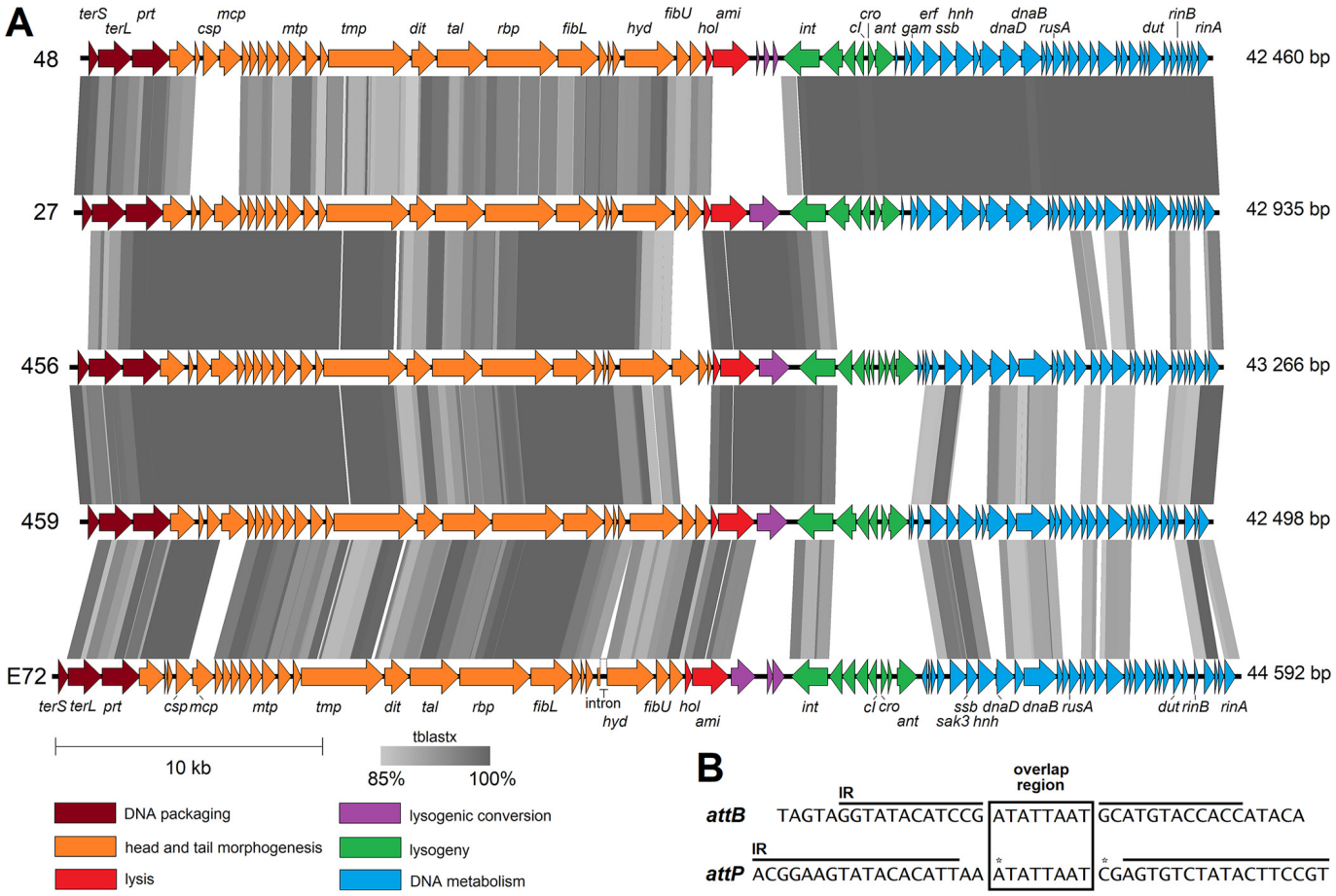

FIG 3 Whole-genome sequence-based comparison of *S. epidermidis* phages 48, 27, 456, 459, and E72. (A) Comparison of the phage genomes. Predicted genes are indicated with full arrows colored according to their modular affiliation. Shaded boxes show the amino acid sequence identity levels between genomes based on tblastx comparison. The genes encoding the following putative products are depicted: terminase small subunit (*terS*), terminase large subunit (*terL*), portal protein (*prt*), capsid scaffolding protein (*csp*), major capsid protein (*mcp*), major tail protein (*mtp*), tape measure protein (*tmp*), distal tail protein (*dit*), tail-associated lysin (*tal*), receptor-binding protein (*rbp*), lower tail fiber (*fibL*), cell wall hydrolase (*hyd*), upper tail fiber (*fibU*), holin (*hol*), amidase (*ami*), integrase (*int*), CI-like repressor (*cI*), Cro-like repressor (*cro*), antirepressor (*ant*), Gam-like nuclease inhibitor (*gam*), ERF-like single-strand annealing protein (*erf*), Sak3-like single-strand annealing protein (*sak3*), single-stranded DNA binding protein (*ssb*), HNHc nuclease (*hnh*), replication protein DnaD (*dnaD*), replicative helicase DnaB (*dnaB*), resolvase (*rusA*), dUTP diphosphatase (*dut*), transcription activator RinB (*rinB*), transcription regulator RinA (*rinA*). (B) Consensus sequences of *attB* sites of *S. epidermidis* strains and *attP* sites of *S. epidermidis* phietaviruses. The overlap region is indicated by the box. Imperfect inverted repeats are indicated with black lines above the sequences. The positions of the substitutions (G and A, respectively) in phage 48 are indicated with asterisks. The hybrid *attL* attachment site (TAGTAGGTATACATCCGATATTAATAGAGTGTCTATACTTCCGT) of strain SE48 lysogenized with phage 48, determined by PCR amplicon *mer-int* sequencing (Table 4), corresponds perfectly to the respective portions of *attB* of strain SE48 and *attP* of phage 48.

other (Fig. 5A). The genes encoding the capsid scaffolding protein (Csp) and the major capsid protein (Mcp) exhibited notable differences when phage 48 is compared with other phages analyzed in this study. Based on the Csp sequence analysis, all of the studied phages except phage 48 grouped into one cluster (Fig. 5B), while they formed two distinct clusters based on Mcp analysis (Fig. 5C). Phylogenetic trees based on alignments of TerS, Csp, and Mcp show reticulate relationships and mosaicism among phietaviruses and the relatedness of *S. epidermidis* phages to those of *S. aureus*, especially 71 and X2 (43) and ETA (44), while *S. aureus* phages NM4 (45) and 80α (46) are more distantly related (Fig. 5).

Baseplate structural components important for host recognition, i.e., receptor-binding proteins (RBP) encoded by the *rbp* gene of phages 459 and 27, are the same and almost identical to the RBP of phages E72 (99.4% identity) and 456 (99.3% identity). They exhibit 97.7% identity to the RBP of phage 48. Similarly, the lower tail fiber protein (FibL) is conserved, exhibiting ≥98% identity. The RBP of *S. aureus* phietavirus 80α (21) exhibits about 25% identity and 37% similarity to those of studied *S. epidermidis* phages, and FibL exhibits about 28% identity and 40% similarity. Another protein

Downloaded from http://msphere.asm.org/ on May 14, 2021 by guest

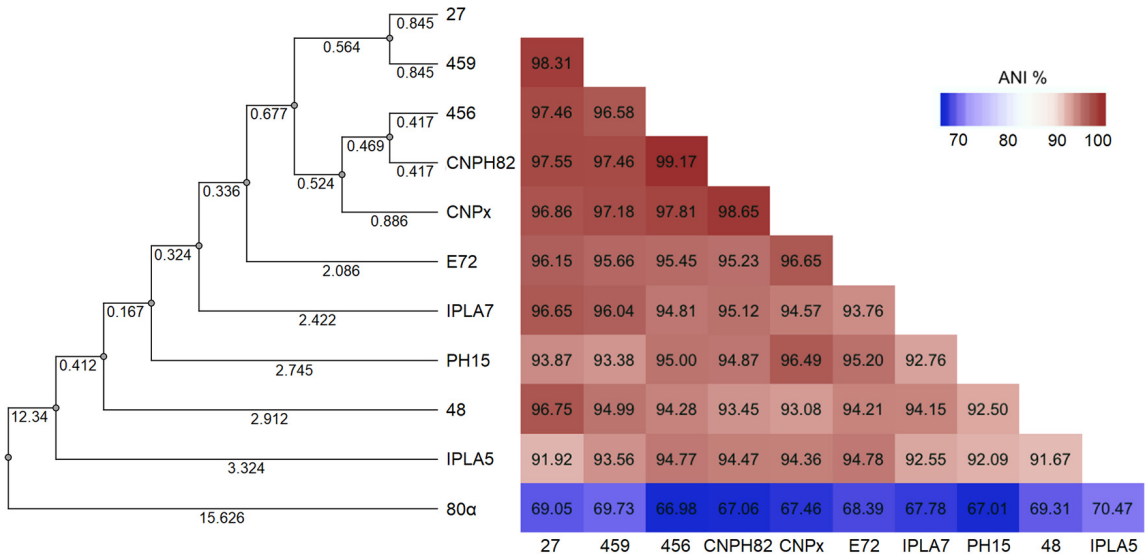

FIG 4 Dendrogram of interphage relatedness of *S. epidermidis* phietaviruses and *S. aureus* phietavirus 80α. The interphage relatedness was calculated with the OrthoANI algorithm, and clustered using unweighted pair group method using average linkages (UPGMA). The corresponding pairwise nucleotide identity heat map is shown, with percentage values.

associated with host range, the cell wall hydrolase (Hyd) encoded by the *hyd* gene, hypothesized to be associated with the baseplate (21), varies slightly across all *S. epidermidis* phages (Table S2). Besides this, a noncoding intron was predicted in the *hyd* gene of phage E72 (Fig. 3A). Genes for upper tail fiber (*fibU*) and a hypothetical protein following the *hyd* gene are replaced by three diverse genes in phage 456. This is manifested as an extra ring of density above the baseplate (Fig. 1G and H).

The lysis module comprising genes for holin (*hol*) and amidase (*ami*) in phage 48 differs significantly from the other *S. epidermidis* phages (Fig. 3A; Table S2). Its amidase gene has only about 50% identity to other *S. epidermidis* phages but exhibits 78% identity to *S. aureus* phage B236 (23).

In the *S. epidermidis* phages studied here, no known genes associated with lysogenic conversion were identified in the region following the lysis genes (Fig. 3A). Phages 27, 456, and 459 harbor the same putative endonuclease gene in this region. In E72, a gene encoding a different putative endonuclease (*gp30*) is located here and is followed by a gene encoding a hypothetical protein and a gene for a putative membrane-associated protein (*gp32*). In this region, the phage 48 genome contains three genes, which encode short hypothetical proteins (Table S2).

The *S. epidermidis* phages studied here have almost identical integrases of the serine-type family (Table S2). An integrase gene with 95% identity was found in a prophage sequence of *S. epidermidis* NCTC 13924 (GenBank accession no. NZ_LR134536). In the laboratory-lysogenized strains prepared in this study, the genomes of all the phages integrated into the same site in the gene encoding a FAD-dependent oxidoreductase (GenBank accession no. WP_080035152 in strain 1457), which in *S. aureus* was annotated as a probable pyridine nucleotide-disulfide oxidoreductase family protein, resulting in the split of this gene into two open reading frames (ORFs). The sequence ATATTAAT of the assumed overlap region, where the crossover between *attB* and *attP* occurs, is flanked by imperfect inverted repeats (Fig. 3B).

Phage growth characteristics. The host range determined on 35 *S. epidermidis* and two *S. aureus* strains (Table 1) and 35 field isolates of seven CoNS species showed that the phages studied here and the previously sequenced phage PH15 (36) were species specific for *S. epidermidis* alone. Most of the susceptible strains were isolated in the 1970s (39, 47), while recent *S. epidermidis* isolates were predominantly resistant (17, 48–52) (Table 1). The broadest host range on *S. epidermidis* strains ($n = 35$) was that of

Downloaded from http://msphere.asm.org/ on May 14, 2021 by guest

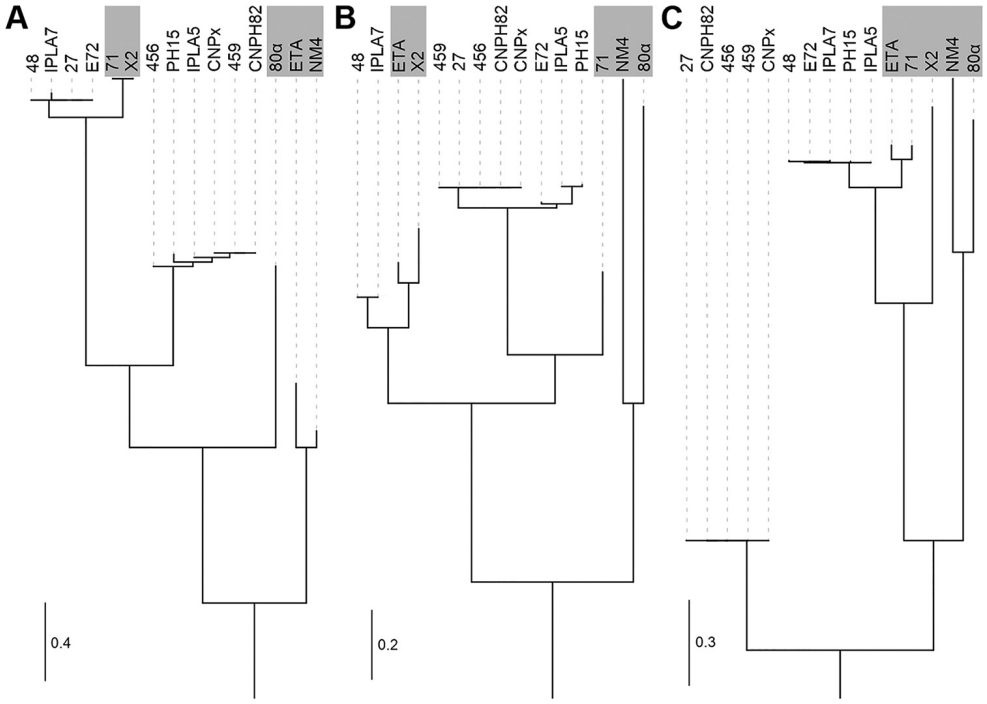

FIG 5 Phylogenetic trees based on multiple-sequence alignment of three phage proteins illustrating different phylogenetic clades within *S. aureus* and *S. epidermidis* phietaviruses and the modular character of their genomes. (A) Terminase small subunit (TerS); (B) capsid scaffolding protein (Csp); (C) major capsid protein (Mcp). *S. aureus* phages ETA, 71, X2, 80α, and NM4 are outlined with a gray background. The trees are the results of the maximum-likelihood-based inference of phylogenetic trees with Smart Model Selection.

phage E72 (34%), followed by 456 (31%) and 27 (26%), and the narrowest were the host ranges of phages 48 and 459 (both 17%). Phage susceptibility testing was conducted by the plate method; however, the ability of phages to effectively propagate on hosts may also depend on the type of culture, i.e., liquid or solid. Strain 1457 did not exhibit sensitivity to phages 27, 48, and 456 (Table 1), but when these phages were incubated with strain 1457 in liquid medium (meat-peptone broth [MPB] or tryptone soy broth [TSB]), they were able to propagate, which enabled their use in transduction experiments. No correlation was found between lytic ability and adsorption kinetics. After 15 min, a portion of the studied *S. epidermidis* phages remained unadsorbed for both phage-resistant and -susceptible strains.

Mobilization and transfer of a chromosomal island. While the sequencing data of phage 48 propagated on *S. epidermidis* strain SE48 were being analyzed, the sequence of a new chromosomal island $SeCI_{SE48}$ was identified. The distribution of its coverage by short Illumina sequencing reads showed that the island was packaged in the phage virions in linear form from the *pac* site by a headful mechanism. The *pac* site of $SeCI_{SE48}$ was predicted at the position between *gp12*, which encodes an unknown protein, and *ptiB*, which encodes a phage transcription inhibitor (Fig. 2B). Using the sequencing data of phage 48, the ratio of mean coverage of $SeCI_{SE48}$ and phage 48 DNA sequences was 1.5×10^{-2}, which indicates that $SeCI_{SE48}$ is packaged at high frequency. In the host chromosome, $SeCI_{SE48}$ is integrated into *att*B at the 3′ end of the *groEL* gene (Fig. 2B). As no antimicrobial resistance factors encoded by $SeCI_{SE48}$ were predicted, the transduction of this island by phage 48 into the recipient strain 1457 was performed without antibiotic selection (Table 2), and the transductants were selected by pulsed-field gel electrophoresis (PFGE) analysis (Fig. 6A). Strain 1457 does not contain any chromosomal island adjacent to the *groEL* gene. After the transfer to strain 1457, the $SeCI_{SE48}$ integrated at the 3′ end of *groEL* gene, which was not altered due to its integration, as the last 18 bp of the gene overlap the $SeCI_{SE48}$ *att* site. PICIs

Downloaded from http://msphere.asm.org/ on May 14, 2021 by guest

TABLE 1 Host range of *S. epidermidis* phages 27, 48, 456, 459, and E72 characterized in this study and phage PH15 described previously

Bacterial strain[a]	Reference or source[b]	Lysis results for phage[c]:					
		PH15	27	48	456	459	E72
S. epidermidis SE15	39	C, C, C	C, C, C	S, C, C	C, C, C	−, −, −	S, C, C
S. epidermidis SE27	39	C, C, C	C, C, C	S, C, C	S, C, C	−, −, −	C, C, C
S. epidermidis A6C	39	C, C, C	C, C, C	S, C, C	C, C, C	−, P, S	C, C, C
S. epidermidis A9C	39	C, C, C	C, C, C	S, C, C	S, C, C	P, S, C	C, C, C
S. epidermidis SE37	39	−, −, −	−, −, −	−, −, −	−, −, −	−, −, −	−, −, −
S. epidermidis SE155	39	−, −, −	−, −, −	−, −, −	−, −, −	−, −, −	−, −, −
S. epidermidis SE48	47	−, −, −	P, P, S	C, C, C	−, −, −	−, −, −	−, −, L
S. epidermidis SE456	47	−, −, −	−, −, −	−, −, −	C, C, C	−, −, −	P, P, S
S. epidermidis SE459	47	P, P, S	P, S, C	P, S, C	P, S, C	S, C, C	P, S, C
S. epidermidis SE471	47	−, −, −	−, −, −	−, −, −	C, C, C	−, −, −	C, C, C
S. epidermidis 1457	49	−, −, −	−, −, −	−, −, −	−, −, −	P, S, C	S, C, C
S. epidermidis 1457 ($SeCI_{SE48}$)	This work	−, −, −	−, −, −	−, −, −	−, −, −	−, −, −	−, −, −
S. epidermidis RP62A	50	−, −, −	−, −, −	−, −, −	−, −, −	−, −, −	−, −, −
S. epidermidis O−47	52	−, −, −	−, −, −	−, −, −	−, −, −	−, −, −	−, −, −
S. epidermidis Tü 3298	48	−, −, −	−, L, L	−, −, −	−, −, −	−, −, −	−, −, L
S. epidermidis CCM 50	CCM	−, −, −	P, S, C	−, −, −	P, S, C	−, −, P	−, −, −
S. epidermidis CCM 4187	CCM	−, −, −	P, P, S	−, −, −	P, P, S	−, −, −	−, −, L
S. epidermidis CCM 2343	CCM	−, −, −	P, S, C	−, −, −	P, P, S	−, P, P	−, −, −
S. epidermidis CCM 4418	CCM	−, −, −	−, −, −	−, −, −	C, C, C	−, −, −	−, L, L
S. epidermidis CCM 7844	CCM	−, −, −	−, −, −	−, −, −	−, −, −	−, −, −	−, S, C
S. epidermidis CCM 7221	CCM	−, −, −	−, −, −	−, −, −	−, −, −	−, −, −	−, −, −
S. epidermidis CCM 2124	CCM	−, −, L	−, −, L	−, −, −	−, −, −	−, −, −	−, −, P
S. epidermidis CCM 4505	CCM	−, −, −	−, −, −	−, −, −	−, −, −	−, −, −	−, P, S
S. epidermidis 4	UPOL	−, −, −	−, −, L	−, −, −	−, −, −	−, −, −	S, C, C
S. epidermidis 2	UPOL	−, −, −		−, −, −	−, −, −	−, −, −	−, −, L
S. epidermidis 18	UPOL	−, −, −	−, −, L	−, −, −	−, −, −	−, −, −	−, −, L
S. epidermidis 58	UPOL	−, −, −	−, −, −	−, −, −	−, −, −	−, −, −	−, −, −
S. epidermidis 221−1	UPOL	−, −, −	−, −, L	−, −, −	−, −, −	−, L, L	L, L, L
S. epidermidis 257−2	UPOL	−, −, −	−, −, −	−, −, −	−, −, −	−, −, −	−, −, L
S. epidermidis 341−5	UPOL	−, −, −	−, −, −	−, −, −	−, −, −	−, −, −	−, −, −
S. epidermidis 348−6	UPOL	−, −, −	−, −, −	−, −, −	−, −, −	−, −, −	−, −, −
S. epidermidis 352−7	UPOL	−, −, −	−, −, −	−, −, −	−, −, −	−, −, −	−, −, −
S. epidermidis 354−8	UPOL	−, −, −	−, −, −	−, −, −	−, −, −	−, −, −	−, −, −
S. epidermidis 357−9	UPOL	−, −, −	−, −, −	−, −, −	−, −, −	−, −, −	−, −, L
S. epidermidis 465−4	UPOL	−, −, −	−, −, −	−, −, −	−, −, −	−, −, −	−, −, L
S. aureus RN4220	51	−, −, −	−, −, −	−, −, −	−, −, −	−, −, −	−, −, −
S. aureus 8325−4	17	−, −, −	−, −, −	−, −, −	−, −, −	−, −, −	−, −, −

[a]"SE" in a strain name indicates a propagating strain for phages.

[b]CCM, Czech Collection of Microorganisms, Masaryk University (Brno, Czech Republic); UPOL, Department of Microbiology, Faculty of Medicine and Dentistry, Palacky University (Olomouc, (Czech Republic) (methicillin-resistant *S. epidermidis* human clinical isolates).

[c]The result of each of the three replicates is given. C, confluent lysis; S, lysis; P, individual plaques; L, lysis from without (early bacterial lysis induced by high-multiplicity virion adsorption without phage propagation or abortive infection, manifested by a turbid zone); −, no lysis. For the C, S, P pattern, the formation of single plaques at higher phage dilution was confirmed for all sensitive strains.

with the same type of integrase and excisionase are localized downstream of the *groEL* gene in several staphylococcal species, including *S. aureus*, *Staphylococcus lugdunensis*, *Staphylococcus pasteuri*, *Staphylococcus warneri*, and *Staphylococcus haemolyticus* (Fig. 2A). Of the chromosomal islands described above, $SeCI_{SE48}$ exhibited the highest similarity with $SePI_{fusB\text{-}857}$, which encodes fusidic acid resistance (12), and a different integrase (Fig. 2B).

The burst size of phage 48 on the transductant strain 1457($SeCI_{SE48}$) was significantly decreased (4.3-fold) compared to that on wild-type strain 1457. $SeCI_{SE48}$ integration also led to a loss of sensitivity of strain 1457($SeCI_{SE48}$) to phages 459 and E72 (Table 1).

Plasmid transductions. All bacterial sequences were obtained using a hybrid assembly of Illumina reads and long Oxford Nanopore reads. All the propagating strains differing in their sequence types (STs) used here carry one or more plasmids, some of which determine antibiotic resistance (Table 3). Phages 27, 48, and 459 transferred naturally occurring plasmids (Table 2; Fig. 6B). Then, a chloramphenicol resistance-

Downloaded from http://msphere.asm.org/ on May 14, 2021 by guest

TABLE 2 Transductions of *S. epidermidis* mobile genetic elements

	Mobile genetic element			Transduction system			
Donor	Name	Size (bp)	Resistance gene(s)	Recipient	Phage	Selection antibiotic	Frequency
SE27	pSE27_S	4,397	*aad(6)*	SE459	27	Streptomycin	NA[a]
SE27	pSE27_T	4,439	*tetK*	1457	48	Tetracycline	5.0×10^{-4}
SE48	$SeCl_{SE48}$	14,835		1457	48		NA[b]
SE459	pSE459_T	18,761	*tetK*	1457	459	Tetracycline	1.6×10^{-7}
1457 (pBTn)	pBTn	11,256	*bla, erm, cat*	A6C	48	Chloramphenicol	5.4×10^{-5}
					456	Chloramphenicol	3.7×10^{-5}
					459	Chloramphenicol	6.9×10^{-5}
					E72	Chloramphenicol	6.1×10^{-5}
1457 (pBTn)	pBTn	11,256	*bla, erm, cat*	1457	48	Chloramphenicol	6.1×10^{-6}
					456	Chloramphenicol	3.9×10^{-7}
					459	Chloramphenicol	2.0×10^{-7}
					E72	Chloramphenicol	9.3×10^{-7}

[a]NA, not applicable due to emergence of spontaneous streptomycin-resistant mutants.
[b]NA, not applicable due to no antibiotic selection.

encoding plasmid, pBTn (53), electroporated into *S. epidermidis* strain 1457 was transferred by all the phages except phage 27 into *S. epidermidis* strains 1457 and A6C (Table 2; Fig. 6B). The transduction efficiency differed according to the phage and recipient strain used (Table 2). Interspecies plasmid transfer from strains SE27, SE48, SE456, and SE459 by phages able to propagate on them (listed in Table 1) into other staphylococcal species, including three strains of *Staphylococcus sciuri*, two strains of *Staphylococcus chromogenes*, two strains of *Staphylococcus xylosus*, one strain each of *Staphylococcus petrasii* and *Staphylococcus simulans*, and seven *S. aureus* strains, was not successful (data not shown).

Application of transducing phages for genetic studies. Our results showed that the transfer of pBTn via electroporation to the 37 clinical *S. epidermidis* strains from University Hospital Tübingen tested here failed in 26 cases (70.3%) (Table S3). Therefore, effectively transducing *S. epidermidis* phages could be considered another laboratory tool for the genetic manipulation of *S. epidermidis*. Phage E72 exhibited high transducing efficiency (up to 10^{-4}) by transferring pBTn from strain 1457 (pBTn) to 21 of 37 (56.8%) *S. epidermidis* strains, including 10 of 19 (52.6%) strains that could not receive pBTn using electroporation or transduction by phage 187 (18) (Table S3). Moreover, we observed that phage E72 could be propagated to a high titer of $\sim 10^{11}$ PFU/ml, which is an advantage for successful genetic manipulation using transduction (54).

DISCUSSION

A detailed genomic and phenotypic analysis of five *S. epidermidis* phietaviruses allowed us to assess their transduction potential and putative impact on the evolution of *S. epidermidis*. Published phietavirus genomes are exclusive to *S. aureus* and *S. epidermidis* phages (searched using NCBI Virus). Before this study, phietaviruses amounted to nine of the 13 *S. epidermidis* siphoviral genomes available in NCBI Virus, which together with the phages described here makes this genus an abundant group of temperate phages in *S. epidermidis*.

Our results confirmed that generalized transduction in *S. epidermidis* is mediated by temperate phages using the headful mechanism for DNA packaging (55). Genomes of the studied phages had no obvious *pac* site, thus resembling *S. aureus* phage 11 (56). During the packaging initiation, the DNA is probably cut not at a precise location but at scattered locations within a large region of up to several kilobases (57). This relaxed specificity enables the packaging of heterogeneous DNA with pseudo-*pac* sites into the virion capsids. Differences in pseudo-*pac* site homology may therefore lead to an altered frequency of transduction. A phage-encoded small terminase subunit (TerS) is essential for phage genome and plasmid packaging into the capsid, but it is not required for the packaging of phage-inducible islands that encode distinct TerS

Downloaded from http://msphere.asm.org/ on May 14, 2021 by guest

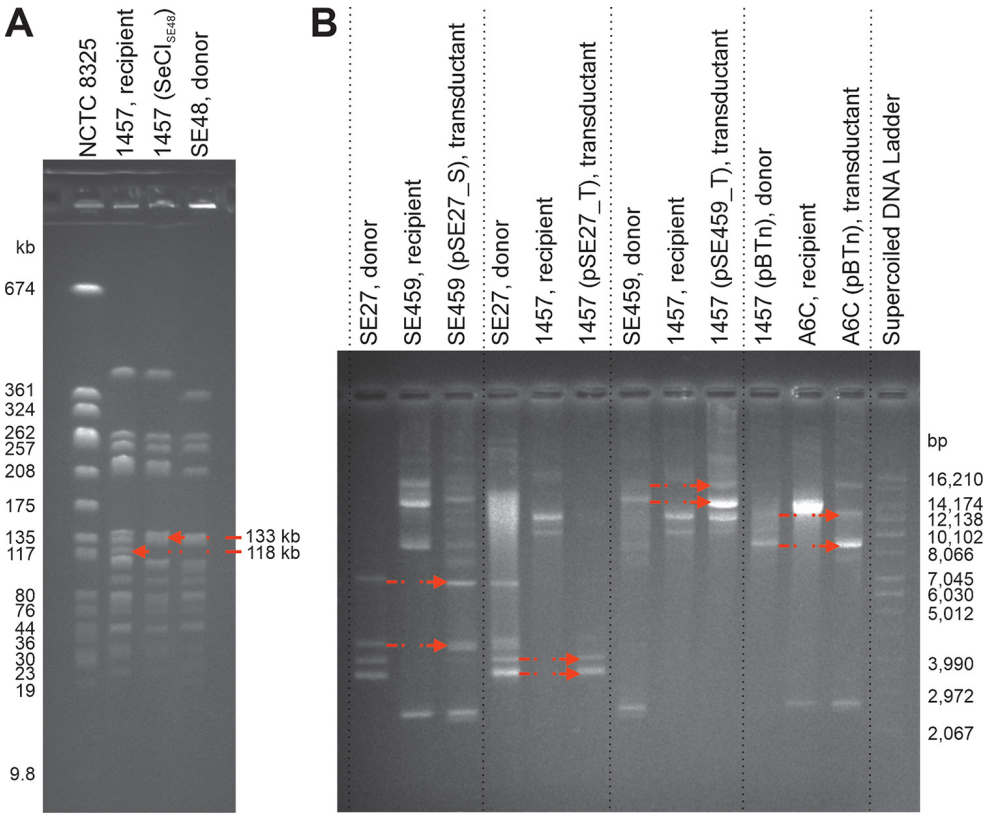

FIG 6 Analysis of transduced mobile elements by agarose gel electrophoresis. (A) PFGE separation of SmaI macrorestriction fragments of genomic DNA of recipient *S. epidermidis* strain 1457 before and after the insertion of SeCI$_{SE48}$, which was transduced by phage 48 from donor *S. epidermidis* strain SE48. The red arrows show a 118-kb fragment of the recipient and the corresponding fragment in the transductant enlarged to 133 kb due to SeCI$_{SE48}$ integration. *S. aureus* strain NCTC 8325 was used as a marker. (B) Plasmid profile of the *S. epidermidis* donor, recipient, and transductant strains in the transductions of plasmids pSE27_S, pSE27_T, pSE459_T, and pBTn, respectively. Detailed information is given in Table 2. The transferred plasmids in their supercoiled and relaxed forms are indicated with arrows.

recognizing their own specific *pac* site (58). We hypothesize that the high efficiency of plasmid transduction by phages 27, 48, and E72 is determined by the same TerS type that is distinct from the other studied phages.

The phage susceptibility of the tested bacterial strains does not always correlate with the adsorption rate of the phage. Therefore, it may depend on many postadsorption factors, as was recently reviewed for *S. aureus* (59). For generalized transduction, the permissivity of a recipient strain to productive phage infection is not required for receiving foreign DNA; however, cell wall penetration is a necessary prerequisite (29). Differences in baseplate structural proteins may relate to the different ability to infect the host (60). Phage 456 differed from other *S. epidermidis* phages except for phage CNPx (61) in several baseplate component-encoding genes, including *fibU* for upper tail fiber protein, which is not essential for either infectivity or assembly of the baseplate in phage 80α (21). We assume it may play a supporting role in host recognition. Phages 456 and E72, which have similar RBP, exhibited the broadest but not identical host ranges. In addition, phage E72 was able to lyse some of the strains resistant to all other tested phages. This could be connected with a small transmembrane domain protein, encoded by *gp24* localized in the tail structure region, which could play a role in the host cell envelope penetration via holin regulation.

Horizontal gene transfer in *S. aureus* is common within clonal lineages, while transfer between them is rare due to specific defense mechanisms, such as restriction-modification systems (62). However, we were able to show that phages 27 and 48 transferred plasmids from *S. epidermidis* CC5 to CC14. Based on our previous findings on

Downloaded from http://msphere.asm.org/ on May 14, 2021 by guest

TABLE 3 Basic genomic properties of *S. epidermidis* propagation strains and their plasmids

Strain	MLST (CC)[a]	Plasmid name	GenBank accession no.	Size (bp)	AR gene(s)[b]	Most similar GenBank entry(ies) (organism), % identity[c]
SE27	ST190 (CC5)	pSE27_T	MW364977	4,439	*tetK*	CP033733 (*S. hominis*), 100; CP038249 (*S. warneri*), 100; GQ900445 (*S. aureus*), 99; AE015930 (*S. epidermidis*), 99
		pSE27_S	MW364976	4,397	*aad(6)*	MH090916 (*S. epidermidis*), 100; CP014406 (*S. aureus*), 100; AP009489 (*Micrococcus caseolyticus*), 100
SE48	ST215[d] (CC14)	pSE48_1	NZ_CP066304	8,255	*fmhA*, *abc*	Novel
		pSE48_2	NZ_CP066305	1,289	*ant(4)*	GQ900442 (*S. aureus*), 99
SE456	ST73 (CC73)	pSE456_1	MW364978	43,075	*abc*	Novel
		pSE456_2	MW364979	13,277	*abc*	Novel
		pSE456_3	MW364980	8,330	*abc*	Novel
		pSE456_4	MW364981	2,348		CP047868 (*S. aureus*), 100
SE459	ST14 (CC14)	pSE459_1	MW364982	20,983		Novel
		pSE459_T	MW364985	18,761	*tetK*, *abc*	Novel
		pSE459_2	MW364983	11,465		Novel
		pSE459_3	MW364984	2,789		Novel
1457	ST86 (CC14)	p1457	NZ_CP020462	15,142		NA

[a]MLST, multilocus sequence type.
[b]Known or putative antibiotic resistance gene. AR, antibiotic resistance. *tetK*, gene encoding tetracycline efflux MFS transporter; *aad(6)*, gene encoding streptomycin aminoglycoside 6-adenyltransferase; *fmhA*, gene encoding aminoacyltransferase possibly involved in methicillin and lysostaphin resistance; *ant(4)*, gene encoding aminoglycoside nucleotidyltransferase; *abc*, gene encoding ABC transporter (may be involved in drug resistance; multiple *abc* genes are present in appropriate plasmids).
[c]If more than one bacterial species is present, one plasmid is given for each of them; plasmids with overall nucleotide sequence identity less than 75% are noted as novel. NA, not performed.
[d]Nearest ST; no match with the *arcC* gene was found.

transduction to *S. aureus* strains insensitive to the lytic action of a transducing phage (29), we analyzed interspecies transfer; however, we found no evidence for such an ability of any of the phages. Nevertheless, the plasmids that were transferred between *S. epidermidis* clonal complexes show high overall identity to plasmids of *Staphylococcus hominis*, *S. warneri*, *S. aureus* and *Macrococcus caseolyticus* (Table 3). Only a few previous studies demonstrated plasmid transfer between different staphylococcal species using electroporation (63) or by transduction (64).

To compare the transduction ability of the tested phages, the transfer frequency of the 11.2-kb chloramphenicol resistance plasmid pBTn was assessed. The transduction rates of the tested phages differed on strain 1457 but not on strain A6C, where all the transducing phages transferred pBTn with a higher rate. Only phage 27 was incapable of transduction into strains 1457 and A6C, which may be connected with host surface structures, as was demonstrated in streptococci (65). In naturally occurring plasmids, more efficient transduction of smaller ones was observed, as was described before (66).

The transfer of PICIs has already been well described for *S. aureus* (SaPIs), but this study provides the first evidence of such a transfer in *S. epidermidis*. Recently, PICIs have also been predicted in genomes of other Gram-positive cocci (67). They are only distantly related to each other and to *S. aureus* SaPIs, but they share a genome organization and content. Therefore, they represent convergent evolution that suggests their high selective value. In the previously described staphylococcal PICIs, the accessory genes encode toxins and/or antibiotic resistance determinants (12, 13, 68), but $SeCI_{SE48}$ harbors genes for putative membrane proteins. $SeCI_{SE48}$ is integrated at the 3′ end of the host *groEL* gene, similar to *S. aureus* and *S. epidermidis* PICIs with the same type of integrase (12–14).

The role of the PICI-encoded proteins PtiA, PtiM, and PtiB in the inhibition of phage late transcription through the interaction with phage transcriptional regulator RinA was demonstrated previously (69). The same mechanism was possibly responsible for the decreased phage susceptibility in strain 1457 after $SeCI_{SE48}$ was integrated into its chromosome. An alteration of the phage life cycle by PICI, leading to the formation of small-headed virions that are unable to carry the entire phage genome, was described (25). In staphylococcal phage 80α, the capsid size change is caused by SaPI1 proteins redirecting the phage capsid architecture from T=7 to T=3 (70). The observed

Downloaded from http://msphere.asm.org/ on May 14, 2021 by guest

formation of small-headed virions in phage 48 suggests a similar architecture shift in *S. epidermidis*. The primary sequence and predicted secondary structure of the $SeCI_{SE48}$-encoded protein, involved in the capsid assembly of small-headed virions, differs from those in SaPI1 (70). This suggests that $SeCI_{SE48}$ uses a different mechanism of phage capsid resizing.

The homologues of phage 80α-encoded PICI derepressors, such as dUTPase, Sri, and ORF15, are encoded by genes in the DNA metabolism module and play an essential role in chromosomal island mobilization (27, 71). In *S. epidermidis* phages 27 and 48, homologues of these PICI mobilization determinants are identical (Fig. 3), but these phages differ significantly in their capsid proteins. While the minor capsid protein has been shown to not affect plasmid or PICI transduction (72), the role of other capsid proteins has been only partially described (70). In phage 48, the capsid scaffolding protein was distinct from all the tested phages. High-frequency transducing phages 48 and E72 encode almost identical major capsid proteins that are very different from all other phages. Thus, the capsid proteins seem to play an important role not only in the mobilization of islands but also in the transfer of plasmids, where the successful transduction is dependent on a complex of genetic determinants of both the mobile element and the phage.

The transfer of plasmids to bacterial cells is an important technique used in research in *S. epidermidis*. However, far fewer clinical *S. epidermidis* than *S. aureus* isolates can be transformed by electroporation, and the efficiency is orders of magnitude lower, despite attempts at optimization (73, 74). While there are many studies of phage-mediated plasmid transduction in *S. aureus*, there is a lack of similar studies in *S. epidermidis*. Recently, Winstel et al. (18) established a plasmid transfer method using phage 187, which is capable of efficient transduction to CoNS strains and specific *S. aureus* strains with CoNS-type wall teichoic acid. The phages used in our study also exhibited a high efficiency of plasmid transduction in strains where phage 187 failed (Table S3). They even transferred relatively large plasmids that generally cannot be easily transferred via electroporation or by phage 187. Therefore, the phages described in this study, especially E72 and 48, could be considered suitable laboratory tools for the transduction of plasmids and chromosomal islands to *S. epidermidis* strains, which could promote future CoNS research.

MATERIALS AND METHODS

Phages and bacterial strains. Bacteriophages PH15 and 27 (39), phages 48, 456, and 459 (40, 47), and their propagating *S. epidermidis* strains SE15, SE27, SE48, SE456, and SE459 were obtained from V. Hájek (Palacký University, Olomouc, Czech Republic). Thirty-seven clinical *S. epidermidis* isolates were obtained from the Medical Microbiology department of the University of Tübingen (Table S3). Phage E72 was induced from *S. epidermidis* strain E72, a clinical isolate from infected teeth of a patient in University Hospital Tübingen, and propagated on *S. epidermidis* strain 1457 (49). *S. aureus* phages 11 and 80α (75) were used in the adsorption assay. Phage 187 (18) was used for the comparison of pBTn transduction efficiency with phage E72.

For the determination of growth properties of tested phages, a collection of *S. epidermidis* strains was used (Table 1). *S. aureus* strains 8325-4 (17) and RN4220 (51) and 35 field isolates of 7 CoNS, including *S. chromogenes*, *S. hominis*, *S. haemolyticus*, *S. petrasii*, *S. sciuri*, *S. simulans* and *S. xylosus*, were used in adsorption and/or host range assays. In addition to natural plasmids, the transposon plasmid pBTn, encoding chloramphenicol resistance (53), was used in a phage transduction assay. All the assays with pBTn were performed at 30°C to avoid loss of the plasmid. The pBTn was transferred to strain 1457 via electroporation, and this strain then served as the donor.

Growth medium and phage propagation. *S. epidermidis* phages were propagated on their propagation strains at 37°C on 1.5% meat peptone agar (MPA), prepared from 13 g nutrient broth CM0001 (Oxoid), 3 g yeast extract LP0021 (Oxoid), 5 g peptone LP0037 (Oxoid), 15 g agar LP0013 (Oxoid), and distilled water to a final volume of 1 liter (pH 7.4), overlaid with a top soft layer of MPA (0.7% agar) containing 2 mM $CaCl_2$. The lysates were centrifuged at 5,000 $\times$ *g* for 15 min and filtered using a polyethersulfone membrane filter with a pore size of 0.45 μm (TPP, Switzerland).

Morphological and proteomic characterization. For electron microscopy, particles of phages E72, 27, 456, and 459 were purified in a CsCl density gradient (16). The transducing lysate of phage 48 was purified by fast protein liquid chromatography (FPLC) and ultrafiltration as described previously (76) with minor modifications. For the FPLC purification, a CIMmultus QA 8-ml monolithic column (Bia Separations, Slovenia) and NGC chromatography system (Bio-Rad, USA) were used. Phage lysate was mixed with 40 mM Tris buffer (pH 7.5) in a 1:1 ratio at a final NaCl concentration of 0.35 M. For

Downloaded from http://msphere.asm.org/ on May 14, 2021 by guest

ultrafiltration, Pellicon XL50 cassettes with a Biomax 300-kDa membrane (Millipore, USA) were used. Retentate and fractions containing phages were desalted and concentrated using Amicon Ultra 0.5-ml centrifugal filters (Millipore, USA) with a 100-kDa cutoff. Phages were diluted to an A_{280} of 0.5 to 1.0, and negatively stained samples were prepared by applying 4 μl of the diluted sample onto copper grids coated with a 12-nm carbon layer, stained with 2% uranyl acetate. Samples were observed using a Tecnai F20 electron microscope (Thermo Fisher Scientific, USA) operated at 200 kV with ×50,000 magnification.

Structural proteins of phage 48 and phage 48-derived small-headed particles purified in a CsCl gradient were determined by LC-MS/MS analysis performed using the Ultimate 3000 RSLCnano system (Thermo Fisher Scientific, USA) connected to an Impact II Qq time-of-flight mass spectrometer (Bruker, Bremen, Germany) as described previously (64). An in-house database of proteins encoded by strain SE48 and phage 48 was used for the final search. Only proteins that were identified based on at least two peptides were reported. Detected bacterial metabolic proteins were filtered out from the final report.

Horizontal gene transfer experiments. For transduction experiments, high-titer phage lysates were prepared in meat-peptone broth (MPB) prepared from 13 g of nutrient broth (Oxoid), 3 g yeast extract (Oxoid), 5 g peptone (Oxoid), and distilled water to a final volume of 1 l (pH 7.4). Alternatively, tryptone soy broth (TSB) (CM0129; Oxoid) was used. Transduction experiments were carried out as described previously (29). Transductants were selected on tryptone soy agar (TSA; CM0131; Oxoid) plates supplemented with sodium citrate (20 mM) and streptomycin (20 mg/liter), tetracycline (5 mg/liter), ampicillin (100 mg/liter), or chloramphenicol (10 mg/liter). The transduction of $SeCI_{SE48}$ was performed without antibiotic selection. Plates were incubated at 37°C (30°C for strains with the plasmid pBTn) for 48 to 72 h. The transductants were verified by colony PCR assays using OneTaq Quick-Load 2× master mix with standard buffer (New England Biolabs, Ipswich, MA, USA) and a 200 nM concentration of each primer (Table 4) (77, 78). The reaction conditions were as follows: 94°C for 30s, followed by 30 cycles of denaturation at 94°C for 40 s, annealing at 53°C for 30 s, and extension at 68°C for 60 s per kb.

Plasmid DNA was isolated from the transductants with a NucleoSpin plasmid kit (Macherey-Nagel, Düren, Germany) according to the manufacturer's protocol using prolonged lysis with lysostaphin as described before (78). Plasmid DNA was analyzed by agarose gel electrophoresis in 1.2% agarose gel (Serva) in 1× Tris-acetate-EDTA (TAE) buffer. SmaI (New England BioLabs, Ipswich, MA, USA) macrorestriction analysis by pulsed-field gel electrophoresis (PFGE) was performed using a CHEF Mapper XA system (Bio-Rad) to confirm the transfer and integration of $SeCI_{SE48}$.

Electroporation. Electroporation was conducted according to the transformation method for *S. epidermidis* described by Monk et al. (79). Briefly, overnight *S. epidermidis* cultures with an optical density at 600 nm (OD_{600}) of 0.5 were chilled on ice, washed in 10% glycerol, and 50 μl was aliquoted to each tube. Before electroporation, competent cells were resuspended in 50 μl of 10% glycerol and 500 mM sucrose. A volume of 5 μl plasmid pBTn DNA (500 ng/μl) was added to the bacterial cells, transferred to a 1-mm electroporation cuvette (Bio-Rad), and then pulsed at 21 kV/cm, 100 Ω, and 25 μF. TSB supplemented with 500 mM sucrose was added to the electroporated bacteria, incubated at 30°C for 1 h before plating on TSA plates with chloramphenicol (10 mg/liter), and incubated at 30°C for 48 h.

Lysogenization. *S. epidermidis* strains SE27, SE48, SE456, SE459, and 1457 were lysogenized with phages 27, 48, 456, 459, and E72, respectively, as described previously (23). Integration sites were identified by PCR (Table 4) and the obtained amplicons were sequenced by Eurofins Genomics (Germany) using the same primers as in the PCR assay.

Determination of host range, phage adsorption, and one-step growth curve. Phage lysates were spotted onto the examined strains at 10×, 100×, and 1,000× routine test dilutions (RTD) (80). Productive phage infection was confirmed by the formation of single plaques. Adsorption curves of the phages were determined as described previously (81) using an input ratio (IR) of 10. The burst size of phage 48 on bacterial strains 1457 and 1457($SeCI_{SE48}$) was determined from the one-step growth curve as described previously (82) with minor modifications. Briefly, overnight bacterial culture was cultivated to an OD_{600} of 0.5 (10^8 CFU/ml). Bacterial cultures were synchronized at 10°C for 30 min. The phage lysate was mixed with the bacterial culture at an IR of 0.01, and the mixture was incubated at 37°C. The titer of free phage particles was determined after 0 to 90 min at 5-min intervals.

Statistical analysis. Plasmid transduction efficiency and phage 48 burst size comparisons were evaluated by statistical analysis using the *t* test. A *P* value of 0.05 was used as the threshold for statistical significance.

Genome analysis. For whole-genome sequencing on the Illumina platform, the phage DNA was isolated using a phenol-chloroform method (83), and bacterial DNA was isolated from cultures cultivated in MPB using a High Pure PCR template preparation kit (Roche Diagnostics, Mannheim, Germany) according to the manufacturer's instructions with the modification of adding lysostaphin (40 μg/ml, Sigma-Aldrich) for cell lysis. The 500-bp sequencing library was prepared with a NEBNext Ultra II DNA library prep kit for Illumina (New England BioLabs). The samples were sequenced using a MID output cartridge in a 150-bp paired-end mode on an Illumina NextSeq sequencing platform (Illumina, San Diego, CA, USA). The quality of sequencing reads was analyzed with FastQC v0.11.8 (84). Bases of lower quality and adapters were trimmed using the sliding window model in Trimmomatic Galaxy v0.36.5 (85).

For sequencing on an Oxford Nanopore platform, the bacterial DNA was isolated using the following steps. First, 10 ml of stationary overnight bacterial culture cultivated in TSB at 37°C was centrifuged at 3,000 × *g* and 10°C for 10 min, washed with 5 ml of wash solution (10 mM Tris-HCl, 10 mM EDTA, 10 mM EGTA, 1 M NaCl [pH 7.5]), and resuspended in Tris-EDTA (TE) buffer with lysostaphin (50 μg/ml), achromopeptidase (1,000 U/ml; Sigma-Aldrich), mutanolysin (40 U/ml; Sigma-Aldrich), and RNase A (200 μg/ml; New

Downloaded from http://msphere.asm.org/ on May 14, 2021 by guest

TABLE 4 PCR assays for verification of plasmid and $SeCI_{SE48}$ transductions, $SeCI_{SE48}$ packaging by *S. epidermidis* phage 48, and identification of prophage integration sites

Construct(s) detected	Target gene(s)	Source sequence	Forward primer	Reverse primer	Product length (bp)	Reference
Tetracycline resistance gene	*tetK*	pSE27_T	TCGATAGGAACAGCAGTA	CAGCAGATCCTACTCCTT	169	77
Chloramphenicol resistance gene	*cat*	pBTn	GCGACGGAGAGTTAGGTT	GCCTATCTGACAATTCCTGA	413	78
Streptomycin resistance gene	*aad(6)*	pSE27_S	ACGTTGAGACACTCCAAAACTC	AAATTATTGCTCTCGAGGGTTCA	429	This study
Plasmid pSE48_2	*rep*	pSE48_2	TTGAGCAAGAGGACGACCAA	AAATGCTACCCTTCGGCTCG	659	This study
S. epidermidis chromosome	*groEL*	*S. epidermidis* 1457	TCAGCGTTACAACATGCAGC	GTTGTCTTTCATAGTTGTATGTGCC	555	This study
S. epidermidis chromosome	*mer*	*S. epidermidis* SE48	ATTCGCACGTGAACCAGTGT	ACATGCTGCTGGTCACGG	343	This study
Integrated PICI	*groEL*, *int*	*S. epidermidis* SE48	TCAGCGTTACAACATGCAGC	GCACTCATTCCGTCACACAC	390	This study
Integrated PICI	*groEL*, *int*	*S. epidermidis* SE48	TCAGCGTTACAACATGCAGC	CGTGCAGGCGAGTTGTTAG	734	This study
$SeCI_{SE48}$	*gp12*, *gp13*	$SeCI_{SE48}$	CGTTGAGGGCTTGAAATGGG	GCACCTAACACTTGGCGTTT	758	This study
Packaged $SeCI_{SE48}$	*gp22*, *int*	$SeCI_{SE48}$	GTCCATACAAGTTAAACGGCGA	GCACTCATTCCGTCACACAC	665	This study
Phage 27 and 48 genomes	*dut*	Phage 48	AGGTGTATCGCAAAGCAGAGTT	TCTAACGGCTTACCTGGTTTCT	266	This study
Phage 456, 459, and E72 genomes	*dnaB*	Phage 459	GGACCAAGCACAAATGACACC	TGCTCAATCCCTCCTGCTTC	282	This study
Prophages 27, 48, 456, 459, and E72	*mer*, *int*	*S. epidermidis* NCTC 13924	ATTCGCACGTGAACCAGTGT	ACAGACGAAACAATCGCAGA	530	This study

Downloaded from http://msphere.asm.org/ on May 14, 2021 by guest

England BioLabs) in a total volume of 500 μl, followed by incubation for 1 to 2 h at 37°C until lysis appeared. Then, 30 μl of 10% SDS and 5 μl of proteinase K (20 mg/ml; Sigma-Aldrich) were added, and the sample was incubated for 60 min at 50°C, followed by heat inactivation for 10 min at 95°C and centrifugation at 9,700 $\times$ *g* for 5 min. DNA was isolated from the supernatant using the phenol-chloroform method (83). The library was prepared using an SQK-RBK004 rapid barcoding kit (Oxford Nanopore Technologies, UK) according to the manufacturer's instructions. Libraries were sequenced with FLO-MIN106 flow cells (R9.4.1) on a MinION device (Oxford Nanopore Technologies, UK). The device was controlled with the software MinKNOW v.2.2.12 (Oxford Nanopore Technologies, UK). Base calling and demultiplexing were performed using Guppy v2.3.5. Reads were trimmed using fastp Galaxy v0.20.1 (86).

Complete genomes were obtained using Unicycler Galaxy v0.4.8.0 (87), including a hybrid assembly of bacterial genome sequences. Genomes were annotated using RAST (88) with manual inspection by BLAST (http://blast.ncbi.nlm.nih.gov/), InterPro (89), Phobius (90), and HHpred (91), which was also used for the secondary structure alignment of putative capsid assembly proteins. The Comprehensive Antibiotic Resistance Database (CARD), the NCBI database, ResFinder, and the virulence factor database (VFDB), accessed through ABRicate Galaxy v1.0.1 (92), were used to search for antibiotic resistance and virulence factor genes with $\geq$80% nucleotide identity and $\geq$60% length coverage. The genomic alignments were constructed using Easyfig v2.4 (93) and GView (94). Phage genome relatedness was calculated by OAT v 0.93.1 (95). The phylogenetic trees were built with the online tool Ngphylogeny.fr (96) as follows. The alignments were computed with Clustal Omega, and low-quality alignments were removed with BMGE (Block Mapping and Gathering with Entropy) software; the trees are the results of the maximum-likelihood-based inference of phylogenetic trees with Smart Model Selection software, and the statistical test for branch support was SH-like aLRT. The EMBOSS tools Needle (https://www.ebi.ac.uk/Tools/psa/emboss_needle/) and Stretcher (https://www.ebi.ac.uk/Tools/psa/emboss_stretcher/) were used for global pairwise sequence comparisons. The heat map was generated using R v3.6.3 (R Core Team). Sequencing reads mapping statistics were computed in CLC Genomic Workbench v3.6.5 (Qiagen Bioinformatics, Denmark). Physical termini of phage and $SeCI_{SE48}$ genophores packaged in the virion capsid were determined from the alignment of Illumina reads with the PhageTerm tool (97). Multilocus sequence typing was performed using MLST v2.0.4 with database version 2.0.0 (98). The assignment of multilocus sequence types into clonal complexes was performed with eBURST v3 (99).

For comparative genomic analyses, the following genomes were used: phages PH15 and CNPH82 (36), CNPx (61), IPLA5 and IPLA7 (38), 71 and X2 (43), ETA (44), NM4 (45), and 80α (46); chromosomal islands of *S. lugdunensis* strain VISLISI_27 (100) and *S. haemolyticus* strain SGAir0252 (101); *S. aureus* pathogenicity islands SaPI1 (25), SaPI2R (102), SaPI3 (103), $SaPI_{N315}$ (104), $SaPI_{IVM10}$, $SaPI_{J11}$, and $SaPI_{No.1}$ (105), SaPI68111 (106), and SaPIeq1 (107); *S. aureus* resistance island SaRIfusB (108); *S. epidermidis* resistance islands SeRIfusB-704, SeRIfusB-2793, SeRIfusB-5907, SeRIfusB-7778 (14), and SeRIfusB-3692 (12); and *S. epidermidis* pathogenicity islands SePIfusB-857 (12) and SePI of strain 14.1.R1 (109).

Data availability. The sequences have been deposited in the GenBank database under the following accession numbers: phage 27 as vB_SepS_27, MW364971; phage 48 as vB_SepS_48, MW364972; phage 456 as vB_SepS_456, MW364973; phage 459 as vB_SepS_459, MW364974; phage E72 as vB_SepS_E72, MW364975; packaged phage-inducible chromosomal island $SeCI_{SE48}$, MW368309; *S. epidermidis* strain SE48, NZ_CP066303; its plasmids pSE48_1, NZ_CP066304, and pSE48_2, NZ_CP066305; pSE27_S, MW364976; pSE27_T, MW364977; pSE456_1, MW364978; pSE456_2, MW364979; pSE456_3, MW364980; pSE456_4, MW364981; pSE459_1, MW364982; pSE459_2, MW364983; pSE459_3, MW364984; and pSE459_T, MW364985.

SUPPLEMENTAL MATERIAL

Supplemental material is available online only.

TABLE S1, PDF file, 0.05 MB.

TABLE S2, PDF file, 0.1 MB.

TABLE S3, PDF file, 0.3 MB.

ACKNOWLEDGMENTS

The research leading to these results received funding from the Czech Science Foundation grant 18-13064S to R.P. We gratefully acknowledge the CIISB, Instruct-CZ Centre of Instruct-ERIC EU consortium, and the NCMG research infrastructure funded by the Ministry of Education, Youth and Sports of the Czech Republic (MEYS CR) projects LM2018127 and LM2018132 for their financial support of the measurements at the Proteomics Core Facility, Cryo-electron Microscopy and Tomography and Genomics Core Facility of CEITEC. This research was partly carried out under project CEITEC 2020 (LQ1601), with financial support from the MEYS CR. Students involved in this study were supported by the Grant Agency of Masaryk University (MUNI/A/1522/2020). A.P. gratefully acknowledges funding by the German Research Foundation (TRR34; TRR156, project ID 246807620; TRR261, project ID 398967434; and PE 805/7-1), Cluster of Excellence EXC2124 'Controlling Microbes to Fight Infections' (project ID 390838134), and the German Center of Infection Research. V.W. acknowledges funding by the German Research Foundation (award WI4582/2-1 to V.W.; project number 449712894).

Downloaded from http://msphere.asm.org/ on May 14, 2021 by guest

TWINCORE is a joint venture between the Hannover Medical School and the Helmholtz Centre for Infection Research.

REFERENCES

1. Otto M. 2009. *Staphylococcus epidermidis*—the 'accidental' pathogen. Nat Rev Microbiol 7:555–567. https://doi.org/10.1038/nrmicro2182.
2. Ziebuhr W, Hennig S, Eckart M, Kranzler H, Batzilla C, Kozitskaya S. 2006. Nosocomial infections by *Staphylococcus epidermidis*: how a commensal bacterium turns into a pathogen. Int J Antimicrob Agents 28(Suppl 1): S14–S20. https://doi.org/10.1016/j.ijantimicag.2006.05.012.
3. Mediano P, Fernandez L, Jimenez E, Arroyo R, Espinosa-Martos I, Rodriguez JM, Marin M. 2017. Microbial diversity in milk of women with mastitis: potential role of coagulase-negative staphylococci, viridans group streptococci, and corynebacteria. J Hum Lact 33:309–318. https://doi.org/10.1177/0890334417692968.
4. Oliveira M, Bexiga R, Nunes SF, Carneiro C, Cavaco LM, Bernardo F, Vilela CL. 2006. Biofilm-forming ability profiling of *Staphylococcus aureus* and *Staphylococcus epidermidis* mastitis isolates. Vet Microbiol 118:133–140. https://doi.org/10.1016/j.vetmic.2006.07.008.
5. Lee JYH, Monk IR, Goncalves da Silva A, Seemann T, Chua KYL, Kearns A, Hill R, Woodford N, Bartels MD, Strommenger B, Laurent F, Dodemont M, Deplano A, Patel R, Larsen AR, Korman TM, Stinear TP, Howden BP. 2018. Global spread of three multidrug-resistant lineages of *Staphylococcus epidermidis*. Nat Microbiol 3:1175–1185. https://doi.org/10.1038/s41564-018-0230-7.
6. Götz F. 2002. *Staphylococcus* and biofilms. Mol Microbiol 43:1367–1378. https://doi.org/10.1046/j.1365-2958.2002.02827.x.
7. Heilmann C, Ziebuhr W, Becker K. 2019. Are coagulase-negative staphylococci virulent? Clin Microbiol Infect 25:1071–1080. https://doi.org/10.1016/j.cmi.2018.11.012.
8. Schoenfelder SM, Lange C, Eckart M, Hennig S, Kozytska S, Ziebuhr W. 2010. Success through diversity—how *Staphylococcus epidermidis* establishes as a nosocomial pathogen. Int J Med Microbiol 300:380–386. https://doi.org/10.1016/j.ijmm.2010.04.011.
9. Schwarz S, Shen J, Wendlandt S, Fessler AT, Wang Y, Kadlec K, Wu CM. 2014. Plasmid-mediated antimicrobial resistance in staphylococci and other Firmicutes. Microbiol Spectr 2:PLAS-0020-2014. https://doi.org/10.1128/microbiolspec.PLAS-0020-2014.
10. Méric G, Miragaia M, de Been M, Yahara K, Pascoe B, Mageiros L, Mikhail J, Harris LG, Wilkinson TS, Rolo J, Lamble S, Bray JE, Jolley KA, Hanage WP, Bowden R, Maiden MC, Mack D, de Lencastre H, Feil EJ, Corander J, Sheppard SK. 2015. Ecological overlap and horizontal gene transfer in *Staphylococcus aureus* and *Staphylococcus epidermidis*. Genome Biol Evol 7:1313–1328. https://doi.org/10.1093/gbe/evv066.
11. Banaszkiewicz S, Calland JK, Mourkas E, Sheppard SK, Pascoe B, Bania J. 2019. Genetic diversity of composite enterotoxigenic *Staphylococcus epidermidis* pathogenicity islands. Genome Biol Evol 11:3498–3509. https://doi.org/10.1093/gbe/evz259.
12. Chen HJ, Chang YC, Tsai JC, Hung WC, Lin YT, You SJ, Tseng SP, Teng LJ. 2013. New structure of phage-related islands carrying *fusB* and a virulence gene in fusidic acid-resistant *Staphylococcus epidermidis*. Antimicrob Agents Chemother 57:5737–5739. https://doi.org/10.1128/AAC.01433-13.
13. Madhusoodanan J, Seo KS, Remortel B, Park JY, Hwang SY, Fox LK, Park YH, Deobald CF, Wang D, Liu S, Daugherty SC, Gill AL, Bohach GA, Gill SR. 2011. An enterotoxin-bearing pathogenicity Island in *Staphylococcus epidermidis*. J Bacteriol 193:1854–1862. https://doi.org/10.1128/JB.00162-10.
14. Chen HJ, Tsai JC, Hung WC, Tseng SP, Hsueh PR, Teng LJ. 2011. Identification of *fusB*-mediated fusidic acid resistance islands in *Staphylococcus epidermidis* isolates. Antimicrob Agents Chemother 55:5842–5849. https://doi.org/10.1128/AAC.00592-11.
15. Haaber J, Penadés JR, Ingmer H. 2017. Transfer of antibiotic resistance in *Staphylococcus aureus*. Trends Microbiol 25:893–905. https://doi.org/10.1016/j.tim.2017.05.011.
16. Mašlaňová I, Doškař J, Varga M, Kuntová L, Mužík J, Malúšková D, Růžičková V, Pantůček R. 2013. Bacteriophages of *Staphylococcus aureus* efficiently package various bacterial genes and mobile genetic elements including SCC*mec* with different frequencies. Environ Microbiol Rep 5:66–73. https://doi.org/10.1111/j.1758-2229.2012.00378.x.
17. Novick R. 1967. Properties of a cryptic high-frequency transducing phage in *Staphylococcus aureus*. Virology 33:155–166. https://doi.org/10.1016/0042-6822(67)90105-5.
18. Winstel V, Kuhner P, Krismer B, Peschel A, Rohde H. 2015. Transfer of plasmid DNA to clinical coagulase-negative staphylococcal pathogens by using a unique bacteriophage. Appl Environ Microbiol 81:2481–2488. https://doi.org/10.1128/AEM.04190-14.
19. Varga M, Pantůček R, Růžičková V, Doškař J. 2016. Molecular characterization of a new efficiently transducing bacteriophage identified in meticillin-resistant *Staphylococcus aureus*. J Gen Virol 97:258–268. https://doi.org/10.1099/jgv.0.000329.
20. Spilman MS, Damle PK, Dearborn AD, Rodenburg CM, Chang JR, Wall EA, Christie GE, Dokland T. 2012. Assembly of bacteriophage 80a capsids in a *Staphylococcus aureus* expression system. Virology 434:242–250. https://doi.org/10.1016/j.virol.2012.08.031.
21. Kizziah JL, Manning KA, Dearborn AD, Dokland T. 2020. Structure of the host cell recognition and penetration machinery of a *Staphylococcus aureus* bacteriophage. PLoS Pathog 16:e1008314. https://doi.org/10.1371/journal.ppat.1008314.
22. Otter JA, Kearns AM, French GL, Ellington MJ. 2010. Panton-Valentine leukocidin-encoding bacteriophage and gene sequence variation in community-associated methicillin-resistant *Staphylococcus aureus*. Clin Microbiol Infect 16:68–73. https://doi.org/10.1111/j.1469-0691.2009.02925.x.
23. Botka T, Růžičková V, Konečná H, Pantůček R, Rychlík I, Zdráhal Z, Petráš P, Doškař J. 2015. Complete genome analysis of two new bacteriophages isolated from impetigo strains of *Staphylococcus aureus*. Virus Genes 51:122–131. https://doi.org/10.1007/s11262-015-1223-8.
24. van Wamel WJ, Rooijakkers SH, Ruyken M, van Kessel KP, van Strijp JA. 2006. The innate immune modulators staphylococcal complement inhibitor and chemotaxis inhibitory protein of *Staphylococcus aureus* are located on beta-hemolysin-converting bacteriophages. J Bacteriol 188:1310–1315. https://doi.org/10.1128/JB.188.4.1310-1315.2006.
25. Ruzin A, Lindsay J, Novick RP. 2001. Molecular genetics of SaPI1—a mobile pathogenicity island in *Staphylococcus aureus*. Mol Microbiol 41:365–377. https://doi.org/10.1046/j.1365-2958.2001.02488.x.
26. Chen J, Novick RP. 2009. Phage-mediated intergeneric transfer of toxin genes. Science 323:139–141. https://doi.org/10.1126/science.1164783.
27. Cervera-Alamar M, Guzmán-Markevitch K, Žiemytė M, Ortí L, Bernabé-Quispe P, Pineda-Lucena A, Pemán J, Tormo-Mas MÁ. 2018. Mobilisation mechanism of pathogenicity islands by endogenous phages in *Staphylococcus aureus* clinical strains. Sci Rep 8:16742. https://doi.org/10.1038/s41598-018-34918-2.
28. Haaber J, Leisner JJ, Cohn MT, Catalan-Moreno A, Nielsen JB, Westh H, Penadés JR, Ingmer H. 2016. Bacterial viruses enable their host to acquire antibiotic resistance genes from neighbouring cells. Nat Commun 7:13333. https://doi.org/10.1038/ncomms13333.
29. Mašlaňová I, Stříbná S, Doškař J, Pantůček R. 2016. Efficient plasmid transduction to *Staphylococcus aureus* strains insensitive to the lytic action of transducing phage. FEMS Microbiol Lett 363:fnw211. https://doi.org/10.1093/femsle/fnw211.
30. Chen J, Ram G, Penadés JR, Brown S, Novick RP. 2015. Pathogenicity island-directed transfer of unlinked chromosomal virulence genes. Mol Cell 57:138–149. https://doi.org/10.1016/j.molcel.2014.11.011.
31. Chen J, Quiles-Puchalt N, Chiang YN, Bacigalupe R, Fillol-Salom A, Chee MSJ, Fitzgerald JR, Penadés JR. 2018. Genome hypermobility by lateral transduction. Science 362:207–212. https://doi.org/10.1126/science.aat5867.
32. Talbot HW, Jr, Parisi JT. 1976. Phage typing of *Staphylococcus epidermidis*. J Clin Microbiol 3:519–523.
33. Rosdahl VT, Gahrn-Hansen B, Moller JK, Kjaeldgaard P. 1990. Phage-typing of coagulase-negative staphylococci. Factors influencing typability. APMIS 98:299–304. https://doi.org/10.1111/j.1699-0463.1990.tb01036.x.
34. Bes M. 1994. Characterization of thirteen *Staphylococcus epidermidis* and *S. saprophyticus* bacteriophages. Res Virol 145:111–121. https://doi.org/10.1016/S0923-2516(07)80013-6.

Downloaded from http://msphere.asm.org/ on May 14, 2021 by guest

35. Lina B, Bes M, Vandenesch F, Greenland T, Etienne J, Fleurette J. 1993. Role of bacteriophages in genomic variability of related coagulase-negative staphylococci. FEMS Microbiol Lett 109:273–277. https://doi.org/10.1111/j.1574-6968.1993.tb06180.x.
36. Daniel A, Bonnen PE, Fischetti VA. 2007. First complete genome sequence of two *Staphylococcus epidermidis* bacteriophages. J Bacteriol 189:2086–2100. https://doi.org/10.1128/JB.01637-06.
37. Deghorain M, Bobay LM, Smeesters PR, Bousbata S, Vermeersch M, Perez-Morga D, Dreze PA, Rocha EPC, Touchon M, Van Melderen L. 2012. Characterization of novel phages isolated in coagulase-negative staphylococci reveals evolutionary relationships with *Staphylococcus aureus* phages. J Bacteriol 194:5829–5839. https://doi.org/10.1128/JB.01085-12.
38. Gutiérrez D, Martínez B, Rodríguez A, García P. 2012. Genomic characterization of two *Staphylococcus epidermidis* bacteriophages with anti-biofilm potential. BMC Genomics 13:228. https://doi.org/10.1186/1471-2164-13-228.
39. Dean BA, Williams RE, Hall F, Corse J. 1973. Phage typing of coagulase-negative staphylococci and micrococci. J Hyg (Lond) 71:261–270. https://doi.org/10.1017/s0022172400022737.
40. Verhoef J, Van Boven CP, Winkler KC. 1972. Phage-typing of coagulase-negative staphylococci. J Med Microbiol 5:9–19. https://doi.org/10.1099/00222615-5-1-9.
41. Casjens SR, Gilcrease EB. 2009. Determining DNA packaging strategy by analysis of the termini of the chromosomes in tailed-bacteriophage virions. Methods Mol Biol 502:91–111. https://doi.org/10.1007/978-1-60327-565-1_7.
42. Sherlock D, Leong JX, Fogg PCM. 2019. Identification of the first gene transfer agent (GTA) small terminase in *Rhodobacter capsulatus* and ilts role in GTA production and packaging of DNA. J Virol 93:e01328-19. https://doi.org/10.1128/JVI.01328-19.
43. Kwan T, Liu J, DuBow M, Gros P, Pelletier J. 2005. The complete genomes and proteomes of 27 *Staphylococcus aureus* bacteriophages. Proc Natl Acad Sci U S A 102:5174–5179. https://doi.org/10.1073/pnas.0501140102.
44. Yamaguchi T, Hayashi T, Takami H, Nakasone K, Ohnishi M, Nakayama K, Yamada S, Komatsuzawa H, Sugai M. 2000. Phage conversion of exfoliative toxin A production in *Staphylococcus aureus*. Mol Microbiol 38:694–705. https://doi.org/10.1046/j.1365-2958.2000.02169.x.
45. Bae T, Baba T, Hiramatsu K, Schneewind O. 2006. Prophages of *Staphylococcus aureus* Newman and their contribution to virulence. Mol Microbiol 62:1035–1047. https://doi.org/10.1111/j.1365-2958.2006.05441.x.
46. Christie GE, Matthews AM, King DG, Lane KD, Olivarez NP, Tallent SM, Gill SR, Novick RP. 2010. The complete genomes of *Staphylococcus aureus* bacteriophages 80 and 80a—implications for the specificity of SaPI mobilization. Virology 407:381–390. https://doi.org/10.1016/j.virol.2010.08.036.
47. Verhoef J, Winkler KC, van Boven CP. 1971. Characters of phages from coagulase-negative staphylococci. J Med Microbiol 4:413–424. https://doi.org/10.1099/00222615-4-4-413.
48. Augustin J, Rosenstein R, Wieland B, Schneider U, Schnell N, Engelke G, Entian KD, Götz F. 1992. Genetic analysis of epidermin biosynthetic genes and epidermin-negative mutants of *Staphylococcus epidermidis*. Eur J Biochem 204:1149–1154. https://doi.org/10.1111/j.1432-1033.1992.tb16740.x.
49. Galac MR, Stam J, Maybank R, Hinkle M, Mack D, Rohde H, Roth AL, Fey PD. 2017. Complete genome sequence of *Staphylococcus epidermidis* 1457. Genome Announc 5:e00450-17. https://doi.org/10.1128/genomeA.00450-17.
50. Gill SR, Fouts DE, Archer GL, Mongodin EF, Deboy RT, Ravel J, Paulsen IT, Kolonay JF, Brinkac L, Beanan M, Dodson RJ, Daugherty SC, Madupu R, Angiuoli SV, Durkin AS, Haft DH, Vamathevan J, Khouri H, Utterback T, Lee C, Dimitrov G, Jiang L, Qin H, Weidman J, Tran K, Kang K, Hance IR, Nelson KE, Fraser CM. 2005. Insights on evolution of virulence and resistance from the complete genome analysis of an early methicillin-resistant *Staphylococcus aureus* strain and a biofilm-producing methicillin-resistant *Staphylococcus epidermidis* strain. J Bacteriol 187:2426–2438. https://doi.org/10.1128/JB.187.7.2426-2438.2005.
51. Kreiswirth BN, Lofdahl S, Betley MJ, O'Reilly M, Schlievert PM, Bergdoll MS, Novick RP. 1983. The toxic shock syndrome exotoxin structural gene is not detectably transmitted by a prophage. Nature 305:709–712. https://doi.org/10.1038/305709a0.
52. Raue S, Fan SH, Rosenstein R, Zabel S, Luqman A, Nieselt K, Götz F. 2020. The genome of *Staphylococcus epidermidis* O47. Front Microbiol 11:2061. https://doi.org/10.3389/fmicb.2020.02061.
53. Li M, Rigby K, Lai Y, Nair V, Peschel A, Schittek B, Otto M. 2009. *Staphylococcus aureus* mutant screen reveals interaction of the human antimicrobial peptide dermcidin with membrane phospholipids. Antimicrob Agents Chemother 53:4200–4210. https://doi.org/10.1128/AAC.00428-09.
54. Olson ME, Horswill AR. 2014. Bacteriophage transduction in *Staphylococcus epidermidis*. Methods Mol Biol 1106:167–172. https://doi.org/10.1007/978-1-62703-736-5_15.
55. Penadés JR, Chen J, Quiles-Puchalt N, Carpena N, Novick RP. 2015. Bacteriophage-mediated spread of bacterial virulence genes. Curr Opin Microbiol 23:171–178. https://doi.org/10.1016/j.mib.2014.11.019.
56. Löfdahl S, Sjöström JE, Philipson L. 1981. Cloning of restriction fragments of DNA from staphylococcal bacteriophage phi 11. J Virol 37:795–801. https://doi.org/10.1128/JVI.37.2.795-801.1981.
57. Casjens SR, Gilcrease EB, Winn-Stapley DA, Schicklmaier P, Schmieger H, Pedulla ML, Ford ME, Houtz JM, Hatfull GF, Hendrix RW. 2005. The generalized transducing *Salmonella bacteriophage* ES18: complete genome sequence and DNA packaging strategy. J Bacteriol 187:1091–1104. https://doi.org/10.1128/JB.187.3.1091-1104.2005.
58. Quiles-Puchalt N, Martinez-Rubio R, Ram G, Lasa I, Penadés JR. 2014. Unravelling bacteriophage phi11 requirements for packaging and transfer of mobile genetic elements in *Staphylococcus aureus*. Mol Microbiol 91:423–437. https://doi.org/10.1111/mmi.12445.
59. Moller AG, Lindsay JA, Read TD, Johnson KN. 2019. Determinants of phage host range in *Staphylococcus* species. Appl Environ Microbiol 85:e00209-19. https://doi.org/10.1128/AEM.00209-19.
60. Koc C, Xia G, Kuhner P, Spinelli S, Roussel A, Cambillau C, Stehle T. 2016. Structure of the host-recognition device of *Staphylococcus aureus* phage phi11. Sci Rep 6:27581. https://doi.org/10.1038/srep27581.
61. Depardieu F, Didier JP, Bernheim A, Sherlock A, Molina H, Duclos B, Bikard D. 2016. A eukaryotic-like serine/threonine kinase protects staphylococci against phages. Cell Host Microbe 20:471–481. https://doi.org/10.1016/j.chom.2016.08.010.
62. McCarthy AJ, Witney AA, Lindsay JA. 2012. *Staphylococcus aureus* temperate bacteriophage: carriage and horizontal gene transfer is lineage associated. Front Cell Infect Microbiol 2:6. https://doi.org/10.3389/fcimb.2012.00006.
63. Fišarová L, Pantůček R, Botka T, Doškař J. 2019. Variability of resistance plasmids in coagulase-negative staphylococci and their importance as a reservoir of antimicrobial resistance. Res Microbiol 170:105–111. https://doi.org/10.1016/j.resmic.2018.11.004.
64. Zeman M, Mašlaňová I, Indráková A, Šiborová M, Mikulášek K, Bendíčková K, Plevka P, Vrbovská V, Zdráhal Z, Doškař J, Pantůček R. 2017. *Staphylococcus sciuri* bacteriophages double-convert for staphylokinase and phospholipase, mediate interspecies plasmid transduction, and package *mecA* gene. Sci Rep 7:46319. https://doi.org/10.1038/srep46319.
65. Skjold SA, Wannamaker LW. 1986. Surface proteins in the transduction of groups A and G streptococci. J Med Microbiol 21:69–74. https://doi.org/10.1099/00222615-21-1-69.
66. Valero-Rello A, Lopez-Sanz M, Quevedo-Olmos A, Sorokin A, Ayora S. 2017. Molecular mechanisms that contribute to horizontal transfer of plasmids by the bacteriophage SPP1. Front Microbiol 8:1816. https://doi.org/10.3389/fmicb.2017.01816.
67. Martinez-Rubio R, Quiles-Puchalt N, Marti M, Humphrey S, Ram G, Smyth D, Chen J, Novick RP, Penadés JR. 2017. Phage-inducible islands in the Gram-positive cocci. ISME J 11:1029–1042. https://doi.org/10.1038/ismej.2016.163.
68. Fillol-Salom A, Martínez-Rubio R, Abdulrahman RF, Chen J, Davies R, Penadés JR. 2018. Phage-inducible chromosomal islands are ubiquitous within the bacterial universe. ISME J 12:2114–2128. https://doi.org/10.1038/s41396-018-0156-3.
69. Ram G, Chen J, Ross HF, Novick RP. 2014. Precisely modulated pathogenicity island interference with late phage gene transcription. Proc Natl Acad Sci U S A 111:14536–14541. https://doi.org/10.1073/pnas.1406749111.
70. Dearborn AD, Wall EA, Kizziah JL, Klenow L, Parker LK, Manning KA, Spilman MS, Spear JM, Christie GE, Dokland T. 2017. Competing scaffolding proteins determine capsid size during mobilization of *Staphylococcus aureus* pathogenicity islands. Elife 6:e30822. https://doi.org/10.7554/eLife.30822.
71. Tormo-Más MA, Mir I, Shrestha A, Tallent SM, Campoy S, Lasa I, Barbé J, Novick RP, Christie GE, Penadés JR. 2010. Moonlighting bacteriophage proteins derepress staphylococcal pathogenicity islands. Nature 465:779–782. https://doi.org/10.1038/nature09065.
72. Manning KA, Dokland T. 2020. The gp44 ejection protein of *Staphylococcus aureus* bacteriophage 80α binds to the ends of the genome

Downloaded from http://msphere.asm.org/ on May 14, 2021 by guest

and protects it from degradation. Viruses 12:563. https://doi.org/10.3390/v12050563.
73. Marraffini LA, Sontheimer EJ. 2008. CRISPR interference limits horizontal gene transfer in staphylococci by targeting DNA. Science 322:1843–1845. https://doi.org/10.1126/science.1165771.
74. Costa SK, Donegan NP, Corvaglia AR, Francois P, Cheung AL. 2017. Bypassing the restriction system to improve transformation of *Staphylococcus epidermidis*. J Bacteriol 199:e00271-17. https://doi.org/10.1128/JB.00271-17.
75. Xia G, Wolz C. 2014. Phages of *Staphylococcus aureus* and their impact on host evolution. Infect Genet Evol 21:593–601. https://doi.org/10.1016/j.meegid.2013.04.022.
76. Štveráková D, Šedo O, Benešík M, Zdráhal Z, Doškař J, Pantůček R. 2018. Rapid identification of intact staphylococcal bacteriophages using matrix-assisted laser desorption ionization-time-of-flight mass spectrometry. Viruses 10:176. https://doi.org/10.3390/v10040176.
77. Ng LK, Martin I, Alfa M, Mulvey M. 2001. Multiplex PCR for the detection of tetracycline resistant genes. Mol Cell Probes 15:209–215. https://doi.org/10.1006/mcpr.2001.0363.
78. Kuntová L, Pantůček R, Rájová J, Růžičková V, Petráš P, Mašlaňová I, Doškař J. 2012. Characteristics and distribution of plasmids in a clonally diverse set of methicillin-resistant *Staphylococcus aureus* strains. Arch Microbiol 194:607–614. https://doi.org/10.1007/s00203-012-0797-y.
79. Monk IR, Shah IM, Xu M, Tan MW, Foster TJ. 2012. Transforming the untransformable: application of direct transformation to manipulate genetically *Staphylococcus aureus* and *Staphylococcus epidermidis*. mBio 3:e00277-11. https://doi.org/10.1128/mBio.00277-11.
80. Blair JE, Williams RE. 1961. Phage typing of staphylococci. Bull World Health Organ 24:771–784.
81. Winstel V, Liang C, Sanchez-Carballo P, Steglich M, Munar M, Broker BM, Penadés JR, Nubel U, Holst O, Dandekar T, Peschel A, Xia G. 2013. Wall teichoic acid structure governs horizontal gene transfer between major bacterial pathogens. Nat Commun 4:2345. https://doi.org/10.1038/ncomms3345.
82. Pajunen M, Kiljunen S, Skurnik M. 2000. Bacteriophage phiYeO3-12, specific for *Yersinia enterocolitica* serotype O:3, is related to coliphages T3 and T7. J Bacteriol 182:5114–5120. https://doi.org/10.1128/jb.182.18.5114-5120.2000.
83. Sambrook J, Fritsch EF, Maniatis T. 1989. Molecular cloning: a laboratory manual. Cold Spring Harbor Laboratory Press, Cold Spring Harbor, NY.
84. Wingett SW, Andrews S. 2018. FastQ Screen: a tool for multi-genome mapping and quality control. F1000Res 7:1338. https://doi.org/10.12688/f1000research.15931.2.
85. Bolger AM, Lohse M, Usadel B. 2014. Trimmomatic: a flexible trimmer for Illumina sequence data. Bioinformatics 30:2114–2120. https://doi.org/10.1093/bioinformatics/btu170.
86. Chen S, Zhou Y, Chen Y, Gu J. 2018. Fastp: an ultra-fast all-in-one FASTQ preprocessor. Bioinformatics 34:i884–i890. https://doi.org/10.1093/bioinformatics/bty560.
87. Wick RR, Judd LM, Gorrie CL, Holt KE. 2017. Unicycler: resolving bacterial genome assemblies from short and long sequencing reads. PLoS Comput Biol 13:e1005595. https://doi.org/10.1371/journal.pcbi.1005595.
88. Brettin T, Davis JJ, Disz T, Edwards RA, Gerdes S, Olsen GJ, Olson R, Overbeek R, Parrello B, Pusch GD, Shukla M, Thomason JA, 3rd, Stevens R, Vonstein V, Wattam AR, Xia F. 2015. RASTtk: a modular and extensible implementation of the RAST algorithm for building custom annotation pipelines and annotating batches of genomes. Sci Rep 5:8365. https://doi.org/10.1038/srep08365.
89. Mitchell AL, Attwood TK, Babbitt PC, Blum M, Bork P, Bridge A, Brown SD, Chang HY, El-Gebali S, Fraser MI, Gough J, Haft DR, Huang H, Letunic I, Lopez R, Luciani A, Madeira F, Marchler-Bauer A, Mi H, Natale DA, Necci M, Nuka G, Orengo C, Pandurangan AP, Paysan-Lafosse T, Pesseat S, Potter SC, Qureshi MA, Rawlings ND, Redaschi N, Richardson LJ, Rivoire C, Salazar GA, Sangrador-Vegas A, Sigrist CJA, Sillitoe I, Sutton GG, Thanki N, Thomas PD, Tosatto SCE, Yong SY, Finn RD. 2019. InterPro in 2019: improving coverage, classification and access to protein sequence annotations. Nucleic Acids Res 47:D351–D360. https://doi.org/10.1093/nar/gky1100.
90. Kall L, Krogh A, Sonnhammer EL. 2007. Advantages of combined transmembrane topology and signal peptide prediction—the Phobius web server. Nucleic Acids Res 35:W429–W432. https://doi.org/10.1093/nar/gkm256.
91. Zimmermann L, Stephens A, Nam SZ, Rau D, Kubler J, Lozajic M, Gabler F, Soding J, Lupas AN, Alva V. 2018. A completely reimplemented MPI bioinformatics toolkit with a new HHpred server at its core. J Mol Biol 430:2237–2243. https://doi.org/10.1016/j.jmb.2017.12.007.
92. Afgan E, Baker D, Batut B, van den Beek M, Bouvier D, Cech M, Chilton J, Clements D, Coraor N, Gruning BA, Guerler A, Hillman-Jackson J, Hiltemann S, Jalili V, Rasche H, Soranzo N, Goecks J, Taylor J, Nekrutenko A, Blankenberg D. 2018. The Galaxy platform for accessible, reproducible and collaborative biomedical analyses: 2018 update. Nucleic Acids Res 46:W537–W544. https://doi.org/10.1093/nar/gky379.
93. Sullivan MJ, Petty NK, Beatson SA. 2011. Easyfig: a genome comparison visualizer. Bioinformatics 27:1009–1010. https://doi.org/10.1093/bioinformatics/btr039.
94. Petkau A, Stuart-Edwards M, Stothard P, Van Domselaar G. 2010. Interactive microbial genome visualization with GView. Bioinformatics 26:3125–3126. https://doi.org/10.1093/bioinformatics/btq588.
95. Lee I, Ouk Kim Y, Park SC, Chun J. 2016. OrthoANI: an improved algorithm and software for calculating average nucleotide identity. Int J Syst Evol Microbiol 66:1100–1103. https://doi.org/10.1099/ijsem.0.000760.
96. Lemoine F, Correia D, Lefort V, Doppelt-Azeroual O, Mareuil F, Cohen-Boulakia S, Gascuel O. 2019. NGPhylogeny.fr: new generation phylogenetic services for non-specialists. Nucleic Acids Res 47:W260–W265. https://doi.org/10.1093/nar/gkz303.
97. Garneau JR, Depardieu F, Fortier LC, Bikard D, Monot M. 2017. PhageTerm: a tool for fast and accurate determination of phage termini and packaging mechanism using next-generation sequencing data. Sci Rep 7:8292. https://doi.org/10.1038/s41598-017-07910-5.
98. Larsen MV, Cosentino S, Rasmussen S, Friis C, Hasman H, Marvig RL, Jelsbak L, Sicheritz-Ponten T, Ussery DW, Aarestrup FM, Lund O. 2012. Multilocus sequence typing of total-genome-sequenced bacteria. J Clin Microbiol 50:1355–1361. https://doi.org/10.1128/JCM.06094-11.
99. Feil EJ, Li BC, Aanensen DM, Hanage WP, Spratt BG. 2004. eBURST: inferring patterns of evolutionary descent among clusters of related bacterial genotypes from multilocus sequence typing data. J Bacteriol 186:1518–1530. https://doi.org/10.1128/jb.186.5.1518-1530.2004.
100. Argemi X, Martin V, Loux V, Dahyot S, Lebeurre J, Guffroy A, Martin M, Velay A, Keller D, Riegel P, Hansmann Y, Paul N, Prevost G. 2017. Whole-genome sequencing of seven strains of *Staphylococcus lugdunensis* allows identification of mobile genetic elements. Genome Biol Evol 9:1183–1189. https://doi.org/10.1093/gbe/evx077.
101. Premkrishnan BNV, Junqueira ACM, Uchida A, Purbojati RW, Houghton JNI, Chenard C, Wong A, Kolundzija S, Clare ME, Kushwaha KK, Panicker D, Putra A, Gaultier NE, Heinle CE, Vettath VK, Drautz-Moses DI, Schuster SC. 2018. Complete genome sequence of *Staphylococcus haemolyticus* type strain SGAir0252. Genome Announc 6:e00229-18. https://doi.org/10.1128/genomeA.00229-18.
102. Khokhlova OE, Hung WC, Wan TW, Iwao Y, Takano T, Higuchi W, Yachenko SV, Teplyakova OV, Kamshilova VV, Kotlovsky YV, Nishiyama A, Reva IV, Sidorenko SV, Peryanova OV, Reva GV, Teng LJ, Salmina AB, Yamamoto T. 2015. Healthcare- and community-associated methicillin-resistant *Staphylococcus aureus* (MRSA) and fatal pneumonia with pediatric deaths in Krasnoyarsk, Siberian Russia: unique MRSA's multiple virulence factors, genome, and stepwise evolution. PLoS One 10:e0128017. https://doi.org/10.1371/journal.pone.0128017.
103. Yarwood JM, McCormick JK, Paustian ML, Orwin PM, Kapur V, Schlievert PM. 2002. Characterization and expression analysis of *Staphylococcus aureus* pathogenicity island 3. Implications for the evolution of staphylococcal pathogenicity islands. J Biol Chem 277:13138–13147. https://doi.org/10.1074/jbc.M111661200.
104. Kuroda M, Ohta T, Uchiyama I, Baba T, Yuzawa H, Kobayashi I, Cui L, Oguchi A, Aoki K-i, Nagai Y, Lian J, Ito T, Kanamori M, Matsumaru H, Maruyama A, Murakami H, Hosoyama A, Mizutani-Ui Y, Takahashi NK, Sawano T, Inoue R-I, Kaito C, Sekimizu K, Hirakawa H, Kuhara S, Goto S, Yabuzaki J, Kanehisa M, Yamashita A, Oshima K, Furuya K, Yoshino C, Shiba T, Hattori M, Ogasawara N, Hayashi H, Hiramatsu K. 2001. Whole genome sequencing of meticillin-resistant *Staphylococcus aureus*. Lancet 357:1225–1240. https://doi.org/10.1016/S0140-6736(00)04403-2.
105. Sato'o Y, Omoe K, Ono HK, Nakane A, Hu DL. 2013. A novel comprehensive analysis method for *Staphylococcus aureus* pathogenicity islands. Microbiol Immunol 57:91–99. https://doi.org/10.1111/1348-0421.12007.
106. Li Z, Stevens DL, Hamilton SM, Parimon T, Ma Y, Kearns AM, Ellis RW, Bryant AE. 2011. Fatal *Staphylococcu aureus* hemorrhagic pneumonia: genetic analysis of a unique clinical isolate producing both PVL and TSST-1. PLoS One 6:e27246. https://doi.org/10.1371/journal.pone.0027246.
107. Viana D, Blanco J, Tormo-Mas MA, Selva L, Guinane CM, Baselga R, Corpa J, Lasa I, Novick RP, Fitzgerald JR, Penadés JR. 2010.

Downloaded from http://msphere.asm.org/ on May 14, 2021 by guest

Adaptation of *Staphylococcus aureus* to ruminant and equine hosts involves SaPI-carried variants of von Willebrand factor-binding protein. Mol Microbiol 77:1583–1594. https://doi.org/10.1111/j.1365-2958.2010.07312.x.

108. O'Neill AJ, Larsen AR, Skov R, Henriksen AS, Chopra I. 2007. Characterization of the epidemic European fusidic acid-resistant impetigo clone of *Staphylococcus aureus*. J Clin Microbiol 45:1505–1510. https://doi.org/10.1128/JCM.01984-06.
109. Lassen SB, Lomholt HB, Bruggemann H. 2017. Complete genome sequence of a *Staphylococcus epidermidis* strain with exceptional antimicrobial activity. Genome Announc 5:e00004-17. https://doi.org/10.1128/genomeA.00004-17.

Downloaded from http://msphere.asm.org/ on May 14, 2021 by guest

APPENDIX 14

Botka T, Pantůček R, Mašlaňová I, Benešík M, Petráš P, Růžičková V, Havlíčková P, Varga M, Žemličková H, Koláčková I, Florianová M, Jakubů V, Karpíšková R, Doškař J (2019) Lytic and genomic properties of spontaneous host-range *Kayvirus* mutants prove their suitability for upgrading phage therapeutics against staphylococci. *Scientific Reports* 9:5475. https://doi.org/10.1038/s41598-019-41868-w

(JCR 2019: IF = 3.998; Q1 – Multidisciplinary Sciences)

CC BY 4.0

SCIENTIFIC REPORTS

OPEN

Lytic and genomic properties of spontaneous host-range *Kayvirus* mutants prove their suitability for upgrading phage therapeutics against staphylococci

Received: 7 December 2018
Accepted: 17 March 2019
Published online: 02 April 2019

Tibor Botka[1], Roman Pantůček[1], Ivana Mašlaňová[1], Martin Benešík[1], Petr Petráš[2], Vladislava Růžičková[1], Pavla Havlíčková[1], Marian Varga[1], Helena Žemličková[2,3], Ivana Koláčková[4], Martina Florianová[4], Vladislav Jakubů[2], Renáta Karpíšková[4] & Jiří Doškař[1]

Lytic bacteriophages are valuable therapeutic agents against bacterial infections. There is continual effort to obtain new phages to increase the effectivity of phage preparations against emerging phage-resistant strains. Here we described the genomic diversity of spontaneous host-range mutants of kayvirus 812. Five mutant phages were isolated as rare plaques on phage-resistant *Staphylococcus aureus* strains. The host range of phage 812-derived mutants was 42% higher than the wild type, determined on a set of 186 methicillin-resistant *S. aureus* strains representing the globally circulating human and livestock-associated clones. Comparative genomics revealed that single-nucleotide polymorphisms from the parental phage 812 population were fixed in next-step mutants, mostly in genes for tail and baseplate components, and the acquired point mutations led to diverse receptor binding proteins in the phage mutants. Numerous genome changes associated with rearrangements between direct repeat motifs or intron loss were found. Alterations occurred in host-takeover and terminal genomic regions or the endolysin gene of mutants that exhibited the highest lytic activity, which implied various mechanisms of overcoming bacterial resistance. The genomic data revealed that *Kayvirus* spontaneous mutants are free from undesirable genes and their lytic properties proved their suitability for rapidly updating phage therapeutics.

Phage therapy is an alternative to antibiotics used against *Staphylococcus aureus* infections, especially for the treatment of chronic infections caused by multidrug-resistant strains. Virulent bacteriophages of the genus *Kayvirus* from the family *Myoviridae* are the most promising due to their high lytic activity, therefore some of them are now commercialized[1–4]. The emergence of phage-resistant bacterial strains requires innovation in phage preparations, which is usually achieved by isolating new phages from the environment[5–7] or time-consuming procedures of phage adaptation such as phage training[8]. Upgraded preparations necessitate the safety assessments required by pharmaceutical authorities[9,10]. Phages adapted to different hosts exhibit distinct phenotypes and their specialization can be manifested as both improved infection of the host used for evolution and decreased infection of the other host types[11]. Phage and host co-evolution, driven by the resistance of bacterial hosts, results in intraspecies heterogeneity in phage genomes via emerging recombination events and single-nucleotide polymorphisms (SNPs) whose frequency and distribution vary depending on the phage and growth conditions[12,13]. The genes for host recognition, attachment, and infection are often affected by SNPs or major re-arrangements[11,14,15]. The fixation of these genome changes by natural selection enables the phages to recognize new hosts[16] and avoid anti-phage systems[17] such as the type II R-M system *Sau*3AI in kayviruses[18].

[1]Department of Experimental Biology, Faculty of Science, Masaryk University, Brno, 611 37, Czech Republic. [2]National Institute of Public Health, Praha, 100 42, Czech Republic. [3]Department of Clinical Microbiology, University Hospital and Faculty of Medicine in Hradec Králové, Charles University, Hradec Králové, 500 05, Czech Republic. [4]Veterinary Research Institute, Brno, 621 00, Czech Republic. Correspondence and requests for materials should be addressed to R.P. (email: pantucek@mail.muni.cz)

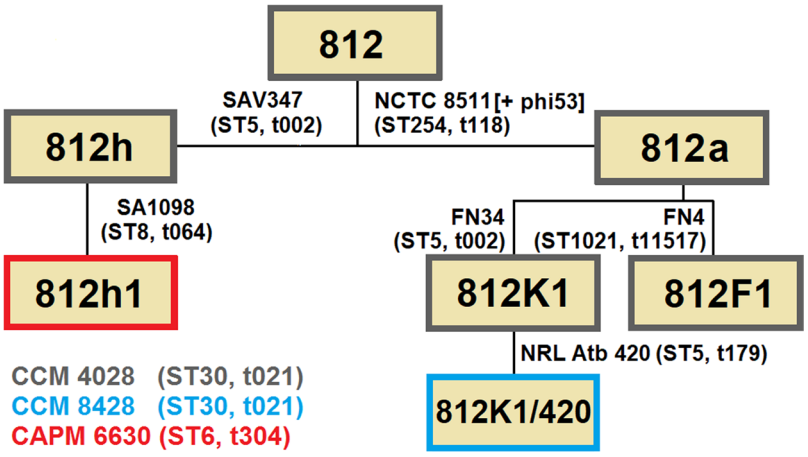

Figure 1. Diagram showing the isolation procedure of spontaneous host-range mutants of phage 812 represented by boxes. All phage mutants were isolated from a single plaque on selection *S. aureus* strains shown next to the corresponding mutants. Phage mutants were then propagated on *S. aureus* strains that are colour coded according to the phage mutant. The sequence type (ST) and the staphylococcal protein A (*spa*)-type of each strain are given in parentheses.

Due to their polyvalence, kayviruses are valuable agents which can be used to treat infections caused by a broad range of *S. aureus* and even non-*S. aureus* staphylococcal species[1,3,7]. Bacteriophage K is the best studied member of the genus *Kayvirus*[18,19]. The unit genomes of kayviruses are about 140 kb in size with more than 200 genes, as was reviewed by Łobocka *et al.*[20]. Early expressed host-takeover genes are located in identical left and right long terminal repeats (L-LTR and R-LTR, respectively), in which R-LTR forms genomic redundancy[21–23]. The majority of *Kayvirus* genomes contain group I introns, often encoding a homing endonuclease, which are located in the genes for DNA metabolism, morphogenesis and lysis[24–26].

In our previous studies, we isolated almost twenty mutants of kayvirus 812, which, when used in cocktails, extended the amount of susceptible *S. aureus* strains of different origin[1,27,28]. Phage 812 was later studied at the proteomic and structural level[29,30], however detailed genomic characterization has not been performed yet. Here, spontaneous mutants of phage 812 exhibiting a broad host range on recently circulating methicillin-resistant *Staphylococcus aureus* (MRSA) strains were isolated. With respect to interest in using the mutants in phage therapy, we focused on deep sequence analysis of their genomes, characterization of genomic variations, and exclusion of potential risks for phage therapy as required by pharmaceuticals authorities[31].

Results

The host range of phage 812 and its mutants. Mutants of phage 812 exhibiting a broader host range were isolated as rare plaques (with frequencies 10^{-6}–10^{-9}) on various *S. aureus* strains resistant to the parental phage (Fig. 1). The mutant phage 812a was a starting phage for several subsequent multi-step mutants isolated on different strains (Fig. 1). As the phage 812a-derived mutants did not exhibit a satisfactory lytic effect on livestock-associated MRSA (LA-MRSA) strains (Supplementary Table S1), a new lineage of mutants represented by phage 812h1 was selected from wild-type phage 812 on phage-resistant LA-MRSA strains (Fig. 1).

To evaluate the efficiency of the phage mutants, their lytic ability was tested on a set of well-characterized MRSA isolates (n = 186) and compared with type phage K and kayviruses isolated from commercial therapeutic preparations Stafal (Bohemia Pharmaceuticals, Czech Republic), PyoPhage (Eliava Biopreparations, Georgia) and StaphPhage (Microgen, Russia). The tested *S. aureus* strains belonged to 18 different sequence types (ST) and 45 staphylococcal protein A gene (*spa*)-types chosen to represent the major global MRSA clones (Supplementary Table S1). The susceptibility to phages varied among the strains of the same ST and even of the same *spa*-type. Of the tested strains, 59.1% (n = 110) were susceptible to all the tested bacteriophages. In contrast, 4.8% (n = 9) of isolates, mostly of ST45, were completely resistant to all the tested phages (Fig. 2, Supplementary Table S1). Overall, the number of tested strains lysed by wild-type phage 812 or at least one of its mutants (n = 177) was higher than phages from commercial preparations Stafal (Bohemia Pharmaceuticals, Czech Republic), PyoPhage (Eliava Biopreparations, Georgia), and StaphPhage (Microgen, Russia) (n = 165) (Supplementary Table S1). The mutant 812h1 exhibited the broadest host range, lysing almost 90% (n = 166) of the strains in total (Fig. 2). Nevertheless, 20 strains remained resistant to this mutant, but 11 of them were susceptible to some other phage 812-derived mutant, mostly to 812K1/420 (Supplementary Table S1).

Genomic analysis of phage 812 and its mutants. The phage 812 unit genome, 141,906 bp in size with a GC content of 30.4%, starts with a 8,484-bp left long terminal repeat (L-LTR) and ends with a tandem repeat with a 35–bp-long repeat unit sequence TATTAYTACTACTAAGTACCTTTGTTATGTACTAC (Figs 3 and 4). The copy number of the repeat unit is variable, ranging from four to more than twenty complete copies in the phage 812 population and down to two copies in the mutant 812K1/420 (Supplementary Fig. S1). The right LTR (R-LTR), identical to L-LTR, comes after the unit genome and forms the terminal redundancy (Fig. 4). In total, 218 coding sequences (CDS), 63 putative promoters, and 30 putative intrinsic terminators were predicted in the

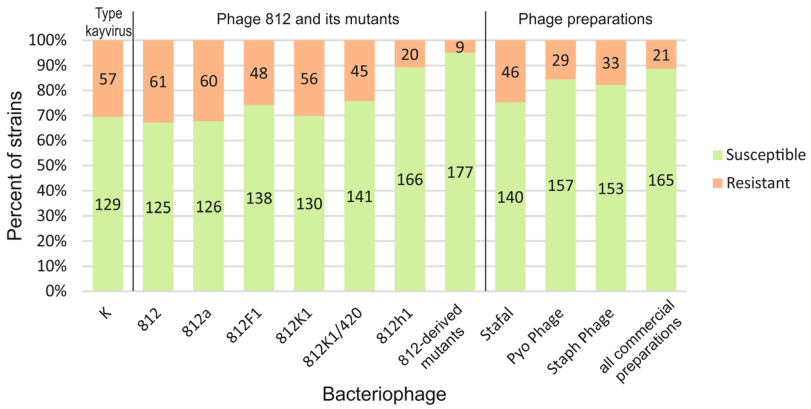

Figure 2. Lytic activity of phages K, 812 and its mutants, and kayviruses from commercial preparations Stafal (Bohemia Pharmaceuticals, Czech Republic), PyoPhage (Eliava Biopreparations, Georgia) and StaphPhage (Microgen, Russia) determined on a set of 186 methicillin-resistant *S. aureus* strains. The number of strains susceptible or resistant to a given phage is shown in each column. The susceptibility patterns of strains are listed in Supplementary Table S1. Susceptibility of strains to at least one of the 812-derived mutants and at least one of the commercial preparations is also shown.

unit genome (Figs 3 and 5). Three genes for tRNA (tRNA-Met-CAT, tRNA-Phe-GAA, and tRNA-Asp-GTC) and one gene for pseudo tRNA with an unknown function were predicted in the phage 812 genome. At least five introns were detected, of which three encode putative endonucleases, as in phage K[23,32]. The genomes of phage 812 and phage K exhibit 98.5% identity; although phage 812 contains two additional non-coding introns in the tail tube protein gene and the adjacent gene for putative endonuclease, which were also localized in phage 812h1 (Fig. 3) and in four previously described kayviruses, i.e. A3R, 676Z, Fi200W, and P4W[20].

In total, 176 variations were identified in the sequencing data of the wild-type phage 812 genome (Supplementary Table S2): 171 single-nucleotide polymorphisms (SNPs) and 5 deletion/insertion polymorphisms (DIPs), often localized in host range-associated genes (Fig. 4, Supplementary Table S2). A lot of minor SNPs and DIPs with a frequency in the genome < 50% of wild-type phage 812 were found to predominate in the mutant 812a and all its derivatives 812F1, 812K1, and 812K1/420 (Table 1). Such polymorphisms are called "fixed" in the text below and some of them affected encoded proteins (Fig. 3).

In addition, a few gene product alterations specific for each of the multi-step mutants were found. Phage 812K1 differs from the others by an 11-aa intrinsic deletion in an encoded ligase and 78-aa deletion along with the substitution of 4 aa in an encoded primase. Both the phages 812F1 and 812K1/420 encode truncated endolysin (a 211-aa deletion) due to a 1509-bp deletion in the endolysin gene as reported previously[26]. The gene for the tail fibre protein complex (*orf119*) of the phage 812K1/420 contains a premature stop codon due to a 77-bp deletion that divides this gene into 2 ORFs. Another premature stop codon caused by a nonsense mutation divides the gene for ribonuclease H of phage 812K1/420 into two ORFs without changing the reading frame.

Genomic analysis of phage 812h1. The phage 812h1 was selected in two steps using two distinct strains (Fig. 1). The unit genome of phage 812h1 is 142,150 bp long with an 8,432-bp-long L-LTR. The unit genome completely lacks the tandem repeat locus typical for phage 812, 812a and its subsequent mutants, as well as for phage K (Fig. 4 and Supplementary Fig. S1). In total, 219 CDS, 62 putative promoters, 31 putative intrinsic terminators, 3 tRNA genes and 1 pseudo tRNA gene were predicted in the unit genome. 255 SNPs and 5 DIPs were identified mostly in the genes for structural proteins and replication, as in phage 812 (Supplementary Tables S2 and S3). On the other hand, many SNPs of phage 812h1 are located in the genes for terminal repeat-encoded proteins (Fig. 4, Supplementary Table S3). One of the most apparent variabilities is the duplication of the gene for terminal repeat-encoded protein (*orf7*) located in the host-takeover region. The *orf7* duplication is bordered by the nucleotide motif TAGGAT, which is present in more than 90 copies in all *Kayvirus* genomes. The next apparent DIP is for a 2-kb-long sequence including *orf195* – *orf200* of unknown function, bordered by a unique direct repeat GGAGGTTAATTWATGAA (Fig. 4). The phage 812h1 genome differed from wild-type phage 812 and all mutants derived from phage 812a in multiple loci (Fig. 3, Supplementary Table S4).

Two different types of genes encoding receptor binding proteins (RBPs) corresponding to phage 812 *orf123* and *orf125* determine the host range of kayviruses through sequence variability and by the adsorption mechanism that may vary even in closely related phages[29,33,34]. These genes exhibit a high variability among *Kayvirus* genomes (Fig. 6), which could help the phages to adapt to a new host strain. The phages 812 and 812h1 differ in both the RBPs (Supplementary Table S4) and by SNPs content in both RBP-encoding genes (Supplementary Tables S2 and S3). The 812a-derived mutants only fixed SNPs of the parental phage 812 in the *orf123* homologue (Table 1).

Safety assessment. Because of the extensive presence of variable genetic elements and virulence or resistance genes in the genome of *S. aureus* strains used for the selection and propagation of the phage 812-derived mutants, it was necessary to check the phage genomes for the possible acquisition of genes with potential safety concerns. None of the isolated phage mutants carried genes for antibiotic resistance, bacterial virulence factors, or

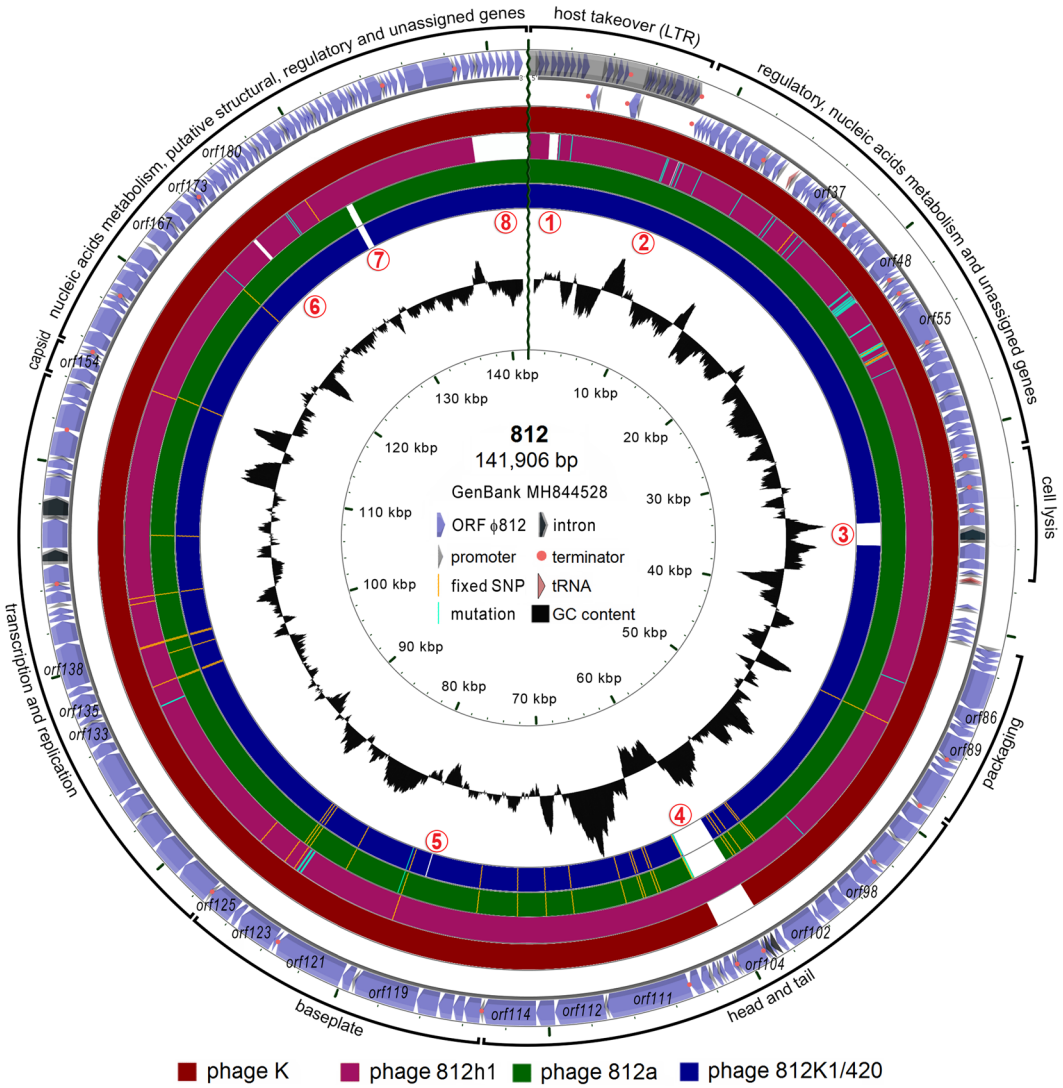

Figure 3. Phage 812 unit genome (GenBank accession number MH844528) and its comparison with phage K (NC_005880), phage mutant 812h1 (MH844529), phage mutant 812a (KJ206560), and 812a-derived mutant 812K1/420 (KJ206563). The major differences are labeled by red numbers: (1) host-takeover region showing low similarity between 812 and 812h1; (2) *orf23* and *orf24* of 812h1 that were not found in phage 812; (3) *orf73* encoding endolysin (LysK) that contains a partial deletion in 812a-derived mutant 812K1/420; (4) *orf103* for a tail tube protein that does not contain non-coding introns in 812a-derived mutants, and *orf104* for a putative intron-encoded nuclease which is missing in phage K and 812a-derived mutants; (5) *orf119* for tail fibre complex that contains a partial deletion in 812K1/420; (6) *orf173* for putative membrane-associated protein which is split into two open reading frames in 812h1 due to a partial deletion; (7) *orf190* and *orf191* deleted in all 812a-derived mutants, which led to fusion of *orf189* for regulatory protein and *orf192* for putative membrane protein; and (8) terminal part of the genome which is highly different from 812h1. Mutations and fixed polymorphisms with impact on protein sequences in compared phages are shown. The genome comparison is based on tblastx with an identity cut-off of 95%.

mobile elements-derived sequences. Similarly, no acquisition of the genes for lysogeny was found in the analysed phage genomes.

To exclude the possibility of generalized transduction, the frequency of packaging of the genes *mecA*, *tetK* and *blaZ* (encoding resistance to methicillin, tetracycline, and penicillin, respectively) into phage particles was analysed by relative quantification (Supplementary Table S5). Kayviruses K, and 812K1/420 as a representative of 812-derived phages, and PyoPhage was propagated on well-characterized MRSA strains: the monolysogenic strain COL with plasmid pT181 (*tetK*) and double lysogenic strain 08/019 of a USA300 clone with penicillinase plasmid pUSA-Houmr-like (*blaZ*). The restriction-deficient prophage-less methicillin-susceptible *S. aureus* (MSSA) strain RN4220 (pT181 and pUSA-Houmr-like) was used to prove the absence of spontaneously induced prophages from the COL and USA300 strains. Compared to simultaneously tested transducing siphovirus 80α, the resistance gene packaging by the studied kayviruses was 1000-fold lower (Supplementary Table S5).

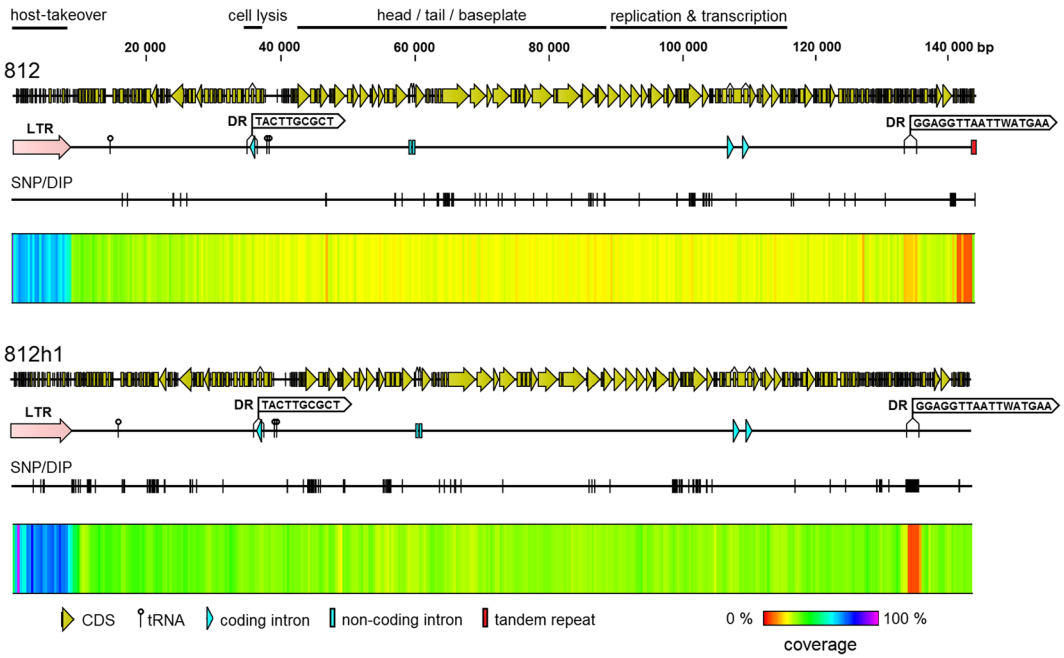

Figure 4. Coverage differences of genomic regions achieved by mapping of sequencing reads to unit genomes of phages 812 and 812h1. Long terminal repeats (LTRs) were delimited according to excessively increased coverage at the left end of the genomes due to the alignment of reads of both the LTRs. The increased coverage at the right end of the phage 812 genome is caused by a variable number of 35-bp tandem repeats. The genome annotations are illustrated on three feature lines: the top line shows coding sequences; the middle line indicates the location of LTR, tRNA genes, introns, and the direct repeats (DR) serving as recombination sites in the endolysin gene of phages 812F1 and 812K1/420, and 2-kb deletion/insertion polymorphism in phage 812h1; and the bottom lines show the positions of all polymorphisms.

Discussion

As shown in this study, the isolation of host-range spontaneous mutants is another and effective way to obtain improved therapeutic phages against almost every *S. aureus* strain. The strains exhibited distinctive phage susceptibility patterns (Supplementary Table S1), which indicates the action of several anti-phage defence mechanisms. This indicates that some of the mechanisms are shared among the strains of different genotypes, as was demonstrated e.g. for strains susceptible only to phage mutants with a truncated endolysin gene[26]. Since there is no apparent association between the strain genotype and the phage susceptibility, it can be assumed that anti-phage defence mechanisms are mainly encoded by the accessory genome. To overcome various defence mechanisms, it seems advantageous to use phage cocktails or apply the phages sequentially during the phage therapy.

Compared to the parental phage, all the isolated mutants exhibited point mutations and/or larger genomic rearrangements, some of which were reported before[27]. Deep sequencing analysis of wild-type phage 812 and the most effective mutant 812h1 showed that numerous genomic polymorphisms emerged during the phage propagation. In agreement with the recent evolutionary study[13], most of the SNPs accumulated in genes with an assumed effect on phage fitness.

Because of the different history of isolation and various genotypes of selection and propagation strains, the conditions for SNP accumulation in the analysed phages were different. The number of SNPs in both the wild-type phage 812 and recently isolated phage mutant 812h1 was higher than reported in *Pseudomonas* phages[13]. The high prevalence of polymorphisms indicates a high mutation rate that enables the diversification of the phage populations. In the genomes of 812a-derived phages obtained by 454-sequencing technology, a deep sequence analysis was not possible, so only the SNP/DIP fixation was evaluated. The procedure for isolating a phage mutant effective against to-date resistant strains were based on natural selection on the phage-resistant strain and the random picking up of a rare single plaque which may lead to genetic drift. Therefore, the understanding of evolutionary processes in natural *Kayvirus* populations requires further study, including the deep sequence analysis of isolates with a unified history.

Sequences of 812h1 distinct from the wild-type phage 812 were found in the genomes of related phages ISP, vB_SauM-fRuSau02, Fi200W, MSA6 or G1[2,3,20,32]. Some of the sequences were also found in wild-type phage 812 sequencing data, but with very low coverage. This suggests that a large pool of phage sequences is maintained in minor genome variants persisting in *Kayvirus* populations.

Numerous direct repeat motifs found across the genomes of kayviruses enable genomic rearrangements, therefore in the phage progeny, the polymorphic loci can be detected in different combinations, which plays an important role in phage diversification. Propagation on strains with different genotypes can cause fixation of the particular polymorphisms beneficial for phage fitness, as was reported in streptococcal phages able to avoid host defence mechanisms[17]. Another repeat-associated change in phage 812-derived mutants is of the copy number

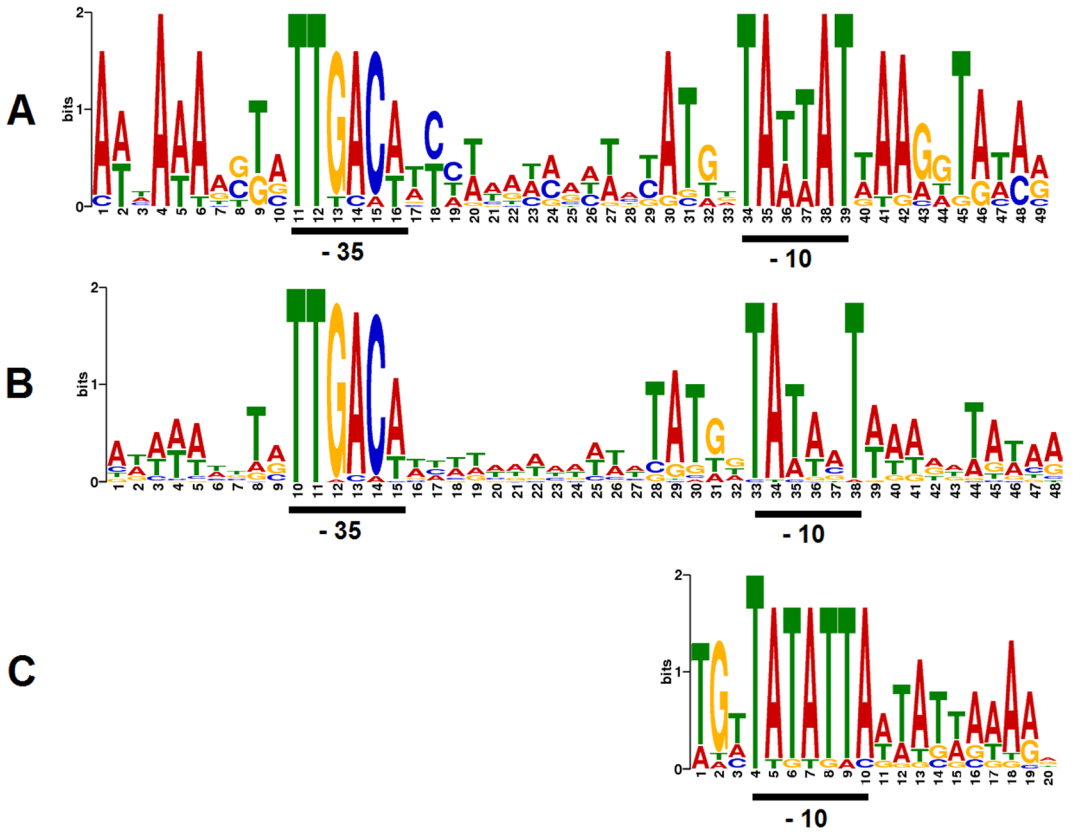

Figure 5. Sequence logos of phage 812 promoters. (**A**) Bacterial promoters in long terminal repeats contain typical −35 and −10 sequences. (**B**) Putative early promoters recognised by host sigma factor. (**C**) Putative late promoters recognised by phage sigma factor. The late promoters drive the transcription of genes for homing endonuclease in long terminal repeat and in the polymerase gene intron, and genes for packaging, the structure of the head, tail and baseplate, and lysis. No conserved −35 sequence was found in phage late promoters.

of tandem repeats in the variable right terminus as a characteristic feature of *Kayvirus* genomes, which probably plays a significant role in replication and packaging[35].

Compared to phage 812, host-range mutant 812h1 exhibited differences in both the genes for RBPs, while in the 812a-derived mutants they were only in one of them (*orf123*). As recently described for bacteriophage SA012, RBP encoded by a gene homologous to *orf125* of phage 812 seems to play an essential role in binding onto the backbone of wall teichoic acids (WTA); the additional binding of RBP encoded by a gene homologous to *orf123* of phage 812 to N-acetyl-α-D-glucosamine (α-GlcNAc) of WTA is required for the effective infection of some phages[34]. In kayviruses, the homologs of the α-GlcNAc-binding RBPs exhibit higher variability than WTA-backbone-binding RBPs, which indicates that they determine the host specificity.

Phages suitable for therapy should not contain genes for the lysogenic life cycle, such as genes for integrases and those for virulence or drug resistance factors, which could be horizontally transferred into the genome of the bacterial host[8,9,31]. A recent comparison of the complete genomes of myoviruses, including 14 kayviruses, proved that they are all strictly lytic and do not carry antibiotic resistance or bacterial virulence genes[36]. Except for the non-spontaneous T4 mutants[37,38], the potential of bacterial gene transduction has not been reported for the strictly virulent phages, some of which even break down the bacterial DNA to generate the building blocks required for the synthesis of progeny DNA[39]. The genomes of these phages feature specific gene products involved in nucleotide metabolism, such as ribonucleotide reductase subunits. It has been shown that the genes for Nrd are host-like auxiliary metabolic genes promoting phage replication[40]. Importantly, the above safety requirements hold for phage 812 and all its host-range mutants described in this paper. Therefore, a shorter assessment time frame, similar to that of the influenza vaccine, should be considered with regard to the data which indicate that bacteriophage strain replacement or addition has no impact on the safety of the preparation[10].

The results of our study help to clarify the molecular basis of differences in phage lytic properties. These findings also contribute to a better understanding of *Kayvirus* genomics and to establishing the rules for updating phage preparations. During commercial phage production, confirmation of the phage identity including its genome consistency is required from the master seed lots to the final products[9]. Since the genomic sequences of host-range phage mutants are almost identical, sequencing PCR amplicons of the most variable regions could distinguish the phages in commercial products from different companies. Alternatively, phage mutants can be distinguished using a multiplex PCR assay designed to target sequences specific for individual phage mutants (Supplementary Fig. S2). Nevertheless, it is necessary to determine the level of acceptable genome variability between the phage master seed lots and the final products. Our results show that the emergence of genomic

ORF of phage 812	Size (nt)	Gene product	Proposed function	Number of fixed SNP or DIP	Mutations in 812a	Number of amino-acid substitutions (sub) and insertions (ins)
orf89	1188	membrane-associated protein	packaging	1	—	2 ins
orf102	1764	tail sheath protein	genome ejection	5	—	5 sub
orf103	426	tail tube protein	genome ejection	0	intron loss	1 sub, 1 ins
orf104	1404	putative intron nuclease	intron homing	—	gene deletion	
orf105	141	hypothetical protein	tail assembly	4	2 nt sub	3 sub
orf110	537	tail morphogenetic protein	tail assembly	6	—	2 sub
orf111	4059	tape measure protein	tail assembly	20	—	6 sub
orf112	2427	tail murein hydrolase	penetration	1	—	1 sub
orf113	888	cysteine protease	penetration	1	—	1 sub
orf114	2547	tail central spike	penetration	1	—	1 sub
orf116	525	baseplate component	adsorption	1	—	1 sub
orf119	3060	tail fiber complex	adsorption	1	1 nt sub	2 sub[1]
orf121	3459	adsorption-associated protein	adsorption	1	—	1 sub
orf123	1923	receptor-binding protein	adsorption	3	—	3 sub
orf135	453	hypothetical protein	DNA metabolism	2	—	2 sub
orf138	2115	ribonucleotide reductase	DNA metabolism	6	—	3 sub
orf141	321	oxidoreductase	DNA metabolism	2	—	1 sub
orf144	3219	DNA polymerase	DNA metabolism	1	—	1 sub
orf154	522	putative capsid component	head assembly	1	—	1 sub
orf167	459	putative structural protein	virion assembly	1	—	1 sub
orf189	294	putative regulatory protein	regulation	0	456-nt deletion	fusion of *orf189* and *orf192*
orf190	288	membrane-associated protein	regulation	0		
orf191	117	putative transcription factor	regulation	0		
orf192	264	membrane-associated protein	regulation	0		

Table 1. Single-nucleotide polymorphisms (SNP) and deletion/insertion polymorphisms (DIP) in phage 812 genome fixed in 812a and its derived mutants 812F1, 812K1, and 812K1/420 and new mutations occurred in 812a. Only genome changes with impact on protein sequences are listed. [1]In phage 812K1/420 a premature stop-codon, due to a 77-nt deletion and 1-nt substitution, split the gene.

alterations in therapeutic phages is a naturally occurring process beneficial for rapidly gaining new host-range mutants. Importantly, we showed that the phage mutants have no undesirable gene acquisitions with impact on the safety of phage therapeutics.

Materials and Methods

Bacterial strains. 186 MRSA strains of various origin (Supplementary Table 1) were obtained from the National Reference Laboratory for Antibiotics and National Reference Laboratory for Staphylococci (National Institute of Public Health, Prague, Czech Republic), University Hospital Brno (Czech Republic), and farm livestock and the environment from different locations in the Czech Republic, deposited in the collection of the Bacteriology Department (Veterinary Research Institute, Brno, Czech Republic). Propagating *S. aureus* strains CCM 4028 and CCM 8428 were provided by the Czech Collection of Microorganisms (Masaryk University, Brno, Czech Republic). Strain RN4220 was obtained from Prof. F. Götz (University of Tübingen, Germany). Strain COL was kindly provided by Prof. Hermínia de Lencastre (Universidade Nova de Lisboa, Portugal and The Rockefeller University, New York, NY). Other propagating and selection strains were isolated in this or earlier studies[1] and are genotypically characterized below. Propagation strain CAPM 6630 for phage 812h1 was deposited in the Collection of Animal Pathogenic Microorganisms (Veterinary Research Institute, Brno, Czech Republic).

Genotyping of *S. aureus* strains. All strains were genotypically characterized using multi-locus sequence typing (MLST) according to Enright *et al.*[41] and *spa*-typing according to the Ridom StaphType standard protocol (www.ridom.org). The software package Ridom StaphType v2.2.1 (Ridom, Germany) was used for *spa*-type assignment. Clonal complex analysis was performed with eBURST v3[42]. All strains were tested for the *mecA* gene as described previously[43]. The prophage content in propagating and selection strains was investigated by multiplex PCR assay[44].

Phages, selection and propagation. Bacteriophage K was obtained from Dr. Christiane Wolz (University of Tübingen, Germany). Phage 812 was described previously[1]. Phages designated Stafal, Pyophage, and StaphPhage were isolated from the commercial therapeutic preparations Stafal (Bohemia Pharmaceuticals, Czech Republic), PyoPhage (Eliava Biopreparations, Georgia), and Staphylococcal bacteriophage liquid (Microgen, Russia), respectively, and propagated on strain CCM 8428 as described previously[45]. Phages 812 and 812h1 were deposited in the Czech Collection of Microorganisms under accession number CCM 7911 and in the Collection

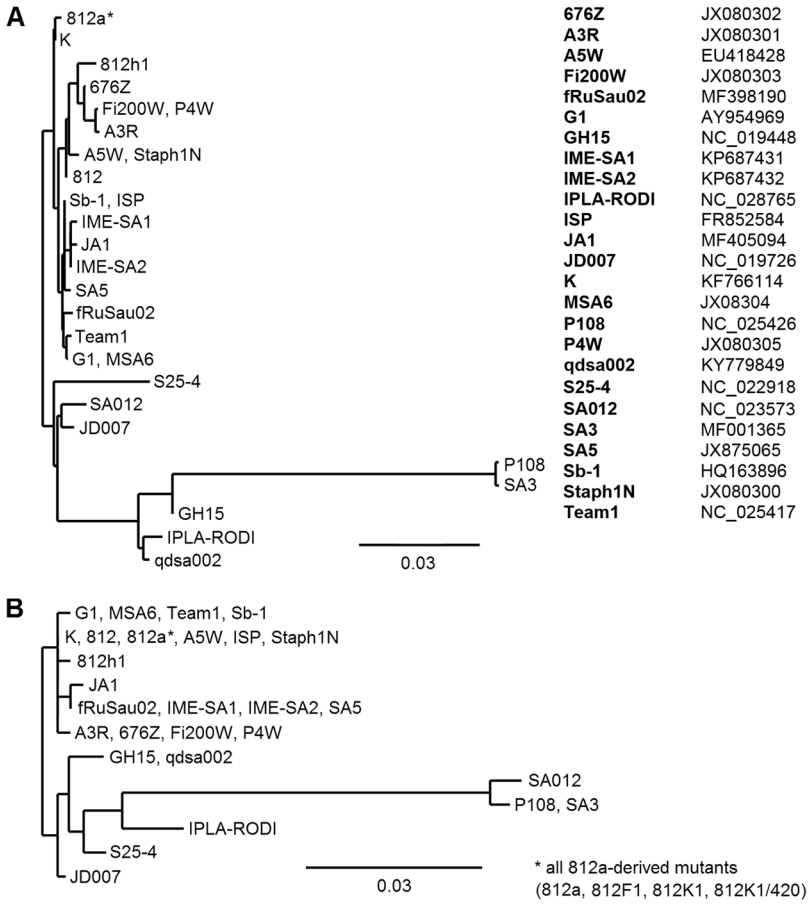

Figure 6. Unrooted phylogenetic trees showing similarity of two *Kayvirus* receptor binding proteins homologous to (**A**) protein encoded by phage 812 *orf123* and (**B**) protein encoded by phage 812 *orf125*. The phylogenetic trees were reconstructed using the maximum likelihood method (aLRT test) performed on the Phylogeny.fr platform. GenBank accession numbers of the compared phage genomes are listed next to the trees. The trees are drawn to scale, with branch lengths measured in the number of substitutions per site.

of Animal Pathogenic Microorganisms under accession number CAPM V-689, respectively. Phage 812K1/420 was patented for treating human MRSA infections[46].

Phage 812 was propagated using stock lysate. After the seeding of the parental phage with a strain resistant to this phage (selection strain) into 0.7% meat-peptone soft agar overlaid on 1.5% meat peptone agar (MPA) plates, individual rare plaques of the mutant phages were picked into 0.1 ml of a liquid medium, meat-peptone broth (MPB), prepared from 13 g of nutrient broth (Oxoid, CM0001), 3 g of yeast extract (Oxoid, LP0021), and 5 g of peptone (Oxoid, LP0037) dissolved in distilled water to a volume of 1000 ml (pH 7.4). Suspensions were purified through a 0.45 µm OlimPeak nylon filter (Teknokroma, Barcelona, Spain) to remove the remaining bacterial cells. Phage mutant 812a was derived from the wild-type phage 812 by selection on *S. aureus* strain NCTC 8511 (ST254, t118) laboratory lysogenized by phage ϕ53[47]. The mutant 812a served as a parental phage to produce the mutants 812K1 and 812F1 isolated on *S. aureus* strains FN34 (ST5, t002) and FN4 (ST1021, t11517), respectively[1]. Phage mutant 812K1/420 was derived from phage 812K1 by selection on human MRSA strain NRL Atb 420 (ST5, t179). Phage 812h1 was selected on MRSA strain 1098 (ST8, t064) from mutant 812h which was selected from phage 812 on MSSA strain 347 (ST5, t002).

Large-scale phage propagation on *S. aureus* strains was performed in 250 ml MPB with aeration. The phages 812, 812a, 812F1, and 812K1 were propagated on strain CCM 4028 (ST30, t021). Phage 812K1/420 was propagated on prophage-less strain CCM 8428 (ST30, t021). Phage 812h1 was propagated on prophage-less MSSA strain CAPM 6630 (ST6, t304). To prove the genetic stability of the obtained phage mutants and to exclude the possibility of phage DNA modification, the phage lytic activity was tested on the selection strain after passaging on the propagation strain, and the efficiency of plating (EOP) was determined. EOP was calculated by dividing the phage titer obtained on selection strains by the phage titer on the propagating strain[1].

Phage susceptibility testing. *S. aureus* strains were grown in MPB to the logarithmic phase at 37 °C. Meat peptone agar plates (1,5% agar) with 2 mM $CaCl_2$ were flooded with the broth culture, drained, and dried. The phage lysates of titer of 10^9 plaque forming units (PFU) per ml were diluted 10^{-2} (i.e. 10^7 PFU/ml) and 10^{-4} (i.e. 10^5 PFU/ml) and applied in triplicate for both the dilutions by spotting 10 µl aliquots onto soft agar lawns

inoculated with tested *S. aureus* strain. Plates were incubated overnight at 37 °C. Then the results were evaluated (Supplementary Fig. S3). If single plaques appeared, the strain was considered susceptible (Supplementary Fig. S3A). If no plaques appeared in any dilution, the strain was considered phage-resistant (Supplementary Fig. S3B).

Phage genome sequencing and analysis. Phenol/chloroform extraction of DNA was performed according to Sambrook *et al.*[48]. The procedure was modified so that Phase Lock Gel tubes (5 PRIME, Hamburg, Germany) were used for separating the aqueous and organic phases. The complete nucleotide sequences (30 to 50-fold coverage) of bacteriophages 812a, 812K1, 812F1, and 812K1/420 were determined using the GS Junior system (Roche, 454 Life Science, USA) according to a previous study[49]. The genomes of phages 812 and 812h1 were determined using the MiSEQ system (Illumina, USA) according to Botka *et al.*[50]. The reads were assembled using the A5-miseq pipeline[51]. The genomes were covered, on average, 2272-fold in phage 812 and 3076-fold in phage 812h1. Sequence gaps were closed using PCR and primer walking. Amplified PCR products were purified using a QIAquick PCR Purification kit (Qiagen, Netherlands) and sequenced by Eurofins MWG Operon (Germany). The same approach was used for PCR assays to verify extensive DIPs of phage 812h1 and to analyse tandem repeat regions. Primers and polymerase chain reaction conditions for differentiation of the phage 812-derived mutants are described in Supplementary Table S6.

The GenBank (NCBI) accession numbers of the phage genomes are as follows: updated genome of phage 812 (MH844528), and genomes of phages 812a (KJ206560), 812K1 (KJ206561), 812F1 (KJ206562), 812K1/420 (KJ206563), and 812h1 (MH844529).

Variations in the genomes obtained with the MiSEQ system were detected using CLC Genomic Workbench v3.6.5 (Qiagen Bioinformatics, Denmark) by analysing the set of pair-end reads aligned to the genome sequence under the following conditions: coverage of reads $\geq$90% and identity $\geq$90%, ignoring non-specific matches. To exclude sequencing errors, only the SNPs and DIPs with at least 10% frequency and, at the same time, a minimum of 30-fold coverage in low-coverage parts were considered. The quality conditions were as follows: quality of central base and average quality of surrounding bases $\geq$Q30. DNA samples were verified by multiplex PCR assay (Supplementary Table S6) to exclude cross-contamination.

Taking into account that the redundant regions exhibit multiplied coverage compared to the rest of the genomes[35], the long terminal repeats were predicted based on a significant change in the MiSEQ read number of the alignments. Open reading frames (ORFs) were identified using GeneMarkS, optimized for phage sequences (http://exon.gatech.edu) and inspected manually. Genomes were annotated using RAST[52], Phobius (http://phobius.sbc.su.se), and BLAST (http://blast.ncbi.nlm.nih.gov/). The EMBOSS tools Needle and Stretcher (https://www.ebi.ac.uk/) were used for pairwise sequence comparisons. The tRNA genes were identified using tRNAscan-SE[53] and RAST. To predict promoters specific for the host and phage sigma factors, 200-bp sequences upstream of start codons were investigated using GLAM2 v.5.0.2 from MEME Suite[54] and BPROM[55], with only the promoters that reached an overall score (LDF) above 5 being considered. Only one promoter per transcription unit was taken into account. ARNold[56] was applied to Rho-independent terminator identification. Only the predicted terminators with a dG value of less than −7.0 kcal/mol and a functional position were taken into consideration. The genome maps were constructed using GCView[57]. The ARDB[58] and VFDB[59] databases were used to search for antibiotic resistance and virulence factor genes. Parameters for ARDB searching were as follows: blastp program, complete database of resistance genes, 40% identity, and an E-value of 0.0001. Parameters for VFDB searching were as follows: tblastn program, using whole phage sequences against DNA sequences from the VFDB datasets A and B. Phylogenetic trees were constructed using the maximum likelihood method (aLRT test) performed in the on-line tool Phylogeny.fr[60]. Genomic sequences of related phages ISP (FR852584), fRuSau02 (MF398190), JD007 (NC_019726), Staph1N (JX080300), A3R (JX080301), 676Z (JX080302), Fi200W (JX080303), P4W (JX080305), K (KF766114), SA012 (NC_023573), G1 (AY954969), IME-SA1 (KP687431), IME-SA2 (KP687432), GH15 (NC_019448), JA1 (MF405094), IPLA-RODI (NC_028765), S25-4 (NC_022918), SA3 (MF001365), SA5 (JX875065), Sb-1 (HQ163896), Team1 (NC_025417), A5W (EU418428), P108 (NC_025426), and qdsa002 (KY779849)[2–4,6,20,23,32,33,34,61–67] were retrieved from the NCBI Nucleotide database (https://www.ncbi.nlm.nih.gov/nucleotide).

qPCR quantification of bacterial genes *blaZ*, *tetK* and *mecA* inside phage particles. Phages K, 812K1/420, PyoPhage and 80α were propagated on MRSA strains COL (pT181) and USA300 08/019 (pUSA-Houmr-like)[68], and the strain RN4220 with plasmids pT181 and pUSA-Houmr-like prepared in this study. Extraction of phage DNA including DNase treatment was performed as described previously[69]. A LightCycler 480 Instrument II (Roche) was used for qPCR performed according to Mašlaňová *et al.*[69]. Reactions were carried out in triplicates in optical 96-well reaction plates. Each reaction mixture (25 µl) contained 12.5 µl LightCycler 480 SYBR Green I Master (Roche), 300 µM of each primer (Supplementary Table S5) and 25 ng of template DNA in a volume of 2.5 µl. Genes encoding distinctive siphoviral and myoviral structural proteins[44] were used as a reference.

Data Availability

All data generated or analysed during this study are included in this published article (and its Supplementary files), or the relevant depository/collection/database is indicated in Materials and Methods. The large datasets (qPCR, raw sequence data) generated during and/or analysed during the current study are available from the corresponding author on request.

References

1. Pantůček, R. *et al*. The polyvalent staphylococcal phage phi 812: its host-range mutants and related phages. *Virology* **246**, 241–252, https://doi.org/10.1006/viro.1998.9203 (1998).
2. Vandersteegen, K. *et al*. Microbiological and molecular assessment of bacteriophage ISP for the control of *Staphylococcus aureus*. *PLoS One* **6**, e24418, https://doi.org/10.1371/journal.pone.0024418 (2011).
3. Leskinen, K. *et al*. Characterization of vB_SauM-fRuSau02, a Twort-like bacteriophage isolated from a therapeutic phage cocktail. *Viruses* **9**, 258, https://doi.org/10.3390/v9090258 (2017).
4. Kvachadze, L. *et al*. Evaluation of lytic activity of staphylococcal bacteriophage Sb-1 against freshly isolated clinical pathogens. *Microb Biotechnol* **4**, 643–650, https://doi.org/10.1111/j.1751-7915.2011.00259.x (2011).
5. Synnott, A. J. *et al*. Isolation from sewage influent and characterization of novel *Staphylococcus aureus* bacteriophages with wide host ranges and potent lytic capabilities. *Appl Environ Microbiol* **75**, 4483–4490, https://doi.org/10.1128/AEM.02641-08 (2009).
6. Cui, Z. *et al*. Characterization and complete genome of the virulent *Myoviridae* phage JD007 active against a variety of *Staphylococcus aureus* isolates from different hospitals in Shanghai, China. *Virol J* **14**, 26, https://doi.org/10.1186/s12985-017-0701-0 (2017).
7. Abatángelo, V. *et al*. Broad-range lytic bacteriophages that kill *Staphylococcus aureus* local field strains. *PLoS One* **12**, e0181671, https://doi.org/10.1371/journal.pone.0181671 (2017).
8. Rohde, C. *et al*. Expert opinion on three phage therapy related topics: bacterial phage resistance, phage training and prophages in bacterial production strains. *Viruses* **10**, 178, https://doi.org/10.3390/v10040178 (2018).
9. Pirnay, J.-P. *et al*. Quality and safety requirements for sustainable phage therapy products. *Pharm Res* **32**, 2173–2179, https://doi.org/10.1007/s11095-014-1617-7 (2015).
10. Pelfrene, E., Willebrand, E., Cavaleiro Sanches, A., Sebris, Z. & Cavaleri, M. Bacteriophage therapy: a regulatory perspective. *J Antimicrob Chemother* **71**, 2071–2074, https://doi.org/10.1093/jac/dkw083 (2016).
11. Enav, H., Kirzner, S., Lindell, D., Mandel-Gutfreund, Y. & Béjà, O. Adaptation to sub-optimal hosts is a driver of viral diversification in the ocean. *Nat Commun* **9**, 4698, https://doi.org/10.1038/s41467-018-07164-3 (2018).
12. Brüssow, H. Population Genomics of Bacteriophages in *Population Genomics: Microorganisms* (eds Polz, M. F. & Rajora, O. P.) 297–334, https://doi.org/10.1007/13836_2018_16 (Springer, 2019).
13. Magill, D. J. *et al*. Localised genetic heterogeneity provides a novel mode of evolution in dsDNA phages. *Sci Rep* **7**, 13731, https://doi.org/10.1038/s41598-017-14285-0 (2017).
14. Essoh, C. *et al*. Investigation of a large collection of *Pseudomonas aeruginosa* bacteriophages collected from a single environmental source in Abidjan, Côte d'Ivoire. *PLoS One* **10**, e0130548, https://doi.org/10.1371/journal.pone.0130548 (2015).
15. Moreno Switt, A. I. *et al*. Genomic characterization provides new insight into *Salmonella* phage diversity. *BMC Genomics* **14**, 481, https://doi.org/10.1186/1471-2164-14-481 (2013).
16. Meyer, J. R. *et al*. Repeatability and contingency in the evolution of a key innovation in phage Lambda. *Science* **335**, 428–432, https://doi.org/10.1126/science.1214449 (2012).
17. Paez-Espino, D. *et al*. CRISPR immunity drives rapid phage genome evolution in *Streptococcus thermophilus*. *mBio* **6**, e00262–15, https://doi.org/10.1128/mBio.00262-15 (2015).
18. O'Flaherty, S. *et al*. Genome of staphylococcal phage K: a new lineage of *Myoviridae* infecting gram-positive bacteria with a low G+C content. *J Bacteriol* **186**, 2862–2871, https://doi.org/10.1128/JB.186.9.2862-2871.2004 (2004).
19. O'Flaherty, S. *et al*. Potential of the polyvalent anti-*Staphylococcus* bacteriophage K for control of antibiotic-resistant staphylococci from hospitals. *Appl Environ Microbiol* **71**, 1836–1842, https://doi.org/10.1128/AEM.71.4.1836-1842.2005 (2005).
20. Łobocka, M. *et al*. Genomics of staphylococcal Twort-like phages-potential therapeutics of the post-antibiotic era. *Adv Virus Res* **83**, 143–216, https://doi.org/10.1016/B978-0-12-394438-2.00005-0 (2012).
21. Stewart, C. R., Yip, T. K. S., Myles, B. & Laughlin, L. Roles of genes 38, 39, and 40 in shutoff of host biosyntheses during infection of *Bacillus subtilis* by bacteriophage SPO1. *Virology* **392**, 271–274, https://doi.org/10.1016/j.virol.2009.06.046 (2009).
22. Stewart, C. R., Deery, W. J., Egan, E. S. K., Myles, B. & Petti, A. A. The product of SPO1 gene 56 inhibits host cell division during infection of *Bacillus subtilis* by bacteriophage SPO1. *Virology* **447**, 249–253, https://doi.org/10.1016/j.virol.2013.09.005 (2013).
23. Gill, J. J. Revised genome sequence of *Staphylococcus aureus* bacteriophage K. *Genome Announc* **2**, e01173–13, https://doi.org/10.1128/genomeA.01173-13 (2014).
24. Lavigne, R. & Vandersteegen, K. Group I introns in *Staphylococcus* bacteriophages. *Future Virol* **8**, 997–1005, https://doi.org/10.2217/fvl.13.84 (2013).
25. Gu, J. *et al*. Genomic characterization of lytic *Staphylococcus aureus* phage GH15: providing new clues to intron shift in phages. *J Gen Virol* **94**, 906–915, https://doi.org/10.1099/vir.0.049197-0 (2013).
26. Benešík, M. *et al*. Role of SH3b binding domain in a natural deletion mutant of *Kayvirus* endolysin LysF1 with a broad range of lytic activity. *Virus Genes* **54**, 130–139, https://doi.org/10.1007/s11262-017-1507-2 (2018).
27. Kašpárek, P., Pantůček, R., Kahánková, J., Růžičková, V. & Doškař, J. Genome rearrangements in host-range mutants of the polyvalent staphylococcal bacteriophage 812. *Folia Microbiol* **52**, 331–338, https://doi.org/10.1007/BF02932087 (2007).
28. Rosypal, S., Rosypalová, A., Doškař, J., Pakrová, E. & Genovová, S. The use of the polyvalent phage 812 and its host-range mutants to the differentiation of *Staphylococcus aureus* from other staphylococci. *Scripta Fac Sci Nat Univ Purk Brun* **16**, 317–336 (1986).
29. Nováček, J. *et al*. Structure and genome release of Twort-like *Myoviridae* phage with a double-layered baseplate. *Proc Natl Acad Sci USA* **113**, 9351–9356, https://doi.org/10.1073/pnas.1605883113 (2016).
30. Eyer, L. *et al*. Structural protein analysis of the polyvalent staphylococcal bacteriophage 812. *Proteomics* **7**, 64–72, https://doi.org/10.1002/pmic.200600280 (2007).
31. Sybesma, W., Pirnay, J.-P. & Expert round table on acceptance and re-implementation of bacteriophage therapy. Silk route to the acceptance and re-implementation of bacteriophage therapy. *Biotechnol J.* **11**, 595–600, https://doi.org/10.1002/biot.201600023 (2016).
32. Kwan, T., Liu, J., DuBow, M., Gros, P. & Pelletier, J. The complete genomes and proteomes of 27 *Staphylococcus aureus* bacteriophages. *Proc Natl Acad Sci USA* **102**, 5174–5179, https://doi.org/10.1073/pnas.0501140102 (2005).
33. Takeuchi, I. *et al*. The presence of two receptor-binding proteins contributes to the wide host range of staphylococcal Twort-like phages. *Appl Environ Microbiol* **82**, 5763–5774, https://doi.org/10.1128/AEM.01385-16 (2016).
34. Azam, A. H., Hoshiga, F., Takeuchi, I., Miyanaga, K. & Tanji, Y. Analysis of phage resistance in *Staphylococcus aureus* SA003 reveals different binding mechanisms for the closely related Twort-like phages ϕSA012 and ϕSA039. *Appl Microbiol Biotechnol* **102**, 8963–8977, https://doi.org/10.1007/s00253-018-9269-x (2018).
35. Zhang, X. *et al*. Conserved termini and adjacent variable region of *Twortlikevirus Staphylococcus* phages. *Virol Sin* **30**, 433–440, https://doi.org/10.1007/s12250-015-3643-y (2015).
36. Cui, Z. *et al*. Safety assessment of *Staphylococcus* phages of the family *Myoviridae* based on complete genome sequences. *Sci Rep* **7**, 41259, https://doi.org/10.1038/srep41259 (2017).
37. Wilson, G. G., Young, K. K. Y., Edlin, G. J. & Konigsberg, W. High-frequency generalised transduction by bacteriophage T4. *Nature* **280**, 80–82, https://doi.org/10.1038/280080a0 (1979).
38. Young, K. K., Edlin, G. J. & Wilson, G. G. Genetic analysis of bacteriophage T4 transducing bacteriophages. *J Virol* **41**, 345–347 (1982).

39. Carlton, R. M., Noordman, W. H., Biswas, B., de Meester, E. D. & Loessner, M. J. Bacteriophage P100 for control of *Listeria monocytogenes* in foods: genome sequence, bioinformatic analyses, oral toxicity study, and application. *Regul Toxicol Pharmacol* **43**, 301–312, https://doi.org/10.1016/j.yrtph.2005.08.005 (2005).
40. Dwivedi, B., Xue, B., Lundin, D., Edwards, R. A. & Breitbart, M. A bioinformatic analysis of ribonucleotide reductase genes in phage genomes and metagenomes. *BMC Evol Biol* **13**, 33, https://doi.org/10.1186/1471-2148-13-33 (2013).
41. Enright, M. C., Day, N. P., Davies, C. E., Peacock, S. J. & Spratt, B. G. Multilocus sequence typing for characterization of methicillin-resistant and methicillin-susceptible clones of *Staphylococcus aureus*. *J Clin Microbiol* **38**, 1008–1015 (2000).
42. Feil, E. J., Li, B. C., Aanensen, D. M., Hanage, W. P. & Spratt, B. G. eBURST: inferring patterns of evolutionary descent among clusters of related bacterial genotypes from multilocus sequence typing data. *J Bacteriol* **186**, 1518–1530, https://doi.org/10.1128/JB.186.5.1518-1530.2004 (2004).
43. Milheiriço, C., Oliveira, D. C. & de Lencastre, H. Update to the multiplex PCR strategy for assignment of mec element types in *Staphylococcus aureus*. *Antimicrob Agents Chemother* **51**, 3374–3377, https://doi.org/10.1128/AAC.00275-07 (2007).
44. Pantůček, R. *et al*. Identification of bacteriophage types and their carriage in *Staphylococcus aureus*. *Arch Virol* **149**, 1689–1703, https://doi.org/10.1007/s00705-004-0335-6 (2004).
45. Štveráková, D. *et al*. Rapid identification of intact staphylococcal bacteriophages using matrix-assisted laser desorption ionization-time-of-flight mass spectrometry. *Viruses* **10**, 176, https://doi.org/10.3390/v10040176 (2018).
46. Moša, M., Boštík, J., Pantůček, R. & Doškař, J. Medicament in the form of anti-*Staphylococcus* phage lysate, process of its preparation and use. CZ201200668-A3. Patent Application (2012).
47. Rosypal, S. & Rosypalová, A. A spontaneus mutant of polyvalent phage 812 capable of growth in *Staphylococcus aureus* NCTC 8511 carrying prophage 53. *Folia Fac Sci Nat Univ Purk Brun* **11**, 37–47 (1970).
48. Sambrook, J., Fritsch, E. F. & Maniatis, T. *Molecular cloning: a laboratory manual*. 2nd ed., (Cold Spring Harbor Laboratory, 1989).
49. Botka, T. *et al*. Complete genome analysis of two new bacteriophages isolated from impetigo strains of *Staphylococcus aureus*. *Virus Genes* **51**, 122–131, https://doi.org/10.1007/s11262-015-1223-8 (2015).
50. Botka, T. *et al*. Two highly divergent lineages of exfoliative toxin B-encoding plasmids revealed in impetigo strains of *Staphylococcus aureus*. *Int J Med Microbiol* **307**, 291–296, https://doi.org/10.1016/j.ijmm.2017.05.005 (2017).
51. Coil, D., Jospin, G. & Darling, A. E. A5-miseq: an updated pipeline to assemble microbial genomes from Illumina MiSeq data. *Bioinformatics* **31**, 587–589, https://doi.org/10.1093/bioinformatics/btu661 (2015).
52. Brettin, T. *et al*. RASTtk: A modular and extensible implementation of the RAST algorithm for building custom annotation pipelines and annotating batches of genomes. *Sci Rep* **5**, 8365, https://doi.org/10.1038/srep08365 (2015).
53. Lowe, T. M. & Chan, P. P. tRNAscan-SE On-line: integrating search and context for analysis of transfer RNA genes. *Nucleic Acids Res* **44**, W54–W57, https://doi.org/10.1093/nar/gkw413 (2016).
54. Frith, M. C., Saunders, N. F. W., Kobe, B. & Bailey, T. L. Discovering Sequence Motifs with Arbitrary Insertions and Deletions. *PLoS Computational Biology* **4**, e1000071, https://doi.org/10.1371/journal.pcbi.1000071 (2008).
55. Solovyev, V. & Salamov, A. Automatic annotation of microbial genomes and metagenomic sequences in *Metagenomics and its applications in agriculture, biomedicine and environmental studies* (ed. Li, R. W.) 61–78 (Nova Science Publishers, 2011).
56. Lesnik, E. A. *et al*. Prediction of rho-independent transcriptional terminators in *Escherichia coli*. *Nucleic Acids Res* **29**, 3583–3594, https://doi.org/10.1093/nar/29.17.3583 (2001).
57. Grant, J. R. & Stothard, P. The CGView Server: a comparative genomics tool for circular genomes. *Nucleic Acids Res* **36**, W181–W184, https://doi.org/10.1093/nar/gkn179 (2008).
58. Liu, B. & Pop, M. ARDB-Antibiotic Resistance Genes Database. *Nucleic Acids Res* **37**, D443–D447, https://doi.org/10.1093/nar/gkn656 (2009).
59. Chen, L., Zheng, D., Liu, B., Yang, J. & Jin, Q. VFDB 2016: hierarchical and refined dataset for big data analysis-10 years on. *Nucleic Acids Res* **44**, D694–D697, https://doi.org/10.1093/nar/gkv1239 (2016).
60. Dereeper, A. *et al*. Phylogeny.fr: robust phylogenetic analysis for the non-specialist. *Nucleic Acids Res* **36**, W465–W469, https://doi.org/10.1093/nar/gkn180 (2008).
61. Gu, J. *et al*. Complete genome sequence of *Staphylococcus aureus* bacteriophage GH15. *J Virol* **86**, 8914–8915, https://doi.org/10.1128/JVI.01313-12 (2012).
62. Ajuebor, J. *et al*. Comparison of *Staphylococcus* phage K with close phage relatives commonly employed in phage therapeutics. *Antibiotics (Basel)*. **7**, 37, https://doi.org/10.3390/antibiotics7020037 (2018).
63. Gutiérrez, D. *et al*. Two phages, phiIPLA-RODI and phiIPLA-C1C, lyse mono- and dual-species staphylococcal biofilms. *Appl Environ Microbiol* **81**, 3336–3348, https://doi.org/10.1128/AEM.03560-14 (2015).
64. Takemura-Uchiyama, I. *et al*. Genomic and phylogenetic traits of *Staphylococcus* phages S25-3 and S25-4 (family *Myoviridae*, genus Twort-like viruses). *Ann Microbiol* **64**, 1453–1456, https://doi.org/10.1007/s13213-013-0762-2 (2014).
65. Kim, S. G. *et al*. Complete genome sequence of *Staphylococcus aureus* bacteriophage pSa-3. *Genome Announc* **5**, e00182–17, https://doi.org/10.1128/genomeA.00182-17 (2017).
66. Kirby, A. E. Synergistic action of gentamicin and bacteriophage in a continuous culture population of *Staphylococcus aureus*. *PLoS One* **7**, e51017, https://doi.org/10.1371/journal.pone.0051017 (2012).
67. El Haddad, L. *et al*. Improving the safety of *Staphylococcus aureus* polyvalent phages by their production on a *Staphylococcus xylosus* strain. *PLoS One* **9**, e102600, https://doi.org/10.1371/journal.pone.0102600 (2014).
68. Varga, M. *et al*. Efficient transfer of antibiotic resistance plasmids by transduction within methicillin-resistant *Staphylococcus aureus* USA300 clone. *FEMS Microbiol Lett* **332**, 146–152, https://doi.org/10.1111/j.1574-6968.2012.02589.x (2012).
69. Mašlaňová, I. *et al*. Bacteriophages of *Staphylococcus aureus* efficiently package various bacterial genes and mobile genetic elements including *SCCmec* with different frequencies. *Environ Microbiol Rep* **5**, 66–73, https://doi.org/10.1111/j.1758-2229.2012.00378.x (2013).

Acknowledgements

The authors would like to thank their colleagues from the participating hospitals for providing the *S. aureus* strains. Thanks are also due to Ms. Eva Kodytková and Dr. Marta Fridrichová (National Institute of Public Health, Prague), Dr. Petra Vídeňská (Veterinary Research Institute, Brno), and Dr. Jiří Jarkovský (Institute of Biostatistics and Analyses at the Masaryk University, Brno) for valuable help. This work was supported by grants from the Czech Science Foundation (18-13064S), Ministry of Agriculture of the Czech Republic (QJ1510216), Ministry of Health of the Czech Republic (16-29916A) and project AdmireVet CZ.1.05/2.1.00/01.0006-ED0006/01/01 from the Czech Ministry of Education, Youth and Sports of the Czech Republic.

Author Contributions

R.P., T.B., I.M., J.D. and V.R. conceived the experiments; T.B., I.M., M.B., P.P., P.H., I.K., M.F. and V.J. conducted the experiments; T.B., R.P., I.M., M.B., M.V., H.Ž. and R.K. analysed the data; T.B., R.P., J.D., V.R. and I.M. wrote the main manuscript; T.B. and R.P. prepared tables and figures. All authors reviewed the manuscript.

Additional Information

Supplementary information accompanies this paper at https://doi.org/10.1038/s41598-019-41868-w.

Competing Interests: The authors declare no competing interests.

Publisher's note: Springer Nature remains neutral with regard to jurisdictional claims in published maps and institutional affiliations.

Open Access This article is licensed under a Creative Commons Attribution 4.0 International License, which permits use, sharing, adaptation, distribution and reproduction in any medium or format, as long as you give appropriate credit to the original author(s) and the source, provide a link to the Creative Commons license, and indicate if changes were made. The images or other third party material in this article are included in the article's Creative Commons license, unless indicated otherwise in a credit line to the material. If material is not included in the article's Creative Commons license and your intended use is not permitted by statutory regulation or exceeds the permitted use, you will need to obtain permission directly from the copyright holder. To view a copy of this license, visit http://creativecommons.org/licenses/by/4.0/.

© The Author(s) 2019

APPENDIX 15

Fišarová L, Pantůček R, Botka T, Doškař J (2019) Variability of resistance plasmids in coagulase-negative staphylococci and their importance as a reservoir of antimicrobial resistance. *Research in Microbiology* 170:105–111.

https://doi.org/10.1016/j.resmic.2018.11.004

(JCR 2019: IF = 3.217; Q2 – Microbiology)

Reproduced with permission from the publisher. Copyright © 2019 Elsevier Masson SAS. All rights reserved.

Research in Microbiology 170 (2019) 105–111

Contents lists available at ScienceDirect

Research in Microbiology

journal homepage: www.elsevier.com/locate/resmic

Original Article

Variability of resistance plasmids in coagulase-negative staphylococci and their importance as a reservoir of antimicrobial resistance

Lenka Fišarová, Roman Pantůček, Tibor Botka, Jiří Doškař*

Masaryk University, Department of Experimental Biology, Kotlářská 2, 611 37 Brno, Czech Republic

ARTICLE INFO

Article history:
Received 15 August 2018
Accepted 22 November 2018
Available online 29 November 2018

Keywords:
Coagulase-negative staphylococci
Resistance plasmids
Antibiotics
Interspecies horizontal gene transfer
Electroporation

ABSTRACT

Coagulase-negative staphylococci (CoNS) are an important cause of human and animal diseases. Treatment of these diseases is complicated by their common antimicrobial resistance, caused by overuse of antibiotics in hospital and veterinary environment. Therefore, they are assumed to serve as a reservoir of resistance genes often located on plasmids. In this study, we analyzed plasmid content in 62 strains belonging to 10 CoNS species of human and veterinary origin. In 48 (77%) strains analyzed, 107 different plasmids were detected, and only some of them showed similarities with plasmids found previously. In total, seven different antimicrobial-resistance genes carried by plasmids were identified. Five of the CoNS staphylococci carried plasmids identical with either those of other CoNS species tested, or a well characterized *Staphylococcus aureus* strain COL, suggesting plasmid dissemination through horizontal transfer. To demonstrate the possibility of horizontal transfer, we performed electroporation of four resistance plasmids among *Staphylococcus epidermidis*, *Staphylococcus petrasii*, and coagulase-positive *S. aureus* strains. Plasmids were transferred unchanged, were stably maintained in recipient strains, and expressed resistance genes. Our work demonstrates a great variability of plasmids in human and veterinary staphylococcal strains and their ability to maintain and express resistance plasmids from other staphylococcal species.

© 2018 Institut Pasteur. Published by Elsevier Masson SAS. All rights reserved.

1. Introduction

CoNS are commonly found on the skin and mucous membranes of humans and animals, and many of them, for example *Staphylococcus epidermidis*, *Staphylococcus haemolyticus*, and *Staphylococcus petrasii*, are a significant cause of various diseases [1–3]. The most severe are usually nosocomial infections connected with biofilm formation on catheters, artificial body parts, and medical devices [4–7]. In the veterinary environment, the species like *Staphylococcus chromogenes* and *Staphylococcus warneri* are also a common cause of mastitis and contaminants of livestock products, food, and the environment [8,9]. A major drawback in the treatment and control of CoNS diseases is multidrug resistance, which is common in the majority of CoNS strains [10–13]. Genes conferring resistance to all classes of antibiotics have been detected in CoNS and are usually located on mobile genetic elements, which are able to transfer among different bacterial species and spread further. They have also been detected in potentially pathogenic strains belonging to species such as *S. epidermidis*, *S. haemolyticus*, and *Staphylococcus sciuri* [14]. Many works identify veterinary strains as a source of these genes for human pathogens because of common drug overuse in the veterinary environment [15–17].

The genes conferring resistance to various antibiotics, such as tetracyclines, amphenicols, macrolides, lincosamides and streptogramin, and aminoglycosides, have also been identified on staphylococcal plasmids [14]. Coagulase-positive and -negative staphylococcal strains carrying such plasmids have been isolated from hospital environment [18], veterinary facilities [19], and polluted water where multidrug resistant CoNS serve as a resistance gene reservoir [20]. Despite significant variability of staphylococcal plasmids, which is reflected in their classification into 15 incompatibility groups [21], the same plasmids have been detected in various species of staphylococci, even over a large geographical distance [22]. High similarity of plasmid DNA sequences, consistency of their structure, and common gene content suggest that plasmids are spread horizontally between strains in different environments.

Even though three mechanisms of horizontal transfer of plasmids are well described, the ways of such transfer among staphylococci in the natural environment still need to be clarified. Transfer of staphylococcal plasmids is best described in *Staphylococcus*

* Corresponding author.
E-mail addresses: lena.fisarova@seznam.cz (L. Fišarová), pantucek@mail.muni.cz (R. Pantůček), tibor.botka@mail.muni.cz (T. Botka), doskar@sci.muni.cz (J. Doškař).

https://doi.org/10.1016/j.resmic.2018.11.004
0923-2508/© 2018 Institut Pasteur. Published by Elsevier Masson SAS. All rights reserved.

aureus. Transduction appears to be common, and mostly small and middle sized plasmids are transferred this way [22]. During transduction, up to 45 kb of chromosomal or plasmid DNA is packaged into the transducing particles [23]. Phages ϕ11 and 80α have been frequently used as tools for transfer. Moreover, phage ϕ187 has been reported to transduce DNA among *S. aureus* strains, other staphylococci and even *Listeria* [24]. Recently, auto-transduction was discovered, during which phages spontaneously released from lysogenic cells infect, lyse, and transfer DNA from a phage-susceptible bacteria back to the lysogenic population [25]. Phages can also help to disseminate SaPIs, which they transfer with very high efficiency [26].

Larger plasmids can be transferred via conjugation, where DNA is delivered to the mating pore by the interaction of the coupling protein and relaxase which binds, cleaves and attaches to *oriT*, forming relaxasome [27]. Some plasmids can be mobilized by carrying sequences that mimic the *oriT* of a conjugative plasmid [28]. About three quarters of non-conjugative *S. aureus* plasmids can be mobilized by either this or the classical mechanism using their own *oriT* and relaxase [29]. The number of mobilizable plasmids can be even higher since in plasmids replicating by rolling-circle replication replicative relaxase (Rep) can act as a mobilization relaxase [23].

Important conjugative elements in staphylococci are ICEs (integrative conjugative elements). Two families of ICEs have been identified – Tn*916* and ICE*6013* [30]. They have a transfer and replication function and can mobilize small plasmids. Tn*916* is a prototypical ICE that has been found in both coagulase-positive and negative staphylococci [31,32]. These elements are common in staphylococci and can inhibit restriction/modification systems, thus facilitating HGT between different bacterial species and genera.

Natural transformation was not known in staphylococci until recently and occurs with a very low frequency [33]. Resistance plasmids are transferred *in vivo* at a higher rate during co-colonization of a host by various bacterial strains [34]. In coagulase-negative staphylococci, only very few cases of plasmid transfer have been described so far. Recent examples are plasmid transductions by *S. aureus* bacteriophage ϕ187 [35] or *S. sciuri* phages [36] into CoNS.

In this study, we characterized resistance plasmids in a representative set of human and veterinary CoNS strains and compared their structures and resistance determinants. In order to confirm that plasmids can be stably maintained in other staphylococcal species and can express resistance genes, electroporation of selected plasmids between species was performed. The work emphasizes the importance of CoNS as a source of resistance determinants and their potential to spread them among different staphylococcal species including human pathogens.

2. Materials and methods

2.1. Bacterial strains and growth media

In total, we analyzed 62 coagulase-negative staphylococcal strains: 12 strains of *S. petrasii*, six of *S. sciuri*, eight of *S. haemolyticus*, 11 of *S. epidermidis*, five of *S. warneri*, six of *S. chromogenes*, six of *Staphylococcus xylosus*, five of *Staphylococcus equorum*, two of *Staphylococcus simulans*, and one of *Staphylococcus caprae*. We also used two methicillin-resistant *S. aureus* strains for comparison. The strains which were resistant to antibiotics and, at the same time, contained plasmids are shown in Table 1. Human strains were isolated from various clinical specimens in 1993–2014 and veterinary strains were recovered at animal farms and during the processing of animal products in 2015–2017. MRSA strains originated from laboratories in Portugal (Universidade Nova de Lisboa, Oeiras; strain COL) and Brno (Veterinary Research Institute, strain S281). As positive controls for PCR, we used MRSA strains E14 and E19 from our laboratory collection. Staphylococci were grown in MPB (1.3% nutrient broth, 0.3% yeast extract, and 0.5% peptone) and on MPA agar plates (MPB with 1.5% agar), except *S. petrasii* strains which were cultured in 2YT (1.6% tryptone, 1% yeast extract, and 0.5% NaCl) and on 2YTA plates (2YT with 1.5% agar).

2.2. Antimicrobial resistance

Antimicrobial resistance was tested by disc diffusion method. We focused on antibiotic resistance where genes located on plasmids are known. For the significance of the resistance to methicillin and vancomycin in staphylococcal strains, we included these antibiotics despite usual location of the resistance genes on the chromosome. Resistance patterns of methicillin-resistant and - susceptible strains were compared to demonstrate a connection between methicillin resistance and multiresistance. Discs with chloramphenicol (30 μg), erythromycin (15 μg), tetracycline (30 μg), oxacillin (1 μg), ampicillin (10 μg), streptomycin (25 μg) and gentamicin (10 μg) were used. Vancomycin resistance was determined by adding the antibiotic into the growth medium as the disc diffusion method is unreliable in this case (www.eucast.org). For the testing, MPA plates were inoculated with 200 μl of overnight bacterial culture diluted to an OD of 0.5 (approximately 3×10^8 CFU/ml), antibiotic discs were placed on the plates and then incubated at 37 °C for 18 h. The measured inhibition zone diameters were compared to the EUCAST reference value.

2.3. Plasmid content determination

Plasmid DNA was isolated using the NucleoSpin Plasmid Kit (Macherey-Nagel, Düren, Germany) and High Pure Plasmid Isolation Kit (Roche Diagnostics, Basel, Switzerland). The procedure was modified for staphylococci – for cell lysis, we added 20 μl of lysostaphin (0.5 mg/ml; Ambi Products, Lawrence, NY, USA) and 2 μl of lysozyme (10 mg/ml; Sigma, St. Louis, USA) while only 20 μl of lysostaphin were used for *S. aureus* strains. Plasmids were then separated by gel electrophoresis in 1% agarose gel (Serva, Heidelberg, Germany) in 1% TAE buffer at 5 V/cm using 2-Log DNA Ladder (New England Biolabs, Ipswich, Massachusetts, USA) as an approximate marker. DNA was stained by ethidium bromide and visualized by UV light. Common resistance genes (*tetK*, *tetM*, *ermA*, *ermB*, *ermC*, *msrA*, *cat*, and *blaZ*) were detected on the isolated plasmid DNA by PCR (according to [37]). Primers were taken from previously published works [38–41].

2.4. Plasmid analysis

The approximate size of plasmids was determined by restriction endonuclease analysis, for which enzymes *Hin*dIII, *Eco*RI, *Bam*HI, *Hae*III, *Alu*I, *Cla*I, *Hpa*I, *Hha*I, *Nde*I, and *Nco*I (New England Biolabs, USA) were used. Size of multiple plasmids in one strain was determined by using several restriction endonucleases which cleaved only some of them and in a few cases plasmid curing was necessary (see below). Plasmids of different strains were compared in terms of size, restriction pattern, and carriage of resistance genes. In case of small plasmids present in more strains or species, we confirmed their identity by determining their DNA sequence in each strain by the MiSeq system using the Nextera XT DNA Sample Preparation Kit and MiSeq Reagent Kit v3 (Illumina, USA). Plasmid DNA sequence was assembled by A5-miseq pipeline [42], annotated using Unipro UGENE version 1.22.0 [43], and manipulated with using the CLC Genomic Workbench software (Qiagen Bioinformatics, Denmark). ORFs were identified by GeneMark (http://opal.biology.gatech.edu/), and the similarity search was done by BLAST (http://blast.ncbi.nlm.nih.gov/). Sequence gaps were closed using PCR and the

Table 1
Plasmids isolated from coagulase-negative staphylococci strains.

Species	Strain	Origin	Plasmids[a]	Antimicrobial resistance	Resistance genes
S. haemolyticus	39	human	12; 4.7; 2.1	chl, ery, str, amp, oxa, gen	*ermC*, *ermA*, *blaZ*
	143	human	25; 6; 3.2; 2.8; 1.4	chl, ery, tet, str, amp, oxa, gen	*tetK*, *blaZ*
	962	veterinary	13; 3.6; 1.7	oxa, gen, str	–
	968	veterinary	14	oxa, gen, str	–
	978	veterinary	3	oxa, gen, amp	–
	980	veterinary	19.5; 3.7	oxa, gen, (amp)	–
	982	veterinary	12	oxa, gen	–
S. petrasii	07/427	human	25; 4.5[b]; 1.5	tet, amp, (str)	*tetK*, *blaZ*
	08/435	human	25; 5; 2.5	tet, amp, str, oxa, gen	*tetK*, *tetM*, *blaZ*, *qacC*
	08/525	human	25; 1.3	tet, str, amp	*tetK*
	12/356	human	24; 2.5	ery, tet, str, amp, oxa, gen	*tetK*, *tetM*, *ermA*, *blaZ*, *qacC*
	12/584	human	27; 15	ery, amp, (str)	*blaZ*
	13/014	human	25; 4; 2.3	(str)	–
	13/057	human	26; 6; 3.2; 1.4	ery, tet, str, amp, oxa, gen	*tetK*, *tetM*, *ermA*, *blaZ*
	13/078	human	26	ery, tet, amp, (str)	*tetK*, *ermC*, *blaZ*
	13/113	human	28; 2.9	ery, amp, (str), (oxa)	*blaZ*
	13/114	human	22; 4; 2.2; 1.5	ery, amp, (str), (oxa)	*ermC*, *blaZ*
	93/321	human	24; 2.5	ery, tet, str, amp, oxa, gen	*tetM*, *ermA*, *blaZ*, *qacC*
	94/190	human	20	(str)	–
S. warner	9S	veterinary	33; 5	ery, amp	*blaZ*
	11S	veterinary	33; 5	ery, amp	*blaZ*
	17S	veterinary	33; 5	ery, amp	*blaZ*
	981	veterinary	17	oxa, (str)	–
	SAV662	veterinary	18	tet	*tetK*
S. chromogenes	976	veterinary	21; 3.2; 1.8	oxa, gen	–
S. xylosus	963	veterinary	30; 20	oxa, gen	–
	971	veterinary	11; 4.6; 2	oxa, (gen)	–
S. equorum	969	veterinary	38.5; 2	oxa, (ery)	–
	970	veterinary	26; 12	oxa, (gen)	–
	972	veterinary	17; 2.5	oxa, (gen), (ery)	–
	973	veterinary	32; 4.6; 1.7; 1.3	oxa, ery, chl	–
S. epidermidis	23S	veterinary	32.5; 3[b]; 2	tet, ery, amp	*tetK*
	24S	veterinary	24; 17	amp	–
	25S	veterinary	26; 4.4[b]; 1.3	str, amp	*aad*(6)
	740	veterinary	1.9; 3; 7; 16	str	–
	957	veterinary	23; 1.7	oxa, gen, amp, ery, tet	*tetK*
	959	veterinary	26; 4.5; 2.8; 2; 1.5; 1.3	oxa, gen, amp, ery, str, tet	*ermC*
S. sciuri	958	veterinary	25; 1.9	oxa, gen	–
	964	veterinary	25; 2.5	oxa, gen	–

[a] Plasmids are represented by sizes in kb.
[b] Plasmids successfully transferred by electroporation. Only strains with both antimicrobial resistance and plasmids are listed. If the strain showed borderline resistance to one or more antibiotics, the respective abbreviation(s) is (are) placed in parentheses. Abbreviations: chl - chloramphenicol, ery - erythromycin, str - streptomycin, amp - ampicillin, oxa - oxacillin, gen - gentamicin, tet – tetracycline.

corresponding designed primers. Amplified PCR products were purified using the QIAquick PCR Purification kit (Qiagen, Hilden, Germany) and sequenced by Eurofins MWG Operon (Germany). The sequences have been deposited in the GenBank database under accession numbers pLF08 (MH090915), pLF25 (MH090916), pLF23/1 (MH090917), and pLF23/2 (MH090918).

2.5. Plasmid curing

To confirm the location of resistance genes on plasmids instead of on the bacterial chromosome, we performed plasmid curing. Plasmid-cured strains were later used as recipients for interstrain plasmid transfer. Plasmid curing was carried out by culture of the test strains in MPB at 40 °C or at 37 °C, after adding 0.002% of SDS, for 18 h [44,45]. This culture was diluted to a suitable concentration and plated on MPA. After 24 h, about 100 colonies were transferred onto plates with the respective antibiotics using a bacteriological stamp. In colonies that did not grow on plates with antibiotics, plasmid loss was confirmed by electrophoresis and antimicrobial susceptibility testing.

2.6. Plasmid transfer by electroporation

Electroporation of *S. aureus* was performed using competent cells prepared in glycerol solution [46]. The competent cells were mixed with plasmid DNA (5 ng–2 μg in 5–20 μl), the mixture was transferred to a cooled cuvette and put into Gene Pulser Xcell (BioRad). After electroporation, the mixture was transferred to SMMP medium (5.5 parts SMM buffer [1 M sucrose, 0.04 M maleic acid, and 0.04 M $MgCl_2$, pH 6.5], 4 parts 7% Panassay broth, and 0.5 parts 10% bovine serum albumin solution) and incubated at 37 °C for 1 h with gentle shaking. Cells were then put on TSA (tryptone soya agar, Oxoid, UK) plates with antibiotics. For electroporation of CoNS, we prepared competent cells in sucrose solution ([47]; modified). Bacterial culture was grown in TSB (tryptone soya broth, Oxoid, UK) for 18 h, transferred to LB broth (1% tryptone, 0.5% yeast extract, and 1% NaCl) incubated to an OD of 0.4–0.7 (approximately 3×10^8 CFU/ml). Cells were centrifuged at 7000× *g* at 4 °C for 10 min, and the pellet was then washed three times in 0.5M sucrose solution and resuspended in 1/40 of the original volume. After electroporation, the cells were incubated in BHI broth (brain heart infusion, Oxoid, UK) at 37 °C for 2 h and plated on TSA plates with antibiotics.

3. Results

3.1. Antimicrobial resistance and plasmid content

Antimicrobial resistance was detected in 47 out of 62 study strains belonging to all species tested (Table 1). Resistance to

ampicillin was the most common (26 strains representing most of the test species), followed by resistance to gentamicin (24 strains), streptomycin and erythromycin (20 strains), and tetracycline (12 strains) while only three strains were resistant to chloramphenicol. Nearly half of all strains also showed resistance to methicillin; however, we did not analyze this resistance further for the typical chromosomal location of the responsible gene. Antimicrobial resistance mostly correlated with the plasmid content of the strains. Plasmids were detected in 48 out of 62 CoNS strains analyzed. In total, 107 plasmids ranging in size between 1.3 and 38.5 kb were detected, and their number in each strain varied between 1 and 6 (Table 1). Six strains of *S. aureus*, *S. haemolyticus*, and *S. petrasii* contained identical plasmids while the remaining 103 plasmids had different restriction endonuclease cleavage patterns. In addition to the previously well-described plasmids (e. g. [14,37,48,49]), we detected plasmids differing in structure and size and carrying multiple resistance genes. For example, we detected tetracycline-resistance plasmids larger than their common size (less than 5 kb) or plasmids over 10 kb carrying multiple resistance genes which are usually located on smaller plasmids. Of the resistance genes detected on these plasmids, *bla*Z for resistance to ampicillin was the most common (13 strains), followed by *tet*K (10 strains) and *tet*M (four strains) genes conferring resistance to tetracycline and *erm*A and *erm*C (four strains each) for resistance to erythromycin. These genes were detected by PCR on isolated plasmid DNA which can still contain residues of chromosomal DNA, however they are usually located on plasmids. We managed to confirm the location of 7 genes by plasmid curing and sequencing. DNA sequencing also revealed the *qac*C gene, which codes for an export pump involved in the resistance to antimicrobials such as quaternary ammonium compounds, ethidium bromide, erythromycin, and tetracycline (in three strains), and *aad*(6) for resistance to streptomycin (in one strain). Moreover, in 18 strains, we found small (1.3–2 kb) plasmids that appear to be cryptic. Apparently cryptic is a 2-kb plasmid in *S. epidermidis* strain 13S which is susceptible to all antibiotics tested. *S. epidermidis* strain 23S also contains a small cryptic plasmid in addition to a tetracycline-resistance plasmid. On this plasmid, we detected three genes for hypothetical proteins with no homology to known plasmids (Fig. 1).

3.2. Plasmid curing

Five *S. petrasii* strains were successfully cured of plasmids; from strain 07/427, we cured a 4.5-kb plasmid carrying a tetracycline-resistance gene, from strains 08/435, 12/356, and 93/321, a 2.5-kb plasmid with genes conferring resistance to both tetracycline and streptomycin, and from strain 08/525, a 1.3-kb plasmid with a streptomycin-resistance gene. From *S. equorum* strain 973, we cured a 1.3-kb plasmid that carried a chloramphenicol-resistance gene, from *S. epidermidis* strain 959, a 1.3-kb plasmid with a streptomycin-resistance gene, and from *S. haemolyticus* strain 980, a 3.7-kb plasmid with an ampicillin-resistance gene. After plasmid curing, all strains became susceptible to the respective antibiotics. Plasmid curing using culture at a higher temperature (40 °C) was unsuccessful in all strains. *S. petrasii* strains which lost plasmids were subsequently used as recipients for electroporation by plasmids from different strains (see below).

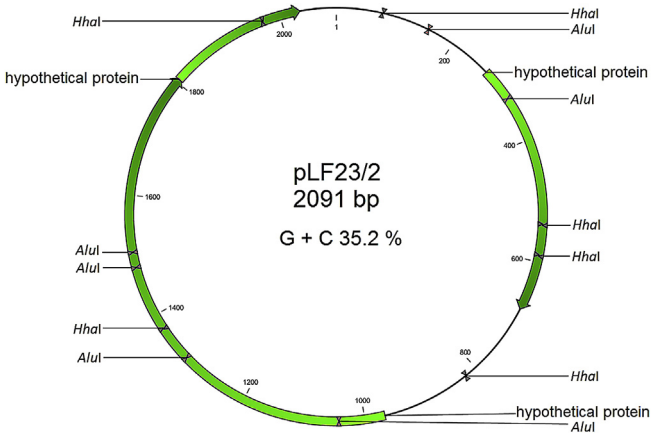

Fig. 1. Circular genetic map of plasmid pLF23/2. The respective gene products are matched with the corresponding ORF. Restriction endonuclease restriction sites are marked.

3.3. Identical plasmids in different staphylococcal species

Seven highly similar plasmids in *S. aureus*, *S. haemolyticus*, and *S. petrasii* strains were selected according to their size, restriction patterns, and resistance genes detected by PCR (Table 2). Plasmids with a size of 4.5 kb carrying a tetracycline resistance gene were detected in *S. aureus* and *S. petrasii* strains. Plasmid DNA sequencing revealed that *S. petrasii* strain 07/427 contained a plasmid identical to the tetracycline resistance plasmid pT181, which was well described in *S. aureus* [50]. Plasmids 2.5 kb in size, showing 99% similarity, encoding tetracycline and streptomycin resistance were found in three different *S. petrasii* strains. We designated this newly described plasmid, carrying a quaternary ammonium compound efflux gene, pLF08 (Fig. 2, Table 3). Plasmids 25 kb in size present in *S. haemolyticus* and *S. petrasii* strains resistant to ampicillin, tetracycline, and streptomycin appeared to be identical too, however they were not sequenced for their large size which makes them unsuitable for electroporation.

3.4. Interspecies plasmid transfer by electroporation

We performed 15 different electroporation experiments 3 times each, using 8 donor and 7 recipient strains. In total, 11 plasmids were selected for the electroporation, 10 from CoNS strains and one from *S. aureus*, out of which four were transformed successfully. First, we transformed a restriction-deficient *S. aureus* strain RN4220, which is commonly used as a recipient when transferring DNA to *S. aureus* strains. This strain was successfully transformed by three tetracycline- and streptomycin-resistance plasmids from *S. petrasii* strain 07/427, *S. epidermidis* strain 23S, and *S. epidermidis* strain 25S. In all cases, the recipient acquired antimicrobial resistance encoded on these plasmids. As another recipient strain, we used plasmid-cured *S. petrasii* 07/427. Its competence for electroporation was proved by successful transfer of the original plasmid back to it. We also transformed *S. petrasii* 07/427 strain by a related tetracycline-resistance plasmid from *S. aureus*, thus demonstrating the possibility of plasmid transfer between coagulase-negative and coagulase-positive staphylococcal species. Plasmids conferred antimicrobial resistance to the same extent as in the donor strains and were stably maintained in all recipient strains. This was proved by passaging the electrotransformed strains 3 times without selection pressure and under the same conditions as the recipient strains. DNA sequencing confirmed that these plasmids originated from the donor strains, they were transferred intact and carried tetracycline and streptomycin-resistance genes (Figs. 3–4 and Table 3).

4. Discussion

Many species of coagulase-negative staphylococci are potential pathogens and are considered a reservoir of antimicrobial

Table 2
Plasmids from different strains with the same size and restriction patterns.

Plasmid	Plasmid size [kb]	Size of restriction fragments [kb]	Strain with identical plasmid
pT181	4.5	*Hin*dIII: 2.5 + 1.5 + 0.5 *Hpa*I: 2.5 + 2 *Nco*I, *Cla*I: 4.5	*S. aureus* COL, *S. petrasii* 07/427
pLF07	25	*Hae*III: 8 + 7 + 6 + 4.5 *Hin*dIII: 12 + 9 + 5	*S. haemolyticus* 143, *S. petrasii* 07/427
pLF08	2.5	*Nde*I, *Hha*I: 2.5	*S. petrasii* 08/435, 12/356, 93/321

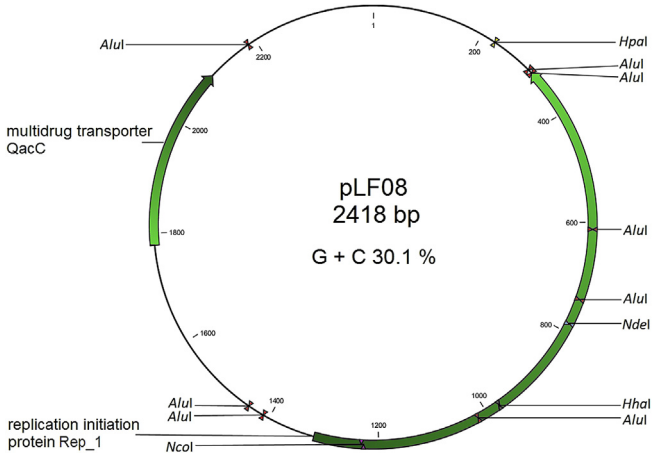

Fig. 2. Circular genetic map of plasmid pLF08. The respective gene products are matched with the corresponding ORF. Restriction endonuclease restriction sites are marked.

resistance genes. In this work, we analyzed CoNS strains from veterinary environment as well as from human clinical specimens, which were resistant to a wide range of antibiotics. The most common resistance was to erythromycin, followed by streptomycin, tetracycline, and ampicillin, similarly to previous studies [10–13]. There was no significant difference in resistance patterns between human and veterinary isolates. In accordance with the resistance patterns detected, we confirmed the presence of the genes *blaZ*, *tet*K, *tet*M, *erm*A, *erm*C, *qac*C, and *aad*(6), which have also been reported in CoNS by other authors [12,51–55]. In our study, the genes *tet*M, *erm*A, and *qac*C were only detected in human strains while the gene *aad*(6) was exclusively found in veterinary strains. Similar antimicrobial resistance patterns in human and veterinary strains can be explained by the use of the same class of antibiotics in both types of environment. Another cause of their similarity can be horizontal transfer of resistance genes since these genes are usually located on plasmids.

Forty-eight out of 62 strains of all CoNS species analyzed contained one or more plasmids which carried various resistance determinants. The presence of such a high number of plasmids implies an essential role for these mobile genetic elements in antimicrobial resistance and in its spread. Compared to previous reports [14], we have found many larger (14–27 kb) plasmids that appear to carry multiple resistance genes. This may be a result of internal rearrangements and interactions between plasmid DNA molecules.

However, large multiresistance plasmids are commonly detected in *S. aureus* [22]. These plasmids are about 10–50 kb in size and carry genes that confer resistance to various antibiotics like aminoglycosides, macrolides, amphenicols, lincosamides, streptogramin, pleuromutilins, trimethoprim, mupirocin, tetracycline and multidrug efflux pumps – for example plasmids pSK41, pGO1, pKKS825, pSCFS1, pMS97, and pTZ2162, as reviewed in [23]. This was in accordance to our findings. Despite that, we detected the *tet*K gene on some plasmids that were significantly larger (about 20–30 kb) than common *tet*K plasmids in *S. aureus*.

It is interesting that tetracycline-resistance *S. epidermidis* plasmid pLF23/1 carried an IS257 element. This insertion sequence has previously been found in association with various antimicrobial resistant determinants [56]. It plays an important role in the incorporation of pT181-like plasmids into the chromosome or larger plasmids, as well as in the expression of resistance genes [57]. This element was originally detected in *S. aureus* [58], but resistance plasmids with similar sequences were found in CoNS [59].

In total, seven different antimicrobial resistance genes as well as genes conferring resistance to heavy metals were detected on these

Table 3
Characteristics of sequenced resistance plasmids and proteins encoded by them.

Plasmid	Source strain	Strain with identical plasmid	Plasmid curing	EP	Gene products	Reference protein ID/identity (%)
pT181h	*S. petrasii* 07/427	*S. aureus* COL (pT181)	+	+	Replication initiation protein (rep7[a]) Tetracycline resistance protein Plasmid recombination enzyme	WP_061391130.1/99 WP_000492285.1/100 WP_031867488.1/98
pLF08	*S. petrasii* 08/435	*S. petrasii* 93/321 *S. petrasii* 12/356	+	–	Replication protein (rep21[a]) Efflux system for quaternary ammonium compounds QacC	WP_001199882.1/100 WP_001146389.1/100
pLF23/1	*S. epidermidis* 23S	–	–	+	Replication initiation protein (rep7[a]) IS6 family transposase IS257R2 Tetracycline resistance MFS efflux pump	EFG38795.1/100 A284_RS24430/97 OHQ30664.1/99
pLF25	*S. epidermidis* 25S	–	–	+	Replication initiation protein (rep7[a]) Streptomycin 6-adenylyltransferase Aad(6) Mobilization protein Rlx protein Transport protein Putative membrane protein	WP_011167206.1/100 CAQ51144.1/99 WP_001002114.1/96 WP_000246202.1/100 WP_080051836.1/68 AIR83875.1/28.5

EP … electroporation.
[a] Rep family determined by PlasmidFinder-2.0.

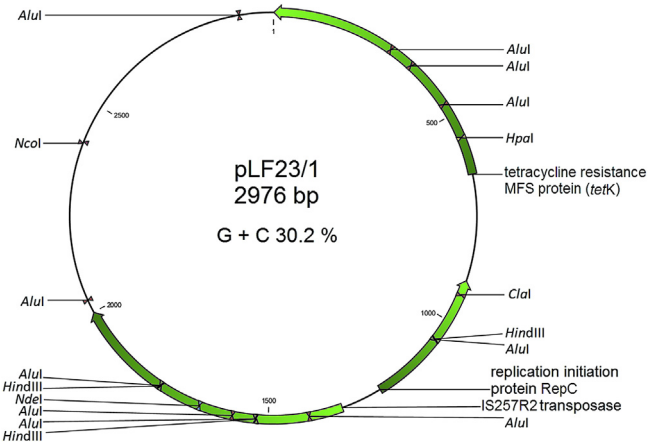

Fig. 3. Circular genetic map of plasmid pLF23/1. The respective gene products are matched with the corresponding ORF. Restriction endonuclease restriction sites are marked.

plasmids, similarly to [60]. We detected almost identical plasmids in strains belonging to different species (*S. petrasii*, *S. haemolyticus*, and *S. aureus*). Kessie et al. [20] also recorded similar plasmids harboring the same resistance genes in different CoNS species. They detected 4.3-kb plasmids carrying a tetracycline resistance gene in five isolates belonging to four species (*S. simulans*, *Staphylococcus lenticus*, *Staphylococcus hyicus*, and *S. xylosus*). We found similar plasmids in six strains including a coagulase-positive *S. aureus*. This fact suggests their horizontal transfer. We therefore attempted to demonstrate that plasmids can be transferred among species and can be stably maintained in recipients.

In staphylococci, plasmids can be naturally transferred mostly by conjugation and transduction. The smallest known conjugative plasmids in staphylococci are about 30 kb in size [61]. In our study, we did not perform conjugation experiments since the majority of detected plasmids was smaller. These small plasmids can be transferred by phages, even to phage non-susceptible strains [62], but in CoNS, interspecies transfer of plasmids by phages has only been described in few cases [35,36]. However, they can also be mobilized by conjugative elements and genes that play a role in this mobilization were detected (Figs. 2–4). To indicate the possibility of plasmid transfer, we used electroporation. This proved that plasmids can be stably maintained and the resistance is expressed in the recipient strains, which shows that CoNS can serve as a reservoir of resistance plasmids.

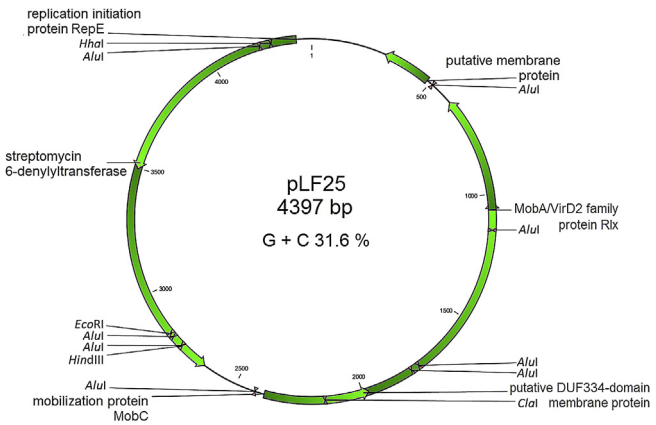

Fig. 4. Circular genetic map of plasmid pLF25. The respective gene products are matched with the corresponding ORF. Restriction endonuclease restriction sites are marked.

When electroporating plasmids into *S. aureus* strains, the restriction-deficient strain RN4220 accepted the foreign DNA more readily than natural strains, which confirmed the important impact of restriction-modification systems on plasmid transfer [63]. Other defensive mechanisms such as CRISPR-Cas systems may also prevent this transfer. However, they have not been detected as extensively in CoNS as in *S. aureus* [64]. Nevertheless, we successfully electroporated a coagulase-negative *S. petrasii* strain of human origin and confirmed that it accepted the plasmid in unaltered form, the plasmid was stably maintained in recipient cells, and expressed resistance genes. Although there is not much evidence for plasmid transfer in the natural environment and its mechanism is not known, the results of our work indicate that genes could be disseminated among staphylococcal species.

In summary, we detected 107 plasmids bearing resistance determinants to all classes of antibiotics in coagulase-negative staphylococcal strains. We confirmed the presence of identical plasmids in strains of different staphylococcal species, which indicates that plasmids can be spread among them horizontally. We successfully electroporated CoNS and *S. aureus* strains by plasmids from different species, which proves that they can accept and replicate them. Our work demonstrates a huge variability of plasmids that carry many resistance determinants and that CoNS serve as a pool of resistance plasmids, can therefore significantly contribute to the spread of this resistance and play a role in the evolution of strains.

Conflicts of interest

The authors declare no conflict of interest.

Acknowledgements

This study was supported by research grants No. QJ1510216 from the Ministry of Agriculture of the Czech Republic and MUNI/A/0824/2017 from the Masaryk University. We thank the Central European Institute of Technology (Masaryk University, Brno) and Eurofins MWG Operon (Germany) for plasmid DNA sequencing and Dr. A. Ševčíková (University Hospital Brno, Bohunice), Dr. M. Klimešová (Dairy Research Institute, Prague), Dr. P. Petráš (National Institute of Public Health, Prague), and animal farms for providing bacterial strains.

References

[1] Kloos WE, Musselwhite MS. Distribution and persistence of *Staphylococcus* and *Micrococcus* species and other aerobic bacteria on human skin. Appl Microbiol 1975;30:381–95.
[2] Becker K, Heilmann C, Peters G. Coagulase-negative staphylococci. Clin Microbiol Rev 2014;27:870–926.
[3] Pantůček R, Švec P, Dajcs JJ, Machová I, Černohlávková J, Šedo O, et al. *Staphylococcus petrasii* sp. nov. including *S. petrasii* subsp. *petrasii* subsp. nov. and *S. petrasii* subsp. *croceilyticus* subsp. nov., isolated from human clinical specimens and human ear infections. Syst Appl Microbiol 2013;36:90–5.
[4] Rewa O, Muscedere J, Reynolds S, Jiang X, Heyland DK. Coagulase-negative *Staphylococcus*, catheter-related, bloodstream infections and their association with acute phase markers of inflammation in the intensive care unit: an observational study. Can J Infect Dis Med Microbiol 2012;23:204–8.
[5] Falcone M, Giannella M, Raponi G, Mancini C, Venditti M. Teicoplanin use and emergence of *Staphylococcus haemolyticus*: is there a link? Clin Microbiol Infect 2006;12:96–7.
[6] del Pozo JL, Patel R. The challenge of treating biofilm-associated bacterial infections. Clin Pharmacol Ther 2007;82:204–9.
[7] Mack D, Davies AP, Harris LG, Jeeves R, Pascoe B, Knobloch JKM, et al. *Staphylococcus epidermidis* in biomaterial-associated infections. In: Moriarty F, Zaat SAJ, editors. Biomaterials associated infection. New York, U. S. A: Springer New York; 2013. p. 25–56.
[8] Hosseinzadeh S, Dastmalchi Saei H. Staphylococcal species associated with bovine mastitis in the North West of Iran: emerging of coagulase-negative staphylococci. Int J Vet Sci Med 2014;2:27–34.
[9] Thorberg B-M, Kühn I, Aarestrup FM, Brändström B, Jonsson P, Danielsson-Tham M-L. Pheno- and genotyping of *Staphylococcus epidermidis* isolated from bovine milk and human skin. Vet Microbiol 2006;115:163–72.

[10] Arslan E, Çelebi A, Açık L, Uçan US. Characterisation of coagulase positive *Staphylococcus* species isolated from bovine mastitis using protein and plasmid patterns. Turk J Vet Anim Sci Turk 2009;33:493–500.
[11] Aslantas O, Ozturk F, Celebi A, Acik L, Ergun Y. Characterization of *Staphylococcus aureus* strains isolated from subclinic bovine mastitis by protein patterns, antibiotic resistance and plasmid profile. Vet J Ank Univ Ank Turk 2006;53:47–51.
[12] Faria C, Vaz-Moreira I, Serapicos E, Nunes OC, Manaia CM. Antibiotic resistance in coagulase negative staphylococci isolated from wastewater and drinking water. Sci Total Environ 2009;407:3876–82.
[13] Koksal F, Yasar H, Samasti M. Antibiotic resistance patterns of coagulase-negative staphylococcus strains isolated from blood cultures of septicemic patients in Turkey. Microbiol Res 2009;164:404–10.
[14] Schwarz S, Shen J, Wendlandt S, Feßler AT, Wang Y, Kadlec K, et al. Plasmid-mediated antimicrobial resistance in staphylococci and other *Firmicutes*. In: Tolmansky ME, Alonso JC, editors. PLASMIDS: biology and impact in biotechnology and discovery. Washington, DC: ASM Press; 2015. p. 421–44.
[15] Aarestrup FM, Seyfarth AM, Emborg H-D, Pedersen K, Hendriksen RS, Bager F. Effect of abolishment of the use of antimicrobial agents for growth promotion on occurrence of antimicrobial resistance in fecal enterococci from food animals in Denmark. Antimicrob Agents Chemother 2001;45:2054–9.
[16] De Liguoro M, Cibin V, Capolongo F, Halling-Sørensen B, Montesissa C. Use of oxytetracycline and tylosin in intensive calf farming: evaluation of transfer to manure and soil. Chemosphere 2003;52:203–12.
[17] Van Boeckel TP, Brower C, Gilbert M, Grenfell BT, Levin SA, Robinson TP, et al. Global trends in antimicrobial use in food animals. Proc Natl Acad Sci USA 2015;112:5649–54.
[18] Akinjogunla OJ, Enabulele IO. Virulence factors, plasmid profiling and curing analysis of multi-drug resistant *Staphylococcus aureus* and coagulase negative *Staphylococcus* spp. isolated from patients with acute otitis media. J Am Sci 2010;6:1022–33.
[19] Sidhu MS, Oppegaard H, Devor TP, Sørum H. Persistence of multidrug-resistant *Staphylococcus haemolyticus* in an animal veterinary teaching hospital clinic. Microb Drug Resist 2007;13:271–80.
[20] Kessie G, Ettayebi M, Haddad AM, Shibl AM, Al-Shammary FJ, Tawfik AF, et al. Plasmid profile and antibiotic resistance in coagulase-negative staphylococci isolated from polluted water. J Appl Microbiol 1998;84:417–22.
[21] Taylor DE, Gibreel A, Lawley TD, Tracz DM. Antibiotic resistance plasmids. In: Funnell BE, Phillips GJ, editors. Plasmid biology. Washington, DC: ASM Press; 2004. p. 473–91.
[22] Shearer JES, Wireman J, Hostetler J, Forberger H, Borman J, Gill J, et al. Major families of multiresistant plasmids from geographically and epidemiologically diverse staphylococci. G3 Genes Genomes Genetics 2011;1:581–91.
[23] Haaber J, Penadés JR, Ingmer H. Transfer of antibiotic resistance in *Staphylococcus aureus*. Trends Microbiol 2017;11:893–905.
[24] Winstel V, Liang C, Sanchez-Carballo P, Steglich M, Munar M, Bröker BM, et al. Wall teichoic acid structure governs horizontal gene transfer between major bacterial pathogens. Nat Commun 2013;4:2345.
[25] Haaber J, Leisner JJ, Cohn MT, Catalan-Moreno A, Nielsen JB, Westh H, et al. Bacterial viruses enable their host to acquire antibiotic resistance genes from neighbouring cells. Nat Commun 2016;7:1–8.
[26] Penadés JR, Christie GE. The phage-inducible chromosomal islands: a family of highly evolved molecular para-sites. Annu Rev Virol 2015;2:181–201.
[27] Goessweiner-Mohr N, Arends K, Keller W, Grohmann E. Conjugation in gram-positive bacteria. Microbiol Spectr 2014;2. PLAS-0004-2013.
[28] O'Brien FG, Yui Eto K, Murphy RJ, Fairhurst HM, Coombs GW, Grubb WB, et al. Origin-of-transfer sequences facilitate mobilization of non-conjugative antimicrobial-resistance plasmids in *Staphylococcus aureus*. Nucleic Acids Res 2015;43:7971–83.
[29] Ramsay JP, Kwong SM, Murphy RJT, Yui Eto K, Price KJ, Nguyen QT, et al. An updated view of plasmid conjugation and mobilization in *Staphylococcus*. Mob Genet Elem 2016;6, e1208317.
[30] Sansevere EA, Robinson DA. Staphylococci on ICE: overlooked agents of horizontal gene transfer. Mob Genet Elem 2017;4:1–10.
[31] Chajecka-Wierzchowska W, Zadernowska A, Nalepa B, Sierpinska, Laniewska-Trokenheim L. Coagulase-negative staphylococci (CoNS) isolated from ready-to-eat food of animal origin–phenotypic and genotypic antibiotic resistance. Food Microbiol 2015;46:222–6.
[32] Stegmann R, Perreten V. Antibiotic resistance profile of *Staphylococcus rostri*, a new species isolated from healthy pigs. Vet Microbiol 2010;1:165–71.
[33] Morikawa K, Takemura AJ, Inose Y, Tsai M, Thi LTN, Ohta T, et al. Expression of a cryptic secondary Sigma factor gene unveils natural competence for DNA transformation in *Staphylococcus aureus*. PLoS Pathog 2012;8, e1003003.
[34] McCarthy AJ, Loeffler A, Witney AA, Gould KA, Lloyd DH, Lindsay JA. Extensive horizontal gene transfer during *Staphylococcus aureus* Co-colonization in vivo. Genome Biol Evol 2014;6:2697–708.
[35] Winstel V, Kühner P, Krismer B, Peschel A, Rohde H. Transfer of plasmid DNA to clinical coagulase-negative staphylococcal pathogens by using a unique bacteriophage. Appl Environ Microbiol 2015;81:2481–8.
[36] Zeman M, Mašlaňová I, Indráková A, Šiborová M, Mikulášek K, Bendíčková K, et al. *Staphylococcus sciuri* bacteriophages double-convert for staphylokinase and phospholipase, mediate interspecies plasmid transduction, and package *mec*A gene. Sci Rep 2017;7:46319.
[37] Kuntová L, Pantůček R, Rájová J, Růžičková V, Petráš P, Mašlaňová I, et al. Characteristics and distribution of plasmids in a clonally diverse set of methicillin-resistant *Staphylococcus aureus* strains. Arch Microbiol 2012;194:607–14.
[38] Ng L-K, Martin I, Alfa M, Mulvey M. Multiplex PCR for the detection of tetracycline resistant genes. Mol Cell Probes 2001;15:209–15.
[39] Martineau F, Picard FJ, Grenier L, Roy PH, Ouellette M, Bergeron MG. Multiplex PCR assays for the detection of clinically relevant antibiotic resistance genes in staphylococci isolated from patients infected after cardiac surgery. The ESPRIT Trial. J Antimicrob Chemother 2000;46:527–34.
[40] Strommenger B, Kettlitz C, Werner G, Witte W. Multiplex PCR assay for simultaneous detection of nine clinically relevant antibiotic resistance genes in *Staphylococcus aureus*. J Clin Microbiol 2003;41:4089–94.
[41] Matsuoka M, Endou K, Kobayashi H, Inoue M, Nakajima Y. A dyadic plasmid that shows MLS and PMS resistance in *Staphylococcus aureus*. FEMS Microbiol Lett 1997;148:91–6.
[42] Coil D, Jospin G, Darling AE. A5-miseq: an updated pipeline to assemble microbial genomes from Illumina MiSeq data. Bioinforma Oxf Engl 2015;31:587–9.
[43] Okonechnikov K, Golosova O, Fursov M. UGENE team. Unipro UGENE: a unified bioinformatics toolkit. Bioinforma Oxf Engl 2012;28:1166–7.
[44] May JW, Houghton RH, Perret CJ. The effect of growth at elevated temperatures on some heritable properties of *Staphylococcus aureus*. J Gen Microbiol 1964;37:157–69.
[45] Sonstein SA, Baldwin JN. Loss of the penicillinase plasmid after treatment of *Staphylococcus aureus* with sodium dodecyl sulfate. J Bacteriol 1972;109:262–5.
[46] Lee JC. Electrotransformation of staphylococci. Meth Mol Biol Clifton NJ 1995;47:209–16.
[47] Lindsay JA. *Staphylococcus*: molecular genetics. Norfolk, UK: Caister Academic Press; 2008.
[48] Lanza VF, Tedim AP, Martínez JL, Baquero F, Coque TM. The plasmidome of *Firmicutes*: impact on the emergence and the spread of resistance to antimicrobials. Microbiol Spectr 2015;3:1–37.
[49] Smith MCA, Thomas CD. An accessory protein is required for relaxosome formation by small staphylococcal plasmids. J Bacteriol 2004;186:3363–73.
[50] Khan SA, Novick RP. Complete nucleotide sequence of pT181, a tetracycline-resistance plasmid from *Staphylococcus aureus*. Plasmid 1983;10:251–9.
[51] Lüthje P, Schwarz S. Antimicrobial resistance of coagulase-negative staphylococci from bovine subclinical mastitis with particular reference to macrolide-lincosamide resistance phenotypes and genotypes. J Antimicrob Chemother 2006;57:966–9.
[52] Cherifi S, Byl B, Deplano A, Nonhoff C, Denis O, Hallin M. Comparative epidemiology of *Staphylococcus epidermidis* isolates from patients with catheter-related bacteremia and from healthy volunteers. J Clin Microbiol 2013;51:1541–7.
[53] Chajecka-Wierzchowska W, Zadernowska A, Nalepa B, Sierpinska M, Laniewska-Trokenheim L. Retail ready-to-eat food as a potential vehicle for *Staphylococcus* spp. harboring antibiotic resistance genes. J Food Protect 2014;77:993–8.
[54] Soares LC, Pereira IA, Pribul BR, Oliva MS, Coelho SMO, Souza MMS. Antimicrobial resistance and detection of *mec*A and *bla*Z genes in coagulase-negative *Staphylococcus* isolated from bovine mastitis. Pesqui Veterinária Bras 2012;32:692–6.
[55] Wendlandt S, Shen J, Kadlec K, Wang Y, Li B, Zhang W-J, et al. Multidrug resistance genes in staphylococci from animals that confer resistance to critically and highly important antimicrobial agents in human medicine. Trends Microbiol 2015;23:44–54.
[56] Firth N, Skurray RA. Mobile elements in the evolution and spread of multiple-drug resistance in staphylococci. Drug Resist Updates 1998;1:49–58.
[57] Skurray RA, Firth N. Molecular evolution of multiply-antibiotic-resistant staphylococci. Ciba Found Symp 1997;207:167–83.
[58] Gillespie MT, Lyon BR, Loo LSL, Matthews PR, Stewart PR, Skurray RA. Homologous direct repeat sequences associated with mercury, methicillin, tetracycline and trimethoprim resistance determinants in *Staphylococcus aureus*. FEMS Microbiol Lett 1987;43:165–71.
[59] Bjorland J, Steinum T, Sunde M, Waage S, Sviland S, Oppegaard H, et al. Deletion of pT181-like sequence in an smr-encoding mosaic plasmid harboured by a persistent bovine *Staphylococcus warneri* strain. Antimicrob Chemother 2006;1:46–51.
[60] Chan CX, Beiko RG, Ragan MA. Lateral transfer of genes and gene fragments in *Staphylococcus* extends beyond mobile elements. J Bacteriol 2011;193:3964–77.
[61] Kennedy AD, Porcella SF, Martens C, Whitney AR, Braughton KR, Chen L, et al. Complete nucleotide sequence analysis of plasmids in strains of *Staphylococcus aureus* clone USA300 reveals a high level of identity among isolates with closely related core genome sequences. J Clin Microbiol 2010;12:4504–11.
[62] Mašlaňová I, Stříbná S, Doškař J, Pantůček R. Efficient plasmid transduction to *Staphylococcus aureus* strains insensitive to the lytic action of transducing phage. FEMS Microbiol Lett 2016;363. pii:fnw211.
[63] Veiga H, Pinho MG. Inactivation of the SauI type I restriction-modification system is not sufficient to generate *Staphylococcus aureus* strains capable of efficiently accepting foreign DNA. Appl Environ Microbiol 2009;75:3034–8.
[64] Rossi CC, Souza-Silva T, Araújo-Alves AV, Giambiagi-deMarval M. CRISPR-cas systems features and the gene-reservoir role of coagulase-negative staphylococci. Front Microbiol 2017;8:1545.

APPENDIX 16

Botka T, Růžičková V, Svobodová K, Pantůček R, Petráš P, Čejková D, Doškař J (2017) Two highly divergent lineages of exfoliative toxin B-encoding plasmids revealed in impetigo strains of *Staphylococcus aureus*. *International Journal of Medical Microbiology* 307:291–296. https://doi.org/10.1016/j.ijmm.2017.05.005

(JCR 2017: IF = 3.298; Q2 – Microbiology)

Reprinted based on the author's right to include this Elsevier article in his own thesis. (https://www.elsevier.com/about/policies-and-standards/copyright)

International Journal of Medical Microbiology 307 (2017) 291–296

Contents lists available at ScienceDirect

International Journal of Medical Microbiology

journal homepage: www.elsevier.com/locate/ijmm

Two highly divergent lineages of exfoliative toxin B-encoding plasmids revealed in impetigo strains of *Staphylococcus aureus*

Tibor Botka[a], Vladislava Růžičková[a,*], Karla Svobodová[a], Roman Pantůček[a], Petr Petráš[b], Darina Čejková[c], Jiří Doškař[a]

[a] Department of Experimental Biology, Faculty of Science, Masaryk University, Kotlářská 2, 611 37 Brno, Czech Republic
[b] National Institute of Public Health, National Reference Laboratory for Staphylococci, Šrobárova 48, 100 42 Prague, Czech Republic
[c] Veterinary Research Institute, Hudcova 70, 621 00 Brno, Czech republic

ARTICLE INFO

Keywords:
Staphylococcus aureus
Exfoliative toxin B
ETB plasmids
Bullous impetigo
Phylogeny

ABSTRACT

Exfoliative toxin B (ETB) encoded by some large plasmids plays a crucial role in epidermolytic diseases caused by *Staphylococcus aureus*. We have found as yet unknown types of *etb* gene-positive plasmids isolated from a set of impetigo strains implicated in outbreaks of pemphigus neonatorum in Czech maternity hospitals. Plasmids from the strains of clonal complex CC121 were related to archetypal plasmid $pETB_{TY4}$. Sharing a 33-kb core sequence including virulence genes for ETB, EDIN C, and lantibiotics, they were assigned to a stand-alone lineage, named $pETB_{TY4}$-based plasmids. Differing from each other in the content of variable DNA regions, they formed four sequence types. In addition to them, a novel unique plasmid pETB608 isolated from a strain of ST130 was described. Carrying conjugative cluster genes, as well as new variants of *etb* and *edinA* genes, pETB608 could be regarded as a source of a new lineage of ETB plasmids. We have designed a helpful detection assay, which facilitates the precise identification of the all described types of ETB plasmids.

1. Introduction

Exfoliative toxin B (ETB), similarly to exfoliative toxin A (ETA), is the active serine protease produced by some strains of *Staphylococcus aureus*. They are closely associated with toxin-mediated epidermolytic skin disorders in humans (Ladhani et al., 1999). While ETA is encoded on a prophage (Yamaguchi et al., 2000; Holochová et al., 2010; Botka et al., 2015), ETB is encoded on a large penicillinase-type plasmid (Yamaguchi et al., 2001). Both the ETs are characterized by splitting the target skin substrate, cadherin-like transmembrane glycoprotein desmoglein 1 (Amagai et al., 2000; Hanakawa et al., 2002). Cleavage of the desmosomal cadherins in the superficial layers of the skin is directly responsible for the clinical manifestation of the blistering skin disease pemphigus neonatorum and/or generalized staphylococcal scalded skin syndrome (SSSS) in neonates, and bullous impetigo in young children and adults (Ladhani et al., 1999).

Multiple reports have shown that ETs are produced approximately by 5% of *S. aureus* strains (reviewed in Bukowski et al., 2010). In a previous study, we have described a set of the 127 impetigo strains of *S. aureus* isolated in 23 maternity hospitals in the Czech Republic (Růžičková et al., 2012). ETB alone was produced by 4.4% of strains, and 17% of strains secreted both ETA and ETB. The *etb* gene was located on the 38–41-kb plasmids, hereinafter termed ETB plasmids, which were characterized only by restriction endonuclease analysis (REAP).

The early studies concerned with the ETB-producing strains described a large *etb* gene-positive plasmid pRW001 (Jackson and Iandolo, 1986), and the complete sequences of the $pETB_{TY4}$ (Yamaguchi et al., 2001) and $pETB_{TY825}$ (Hisatsune et al., 2013) have been determined. However, recent data on the structural diversity and evolutional course of ETB plasmids are not available.

In this study, we present a molecular characterization of 13 *etb* gene-positive clinical strains of *S. aureus* isolated in Czech maternity hospitals from 1999 to 2015. Their plasmids were analyzed and compared with the already published ETB plasmids to determine their similarity and elucidate their phylogeny and impact on the pathogenicity of the host bacteria. To differentiate between ETB plasmids, a helpful PCR method was designed.

* Corresponding author at: Department of Experimental Biology, Laboratory of Molecular Diagnostics of Microorganisms, Faculty of Science, Masaryk University, Kotlářská 2, CZ-611 37 Brno, Czech Republic.
E-mail address: vladkar@sci.muni.cz (V. Růžičková).

http://dx.doi.org/10.1016/j.ijmm.2017.05.005
Received 9 March 2017; Received in revised form 17 May 2017; Accepted 24 May 2017
1438-4221/ © 2017 Elsevier GmbH. All rights reserved.

Table 1
Characteristics of 13 ETB-producing impetigo strains of *Staphylococcus aureus*.

Strain[a]	Hospital no.[b]	Clinical origin	Year of isolation	MLST	*spa* type	*agr* type	Plasmids		Prophages[c]	*etb* gene	*eta* gene	ETA-B-phage type	SAgs genes[d]
							No.	pETB type					
791*	9	Child, blister	2013	ST121	t159	IV	1	I	B, Fb	+	+	B5	*seg, sei*
445	2	Nurse, nose	2013	ST121	t159	IV	2	II	A, B, Fb	+	+	B1	*sei*
507	25	Child, blister	2010	ST121	t159	IV	1	III	Fb	+	−	−	*seg, sei*
586	9	Child, blister	2014	ST121	t169	IV	3	I	B, Fb	+	+	B5	*seg, sei*
013	26	Child, blister	2014	ST121	t169	IV	1	II	−	+	−	−	*sei*
459*	17	Child, blister	2003	ST121	t169	IV	1	III	Fb	+	−	−	*seg, sei*
049*	14	Child, SSSS	1999	ST121	t916	IV	1	II	A, B, Fb	+	+	B1	*seg, sea, sei*
797*	1	Child, blister	2008	ST121	t916	IV	1	II	A, B, Fb	+	+	B1	*seg, sei*
497	3	Child, SSSS	2011	ST121	t272	IV	1	II	−	+	−	−	*sei*
151	18	Child, blister	2008	ST121	t645	IV	1	II	Fb	+	−	−	*sei*
618	15	Child, nose	2015	ST123	t1688	IV	2	II	Fb	+	−	−	*seg, sei*
420	27	Child, blister	2013	ST2276	t876	IV	1	II	B, Fb	+	+	B1	*seg, sei*
608*	26	Child, blister	2011	ST130	t843	III	1	V	−	+	−	−	−

[a] Host strains of fully-sequenced ETB plasmids are marked with asterisks.
[b] Czech hospitals are numbered according to Růžičková et al. (2012).
[c] Prophage serogroups were classified according to Pantůček et al. (2004).
[d] Genes *seg* and *sei* were detected according to Banks et al. (2003), and Becker et al. (2003) respectively.

2. Materials and methods

2.1. Bacterial strains

Thirteen ETB-producing *S. aureus* strains were isolated from skin blisters of the Czech pediatric patients between 1999 and 2015. Two of them originated from skin lesions of pediatric patients diagnosed with SSSS and one from a nurse (Table 1). Seven of these strains and other fourteen ETB-producing collection strains, tested in the multiplex PCR assays of all ETB plasmid types, were previously published by Růžičková et al. (2012). The production of exfoliative toxin serotypes A and B was verified by using the Reverse Passive Latex Agglutination Kit (Denka Seiken for Unipath, Tokyo, Japan).

2.2. Isolation and restriction endonuclease profiling of plasmids

Plasmid DNA for whole genome sequencing and restriction analysis was isolated from bacterial cells by the High Pure Plasmid Isolation Kit (Roche Diagnostics, Germany) according to the manufacturer's protocol with minute modifications as described previously (Varga et al., 2012). The plasmid DNA was digested with EcoRI, HindIII, PstI, and XbaI restriction endonuclease (Roche Diagnostics, Germany) according to the manufacturer's protocol and electrophoresed as described previously (Doškař et al., 2000). Restriction endonuclease analysis of plasmids (REAP) was used for plasmid typing.

2.3. PCR genotyping

Bacterial DNA was isolated by the High Pure PCR Template Preparation Kit (Roche Diagnostics, Germany) according to the manufacturer's protocol. Multilocus sequence typing (MLST) of *S. aureus* strains was carried out as described previously (Enright et al., 2000), *spa* typing was performed according to the Ridom StaphType standard protocol (www.ridom.org), and the Ridom StaphType software package (Ridom, Germany) was used for assignment. For the detection of *agr* type and staphylococcal genes *mecA*, *eta*, *etb*, *etd*, *sea*, *sej*, *see*, *sec*, *seh*, *seb*, *seg*, *sed*, *sei*, *tst*, and Panton Valentine leukocidin (PVL) genes *lukS-PV* and *lukF-PV*, the polymerase chain reactions were carried out as described previously (Jarraud et al., 2002; Murakami et al., 1991; Růžičková et al., 2005; Monday and Bohach, 1999; Banks et al., 2003; Becker et al., 2003 and Lina et al., 1999). Prophage serogroups and ETA-B types were identified as described previously (Pantůček et al., 2004; Holochová et al., 2010). PCR products for MLST and *spa* typing were sequenced by Eurofins MWG Operon (Germany).

2.4. Identification of ETB plasmids

To distinguish between $pETB_{TY4}$-based plasmids and pETB608, a novel multiplex PCR assay mapping plasmid sequence structure was designed. Primers targeting typical sites of the core sequence of $pETB_{TY4}$-based plasmids and the common part of the *etb* genes of both types were used. The cycling scheme was as follows: 95 °C for 10 min, followed by 30 cycles at 94 °C for 90 s, 58 °C for 70 s, 72 °C for 60 s, and finally 72 °C for 3 min. Another multiplex PCR assay was developed for classifying ETB plasmids into five pETB types. Primers, targeting a common part of the core sequence from one side and the variable DNA sequence from the other side, were designed to maintain the specificity to ETB plasmids. The cycling scheme was as follows: 95 °C for 10 min, followed by 30 cycles at 94 °C for 80 s, 58 °C for 50 s, 72 °C for 60 s, and finally 72 °C for 5 min. Both assays were verified using plasmid DNA as well as whole bacterial genome DNA. Primers used in both assays are shown in Table S1. The amplicon spectra are illustrated in Fig. S1.

2.5. DNA sequencing and analysis software

Sequencing libraries were prepared from 1 ng of plasmid DNA using the Nextera XT DNA Sample Preparation kit (Illumina, USA). Sequencing reactions were performed using the MiSeq Reagent Kit v3 in the MiSEQ system (Illumina). Raw sequencing reads were trimmed using the sliding window model in Trimmomatic (Version 0.32; Bolger et al., 2014) in order to remove low-quality reads. Trimmed paired-end reads were assembled by *de novo* assembler IDBA_UD (Version 1.1.1; Peng et al., 2012) with a modification to the default settings; k-mer sizes ranged from 20 to 120 with an increment of 10. Contigs were assembled using the CLC Genomics Workbench software (CLC, Inc., Denmark). Sequence gaps were closed using PCR and the corresponding designed primers. Amplified PCR products were purified using the QIAquick PCR Purification kit (Qiagen) and sequenced by Eurofins MWG Operon (Germany). The sequences have been deposited in the GenBank database under accession nos.: pETB049 (KY436021), pETB459 (KY436022), pETB608 (KY436023), pETB791 (KY436024), and pETB797 (KY436025).

Open reading frames were identified by GeneMark.hmm with Heuristic models (http://exon.gtech.edu) and annotated by BLAST (http://blast.ncbi.nlm.nih.gov), InterPro (http://www.ebi.ac.uk/interpro), Phobius (http://phobius.sbc.su.se), and IS Finder database (Siguier et al., 2006). BPROM (Solovyev and Salamov, 2011) was applied to promoter prediction. Only the promoters with an overall score above 3.5 and located in the close vicinity of ORF were

considered. ARNold (Lesnik et al., 2001) was applied to Rho-independent terminator identification. Only the predicted terminators with a dG value of less than −10 kcal/mol and a functional position were considered.

Nucleotide sequence similarity comparisons were calculated using megablast algorithm, and protein similarity comparisons were made using blastp (http://blast.ncbi.nlm.nih.gov). *In silico* PCR was carried out by the on-line tool "*In silico* analysis of complete bacterial genomes: PCR, AFLP-PCR, and endonuclease restriction" (Bikandi et al., 2004). *In silico* restriction endonuclease profiling was performed by NEBcutter V2.0 (http://nc2.neb.com/NEBcutter2). Protein models were generated by the SWISS-MODEL (https://swissmodel.expasy.org). Clonal complex analysis was performed by eBURST v3 (http://saureus.mlst.net/eburst). The genome maps were constructed by GCView (Grant and Stothard, 2008) and Easyfig 2.1 (Sullivan et al., 2011).

The phylogenetic tree was constructed in MEGA7 (Kumar et al., 2016) from multiple alignment by Clustal Omega (http://www.ebi.ac.uk/Tools/msa/clustalo). Molecular phylogenetic analysis was performed by the maximum likelihood method. The tree with the highest log likelihood (- 43193.6755) is presented. Codon positions included were 1st + 2nd + 3rd + noncoding. All positions containing gaps were eliminated. In total 33,233 positions in the final dataset corresponded to the stable common core sequence of $pETB_{TY4}$-based plasmids. It was gained from plasmid DNA sequences clear of variable parts between the genes for resolvase and replication-associated protein (ORF2 and ORF3 of pETB791) and between *abiK* and transposase (ORF23 and ORF33 of pETB791).

3. Results and discussion

3.1. General overview of ETB-producing strains

All investigated strains were proved as ETB producers by the RPLA assay. They were characterized by MLST, *spa* typing, *agr* typing, and prophage carriage, plasmid contents, and PCR detection of virulence genes (Table 1). Ten strains of prevalent sequence type ST121, as well as the singles, ST2276 and ST123, belong to the same clonal complex CC121. Six strains were proved as producers of ETB along with ETA. The *eta* gene in these isolates was harboured by prophages, exclusively belonging to group ETA-B1 and/or ETA-B5, which is in accordance with our previous study (Růžičková et al., 2012). We have found that phages of these two groups carry genes of DNA replication and packaging module which are completely different from those of other ETA phages (Botka et al., 2015). Of many probed virulence genes, only three superantigen (SAg) genes, i.e. *sea*, *seg*, and *sei*, were detected (Table 1).

Prophage-less strain 608 belonging to genotype ST130/*spa* t843 was isolated from an impetigo patient in 2011. It produced only ETB and carried one, as yet not characterized ETB plasmid. Unlike other strains, which are *agr* type IV, it contains the *agr* locus of type III.

3.2. Comparison and phylogeny of plasmids related to $pETB_{TY4}$

The first restriction endonuclease analysis revealed various patterns of ETB plasmids (Table 2). The complete nucleotide sequences of the representative plasmids, named pETB049, pETB791, pETB797, and pETB459, whose size ranged from 37.3 to 45.7 kb, were determined. We compared them with the already known sequences of the *etb*-carrying plasmids $pETB_{TY4}$ (AP003088), $pETB_{TY825}$ (AP012457), and SAP057A (GQ900415) described previously (Yamaguchi et al., 2001; Hisatsune et al., 2013). As all these plasmids share a common 33-kb core sequence, we denominated them as $pETB_{TY4}$-based plasmids. They differ from each other in the content of two variable DNA regions (Fig. 1A, Table 2). The $pETB_{TY4}$-based plasmids could be classified into four pETB types. Plasmids of types I and IV lack any insertion between the ORFs for resolvase and replication-associated protein. On the other hand, the plasmids of types II and III have *repA* genes inserted in that position. Those of type III have there another insert of beta-lactamase-encoding transposon Tn552 described by Rowland and Dyke (1990). The region, located between the phage resistance gene *abiK* and transposase gene, contains cadmium resistance genes. Plasmid $pETB_{TY825}$ of type IV has at this site an additional large multi-resistance segment (Hisatsune et al., 2013).

As shown in Table 2, all $pETB_{TY4}$-based plasmids contain genetic determinants of epidermal cell differentiation inhibitor (EDIN) C, bacteriocin, and cadmium resistance (*cadD* and *cadX*). Nevertheless, the cadmium resistance genes in $pETB_{TY825}$ and other $pETB_{TY4}$-based plasmids do not have a common origin. For example, the *cadD* of $pETB_{TY825}$ is more similar to that in the plasmids of *Staphylococcus epidermidis* (GQ900456) and *S. lugdunensis* (KU882685). Compared to other $pETB_{TY4}$-based plasmids, the cadmium resistance operon-containing region in $pETB_{TY825}$ has a different structure.

The phylogenetic analysis of the core sequence of $pETB_{TY4}$-based plasmids divided them into two groups corresponding to the geographical distribution of their host strains (Fig. 2). One group associated with isolates from Europe and the other with Asian (Japan) isolates. The European clade branches into a subgroup of Czech isolates and British isolate SAP057A. Plasmids of pETB type II containing the *repA* genes are prevalent and seem to be evolutionarily ancestral. Plasmids of type III probably subsequently gained Tn552.

3.3. Genome analysis and phylogeny of pETB608

The determination of the complete DNA sequence revealed that novel pETB608 is noticeably different from the $pETB_{TY4}$-based plasmids (Figs. 1 B, 3). This plasmid, assigned to the pETB type V, is markedly shorter in size (30.6 kb) and has higher GC content (30.1%) than the others (Table 2, Figs. 1 B; 3). In pETB608, 37 ORFs, 18 promoters, and 4 intrinsic terminators were predicted (Fig. 1B, Table S2). A novel insertion sequence, named IS608, was identified. Unlike in $pETB_{TY4}$-based plasmids, no metal or antibiotic resistance genes were found in pETB608.

While all $pETB_{TY4}$-based plasmids encode identical exfoliative toxin B, the same-sized protein of pETB608, proved as ETB by the RPLA assay, showed 84% protein sequence similarity with it. In addition to ETB, two trypsin-like serine protease (SP) domain proteins belonging to the Peptidase S1B family are encoded by pETB608. SP608A encoded by ORF2 shows 50% similarity to serine protease of *Streptococcus didelphis* (WP_018367156). SP608B encoded by ORF37 shows about 55% similarity to glutamyl endopeptidase of *Staphylococcus pseudintermedius* (WP_015728600). Multiple alignment of ETB, SP608A, SP608B, and ETA protein sequences showed conserved regions harbouring catalytic triad (Fig. S2).

Plasmid pETB608 encodes two EDIN A-like proteins with VIP2 domain and ADP-ribosyltransferase (ART) domain. The product of ORF1, named ART608A, shows 93% similarity to the same-sized precursor of EDIN A (Inoue et al., 1991) and could be considered as its new variant. The protein of ORF35, designated ART608B, shows 65% similarity to EDIN A. It is probably truncated due to genomic rearrangements, visible in Fig. 3, as a possible result of recombination events.

In spite of the same dermatologic effect of epidermolysins A and B, ETB-producing strains are assumed to be more virulent (Mulligan et al., 1993). Yamaguchi et al. (2001) have reported that the activity of ETB could be increased by EDIN C. The effect of EDIN A and EDIN C on endothelial wound repair and epidermal differentiation and growth has been demonstrated previously (Aepfelbacher et al., 1997; Yamaguchi et al., 2001). EDIN, facilitating formation of disseminated infection foci, is a risk factor for deep-seated staphylococcal tissue infections following bacteremia (Munro et al., 2010). The predicted EDIN A-like proteins and trypsin-like serine proteases of pETB608 could be associated with more staphylococcal infections than only bullous impetigo, but it needs to be elucidated.

Table 2
Comparison of *etb* gene-positive plasmids belonging to five pETB types.

pETB type	Name[a]	Size (kb)	G + C (%)	No. of ORFs	Location in ORF[b]			No. of restriction fragments[c]				Factors of		Other typical sequences
					edinC	*etb*	*cadD*	EcoRI	HindIII	PstI	XbaI	resistance	virulence	
I	pETB791	37.9	27.8	44	4	8	31	5	22	4	5	cadmium	EDIN C, ETB, bacteriocin	IS257
	$pETB_{TY4}$	38.2	27.7	50	2	7	34		23					
II	pETB049	39.3	27.7	47	7	11	34	5	23	4	5	cadmium	EDIN C, ETB, bacteriocin	IS257, *repA*
	pETB797	39.4	27.7		7	11	34							
	SAP057A	39.3	27.7	48	7	11	35							
III	pETB459	45.7	27.9	52	13	17	39	5	24	4	7	cadmium, penicillin	EDIN C, ETB, bacteriocin	IS257, Tn552, *repA*
IV	$pETB_{TY825}$	60.6	28.2	63	51	55	9	8	31	5	6	cadmium, penicillin, aminoglycosides, macrolides	EDIN C, ETB, bacteriocin	IS257, IS256, 22-kb insertion, *cad* operon
V	pETB608	30.6	30.1	37	–	5	–	6	15	2	7	–	ETB, EDIN A-like proteins, trypsin-like serine proteases	IS608, *tra* operon

[a] $pETB_{TY4}$ (NC_003265) published by Yamaguchi et al. (2001); $pETB_{TY825}$ (NC_0022598) published by Hisatsune et al. (2013); SAP057A (NC_013334).
[b] Localization of genes according to GenBank records.
[c] HindIII restriction fingerprint of pETB791 differ from $pETB_{TY4}$ due to deletion of one restriction site.

We showed that all investigated ETB plasmids carried the *edin* or *edin*-like genes. The chromosomally located EDIN B is the most prevalent in Europe while EDIN A seems to be very rare there (Czech et al., 2001). On the other hand, it is the second most common in Japan, following EDIN C. Czech et al. (2001) have presumed a close relationship between the EDIN A- and EDIN C-positive strains. This is in accordance with our hypothesis that the genome of pETB608 probably originates from ancestral conjugative plasmid WBG707 isolated from Malaysian *S. aureus* strain in 1992 (Udo et al., 1992; Ramsay et al., 2016). The sequence of pETB608 has developed through the following events: (i) deletion of the part including the trimethoprim-resistance dihydrofolate reductase gene *dhfr*, *radC* (DNA repair protein), and conjugation cluster *detU*; (ii) multiple recombination leading to truncation of some ORFs, (iii) acquisition of virulence genes (Figs. 1 B, 3). These events probably happened in Asian *S. aureus* strains carrying $pETB_{TY4}$-based and *edinA*-positive plasmids.

3.4. Horizontal transfer of ETB plasmids

The presence of the *tra* operon in pETB608 implies its ability of self-transmission by conjugation. The presence of the plasmid conjugation transfer (tra)A–M genes is not associated with *S. aureus* lineage (McCarthy and Lindsay, 2012). It indicates that the pETB608 is not tied up only to strains of ST130.

The mechanism of horizontal transfer of $pETB_{TY4}$-based plasmids is not known. These plasmids have no *tra* or *mob* operon genes, except $pETB_{TY825}$ which contains the relaxase gene. Ramsay et al. (2016) have shown that most of the known non-conjugative plasmids are potentially mobilizable by pWBG749-family and pSK41-family plasmids through a relaxase-*in trans* mechanism. Despite the presence of *oriT* mimic

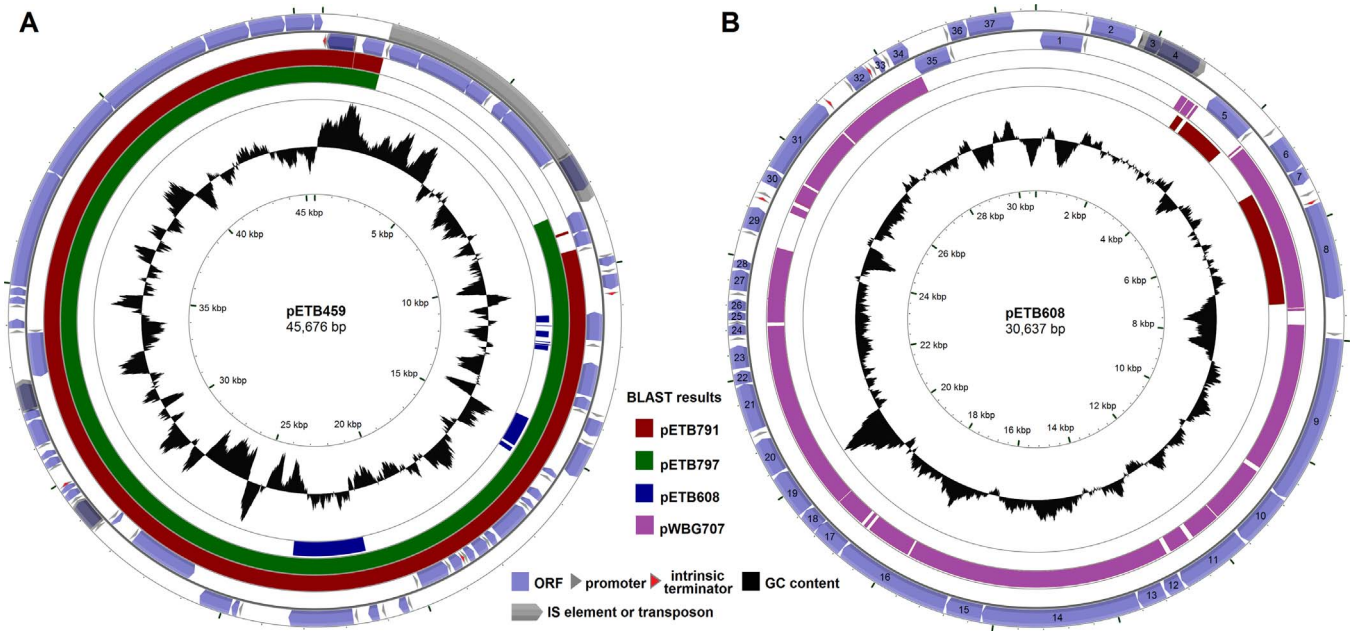

Fig. 1. Circular maps of plasmid nucleotide sequences: (A) pETB459 (type III) and (B) pETB608 (type V). Nucleotide sequence similarities to $pETB_{TY4}$-based plasmids of pETB type I (pETB791), II (pETB797), and to conjugative plasmid pWBG707 are shown with a 70% (A) and 85% (B) identity cut-offs. Detailed information about proteins encoded by pETB608 is in Table S2.

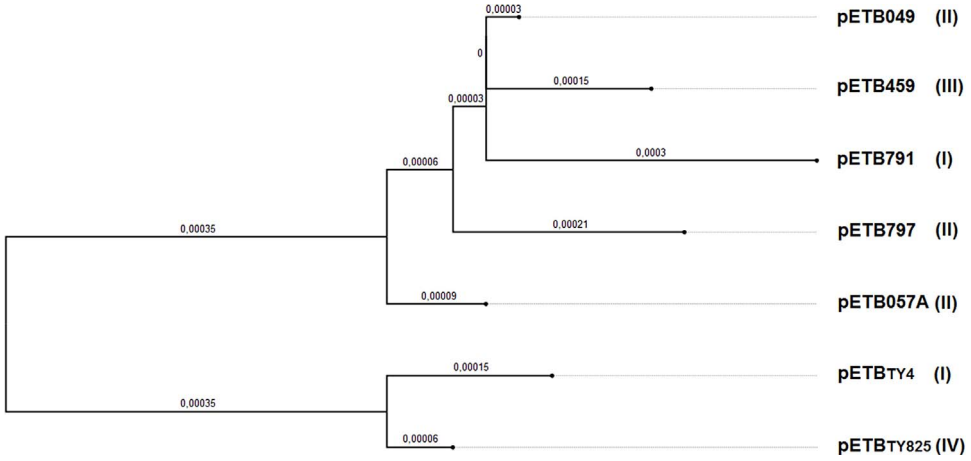

Fig. 2. Molecular phylogenetic analysis of $pETB_{TY4}$-based plasmids by the maximum likelihood method. The tree is drawn to scale, with branch lengths measured in the number of substitutions per site (next to the branches); pETB types are shown in parenthesis next to plasmid names. Formed groups correspond to geographical distribution of plasmid isolation – the upper group of European isolates and lower group of Asian isolates.

sequences in all $pETB_{TY4}$-based plasmids, none of the investigated *S. aureus* strains carried an additional conjugative plasmid (Table 1). As reported by Roberts and Mullany (2011), the mobilization by a conjugative transposon element could also be considered, but it awaits further research. The bacteriophage-mediated horizontal transfer via transduction remains the most probable way of dissemination of plasmids among staphylococci (Varga et al., 2012).

3.5. Identification of ETB plasmids in S. aureus

We have developed two multiplex PCR assays to determine the distribution of ETB plasmid types in Czech clinical isolates of *S. aureus*. We have probed 13 strains characterized in this paper (Table 1), and other fourteen ETB-producing strains from our laboratory collection. The bacterial DNA as well as plasmid DNA was used in both assays. The first multiplex PCR allowed us to distinguish between two different ETB plasmid lineages. It showed that all of the plasmids but pETB608 have the same genomic organization corresponding to that of the $pETB_{TY4}$-based plasmids (Fig. S1A). The second multiplex PCR is based on the amplification of sequences, typical for every single pETB type (Table 2, Fig. S1B). The most abundant was pETB type II (14 plasmids), followed by pETB type I (eight plasmids), pETB type III (four plasmids), and pETB type V (one plasmid pETB608). No plasmid of pETB type IV was detected in strains probed in this work.

Primers used for PCR detection of *etb* according to Jarraud et al. (2002) and Růžičková et al. (2005) showed multiple mismatches in target sites of pETB608 leading to inconsistent results. The multiplex PCR assay designed in this study proved to be much more suitable for the detection of the *etb* gene, including its newly described variant.

4. Conclusions

In this study, we established that all $pETB_{TY4}$-based plasmids resided in strains of clonal complex CC121 including types ST121, ST2276, and ST123. The existence of only a few variants in this ETB plasmid lineage suggests that a vertical transfer is the almost exclusive way of their spread. All $pETB_{TY4}$-based plasmids share a common core sequence, but they differ from each other in variable DNA content inserted at specific sites. Despite the uncertainty of whether one or another ETB plasmid type was primordial, their role in ETB-producing *S. aureus* strains as a cause of epidermolytic diseases is substantial. Moreover, unique pETB608 described in this study represents a novel type of ETB plasmids. It was detected in only one *S. aureus* strain of ST130 and hence seems to be an evolutionarily recent plasmid. Sequence variations, identified in all ETB plasmid types, served as identification markers in the development of a multiplex PCR assay. This effective method, which is able to detect the newly described *etb* gene variant, enabled us to reveal the diversity of ETB plasmids in the

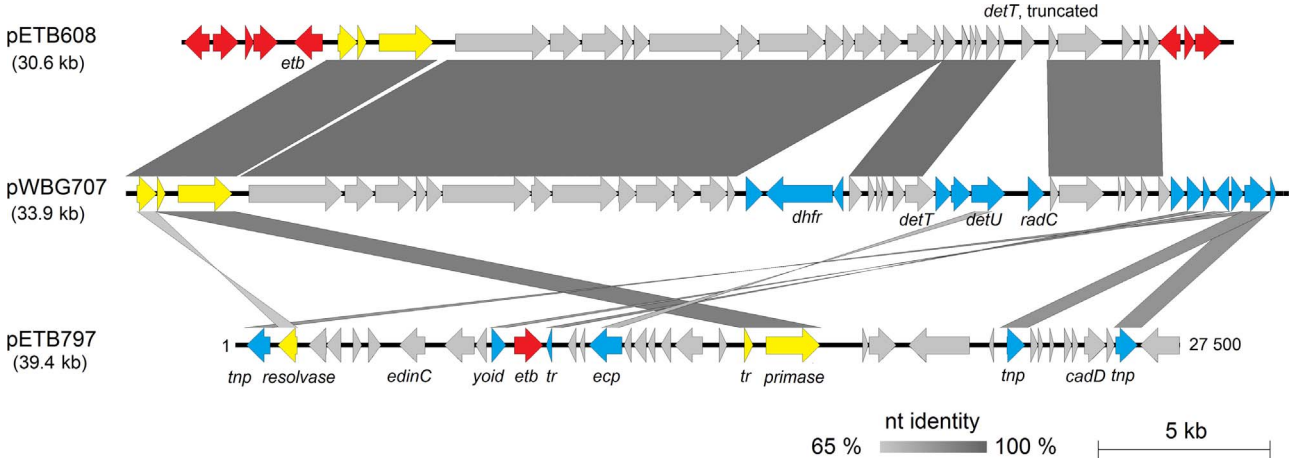

Fig. 3. Comparative sequence analysis of pETB608, pWBG707 (KX149097), and pETB797. ORFs are represented by full arrows. Sequence identity is expressed by shading levels. ORFs of pETB608 virulence region and their homologs are colored in red. ORFs common to all ETB plasmids and pWBG707 are colored in yellow. ORFs unique to pWBG707 with respect to pETB608 and their homologs are colored in blue. Lantibiotic cluster of pETB797 is not displayed due to absent similarity with compared plasmid sequences. Gene abbreviations: *det,* conjugation cluster; *dhfr*, dihydrofolate reductase; *radC*, DNA repair protein; *tnp*, transposase; *yoid*, YoID-like protein; *tr*, transcriptional regulator; *ecp*, extracellular protein.

natural population of *S. aureus* strains.

Conflict of interest

Authors have no conflict of interest

Acknowledgments

The authors would like to thank their colleagues from the participating hospitals for providing the strains of *S. aureus*. Thanks are also due to Ms. Eva Kodytková for valuable help. This work was supported by Grant from Masaryk UniversityMUNI/A/0967/2015, Ministry of Agriculture of the Czech Republic (QJ1510216), and AdmireVetCZ.1.05/2.1.00/01.0006–ED0006/01/01.

Appendix A. Supplementary data

Supplementary data associated with this article can be found, in the online version, at http://dx.doi.org/10.1016/j.ijmm.2017.05.005.

References

Aepfelbacher, M., Essler, M., Huber, E., Sugai, M., Weber, P.C., 1997. Bacterial toxins block endothelial wound repair. Evidence that Rho GTPases control cytoskeletal rearrangements in migrating endothelial cells. Arterioscler. Thromb. Vasc. Biol. 17, 1623–1629.

Amagai, M., Matsuyoshi, N., Wang, Z.H., Andl, C., Stanley, J.R., 2000. Toxin in bullous impetigo and staphylococcal scalded-skin syndrome targets desmoglein 1. Nat. Med. 6, 1275–1277.

Banks, M.C., Kamel, N.S., Zabriskie, J.B., Larone, D.H., Ursea, D., Posnett, D.N., 2003. *Staphylococcus aureus* express unique superantigens depending on the tissue source. J. Infect. Dis. 187, 77–86.

Becker, K., Friedrich, A.W., Lubritz, G., Weilert, M., Peters, G., von Eiff, Ch., 2003. Prevalence of genes encoding pyrogenic toxin superantigens and exfoliative toxins among strains of Staphylococcus aureus isolated from blood and nasal specimens. J. Clin. Microbiol. 41, 1434–1439.

Bikandi, J., San Millán, R., Rementeria, A., Garaizar, J., 2004. *In silico* analysis of complete bacterial genomes PCR. AFLP-PCR and endonuclease restriction. Bioinf. Oxf. Engl. 20, 798–799.

Bolger, A.M., Lohse, M., Usadel, B., 2014. Trimmomatic: a flexible trimmer for Illumina sequence data. Bioinformatics 30, 2114–2120.

Botka, T., Růžičková, V., Konečná, H., Pantůček, R., Rychlík, I., Zdráhal, Z., Petráš, P., Doškař, J., 2015. Complete genome analysis of two new bacteriophages isolated from impetigo strains of Staphylococcus aureus. Virus Genes 51, 122–131.

Bukowski, M., Wladyka, B., Dubin, G., 2010. Exfoliative toxins of *Staphylococcus aureus*. Toxins 2, 1148–1165.

Czech, A., Yamaguchi, T., Bader, L., Linder, S., Kaminski, K., Sugai, M., Aepfelbacher, M., 2001. Prevalence of Rho-inactivating epidermal cell differentiation inhibitor toxins in clinical *Staphylococcus aureus* isolates. J. Infect. Dis. 184, 785–788.

Doškař, J., Pallová, P., Pantůček, R., Rosypal, S., Růžičková, V., Pantůčková Kailerová, J., Klepárník, K., Malá, Z., Bocek, P., 2000. Genomic relatedness of *Staphylococcus aureus* phages of the international typing set and detection of serogroup A B, and F prophages in lysogenic strains. Can. J. Microbiol. 46, 1066–1076.

Enright, M.C., Day, N.P., Davies, C.E., Peacock, S.J., Spratt, B.G., 2000. Multilocus sequence typing for characterization of methicillin-resistant and methicillin-susceptible clones of *Staphylococcus aureus*. J. Clin. Microbiol. 38, 1008–1015.

Grant, J.R., Stothard, P., 2008. The CGView Server: a comparative genomics tool for circular genomes. Nucleic Acids Res. 36, W181–184.

Hanakawa, Y., Schechter, N.M., Lin, C., Garza, L., Li, H., Yamaguchi, T., Fudaba, Y., Nishifuji, K., Sugai, M., Amagai, M., Stanley, J.R., 2002. Molecular mechanisms of blister formation in bullous impetigo and staphylococcal scalded skin syndrome. J. Clin. Invest. 110, 53–60.

Hisatsune, J., Hirakawa, H., Yamaguchi, T., Fudaba, Y., Oshima, K., Hattori, M., Kato, F., Kayama, S., Sugai, M., 2013. Emergence of *Staphylococcus aureus* carrying multiple drug resistance genes on a plasmid encoding exfoliative toxin B. Antimicrob. Agents Chemother. 57, 6131–6140.

Holochová, P., Růžičková, V., Dostálová, L., Pantůček, R., Petráš, P., Doškař, J., 2010. Rapid detection and differentiation of the exfoliative toxin A-producing *Staphylococcus aureus* strains based on phiETA prophage polymorphisms. Diagn. Microbiol. Infect. Dis. 66, 248–252.

Inoue, S., Sugai, M., Murooka, Y., Paik, S.-Y., Hong, Y.-M., Ohgai, H., Suginaka, H., 1991. Molecular cloning and sequencing of the epidermal cell differentiation inhibitor gene from *Staphylococcus aureus*. Biochem. Biophys. Res. Commun. 174, 459–464.

Jackson, M.P., Iandolo, J.J., 1986. Cloning and expression of the exfoliative toxin B gene from *Staphylococcus aureus*. J. Bacteriol. 166, 574–580.

Jarraud, S., Mougel, C., Thioulouse, J., Lina, G., Meugnier, H., Forey, F., Nesme, X., Etienne, J., Vandenesch, F., 2002. Relationships between *Staphylococcus aureus* genetic background, virulence factors, *agr* groups (alleles), and human disease. Infect. Immun. 70, 631–641.

Kumar, S., Stecher, G., Tamura, K., 2016. MEGA7: molecular evolutionary genetics analysis version 7.0 for bigger datasets. Mol. Biol. Evol. 33, 1870–1874.

Ladhani, S., Joannou, C.L., Lochrie, D.P., Evans, R.W., Poston, S.M., 1999. Clinical, microbial, and biochemical aspects of the exfoliative toxins causing staphylococcal scalded-skin syndrome. Clin. Microbiol. Rev. 12, 224–242.

Lesnik, E.A., Sampath, R., Levene, H.B., Henderson, T.J., McNeil, J.A., Ecker, D.J., 2001. Prediction of rho-independent transcriptional terminators in *Escherichia coli*. Nucleic Acids Res. 29, 3583–3594.

Lina, G., Piémont, Y., Godail-Gamot, F., Bes, M., Peter, M.O., Gauduchon, V., Vandenesch, F., Etienne, J., 1999. Involvement of Panton-Valentine leukocidin-producing *Staphylococcus aureus* in primary skin infections and pneumonia. Clin. Infect. Dis. 29, 1128–1132.

McCarthy, A.J., Lindsay, J.A., 2012. The distribution of plasmids that carry virulence and resistance genes in *Staphylococcus aureus* is lineage associated. BMC Microbiol. 12, 104.

Monday, S.R., Bohach, G.A., 1999. Use of multiplex PCR to detect classical and newly described pyrogenic toxin genes in staphylococcal isolates. J. Clin. Microbiol. 37, 3411–3414.

Mulligan, M.E., Murray-Leisure, K.A., Ribner, B.S., Standiford, H.C., John, J.F., Korvick, J.A., Kauffman, C.A., Yu, V.L., 1993. Methicillin-resistant *Staphylococcus aureus*: a consensus review of the microbiology, pathogenesis, and epidemiology with implications for prevention and management. Am. J. Med. 94, 313–328.

Munro, P., Benchetrit, M., Nahori, M.-A., Stefani, C., Clément, R., Michiels, J.-F., Landraud, L., Dussurget, O., Lemichez, E., 2010. The *Staphylococcus aureus* epidermal cell differentiation inhibitor toxin promotes formation of infection foci in a mouse model of bacteremia. Infect. Immun. 78, 3404–3411.

Murakami, K., Minamide, W., Wada, K., Nakamura, E., Teraoka, H., Watanabe, S., 1991. Identification of methicillin-resistant strains of staphylococci by polymerase chain reaction. J. Clin. Microbiol. 29, 2240–2244.

Pantůček, R., Doškař, J., Růžičková, V., Kašpárek, P., Oráčová, E., Kvardová, V., Rosypal, S., 2004. Identification of bacteriophage types and their carriage in *Staphylococcus aureus*. Arch. Virol. 149, 1689–1703.

Peng, Y., Leung, H.C., Yiu, S.M., Chin, F.Y., 2012. IDBA-UD: a *de novo* assembler for single-cell and metagenomic sequencing data with highly uneven depth. Bioinformatics 28, 1420–1428.

Růžičková, V., Voller, J., Pantůček, R., Petráš, P., Doškař, J., 2005. Multiplex PCR for detection of three exfoliative toxin serotype genes in *Staphylococcus aureus*. Folia Microbiol. 50, 499–502.

Růžičková, V., Pantůček, R., Petráš, P., Machová, I., Kostýlková, K., Doškař, J., 2012. Major clonal lineages in impetigo *Staphylococcus aureus* strains isolated in Czech and Slovak maternity hospitals. Int. J. Med. Microbiol. 30, 237–241.

Ramsay, J.P., Kwong, S.M., Murphy, R.J.T., Yui Eto, K., Price, K.J., Nguyen, Q.T., O'Brien, F.G., Grubb, W.B., Coombs, G.W., Firth, N., 2016. An updated view of plasmid conjugation and mobilization in *Staphylococcus*. Mob. Genet. Elem. 6, e1208317.

Roberts, A.P., Mullany, P., 2011. Tn916-like genetic elements: a diverse group of modular mobile elements conferring antibiotic resistance. FEMS Microbiol. Rev. 35, 856–871.

Rowland, S.J., Dyke, K.G., 1990. Tn552, a novel transposable element from *Staphylococcus aureus*. Mol. Microbiol. 4, 961–975.

Siguier, P., Perochon, J., Lestrade, L., Mahillon, J., Chandler, M., 2006. ISfinder: the reference centre for bacterial insertion sequences. Nucleic Acids Res. 34, D32–36.

Solovyev, V., Salamov, A., 2011. Automatic annotation of microbial genomes and metagenomic sequences. In: Li, R.W. (Ed.), Metagenomics and Its Applications in Agriculture, Biomedicine and Environmental Studies. Nova Science Publishers, pp. 61–78.

Sullivan, M.J., Petty, N.K., Beatson, S.A., 2011. Easyfig: a genome comparison visualizer. Bioinf. Oxf. Engl. 27, 1009–1010.

Udo, E.E., Wei, M.Q., Grubb, W.B., 1992. Conjugative trimethoprim resistance in *Staphylococcus aureus*. FEMS Microbiol. Lett. 76, 243–248.

Varga, M., Kuntová, L., Pantůček, R., Mašlaňová, I., Růžičková, V., Doškař, J., 2012. Efficient transfer of antibiotic resistance plasmids by transduction within methicillin-resistant *Staphylococcus aureus* USA300 clone. FEMS Microbiol. Lett. 332, 146–152.

Yamaguchi, T., Hayashi, T., Takami, H., Nakasone, K., Ohnishi, M., Nakayama, K., Yamada, S., Komatsuzawa, H., Sugai, M., 2000. Phage conversion of exfoliative toxin A production in *Staphylococcus aureus*. Mol. Microbiol. 38, 694–705.

Yamaguchi, T., Hayashi, T., Takami, H., Ohnishi, M., Murata, T., Nakayama, K., Asakawa, K., Ohara, M., Komatsuzawa, H., Sugai, M., 2001. Complete nucleotide sequence of a *Staphylococcus aureus* exfoliative toxin B plasmid and identification of a novel ADP-ribosyltransferase. EDIN-C. Infect. Immun. 69, 7760–7771.

APPENDIX 17

Botka T, Růžičková V, Konečná H, Pantůček R, Rychlík I, Zdráhal Z, Petráš P, Doškař J (2015) Complete genome analysis of two new bacteriophages isolated from impetigo strains of *Staphylococcus aureus*. *Virus Genes* 51:122–131. https://doi.org/10.1007/s11262-015-1223-8 (JCR 2015: IF = 1.285; Q4 – Genetics & Heredity)

Reproduced with permission from Springer Nature.

Virus Genes (2015) 51:122–131
DOI 10.1007/s11262-015-1223-8

Complete genome analysis of two new bacteriophages isolated from impetigo strains of *Staphylococcus aureus*

Tibor Botka[1] · Vladislava Růžičková[1] · Hana Konečná[2] · Roman Pantůček[1] · Ivan Rychlík[3] · Zbyněk Zdráhal[2] · Petr Petráš[4] · Jiří Doškař[1]

Received: 1 April 2015 / Accepted: 23 June 2015 / Published online: 2 July 2015
© Springer Science+Business Media New York 2015

Abstract Exfoliative toxin A (ETA)-coding temperate bacteriophages are leading contributors to the toxic phenotype of impetigo strains of *Staphylococcus aureus*. Two distinct *eta* gene-positive bacteriophages isolated from *S. aureus* strains which recently caused massive outbreaks of pemphigus neonatorum in Czech maternity hospitals were characterized. The phages, designated ϕB166 and ϕB236, were able to transfer the *eta* gene into a prophageless *S. aureus* strain which afterwards converted into an ETA producer. Complete phage genome sequences were determined, and a comparative analysis of five designed genomic regions revealed major variances between them. They differed in the genome size, number of open reading frames, genome architecture, and virion protein patterns. Their high mutual sequence similarity was detected only in the terminal regions of the genome. When compared with the so far described *eta* phage genomes, noticeable differences were found. Thus, both phages represent two new lineages of as yet not characterized bacteriophages of the *Siphoviridae* family having impact on pathogenicity of impetigo strains of *S. aureus*.

Keywords ETA-converting bacteriophages · *Staphylococcus aureus* · Complete genome sequences · Virion protein patterns

Edited by Joachim Jakob Bugert.

Electronic supplementary material The online version of this article (doi:10.1007/s11262-015-1223-8) contains supplementary material, which is available to authorized users.

✉ Vladislava Růžičková
vladkar@sci.muni.cz

[1] Department of Experimental Biology, Faculty of Science, Masaryk University, Kotlářská 2, 611 37 Brno, Czech Republic

[2] Central European Institute of Technology, Masaryk University, Kamenice 5, 625 00 Brno, Czech Republic

[3] Veterinary Research Institute, Hudcova 70, 621 00 Brno, Czech Republic

[4] National Reference Laboratory for Staphylococci, National Institute of Public Health, Šrobárova 48, 100 42 Prague, Czech Republic

Introduction

Bacteriophages are the most abundant microorganisms in the biosphere that play an important role in bacterial biology, pathogenicity, and evolution. While many phages simply infect bacteria, lyse them, and spread, others take up long-term residence in their host. As far as *Staphylococcus aureus* is concerned, most strains harbour at least one prophage that replicates along with the host chromosome [1–6]. More than 1880 complete genomes of bacteriophages are reported; hereof, 96 belong to staphylococcal phages (EMBL-EBI Genomes, 2015). Recent sequence analyses indicate that many strains carry a large spectrum of prophages encoding additional factors which enhance bacterial virulence as well as survival ability in various hosts. Staphylophages participate in the mediation of horizontal transfer of pathogenicity islands and raise intra-strain and inter-strain exchange frequency of toxic or resistance genes [7–11].

Some human and animal strains of *S. aureus* produce an exfoliative toxin (ET) [12, 13]. Of the four known ETs-causing epidermal splitting in infected neonatal mice [14, 15], two (ETA and ETB) have been identified as the major causative agents of the blistering skin disease pemphigus neonatorum and/or generalised staphylococcal scalded skin

syndrome (SSSS) [16]. Only the *eta* gene encoding ETA is located on a *S. aureus* prophage [17, 18], while other ET genes were localized on other accessory elements such as a plasmid (*etb*) [19] and/or a pathogenicity island (*etd*) [15].

The staphylococcal bacteriophages belonging to the *Siphoviridae* family, the genus "Phietalikevirus" commonly have a linear double-stranded DNA with a size ranging from 42 to 44 kb, the modular structure of genome, and the B1 morphotype showing an isometric head with non-contractile tail [13, 17, 20, 21]. Most of the impetigo strains of *S. aureus* isolated in 23 maternity hospitals in the Czech Republic contained *eta* gene-positive prophages [12, 22], which can be classified into six ETA-B groups [23].

In this study, the two *eta* gene-positive phages (hereinafter termed *eta* phages) isolated from *S. aureus* strains implicated in massive pemphigus neonatorum outbreaks in two Czech geographically distant maternity hospitals were characterized. Their whole-genome sequences were analysed and compared with the published genomes of three *eta* phages and 24 staphylococcal *eta* gene-negative phages of the *Siphoviridae* family to determine their relatedness and elucidate their impact on the pathogenicity of the host bacteria.

Materials and methods

Bacterial strains

Two ETA-producing *S. aureus* strains (SA 166 and SA 236) were recovered from the skin blisters of child patients in 2008 and 2009 [12]. Both the strains carried prophage B along with prophage F. Strain SA 236 of clonal lineage CC121 harboured the *eta* and *etb* genes, while SA 166 of clonal lineage CC9 carried only *eta*. Prophageless and non-toxigenic *S. aureus* strain CCM 4890, originally designated 1039, was kindly provided by Dr Y. Yoshizawa (Jikei University School of Medicine, Tokyo, Japan).

Isolation of phages

The particles of phages, designated ϕB166 and ϕB236, were isolated from bacterial cells as described previously [20, 24]. The phage stock lysates, prepared by propagation of phages on strain CCM 4890, were used for the isolation of DNA, virion protein analysis, and lysogenization experiments.

Isolation of phage DNA

High-titre lysates of 10^9 pfu/ml were prepared on the propagation strain CCM 4890 growing in BHI broth (Oxoid, UK). Phage lysates were centrifuged at $5000\times g$ for 15 min and filtered by 0.45 μm pore size filter to remove cell debris. The phage DNA was purified as described previously [25].

Restriction endonuclease profiling and PCR genotyping

The phage DNA was digested with *Hin*dIII restriction endonuclease (Roche Diagnostics, Germany) and electrophoresed as described previously [26]. Phage ETA-B type, serogroup, and the *eta* gene were identified by PCR as described previously [23, 27, 28].

DNA sequencing

Phage genome sequences were obtained by the 454 sequencing method. A GS Junior System (Roche 454 Life Science, USA) was used. Samples of DNA were prepared as described previously [25]. Fully covered genome sequences of ϕB166 and ϕB236, with more than 28,300 numreads each, were obtained and assembled using the GS De Novo Assembler, version 2.6. The sequences have been deposited in the GenBank database under accession nos. KP893289 and KP893290.

Genome analysis software

To handle and visualize sequence data, the CLC Genomics Workbench software (CLC, Inc., Aarhus, Denmark) was used. ORFs were identified by GeneMarkS, optimized for phage sequences (http://exon.gatech.edu), and annotated by BLAST (http://blast.ncbi.nlm.nih.gov/) and InterPro (http://www.ebi.ac.uk/interpro/). Nucleotide sequence similarity comparisons are based on megablast algorithm calculations. BPROM [29] was applied to promoter prediction. Only the promoters with an overall score above 3.5 and located in close vicinity to ORF were considered. ARNold [30] was applied to Rho-independent terminator identification. Only the predicted terminators with a dG value of less than −11 kcal/mol and with functional position were considered. The GC content and its variation in the phage genomes were analysed by GC-Profile [31].

Lysogenic conversion and detection of ETA production

Staphylococcus aureus strain CCM 4890 was lysogenized with induced phages as described previously [20]. Lysogenic strains were incubated in BHI medium at 37 °C for 24 h. Single colonies were cultivated three times in medium with 10^{-3} M Na citrate to obtain pure culture of lysogens. PCR detection of prophages and the *eta* gene as well as PFGE of *Sma*I macrorestriction fragments

confirmed the presence of integrated prophages. ETA produced by the lysogens was detected using the Reverse Passive Latex Agglutination Kit (RPLA, Denka Seiken for Unipath, Japan).

PFGE analysis

Genomic DNA of lysogenized strains was prepared as described previously [32]. *Sma*I macrorestriction fragments were separated with a CHEF Mapper (Bio-Rad Laboratories) under the following conditions: 1.2 % agarose in 1× TAE electrophoresis buffer (0.04 M Tris/acetate, 0.001 M EDTA, pH 8.2) at 14 °C, 6 V cm^{-1}, pulse times of 1–55 s for 24 h.

Structure proteins analysis

Virion proteins were isolated from phage lysate according to Eyer et al. [33]. Vertical one-dimensional electrophoresis (1-DE), using the Bio-Rad equipment and reagents, was performed in Protean II xi Cell (discontinuous 12 % T SDS-PAGE). Precision Plus Protein Standard (catalogue no. 161-0363) was applied as the molecular weight marker. Proteins were stained with Bio-Safe Coomassie Stain. The GS-900 calibrated densitometer and Image Lab 5.1 software (cubic spline regression) were used for image analysis. Protein bands were excised and subjected to tryptic digestion (40 °C, 2 h). Tryptic peptides were analysed by LC–MS/MS system consisting of RSLCnano chromatograph (Thermo Fisher Scientific) connected to Impact II Ultra-High Resolution Qq-Time-Of-Flight mass spectrometer (Bruker). After desalting and concentration on trap column, the peptides were separated using Acclaim Pepmap100 C18 column (2 µm particles, 75 µm × 500 mm; Thermo Fisher Scientific, 300 nl/min) and 0.1 % FA/acetonitrile gradient. MS data were acquired in a data-dependent strategy with 3 s long cycle time. Mass range was set to 150–2200 m/z, and precursors were selected from 300 to 2000 m/z. Mascot search engine was used in combination of phage translated sequence data for protein identification. Mass tolerance for peptides and MS/MS fragments were 15 ppm and 0.05 Da, respectively.

Results and discussion

The present study focused on the characterization of two as yet undescribed bacteriophages, ϕB166 and ϕB236, originating from staphylococcal impetigo strains isolated from the skin blisters of two neonatal patients. The phages, identified by PCR as B phages carrying the *eta* gene, were investigated by whole-genome sequencing and assayed for *eta* gene transfer activity and lysogenic conversion of ETA production. The phage ϕB236 was assigned to type ETA-B5 and ϕB166 to ETA-B6. Prophages of the ETA-B5 type were found in 24 *S. aureus* strains isolated in eight maternity hospitals, and prophages of the ETA-B6 type have been reported in 17 impetigo strains from two distant Czech maternity hospitals [12].

In accordance with previous study [20], the ϕB166 as well as ϕB236 genome integrated into the 365-kb *Sma*I fragment of the recipient strain (Fig. 1). Selected *eta* gene-positive lysogens turned out to be producers of exfoliative toxin A. These results proved the induced *eta* phages to be efficient ETA-converting phages. Two lysogenized strains designated CCM 8515 (1039/ϕ166+) and CCM 8512 (1039/ϕ236+), and both phages, ϕB166 (CCM 8513) and ϕB236 (CCM 8514), were deposited into the Czech Collection of Microorganisms.

The genomes and virion protein patterns of ϕB166 and ϕB236

Restriction endonuclease analysis of the phage genomes gave the first evidence that ϕB166 and ϕB236 are not identical (Supplementary material, Fig. S1). Description of the genome sequences, their characteristics, and predicted gene products are summarized in Table 1 and Fig. 2. The sequences of these

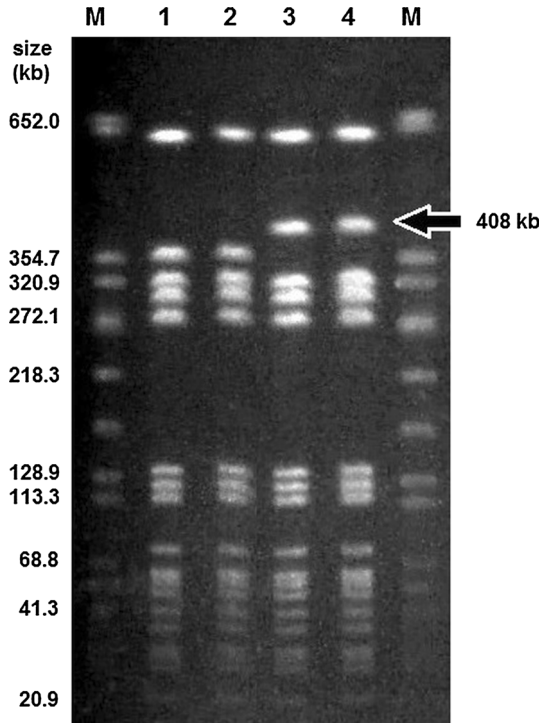

Fig. 1 A pulsed-field electrophoresis agarose gel of DNAs from prophageless *S. aureus* strain CCM 4890 (*lines 1* and *2*) and lysogens CCM 8515 [+ϕB166] (*line 3*) and CCM 8512 [+ϕB236] (*line 4*). M, size standard (DNA of *S. aureus* NCTC 8325); the *Sma*I restriction fragment with integrated *eta* prophage is indicated by a *full arrow*

Table 1 Predicted phage ϕB166 and ϕB236 products categorized into five genomic regions

ORF	ϕB166[a]		ORF	ϕB236[b]	
	Predicted function Region I (1–9097)	aa		Predicted function Region I (1–8404)	aa
01	Integrase	349	01	Integrase	349
02	Hypothetical protein	156	02	PemK-like phage protein	226
03	Hypothetical protein	173	03	cI-like repressor	239
04	Putative bacterial membrane protein	46	04	cro-like repressor	72
05	cI-like repressor	212	05	Antirepressor	263
06	cro-like repressor	84	06	Hypothetical protein	74
07	Putative antirepressor	262	07	Hypothetical protein	59
08	Hypothetical protein	67	08	Putative bacterial membrane protein	160
09	Hypothetical protein	46	09	XRE transcriptional regulator	61
10	Hypothetical protein	66	10	Putative antirepressor	250
11	Hypothetical protein	73	11	Hypothetical protein	71
12	DUF 1270 hypothetical protein	53	12	Hypothetical protein	84
13	DUF 2482 hypothetical protein	100	13	Hypothetical protein	73
14	DUF1108 hypothetical protein	85	14	DUF1270 hypothetical protein	53
15	Hypothetical protein	92	15	DUF1108 hypothetical protein	98
16	ATPase	651	16	DUF2483 hypothetical protein	73
17	ssDNA annealing protein RecT	306	17	SAK3-like protein	207
ORF	ϕB166[a]		ORF	ϕB236[b]	
	Predicted function Region II (9185–16,920)	aa		Predicted function Region II (8405–17,114)	aa
18	Metallo-hydrolase	161	18	ssDNA-binding protein	141
19	ssDNA-binding protein	156	19	DUF968 hypothetical protein	231
20	Replication protein	297	20	Replication protein	268
21	Hypothetical protein	72	21	Helicase inhibitor G39P-like protein	118
22	RusA-like protein	138	22	Replicative DNA helicase	413
23	ϕPVL_ORF50-like protein	125	23	Hypothetical protein	71
24	Phage_ORF51 superfamily protein	80	24	DUF3269 hypothetical protein	76
25	Hypothetical protein	68	25	DUF1064 hypothetical protein	134
26	Hypothetical protein	134	26	DUF3113 hypothetical protein	61
27	Hypothetical protein	64	27	ϕPVL_ORF50-like protein	119
28	Hypothetical protein	150	28	Phage_ORF51 superfamily protein	82
29	Hypothetical protein	167	29	DUF1024 hypothetical protein	87
30	Hypothetical protein	65	30	Hypothetical protein	66
31	DUF1024 hypothetical protein	82	31	Hypothetical protein	79
32	dUTPase	184	32	HNH endonuclease domain protein	184
33	Putative bacterial membrane protein	81	33	dUTPase	186
34	DUF1523 hypothetical protein	131	34	Hypothetical protein	57
35	Transcriptional activator RinB	57	35	Hypothetical protein	88
36	Hypothetical protein	133	36	DUF1381 hypothetical protein	96
			37	Hypothetical protein	78
			38	Transcriptional activator RinB	58
			39	Hypothetical protein	133

Table 1 continued

ORF	ϕB166[a]		ORF	ϕB236[b]	
	Predicted function Region III (16,903–24,920)	aa		Predicted function Region III (17,115–25,245)	aa
37	Terminase small subunit	164	40	Terminase small subunit	164
38	Terminase large subunit	407	41	Terminase large subunit	403
39	Portal protein	474	42	Portal protein	492
40	Head morphogenesis protein	316	43	Head morphogenesis protein	326
41	Hypothetical protein	194	44	Minor structural protein GP20	198
42	Major capsid protein	304	45	Capsid protein	274
43	Hypothetical protein	48	46	Rho domain protein	108
44	Head–tail connector	116	47	Head–tail connector	104
45	Head–tail adaptor	111	48	Head–tail adaptor	111
46	Putative tail component	135	49	Putative tail component	137
47	DUF3168 hypothetical protein	141	50	DUF3168 hypothetical protein	145
48	Tail protein	185	51	Putative major tail protein	186
ORF	ϕB166[a]		ORF	ϕB236[b]	
	Predicted function Region IV (24,886–36,266)	aa		Predicted function Region IV (25,224–36,614)	aa
49	DUF3647 hypothetical protein	168	52	DUF3647 hypothetical protein	164
50	Hypothetical protein	107	53	Hypothetical protein	105
51	Tape measure protein	961	54	Tape measure protein	961
52	Siphovirus-type tail component	313	55	Siphovirus-type tail component	311
53	Tail endopeptidase	628	56	Tail endopeptidase	628
54	Putative minor structural protein	632	57	Putative minor structural protein	632
55	DUF2479 hypothetical protein	607	58	DUF2479 hypothetical protein	607
56	DUF2977 hypothetical protein	125	59	DUF2977 hypothetical protein	125
57	XkdX superfamily protein	58	60	XkdX superfamily protein	60
58	DUF2951 hypothetical protein	99	61	DUF2951 hypothetical protein	77
ORF	ϕB166[a]		ORF	ϕB166[a]	
	Predicted function Region V (36,241–42,881)	aa		Predicted function Region V (36,590–43,228)	aa
59	Tail tip cell wall hydrolase	624	62	Tail tip cell wall hydrolase	624
60	Tail fibre protein	412	63	Tail fibre protein	412
61	phiETA ORF63-like protein	131	64	phiETA ORF63-like protein	131
62	Holin	91	65	Holin	91
63	Amidase	473	66	Amidase	473
64	Exfoliative toxin A	280	67	Exfoliative toxin A	280

Position of each region in the phage genome is indicated in brackets

[a] ORFs 01–05 and 09 were localized on the negative strand

[b] ORFs 01–03, 08, and 12 were localized on the negative strand

phages were divided into five genomic regions, which were designed with respect to the functional genomic architecture, based on the predicted regulatory elements and modular arrangement. Each of the five regions carries specific genes as follows: Region I: genes for lysogeny and regulation of transcription, region II: genes for products involved in DNA replication, region III: genes for terminase and capsid structure proteins, region IV: genes for tail proteins, and the smallest region V: genes for host lysis and the *eta* gene encoding exfoliative toxin A (Table 1; Fig. 3).

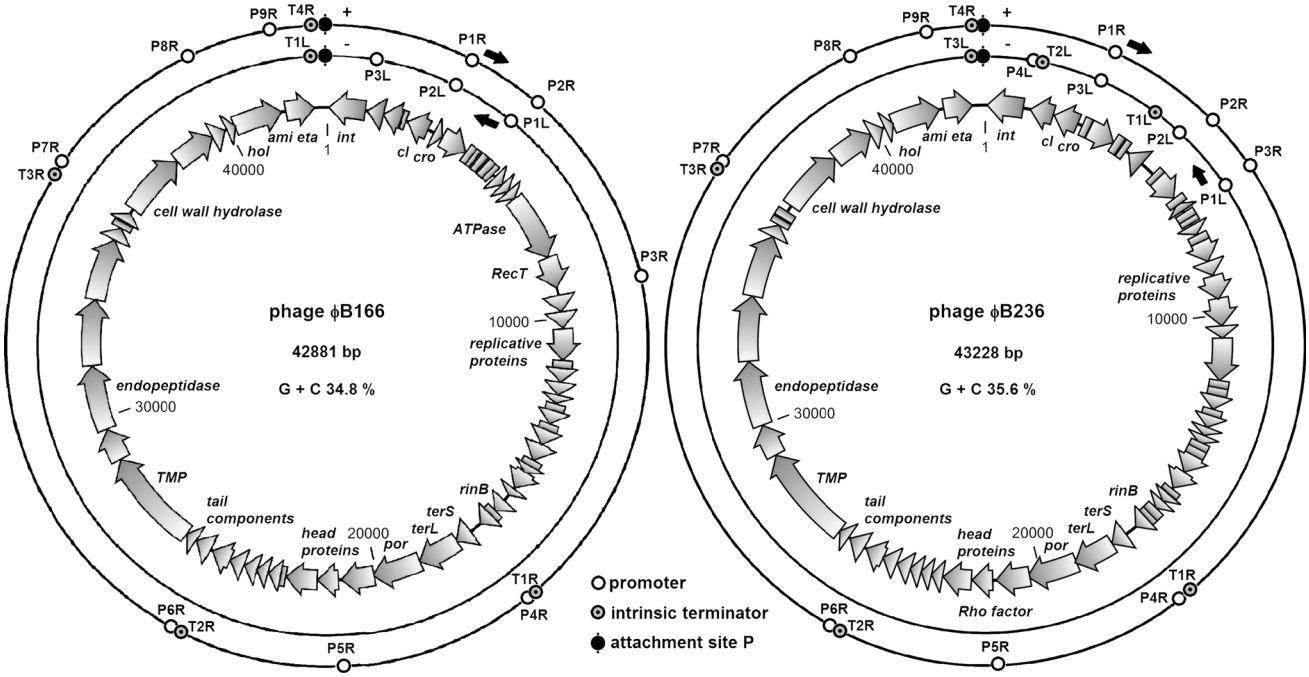

Fig. 2 Circular maps of the ϕB166 and ϕB236 genomes. ORFs are represented by *dark arrows* on *inner circles*. Promoters and terminators are marked on *outer circles*. Directions of transcription are indicated by *black arrows*. The main (+) and complementary (−) strands are distinguished. The attachment site P is indicated at the *top* of each map. The whole-genome size and GC content are provided. Positions are shown in bp. Detailed information is in Table 1 and Supplementary material in Table S1

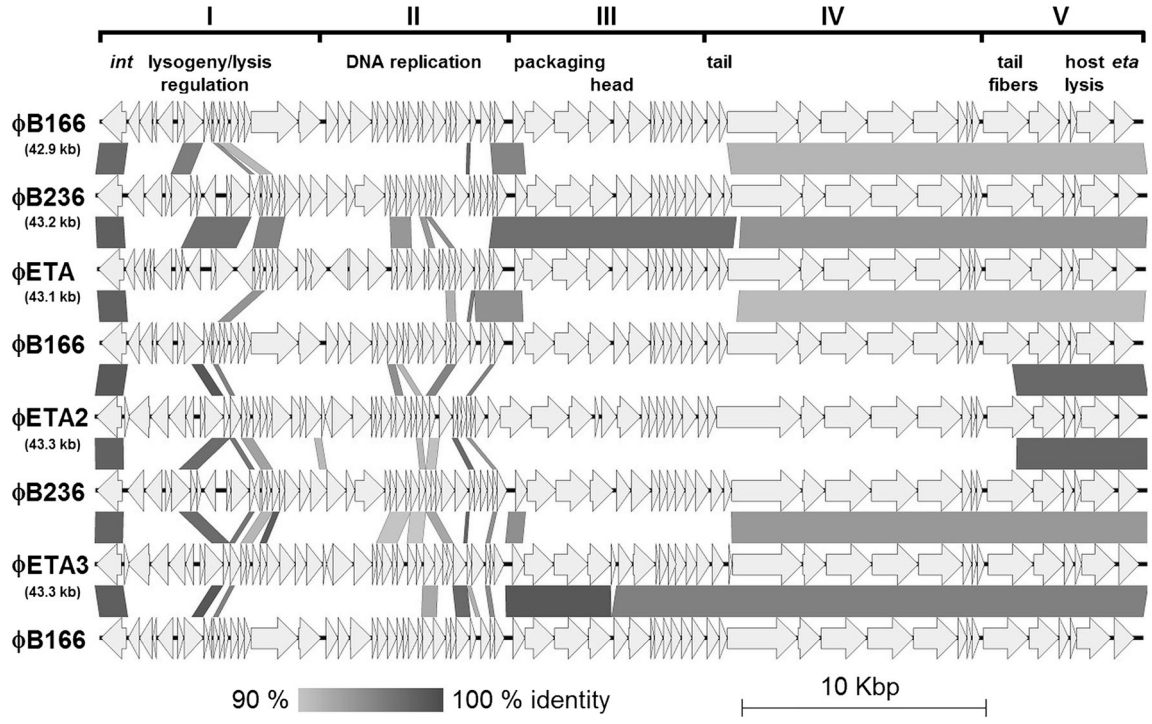

Fig. 3 Alignment of the genome maps of ϕB166 and ϕB236 and ϕETA, ϕETA2, and ϕETA3. Regions I−V and modules are depicted on the *top line*. ORFs are represented by *full arrows* and intergenic sequences by abscissa. *Shaded boxes* express the sequence identity levels between genomes. The phage genome sizes are noted in *brackets*

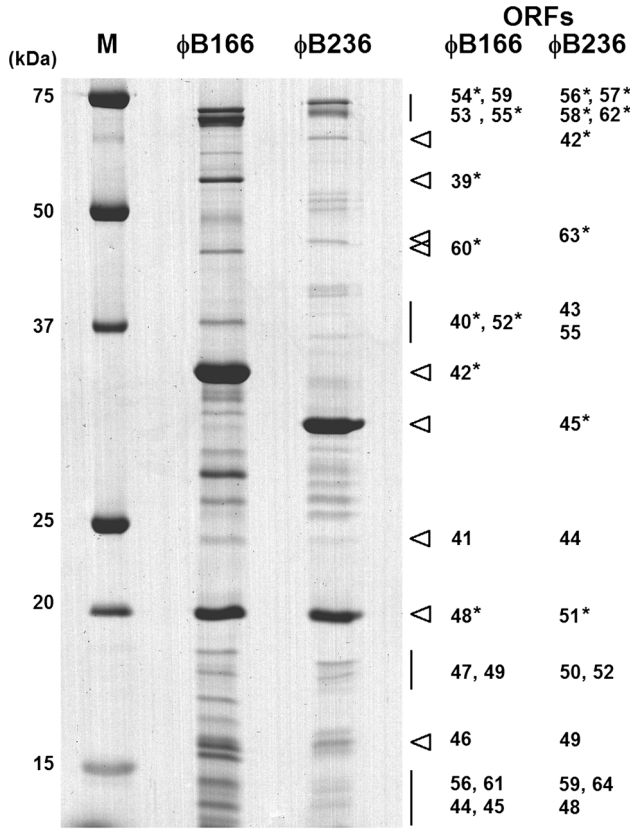

Fig. 4 SDS-PAGE patterns of virion proteins. M = Precision Plus Protein Standard. ORFs corresponding to protein bands are noted on the right. Described positions are marked by empty *arrow heads* or *vertical lines*. Protein bands used for MS analysis are marked by *asterisk*. Fragments of tape measure protein were detected only by MS. TerL and amidase fragments were identified only in the ϕB166 pattern. Details of ORFs are given in Table 1

The determination of the complete genome sequences revealed that ϕB166 and ϕB236 have genome sizes of 42.9 and 43.2 kb, respectively. The coding sequences (ORFs) take over 94.4 % of the genome of ϕB166 and 93.7 % of the genome of ϕB236. In addition, 12 promoters and five Rho-independent terminators were predicted in the genome of ϕB166, and 13 promoters and seven Rho-independent terminators were predicted in the ϕB236 genome (Fig. 2; Supplementary Material, Table S1).

The whole GC content corresponds to those in other B phages and is slightly superior to those in *S. aureus* (approximately 32.7 %). Based on the low percentage of G+C, genome location, and InterPro prediction, some ORFs seem to have a diverse origin. A good example is ϕB236-ORF08 and its promoter P2L (27.5 % G+C).

SDS-PAGE analysis of ϕB166 and ϕB236 virion proteins revealed major differences between the molecular weights of the capsid proteins which correlated with gene sequence variability detected in the respective ORFs (Fig. 4). The differences between SDS-PAGE patterns were also observed in the previously characterized *eta* phages ϕB557 and ϕB122 [20]. On the other hand, a resemblance was found between the tail and tail fibre components.

Comparison of ϕB166 and ϕB236 with *eta*-positive and *eta*-negative phages

Sequence analyses revealed that ϕB166 and ϕB236 are not closely related to each other or to other previously reported *eta* phages (Fig. 3; Table 2). The phage ϕB166 showed the following levels of total sequence similarity: 51 % to ϕETA, 36 % to ϕETA2, 67 % to ϕETA3, and 54 % to ϕB236. In respect of non-*eta* phages, the highest similarities were found between ϕB166 and the ϕNM4 (62 %), ϕ96 (63 %), ϕ71, and ϕ55 (51 % each). The region III showed 98 % homology to ϕNM4 and ϕ96; therefore, it may originate from a common ancestor or could have been acquired as a result of recombination exchange between phages during co-replication.

Whole-genome comparison of ϕB236 with other *eta* phages revealed the following identity levels: 78 % with ϕETA, 37 % with ϕETA2, 58 % with ϕETA3, and 53 % with ϕB166. As far as non-*eta* phages are concerned, the highest similarities were found between ϕB236 and ϕ71 (72 %), ϕ29 (70 %), ϕ55 (69 %), and StauST398-1 (67 %). The regions I and II of ϕB166 and ϕB236 are the most variable and distinct from those of other *eta* phages and non-*eta* phages.

Despite genome variability, all *eta* phages share highly similar sequences of the region V harbouring the major virulence gene encoding ETA. The phages ϕB166 and ϕB236 demonstrated the same type of integrase locus as ϕETA, ϕETA2, and ϕETA3. Much like ϕETA, these phages did not share the *xis* gene with ϕETA2 and ϕETA3, which indicates that the excisionase does not play a crucial role in releasing an *eta* prophage from the host chromosome.

The gene for Rho-termination factor domain protein was identified in ϕB236, but not in ϕB166. The same and/or very similar gene was found in ϕETA and in the non-*eta* phages ϕ88, ϕ92, StauST398-1, StauST398-5, ϕ55, ϕ71, ϕ29, and ϕ52A. The promoter and terminator sequences of phages showed reciprocal similarities almost analogously as the nearby ORFs. Differences between regulatory sequences are caused by variation in region II and the presence of presumptive morons (e.g. ϕB166 ORF09 or ϕB236 ORFs 08 and 12) flanked by their own promoters and/or terminators.

Table 2 Percentages of similarities between the genomic regions of ϕB166, ϕB236, and selected phages

Phage[a]		ϕB166 region[b]					ϕB236 region[b]				
Name	ID	I	II	III	IV	V	I	II	III	IV	V
eta-phages											
ϕB166 (Sa1, B)	KP893289	100	100	100	100	100	31	16	18	79	**98**
ϕB236 (Sa1, B)	KP893290	**28**	19	18	79	98	100	100	100	100	100
ϕETA (Sa1, B)	NC_003288	18	**32**	15	77	98	**50**	32	**97**	**90**	**98**
ϕETA2 (Sa1, B)	NC_008798	**28**	17	–	39	80	33	25	–	41	80
ϕETA3 (Sa1, B)	NC_008799	27	30	**98**	**93**	**99**	33	**34**	24	83	**98**
non eta-phages											
55 (Sa1, B)	NC_007060	17	42	15	75	56	38	34	**97**	90	55
71 (Sa1, B)	NC_007059	18	30	10	77	**81**	42	**62**	53	**93**	**80**
SAP-26 (Sa1, B)	NC_014460	40	19	–	41	38	40	25	–	43	38
StauST398-1 (Sa3, B)	NC_021326	4	36	25	76	77	13	34	**97**	89	77
TEM126 (Sa3, B)	HQ127381	31	35	–	39	34	21	10	–	42	35
ϕ11 (Sa5, B)	NC_004615	17	10	–	41	34	34	54	–	43	36
29 (Sa5, B)	NC_007061	7	17	15	77	55	30	56	84	**93**	54
69 (Sa5, B)	NC_007048	10	18	–	43	36	33	31	–	42	37
88 (Sa5, B)	NC_007063	14	34	10	77	55	27	47	62	92	55
ϕMR25 (Sa5, B)	NC_010808	15	24	–	42	35	**45**	37	–	42	36
52A (Sa6, B)	NC_007062	7	27	15	77	53	5	33	84	**93**	53
80 (Sa6, B)	DQ908929	8	25	–	77	53	10	33	84	**93**	53
ϕNM4 (Sa6, B)	DQ530362	3	49	**98**	90	34	27	34	24	80	33
92 (Sa7, B)	NC_007064	7	34	10	77	54	30	47	62	92	53
TEM123 (Sa7, B)	NC_017968	**60**	60	–	39	34	21	10	–	42	35
96 (Sa9, B)	NC_007057	7	31	**98**	**91**	53	3	56	24	79	54
StauST398-5 (-, B)	NC_023500	3	36	25	76	77	3	34	**97**	89	77
ϕPVL (Sa2, F)	NC_002321	35	50	–	–	<1	17	8	–	–	<1
ϕBU01 (Sa3, F)	KF831354	34	61	–	–	<1	11	12	–	–	<1
JS01 (Sa3, F)	NC_021773	49	**66**	15	–	–	16	13	–	–	–
ϕ13 (Sa3, F)	NC_004617	4	16	–	2	–	22	27	–	–	–
ϕNM3 (Sa3, F)	NC_008617	42	46	–	–	<1	12	9	–	–	<1
StauST398-4 (Sa3, F)	NC_023499	42	46	–	–	<1	12	9	–	–	–
P954 (Sa7, F)	NC_013195	2	24	–	2	<1	26	50	–	–	<1

[a] Phages are listed in order of assignment to serogroup and integrase family according to Kahánková et al. [27]

[b] The highest similarities determined in each region are highlighted in bold; (–) no significant similarity was found

Phage genomic mosaicism

In agreement with the known extensive mosaic structure of prophages resulting from the recombination among members of a phage species and horizontal transfer of sequences [34–36], many non-homologous ORFs and/or sequences located in the genomes of ϕB166 and ϕB236 were identified. In ϕB166, these were ORFs 2–4 and ORFs 29–30. In ϕB236, ORFs 31, 32, and 35 were unique. Both phages use the ϕETA-like *pac*-site located within the *terS* sequence as reported by Yamaguchi et al. [17]. In accordance with the recently proposed division of the *Siphoviridae* family [21], both phages studied have a tail protein architecture and catalytic domain distribution corresponding to the genus "Phietalikevirus", subgroup I. In contrast, there is a HNH domain in the ϕB236-ORF32 product, which is considered a typical characteristic of the proposed genus "3alikevirus".

Except the *eta* gene and its promoter, conserved region V is highly similar to that of the prophage of *S. aureus* strain 04-02981 (CP001844). Its genome contains the *ami* gene and a nearby sequence, highly similar to the terminal part of *eta* phages. It indicates that the *eta* gene and its promoter could be incorporated between the *ami* gene and the *eta*-terminator by recombination, which is inconsistent with the previously assumed aberrant excision [17].

Recombination events in *eta* phages are supported by the finding that a large part of the ϕB166 genome (ORF 14–22) is very similar to that of F phages (ϕPVL and ϕJS01). ORFs 13 and 23 in ϕB166 can be considered as the most probable recombination sites. They resemble those of some F phages (i.e. JS01, BU01, and ϕNM3), prophage StauST398-4 [37], and B phage ϕETA3. The genes involved in recombination were found in both phages studied. The ϕB166 genome contains the genes for RecT and RusA-like proteins, while ϕB236 contains Sak3-like and HNH endonuclease domain proteins. These proteins can mediate new rearrangements in the phage genomes, especially in polylysogenic strains or strains with defective prophages [36].

Conclusions

The emerging data strongly suggest that ETA-converting phages are crucial in the pathogenesis of staphylococcal skin blistering infections because of the extensive prevalence of ETA-producing impetigo strains of *S. aureus*. This work reports detailed genomic characteristics of two *eta* gene-positive bacteriophages as new members of a large group of diverse temperate phages encoding exfoliative toxin A. Based on the genomic comparisons between phages isolated in this work and those formerly characterized as *S. aureus* ETA-like B bacteriophages, it can be concluded that ϕB166 and ϕB236 represent the recent new lineages of as yet undescribed ETA-converting bacteriophages. Polymorphisms detected in their genomic sequences could be used as an identification tool for detailed classification of the *eta* phages. Their genomic mosaicism reveals them as a fluid gene pool to confer new properties to co-replicating phages and also as mediators of the *S. aureus* pathogenicity.

Acknowledgments The authors would like to thank their colleagues from the participating hospitals for providing the strains of *S. aureus*. Thanks are also due to Ms Eva Kodytková for valuable help. This work was supported by Grant No. NT12395-5 from the Internal Grant Agency of the Ministry of Health of the Czech Republic and project AdmireVet CZ.1.05/2.1.00/01.0006-ED0006/01/01 from the Czech Ministry of Education, Youth and Sports. The proteomic part was carried out with the support of the CEITEC (Central European Institute of Technology) Proteomics Core Facility, ID No. CZ.1.05/1.1.00/02.0068, financed from the European Regional Development Fund and Czech Science Foundation (Project No. P206-12-G151).

References

1. T. Bae, T. Baba, K. Hiramatsu, O. Schneewind, Mol. Microbiol. **62**, 1035–1047 (2006)
2. C. Goerke, R. Pantůček, S. Holtfreter, B. Schulte, M. Zink, D. Grumann, B.M. Broker, J. Doškař, C. Wolz, J. Bacteriol. **191**, 3462–3468 (2009)
3. R. Hrstka, V. Růžičková, P. Petráš, R. Pantůček, S. Rosypal, J. Doškař, Int. J. Med. Microbiol. **296**, 49–54 (2006)
4. J.J. Iandolo, V. Worrel, K.H. Groicher, Y. Qian, R. Tian, S. Kenton, A. Dorman, H. Ji, S. Lin, P. Loh, S. Qi, H. Zhu, B.A. Roe, Gene **289**, 109–118 (2002)
5. R. Pantůček, J. Doškař, V. Růžičková, P. Kašpárek, E. Oráčová, V. Kvardová, S. Rosypal, Arch. Virol. **149**, 1689–1703 (2004)
6. V. Růžičková, R. Karpíšková, R. Pantůček, M. Pospíšilová, P. Černíková, J. Doškař, Int. J. Food Microbiol. **121**, 60–65 (2008)
7. R.P. Novick, G.E. Christie, J.R. Penadés, Nat. Rev. Microbiol. **8**, 541–551 (2010)
8. A.J. McCarthy, A.A. Witney, J.A. Lindsay, Front. Cell. Infect. Microbiol. **2**, 1–10 (2012)
9. A.D. Dearborn, T. Dokland, Bacteriophage **2**, 70–78 (2012)
10. M. Varga, L. Kuntová, R. Pantůček, I. Mašlaňová, V. Růžičková, J. Doškař, FEMS Microbiol. Lett. **332**, 146–152 (2012)
11. I. Mašlaňová, J. Doškař, M. Varga, L. Kuntová, J. Mužík, D. Malúšková, V. Růžičková, R. Pantůček, Environ. Microbiol. Rep. **5**, 66–73 (2013)
12. V. Růžičková, R. Pantůček, P. Petráš, I. Machová, K. Kostýlková, J. Doškař, Int. J. Med. Microbiol. **302**, 237–241 (2012)
13. Y. Endo, T. Yamada, K. Matsunaga, Y. Hayakawa, T. Kaidoh, S. Takeuchi, Vet. Microbiol. **96**, 81–90 (2003)
14. M. Amagai, N. Matsuyoshi, Z.H. Wang, C. Andl, J.R. Stanley, Nat. Med. **6**, 1275–1277 (2000)
15. T. Yamaguchi, K. Nishifuji, M. Sasaki, Y. Fudaba, M. Aepfelbacher, T. Takata, M. Ohara, H. Komatsuzawa, M. Amagai, M. Sugai, Infect. Immun. **70**, 5835–5845 (2002)
16. S. Ladhani, R.W. Evans, Arch. Dis. Child. **78**, 85–88 (1998)
17. T. Yamaguchi, T. Hayashi, H. Takami, K. Nakasone, M. Ohnishi, K. Nakayama, S. Yamada, H. Komatsuzawa, M. Sugai, Mol. Microbiol. **38**, 694–705 (2000)
18. Y. Yoshizawa, J. Sakurada, S. Sakurai, K. Machida, I. Kondo, S. Masuda, Microbiol. Immunol. **44**, 189–191 (2000)
19. T. Yamaguchi, T. Hayashi, H. Takami, M. Ohnishi, T. Murata, K. Nakayama, K. Asakawa, M. Ohara, H. Komatsuzawa, M. Sugai, Infect. Immun. **69**, 7760–7771 (2001)
20. P. Holochová, V. Růžičková, R. Pantůček, P. Petráš, R. Janisch, J. Doškař, Res. Microbiol. **161**, 260–267 (2010)
21. D. Gutiérrez, E.M. Adriaenssens, B. Martínez, A. Rodríguez, R. Lavigne, A.M. Kropinski, P. García, Arch. Virol. **159**, 389–398 (2014)
22. V. Růžičková, R. Pantůček, P. Petráš, J. Doškař, I. Sedláček, S. Rosypal, Int. J. Med. Microbiol. **292**, 541–545 (2003)
23. P. Holochová, V. Růžičková, L. Dostálová, R. Pantůček, P. Petráš, J. Doškař, Diagn. Microbiol. Infect. Dis. **66**, 248–252 (2010)
24. Y. Duval-Iflah, Can. J. Microbiol. **18**, 1491–1497 (1972)
25. J. Sambrook, E.F. Fritsch, T. Maniatis, *Molecular cloning: a laboratory manual*, 2nd edn. (Cold Spring Harbor Laboratory, New York, 1989)
26. J. Doškař, P. Pallová, R. Pantůček, S. Rosypal, V. Růžičková, P. Pantůčková, J. Kailerová, K. Klepárník, Z. Malá, P. Bocek, Can. J. Microbiol. **46**, 1066–1076 (2000)
27. J. Kahánková, R. Pantůček, C. Goerke, V. Růžičková, P. Holochová, J. Doškař, Environ. Microbiol. **12**, 2527–2538 (2010)
28. V. Růžičková, J. Voller, R. Pantůček, P. Petráš, J. Doškař, Folia Microbiol. **50**, 499–502 (2005)
29. V. Solovyev, A. Salamov, in *Metagenomics and its applications in agriculture, biomedicine and environmental studies*, ed. by R.W. Li (Nova Science Publishers, New York, 2011), pp. 61–78
30. E.A. Lesnik, R. Sampath, H.B. Levene, T.J. Henderson, J.A. McNeil, D.J. Ecker, Nucleic Acids Res. **29**, 3583–3594 (2001)
31. F. Gao, C.T. Zhang, Nucleic Acids Res. **34**, 686–691 (2006)
32. R. Pantůček, F. Götz, J. Doškař, S. Rosypal, Int. J. Syst. Bacteriol. **46**, 216–222 (1996)

33. L. Eyer, R. Pantůček, Z. Zdráhal, H. Konečná, P. Kašpárek, V. Růžičková, L. Hernychová, J. Preisler, J. Doškař, Proteomics **7**, 64–72 (2007)
34. R.W. Hendrix, M.C. Smith, R.N. Burns, M.E. Ford, G.F. Hatfull, Proc. Natl. Acad. Sci. U.S.A. **96**, 2192–2197 (1999)
35. T. Kwan, J. Liu, M. DuBow, P. Gros, J. Pelletier, Proc. Natl. Acad. Sci. U.S.A. **102**, 5174–5179 (2005)
36. M. De Paepe, G. Hutinet, O. Son, J. Amarir-Bouhram, S. Schbath, M.-A. Petit, PLoS Genet. (2014). doi:10.1371/journal.pgen.1004181
37. N. Van Der Mee-Marquet, A.-R. Corvaglia, A.-S. Valentin, D. Hernandez, X. Bertrand, M. Girard, J. Kluytmans, P.Y. Donnio, R. Quentin, P. Francois, Infect. Genet. Evol. **18**, 299–308 (2013)

APPENDIX 18

Tkadlec J, Vařeková E, Pantůček R, Doškař J, Růžičková V, Botka T, Fila L, Melter O (2015) Characterization of *Staphylococcus aureus* strains isolated from Czech cystic fibrosis patients: High rate of ribosomal mutation conferring resistance to MLS(B) antibiotics as a result of long-term and low-dose azithromycin treatment. *Microbial Drug Resistance* 21:416–423. https://doi.org/10.1089/mdr.2014.0276

(JCR 2015: IF = 2.529; Q2 – Infectious Diseases)

Copyright © 2015 by Sage Publications. Reprinted by Permission of Sage Publications.

MICROBIAL DRUG RESISTANCE
Volume 21, Number 4, 2015
© Mary Ann Liebert, Inc.
DOI: 10.1089/mdr.2014.0276

Characterization of *Staphylococcus aureus* Strains Isolated from Czech Cystic Fibrosis Patients: High Rate of Ribosomal Mutation Conferring Resistance to MLS_B Antibiotics as a Result of Long-Term and Low-Dose Azithromycin Treatment

Jan Tkadlec,[1] Eva Vařeková,[1] Roman Pantůček,[2] Jiří Doškař,[2] Vladislava Růžičková,[2] Tibor Botka,[2] Libor Fila,[3] and Oto Melter[1]

Staphylococcus aureus is one of the most frequent pathogens infecting the respiratory tract of patients with cystic fibrosis (CF). This study was the first to examine *S. aureus* isolates from CF patients in the Czech Republic. Among 100 *S. aureus* isolates from 92 of 107 observed patients, we found a high prevalence of resistance to macrolide–lincosamide–streptogramin B (MLS_B) antibiotics (56%). More than half of the resistant strains (29 of 56) carried a mutation in the MLS_B target site. The emergence of MLS_B resistance and mutations conferring resistance to MLS_B antibiotics was associated with azithromycin treatment ($p = 0.000000184$ and $p = 0.000681$, respectively). Methicillin resistance was only detected in 3% of isolates and the rate of resistance to other antibiotics did not exceed 12%. The prevalence of small-colony variant (SCV) strains was relatively low (9%) and eight of nine isolates with the SCV phenotype were thymidine dependent. The study population of *S. aureus* was heterogeneous in structure and both the most prevalent community-associated and hospital-acquired clonal lineages were represented. Of the virulence genes, enterotoxin genes *seg* ($n = 52$), *sei* ($n = 49$), and *sec* ($n = 16$) were the most frequently detected among the isolates. The PVL genes (*lukS-PV* and *lukF-PV*) have not been revealed in any of the isolates.

Introduction

Cystic fibrosis (CF) is the most common life-shortening genetic disorder in Caucasians. It is caused by mutations in the cystic fibrosis transmembrane conductance regulator (CFTR) gene encoding a chloride channel resulting in abnormal ion transport. CF targets many organs, including the pancreas, liver, and intestine, but the most commonly affected are the lungs. Production of thick mucus on the respiratory epithelial surface is the cause of decreased mucociliary clearance which, in turn, leads to chronic respiratory infection. This ongoing infection together with an inflammatory response leads to irreversible progressive lung damage, and pulmonary insufficiency is the primary cause of death in the majority of patients with CF.[31] *Pseudomonas aeruginosa, Haemophilus influenzae, Staphylococcus aureus, Stenotrophomonas maltophilia, Burkholderia cepacia* complex (*Bcc*), and *Achromobacter xylosoxidans* are the most common pathogens infecting the lungs of these patients.[36]

S. aureus, historically the first bacterial pathogen to be associated with respiratory infections in patients with CF,[1] is still one of the most common isolates recovered from the sputum of these patients, and children in particular, with a prevalence ranging between 50% and 70% across Europe.[3,20,43] Recently, increasing prevalence of *S. aureus*, including methicillin-resistant *S. aureus* (MRSA), at some US CF care centers is an emerging challenge in CF.[10,36]

S. aureus small-colony variants (SCVs) are often recovered from chronic and persistent infections, including CF lung infection.[19] SCVs represent a persistent subpopulation

[1]Department of Medical Microbiology, 2nd Faculty of Medicine, Charles University in Prague and Motol University Hospital, Prague, Czech Republic.
[2]Department of Experimental Biology, Faculty of Science, Masaryk University, Brno, Czech Republic.
[3]Department of Pneumology, 2nd Faculty of Medicine, Charles University in Prague and Motol University Hospital, Prague, Czech Republic.

of metabolically deficient/auxotrophic bacteria that usually grow slowly in nonpigmented and nonhemolytic colonies with pinpoint or fried egg morphology. A pinpoint colony isolate is approximately 10 times smaller in size than the parent strain.[8] SCV formation is associated with prolonged antibiotic treatment with trimethoprim–sulfamethoxazole (TMP-SXT) or aminoglycosides.[9,20] The underlying mechanisms for SCV formation appear to be disruption of the electron transport chain or thymidylate synthase pathway for menadione/hemin- and thymidine-dependent SCVs, respectively.[22,33] These metabolic defects are responsible for SCV resistance or tolerance to TMP-SXT and aminoglycosides and because of slow growth of the affected cells also to the antibiotics targeting exponentially growing bacteria. The significance of SCVs in the context of chronic infections is also supported by their increased ability to persist intracellularly in different cell lines. Moreover, SCVs in CF were found to be associated with hypermutability which, in turn, results in a high rate of Macrolide–Lincosamide–Streptogramin B (MLS_B) resistance in these strains.[4,35] The high rate of MLS_B resistance could be a result of the long-term low-dose azithromycin therapy. Azithromycin is frequently used in CF patients for its beneficial effects on inflammation and lung physiology and also the potential to reduce *P. aeruginosa* biofilm formation.[7]

The impact of *S. aureus* on the pathogenesis of respiratory tract infections in CF patients is not fully understood, with the exception of MRSA and SCV strains, which are associated with poor clinical outcome.[5,42] Although the presence of pathogenic bacteria such as *S. aureus* in the respiratory tract is not normal, different studies disagree on the impact of *S. aureus* on the progression of CF.[13,25,39]

The goal of our study was to analyze the prevalence of SCVs, virulence factors, and antibiotic resistance (together with the mechanisms underlying the resistance) among *S. aureus* isolates from Czech CF patients.

Methods

Patients and isolates

Between July 2011 and March 2013, 100 *S. aureus* isolates were recovered from 92 of 107 selected children and adult patients followed up at the Centre for CF of the Motol University Hospital, when presenting for periodical check-ups or with exacerbation. The study group consists of patients with documented staphylococcal infection in their medical records followed up at the Prague CF Centre and selected in an attempt to maximize the number of *S. aureus* isolates to analyze. Written informed consent was obtained from all study participants or their parents.

The *S. aureus*-positive group included 44 males and 48 females and the median age when sampled was 16 years (age range from below one year to 37 years). Single unique *S. aureus* isolates were recovered from 84 patients and two phenotypically different (in colony size, shape, or pigmentation) isolates from the same sputum sample were available from eight patients. Most patients ($n=85$) had chronic staphylococcal infection as defined according to the modified Leeds criteria: $>50\%$ of the sputum samples positive during the last 12 months. At least four sputum samples were collected during that period.[44]

Species identification was performed by matrix-assisted laser desorption/ionization time-of-flight mass spectrometry (MALDI-TOF MS) (Bruker Daltonics). Nonhemolytic and nonpigmented isolates with a small colony size or fried egg morphology were considered to be *S. aureus* SCVs. These isolates were also tested by the Pastorex Staph Plus© latex agglutination test (Bio-Rad Laboratories) and biochemical STAPHYtest 16 (Erba Lachema).

When sampled or within three months, coinfection with *S. aureus* and the following bacteria was detected: *P. aeruginosa* ($n=21$), *Bcc* ($n=5$), *S. maltophilia* ($n=8$), *P. aeruginosa* and *Bcc* ($n=1$), and *P. aeruginosa* and *S. maltophilia* ($n=3$). Within one year before the sampling date, the patients were treated with long-term azithromycin ($n=22$), trimethoprim–sulfamethoxazole (TMP-SXT, $n=55$, for 25 days on an average, for a median of 20 days, long-term TMP-SXT in one patient), and other MLS_B antibiotics (clindamycin, clarithromycin, and spiramycin) ($n=23$, for 21 days on an average, for a median of 14 days). The use of other antibiotics was not reported.

Susceptibility testing

Antimicrobial susceptibility of the strains was determined by the disk diffusion method (DDM) according to the EUCAST guidelines for oxacillin, cefoxitin, erythromycin, clindamycin, gentamicin, tetracycline, amoxicillin/clavulanic acid, rifampicin, ofloxacin, vancomycin, teicoplanin, TMP-SXT, linezolid, azithromycin, and quinupristin/dalfopristin.[12] In addition, the minimum inhibitory concentrations (MICs) for oxacillin, vancomycin, gentamicin, erythromycin, or clindamycin were measured for strains with a borderline DDM value and for MRSA strains (vancomycin) using M.I.C. Evaluator strips (Oxoid). Inducible MLS_B resistance was tested by the D-test. *S. aureus* and SCV isolates were cultured on Mueller Hinton (MH) agar and Columbia agar supplemented with sheep blood (Oxoid), respectively. Plates were incubated at 37°C for 24 and 48 hours. *S. aureus* strain ATCC 25923 was used as a quality control.

Polymerase chain reaction detection of MLS_B, aminoglycoside, and methicillin resistance genes

Bacterial genomic DNA was extracted using the Amplicor® Respiratory Specimen Preparation Kit (Roche) and used as a template for polymerase chain reaction (PCR).

Detection of the methicillin resistance gene *mecA*, MLS_B resistance genes *ermA*, *ermB*, *ermC*, *ermT*, and *msrA*, and aminoglycoside resistance genes *aadC, aphA3,* and *aac-aphD* was performed as described previously.[17,23,30,41]

PCR amplicons were resolved in 2% (w/v) agarose gels in Tris-boric acid-EDTA (TBE) buffer at constant voltage (6 V/cm) and stained with ethidium bromide (0.5 mg/ml). Images were photographed under UV light using a gel documentation system.

Detection of mutations conferring resistance to MLS_B

Amplification and sequencing were conducted using the respective primers specific for the domain V of the 23S rRNA (*rrl*) and the genes for ribosomal proteins L4 (*rplD*) and L22 (*rplV*), as described previously.[35] PCR products were purified using MagneSil Paramagnetic Particles

(Biomek 3000; Beckman Coulter) and sequenced by ABI 3130xl Genetic Analyzer (Biotechnology Center).

The sequence of each gene was compared with sequences of genes from susceptible strain *Staphylococcus aureus* subsp. *aureus* NCTC 8325 (GenBank accession number NC_007795) for the detection of mutations.

spa, *MLST, and SCC*mec *typing*

Single-locus DNA sequencing of the repeat region of the *Staphylococcus* protein A gene (*spa*) was performed on all 100 isolates according to the protocol described on the European Network of Laboratories for sequence-based typing of microbial pathogens website (www.seqnet.org). *spa* types were assigned by the Ridom StaphType software (Ridom). The BURP (Based Upon Repeat Pattern) algorithm was used to define *spa* clonal complexes (*spa*-CC). Multilocus sequence types (ST) and clonal complexes (CC) were inferred from the *spa* type in the *spa* server database (http://spaserver. ridom.de/). SCC*mec* and MLST typing of the MRSA isolates was performed as described previously.[11,26]

Virulence gene detection

The exfoliatin genes *eta*, *etb*, and *etd,* staphylococcal enterotoxin genes *sea*, *sej*, *see*, *sec*, *seh*, *seb*, *seg*, *sed*, and *sei*, toxic shock syndrome gene *tst*, and Panton-Valentine leukocidin (PVL) genes *lukS-PV* and *lukF-PV* were detected using PCR and multiplex PCR, as described previously.[24,28,38]

SCV auxotrophy tests

SCV strains were screened for auxotrophy using standard 5-μg hemin disks (ITEST plus) and sterile blank disks impregnated with 15 μl of thymidine or menadione solution (Sigma-Aldrich) at a concentration of 100 μg/ml, as described previously.[3] Isolates were plated in duplicate on MH agar (Oxoid), with disks with auxotrophy supplements placed on one plate and the other plate serving as a negative control. The isolates growing only in the presence of an auxotrophic supplement were classified as auxotrophic.

Statistical analyses

Two-tailed Fisher's exact test was used to analyze binary variables, whereas continuous scaled variables were evaluated with the nonparametric Kruskal–Wallis test. A p-value of ≤ 0.05 was considered to be statistically significant for all analyses. Statistical analyses were performed using *STATISTICA* software, version 12 (StatSoft).

Results

Patients

During the study period, the number of CF patients in the Czech Republic varied from 542 in 2011 to 586 in 2013 and more than half of these patients (325) were followed up at the Centre for CF of the Motol University Hospital (data derived from the Czech Cystic Fibrosis Patient Registry www.cfregistr.cz/). The prevalence of *S. aureus* in our CF patients could not be determined due to incomplete data, but *S. aureus* was recovered at least once from at least 124 (38.8%) of about 325 patients. In our study, we screened samples from 107 selected patients for the presence of *S. aureus*. From July 2011 to March 2013, we collected 100 *S. aureus* isolates from 92 of the 107 patients. SCV phenotype prevalence among *S. aureus* isolates was about 9% ($n=9$).

Susceptibility to antibiotics

The prevalence of resistance to oxacillin/cefoxitin (MRSA) was 3.26% among patients ($n=3$) and 3% among *S. aureus* isolates ($n=3$). The respective rates of resistance to most other antibiotics tested ranged from 1% to 12% (Table 1), with the exception of resistance to MLS_B antibiotics found in 55% of isolates. Of the MLS_B-resistant isolates, 48% showed constitutive resistance to macrolides and lincosamides ($cMLS_B$), 32% possessed inducible resistance ($iMLS_B$), and 20% were resistant to macrolides only (ERY).

MLS_B-resistant *S. aureus* was recovered from all patients treated with long-term azithromycin and the association between MLS_B resistance and azithromycin treatment reached unambiguous statistical significance ($p=0.000000184$). All of the 22 azithromycin-treated patients harbored MLS_B-resistant strains.

Resistance determinants

All oxacillin- and cefoxitin-resistant strains ($n=3$) harbored the *mecA* gene. The presence of the *aphA3*, *aac-aphD*, and *aadC* genes either alone or in combination was identified as the cause of resistance to aminoglycosides in 10 isolates. One aminoglycoside-resistant isolate with the SCV phenotype did not possess any aminoglycoside resistance determinant. A possible explanation is decreased aminoglycoside susceptibility in SCV strains. Disruption of the respiratory chain in SCV strains is resulting in changes in the membrane potential and the consequent decreased transport of the aminoglycosides into the bacterial cell that eventually leads to the resistance to the aminoglycosides.[33]

Table 1. Prevalence of Antibiotic Resistance and Small-Colony Variant Isolates

Resistance	*MRSA*	*TMP-SXT*	*GEN*	*TET*	*OFX*	*RIF*	*Total MLS_B*	*$iMLS_B$*	*$cMLS_B$*	*ERY*	*SCV*
No. of isolates	3	12	11	5	4	1	56	18	27	11	9
No. of pts (%)	3 (3.26)	11 (11.96)	11 (11.96)	4 (4.35)	4 (4.35)	1 (1.09)	51 (55.43)	17 (18.48)	24 (26.09)	10 (10.87)	9 (9.78)

$cMLS_B$, constitutive MLS_B resistance; ERY, erythromycin; GEN, gentamicin; $iMLS_B$, inducible MLS_B resistance; MLS_B, macrolide-lincosamide-streptogramin B; MRSA, methicillin-resistant *Staphylococcus aureus*; OFX, ofloxacin; RIF, rifampin; SCV, small-colony variant; TET, tetracycline; TMP-SXT, trimethoprim–sulfamethoxazole.

TABLE 2. MECHANISM OF MLS_B RESISTANCE

Resistance mechanism	*Profile*	*No. of isolates (%)*	spa-*types*
Gene		26 (46.43%)	
ermA		9 (16.07%)	t003, t209, t786, t5098, t8826, t13812
	$iMLS_B$	5	
	$cMLS_B$	4	
ermC		10 (17.86%)	t002, t084, t091, t095, t177, t548, t579, t13495
	$iMLS_B$	9	
	$cMLS_B$	1	
ermA + ermC	$cMLS_B$	1 (1.79%)	t2249
ermT	$iMLS_B$	2 (3.57%)	t571, t1451
msrA	ERY	4 (7.14%)	t024, t091, t398, t550
Target-site alteration		29 (51.79%)	t002, t012, t015, t024, t056, t065, t091, t095, t153,
23S RNA	$cMLS_B$	23 (41.07%)	t164, t311, t386, t643, t831, t1365, t1510, t1671, t2275,
L4	ERY	6 (10.71%)	t2449, t6906, t10146, t12062, t13497, t13498, t13503
Unknown	ERY	1 (1.79%)	t10146
Total of isolates		56	

The *ermA*, *ermC*, *ermT*, and *msrA* genes as well as antibiotic target-site mutations—domain V of the 23S rRNA (*rrl*) and ribosomal protein L4 gene (*rplD*) mutations—were identified as MLS_B resistance determinants. In one isolate, the cause of resistance was not determined (Table 2). The mutations conferring MLS_B resistance were associated with azithromycin treatment (13 of 26 patients with such mutations were treated with azithromycin, $p = 0.000681$). The *erm* and *msrA* genes were not associated with azithromycin treatment ($p = 0.1078$).

Small-colony variant

Eight of nine *S. aureus* isolates with the SCV phenotype appeared to be thymidine auxotrophic and one readily reverted to wild type after subculture. All isolates exhibited resistance to TMP-SXT. The SCV-positive patients at a median age of 17 years (range from four to 31 years) were older than the remaining patients, but the difference did not reach statistical significance ($p = 0.5361$). No association was observed between SCV positivity and TMP-SXT treatment ($p = 0.079$), sex ($p = 0.302$), or coinfection with *P. aeruginosa* ($p = 0.4419$), *S. maltophilia* ($p = 0.0723$), or *Bcc* ($p = 0.470$).

Typing

The *spa* typing revealed 65 *spa* types among 100 *S. aureus* isolates from CF patients ($n = 92$). The most common *spa* types were t065 and t127, each detected in five isolates. The *spa* types were further divided using the BURP algorithm of the Ridom Staph Type software (Fig. 1) into 12 clusters (spa-CC) and 16 singletons (*spa* types not assigned to any of the clusters). Five isolates were excluded from the cluster analysis due to an insufficient number of repeats. For the *spa*-CC, where both *spa* types and ST were assigned, the respective MLST CC are also indicated. The largest cluster CC-t065 (MLST CC45) included 19 isolates from 18 patients, followed by CC-t002 (MLST CC5) comprising 10 isolates from 10 patients (Table 3).

MLST and SCC*mec* typing was performed on all MRSA isolates ($n = 3$). All of them showed identical ST225 and identical SCCmec type II, respectively. Because of their shared genetic background (*spa* type t003, SCCmec type II and MLST type ST225), all MRSA strains were assigned to the widespread clonal complex CC5. Detected strain ST225-MRSA-II is a single-locus variant of ST5-MRSA-II known also as UK-EMRSA-3, New York-Japan Clone, and Rhine-Hesse Epidemic Strain.[29]

Virulence genes

The most prevalent virulence genes detected in the study isolates were the staphylococcal enterotoxin genes *seg* ($n = 52$), *sei* ($n = 49$), and *sec* ($n = 16$). The staphylococcal

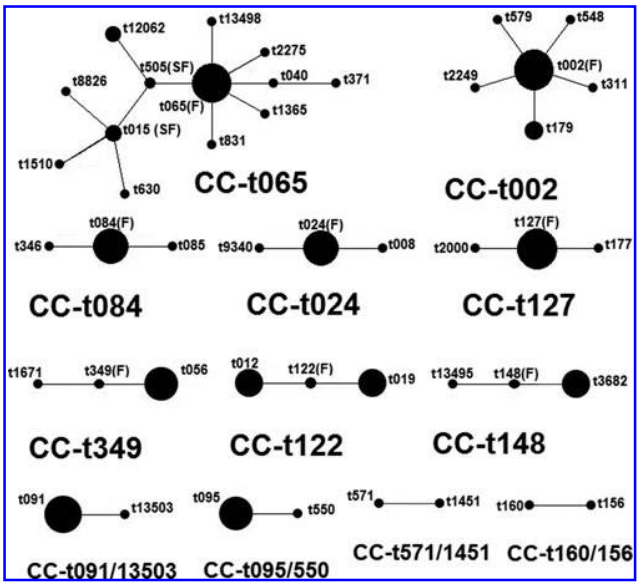

FIG. 1. BURP clustering of *spa* types. The *spa* typing data from *S. aureus* isolates were analyzed by the BURP algorithm (http://spaserver.ridom.de/, StaphType software v. 1.5, Ridom). Each spa type identified is depicted with a *circle*. The size of the *circle* is proportional to the frequency of the *spa* type in the population. Related *spa* types are connected with a *black* line. (F) or (SF) founder or subfounder of each clonal complex.

Table 3. *spa* and MLST Clonal Complexes and Their Frequency

spa-*CC*	*MLST CC (STs)*	*Origin*	spa-*types*	*Frequency% (no.)*	
CC-t065	CC45 (ST45,ST46)	HA	t015, t040, t065, t371, t505, t630, t831, t1365, t1510, t2275, t8826, t12062, t13498	19 (19)	
CC-t002	CC5 (ST5, ST231)	HA	t002, t179, t311, t548, t579, t2249	10 (10)	
CC-t084	CC15 (ST1, ST15, ST18, ST772)	CA	t084, t085, t346	5 (5)	
CC-t024	CC8 (ST8, ST247, ST250, ST254)	CA	t008, t024, t9340	5 (5)	
CC-t127	CC15 (ST1, ST3)	CA	t127, t2000	7 (7)	
CC-t349	(ST101)	ND	t056, t349, t1671	5 (5)	
CC-t122	CC30 (ST30, ST34, ST1472)	CA	t012, t019, t122	5 (5)	
CC-t148	CC8 (ST8, ST72)	CA	t148, t3682, t13495	4 (4)	
CC-t091/13503	CC7 (ST7, ST1867)	CA	t091, t13503	5 (5)	
CC-t095/550	CC45 (ST45)	HA	t095, t550	4 (4)	
CC-t571/1451	CC398 (ST398)	LA	t571, t1451	2 (2)	
CC-t160/156	(ST12, ST13)	ND	t156, t160	2 (2)	
Singletons	CC5 (ST225)	HA	t003	3	22 (22)
	(ST20)	ND	t164	2	
	(ST97)	ND	t224	1	
	(ST109)	ND	t209	2	
	CC45(ST45)	HA	t10146	14	
	ND	ND	t786, t2449, t5098, t6155, t6906, t153, t13497, t13500, t13502, t13505, t13812		
Excluded	CC15 (ST1)	CA	t386	2	5 (5)
	ND	ND	t398, t586, t643	3	

spa type of the MRSA strains is underlined.
CA, community-associated strains of *S. aureus*; HA, healthcare-associated strains of *S. aureus;* LA–livestock-associated strains of *S. aureus*, ND, not determined.

enterotoxin genes *sea* ($n=8$), *seb* ($n=1$), *sed* ($n=6$), *seh* ($n=10$), and *sej* ($n=5$), exfoliatin genes *eta* ($n=2$) and *etd* ($n=3$), and toxic shock syndrome toxin gene *tst* ($n=1$) were found sporadically in one to 10 isolates. The PVL genes (*lukS-PV* and *lukF-PV*), exfoliatin B gene (*etb*), or staphylococcal enterotoxin E gene (*see*) were not detected in any of the isolates.

Discussion

This is the first detailed study of *S. aureus* isolates from CF patients to be conducted in the Czech Republic. The study objective was to analyze the population structure of *S. aureus* isolates from CF patients and to investigate in detail antibiotic resistance and virulence of these isolates, with emphasis on the study of the MLS_B resistance mechanisms and occurrence of SCVs.

S. aureus is among the most commonly isolated bacterial pathogens in CF patients, with a prevalence rate ranging between 30 and 70% across Europe.[3,20,21,43] *S. aureus* isolates from CF patients included MRSA and SCV strains known to be associated with worse lung disease in CF patients.[5,42] Increasing prevalence of MRSA in some US CF care centers is an emerging challenge in CF.[18] In comparison with the US data, the MRSA prevalence of 3.26% (three patients) in our study cohort was relatively low. All MRSA-positive patients were infected with the ST225-MRSA-II strain (t003/ST225/SCCmecII) assigned to the globally widespread hospital-acquired MRSA (HA-MRSA) CC5.[40]

The prevalence of SCV strains in *S. aureus*-positive CF patients has been reported to range between 17% and 52%.[3,20,43] In our study cohort, the respective rate was 9.78% only (nine patients). However, the study design with the prospective collection of single-patient isolates only can be responsible for a slight underestimation of the overall prevalence of SCV strains. In six additional patients, SCV strains were detected in samples collected outside the time frame of this study. When taking into account these six patients, the SCV prevalence reaches 16.3%, which does not differ significantly from the data reported by other countries. Most SCV isolates (eight of nine) were recovered along with the normal colony variant (NCV) strain, isogenic in six cases, from the same sample. Prophylactic TMP-SXT, older age, and *P. aeruginosa* coinfection have been identified previously as the factors associated with SCV isolation.[3,27] In total, 55 patients were treated with TMP-SXT (from 10 days to continuous treatment, average duration of 26 days) and only eight of them harbored SCV strains; thus, correlation between TMP-SXT and SCV formation did not reach statistical significance ($p=0.079$). However, our findings are not in conflict with previous studies that confirmed an association between long-term prophylactic TMP-SXT treatment and the presence of SCV.[3,20] Eight of our nine patients with SCVs were treated with TMP-SXT, but none of them prophylactically. Since the SCV formation is caused by mutation[22] and the mutations are stochastical processes, it is not surprising that without strong selective pressure of continuous prophylactic TMP-SXT treatment SCV appears only in a fraction of patients occasionally treated with TMP-SXT. *P. aeruginosa* coinfection was only detected in one patient. The mean age was higher in SCV patients than in non-SCV patients, but the difference did not reach statistical significance. These discrepancies from the data reported by others can be explained by the small number of SCV-

positive patients as well as by long-term persistence of *S. aureus* along with SCV strains as a possible persistence mechanism.[16] The factors associated with the emergence of the SCV phenotype may have played a role outside the time frame delimited for this study.

From the perspective of the population structure, the study collection was heterogeneous and consisted of six major clones of methicillin-sensitive *S. aureus* (MSSA) with hospital-acquired (HA)-MSSA (33 strains) represented by CC5 and CC45 and community-associated (CA)-MSSA (35 strains) represented by CC7, CC8, CC15, and CC30.[6,14,37] The proportion of the CA and HA strains is likely to reflect the probability of *S. aureus* transmission to CF patients from the community and hospital environment.

Increased prevalence of resistance to MLS_B antibiotics in *S. aureus* isolates from CF patients treated with azithromycin has been reported by several studies.[15,32] Nevertheless, the MLS_B resistance mechanisms in CF isolates have been studied insufficiently. The most frequent of the MLS_B resistance mechanisms are MLS_B target-site alteration due to *erm* methylase action or *msrA* efflux pump.[23] Prunier *et al.*[34,35] have also reported MLS_B target-site mutations in the ribosomal genes *rrl* (23S rRNA), *rplD* (L4 protein), and *rplV* (L22 protein) as the cause of resistance in CF isolates. Isolates in their study were from CF patients treated with azithromycin.[35] A limitation of both studies is a relatively small sample of CF patients (five and nine patients, respectively) from whom the isolates were collected and, moreover, neither of them has reported the prevalence of these mutations among the *S. aureus* isolates from CF patients. In our study, we also found a high prevalence of MLS_B resistance (56%), with nearly half of the isolates carrying a resistance gene from the *erm* methylase group or *msrA* efflux pump. A greater half of MLS_B-resistant isolates (52%) had a mutation in the gene encoding 23S rRNA or ribosomal protein L4. A relevant finding is the association between azithromycin treatment and MLS_B resistance and mutations conferring this resistance.

PVL-positive *S. aureus* has recently been reported as a possible severe pathogen in CF patients.[2] In our study, the PVL genes have not been detected in any CF isolate, but a large proportion of isolates carried enterotoxin genes, a smaller proportion of isolates possessed exfoliatin genes, and one isolate harbored gene for toxic shock syndrome toxin (*tst*). However, no study of the impact of these virulence factors on the severity of CF has been conducted to date.

In conclusion, this is the first report to provide information about *S. aureus* isolates from Czech patients with CF, that is, about their clonal structure, distribution of resistance mechanisms, virulence genes, and the presence of SCV. High prevalence of MLS_B resistance emerged as a major finding. Most significantly, the connection between long-term prophylactic use of azithromycin and increase in MLS_B resistance in *S. aureus* was described, in agreement with previous studies. Nevertheless, we were the first to observe mutation of the MLS_B target site as a major resistance mechanism selected by azithromycin treatment. Further studies are needed to characterize the evolution of antibiotic resistance during antibiotic treatment with respect to SCV formation and mutation of the antibiotic target sites under specific circumstances as crucial mechanisms.

Acknowledgment

Supported by grant No. NT12395-5/2011 from the Internal Grant Agency (IGA) of the Ministry of Health of the Czech Republic.

Disclosure Statement

No competing financial interests exist.

References

1. **Andersen, D.H.** 1949. The present diagnosis and therapy of cystic fibrosis of the pancreas. Proc. R. Soc. Med. **42:**25–32.
2. **Barry, P.J., B.J. Isalska, and A.M. Jones.** 2014. Panton-Valentine Leukocidin-positive *Staphylococcus aureus*: a potentially significant pathogen in cystic fibrosis. Paediatr. Respir. Rev. **15 Suppl 1:**22–25.
3. **Besier, S., C. Smaczny, C. von Mallinckrodt, A. Krahl, H. Ackermann, V. Brade, *et al.*** 2007. Prevalence and clinical significance of *Staphylococcus aureus* small-colony variants in cystic fibrosis lung disease. J. Clin. Microbiol. **45:**168–172.
4. **Besier, S., J. Zander, B.C. Kahl, P. Kraiczy, V. Brade, and T.A Wichelhaus.** 2008. The thymidine-dependent small-colony-variant phenotype is associated with hypermutability and antibiotic resistance in clinical *Staphylococcus aureus* isolates. Antimicrob. Agents Chemother. **52:**2183–2189.
5. **Dasenbrook, E.C., W. Checkley, C.A. Merlo, M.W. Konstan, N. Lechtzin, and M.P. Boyle.** 2010. Association between respiratory tract methicillin-resistant *Staphylococcus aureus* and survival in cystic fibrosis. JAMA **303:**2386–2392.
6. **Deurenberg, R.H., and E.E. Stobberingh.** 2008. The evolution of *Staphylococcus aureus*. Infect. Genet. Evol. **8:**747–763.
7. **Döring, G., P. Flume, H. Heijerman, and J.S. Elborn.** 2012. Treatment of lung infection in patients with cystic fibrosis: current and future strategies. J. Cyst. Fibros. **11:**461–479.
8. **Eiff C. Von.** 2008. *Staphylococcus aureus* small colony variants: a challenge to microbiologists and clinicians. Int. J. Antimicrob. Agents **31:**507–510.
9. **Eiff C. Von, D. Bettin, R.A. Proctor, B. Rolauffs, N. Lindner, W. Winkelmann, *et al.*** 1997. Recovery of small colony variants of *Staphylococcus aureus* following gentamicin bead placement for osteomyelitis. Clin. Infect. Dis. **25:**1250–1251.
10. **Emerson, J., S. McNamara, A.M. Buccat, K. Worrell, and J.L. Burns.** 2010. Changes in cystic fibrosis sputum microbiology in the United States between 1995 and 2008. Pediatr. Pulmonol. **45:**363–370.
11. **Enright, M.C., N.P.J. Day, C.E. Davies, S.J. Peacock, and B.G. Spratt.** 2000. Multilocus sequence typing for characterization of methicillin-resistant and methicillin-susceptible clones of *Staphylococcus aureus*. J. Clin. Microbiol. **38:**1008–1015.
12. **European Committee on Antimicrobial Susceptibility Testings (EUCAST).** 2014. Breakpoint Tables for Interpretation of MICs and Zone Diameters, Version 4.0. 0–79. Available at http://www.eucast.org/fileadmin/src/media/PDFs/EUCAST_files/Breakpoint_tables/Breakpoint_table_v_4.0.pdf (Online).
13. **Gangell, C., S. Gard, T. Douglas, J. Park, N. de Klerk, T. Keil, *et al.*** 2011. Inflammatory responses to individual

microorganisms in the lungs of children with cystic fibrosis. Clin. Infect. Dis. **53:**425–432.

14. **Grundmann, H., D.M. Aanensen, C.C. van den Wijngaard, B.C. Spratt, D. Harmsen, A.W. Friedrich, *et al.*** 2010. Geographic distribution of *Staphylococcus aureus* causing invasive infections in Europe: a molecular-epidemiological analysis. PLoS Med. **7:** e1000215.
15. **Hansen, C.R., T. Pressler, N. Hoiby, and H.K. Johansen.** 2009. Long-term, low-dose azithromycin treatment reduces the incidence but increases macrolide resistance in *Staphylococcus aureus* in Danish CF patients. J. Cyst. Fibros. **8:**58–62.
16. **Hirschhausen, N., D. Block, I. Bianconi, A. Bragonzi, J. Birtel, J.C. Lee, *et al.*** 2013. Extended *Staphylococcus aureus* persistence in cystic fibrosis is associated with bacterial adaptation. Int. J. Med. Microbiol. **303:**685–692.
17. **Chen, J., Z. Yu, F.C. Michel, T. Wittum, and M. Morrison.** 2007. Development and application of real-time PCR assays for quantification of erm genes conferring resistance to macrolides-lincosamides-streptogramin B in livestock manure and manure management systems. Appl. Environ. Microbiol. **73:**4407–4416.
18. **Jennings, M.T., K.A. Riekert, and M.P. Boyle.** 2014. Update on key emerging challenges in cystic fibrosis. Med. Princ. Pract. **23:**393–402.
19. **Kahl, B.C., M. Herrmann, A. Schulze-Everding, H.G. Koch, K. Becker, E. Harms, *et al.*** 1998. Persistent infection with small colony variant strains of *Staphylococcus aureus* in patients with cystic fibrosis. J. Infect. Dis. **177:**1023–1029.
20. **Kahl, B.C., A. Duebbers, G. Lubritz, J. Haeberle, H.G. Koch, B. Ritzerfeld, *et al.*** 2003. Population dynamics of persistent *Staphylococcus aureus* isolated from the airways of cystic fibrosis patients during a 6-year prospective study. J. Clin. Microbiol. **41:**4424–4427.
21. **Kahl, B.C.** 2010. Impact of *Staphylococcus aureus* on the pathogenesis of chronic cystic fibrosis lung disease. Int. J. Med. Microbiol. **300:**514–519.
22. **Kriegeskorte, A., D. Block, M. Drescher, N. Windmüller, A. Mellmann, C. Baum, *et al.*** 2014. Inactivation of *thyA* in *Staphylococcus aureus* attenuates virulence and has a strong impact on metabolism and virulence gene expression. MBio **5:**e01447–14.
23. **Lina, G., A. Quaglia, M.-E. Reverdy, R. Leclercq, F. Vandenesch, and J. Etienne.** 1999. Distribution of genes encoding resistance to macrolides, lincosamides, and streptogramins among staphylococci. Antimicrob. Agents Chemother. **43:**1062–1066.
24. **Lina, G., Y. Piémont, F. Godail-Gamot, M. Bes, M.O. Peter, V. Gauduchon, *et al.*** 1999. Involvement of Panton-Valentine leukocidin-producing *Staphylococcus aureus* in primary skin infections and pneumonia. Clin. Infect. Dis. **29:**1128–1132.
25. **Liou, T.G., F.R. Adler, S.C. Fitzsimmons, B.C. Cahill, J.R. Hibbs, and B.C. Marshall.** 2001. Predictive 5-year survivorship model of cystic fibrosis. Am. J. Epidemiol. **153:**345–352.
26. **Milheiriço, C., D.C. Oliveira, and H. de Lencastre.** 2007. Update to the multiplex PCR strategy for assignment of *mec* element types in *Staphylococcus aureus.* Antimicrob. Agents Chemother. **51:**3374–3377.
27. **Mitchell, G., D.L. Séguin, A.-E. Asselin, E. Déziel, A.M. Cantin, E.H. Frost, *et al.*** 2010. *Staphylococcus aureus* sigma B-dependent emergence of small-colony variants and biofilm production following exposure to Pseudomonas aeruginosa 4-hydroxy-2-heptylquinoline-N-oxide. BMC Microbiol. **10:**33.
28. **Monday, S.R., and G.A. Bohach.** 1999. Use of multiplex PCR to detect classical and newly described pyrogenic toxin genes in staphylococcal isolates. J. Clin. Microbiol. **37:**3411–3414.
29. **Monecke, S., G. Coombs, A.C. Shore, D.C. Coleman, P. Akpaka, M. Borg, *et al.*** 2011. A field guide to pandemic, epidemic and sporadic clones of methicillin-resistant *Staphylococcus aureus*. PLoS One **6:**e17936.
30. **Murakami, K., W. Minamide, K. Wada, E. Nakamura, H. Teraoka, and S. Watanabe.** 1991. Identification of methicillin-resistant strains of staphylococci by polymerase chain reaction. J. Clin. Microbiol. **29:**2240–2244.
31. **O'Sullivan, B.P., and S.D. Freedman.** 2009. Cystic fibrosis. Lancet **373:**1891–1904.
32. **Phaff, S.J., H.A. Tiddens, H.A. Verbrugh, and A. Ott.** 2006. Macrolide resistance of *Staphylococcus aureus* and *Haemophilus* species associated with long-term azithromycin use in cystic fibrosis. J. Antimicrob. Chemother. **57:**741–746.
33. **Proctor, R.A., C. Von Eiff, B.C. Kahl, K. Becker, P. McNamara, M. Herrmann, *et al.*** 2006. Small colony variants: a pathogenic form of bacteria that facilitates persistent and recurrent infections. Nat. Rev. Microbiol. **4:**295–305.
34. **Prunier, A., B. Malbruny, D. Tande, B. Picard, and R. Leclercq.** 2002. Clinical isolates of *Staphylococcus aureus* with ribosomal mutations conferring resistance to macrolides. Antimicrob. Agents Chemother. **46:**3054–3056.
35. **Prunier, A.-L., B. Malbruny, M. Laurans, J. Brouard, J.-F. Duhamel, and R. Leclercq.** 2003. High rate of macrolide resistance in *Staphylococcus aureus* strains from patients with cystic fibrosis reveals high proportions of hypermutable strains. J. Infect. Dis. **187:**1709–1716.
36. **Razvi, S., L. Quittell, A. Sewall, H. Quinton, B. Marshall, and L. Saiman.** 2009. Respiratory microbiology of patients with cystic fibrosis in the United States, 1995 to 2005. Chest **136:**1554–1560.
37. **Rolo, J., M. Miragaia, A. Turlej-Rogacka, J. Empel, O. Bouchami, N.A. Faria, *et al.*** 2012. High genetic diversity among community-associated *Staphylococcus aureus* in Europe: results from a multicenter study. PLoS One **7:**e34768.
38. **Růžičková, V., J. Voller, R. Pantůček, P. Petráš, and J. Doškař.** 2005. Multiplex PCR for detection of three exfoliative toxin serotype genes in *Staphylococcus aureus*. Folia Microbiol. (Praha). **50:**499–502.
39. **Sagel, S.D., R.L. Gibson, J. Emerson, S. McNamara, J.L. Burns, J.S. Wagener, *et al.*** 2009. Impact of *Pseudomonas* and *Staphylococcus* infection on inflammation and clinical status in young children with cystic fibrosis. J. Pediatr. **154:**183–188.
40. **Stefani, S., D. Ryeon, J.A. Lindsay, A.W. Friedrich, A.M. Kearns, H. Westh, *et al.*** 2012. Meticillin-resistant *Staphylococcus aureus* (MRSA): global epidemiology and harmonisation of typing methods. Int. J. Antimicrob. Agents **39:**273–282.
41. **Vanhoof, R., C. Godard, J. Content, H.J. Nyssen, and E. Hannecart-Pokorni.** 1994. Detection by polymerase chain reaction of genes encoding aminoglycoside-modifying enzymes in methicillin-resistant *Staphylococcus aureus* isolates of epidemic phage types. J. Med. Microbiol. **41:**282–290.
42. **Wolter, D.J., J.C. Emerson, S. McNamara, A.M. Buccat, X. Qin, E. Cochrane, *et al.*** 2013. *Staphylococcus aureus* small-colony variants are independently associated

with worse lung disease in children with cystic fibrosis. Clin. Infect. Dis. **57:**384–391.
43. **Yagci, S., G. Hascelik, D. Dogru, U. Ozcelik, and B. Sener.** 2011. Prevalence and genetic diversity of *Staphylococcus aureus* small-colony variants in cystic fibrosis patients. Clin. Microbiol. Infect. **19:**77–84.
44. **Zolin, A., E. McKone, J. van Rens, A. Fox, P. Iansa, A. Preftitsi, *et al.*** 2014. European Cystic Fibrosis Society (ECFS) Patient Registry Annual Report 2010. Available at https://www.ecfs.eu/files/webfm/webfiles/File/ecfs_registry/ECFSPR_Report10_v12014_final_020617.pdf (Online).

Address correspondence to:
Jan Tkadlec, MSc
Department of Medical Microbiology
2nd Faculty of Medicine
Charles University in Prague
V Úvalu 84
Prague 150 06
Czech Republic

E-mail: tkadlecjan@gmail.com